INVOLVEMENT OF BLOOD BRAIN BARRIER EFFICACY, NEUROVASCULAR COUPLING AND ANGIOGENESIS IN THE HEALTHY AND DISEASED BRAIN

EDITED BY: Jean-luc Morel, Daniela Carnevale, Fabrice Dabertrand and Clotilde Lecrux

PUBLISHED IN: Frontiers in Physiology and Frontiers in Cellular Neuroscience

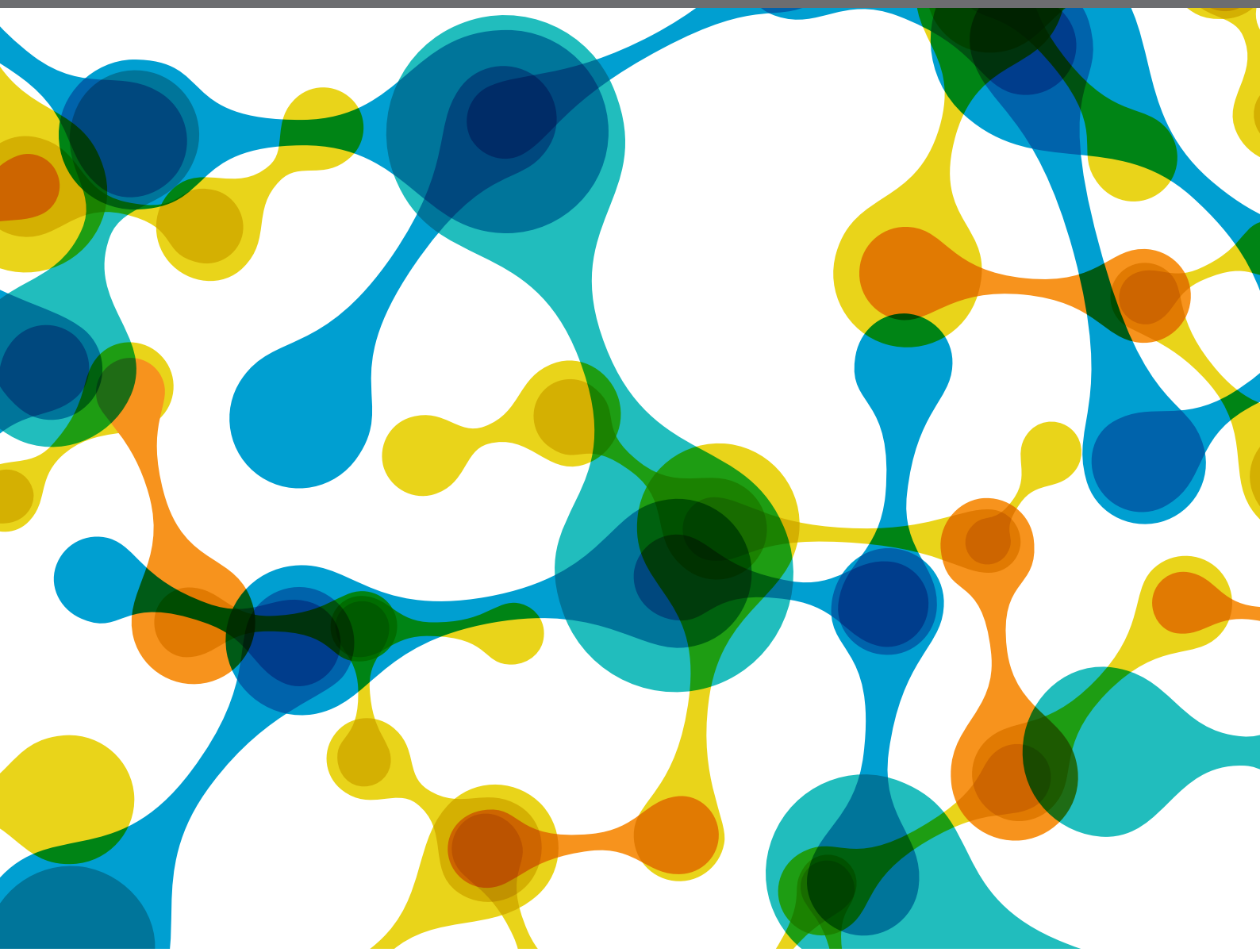

frontiers Research Topics

ISSN 1664-8714
ISBN 978-2-88971-891-7
DOI 10.3389/978-2-88971-891-7

About Frontiers

Frontiers is more than just an open-access publisher of scholarly articles: it is a pioneering approach to the world of academia, radically improving the way scholarly research is managed. The grand vision of Frontiers is a world where all people have an equal opportunity to seek, share and generate knowledge. Frontiers provides immediate and permanent online open access to all its publications, but this alone is not enough to realize our grand goals.

Frontiers Journal Series

The Frontiers Journal Series is a multi-tier and interdisciplinary set of open-access, online journals, promising a paradigm shift from the current review, selection and dissemination processes in academic publishing. All Frontiers journals are driven by researchers for researchers; therefore, they constitute a service to the scholarly community. At the same time, the Frontiers Journal Series operates on a revolutionary invention, the tiered publishing system, initially addressing specific communities of scholars, and gradually climbing up to broader public understanding, thus serving the interests of the lay society, too.

Dedication to Quality

Each Frontiers article is a landmark of the highest quality, thanks to genuinely collaborative interactions between authors and review editors, who include some of the world's best academicians. Research must be certified by peers before entering a stream of knowledge that may eventually reach the public - and shape society; therefore, Frontiers only applies the most rigorous and unbiased reviews.
Frontiers revolutionizes research publishing by freely delivering the most outstanding research, evaluated with no bias from both the academic and social point of view. By applying the most advanced information technologies, Frontiers is catapulting scholarly publishing into a new generation.

What are Frontiers Research Topics?

Frontiers Research Topics are very popular trademarks of the Frontiers Journals Series: they are collections of at least ten articles, all centered on a particular subject. With their unique mix of varied contributions from Original Research to Review Articles, Frontiers Research Topics unify the most influential researchers, the latest key findings and historical advances in a hot research area! Find out more on how to host your own Frontiers Research Topic or contribute to one as an author by contacting the Frontiers Editorial Office: frontiersin.org/about/contact

INVOLVEMENT OF BLOOD BRAIN BARRIER EFFICACY, NEUROVASCULAR COUPLING AND ANGIOGENESIS IN THE HEALTHY AND DISEASED BRAIN

Topic Editors:
Jean-luc Morel, Centre National de la Recherche Scientifique (CNRS), France
Daniela Carnevale, Sapienza University of Rome, Italy
Fabrice Dabertrand, University of Colorado, United States
Clotilde Lecrux, McGill University, Canada

Citation: Morel, J.-L., Carnevale, D., Dabertrand, F., Lecrux, C., eds. (2021). Involvement of Blood Brain Barrier Efficacy, Neurovascular Coupling and Angiogenesis in the Healthy and Diseased Brain. Lausanne: Frontiers Media SA. doi: 10.3389/978-2-88971-891-7

Table of Contents

frontiers in Physiology

EDITORIAL
published: 26 October 2021
doi: 10.3389/fphys.2021.771069

Editorial: Involvement of Blood Brain Barrier Efficacy, Neurovascular Coupling and Angiogenesis in the Healthy and Diseased Brain

Daniela Carnevale[1,2]*, *Fabrice Dabertrand*[3,4]*, *Clotilde Lecrux*[5]* and *Jean-Luc Morel*[6]*

[1] Department of Molecular Medicine, Sapienza University of Rome, Rome, Italy, [2] Research Unit of Neuro and Cardiovascular Pathophysiology, IRCCS Neuromed, Pozzilli, Italy, [3] Department of Anesthesiology, University of Colorado Anschutz Medical Campus, Aurora, CO, United States, [4] Department of Pharmacology, University of Colorado Anschutz Medical Campus, Aurora, CO, United States, [5] Montreal Neurological Institute, McGill University, Montreal, QC, Canada, [6] Univ. Bordeaux, CNRS, IMN, UMR 5293, Bordeaux, France

Keywords: blood brain barrier, neurovascular coupling, neurodegenerative disorders, stroke, traumatic brain injury, pericyte

Editorial on the Research Topic

Involvement of Blood Brain Barrier Efficacy, Neurovascular Coupling and Angiogenesis in the Healthy and Diseased Brain

As we wrote to introduce this topic, the complexity of the neurovascular unit (NVU) ensure two crucial function's in brain: the blood brain barrier (BBB) and neurovascular coupling (NVC). In this first volume, reviews and articles, reporting original research and methods, address the theme of this Research Topic through pathologies such as stroke or traumatic brain injury (TBI) by *in vivo* or post-mortem techniques both in animal models and in humans. Original points of view are presented on the functions of pericytes, glycocalyx, and Wnt pathways, as well as on vascular alterations and their link with the loss of nervous system functions in preeclampsia, amyotrophic lateral sclerosis, and Parkinson's disease.

Single-cell omic analyses have shown a radically increased vascular diversity along the arterial-venous axis compared to our previous understanding. This diversity should be considered in studies of neurovascular functions. The diverse functions of the endothelial cells (ECs), pericytes, and vascular smooth muscle cells (VSMC) should be considered alongside the perivascular macrophages that reside in the Virchow-Robin space. Moreover, the perivascular fibroblast-like cells, identified by RNAseq on arteries and veins (but not capillaries), are also described and proposed to be the pericyte precursors. Finally, astrocytes are included in the list because of the direct interaction between their endfoot processes and the ECs. The review of all cells participating in the neurovascular unit (NVU) is a good entry into the field of NVC and to understand the complexity of the links between cerebrovascular disorders and neurodegenerative diseases (Ross et al.). The functional importance of heterogeneity of cell subtypes reported by transcriptomic analysis is illustrated here with heterogeneity of calcium responses of astrocytes induced by cortical hyperemia due to whisker stimulation (Sharma et al.). This work suggests that the heterogeneity of calcium response is able to transduce multiple specific signals to fine-tune the NVC process.

The role of pericytes in NVC is under development not only because of its function in the regulation of brain flow, but also because of other currently unknown functions involved in pathologies. In fact, pericytes cover 90% of the length of capillary beds. The recent research using RNAseq approaches has proposed that several pericyte lines present in the brain that regulate cerebral blood flow also have potential other functions. The comparison of available RNAseq

Edited and reviewed by:
Gerald A. Meininger, University of Missouri, United States

***Correspondence:**
Daniela Carnevale
daniela.carnevale@uniroma1.it
Fabrice Dabertrand
fabrice.dabertrand@cuanschutz.edu
Clotilde Lecrux
clotilde.lecrux@gmail.com
Jean-Luc Morel
jean-luc.morel@u-bordeaux.fr

Specialty section:
This article was submitted to Vascular Physiology, a section of the journal Frontiers in Physiology

Received: *05 September 2021*
Accepted: *27 September 2021*
Published: *26 October 2021*

Citation:
Carnevale D, Dabertrand F, Lecrux C and Morel J-L (2021) Editorial: Involvement of Blood Brain Barrier Efficacy, Neurovascular Coupling and Angiogenesis in the Healthy and Diseased Brain. Front. Physiol. 12:771069. doi: 10.3389/fphys.2021.771069

to characterize pericyte subtypes is exhaustively presented (Hariharan et al.). The diversity of potassium channels expressed in pericytes around brain capillaries suggest their important role in metabolism-electrical coupling required for cerebral blood flow (CBF) regulation. Moreover, the putative roles of TRP-, voltage-gated calcium- and chloride channels, as well as the reticulum calcium channels inositol trisphosphate receptors (InsP3R) are also discussed. The regulation of these channels is assumed by the variety of G protein-coupled receptors (GPCRs) expressed in pericytes in response to external stimuli (Hariharan et al.). As presented in other articles (see below), disorders affecting brain function could be linked to alteration of the NVU and especially pericytes. As mentioned in the perspectives in Hariharan et al., "pericytes appear exceptionally sensitive to pathological perturbations," but the specific pharmacological targeting of ion channels and GPCRs expressed in pericytes could represent new therapeutic approaches. One research article illustrates this by the description of the role of NLRP3 on pericytes. In fact, its deficiency in transgenic mice induced a decrease in the number of pericytes as well as reduced collagen-IV platelet-derived growth factor receptor β (PDGFRβ), and CD13 expression. Moreover, in cultured pericytes, the process is inhibited by MCC950, the antagonist of NLRP3 and Il-1β treatment (Quan et al.). Research on pericytes and other cells that compose the NVU has benefited greatly from the development of technologies that allow *in vivo* monitoring of cellular activity in animal models using various techniques, including two-photon microscopy. These techniques require the installation of a cranial window according to standardized procedures (Kiliç et al.). The time-controlled focal photothrombosis has classically been used to described the acute effect of ischemia, but it can also be used to follow the time course of the BBB alterations in the penumbra and to measure the distance of effect, including the contralateral hemisphere, in order to describe the possible spatiotemporal progression of the damages correlated to the intensity of the ischemia (Weber et al.). By coupling two-photon microscopy with the use of fluorescein isothiocyanate (FITC)-gelatin (as a MMP9-activity probe) and photothrombosis (using Rose Bengal) in a mouse model expressing tdTomato in pericytes, it has been possible to follow the time course of capillary occlusion and its physiological consequences (Underly and Shih). During ischemia, the pericytes are immediately affected and participate in the protein degradation via MMP9-dependent mechanism. L-NIL (inhibitor of nitric oxide (NO) synthases) attenuated capillary leakage and the addition of anisomycin (inhibitor of protein synthesis), led to near complete elimination of FITC-gelatin cleavage and vascular leakage. These results indicate that both NO synthase and new protein synthesis are involved in the rapid activation of MMP-9 during ischemia (Underly and Shih).

Stroke is the most important acute event that induces NVU remodeling. Freitas-Andrade et al. present a comprehensive update on this remodeling. General concepts about stroke and therapeutic approaches are linked to the endocrine function of ECs to induce neuronal development. However, how neuronal activity is responsible for plasticity and remodeling of cerebrovascular network (angiogenesis and barriergenesis) has also been studied. The time course of the ischemia-reperfusion effects is important to understand the alterations of EC structure and functions; the roles of pericytes, astrocytes, microglial cells, and the perivascular macrophages' roles on the BBB and NVC efficacies. Where and when these processes are engaged is crucial to understand the importance of biological processes such as degradation of the basement membrane or angiogenesis following ischemic and hemorrhagic strokes. The authors also addressed the issue of sexual differences in cerebrovascular outcomes of stroke through the prism of the effects of hormones on CBF and risk of ischemic stroke. Finally, limitations of preclinical stroke research concerning models of stroke are discussed. This review is well-completed by another article focused on glycocalyx, which is proposed to be responsible for endothelial mechanobiology in collaboration with channels specialized in mechanosensitivity. Variations of pressure on the BBB (or cells of the NVU) is one of the pathways that signals pathological changes (Nian et al.). Collagen-IV and fibronectin could represent markers of extracellular matrix reorganization due to ischemia as shown by immunohistochemistry in preclinical animal models and in the human brain (Michalski et al.). To test a new therapeutic pathway, more than one parameter should be followed. After ischemia, DL-3n-butylphthalide promotes angiogenesis in the perifocal region to restore the vasculature, but it can also acutely protect the BBB integrity as suggested in rat models by oral administration 1 h after the beginning of reperfusion process starting 2 h from a transient middle cerebral artery occlusion (Mamtilahun et al.).

The second severe alteration to the NVU is due to TBI. The review of preclinical experiments performed on mice have shown that alterations of the BBB can trigger or enhance the neurodegenerative disorders following mild TBI (Wu et al.). Because TBI and ischemic and hemorrhagic strokes have some similarities, Menet et al. recapitulated the works on genetic variants of Wnt partners representing risk factors of stroke as well as preclinical studies on animal models reporting Wnt partners as biomarkers or targets to reduce the deleterious effects of ischemic and hemorrhagic stroke and their implications in TBI. Because Wnt pathways are involved in the regulation of neurogenesis, synaptogenesis, angiogenesis, and BBB formation and stabilization as well as in dendritic cells implicated in immunity and inflammation, they are potentially "druggable targets" (Menet et al.).

Alterations of the NVU and NVC are also observed in neurodegenerative disorders. The accumulation of amyloid peptides is considered to drive the pathogenesis of Alzheimer's disease and cerebral amyloid angiopathy (CAA). Interestingly, the amyloid precursor protein (APP) could have a role in BBB maintenance (Ristori et al.). The links between nitric oxide and amyloid pathways in ECs, vascular disorders observed in transgenic mice with APP alterations (KO, expression of mutations-induced neurodegeneration, etc.), the APP physiological role in ECs (particularly in angiogenesis even if the functionality of the new vessels is always moot), and cell adhesion and transcription factors (AICD provided from

the cleavage of APP is a regulator of transcription and calcium signaling) are reviewed. CAA could also be induced by the impairment of the transport of amyloid peptides through the basement membrane, and the molecular interactions between amyloid peptides and basement membrane proteins could be responsible for their aggregation and pathogenicity (Howe et al.).

The alteration of the BBB is now well-documented in AD patients and animal models, but it is also observed in Parkinson's disease (PD) animal models. Alterations of blood pressure, angiogenesis and vascular remodeling are reported in PD patients, and now BBB disruption is reported in the white matter of PD patients by MRI study (Al-Bachari et al.).

Since the nervous and vascular systems are developed together and because of the crucial role of NVC to sense the neuronal function, it is essential to know the development of the vascular network of the spinal cord to better consider the post-traumatic repair of this nervous tissue and also to understand pathologies such as amyotrophic lateral sclerosis or arteriovenous malformations (Vieira et al.).

Finally, vascular pathologies can induce or exacerbate cognitive problems as shown with hypertension. For example, préclampsia is a common hypertensive disorder in pregnant women potentially linked with cognitive disorders. Mice, chronically overexpressing human angiotensinogen and renin (R^+A^+ mice), display characteristics of preeclampsia and have now been validated to investigate cognitive alterations in post-partum females and their pups (Trigiani et al.).

In conclusion, as we can read in this first volume of "Involvement of Blood Brain Barrier Efficacy, Neurovascular Coupling and Angiogenesis in the Healthy and Diseased Brain," many questions are still open to better understanding the interactions between cells of the NVU to study the efficacy of brain functions, the activated molecular pathways, and the time course of their alterations after vascular trauma or in neurodegenerative disorders.

AUTHOR CONTRIBUTIONS

All authors listed have made a substantial, direct, and intellectual contribution to the work, and approved it for publication.

FUNDING

FD received awards from the CADASIL Together We Have Hope non-profit organization; a research grant from the Center for Women's Health Research located at the University of Colorado Anschutz Medical Campus; a research grant from the University of Pennsylvania Orphan Disease Center in partnership with the cureCADASIL, and the National Heart, Lung, and Blood Institute R01HL136636. J-LM received grants from Center National de la Recherche Scientifique (CNRS) and Centre National des études spatiales (CNES). DC received grants from the Italian Ministry of Health (MOH) for the ricerca corrente program.

ACKNOWLEDGMENTS

The authors thank all the reviewers who have taken time to analyze the manuscript and discuss with the authors.

Conflict of Interest: The authors declare that the research was conducted in the absence of any commercial or financial relationships that could be construed as a potential conflict of interest.

Publisher's Note: All claims expressed in this article are solely those of the authors and do not necessarily represent those of their affiliated organizations, or those of the publisher, the editors and the reviewers. Any product that may be evaluated in this article, or claim that may be made by its manufacturer, is not guaranteed or endorsed by the publisher.

frontiers in Physiology

REVIEW
published: 07 August 2020
doi: 10.3389/fphys.2020.00948

Structural and Functional Remodeling of the Brain Vasculature Following Stroke

*Moises Freitas-Andrade[1], Joanna Raman-Nair[1] and Baptiste Lacoste[1,2,3]**

[1] Neuroscience Program, Ottawa Hospital Research Institute, Ottawa, ON, Canada, [2] Department of Cellular and Molecular Medicine, Faculty of Medicine, University of Ottawa, Ottawa, ON, Canada, [3] Brain and Mind Research Institute, University of Ottawa, Ottawa, ON, Canada

OPEN ACCESS

Edited by:
Fabrice Dabertrand, University of Colorado School of Medicine, United States

Reviewed by:
William J. Pearce, Loma Linda University School of Medicine, United States
Anne Dorrance, Michigan State University, United States

***Correspondence:**
Baptiste Lacoste
blacoste@uottawa.ca

Specialty section:
This article was submitted to Vascular Physiology, a section of the journal Frontiers in Physiology

Received: *11 May 2020*
Accepted: *14 July 2020*
Published: *07 August 2020*

Citation:
Freitas-Andrade M, Raman-Nair J and Lacoste B (2020) Structural and Functional Remodeling of the Brain Vasculature Following Stroke. Front. Physiol. 11:948. doi: 10.3389/fphys.2020.00948

Maintenance of cerebral blood vessel integrity and regulation of cerebral blood flow ensure proper brain function. The adult human brain represents only a small portion of the body mass, yet about a quarter of the cardiac output is dedicated to energy consumption by brain cells at rest. Due to a low capacity to store energy, brain health is heavily reliant on a steady supply of oxygen and nutrients from the bloodstream, and is thus particularly vulnerable to stroke. Stroke is a leading cause of disability and mortality worldwide. By transiently or permanently limiting tissue perfusion, stroke alters vascular integrity and function, compromising brain homeostasis and leading to widespread consequences from early-onset motor deficits to long-term cognitive decline. While numerous lines of investigation have been undertaken to develop new pharmacological therapies for stroke, only few advances have been made and most clinical trials have failed. Overall, our understanding of the acute and chronic vascular responses to stroke is insufficient, yet a better comprehension of cerebrovascular remodeling following stroke is an essential prerequisite for developing novel therapeutic options. In this review, we present a comprehensive update on post-stroke cerebrovascular remodeling, an important and growing field in neuroscience, by discussing cellular and molecular mechanisms involved, sex differences, limitations of preclinical research design and future directions.

Keywords: stroke, cerebrovascular, neurovascular unit, vascular remodeling, angiogenesis, blood–brain barrier

GENERAL CONCEPTS

Stroke is an injury to the central nervous system (CNS) with a vascular cause, leading to high rates of disability and representing the second leading cause of death worldwide (Mittmann et al., 2012; Krueger et al., 2015; Mozaffarian et al., 2015). Stroke compromises cerebral blood flow (CBF) following either blood vessel occlusion (i.e., *ischemic stroke*) or blood vessel rupture

(i.e., *hemorrhagic stroke*), which includes intracerebral hemorrhage (ICH) or subarachnoid hemorrhage (SAH) (Sacco et al., 2013). Hemorrhagic strokes represent ∼20% of cases, while ischemic lesions account for almost 80% of all strokes (Qureshi et al., 2009; Donkor, 2018). Most stroke survivors are left with residual impairments requiring chronic rehabilitation therapy (Bernhardt et al., 2019; Hayward et al., 2019). Moreover, the 30-day mortality rate of ischemic stroke has been estimated at ∼15% in high-income countries (Gattringer et al., 2019), which may vary depending on sex-specific factors (Arnao et al., 2016) and economic disparities (Osypuk et al., 2017). A recent study from the Netherlands showed that in >15,000 patients who had a first stroke at age 18–49 in 1998–2010, cumulative 15-year mortality among 30-day survivors was 13.3 per 1,000 person-years, compared with an expected mortality of 2.4 per 1,000 person-years in the general population (Ekker et al., 2019). In addition, brain microinfarcts (<5 mm lesions) play an insidious role in aging and dementia, since these microscopic strokes may accumulate over several years before manifesting as detectable symptoms (Hakim, 2014; Ferro et al., 2019).

By limiting tissue perfusion, stroke affects both neuronal health and vascular health (Iadecola and Anrather, 2011a,b; Tymianski, 2011; Silasi and Murphy, 2014) with widespread consequences. While numerous lines of investigation have aimed to develop neuroprotective therapies for stroke (Dirnagl et al., 2013; Willis and Hakim, 2013; Corbett et al., 2014; Meschia et al., 2014; Ploughman et al., 2015), there were too few significant advances. For instance, only thrombolysis with recombinant tissue plasminogen activator rtPA (Hebert et al., 2016) or acute endovascular treatment (Goyal et al., 2015) have led to significant benefit for ischemic stroke (Richardson et al., 2014; Teasell et al., 2014a,b; Gurewich, 2016). Within the first hours after ischemic stroke, the goal is to promptly restore perfusion (Lin and Sanossian, 2015; Prabhakaran et al., 2015), and intravenous administration of rtPA has been the first line of intervention for years (The National Institute of Neurological Disorders, and Stroke rt-Pa Stroke Study Group, 1995; Gurewich, 2016). Unfortunately, rtPA must be administered within a narrow therapeutic window (∼4 h following stroke). Moreover, due to safety concerns, its use is limited to 10–15% of stroke victims (Jauch et al., 2013; Gurewich, 2016; Suzuki et al., 2016).

Maintenance of brain health is ensured by key vascular features: (i) The safeguarding of vascular networks for efficient perfusion; (ii) The function of the blood–brain barrier (BBB) to preserve brain homeostasis; and (iii) The regulation of CBF to match energy demands of brain cells (Andreone et al., 2015). During development, neuronal and vascular network formation share similar mechanisms of growth and maturation (Carmeliet and Tessier-Lavigne, 2005; Gu et al., 2005; Eichmann and Thomas, 2013). Endothelial cells (ECs) secrete factors that modulate neurogenesis (Goldman and Chen, 2011; Delgado et al., 2014; Licht and Keshet, 2015; Walchli et al., 2015) and neuronal activity controls brain angiogenesis and barriergenesis (Lacoste, 2014; Biswas et al., 2020). In the mature brain, relationships between neural and vascular cells ensure a functional matching such that changes in neuronal activity are coupled to changes in CBF (i.e., neurovascular coupling) (Hillman, 2014). This involves balanced secretions of vasoconstrictor and vasodilator molecules including, but not limited to, endothelial-derived nitric oxide (NO), or astrocyte-derived prostaglandin E_2 (PGE_2) (Attwell et al., 2010; Cauli and Hamel, 2010; Mishra et al., 2016). The underlying structure of neurovascular coupling is the neurovascular unit (NVU), which corresponds to a multicellular ensemble in which ECs, neurons, pericytes, astrocytes, and microglia orchestrate brain function (Zlokovic, 2010; Lind et al., 2013; ElAli et al., 2014; Howarth, 2014) (**Figure 1**). The NVU also constitutes the BBB which controls the efflux/influx of substances for a controlled brain homeostasis (Daneman, 2012; Ben-Zvi et al., 2014; Andreone et al., 2015; Profaci et al., 2020). The structural and functional interdependence between brain cells and blood vessels renders the brain particularly vulnerable to declines in CBF that result from stroke.

Post-stroke NVU remodeling represents a growing field in neuropathophysiology (Maki et al., 2013; Knowland et al., 2014; Liu et al., 2014; Prakash and Carmichael, 2015; Munji et al., 2019). While the mechanisms underlying ischemia-induced neuronal plasticity are an ongoing focus in stroke research (Mostany et al., 2010; Swayne and Wicki-Stordeur, 2012; Silasi and Murphy, 2014; Felling and Song, 2015), our understanding of acute and chronic vascular responses to stroke is only in its infancy. NVU remodeling is rapidly activated after stroke and occurs at the molecular and cellular levels. Within minutes following an ischemic insult, proangiogenic genes are upregulated and growth factors are secreted to promote both angiogenesis and survival of glial and neuronal cells within peri-infarct tissues (Ergul et al., 2012; Gutierrez-Fernandez et al., 2012; Talwar and Srivastava, 2014). These events stimulate neurogenesis, synaptogenesis and neuronal plasticity, improving functional outcome (Ergul et al., 2012). In addition, changes in mechanical shear stress due to arterial occlusion result in increased flow through pre-existing collaterals and trigger significant changes in blood vessels (Nishijima et al., 2015). Paradoxically, endogenous repair mechanisms also have detrimental effects on the brain vasculature, as we will discuss in this review. Altogether, these cellular and molecular responses to stroke contribute to vascular and neuronal injury (Haley and Lawrence, 2016; Nahirney et al., 2016).

Despite recent advances in significant areas of stroke pathophysiology, certain aspects of stroke, and particularly spatiotemporal cerebrovascular responses, require further attention. Stroke doubles the risk for dementia (post-stroke dementia), and approximately 30% of stroke survivors develop cognitive dysfunction within 3 years (Allan et al., 2011; Vijayan and Reddy, 2016). The link between stroke and dementia was also observed in patients younger than 50 years, up to 50% of whom exhibit cognitive deficits after a decade (Schaapsmeerders et al., 2013). There is also mounting evidence indicating that stroke can precipitate the likelihood of developing neurodegeneration (Vijayan and Reddy, 2016). Vascular vulnerabilities caused by stroke result in neurovascular uncoupling and affect the integrity of the BBB; these changes impact proper brain functioning and are characteristics found in the early stages of several neurological disorders including Alzheimer's disease. Therefore, understanding the mechanisms involved in cerebrovascular

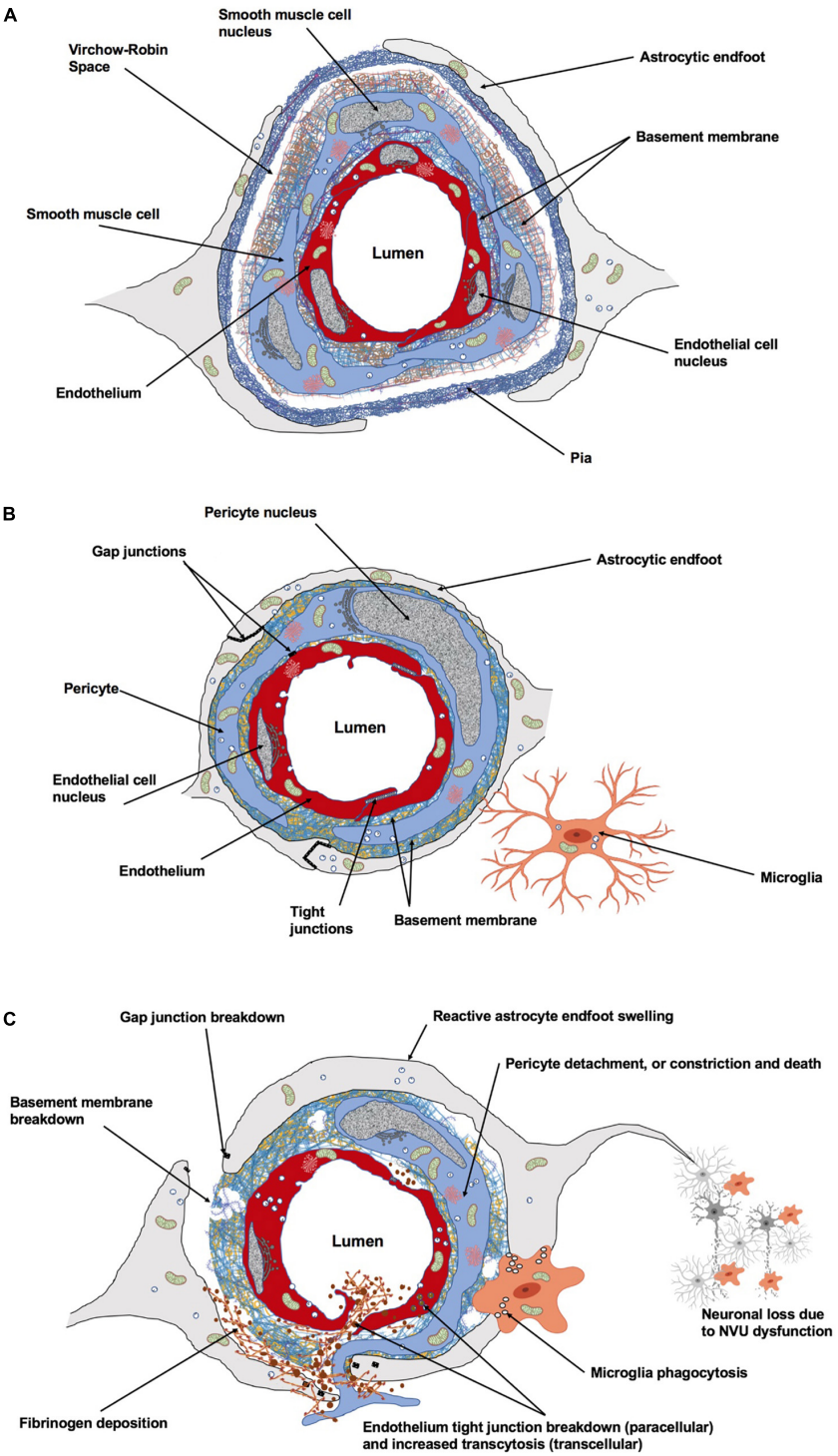

FIGURE 1 | Cellular and acellular constituents of the neurovascular unit (NVU). **(A)** At the level of penetrating arteries, upstream capillaries, endothelial cells (ECs) are surrounded by vascular smooth muscle cells. At this level, cerebral vessels are still surrounded by the pia. The Virchow–Robin space is located between the pia and the glial limitans formed by the astrocytic endfeet. This perivascular space plays an important role in waste removal and in regulation of the interstitial fluid of the brain. **(B)** At the level of intracerebral capillaries, the NVU is comprised of ECs, pericytes, astrocytes, microglia, and the basement membrane. Both the ECs and surrounding pericytes are unsheathed by a common basement membrane. Pericyte processes encase most of the endothelial surface. Astrocytic endfeet completely surround the capillary wall. Resting microglial have a ramified morphology and are in constant surveillance around brain microvessels. Gap junction channels enable cytoplasmic continuity between astrocytic endfeet, and also exist between pericytes and ECs at peg-socket structures providing quick communication between these cells. Specialized tight junctions between ECs prevent paracellular leakage into the brain parenchyma. **(C)** The NVU undergoes dramatic structural changes following stroke, affecting cerebrovascular integrity, neuro-vascular coupling and neuronal survival within the peri-infarct territory. *Figure prepared with BioRender.*

adaptation to brain injury may have profound long-term clinical outcomes. In this review, we present an overview of recent advances in cerebrovascular research on stroke, and we discuss limitations and ideas for future investigation.

EFFECTS OF STROKE ON THE NEUROVASCULAR UNIT

Capillary brain ECs and surrounding pericytes, astrocytes, microglia, neurons, and extracellular matrix (ECM) of the basement membrane altogether compose the NVU. The multiple interactions between these cellular and acellular elements are disrupted after stroke.

Effects of Stroke on Endothelial Cells

Effects of Stroke on Endothelial Cell Structure and Molecular Profile

The EC layer provides the CNS with an important physical, functional, and metabolic barrier, which limits the entry of circulating hydrophilic molecules, such as peptides and proteins into the brain parenchyma. Gaseous molecules such as oxygen (O_2) and carbon dioxide (CO_2), as well as small lipophilic molecules less than 500 Da can diffuse freely through brain ECs. Brain ECs are attached to each other by specialized 'tight' junctions (TJs) consisting of various molecular components (Chow and Gu, 2015; Delaney and Campbell, 2017). The TJs form the physical barrier of the BBB (Reese and Karnovsky, 1967) and regulate permeability of the endothelial layer. TJ proteins have also been implicated in regulation of gene expression, cell proliferation and differentiation (Zlokovic, 2008; Sweeney et al., 2019). Brain ECs also express gap junction proteins, such as connexin (Cx)-37, Cx40 and Cx43 that contribute to TJ integrity (Nagasawa et al., 2006; De Bock et al., 2011) and cell–cell communication (Figueroa and Duling, 2009; De Bock et al., 2014). The role of endothelial Cxs in BBB function, particularly during aging, remains poorly explored (De Bock et al., 2014).

TJ disruption is a hallmark of both ischemic and hemorrhagic stroke and is typically associated with increased vascular permeability and homeostatic changes in the neuronal microenvironment. It was shown in an ischemia/reperfusion model that BBB permeability exhibited a biphasic pattern (permeability occurring at 3 and 72 h of reperfusion), which was linked to changes in claudin-5, occludin and ZO-1 protein levels (Jiao et al., 2011). More recently, Knowland et al. (2014) used transgenic mice expressing a fusion protein of eGFP with claudin-5 and elegantly demonstrated that TJs were stable during the early phase of reperfusion (up to 24 h) following 30 min of transient middle cerebral artery occlusion (tMCAo), but underwent significant remodeling and breakdown from 48 to 58 h after reperfusion (Knowland et al., 2014). This study demonstrates the stepwise dysfunction that occurs initially at the transcellular level followed by paracellular impairment that accounts for BBB deficits in stroke. Furthermore, it links caveolin-1 (cav-1) to impaired transcellular route.

Caveolae-mediated transcytosis is a major pathway for transport across ECs and it is normally suppressed in the healthy brain (Drab et al., 2001; Predescu et al., 2001; Schnitzer, 2001; Tuma and Hubbard, 2003; Ben-Zvi et al., 2014). Caveolae are 50–100 nm invaginations in the plasma membrane and are highly enriched in saturated phospholipids, sphingolipids, ethanolamine plasmalogens and cholesterol (Andreone et al., 2017). The formation of caveolae vesicles requires both caveolin coat proteins and cytosolic adaptor proteins belonging to the cavin family (Ayloo and Gu, 2019). Under physiological conditions, major facilitator super family domain containing 2a (MFSD2A) is selectively expressed in brain endothelium (Ben-Zvi et al., 2014). MFSD2A acts as a lipid flippase, transporting phospholipids, from the outer to inner plasma membrane leaflet thus altering the plasma membrane composition in such a way that caveolae vesicles are unable to form (Andreone et al., 2017). Inhibition of caveolae formation and trafficking ensures BBB integrity under normal conditions. However, caveolae-mediated transcytosis is activated following tMCAo, and cav-1 expression increases early following stroke or brain injury, prior to TJ disassembly (Knowland et al., 2014). A significant correlation between the extent of BBB disruption following brain ischemia and cav-1 expression was recently confirmed in mice subjected to focal cortical ischemia induced by photothrombosis (Choi et al., 2016). In summary, ischemia/reperfusion-induced BBB disruption in the peri-infarct region involves (i) upregulation of caveolae-mediated endothelial transcytosis in the early phase of reperfusion (between 0 and 12 h); (ii) major TJ remodeling in the late phase (48–60 h) (Cipolla et al., 2004; Knowland et al., 2014; Haley and Lawrence, 2016; Nahirney et al., 2016). The first phase, which peaks at 6 h, leads to non-selective vesicular transport of blood-borne molecules across ECs. The second phase leads to breakdown of the vessel wall, exacerbating BBB dysfunction. It remains unclear why ECs respond in two phases and whether increased transcytosis provides a signal to the NVU. An enticing notion would be to test whether stroke disrupts the unique endothelial cell membrane lipid composition in such a way that induces cav-1 dependent transcytosis. Other factors can also be at play, for example, in a mouse model of retinal vein occlusion, activated ECs expressed caspase-9, the caspase-9 induced non-apoptotic endothelial dysfunction, and barrier breakdown (Avrutsky et al., 2020). Nonetheless, BBB disruption via increased caveolae-mediated bulk-flow fluid transcytosis allows free mobility of toxic substances and accumulation into the brain of plasma proteins that notably include immunoglobulins, albumin, laminin, thrombin and ferritin, collectively leading to neuroinflammation, neuronal death and functional impairment (Zlokovic, 2010).

Other important endothelial players are involved in vascular responses to stroke. Rho-associated coiled-coil kinase (ROCK), a downstream effector of the small GTPase RhoA, is a major regulator of endothelial function (van Nieuw Amerongen et al., 2003; Allen et al., 2010; Mikelis et al., 2015; De Silva et al., 2016) and is involved in the pathogenesis of vascular diseases (Yao et al., 2010; Hartmann et al., 2015; Kajikawa et al., 2015). ROCKs belong to the serine-threonine family of kinases, with two isoforms (1 and 2) that play different pathophysiological roles (Hartmann et al., 2015). Both ROCK1 and ROCK2 are expressed in ECs (Montalvo et al., 2013), and

ROCK2 is abundantly found in the brain (Nakagawa et al., 1996) where it plays a pivotal role in endothelial homeostasis. ROCKs play integral roles in cell adhesion, migration and proliferation (Riento and Ridley, 2003) and when activated by RhoA it regulates assembly of the actin cytoskeleton and smooth muscle cell contractility (Noma et al., 2012). In rodent tMCAo, ischemia-reperfusion promotes RhoA/ROCK signaling (Cui et al., 2013; Canazza et al., 2014). Pathological RhoA/ROCK2 activation in ECs promotes the association between endothelial NO synthase (eNOS) and cav-1 and their translocation to membrane caveolae compartments (Zhu et al., 2003) where eNOS is inhibited (Ju et al., 1997; Drab et al., 2001; Ming et al., 2002), which might in turn impair permeability (Siddiqui et al., 2011). *In vivo* evidence from pharmacological studies in mice show that non-selective inhibition of ROCKs following tMCAo exerts neurovascular protection by significantly reducing lesion volumes and improving CBF, in an endothelium-dependent manner (Rikitake et al., 2005; Shin et al., 2007; Sugimoto et al., 2007; Satoh et al., 2010; Vesterinen et al., 2013). Non-selective inhibition of ROCKs by hydroxyfasudil also attenuates early BBB disruption following intracerebral hemorrhage in rats (Fujii et al., 2012; Fu et al., 2014). Selective pharmacological ROCK2 inhibition by KD025 (SLx-2119) was recently demonstrated as efficacious and safe acutely after tMCAo in mice (Lee et al., 2014). ROCK also directly inhibits expression of eNOS (*Nos3*) by decreasing the mRNA stability of eNOS (Noma et al., 2012). Interestingly, expression and activity of eNOS are constitutively enhanced in brain ECs from heterozygous ROCK2 knockout ($Rock2^{+/-}$) mice that display reduced infarct volume following tMCAo (Hiroi et al., 2018). Accumulating *in vitro* evidence also shows that increased expression and activity of ROCKs in ECs account for ischemia-induced barrier dysfunction, for instance following oxygen-glucose deprivation (OGD) (Allen et al., 2010; Gibson et al., 2014; Yang et al., 2016). Pathological activation of ROCK2 also promotes oxidative stress (Rivera et al., 2007; Soliman et al., 2012), and pharmacological blockade of ROCKs reduces OGD-induced hyperpermeability via inhibition of endothelial oxidative stress (Gibson et al., 2014).

As a result of a tightly sealed BBB, brain ECs express specialized transporter proteins on both their luminal and abluminal surfaces. Efflux transporters, primarily localized on the luminal surface, include ATP-binding cassette (ABC) transporters, the multidrug resistance transporter P-glycoprotein (Pgp) and several multidrug resistance-associated proteins (MRPs) that work together to reduce penetration of toxic compounds into the brain (Shen and Zhang, 2010). Among many other transport systems, brain ECs also express the glucose transporter-1 (GLUT1), involved in delivering glucose into the brain (Winkler et al., 2015; Tang M. et al., 2017; Vaudano et al., 2017). For instance, isolated bovine brain capillaries subjected to an OGD paradigm displayed decreased Pgp and MRP expression after 24 h of reoxygenation (Tornabene et al., 2019). Interestingly, vitamin E α-tocotrienol was reported as protective against tMCAo in mice through upregulation of MRP-1, resulting in an increase in efflux of toxic oxidized glutathione (Park et al., 2011). In this study, the authors investigated the effects of α-tocotrienol on neuronal MRP-1, but the role of endothelial MRP-1 in the context of ischemia/reperfusion remains to be explored.

Cerebral ECs also express a wide array of ion transporters and channels, asymmetrically distributed between the luminal and abluminal plasma membranes. This polarized arrangement of channels and transporters allows ECs to participate in the regulation of brain interstitial fluid volume and composition. During the early hours following ischemic stroke in animal models, edema builds up via processes involving stimulation of EC ion transporters on the luminal side and increased secretion of Na^+, Cl^-, followed by water from the blood stream into the brain across the BBB (O'Donnell, 2014). These transporters also represent possible targets for therapeutic intervention in stroke (O'Donnell, 2014; Brzica et al., 2017).

As mentioned earlier, endogenous mechanisms recruited following brain ischemia have detrimental effects on the brain vasculature (Beck and Plate, 2009). Vascular endothelial growth factor (VEGF) is a potent inducer of microvascular permeability (Dvorak, 1995; Zhang et al., 2002) via rapid (within minutes) stimulation of caveolae-mediated transcytosis (Feng et al., 1999; Chen et al., 2002). Moreover, oxidative stress is promptly elevated in the peri-infarct region (Carbonell and Rama, 2007; Shi and Liu, 2007; Pradeep et al., 2012; Rodrigo et al., 2013) and represents a major cause of vascular dysfunction through neutralization of NO by reactive oxygen species. This decreases NO bioavailability and inhibition of its modulatory role in angiogenesis and vascular reactivity (Nedeljkovic et al., 2003; Park et al., 2005; Fisher, 2008; Xu C. et al., 2016; van Leeuwen et al., 2020). Interestingly, in patients with acute stroke, low NO levels following stroke correlate with outcome severity (Rashid et al., 2003). Oxidative stress also induces vascular hyperpermeability through oxidant-induced phosphorylation of cav-1 and increased caveolae-mediated transcytosis in ECs in culture (Takeuchi et al., 2013). Altogether, these mechanisms contribute to the early-onset vascular injury observed in the peri-infarct region (Haley and Lawrence, 2016; Nahirney et al., 2016).

Collectively, these studies reveal a high complexity at the level of the BBB, which raises challenges but also new opportunities for stroke therapy (Abdullahi et al., 2018; Liberale et al., 2020). Recent publications are unmasking novel endothelial metabolic pathways that are conserved across diseases and species (Rohlenova et al., 2020). Interestingly, Munji et al. (2019) recently investigated brain EC transcriptomic changes in four different brain injury models associated with BBB disruption: permanent MCAo (coagulation of the distal portion of the left middle cerebral artery), experimental encephalomyelitis, traumatic brain injury and kainate-induced seizures (Munji et al., 2019). Remarkably, 2 days following injury onset, when the most severe BBB dysfunction was observed, 54 common genes were upregulated in all four injury models, and 136 genes appeared upregulated in at least three models. These include genes that regulate leukocyte trafficking and proteolytic cleavage of ECM. Multiple members of several gene families were upregulated: extracellular proteases of the Serpin family (Serpine1 and Serping1), Adams and Adamts families (Adam12, Adam19, Adamts4, and Adamts8), collagens (Col1a1, Col1a2,

Col3a1, Col5a1, Col5a2, and Col12a1), centromere proteins (Cenpe and Cenpf), Igf-binding proteins (Igfbp4 and Igfbp5), kinesins (Kif11, Kif15, and Kif20b), lysyl oxidases (lox, Loxl2, and Lox3), sulfatases (Sulf1 and Sulf2), thrombospondins (Thbs1 and Thbs2), and pleckstrin domain-containing genes (Plekho1 and Plekho2). Taken together, BBB dysfunction-induced changes in gene expression affect cell division, blood vessel development, inflammatory response, wound healing, leukocyte migration and focal adhesion, highlighting a role for angiogenesis and inflammation in this response (Munji et al., 2019). In addition, mesenchyme homeobox 1 (Meox1), placental growth factor (pgf) and insulin-like growth factor binding protein 4 and 5 (Igfpb4 and 5) were among the genes associated with angiogenesis and upregulated following stroke (Freitas-Andrade et al., 2012; Smith et al., 2018; Wu et al., 2018; Munji et al., 2019). The authors also found that, in each disease model, brain ECs acquired a "peripheral" (i.e., leakier) endothelial gene expression profile. These findings highlight the importance of transcriptomic studies that reveal novel pathways involved in brain endothelial dysfunction and unmask common pathways that may be significant targets for stroke therapy. Of note, while this elegant study provides invaluable molecular insights into BBB dysfunction, the animals used for MCAo were all young, 2–3-month-old males (Munji et al., 2019). Limitations related to the age of animal models are discussed later in this review.

Effects of Stroke on Endothelial Cell Function

Endothelial cells are master regulators of neurovascular coupling and CBF (defined as the blood volume that flows per unit mass or volume of brain tissue per time unit) in the healthy brain, in particular through production of vasodilatory NO via eNOS (Yamada et al., 2000). However, other factors produced by ECs such as, epoxyeicosatetraenoic acids (EETs), prostacyclin as well as endothelium-derived hyperpolarizing factor (EDHF) can also trigger vasodilation (Kisler et al., 2017). For example, mechanical shear stress in vessel lumen activates EC production of arachidonic acid (AA) and its metabolic products EETs via cytochrome P450 activity, and prostacyclin via cyclooxygenase 1 (COX1) activity. These by-products act on the surrounding vascular smooth muscle cells (VSMCs) and induce vasodilation (Kisler et al., 2017). Under pathological conditions, dysregulation of eNOS activity is involved in cardiovascular disease, vascular aging, vascular dementia and stroke (Huang et al., 1995; Lange-Asschenfeldt and Kojda, 2008; Sawada and Liao, 2009; Toda et al., 2009; Toda, 2012; Zhu et al., 2016; Wang et al., 2018). eNOS is constitutively expressed in ECs, briefly activated by increases in intracellular calcium, and underlies agonist (e.g., acetylcholine)-induced endothelium-dependent vasodilation. NO released by ECs triggers relaxation of VSMCs, and a partial modulation of eNOS is sufficient to induce large changes in CBF (Samdani et al., 1997).

Ischemic stroke, resulting in acute loss of regional CBF, rapidly initiates vascular remodeling via eNOS (Liu et al., 2014; Hoffmann et al., 2015; Lapi and Colantuoni, 2015; Prakash and Carmichael, 2015). Following MCAo in rats, while eNOS inhibitors reduce CBF and increase infarct volume, intra-arterial administration of NO donors increases CBF and decreases infarct volume (Dalkara and Moskowitz, 1994; Dawson, 1994; Iadecola, 1997). As such, eNOS activation is considered neuroprotective (Zhu et al., 2016). The Statin class of drugs, which upregulate eNOS, have neuroprotective properties in experimental animal models of stroke (Vaughan and Delanty, 1999). The upregulation of eNOS by Statins is mediated by inhibition of small GTPase RhoA (Sawada and Liao, 2009), reducing activation of RhoA's downstream effector ROCK2 (Hao et al., 2016; Tang F. C. et al., 2017). Using pharmacological intervention to directly target eNOS function might represent an interesting avenue to promote stroke recovery. This is important as direct eNOS modulation may prevent expansion of penumbral cell death, a notorious clinical problem. The effects of eNOS enhancers on stroke recovery have not yet been tested in animal models of stroke. AVE3085 and AVE9488 are small-molecule eNOS enhancers that are protective in rodent models of cardiovascular disease, including heart failure, myocardial infarction and diabetes (Bauersachs and Widder, 2008; Fraccarollo et al., 2008; Wohlfart et al., 2008; Frantz et al., 2009; Schafer et al., 2009; Cheang et al., 2011). These therapeutic benefits were attributed to ameliorated endothelial function via increased NO bioavailability and reduced oxidative stress.

In the cerebral vasculature, direct intercellular communication through gap junctions is instrumental, as synchronization of VSMCs and ECs along the vessel is required for proper vasomotor tone. Indeed, the low electrical resistance of these channels allows for faster signaling over long distances such as retrograde propagation of dilation to upstream arteries; gap junctions are hence critical in conducting a hyperpolarizing, electrical wave between ECs that modulates vascular tone (Behringer and Segal, 2012). Gap junction communication between the endothelium and astrocytes, as well as between ECs and pericytes, mediate neurovascular coupling and vasomotor control, respectively (De Bock et al., 2017; Pohl, 2020). For example, several endothelial signaling factors that control vasomotor function, such as prostacyclin and NO, rely on the increase in endothelial intracellular Ca^{2+} concentration. Gap junctional transfer of Ca^{2+} (or Ca^{2+} releasing compounds) plays an important role in controlling endothelial-dependent vasomotor function (Pohl, 2020). Under stroke conditions, this finely tuned coupling between cells is disrupted (Bolon et al., 2005; Yu et al., 2010). The role of endothelial gap junctions in CBF after stroke remains to be fully elucidated.

Collateral vascular remodeling, a process known as arteriogenesis, is initiated by fluid shear stress rather than hypoxia (Nishijima et al., 2015). ECs lining the collateral vasculature detect increased flow shear stress, which triggers the expression of transient receptor potential cation channel, subfamily V, member 4 (Trpv4) (Schierling et al., 2011). This mechanosensitive Ca^{2+} channel has been shown to induce significant collateral growth length and diameter in rats subjected to bilateral common carotid artery occlusion. Indeed, proper collateral vascular responses in stroke can significantly affect stroke outcome and mortality (Kimmel et al., 2019; Nannoni

et al., 2019). However, current understanding of collateral vessel dynamics is not clear; interestingly, a recent study reported that collateral vessels have distinct endothelial and smooth muscle cell phenotypes (Zhang et al., 2019). Understanding the molecular factors that govern collateral responses to brain injury may illuminate new avenues for therapeutic approaches.

Effects of Stroke on Pericytes

Effects of Stroke on Pericyte Structure

Pericytes are cells located within the basement membrane surrounding cerebral capillaries, and are in intimate contact with ECs through gap junctional complexes, called peg-socket contacts where the basement membrane is absent (**Figure 1B**). Pericytes represent a heterogeneous cell population with differences in morphology, location within the vascular tree and function (Winkler et al., 2014). Pericyte subtypes include 'mid-capillary' pericytes in the vast majority of the capillary bed, 'transitional' pericytes close to VSMCs and 'stellate' pericytes on post-capillary venules (Hartmann et al., 2020). Whether different pericyte subtypes have different functions, for example regulation of BBB permeability or control of CBF remains to be determined (Kisler et al., 2017).

Pericytes can constrict or relax, affecting capillary diameter, as discussed later in this review. Pericytes also promote vascular stability (Nishioku et al., 2009; Thomas and Augustin, 2009; Bell et al., 2010) and secrete basement membrane components (Virgintino et al., 2007). Studies have also underscored the importance of pericytes in modulating BBB integrity (Armulik et al., 2010; Daneman et al., 2010). Daneman et al. (2010) demonstrated that pericytes do not induce BBB-specific genes in ECs, but rather inhibit the expression of genes that promote vessel permeability. Pericytes have also been shown to affect functional aspects of the BBB, controlling both the structure of TJs and the rate of vesicular trafficking. Lack of pericytes (pericyte coverage between 20 and 40%) resulted in increased BBB permeability to water and a range of tracers of different molecular weights via increased endothelial transcytosis (Armulik et al., 2010). Similarly, a study using pericyte-specific Cre line crossed with mice carrying Cre-dependent human diphtheria toxin receptor showed that 40% pericyte coverage resulted in circulatory failure including BBB disruption, development of vasogenic edema and loss of CBF (Nikolakopoulou et al., 2019).

Following stroke, pericytes play a role in BBB remodeling and vessel stability (Su et al., 2019). Pericytes were shown to migrate away from brain microvessels in the first 2 h after occlusion of the internal carotid artery in cats (Gonul et al., 2002). Following photothrombotic occlusion of superficial cortical capillaries in mice, it was demonstrated that ischemia resulted in rapid activation of matrix metalloproteinase-9 (MMP-9) and plasma leakage at places where pericyte somata adjoined the capillary wall (Underly et al., 2017). The authors postulated that MMP-9 secreted from pericyte somata degraded underlying TJ complexes. This process was suggested as an intermediate step between leakage by transcytosis (transcellular leakage) and eventual TJ degradation (paracellular leakage). An important point raised by the authors, which would support findings from Gonul et al. (2002), is that pericytes may use MMP-9 to actively migrate from the endothelium to participate in revascularization (Underly et al., 2017). In addition, activation of PDGFR-β and Ang1/Tie2 signaling pathways are triggered by ischemic stroke, enhancing pericyte survival as well expression of TJ proteins in ECs, as reviewed elsewhere (ElAli et al., 2014). Finally, the control of endothelial transcytosis by pericytes following stroke requires further investigation. It has been proposed that pericytes may regulate transcytosis via expression of MFSD2A in brain ECs (Ben-Zvi et al., 2014; Keaney and Campbell, 2015; Sweeney et al., 2016; Chow and Gu, 2017). Importance of this cell–cell interaction in stroke remains to be comprehended, particularly in light of a recent study demonstrating the protective role of MFSD2A upregulation in rodent SAH (Zhao et al., 2020).

Effects of Stroke on Pericyte Function

The role of pericyte-dependent CBF regulation at the level of capillaries is currently debated, pericytes have the capacity to contract or relax, affecting capillary diameter in various physiological or pathological conditions (Hall et al., 2014; Hill et al., 2015; Cai et al., 2018). They possess the machinery necessary for cytoskeletal plasticity, including alpha-smooth muscle actin (α-SMA), tropomyosin and myosin. Pericytes are also sensitive to direct electrical stimulation or to neuronal activity via transmitters including NO, glutamate, noradrenalin, PGE2 or ATP (Peppiatt et al., 2006; Puro, 2007; Hall et al., 2014), and they respond by changes in intracellular Ca^{2+} by relaxation or constriction around the endothelium (Kawamura et al., 2003, 2004). A recent study reported that genetic ablation of pericytes in the mouse cerebral cortex correlated with 50% reductions in CBF responses to sensory stimulation (Kisler et al., 2020). A study by Hartmann et al. (2020) elegantly demonstrated, using two-photon live imaging, that optogenetic stimulation of pericytes decreased lumen diameter and CBF, but with slower kinetics than mural cells from upstream vascular beds.

The reactivity of pericytes is affected by stroke. Both physiological hypoxia and short-term hypoxia after stroke induce pericyte relaxation, a process modulated by PDGF-β, ATP, NO, and oxygen (Arimura et al., 2012; Cai et al., 2017). However, sustained hypoxic-ischemic damage leads to constriction and death of pericytes. Fernandez-Klett et al. (2013) reported that pericytes are rapidly lost 24 h after cerebral ischemia in both experimental (1-h tMCAo) and human stroke. *In vivo*, pericyte constriction/injury following ischemia-reperfusion was attributed to increased oxidative stress (Shojaee et al., 1999; Yemisci et al., 2009). OGD-induced ischemia in rat cerebellar slices triggered capillary constriction by pericytes followed by pericyte death, similarly 90 min of tMCAo in rats led to increased pericyte death in the lesioned hemisphere (Hall et al., 2014). Loss of pericytes also have profound effects on neurotrophic-dependent neuronal survival. This was demonstrated by genetic ablation of pericytes resulting in loss of pleiotrophin (PTN) expression; PTN is a pericyte-secreted growth factor

and loss of this factor contributed to neuronal death in this study (Nikolakopoulou et al., 2019). Hence, pericytes can play a detrimental role in ischemia-reperfusion injury and thus represent a promising therapeutic target, as reviewed elsewhere (Cai et al., 2017; Su et al., 2019; Uemura et al., 2020).

Effects of Stroke on Astrocytes

Effects of Stroke on Astrocyte Structure

Located between synapses and capillaries, astrocytes extend processes that physically link neighboring neurons with their surrounding blood vessels (**Figure 1**), allowing them to sense changes in the neuronal microenvironment and adjust the microvasculature accordingly (Attwell et al., 2010; Gordon et al., 2011; He et al., 2012). Several lines of evidence have implicated astrocytes in promoting and modulating the BBB identity of brain ECs (Abbott et al., 2006; Al Ahmad et al., 2011). In brief, perivascular astrocytes increase the tightness of TJs (Lee et al., 2003), promote the expression and localization of endothelial transporters (McAllister et al., 2001) and induce the expression of enzymes associated with the metabolic endothelial barrier (Abbott et al., 2006). Astrocytes are critical to neuronal survival and repair, a large part of this function being mediated through gap junction proteins that connect astrocyte networks into a cooperative functional syncytium (De Bock et al., 2017; Laird et al., 2017; Freitas-Andrade et al., 2019; Freitas-Andrade et al., 2020).

Generally, astrocytes are more resistant to hypoxic conditions than other CNS cells (Anderson and Nedergaard, 2003; Chen and Swanson, 2003). However, they are highly vulnerable to the coupling of acidosis and hypoxia during cerebral ischemia (Bondarenko and Chesler, 2001). In cell culture and *in vivo*, differences in sensitivity to hypoxia have been reported between different populations of astrocytes from different parts of the brain (Zhao and Flavin, 2000; Lukaszevicz et al., 2002; Shannon et al., 2007). Indeed, astrocytes differ between various regions of gray matter, or within a single brain region (Molofsky et al., 2012; Tsai et al., 2012; Clavreul et al., 2019; Batiuk et al., 2020). Astrocytes express gap junction proteins (Belliveau and Naus, 1994), neurotransmitter receptors, transporters (Zhou and Kimelberg, 2001; Matthias et al., 2003) and ion channels (Verkhratsky and Steinhauser, 2000). These specific molecular characteristics allow astrocytes to fulfill a range of homeostatic functions. However, this molecular diversity may bestow, to some astrocyte subtypes, vulnerabilities to stroke. One can also postulate that astrocytes are regulated by different cell types. For example, in a recent study, rats were subjected to global cerebral ischemia, performed by cardiac arrest of 10 min duration, then allowed to survive 2 years post-ischemia. After the 2 years, the authors found that in the hippocampal CA1 and CA3, and in the motor cortex, co-activation of both microglia and astrocytes was significant; however, in the resistant brain areas (that is, the dentate gyrus, sensory cortex, striatum, and dorso-lateral nucleus of the thalamus), significant activation was observed for astrocytes only (Radenovic et al., 2020). Similarly, in mice subjected to permanent MCAo, pericytes within the infarct area produced trophic factors activating astrocytes, thereby enhancing peri-infarct astrogliosis (Shibahara et al., 2020). This interplay between astrocyte and microglial and/or pericytes following ischemia remains elusive. Emerging technologies such as single-cell RNA sequencing, coupled with quantitative transcriptional genome-profiling, could molecularly define astrocytic subtypes and unmask mechanisms that affect astrocyte sensitivity to stroke.

In pathological conditions such as stroke, astrocyte survival has been correlated with neuronal survival (Chen and Swanson, 2003). Astrocytes secrete neurotrophic factors and, along with perivascular stromal cells, minimize damage to neighboring cells through formation of a glial scar (Krum et al., 2008; Fernandez-Klett et al., 2013). However, the glial scar can also be detrimental to functional recovery, by acting as a barrier to neuronal regeneration (Beck et al., 2008). Under ischemic conditions, astrocytes also secrete pro-angiogenic factors that promote the growth of new capillaries toward the infarcted tissue (Chow et al., 2001). Following brain injury, astrocytes upregulate glial fibrillary acidic protein (GFAP), an intermediate filament involved in astrocyte activation (Li et al., 2008). Interestingly, mice exposed to 1 hr of tMCAo coupled with a novel live imaging approach, Cordeau et al. (2008) reported that GFAP upregulation following ischemic brain injury may not have the same functional significance in male versus female mice (Cordeau et al., 2008). The authors showed that chronic estrogen deprivation (40 days after ovariectomy) resulted in a significant increase in GFAP upregulation in astrocytes after 24–72 h after reperfusion, compared with mice that were subjected to only 14 days of estrogen deprivation. However, the extent to which sexually dimorphic mechanisms affect astrocytic responses to stroke requires further investigation (Roy-O'Reilly and McCullough, 2018).

Effects of Stroke on Astrocyte Function

Astrocytes play important roles in homeostatic control of arterial blood pressure and CBF (Marina et al., 2020). Astrocytes are intimately associated with tens of thousands of synapses through highly ramified branches (Fields et al., 2015) and modulate CBF in response to synaptic activity (Anderson and Nedergaard, 2003). Astrocytes express metabotropic glutamate receptors (mGluRs) and sense glutamate release from synaptic clefts, and activation of mGluRs induces an increase in intracellular Ca^{2+} concentration spreading to the astrocytic endfeet (Zonta et al., 2003). These increases in Ca^{2+} concentration induce release of vasoactive factors from astrocytic endfeet and are dependent on the metabolic state of the neuronal microenvironment (Mulligan and MacVicar, 2004; Gordon et al., 2008).

Following stroke, profound functional changes occur at the level of astrocytes, which significantly affects neurovascular coupling. At the cellular level, post-stroke astrogliosis is noticeable around brain vessels (McConnell et al., 2019). At the molecular level, intracellular factors in astrocytes affect their ability to respond to neurometabolic needs. For instance,

Howarth et al. (2017) demonstrated a novel mechanism of CBF regulation involving astrocytes and dependent on glutathione, a factor that is substantially reduced after stroke. When glutathione levels are reduced in conditions such as stroke, Ca^{2+}-evoked release of PGE2 by astrocytic endfeet was decreased and vasodilation inhibited, an effect dependent of microsomal prostaglandin E synthase-1, downstream of COX-1 (Howarth et al., 2017).

A critical factor contributing to decreased CBF following stroke and implicating astrocytes are injury depolarizations, also known as Cortical Spreading Depressions or CSDs (Takano et al., 2007; Attwell et al., 2010). CSDs are slowly propagating waves of neuronal and glial depolarization (Lauritzen et al., 2011; Ayata and Lauritzen, 2015) that spontaneously occur within minutes after ischemic stroke and originate from the peri-infarct region (Dreier, 2011; Lauritzen et al., 2011; Kao et al., 2014; Lauritzen and Strong, 2016; Kirov et al., 2020). CSDs impair recovery in rodent stroke models (Risher et al., 2010; von Bornstadt et al., 2015) and correlate with clinical deterioration in stroke patients (Nakamura et al., 2010; Lauritzen and Strong, 2016). In the rat cerebral cortex, CSDs were shown to increase the vasoconstrictor 20-hydroxyeicosatetraenoic acid (20-HETE) which is generated in astrocytes from arachidonic acid, and known to induce constriction of VSMCs (Attwell et al., 2010; Fordsmann et al., 2013). It was postulated that 20-HETE secreted by astrocytes could have a significant impact on vascular function during stroke (Attwell et al., 2010). Astrocytic gap junctions have also been implicated in propagating CSDs and brain damage (Martinez and Saez, 2000; Rovegno and Saez, 2018).

Collectively, these studies show that cellular and molecular mechanisms normally associated with astrocytic regulation of CBF are hijacked following stroke. Dissection and understanding of these mechanisms represent another critical avenue for stroke research.

Effects of Stroke on Microglia

Microglia play critical roles in both innate and adaptive immune responses in the CNS. They vigilantly monitor their microenvironment and perform homeostatic functions that are necessary for proper brain homeostasis (Nimmerjahn et al., 2005; Wake et al., 2009). Microglia are also involved in brain development, playing important roles in synaptic pruning, modulation of neurogenesis and myelination, as reviewed elsewhere (Tremblay et al., 2011; Wu et al., 2015; Hammond et al., 2018). A recent study using single cell transcriptomics discovered that mouse microglia are far more diverse than originally thought, comprising distinct subpopulations with unique molecular signatures (Hammond et al., 2019). While microglial ablation in the mature mouse brain does not affect BBB function (Parkhurst et al., 2013; Haruwaka et al., 2019), microglia can modulate BBB integrity in opposite ways during inflammation.

Following ischemic or hemorrhagic stroke, microglia dynamically transition into a reactive state (Eldahshan et al., 2019; Rawlinson et al., 2020). The initial leakage of blood serum components such as fibrinogen induces local activation of microglia. Microglia are finely tuned to sense any small disturbance in the BBB (Hines et al., 2009; Petersen et al., 2018), and their recruitment to blood vessels occurs within 6 h of reperfusion with significant accumulation in perilesional tissue. After 24 h of reperfusion, microglia fully enwrap small blood vessels in the peri-infarct region (Jolivel et al., 2015). Individual perivascular microglia displayed intracellular vesicles containing CD31-positive inclusions, suggesting phagocytosis of brain ECs, which was correlated with BBB breakdown as shown by the extravasation of Evans blue from perfused vessels. At 72 h post-MCAo, blood vessel degradation was complete and remaining vascular debris were cleared by microglia and invading immune cells (Jolivel et al., 2015). Following stroke, reactive microglia also secrete MMP-9 and MMP-3, proteases that can break down the basement membrane surrounding brain–blood vessels and exacerbate BBB leakage (Yenari et al., 2010), as discussed below.

Following ICH, blood invading the brain parenchyma induces a rapid inflammatory response from microglia. Activated microglia develop into an M1-like phenotype resulting in production of pro-inflammatory cytokines such as [interleukin (IL)-1β, IL-6, IL-12, IL-23, tumor necrosis factor alpha (TNF-α)], chemokines, redox molecules (NADPH oxidase, phagocyte oxidase, inducible NO synthase), costimulatory proteins (CD40), and major histocompatibility complex II (MHC-II) (Zhang et al., 2017). In the acute phase of ICH, both in the clinical and experimental rodent models, proinflammatory factors are present in the brain starting 3 h after ICH and peaking at 3 days. Due to their proinflammatory phenotype, M1 microglia are linked to short-term brain damage. Within 1 week, a M1-to-M2 microglial phenotypic switch occurs (Lan et al., 2017). M2-like microglia are associated with anti-inflammatory and phagocytic functions and assist in the clearance of the haematoma. Microglia can also be activated by IL4/IL3 to the M2 polarization state, which produces anti-inflammatory mediators IL-10, transforming growth factor beta (TGFβ), and glucocorticoids (Zhang et al., 2017). Several factors have been implicated in inducing microglial polarization including, nuclear factor-κB (NF-κB), signal transducer and activator of transcription (STAT1–STAT6), high mobility group protein B1 (HMGB1) as well as PGE2 (Lan et al., 2017). Finally, studies have shown that age, environmental factors and sex differences can influence microglial responses and polarization to injury (Crain et al., 2013; Bisht et al., 2016; Lan et al., 2017). Taken together, this shows that various conditions may have a profound impact on the responsiveness of microglia following stroke.

Effects of Stroke on Perivascular Macrophages

Although different from microglia, the function of brain perivascular macrophages (PVMs) are of growing interest in stroke research. PVMs are myeloid cells located in the perivascular space surrounding cerebral blood vessels (Faraco et al., 2017). In the healthy brain, PVMs contribute to BBB integrity and help regulate infiltration of large molecules into the brain through scavenger activity (Mendes-Jorge et al., 2009). PVMs have largely been implicated in their role as scavengers in

the context of Alzheimer's disease and CNS infection, however, there is increasing evidence for their role in the regulation of CBF, vascular function and stroke pathogenesis. Depletion of PVM has been shown to prevent changes in vascular structure associated with chronic hypertension (Pires et al., 2013). Additionally, PVMs were shown to promote BBB degradation through ROS production in a mouse model of hypertension, which could be reversed by depleting PVMs, effectively reducing oxidative stress, improving CBF dysfunction, restoring neurovascular coupling, and rescuing cognitive impairment (Faraco et al., 2016). In post-mortem tissues, cells positive for the PVM marker CD163 were found accumulated in brains with ischemic, but not hemorrhagic, lesions (Holfelder et al., 2011). Furthermore, CD163-positive cells isolated from rats following 1-h tMCAo followed by 16-h reperfusion showed upregulation of the HIF-1 pathway, as well as of genes encoding the ECM and leukocyte chemoattractants (Pedragosa et al., 2018). Depletion of PVMs reduced granulocyte infiltration, BBB permeability and VEGF expression (Pedragosa et al., 2018). Because VEGF promotes migration of cells to participate in angiogenesis, it is possible upregulation of HIF-1 and VEGF by PVMs is pathological in the acute phase following ischemic stroke. It has been hypothesized that activation of PVMs in cerebrovascular pathologies may initially be protective through their phagocytic activity, but may in turn be detrimental with repeated long-term activation (Koizumi et al., 2019). Further research is required to fully elucidate the role of PVMs in the context of stroke.

Effects of Stroke on the Basement Membrane

The basement membrane forms a three-dimensional protein network composed of laminins, collagen, nidogen and heparan sulfate proteoglycans (HSPGs) that mutually support interactions between ECs, pericytes and astrocytes (**Figure 1**) (Thomsen et al., 2017). The basement membrane functions as a second barrier, limiting movement between the blood and the brain. At the NVU, ECs, astrocytes and pericytes synthesize and deposit different laminin isoforms in the basement membrane, which have been shown to modulate BBB function (Gautam et al., 2016, 2019). Penetrating arteries and parenchymal arterioles are surrounded by a basement membrane composed of two distinct entities: the basement membrane produced by the endothelium, and the parenchymal membrane located between vascular smooth muscle cells (VSMCs) and astrocytes, produced by pial cells and astrocytic endfeet. Pericytes also contribute to basement membrane formation by producing and secreting ECM proteins (Yao, 2019).

Several lines of evidence suggest that integrin matrix adhesion receptors expressed by ECs and astrocytes exhibit dynamic cellular influences (Milner et al., 2008; McCarty, 2020). In addition, matrix adhesion by endothelial β1-integrin receptors affect claudin-5 expression and regulate BBB permeability (Osada et al., 2011). Interestingly, studies have also indicated the importance of the basement membrane in cerebrospinal fluid regulation (Morris et al., 2016; Albargothy et al., 2018; Howe et al., 2019). Impaired basement membrane integrity is a significant contributor to neuronal loss after stroke.

The ECM of the basement membrane plays a role in limiting the transmigration of erythrocytes during hemorrhage, and of leukocytes during inflammation. Following ischemic stroke, MMPs produced by activated ECs and pericytes degrade the basement membrane (Thomsen et al., 2017; Kang and Yao, 2020). Other proteinases, including plasminogen activators, heparinases and cathepsins also contribute to ECM degradation. The proteolytic breakdown of ECM proteins such as laminin-5 or type IV collagen exposes cryptic epitopes that promote EC and pericyte migration (Hangai et al., 2002). A recent study highlighted the complex molecular cascades and plethora of genes induced by stroke that are in relation to ECM and NVU integrity (Aleithe et al., 2019). Aging is also an important factor in basement membrane integrity after stroke. TGF-β signaling in hypoxic astrocytes induces basement membrane fibrosis and chronically impairs perivascular CSF distribution, specifically in aged animals after permanent MCAo (Howe et al., 2019), providing a new mechanism by which brain injury can lead to prolonged functional impairment in the elderly.

Interestingly, disruption of astrocyte-derived laminin expression resulted in spontaneous hemorrhagic stroke in deep brain regions (basal ganglia), which are similarly affected in human patients. Chen et al. (2013) generated conditional knockout mice in which astrocytes do not express laminin γ1 chain, an essential subunit of most laminins (Durbeej, 2010). Lack of astrocyte-derived laminin γ1 resulted in impaired VSMC differentiation and decreased levels of contractile proteins in VSMCs around small arteries and arterioles (diameter 8–20 μm), but only in the striatum. The authors observed that while mutant astrocytes throughout the brain did not produce laminin, hemorrhaging occurred only in the basal ganglia. In the normal brain, penetrating arteries and arterioles are surrounded by a basement membrane composed of two distinct entities: the basement membrane produced by the endothelium and the parenchymal membrane. As arteries branch into small arteries, and small arteries ramify into arterioles, the contribution of the pia meninges decrease. At the capillary level, there are no pia meninges, and the basement membrane between the astrocytic endfeet and VSMC become very thin, at some points along the capillary endfeet directly contact VSMCs or ECs (Yao, 2019). It was postulated that, due to the close relationship between astrocytes and VSMCs in the striatal vasculature, the lack of astrocyte-derived laminins had a direct effect on the underlying VSMCs within this brain region (Chen et al., 2013). In contrast, this close relationship between astrocytes and VSMCs was not observed in the cerebral cortex. The phenotype presented by the transgenic animals appears similar to abnormalities found in human hypertensive hemorrhagic patients in the striatum (Chen et al., 2013). More recently, Gautam et al. (2020) demonstrated in mutant mice lacking mural cell-derived laminin that the latter attenuates BBB damage in ICH via decreasing caveolin-1 and transcytosis.

Following 6 h of tMCAo, basement membrane degradation was observed 10 min after reperfusion, and basement membrane loss was detected as early as 1–3 h after ischemia (Yao, 2019). In a non-human primate study after middle cerebral artery occlusion/reperfusion both MMP-2 and -9 are significantly upregulated and digest ECM proteins of the basement

membrane, affecting BBB integrity (Heo et al., 1999). A possible harmful consequence of MMP-9 activation during acute stroke treatment is that rtPA can leak out of the vessel through the permeable BBB and substantially further enhance MMP-9 levels, resulting in hemorrhage (Tsuji et al., 2005; Yao, 2019).

Cathepsin B and L proteases are enhanced soon after stroke onset and degrade heparan sulfate proteoglycans (HSPGs) (Becker et al., 2015). Reduction of HSPG has a dramatic effect on the BBB, as the HSPG Agrin is known to stabilize adherens junctions in mouse brain ECs (Steiner et al., 2014). While proteases activated during stroke may have detrimental effects during initial stages, they also play an important role in angiogenesis and vascular remodeling (Thomsen et al., 2017). MMPs are integral players in angiogenesis, breaking down ECM proteins to facilitate endothelial tip cell and pericyte migration. It has also been demonstrated that degraded fragments of the HSPG Perlecan reduce neuronal death and infarct volume, as well as enhance angiogenesis (Lee et al., 2011; Bix et al., 2013).

Targeting MMPs has some potential therapeutic benefits (Chaturvedi and Kaczmarek, 2014). Minocycline is a lipophilic tetracycline and was shown to inhibit MMP-9 activity and expression in rats subjected to 3 h of tMCAo (Machado et al., 2006). In this study, minocycline was administered after the stroke and given at a clinically relevant concentration (intra-peritoneal minocycline 45 mg/kg). Although, the authors did not show whether minocycline reduced infarct damage, minocycline later appeared neuroprotective in several models of brain injury (Naderi et al., 2020) with demonstrated efficacy in acute stroke patients (Malhotra et al., 2018). Moreover, as mentioned previously, MMP-9 has been associated with hemorrhagic transformation in the setting of tPA therapy (Aoki et al., 2002). MMP-9 is associated with BBB breakdown and subsequent vasogenic edema, and an MMP-9 polymorphism was shown to confer susceptibility to ischemic stroke in a Chinese population (Jiang et al., 2020). HIBISCUS-STROKE is a cohort study including acute ischemic stroke patients with large vessel occlusion treated with mechanical thrombectomy following admission magnetic resonance imaging (MRI) (Mechtouff et al., 2020). In this study, MMP-9 levels were assessed to determine whether it correlated with infarct growth and hemorrhagic transformation. The study showed that MMP-9 levels measured 6 h after admission predicted infarct growth and hemorrhagic transformation (Mechtouff et al., 2020).

In summary, sudden and sustained interruption of blood flow to the brain induces dynamic highly complex cellular and molecular responses in the NVU (**Figure 1C** and **Table 1**). While the disruption at the NVU is catastrophic, the mechanisms triggered by ischemia or hemorrhage are set in motion in order to restore homeostatic balance. Increased BBB permeability and basement membrane breakdown due to secretion of MMPs by ECs, pericytes and astrocytes facilitate cell migration and vascular remodeling. Fibrinogen and other blood components leaking into the parenchyma activates microglia and promote phagocytosis of cellular debris. Secreted factors by these cells as well as components of the basement membrane induces angiogenesis and capillary network formation after stroke.

Regulation of Angiogenesis Following Stroke

Lessons From Developmental Biology

To gain further insight into angiogenesis in the injured/ischemic adult brain, it is critical to understand developmental angiogenesis, given that developmental processes are re-activated following stroke (Lee et al., 2004; Gonzenbach and Schwab, 2008; Milner et al., 2008).

Stroke triggers a complex set of cellular and molecular responses that evolve from minutes to days. Energy supply and ionic balance are immediately compromised in the ischemic core, leading to rapid neuronal demise. Directly surrounding the infarct core, the peri-infarct region (also referred to as "ischemic penumbra") is a territory that still receives limited perfusion by collateral blood vessels. Due to the inadequate blood supply, this peri-infarct region is functionally silent, yet potentially salvageable (del Zoppo et al., 2011). In the early 1990's, a post-mortem study on human brains demonstrated that stroke activates angiogenesis mostly in the peri-infarct region, and a higher blood vessel count correlated with longer survival time (Krupinski et al., 1994). Subsequent human studies demonstrated a correlation between improved stroke outcome and levels of circulating pro-angiogenic factors (Lee et al., 2010; Navarro-Sobrino et al., 2011).

During early development, brain vascularization is mediated through ingression of blood vessels in the presumptive cerebral cortex from a superficial vascular plexus, with hypoxia and genetic programs as driving forces. Blood vessels within the brain then sprout and expand into vast highly connected networks and remodel into a complex vascular tree characterized by an arterial and venous hierarchy (Carmeliet and Tessier-Lavigne, 2005; Tata et al., 2015). As brain tissue expands and oxygen diffusion from neighboring capillaries is insufficient, a mild hypoxia promotes activation of hypoxia-inducible transcription factors (HIFs). HIFs are heterodimeric proteins consisting of a constitutive subunit HIF-1β as well as either a HIF-1α or HIF-2α subunit. HIF-1α and -2α subunits are rapidly degraded in normoxia, which is initiated by the hydroxylation of two conserved prolyl residues in the HIF-α subunits (Tomita et al., 2003). When cellular oxygen concentration is reduced, HIF-1α and -2α protein levels increase dramatically. More than 1,000 genes are directly transactivated by HIFs in response to hypoxia (Semenza, 2014; Rattner et al., 2019). HIFs induce the expression of angiogenic genes that act both on the nascent cerebrovascular system, as well as developing neurons. The intimate relationship between the vasculature and neurons is established early during development. For example, signaling factors associated with axonal guidance (Netrins, Semaphorins, and Ephrins) as well as angiogenic factors (VEGFs) are common signals orchestrating the regulation of both vessels and neuronal development (Gu et al., 2005; Oh and Gu, 2013). Detailed reviews about neuro-vascular development can be consulted (Tam and Watts, 2010; Eichmann and Thomas, 2013; Andreone et al., 2015; He et al., 2018; Paredes et al., 2018; Coelho-Santos and Shih, 2020).

TABLE 1 | Major features (non-exhaustive list) of structural and functional remodeling of the neurovascular unit following stroke.

		Selected references
Structural NVU Remodeling		
Ischemic Stroke	– Reparative angiogenesis primarily in the peri-infarct. – Biphasic BBB breakdown: (1) Increased caveolae-mediated transcytosis. (2) Tight junction breakdown. – Secretion of MMPs by pericytes, ECs, and microglia promotes degradation of the basement membrane and TJ disruption, leading, to increased BBB permeability and edema. – Secreted MMPs also facilitate angiogenesis and vascular remodeling by promoting EC and pericyte migration. – Basement membrane fibrosis induced by TGF-β. – Astrocytes contribute to glial scar formation which is both beneficial and detrimental to nearby cells. – Astrocytes upregulate GFAP soon after stroke and secrete neurotrophic and proangiogenic factors. – Pericytes secrete trophic factors that contribute to astrogliosis. – Leakage of blood-borne factors into brain parenchyma results in rapid microglia activation that enwrap and phagocytose ECs in the peri-infarct region.	Chow et al., 2001; Hangai et al., 2002; Beck et al., 2008; Krum et al., 2008; Yu et al., 2010; Yenari et al., 2010; Jiao et al., 2011; Ben-Zvi et al., 2014; ElAli et al., 2014; Knowland et al., 2014; Jolivel et al., 2015; Choi et al., 2016; Nahirney et al., 2016; Thomsen et al., 2017; Underly et al., 2017; Eldahshan et al., 2019; Howe et al., 2019; Munji et al., 2019; Yao, 2019; Shibahara et al., 2020.
Hemorrhagic stroke	– ECs proliferate around hematoma following ICH. – BBB breakdown and tight junction disruption. – Blood in parenchyma results in rapid microglia activation to a pro-inflammatory phenotype, which eventually polarize to an anti-inflammatory phenotype. – Mutations in genes that encode basement membrane proteins are associated with ICH. – Loss of astrocyte-derived basement membrane proteins is associated with hemorrhagic stroke in deep brain regions. – MMP-9 implicated in hemorrhagic transformation following treatment for ischemic stroke. – VEGF can also increase BBB permeability, which may help peripheral macrophages infiltrate into the brain.	Manoonkitiwongsa et al., 2001; Gould et al., 2006; Chen et al., 2013; Fu et al., 2014; Lan et al., 2017; Zhang et al., 2017; Gautam et al., 2020; Mechtouff et al., 2020.
Functional NVU Remodeling		
Ischemic stroke	– Acute loss of CBF initiates vascular remodeling via eNOS. – Acute hypoxia induces pericyte relaxation, however, sustained hypoxia leads to pericyte constriction and death. – Functional changes in astrocytes significantly affect NVC. – Decrease in glutathione impairs astrocytic regulation of CBF. – Astrocytes implicated in propagating CSD and VSMC constriction contributing to decreased CBF. – Cell death of perivascular neurons exacerbates brain damage and leads to neurovascular uncoupling. – Hypoxia activates and stabilizes HIFs, upregulating VEGF signaling and promoting angiogenesis. – Angiogenic response provides a scaffold for neuronal regeneration, mediated by neural precursor cells.	Marti et al., 2000; Attwell et al., 2010; Arimura et al., 2012; Fernandez-Klett et al., 2013; Hall et al., 2014; O'Donnell, 2014; Hoffmann et al., 2015; Reeson et al., 2015; Howarth et al., 2017; Cai et al., 2018; Rovegno and Saez, 2018; McConnell et al., 2019; Tornabene et al., 2019.
Hemorrhagic stroke	– VEGF and its receptors upregulated persistently. – Increased VEGF increases vessel density and improves stroke outcome. – Beneficial effects of VEGF mediated through aquaporin-4. – Morphology of newly formed vessels resemble that of the developing brain.	Josko, 2003; Tang et al., 2007; Chu et al., 2013; Sugimoto and Chung, 2020.

Selected references are displayed. BBB, blood–brain barrier; TJ: tight junction; MMPs, matrix metalloproteinases; EC, endothelial cell; ICH, intracerebral hemorrhage; NVC, neurovascular coupling; NVU, neurovascular unit; CBF, cerebral blood flow; CSD, cortical spreading depression; VSMC, vascular smooth muscle cell; HIF, hypoxia-inducible transcription factors; VEGF, vascular endothelial growth factor.

Angiogenesis After Ischemic Stroke

Similar to the developing brain, low O_2 levels increase the stability and activity of HIFs in vulnerable cells of the peri-infarct region, triggering angiogenesis from non-affected tissue and pial vessels. New vessels grow through the hypoxic micro-environment of the penumbra into the core of the infarct (Marti et al., 2000). Post-stroke HIF activation induces the expression of several angiogenic and inflammatory factors including VEGF. Serum VEGF is significantly increased in ischemic stroke patients (Dassan et al., 2012; Paczkowska et al., 2013), in whom highest VEGF expression occurs 7 days post-stroke, and remains significantly elevated 14 days after stroke (Slevin et al., 2000; Matsuo et al., 2013). VEGF and its receptors (VEGFR-1 and -2) play a central role in initiating CNS angiogenesis,

stimulating endothelial cell survival, proliferation and migration. In permanent MCAo mouse model, VEGF expression was detected within the first 24 h after occlusion in hypoxic peri-infarct tissues and in the pia above the infarcted area. Within the same brain regions, VEGFR-1 and subsequently VEGFR-2 were increased 48 h after MCAo (Marti et al., 2000). After 48 and 72 h of ischemia, a dramatic increase in proliferating ECs was measured within the peri-infarct area as well as the pial surface. The authors reported that VEGFRs were induced mainly in ECs, but that VEGFR-2 was also detected in hippocampal neurons in both the ipsilateral and contralateral hemispheres, suggesting that the VEGF/VEGFR pathway could be associated with neuroprotection. Other studies using either permanent or transient MCAo showed similar spatio-temporal dynamics in VEGF/VEGFR expression (Plate et al., 1999; Beck et al., 2002). Taken together, these studies indicate that ischemia is a significant driving force of angiogenesis during the initial stages of stroke and is mediated by VEGF and its receptors.

While VEGFR-1 is involved in attenuating the effects of VEGF (Kearney et al., 2002; Meyer et al., 2006) and modulating inflammatory responses (Cardenas-Rivera et al., 2019), VEGFR-2 activation, induces intracellular pathways associated with EC activation and neuroprotection. VEGFR-2-PI3K-Akt signaling pathway was linked to neuronal survival and reduced infarct size in mice subjected to 90 min of tMCAo (Kilic et al., 2006). However, it was also shown that VEGFR-2 mediated PI3K-Akt signaling induced BBB permeability (Kilic et al., 2006). While the benefits of VEGF-dependent activation of VEGFR-2 have been demonstrated, the detrimental effects on vascular permeability are also well known (Zhang et al., 2002; Reeson et al., 2015; Geiseler and Morland, 2018). Due to these contrasting effects, the use of VEGF as a therapeutic strategy in stroke has been challenging.

In addition, a role for ADAMTS13 in reparative angiogenesis after ischemic stroke was recently discovered *in vivo*. Normally after vascular injury, von Willebrand factor is secreted as hyperactive ultralarge multimers that are rapidly cleaved by ADAMTS13 into less reactive fragments (Crawley et al., 2011). Following permanent MCAo, *Adamts13*$^{-/-}$ mice displayed reduced neovascularization, reduced brain capillary perfusion, as well as accelerated BBB breakdown (Xu et al., 2017).

Angiogenesis After Hemorrhagic Stroke

The two types of hemorrhagic stroke are: intracerebral hemorrhage (ICH), defined as bleeding into the brain parenchyma, and subarachnoid hemorrhage (SAH) caused by bleeding into the cerebrospinal fluid (CSF)-containing sulci, fissures and cisterns (Smith and Eskey, 2011). There are marked differences in neurological cascade of events between ischemic and hemorrhagic strokes (Qureshi et al., 2009). However, both hemorrhagic and ischemic strokes share common angiogenic mechanisms. Tang et al. (2007) demonstrated that angiogenesis in rat brains subjected to collagenase-induced ICH was similar to those observed following ischemic stroke. Seven days after collagenase injection into the right globus pallidus, enlarged and thin-walled microvessels appeared along the border of the hematoma and continued to grow into the core, and then spread all over the clot by 21 days. Endothelial cell proliferation was also observed around the hematoma 2 days after collagenase injection and peaked from 7 to 14 days. Within the same time frame, VEGF as well as VEGFR-1 and -2 mRNA were detected as early as 2 days after ICH; mRNA levels peaked at 21 days and persisted for at least 28 days post-ICH (Tang et al., 2007). Interestingly, the authors noted that newly formed microvessels displayed an enlarged and thin-walled morphology, reminiscent of those found in the developing brain. Similarly, angiogenesis was observed in rats subjected to a SAH stroke paradigm, and expression of VEGF was induced by hypoxia resulting from vasospasm (Josko, 2003). Similar to ischemic stroke, CSD also occurs in hemorrhagic stroke (Sugimoto and Chung, 2020). Subsequent ICH studies suggested that angiogenesis may have therapeutic benefits (Lei et al., 2013; Pan et al., 2018). For instance, treatment with EGb761, a Ginkgo biloba extract, increased microvessel density and promoted neuroprotection in mice subjected to ICH induced by collagenase injection (Pan et al., 2018). EGb761 treatment enhanced VEGF expression, while inhibition of this VEGF expression negatively affected stroke outcome (Pan et al., 2018). Similarly, the effects of VEGF inhibition on collagenase-induced ICH in rats was demonstrated through pharmacological inhibition of high-mobility group box 1 protein (HMGB1), a member of the damage-associated-molecular-pattern (DAMP) family of proteins. Inhibition of HMGB1 resulted in reduced levels of VEGF and nerve growth factor (NGF), and reduced recovery of neurological function following ICH (Lei et al., 2013). Beneficial effects of VEGF on brain edema following ICH were also reported (Chu et al., 2013). In this particular study, ICH was induced by microinjecting autologous whole blood into the right striatum of transgenic aquaporin-4 (AQP4) Wild-Type (AQP4$^{+/+}$) and knockout (AQP4$^{-/-}$) mice. One day after injury, recombinant human VEGF injected intracerebroventricularly induced AQP4 expression in the striatum of AQP4$^{+/+}$ mice 1 day after VEGF injection, and peaked at 3 days. AQP4 was still present 7 days post-injection and concentrated in glial endfeet surrounding the hematoma (Chu et al., 2013). While AQP4$^{+/+}$ mice injected with VEGF showed reduced neurological deficits and decreased brain edema following ICH at 1, 3, and 7 days post-treatment, AQP4$^{-/-}$ ICH mice did not benefit from VEGF injection. Moreover, this study demonstrated that VEGF did not affect BBB permeability after ICH. In view of these studies, VEGF may have therapeutic potential for ICH.

Reparative Angiogenesis as Support for Post-stroke Neurogenesis

A key role for angiogenic responses to ischemic injury is to provide a scaffold for neuronal regeneration. Proper cell–cell communication within vascular niches of neurogenesis is crucial for regenerative mechanisms in the adult brain. Close reciprocal relationships between brain ECs and neural progenitor cells (NPCs) regulate neurogenesis in both the developing and adult brain (Goldman and Chen, 2011; Licht and Keshet, 2015; Segarra et al., 2015, 2018; Tata and Ruhrberg, 2018). NPCs secrete proangiogenic factors that promote brain vascularization, and brain ECs instruct NPCs to proliferate, differentiate, or remain quiescent through release of angiocrine messengers including NO, BDNF, stromal-derived factor 1, or angiopoietin

1 (Ohab et al., 2006; Goldman and Chen, 2011). Stroke triggers a regenerative response in the peri-infarct region, adjacent to the core area of cell death. A focal cortical stroke in mice induced a strong neurogenic response with induction of GFAP-expressing NPCs in the subventricular zone, followed by migration of neuroblasts along existing and newly formed vascular beds toward the peri-infarct cortex (Ohab et al., 2006; Ohab and Carmichael, 2008). Following this important discovery that angiogenesis and neurogenesis are causally linked in the post-stroke niche, several studies have investigated these complex structural and molecular neuro-vascular interactions, as recently reviewed elsewhere (Fujioka et al., 2019; Hatakeyama et al., 2020). Overall, this supports the idea that enhancing post-stroke angiogenesis might represent a valuable strategy to promote post-stroke functional recovery.

In summary, angiogenesis is a multistep process involving basement membrane breakdown, cell proliferation and migration, capillary morphogenesis, vascular maturation and vascular pruning and cellular apoptosis. Similar angiogenic mechanisms are triggered in both ischemic and hemorrhagic brain injury. Many of these mechanisms are also critical during brain development and are similarly induced by ischemia. Importantly, formation of new capillaries, through angiogenic processes, provide a scaffold for neuronal stem cell recruitment both during brain injury and CNS development.

SEX DIFFERENCES IN CEREBROVASCULAR OUTCOMES OF STROKE

Sex differences in brain morphology, function and disease are eliciting growing interest, but very little is known about the cellular and molecular underpinnings of sex differences in vascular outcomes of stroke. Biological sex markedly influences CBF as well as the prevalence and progression of cardiovascular diseases, including stroke (Krause et al., 2006; Cosgrove et al., 2007; Hofer et al., 2007; Cowan et al., 2017). It is well recognized that stroke differentially affects women and men. Although men have a higher incidence of stroke compared to age-matched pre-menopausal women, epidemiological studies show that most women have strokes when they are post-menopausal, resulting in increased stroke severity, worse psychological outcomes, and higher rates of disability (Persky et al., 2010; Turtzo and McCullough, 2010; Barker-Collo et al., 2015; Ahnstedt et al., 2016; Madsen et al., 2019; Wang et al., 2019). Despite this, the effects of sex hormones on cerebrovascular regulation in the healthy and ischemic brain have yet to be fully comprehended.

The concept of sex differences in neuro-vascular research was not well appreciated until recently. A common finding is an increased baseline CBF in women versus men (Cosgrove et al., 2007; Ghisleni et al., 2015). Women also display greater perfusion during cognitive tasks (Gur et al., 1982; Esposito et al., 1996), and better autoregulation of CBF as they age (Deegan et al., 2011). Yet, the underlying causes of these sex differences are unknown. Sex differences in CBF are due in part to the combined modulation by steroid hormones. Estradiol, testosterone and dehydroepiandrosterone sulfate are modulators of brain perfusion (Ghisleni et al., 2015). Testosterone mainly exerts vasoconstrictive effects, and its supplementation decreases CBF in post-menopausal women. 17β-estradiol (E2) is the most abundant and potent estrogen in mammals. Binding of E2 to its receptor ERα increases NO production through upregulation of eNOS (Miyazaki-Akita et al., 2007), as well as via decreasing the concentration of NO-scavenging superoxide anion (Novella et al., 2012). eNOS is modulated by ERα activation via: (1) typical ERα signaling with nuclear translocation of intracellular receptors, leading to increased eNOS gene (*Nos3*) expression, or (2) the lesser-studied stimulation of membrane-bound ERα leading to phosphatidylinositol-3-kinase pathway stimulation and eNOS activation (Novella et al., 2012). Signaling through these pathways results in increased bioavailability of NO, a potent relaxant of VSMCs and therefore vasodilator (Chen et al., 2008; Moncada and Higgs, 1993).

Lower incidence rates of stroke in pre-menopausal women has been linked to a protective effect of estrogens (Turtzo and McCullough, 2010), and after menopause rates of stroke dramatically increase (Lisabeth and Bushnell, 2012; Xu J. et al., 2016). As women have a longer life expectancy, they account for 60% of stroke events when incidence rates are adjusted for age (Reeves et al., 2008). Following menopause, estrogen production by the ovaries decreases by >50%. This has supported the theory that estrogens are protective in CVD, which has been attributed in part to the ability of estrogens to enhance NO production via stimulation of eNOS (Krause et al., 2006; Nevzati et al., 2015).

Protective roles of estrogens have been reported in a variety of animal models of cerebral ischemia. Numerous studies show that estrogen treatment or activation of estrogen receptors reduces lesion size in these animal models (Yang et al., 2000; McCullough et al., 2001; Selvaraj et al., 2018; Xiao et al., 2018) while removing endogenous estrogen through ovariectomy (Ovx) worsens their outcomes (Alkayed et al., 1998; Fukuda et al., 2000). Furthermore, female rats that undergo tMCAo during the proestrus phase of their estrous cycle (i.e., highest estradiol levels) have smaller infarcts than females in other phases of the cycle (Liao et al., 2001). Estrogen supplementation of Ovx rodents prior to stroke has also been found to preserve BBB integrity by reducing EC death and preventing the loss of TJ proteins (Liu et al., 2005; Shin et al., 2016). *In vitro*, estradiol protects the endothelium by reducing mitochondrial reactive oxygen species (ROS) production following ischemic injury (Razmara et al., 2008; Guo et al., 2010). These protective mechanisms may contribute to preserving not only neuronal health, but also vascular health, during and following cerebral ischemia.

Overall, there are very few mechanistic investigations on disparities between sexes in post-stroke CBF outcome. Ovx rats displayed significantly lower CBF following tMCAo compared to intact females. Upon estrogen supplementation, CBF in Ovx rats could be rescued 1 day post-stroke (Yang et al., 2000). Long-term estrogen treatment increases eNOS expression in cerebral blood vessels from male and female rats (McNeill et al., 1999), suggesting that NO may play a protective role through vasorelaxation. In contrast, males treated with estrogen immediately following tMCAo had increased CBF up to 10 min following stroke, but not past 90 min (McCullough

et al., 2001), but not past 90 min, suggesting that modulation of hormones might not be a viable therapeutic option. Additionally, following photothrombotic distal MCAo, female rats showed quicker vascular remodeling of occluded and peripheral vessels compared to males (Yang et al., 2019). Only one study has shown that CBF values of females are higher following stroke compared to males and Ovx females, and the mechanism behind this difference has yet to be elucidated (Alkayed et al., 1998).

Despite the promising effects of estrogens in rodent stroke models, hormone therapy containing either combined estrogen and progesterone, or estrogen alone, increases the risk of ischemic stroke by 40–50% in healthy postmenopausal women (Wassertheil-Smoller et al., 2003; Hendrix et al., 2006; Hale and Shufelt, 2015). In this case, the stroke is most often thrombotic, which is attributed to decreased plasma levels of endogenous circulating anticoagulants in response to high estrogen levels (Mendelsohn and Karas, 1999). There is also the timing hypothesis for hormone therapy, which suggests that treatment with exogenous estrogens and progesterone causes more harm when EC viability is already compromised, as is often the case in aging women (Lisabeth and Bushnell, 2012). Additionally, hormone replacement therapy using estrogens can increase the risk of ovarian and breast cancer (Brown et al., 2018). For these reasons, hormone replacement therapy to reduce stroke risk in post-menopausal women is not recommended. Therefore, it is critical to better understand how sex hormones regulate vascular function in order to refine future therapies. Switching to novel targets might represent safer options, but further preclinical research is warranted. Known eNOS enhancers (e.g., AVE3085 and AVE9488) that have been beneficial for peripheral cardiovascular disease (CVD) in animal studies might prove particularly efficient in post-menopausal women.

In summary, although existing literature on sex differences in stroke severity and mortality are somewhat contradictory, women suffer from worse functional outcomes and have high levels of long-term disability. Animal models do not entirely reflect what is observed in the clinic and estrogen therapy, while beneficial in rodent experiments, failed to translate into the clinical setting. Many factors may influence sex-specific responses to stroke including epigenetics, immune responsiveness, inflammation and chromosomal contributions. This area of research has been largely overlooked, and given the significant impact stroke has in women it is imperative that more research is conducted.

CONCLUDING REMARKS

Limitations of Preclinical Stroke Research

The majority of preclinical work on cerebrovascular stroke outcomes has been performed in anesthetized healthy rodents, often using solely males. Moreover, two important limitations of preclinical studies on sex differences in stroke have been (i) the use of young animals and (ii) the misconception that Ovx (i.e., model of reduced steroid influence) mimics human menopause. Aging is a key risk factor for stroke, together with several comorbidities such as hypertension and atherosclerosis that develop with age. The use of young healthy male rodent models, not reflective of the human condition, is a contributing factor to the failure to translate drugs into the clinic. While these concerns are addressable by using rodent cohorts that better mimic the human population most often affected by stroke, there are inherent problems that must be accounted for in preclinical stroke models.

Experimental MCAo is the most commonly used animal model of ischemic stroke, which consists of either permanent (without reperfusion) or transient (with reperfusion) occlusion of the middle cerebral artery (MCA). While reproducible, MCAo has important translational limitations. As typically used, MCAo creates large infarcts equivalent to malignant human brain infarction (Carmichael, 2005). Furthermore, permanent and complete occlusion of the MCA does not accurately represent human ischemic stroke, and the transient model that allows for quick reperfusion is more representative of global ischemia conditions rather than a focal ischemic stroke (Sommer, 2017). While MCAo has a similar inflammatory profile as seen in humans and is useful to assess neuroprotection, as it allows for sensitive measures of neuronal death, it is not recommended for stroke recovery studies that rely on behavioral outcomes (Corbett et al., 2017; McCabe et al., 2018). However, it has recently been suggested that the MCAo model may be useful for mimicking the conditions associated with endovascular treatment of ischemic stroke (Sommer, 2017).

Accordingly, it is preferable to create focal ischemia using the photothrombotic (PT) or endothelin-1 (ET-1) stroke models, which are both highly recommended by recent international consensus panels (Tennant and Jones, 2009; Roome et al., 2014; Corbett et al., 2017). Stereotaxic injection of the peptide ET-1, a potent vasoconstrictor, restricts blood flow to the region. This is followed by reperfusion when the effects of ET-1 wear off after several hours (Biernaskie et al., 2001). The reperfusion creates an ischemic penumbra (Weinstein et al., 2004; Gauberti et al., 2016), largely absent in PT stroke, corresponding to a region where neurons remain at risk but are salvageable (Heiss, 2012; Wetterling et al., 2016). PT strokes are induced by cortical photoactivation of a light-sensitive dye that is administered peripherally, resulting in singlet oxygen production, endothelial damage, platelet activation and aggregation, causing permanent occlusion of vessels in the irradiated region of the brain (Uzdensky, 2018). ET-1 and PT stroke models precisely target cortical regions relevant to cerebrovascular and behavioral recovery, are reproducible, and more closely mimic the size (on a proportional basis) of human strokes, with or without reperfusion. There is minimal edema associated with the ET-1 model (Schirrmacher et al., 2016) and lack of BBB disruption (Hughes et al., 2003), while PT stroke is associated with simultaneous cytotoxic edema due to cell death and vasogenic edema due to BBB disruption (Chen et al., 2007). This varies from the primarily cytotoxic edema seen initially in human stroke which is later followed by vasogenic edema (Provenzale et al., 2003). Furthermore, PT stroke corresponds with a strong

immunogenic response characterized by increased infiltration of circulating leukocytes, as well as high levels of ROS and pro-inflammatory cytokines (Cotrina et al., 2017). Both PT and ET-1 are reproducible, convenient, and minimally invasive, however, they must be used accordingly regarding these considereations.

Perhaps the most accurate representation of ischemic stroke as seen in humans is the thromboembolic model of embolic stroke, whereby spontaneous or thrombin-induced clots of heterologous or autologous blood are injected into a cerebral artery. Alternatively, thrombin can be directly injected into the MCA or internal carotid artery to induce vascular occlusion. This accurately represents vascular occlusion most often seen in humans; however, the thrombi are mainly composed of polymerized fibrin, and therefore differ from thrombi in human patients that contain large amounts of both thrombin and erythrocytes (Duffy et al., 2019). Nevertheless, use of thrombolytic agents in this stroke model has the potential to mimic reperfusion following treatment that current stroke models do not as accurately represent (Fluri et al., 2015). Additionally, variability in clot size and stability results in variable infarct size and location. While thromboembolic stroke provides an accurate clinical representation of stroke in terms of edema, BBB breakdown, and inflammatory response, the inherent variability of the model requires large sample sizes to overcome this (Sommer, 2017).

In addition, the choice of anesthetic regimen is crucial when performing stroke surgery in rodents, as it can strongly influence CBF and stroke outcome, and may contribute to translational failure (O'Collins et al., 2006). For instance, isoflurane is a potent vasodilator with neuroprotective effects (Tsuda, 2010; Gaidhani et al., 2017; Jiang et al., 2017; Lu et al., 2017) via modulation of eNOS activity (Kehl et al., 2002; Krolikowski et al., 2006), which strongly confounds results. Ketamine/Xylazine (K/X) anesthesia affects baseline CBF to a lesser extent, but has also been shown to modulate eNOS (Chen et al., 2005). To circumvent these methodological obstacles, one should compare stroke outcomes in anesthetized versus awake mice when possible.

Overall, there is an urgent need to carefully refine experimental designs to prevent translational failure. In depth comparisons of the advantages and disadvantages of currently used stroke models and their applications in different areas of research has been reviewed elsewhere (Fluri et al., 2015; Sommer, 2017). Choosing the appropriate stroke model is essential to provide meaningful data and avoid translational failure.

What the Future Holds for Cerebrovascular Stroke Research

Unfortunately, stroke research has suffered many setbacks, primarily due to a number of potential therapeutic candidates that have not delivered the expected benefits. As such, industry investment in the field dwindled owing to the perception of stroke research as a high-risk/low reward investment. Most negative results stemmed from failure of scientists to apply the information supplied by animal models to clinical trials. One compelling example, *N*-methyl-D-aspartate (NMDA) antagonists were only found to be neuroprotective when given to rats up to 90 min after blood vessel occlusion. However, in clinical trials patients were not given these drugs until 6 h later (Green and Shuaib, 2006). Despite these setbacks, researchers are continuously developing new methods and refining models, as well as investigating novel avenues of research that hold significant promise in improving stroke outcome (Silasi et al., 2015; Gouveia et al., 2017; Kannangara et al., 2018; Freitas-Andrade et al., 2019; Hill et al., 2020; Mendonca et al., 2020; Rayasam et al., 2020; Zhang et al., 2020). A greater appreciation for the role of physical rehabilitation and insight into the molecular mechanisms at play has led to a significant impact on the quality of life after stroke (Fang et al., 2019; McDonald et al., 2019; Sun and Zehr, 2019).

Novel molecules and new approaches focused on manipulating the cerebral vasculature to mitigate the effects of stroke are ongoing (Stanimirovic et al., 2018; Kanazawa et al., 2019). For example, Salvinorin A (derived from the ethnomedical plant Salvia divinorum), a selective kappa opioid receptor (KOR) agonist (Butelman and Kreek, 2015), has been shown to reduce cerebral vasospasm and alleviate brain injury after SAH via increasing expression of eNOS, and decreasing ET-1 concentration and AQP-4 protein expression (Sun et al., 2018). A recent study also showed that this drug can protect EC mitochondrial function following stroke (Dong et al., 2019). Remarkably, cutting-edge techniques, such as, single-cell RNA sequencing are unmasking the inner workings of ECs at an unprecedented level (Vanlandewijck et al., 2018; Munji et al., 2019; Kalucka et al., 2020; Kirst et al., 2020; Rohlenova et al., 2020). Finally, rigorous guidelines for effective translational research have been proposed, including the use of rodent models that are more representative of human strokes integrating comorbidities (Lapchak et al., 2013; Reeson et al., 2015). Given that the incidence of stroke increases with vascular diseases, animal models that incorporate comorbidities are critical in stroke research. A clinical study demonstrated that patients with chronic cerebral small vessel disease were associated with poor recruitment of collaterals in large vessel occlusion stroke (Lin et al., 2020). Another comorbidity, hypertension, is a modifiable risk factor for stroke. Hypertension is prevalent in the stroke population and is an important comorbidity to investigate (Cipolla et al., 2018). Hypertension promotes stroke through increased shear stress, endothelial cell dysfunction and large artery stiffness that transmits pulsatile flow to the microcirculation in the brain. Indeed, dysfunctional angiogenesis may occur in diabetic and/or hypertensive elderly patients in the recovering penumbra following stroke (Ergul et al., 2012).

While exciting new developments are in the pipeline, several lines of investigation indicate a significant impact lifestyle has on vascular health (Hakim, 2014, 2019) and particularly on brain angiogenesis and stroke outcome (Schmidt et al., 2013). A short interval of exercise prior to stroke was shown to improve functional outcomes by enhancing angiogenesis (Pianta et al., 2019). A possible mechanism of action was demonstrated to result from exercise-induced increase in VEGF expression via the lactate receptor HCAR1 in the brain (Morland et al., 2017). However, other mechanisms including growth factors or eNOS-dependent pathways have been reported (Geiseler and Morland, 2018).

Therefore, the scientific community must emphasize the importance of lifestyle in reducing the burden of stroke; we have the knowledge and responsibility to urge implementation of more extensive public health awareness and strategies to promote healthy vascular aging.

AUTHOR CONTRIBUTIONS

BL chose the theme of the review. MF-A, JR-N, and BL wrote the manuscript. All authors contributed to the article and approved the submitted version.

FUNDING

This publication was possible thanks to funding by a Heart and Stroke Foundation of Canada research grant to BL (G-17-0018290).

ACKNOWLEDGMENTS

We thank Dr. Antoine M. Hakim for his feedback on the manuscript.

REFERENCES

Abbott, N. J., Ronnback, L., and Hansson, E. (2006). Astrocyte-endothelial interactions at the blood-brain barrier. *Nat. Rev. Neurosci.* 7, 41–53. doi: 10.1038/nrn1824

Abdullahi, W., Tripathi, D., and Ronaldson, P. T. (2018). Blood-brain barrier dysfunction in ischemic stroke: targeting tight junctions and transporters for vascular protection. *Am. J. Physiol. Cell Physiol.* 315, C343–C356.

Ahnstedt, H., McCullough, L. D., and Cipolla, M. J. (2016). The importance of considering sex differences in translational stroke research. *Transl. Stroke Res.* 7, 261–273. doi: 10.1007/s12975-016-0450-1

Al Ahmad, A., Taboada, C. B., Gassmann, M., and Ogunshola, O. O. (2011). Astrocytes and pericytes differentially modulate blood-brain barrier characteristics during development and hypoxic insult. *J. Cereb. Blood Flow Metab.* 31, 693–705. doi: 10.1038/jcbfm.2010.148

Albargothy, N. J., Johnston, D. A., MacGregor-Sharp, M., Weller, R. O., Verma, A., Hawkes, C. A., et al. (2018). Convective influx/glymphatic system: tracers injected into the CSF enter and leave the brain along separate periarterial basement membrane pathways. *Acta Neuropathol.* 136, 139–152. doi: 10.1007/s00401-018-1862-7

Aleithe, S., Blietz, A., Mages, B., Hobusch, C., Hartig, W., and Michalski, D. (2019). Transcriptional response and morphological features of the neurovascular unit and associated extracellular matrix after experimental stroke in mice. *Mol. Neurobiol.* 56, 7631–7650. doi: 10.1007/s12035-019-1604-4

Alkayed, N. J., Harukuni, I., Kimes, A. S., London, E. D., Traystman, R. J., and Hurn, P. D. (1998). Gender-linked brain injury in experimental stroke. *Stroke* 29, 159–165; discussion166.

Allan, L. M., Rowan, E. N., Firbank, M. J., Thomas, A. J., Parry, S. W., Polvikoski, T. M., et al. (2011). Long term incidence of dementia, predictors of mortality and pathological diagnosis in older stroke survivors. *Brain* 134, 3716–3727. doi: 10.1093/brain/awr273

Allen, C., Srivastava, K., and Bayraktutan, U. (2010). Small GTPase RhoA and its effector rho kinase mediate oxygen glucose deprivation-evoked in vitro cerebral barrier dysfunction. *Stroke* 41, 2056–2063. doi: 10.1161/strokeaha.109.574939

Anderson, C. M., and Nedergaard, M. (2003). Astrocyte-mediated control of cerebral microcirculation. *Trends Neurosci.* 26, 340–344; authorrely344–345.

Andreone, B. J., Chow, B. W., Tata, A., Lacoste, B., Ben-Zvi, A., Bullock, K., et al. (2017). Blood-brain barrier permeability is regulated by lipid transport-dependent suppression of caveolae-mediated transcytosis. *Neuron* 94, 581.e5–594.e5.

Andreone, B. J., Lacoste, B., and Gu, C. (2015). Neuronal and vascular interactions. *Annu. Rev. Neurosci.* 38, 25–46. doi: 10.1146/annurev-neuro-071714-033835

Aoki, T., Sumii, T., Mori, T., Wang, X., and Lo, E. H. (2002). Blood-brain barrier disruption and matrix metalloproteinase-9 expression during reperfusion injury: mechanical versus embolic focal ischemia in spontaneously hypertensive rats. *Stroke* 33, 2711–2717. doi: 10.1161/01.str.0000033932.34467.97

Arimura, K., Ago, T., Kamouchi, M., Nakamura, K., Ishitsuka, K., Kuroda, J., et al. (2012). PDGF receptor beta signaling in pericytes following ischemic brain injury. *Curr. Neurovasc. Res.* 9, 1–9. doi: 10.2174/156720212799297100

Armulik, A., Genove, G., Mae, M., Nisancioglu, M. H., Wallgard, E., Niaudet, C., et al. (2010). Pericytes regulate the blood-brain barrier. *Nature* 468, 557–561.

Arnao, V., Acciarresi, M., Cittadini, E., and Caso, V. (2016). Stroke incidence, prevalence and mortality in women worldwide. *Int. J. Stroke* 11, 287–301. doi: 10.1177/1747493016632245

Attwell, D., Buchan, A. M., Charpak, S., Lauritzen, M., Macvicar, B. A., and Newman, E. A. (2010). Glial and neuronal control of brain blood flow. *Nature* 468, 232–243. doi: 10.1038/nature09613

Avrutsky, M. I., Ortiz, C. C., Johnson, K. V., Potenski, A. M., Chen, C. W., Lawson, J. M., et al. (2020). Endothelial activation of caspase-9 promotes neurovascular injury in retinal vein occlusion. *Nat. Commun.* 11:3173.

Ayata, C., and Lauritzen, M. (2015). Spreading depression, spreading depolarizations, and the cerebral vasculature. *Physiol. Rev.* 95, 953–993. doi: 10.1152/physrev.00027.2014

Ayloo, S., and Gu, C. (2019). Transcytosis at the blood-brain barrier. *Curr. Opin. Neurobiol.* 57, 32–38. doi: 10.1016/0006-8993(87)90236-8

Barker-Collo, S., Bennett, D. A., Krishnamurthi, R. V., Parmar, P., Feigin, V. L., Naghavi, M., et al. (2015). Sex differences in stroke incidence, prevalence, mortality and disability-adjusted life years: results from the global burden of disease study 2013. *Neuroepidemiology* 45, 203–214. doi: 10.1159/000441103

Batiuk, M. Y., Martirosyan, A., Wahis, J., de Vin, F., Marneffe, C., Kusserow, C., et al. (2020). Identification of region-specific astrocyte subtypes at single cell resolution. *Nat. Commun.* 11:1220.

Bauersachs, J., and Widder, J. D. (2008). Endothelial dysfunction in heart failure. *Pharmacol. Rep.* 60, 119–126.

Beck, H., Acker, T., Puschel, A. W., Fujisawa, H., Carmeliet, P., and Plate, K. H. (2002). Cell type-specific expression of neuropilins in an MCA-occlusion model in mice suggests a potential role in post-ischemic brain remodeling. *J. Neuropathol. Exp. Neurol.* 61, 339–350. doi: 10.1093/jnen/61.4.339

Beck, H., and Plate, K. H. (2009). Angiogenesis after cerebral ischemia. *Acta Neuropathol.* 117, 481–496. doi: 10.1007/s00401-009-0483-6

Beck, H., Semisch, M., Culmsee, C., Plesnila, N., and Hatzopoulos, A. K. (2008). Egr-1 regulates expression of the glial scar component phosphacan in astrocytes after experimental stroke. *Am. J. Pathol.* 173, 77–92. doi: 10.2353/ajpath.2008.070648

Becker, B. F., Jacob, M., Leipert, S., Salmon, A. H., and Chappell, D. (2015). Degradation of the endothelial glycocalyx in clinical settings: searching for the sheddases. *Br. J. Clin. Pharmacol.* 80, 389–402. doi: 10.1111/bcp.12629

Behringer, E. J., and Segal, S. S. (2012). Tuning electrical conduction along endothelial tubes of resistance arteries through Ca(2+)-activated K(+) channels. *Circ. Res.* 110, 1311–1321. doi: 10.1161/circresaha.111.262592

Bell, R. D., Winkler, E. A., Sagare, A. P., Singh, I., LaRue, B., Deane, R., et al. (2010). Pericytes control key neurovascular functions and neuronal phenotype in the adult brain and during brain aging. *Neuron* 68, 409–427. doi: 10.1016/j.neuron.2010.09.043

Belliveau, D. J., and Naus, C. C. (1994). Cortical type 2 astrocytes are not dye coupled nor do they express the major gap junction genes found in the central nervous system. *Glia* 12, 24–34. doi: 10.1002/glia.440120104

Ben-Zvi, A., Lacoste, B., Kur, E., Andreone, B. J., Mayshar, Y., Yan, H., et al. (2014). Mfsd2a is critical for the formation and function of the blood-brain barrier. *Nature* 509, 507–511. doi: 10.1038/nature13324

Bernhardt, J., Borschmann, K. N., Kwakkel, G., Burridge, J. H., Eng, J. J., Walker, M. F., et al. (2019). Setting the scene for the second stroke recovery

and rehabilitation roundtable. *Int. J. Stroke* 14, 450–456. doi: 10.1177/1747493019851287

Biernaskie, J., Corbett, D., Peeling, J., Wells, J., and Lei, H. (2001). A serial MR study of cerebral blood flow changes and lesion development following endothelin-1-induced ischemia in rats. *Magn. Reson. Med.* 46, 827–830. doi: 10.1002/mrm.1263

Bisht, K., Sharma, K. P., Lecours, C., Sanchez, M. G., El Hajj, H., Milior, G., et al. (2016). Dark microglia: a new phenotype predominantly associated with pathological states. *Glia* 64, 826–839. doi: 10.1002/glia.22966

Biswas, S., Cottarelli, A., and Agalliu, D. (2020). Neuronal and glial regulation of CNS angiogenesis and barriergenesis. *Development* 147, 1–13.

Bix, G. J., Gowing, E. K., and Clarkson, A. N. (2013). Perlecan domain V is neuroprotective and affords functional improvement in a photothrombotic stroke model in young and aged mice. *Transl. Stroke Res.* 4, 515–523. doi: 10.1007/s12975-013-0266-1

Bolon, M. L., Ouellette, Y., Li, F., and Tyml, K. (2005). Abrupt reoxygenation following hypoxia reduces electrical coupling between endothelial cells of wild-type but not connexin40 null mice in oxidant- and PKA-dependent manner. *FASEB J.* 19, 1725–1727. doi: 10.1096/fj.04-3446fje

Bondarenko, A., and Chesler, M. (2001). Rapid astrocyte death induced by transient hypoxia, acidosis, and extracellular ion shifts. *Glia* 34, 134–142. doi: 10.1002/glia.1048

Brown, K. F., Rumgay, H., Dunlop, C., Ryan, M., Quartly, F., Cox, A., et al. (2018). The fraction of cancer attributable to modifiable risk factors in England, Wales, Scotland, Northern Ireland, and the United Kingdom in 2015. *Br. J. Cancer* 118, 1130–1141. doi: 10.1038/s41416-018-0029-6

Brzica, H., Abdullahi, W., Ibbotson, K., and Ronaldson, P. T. (2017). Role of transporters in central nervous system drug delivery and blood-brain barrier protection: relevance to treatment of stroke. *J. Cent. Nerv. Syst. Dis.* 9:1179573517693802.

Butelman, E. R., and Kreek, M. J. (2015). Salvinorin A, a kappa-opioid receptor agonist hallucinogen: pharmacology and potential template for novel pharmacotherapeutic agents in neuropsychiatric disorders. *Front. Pharmacol.* 6:190. doi: 10.3389/fphar.2015.00190

Cai, C., Fordsmann, J. C., Jensen, S. H., Gesslein, B., Lonstrup, M., Hald, B. O., et al. (2018). Stimulation-induced increases in cerebral blood flow and local capillary vasoconstriction depend on conducted vascular responses. *Proc. Natl. Acad. Sci. U.S.A.* 115, E5796–E5804.

Cai, W., Liu, H., Zhao, J., Chen, L. Y., Chen, J., Lu, Z., et al. (2017). Pericytes in brain injury and repair after ischemic stroke. *Transl. Stroke Res.* 8, 107–121. doi: 10.1007/s12975-016-0504-4

Canazza, A., Minati, L., Boffano, C., Parati, E., and Binks, S. (2014). Experimental models of brain ischemia: a review of techniques, magnetic resonance imaging, and investigational cell-based therapies. *Front. Neurol.* 5:19. doi: 10.3389/fneur.2014.00019

Carbonell, T., and Rama, R. (2007). Iron, oxidative stress and early neurological deterioration in ischemic stroke. *Curr. Med. Chem.* 14, 857–874. doi: 10.2174/092986707780363014

Cardenas-Rivera, A., Campero-Romero, A. N., Heras-Romero, Y., Penagos-Puig, A., Rincon-Heredia, R., and Tovar, Y. R. L. B. (2019). Early post-stroke activation of vascular endothelial growth factor receptor 2 hinders the receptor 1-dependent neuroprotection afforded by the endogenous ligand. *Front. Cell. Neurosci.* 13:270. doi: 10.3389/fncel.2019.00270

Carmeliet, P., and Tessier-Lavigne, M. (2005). Common mechanisms of nerve and blood vessel wiring. *Nature* 436, 193–200. doi: 10.1038/nature03875

Carmichael, S. T. (2005). Rodent models of focal stroke: size, mechanism, and purpose. *NeuroRx* 2, 396–409. doi: 10.1602/neurorx.2.3.396

Cauli, B., and Hamel, E. (2010). Revisiting the role of neurons in neurovascular coupling. *Front. Neuroenerg.* 2:9. doi: 10.3389/fnene.2010.00009

Chaturvedi, M., and Kaczmarek, L. (2014). Mmp-9 inhibition: a therapeutic strategy in ischemic stroke. *Mol. Neurobiol.* 49, 563–573. doi: 10.1007/s12035-013-8538-z

Cheang, W. S., Wong, W. T., Tian, X. Y., Yang, Q., Lee, H. K., He, G. W., et al. (2011). Endothelial nitric oxide synthase enhancer reduces oxidative stress and restores endothelial function in db/db mice. *Cardiovasc. Res.* 92, 267–275. doi: 10.1093/cvr/cvr233

Chen, F., Suzuki, Y., Nagai, N., Jin, L., Yu, J., Wang, H., et al. (2007). Rodent stroke induced by photochemical occlusion of proximal middle cerebral artery: evolution monitored with MR imaging and histopathology. *Eur. J. Radiol.* 63, 68–75. doi: 10.1016/j.ejrad.2007.01.005

Chen, J., Braet, F., Brodsky, S., Weinstein, T., Romanov, V., Noiri, E., et al. (2002). VEGF-induced mobilization of caveolae and increase in permeability of endothelial cells. *Am. J. Physiol. Cell Physiol.* 282, C1053–C1063.

Chen, K., Pittman, R. N., and Popel, A. S. (2008). Nitric oxide in the vasculature: where does it come from and where does it go? A quantitative perspective. *Antioxid. Redox. Signal.* 10, 1185–1198. doi: 10.1089/ars.2007.1959

Chen, R. M., Chen, T. L., Lin, Y. L., Chen, T. G., and Tai, Y. T. (2005). Ketamine reduces nitric oxide biosynthesis in human umbilical vein endothelial cells by down-regulating endothelial nitric oxide synthase expression and intracellular calcium levels. *Crit. Care Med.* 33, 1044–1049. doi: 10.1097/01.ccm.0000163246.33366.51

Chen, Y., and Swanson, R. A. (2003). Astrocytes and brain injury. *J. Cereb. Blood Flow Metab.* 23, 137–149.

Chen, Z. L., Yao, Y., Norris, E. H., Kruyer, A., Jno-Charles, O., Akhmerov, A., et al. (2013). Ablation of astrocytic laminin impairs vascular smooth muscle cell function and leads to hemorrhagic stroke. *J. Cell Biol.* 202, 381–395. doi: 10.1083/jcb.201212032

Choi, K. H., Kim, H. S., Park, M. S., Kim, J. T., Kim, J. H., Cho, K. A., et al. (2016). Regulation of caveolin-1 expression determines early brain edema after experimental focal cerebral ischemia. *Stroke* 47, 1336–1343. doi: 10.1161/strokeaha.116.013205

Chow, B. W., and Gu, C. (2015). The molecular constituents of the blood-brain barrier. *Trends Neurosci.* 38, 598–608. doi: 10.1016/j.tins.2015.08.003

Chow, B. W., and Gu, C. (2017). Gradual suppression of transcytosis governs functional blood-retinal barrier formation. *Neuron* 93, 1325.e3–1333.e3.

Chow, J., Ogunshola, O., Fan, S. Y., Li, Y., Ment, L. R., and Madri, J. A. (2001). Astrocyte-derived VEGF mediates survival and tube stabilization of hypoxic brain microvascular endothelial cells in vitro. *Brain Res. Dev. Brain Res.* 130, 123–132. doi: 10.1016/s0165-3806(01)00220-6

Chu, H., Tang, Y., and Dong, Q. (2013). Protection of vascular endothelial growth factor to brain edema following intracerebral hemorrhage and its involved mechanisms: effect of aquaporin-4. *PLoS One* 8:e66051. doi: 10.1371/journal.pone.0066051

Cipolla, M. J., Crete, R., Vitullo, L., and Rix, R. D. (2004). Transcellular transport as a mechanism of blood-brain barrier disruption during stroke. *Front. Biosci.* 9:777–785. doi: 10.2741/1282

Cipolla, M. J., Liebeskind, D. S., and Chan, S. L. (2018). The importance of comorbidities in ischemic stroke: impact of hypertension on the cerebral circulation. *J. Cereb. Blood Flow Metab.* 38, 2129–2149. doi: 10.1177/0271678x18800589

Clavreul, S., Abdeladim, L., Hernandez-Garzon, E., Niculescu, D., Durand, J., Ieng, S. H., et al. (2019). Cortical astrocytes develop in a plastic manner at both clonal and cellular levels. *Nat. Commun.* 10:4884.

Coelho-Santos, V., and Shih, A. Y. (2020). Postnatal development of cerebrovascular structure and the neurogliovascular unit. *Wiley Interdiscip. Rev. Dev. Biol.* 9:e363.

Corbett, D., Carmichael, S. T., Murphy, T. H., Jones, T. A., Schwab, M. E., Jolkkonen, J., et al. (2017). Enhancing the alignment of the preclinical and clinical stroke recovery research pipeline: consensus-based core recommendations from the stroke recovery and rehabilitation roundtable translational working group. *Neurorehabil. Neural Repair* 31, 699–707. doi: 10.1177/1545968317724285

Corbett, D., Nguemeni, C., and Gomez-Smith, M. (2014). How can you mend a broken brain? Neurorestorative approaches to stroke recovery. *Cerebrovasc. Dis.* 38, 233–239. doi: 10.1159/000368887

Cordeau, P. Jr., Lalancette-Hebert, M., Weng, Y. C., and Kriz, J. (2008). Live imaging of neuroinflammation reveals sex and estrogen effects on astrocyte response to ischemic injury. *Stroke* 39, 935–942. doi: 10.1161/strokeaha.107.501460

Cosgrove, K. P., Mazure, C. M., and Staley, J. K. (2007). Evolving knowledge of sex differences in brain structure, function, and chemistry. *Biol. Psychiatry* 62, 847–855. doi: 10.1016/j.biopsych.2007.03.001

Cotrina, M. L., Lou, N., Tome-Garcia, J., Goldman, J., and Nedergaard, M. (2017). Direct comparison of microglial dynamics and inflammatory profile in photothrombotic and arterial occlusion evoked stroke. *Neuroscience* 343, 483–494. doi: 10.1016/j.neuroscience.2016.12.012

Cowan, R. L., Beach, P. A., Atalla, S. W., Dietrich, M. S., Bruehl, S. P., Deng, J., et al. (2017). Sex differences in the psychophysical response to contact heat in moderate cognitive impairment alzheimer's disease: a cross-sectional brief report. *J. Alzheimers Dis.* 60, 1633–1640. doi: 10.3233/jad-170532

Crain, J. M., Nikodemova, M., and Watters, J. J. (2013). Microglia express distinct M1 and M2 phenotypic markers in the postnatal and adult central nervous system in male and female mice. *J. Neurosci. Res.* 91, 1143–1151. doi: 10.1002/jnr.23242

Crawley, J. T., de Groot, R., Xiang, Y., Luken, B. M., and Lane, D. A. (2011). Unraveling the scissile bond: how ADAMTS13 recognizes and cleaves von Willebrand factor. *Blood* 118, 3212–3221. doi: 10.1182/blood-2011-02-306597

Cui, Q., Zhang, Y., Chen, H., and Li, J. (2013). Rho kinase: a new target for treatment of cerebral ischemia/reperfusion injury. *Neural Regen. Res.* 8, 1180–1189.

Dalkara, T., and Moskowitz, M. A. (1994). The complex role of nitric oxide in the pathophysiology of focal cerebral ischemia. *Brain Pathol.* 4, 49–57. doi: 10.1111/j.1750-3639.1994.tb00810.x

Daneman, R. (2012). The blood-brain barrier in health and disease. *Ann. Neurol.* 72, 648–672.

Daneman, R., Zhou, L., Kebede, A. A., and Barres, B. A. (2010). Pericytes are required for blood-brain barrier integrity during embryogenesis. *Nature* 468, 562–566. doi: 10.1038/nature09513

Dassan, P., Keir, G., Jager, H. R., and Brown, M. M. (2012). Value of measuring serum vascular endothelial growth factor levels in diagnosing acute ischemic stroke. *Int. J. Stroke* 7, 454–459. doi: 10.1111/j.1747-4949.2011.00677.x

Dawson, D. A. (1994). Nitric oxide and focal cerebral ischemia: multiplicity of actions and diverse outcome. *Cerebrovasc. Brain Metab. Rev.* 6, 299–324.

De Bock, M., Culot, M., Wang, N., Bol, M., Decrock, E., De Vuyst, E., et al. (2011). Connexin channels provide a target to manipulate brain endothelial calcium dynamics and blood-brain barrier permeability. *J. Cereb. Blood Flow Metab.* 31, 1942–1957. doi: 10.1038/jcbfm.2011.86

De Bock, M., Leybaert, L., and Giaume, C. (2017). Connexin channels at the glio-vascular interface: gatekeepers of the brain. *Neurochem. Res.* 42, 2519–2536. doi: 10.1007/s11064-017-2313-x

De Bock, M., Vandenbroucke, R. E., Decrock, E., Culot, M., Cecchelli, R., and Leybaert, L. (2014). A new angle on blood-CNS interfaces: a role for connexins? *FEBS Lett.* 588, 1259–1270. doi: 10.1016/j.febslet.2014.02.060

De Silva, T. M., Kinzenbaw, D. A., Modrick, M. L., Reinhardt, L. D., and Faraci, F. M. (2016). Heterogeneous impact of ROCK2 on carotid and cerebrovascular function. *Hypertension* 68, 809–817. doi: 10.1161/hypertensionaha.116.07430

Deegan, B. M., Sorond, F. A., Galica, A., Lipsitz, L. A., O'Laighin, G., and Serrador, J. M. (2011). Elderly women regulate brain blood flow better than men do. *Stroke* 42, 1988–1993. doi: 10.1161/strokeaha.110.605618

del Zoppo, G. J., Sharp, F. R., Heiss, W. D., and Albers, G. W. (2011). Heterogeneity in the penumbra. *J. Cereb. Blood Flow Metab.* 31, 1836–1851.

Delaney, C., and Campbell, M. (2017). The blood brain barrier: insights from development and ageing. *Tissue Barr.* 5:e1373897. doi: 10.1080/21688370.2017.1373897

Delgado, A. C., Ferron, S. R., Vicente, D., Porlan, E., Perez-Villalba, A., Trujillo, C. M., et al. (2014). Endothelial NT-3 delivered by vasculature and CSF promotes quiescence of subependymal neural stem cells through nitric oxide induction. *Neuron* 83, 572–585. doi: 10.1016/j.neuron.2014.06.015

Dirnagl, U., Hakim, A., Macleod, M., Fisher, M., Howells, D., Alan, S. M., et al. (2013). A concerted appeal for international cooperation in preclinical stroke research. *Stroke* 44, 1754–1760. doi: 10.1161/strokeaha.113.000734

Dong, H., Zhou, W., Xin, J., Shi, H., Yao, X., He, Z., et al. (2019). Salvinorin A moderates postischemic brain injury by preserving endothelial mitochondrial function via AMPK/Mfn2 activation. *Exp. Neurol.* 322:113045. doi: 10.1016/j.expneurol.2019.113045

Donkor, E. S. (2018). Stroke in the 21(st) Century: a snapshot of the burden, epidemiology, and quality of life. *Stroke Res. Treat.* 2018, 3238165.

Drab, M., Verkade, P., Elger, M., Kasper, M., Lohn, M., Lauterbach, B., et al. (2001). Loss of caveolae, vascular dysfunction, and pulmonary defects in caveolin-1 gene-disrupted mice. *Science* 293, 2449–2452. doi: 10.1126/science.1062688

Dreier, J. P. (2011). The role of spreading depression, spreading depolarization and spreading ischemia in neurological disease. *Nat. Med.* 17, 439–447. doi: 10.1038/nm.2333

Duffy, S., McCarthy, R., Farrell, M., Thomas, S., Brennan, P., Power, S., et al. (2019). Per-Pass analysis of thrombus composition in patients with acute ischemic stroke undergoing mechanical thrombectomy. *Stroke* 50, 1156–1163. doi: 10.1161/strokeaha.118.023419

Durbeej, M. (2010). Laminins. *Cell Tissue Res.* 339, 259–268.

Dvorak, J. (1995). Mortality from major civilised diseases in adult and pediatric populations in the CSFR CR and SR in the period from 1950-1985. *Acta Univ. Palacki Olomuc. Fac. Med.* 139, 43–47.

Eichmann, A., and Thomas, J. L. (2013). Molecular parallels between neural and vascular development. *Cold Spring Harb. Perspect. Med.* 3:a006551. doi: 10.1101/cshperspect.a006551

Ekker, M. S., Verhoeven, J. I, Vaartjes, I., Jolink, W. M. T., Klijn, C. J. M., and de Leeuw, F. E. (2019). Association of stroke among adults aged 18 to 49 years with long-term mortality. *JAMA* 321, 2113–2123.

ElAli, A., Theriault, P., and Rivest, S. (2014). The role of pericytes in neurovascular unit remodeling in brain disorders. *Int. J. Mol. Sci.* 15, 6453–6474. doi: 10.3390/ijms15046453

Eldahshan, W., Fagan, S. C., and Ergul, A. (2019). Inflammation within the neurovascular unit: focus on microglia for stroke injury and recovery. *Pharmacol. Res.* 147:104349. doi: 10.1016/j.phrs.2019.104349

Ergul, A., Alhusban, A., and Fagan, S. C. (2012). Angiogenesis: a harmonized target for recovery after stroke. *Stroke* 43, 2270–2274. doi: 10.1161/strokeaha.111.642710

Esposito, G., Van Horn, J. D., Weinberger, D. R., and Berman, K. F. (1996). Gender differences in cerebral blood flow as a function of cognitive state with PET. *J. Nucl. Med.* 37, 559–564.

Fang, M., Zhong, L., Jin, X., Cui, R., Yang, W., Gao, S., et al. (2019). Effect of inflammation on the process of stroke rehabilitation and poststroke depression. *Front. Psychiatry* 10:184. doi: 10.3389/fpsyt.2019.00184

Faraco, G., Park, L., Anrather, J., and Iadecola, C. (2017). Brain perivascular macrophages: characterization and functional roles in health and disease. *J. Mol. Med.* 95, 1143–1152. doi: 10.1007/s00109-017-1573-x

Faraco, G., Sugiyama, Y., Lane, D., Garcia-Bonilla, L., Chang, H., Santisteban, M. M., et al. (2016). Perivascular macrophages mediate the neurovascular and cognitive dysfunction associated with hypertension. *J. Clin. Invest.* 126, 4674–4689. doi: 10.1172/JCI86950

Felling, R. J., and Song, H. (2015). Epigenetic mechanisms of neuroplasticity and the implications for stroke recovery. *Exp. Neurol.* 268, 37–45. doi: 10.1016/j.expneurol.2014.09.017

Feng, Y., Venema, V. J., Venema, R. C., Tsai, N., Behzadian, M. A., and Caldwell, R. B. (1999). VEGF-induced permeability increase is mediated by caveolae. *Invest. Ophthalmol. Vis. Sci.* 40, 157–167.

Fernandez-Klett, F., Potas, J. R., Hilpert, D., Blazej, K., Radke, J., Huck, J., et al. (2013). Early loss of pericytes and perivascular stromal cell-induced scar formation after stroke. *J. Cereb. Blood Flow Metab.* 33, 428–439. doi: 10.1038/jcbfm.2012.187

Ferro, D., Heinen, R., de Brito Robalo, B., Kuijf, H., Biessels, G. J., and Reijmer, Y. (2019). Cortical microinfarcts and white matter connectivity in memory clinic patients. *Front. Neurol.* 10:571. doi: 10.3389/fneur.2019.00571

Fields, R. D., Woo, D. H., and Basser, P. J. (2015). Glial regulation of the neuronal connectome through local and long-distant communication. *Neuron* 86, 374–386. doi: 10.1016/j.neuron.2015.01.014

Figueroa, X. F., and Duling, B. R. (2009). Gap junctions in the control of vascular function. *Antioxid. Redox. Signal.* 11, 251–266. doi: 10.1089/ars.2008.2117

Fisher, M. (2008). Injuries to the vascular endothelium: vascular wall and endothelial dysfunction. *Rev. Neurol. Dis.* 5(Suppl. 1), S4–S11.

Fluri, F., Schuhmann, M. K., and Kleinschnitz, C. (2015). Animal models of ischemic stroke and their application in clinical research. *Drug Des. Dev. Ther.* 9, 3445–3454.

Fordsmann, J. C., Ko, R. W., Choi, H. B., Thomsen, K., Witgen, B. M., Mathiesen, C., et al. (2013). Increased 20-HETE synthesis explains reduced cerebral blood flow but not impaired neurovascular coupling after cortical spreading depression in rat cerebral cortex. *J. Neurosci.* 33, 2562–2570. doi: 10.1523/jneurosci.2308-12.2013

Fraccarollo, D., Widder, J. D., Galuppo, P., Thum, T., Tsikas, D., Hoffmann, M., et al. (2008). Improvement in left ventricular remodeling by the endothelial nitric oxide synthase enhancer AVE9488 after experimental myocardial infarction. *Circulation* 118, 818–827. doi: 10.1161/circulationaha.107.717702

Frantz, S., Adamek, A., Fraccarollo, D., Tillmanns, J., Widder, J. D., Dienesch, C., et al. (2009). The eNOS enhancer AVE 9488: a novel cardioprotectant against ischemia reperfusion injury. *Basic Res. Cardiol.* 104, 773–779. doi: 10.1007/s00395-009-0041-3

Freitas-Andrade, M., Bechberger, J., Wang, J., Yeung, K. K. C., Whitehead, S. N., Hansen, R. S., et al. (2020). Danegaptide enhances astrocyte gap junctional coupling and reduces ischemic reperfusion brain injury in mice. *Biomolecules* 10:353. doi: 10.3390/biom10030353

Freitas-Andrade, M., Carmeliet, P., Charlebois, C., Stanimirovic, D. B., and Moreno, M. J. (2012). PlGF knockout delays brain vessel growth and maturation upon systemic hypoxic challenge. *J. Cereb. Blood Flow Metab.* 32, 663–675. doi: 10.1038/jcbfm.2011.167

Freitas-Andrade, M., Wang, N., Bechberger, J. F., De Bock, M., Lampe, P. D., Leybaert, L., et al. (2019). Targeting MAPK phosphorylation of connexin43 provides neuroprotection in stroke. *J. Exp. Med.* 216, 916–935. doi: 10.1084/jem.20171452

Fu, Z., Chen, Y., Qin, F., Yang, S., Deng, X., Ding, R., et al. (2014). Increased activity of Rho kinase contributes to hemoglobin-induced early disruption of the blood-brain barrier in vivo after the occurrence of intracerebral hemorrhage. *Int. J. Clin. Exp. Pathol.* 7, 7844–7853.

Fujii, M., Duris, K., Altay, O., Soejima, Y., Sherchan, P., and Zhang, J. H. (2012). Inhibition of Rho kinase by hydroxyfasudil attenuates brain edema after subarachnoid hemorrhage in rats. *Neurochem. Int.* 60, 327–333. doi: 10.1016/j.neuint.2011.12.014

Fujioka, T., Kaneko, N., and Sawamoto, K. (2019). Blood vessels as a scaffold for neuronal migration. *Neurochem. Int.* 126, 69–73. doi: 10.1016/j.neuint.2019.03.001

Fukuda, K., Yao, H., Ibayashi, S., Nakahara, T., Uchimura, H., Fujishima, M., et al. (2000). Ovariectomy exacerbates and estrogen replacement attenuates photothrombotic focal ischemic brain injury in rats. *Stroke* 31, 155–160. doi: 10.1161/01.str.31.1.155

Gaidhani, N., Sun, F., Schreihofer, D., and Uteshev, V. V. (2017). Duration of isoflurane-based surgical anesthesia determines severity of brain injury and neurological deficits after a transient focal ischemia in young adult rats. *Brain Res. Bull.* 134, 168–176. doi: 10.1016/j.brainresbull.2017.07.018

Gattringer, T., Posekany, A., Niederkorn, K., Knoflach, M., Poltrum, B., Mutzenbach, S., et al. (2019). Predicting early mortality of acute ischemic stroke. *Stroke* 50, 349–356. doi: 10.1161/strokeaha.118.022863

Gauberti, M., De Lizarrondo, S. M., and Vivien, D. (2016). The "inflammatory penumbra" in ischemic stroke: from clinical data to experimental evidence. *Eur. Stroke J.* 1, 20–27. doi: 10.1177/2396987316630249

Gautam, J., Miner, J. H., and Yao, Y. (2019). Loss of endothelial laminin alpha5 exacerbates hemorrhagic brain injury. *Transl. Stroke Res.* 10, 705–718. doi: 10.1007/s12975-019-0688-5

Gautam, J., Xu, L., Nirwane, A., Nguyen, B., and Yao, Y. (2020). Loss of mural cell-derived laminin aggravates hemorrhagic brain injury. *J. Neuroinflamm.* 17, 103.

Gautam, J., Zhang, X., and Yao, Y. (2016). The role of pericytic laminin in blood brain barrier integrity maintenance. *Sci. Rep.* 6:36450.

Geiseler, S. J., and Morland, C. (2018). The janus face of VEGF in stroke. *Int. J. Mol. Sci.* 19:1362. doi: 10.3390/ijms19051362

Ghisleni, C., Bollmann, S., Biason-Lauber, A., Poil, S. S., Brandeis, D., Martin, E., et al. (2015). Effects of steroid hormones on sex differences in cerebral perfusion. *PLoS One* 10:e0135827. doi: 10.1371/journal.pone.0135827

Gibson, C. L., Srivastava, K., Sprigg, N., Bath, P. M., and Bayraktutan, U. (2014). Inhibition of Rho-kinase protects cerebral barrier from ischaemia-evoked injury through modulations of endothelial cell oxidative stress and tight junctions. *J. Neurochem.* 129, 816–826. doi: 10.1111/jnc.12681

Goldman, S. A., and Chen, Z. (2011). Perivascular instruction of cell genesis and fate in the adult brain. *Nat. Neurosci.* 14, 1382–1389. doi: 10.1038/nn.2963

Gonul, E., Duz, B., Kahraman, S., Kayali, H., Kubar, A., and Timurkaynak, E. (2002). Early pericyte response to brain hypoxia in cats: an ultrastructural study. *Microvasc. Res.* 64, 116–119. doi: 10.1006/mvre.2002.2413

Gonzenbach, R. R., and Schwab, M. E. (2008). Disinhibition of neurite growth to repair the injured adult CNS: focusing on Nogo. *Cell Mol. Life Sci.* 65, 161–176. doi: 10.1007/s00018-007-7170-3

Gordon, G. R., Choi, H. B., Rungta, R. L., Ellis-Davies, G. C., and MacVicar, B. A. (2008). Brain metabolism dictates the polarity of astrocyte control over arterioles. *Nature* 456, 745–749. doi: 10.1038/nature07525

Gordon, G. R., Howarth, C., and MacVicar, B. A. (2011). Bidirectional control of arteriole diameter by astrocytes. *Exp. Physiol.* 96, 393–399. doi: 10.1113/expphysiol.2010.053132

Gould, D. B., Phalan, F. C., van Mil, S. E., Sundberg, J. P., Vahedi, K., Massin, P., et al. (2006). Role of COL4A1 in small-vessel disease and hemorrhagic stroke. *N. Engl. J. Med.* 354, 1489–1496. doi: 10.1056/NEJMoa053727

Gouveia, A., Seegobin, M., Kannangara, T. S., He, L., Wondisford, F., Comin, C. H., et al. (2017). The aPKC-CBP pathway regulates post-stroke neurovascular remodeling and functional recovery. *Stem Cell Rep.* 9, 1735–1744. doi: 10.1016/j.stemcr.2017.10.021

Goyal, M., Demchuk, A. M., Menon, B. K., Eesa, M., Rempel, J. L., Thornton, J., et al. (2015). Randomized assessment of rapid endovascular treatment of ischemic stroke. *N. Engl. J. Med.* 372, 1019–1030.

Green, A. R., and Shuaib, A. (2006). Therapeutic strategies for the treatment of stroke. *Drug Discov. Today* 11, 681–693. doi: 10.1016/j.drudis.2006.06.001

Gu, C., Yoshida, Y., Livet, J., Reimert, D. V., Mann, F., Merte, J., et al. (2005). Semaphorin 3E and plexin-D1 control vascular pattern independently of neuropilins. *Science* 307, 265–268. doi: 10.1126/science.1105416

Guo, J., Krause, D. N., Horne, J., Weiss, J. H., Li, X., and Duckles, S. P. (2010). Estrogen-receptor-mediated protection of cerebral endothelial cell viability and mitochondrial function after ischemic insult in vitro. *J. Cereb. Blood Flow Metab.* 30, 545–554. doi: 10.1038/jcbfm.2009.226

Gur, R. C., Gur, R. E., Obrist, W. D., Hungerbuhler, J. P., Younkin, D., Rosen, A. D., et al. (1982). Sex and handedness differences in cerebral blood flow during rest and cognitive activity. *Science* 217, 659–661. doi: 10.1126/science.7089587

Gurewich, V. (2016). Thrombolysis: a critical first-line therapy with an unfulfilled potential. *Am. J. Med.* 129, 573–575. doi: 10.1016/j.amjmed.2015.11.033

Gutierrez-Fernandez, M., Fuentes, B., Rodriguez-Frutos, B., Ramos-Cejudo, J., Vallejo-Cremades, M. T., and Diez-Tejedor, E. (2012). Trophic factors and cell therapy to stimulate brain repair after ischaemic stroke. *J. Cell Mol. Med.* 16, 2280–2290. doi: 10.1111/j.1582-4934.2012.01575.x

Hakim, A. M. (2014). Perspective: silent, but preventable, perils. *Nature* 510:S12.

Hakim, A. M. (2019). Small vessel disease. *Front. Neurol.* 10:1020. doi: 10.3389/fneur.2019.01020

Hale, G. E., and Shufelt, C. L. (2015). Hormone therapy in menopause: an update on cardiovascular disease considerations. *Trends Cardiovasc. Med.* 25, 540–549. doi: 10.1016/j.tcm.2015.01.008

Haley, M. J., and Lawrence, C. B. (2016). The blood-brain barrier after stroke: structural studies and the role of transcytotic vesicles. *J. Cereb. Blood Flow Metab.* 37, 456–470. doi: 10.1177/0271678x16629976

Hall, C. N., Reynell, C., Gesslein, B., Hamilton, N. B., Mishra, A., Sutherland, B. A., et al. (2014). Capillary pericytes regulate cerebral blood flow in health and disease. *Nature* 508, 55–60. doi: 10.1038/nature13165

Hammond, T. R., Dufort, C., Dissing-Olesen, L., Giera, S., Young, A., Wysoker, A., et al. (2019). Single-Cell RNA sequencing of microglia throughout the mouse lifespan and in the injured brain reveals complex cell-state changes. *Immunity* 50, 253.e6–271.e6.

Hammond, T. R., Robinton, D., and Stevens, B. (2018). Microglia and the brain: complementary partners in development and disease. *Annu. Rev. Cell Dev. Biol.* 34, 523–544. doi: 10.1146/annurev-cellbio-100616-060509

Hangai, M., Kitaya, N., Xu, J., Chan, C. K., Kim, J. J., Werb, Z., et al. (2002). Matrix metalloproteinase-9-dependent exposure of a cryptic migratory control site in collagen is required before retinal angiogenesis. *Am. J. Pathol.* 161, 1429–1437. doi: 10.1016/s0002-9440(10)64418-5

Hao, Z., Liu, Y., Liao, H., Zheng, D., Xiao, C., and Li, G. (2016). Atorvastatin plus metformin confer additive benefits on subjects with dyslipidemia and overweight/obese via reducing ROCK2 concentration. *Exp. Clin. Endocrinol. Diabetes* 124, 246–250. doi: 10.1055/s-0035-1569364

Hartmann, D. A., Berthiaume, A.-A., Grant, R. I., Harrill, S. A., Noonan, T., Costello, J., et al. (2020). Brain capillary pericytes exert a substantial but slow influence on blood flow. *bioRxiv*

Hartmann, S., Ridley, A. J., and Lutz, S. (2015). The function of Rho-associated kinases ROCK1 and ROCK2 in the pathogenesis of cardiovascular disease. *Front. Pharmacol.* 6:276. doi: 10.3389/fphar.2015.00276

Haruwaka, K., Ikegami, A., Tachibana, Y., Ohno, N., Konishi, H., Hashimoto, A., et al. (2019). Dual microglia effects on blood brain barrier permeability induced by systemic inflammation. *Nat. Commun.* 10:5816.

Hatakeyama, M., Ninomiya, I., and Kanazawa, M. (2020). Angiogenesis and neuronal remodeling after ischemic stroke. *Neural Regen. Res.* 15, 16–19.

Hayward, K. S., Kramer, S. F., Thijs, V., Ratcliffe, J., Ward, N. S., Churilov, L., et al. (2019). A systematic review protocol of timing, efficacy and cost effectiveness of upper limb therapy for motor recovery post-stroke. *Syst. Rev.* 8:187.

He, L., Linden, D. J., and Sapirstein, A. (2012). Astrocyte inositol triphosphate receptor type 2 and cytosolic phospholipase A2 alpha regulate arteriole responses in mouse neocortical brain slices. *PLoS One* 7:e42194. doi: 10.1371/journal.pone.0042194

He, L., Vanlandewijck, M., Mae, M. A., Andrae, J., Ando, K., Del Gaudio, F., et al. (2018). Single-cell RNA sequencing of mouse brain and lung vascular and vessel-associated cell types. *Sci. Data* 5:180160.

Hebert, M., Lesept, F., Vivien, D., and Macrez, R. (2016). The story of an exceptional serine protease, tissue-type plasminogen activator (tPA). *Rev. Neurol.* 172, 186–197. doi: 10.1016/j.neurol.2015.10.002

Heiss, W. D. (2012). The ischemic penumbra: how does tissue injury evolve? *Ann. N. Y. Acad. Sci.* 1268, 26–34. doi: 10.1111/j.1749-6632.2012.06668.x

Hendrix, S. L., Wassertheil-Smoller, S., Johnson, K. C., Howard, B. V., Kooperberg, C., Rossouw, J. E., et al. (2006). Effects of conjugated equine estrogen on stroke in the Women's Health Initiative. *Circulation* 113, 2425–2434.

Heo, J. H., Lucero, J., Abumiya, T., Koziol, J. A., Copeland, B. R., and del Zoppo, G. J. (1999). Matrix metalloproteinases increase very early during experimental focal cerebral ischemia. *J. Cereb. Blood Flow Metab.* 19, 624–633. doi: 10.1097/00004647-199906000-00005

Hill, M. D., Goyal, M., Menon, B. K., Nogueira, R. G., McTaggart, R. A., Demchuk, A. M., et al. (2020). Efficacy and safety of nerinetide for the treatment of acute ischaemic stroke (ESCAPE-NA1): a multicentre, double-blind, randomised controlled trial. *Lancet* 395, 878–887.

Hill, R. A., Tong, L., Yuan, P., Murikinati, S., Gupta, S., and Grutzendler, J. (2015). Regional blood flow in the normal and ischemic brain is controlled by arteriolar smooth muscle cell contractility and not by capillary pericytes. *Neuron* 87, 95–110. doi: 10.1016/j.neuron.2015.06.001

Hillman, E. M. (2014). Coupling mechanism and significance of the BOLD signal: a status report. *Annu. Rev. Neurosci.* 37, 161–181. doi: 10.1146/annurev-neuro-071013-014111

Hines, D. J., Hines, R. M., Mulligan, S. J., and Macvicar, B. A. (2009). Microglia processes block the spread of damage in the brain and require functional chloride channels. *Glia* 57, 1610–1618. doi: 10.1002/glia.20874

Hiroi, Y., Noma, K., Kim, H. H., Sladojevic, N., Tabit, C. E., Li, Y., et al. (2018). Neuroprotection mediated by upregulation of endothelial nitric oxide synthase in Rho-Associated, coiled-coil-containing kinase 2 deficient mice. *Circ. J.* 82, 1195–1204. doi: 10.1253/circj.cj-17-0732

Hofer, A., Siedentopf, C. M., Ischebeck, A., Rettenbacher, M. A., Verius, M., Felber, S., et al. (2007). Sex differences in brain activation patterns during processing of positively and negatively valenced emotional words. *Psychol. Med.* 37, 109–119. doi: 10.1017/s0033291706008919

Hoffmann, C. J., Harms, U., Rex, A., Szulzewsky, F., Wolf, S. A., Grittner, U., et al. (2015). Vascular signal transducer and activator of transcription-3 promotes angiogenesis and neuroplasticity long-term after stroke. *Circulation* 131, 1772–1782. doi: 10.1161/circulationaha.114.013003

Holfelder, K., Schittenhelm, J., Trautmann, K., Haybaeck, J., Meyermann, R., and Beschorner, R. (2011). *De novo* expression of the hemoglobin scavenger receptor CD163 by activated microglia is not associated with hemorrhages in human brain lesions. *Histol. Histopathol.* 26, 1007–1017. doi: 10.14670/HH-26.1007

Howarth, C. (2014). The contribution of astrocytes to the regulation of cerebral blood flow. *Front. Neurosci.* 8:103. doi: 10.3389/fnins.2014.00103

Howarth, C., Sutherland, B., Choi, H. B., Martin, C., Lind, B. L., Khennouf, L., et al. (2017). A critical role for astrocytes in hypercapnic vasodilation in brain. *J. Neurosci.* 37, 2403–2414. doi: 10.1523/jneurosci.0005-16.2016

Howe, M. D., Furr, J. W., Munshi, Y., Roy-O'Reilly, M. A., Maniskas, M. E., Koellhoffer, E. C., et al. (2019). Transforming growth factor-beta promotes basement membrane fibrosis, alters perivascular cerebrospinal fluid distribution, and worsens neurological recovery in the aged brain after stroke. *Geroscience* 41, 543–559. doi: 10.1007/s11357-019-00118-7

Huang, P. L., Huang, Z., Mashimo, H., Bloch, K. D., Moskowitz, M. A., Bevan, J., et al. (1995). Hypertension in mice lacking the gene for endothelial nitric oxide synthase. *Nature* 377, 239–242.

Hughes, P. M., Anthony, D. C., Ruddin, M., Botham, M. S., Rankine, E. L., Sablone, M., et al. (2003). Focal lesions in the rat central nervous system induced by endothelin-1. *J. Neuropathol. Exp. Neurol.* 62, 1276–1286. doi: 10.1093/jnen/62.12.1276

Iadecola, C. (1997). Bright and dark sides of nitric oxide in ischemic brain injury. *Trends Neurosci.* 20, 132–139. doi: 10.1016/s0166-2236(96)10074-6

Iadecola, C., and Anrather, J. (2011b). The immunology of stroke: from mechanisms to translation. *Nat. Med.* 17, 796–808. doi: 10.1038/nm.2399

Iadecola, C., and Anrather, J. (2011a). Stroke research at a crossroad: asking the brain for directions. *Nat. Neurosci.* 14, 1363–1368. doi: 10.1038/nn.2953

Jauch, E. C., Saver, J. L., Adams, H. P. Jr., Bruno, A., Connors, J. J., Demaerschalk, B. M., et al. (2013). Guidelines for the early management of patients with acute ischemic stroke: a guideline for healthcare professionals from the American Heart Association/American Stroke Association. *Stroke* 44, 870–947.

Jiang, M., Sun, L., Feng, D. X., Yu, Z. Q., Gao, R., Sun, Y. Z., et al. (2017). Neuroprotection provided by isoflurane pre-conditioning and post-conditioning. *Med. Gas Res.* 7, 48–55.

Jiang, Y., Liu, H., Wang, Y., Shi, X., Shao, Y., and Xu, Z. (2020). Meta-analysis of matrix metalloproteinase (MMP)-9 C1562T polymorphism and susceptibility to ischemic stroke in the Chinese population. *J. Int. Med. Res.* 48:0300060520926427.

Jiao, H., Wang, Z., Liu, Y., Wang, P., and Xue, Y. (2011). Specific role of tight junction proteins claudin-5, occludin, and ZO-1 of the blood-brain barrier in a focal cerebral ischemic insult. *J. Mol. Neurosci.* 44, 130–139. doi: 10.1007/s12031-011-9496-4

Jolivel, V., Bicker, F., Biname, F., Ploen, R., Keller, S., Gollan, R., et al. (2015). Perivascular microglia promote blood vessel disintegration in the ischemic penumbra. *Acta Neuropathol.* 129, 279–295. doi: 10.1007/s00401-014-1372-1

Josko, J. (2003). Cerebral angiogenesis and expression of VEGF after subarachnoid hemorrhage (SAH) in rats. *Brain Res.* 981, 58–69. doi: 10.1016/s0006-8993(03)02920-2

Ju, H., Zou, R., Venema, V. J., and Venema, R. C. (1997). Direct interaction of endothelial nitric-oxide synthase and caveolin-1 inhibits synthase activity. *J. Biol. Chem.* 272, 18522–18525. doi: 10.1074/jbc.272.30.18522

Kajikawa, M., Noma, K., Nakashima, A., Maruhashi, T., Iwamoto, Y., Matsumoto, T., et al. (2015). Rho-associated kinase activity is an independent predictor of cardiovascular events in acute coronary syndrome. *Hypertension* 66, 892–899. doi: 10.1161/hypertensionaha.115.05587

Kalucka, J., de Rooij, L., Goveia, J., Rohlenova, K., Dumas, S. J., Meta, E., et al. (2020). Single-cell transcriptome atlas of murine endothelial cells. *Cell* 180, 764.e20–779.e20.

Kanazawa, M., Takahashi, T., Ishikawa, M., Onodera, O., Shimohata, T., and Del Zoppo, G. J. (2019). Angiogenesis in the ischemic core: a potential treatment target? *J. Cereb. Blood Flow Metab.* 39, 753–769. doi: 10.1177/0271678x19834158

Kang, M., and Yao, Y. (2020). Basement membrane changes in ischemic stroke. *Stroke* 51, 1344–1352. doi: 10.1161/strokeaha.120.028928

Kannangara, T. S., Carter, A., Xue, Y., Dhaliwal, J. S., Beique, J. C., and Lagace, D. C. (2018). Excitable adult-generated GABAergic neurons acquire functional innervation in the cortex after stroke. *Stem Cell Rep.* 11, 1327–1336. doi: 10.1016/j.stemcr.2018.10.011

Kao, Y. C., Li, W., Lai, H. Y., Oyarzabal, E. A., Lin, W., and Shih, Y. Y. (2014). Dynamic perfusion and diffusion MRI of cortical spreading depolarization in photothrombotic ischemia. *Neurobiol. Dis.* 71, 131–139. doi: 10.1016/j.nbd.2014.07.005

Kawamura, H., Kobayashi, M., Li, Q., Yamanishi, S., Katsumura, K., Minami, M., et al. (2004). Effects of angiotensin II on the pericyte-containing microvasculature of the rat retina. *J. Physiol.* 561, 671–683. doi: 10.1113/jphysiol.2004.073098

Kawamura, H., Sugiyama, T., Wu, D. M., Kobayashi, M., Yamanishi, S., Katsumura, K., et al. (2003). ATP: a vasoactive signal in the pericyte-containing microvasculature of the rat retina. *J. Physiol.* 551, 787–799. doi: 10.1113/jphysiol.2003.047977

Keaney, J., and Campbell, M. (2015). The dynamic blood-brain barrier. *FEBS J.* 282, 4067–4079.

Kearney, J. B., Ambler, C. A., Monaco, K. A., Johnson, N., Rapoport, R. G., and Bautch, V. L. (2002). Vascular endothelial growth factor receptor Flt-1 negatively regulates developmental blood vessel formation by modulating endothelial cell division. *Blood* 99, 2397–2407. doi: 10.1182/blood.v99.7.2397

Kehl, F., Shen, H., Moreno, C., Farber, N. E., Roman, R. J., Kampine, J. P., et al. (2002). Isoflurane-induced cerebral hyperemia is partially mediated by nitric oxide and epoxyeicosatrienoic acids in mice in vivo. *Anesthesiology* 97, 1528–1533. doi: 10.1097/00000542-200212000-00027

Kilic, E., Kilic, U., Wang, Y., Bassetti, C. L., Marti, H. H., and Hermann, D. M. (2006). The phosphatidylinositol-3 kinase/Akt pathway mediates VEGF's neuroprotective activity and induces blood brain barrier permeability after focal cerebral ischemia. *FASEB J.* 20, 1185–1187. doi: 10.1096/fj.05-4829fje

Kimmel, E. R., Al Kasab, S., Harvey, J. B., Bathla, G., Ortega-Gutierrez, S., Toth, G., et al. (2019). Absence of collaterals is associated with larger infarct volume and worse outcome in patients with large vessel occlusion and mild symptoms. *J. Stroke Cerebrovasc. Dis.* 28, 1987–1992. doi: 10.1016/j.jstrokecerebrovasdis.2019.03.032

Kirov, S. A., Fomitcheva, I. V., and Sword, J. (2020). Rapid neuronal ultrastructure disruption and recovery during spreading depolarization-induced cytotoxic edema. *Cereb. Cortex* [Epub ahead of print]. doi: 10.1093/cercor/bhaa134

Kirst, C., Skriabine, S., Vieites-Prado, A., Topilko, T., Bertin, P., Gerschenfeld, G., et al. (2020). Mapping the fine-scale organization and plasticity of the brain vasculature. *Cell* 180, 780.e25–795.e25.

Kisler, K., Nelson, A. R., Montagne, A., and Zlokovic, B. V. (2017). Cerebral blood flow regulation and neurovascular dysfunction in Alzheimer disease. *Nat. Rev. Neurosci.* 18, 419–434. doi: 10.1038/nrn.2017.48

Kisler, K., Nikolakopoulou, A. M., Sweeney, M. D., Lazic, D., Zhao, Z., and Zlokovic, B. V. (2020). Acute ablation of cortical pericytes leads to rapid neurovascular uncoupling. *Front. Cell Neurosci.* 14:27. doi: 10.3389/fncel.2020.00027

Knowland, D., Arac, A., Sekiguchi, K. J., Hsu, M., Lutz, S. E., Perrino, J., et al. (2014). Stepwise recruitment of transcellular and paracellular pathways underlies blood-brain barrier breakdown in stroke. *Neuron* 82, 603–617. doi: 10.1016/j.neuron.2014.03.003

Koizumi, T., Kerkhofs, D., Mizuno, T., Steinbusch, H. W., and Foulquier, S. (2019). Vessel-associated immune cells in cerebrovascular diseases: From perivascular macrophages to vessel-associated microglia. *Front. Neurosci.* 13:1291. doi: 10.3389/fnins.2019.01291

Krause, D. N., Duckles, S. P., and Pelligrino, D. A. (2006). Influence of sex steroid hormones on cerebrovascular function. *J. Appl. Physiol.* 101, 1252–1261. doi: 10.1152/japplphysiol.01095.2005

Krolikowski, J. G., Weihrauch, D., Bienengraeber, M., Kersten, J. R., Warltier, D. C., and Pagel, P. S. (2006). Role of Erk1/2, p70s6K, and eNOS in isoflurane-induced cardioprotection during early reperfusion in vivo. *Can. J. Anaesth.* 53, 174–182. doi: 10.1007/bf03021824

Krueger, H., Koot, J., Hall, R. E., O'Callaghan, C., Bayley, M., and Corbett, D. (2015). Prevalence of individuals experiencing the effects of stroke in canada: trends and projections. *Stroke* 46, 2226–2231. doi: 10.1161/strokeaha.115.009616

Krum, J. M., Mani, N., and Rosenstein, J. M. (2008). Roles of the endogenous VEGF receptors flt-1 and flk-1 in astroglial and vascular remodeling after brain injury. *Exp. Neurol.* 212, 108–117. doi: 10.1016/j.expneurol.2008.03.019

Krupinski, J., Kaluza, J., Kumar, P., Kumar, S., and Wang, J. M. (1994). Role of angiogenesis in patients with cerebral ischemic stroke. *Stroke* 25, 1794–1798. doi: 10.1161/01.str.25.9.1794

Lacoste, B. (2014). Neuronal activity influences the development of blood vessels in the brain. *Med. Sci.* 30, 1063–1066.

Laird, D. W., Naus, C. C., and Lampe, P. D. (2017). SnapShot: connexins and disease. *Cell* 170, 1260.e1–1260.e1.

Lan, X., Han, X., Li, Q., Yang, Q. W., and Wang, J. (2017). Modulators of microglial activation and polarization after intracerebral haemorrhage. *Nat. Rev. Neurol.* 13, 420–433. doi: 10.1038/nrneurol.2017.69

Lange-Asschenfeldt, C., and Kojda, G. (2008). Alzheimer's disease, cerebrovascular dysfunction and the benefits of exercise: from vessels to neurons. *Exp. Gerontol.* 43, 499–504. doi: 10.1016/j.exger.2008.04.002

Lapchak, P. A., Zhang, J. H., and Noble-Haeusslein, L. J. (2013). RIGOR guidelines: escalating STAIR and STEPS for effective translational research. *Transl. Stroke Res.* 4, 279–285. doi: 10.1007/s12975-012-0209-2

Lapi, D., and Colantuoni, A. (2015). Remodeling of cerebral microcirculation after ischemia-reperfusion. *J. Vasc. Res.* 52, 22–31. doi: 10.1159/000381096

Lauritzen, M., Dreier, J. P., Fabricius, M., Hartings, J. A., Graf, R., and Strong, A. J. (2011). Clinical relevance of cortical spreading depression in neurological disorders: migraine, malignant stroke, subarachnoid and intracranial hemorrhage, and traumatic brain injury. *J. Cereb. Blood Flow Metab.* 31, 17–35. doi: 10.1038/jcbfm.2010.191

Lauritzen, M., and Strong, A. J. (2016). 'Spreading depression of Leao' and its emerging relevance to acute brain injury in humans. *J. Cereb. Blood Flow Metab.* 37, 1553–1570. doi: 10.1177/0271678x16657092

Lee, B., Clarke, D., Al Ahmad, A., Kahle, M., Parham, C., Auckland, L., et al. (2011). Perlecan domain V is neuroprotective and proangiogenic following ischemic stroke in rodents. *J. Clin. Invest.* 121, 3005–3023. doi: 10.1172/jci46358

Lee, J. H., Zheng, Y., von Bornstadt, D., Wei, Y., Balcioglu, A., Daneshmand, A., et al. (2014). Selective ROCK2 inhibition in focal cerebral ischemia. *Ann. Clin. Transl. Neurol.* 1, 2–14. doi: 10.1002/acn3.19

Lee, J. K., Kim, J. E., Sivula, M., and Strittmatter, S. M. (2004). Nogo receptor antagonism promotes stroke recovery by enhancing axonal plasticity. *J. Neurosci.* 24, 6209–6217. doi: 10.1523/jneurosci.1643-04.2004

Lee, S. C., Lee, K. Y., Kim, Y. J., Kim, S. H., Koh, S. H., and Lee, Y. J. (2010). Serum VEGF levels in acute ischaemic strokes are correlated with long-term prognosis. *Eur. J. Neurol.* 17, 45–51. doi: 10.1111/j.1468-1331.2009.02731.x

Lee, S. W., Kim, W. J., Choi, Y. K., Song, H. S., Son, M. J., Gelman, I. H., et al. (2003). SSeCKS regulates angiogenesis and tight junction formation in blood-brain barrier. *Nat. Med.* 9, 900–906. doi: 10.1038/nm889

Lei, C., Lin, S., Zhang, C., Tao, W., Dong, W., Hao, Z., et al. (2013). Effects of high-mobility group box1 on cerebral angiogenesis and neurogenesis after intracerebral hemorrhage. *Neuroscience* 229, 12–19. doi: 10.1016/j.neuroscience.2012.10.054

Li, L., Lundkvist, A., Andersson, D., Wilhelmsson, U., Nagai, N., Pardo, A. C., et al. (2008). Protective role of reactive astrocytes in brain ischemia. *J. Cereb. Blood Flow Metab.* 28, 468–481.

Liao, S., Chen, W., Kuo, J., and Chen, C. (2001). Association of serum estrogen level and ischemic neuroprotection in female rats. *Neurosci. Lett.* 297, 159–162. doi: 10.1016/s0304-3940(00)01704-3

Liberale, L., Gaul, D. S., Akhmedov, A., Bonetti, N. R., Nageswaran, V., Costantino, S., et al. (2020). Endothelial SIRT6 blunts stroke size and neurological deficit by preserving blood-brain barrier integrity: a translational study. *Eur. Heart J.* 41, 1575–1587. doi: 10.1093/eurheartj/ehz712

Licht, T., and Keshet, E. (2015). The vascular niche in adult neurogenesis. *Mech. Dev.* 138(Pt 1), 56–62. doi: 10.1016/j.mod.2015.06.001

Lin, M. P., Brott, T. G., Liebeskind, D. S., Meschia, J. F., Sam, K., and Gottesman, R. F. (2020). Collateral recruitment is impaired by cerebral small vessel disease. *Stroke* 51, 1404–1410. doi: 10.1161/strokeaha.119.027661

Lin, M. P., and Sanossian, N. (2015). Reperfusion therapy in the acute management of ischemic stroke. *Cardiol. Clin.* 33, 99–109. doi: 10.1016/j.ccl.2014.09.009

Lind, B. L., Brazhe, A. R., Jessen, S. B., Tan, F. C., and Lauritzen, M. J. (2013). Rapid stimulus-evoked astrocyte Ca2+ elevations and hemodynamic responses in mouse somatosensory cortex in vivo. *Proc. Natl. Acad. Sci. U.S.A.* 110, E4678–E4687.

Lisabeth, L., and Bushnell, C. (2012). Stroke risk in women: the role of menopause and hormone therapy. *Lancet Neurol.* 11, 82–91. doi: 10.1016/s1474-4422(11)70269-1

Liu, J., Wang, Y., Akamatsu, Y., Lee, C. C., Stetler, R. A., Lawton, M. T., et al. (2014). Vascular remodeling after ischemic stroke: mechanisms and therapeutic potentials. *Prog. Neurobiol.* 115, 138–156. doi: 10.1016/j.pneurobio.2013.11.004

Liu, R., Wen, Y., Perez, E., Wang, X., Day, A. L., Simpkins, J. W., et al. (2005). 17beta-Estradiol attenuates blood-brain barrier disruption induced by cerebral ischemia-reperfusion injury in female rats. *Brain Res.* 1060, 55–61. doi: 10.1016/j.brainres.2005.08.048

Lu, H., Li, Y., Bo, B., Yuan, L., Lu, X., Li, H., et al. (2017). Hemodynamic effects of intraoperative anesthetics administration in photothrombotic stroke model:

a study using laser speckle imaging. *BMC Neurosci.* 18:10. doi: 10.1186/s12868-016-0327-y

Lukaszevicz, A. C., Sampaio, N., Guegan, C., Benchoua, A., Couriaud, C., Chevalier, E., et al. (2002). High sensitivity of protoplasmic cortical astroglia to focal ischemia. *J. Cereb. Blood Flow Metab.* 22, 289–298. doi: 10.1097/00004647-200203000-00006

Machado, L. S., Kozak, A., Ergul, A., Hess, D. C., Borlongan, C. V., and Fagan, S. C. (2006). Delayed minocycline inhibits ischemia-activated matrix metalloproteinases 2 and 9 after experimental stroke. *BMC Neurosci.* 7:56. doi: 10.1186/1471-2202-7-56

Madsen, T. E., Khoury, J. C., Alwell, K., Moomaw, C. J., Rademacher, E., Flaherty, M. L., et al. (2019). Temporal trends of sex differences in transient ischemic attack incidence within a population. *J. Stroke Cerebrovasc. Dis.* 28, 2468–2474. doi: 10.1016/j.jstrokecerebrovasdis.2019.06.020

Maki, T., Hayakawa, K., Pham, L. D., Xing, C., Lo, E. H., and Arai, K. (2013). Biphasic mechanisms of neurovascular unit injury and protection in CNS diseases. *CNS Neurol. Disord. Drug Targets* 12, 302–315. doi: 10.2174/18715273113120300004

Malhotra, K., Chang, J. J., Khunger, A., Blacker, D., Switzer, J. A., Goyal, N., et al. (2018). Minocycline for acute stroke treatment: a systematic review and meta-analysis of randomized clinical trials. *J. Neurol.* 265, 1871–1879. doi: 10.1007/s00415-018-8935-3

Manoonkitiwongsa, P. S., Jackson-Friedman, C., McMillan, P. J., Schultz, R. L., and Lyden, P. D. (2001). Angiogenesis after stroke is correlated with increased numbers of macrophages: the clean-up hypothesis. *J. Cereb. Blood Flow Metab.* 21, 1223–1231. doi: 10.1097/00004647-200110000-00011

Marina, N., Christie, I. N., Korsak, A., Doronin, M., Brazhe, A., Hosford, P. S., et al. (2020). Astrocytes monitor cerebral perfusion and control systemic circulation to maintain brain blood flow. *Nat. Commun.* 11:131.

Marti, H. J., Bernaudin, M., Bellail, A., Schoch, H., Euler, M., Petit, E., et al. (2000). Hypoxia-induced vascular endothelial growth factor expression precedes neovascularization after cerebral ischemia. *Am. J. Pathol.* 156, 965–976. doi: 10.1016/s0002-9440(10)64964-4

Martinez, A. D., and Saez, J. C. (2000). Regulation of astrocyte gap junctions by hypoxia-reoxygenation. *Brain Res. Rev.* 32, 250–258. doi: 10.1016/s0165-0173(99)00086-7

Matsuo, R., Ago, T., Kamouchi, M., Kuroda, J., Kuwashiro, T., Hata, J., et al. (2013). Clinical significance of plasma VEGF value in ischemic stroke - research for biomarkers in ischemic stroke (REBIOS) study. *BMC Neurol.* 13:32. doi: 10.1186/1471-2377-13-32

Matthias, K., Kirchhoff, F., Seifert, G., Huttmann, K., Matyash, M., Kettenmann, H., et al. (2003). Segregated expression of AMPA-type glutamate receptors and glutamate transporters defines distinct astrocyte populations in the mouse hippocampus. *J. Neurosci.* 23, 1750–1758. doi: 10.1523/jneurosci.23-05-01750.2003

McAllister, M. S., Krizanac-Bengez, L., Macchia, F., Naftalin, R. J., Pedley, K. C., Mayberg, M. R., et al. (2001). Mechanisms of glucose transport at the blood-brain barrier: an in vitro study. *Brain Res.* 904, 20–30. doi: 10.1016/s0006-8993(01)02418-0

McCabe, C., Arroja, M. M., Reid, E., and Macrae, I. M. (2018). Animal models of ischaemic stroke and characterisation of the ischaemic penumbra. *Neuropharmacology* 134, 169–177. doi: 10.1016/j.neuropharm.2017.09.022

McCarty, J. H. (2020). alphavbeta8 integrin adhesion and signaling pathways in development, physiology and disease. *J. Cell Sci.* 133:jcs239434. doi: 10.1242/jcs.239434

McConnell, H. L., Li, Z., Woltjer, R. L., and Mishra, A. (2019). Astrocyte dysfunction and neurovascular impairment in neurological disorders: correlation or causation? *Neurochem. Int.* 128, 70–84. doi: 10.1016/j.neuint.2019.04.005

McCullough, L. D., Alkayed, N. J., Traystman, R. J., Williams, M. J., and Hurn, P. D. (2001). Postischemic estrogen reduces hypoperfusion and secondary ischemia after experimental stroke. *Stroke* 32, 796–802. doi: 10.1161/01.str.32.3.796

McDonald, M. W., Black, S. E., Copland, D. A., Corbett, D., Dijkhuizen, R. M., Farr, T. D., et al. (2019). Cognition in stroke rehabilitation and recovery research: consensus-based core recommendations from the second stroke recovery and rehabilitation roundtable. *Int. J. Stroke* 14, 774–782. doi: 10.1177/1747493019873600

McNeill, A. M., Kim, N., Duckles, S. P., Krause, D. N., and Kontos, H. A. (1999). Chronic estrogen treatment increases levels of endothelial nitric oxide synthase protein in rat cerebral microvessels. *Stroke* 30, 2186–2190. doi: 10.1161/01.str.30.10.2186

Mechtouff, L., Bochaton, T., Paccalet, A., Crola Da Silva, C., Buisson, M., Amaz, C., et al. (2020). Matrix metalloproteinase-9 relationship with infarct growth and hemorrhagic transformation in the era of thrombectomy. *Front. Neurol.* 11:473. doi: 10.3389/fneur.2020.00473

Mendelsohn, M. E., and Karas, R. H. (1999). The protective effects of estrogen on the cardiovascular system. *N. Engl. J. Med.* 340, 1801–1811. doi: 10.1056/nejm199906103402306

Mendes-Jorge, L., Ramos, D., Luppo, M., Llombart, C., Alexandre-Pires, G., Nacher, V., et al. (2009). Scavenger function of resident autofluorescent perivascular macrophages and their contribution to the maintenance of the blood-retinal barrier. *Invest. Ophthalmol. Vis. Sci.* 50, 5997–6005. doi: 10.1167/iovs.09-3515

Mendonca, B. P., Cardoso, J. D. S., Michels, M., Vieira, A. C., Wendhausen, D., Manfredini, A., et al. (2020). Neuroprotective effects of ammonium tetrathiomolybdate, a slow-release sulfide donor, in a rodent model of regional stroke. *Intensive Care Med. Exp.* 8:13.

Meschia, J. F., Bushnell, C., Boden-Albala, B., Braun, L. T., Bravata, D. M., Chaturvedi, S., et al. (2014). Guidelines for the primary prevention of stroke: a statement for healthcare professionals from the American Heart Association/American Stroke Association. *Stroke* 45, 3754–3832.

Meyer, R. D., Mohammadi, M., and Rahimi, N. (2006). A single amino acid substitution in the activation loop defines the decoy characteristic of VEGFR-1/FLT-1. *J. Biol. Chem.* 281, 867–875. doi: 10.1074/jbc.m506454200

Mikelis, C. M., Simaan, M., Ando, K., Fukuhara, S., Sakurai, A., Amornphimoltham, P., et al. (2015). RhoA and ROCK mediate histamine-induced vascular leakage and anaphylactic shock. *Nat. Commun.* 6:6725.

Milner, R., Hung, S., Erokwu, B., Dore-Duffy, P., LaManna, J. C., and del Zoppo, G. J. (2008). Increased expression of fibronectin and the alpha 5 beta 1 integrin in angiogenic cerebral blood vessels of mice subject to hypobaric hypoxia. *Mol. Cell. Neurosci.* 38, 43–52. doi: 10.1016/j.mcn.2008.01.013

Ming, X. F., Viswambharan, H., Barandier, C., Ruffieux, J., Kaibuchi, K., Rusconi, S., et al. (2002). Rho GTPase/Rho kinase negatively regulates endothelial nitric oxide synthase phosphorylation through the inhibition of protein kinase B/Akt in human endothelial cells. *Mol. Cell. Biol.* 22, 8467–8477. doi: 10.1128/mcb.22.24.8467-8477.2002

Mishra, A., Reynolds, J. P., Chen, Y., Gourine, A. V., Rusakov, D. A., and Attwell, D. (2016). Astrocytes mediate neurovascular signaling to capillary pericytes but not to arterioles. *Nat. Neurosci.* 19, 1619–1627. doi: 10.1038/nn.4428

Mittmann, N., Seung, S. J., Hill, M. D., Phillips, S. J., Hachinski, V., Cote, R., et al. (2012). Impact of disability status on ischemic stroke costs in Canada in the first year. *Can. J. Neurol. Sci.* 39, 793–800. doi: 10.1017/s0317167100015638

Miyazaki-Akita, A., Hayashi, T., Ding, Q. F., Shiraishi, H., Nomura, T., Hattori, Y., et al. (2007). 17beta-estradiol antagonizes the down-regulation of endothelial nitric-oxide synthase and GTP cyclohydrolase I by high glucose: relevance to postmenopausal diabetic cardiovascular disease. *J. Pharmacol. Exp. Ther.* 320, 591–598. doi: 10.1124/jpet.106.111641

Molofsky, A. V., Krencik, R., Ullian, E. M., Tsai, H. H., Deneen, B., Richardson, W. D., et al. (2012). Astrocytes and disease: a neurodevelopmental perspective. *Genes Dev.* 26, 891–907. doi: 10.1101/gad.188326.112

Moncada, S., and Higgs, A. (1993). The L-arginine-nitric oxide pathway. *N. Engl. J. Med.* 329, 2002–2012.

Montalvo, J., Spencer, C., Hackathorn, A., Masterjohn, K., Perkins, A., Doty, C., et al. (2013). ROCK1 and 2 perform overlapping and unique roles in angiogenesis and angiosarcoma tumor progression. *Curr. Mol. Med.* 13, 205–219. doi: 10.2174/1566524011307010205

Morland, C., Andersson, K. A., Haugen, O. P., Hadzic, A., Kleppa, L., Gille, A., et al. (2017). Exercise induces cerebral VEGF and angiogenesis via the lactate receptor HCAR1. *Nat. Commun.* 8:15557.

Morris, A. W., Sharp, M. M., Albargothy, N. J., Fernandes, R., Hawkes, C. A., Verma, A., et al. (2016). Vascular basement membranes as pathways for the passage of fluid into and out of the brain. *Acta Neuropathol.* 131, 725–736. doi: 10.1007/s00401-016-1555-z

Mostany, R., Chowdhury, T. G., Johnston, D. G., Portonovo, S. A., Carmichael, S. T., and Portera-Cailliau, C. (2010). Local hemodynamics dictate long-term dendritic plasticity in peri-infarct cortex. *J. Neurosci.* 30, 14116–14126. doi: 10.1523/jneurosci.3908-10.2010

Mozaffarian, D., Benjamin, E. J., Go, A. S., Arnett, D. K., Blaha, M. J., Cushman, M., et al. (2015). Heart disease and stroke statistics–2015 update: a report from the American Heart Association. *Circulation* 131, e29–e322.

Mulligan, S. J., and MacVicar, B. A. (2004). Calcium transients in astrocyte endfeet cause cerebrovascular constrictions. *Nature* 431, 195–199. doi: 10.1038/nature02827

Munji, R. N., Soung, A. L., Weiner, G. A., Sohet, F., Semple, B. D., Trivedi, A., et al. (2019). Profiling the mouse brain endothelial transcriptome in health and disease models reveals a core blood-brain barrier dysfunction module. *Nat. Neurosci.* 22, 1892–1902. doi: 10.1038/s41593-019-0497-x

Naderi, Y., Panahi, Y., Barreto, G. E., and Sahebkar, A. (2020). Neuroprotective effects of minocycline on focal cerebral ischemia injury: a systematic review. *Neural Regen. Res.* 15, 773–782.

Nagasawa, K., Chiba, H., Fujita, H., Kojima, T., Saito, T., Endo, T., et al. (2006). Possible involvement of gap junctions in the barrier function of tight junctions of brain and lung endothelial cells. *J. Cell. Physiol.* 208, 123–132. doi: 10.1002/jcp.20647

Nahirney, P. C., Reeson, P., and Brown, C. E. (2016). Ultrastructural analysis of blood-brain barrier breakdown in the peri-infarct zone in young adult and aged mice. *J. Cereb. Blood Flow Metab.* 36, 413–425. doi: 10.1177/0271678x15608396

Nakagawa, O., Fujisawa, K., Ishizaki, T., Saito, Y., Nakao, K., and Narumiya, S. (1996). ROCK-I and ROCK-II, two isoforms of Rho-associated coiled-coil forming protein serine/threonine kinase in mice. *FEBS Lett.* 392, 189–193. doi: 10.1016/0014-5793(96)00811-3

Nakamura, H., Strong, A. J., Dohmen, C., Sakowitz, O. W., Vollmar, S., Sue, M., et al. (2010). Spreading depolarizations cycle around and enlarge focal ischaemic brain lesions. *Brain* 133, 1994–2006. doi: 10.1093/brain/awq117

Nannoni, S., Cereda, C. W., Sirimarco, G., Lambrou, D., Strambo, D., Eskandari, A., et al. (2019). Collaterals are a major determinant of the core but not the penumbra volume in acute ischemic stroke. *Neuroradiology* 61, 971–978. doi: 10.1007/s00234-019-02224-x

Navarro-Sobrino, M., Rosell, A., Hernandez-Guillamon, M., Penalba, A., Boada, C., Domingues-Montanari, S., et al. (2011). A large screening of angiogenesis biomarkers and their association with neurological outcome after ischemic stroke. *Atherosclerosis* 216, 205–211. doi: 10.1016/j.atherosclerosis.2011.01.030

Nedeljkovic, Z. S., Gokce, N., and Loscalzo, J. (2003). Mechanisms of oxidative stress and vascular dysfunction. *Postgrad. Med. J.* 79, 195–199; quiz198–200.

Nevzati, E., Shafighi, M., Bakhtian, K. D., Treiber, H., Fandino, J., and Fathi, A. R. (2015). Estrogen induces nitric oxide production via nitric oxide synthase activation in endothelial cells. *Acta Neurochir. Suppl.* 120, 141–145. doi: 10.1007/978-3-319-04981-6_24

Nikolakopoulou, A. M., Montagne, A., Kisler, K., Dai, Z., Wang, Y., Huuskonen, M. T., et al. (2019). Pericyte loss leads to circulatory failure and pleiotrophin depletion causing neuron loss. *Nat. Neurosci.* 22, 1089–1098. doi: 10.1038/s41593-019-0434-z

Nimmerjahn, A., Kirchhoff, F., and Helmchen, F. (2005). Resting microglial cells are highly dynamic surveillants of brain parenchyma in vivo. *Science* 308, 1314–1318. doi: 10.1126/science.1110647

Nishijima, Y., Akamatsu, Y., Weinstein, P. R., and Liu, J. (2015). Collaterals: Implications in cerebral ischemic diseases and therapeutic interventions. *Brain Res.* 1623, 18–29. doi: 10.1016/j.brainres.2015.03.006

Nishioku, T., Dohgu, S., Takata, F., Eto, T., Ishikawa, N., Kodama, K. B., et al. (2009). Detachment of brain pericytes from the basal lamina is involved in disruption of the blood-brain barrier caused by lipopolysaccharide-induced sepsis in mice. *Cell Mol. Neurobiol.* 29, 309–316. doi: 10.1007/s10571-008-9322-x

Noma, K., Kihara, Y., and Higashi, Y. (2012). Striking crosstalk of ROCK signaling with endothelial function. *J. Cardiol.* 60, 1–6. doi: 10.1016/j.jjcc.2012.03.005

Novella, S., Dantas, A. P., Segarra, G., Medina, P., and Hermenegildo, C. (2012). Vascular aging in women: is estrogen the fountain of youth? *Front. Physiol.* 3:165. doi: 10.3389/fphys.2012.00165

O'Collins, V. E., Macleod, M. R., Donnan, G. A., Horky, L. L., van der Worp, B. H., and Howells, D. W. (2006). 1,026 experimental treatments in acute stroke. *Ann. Neurol.* 59, 467–477.

O'Donnell, M. E. (2014). Blood-brain barrier Na transporters in ischemic stroke. *Adv. Pharmacol.* 71, 113–146. doi: 10.1016/bs.apha.2014.06.011

Oh, W. J., and Gu, C. (2013). The role and mechanism-of-action of Sema3E and Plexin-D1 in vascular and neural development. *Semin. Cell Dev. Biol.* 24, 156–162. doi: 10.1016/j.semcdb.2012.12.001

Ohab, J. J., and Carmichael, S. T. (2008). Poststroke neurogenesis: emerging principles of migration and localization of immature neurons. *Neuroscientist* 14, 369–380. doi: 10.1177/1073858407309545

Ohab, J. J., Fleming, S., Blesch, A., and Carmichael, S. T. (2006). A neurovascular niche for neurogenesis after stroke. *J. Neurosci.* 26, 13007–13016. doi: 10.1523/jneurosci.4323-06.2006

Osada, T., Gu, Y. H., Kanazawa, M., Tsubota, Y., Hawkins, B. T., Spatz, M., et al. (2011). Interendothelial claudin-5 expression depends on cerebral endothelial cell-matrix adhesion by beta(1)-integrins. *J. Cereb. Blood Flow Metab.* 31, 1972–1985. doi: 10.1038/jcbfm.2011.99

Osypuk, T. L., Ehntholt, A., Moon, J. R., Gilsanz, P., and Glymour, M. M. (2017). Neighborhood differences in post-stroke mortality. *Circ. Cardiovasc. Qual. Outcomes* 10:e002547.

Paczkowska, E., Golab-Janowska, M., Bajer-Czajkowska, A., Machalinska, A., Ustianowski, P., Rybicka, M., et al. (2013). Increased circulating endothelial progenitor cells in patients with haemorrhagic and ischaemic stroke: the role of endothelin-1. *J. Neurol. Sci.* 325, 90–99. doi: 10.1016/j.jns.2012.12.005

Pan, C., Liu, N., Zhang, P., Wu, Q., Deng, H., Xu, F., et al. (2018). EGb761 ameliorates neuronal apoptosis and promotes angiogenesis in experimental intracerebral hemorrhage via RSK1/GSK3beta pathway. *Mol. Neurobiol.* 55, 1556–1567. doi: 10.1007/s12035-016-0363-8

Paredes, I., Himmels, P., and Ruiz de Almodovar, C. (2018). Neurovascular communication during CNS development. *Dev. Cell* 45, 10–32. doi: 10.1016/j.devcel.2018.01.023

Park, H. A., Kubicki, N., Gnyawali, S., Chan, Y. C., Roy, S., Khanna, S., et al. (2011). Natural vitamin E alpha-tocotrienol protects against ischemic stroke by induction of multidrug resistance-associated protein 1. *Stroke* 42, 2308–2314. doi: 10.1161/strokeaha.110.608547

Park, L., Anrather, J., Zhou, P., Frys, K., Pitstick, R., Younkin, S., et al. (2005). NADPH-oxidase-derived reactive oxygen species mediate the cerebrovascular dysfunction induced by the amyloid beta peptide. *J. Neurosci.* 25, 1769–1777. doi: 10.1523/jneurosci.5207-04.2005

Parkhurst, C. N., Yang, G., Ninan, I., Savas, J. N., Yates, J. R. III, Lafaille, J. J., et al. (2013). Microglia promote learning-dependent synapse formation through brain-derived neurotrophic factor. *Cell* 155, 1596–1609. doi: 10.1016/j.cell.2013.11.030

Pedragosa, J., Salas-Perdomo, A., Gallizioli, M., Cugota, R., Miró-Mur, F., Briansó, F., et al. (2018). CNS-border associated macrophages respond to acute ischemic stroke attracting granulocytes and promoting vascular leakage. *Acta Neuropathol. Commun.* 6:76. doi: 10.1186/s40478-018-0581-6

Peppiatt, C. M., Howarth, C., Mobbs, P., and Attwell, D. (2006). Bidirectional control of CNS capillary diameter by pericytes. *Nature* 443, 700–704. doi: 10.1038/nature05193

Persky, R. W., Turtzo, L. C., and McCullough, L. D. (2010). Stroke in women: disparities and outcomes. *Curr. Cardiol. Rep.* 12, 6–13. doi: 10.1007/s11886-009-0080-2

Petersen, M. A., Ryu, J. K., and Akassoglou, K. (2018). Fibrinogen in neurological diseases: mechanisms, imaging and therapeutics. *Nat. Rev. Neurosci.* 19, 283–301. doi: 10.1038/nrn.2018.13

Pianta, S., Lee, J. Y., Tuazon, J. P., Castelli, V., Mantohac, L. M., Tajiri, N., et al. (2019). A short bout of exercise prior to stroke improves functional outcomes by enhancing angiogenesis. *Neuromol. Med.* 21, 517–528. doi: 10.1007/s12017-019-08533-x

Pires, P. W., Girgla, S. S., McClain, J. L., Kaminski, N. E., van Rooijen, N., and Dorrance, A. M. (2013). Improvement in middle cerebral artery structure and endothelial function in stroke-prone spontaneously hypertensive rats after macrophage depletion. *Microcirculation* 20, 650–661. doi: 10.1111/micc.12064

Plate, K. H., Beck, H., Danner, S., Allegrini, P. R., and Wiessner, C. (1999). Cell type specific upregulation of vascular endothelial growth factor in an MCA-occlusion model of cerebral infarct. *J. Neuropathol. Exp. Neurol.* 58, 654–666. doi: 10.1097/00005072-199906000-00010

Ploughman, M., Austin, M. W., Glynn, L., and Corbett, D. (2015). The effects of poststroke aerobic exercise on neuroplasticity: a systematic review of animal and clinical studies. *Transl. Stroke Res.* 6, 13–28. doi: 10.1007/s12975-014-0357-7

Pohl, U. (2020). Connexins: key players in the control of vascular plasticity and function. *Physiol. Rev.* 100, 525–572. doi: 10.1152/physrev.00010.2019

Prabhakaran, S., Ruff, I., and Bernstein, R. A. (2015). Acute stroke intervention: a systematic review. *JAMA* 313, 1451–1462.

Pradeep, H., Diya, J. B., Shashikumar, S., and Rajanikant, G. K. (2012). Oxidative stress–assassin behind the ischemic stroke. *Folia Neuropathol.* 50, 219–230. doi: 10.5114/fn.2012.30522

Prakash, R., and Carmichael, S. T. (2015). Blood-brain barrier breakdown and neovascularization processes after stroke and traumatic brain injury. *Curr. Opin. Neurol.* 28, 556–564. doi: 10.1097/wco.0000000000000248

Predescu, S. A., Predescu, D. N., and Palade, G. E. (2001). Endothelial transcytotic machinery involves supramolecular protein-lipid complexes. *Mol. Biol. Cell* 12, 1019–1033. doi: 10.1091/mbc.12.4.1019

Profaci, C. P., Munji, R. N., Pulido, R. S., and Daneman, R. (2020). The blood-brain barrier in health and disease: important unanswered questions. *J. Exp. Med.* 217:e20190062.

Provenzale, J. M., Jahan, R., Naidich, T. P., and Fox, A. J. (2003). Assessment of the patient with hyperacute stroke: imaging and therapy. *Radiology* 229, 347–359. doi: 10.1148/radiol.2292020402

Puro, D. G. (2007). Physiology and pathobiology of the pericyte-containing retinal microvasculature: new developments. *Microcirculation* 14, 1–10. doi: 10.1080/10739680601072099

Qureshi, A. I., Mendelow, A. D., and Hanley, D. F. (2009). Intracerebral haemorrhage. *Lancet* 373, 1632–1644.

Radenovic, L., Nenadic, M., Ulamek-Koziol, M., Januszewski, S., Czuczwar, S. J., Andjus, P. R., et al. (2020). Heterogeneity in brain distribution of activated microglia and astrocytes in a rat ischemic model of Alzheimer's disease after 2 years of survival. *Aging* 12, 12251–12267. doi: 10.18632/aging.103411

Rashid, P. A., Whitehurst, A., Lawson, N., and Bath, P. M. (2003). Plasma nitric oxide (nitrate/nitrite) levels in acute stroke and their relationship with severity and outcome. *J. Stroke Cerebrovasc. Dis.* 12, 82–87. doi: 10.1053/jscd.2003.9

Rattner, A., Williams, J., and Nathans, J. (2019). Roles of HIFs and VEGF in angiogenesis in the retina and brain. *J. Clin. Invest.* 130, 3807–3820. doi: 10.1172/jci126655

Rawlinson, C., Jenkins, S., Thei, L., Dallas, M. L., and Chen, R. (2020). Post-ischaemic immunological response in the brain: targeting microglia in ischaemic stroke therapy. *Brain Sci.* 10:159. doi: 10.3390/brainsci10030159

Rayasam, A., Faustino, J., Lecuyer, M., and Vexler, Z. S. (2020). Neonatal stroke and TLR1/2 ligand recruit myeloid cells through the choroid plexus in a CX3CR1(-)CCR2 and context specific manner. *J. Neurosci.* 40, 3849–3861. doi: 10.1523/jneurosci.2149-19.2020

Razmara, A., Sunday, L., Stirone, C., Wang, X. B., Krause, D. N., Duckles, S. P., et al. (2008). Mitochondrial effects of estrogen are mediated by estrogen receptor alpha in brain endothelial cells. *J. Pharmacol. Exp. Ther.* 325, 782–790. doi: 10.1124/jpet.107.134072

Reese, T. S., and Karnovsky, M. J. (1967). Fine structural localization of a blood-brain barrier to exogenous peroxidase. *J. Cell Biol.* 34, 207–217. doi: 10.1083/jcb.34.1.207

Reeson, P., Tennant, K. A., Gerrow, K., Wang, J., Weiser Novak, S., Thompson, K., et al. (2015). Delayed inhibition of VEGF signaling after stroke attenuates blood-brain barrier breakdown and improves functional recovery in a comorbidity-dependent manner. *J. Neurosci.* 35, 5128–5143. doi: 10.1523/jneurosci.2810-14.2015

Reeves, M. J., Bushnell, C. D., Howard, G., Gargano, J. W., Duncan, P. W., Lynch, G., et al. (2008). Sex differences in stroke: epidemiology, clinical presentation, medical care, and outcomes. *Lancet Neurol.* 7, 915–926. doi: 10.1016/s1474-4422(08)70193-5

Richardson, M., Meyer, M., and Teasell, R. (2014). The effect of tPA on inpatient rehabilitation after stroke: a cost comparison. *Can. J. Neurol. Sci.* 41, 482–485. doi: 10.1017/s0317167100018527

Riento, K., and Ridley, A. J. (2003). Rocks: multifunctional kinases in cell behaviour. *Nat. Rev. Mol. Cell Biol.* 4, 446–456. doi: 10.1038/nrm1128

Rikitake, Y., Kim, H. H., Huang, Z., Seto, M., Yano, K., Asano, T., et al. (2005). Inhibition of Rho kinase (ROCK) leads to increased cerebral blood flow and stroke protection. *Stroke* 36, 2251–2257. doi: 10.1161/01.str.0000181077.84981.11

Risher, W. C., Ard, D., Yuan, J., and Kirov, S. A. (2010). Recurrent spontaneous spreading depolarizations facilitate acute dendritic injury in the ischemic penumbra. *J. Neurosci.* 30, 9859–9868. doi: 10.1523/jneurosci.1917-10.2010

Rivera, P., Ocaranza, M. P., Lavandero, S., and Jalil, J. E. (2007). Rho kinase activation and gene expression related to vascular remodeling in normotensive rats with high angiotensin I converting enzyme levels. *Hypertension* 50, 792–798. doi: 10.1161/hypertensionaha.107.095117

Rodrigo, R., Fernandez-Gajardo, R., Gutierrez, R., Matamala, J. M., Carrasco, R., Miranda-Merchak, A., et al. (2013). Oxidative stress and pathophysiology of ischemic stroke: novel therapeutic opportunities. *CNS Neurol. Disord. Drug Targets* 12, 698–714. doi: 10.2174/18715273113120500015

Rohlenova, K., Goveia, J., Garcia-Caballero, M., Subramanian, A., Kalucka, J., Treps, L., et al. (2020). Single-Cell RNA sequencing maps endothelial metabolic plasticity in pathological angiogenesis. *Cell Metab.* 31, 862.e14–877.e14.

Roome, R. B., Bartlett, R. F., Jeffers, M., Xiong, J., Corbett, D., and Vanderluit, J. L. (2014). A reproducible endothelin-1 model of forelimb motor cortex stroke in the mouse. *J. Neurosci. Methods* 233, 34–44. doi: 10.1016/j.jneumeth.2014.05.014

Rovegno, M., and Saez, J. C. (2018). Role of astrocyte connexin hemichannels in cortical spreading depression. *Biochim. Biophys. Acta Biomembr.* 1860, 216–223. doi: 10.1016/j.bbamem.2017.08.014

Roy-O'Reilly, M., and McCullough, L. D. (2018). Age and sex are critical factors in ischemic stroke pathology. *Endocrinology* 159, 3120–3131. doi: 10.1210/en.2018-00465

Sacco, R. L., Kasner, S. E., Broderick, J. P., Caplan, L. R., Connors, J. J., Culebras, A., et al. (2013). An updated definition of stroke for the 21st century: a statement for healthcare professionals from the American Heart Association/American Stroke Association. *Stroke* 44, 2064–2089.

Samdani, A. F., Dawson, T. M., and Dawson, V. L. (1997). Nitric oxide synthase in models of focal ischemia. *Stroke* 28, 1283–1288. doi: 10.1161/01.str.28.6.1283

Satoh, S., Hitomi, A., Ikegaki, I., Kawasaki, K., Nakazono, O., Iwasaki, M., et al. (2010). Amelioration of endothelial damage/dysfunction is a possible mechanism for the neuroprotective effects of Rho-kinase inhibitors against ischemic brain damage. *Brain Res. Bull.* 81, 191–195. doi: 10.1016/j.brainresbull.2009.08.021

Sawada, N., and Liao, J. K. (2009). Targeting eNOS and beyond: emerging heterogeneity of the role of endothelial Rho proteins in stroke protection. *Expert Rev. Neurother.* 9, 1171–1186. doi: 10.1586/ern.09.70

Schaapsmeerders, P., Maaijwee, N. A., van Dijk, E. J., Rutten-Jacobs, L. C., Arntz, R. M., Schoonderwaldt, H. C., et al. (2013). Long-term cognitive impairment after first-ever ischemic stroke in young adults. *Stroke* 44, 1621–1628. doi: 10.1161/strokeaha.111.000792

Schafer, A., Fraccarollo, D., Widder, J., Eigenthaler, M., Ertl, G., and Bauersachs, J. (2009). Inhibition of platelet activation in rats with severe congestive heart failure by a novel endothelial nitric oxide synthase transcription enhancer. *Eur. J. Heart Fail.* 11, 336–341. doi: 10.1093/eurjhf/hfp005

Schierling, W., Troidl, K., Apfelbeck, H., Troidl, C., Kasprzak, P. M., Schaper, W., et al. (2011). Cerebral arteriogenesis is enhanced by pharmacological as well as fluid-shear-stress activation of the Trpv4 calcium channel. *Eur. J. Vasc. Endovasc. Surg.* 41, 589–596. doi: 10.1016/j.ejvs.2010.11.034

Schirrmacher, R., Dea, M., Heiss, W. D., Kostikov, A., Funck, T., Quessy, S., et al. (2016). Which aspects of stroke do animal models capture? A Multitracer Micro-PET study of focal ischemia with endothelin-1. *Cerebrovasc. Dis.* 41, 139–147. doi: 10.1159/000442997

Schmidt, W., Endres, M., Dimeo, F., and Jungehulsing, G. J. (2013). Train the vessel, gain the brain: physical activity and vessel function and the impact on stroke prevention and outcome in cerebrovascular disease. *Cerebrovasc. Dis.* 35, 303–312. doi: 10.1159/000347061

Schnitzer, J. E. (2001). Caveolae: from basic trafficking mechanisms to targeting transcytosis for tissue-specific drug and gene delivery in vivo. *Adv. Drug Deliv. Rev.* 49, 265–280. doi: 10.1016/s0169-409x(01)00141-7

Segarra, M., Aburto, M. R., Cop, F., Llao-Cid, C., Hartl, R., Damm, M., et al. (2018). Endothelial Dab1 signaling orchestrates neuro-glia-vessel communication in the central nervous system. *Science* 361:eaao2861. doi: 10.1126/science.aao2861

Segarra, M., Kirchmaier, B. C., and Acker-Palmer, A. (2015). A vascular perspective on neuronal migration. *Mech. Dev.* 138(Pt 1), 17–25. doi: 10.1016/j.mod.2015.07.004

Selvaraj, U. M., Zuurbier, K. R., Whoolery, C. W., Plautz, E. J., Chambliss, K. L., Kong, X., et al. (2018). Selective nonnuclear estrogen receptor activation decreases stroke severity and promotes functional recovery in female mice. *Endocrinology* 159, 3848–3859. doi: 10.1210/en.2018-00600

Semenza, G. L. (2014). Oxygen sensing, hypoxia-inducible factors, and disease pathophysiology. *Annu. Rev. Pathol.* 9, 47–71. doi: 10.1146/annurev-pathol-012513-104720

Shannon, C., Salter, M., and Fern, R. (2007). GFP imaging of live astrocytes: regional differences in the effects of ischaemia upon astrocytes. *J. Anat.* 210, 684–692. doi: 10.1111/j.1469-7580.2007.00731.x

Shen, S., and Zhang, W. (2010). ABC transporters and drug efflux at the blood-brain barrier. *Rev. Neurosci.* 21, 29–53.

Shi, H., and Liu, K. J. (2007). Cerebral tissue oxygenation and oxidative brain injury during ischemia and reperfusion. *Front. Biosci.* 12:1318–1328. doi: 10.2741/2150

Shibahara, T., Ago, T., Nakamura, K., Tachibana, M., Yoshikawa, Y., Komori, M., et al. (2020). Pericyte-Mediated tissue repair through pdgfrbeta promotes peri-infarct astrogliosis, oligodendrogenesis, and functional recovery after acute ischemic stroke. *eNeuro* 7:ENEURO.474-19.2020.

Shin, H. K., Salomone, S., Potts, E. M., Lee, S. W., Millican, E., Noma, K., et al. (2007). Rho-kinase inhibition acutely augments blood flow in focal cerebral ischemia via endothelial mechanisms. *J. Cereb. Blood Flow Metab.* 27, 998–1009. doi: 10.1038/sj.jcbfm.9600406

Shin, J. A., Yoon, J. C., Kim, M., and Park, E. M. (2016). Activation of classical estrogen receptor subtypes reduces tight junction disruption of brain endothelial cells under ischemia/reperfusion injury. *Free Radic. Biol. Med.* 92, 78–89. doi: 10.1016/j.freeradbiomed.2016.01.010

Shojaee, N., Patton, W. F., Hechtman, H. B., and Shepro, D. (1999). Myosin translocation in retinal pericytes during free-radical induced apoptosis. *J. Cell. Biochem.* 75, 118–129. doi: 10.1002/(sici)1097-4644(19991001)75:1<118::aid-jcb12>3.0.co;2-u

Siddiqui, M. R., Komarova, Y. A., Vogel, S. M., Gao, X., Bonini, M. G., Rajasingh, J., et al. (2011). Caveolin-1-eNOS signaling promotes p190RhoGAP-A nitration and endothelial permeability. *J. Cell Biol.* 193, 841–850. doi: 10.1083/jcb.201012129

Silasi, G., and Murphy, T. H. (2014). Stroke and the connectome: how connectivity guides therapeutic intervention. *Neuron* 83, 1354–1368. doi: 10.1016/j.neuron.2014.08.052

Silasi, G., She, J., Boyd, J. D., Xue, S., and Murphy, T. H. (2015). A mouse model of small-vessel disease that produces brain-wide-identified microocclusions and regionally selective neuronal injury. *J. Cereb. Blood Flow Metab.* 35, 734–738. doi: 10.1038/jcbfm.2015.8

Slevin, M., Krupinski, J., Slowik, A., Kumar, P., Szczudlik, A., and Gaffney, J. (2000). Serial measurement of vascular endothelial growth factor and transforming growth factor-beta1 in serum of patients with acute ischemic stroke. *Stroke* 31, 1863–1870. doi: 10.1161/01.str.31.8.1863

Smith, S. D., and Eskey, C. J. (2011). Hemorrhagic stroke. *Radiol. Clin. North Am.* 49, 27–45.

Smith, Y. E., Toomey, S., Napoletano, S., Kirwan, G., Schadow, C., Chubb, A. J., et al. (2018). Recombinant PAPP-A resistant insulin-like growth factor binding protein 4 (dBP4) inhibits angiogenesis and metastasis in a murine model of breast cancer. *BMC Cancer* 18:1016. doi: 10.1186/s12885-018-4950-0

Soliman, H., Gador, A., Lu, Y. H., Lin, G., Bankar, G., and MacLeod, K. M. (2012). Diabetes-induced increased oxidative stress in cardiomyocytes is sustained by a positive feedback loop involving Rho kinase and PKCbeta2. *Am. J. Physiol. Heart Circ. Physiol.* 303, H989–H1000.

Sommer, C. J. (2017). Ischemic stroke: experimental models and reality. *Acta Neuropathol.* 133, 245–261. doi: 10.1007/s00401-017-1667-0

Stanimirovic, D. B., Sandhu, J. K., and Costain, W. J. (2018). Emerging technologies for delivery of biotherapeutics and gene therapy across the blood-brain barrier. *BioDrugs* 32, 547–559. doi: 10.1007/s40259-018-0309-y

Steiner, E., Enzmann, G. U., Lyck, R., Lin, S., Ruegg, M. A., Kroger, S., et al. (2014). The heparan sulfate proteoglycan agrin contributes to barrier properties of mouse brain endothelial cells by stabilizing adherens junctions. *Cell Tissue Res.* 358, 465–479. doi: 10.1007/s00441-014-1969-7

Su, X., Huang, L., Qu, Y., Xiao, D., and Mu, D. (2019). Pericytes in cerebrovascular diseases: an emerging therapeutic target. *Front. Cell. Neurosci.* 13:519. doi: 10.3389/fncel.2019.00519

Sugimoto, K., and Chung, D. Y. (2020). Spreading depolarizations and subarachnoid hemorrhage. *Neurotherapeutics* 17, 497–510. doi: 10.1007/s13311-020-00850-5

Sugimoto, M., Nakayama, M., Goto, T. M., Amano, M., Komori, K., and Kaibuchi, K. (2007). Rho-kinase phosphorylates eNOS at threonine 495 in endothelial cells. *Biochem. Biophys. Res. Commun.* 361, 462–467. doi: 10.1016/j.bbrc.2007.07.030

Sun, J., Zhang, Y., Lu, J., Zhang, W., Yan, J., Yang, L., et al. (2018). Salvinorin A ameliorates cerebral vasospasm through activation of endothelial nitric oxide synthase in a rat model of subarachnoid hemorrhage. *Microcirculation* 25:e12442. doi: 10.1111/micc.12442

Sun, Y., and Zehr, E. P. (2019). Training-induced neural plasticity and strength are amplified after stroke. *Exerc. Sport Sci. Rev.* 47, 223–229. doi: 10.1249/jes.0000000000000199

Suzuki, Y., Nagai, N., and Umemura, K. (2016). A review of the mechanisms of blood-brain barrier permeability by tissue-type plasminogen activator treatment for cerebral ischemia. *Front. Cell Neurosci.* 10:2. doi: 10.3389/fncel.2016.00002

Swayne, L. A., and Wicki-Stordeur, L. (2012). Ion channels in postnatal neurogenesis: potential targets for brain repair. *Channels* 6, 69–74. doi: 10.4161/chan.19721

Sweeney, M. D., Ayyadurai, S., and Zlokovic, B. V. (2016). Pericytes of the neurovascular unit: key functions and signaling pathways. *Nat. Neurosci.* 19, 771–783. doi: 10.1038/nn.4288

Sweeney, M. D., Zhao, Z., Montagne, A., Nelson, A. R., and Zlokovic, B. V. (2019). Blood-brain barrier: from physiology to disease and back. *Physiol. Rev.* 99, 21–78. doi: 10.1152/physrev.00050.2017

Takano, T., Tian, G. F., Peng, W., Lou, N., Lovatt, D., Hansen, A. J., et al. (2007). Cortical spreading depression causes and coincides with tissue hypoxia. *Nat. Neurosci.* 10, 754–762. doi: 10.1038/nn1902

Takeuchi, K., Morizane, Y., Kamami-Levy, C., Suzuki, J., Kayama, M., Cai, W., et al. (2013). AMP-dependent kinase inhibits oxidative stress-induced caveolin-1 phosphorylation and endocytosis by suppressing the dissociation between c-Abl and Prdx1 proteins in endothelial cells. *J. Biol. Chem.* 288, 20581–20591. doi: 10.1074/jbc.m113.460832

Talwar, T., and Srivastava, M. V. (2014). Role of vascular endothelial growth factor and other growth factors in post-stroke recovery. *Ann. Indian Acad Neurol.* 17, 1–6.

Tam, S. J., and Watts, R. J. (2010). Connecting vascular and nervous system development: angiogenesis and the blood-brain barrier. *Annu. Rev. Neurosci.* 33, 379–408. doi: 10.1146/annurev-neuro-060909-152829

Tang, F. C., Wang, H. Y., Ma, M. M., Guan, T. W., Pan, L., Yao, D. C., et al. (2017). Simvastatin attenuated rat thoracic aorta remodeling by decreasing ROCK2mediated CyPA secretion and CD147ERK1/2cyclin pathway. *Mol. Med. Rep.* 16, 8123–8129. doi: 10.3892/mmr.2017.7640

Tang, M., Gao, G., Rueda, C. B., Yu, H., Thibodeaux, D. N., Awano, T., et al. (2017). Brain microvasculature defects and Glut1 deficiency syndrome averted by early repletion of the glucose transporter-1 protein. *Nat. Commun.* 8: 14152.

Tang, T., Liu, X. J., Zhang, Z. Q., Zhou, H. J., Luo, J. K., Huang, J. F., et al. (2007). Cerebral angiogenesis after collagenase-induced intracerebral hemorrhage in rats. *Brain Res.* 1175, 134–142. doi: 10.1016/j.brainres.2007.08.028

Tata, M., and Ruhrberg, C. (2018). Cross-talk between blood vessels and neural progenitors in the developing brain. *Neuronal Signal.* 2:NS20170139.

Tata, M., Ruhrberg, C., and Fantin, A. (2015). Vascularisation of the central nervous system. *Mech. Dev.* 138(Pt 1), 26–36. doi: 10.1016/j.mod.2015.07.001

Teasell, R., Hussein, N., McClure, A., and Meyer, M. (2014a). Stroke: more than a 'brain attack'. *Int J Stroke* 9, 188–190. doi: 10.1111/ijs.12233

Teasell, R., Rice, D., Richardson, M., Campbell, N., Madady, M., Hussein, N., et al. (2014b). The next revolution in stroke care. *Expert Rev. Neurother.* 14, 1307–1314.

Tennant, K. A., and Jones, T. A. (2009). Sensorimotor behavioral effects of endothelin-1 induced small cortical infarcts in C57BL/6 mice. *J. Neurosci. Methods* 181, 18–26. doi: 10.1016/j.jneumeth.2009.04.009

The National Institute of Neurological Disorders, and Stroke rt-Pa Stroke Study Group (1995). Tissue plasminogen activator for acute ischemic stroke. *N. Engl. J. Med.* 333, 1581–1587.

Thomas, M., and Augustin, H. G. (2009). The role of the Angiopoietins in vascular morphogenesis. *Angiogenesis* 12, 125–137. doi: 10.1007/s10456-009-9147-3

Thomsen, M. S., Routhe, L. J., and Moos, T. (2017). The vascular basement membrane in the healthy and pathological brain. *J. Cereb. Blood Flow Metab.* 37, 3300–3317. doi: 10.1177/0271678x17722436

Toda, N. (2012). Age-related changes in endothelial function and blood flow regulation. *Pharmacol. Ther.* 133, 159–176. doi: 10.1016/j.pharmthera.2011.10.004

Toda, N., Ayajiki, K., and Okamura, T. (2009). Cerebral blood flow regulation by nitric oxide in neurological disorders. *Can. J. Physiol. Pharmacol.* 87, 581–594. doi: 10.1139/y09-048

Tomita, S., Ueno, M., Sakamoto, M., Kitahama, Y., Ueki, M., Maekawa, N., et al. (2003). Defective brain development in mice lacking the Hif-1alpha gene in neural cells. *Mol. Cell. Biol.* 23, 6739–6749. doi: 10.1128/mcb.23.19.6739-6749.2003

Tornabene, E., Helms, H. C. C., Pedersen, S. F., and Brodin, B. (2019). Effects of oxygen-glucose deprivation (OGD) on barrier properties and mRNA transcript levels of selected marker proteins in brain endothelial cells/astrocyte co-cultures. *PLoS One* 14:e0221103. doi: 10.1371/journal.pone.0221103

Tremblay, M. E., Stevens, B., Sierra, A., Wake, H., Bessis, A., and Nimmerjahn, A. (2011). The role of microglia in the healthy brain. *J. Neurosci.* 31, 16064–16069. doi: 10.1523/jneurosci.4158-11.2011

Tsai, H. H., Li, H., Fuentealba, L. C., Molofsky, A. V., Taveira-Marques, R., Zhuang, H., et al. (2012). Regional astrocyte allocation regulates CNS synaptogenesis and repair. *Science* 337, 358–362. doi: 10.1126/science.1222381

Tsuda, K. (2010). Neuroprotective effect of isoflurane and N-methyl-D-aspartate receptors in ischemic brain injury. *Stroke* 41, e578; authorrelye579.

Tsuji, K., Aoki, T., Tejima, E., Arai, K., Lee, S. R., Atochin, D. N., et al. (2005). Tissue plasminogen activator promotes matrix metalloproteinase-9 upregulation after focal cerebral ischemia. *Stroke* 36, 1954–1959. doi: 10.1161/01.str.0000177517.01203.eb

Tuma, P., and Hubbard, A. L. (2003). Transcytosis: crossing cellular barriers. *Physiol. Rev.* 83, 871–932. doi: 10.1152/physrev.00001.2003

Turtzo, L. C., and McCullough, L. D. (2010). Sex-specific responses to stroke. *Future Neurol.* 5, 47–59. doi: 10.2217/fnl.09.6

Tymianski, M. (2011). Emerging mechanisms of disrupted cellular signaling in brain ischemia. *Nat. Neurosci.* 14, 1369–1373. doi: 10.1038/nn.2951

Uemura, M. T., Maki, T., Ihara, M., Lee, V. M. Y., and Trojanowski, J. Q. (2020). Brain microvascular pericytes in vascular cognitive impairment and dementia. *Front. Aging Neurosci.* 12:80. doi: 10.3389/fnagi.2020.00080

Underly, R. G., Levy, M., Hartmann, D. A., Grant, R. I, Watson, A. N., and Shih, A. Y. (2017). Pericytes as inducers of rapid, matrix metalloproteinase-9-dependent capillary damage during Ischemia. *J. Neurosci.* 37, 129–140. doi: 10.1523/jneurosci.2891-16.2016

Uzdensky, A. B. (2018). Photothrombotic stroke as a model of ischemic stroke. *Transl. Stroke Res.* 9, 437–451. doi: 10.1007/s12975-017-0593-8

van Leeuwen, E., Hampton, M. B., and Smyth, L. C. D. (2020). Redox signalling and regulation of the blood-brain barrier. *Int. J. Biochem. Cell Biol.* 125, 105794. doi: 10.1016/j.biocel.2020.105794

van Nieuw Amerongen, G. P., Koolwijk, P., Versteilen, A., and van Hinsbergh, V. W. (2003). Involvement of RhoA/Rho kinase signaling in VEGF-induced endothelial cell migration and angiogenesis in vitro. *Arterioscler. Thromb. Vasc. Biol.* 23, 211–217. doi: 10.1161/01.atv.0000054198.68894.88

Vanlandewijck, M., He, L., Mae, M. A., Andrae, J., Ando, K., Del Gaudio, F., et al. (2018). A molecular atlas of cell types and zonation in the brain vasculature. *Nature* 554, 475–480. doi: 10.1038/nature25739

Vaudano, A. E., Olivotto, S., Ruggieri, A., Gessaroli, G., De Giorgis, V., Parmeggiani, A., et al. (2017). Brain correlates of spike and wave discharges in GLUT1 deficiency syndrome. *Neuroimage Clin.* 13, 446–454. doi: 10.1016/j.nicl.2016.12.026

Vaughan, C. J., and Delanty, N. (1999). Neuroprotective properties of statins in cerebral ischemia and stroke. *Stroke* 30, 1969–1973. doi: 10.1161/01.str.30.9.1969

Verkhratsky, A., and Steinhauser, C. (2000). Ion channels in glial cells. *Brain research reviews* 32, 380–412. doi: 10.1016/s0165-0173(99)00093-4

Vesterinen, H. M., Currie, G. L., Carter, S., Mee, S., Watzlawick, R., Egan, K. J., et al. (2013). Systematic review and stratified meta-analysis of the efficacy of RhoA and Rho kinase inhibitors in animal models of ischaemic stroke. *Syst. Rev.* 2:33. doi: 10.1186/2046-4053-2-33

Vijayan, M., and Reddy, P. H. (2016). Stroke, vascular dementia, and alzheimer's disease: molecular links. *J. Alzheimers Dis.* 54, 427–443. doi: 10.3233/jad-160527

Virgintino, D., Girolamo, F., Errede, M., Capobianco, C., Robertson, D., Stallcup, W. B., et al. (2007). An intimate interplay between precocious, migrating pericytes and endothelial cells governs human fetal brain angiogenesis. *Angiogenesis* 10, 35–45. doi: 10.1007/s10456-006-9061-x

von Bornstadt, D., Houben, T., Seidel, J. L., Zheng, Y., Dilekoz, E., Qin, T., et al. (2015). Supply-demand mismatch transients in susceptible peri-infarct hot zones explain the origins of spreading injury depolarizations. *Neuron* 85, 1117–1131. doi: 10.1016/j.neuron.2015.02.007

Wake, H., Moorhouse, A. J., Jinno, S., Kohsaka, S., and Nabekura, J. (2009). Resting microglia directly monitor the functional state of synapses in vivo and determine the fate of ischemic terminals. *J. Neurosci.* 29, 3974–3980. doi: 10.1523/jneurosci.4363-08.2009

Walchli, T., Wacker, A., Frei, K., Regli, L., Schwab, M. E., Hoerstrup, S. P., et al. (2015). Wiring the vascular network with neural cues: a CNS perspective. *Neuron* 87, 271–296. doi: 10.1016/j.neuron.2015.06.038

Wang, F., Cao, Y., Ma, L., Pei, H., Rausch, W. D., and Li, H. (2018). Dysfunction of cerebrovascular endothelial cells: prelude to vascular dementia. *Front. Aging Neurosci.* 10:376. doi: 10.3389/fnagi.2018.00376

Wang, Y., Dai, Y., Zheng, J., Xie, Y., Guo, R., Guo, X., et al. (2019). Sex difference in the incidence of stroke and its corresponding influence factors: results from a follow-up 8.4 years of rural China hypertensive prospective cohort study. *Lipids Health Dis.* 18:72.

Wassertheil-Smoller, S., Hendrix, S. L., Limacher, M., Heiss, G., Kooperberg, C., Baird, A., et al. (2003). Effect of estrogen plus progestin on stroke in postmenopausal women: the Women's Health Initiative: a randomized trial. *JAMA* 289, 2673–2684.

Weinstein, P. R., Hong, S., and Sharp, F. R. (2004). Molecular identification of the ischemic penumbra. *Stroke* 35, 2666–2670. doi: 10.1161/01.str.0000144052.10644.ed

Wetterling, F., Chatzikonstantinou, E., Tritschler, L., Meairs, S., Fatar, M., Schad, L. R., et al. (2016). Investigating potentially salvageable penumbra tissue in an in vivo model of transient ischemic stroke using sodium, diffusion, and perfusion magnetic resonance imaging. *BMC Neurosci.* 17:82. doi: 10.1186/s12868-016-0316-1

Willis, K. J., and Hakim, A. M. (2013). Stroke prevention and cognitive reserve: emerging approaches to modifying risk and delaying onset of dementia. *Front. Neurol.* 4:13. doi: 10.3389/fneur.2013.00013

Winkler, E. A., Nishida, Y., Sagare, A. P., Rege, S. V., Bell, R. D., Perlmutter, D., et al. (2015). GLUT1 reductions exacerbate Alzheimer's disease vasculo-neuronal dysfunction and degeneration. *Nat. Neurosci.* 18, 521–530. doi: 10.1038/nn.3966

Winkler, E. A., Sagare, A. P., and Zlokovic, B. V. (2014). The pericyte: a forgotten cell type with important implications for Alzheimer's disease? *Brain Pathol.* 24, 371–386. doi: 10.1111/bpa.12152

Wohlfart, P., Xu, H., Endlich, A., Habermeier, A., Closs, E. I., Hubschle, T., et al. (2008). Antiatherosclerotic effects of small-molecular-weight compounds enhancing endothelial nitric-oxide synthase (eNOS) expression and preventing eNOS uncoupling. *J. Pharmacol. Exp. Ther.* 325, 370–379. doi: 10.1124/jpet.107.128009

Wu, B., Zhang, L., Zhu, Y. H., Zhang, Y. E., Zheng, F., Yang, J. Y., et al. (2018). Mesoderm/mesenchyme homeobox gene l promotes vascular smooth muscle cell phenotypic modulation and vascular remodeling. *Int. J. Cardiol.* 251, 82–89. doi: 10.1016/j.ijcard.2017.10.098

Wu, Y., Dissing-Olesen, L., MacVicar, B. A., and Stevens, B. (2015). Microglia: dynamic mediators of synapse development and plasticity. *Trends Immunol.* 36, 605–613. doi: 10.1016/j.it.2015.08.008

Xiao, H., Deng, M., Yang, B., Hu, Z., and Tang, J. (2018). Pretreatment with 17beta-Estradiol attenuates cerebral ischemia-induced blood-brain barrier disruption

in aged rats: involvement of antioxidant signaling. *Neuroendocrinology* 106, 20–29. doi: 10.1159/000455866

Xu, C., Tang, F., Lu, M., Yang, J., Han, R., Mei, M., et al. (2016). Astragaloside IV improves the isoproterenol-induced vascular dysfunction via attenuating eNOS uncoupling-mediated oxidative stress and inhibiting ROS-NF-kappaB pathways. *Int. Immunopharmacol.* 33, 119–127. doi: 10.1016/j.intimp.2016.02.009

Xu, J., Murphy, S. L., Kochanek, K. D., and Bastian, B. A. (2016). Deaths: final data for 2013. *Natl. Vital Stat. Rep.* 64, 1–119.

Xu, H., Cao, Y., Yang, X., Cai, P., Kang, L., Zhu, X., et al. (2017). ADAMTS13 controls vascular remodeling by modifying VWF reactivity during stroke recovery. *Blood* 130, 11–22. doi: 10.1182/blood-2016-10-747089

Yamada, M., Huang, Z., Dalkara, T., Endres, M., Laufs, U., Waeber, C., et al. (2000). Endothelial nitric oxide synthase-dependent cerebral blood flow augmentation by L-arginine after chronic statin treatment. *J. Cereb. Blood Flow Metab.* 20, 709–717. doi: 10.1097/00004647-200004000-00008

Yang, G., Qian, C., Wang, N., Lin, C., Wang, Y., Wang, G., et al. (2016). Tetramethylpyrazine protects against oxygen-glucose deprivation-induced brain microvascular endothelial cells injury via rho/rho-kinase signaling pathway. *Cell Mol. Neurobiol.* 37, 619–633. doi: 10.1007/s10571-016-0398-4

Yang, S., Liu, K., Ding, H., Gao, H., Zheng, X., Ding, Z., et al. (2019). Longitudinal in vivo intrinsic optical imaging of cortical blood perfusion and tissue damage in focal photothrombosis stroke model. *J. Cereb. Blood Flow Metab.* 39, 1381–1393. doi: 10.1177/0271678x18762636

Yang, S. H., Shi, J., Day, A. L., and Simpkins, J. W. (2000). Estradiol exerts neuroprotective effects when administered after ischemic insult. *Stroke* 31, 745–749; discussion749–750.

Yao, L., Romero, M. J., Toque, H. A., Yang, G., Caldwell, R. B., and Caldwell, R. W. (2010). The role of RhoA/Rho kinase pathway in endothelial dysfunction. *J. Cardiovasc. Dis. Res.* 1, 165–170. doi: 10.4103/0975-3583.74258

Yao, Y. (2019). Basement membrane and stroke. *J. Cereb. Blood Flow Metab.* 39, 3–19. doi: 10.1177/0271678x18801467

Yemisci, M., Gursoy-Ozdemir, Y., Vural, A., Can, A., Topalkara, K., and Dalkara, T. (2009). Pericyte contraction induced by oxidative-nitrative stress impairs capillary reflow despite successful opening of an occluded cerebral artery. *Nat. Med.* 15, 1031–1037. doi: 10.1038/nm.2022

Yenari, M. A., Kauppinen, T. M., and Swanson, R. A. (2010). Microglial activation in stroke: therapeutic targets. *Neurotherapeutics* 7, 378–391. doi: 10.1016/j.nurt.2010.07.005

Yu, G., Bolon, M., Laird, D. W., and Tyml, K. (2010). Hypoxia and reoxygenation-induced oxidant production increase in microvascular endothelial cells depends on connexin40. *Free Radic. Biol. Med.* 49, 1008–1013. doi: 10.1016/j.freeradbiomed.2010.06.005

Zhang, H., Chalothorn, D., and Faber, J. E. (2019). Collateral vessels have unique endothelial and smooth muscle cell phenotypes. *Int. J. Mol. Sci.* 20:3608. doi: 10.3390/ijms20153608

Zhang, H., Pan, Q., Xie, Z., Chen, Y., Wang, J., Bihl, J., et al. (2020). Implication of MicroRNA503 in brain endothelial cell function and ischemic stroke. *Transl. Stroke Res.* [Epub ahead of print]. doi: 10.1007/s12975-020-00794-0

Zhang, Z., Zhang, Z., Lu, H., Yang, Q., Wu, H., and Wang, J. (2017). Microglial polarization and inflammatory mediators after intracerebral hemorrhage. *Mol. Neurobiol.* 54, 1874–1886. doi: 10.1007/s12035-016-9785-6

Zhang, Z. G., Zhang, L., Tsang, W., Soltanian-Zadeh, H., Morris, D., Zhang, R., et al. (2002). Correlation of VEGF and angiopoietin expression with disruption of blood-brain barrier and angiogenesis after focal cerebral ischemia. *J. Cereb. Blood Flow Metab.* 22, 379–392. doi: 10.1097/00004647-200204000-00002

Zhao, C., Ma, J., Wang, Z., Li, H., Shen, H., Li, X., et al. (2020). Mfsd2a attenuates blood-brain barrier disruption after sub-arachnoid hemorrhage by inhibiting caveolae-mediated transcellular transport in rats. *Transl Stroke Res.* [Epub ahead of print]. doi: 10.1007/s12975-019-00775-y

Zhao, G., and Flavin, M. P. (2000). Differential sensitivity of rat hippocampal and cortical astrocytes to oxygen-glucose deprivation injury. *Neurosci. Lett.* 285, 177–180. doi: 10.1016/s0304-3940(00)01056-9

Zhou, M., and Kimelberg, H. K. (2001). Freshly isolated hippocampal CA1 astrocytes comprise two populations differing in glutamate transporter and AMPA receptor expression. *J. Neurosci.* 21, 7901–7908. doi: 10.1523/jneurosci.21-20-07901.2001

Zhu, J., Song, W., Li, L., and Fan, X. (2016). Endothelial nitric oxide synthase: a potential therapeutic target for cerebrovascular diseases. *Mol. Brain* 9:30.

Zhu, Y., Liao, H. L., Niu, X. L., Yuan, Y., Lin, T., Verna, L., et al. (2003). Low density lipoprotein induces eNOS translocation to membrane caveolae: the role of RhoA activation and stress fiber formation. *Biochim. Biophys. Acta* 1635, 117–126. doi: 10.1016/j.bbalip.2003.10.011

Zlokovic, B. V. (2008). The blood-brain barrier in health and chronic neurodegenerative disorders. *Neuron* 57, 178–201. doi: 10.1016/j.neuron.2008.01.003

Zlokovic, B. V. (2010). Neurodegeneration and the neurovascular unit. *Nat. Med.* 16, 1370–1371. doi: 10.1038/nm1210-1370

Zonta, M., Angulo, M. C., Gobbo, S., Rosengarten, B., Hossmann, K. A., Pozzan, T., et al. (2003). Neuron-to-astrocyte signaling is central to the dynamic control of brain microcirculation. *Nat. Neurosci.* 6, 43–50. doi: 10.1038/nn980

Conflict of Interest: The authors declare that the research was conducted in the absence of any commercial or financial relationships that could be construed as a potential conflict of interest.

frontiers in Cellular Neuroscience

ORIGINAL RESEARCH
published: 21 August 2020
doi: 10.3389/fncel.2020.00276

NLRP3 Is Involved in the Maintenance of Cerebral Pericytes

*Wenqiang Quan[1,2], Qinghua Luo[2], Qiqiang Tang[3], Tomomi Furihata[4], Dong Li[1], Klaus Fassbender[2] and Yang Liu[1,2]**

[1]Department of Clinical Laboratory, Tongji Hospital, Tongji University Medical School, Shanghai, China, [2]Department of Neurology, Saarland University, Homburg, Germany, [3]Department of Neurology, The First Affiliated Hospital of University of Science and Technology of China (Anhui Provincial Hospital), Hefei, China, [4]Department of Clinical Pharmacy and Experimental Therapeutics, School of Pharmacy, Tokyo University of Pharmacy and Life Sciences, Tokyo, Japan

Pericytes play a central role in regulating the structure and function of capillaries in the brain. However, molecular mechanisms that drive pericyte proliferation and differentiation are unclear. In our study, we immunostained NACHT, LRR and PYD domains-containing protein 3 (NLRP3)-deficient and wild-type littermate mice and observed that NLRP3 deficiency reduced platelet-derived growth factor receptor β (PDGFRβ)-positive pericytes and collagen type IV immunoreactive vasculature in the brain. In Western blot analysis, PDGFRβ and CD13 proteins in isolated cerebral microvessels from the NLRP3-deficient mouse brain were decreased. We further treated cultured pericytes with NLRP3 inhibitor, MCC950, and demonstrated that NLRP3 inhibition attenuated cell proliferation but did not induce apoptosis. NLRP3 inhibition also decreased protein levels of PDGFRβ and CD13 in cultured pericytes. On the contrary, treatments with IL-1β, the major product of NLRP3-contained inflammasome, increased protein levels of PDGFRβ, and CD13 in cultured cells. The alteration of PDGFRβ and CD13 protein levels were correlated with the phosphorylation of AKT. Inhibition of AKT reduced both protein markers and abolished the effect of IL-1β activation in cultured pericytes. Thus, NLRP3 activation might be essential to maintain pericytes in the healthy brain through phosphorylating AKT. The potential adverse effects on the cerebral vascular pericytes should be considered in clinical therapies with NLRP3 inhibitors.

Keywords: Alzheimer's disease, neuroinflammation, NLRP3, pericyte, cerebral perfusion

OPEN ACCESS

Edited by:
Fabrice Dabertrand, University of Colorado, United States

Reviewed by:
Kuniyuki Nakamura, Kyushu University, Japan
Albert L. Gonzales, University of Vermont, United States

****Correspondence:***
Yang Liu
a.liu@mx.uni-saarland.de

Specialty section:
This article was submitted to Non-Neuronal Cells, a section of the journal Frontiers in Cellular Neuroscience

Received: *17 May 2020*
Accepted: *05 August 2020*
Published: *21 August 2020*

Citation:
Quan W, Luo Q, Tang Q, Furihata T, Li D, Fassbender K and Liu Y (2020) NLRP3 Is Involved in the Maintenance of Cerebral Pericytes. Front. Cell. Neurosci. 14:276. doi: 10.3389/fncel.2020.00276

INTRODUCTION

Brain pericytes wrapping around endothelial cells regulate various functions in the brain, which include blood-brain barrier (BBB) permeability, angiogenesis, and capillary hemodynamic responses (Sweeney et al., 2016). Pericytes express platelet-derived growth factor receptor β (PDGFRβ) and CD13. The binding of PDGFRβ with endothelial cells-released platelet-derived growth factor (PDGF)-B is essential for pericyte proliferation and integration into the blood vessel (Lindahl et al., 1997). CD13 promotes angiogenesis in hypoxic tissues, and response to stimulation of angiogenic growth factors, such as vascular endothelial growth

Abbreviations: Aβ, amyloid β peptide; AD, Alzheimer's disease; APP, Alzheimer's precursor protein; BBB, blood-brain barrier; BDNF, brain-delivered neurotrophic factor; HBPC, human primary brain vascular pericytes; HBSS, Hanks' balanced salt solution; IL-1β, interleukin-1β; LPS, lipopolysaccharide; MyD88, myeloid differentiation primary response 88; NLRP, NACHT, LRR and PYD domains-containing protein; PCNA, proliferating cell nuclear antigen; PDGFRβ, platelet-derived growth factor receptor β; TLR, Toll-like receptor; TNF-α, tumor necrosis factor α.

factor, basic fibroblast growth factor, and transforming growth factor (Rangel et al., 2007). Deficiency of PDGFRβ decreases pericyte number, accumulates blood-derived fibrin/fibrinogen, reduces vasculature, and attenuates blood flow in the mouse brain, which finally leads to the white matter lesions characterized by loss of oligodendrocytes, demyelination, and axonal degeneration (Montagne et al., 2018). Growing evidence suggests that pericyte impairment mediates vascular dysfunction and contributes to the pathogenesis of Alzheimer's disease (AD; Love and Miners, 2016). In the AD human brain, pericytes are lost in association with increased BBB permeability at a very early disease stage (Sengillo et al., 2013; Nation et al., 2019). In AD mouse models that overexpress Alzheimer's precursor protein (APP) in neurons, the deletion of pericytes increases deposition of amyloid β peptide (Aβ) in both brain parenchyma and blood vessels, which potentially exaggerates cognitive deficits (Sagare et al., 2013). However, molecular mechanisms that regulate pericyte survival and activation in the brain are largely unknown.

Pericytes express pattern recognition receptors, such as Toll-like receptor 2 and 4 (TLR-2 and -4) and NACHT, LRR and PYD domains-containing protein 1 and 3 (NLRP-1 and -3; Guijarro-Muñoz et al., 2014; Leaf et al., 2017; Nyúl-Tóth et al., 2017). Cultured brain pericytes release cytokines and chemokines after being challenged with lipopolysaccharide (LPS), tumor necrosis factor (TNF)-α or *E. coli* infection (Kovac et al., 2011; Guijarro-Muñoz et al., 2014; Nyúl-Tóth et al., 2017). Cultured pericytes secret active interleukin (IL)-1β when they are intracellularly stimulated with LPS, although how NLRP3-contained inflammasome is activated remains unclear (Nyúl-Tóth et al., 2017). It is interesting to ask whether innate immune signaling regulates cell fate and functions of pericytes in the brain.

In AD research, NLRP3-contained inflammasome attracted great attention, as it is activated in AD brain and potentially mediates microglial inflammatory responses, exaggerates Aβ and Tau protein aggregation in APP or Tau-transgenic mice (Heneka et al., 2013; Venegas et al., 2017; Ising et al., 2019; Stancu et al., 2019). NLRP3 is considered as a promising therapeutic target for AD patients (Dempsey et al., 2017). However, the effects of NLRP3 activation on pericytes and vascular dysfunction were not addressed. The animal models used in published studies have also limited AD-associated vascular pathology. Thus, whether NLRP3 inhibition protects or damages microvascular circulation in the AD brain remains unclear. Moreover, AD pathology is mainly localized in temporal and parietal lobes, instead of covering the whole brain. Between AD lesion sites as shown with Aβ deposits, neurofibrillary tangles, and gliosis, the brain tissues are relatively or absolutely healthy (Deture and Dickson, 2019). It is, therefore, necessary to understand the physiological function of NLRP3 in brain pericytes, which is helpful to predict potential off-target effects of NLRP3 inhibitors in the future anti-AD therapies.

In this study, we used NLRP3-knockout mice and treated cultured pericytes with NLRP3 inhibitor, MCC950, or IL-1β, a major product of NLRP3-contained inflammasome. We observed that NLRP3 might be essential for the maintenance of healthy pericytes in the brain. We further observed that AKT (also known as protein kinase B) might mediate the physiological function of NLRP3 in pericytes.

MATERIALS AND METHODS

Mice

NLRP3-encoding gene knockout (NLRP3$^{-/-}$) mice were kindly provided by N. Fasel (University of Lausanne, Lausanne, Switzerland; Martinon et al., 2006). Mice with the knockout of gene encoding myeloid differentiation primary response 88 (MyD88$^{-/-}$) were originally provided by S. Akira and K. Takeda (Osaka University, Osaka, Japan; Adachi et al., 1998). Breeding between heterozygous mutants (+/−) on a C57BL/6 background was used to maintain mouse colonies. Mice were compared only between littermates. Animal experiments were performed following all relevant national rules and were authorized by the local research ethics committee.

Tissue Collection and Isolation of Blood Vessels

Animals were euthanized by inhalation of isoflurane and perfused with ice-cold phosphate-buffered saline. The brain was removed and divided. The left hemisphere was immediately fixed in 4% paraformaldehyde (Sigma-Aldrich Chemie GmbH, Taufkirchen, Germany) for immunohistochemistry. The cortex and hippocampus from the right hemisphere were carefully dissected and brain vessel fragments were isolated according to the published protocol (Boulay et al., 2015). Briefly, brain tissues were homogenized in HEPES-contained Hanks' balanced salt solution (HBSS) and centrifuged at 4,400 *g* in HEPES-HBSS buffer supplemented with dextran from Leuconostoc spp. (molecular weight ∼70,000; Sigma-Aldrich) to delete myelin. The vessel pellet was re-suspended in HEPES-HBSS buffer supplemented with 1% bovine serum albumin (Sigma-Aldrich) and filtered with 20 μm-mesh. The blood vessel fragments were collected on the top of the filter for biochemical analysis and stored at −80°C for biochemical analysis.

Histological Analysis

To analyze pericytes in capillaries, serial 30-μm-thick sagittal sections were cut from the dehydrated and cryoembedded left brain hemisphere with a Leica cryostat (Leica Mikrosysteme Vertrieb, Wetzlar, Germany). Three sections per mouse with 300 μm of an interval between neighboring layers were used. Antigen retrieval was performed by heating sections in 10 μM citrate buffer (pH = 6). After blocking with 5% goat serum in PBS/0.3% Triton X-100, brain sections were incubated with rabbit anti-PDGFRβ monoclonal antibody (clone: 28E1; Cell Signaling Technology Europe, Frankfurt am Main, Germany) at 4°C overnight and then Alexa488-conjugated goat anti-rabbit IgG (Thermo Fisher Scientific, Darmstadt, Germany) at room temperature for 1 h. Thereafter, brain sections were further stained with biotin-labeled *Griffonia simplicifolia* Lectin I isolectin B4 (Catalog: B-1205; Vector Laboratories, Burlingame, CA, USA) and Cy3-conjugated streptavidin (Roche Applied Science, Mannheim, Germany). The whole cortex was imaged under a Zeiss AxioImager.Z2 microscope (Carl

Zeiss Microscopy GmbH, Göttingen, Germany) equipped with a Stereo Investigator system (MBF Bioscience, Williston, VT, USA). Ten regions per section were randomly chosen under a 40× objective. Blood vessels with <6 μm of diameter were examined. Fluorescence-labeled areas were measured with ImageJ software[1]. The coverage of pericytes was calculated as a ratio of PDGFRβ/isolectin B4-positive staining area.

To detect the expression of NLRP3 in pericytes, brain sections were incubated at 4°C overnight with mouse anti-NLRP3 monoclonal antibody (clone: Cryo-2; AdipoGen Life Sciences, San Diego, CA, USA), which was followed by incubation with Cy3-conjugated goat anti-mouse IgG (Jackson ImmunoResearch Europe Ltd., Cambridgeshire, UK) at room temperature for 1 h. Thereafter, brain sections were further stained with rabbit anti-PDGFRβ monoclonal antibody and Alexa488-conjugated goat anti-rabbit IgG as described above. Stack images were acquired with a Zeiss AxioImager.Z2 microscope under a 63× oil objective with an interval of 0.2 μm between neighboring layers, processed with deconvolution and finally Z-projected with maximum intensity.

For analysis of the impairment of BBB in NLRP3-deficient mice, brain sections from NLRP3 - knockout and wild-type mice were stained with Alexa488-conjugated goat anti-mouse IgG (Thermo Fisher Scientific) after blocking with goat serum as we did in a previous study (Hao et al., 2011), and co-stained with biotinylated isolectin B4 and Cy3-conjugated streptavidin.

To quantify vasculature in the brain, our established protocol was used (Decker et al., 2018). The left hemisphere was embedded in paraffin and 40-μm-thick sagittal sections were serially cut. Four serial sections per mouse with 400 μm of distance in between were deparaffinized, heated at 80°C in citrate buffer (10 mM, pH = 6) for 1 h, and digested with Digest-All 3 (Pepsin; Thermo Fisher Scientific) for 20 min. Thereafter, brain sections were stained with rabbit anti-collagen IV polyclonal antibody (Catalog: #ab6586; Abcam, Cambridge, UK) and Alexa488-conjugated goat anti-rabbit IgG (Thermo Fisher Scientific). After being mounted, the whole brain including the hippocampus and cortex was imaged with Microlucida (MBF Bioscience). The length and branching points of collagen type IV staining-positive blood vessels were analyzed with free software, AngioTool[2] (Zudaire et al., 2011). The parameters of analysis for all compared samples were kept constant. The length and branching points were adjusted with an area of interest.

Western Blot Analysis

Isolated blood vessels were lysed in RIPA buffer [50 mM Tris (pH 8.0), 150 mM NaCl, 0.1% SDS, 0.5% sodium deoxycholate, 1% NP-40, and 5 mM EDTA] supplemented with protease inhibitor cocktail (Roche Applied Science) on ice. The tissue lysate was sonicated before being loaded onto 10% SDS-PAGE. For Western blot detection, rabbit monoclonal antibodies against PDGFRβ and CD13/APN (clone: 28E1 and D6V1W, respectively; Cell Signaling Technology Europe) were used. In the same sample, β-actin was detected as a loading control using a rabbit monoclonal antibody (clone: 13E5; Cell Signaling Technology Europe). Western blots were visualized *via* the ECL method (PerkinElmer LAS GmbH, Rodgau, Germany). Densitometric analysis of band densities was performed with ImageJ software. For each sample, the protein level was calculated as a ratio of target protein/β-actin.

Culture of Pericytes

Human primary brain vascular pericytes (HBPC) were immortalized by infecting cells with tsSV40T lentiviral particles (Umehara et al., 2018). The selected immortalized HBPC clone 37 (hereafter referred to as HBPC/ci37) was used for our study. HBPC/ci37 cells were cultured at 33°C with 5% CO_2/95% air in pericyte medium (Catalog: #1201; Sciencell Research Laboratories, Carlsbad, CA, USA) containing 2% (v/v) fetal bovine serum, 1% (w/v) pericyte growth factors, and penicillin-streptomycin. Culture flasks and plates were treated with Collagen Coating Solution (Catalog: #125-50; Sigma-Aldrich). HBPC/ci37 cells were used at 40–60 passages in this study.

Analysis of Pericyte Proliferation and Apoptosis

Pericytes were seeded at 1.0×10^4 cells on 96-well plate/100 μl (day 0), and cultured in pericyte medium containing NLRP3 inhibitor, MCC950 (Catalog: #PZ0280; Sigma-Aldrich), at 0, 25, 50 and 100 nM, or containing recombinant human IL-1β (Catalog: #201-LB; R&D Systems, Wiesbaden, Germany) at 0, 5, 10 and 50 ng/ml. The cell survival was detected with MTT-based Cell Proliferation Kit I (Catalog: #11465007001; Sigma-Aldrich) on days 1, 2, 3, 4, 5, 6 and 7. In MTT assay, yellow and water-soluble 3-(4,5-dimethylthiazol-2-yl)-2,5-diphenyl tetrazolium bromide (MTT) enters viable cells and passes into the mitochondria where it is reduced by succinate dehydrogenase to an insoluble, dark purple formazan product. The measured absorbance as shown with optical density (OD) at 590 nm is proportional to the number of viable cells.

To further detect cell death and proliferation of pericytes, cells were cultured in 12-well plate at 5.0×10^5 cells/well, and treated with MCC950 as described in MTT assay. After 24 h, pericytes were collected and lysed in RIPA buffer. Quantitative Western blot was used with rabbit monoclonal antibody against cleaved caspase-3 (clone: 5A1E; Cell Signaling Technology Europe), mouse monoclonal antibody against proliferating cell nuclear antigen (PCNA; clone: PC10; Cell Signaling Technology Europe) and rabbit monoclonal antibody against Ki-67 (clone: SP6; Abcam). α-tubulin and β-actin were detected as internal control with mouse monoclonal antibody (clone: DM1A; Abcam) and rabbit monoclonal antibody (clone: 13E5; Cell Signaling Technology Europe), respectively.

In this experiment, we also detected NLRP3 and cleaved caspase-1 in the cell lysate from pericytes with and without treatment of MCC950, with rabbit monoclonal antibodies against NLRP3 and cleaved caspase-1 (Asp297; clone D4D8T and D57A2; Cell Signaling Technology Europe), respectively.

[1]https://imagej.nih.gov/ij/

[2]https://ccrod.cancer.gov/confluence/display/ROB2/

Treatments of Pericytes for Detection of PDGFRβ and CD13 and Phosphorylated Kinases

Pericytes were cultured in a 12-well plate at 5.0×10^5 cells/well. Before experiments, we replaced the culture medium with serum-free pericyte medium and cultured cells at 37°C for 3 days to facilitate cell differentiation (Umehara et al., 2018). Thereafter, pericytes were treated for 24 h with MCC950, at 0, 25, 50 and 100 nM, recombinant human IL-1β (Catalog: #201-LB; R&D Systems) at 0, 5, 10 and 50 ng/ml, or AKT Inhibitor VIII (Catalog: #124018; Sigma-Aldrich) at 0, 0.5, 1 and 5 μM. To investigate whether AKT mediates the effect of IL-1β, pericytes were pre-treated with 1 μM AKT inhibitor VIII for 1 h and then incubated with IL-1β at various concentrations in the presence of AKT inhibitor for 24 h. The cell lysate was prepared in RIPA buffer supplemented with protease inhibitor cocktail (Roche Applied Science) and phosphatase inhibitors (50 nM okadaic acid, 5 mM sodium pyrophosphate, and 50 mM NaF; Sigma-Aldrich). For quantitative Western blot, the following antibodies were used: rabbit monoclonal antibodies against PDGFRβ, CD13/APN, phosphorylated AKT (Ser473), phosphorylated ERK1/2 (Thr202/Tyr204), phosphorylated NFκB p65 (S536), NFκB p65, β-actin, GAPDH (clone: 28E1, D6V1W, D9E, D13.14.4E, 93H1, D14E12, 13E5, and 14C10, respectively; Cell Signaling Technology Europe), rabbit polyclonal antibodies against AKT and phosphorylated GSK-3β (Ser9; Catalog: #9272 and Catalog: #9336, respectively; Cell Signaling Technology Europe) and mouse monoclonal antibodies against ERK1/2 and GSK-3β (clone: L34F12 and 3D10, respectively; Cell Signaling Technology Europe) and α-tubulin (clone: DM1A; Abcam).

Statistics

Data were presented as mean ± SEM for mice and mean ± SD for cells. For multiple comparisons, one-way or two-way ANOVA followed by Bonferroni or Tukey *post hoc* test. Two independent-samples Students *t*-test was used to compare means for two groups of cases. All statistical analyses were performed with GraphPad Prism 5 version 5.01 for Windows (GraphPad Software, San Diego, CA, USA). Statistical significance was set at $p < 0.05$.

RESULTS

NLRP3 Deficiency Reduces Pericyte Cell Coverage and Decreases Protein Levels of PDGFRβ and CD13 in the Brain

To explore the effects of NLRP3 on the maintenance of pericytes in the brain, we first detected the expression of NLRP3 in pericytes. In brain sections, we observed widely distributed NLRP3-immune reactive cell bodies and processes, part of which were co-stained by PDGFRβ-specific antibodies (**Figure 1A**), which suggests that pericytes express NLRP3. Then, we estimated the coverage of PDGFRβ-positive cells in brains from 9-month-old NLRP3-knockout ($NLRP3^{-/-}$ and $NLRP3^{+/-}$) and wild-type ($NLRP3^{+/+}$) littermate mice. As shown in **Figures 1B,C**, deficiency of NLRP3 significantly decreased the coverage of PDGFRβ-immune reactive cells in microvessels with < 6 μm of diameter in a gene dose-dependent manner as compared with that in NLRP3-wildtype mice (one-way ANOVA, $p < 0.05$; $n = 4$ per group). We continued to isolate blood vessels from brains of 9-month-old $NLRP3^{-/-}$, $NLRP3^{+/-}$ and $NLRP3^{+/+}$ littermate mice for the detection of pericyte protein markers, PDGFRβ, and CD13. We observed that the deletion of NLRP3 significantly reduced PDGFRβ and CD13 proteins in the cerebral blood vessels also in a gene dose-dependent manner (**Figures 1D,E**; one-way ANOVA, $p < 0.05$; $n \geq 7$ per group). Unfortunately, we failed to detect cleaved caspase-3 and PCNA in the tissue lysate of blood vessels (data not shown), which are markers for cell apoptosis and cell proliferation, respectively.

In further experiments, we asked whether innate immune signaling serves a common effect on pericyte survival in the brain. We detected PDGFRβ and CD13 proteins in cerebral blood vessels isolated from 6-month-old $MyD88^{-/-}$, $MyD88^{+/-}$ and $MyD88^{+/+}$ littermate mice. MyD88 is a common adaptor down-stream to most TLRs and mediates the inflammatory activation of IL-1β (O'Neill and Bowie, 2007). We observed that protein levels of CD13 and PDGFRβ were significantly lower in MyD88-deficient mice than in MyD88-wildtype controls (**Figures 1F,G**; one-way ANOVA, $p < 0.05$; $n \geq 6$ per group).

NLRP3 Deficiency Reduces Vasculature in the Brain

Pericytes are essential for the development of cerebral circulation. Dysfunction of pericytes reduces vasculature and increases the permeability of BBB (Sweeney et al., 2016; Montagne et al., 2018). We asked whether NLRP3 deficiency affects the structure of cerebral blood vessels. We observed that, in 9-month-old mouse brains, deficiency of NLRP3 significantly reduced the total length and branching points of collagen type IV-positive blood vessels (**Figures 2A–C**; one-way ANOVA, $p < 0.05$; $n \geq 6$ per group). The reduction of brain vasculature was dependent on the copies of the NLRP3-encoding gene. However, we did not detect IgG leakage into the brain parenchyma, which suggested that the intactness of BBB in NLRP3-deficient mice was not severely damaged (see **Figure 2D**).

NLRP3 Inhibition Attenuates Cell Proliferation in Cultured Pericytes

After we observed that NLRP3 deficiency decreased the number of pericytes in the brain, we continued to investigate whether NLRP3 directly regulates the proliferation and death of pericytes. We detected NLRP3 proteins in our cultured pericytes with different passaging numbers (**Figure 3A**). We also detected cleaved caspase-1 in pericytes, with the remarked reduction of proteins after cells were treated with NLRP3 inhibitor, MCC950 (**Figure 3B**). Thus, the NLRP3-caspase-1 signaling pathway is active in pericytes and potentially regulates the cellular function. Activated caspase-1 cleaves pro-IL-1β into active IL-1β

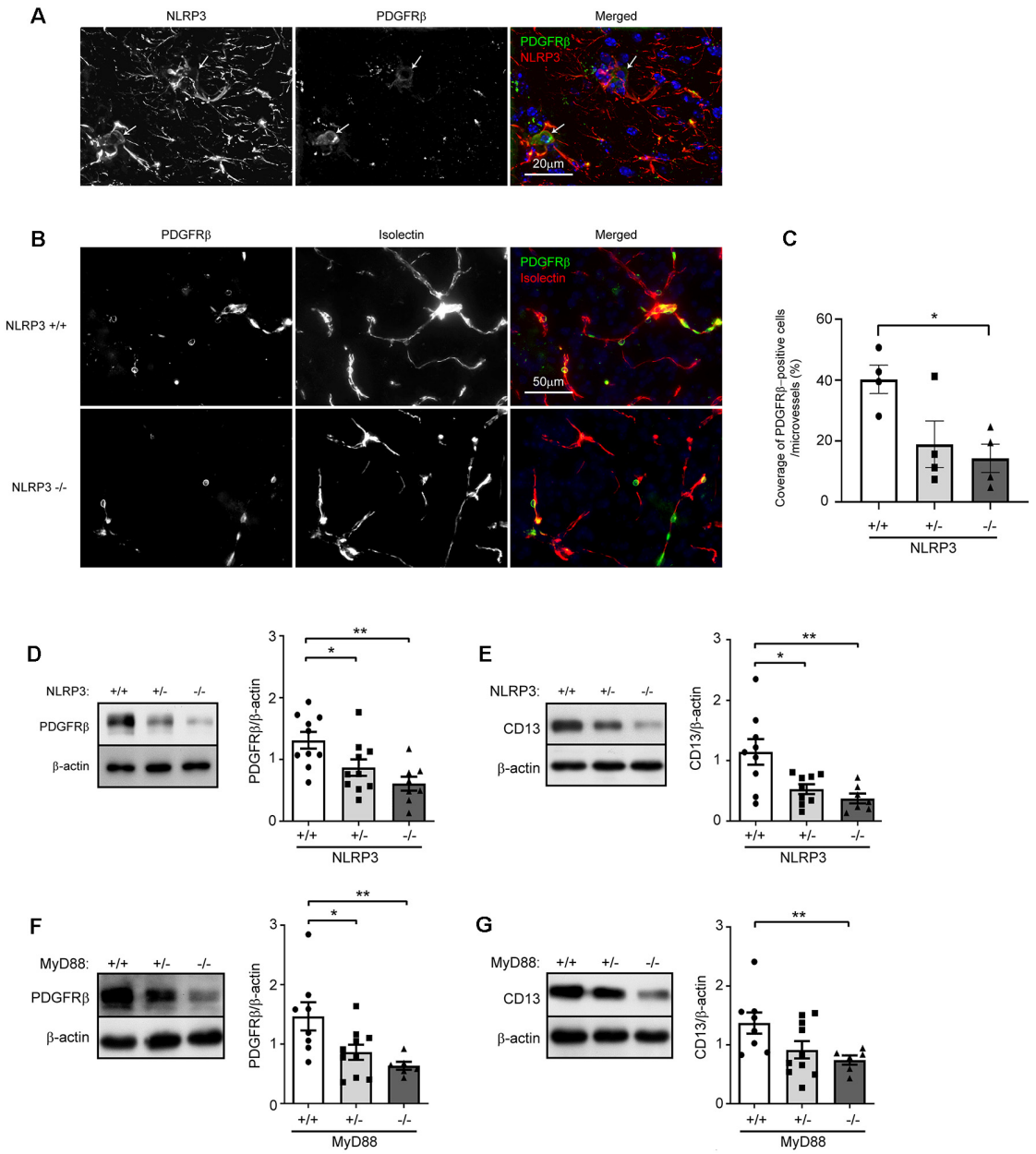

FIGURE 1 | NLRP3 deficiency reduces pericyte cell coverage and decreases protein levels of PDGFRβ and CD13 in the brain. **(A)** Nine-month-old mouse brains were co-stained for NLRP3 and PDGFRβ. PDGFRβ-immune reactive cell bodies (in green; marked with arrows) were stained by NLRP3-specific antibodies (in red). **(B)** Brain tissues from 9-month-old NLRP3-knockout (−/− and +/−) and wild-type (+/+) littermate mice were then co-stained for PDGFRβ (with anti-PDGFRβ antibodies, in green) and endothelial cells (with isolectin B4, in red). **(C)** The coverage of PDGFRβ-positive pericytes was calculated as a ratio of PDGFRβ/isolectin B4-positive area. One-way ANOVA followed by Tukey *post hoc* test, $n = 4$ per group. **(D–G)** Nine-month-old NLRP3, and 6-month-old MyD88 littermate mice with homozygous (−/−) and heterozygous (+/−) knockout, and wild-type (+/+) of *nlrp3* and *myd88* genes, respectively, were analyzed for protein levels of PDGFRβ and CD13 in isolated cerebral blood vessels. One-way ANOVA followed by Bonferroni *post hoc* test, $n = 10$, 10 and 8 for NLRP3 (+/+, +/− and −/−) mice in PDGFRβ detection and $n = 9$, 9 and 7 for NLRP3 (+/+, +/− and −/−) mice in CD13 detection; $n = 8$, 10 and 6 for MyD88 (+/+, +/− and −/−) mice in the detection of both PDGFRβ and CD13. *$p < 0.05$ and **$p < 0.01$.

(Gross et al., 2011). However, we were not able to show that NLRP3 inhibition reduced IL-1β secretion as the IL-1β release from non-activated pericytes was undetectable (data are not shown).

Then, we investigated whether NLRP3 regulates pericyte proliferation. After treating cultured pericytes with MCC950 at different concentrations, we observed that NLRP3 inhibition significantly reduced the conversion of MTT into its colorful

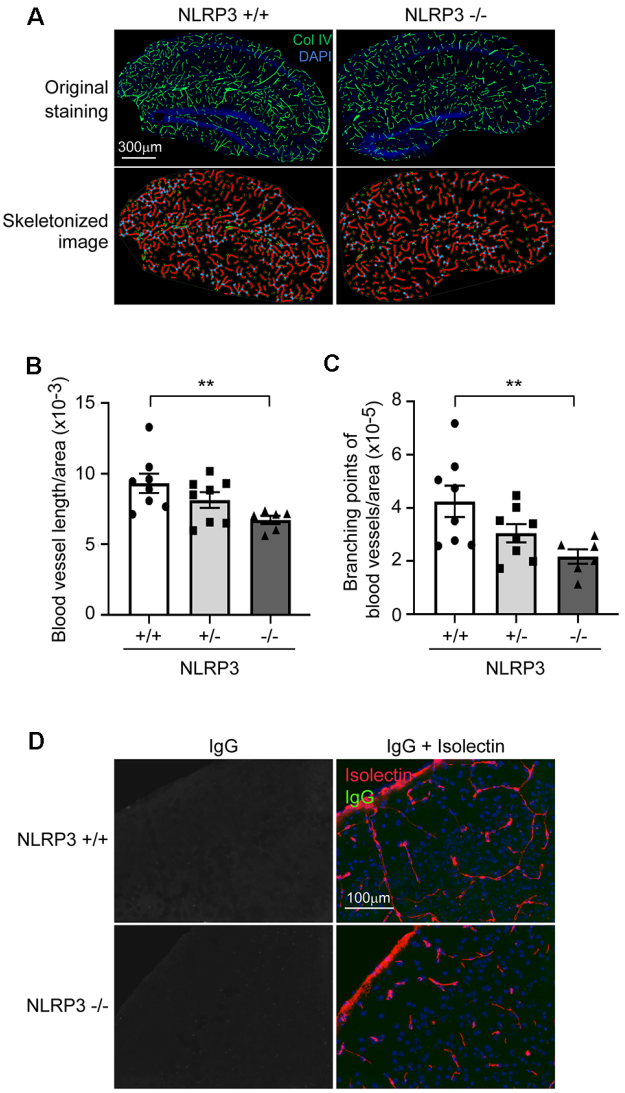

FIGURE 2 | NLRP3 deficiency reduces vasculature in the brain. **(A)** The brains of 9-month-old littermate mice with homozygous (−/−), heterozygous (+/−), and wild-type (+/+) of *nlrp3* gene were stained for collagen type IV (Col IV). The blood vessels in the hippocampus were thresholded and skeletonized. The skeleton representation of vasculature is shown in red and branching points of blood vessels are in blue. **(B,C)** The total length and branching points of blood vessels were calculated and adjusted by area of analysis. One-way ANOVA followed by Bonferroni *post hoc* test, $n = 8$, 8, and 6 for NLRP3 (+/+, +/− and −/−) mice, respectively. $^{**}p < 0.01$. **(D)** Nine-month-old NLRP3-deficient and wild-type mouse brains were further stained for mouse IgG and isolectin B4. We could not detect mouse IgG in the brain parenchyma.

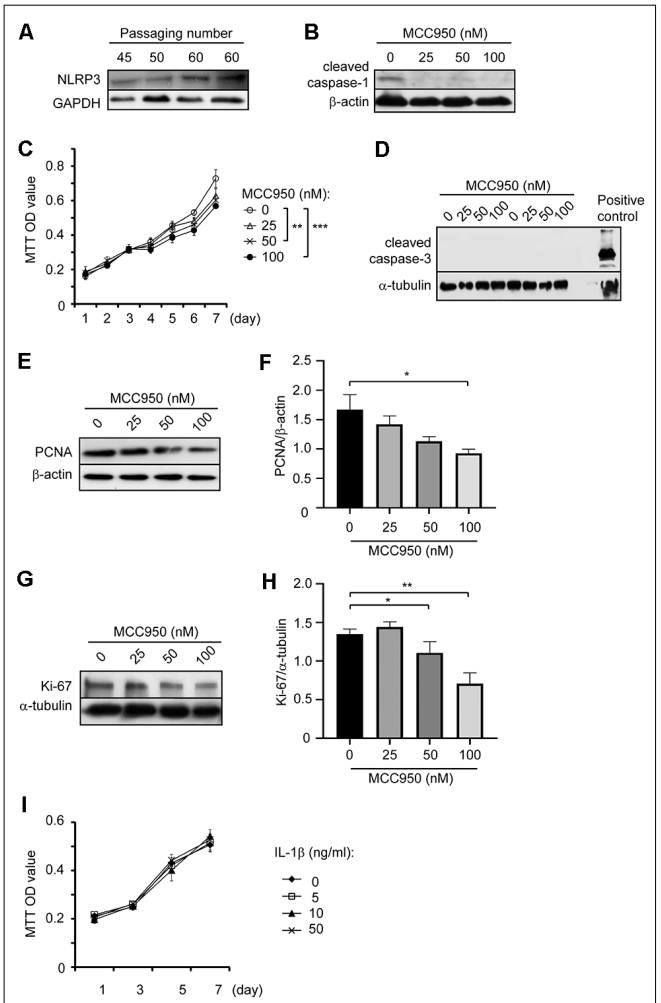

FIGURE 3 | NLRP3 inhibition attenuates cell proliferation in cultured pericytes. **(A)** The cell lysates collected from cultured pericytes with different passaging numbers were detected for NLRP3 with Western blot. **(B)** Pericytes were treated with NLRP3 inhibitor, MCC950, at 0, 25, 50, and 100 nM for 24 h and then detected for cleaved caspase-1. After inhibition of NLRP3, cleaved caspase-1 was nearly undetectable. **(C)** Cultured pericytes were treated with MCC950 with various doses and analyzed for proliferation with MTT assay every day for 7 days. Two-way ANOVA followed by Tukey *post hoc* test, $n = 4$ per group. $^{**}p < 0.01$ and $^{***}p < 0.001$. **(D–H)** Pericytes were cultured and treated with MCC950 at indicated concentrations for 24 h. Cell lysates were detected for cleaved caspase-3, PCNA, and Ki-67 with a quantitative Western blot. As a positive control for cleavage of caspase-3, the brain lysate from neuronal ATG5-deficient mice was used. The result in **(D)** shows one experiment representative of four independent experiments. The inhibition of NLRP3 reduces protein levels of PCNA and Ki-67 in a dose-dependent manner. One-way ANOVA followed by Tukey *post hoc* test, $n = 3$ per group for PCNA, and $n = 4$ per group for Ki-67. $^{*}p < 0.05$ and $^{**}p < 0.01$. **(I)** cultured pericytes were further treated with recombinant IL-1β at 0, 5, 10, and 50 ng/ml and analyzed with MTT assay every 2 days for 7 days. Two-way ANOVA analysis did not show the effects of IL-1β on cell proliferation, $n = 3$ per group.

product, formazan, in a dose-dependent manner (**Figure 3C**; two-way ANOVA, $p < 0.05$; $n = 4$ per group). The amount of formazan as shown with OD values is proportional to the number of viable cells. In further experiments, we detected no cleavage of caspase-3 in MCC950-treated cells (**Figure 3D**), while MCC950 treatments significantly decreased protein levels of both PCNA (**Figures 3E,F**; one-way ANOVA, $p < 0.05$; $n = 3$ per group) and Ki-67 (**Figures 3G,H**; one-way ANOVA, $p < 0.05$; $n = 4$ per group), which are two typical protein markers for cell proliferation. Thus, inhibition of NLRP3 suppresses the proliferation of pericytes.

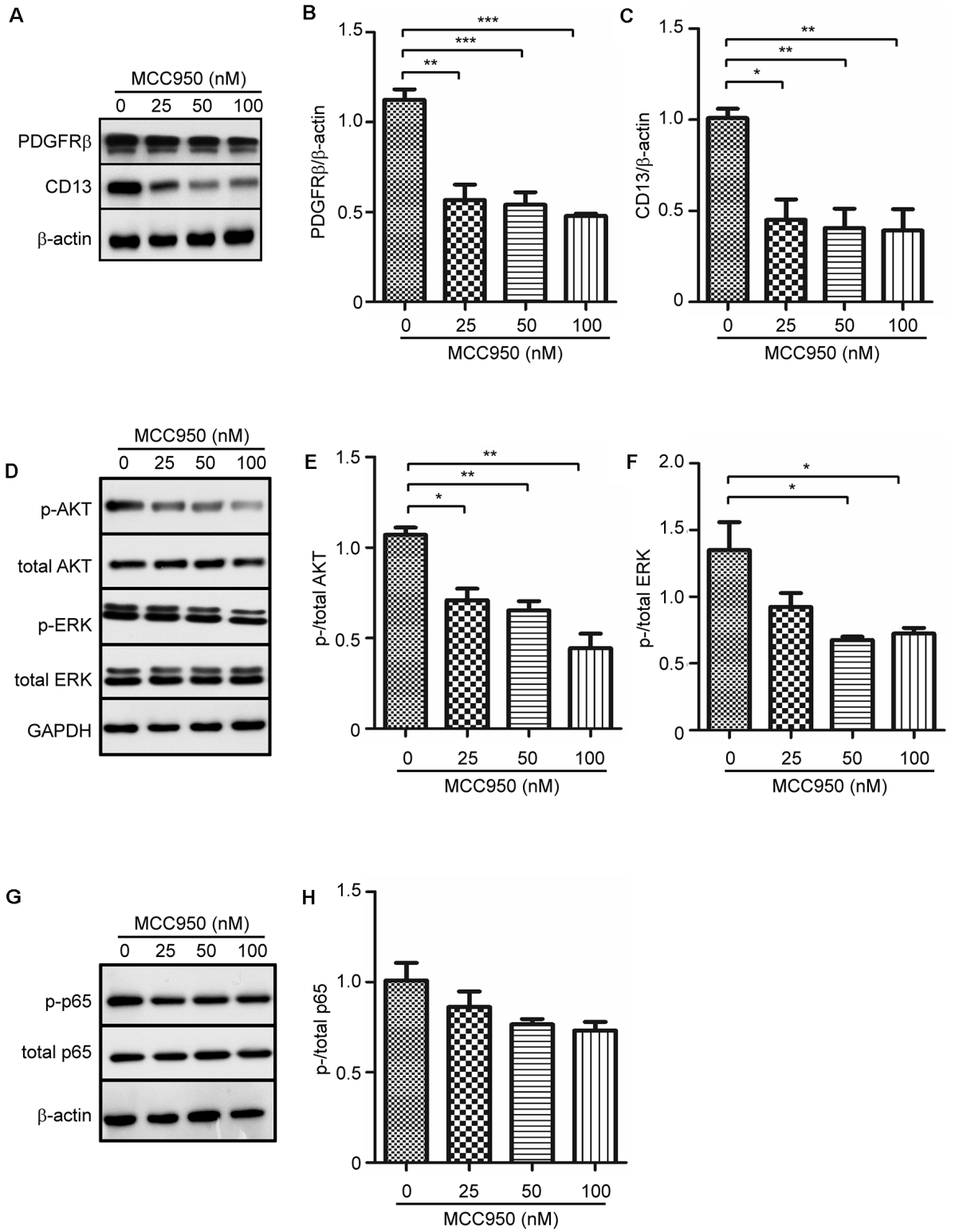

FIGURE 4 | NLRP3 inhibition attenuates protein expression of PDGFRβ and CD13 and inhibits phosphorylation of AKT and ERK in cultured pericytes. Pericytes were cultured and treated with MCC950 at 0, 25, 50, and 100 nM for 24 h. **(A,D,G)** Western blot was used to detect PDGFRβ and CD13, as well as phosphorylated and total protein levels of AKT, ERK, and NFκB p65. **(B,C,E,F)** Inhibition of NLRP3 reduces protein levels of PDGFRβ and CD13 and inhibits phosphorylation of AKT and ERK with a dose-dependent pattern. one-way ANOVA followed by Tukey *post hoc* test, $n = 4$ per group. $^{*}p < 0.05$, $^{**}p < 0.01$ and $^{***}p < 0.001$. **(H)** Phosphorylation of NFκB p65 is not significantly changed by inhibition of NLRP3. One-way ANOVA, $n = 3$ per group.

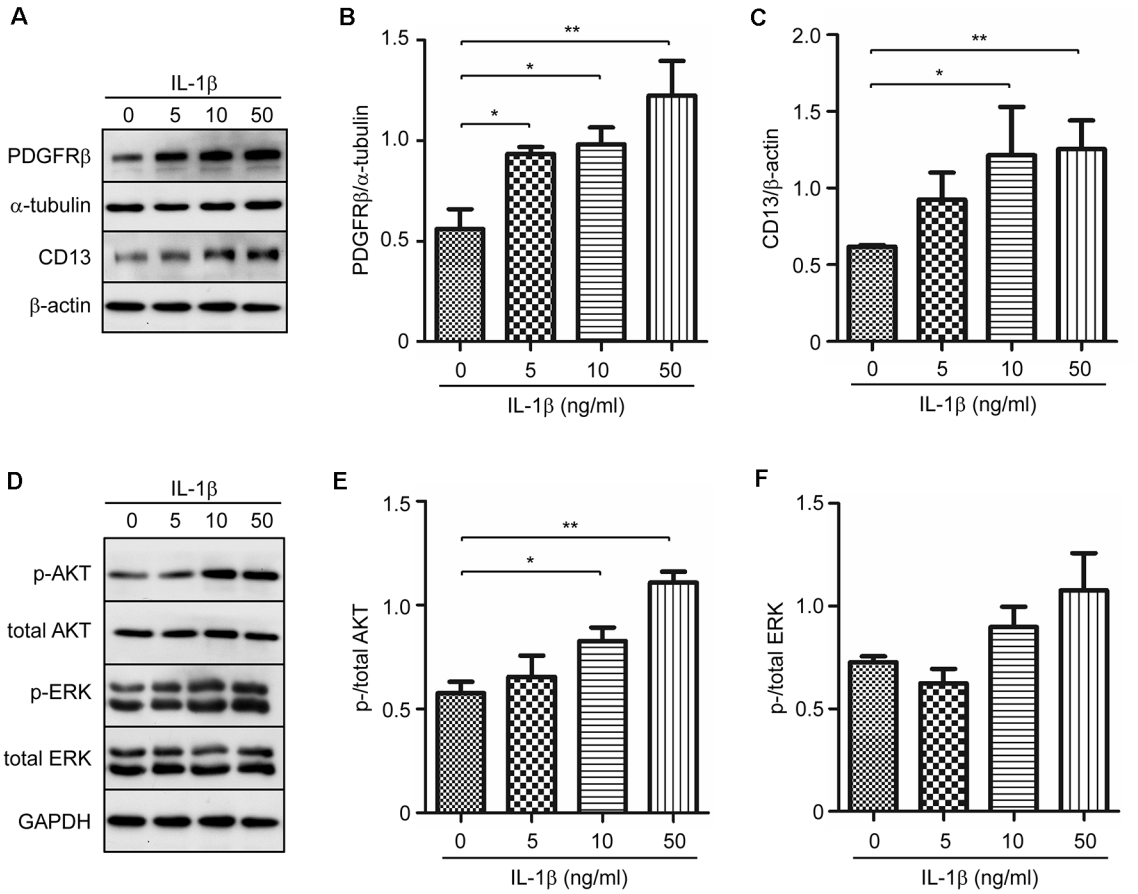

FIGURE 5 | IL-1β increases protein expression of PDGFRβ and CD13 in cultured pericytes. Pericytes were cultured and treated with recombinant human IL-1β at 0, 5, 10, and 50 ng/ml for 24 h. **(A,D)** Western blot was used to detect PDGFRβ and CD13, as well as phosphorylated and total protein levels of AKT and ERK. **(B,C,E,F)** Stimulation of IL-1β increases protein levels of PDGFRβ and CD13, and activates phosphorylation of AKT, but not ERK, in a dose-dependent manner. One-way ANOVA followed by Tukey *post hoc* test, $n = 3$ per group. $^{*}p < 0.05$ and $^{**}p < 0.01$.

In additional experiments, we treated cultured pericytes with recombinant IL-1β cytokine. IL-1β at 5, 10 and 50 ng/ml did not alter the cell proliferation as measured with MTT assay (**Figure 3I**; $n = 3$ per group).

NLRP3 Inhibition Attenuates the Expression of PDGFRβ and CD13 in Cultured Pericytes

PDGFRβ and CD13 are two protein markers of pericytes in the brain, which mediate the physiological and pathophysiological functions of pericytes (Lindahl et al., 1997; Rangel et al., 2007). We observed that treatments with MCC950 inhibited expression of PDGFRβ and CD13 in pericytes in a dose-dependent manner (**Figures 4A–C**; one-way ANOVA, $p < 0.05$; $n = 4$ per group). To analyze underlying mechanisms, through which NLRP3 drives pericyte differentiation, we detected phosphorylation of AKT, ERK, and NF-κB in MCC950-treated cells. Activation of AKT and ERK is involved in pericyte proliferation and migration (Bonacchi et al., 2001; Yao et al., 2014). We observed that inhibition of NLRP3 reduced the protein levels of both phosphorylated AKT and ERK in a dose-dependent manner (**Figures 4D–F**; one-way ANOVA, $p < 0.05$; $n = 4$ per group). However, phosphorylation of NF-κB in pericytes was not significantly altered by treatments with MCC950 (**Figures 4G,H**; one-way ANOVA, $p = 0.094$; $n = 3$ per group).

IL-1β Increases the Expression of PDGFRβ and CD13 in Cultured Pericytes

Although IL-1β did not increase pericyte proliferation (**Figure 3I**), we hypothesized that IL-1β might affect the differentiation of pericytes. We treated cultured pericytes with IL-1β at different concentrations. IL-1β did increase the protein expression of PDGFRβ and CD13 also with a concentration-dependent pattern (**Figures 5A–C**; one-way ANOVA, $p < 0.05$; $n = 3$ per group). As potential mechanisms mediating effects of IL-1β activation, we observed that IL-1β treatments significantly increased phosphorylation of AKT but not of ERK (**Figures 5D–F**; one-way ANOVA, $p < 0.05$; $n = 3$ per group).

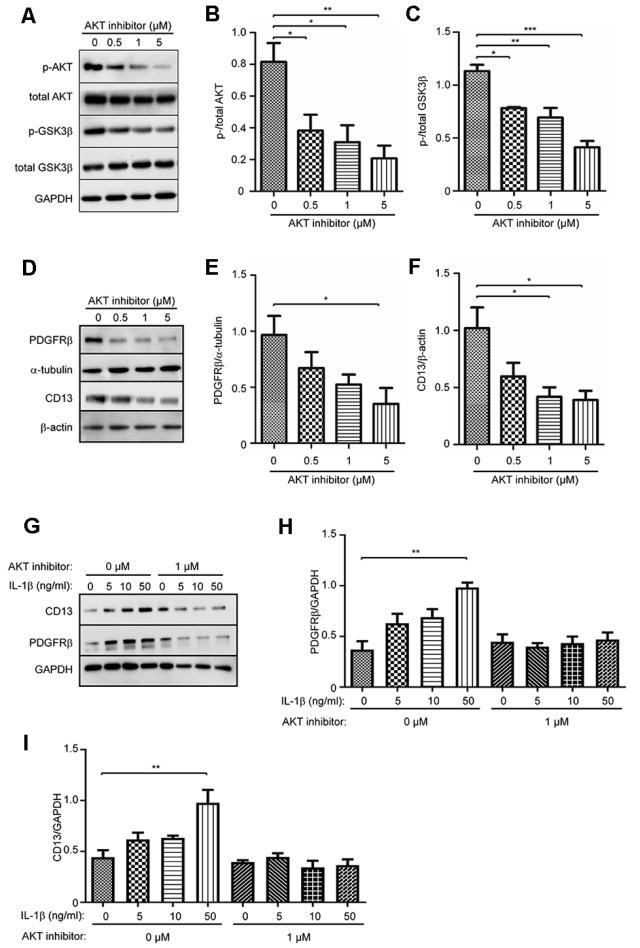

FIGURE 6 | Inhibition of AKT signaling pathway suppresses protein expression of PDGFRβ and CD13 and abolishes the effect of IL-1β in cultured pericytes. Pericytes were cultured and treated with AKT inhibitor at 0, 0.5, 1, and 5 μM for 24 h. **(A–C)** Western blot was used to detect phosphorylated and total AKT, and GSK3β, which shows that phosphorylation of both AKT and GSK3β was significantly inhibited by treatments with AKT inhibitors. One-way ANOVA followed by Tukey *post hoc* test, $n = 4$ per group. **(D–F)** The cell lysate from AKT inhibitor-treated pericytes were detected for protein levels of PDGFRβ and CD13 with a quantitative Western blot. The inhibition of AKT decreases protein levels of PDGFRβ and CD13 in a dose-dependent manner. One-way ANOVA followed by Tukey *post hoc* test, $n = 3$ per group. $^{*}p < 0.05$, $^{**}p < 0.01$ and $^{***}p < 0.001$. **(G–I)** Cultured pericytes were pre-treated with 1 μM AKT inhibitor and then incubated with IL-1β at 0, 5, 10, and 50 ng/ml, in the presence of AKT inhibitor for 24 h. AKT inhibition abolished the effect of IL-1β on the up-regulation of PDGFRβ and CD13 expression. one-way ANOVA followed by Tukey *post hoc* test, $n = 3$ per group. $^{**}p < 0.01$.

Inhibition of AKT Suppresses Expression of PDGFRβ and CD13 in Cultured Pericytes

As activation of AKT in pericytes was suppressed by NLRP3 inhibition but enhanced upon IL-1β activation, we supposed that AKT signaling plays a key role in the differentiation of pericytes. We treated pericytes with AKT inhibitors at 0, 0.5, 1, and 5 μM. Phosphorylation of AKT and phosphorylation of GSK3β, a kinase down-stream to AKT, were both reduced (**Figures 6A–C**; one-way ANOVA, $p < 0.05$; $n = 4$ per group), which verified the successful inhibition of AKT signaling. With such an inhibition, expression of both PDGFRβ and CD13 was significantly down-regulated in a dose-dependent manner (**Figures 6D–F**; one-way ANOVA, $p < 0.05$; $n = 3$ per group).

In the following experiments, we treated cultured pericytes with IL-1β at different concentrations in the presence and absence of 1 μM AKT inhibitor. Without co-treatment of AKT inhibitor, IL-1β activation did increase the expression of PDGFRβ and CD13 in pericytes (**Figures 6G–I**; one-way ANOVA, $p < 0.05$; $n = 3$ per group), which corroborated our previous experiments (see **Figure 5**). Interestingly, inhibition of AKT abolished the effect of IL-1β on the up-regulation of PDGFRβ and CD13 proteins in pericytes (**Figures 6G–I**; one-way ANOVA, $p > 0.05$; $n = 3$ per group).

DISCUSSION

Pericytes play a central role in regulating microvascular circulation and BBB function in the brain (Sweeney et al., 2016). Our study demonstrated that the deletion of NLRP3 under physiological conditions decreases the coverage of pericytes and protein levels of PDGFRβ and CD13 in cerebral blood vessels. PDGFRβ and CD13, together with neural/glial antigen-2 and CD146 are expressed in capillary-associated pericytes, and often used as protein markers of brain pericytes (Smyth et al., 2018). PDGFRβ and CD13 also trigger proliferation and migration of pericytes after stimulation with angiogenesis-associated growth factors (Lindahl et al., 1997; Rangel et al., 2007). Thus, the reduction of CD13 and PDGFRβ represents not only the loss of pericytes but also the dysfunction of pericytes in the brain. Indeed, we observed that the deletion of NLRP3 reduces the vasculature in the brain, which corroborates a recent observation that the dysfunction of pericytes decreases the length of cerebral blood vessels in PDGFRβ-mutated mouse brain (Montagne et al., 2018). Our study suggests that NLRP3 is essential in the maintenance of functional pericytes in healthy brains. We did not observe the leakage of IgG from serum into brain parenchyma in NLRP3-deficient mice. However, we could not exclude the impairment in the ultrastructure of BBB, which might be caused by the lack of NLRP3.

NLRP3-contained inflammasome activates caspase-1 and produces active IL-1β (Gross et al., 2011). MyD88 mediates inflammatory activation after the challenges of TLRs ligands and IL-1β (O'Neill and Bowie, 2007). We observed that deficiency of either NLRP3 or MyD88 decreases protein levels of PDGFRβ and CD13 in the mouse brain. We supposed that NLRP3 drives a basal inflammatory activation in pericytes and promotes pericyte survival, although it was difficult to detect the secretion of IL-1β from pericytes in the brain. In cultured pericytes, we did observe that caspase-1 is activated and inhibition of NLRP3 attenuates

phosphorylation of multiple inflammation-related kinases, such as AKT and ERK, and perhaps also NFκB (p = 0.094), which is correlated with decreased cell proliferation and PDGFRβ and CD13 expression. Moreover, treatments with IL-1β increase PDGFRβ and CD13 expression in our cultured pericytes. It is consistent with a report that TNF-α at 10 ng/ml promotes cultured pericytes to proliferate and migrate (Tigges et al., 2013). Thus, it is not surprising that angiogenesis is activated with pericyte proliferation in inflammatory lesion sites of multiple sclerosis (Girolamo et al., 2014). However, we observed that IL-1β treatments did not increase pericyte proliferation, which suggests that the regulation of pericyte proliferation by NLRP3 might not depend on IL-1β production. During early wound healing, NLRP3 facilitates angiogenesis; and the production of IL-1β was not always necessary for this repair process, either (Weinheimer-Haus et al., 2015).

As there are no pericyte-specific NLRP3-knockout mice available, we had to work on animals with an overall deficiency of NLRP3. We know that NLRP3 is expressed also in non-pericyte brain cells, i.e., microglia (Heneka et al., 2013). We cannot exclude the possibility that NLRP3 deficiency in microglia decreases the coverage of pericytes in brain vessels. Microglia, located at the perivascular space, is the major component of the neurovascular unit. In response to systemic inflammation, microglia protect BBB integrity in an initial phase by expressing tight-junction protein Claudin-5 and turn to damage BBB through phagocytizing astrocytic end-feet after the inflammation is sustained (Haruwaka et al., 2019). However, the regulation of BBB function and especially pericyte activation by blood vessel-associated microglia under physiological conditions has not been fully explored.

It should be noted that NLRP3 might not fully offer protective effects on pericytes when the inflammatory activation surrounding pericytes is uncontrolled. In the AD brain, NLRP3-contained inflammasome is activated (Heneka et al., 2013), whereas, pericytes are impaired and lost (Sengillo et al., 2013; Nation et al., 2019). There must be other mechanisms, which damage pericytes, compensating for the protective effects of NLRP3 activation. For example, brain-delivered neurotrophic factor (BDNF) drops down and the activation of the BDNF receptor, TrkB, is impaired in the AD brain (Tanila, 2017). TrkB signaling regulates pericyte migration. The deletion of TrkB in pericytes reduces pericyte density and causes abnormal vasculogenesis in the heart (Anastasia et al., 2014). The deletion of NLRP3 in APP or Tau-transgenic mice was reported to rescue neuronal functions and shift microglial activation from pro-inflammatory to anti-inflammatory profile (Heneka et al., 2013; Ising et al., 2019). Unfortunately, the microvascular circulation in NLRP3-deficient AD mice has not been investigated.

AKT is a known kinase to regulate cell survival, proliferation, and angiogenesis in response to extracellular signals (Manning and Cantley, 2007). AKT activation prevents pericyte loss in diabetic retinopathy (Yun et al., 2018). In our experiments, AKT phosphorylation is reduced by NLRP3 inhibition but enhanced by IL-1β activation. Inhibition of AKT directly down-regulates the expression of PDGFRβ and CD13 and also abolishes the effect of IL-1β to elevate the protein levels of PDGFRβ and CD13 in pericytes. Thus, AKT activation might mediate the protective effects of NLRP3 in pericytes. As PDGFRβ activation induces phosphorylation of AKT (Lehti et al., 2005), PDGFRβ and AKT even activate each other and form positive feedback to maintain the healthy pericytes in the brain.

In summary, our study suggested that NLRP3 activation maintains healthy pericytes in the brain through activating AKT signaling pathway. In the following studies, we are evaluating potential cerebral vascular impairment in AD mice with both genetic and pharmacological inhibitions of NLRP3. The potential adverse effects of NLRP3 inhibition on pericyte function and microcirculation should be considered when NLRP3 inhibitors are administered to treat AD or other inflammatory disorders.

DATA AVAILABILITY STATEMENT

The original contributions presented in the study are included in the article, further inquiries can be directed to the corresponding author.

ETHICS STATEMENT

The animal study was reviewed and approved by Landesamt für Verbraucherschutz, Saarland.

AUTHOR CONTRIBUTIONS

YL designed the study and wrote the manuscript. WQ, QL and QT conducted experiments, acquired data and analyzed data. TF provided pericyte cell line. DL and KF supervised the study. All authors contributed to the article and approved the submitted version.

FUNDING

This work was funded by National Natural Science Foundation of China (Grant 81771371 to YL and Grant 81902984 to WQ), SNOWBALL, an EU Joint Programme for Neurodegenerative Disease (JPND; 01ED1617B; to YL and KF) and China Scholarship Council (CSC; 201906820011; to QL). We acknowledge support by the Deutsche Forschungsgemeinschaft (DFG, German Research Foundation) and Saarland University within the funding programme Open Access Publishing. The older version of this manuscript has been released as a pre-print at Research Square (Quan et al., 2019).

ACKNOWLEDGMENTS

We thank Inge Tomic and Isabel Euler for their perfect technical support.

REFERENCES

Adachi, O., Kawai, T., Takeda, K., Matsumoto, M., Tsutsui, H., Sakagami, M., et al. (1998). Targeted disruption of the MyD88 gene results in loss of IL-1- and IL-18-mediated function. *Immunity* 9, 143–150. doi: 10.1016/s1074-7613(00)80596-8

Anastasia, A., Deinhardt, K., Wang, S., Martin, L., Nichol, D., Irmady, K., et al. (2014). Trkb signaling in pericytes is required for cardiac microvessel stabilization. *PLoS One* 9:e87406. doi: 10.1371/journal.pone.0087406

Bonacchi, A., Romagnani, P., Romanelli, R. G., Efsen, E., Annunziato, F., Lasagni, L., et al. (2001). Signal transduction by the chemokine receptor CXCR3: activation of Ras/ERK, Src and phosphatidylinositol 3-kinase/Akt controls cell migration and proliferation in human vascular pericytes. *J. Biol. Chem.* 276, 9945–9954. doi: 10.1074/jbc.m010303200

Boulay, A. C., Saubamea, B., Decleves, X., and Cohen-Salmon, M. (2015). Purification of mouse brain vessels. *J. Vis. Exp.* 105:e53208. doi: 10.3791/53208

Decker, Y., Muller, A., Nemeth, E., Schulz-Schaeffer, W. J., Fatar, M., Menger, M. D., et al. (2018). Analysis of the vasculature by immunohistochemistry in paraffin-embedded brains. *Brain Struct. Funct.* 223, 1001–1015. doi: 10.1007/s00429-017-1595-8

Dempsey, C., Rubio Araiz, A., Bryson, K. J., Finucane, O., Larkin, C., Mills, E. L., et al. (2017). Inhibiting the NLRP3 inflammasome with MCC950 promotes non-phlogistic clearance of amyloid-beta and cognitive function in APP/PS1 mice. *Brain Behav. Immun.* 61, 306–316. doi: 10.1016/j.bbi.2016.12.014

Deture, M. A., and Dickson, D. W. (2019). The neuropathological diagnosis of Alzheimer's disease. *Mol. Neurodegener.* 14:32. doi: 10.1186/s13024-019-0333-5

Girolamo, F., Coppola, C., Ribatti, D., and Trojano, M. (2014). Angiogenesis in multiple sclerosis and experimental autoimmune encephalomyelitis. *Acta Neuropathol. Commun.* 2:84. doi: 10.1186/s40478-014-0084-z

Gross, O., Thomas, C. J., Guarda, G., and Tschopp, J. (2011). The inflammasome: an integrated view. *Immunol. Rev.* 243, 136–151. doi: 10.1111/j.1600-065x.2011.01046.x

Guijarro-Muñoz, I., Compte, M., Alvarez-Cienfuegos, A., Alvarez-Vallina, L., and Sanz, L. (2014). Lipopolysaccharide activates Toll-like receptor 4 (TLR4)-mediated NF-κB signaling pathway and proinflammatory response in human pericytes. *J. Biol. Chem.* 289, 2457–2468. doi: 10.1074/jbc.m113.521161

Hao, W., Liu, Y., Liu, S., Walter, S., Grimm, M. O., Kiliaan, A. J., et al. (2011). Myeloid differentiation factor 88-deficient bone marrow cells improve Alzheimer's disease-related symptoms and pathology. *Brain* 134, 278–292. doi: 10.1093/brain/awq325

Haruwaka, K., Ikegami, A., Tachibana, Y., Ohno, N., Konishi, H., Hashimoto, A., et al. (2019). Dual microglia effects on blood brain barrier permeability induced by systemic inflammation. *Nat. Commun.* 10:5816. doi: 10.1038/s41467-019-13812-z

Heneka, M. T., Kummer, M. P., Stutz, A., Delekate, A., Schwartz, S., Vieira-Saecker, A., et al. (2013). NLRP3 is activated in Alzheimer's disease and contributes to pathology in APP/PS1 mice. *Nature* 493, 674–678. doi: 10.1038/nature11729

Ising, C., Venegas, C., Zhang, S., Scheiblich, H., Schmidt, S. V., Vieira-Saecker, A., et al. (2019). NLRP3 inflammasome activation drives tau pathology. *Nature* 575, 669–673. doi: 10.1038/s41586-019-1769-z

Kovac, A., Erickson, M. A., and Banks, W. A. (2011). Brain microvascular pericytes are immunoactive in culture: cytokine, chemokine, nitric oxide and LRP-1 expression in response to lipopolysaccharide. *J. Neuroinflammation* 8:139. doi: 10.1186/1742-2094-8-139

Leaf, I. A., Nakagawa, S., Johnson, B. G., Cha, J. J., Mittelsteadt, K., Guckian, K. M., et al. (2017). Pericyte MyD88 and IRAK4 control inflammatory and fibrotic responses to tissue injury. *J. Clin. Invest.* 127, 321–334. doi: 10.1172/jci87532

Lehti, K., Allen, E., Birkedal-Hansen, H., Holmbeck, K., Miyake, Y., Chun, T. H., et al. (2005). An MT1-MMP-PDGF receptor-beta axis regulates mural cell investment of the microvasculature. *Genes Dev.* 19, 979–991. doi: 10.1101/gad.1294605

Lindahl, P., Johansson, B. R., Leveen, P., and Betsholtz, C. (1997). Pericyte loss and microaneurysm formation in PDGF-B-deficient mice. *Science* 277, 242–245. doi: 10.1126/science.277.5323.242

Love, S., and Miners, J. S. (2016). Cerebrovascular disease in ageing and Alzheimer's disease. *Acta Neuropathol.* 131, 645–658. doi: 10.1007/s00401-015-1522-0

Manning, B. D., and Cantley, L. C. (2007). AKT/PKB signaling: navigating downstream. *Cell* 129, 1261–1274. doi: 10.1016/j.cell.2007.06.009

Martinon, F., Petrilli, V., Mayor, A., Tardivel, A., and Tschopp, J. (2006). Gout-associated uric acid crystals activate the NALP3 inflammasome. *Nature* 440, 237–241. doi: 10.1038/nature04516

Montagne, A., Nikolakopoulou, A. M., Zhao, Z., Sagare, A. P., Si, G., Lazic, D., et al. (2018). Pericyte degeneration causes white matter dysfunction in the mouse central nervous system. *Nat. Med.* 24, 326–337. doi: 10.1038/nm.4482

Nation, D. A., Sweeney, M. D., Montagne, A., Sagare, A. P., D'Orazio, L. M., Pachicano, M., et al. (2019). Blood-brain barrier breakdown is an early biomarker of human cognitive dysfunction. *Nat. Med.* 25, 270–276. doi: 10.1038/s41591-018-0297-y

Nyúl-Tóth, A., Kozma, M., Nagyőszi, P., Nagy, K., Fazakas, C., Haskó, J., et al. (2017). Expression of pattern recognition receptors and activation of the non-canonical inflammasome pathway in brain pericytes. *Brain Behav. Immun.* 64, 220–231. doi: 10.1016/j.bbi.2017.04.010

O'Neill, L. A., and Bowie, A. G. (2007). The family of five: TIR-domain-containing adaptors in Toll-like receptor signalling. *Nat. Rev. Immunol.* 7, 353–364. doi: 10.1038/nri2079

Quan, W. Q., Luo, Q. H., Tang, Q. Q., Furihata, T., Li, D., Fassbender, K., et al. (2019). NLRP3 maintains healthy pericytes in the brain. [Preprint]. (Version 1). doi: 10.21203/rs.2.18793/v1

Rangel, R., Sun, Y., Guzman-Rojas, L., Ozawa, M. G., Sun, J., Giordano, R. J., et al. (2007). Impaired angiogenesis in aminopeptidase N-null mice. *Proc. Natl. Acad. Sci. U S A* 104, 4588–4593. doi: 10.1073/pnas.0611653104

Sagare, A. P., Bell, R. D., Zhao, Z., Ma, Q., Winkler, E. A., Ramanathan, A., et al. (2013). Pericyte loss influences Alzheimer-like neurodegeneration in mice. *Nat. Commun.* 4:2932. doi: 10.1038/ncomms3932

Sengillo, J. D., Winkler, E. A., Walker, C. T., Sullivan, J. S., Johnson, M., and Zlokovic, B. V. (2013). Deficiency in mural vascular cells coincides with blood-brain barrier disruption in Alzheimer's disease. *Brain Pathol.* 23, 303–310. doi: 10.1111/bpa.12004

Smyth, L. C. D., Rustenhoven, J., Scotter, E. L., Schweder, P., Faull, R. L. M., Park, T. I. H., et al. (2018). Markers for human brain pericytes and smooth muscle cells. *J. Chem. Neuroanat.* 92, 48–60. doi: 10.1016/j.jchemneu.2018.06.001

Stancu, I. C., Cremers, N., Vanrusselt, H., Couturier, J., Vanoosthuyse, A., Kessels, S., et al. (2019). Aggregated Tau activates NLRP3-ASC inflammasome exacerbating exogenously seeded and non-exogenously seeded Tau pathology *in vivo*. *Acta Neuropathol.* 137, 599–617. doi: 10.1007/s00401-018-01957-y

Sweeney, M. D., Ayyadurai, S., and Zlokovic, B. V. (2016). Pericytes of the neurovascular unit: key functions and signaling pathways. *Nat. Neurosci.* 19, 771–783. doi: 10.1038/nn.4288

Tanila, H. (2017). The role of BDNF in Alzheimer's disease. *Neurobiol. Dis.* 97, 114–118. doi: 10.1016/j.nbd.2016.05.008

Tigges, U., Boroujerdi, A., Welser-Alves, J. V., and Milner, R. (2013). TNF-α promotes cerebral pericyte remodeling *in vitro*, *via* a switch from α1 to α2 integrins. *J. Neuroinflammation* 10:33. doi: 10.1186/1742-2094-10-33

Umehara, K., Sun, Y., Hiura, S., Hamada, K., Itoh, M., Kitamura, K., et al. (2018). A new conditionally immortalized human fetal brain pericyte cell line: establishment and functional characterization as a promising tool for human brain pericyte studies. *Mol. Neurobiol.* 55, 5993–6006. doi: 10.1007/s12035-017-0815-9

Venegas, C., Kumar, S., Franklin, B. S., Dierkes, T., Brinkschulte, R., Tejera, D., et al. (2017). Microglia-derived ASC specks cross-seed amyloid-β in Alzheimer's disease. *Nature* 552, 355–361. doi: 10.1038/nature25158

Weinheimer-Haus, E. M., Mirza, R. E., and Koh, T. J. (2015). Nod-like receptor protein-3 inflammasome plays an important role during early stages of wound healing. *PLoS One* 10:e0119106. doi: 10.1371/journal.pone.0119106

Yao, Q., Renault, M. A., Chapouly, C., Vandierdonck, S., Belloc, I., Jaspard-Vinassa, B., et al. (2014). Sonic hedgehog mediates a novel pathway of PDGF-BB-dependent vessel maturation. *Blood* 123, 2429–2437. doi: 10.1182/blood-2013-06-508689

Yun, J. H., Jeong, H. S., Kim, K. J., Han, M. H., Lee, E. H., Lee, K., et al. (2018). β-Adrenergic receptor agonists attenuate pericyte loss in diabetic retinas through Akt activation. *FASEB J.* 32, 2324–2338. doi: 10.1096/fj.201700570rr

Zudaire, E., Gambardella, L., Kurcz, C., and Vermeren, S. (2011). A computational tool for quantitative analysis of vascular networks. *PLoS One* 6:e27385. doi: 10.1371/journal.pone.0027385

Conflict of Interest: The authors declare that the research was conducted in the absence of any commercial or financial relationships that could be construed as a potential conflict of interest.

frontiers in Physiology

MINI REVIEW
published: 21 August 2020
doi: 10.3389/fphys.2020.01030

Blood–Brain Barrier Dysfunction in Mild Traumatic Brain Injury: Evidence From Preclinical Murine Models

Yingxi Wu[1†], Haijian Wu[1,2†], Xinying Guo[1], Brock Pluimer[1,3] and Zhen Zhao[1,3]*

[1] Center for Neurodegeneration and Regeneration, Zilkha Neurogenetic Institute and Department of Physiology and Neuroscience, Keck School of Medicine, University of Southern California, Los Angeles, CA, United States, [2] Department of Neurosurgery, Second Affiliated Hospital, School of Medicine, Zhejiang University, Hangzhou, China, [3] Neuroscience Graduate Program, Keck School of Medicine, University of Southern California, Los Angeles, CA, United States

OPEN ACCESS

Edited by:
Clotilde Lecrux, McGill University, Canada

Reviewed by:
Jerome Badaut, UMR 5287 Institut de Neurosciences Cognitives et Intégratives d'Aquitaine (INCIA), France
Stefano Tarantini, University of Oklahoma Health Sciences Center, United States

***Correspondence:**
Zhen Zhao
zzhao@usc.edu

[†] These authors have contributed equally to this work

Specialty section:
This article was submitted to Vascular Physiology, a section of the journal Frontiers in Physiology

Received: *09 April 2020*
Accepted: *28 July 2020*
Published: *21 August 2020*

Citation:
Wu Y, Wu H, Guo X, Pluimer B and Zhao Z (2020) Blood–Brain Barrier Dysfunction in Mild Traumatic Brain Injury: Evidence From Preclinical Murine Models. Front. Physiol. 11:1030. doi: 10.3389/fphys.2020.01030

Mild traumatic brain injury (mTBI) represents more than 80% of total TBI cases and is a robust environmental risk factor for neurodegenerative diseases including Alzheimer's disease (AD). Besides direct neuronal injury and neuroinflammation, blood–brain barrier (BBB) dysfunction is also a hallmark event of the pathological cascades after mTBI. However, the vascular link between BBB impairment caused by mTBI and subsequent neurodegeneration remains undefined. In this review, we focus on the preclinical evidence from murine models of BBB dysfunction in mTBI and provide potential mechanistic links between BBB disruption and the development of neurodegenerative diseases.

Keywords: mild traumatic brain injury, blood-brain barrier, murine model, vascular link, neurodegenerative diseases

INTRODUCTION

Traumatic brain injury (TBI) is a leading cause of death and long-term disability around the world (Hackenberg and Unterberg, 2016). Based on the severity, TBI can be classified as mild, moderate, and severe TBI (Chamelian and Feinstein, 2004). As more than 80% of cases are estimated to be mild cases (Rutland-Brown et al., 2006), it is particularly important to understand the pathophysiological mechanisms of mild TBI (mTBI) and develop novel and effective therapeutic approaches. Accumulating evidence has demonstrated that mTBI can result in a series of pathologic events, including neuroinflammation, oxidative stress (Katz et al., 2015), cerebrovascular impairment such as edema, circulatory insufficiency, and blood–brain barrier (BBB) breakdown (Doherty et al., 2016). These events are highly interactive, and all contribute to the long-term cognitive and emotional impairments in mTBI patients (Riggio, 2011).

The BBB is a highly selective membrane that mainly encompasses endothelial cells, sealed by tight junctions, and fortified by pericytes and astrocytic endfeet (Daneman and Prat, 2015). This coordinated network of cells plays an important role in the brain's physiological homeostasis and functions, while disruption of this network can trigger multiple pathologic events (Zhao et al., 2015). In fact, BBB dysfunction has been increasingly noticed in many neurological conditions of

the central nervous system (CNS), including acute injuries such as TBI and stroke, and chronic neurodegenerative disorders such as Alzheimer's disease (AD), Parkinson's disease (PD), and chronic traumatic encephalopathy (CTE) (Sweeney et al., 2019). It is worth noting that BBB dysfunction was commonly observed in both mTBI patients and experimental animal models (Sandsmark et al., 2019). For instance, histological evidence from human patients indicated that microvascular dysfunction widely occurred from mild to moderate and severe TBI, and not only in the acute and subacute stages after the primary injury but also in the chronic stage in long-term survivors (O'Keeffe et al., 2020). These clinical findings are in general backed up by the evidence from preclinical animal models (Sandsmark et al., 2019), which demonstrated that mTBI induces cellular and molecular events at the BBB, including alteration of endothelial transport functions (Villalba et al., 2017), disruption of the crosstalk between endothelial cells and pericytes (Bhowmick et al., 2019), pericyte loss (Zehendner et al., 2015), cerebral blood flow (CBF) reduction, and tissue hypoxia (Han et al., 2020; O'Keeffe et al., 2020). These vascular pathological events interact and evolve with neuroinflammation (Blennow et al., 2012) and contribute to chronic neurodegeneration post-injury.

More importantly, clinical data indicated that BBB impairment can persist for many years and is highly associated with long-term neurological deficits in mTBI patients (Shlosberg et al., 2010). Therefore, it is crucial to evaluate the extent of BBB disruption after mTBI and elucidate the underlying molecular cascades in preclinical models. Such knowledge will not only define a clear vascular link between mTBI and long-term neurological impairments, as well as build up a foundation for developing novel therapeutic approaches. Animal models, more specifically murine models, often closely mimic key neuropathological features in human patients and allow us to study the underlying mechanisms of BBB dysfunction and its associated pathophysiologies in CNS diseases. Therefore, in this review, we summarize recent evidence in the last 10 years obtained from experimental murine models of mTBI, address the BBB disruptions and its associated pathologic changes in mTBI, and depict the vascular link between mTBI and subsequent neurodegeneration (**Figure 1**). The criteria used for mTBI (include repetitive mTBI) are mainly based on the recent systematic review (Bodnar et al., 2019). Only studies with histological and/or behavioral validation of mTBI were included to ensure a closer recapitulation of clinical observations under the mTBI category (Bodnar et al., 2019).

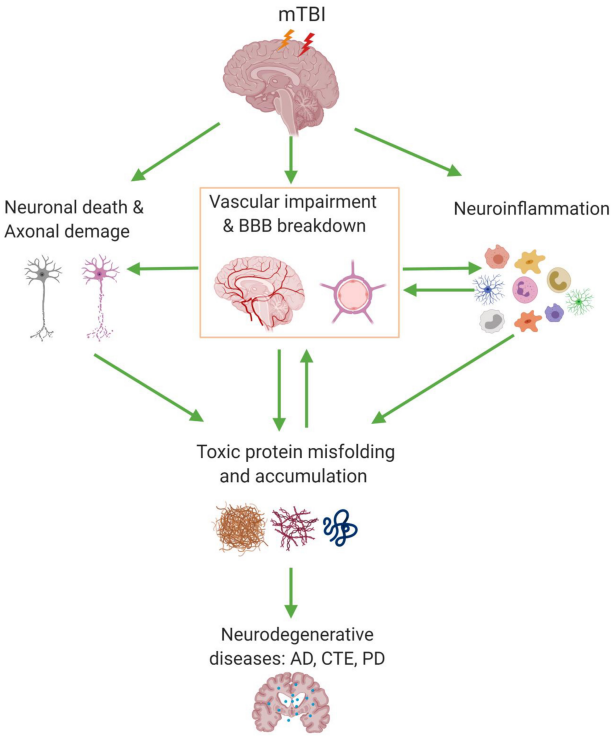

FIGURE 1 | Blood–brain barrier (BBB) dysfunction and its associated pathologic events involved in mild traumatic brain injury (mTBI). mTBI can cause a series of pathologic changes including cerebrovascular impairment and BBB dysfunction, neuronal cell death, and axonal damage, as well as gliosis and neuroinflammation. Also, BBB dysfunction can accelerate the accumulation of pathologic products such as Aβ, tau, and α-synuclein; on the other hand, their deposition around the cerebral vessel has a chronic toxic effect which enhances the BBB disruption and ultimately may lead to neurodegenerative diseases. AD, Alzheimer's disease; CTE, chronic traumatic encephalopathy; PD, Parkinson's disease.

BLOOD–BRAIN BARRIER DYSFUNCTION IN MURINE MODELS OF MILD TRAUMATIC BRAIN INJURY

Murine models have helped us tremendously to understand the pathogenic events after mTBI, including cerebral microvascular injury and BBB dysfunction. We searched over 6,000 publications related to mTBI on PubMed and found 232 studies potentially covering cerebrovascular impairment and BBB dysfunction (**Figure 2**). Among them, 17 research articles in the last 10 years were based on murine models of mTBI (**Table 1**) and selected. The models include not only the well-established weight drop and piston-driven models (Bodnar et al., 2019) but also the increasingly appreciated models including modified controlled cortical impact (CCI), mild blast injury, and fluid percussion (Lifshitz et al., 2016; Bharadwaj et al., 2018). The results were organized by the timing of assessments and mechanism of pathogenesis and discussed in the context of methods used to generate the impact and detection of the vascular impairment.

We surveyed the BBB dysfunction and relevant pathologic changes found in mouse or rat models, covering the acute and subacute stages that evolve within the first 2 weeks after mTBI and the chronic stage that usually takes place 2 weeks after mTBI. The methods commonly used for BBB functional analysis in murine models are (i) histological assessment using plasma proteins such as immunoglobulin G (IgG) and/or exogenous tracers such as Evans blue dye, horseradish peroxidase (HRP), or fluoresce labeled albumin; (ii) *in vivo* imaging techniques including magnetic resonance imaging (MRI) and multi-photon imaging; and (iii) additional methods such as brain water content

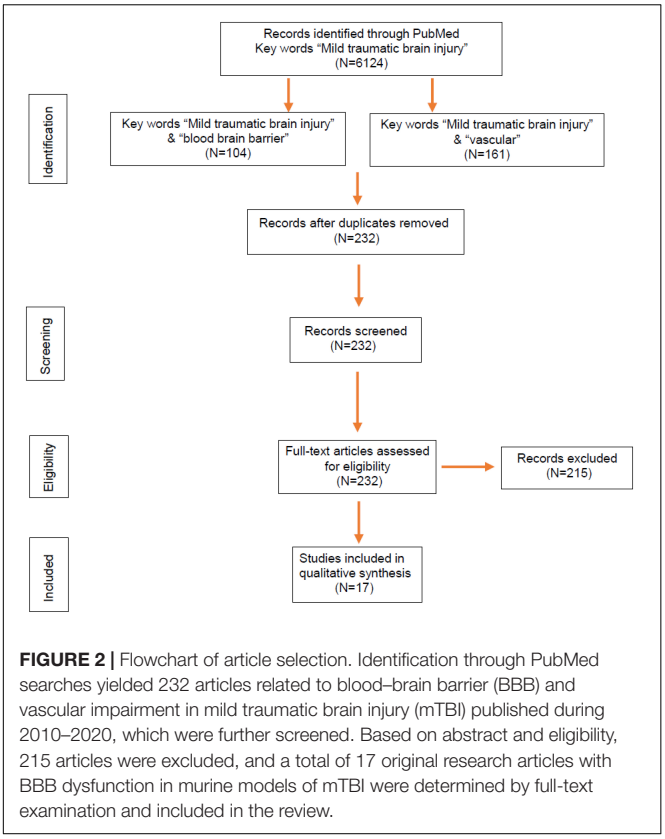

FIGURE 2 | Flowchart of article selection. Identification through PubMed searches yielded 232 articles related to blood–brain barrier (BBB) and vascular impairment in mild traumatic brain injury (mTBI) published during 2010–2020, which were further screened. Based on abstract and eligibility, 215 articles were excluded, and a total of 17 original research articles with BBB dysfunction in murine models of mTBI were determined by full-text examination and included in the review.

calculation for cerebral edema (wet/dry weight ratio). Analysis of the protein and mRNA expression of tight junction protein was also reported.

BLOOD–BRAIN BARRIER DYSFUNCTION IN ACUTE AND SUBACUTE STAGES OF MILD TRAUMATIC BRAIN INJURY

Twelve out of 17 of these mTBI studies showed that the BBB breakdown is an early event in murine models of mTBI, even as early as 5 min post-injury. For example, Li et al. (2016) examined the integrity of BBB in a modified CCI model of mTBI *via* the *in vivo* two-photon imaging of intravenously injected rhodamine B. They showed that BBB disruption in wild-type C57BL/6 mice occurred at a very early stage of mTBI (between 5 and 60 min), which was even exacerbated in Slit2-Tg mice (Li et al., 2016). Using peripherally injected radiotracer, ^{14}C-sucrose and ^{99m}Tc-albumin, Logsdon et al. (2018) found BBB disruption by mild blast exposure in just 15 min. Moreover, based on immunostaining of endogenous IgG, BBB disruption was detected in both adult and juvenile mice from 6 h to 2 days after mTBI (Laurer et al., 2001; Huh et al., 2008; Ichkova et al., 2020). By administering exogenous tracers Evans blue dye or fluoresce labeled albumin, the BBB breakdown was also detected from the mTBI between 1 and 24 h after mTBI based on extravascular leakages (Yang et al., 2013; Chen et al., 2014; Katz et al., 2015; Yates et al., 2017). Tagge et al. (2018) applied a novel closed-head concussive left-lateral impact injury mouse model to investigate the microvascular injury after mTBI. Both Evans blue extravasation and *in vivo* dynamic MRI of systemically administered gadolinium-based contrast agent confirmed acute and persistent BBB disruption in the ipsilateral cortex of impacted mice. They also examined the postmortem neuropathological changes and did not find the evidence of hemorrhagic contusion, suggesting BBB dysfunction rather than intraparenchymal hemorrhage resulted in permeability changes (Tagge et al., 2018). These data indicate that BBB breakdown occurs within minutes after mTBI; however, it may only be detected by more sensitive methods than classic histological analysis.

The mechanism of the BBB dysfunction after mTBI was also investigated in some of the studies. For example, reduced expression of tight junction protein claudin-5 and BBB disruption were detected in an mTBI model with a blast method, and inhibiting nitric oxide-dependent signaling pathways and preserving tight junction integrity were helpful to maintain BBB integrity after injury (Logsdon et al., 2018). mTBI-induced acute BBB disruption was also associated with microvascular structural damages including swollen astrocyte endfeet and deformation of pericytes in cortical regions 6 h post-injury (Bashir et al., 2020). Using a closed-head TBI model, Tagge et al. (2018) described that mTBI induced capillary retraction, changes in the extracellular matrix and basal lamina, and astrocytic endfeet engorgement, which all contribute to BBB disruption. Interestingly, these vascular structural changes such as loss of tight junctions and pericytes and swollen endfeet (**Figure 3**, left) are commonly seen in neurodegenerative diseases such as AD, suggesting that a shared underlying mechanism may exist in these distinct pathological conditions.

However, five recent studies found no evident BBB disruption after mTBI (**Table 1**). For example, Kane et al. (2012) found mild astrocytic activation but lack of BBB disruption to IgG or edema in weight drop model of mTBI in mice, while Whalen's group reported that the BBB integrity was not compromised after single or repetitive closed head injury by immunohistochemical analysis of Evans blue or intracerebral levels of mouse IgG (Meehan et al., 2012; Chung et al., 2019; Wu et al., 2019). In a long-term study, Lynch et al. (2016) also found no BBB leakage to Evans blue at 7 months after repetitive midline mTBI, despite vascular abnormality still existed at that time. These different results may reflect the differences in animal models, methodology in detecting BBB changes, and observation time points.

BLOOD–BRAIN BARRIER DYSFUNCTION IN THE CHRONIC STAGE OF MILD TRAUMATIC BRAIN INJURY

In addition to its breakdown during the acute and subacute phases of mTBI, the pathological changes of BBB integrity in the chronic phase of mTBI have been well documented in human patients, yet underexplored in animal models (Jullienne et al., 2016; Sandsmark et al., 2019). For example, Tomkins et al. (2011) found that 13 of 27 mTBI patients showed parenchymal regions with BBB disruption based on MRI scans, which were

TABLE 1 | An update on mTBI studies in murine models in recent 10 years.

Study	Animal	Model	BBB Impairment	Neuropathology	Neuroinflammation	Motor function	Cognitive function
Yang et al., 2013	Mouse	Weight drop	BBB disruption detected by Lucifer yellow and FITC-albumin at 1.5–6 h	Increased expression of serum NSE at 1.5–6 h, 1 day	Increased expression of brain MDC and MIP-1α on 1 day	Deficit in rotarod test on 1–5 days	Impairment (NOR: 1–4 days)
Chen et al., 2014	Mouse	Modified CCI	BBB disruption detected by Evan blue at 1 h	Axonal injury on 1 day; Increased neuronal degeneration on 1–8 days	Activation of astrocytes and microglia on 8 days	Deficit in rotarod test on 1–3 days	No impairment (SOR and contextual fear conditioning: 5–8 days)
Gama Sosa et al., 2014	Rat	Blast exposure; RHI	Altered microvascular ECM, microvascular occlusion and degeneration, intraventricular hemorrhage at 6–10 months	n/a	Activation of astrocytes in 10 months	n/a	n/a
Katz et al., 2015	Rat	LFP	BBB disruption detected by Evan blue at 24 h	n/a	Activation of astrocytes at 24 h; Cytokine upregulation at 24 h	n/a	Impairment in NBS and NSS tests at 2–24 h
Li et al., 2016	Mouse	Micro TBI compression	BBB disruption detected by rhodamine B at 5–60 min	Increased cell death at 6–24 h	n/a	n/a	n/a
Logsdon et al., 2018	Mouse	Blast exposure; RHI	BBB disruption detected by ^{14}C-sucrose and ^{99m}Tc-albumin at 0.25 h, 3 days	n/a	Activation of astrocytes and microglia on 3 days	n/a	n/a
Adams et al., 2018	Mouse	CHI; RHI	Decreased CBF and CVR detected by MRI on 14 days	Reduced evoked neuronal responses without changes in neuronal density on 14 days	Activation of astrocytes on 14 days	n/a	n/a
Bharadwaj et al., 2018	Mouse	MFP	BBB disruption detected by HRP staining and nanoparticles at 3 h	n/a	n/a	n/a	n/a
Tagge et al., 2018	Mouse	Lateral CHI	BBB disruption detected by Evans blue, extravasated serum albumin, and DCE-MRI at 24 h	Neuronal damage on 1 day; Decreased neuronal density on 3–14 days	Activation of astrocytes and microglia on 1–3 days	Transient impairments in neurobehavioral response tests	n/a

(Continued)

TABLE 1 | Continued

Study	Animal	Model	BBB Impairment	Neuropathology	Neuroinflammation	Motor function	Cognitive function
Wendel et al., 2018	Mouse (juvenile)	CHI	Increased vessel density and length detected by IHC on 4–60 days	White matter disruption on 4–14 days	n/a	n/a	n/a
Yates et al., 2017	Rat	Weight drop; RHI	BBB disruption detected by Evan blue on 3 days	n/a	No activation of astrocytes and microglia on 4 days	Deficit in Foot-fault test on 1 day	Impairment in MWM on 4 days
Ichkova et al., 2020	Mouse (juvenile)	CHI	BBB disruption and altered cortical cerebrovascular reactivity detected by IgG staining on 1–3 days	Axonal pathology on 30 days; No neuronal loss on 1, 3, 7, 30 days	n/a	n/a	Deficit in open-field test on 1–30 days
Kane et al., 2012	Mouse	Weight drop; RHI	No BBB disruption by IgG staining on 7 days	n/a	Mild activation of astrocytes on 7 days	Deficit in rotarod test on 1 day and locomotor activity on 5 days	n/a
Meehan et al., 2012	Mouse	Weight drop; RHI	No BBB disruption by IgG staining at 1 h, 24 h	No changes in neuronal degeneration and axonal injury at 1 h, 24 h	n/a	n/a	Impairment in MWM at 1 month
Lynch et al., 2016	Mouse (aged)	CHI; RHI	No BBB disruption by S100β ELISA or occludin at 7 months	n/a	Activation of astrocytes and microglia in the CC	n/a	Spatial memory deficits in Barnes Maze task at 1–6 months
Chung et al., 2019	Mouse	CHI	No BBB disruption by IgG staining at 24 h	No changes in neuronal degeneration at 24 h, 48 h	Increased infiltration of $CD11b^+/CD45^+$ leukocytes at 72 h	No deficit in Foot-fault test on 1–14 days	Impairment in MWM on 3–42 days
Wu et al., 2019	Mouse (adolescent)	CHI; RHI	No BBB disruption by Evan blue at 4 h	No changes in neuronal degeneration at 1 year	No activation of astrocytes and microglia at 4 h–1 year	n/a	Impairment in MWM on 7 days–9 months

BBB, blood–brain barrier; CBF, cerebral blood flow; CC, corpus callosum; CCI, controlled cortical impact; CHI, closed head injury; CVR, cerebrovascular reactivity; DCE-MRI, dynamic contrast-enhanced MRI; ECM, extracellular matrix; ELISA, enzyme-linked immunosorbent assay; FITC, fluorescein isothiocyanate; HRP, horseradish peroxidase; IHC, immunohistochemistry; LFP, lateral fluid percussion; MDC, macrophage-derived chemokine; MFP, midline fluid percussion; MIP-1α, macrophage inflammatory protein-1α; MRI, magnetic resonance imaging; mTBI, mild traumatic brain injury; MWM, Morris water maze; NBS, neurobehavioral scores; NSS, neurological severity scores; NOR, novel object recognition; NSE, neuron-specific enolase; RHI, repetitive head injury; SOR, spatial object recognition.

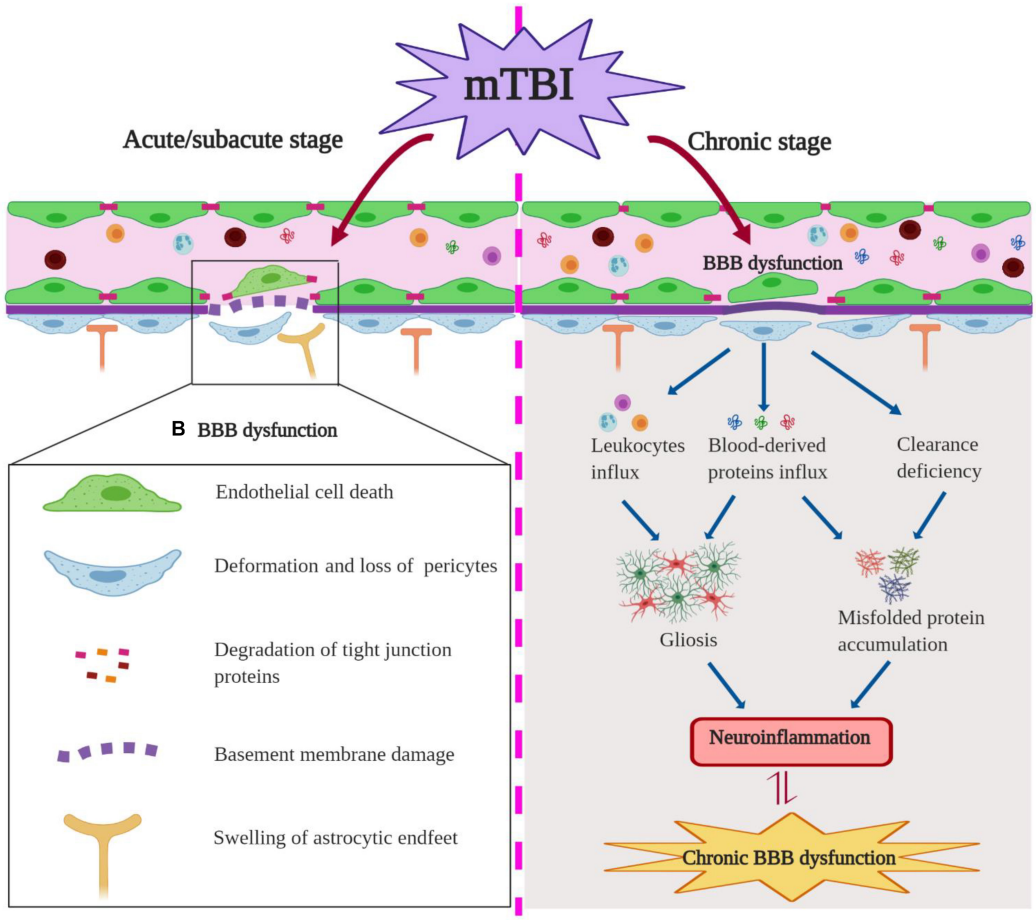

FIGURE 3 | Blood–brain barrier (BBB) dysfunction in the acute/subacute stage **(Left)** and chronic stage **(Right)** of mild traumatic brain injury (mTBI). In the acute/subacute stage, mTBI induces the endothelial cell (EC) death, loss of pericytes and tight junction proteins, astrocytic endfeet swelling, as well as basement membrane damage and ultimately an impairment of BBB permeability. In the chronic stage, mTBI causes BBB leakage and influx of neurotoxic blood-derived proteins and cells into the brain parenchyma, which can induce gliosis and misfolded protein accumulation post-insult; mTBI-induced clearance deficiency of BBB promotes misfolded protein accumulation.

identified up to a median of 2.5 months after the initial trauma event, indicating that lasting BBB disruption exists in nearly half of the mTBI patients. In a different cohort of 17 mTBI patients with post-concussion syndromes (PCSs), eight of them exhibited abnormal BBB permeability based on single-photon emission computed tomography (SPECT) of ^{99m}Tc-diethylenetriaminepentaacetic acid radiotracer (Korn et al., 2005). These patients were scanned between 1 month and 7 years after their respective head injuries. More recently, Yoo et al. (2019) demonstrated that mTBI patients with PCS, who had a median of 4-month time interval between injury and MRI examinations, exhibited much higher BBB permeability based on K^{trans} measurement from dynamic contrast-enhanced MRI (DCE-MRI) when compared with controls. Similar situations were also reported from patients diagnosed with concussion in adolescent sports (O'Keeffe et al., 2020) and football players (Weissberg et al., 2014).

Consistent with observations in human patients, cerebrovascular dysfunction was detected in a repeated mTBI mouse model at 2 weeks after the insult (Adams et al., 2018). Functional assessments revealed that repeated impacts cause sustained decreases of CBF and cerebrovascular reactivity, along with neuronal function deficits and astrogliosis in peri-contusion areas (Adams et al., 2018). In addition, mTBI can elicit an early and long-lasting cerebrovascular dysfunction in juvenile mice (Wendel et al., 2018; Ichkova et al., 2020), accompanied by astrocyte response and gliovascular changes (Rodriguez-Grande et al., 2018; Clément et al., 2020). Furthermore, pediatric mTBI can morphologically alter the vasculature of the ipsilateral corpus callosum differentially between the acute/subacute stage and the chronic stage (Wendel et al., 2018). As demonstrated, mTBI induced an initial increase in vessel parameters (e.g., vessel density and length) at 4 days post-injury (DPI), which was followed by a transient decrease at 14 DPI but with a subsequent increase in vessel density at 60 DPI (Wendel et al., 2018). It suggested that these microvascular alterations contribute to the long-term reorganization of the ipsilateral corpus callosum after mTBI (Wendel et al., 2018). Finally, chronic changes

in the microvasculature were also reported in rats several months after the initial blast exposure (Gama Sosa et al., 2014). In particular, intraventricular hemorrhage was observed in four out of 23 blast-exposed animals examined between 6 and 10 months after the last blast exposure, which may be attributed to continued vascular fragility within the choroid plexus post-injury (Gama Sosa et al., 2014). As suggested, blast exposure may induce the degradation and remodeling of the extracellular matrix, which contributes to chronic microvascular pathology after injury (Gama Sosa et al., 2014). Due to the limited number of reports, the potential molecular and cellular mechanisms of BBB dysfunction in the chronic phase of murine mTBI remain largely unknown. Abnormal expressions of junctional proteins and matrix metallopeptidases may potentially involve the degradation of the extracellular matrix and prolonged BBB breakdown, and chronic inflammation may also play a crucial role. More importantly, the crosstalk between vascular impairment and neuroinflammation in the context of persistent BBB dysfunction after mTBI is yet to be determined (**Figure 3**, right).

BLOOD–BRAIN BARRIER DYSFUNCTION OF MILD TRAUMATIC BRAIN INJURY MODEL IN THE HIGH-THROUGHPUT SEQUENCING ERA

Over the past decade, high-throughput sequencing methods have revolutionized the entire field of biology. The RNA sequencing to study the entire transcriptomes in detail has driven many important discoveries for various neurological disorders (von Gertten et al., 2005; Redell et al., 2013; Lipponen et al., 2016; Meng et al., 2017). The brain microvascular endothelial cells are the major component of the BBB and play critical roles to maintain its normal function and integrity. Therefore, understanding endothelial cell-specific transcriptional profiles can help us to identify novel mechanisms of TBI-induced changes within the BBB. As most of the previous genomic profiling studies of TBI are based on heterogeneous mixtures of brain cell types, Munji et al. (2019) recently used endothelial cell enrichment for deep RNA sequencing to decipher the transcriptome differences at 24 h (acute), 72 h (subacute), and 1 month (chronic) after TBI in mice. They found that most unique and dramatic changes were at the acute time point, whereas few overlapped genes were observed between acute and chronic periods. These findings reflect the severity of the initial insult on the endothelial functions and BBB integrity and immediate response at the early stage, yet clearly point out to the distinct molecular mechanisms that are involved in acute/subacute and chronic phases of TBI. In addition, they also found that the synthesis of extracellular matrix molecules and activation of proteases further contributed to the BBB changes in the acute and subacute period. On the other hand, the immune response may play a more prominent role in the chronic period. These findings provided us further directions for investigating the endothelial dysfunction in TBI.

The diversity of cell types at the BBB (Vanlandewijck et al., 2018), only focusing on endothelial cells, will mask crucial signals from other BBB-related cell types. Therefore, single-cell RNA sequencing represents an approach to overcome this problem. Arneson et al. (2018) firstly investigated the mTBI pathogenesis in thousands of individual brain cells in parallel using single-cell RNA sequencing. Unsupervised clustering analysis identified BBB-associated cell types such as endothelial cells and mural cells. Besides, they also found a previously unknown cell type after mTBI, which likely is a migrating endothelial cell, as it carries key signatures of cell growth and migration as well as endothelial identity. This is consistent with previous research that endothelial cell is a main component of BBB that is destroyed after mTBI (Shlosberg et al., 2010), and the proliferation and migration of endothelial cells are inherent aspects of neovascularization after injuries (Salehi et al., 2017). More importantly, pathway analysis informed by genes with significant changes from both endothelial cells and astrocytes implicates endoplasmic reticulum dysfunction after mTBI. As endoplasmic reticulum stress is a key contributor to the injury-induced neurodegeneration (Oakes and Papa, 2015), the single-cell RNA sequencing data indicated that endoplasmic reticulum dysfunction in BBB may be an overlooked mechanism in mTBI. In addition, their data also demonstrated that cellular interactions based on extracellular matrix of endothelial cells are also heavily impacted after mTBI (Arneson et al., 2018), which is consistent with a recent report (Munji et al., 2019). Taken together, deep RNA sequencing and single-cell RNA sequencing data have become valuable resources to explore BBB dysfunction in mTBI, which will likely bring new insights to the true mechanism of vascular impairment after mTBI.

BLOOD–BRAIN BARRIER DYSFUNCTION AND NEUROINFLAMMATION IN MILD TRAUMATIC BRAIN INJURY

In animal models of mTBI, BBB dysfunction is closely associated with neuroinflammation in both acute/subacute stage and chronic period. In the event of mTBI, the tight junction complexes and basement membrane are disrupted, which results in increased permeability of BBB and inflammatory response after injury (Chodobski et al., 2011). Activation of microglia, stimulation of astrocytes, and neuronal cell death are closely associated with neurodegeneration after mTBI (Ramos-Cejudo et al., 2018; **Figure 1**). Notably, many studies reported that microglia and astrocytes are activated in the acute period after mTBI. For example, in a lateral impact of closed head injury mouse model, Tagge et al. (2018) reported that activated microglia and reactive astrocytes were detected at 24 h post-injury in the ipsilateral cortex, which peaked around 3 DPI and started to be resolved in 2 weeks, although perivascular accumulation of hemosiderin-laden macrophages may persist.

Limited evidence has indicated that BBB dysfunction precedes gliosis and neuroinflammation at least in murine models of mTBI. For example, Huh et al. (2008) showed that BBB disruption in their midline CCI rat model of mTBI occurs within

6 h after impact, while glial fibrillary acidic protein (GFAP) immunoreactivity in the cortex at 24 h was comparable to that observed in sham-injured animals, and astrogliosis was only observed on day 3 and day 8 post-injury. As BBB breakdown and extravasation of plasma proteins such as fibrinogen are a driving force of microglia activation after injury (Davalos et al., 2012) and capable of inducing neurotoxic reactive astrocytes after TBI (Liddelow and Barres, 2017; Liddelow et al., 2017) and cognitive impairment (Fulop et al., 2019), the vascular link between mTBI and neuroinflammation should be defined in future studies.

BLOOD–BRAIN BARRIER DYSFUNCTION AND COGNITIVE IMPAIRMENT IN MURINE MILD TRAUMATIC BRAIN INJURY MODELS

Among the 17 articles of BBB dysfunction in mTBI, nine of them studied whether mTBI-induced BBB dysfunction was related to cognitive impairment in mice and rats. Meehan et al. (2012) and Yates et al. (2017) used a weight drop model of mTBI as well as Huh et al. (2008) used a midline brain injury model and found that mTBI induced BBB dysfunction and significant reduction in Morris water maze (MWM) performance from injured mice and rats when compared with sham-operated controls. Yang et al. (2013) also found that mTBI mice with BBB impairment spent significantly less time in investigating a novel object during the novel object recognition test in the first few days. In addition, Katz et al. (2015) used a lateral fluid percussion model to induce mTBI in rats and noted that mTBI rats displayed significant BBB leakage as well as acute cognitive impairment. These injured rats exhibited significantly lower neurological severity score (NSS) and neurobehavioral score (NBS) at 2 and 24 h after injury (Katz et al., 2015). Additionally, Ichkova et al. (2020) found that an early cerebrovascular pathology including BBB disruption may contribute to long-term behavioral deficits in mice following experimental juvenile mTBI, while the exact topographical coherence and the direct causality between these two events require further investigation.

However, Chen et al. (2014) and Laurer et al. (2001) found mTBI caused no significant impairments in either acute or long-term cognitive ability in the CCI models, although BBB dysfunction was reported in these animals. On the other hand, although Kane et al. (2012) and Meehan et al. (2012) found motor and cognitive deficits in mTBI animals, no BBB disruption was observed. While the different injury methodologies between groups may underlie the discrepancies in behavioral outcomes, further studies should still address the link between BBB dysfunction and cognitive impairment in animal models of mTBI.

DISCUSSION

Mild traumatic brain injury commonly occurs in professional sports (such as American football and boxing) and military service, which can be exacerbated by repetitive mild trauma injury (Baker and Patel, 2000). There are growing interests to investigate the acute/subacute and long-term pathologic changes after mTBI, as well as a focus on motor and cognitive impairments. In this study, we collected preclinical evidence from murine models to describe the role of BBB dysfunction in mTBI. BBB plays a key role in maintaining brain function stability, the integrity of BBB may be compromised under pathologic conditions such as TBI, stroke, brain tumor, and AD (Sweeney et al., 2019). For example, previous research showed BBB leakage was detected in a stroke model of rat (Michalski et al., 2010). In our review, we included 17 representative studies that described the BBB breakdown after mTBI. Twelve of them reported that the BBB was compromised after mTBI; however, five studies indicated that BBB breakdown was not detected in mTBI, even in receptive mTBI models. Up to now, it is still unclear whether the minor discrepancy was a result of the differences in mTBI animal models, animal ages, procedures, time points of observation, or methodology.

Mechanistically, impairment of BBB can initiate a series of adverse events, including the leakage of serum-derived circulating agents into the brain parenchyma and improper activation of signaling pathways (Manev, 2009). As some studies indicated that mTBI can induce sustained shear stress located within the impact zone, capillary retraction, pericyte degeneration, and astrocytic endfeet swelling, which all contribute to microvascular injury and BBB breakdown post-insult (Tagge et al., 2018), the exact mechanism of BBB impairment in different models of mTBI could still vary and depend on the severity. Importantly, emerging evidence from human genome-wide association studies suggests that many signature genes and network regulators of TBI may be associated with neurological disorders, which could be used as elements of prognosis and plausible interventional targets for TBI (Meng et al., 2017). Single-cell molecular alterations were reported after mTBI by using unbiased single-cell sequencing, which provides new insights to the molecular pathway mechanism and therapeutics in mTBI and its related neurodegeneration (Arneson et al., 2018).

Mild traumatic brain injury is considered a long-term risk for neurobehavioral changes, cognitive decline, and neurodegenerative disease including AD (McAllister and McCrea, 2017). Cognitive and motor function changes commonly occur after mTBI and may have lifelong consequences, which are still difficult to detect and trace in clinical settings. On the other hand, murine animal models of mTBI provide us quantitative measures and longitudinal follow-ups. Most used methods for motor function tests include Foot-fault, rotarod, and beam walking assays, and cognitive function tests include nest construction, food burrowing, novel object recognition, fear conditioning, MWM, etc. In our review, we found that most studies reported the motor deficit and cognitive impairment after mTBI range from 1 day to several months. However, few studies indicated the absence of motor or cognitive function impairment, which may be due to differences in animal models or procedures as described above. Vascular dysfunction and BBB breakdown are associated with cognitive impairments in aging and neurodegenerative diseases such as AD

(Iadecola, 2004). In the mTBI event, cerebrovascular dysfunction can result in circulatory insufficiency and cause neuronal dysfunction (Jullienne et al., 2016). Edema formation and BBB breakdown after mTBI can also disturb the brain homeostasis and the clearance of toxic products such as β-amyloid, which will accelerate the neuronal damage and contribute to the mTBI-associated late-life neurodegeneration. Can we target vascular dysfunctions in mTBI as a potential therapeutic intervention? Histological and genetic profiling evidence has indicated changes in different BBB modalities after mTBI (Meng et al., 2017; Arneson et al., 2018; Munji et al., 2019; Sandsmark et al., 2019), including alteration of extracellular matrix and basement membrane, metalloproteinase, etc. Targeting these endophenotypes may offer novel therapeutic opportunities. But the journey is still out there.

CONCLUSION

In this review, we focused on BBB dysfunction after mTBI in murine models and found that BBB breakdown and microvascular impairment are important pathological mechanisms for cognitive impairment after mTBI. Restoring vascular functions might be beneficial for patients with mTBI and reduce the risk of developing cognitive impairments post-insult.

AUTHOR CONTRIBUTIONS

ZZ and YW designed the review outline, wrote and reviewed the review, did the literature search, and data extraction and interpretation. HW, XG, and BP provided critical reviews, revised the manuscript, and provided relevant insights and edits. All authors read and approved the final version of the manuscript.

FUNDING

The work of ZZ is supported by the National Institutes of Health (NIH) grant nos. R01AG061288, R01NS110687, R03AG063287, and R21AG066090; Department of Defense (DOD) grant AZ190072; and Bright Focus Foundation grant A2019218S.

REFERENCES

Adams, C., Bazzigaluppi, P., Beckett, T. L., Bishay, J., Weisspapir, I., Dorr, A., et al. (2018). Neurogliovascular dysfunction in a model of repeated traumatic brain injury. *Theranostics* 8, 4824–4836. doi: 10.7150/thno.24747

Arneson, D., Zhang, G., Ying, Z., Zhuang, Y., Byun, H. R., Ahn, I. S., et al. (2018). Single cell molecular alterations reveal target cells and pathways of concussive brain injury. *Nat. Commun.* 9:3894. doi: 10.1038/s41467-018-06222-0

Baker, R. J., and Patel, D. R. (2000). Sports related mild traumatic brain injury in adolescents. *Indian J. Pediatr.* 67, 317–321. doi: 10.1007/bf02820676

Bashir, A., Abebe, Z. A., McInnes, K. A., Button, E. B., Tatarnikov, I., Cheng, W. H., et al. (2020). Increased severity of the CHIMERA model induces acute vascular injury, sub-acute deficits in memory recall, and chronic white matter gliosis. *Exp. Neurol.* 324:113116. doi: 10.1016/j.expneurol.2019.113116

Bharadwaj, V. N., Rowe, R. K., Harrison, J., Wu, C., Anderson, T. R., Lifshitz, J., et al. (2018). Blood–brain barrier disruption dictates nanoparticle accumulation following experimental brain injury. *Nanomedicine* 14, 2155–2166. doi: 10.1016/j.nano.2018.06.004

Bhowmick, S., D'Mello, V., Caruso, D., Wallerstein, A., and Abdul-Muneer, P. M. (2019). Impairment of pericyte-endothelium crosstalk leads to blood-brain barrier dysfunction following traumatic brain injury. *Exp. Neurol.* 317, 260–270. doi: 10.1016/j.expneurol.2019.03.014

Blennow, K., Hardy, J., and Zetterberg, H. (2012). The neuropathology and neurobiology of traumatic brain injury. *Neuron* 76, 886–899. doi: 10.1016/j.neuron.2012.11.021

Bodnar, C. N., Roberts, K. N., Higgins, E. K., and Bachstetter, A. D. (2019). A systematic review of closed head injury models of mild traumatic brain injury in mice and rats. *J. Neurotrauma* 36, 1683–1706. doi: 10.1089/neu.2018.6127

Chamelian, L., and Feinstein, A. (2004). Outcome after mild to moderate traumatic brain injury: the role of dizziness. *Arch. Phys. Med. Rehabil.* 85, 1662–1666. doi: 10.1016/j.apmr.2004.02.012

Chen, Y., Mao, H., Yang, K. H., Abel, T., and Meaney, D. F. (2014). A modified controlled cortical impact technique to model mild traumatic brain injury mechanics in mice. *Front. Neurol.* 5:100. doi: 10.3389/fneur.2014.00100

Chodobski, A., Zink, B. J., and Szmydynger-Chodobska, J. (2011). Blood-brain barrier pathophysiology in traumatic brain injury. *Transl. Stroke Res.* 2, 492–516. doi: 10.1007/s12975-011-0125-x

Chung, J. Y., Krapp, N., Wu, L., Lule, S., McAllister, L. M., Edmiston, W. J., et al. (2019). Interleukin-1 receptor 1 deletion in focal and diffuse experimental traumatic brain injury in mice. *J. Neurotrauma* 36, 370–379. doi: 10.1089/neu.2018.5659

Clément, T., Lee, J. B., Ichkova, A., Rodriguez-Grande, B., Fournier, M.-L., Aussudre, J., et al. (2020). Juvenile mild traumatic brain injury elicits distinct spatiotemporal astrocyte responses. *Glia* 68, 528–542. doi: 10.1002/glia.23736

Daneman, R., and Prat, A. (2015). The blood-brain barrier. *Cold Spring Harb. Perspect. Biol.* 7:a020412. doi: 10.1101/cshperspect.a020412

Davalos, D., Kyu Ryu, J., Merlini, M., Baeten, K. M., Le Moan, N., Petersen, M. A., et al. (2012). Fibrinogen-induced perivascular microglial clustering is required for the development of axonal damage in neuroinflammation. *Nat. Commun.* 3:1227. doi: 10.1038/ncomms2230

Doherty, C. P., O'Keefe, E., Wallace, E., Loftus, T., Keaney, J., Kealy, J., et al. (2016). Blood-brain barrier dysfunction as a hallmark pathology in chronic traumatic encephalopathy. *J. Neuropathol. Exp. Neurol.* 75, 656–662. doi: 10.1093/jnen/nlw036

Fulop, G. A., Ahire, C., Csipo, T., Tarantini, S., Kiss, T., Balasubramanian, P., et al. (2019). Cerebral venous congestion promotes blood-brain barrier disruption and neuroinflammation, impairing cognitive function in mice. *Geroscience* 41, 575–589. doi: 10.1007/s11357-019-00110-1

Gama Sosa, M. A., De Gasperi, R., Janssen, P. L., Yuk, F. J., Anazodo, P. C., Pricop, P. E., et al. (2014). Selective vulnerability of the cerebral vasculature to blast injury in a rat model of mild traumatic brain injury. *Acta Neuropathol. Commun.* 2:67. doi: 10.1186/2051-5960-2-67

Hackenberg, K., and Unterberg, A. (2016). [Traumatic brain injury]. *Nervenarzt* 87, 203–216. doi: 10.1007/s00115-015-0051-3

Han, X., Chai, Z., Ping, X., Song, L.-J., Ma, C., Ruan, Y., et al. (2020). In vivo two-photon imaging reveals acute cerebral vascular spasm and microthrombosis after mild traumatic brain injury in mice. *Front. Neurosci.* 14:210. doi: 10.3389/fnins.2020.00210

Huh, J. W., Widing, A. G., and Raghupathi, R. (2008). Midline brain injury in the immature rat induces sustained cognitive deficits, bihemispheric axonal injury and neurodegeneration. *Exp. Neurol.* 213, 84–92. doi: 10.1016/j.expneurol.2008.05.009

Iadecola, C. (2004). Neurovascular regulation in the normal brain and in Alzheimer's disease. *Nat. Rev. Neurosci.* 5, 347–360. doi: 10.1038/nrn1387

Ichkova, A., Rodriguez-Grande, B., Zub, E., Saudi, A., Fournier, M.-L., Aussudre, J., et al. (2020). Early cerebrovascular and long-term neurological modifications ensue following juvenile mild traumatic brain injury in male mice. *Neurobiol. Dis.* 141:104952. doi: 10.1016/j.nbd.2020.104952

Jullienne, A., Obenaus, A., Ichkova, A., Savona-Baron, C., Pearce, W. J., and Badaut, J. (2016). Chronic cerebrovascular dysfunction after traumatic brain injury. *J. Neurosci. Res.* 94, 609–622. doi: 10.1002/jnr.23732

Kane, M. J., Angoa-Pérez, M., Briggs, D. I., Viano, D. C., Kreipke, C. W., and Kuhn, D. M. (2012). A mouse model of human repetitive mild traumatic brain injury. *J. Neurosci. Methods* 203, 41–49. doi: 10.1016/j.jneumeth.2011.09.003

Katz, P. S., Sulzer, J. K., Impastato, R. A., Teng, S. X., Rogers, E. K., and Molina, P. E. (2015). Endocannabinoid degradation inhibition improves neurobehavioral function, blood-brain barrier integrity, and neuroinflammation following mild traumatic brain injury. *J. Neurotrauma* 32, 297–306. doi: 10.1089/neu.2014.3508

Korn, A., Golan, H., Melamed, I., Pascual-Marqui, R., and Friedman, A. (2005). Focal cortical dysfunction and blood-brain barrier disruption in patients with Postconcussion syndrome. *J. Clin. Neurophysiol.* 22, 1–9. doi: 10.1097/01.wnp.0000150973.24324.a7

Laurer, H. L., Bareyre, F. M., Lee, V. M., Trojanowski, J. Q., Longhi, L., Hoover, R., et al. (2001). Mild head injury increasing the brain's vulnerability to a second concussive impact. *J. Neurosurg.* 95, 859–870. doi: 10.3171/jns.2001.95.5.0859

Li, S., Li, H., He, X.-F., Li, G., Zhang, Q., Liang, F.-Y., et al. (2016). Transgenic over-expression of slit2 enhances disruption of blood-brain barrier and increases cell death after traumatic brain injury in mice. *Neurosci. Lett.* 631, 85–90. doi: 10.1016/j.neulet.2016.08.013

Liddelow, S. A., and Barres, B. A. (2017). Reactive astrocytes: production, function, and therapeutic potential. *Immunity* 46, 957–967. doi: 10.1016/j.immuni.2017.06.006

Liddelow, S. A., Guttenplan, K. A., Clarke, L. E., Bennett, F. C., Bohlen, C. J., Schirmer, L., et al. (2017). Neurotoxic reactive astrocytes are induced by activated microglia. *Nature* 541, 481–487. doi: 10.1038/nature21029

Lifshitz, J., Rowe, R. K., Griffiths, D. R., Evilsizor, M. N., Thomas, T. C., Adelson, P. D., et al. (2016). Clinical relevance of midline fluid percussion brain injury: acute deficits, chronic morbidities and the utility of biomarkers. *Brain Injury* 30, 1293–1301. doi: 10.1080/02699052.2016.1193628

Lipponen, A., Paananen, J., Puhakka, N., and Pitkänen, A. (2016). Analysis of post-traumatic brain injury gene expression signature reveals tubulins, Nfe2l2, Nfkb, Cd44, and S100a4 as treatment targets. *Sci. Rep.* 6:31570. doi: 10.1038/srep31570

Logsdon, A. F., Meabon, J. S., Cline, M. M., Bullock, K. M., Raskind, M. A., Peskind, E. R., et al. (2018). Blast exposure elicits blood-brain barrier disruption and repair mediated by tight junction integrity and nitric oxide dependent processes. *Sci. Rep.* 8:11344. doi: 10.1038/s41598-018-29341-6

Lynch, C. E., Crynen, G., Ferguson, S., Mouzon, B., Paris, D., Ojo, J., et al. (2016). Chronic cerebrovascular abnormalities in a mouse model of repetitive mild traumatic brain injury. *Brain Injury* 30, 1414–1427. doi: 10.1080/02699052.2016.1219060

Manev, H. (2009). Hypotheses on mechanisms linking cardiovascular and psychiatric/neurological disorders. *Cardiovasc. Psychiatry Neurol.* 2009:197132. doi: 10.1155/2009/197132

McAllister, T., and McCrea, M. (2017). Long-term cognitive and neuropsychiatric consequences of repetitive concussion and head-impact exposure. *J. Athl. Train* 52, 309–317. doi: 10.4085/1062-6050-52.1.14

Meehan, W. P., Zhang, J., Mannix, R., and Whalen, M. J. (2012). Increasing recovery time between injuries improves cognitive outcome after repetitive mild concussive brain injuries in mice. *Neurosurgery* 71, 885–891. doi: 10.1227/NEU.0b013e318265a439

Meng, Q., Zhuang, Y., Ying, Z., Agrawal, R., Yang, X., and Gomez-Pinilla, F. (2017). Traumatic brain injury induces genome-wide transcriptomic, methylomic, and network perturbations in brain and blood predicting neurological disorders. *EBioMedicine* 16, 184–194. doi: 10.1016/j.ebiom.2017.01.046

Michalski, D., Grosche, J., Pelz, J., Schneider, D., Weise, C., Bauer, U., et al. (2010). A novel quantification of blood-brain barrier damage and histochemical typing after embolic stroke in rats. *Brain Res.* 1359, 186–200. doi: 10.1016/j.brainres.2010.08.045

Munji, R. N., Soung, A. L., Weiner, G. A., Sohet, F., Semple, B. D., Trivedi, A., et al. (2019). Profiling the mouse brain endothelial transcriptome in health and disease models reveals a core blood–brain barrier dysfunction module. *Nat. Neurosci.* 22, 1892–1902. doi: 10.1038/s41593-019-0497-x

Oakes, S. A., and Papa, F. R. (2015). The role of endoplasmic reticulum stress in human pathology. *Annu. Rev. Pathol. Mech. Dis.* 10, 173–194. doi: 10.1146/annurev-pathol-012513-104649

O'Keeffe, E., Kelly, E., Liu, Y., Giordano, C., Wallace, E., Hynes, M., et al. (2020). Dynamic blood-brain barrier regulation in mild traumatic brain injury. *J. Neurotrauma* 37, 347–356. doi: 10.1089/neu.2019.6483

Ramos-Cejudo, J., Wisniewski, T., Marmar, C., Zetterberg, H., Blennow, K., de Leon, M. J., et al. (2018). Traumatic brain injury and Alzheimer's disease: the cerebrovascular link. *EBioMedicine* 28, 21–30.

Redell, J. B., Moore, A. N., Grill, R. J., Johnson, D., Zhao, J., Liu, Y., et al. (2013). Analysis of functional pathways altered after mild traumatic brain injury. *J. Neurotrauma* 30, 752–764. doi: 10.1089/neu.2012.2437

Riggio, S. (2011). Traumatic brain injury and its neurobehavioral sequelae. *Neurol. Clin.* 29, 35–47. doi: 10.1016/j.ncl.2010.10.008

Rodriguez-Grande, B., Obenaus, A., Ichkova, A., Aussudre, J., Bessy, T., Barse, E., et al. (2018). Gliovascular changes precede white matter damage and long-term disorders in juvenile mild closed head injury. *Glia* 66, 1663–1677. doi: 10.1002/glia.23336

Rutland-Brown, W., Langlois, J. A., Thomas, K. E., and Xi, Y. L. (2006). Incidence of traumatic brain injury in the United States, 2003. *J. Head Trauma Rehabil.* 21, 544–548. doi: 10.1097/00001199-200611000-00009

Salehi, A., Zhang, J. H., and Obenaus, A. (2017). Response of the cerebral vasculature following traumatic brain injury. *J. Cereb. Blood Flow Metab.* 37, 2320–2339. doi: 10.1177/0271678X17701460

Sandsmark, D. K., Bashir, A., Wellington, C. L., and Diaz-Arrastia, R. (2019). Cerebral microvascular injury: a potentially treatable endophenotype of traumatic brain injury-induced neurodegeneration. *Neuron* 103, 367–379. doi: 10.1016/j.neuron.2019.06.002

Shlosberg, D., Benifla, M., Kaufer, D., and Friedman, A. (2010). Blood-brain barrier breakdown as a therapeutic target in traumatic brain injury. *Nat. Rev. Neurol.* 6, 393–403. doi: 10.1038/nrneurol.2010.74

Sweeney, M. D., Zhao, Z., Montagne, A., Nelson, A. R., and Zlokovic, B. V. (2019). Blood-brain barrier: from physiology to disease and back. *Physiol. Rev.* 99, 21–78. doi: 10.1152/physrev.00050.2017

Tagge, C. A., Fisher, A. M., Minaeva, O. V., Gaudreau-Balderrama, A., Moncaster, J. A., Zhang, X.-L., et al. (2018). Concussion, microvascular injury, and early tauopathy in young athletes after impact head injury and an impact concussion mouse model. *Brain* 141, 422–458. doi: 10.1093/brain/awx350

Tomkins, O., Feintuch, A., Benifla, M., Cohen, A., Friedman, A., and Shelef, I. (2011). Blood-brain barrier breakdown following traumatic brain injury: a possible role in posttraumatic epilepsy. *Cardiovasc. Psychiatry Neurol.* 2011:765923. doi: 10.1155/2011/765923

Vanlandewijck, M., He, L., Mäe, M. A., Andrae, J., Ando, K., Del Gaudio, F., et al. (2018). A molecular atlas of cell types and zonation in the brain vasculature. *Nature* 554, 475–480. doi: 10.1038/nature25739

Villalba, N., Sackheim, A. M., Nunez, I. A., Hill-Eubanks, D. C., Nelson, M. T., Wellman, G. C., et al. (2017). Traumatic Brain Injury Causes Endothelial Dysfunction in the Systemic Microcirculation through Arginase-1-Dependent Uncoupling of Endothelial Nitric Oxide Synthase. *J. Neurotrauma* 34, 192–203. doi: 10.1089/neu.2015.4340

von Gertten, C., Flores Morales, A., Holmin, S., Mathiesen, T., and Nordqvist, A.-C. S. (2005). Genomic responses in rat cerebral cortex after traumatic brain injury. *BMC Neurosci.* 6:69. doi: 10.1186/1471-2202-6-69

Weissberg, I., Veksler, R., Kamintsky, L., Saar-Ashkenazy, R., Milikovsky, D. Z., Shelef, I., et al. (2014). Imaging blood-brain barrier dysfunction in football players. *JAMA Neurol.* 71, 1453–1455. doi: 10.1001/jamaneurol.2014.2682

Wendel, K. M., Lee, J. B., Affeldt, B. M., Hamer, M., Harahap-Carrillo, I. S., Pardo, A. C., et al. (2018). Corpus callosum vasculature predicts white matter microstructure abnormalities after pediatric mild traumatic brain injury. *J. Neurotrauma* [Online ahead of print]. doi: 10.1089/neu.2018.5670

Wu, L., Chung, J. Y., Saith, S., Tozzi, L., Buckley, E. M., Sanders, B., et al. (2019). Repetitive head injury in adolescent mice: a role for vascular inflammation. *J. Cereb. Blood Flow Metab.* 39, 2196–2209. doi: 10.1177/0271678X18786633

Yang, S. H., Gustafson, J., Gangidine, M., Stepien, D., Schuster, R., Pritts, T. A., et al. (2013). A murine model of mild traumatic brain injury exhibiting cognitive and motor deficits. *J. Surg. Res.* 184, 981–988. doi: 10.1016/j.jss.2013.03.075

Yates, N. J., Lydiard, S., Fehily, B., Weir, G., Chin, A., Bartlett, C. A., et al. (2017). Repeated mild traumatic brain injury in female rats increases lipid peroxidation in neurons. *Exp. Brain Res.* 235, 2133–2149. doi: 10.1007/s00221-017-4958-8

Yoo, R.-E., Choi, S. H., Oh, B.-M., Do Shin, S., Lee, E. J., Shin, D. J., et al. (2019). Quantitative dynamic contrast-enhanced MR imaging shows widespread

blood-brain barrier disruption in mild traumatic brain injury patients with post-concussion syndrome. *Eur. Radiol.* 29, 1308–1317. doi: 10.1007/s00330-018-5656-z

Zehendner, C. M., Sebastiani, A., Hugonnet, A., Bischoff, F., Luhmann, H. J., and Thal, S. C. (2015). Traumatic brain injury results in rapid pericyte loss followed by reactive pericytosis in the cerebral cortex. *Sci. Rep.* 5:13497. doi: 10.1038/srep13497

Zhao, Z., Nelson, A. R., Betsholtz, C., and Zlokovic, B. V. (2015). Establishment and dysfunction of the blood-brain barrier. *Cell* 163, 1064–1078. doi: 10.1016/j.cell.2015.10.067

Conflict of Interest: The authors declare that the research was conducted in the absence of any commercial or financial relationships that could be construed as a potential conflict of interest.

frontiers in Physiology

MINI REVIEW
published: 27 August 2020
doi: 10.3389/fphys.2020.01056

New Insights Into Blood-Brain Barrier Maintenance: The Homeostatic Role of β-Amyloid Precursor Protein in Cerebral Vasculature

*Emma Ristori[1], Sandra Donnini[1]*and Marina Ziche[2]**

[1]Department of Life Sciences, University of Siena, Siena, Italy, [2]Department of Medicine, Surgery and Neuroscience, University of Siena, Siena, Italy

OPEN ACCESS

Edited by:
Clotilde Lecrux, McGill University, Canada

Reviewed by:
Satoshi Saito, National Cerebral and Cardiovascular Center, Japan
Alla B. Salmina, Krasnoyarsk State Medical University named after Prof. V.F.Voino-Yasenetski, Russia

***Correspondence:**
Sandra Donnini
sandra.donnini@unisi.it
Marina Ziche
marina.ziche@unisi.it

Specialty section:
This article was submitted to Vascular Physiology, a section of the journal Frontiers in Physiology

Received: *03 April 2020*
Accepted: *31 July 2020*
Published: *27 August 2020*

Citation:
Ristori E, Donnini S and Ziche M (2020) New Insights Into Blood-Brain Barrier Maintenance: The Homeostatic Role of β-Amyloid Precursor Protein in Cerebral Vasculature. Front. Physiol. 11:1056. doi: 10.3389/fphys.2020.01056

Cerebrovascular homeostasis is maintained by the blood-brain barrier (BBB), a highly selective structure that separates the peripheral blood circulation from the brain and protects the central nervous system (CNS). Dysregulation of BBB function is the precursor of several neurodegenerative diseases including Alzheimer's disease (AD) and cerebral amyloid angiopathy (CAA), both related to β-amyloid (Aβ) accumulation and deposition. The origin of BBB dysfunction before and/or during CAA and AD onset is not known. Several studies raise the possibility that vascular dysfunction could be an early step in these diseases and could even precede significant Aβ deposition. Though accumulation of neuron-derived Aβ peptides is considered the primary influence driving AD and CAA pathogenesis, recent studies highlighted the importance of the physiological role of the β-amyloid precursor protein (APP) in endothelial cell homeostasis, suggesting a potential role of this protein in maintaining vascular stability. In this review, we will discuss the physiological function of APP and its cleavage products in the vascular endothelium. We further suggest how loss of APP homeostatic regulation in the brain vasculature could lead toward pathological outcomes in neurodegenerative disorders.

Keywords: blood-brain barrier, β-Amyloid precursor protein, Alzheimer's disease, cerebral amyloid angiopathy, vascular homeostasis, β-Amyloid

INTRODUCTION

The brain vasculature is characterized by the presence of the blood-brain barrier (BBB), a specialized structure that maintains the separation between the circulating blood and central nervous system (CNS). The BBB surrounds most of the vessels in the brain and is characterized by the establishment of specialized endothelial tight junctions that consist of transmembrane proteins (claudin3/5, occludins, and JAMs) and cytoplasmic scaffolding proteins (e.g., ZO-1, ZO-2, and ZO-3), involved in cell-to-cell contacts and interacting with actin cytoskeleton and associated proteins (G-proteins, protein kinases, and small GTPases). The tightly interconnected endothelial cells that form the inner lining of BBB vessels not only deliver nutrients and oxygen to brain tissues to ensure neuronal function but also protect the brain by limiting entry of

toxins, pathogen, and inflammatory cells. BBB is not the same in all the regions through the brain. While most blood vessels in the brain are situated in the BBB, there are some regions, like the circum-ventricular organs where the microvessels are permeable and lack this specialized structure, allowing the free passage of substances (Wilhelm et al., 2016). The BBB is an essential part of the neurovascular unit (NVU), defined as a complex functional and anatomical structure composed of BBB endothelium, basement membranes (basal lamina and extracellular membranes), astrocytes, pericytes, microglial cells, and neurons. In this context, the neuronal-vascular interaction is critical for proper brain function, and the structural and functional integrity of blood vessels is essential to maintain appropriate brain perfusion and to preserve normal neurological function. Pathological changes in the NVU, including impairment of neurovascular coupling and BBB dysfunction, are present in a variety of neurovascular diseases (Chou et al., 2015; Cai et al., 2017; Iadecola, 2017; Liu et al., 2019; Nizari et al., 2019; Nortley et al., 2019). Increasing evidence supports the hypothesis that vascular dysfunction plays a major role in β-amyloid (Aβ) diseases such as cerebral amyloid angiopathy (CAA) and Alzheimer's disease (AD) (de la Torre, 2018; Klohs, 2020). While AD is characterized by formation of amyloid plaques in the brain parenchyma, CAA refers to Aβ deposits on the walls of cerebrovasculature. CAA is a common comorbidity of patients with AD. Though accumulation of neuron-derived Aβ in the brain and vessel walls is considered the primary influence driving CAA and AD pathogenesis, clinical trials based on immunotherapy that target and clear Aβ have failed to reverse cognitive loss. The most-cited explanation for the failure of such trials is that the drugs were given too late in the progression of the disease, when the process of Aβ deposition was advanced and at a point of no return in the progression of the disease. This is due in part to an incomplete understanding of the mechanisms that trigger Aβ aggregation and deposition and a lack of notions about the functional role of this peptide and its precursor protein, the amyloid precursor protein (APP) in the cerebrovascular homeostasis. Interestingly, immunotherapy with bapineuzumab, a monoclonal antibody targeting both fibrillar and soluble Aβ, showed severe vascular adverse events like brain vasogenic edema and microhemorrhages, possibly due to a loss in cerebrovascular integrity (Gustafsson et al., 2018). This suggests that physiological levels of Aβ are necessary for normal vascular homeostasis. Furthermore, several studies showed the importance of Aβ and APP for proper physiological function of endothelium, and APP has been hypothesized to play a protective role in vascular dysfunction. In this work, we summarize these findings and highlight the importance of APP and its metabolites on the normal physiology of the vascular system.

APP PROCESSING IN HEALTH AND DISEASE

APP belongs to a conserved gene family that includes two mammalian homologues, the APP-like proteins (APLPs), APLP1 and APLP2. These proteins are type I integral membrane proteins that share similar structural organization and partially overlapping functions, and this may explain why single-gene-knockout animal models have failed to show any major phenotype (Shariati and De Strooper, 2013). Structurally, APP and APLPs share conserved regions, although APP is the only family member containing the sequence encoding Aβ peptides (d'Uscio et al., 2017). APP presents three major isoforms, generated by alternative splicing: APP695, APP751, and APP770. The APP695 isoform is mainly expressed in neurons, whereas APP751 and APP770 are the predominant forms expressed in non-neuronal cells, including endothelial cells and platelets (Van Nostrand et al., 1994). Under physiological conditions, APP is cleaved by different secretases through two main proteolytic pathways: the amyloidogenic and non-amyloidogenic processing (**Figure 1**). The latter leads to the release in the extracellular space of the soluble form soluble amyloid precursor protein (sAPP-α) generated by α-secretase (ADAM10) cleavage and the p3 peptide through cleavage of α-secretase and the γ-secretase complex (composed of four subunits: presenilins, nicastrin, Aph-1, and Pen-2). By contrast, in the amyloidogenic processing, β-secretase (BACE1) cleavage releases soluble amyloid precursor protein cleaved by β-secretase (sAPP-β; another soluble form with different structure and physiological properties), and subsequent cleavage of BACE1 and γ-secretase generates different Aβ isoforms of various lengths. Moreover, γ-secretase cleavage in the APP transmembrane region yields the biologically active APP intracellular domain (AICD) in both the proteolytic pathways. The main species of Aβ peptides involved in CAA and AD are Aβ1-40 and Aβ1-42. The Aβ1-42 peptides are the predominant form in AD neuronal plaques, whereas deposition of Aβ1-40 peptides on the cerebral vasculature contributes to the onset of CAA (Stakos et al., 2020). While the neuronal origin of Aβ deposits observed in

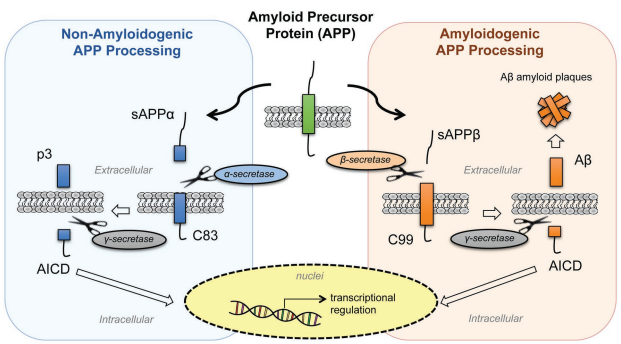

FIGURE 1 | Processing of amyloid precursor protein (APP). APP is processed by two proteolytic pathways: the non-amyloidogenic processing (in blue) and the amyloidogenic processing (in orange). The non-amyloidogenic processing releases in the extracellular space sAPPα and p3 fragments, while the amyloidogenic processing releases sAPPβ and β-amyloid (Aβ) peptides. Both pathways release APP intracellular domain (AICD) fragments into the intracellular space that then translocate to the nuclei and regulate cellular transcription. [sAPPα, soluble amyloid precursor protein; p3, APP non-amyloidogenic extracellular fragment; C83 (βCTF), APP C-terminal fragment beta; AICD, APP intracellular domain; sAPPβ, soluble amyloid precursor protein cleaved by β-secretase; Aβ, beta-amyloid peptide; C89 (αCTF), APP C-terminal fragment alpha].

AD and CAA is well established, evidences show that activated endothelial cells and platelets are also able to release Aβ1-40 peptides (Kitazume et al., 2012; Canobbio et al., 2015). Under normal physiological conditions, APP is predominantly processed through the non-amyloidogenic pathway, and the Aβ peptide is constitutively generated at relatively low levels. In addition, several mechanisms of Aβ clearance involving the cerebrovasculature contribute to maintain the concentrations of these peptides to physiological levels in the brain. Some of these mechanisms include Aβ degradation by proteolytic enzymes, phagocytosis by macrophages, intramural periarterial drainage, and receptor mediated Aβ transport across the BBB in which the main transport proteins are: the P-glycoprotein (P-gp), the low-density lipoprotein receptor related protein-1 (LRP-1), and the receptor for advanced glycation end-products (RAGE). While LRP-1 mediates the efflux of Aβ from the brain to the blood circulation, RAGE plays an opposite role by promoting the influx to the brain, thus promoting its accumulation in the parenchyma (Deane et al., 2004; Wan et al., 2014; Wang et al., 2016). Impaired clearance of Aβ across the cerebrovascular endothelium is considered the main cause of CAA (Qi and Ma, 2017). Recent studies suggested the involvement of heparan sulfate proteoglycans (HSPGs) in modulating Aβ clearance and that the altered distribution and increased levels of HSPGs in AD brains might contribute to Aβ aggregation and plaque formation (Zhang et al., 2014; Liu et al., 2016). Interestingly, APP processing is influenced by its cellular distribution: the cell-surface accumulation of APP favors non-amyloidogenic processing (Jiang et al., 2014). On the contrary, the retention of APP in acidic compartments, such as early endosomes, promotes amyloidogenic processing (O'Brien and Wong, 2011). Furthermore, the soluble fragment sAPP-α has a role in the auto regulation of APP processing. One of the proposed mechanisms is that the sAPP-α modulates BACE1 activity promoting the non-amyloidogenic process of APP, thus decreasing Aβ production (Kaden et al., 2008; Gralle et al., 2009; Obregon et al., 2012). All cell types in the NVU express APP and release biologically active APP metabolites, however increasing evidence suggests that dysregulation of APP homeostasis in the brain vasculature would shift the balance toward pathological outcomes. In fact, reduced expression of APP in senescent brain microvascular endothelium contributes to downregulation of sAPPα and promotes the amyloidogenic processing of APP, suggesting that aging-induced loss of APP function might increase the susceptibility to neurovascular dysfunction (Kern et al., 2006; Sun et al., 2018). Moreover, the amyloidogenic secretase BACE1 shows an age-related increased expression and activity in specific brain regions (e.g., cortex) in a mouse model, probably due to alterations of the cellular microenvironment (Chiocco and Lamb, 2007). Not only Aβ production but also its accumulation appears to follow an age-related specific regional pattern (e.g., leptomeningeal and parenchymal vessels), indicating age- and spatial-related efficiency of BBB mechanisms for Aβ clearance and degradation (Lewis et al., 2006; van Assema et al., 2012; Zoufal et al., 2020). Based on this evidence, the alteration of APP expression and processing affects the integrity and functionality of neurovascular tissues, and this may be a critical step in the pathogenesis of neurodegenerative diseases.

APP AND CEREBRAL VASCULATURE

APP is highly expressed in embryonic endothelium, suggesting an important role of this macromolecule and its metabolites in early angiogenesis (Ott and Bullock, 2001). A strong correlation between APP loss-of-function models and vascular dysfunction has been reported, supporting the importance of this protein and its metabolites on vascular homeostasis. In the zebrafish embryo, knockdown of APP by morpholino causes diffused angiogenic defects especially in the brain. This phenotype can be rescued by reintroducing Aβ peptides supporting the hypothesis that these peptides have an essential role in angiogenesis during embryonic development (Luna et al., 2013). Indeed, blocking Aβ production by inhibition of BACE1 or γ-secretase activity causes reduced angiogenesis both *in vitro* and *in vivo* (Paris et al., 2005). Several studies showed that APP exerts vascular protective properties under physiological conditions. APP regulates expression and function of endothelial nitric oxide synthase (eNOS) in cerebrovascular endothelium (d'Uscio et al., 2018). Loss of APP leads to a loss of eNOS protein expression and to an increase of oxidative stress both *in vivo* and *in vitro* models (d'Uscio et al., 2018; d'Uscio and Katusic, 2019). On the other hand, in $eNOS^{+/-}$ mouse model, reduced availability of endothelial NO leads to increased cerebrovascular concentrations of Aβ (Austin and Katusic, 2020) and transgenic mice overexpressing APP show increased oxidative stress and cerebrovascular dysfunction, associated with altered vasoactive signaling (Tong et al., 2005). In experimental models of stroke, the compensatory increase in cerebrovascular blood flow induced by the occlusion of the common carotid artery is attenuated in $APP^{-/-}$ mice (Koike et al., 2012). Due to this reduced ability to adjust blood flow, $APP^{-/-}$ mice die shortly after the common carotid artery occlusion, whereas wild-type mice survive. Conversely, in transgenic-AD rats, the overexpression of wild-type APP in neuronal tissue exerts neuroprotective effect from ischemic damage (Clarke et al., 2007). APP may also play a role in pathogenesis of atherosclerosis. APP and Aβ can be found in advanced human carotid plaques and in atherosclerotic aortas of Apolipoprotein E-deficient ($apoE^{-/-}$) mice, where the APP overexpression in this mouse model accelerates the development of aortic atherosclerotic (De Meyer et al., 2002; Austin et al., 2009; Tibolla et al., 2010). Moreover, transgenic B6Tg2576 mice overexpressing double Swedish mutated human APP (K670N/M671L) develop non-dietary induced early atherosclerotic (Li et al., 2003). On the contrary, the lack of APP attenuated atherogenesis and leads to plaque stability in double knockout mice $APP^{-/-}/apoE^{-/-}$ (Van De Parre et al., 2011). A recent study suggested that the increased pulsatile stretch on the microvessel walls induced by hypertension functions as a mechanic stimulus that modifies the expression and processing of APP, promoting APP overexpression, and favoring APP amyloidogenic processing, and linking APP processing with hypertension (Gangoda et al., 2018). Moreover, modifications of vascular tone could be caused by an alteration of normal

neurovascular coupling. Since components of the NVU, such as astrocytes and neurons, control vasodilation by releasing vasoactive molecules, altered vasomotor signals might affect APP processing in cerebral microvasculature (Niwa et al., 2001, 2002; Park et al., 2004, 2005). These studies suggest that several vascular risk factors are linked to APP dysfunction. Although the vascular function of APP has not been defined yet, these evidences suggest the importance of this protein on vascular development and on maintaining the normal tissue homeostasis.

APP PHYSIOLOGICAL ROLES IN CEREBRAL VASCULATURE

Several physiological roles have been attributed to APP and its processing products, some of which impact neurovascular development and function. Even if APP is notoriously known for its contribution to pathogenesis of neurodegenerative diseases, and many physiological roles have been identified in neural cells (Perez et al., 1997; Nicolas and Hassan, 2014; Nhan et al., 2015; Habib et al., 2017; Coronel et al., 2018), little is known on its function on endothelial cells and cerebral vasculature (**Figure 2**). Growing evidence suggests that perturbations of some of APP functional activities may contribute to cerebral angiopathy and neurodegeneration (Pearson and Peers, 2006; Thinakaran and Koo, 2008; d'Uscio et al., 2017; Muller et al., 2017). Studying APP cellular functions is complex since both the full-length protein and the secreted or intracellular metabolites have biological activity. The Aβ peptide appears to be involved in protecting the body from various types of infections, sealing leaks in the BBB, improving outcomes after injury, and stimulating angiogenesis by modifying the response to angiogenic factors (Cantara et al., 2004; Brothers et al., 2018). Full-length APP protein has been suggested to function as an important factor for proper migration of neuronal precursors into the cortical plate during the development of mammalian brain (Young-Pearse et al., 2007). The secreted ectodomain sAPP-α is sufficient to rescue prominent deficits in $APP^{-/-}$ mice such as reduction in brain and body weight, impairment in spatial learning, and long-term potentiation (Ring et al., 2007). Moreover, different APP isoforms may have distinct roles in various cell types. While the intracellular C-terminus is conserved in all APP isoforms, the extracellular N-terminus of APP differs between isoforms. The endothelial-specific isoforms, APP751 and APP770, contain two conserved extracellular regions (E1 and E2) connected by an acidic domain (AcD), a Kunitz protease inhibitor (KPI) region, and an OX-2 antigen domain, while the neuronal isoform APP695 lacks the KPI and OX-2 domains. The N-terminal of all APP isoforms presents functional binding sites for metals (zinc and copper) and extracellular matrix (ECM) proteins (heparin, collagen, and laminin; Zheng and Koo, 2011; van der Kant and Goldstein, 2015). Here, we summarize the physiological roles of APP full-length protein and its metabolites in cerebral vasculature.

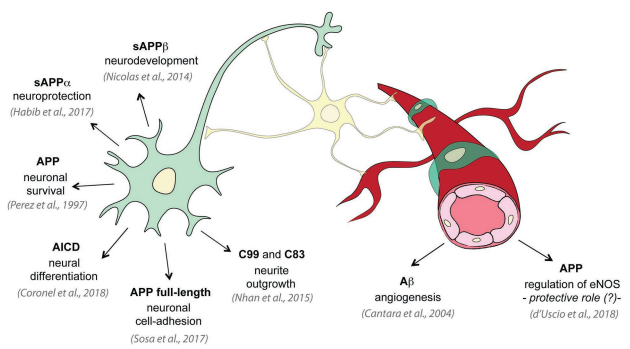

FIGURE 2 | Physiological roles of APP and its metabolites. Several studies investigated the physiological functions of APP on neural tissue: APP promotes neuron viability and axonogenesis (Perez et al., 1997); membrane APP full-length protein shows cell-adhesive properties in neurons (Sosa et al., 2017); sAPPα has been shown to be neuroprotective and to have neuronal trophic properties (Habib et al., 2017); sAPPβ is important for neuronal development (Nicolas and Hassan, 2014); C99 and C83 fragments are involved in neurite outgrowth (Nhan et al., 2015); AICD controls neural differentiation (Coronel et al., 2018). On the contrary only few studies investigated the physiological role of APP in vascular tissue: low concentrations of Aβ promote endothelial cells migration and proliferation and angiogenesis (Cantara et al., 2004); and APP regulates expression of endothelial nitric oxide synthase (eNOS) and may exert a protective role (d'Uscio et al., 2018).

APP and Angiogenesis

Many studies have clearly shown the detrimental role of Aβ accumulation on vascular stability; however, evidences suggest that APP mediates endothelial cells' response to angiogenic growth factors and modulates angiogenesis. Different APP metabolites have been shown to have different roles in angiogenesis and vascular maintenance. Aβ peptides, for example, show both anti-angiogenic and pro-angiogenic effects in a dose-dependent manner *in vitro*. In fact, high micromolar concentrations of different Aβ variants impair angiogenesis, while low nanomolar concentrations of either Aβ1-40 or Aβ1-42 promote angiogenesis in cultured cerebral and peripheral endothelial cells by promoting cell proliferation, migration, and tube formation (Cantara et al., 2004; Cameron et al., 2012). However, the role of Aβ on angiogenesis *in vivo* is still controversial since cerebral hyper-vascularization was observed in human AD brains and transgenic animals overexpressing APP (Biron et al., 2011). To note, the majority of neo-formed vessels observed in AD is so called "string vessels," non-functional capillaries composed by connecting tissue and lacking endothelial cells (Brown, 2010; Forsberg et al., 2018). It has been proposed that the Aβ-induced aberrant angiogenesis may be the basis for BBB disruption in AD (Biron et al., 2011). Aβ peptides can modulate angiogenesis by functionally interacting with important angiogenic signaling pathways, such as the FGF-2, the vascular endothelial growth factor (VEGF), and the notch signaling (Cantara et al., 2004; Patel et al., 2010; Cameron et al., 2012); however, *in vivo* and *in vitro* studies showed once again controversial results. While brains of patients with AD show upregulation of the VEGF suggesting an interaction of VEGF

with APP processing (Burger et al., 2009), *in vitro* studies revealed that high concentrations of Aβ act as a VEGF antagonist, inhibiting VEGR receptor (VEGFR2) activation as well as VEGF-stimulated activation of eNOS in endothelium (Patel et al., 2010; Lamoke et al., 2015; Cho et al., 2017). Another APP metabolite, the secreted APP-α ectodomain, sAPP-α, has been proposed to modulate angiogenesis by binding to the FGF-2 receptor (FGFR-1). In particular, sAPP-α may counterbalance Aβ anti-angiogenic effect by competing with Aβ and FGF-2 for binding to FGFR-1 (Reinhard et al., 2013). More studies are needed to unravel the dichotomy of Aβ roles on angiogenesis and to establish the exact role of each APP metabolite on angiogenesis.

APP and Cell Adhesion

While the APP soluble metabolites act mostly as ligands, the APP full-length membrane protein functions as a membrane receptor and interacts with cell-adhesion molecules and the ECM. APP extracellular domain binds a series of ECM molecules, including collagen, spondin, laminin, reelin, and HSPGs (glypican and syndecans), and to cell adhesion molecules (CAMs) expressed in neighbor cells, suggesting an important function of APP as an adhesion molecule (Sosa et al., 2017). Many of these interactions stimulate neuronal migration and neurite outgrowth, and we can assume a similar function in endothelial cells (Sosa et al., 2017). The APP extracellular domain is also able to self-dimerize and bind to cell surface receptors, promoting APP surface localization (Deyts et al., 2016). As already discussed, cell-surface accumulation of APP favors non-amyloidogenic processing, thus cell-surface dimerization of APP as well as binding to ECM appears to modulate APP proteolytic processing by secretases. This suggests that APP-dependent adhesive contacts contribute to the control of the dynamics of APP extracellular and intracellular fragments generation. Moreover, APP connects the extracellular environment to the cellular cytoskeleton by physically linking ECM and CAMs elements to the actin cytoskeleton through intracellular scaffold proteins. The cytosolic region of APP presents a YENPTY amino acid sequence motif that is recognized by adaptor proteins (such as Fe65, Mint/X11, and Dab1) capable to link with the actin cytoskeleton and Eb41 (component of cortical cytoskeleton that directly interacts with alpha-actin). Based on this evidence, APP acts as a cell adhesion molecule; however, this physiological role in endothelial cells has not yet been explored.

APP and Transcription Factors

The AICD plays an important role as a transcriptional regulator and shares many structural and functional similarities with the receptor Notch, a key regulator of endothelial cell phenotype. The cleavage of APP by γ-secretase acts as a receptor processing of APP transmembrane region yielding the biologically active cytosolic fragment AICD that participates in cell signaling. This processing step is shared by many membrane-anchored proteins, included Notch (Kopan and Ilagan, 2004). AICD has a short half-life and is rapidly degraded resulting in low steady-state concentrations. Analogous to Notch receptor signaling, AICD regulates gene expression interacting with transcription factors. In particular, AICD interacts with Fe65 and Tip60 to form a transcriptionally active complex that has been reported to promote glycogen synthase kinase 3 β (GSK3β) gene expression (Cao and Sudhof, 2001; Deyts et al., 2016). APP activates or inhibits GSK3β depending on its subcellular localization: The signaling associated with AICD transcription promotes GSK3β activation, while retaining AICD at the membrane favors inhibition of GSK3β signaling (Chang et al., 2006; Deyts et al., 2012). Dysregulation of GSK3β is involved in several aspects of AD development and progression, pointing out the importance of a correct regulation of APP interacting proteins (Llorens-Martin et al., 2014). Similar to the Notch intracellular domain (NICD), the AICD has been also found to regulate cellular calcium homeostasis through a γ-secretase dependent mechanism (Leissring et al., 2002; Hamid et al., 2007). Notch is an essential protein for endothelial cells, and Notch signaling controls fundamental aspects of angiogenic blood vessel growth and regulates vascular remodeling, vessels stabilization, and endothelial cells quiescence (Mack and Iruela-Arispe, 2018). Similarly, AICD may contribute to the stability of endothelial phenotype by modulating various APP physiological functions including trafficking and signal transduction. The complete understanding of AICD-mediated intracellular molecular mechanisms promoting vascular functionality and BBB integrity requires further investigation.

CONCLUSION

APP is a very complex protein that can function as a full-length membrane protein but also through its processing metabolites (included Aβ). While the APP soluble metabolites function mostly as ligands, the APP full-length membrane protein functions as a membrane receptor and interacts with cell-adhesion molecules and the ECM. The processing of this protein through an amyloidogenic or non-amyloidogenic pathway is a key point for the development of amyloid deposits observed in AD and CAA. The failure of clinical trials targeting the amyloidogenic processing and Aβ clearance suggests that more effort is needed to understand the physiological function of APP and modulation of APP processing in cell homeostasis. Even if all cell types of the NVU express APP, experimental *in vivo* and *in vitro* evidence show that endothelial cells dysfunction is related to loss of vascular APP homeostasis. Vascular risk factors such as aging and hypertension can alter APP homeostasis in cerebrovascular tissue not only by modulating APP expression and processing but also by affecting APP protein interaction network. In conclusion, the loss of the physiological activity of APP and its metabolites may have a very important clinical significance. Understanding the influence of APP roles on the functionality of the vascular system might shed light on new therapeutic targets and provide a new perspective on treatment options of neurodegenerative diseases.

AUTHOR CONTRIBUTIONS

ER wrote the manuscript. SD and MZ critically reviewed and edited the manuscript. All authors contributed to the article and approved the submitted version.

FUNDING

This review was supported by Italian Ministry of Education, University and Research (grant MIUR-PRIN n. 20152HKF3Z to MZ).

REFERENCES

Austin, S. A., and Katusic, Z. S. (2020). Partial loss of endothelial nitric oxide leads to increased cerebrovascular beta amyloid. *J. Cereb. Blood Flow Metab.* 40, 392–403. doi: 10.1177/0271678X18822474

Austin, S. A., Sens, M. A., and Combs, C. K. (2009). Amyloid precursor protein mediates a tyrosine kinase-dependent activation response in endothelial cells. *J. Neurosci.* 29, 14451–14462. doi: 10.1523/JNEUROSCI.3107-09.2009

Biron, K. E., Dickstein, D. L., Gopaul, R., and Jefferies, W. A. (2011). Amyloid triggers extensive cerebral angiogenesis causing blood brain barrier permeability and hypervascularity in Alzheimer's disease. *PLoS One* 6:e23789. doi: 10.1371/journal.pone.0023789

Brothers, H. M., Gosztyla, M. L., and Robinson, S. R. (2018). The physiological roles of amyloid-beta peptide hint at new ways to treat Alzheimer's disease. *Front. Aging Neurosci.* 10:118. doi: 10.3389/fnagi.2018.00118

Brown, W. R. (2010). A review of string vessels or collapsed, empty basement membrane tubes. *J. Alzheimers Dis.* 21, 725–739. doi: 10.3233/JAD-2010-100219

Burger, S., Noack, M., Kirazov, L. P., Kirazov, E. P., Naydenov, C. L., Kouznetsova, E., et al. (2009). Vascular endothelial growth factor (VEGF) affects processing of amyloid precursor protein and beta-amyloidogenesis in brain slice cultures derived from transgenic Tg2576 mouse brain. *Int. J. Dev. Neurosci.* 27, 517–523. doi: 10.1016/j.ijdevneu.2009.06.011

Cai, W., Zhang, K., Li, P., Zhu, L., Xu, J., Yang, B., et al. (2017). Dysfunction of the neurovascular unit in ischemic stroke and neurodegenerative diseases: an aging effect. *Ageing Res. Rev.* 34, 77–87. doi: 10.1016/j.arr.2016.09.006

Cameron, D. J., Galvin, C., Alkam, T., Sidhu, H., Ellison, J., Luna, S., et al. (2012). Alzheimer's-related peptide amyloid-beta plays a conserved role in angiogenesis. *PLoS One* 7:e39598. doi: 10.1371/journal.pone.0039598

Canobbio, I., Abubaker, A. A., Visconte, C., Torti, M., and Pula, G. (2015). Role of amyloid peptides in vascular dysfunction and platelet dysregulation in Alzheimer's disease. *Front. Cell. Neurosci.* 9:65. doi: 10.3389/fncel.2015.00065

Cantara, S., Donnini, S., Morbidelli, L., Giachetti, A., Schulz, R., Memo, M., et al. (2004). Physiological levels of amyloid peptides stimulate the angiogenic response through FGF-2. *FASEB J.* 18, 1943–1945. doi: 10.1096/fj.04-2114fje

Cao, X., and Sudhof, T. C. (2001). A transcriptionally [correction of transcriptively] active complex of APP with Fe65 and histone acetyltransferase Tip60. *Science* 293, 115–120. doi: 10.1126/science.1058783

Chang, K. A., Kim, H. S., Ha, T. Y., Ha, J. W., Shin, K. Y., Jeong, Y. H., et al. (2006). Phosphorylation of amyloid precursor protein (APP) at Thr668 regulates the nuclear translocation of the APP intracellular domain and induces neurodegeneration. *Mol. Cell. Biol.* 26, 4327–4338. doi: 10.1128/MCB.02393-05

Chiocco, M. J., and Lamb, B. T. (2007). Spatial and temporal control of age-related APP processing in genomic-based beta-secretase transgenic mice. *Neurobiol. Aging* 28, 75–84. doi: 10.1016/j.neurobiolaging.2005.11.011

Cho, S. J., Park, M. H., Han, C., Yoon, K., and Koh, Y. H. (2017). VEGFR2 alteration in Alzheimer's disease. *Sci. Rep.* 7:17713. doi: 10.1038/s41598-017-18042-1

Chou, C. H., Fan, H. C., and Hueng, D. Y. (2015). Potential of neural stem cell-based therapy for Parkinson's disease. *Parkinsons Dis.* 2015:571475. doi: 10.1155/2015/571475

Clarke, J., Thornell, A., Corbett, D., Soininen, H., Hiltunen, M., and Jolkkonen, J. (2007). Overexpression of APP provides neuroprotection in the absence of functional benefit following middle cerebral artery occlusion in rats. *Eur. J. Neurosci.* 26, 1845–1852. doi: 10.1111/j.1460-9568.2007.05807.x

Coronel, R., Bernabeu-Zornoza, A., Palmer, C., Muniz-Moreno, M., Zambrano, A., Cano, E., et al. (2018). Role of amyloid precursor protein (APP) and its derivatives in the biology and cell fate specification of neural stem cells. *Mol. Neurobiol.* 55, 7107–7117. doi: 10.1007/s12035-018-0914-2

de la Torre, J. (2018). The vascular hypothesis of Alzheimer's disease: a key to preclinical prediction of dementia using neuroimaging. *J. Alzheimers Dis.* 63, 35–52. doi: 10.3233/JAD-180004

De Meyer, G. R., De Cleen, D. M., Cooper, S., Knaapen, M. W., Jans, D. M., Martinet, W., et al. (2002). Platelet phagocytosis and processing of beta-amyloid precursor protein as a mechanism of macrophage activation in atherosclerosis. *Circ. Res.* 90, 1197–1204. doi: 10.1161/01.RES.0000020017.84398.61

Deane, R., Wu, Z., Sagare, A., Davis, J., Du Yan, S., Hamm, K., et al. (2004). LRP/amyloid beta-peptide interaction mediates differential brain efflux of Abeta isoforms. *Neuron* 43, 333–344. doi: 10.1016/j.neuron.2004.07.017

Deyts, C., Thinakaran, G., and Parent, A. T. (2016). APP receptor? To be or not to be. *Trends Pharmacol. Sci.* 37, 390–411. doi: 10.1016/j.tips.2016.01.005

Deyts, C., Vetrivel, K. S., Das, S., Shepherd, Y. M., Dupre, D. J., Thinakaran, G., et al. (2012). Novel GalphaS-protein signaling associated with membrane-tethered amyloid precursor protein intracellular domain. *J. Neurosci.* 32, 1714–1729. doi: 10.1523/JNEUROSCI.5433-11.2012

d'Uscio, L. V., He, T., and Katusic, Z. S. (2017). Expression and processing of amyloid precursor protein in vascular endothelium. *Physiology* 32, 20–32. doi: 10.1152/physiol.00021.2016

d'Uscio, L. V., He, T., Santhanam, A. V., and Katusic, Z. S. (2018). Endothelium-specific amyloid precursor protein deficiency causes endothelial dysfunction in cerebral arteries. *J. Cereb. Blood Flow Metab.* 38, 1715–1726. doi: 10.1177/0271678X17735418

d'Uscio, L. V., and Katusic, Z. S. (2019). Vascular phenotype of amyloid precursor protein-deficient mice. *Am. J. Physiol. Heart Circ. Physiol.* 316, H1297–H1308. doi: 10.1152/ajpheart.00539.2018

Forsberg, K. M. E., Zhang, Y., Reiners, J., Ander, M., Niedermayer, A., Fang, L., et al. (2018). Endothelial damage, vascular bagging and remodeling of the microvascular bed in human microangiopathy with deep white matter lesions. *Acta Neuropathol. Commun.* 6:128. doi: 10.1186/s40478-018-0632-z

Gangoda, S. V. S., Avadhanam, B., Jufri, N. F., Sohn, E. H., Butlin, M., Gupta, V., et al. (2018). Pulsatile stretch as a novel modulator of amyloid precursor protein processing and associated inflammatory markers in human cerebral endothelial cells. *Sci. Rep.* 8:1689. doi: 10.1038/s41598-018-20117-6

Gralle, M., Botelho, M. G., and Wouters, F. S. (2009). Neuroprotective secreted amyloid precursor protein acts by disrupting amyloid precursor protein dimers. *J. Biol. Chem.* 284, 15016–15025. doi: 10.1074/jbc.M808755200

Gustafsson, S., Gustavsson, T., Roshanbin, S., Hultqvist, G., Hammarlund-Udenaes, M., Sehlin, D., et al. (2018). Blood-brain barrier integrity in a mouse model of Alzheimer's disease with or without acute 3D6 immunotherapy. *Neuropharmacology* 143, 1–9. doi: 10.1016/j.neuropharm.2018.09.001

Habib, A., Sawmiller, D., and Tan, J. (2017). Restoring soluble amyloid precursor protein alpha functions as a potential treatment for Alzheimer's disease. *J. Neurosci. Res.* 95, 973–991. doi: 10.1002/jnr.23823

Hamid, R., Kilger, E., Willem, M., Vassallo, N., Kostka, M., Bornhovd, C., et al. (2007). Amyloid precursor protein intracellular domain modulates cellular calcium homeostasis and ATP content. *J. Neurochem.* 102, 1264–1275. doi: 10.1111/j.1471-4159.2007.04627.x

Iadecola, C. (2017). The neurovascular unit coming of age: a journey through neurovascular coupling in health and disease. *Neuron* 96, 17–42. doi: 10.1016/j.neuron.2017.07.030

Jiang, S., Li, Y., Zhang, X., Bu, G., Xu, H., and Zhang, Y. W. (2014). Trafficking regulation of proteins in Alzheimer's disease. *Mol. Neurodegener.* 9:6. doi: 10.1186/1750-1326-9-6

Kaden, D., Munter, L. M., Joshi, M., Treiber, C., Weise, C., Bethge, T., et al. (2008). Homophilic interactions of the amyloid precursor protein (APP) ectodomain are regulated by the loop region and affect beta-secretase cleavage of APP. *J. Biol. Chem.* 283, 7271–7279. doi: 10.1074/jbc.M708046200

Kern, A., Roempp, B., Prager, K., Walter, J., and Behl, C. (2006). Down-regulation of endogenous amyloid precursor protein processing due to cellular aging. *J. Biol. Chem.* 281, 2405–2413. doi: 10.1074/jbc.M505625200

Kitazume, S., Yoshihisa, A., Yamaki, T., Oikawa, M., Tachida, Y., Ogawa, K., et al. (2012). Soluble amyloid precursor protein 770 is released from inflamed

endothelial cells and activated platelets: a novel biomarker for acute coronary syndrome. *J. Biol. Chem.* 287, 40817–40825. doi: 10.1074/jbc.M112.398578

Klohs, J. (2020). An integrated view on vascular dysfunction in Alzheimer's disease. *Neurodegener. Dis.* 19, 109–127. doi: 10.1159/000505625

Koike, M. A., Lin, A. J., Pham, J., Nguyen, E., Yeh, J. J., Rahimian, R., et al. (2012). APP knockout mice experience acute mortality as the result of ischemia. *PLoS One* 7:e42665. doi: 10.1371/journal.pone.0042665

Kopan, R., and Ilagan, M. X. (2004). Gamma-secretase: proteasome of the membrane? *Nat. Rev. Mol. Cell Biol.* 5, 499–504. doi: 10.1038/nrm1406

Lamoke, F., Mazzone, V., Persichini, T., Maraschi, A., Harris, M. B., Venema, R. C., et al. (2015). Amyloid beta peptide-induced inhibition of endothelial nitric oxide production involves oxidative stress-mediated constitutive eNOS/HSP90 interaction and disruption of agonist-mediated Akt activation. *J. Neuroinflammation* 12, 84. doi: 10.1186/s12974-015-0304-x

Leissring, M. A., Murphy, M. P., Mead, T. R., Akbari, Y., Sugarman, M. C., Jannatipour, M., et al. (2002). A physiologic signaling role for the gamma-secretase-derived intracellular fragment of APP. *Proc. Natl. Acad. Sci. U. S. A.* 99, 4697–4702. doi: 10.1073/pnas.072033799

Lewis, H., Beher, D., Cookson, N., Oakley, A., Piggott, M., Morris, C. M., et al. (2006). Quantification of Alzheimer pathology in ageing and dementia: age-related accumulation of amyloid-beta(42) peptide in vascular dementia. *Neuropathol. Appl. Neurobiol.* 32, 103–118. doi: 10.1111/j.1365-2990.2006.00696.x

Li, L., Cao, D., Garber, D. W., Kim, H., and Fukuchi, K. (2003). Association of aortic atherosclerosis with cerebral beta-amyloidosis and learning deficits in a mouse model of Alzheimer's disease. *Am. J. Pathol.* 163, 2155–2164. doi: 10.1016/s0002-9440(10)63572-9

Liu, X., Hou, D., Lin, F., Luo, J., Xie, J., Wang, Y., et al. (2019). The role of neurovascular unit damage in the occurrence and development of Alzheimer's disease. *Rev. Neurosci.* 30, 477–484. doi: 10.1515/revneuro-2018-0056

Liu, C. C., Zhao, N., Yamaguchi, Y., Cirrito, J. R., Kanekiyo, T., Holtzman, D. M., et al. (2016). Neuronal heparan sulfates promote amyloid pathology by modulating brain amyloid-beta clearance and aggregation in Alzheimer's disease. *Sci. Transl. Med.* 8:332ra344. doi: 10.1126/scitranslmed.aad3650

Llorens-Martin, M., Jurado, J., Hernandez, F., and Avila, J. (2014). GSK-3beta, a pivotal kinase in Alzheimer disease. *Front. Mol. Neurosci.* 7:46. doi: 10.3389/fnmol.2014.00046

Luna, S., Cameron, D. J., and Ethell, D. W. (2013). Amyloid-beta and APP deficiencies cause severe cerebrovascular defects: important work for an old villain. *PLoS One* 8:e75052. doi: 10.1371/journal.pone.0075052

Mack, J. J., and Iruela-Arispe, M. L. (2018). NOTCH regulation of the endothelial cell phenotype. *Curr. Opin. Hematol.* 25, 212–218. doi: 10.1097/MOH.0000000000000425

Muller, U. C., Deller, T., and Korte, M. (2017). Not just amyloid: physiological functions of the amyloid precursor protein family. *Nat. Rev. Neurosci.* 18, 281–298. doi: 10.1038/nrn.2017.29

Nhan, H. S., Chiang, K., and Koo, E. H. (2015). The multifaceted nature of amyloid precursor protein and its proteolytic fragments: friends and foes. *Acta Neuropathol.* 129, 1–19. doi: 10.1007/s00401-014-1347-2

Nicolas, M., and Hassan, B. A. (2014). Amyloid precursor protein and neural development. *Development* 141, 2543–2548. doi: 10.1242/dev.108712

Niwa, K., Kazama, K., Younkin, L., Younkin, S. G., Carlson, G. A., and Iadecola, C. (2002). Cerebrovascular autoregulation is profoundly impaired in mice overexpressing amyloid precursor protein. *Am. J. Physiol. Heart Circ. Physiol.* 283, H315–H323. doi: 10.1152/ajpheart.00022.2002

Niwa, K., Porter, V. A., Kazama, K., Cornfield, D., Carlson, G. A., and Iadecola, C. (2001). A beta-peptides enhance vasoconstriction in cerebral circulation. *Am. J. Physiol. Heart Circ. Physiol.* 281, H2417–H2424. doi: 10.1152/ajpheart.2001.281.6.H2417

Nizari, S., Carare, R. O., Romero, I. A., and Hawkes, C. A. (2019). 3D reconstruction of the neurovascular unit reveals differential loss of cholinergic innervation in the cortex and hippocampus of the adult mouse brain. *Front. Aging Neurosci.* 11:172. doi: 10.3389/fnagi.2019.00172

Nortley, R., Korte, N., Izquierdo, P., Hirunpattarasilp, C., Mishra, A., Jaunmuktane, Z., et al. (2019). Amyloid beta oligomers constrict human capillaries in Alzheimer's disease via signaling to pericytes. *Science* 365:eaav9518. doi: 10.1126/science.aav9518

Obregon, D., Hou, H., Deng, J., Giunta, B., Tian, J., Darlington, D., et al. (2012). Soluble amyloid precursor protein-alpha modulates beta-secretase activity and amyloid-beta generation. *Nat. Commun.* 3:777. doi: 10.1038/ncomms1781

O'Brien, R. J., and Wong, P. C. (2011). Amyloid precursor protein processing and Alzheimer's disease. *Annu. Rev. Neurosci.* 34, 185–204. doi: 10.1146/annurev-neuro-061010-113613

Ott, M. O., and Bullock, S. L. (2001). A gene trap insertion reveals that amyloid precursor protein expression is a very early event in murine embryogenesis. *Dev. Genes Evol.* 211, 355–357. doi: 10.1007/s004270100158

Paris, D., Quadros, A., Patel, N., DelleDonne, A., Humphrey, J., and Mullan, M. (2005). Inhibition of angiogenesis and tumor growth by beta and gamma-secretase inhibitors. *Eur. J. Pharmacol.* 514, 1–15. doi: 10.1016/j.ejphar.2005.02.050

Park, L., Anrather, J., Forster, C., Kazama, K., Carlson, G. A., and Iadecola, C. (2004). Abeta-induced vascular oxidative stress and attenuation of functional hyperemia in mouse somatosensory cortex. *J. Cereb. Blood Flow Metab.* 24, 334–342. doi: 10.1097/01.WCB.0000105800.49957.1E

Park, L., Anrather, J., Zhou, P., Frys, K., Pitstick, R., Younkin, S., et al. (2005). NADPH-oxidase-derived reactive oxygen species mediate the cerebrovascular dysfunction induced by the amyloid beta peptide. *J. Neurosci.* 25, 1769–1777. doi: 10.1523/JNEUROSCI.5207-04.2005

Patel, N. S., Mathura, V. S., Bachmeier, C., Beaulieu-Abdelahad, D., Laporte, V., Weeks, O., et al. (2010). Alzheimer's beta-amyloid peptide blocks vascular endothelial growth factor mediated signaling via direct interaction with VEGFR-2. *J. Neurochem.* 112, 66–76. doi: 10.1111/j.1471-4159.2009.06426.x

Pearson, H. A., and Peers, C. (2006). Physiological roles for amyloid beta peptides. *J. Physiol.* 575, 5–10. doi: 10.1113/jphysiol.2006.111203

Perez, R. G., Zheng, H., Van der Ploeg, L. H., and Koo, E. H. (1997). The beta-amyloid precursor protein of Alzheimer's disease enhances neuron viability and modulates neuronal polarity. *J. Neurosci.* 17, 9407–9414. doi: 10.1523/JNEUROSCI.17-24-09407.1997

Qi, X. M., and Ma, J. F. (2017). The role of amyloid beta clearance in cerebral amyloid angiopathy: more potential therapeutic targets. *Transl. Neurodegener.* 6:22. doi: 10.1186/s40035-017-0091-7

Reinhard, C., Borgers, M., David, G., and De Strooper, B. (2013). Soluble amyloid-beta precursor protein binds its cell surface receptor in a cooperative fashion with glypican and syndecan proteoglycans. *J. Cell Sci.* 126, 4856–4861. doi: 10.1242/jcs.137919

Ring, S., Weyer, S. W., Kilian, S. B., Waldron, E., Pietrzik, C. U., Filippov, M. A., et al. (2007). The secreted beta-amyloid precursor protein ectodomain APPs alpha is sufficient to rescue the anatomical, behavioral, and electrophysiological abnormalities of APP-deficient mice. *J. Neurosci.* 27, 7817–7826. doi: 10.1523/JNEUROSCI.1026-07.2007

Shariati, S. A., and De Strooper, B. (2013). Redundancy and divergence in the amyloid precursor protein family. *FEBS Lett.* 587, 2036–2045. doi: 10.1016/j.febslet.2013.05.026

Sosa, L. J., Caceres, A., Dupraz, S., Oksdath, M., Quiroga, S., and Lorenzo, A. (2017). The physiological role of the amyloid precursor protein as an adhesion molecule in the developing nervous system. *J. Neurochem.* 143, 11–29. doi: 10.1111/jnc.14122

Stakos, D. A., Stamatelopoulos, K., Bampatsias, D., Sachse, M., Zormpas, E., Vlachogiannis, N. I., et al. (2020). The Alzheimer's disease amyloid-beta hypothesis in cardiovascular aging and disease: JACC focus seminar. *J. Am. Coll. Cardiol.* 75, 952–967. doi: 10.1016/j.jacc.2019.12.033

Sun, R., He, T., Pan, Y., and Katusic, Z. S. (2018). Effects of senescence and angiotensin II on expression and processing of amyloid precursor protein in human cerebral microvascular endothelial cells. *Aging* 10, 100–114. doi: 10.18632/aging.101362

Thinakaran, G., and Koo, E. H. (2008). Amyloid precursor protein trafficking, processing, and function. *J. Biol. Chem.* 283, 29615–29619. doi: 10.1074/jbc.R800019200

Tibolla, G., Norata, G. D., Meda, C., Arnaboldi, L., Uboldi, P., Piazza, F., et al. (2010). Increased atherosclerosis and vascular inflammation in APP transgenic mice with apolipoprotein E deficiency. *Atherosclerosis* 210, 78–87. doi: 10.1016/j.atherosclerosis.2009.10.040

Tong, X. K., Nicolakakis, N., Kocharyan, A., and Hamel, E. (2005). Vascular remodeling versus amyloid beta-induced oxidative stress in the cerebrovascular dysfunctions associated with Alzheimer's disease. *J. Neurosci.* 25, 11165–11174. doi: 10.1523/JNEUROSCI.4031-05.2005

van Assema, D. M., Lubberink, M., Boellaard, R., Schuit, R. C., Windhorst, A. D., Scheltens, P., et al. (2012). P-glycoprotein function at the blood-brain barrier: effects of age and gender. *Mol. Imaging Biol.* 14, 771–776. doi: 10.1007/s11307-012-0556-0

Van De Parre, T. J., Guns, P. J., Fransen, P., Martinet, W., Bult, H., Herman, A. G., et al. (2011). Attenuated atherogenesis in apolipoprotein E-deficient mice lacking amyloid precursor protein. *Atherosclerosis* 216, 54–58. doi: 10.1016/j.atherosclerosis.2011.01.032

van der Kant, R., and Goldstein, L. S. (2015). Cellular functions of the amyloid precursor protein from development to dementia. *Dev. Cell* 32, 502–515. doi: 10.1016/j.devcel.2015.01.022

Van Nostrand, W. E., Schmaier, A. H., Neiditch, B. R., Siegel, R. S., Raschke, W. C., Sisodia, S. S., et al. (1994). Expression, purification, and characterization of the kunitz-type proteinase inhibitor domain of the amyloid beta-protein precursor-like protein-2. *Biochim. Biophys. Acta* 1209, 165–170. doi: 10.1016/0167-4838(94)90180-5

Wan, W., Chen, H., and Li, Y. (2014). The potential mechanisms of Abeta-receptor for advanced glycation end-products interaction disrupting tight junctions of the blood-brain barrier in Alzheimer's disease. *Int. J. Neurosci.* 124, 75–81. doi: 10.3109/00207454.2013.825258

Wang, W., Bodles-Brakhop, A. M., and Barger, S. W. (2016). A role for P-glycoprotein in clearance of Alzheimer amyloid beta-peptide from the brain. *Curr. Alzheimer Res.* 13, 615–620. doi: 10.2174/1567205013666160314151012

Wilhelm, I., Nyul-Toth, A., Suciu, M., Hermenean, A., and Krizbai, I. A. (2016). Heterogeneity of the blood-brain barrier. *Tissue Barriers* 4:e1143544. doi: 10.1080/21688370.2016.1143544

Young-Pearse, T. L., Bai, J., Chang, R., Zheng, J. B., LoTurco, J. J., and Selkoe, D. J. (2007). A critical function for beta-amyloid precursor protein in neuronal migration revealed by in utero RNA interference. *J. Neurosci.* 27, 14459–14469. doi: 10.1523/JNEUROSCI.4701-07.2007

Zhang, G. L., Zhang, X., Wang, X. M., and Li, J. P. (2014). Towards understanding the roles of heparan sulfate proteoglycans in Alzheimer's disease. *Biomed. Res. Int.* 2014:516028. doi: 10.1155/2014/516028

Zheng, H., and Koo, E. H. (2011). Biology and pathophysiology of the amyloid precursor protein. *Mol. Neurodegener.* 6:27. doi: 10.1186/1750-1326-6-27

Zoufal, V., Wanek, T., Krohn, M., Mairinger, S., Filip, T., Sauberer, M., et al. (2020). Age dependency of cerebral P-glycoprotein function in wild-type and APPPS1 mice measured with PET. *J. Cereb. Blood Flow Metab.* 40, 150–162. doi: 10.1177/0271678X18806640

Conflict of Interest: The authors declare that the research was conducted in the absence of any commercial or financial relationships that could be construed as a potential conflict of interest.

frontiers in Physiology

REVIEW
published: 18 September 2020
doi: 10.3389/fphys.2020.565667

Wnt Pathway: An Emerging Player in Vascular and Traumatic Mediated Brain Injuries

Romain Menet[1,2], *Sarah Lecordier*[1,2] *and Ayman ElAli*[1,2]*

[1] Neuroscience Axis, Research Center of CHU de Québec – Université Laval, Quebec City, QC, Canada, [2] Department of Psychiatry and Neuroscience, Faculty of Medicine, Université Laval, Quebec City, QC, Canada

The Wnt pathway, which comprises the canonical and non-canonical pathways, is an evolutionarily conserved mechanism that regulates crucial biological aspects throughout the development and adulthood. Emergence and patterning of the nervous and vascular systems are intimately coordinated, a process in which Wnt pathway plays particularly important roles. In the brain, Wnt ligands activate a cell-specific surface receptor complex to induce intracellular signaling cascades regulating neurogenesis, synaptogenesis, neuronal plasticity, synaptic plasticity, angiogenesis, vascular stabilization, and inflammation. The Wnt pathway is tightly regulated in the adult brain to maintain neurovascular functions. Historically, research in neuroscience has emphasized essentially on investigating the pathway in neurodegenerative disorders. Nonetheless, emerging findings have demonstrated that the pathway is deregulated in vascular- and traumatic-mediated brain injuries. These findings are suggesting that the pathway constitutes a promising target for the development of novel therapeutic protective and restorative interventions. Yet, targeting a complex multifunctional signal transduction pathway remains a major challenge. The review aims to summarize the current knowledge regarding the implication of Wnt pathway in the pathobiology of ischemic and hemorrhagic stroke, as well as traumatic brain injury (TBI). Furthermore, the review will present the strategies used so far to manipulate the pathway for therapeutic purposes as to highlight potential future directions.

Keywords: Wnt pathway, cerebrovascular diseases, traumatic brain injury, signal transduction, neurovascular interactions

OPEN ACCESS

Edited by:
Jean-luc Morel,
Centre National de la Recherche Scientifique (CNRS), France

Reviewed by:
Prasad V. Katakam,
Tulane University School of Medicine, United States
Daniela Carnevale,
Sapienza University of Rome, Italy

***Correspondence:**
Ayman ElAli
ayman.el-ali@crchudequebec.ulaval.ca

Specialty section:
This article was submitted to Vascular Physiology, a section of the journal Frontiers in Physiology

Received: *25 May 2020*
Accepted: *18 August 2020*
Published: *18 September 2020*

Citation:
Menet R, Lecordier S and ElAli A (2020) Wnt Pathway: An Emerging Player in Vascular and Traumatic Mediated Brain Injuries. Front. Physiol. 11:565667. doi: 10.3389/fphys.2020.565667

INTRODUCTION

The Wnt pathway regroups evolutionarily conserved intracellular signal transduction cascades that regulate key biological aspects, such as cell proliferation, polarity, migration, and fate determination during development (Willert and Nusse, 2012). Wnt proteins have been discovered 30 years ago (Nusse and Varmus, 1982), and the name is an abbreviation resulting from the fusion of the name of Drosophila segment polarity gene "*Wingless*" and that of its vertebrate proto-oncogene orthologous gene "*Integrated, Int-1*" (Nusse and Varmus, 1982). Nineteen Wnt genes have been identified so far in humans and rodents, clustering into 12 subfamilies (Foulquier et al., 2018). Wnts are secreted glycoproteins that activate intracellular signals upon binding to cell-specific transmembrane receptors (Hermann and ElAli, 2012). Wnt proteins activate different pathways that comprise the canonical pathway, which depends upon β-catenin-mediated gene regulation, and the non-canonical pathway that includes the planar cell polarity (PCP) and calcium (Ca^{2+})

pathways, which are both β-catenin-independent (Croce and McClay, 2008). The canonical Wnt pathway is mediated essentially by the action of Wnt1, Wnt3, Wnt3a, Wnt7a, Wnt7b, Wnt8 and Wnt9 ligands, and involves the recruitment of low-density lipoprotein receptor-related protein-5/6 (LRP5/6) to Frizzled (Fzd) receptors to form a transmembrane receptor complex, and the non-canonical Wnt pathway is mediated essentially by Wnt4, Wnt5a, Wnt6, and Wnt11 ligands, without the involvement of LRP5/6 (Croce and McClay, 2008). In the brain, Wnt proteins are secreted essentially by neurons and astrocytes, and act as cell-specific ligands that orchestrate a wide range of biological processes during development and adulthood (Hermann and ElAli, 2012; Noelanders and Vleminckx, 2017). In the developing brain, Wnt pathway has been shown to regulate neural patterning, neurogenesis, axon guidance, synaptogenesis, and vascular development (Hermann and ElAli, 2012; Lambert et al., 2016; Noelanders and Vleminckx, 2017; Jaworski et al., 2019). Recent evidence is demonstrating that Wnt pathway is required to maintain brain homeostasis and functioning during lifespan by fine-tuning adult neurogenesis, synaptic plasticity, vascular stability, blood-brain barrier (BBB) integrity, and inflammation (Hermann and ElAli, 2012; Noelanders and Vleminckx, 2017). The emerging findings are indicating that the Wnt pathway is deregulated in several brain disorders, namely Alzheimer's disease (AD), anticipating its importance as a novel target for the development of new therapies (Hermann and ElAli, 2012). Dysfunction of the Wnt pathway in neurodegenerative disorders is largely covered in the literature. In the recent years, deregulation of the Wnt pathway has been reported in vascular- and traumatic-mediated brain injuries, outlining a direct and major impact on the mechanisms related to injury, as well as protection and regeneration. Yet, there is still a gap in the literature in this particular field. In this review, we will summarize the implication of Wnt pathway in the pathobiology of ischemic and hemorrhagic stroke, as well as traumatic brain injury (TBI), and outline its role in the development of novel therapeutic interventions for these neurological conditions.

THE CANONICAL Wnt PATHWAY

In the canonical Wnt pathway, Wnt ligands bind to 10 different Fzd receptors (Wang et al., 2006). The interaction between Wnt and Fzd receptors requires LRP5/6, which acts as a co-receptor. The complex Wnt-Fzd-LRP5/6 recruits and activates the scaffold protein Disheveled (Dvl), which induces the disassembly of β-catenin destruction complex, which comprises the adenomatous polyposis coli (APC), Axin, casein kinase-1α (CK1α), and glycogen synthase kinase3-β (GSK3β) (Croce and McClay, 2008). LRP5/6 phosphorylation by CK1α induces inhibition of the destruction complex (Croce and McClay, 2008). In the presence of Wnt ligands, the serine kinase activity of GSK3β is inhibited, resulting in the disassembly of the destruction complex, leading to the stabilization and accumulation of β-catenin in the cytosol and subsequent translocation into the nucleus (Hermann and ElAli, 2012). In the nucleus, β-catenin binds and activates the lymphoid enhancer factor (LEF)/T cell factor (TCF) transcription factor to regulate the expression of Wnt target genes (Niehrs, 2012). TCF/LEF activation by β-catenin regulates several genes implicated in neurogenesis, synaptogenesis, neuronal plasticity, synaptic plasticity, BBB formation, cell survival, and inflammation (Liebner et al., 2008; Hur and Zhou, 2010; Marchetti and Pluchino, 2013; Zhou Y. et al., 2014; Ma and Hottiger, 2016). The interaction of Wnt with Fzd-LRP5/6 receptor complex is tightly regulated to assure an adequate activation of the pathway (He et al., 2016; Lambert et al., 2016). The endogenous secreted proteins Dickkopf-1 (Dkk1) and sclerostin (Scl) play particular important roles in modulating pathway activation (He et al., 2016; Lambert et al., 2016).

LRP5 and LRP6 are 70% identical and represent a unique group of the LDLR family (He et al., 2004; MacDonald and He, 2012). These single transmembrane receptors have an extracellular domain containing 4-tandem β-propeller (E1–E4) (MacDonald and He, 2012). Some Wnt ligands such as Wnt1, Wnt2, Wnt2b, Wnt6, Wnt8a, Wnt9a and Wnt9b interact with E1, whereas others such as Wnt3 and Wnt3a prefer E3 and E4 (Takanari et al., 1990; Bourhis et al., 2010; Rochefort, 2014). The domains that are implicated in binding other Wnt ligands such as Wnt7a and Wnt7b remain unknown (Takanari et al., 1990). It has been shown that Dkk1 binds to all β-propeller domains of LRP5 and LRP6, thus inhibiting Wnt1, Wnt9b, and Wnt3a for binding to LRP5/6 and consequently preventing pathway activation (Bourhis et al., 2010; Rochefort, 2014). Furthermore, Dkk1 binds to E3 and E4 fragments, thus competing with Wnt3a for binding to LRP6, and preventing the formation of the Wnt3a-Fzd8-LRP6 complex. Inhibition of Wnt3a binding to LRP6 by Dkk1 does not disrupt Wnt3a-Fzd8 interaction, but rather prevents the formation of Wnt-Fzd-LRP5/6 complex (Bourhis et al., 2010; Rochefort, 2014). Scl binds the first β-propeller of LRP5 and LRP6 to inhibit the biological activity of Wnt1 (Rochefort, 2014), and Wnt9b (Bourhis et al., 2010), respectively, and similar to Dkk1, prevents pathway activation. In addition, Dkk1 and Scl can use co-receptors, such as Kremen-1/2, to increase their inhibitory activity by facilitating the internalization of the Fzd-LRP5/6 receptor complex (Mao et al., 2002). In the healthy brain, Wnt pathway basal activity is required to maintain tissue homeostasis. However, accumulating evidence is suggesting that the pathway is deregulated in brain injuries associated to cerebrovascular diseases and trauma, impacting adult neurogenesis, neuronal plasticity, synaptic plasticity, angiogenesis, vascular stability and the immune response (He et al., 2016; Lambert et al., 2016).

THE NON-CANONICAL Wnt PATHWAY

The non-canonical Wnt pathway comprises Wnt/PCP and Wnt/Ca^{2+} pathways, which are β-catenin-independent, and are largely associated to cell mobility and differentiation (Ng et al., 2019). The Wnt/PCP pathway is initiated when Fzd receptors activate a cascade of intracellular cascades involving the small guanosine triphosphate (GTP)ases, Ras-related C3 botulinum toxin substrate-1 (RAC1), and Ras homolog gene family member A (RHOA), cell division cycle 42 (CDC42), as well as the c-Jun N-terminal-kinase (JNK), independently of LRP5/6 (Habas

and Dawid, 2005). The Wnt/PCP pathway is divided into two sub-branches: the RHOA and its effector Rho-associated protein kinase-1/2 (ROCK1/2) "RHOA/ROCK pathway" and JNK effector c-Jun "JNK/c-Jun pathway." RHOA/ROCK pathway does not always involve the recruitment of key components of the canonical pathway including Wnt itself, but involves mostly Dvl and specifically its PDZ (post-synaptic density protein-95, PSD95/disks large homolog, DLG/zonula occludens-1, ZO1) and DEP (Dvl/EGg laying defective, EGL-10/Pleckstrin) domains, as well as the Dvl-associated activator of morphogenesis-1 (DAAM1) (Habas et al., 2001). These domains link Fzd and Dvl to the small GTPases RHO, which in turn activate their effector ROCK, leading to cytoskeletal reorganization (Veeman et al., 2003). The JNK/c-Jun pathway involves as well Dvl that interacts through its DEP domain with RAC1 to form a complex independently of DAAM1, stimulating JNK activity and mediating profilin binding to actin (Habas et al., 2001; Veeman et al., 2003). The PCP pathway regulates a variety of cellular processes including planar polarity, cell mobility, and cell migration of neural crest cells (Veeman et al., 2003; Komiya and Habas, 2008; Ng et al., 2019).

The Wnt/Ca^{2+} pathway shares several components with the PCP pathway. The pathway is activated when Wnt ligands bind to the Fzd receptors, which activates heterotrimeric G proteins, stimulating the release of Ca^{2+} from intracellular stores (Marchetti and Pluchino, 2013). The increased Ca^{2+} concentration subsequently activates various Ca^{2+}-dependent effectors, namely protein kinase C (PKC), Ca^{2+}-calmodulin-dependent protein kinase II (CaMKII), and the Ca^{2+}-calmodulin-sensitive protein phosphatase calcineurin (Marchetti and Pluchino, 2013; Ng et al., 2019). Several downstream components of the Wnt/Ca^{2+} pathway have been shown to interact with the canonical Wnt pathway. Furthermore, the association of Fzd receptors with Knypek (Kny), RAR-related orphan receptor-2 (ROR2), or related to receptor tyrosine kinase (RYK) receptors can activate JNK, promoting target gene expression through Activator protein-1 (AP1) (Marchetti and Pluchino, 2013). The Wnt/Ca^{2+} pathway is implicated in regulating dorsal axis formation, cell adhesion, migration, and tissue separation during embryogenesis (Komiya and Habas, 2008). Little is known about the physiological role of the non-canonical Wnt pathway in the adult brain. Nonetheless, the recent findings suggest that the pathway is deregulated in brain injuries, such as cerebrovascular diseases and trauma, impacting adult neurogenesis, angiogenesis, BBB permeability and the immune response (Johnson and Nakamura, 2007).

THE Wnt PATHWAY IN BRAIN PHYSIOLOGY

Implication in Neurogenesis

The adult hippocampal stem/progenitor cells (AHPs) express receptors and several components for the Wnt pathway (Lie et al., 2005). It has been shown that the canonical Wnt pathway exhibits a basal activity, and Wnt3 is expressed in the hippocampal neurogenic niche (Lie et al., 2005). Importantly, Wnt3 overexpression was sufficient to increase neurogenesis from AHPs *in vitro* and *in vivo* (Lie et al., 2005), outlining the importance of the pathway in regulating this process. In addition, β-catenin was detected in progenitor cells within the adult sub-ventricular zone (SVZ) of Axin2-d2EGFP transgenic mice, a mouse line reporter for Wnt pathway activity (Lie et al., 2005). Indeed, when canonical Wnt pathway is blocked via the expression of a dominant negative LEF1 (dnLEF1) in AHPs, a reduction of neuronal differentiation was observed in hippocampal cultures (Lie et al., 2005). The presence of astrocyte-derived secreted Fzd receptor progenitor-2/3 (sFRP2/3), which acts as decoy receptor negatively regulating pathway activity, decreased the percentage of AHPs, outlining canonical Wnt pathway participation to the differentiation of AHPs through factors derived from the hippocampal astrocytes (Lie et al., 2005). Furthermore, inhibition of GSK3β promoted both the proliferation and neuronal differentiation of human neural progenitor cells (NPCs) (Esfandiari et al., 2012), and increased neurogenesis in the sub-granular zone (SGZ) of adult mice (Adachi et al., 2007). Inhibition of Wnt signaling using dominant negative Wnt (dnWnt) (Jessberger et al., 2009), and dnWnt1 (Lie et al., 2005) reduced the level of adult hippocampal neurogenesis, and impaired the cognitive functions of mice. Importantly, the retroviral injection of Dkk1 into the SVZ reduced the proliferation of mammalian achaete-scute homolog-1 $(MASH1)^{+}$ NPCs (Adachi et al., 2007). Furthermore, in Nestin-Dkk1 mice in which Dkk1 is specifically depleted in NPCs, neurons and glial cells, an increased number of neural progenitors was observed, accompanied by an enhanced dendritic complexity and neuronal activity in the dentate gyrus (DG) (Seib et al., 2013). Interestingly, reduction of the paracrine Wnt3 during aging has been shown to impair adult neurogenesis by modulating expression of the neuronal-lineage factors NeuroD1, retrotransposon L1, and doublecortin (Dcx) (Okamoto et al., 2011). Finally, the loss of Wnt7a expression reduced the expansion of NPCs *in vitro*, and in $Wnt7a^{-/-}$ mice a decreased number of newborn neurons at the SGZ was observed, accompanied by altered neuronal maturation translated by an impaired dendritic development, thus linking Wnt7a to self-renewal and differentiation (Qu et al., 2013).

Implication in Synaptogenesis

Wnt ligands have been shown directly modulate the function as well as the architecture of the pre-synaptic regions (Cerpa et al., 2008). Wnt3a and Wnt7a have been reported to stimulate exocytosis and recycling of synaptic vesicles in hippocampal neurons, thus enhancing the synaptic transmission and plasticity (Cerpa et al., 2008; Rosso and Inestrosa, 2013). Wnt3a and Wnt7a, which are expressed as well by post-synaptic components, have been shown to promote the assembly of pre-synaptic structures at the early stages of synapse formation (Cerpa et al., 2008). Wnt7a stimulated the pre-synaptic assembly via inhibition of GSK3β, without transcriptional regulation (Cerpa et al., 2008), and promoted dendritic spine growth and synaptic strength via a CaMKII-dependent mechanism *in vitro* and *in vivo* (Ciani et al., 2011). Wnt7a increased the density and maturity of dendritic spines, whereas Wnt7a-Dvl1 deficient

mice exhibited several defects in spine morphogenesis and mossy fiber CA3 synaptic transmission in the hippocampus (Ciani et al., 2011). Furthermore, Wnt5a induced short-term changes in the clustering of PSD95 and modulated glutamatergic synaptic transmission (Farías et al., 2009). In cultured hippocampal neurons, the tyrosine-protein kinase transmembrane receptors, receptor tyrosine kinase-like orphan receptor-1/2 (Ror1/2), have been demonstrated to play an important role in synapse formation by interacting with Wnt5a to increase synapse formation (Paganoni et al., 2010). The length and number of synapses significantly decreased when Ror1/2 were depleted (Paganoni et al., 2010). Overexpression of Fzd1 receptor increased the pre-synaptic clustering (Varela-Nallar et al., 2009). Interestingly, it has been shown that the astrocytic layers in the DG play an essential role in triggering neuronal differentiation of hippocampal neural stem cells (NSCs) (Kuwabara et al., 2009). Astrocyte-derived Wnt3 has been shown to promote NSC differentiation in a paracrine manner by increasing the expression of synapsin-I and tubulin-III (Okamoto et al., 2011). Wnt3 overexpression in aged primary astrocytes using lentivirus (LV)-expressing Wnt3 significantly improved neurogenesis (Okamoto et al., 2011). Furthermore, GSK3β overexpression has been shown to alter dendritic branching and reducing the number of functional synapses of granule cells in DG (Llorens-Martín et al., 2013). In contrast, GSK3β depletion in the cortex and hippocampus of mice potently reduced spine density associated to loss of persistent spines and destabilization of the new spines (Ochs et al., 2015). These changes were accompanied with an impaired α-amino-3-hydroxy-5-methyl-4-isoxazolepropionic acid (AMPA) receptor-dependent excitatory post-synaptic currents (Ochs et al., 2015). Finally, TAT-TI-JIP, a JNK inhibitor, prevented the increase in the number of PSD95 clusters induced by Wnt5a (Farías et al., 2009).

Implication in Angiogenesis

The Wnt pathway has been shown to play an important role in angiogenesis. Indeed, cadherin-5 (Cdh5)(PAC)-Cre^{ERT2};$Ctnnb1^{floxed}$, or $Ctnnb1^{i\Delta EC}$ transgenic mice, in which β-catenin depletion is specifically induced in endothelial cells, showed low vessel area and reduced number of vascular branch points (Martowicz et al., 2019). In addition, Wnt7a and Wnt7b have been identified as key regulator of normal angiogenesis in the ventral region of the brain, as the combined inactivation of both ligands caused severe defects in brain angiogenesis (Engelhardt, 2003). Indeed, Wnt7a and Wnt7b depletion caused vascular malformations in mice (Daneman et al., 2009). For instance, in $Wnt7a^{+/-}$;$Wnt7b^{-/-}$ mice, which are deficient in Wnt7b, a thickened vascular plexus was observed, whereas in $Wnt7a^{-/-}$;$Wnt7b^{-/-}$ mice, which are deficient for both Wnt7a and Wnt7b, large vascular plexus dilations were observed (Daneman et al., 2009). Wnt3a also plays a major role in angiogenesis but has a moderate effect compared to the two others Wnt7 ligands. Treatment of the human endothelial cell line EAhy926 with Wnt3a up-regulated the nuclear levels of nuclear β-catenin, accompanied by an enhanced transcriptional activity of LEF1, which induced matrix metalloproteinase-2 (MMP2) expression, an effect that was completely abrogated in the presence of LEF1 siRNA (Planutiene et al., 2011). In $Fzd7^{iECKO}$ mice, which are deficient in Fzd7 in endothelial cells, a reduced level of the activated form of β-catenin was observed, and accompanied by a downregulation of Axin2 and LEF1 gene expression (Peghaire et al., 2016). In these mice, the spreading and the percentage of vascularization showed a strong delay in vascular formation in the retina (Peghaire et al., 2016). In $Fzd4^{-/-}$ mice, the neuronal degeneration observed in the brain was essentially caused by vascular dysfunction, due to misshapen capillaries and protrusions of the endothelial processes into the vessel lumen (Ye et al., 2009). Interestingly, the canonical Wnt pathway has been shown to suppress early sphingosine-1-phosphate receptor (S1PR) signaling during angiogenesis to enable the dynamic cell-cell junction formation during anastomosis (Hübner et al., 2018). However, at later stages S1PR signaling regulated BBB maturation and VE-cadherin stabilization (Hübner et al., 2018). Interesting, the E3 ubiquitin ligase PDZ domain–containing ring finger 3 (Pdzrn3), which regulates Dvl3 ubiquitinylation, regulated endothelial intercellular junction integrity. Endothelial cell-specific overexpression of Pdzrn3 led to early embryonic lethality with severe hemorrhaging and altered organization of endothelial intercellular junctions (Sewduth et al., 2017). Treatment of the human umbilical vein endothelial cells (HUVEC) with Wnt3a, significantly increased the level of β-catenin and this upregulation was higher when Pdzrn3 was depleted by siRNA and reduced in Pdzrn3 lentiviral-transduced endothelial cells (Sewduth et al., 2014). Very interestingly, treatment of HUVEC with Wnt5a increased the level of p-c-jun which was impaired in Pdzrn3-depleted cells. In addition, Wnt5a treatment induced AP1 response in HUVEC and this induction was repressed by siPdzrn3-treatment and induced in Pdzrn3 lentiviral-transduced endothelial cells (Sewduth et al., 2014). These results outline the regulatory role of Wnt pathway in temporally linking angiogenesis to BBB formation and in anastomosis (Hübner et al., 2018).

Implication in BBB Formation

The canonical Wnt pathway was shown to act as master regulator of BBB formation and maturation during ontogeny (Liebner et al., 2008). Initial reports showed that β-catenin in human cerebral microvascular endothelial cells (hCMEC/D3) was capable of binding directly to the promoter region of the multidrug resistance protein-1 (MDR1; i.e., ATP-binding cassette sub-family B member-1, ABCB1) gene, a marker of BBB functionality (Pinzón-Daza et al., 2014). In $Ctnnb1^{i\Delta EC}$ transgenic mice, expression of the tight junction protein claudin-5, glucose transporter-1 (GLUT1), and the major facilitator superfamily domain-containing protein 2 (MFSD2A) a key lipid transporter expressed in brain endothelial cells that is vital for brain lipid uptake, were all significantly decreased, associated to defective BBB structural and functional integrity (Martowicz et al., 2019). The stimulation of hCMEC/D3 endothelial cells with Wnt activators increased the gene expression of the multidrug resistance-associated protein-1 (MRP1; ATP-binding cassette sub-family C member-1, ABCC1), as well as ROCK,

whereas Dkk1 induced opposite effects, thus suggesting that the biological activities of the canonical and non-canonical Wnt pathways vary in response to Wnt activators and inhibitors (Pinzón-Daza et al., 2014). Administration of Wnt3aCM in the brain of mice upregulated the expression of the tight junction protein claudin-3, whereas it downregulated the expression of plasmalemma vesicle associated protein (PLVAP), which is involved in endothelial cell fenestration and permeability (Liebner et al., 2008). Furthermore, Wnt7a has been shown to regulate the expression of the BBB-specific GLUT1 in purified endothelial cells *in vitro*, and that β-catenin was required to mediate GLUT1 expression *in vivo* (Engelhardt, 2003). The conditional activation or deactivation of endothelial β-catenin *in vivo* confirmed latter's requirement in regulating the expression of ABCB1, claudin-3, and PLVAP at the BBB (Liebner et al., 2008). The results showed that the transcriptional activity of β-catenin is necessary and sufficient to upregulate the expression of claudin-3, ABCB1 and downregulate PLVAP in brain endothelial cells, thus inducing the structural and functional properties of the BBB (Liebner et al., 2008). Interestingly, the canonical Wnt pathway is essential for maintaining BBB integrity in adulthood as well. Indeed, using a transgenic mouse model with tamoxifen-inducible endothelial cell-restricted disruption of Ctnnb1 (iCKO), it has been shown that β-catenin depletion in endothelial cells caused neuronal damage and multiple intracerebral petechial hemorrhages associated to a downregulation of the tight junction proteins claudin-1 and -3 in the adult brain endothelial cells (Yi et al., 2015).

Implication in Immunity

Several findings have outlined the role of Wnt pathway in regulating different immune functions. In cultured human aortic endothelial cells (HAEC), exposure to Wnt5a has been shown to increase the level of cyclooxygenase-2 (COX2) (Kim et al., 2010). Wnt3a ligand was reported to exert an anti-inflammatory effects in murine mycobacteria-infected macrophages, and mycobacterium tuberculosis-infected macrophages, notably by regulating the expression of tumor necrosis factor (TNF) (Neumann et al., 2010). Wnt pathway plays an important role in dendritic cells (DCs) differentiation (Zhou et al., 2009). More precisely, β-catenin-TCF/LEF signaling has been demonstrated to interact with Notch signaling to promote the differentiation of DCs (Zhou et al., 2009). Interestingly, activation of the non-canonical Wnt pathway mediated by Wnt5a attenuated DCs differentiation (Zhou et al., 2009). Wnt pathway has been shown to promote as well immune tolerance in DCs (Swafford and Manicassamy, 2016). DCs play an important role in regulating the balance between inflammatory and regulatory responses in the periphery. In LRP5/6$^{i\Delta DC}$ mice, in which LRP5 and LRP6 are specifically depleted in DCs, the mRNA levels of interleukin (IL)17A, IL22, TNFα increased, whereas the mRNA levels of IL10 and TNFβ were reduced (Suryawanshi et al., 2015). In β-cat$^{\Delta DC}$ mice, which specifically lack β-catenin expression in DCs, a higher frequency of T helper 1 (Th1), Th17, TNFα^{+};CD4^{+} T cells, and TNFα^{+};CD8^{+} T cells was observed (Manicassamy et al., 2010). The stimulation of DCs with Wnt3a has been shown to limit the expression of pro-inflammatory cytokines and to increase the expression of anti-inflammatory factors in response to *M. tuberculosis* (Suryawanshi et al., 2015). The Wnt pathway could modulate the immune response through the interaction with other signaling pathways. Indeed, a cross-regulation between the Wnt and nuclear factor-kappa B (NF-κB) signaling cascades has been demonstrated, showing that β-catenin exerted an anti-inflammatory effect by physically inhibiting the NF-κB-mediated transcription of pro-inflammatory genes (Ma and Hottiger, 2016). Wnt5a seems to elicit pro-inflammatory responses via Fzd5, whereas Wnt3a-Fzd1 signaling elicited anti-inflammatory responses (Schaale et al., 2011). Nonetheless, in cultured mouse microglial cells that express the Fzd4/5/7/8 receptors as well as LRP5/6, Wnt3a stimulation activated β-catenin signaling, increasing the expression of pro-inflammatory mediators such as IL6, IL12, and TNFα (Halleskog et al., 2011). However, recent findings have demonstrated that deactivation of the β-catenin signaling induced a pro-inflammatory phenotype in microglial cells (Van Steenwinckel et al., 2019). Interestingly, delivery into the brain of a Wnt agonist that mediates canonical pathway activation specifically in microglia by using a microglia-specific targeting nano-carrier, microglial cell pro-inflammatory phenotype was attenuated (Van Steenwinckel et al., 2019). More investigations are required to clearly address the complex role of Wnt pathway in regulating microglial cell activation.

THE Wnt PATHWAY IN ISCHEMIC STROKE

Stroke constitutes a leading cause of death and long-term disability in adults in the industrialized world. Ischemic stroke accounts for the majority of cases, approximately 85%, and occurs when the cerebral blood flow (CBF) is interrupted due to the sudden obstruction of a cerebral artery caused by an embolus or thrombus (Dirnagl et al., 1999; Moskowitz et al., 2010). The disruption of the regional cerebral blood supply initiates a cascade of events that evolve following three major phases (Dirnagl et al., 1999; Moskowitz et al., 2010). The acute phase, which takes place minutes upon occlusion, is characterized by BBB disruption caused by MMPs activation, oxidative stress, and excitotoxicity, leading to neuronal dysfunction and death (Dirnagl et al., 1999; Moskowitz et al., 2010; ElAli, 2016). The second phase, which takes place hours and days upon occlusion, is characterized by apoptosis, neuroinflammation and exacerbation of BBB breakdown, contributing to the secondary progression of injury (Dirnagl et al., 1999; Moskowitz et al., 2010; ElAli, 2016). The third phase, which takes place days and weeks following upon occlusion, is characterized by the activation of various reparative and regenerative processes that include neuronal plasticity, neurogenesis, angiogenesis and tissue scarring (Dirnagl et al., 1999; Moskowitz et al., 2010; ElAli, 2016). The severity of the early pathological events decelerates brain recovery in the chronic phase, thus significantly worsening outcomes (Dirnagl et al., 1999; Moskowitz et al., 2010). Importantly, ischemic stroke results in two major zones

of injury, the infarct core associated to a dramatic reduction of the CBF causing immediate cell death by necrosis, and the peri-infarct penumbra associated to a moderately reduced CBF causing neuronal paralysis that could evolve to cell death (Lo, 2008). Currently, recombinant tissue-plasminogen activator (rtPA)-induced thrombolysis constitutes the only food and drug administration (FDA) approved approach used in clinics to restore CBF (Lo, 2008). The recent evidence is suggesting that Wnt pathway is implicated in ischemic stroke pathobiology, outlining its potential as novel target for the development of new therapeutic interventions.

Implication in Ischemic Stroke Pathobiology

Several studies have suggested that Wnt pathway is regulated in ischemic stroke patients. The Ischemic Stroke Genetics Study (ISGS) has identified some genetic variants in LRP6 to play a role in determining the risk of ischemic stroke (Harriott et al., 2015). Furthermore, the levels of Dkk1 in the plasma of patients with acute ischemic stroke have been reported to significantly increase in comparison to healthy individuals, as well as patients with stable cerebrovascular disease (Seifert-Held et al., 2011). Interestingly, Dkk1 plasma levels were higher in patients with stable cerebrovascular disease when compared to healthy individuals (Seifert-Held et al., 2011). These findings were confirmed in another independent study showing that the serum levels Scl and Dkk1 were significantly higher in patients with ischemic stroke caused by large artery atherosclerotic (LAA) or small-artery occlusion (SAO) stroke (He et al., 2016) in comparison to healthy individuals. However, no difference in the serum levels of Scl and Dkk1 were detected between the stroke sub-types (He et al., 2016). Both studies did not detect any correlation between Scl or Dkk1 levels and stroke severity or outcome. Nonetheless, recent evidence is suggesting that the elevated levels of serum Dkk1 at baseline were associated with poor prognosis 1 year after ischemic stroke, suggesting that initial Dkk1 levels in the serum could constitute a biomarker for ischemic stroke prognosis (Zhu Z. et al., 2019). In a recent study, miR-150-5p, a regulator of β-catenin and thereby the canonical Wnt pathway, was shown to be upregulated in the blood plasma of hospitalized patient with cerebral infarction (Sun et al., 2020).

The overwhelming experimental findings are indicating that the Wnt pathway is potently and dynamically regulated upon ischemic stroke and is critically involved in disease's pathogenesis. For instance, Wnt1 levels have been reported to significantly increase 1 to 6 h within the penumbra of rodents subjected to middle artery occlusion (MCAo) (Chong et al., 2010). The re-emergence of the canonical Wnt pathway activity was interpreted as an intrinsic compensatory mechanism to preserve brain homeostasis upon injury (Chong et al., 2010). Indeed, our group has recently demonstrated that β-catenin levels significantly increased in the brain endothelial cells as early as 3 h after MCAo (Jean LeBlanc et al., 2019). Importantly, the early deactivation of the pathway using the potent Wnt inhibitor XAV939 exacerbated BBB breakdown and edema formation, indicating that the pathway re-emerged to preserve BBB structure and function upon injury (Jean LeBlanc et al., 2019). Following the early activation of the pathway, a tendency toward deactivation has been reported and was associated to an upregulation of GSK3β (Jean LeBlanc et al., 2019), and a downregulation of β-catenin and Dvl (Xing et al., 2012) as well as Wnt3a (Wei et al., 2018) within the infarct region. Furthermore, Dkk1 expression was detected within the ischemic region as early as 3 h after MCAo and continued to steadily increase during the following hours (Mastroiacovo et al., 2009). Dkk1-induced expression was correlated with reduced levels of β-catenin in ischemic neurons, outlining Dkk1 potency in modulating canonical Wnt pathway (Mastroiacovo et al., 2009). In the SVZ, β-catenin and Wnt3a expression was shown to decrease during the sub-acute phase after ischemic stroke (Wei et al., 2018). In LRP6$^{+/-}$ mice, which are LRP6 haplo-insufficient, a larger infarct and severe motor deficits as well as increased inflammatory gene expression were reported after MCAo (Abe et al., 2013). Interestingly, Gpr124$^{flox/-}$ mice, which are deficient for the endothelial-specific G-protein-coupled receptor (GPCR) Gpr124, exposed to MCAo exhibited rapid BBB breakdown accompanied by hemorrhagic transformation (Chang et al., 2017). Importantly, BBB breakdown following MCAo was potently rescued in Gpr124$^{flox/-}$Ctnnb1$^{lox(ex3)/+}$;Cdh5-Cre^{ERT2} mice in which β-catenin signaling is specifically activated in endothelial cells (Chang et al., 2017). The induced activation of β-catenin signaling in Gpr124$^{flox/-}$ mice attenuated hemorrhagic transformation and restored the pericyte-endothelial cell crosstalk (Chang et al., 2017). Interestingly, Wnt7a/b, two of the most potent factors implicated in physiological angiogenesis are not activated during post-stroke angiogenesis, suggesting that the latter does not constitute a simple recapitulation of developmental angiogenesis (Buga et al., 2014). Transcriptomic studies have shown that the proliferation of vascular smooth muscle cells (VSMCs), which contribute to post-stroke angiogenesis, is modulated by LEF1 and Wnt4a, and that this modulation was more important in young animals compared to aged animals after MCAo, whereas Wnt5 was specifically increased in the brain of aged animals (Buga et al., 2014). Furthermore, the deposition of the extracellular matrix proteins (ECM) limits the plasticity and remodeling capability of the microvasculature within the scarring zone upon MCAo, was exacerbated in aged animals (Johnson and DiPietro, 2013), accompanied by an increased expression of Wnt5b gene in the peri-lesional region in the cortex (Buga et al., 2014). Dkk1 is induced in neurons within the infarct core and the penumbra and was associated to a reduced expression of β-catenin (Mastroiacovo et al., 2009). Treatment with lithium ions rescued canonical Wnt pathway activity and was highly protective against ischemia (Mastroiacovo et al., 2009). Importantly, doubleridge mice, which have a reduced basal expression of Dkk1, showed an attenuated reduction of β-catenin and a reduced infarct volume following MCAo, providing a direct proof that Dkk1 contributes to the injury progression in ischemic stroke (Mastroiacovo et al., 2009). It is well established that 17β-estradiol (i.e., E2, estrogen) exerts neuroprotective effects following cerebral ischemia (Zhang et al., 2008). E2 mediates its neuroprotective effects, at least partly, by attenuating the post-ischemic induction of Dkk1

(Zhang et al., 2008). Indeed, E2 reduced ischemia-induced Dkk1 expression, which correlated with elevated levels of nuclear β-catenin, and enhanced the expression of Wnt3 at the lesion site (Zhang et al., 2008). These effects were associated as well to the modulation of JNK/c-Jun signaling (Zhang et al., 2008). It is well known that the pre-menopausal women are somehow protected against ischemic stroke in comparison to age-matching men (Roquer et al., 2003). This tendency is drastically inverted after menopause, and aged women have worse stroke outcomes when compared with men (Di Carlo et al., 2003). The functional link between E2 and Wnt pathway via Dkk1 is highly interesting, as it might accounts for the sex-dependent disparities observed in ischemic stroke recovery, thereby constituting a novel target for the development of therapeutic interventions that are tailored for the biological sex.

The accumulating evidence is indicating that the non-canonical Wnt pathway is deregulated in ischemic stroke (Wang and Liao, 2012). Among the various signaling components, ROCK pathway seems to play a particularly important role. Indeed, in global hemizygous ROCK2$^{+/-}$ and endothelial-specific (EC-ROCK2)$^{-/-}$ mice, endothelial nitric oxide synthase (eNOS) mRNA stability and expression were increased after MCAo (Hiroi et al., 2018). This was correlated with an enhanced endothelium-dependent relaxation and neuroprotection (Hiroi et al., 2018). The neuroprotective effects observed in ROCK2$^{+/-}$ were totally abolished upon eNOS depletion (Hiroi et al., 2018). These findings indicate that ROCK2 plays important role in regulating eNOS expression and NO-mediated maintenance of the neurovascular functions after ischemic stroke (Hiroi et al., 2018). In a recent study, the depletion of profilin-1 (Pfn1), which is an actin-binding protein involved in the dynamic transformation and reorganization of cytoskeleton, attenuated damage upon cerebral ischemia via modulation of microglial cell function associated with the RHOA/ROCK pathway (Lu et al., 2020). Furthermore, it has been shown that JNK and c-Jun phosphorylation is increased very early within the infarct core and peri-lesional region in the brain of rats after MCAo (Ferrer et al., 2003). Moreover, in JNK1$^{-/-}$ mice the infarct size is exacerbated following MCAo (Brecht et al., 2005). The expression of TNF receptor-associated factor-6 (TRAF6) was markedly increased after cerebral ischemia in mice (Li T. et al., 2017). TRAF6 induced RAC1 activation and consequently exacerbated ischemic injury by directly binding and ubiquitinating RAC1 (Li T. et al., 2017). TRAF6 depletion reduced the infarct volume and ameliorated the neurological functions following MCAo (Li T. et al., 2017). TRAF6 depletion attenuated the pro-inflammatory response, oxidative stress, and neuronal death (Li T. et al., 2017). More investigations are still needed to decipher and fully address the complex role of the non-canonical Wnt pathway in ischemic stroke pathobiology (**Figure 1**).

Implication in Ischemic Stroke Therapy

In anticipation of its potential as a major therapeutic target, there is currently a growing interest in investigating the impact of Wnt pathway modulation on structural and functional recovery after ischemic stroke. Ischemic stroke induces neurogenesis in the SVZ where stem/progenitor cells shift from asymmetric to symmetric cell division, and migrate toward the peri-lesional zone in attempt to integrate and replace the lost neurons (Marchetti and Pluchino, 2013). Moreover, NPCs have been shown to use the vasculature as scaffold to migrate to the lesion site within specialized neurovascular niches (Ohab et al., 2006; Hermann and Chopp, 2012; ElAli et al., 2014). Ischemic stroke induces as well angiogenesis within the lesion site as an attempt to ameliorate cerebral blood perfusion, enhance the uptake of nutrients, and promote the secretion of neurotrophic factors (Ohab et al., 2006; Hermann and Chopp, 2012). Unfortunately, these responses do not improve recovery after stroke, as NPCs have slow proliferation rate, newborn neurons do not survive the ischemic "milieu," and density of the new microvasculature is not sufficient to adequately perfuse the injured tissue (Ohab et al., 2006; Wu et al., 2017). These processes are associated to an activation of the canonical Wnt pathway, translating an intrinsic attempt from the brain to repair itself via re-emergence of specialized developmental mechanisms (Piccin and Morshead, 2011; Hermann and ElAli, 2012). It has been proposed that amplification of the Wnt pathway activity would allow boosting the endogenous protective and restorative processes. Indeed, the exogenous delivery of recombinant Wnt3a into the brain of mice improved short- and long-term tissue repair and regeneration following MCAo (Wei et al., 2018). This was attributed to an upregulation of the brain-derived growth factor (BDNF), and stimulation of the proliferation and migration of NPCs from the SVZ toward the peri-lesional zone, thus increasing the number of newborn neurons at the injured site (Wei et al., 2018). Additionally, Wnt3a administration enhanced the regional CBF within the peri-lesional zone (Wei et al., 2018). Importantly, Dkk1 abolished most of the beneficial effects of Wnt3a administration (Wei et al., 2018). MiRNA-148b has been reported to be overexpressed in the SVZ of rats upon MCAo (Wang et al., 2017). MiRNA-148b has been shown to suppress the expression of Wnt1 and β-catenin, hence acting as negative regulator of the canonical Wnt pathway (Wang et al., 2017). Inhibition of miRNA-148b expression using a LV-miR-148b inhibitor promoted the proliferation and differentiation of NSCs into neurons and astrocytes, and improved functional recovery (Wang et al., 2017). These effects were abolished upon depletion of Wnt1 (Wang et al., 2017). The delivery of LV-Wnt3a-HA directly into the striatum of mice enhanced long-term functional recovery after cerebral ischemia, and increased the number of bromodeoxyuridine (BrdU)$^{+}$ cells that differentiated into mature neurons in the ischemic striatum (Shruster et al., 2012). On the other hand, delivery of LV-Wnt3a-HA into the SVZ enhanced functional recovery early after cerebral ischemia and increased the number of immature neurons in the striatum as well as SVZ, accompanied by attenuation of neuronal injury (Shruster et al., 2012). The delayed effects following intra-striatal LV-Wnt3a-HA administration, up to 1 month after ischemia, suggest that the observed functional recovery was not attributable to the rescuing of pre-existing damaged neurons but rather to the improved neurogenesis within the neurogenic niches (Shruster et al., 2012). This might be attributed to Dkk1-induced expression within the ischemic striatum, which prevented Wnt3a from binding

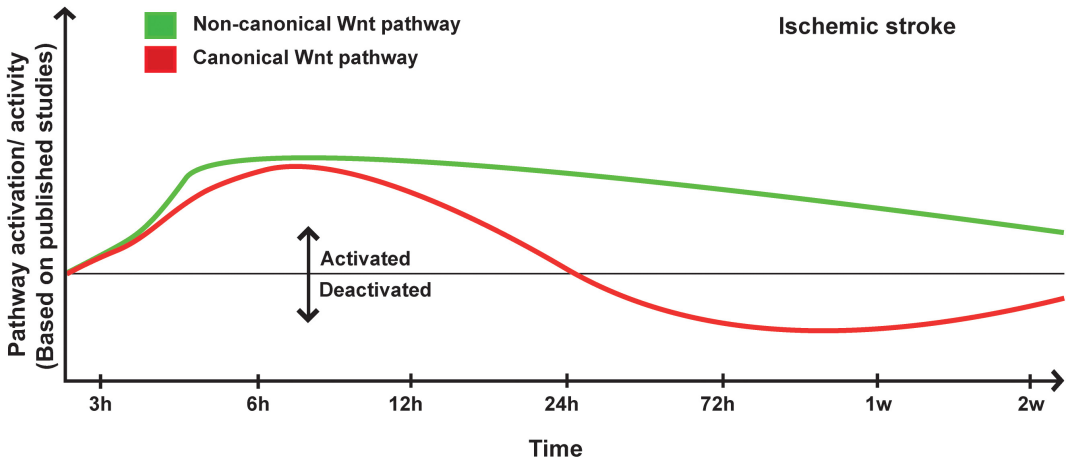

FIGURE 1 | Proposed scheme for Wnt pathway regulation in ischemic stroke. A representation of canonical and non-canonical Wnt pathways temporal regulation following ischemic stroke onset based on pathway activation (i.e., modulation of pathway's key components) and activity (i.e., regulation of specific target genes) as reported in the different published studies.

to LRP5/6 (Shruster et al., 2012). Galangin, a natural flavonoid isolated from the rhizome of *Alpinia officinarum Hance*, has been shown as well to improve neurovascular functions after cerebral ischemia, and to ameliorate neurological functions through activation of the canonical Wnt pathway coupled with hypoxia-inducible factor-1α (HIF1α) and vascular endothelial growth factor (VEGF) (Wu et al., 2015). Interestingly, hypoxic post-conditioning (HPC) increased the levels of nuclear β-catenin and the expression of Wnt3a, while decreasing the expression of Dkk1 after cerebral ischemia in rats (Zhan et al., 2019). The effects of HPC were abolished by the LV-mediated overexpression of Dkk1 in the brain (Zhan et al., 2019). HPC reduced the activity of GSK3β, an effect that was recapitulated following the pharmacological inhibition of GSK3β using SB216763 (Zhan et al., 2019). These results suggest that activation of the canonical Wnt pathway through Dkk1 inhibition and GSK3β deactivation jointly contribute to the neuroprotective effects of HPC against ischemic injury (Zhan et al., 2019). Moreover, the acute administration of 4,6-disubstituted pyrrolopyrimidine (TWS119), a specific inhibitor of GSK3β, has been shown to provide neuroprotection by decreasing the infarct volume and reducing BBB permeability after cerebral ischemia in rodents (Wang W. et al., 2016). These effects were associated to canonical Wnt signaling pathway activation, which increased the expression of tight junction proteins claudin-3 and ZO1 (Wang W. et al., 2016). In parallel, the delayed administration of TWS119 has been shown to improve long-term neurological functions associated to enhanced angiogenesis and neural plasticity after ischemic stroke (Song et al., 2019). Furthermore, pathway delayed activation enhanced the expression of PSD95, the pre-synaptic marker synaptophysin, as well as the growth-associated protein-43 (GAP43) (Song et al., 2019). Additionally, canonical Wnt pathway delayed activation stimulated microglia cell polarization toward a reparative phenotype in the sub-acute phase translated by an increased expression of CD206, Arginase-1 (Arg1) and chitinase3-like 3 (YM1/2) (Song et al., 2019). This was accompanied by an enhanced expression of various anti-inflammatory mediators, including IL10 and TGFβ (Song et al., 2019). Indeed, previous studies have shown that Wnt3a induced an anti-inflammatory M2-like phenotype in microglial cells via canonical Wnt pathway activation, which increased the expression of Arg1 (Matias et al., 2019). In this regard, the delivery of Wnt3a attenuated the inflammatory response upon MCAo by modulating microglial cell activation and phenotype (Zhang et al., 2019). Wnt3a administration downregulated the expression of pro-inflammatory markers, such as the inducible NOS (iNOS) and TNFα, whereas upregulated the expression of anti-inflammatory markers, such as CD206 and Arg1 (Zhang et al., 2019). The immunomodulatory potential of canonical Wnt pathway activation could be associated to an activation of autophagy through Beclin-1 and the microtubule-associated protein light chain-3 (LC3)-II (Zhou et al., 2011). Ischemic stroke strongly induces the activation of astrocytes that contribute to scar formation, thus physically separating the injured tissue from the intact region (Liu and Chopp, 2016). Importantly, Wnt3a treatment was efficient in decreasing the number of neurotoxic activated astrocytes (A1 phenotype) and to increase the number of neuroprotective activated astrocytes (A2 phenotype), via reduction of glial fibrillary acidic protein (GFAP) expression (Zhang et al., 2019). This was accompanied by reducing the expression of IL15, which induces neurotoxic glial activation, and by increasing the expression of IL33, which promotes neuroprotective glial activation (Zhang et al., 2019). In a previous study, it has been reported that administration of Sulindac, a non-steroidal anti-inflammatory drug, in rats after MCAo activated the canonical Wnt pathway by inducing the expression of Dvl and β-catenin, and provided anti-apoptotic effect by increasing the expression of B-cell lymphoma-2 (BCL2) and decreasing the expression of Bcl-2-associated X (BAX) in the ischemic brain (Xing et al., 2012). Importantly, BCL2 has been shown to stimulate neurogenesis in rats upon MCAo by inhibiting the function of

bone morphogenetic protein-4 (BMP4), which has been shown to negatively regulate adult brain neurogenesis and to direct neural progenitors to a glial fate, via activation of β-catenin signaling (Lei et al., 2012). In a recent study, it has been shown that the transplantation of oligodendrocyte precursor cells (OPCs) in the brain of mice after MCAo reduced the infarct and edema volumes, and improved the neurological functions (Wang et al., 2020). OPCs transplantation attenuated BBB breakdown by increasing the expression of claudin-5 and occludin (Wang et al., 2020). These effects were mediated via the activation of the canonical Wnt pathway, as OPCs transplantation increased the expression of β-catenin and Wnt7a in the ischemic brain (Wang et al., 2020). Pharmacological inhibition of the canonical Wnt pathway totally abolished the beneficial effects of OPCs transplantation (Wang et al., 2020).

As mentioned earlier, ischemic stroke induces BBB breakdown, which promotes complications such as edema formation and inflammation (ElAli et al., 2011; Jean LeBlanc et al., 2019). Currently, thrombolysis via rtPA administration constitutes the only existing approach approved by the FDA to treat acute ischemic stroke (Jean LeBlanc et al., 2019). rtPA significantly enhances stroke outcomes by restoring CBF to the ischemic region (Wang et al., 2004; Jean LeBlanc et al., 2019). However, rtPA should be administered within a narrow therapeutic window of 4.5 h after onset due to the elevated risk of causing hemorrhagic transformation (HT), a life-threatening post-stoke complication (Sussman and Connolly, 2013). Therefore, only around 5% of eligible stroke patients could benefit from thrombolysis (Wang et al., 2004). It has been demonstrated that HT associated to rtPA administration is mediated via the activity of MMPs, namely MMP9, which exacerbates BBB breakdown via excessive degradation of the ECM and tight junction proteins (Wang et al., 2004). Furthermore, our group has recently demonstrated that rtPA increased the hypoxia-induced expression of PLVAP, increasing vascular permeability and leakage (Jean LeBlanc et al., 2019). Interestingly, the administration of the GSK3β inhibitor, TWS119, to activate the canonical Wnt pathway attenuated rtPA-induced HT in rats upon MCAo. Indeed, TWS119 administration reduced BBB breakdown and improved structural and functional recovery by increasing the expression of claudin-3, and ZO1 (Wang W. et al., 2016). These results suggest that pathway activation could prevent tPA-induced HT after acute ischemic stroke. However, in this study the pathway was activated 4 h after MCAo, thus within the approved therapeutic window for rtPA administration, limiting its clinical relevance. Our group has recently demonstrated that canonical Wnt pathway activation using a potent agonist, 6-bromoindirubin-3′-oxime (6-BIO), attenuated BBB breakdown and reduced the incidence of HT associated to delayed rtPA administration (Jean LeBlanc et al., 2019). In this study, rtPA was administered 6 h after MCAo, thus beyond the current therapeutic window. Canonical pathway activation, which was translated by increased levels of β-catenin restored the expression of claudin-3 and claudin-5, and attenuated the basal endothelial permeability by repressing PLVAP expression (Jean LeBlanc et al., 2019). These findings suggest that activation of the canonical Wnt pathway could extend the therapeutic window of rtPA via attenuation of BBB breakdown (Jean LeBlanc et al., 2019).

Using a potent cell-penetrating peptide D-JNKI1, which selectively block the access of JNK to c-Jun, it has been shown that deactivation of JNK/c-Jun pathway significantly attenuated NMDA receptor-mediated excitotoxicity and subsequent cell death in the brain of rodents after MCAo (Borsello et al., 2003). In another study, D-JNKI1 has been demonstrated to markedly prevent c-Jun phosphorylation after MCAo in rats, in the core and the peri-lesional zone, resulting in a strong inhibition of caspase-3 activation in the core (Repici et al., 2007). The administration of JNK-IN-8, a potent JNK inhibitor with high specificity, improved structural and functional recovery through suppressing of neuroinflammation in the brain of rats following MCAo (Zheng et al., 2020). JNK-IN-8 administration exerted anti-inflammatory effects by attenuating the activation of microglia and reducing expression of IL6, IL1β, and TNFα expression (Zheng et al., 2020). Furthermore, JNK-IN-8 suppressed the activation of NF-κB signaling, translated by reduced levels of p65 (Zheng et al., 2020). These findings suggest that deactivation of the non-canonical Wnt pathway provided protection in the context of ischemic stroke. Indeed, it is well established that ROCK, which is a main downstream effector in the non-canonical Wnt pathway, plays a negative role in ischemic stroke (Sladojevic et al., 2017). The administration of fasudil and Y-27632, which are potent ROCK inhibitors, has been shown to ameliorate the CBF to both ischemic and non-ischemic brain of mice after MCAo, reduced infarct size and improved neurological functions (Rikitake et al., 2005). These observations were associated to a reduced ROCK activity within the vasculature as well as brain parenchyma, and an increased eNOS expression and activity (Rikitake et al., 2005). The protective effects of ROCK inhibition were abolished upon eNOS genetic depletion in mice (Rikitake et al., 2005). ROCK inhibition using fasudil after MCAo in rats reduced infarct size, neuronal apoptosis as well as caspase-3 activity, subsequently improving neurological recovery (Wu J. et al., 2012). ROCK has been shown to mediate inflammation, thrombosis formation, and vasospasm by affecting the function of vascular and inflammatory cells (Wang and Liao, 2012). For instance, peripheral leukocyte ROCK activity was reported to increase in acute stroke patients compared to healthy individuals with maximal activity occurring about 48 h after stroke onset (Feske et al., 2009). ROCK inhibition using Y-27632 after MCAo in rats decreased infarct size, reduced oxidative stress and alleviated the inflammatory response in the ischemic brain (Li and Liu, 2019). ROCK inhibition attenuated neuronal apoptosis by modulating the expression of caspase-3/8/9 as well as BAX/BCL2 ratio (Li and Liu, 2019). Furthermore, ROCK inhibition attenuated as well the activation of astrocytes and microglial cells at the lesion site (Li and Liu, 2019). Importantly, inhibition of ROCK activity was proposed to account for the pleiotropic non-cholesterol protective effects of statins in ischemic stroke (Sacco and Liao, 2005). For example, some of the beneficial effects of statins in ischemic stroke are attributed to the inhibition of geranylgeranyl pyrophosphate formation required for the function of RHO-GTPases, thus altering RHO/ROCK pathway (Wang and Liao,

2012). Outlining the clinical relevance of ROCK inhibition in ischemic stroke therapies, fasudil was assessed in clinical studies and has been shown to improve the outcomes of ischemic stroke patients when administered within 48 h after onset (Shibuya et al., 2005). Sanggenon C (SC), a natural flavonoid extracted from the Cortex Mori *Sang Bai Pi*, was reported to possess anti-inflammatory and antioxidant properties under hypoxic conditions (Zhao and Xu, 2020). SC administration in rats after MCAo improved structural and functional recovery by reducing inflammation, oxidative stress, and apoptosis (Zhao and Xu, 2020). RHOA overexpression abolished SC properties, indicating that SC mediated its protective effects by inhibiting RHOA/ROCK pathway (Zhao and Xu, 2020).

The recent findings are suggesting that CaMKII activity, which is another major component of the non-canonical Wnt pathway, constitutes a potential target for neuroprotection after ischemic stroke (Coultrap et al., 2011). CaMKII, which has been shown to mediate major effects of physiological NMDA-receptor stimulation, is implicated in the pathological glutamate signaling after ischemic stroke (Vest et al., 2010). Indeed, inhibition of stimulated and autonomous CaMKII activity in the brain of mice after MCAo using tatCN21 attenuated glutamate-mediated neuronal cell death in the ischemic brain (Vest et al., 2010). However, another study has demonstrated that the neuroprotection observed upon CaMKII inhibition could be seen only acutely immediately, whereas a sustained CaMKII inhibition associated to excitotoxicity could exacerbate neuronal death by increasing neuronal vulnerability to glutamate (Ashpole and Hudmon, 2011). Collectively, these findings highlight the promises of targeting the non-canonical Wnt pathway in ischemic stroke (**Supplementary Table 1**).

THE Wnt PATHWAY IN HEMORRHAGIC STROKE

Hemorrhagic stroke, which comprises essentially intra-cerebral hemorrhage (ICH) and subarachnoid hemorrhage (SAH), accounts for approximately 15% of stroke cases (Qureshi et al., 2009). Hemorrhagic stroke is a devastating pathological condition as it is more likely to result in fatality or severe disability in survivors (Morioka et al., 2017). During hemorrhagic stroke, a rapid accumulation of blood within the brain parenchyma leads to disruption of the normal anatomy, and increases local pressure (Aronowski and Zhao, 2011). When hemorrhagic volume exceeds 150 mL acutely, cerebral perfusion pressure falls to zero and the patient dies. If the hemorrhagic volume is smaller than 140 mL, most patients survive the initial insult (Xi et al., 2006). ICH evolves within three distinct phases; (1) initial hemorrhage, which is caused by the rupture of cerebral arteries, (2) hematoma expansion, which occurs during the first hours after initial hemorrhage onset and is implicated in the increased intra-cranial pressure that disrupts local tissue integrity and the BBB, and (3) the peri-hematomal edema, which is formed around the hematoma causing secondary insult (Magistris et al., 2013). During the secondary insult, some biological modification appears such as cytotoxicity of blood, hyper-metabolism, excitotoxicity, spreading depression, oxidative stress, inflammation, and exacerbated BBB disruption (Aronowski and Zhao, 2011). This peri-hematomal edema is the primary etiology for neurological deterioration and develops over days following the initial insult that itself can lead to secondary brain injury resulting in severe neurological deficits and sometimes delayed fatality (Xi et al., 2006). Ultimately, this pathogenesis leads to irreversible disruption of the components of the neurovascular unit, leading to deadly brain edema with massive brain cell death. Whereas inflammatory mediators generated locally in response to brain tissue injury have the capacity to increase damage caused by ICH, inflammatory cells are vital for the removal of cell debris from hematoma (Aronowski and Zhao, 2011). In more than 40% of intra-cerebral hemorrhage cases, hemorrhage extends into the cerebral ventricles causing intra-ventricular hemorrhage. This is associated with acute obstructive hydrocephalus and substantially worsening the prognosis (Magistris et al., 2013). The recent evidence is suggesting that Wnt pathway is implicated in hemorrhagic stroke pathobiology, thus outlining its potential as novel target for the development of new therapeutic interventions.

Implication in Hemorrhagic Stroke Pathobiology

Several studies have suggested that Wnt pathway is deregulated in hemorrhagic stroke. Indeed, in hemorrhagic stroke patients with spontaneous non-traumatic ICH, a decreased level of nuclear β-catenin in brain endothelial cells located near the bleeding site was reported, suggesting a deactivation of the canonical Wnt pathway at the BBB (Tran et al., 2016). Moreover, the protein expression of APC was decreased in the brain of intra-cranial aneurysm type of patients, independently of biological sex and age, and was associated to the intra-cranial aneurysm diameter (Lai et al., 2019). In addition, RHOA expression was significantly increased in the peripheral blood mononuclear cells (PBMCs) on days 0, 2, and 4 after aneurysmal SAH patients (González-Montelongo et al., 2018). Interestingly, a strong correlation between RHOA expression/activity and injury severity was observed in patients at days 2 and 4 (González-Montelongo et al., 2018). There was no significant increase in activated RHOA in patients who developed vasospasm versus patients without vasospasm on day 0 as well as on day 2 whereas active RHOA was significantly increased on day 4 (González-Montelongo et al., 2018).

The overwhelming experimental findings are indicating that Wnt pathway is potently regulated upon hemorrhagic stroke, and is critically involved in disease pathogenesis. Indeed, expression of Norrin, a key protein implicated in BBB formation, which activates Fzd4 receptor, has been shown to significantly increase 6 to 24 h after SAH, which was induced by endovascular perforation in rats (Chen et al., 2015). Aldolase C, a positive regulator of Wnt signaling that acts through destabilization of Axin, significantly increased during early brain injury associated to SAH, subsequently increasing the expression of Axin (Ruan et al., 2020). Following SAH, Wnt1 and Wnt3a levels significantly

decreased 12 h after onset (Wang Y. et al., 2019; Ruan et al., 2020), whereas the levels of β-catenin, Fzd1 decreased as early as 6 h after onset (Wang Y. et al., 2019; Ruan et al., 2020). Twenty-four hours after ICH and SAH, the ratio of p-tyrosine-GSK3β/GSK3β (i.e., indicating an enhanced kinase activity) (Krafft et al., 2012, 2013; Zuo et al., 2017), and p-serine-β-catenin/β-catenin were increased (Krafft et al., 2013; Zuo et al., 2017; Li et al., 2018), whereas the ratio p-serine-GSK3β/GSK3β (i.e., indicating a reduced kinase activity) was decreased (Li et al., 2018). Interestingly, another study has reported that in the peri-hematomal β-catenin expression in endothelial cells is downregulated, whereas GSK3β expression and activity remained unchanged (Zhao et al., 2017). On the other hand, Dkk1 expression in the basal ganglia and peri-hematomal remarkably increased during early brain injury associated to ICH, whereas it remains unchanged in the contralateral basal ganglia and in the blood serum (Li Z. et al., 2017; Wang G. et al., 2019). Interestingly, Dkk1 expression was found in the neuron and microglia but not in astrocytes (Wang G. et al., 2019), and correlated with a decreased level of Wnt1 in neurons (Wang Y. et al., 2019). GSK3β was activated as well in early brain injury as well as in the second phase of hemorrhagic stroke within the CA1, CA3, and DG regions of the hippocampus (Liu et al., 2018). Early deactivation of the canonical Wnt pathway using Wnt1 or Fzd1 siRNA worsened brain edema after SAH and exacerbated neurological deficits (Ruan et al., 2020), outlining the importance of canonical Wnt pathway after hemorrhagic stroke. In tamoxifen-inducible endothelial cell-restricted disruption of ctnnb1 (iCKO) mice in which β-catenin is completely depleted, the expression of both claudin-1 and claudin-3 were diminished in brain endothelial cells (Tran et al., 2016). Loss of 60% of claudin-1 expression was associated to an increased permeability of the BBB in iCKO mice, leading to petechial hemorrhage in the brain of mutant mice (Tran et al., 2016).

Recent studies have demonstrated an important role as well of the non-canonical Wnt in hemorrhagic stroke. For instance, the expression and activity of ROCK and RHOA significantly increased 24 h after SAH (Fujii et al., 2012; Huang et al., 2012; Zhao H. et al., 2016), whereas RAC1, which counteracts the biological activity of RHOA, remained unchanged, correlating with low levels of β-catenin within the adherent junctions (Huang et al., 2012). Ephrin receptor-A4 (EphA4) activation has been shown to induce the phosphorylation of Ephexin1, which preferentially activates RHOA (Fan et al., 2017). Furthermore, EphA4 has been shown to promote cell death and apoptosis (Conover et al., 2000; Lemmens et al., 2013). EphA4 expression increased as well as Ephexin1, RHOA and ROCK2 (Fan et al., 2017) in the brain of rats after SAH, and EphA4 was strongly expressed in neurons, astrocytes, and microglia (Fan et al., 2017). Importantly, hemoglobin (Hb) extravasation after ICH has been demonstrated to exacerbate BBB disruption as well as edema formation within the peri-hematomal region as early as 24 h after onset (Koeppen et al., 1995). Six and 24 h following Hb intra-cerebral injection, RHOA and ROCK2 activities were significantly increased, and ROCK2 activity positively correlated with MMP9 expression levels (Fu et al., 2014). In addition, the purinergic receptor P2X7, which is implicated in modulating BBB integrity, was upregulated following hemorrhagic stroke via the activity of RHOA (Zhao H. et al., 2016). RHOA/ROCK pathway plays key role in mediating the contraction of the VSMCs of the basilar arteries in SAH animals during the early brain injury phase (Egea-Guerrero et al., 2015), as well as in the second phase of hemorrhagic stroke (Naraoka et al., 2013). Moreover, it has been shown that the Wnt/PCP pathway is regulated as well following hemorrhagic stroke, translated by increased levels of JNK and c-Jun phosphorylation at the early stages after onset within the basal ganglia and cortical basal brain (Wan et al., 2009; Ling et al., 2019; Xu et al., 2020, p. 3), as well as within the basilar arteries at least until day 7 after onset (Yatsushige et al., 2005, 2008). However, another study reported no changes in JNK and c-Jun phosphorylation, as well as no correlation with P2X7 upregulation (Wen et al., 2017). The expression of Dkk3, which acts as a negative regulator for the canonical Wnt signaling similarly to Dkk1, and Dvl were downregulated very early after ICH, whereas JNK/AP1 signaling was induced (Xu et al., 2020, p. 3). Interestingly, CaMKII, which is another component of the non-canonical Wnt pathway, plays an important role in the regulation of intracellular Ca^{2+} homeostasis VSMCs contraction and vascular inflammation (House et al., 2008). It has been shown that CaMKII phosphorylation increased 1 h after SAH in the cerebral arteries whereas CaMKII protein expression increased after 3 days within the same arteries (Edvinsson et al., 2014). CaMKIIα, which is one of the major isoforms of CaMKII, was shown to modulate the inflammatory response of microglial cells (Huang et al., 2015). Tyrosine phosphorylation of CaMKIIα, which modulate protein kinase activity, was shown to increase immediately after SAH induction essentially in neurons and microglia within the lesion site (Makino et al., 2015; Zhou et al., 2018) (**Figure 2**).

Implication in Hemorrhagic Stroke Therapy

In the recent years, several studies have evaluated the impact of the Wnt pathway modulation on structural and functional recovery after hemorrhagic stroke. It has been proposed that amplifying the activity of the canonical Wnt pathway or attenuating that of the non-canonical Wnt pathway could promote the reparative and restorative processes. Indeed, the exogenous intranasal delivery of Wnt3a into the brain of SAH rats improved short-, mid- and long-term neuronal function and reduced brain edema without influencing SAH severity (Ruan et al., 2020). Administration of the Wnt inhibitor XAV939 counteracted most of the beneficial effect of Wnt3a after SAH (Ruan et al., 2020). On the other hand, the exogenous delivery of recombinant human Wnt1 (rhWnt1) into the ventricle of SAH rats decreased brain edema and ameliorated neurological functions (Wang Y. et al., 2019). Interestingly, these beneficial effects were totally abolished after administration of Wnt1 siRNA or a neutralizing monoclonal antibody anti-Fzd1 (Wang Y. et al., 2019). These results highlight the importance of the canonical Wnt pathway as a therapeutic target to promote neurovascular repair following hemorrhagic stroke. In both studies, SAH was associated to a deactivation of the canonical

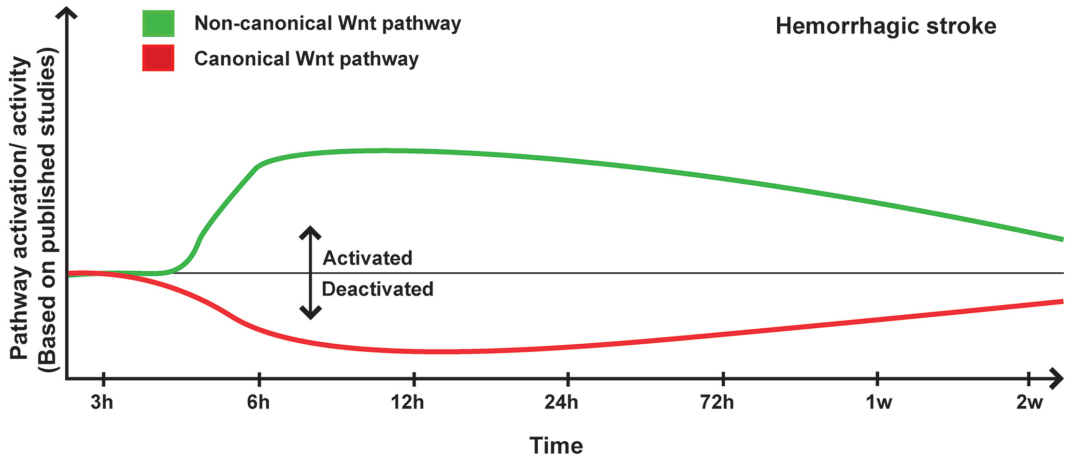

FIGURE 2 | Proposed scheme for Wnt pathway regulation in hemorrhagic stroke. A representation of canonical and non-canonical Wnt pathways temporal regulation following hemorrhagic stroke onset based on pathway activation (i.e., modulation of pathway's key components) and activity (i.e., regulation of specific target genes) as reported in the different published studies.

Wnt pathway translated by reduced levels of Wnt1, Wnt3a and Fzd1. In this regard, the intraperitoneal delivery of 6-BIO, a GSK3β inhibitor, improved neurological functions, reduced brain hematoma volume, and stimulated regeneration after ICH (Zhao et al., 2017). This was attributed to an upregulation of BDNF, which stimulates the proliferation and migration of neuronal progenitors from the SVZ toward the injured zone, thus increasing the number of newborn neurons within in the peri-hematomal brain region (Zhao et al., 2017). 6-BIO also improved angiogenesis by an increase number of $BrdU^{+}/GLUT1^{+}$ cells in the peri-hematomal zone during the second phase of hemorrhagic stroke (Zhao et al., 2017). As mentioned, the expression Dkk1, a potent endogenous inhibitor of the canonical Wnt pathway, increased in the basal ganglia early after ICH (Li Z. et al., 2017), and was expressed essentially in neurons, and microglia (Wang G. et al., 2019). The administration of Dkk1 siRNA into the brain ventricles of rats attenuated BBB disruption after ICH by increasing the expression of ZO1, consequently decreasing brain edema and attenuating neurological deficits (Li Z. et al., 2017). These results suggest that Dkk1 neutralization is neuroprotective against the secondary injury following ICH, and that the underlying mechanisms are associated with an improved integrity of the BBB (Li Z. et al., 2017). These observations might be associated with enhanced biological activities of Wnt1 or Wnt3a, as Dkk1 prevents Wnt1 and Wnt3a binding to LRP5/6 (Shruster et al., 2012). In this regard, our group has recently demonstrated that deactivation of the canonical Wnt pathway using XAV939 increased the risk of spontaneous intra-cerebral HT following ischemic stroke by exacerbating BBB permeability (Jean LeBlanc et al., 2019). Furthermore, minocycline, a semi-synthetic tetracycline derivative, alleviated the severity of brain edema and BBB disruption, thus ameliorating neurological functions, notably by upregulating the expression of occludin in a rodent collagenase-induced ICH model (Wang G. et al., 2019). Minocycline activated the canonical Wnt pathway by increasing the abundance of β-catenin and Wnt1, and reducing the expression of Dkk1, thereby inducing the expression of the tight junction occludin (Wang G. et al., 2019). Interestingly, the administration Dkk1 siRNA amplified the protective effects of minocycline (Wang G. et al., 2019). These results suggest that reducing Dkk1 expression constitutes an interesting strategy to attenuate brain damage after hemorrhagic stroke (Wang G. et al., 2019). Norrin is a secreted protein that plays an important role in regulating angiogenesis via activation of the Fzd4, a receptor implicated in canonical Wnt pathway (Chen et al., 2015). Exogenous delivery of recombinant Norrin (rNorrin) into the ventricles of rats after SAH has been shown to provide neuroprotection by reducing brain edema and attenuating BBB permeability via activation of the canonical Wnt pathway, translated by an increased level of nuclear β-catenin (Chen et al., 2015). This was associated to an increased expression of tight junction proteins, namely occludin, ZO1, and VE-cadherin (Chen et al., 2015). Interestingly, Fzd4 siRNA prophylactic treatment attenuated the beneficial effects of rNorrin (Chen et al., 2015). The α7 nicotinic acetylcholine receptor (α7nAChR) has been shown to activate the phosphatidylinositol 3-kinase (PI3K)/Akt signaling pathway, which mediates GSK3β inhibition and thus β-catenin stabilization (Moccia et al., 2004). Importantly, functional α7nAChR was detected in the cerebral microvasculature (Moccia et al., 2004), and its activation attenuated BBB disruption after hemorrhagic stroke (Krafft et al., 2013). Indeed, PHA-543613, an agonist of α7nAChR, decreased GSK3β expression and subsequently stabilized β-catenin, reducing the peri-hematomal brain edema and improving the BBB functional integrity by increasing the expression of claudin-3 and claudin-5 (Krafft et al., 2013). On the other hand, administration of the GSK3β inhibitors, lithium and TWS119, attenuated the sensorimotor deficits and reduced brain edema by increasing β-catenin nuclear expression, which upregulated claudin-1 and claudin-3 expression, consequently improving BBB integrity after ICH (Li et al., 2018). Moreover, lithium reduced the number of

OX6-positive cells microglia in the peri-hematomal zone as well as decreased the expression of the pro-inflammatory mediator COX2 during the early brain injury phase (Kang et al., 2012). M1-type microglia promote the inflammatory response by releasing pro-inflammatory mediators, such as TNFα, IL1β, and IL6, exacerbating tissue damage (Ueba et al., 2018), whereas M2-type microglia exert protective effects by promoting the release of anti-inflammatory mediators and trophic factors, and contribute to tissue repair (Yang et al., 2018). Increasing the brain levels of Wnt1 via the delivery of rhWnt1 alleviated early brain injury associated to SAH in rats, which was accompanied by increased expression of β-catenin (Wang Y. et al., 2019). Activation of the canonical Wnt pathway via rhWnt1 delivery stimulated microglia cell polarization toward a M2-type reparative phenotype during the early brain injury phase by increasing the expression of CD36, CD206 and peroxisome proliferator-activated receptor-γ (PPARγ), and decreasing the protein levels of NF-κB (Wang Y. et al., 2019). Delivery of rhWnt1 reduced as well the release of pro-inflammatory cytokines such as IL1β, IL6, and TNFα (Wang Y. et al., 2019). In contrast, administration Wnt1 siRNA or neutralizing monoclonal antibody anti-Fzd1 resulted in opposite effects (Wang Y. et al., 2019). The intranasal injection of Wnt3a in rats after SAH activated the canonical Wnt pathway translated by the increased expression of β-catenin, Fzd1, aldolase C, PPAN, and the decreased expression of Axin (Ruan et al., 2020). Wnt3a in delivery into the brain via the intranasal route mediated anti-apoptotic effects during the early brain injury phase by increasing BCL2/BAX ratio and decreasing cleaved caspase-3 expression (Ruan et al., 2020). The anti-apoptotic effects of Wnt3a were further evidenced by the reduced density of terminal deoxynucleotidyl transferase dUTP nick end labeling $(TUNEL)^+$ neurons (Ruan et al., 2020). The administration of Fzd1 or aldolase C siRNA counteracted the beneficial effects of Wnt3a intranasal delivery (Ruan et al., 2020). These results indicate that Wnt3a exerted its neuroprotective effects by alleviating neuronal apoptosis at the cellular and subcellular levels through canonical Wnt pathway activation (Ruan et al., 2020). Interestingly, it has been reported that the number of apoptotic cells positively correlated with Wnt3a and β-catenin mRNA expression, whereas the proliferating cell nuclear antigen $(PCNA)^+$ cells negatively correlated with Wnt3a and β-catenin mRNAs during the early brain injury phase and the second phase of hemorrhagic stroke (Zhou L. et al., 2014). Collectively these findings suggest that the canonical Wnt pathway regulate the subtle balance between cell apoptosis and survival within the damaged region after hemorrhagic stroke (Zhou L. et al., 2014).

Using the potent cell-penetrating peptide D-JNKI-1, which selectively blocks JNK and c-Jun interaction, it has been shown that deactivation of the JNK/c-Jun pathway significantly decreased the lesion volume, hemispheric swelling and improved the neurological functions after ICH, correlating with an increased expression of aquaporin-4 (AQP4) in astrocyte endfeet (Michel-Monigadon et al., 2010). Iron contributes to ICH-induced brain injury (Xi et al., 2006), as free iron facilitates free radical formation and oxidative brain damage via activation of the JNK/c-Jun pathway (Wan et al., 2009). Administration of deferoxamine (DFX), an iron chelator, decreased the level of p-JNK in the basal ganglia of rats after SAH during the early brain injury phase, reduced free iron contents in the cerebral spinal fluid (CSF), and improved neurological recovery (Wan et al., 2009). In addition, administration of SP600125, a JNK inhibitor, in rats after SAH increased the density of $NeuN^+$ cells within the periphery of the hematoma, without affecting the hematoma size and brain water content (Ohnishi et al., 2007). Interestingly, attenuation of JNK activation via SP600125 administration increased microglial cell death (Ohnishi et al., 2007), and reduced the pro-inflammatory response following SAH notably by decreasing the levels of IL6 in the CSF during the early brain injury phase as well as the second phase of hemorrhagic stroke in dogs (Yatsushige et al., 2005). In another study, JNK inhibition using SP600125 has been shown to reduce the levels of JNK and c-Jun phosphorylation, correlating with an attenuation of the angiographic and morphological vasospasm of the basilar artery in the brain of dogs after SAH (Yatsushige et al., 2005, 2008). Furthermore, SP600125 administration significantly attenuated the infiltration of leukocytes, namely T cells, neutrophils, and macrophages, associated to a reduced apoptosis (Yatsushige et al., 2005, 2008). The exogenous intranasal injection of recombinant Dkk3 (rDkk3), also called SRP6268, decreased JNK phosphorylation and AP1 expression, reduced the brain water content during the early brain injury phase, and improved long-term neurological functions after ICH (Xu et al., 2020). In addition, rDkk3 exerted anti-inflammatory effects within the peri-hematomal zone after ICH induction translated by a reduced expression of TNFα and IL1β (Xu et al., 2020). Interestingly, these beneficial effects were abolished following the injection of Kremen1 or Dvl1 siRNAs (Xu et al., 2020). The early administration of JNK1 siRNA improved the neurological recovery and survival rate after SAH, indicating that interruption of the early brain injury process support neuronal survival in the subsequent phases of SAH (Ling et al., 2019). Indeed, JNK1 siRNA attenuated neuronal apoptosis by decreasing p53 phosphorylation as well as mitochondrial apoptotic pathways via the downregulation of BAX, upregulation of BCL2, and downregulation of cleaved-caspase-3, thus preserving neurons from undergoing apoptosis after SAH (Ling et al., 2019). These findings suggest that deactivation of the non-canonical Wnt pathway provides protection in the context of hemorrhagic stroke. Indeed, it has been shown that the RHOA/ROCK pathway was also activated after hemorrhagic stroke. Recent clinical studies have reported a slight improvement in the clinical outcomes of patients treated with the ROCK inhibitor fasudil 24 h following hemorrhagic stroke onset (Zhao et al., 2011, 2006). In experimental studies, administration of fasudil or ROCK2 specific inhibitor KD025, did not affect the neurological outcome or the size of hematoma after ICH (Akhter et al., 2018). It is noteworthy to mention that KD025 was less potent than fasudil in stopping intracerebral bleeding, whereas it was more potent in reducing the hematoma size (Akhter et al., 2018). In another study, fasudil alone did not inhibit the RHOA activity, whereas pitavastatin attenuated RHOA activation in VSMCs following SAH (Naraoka et al., 2013). The combination of fasudil and pitavastatin strongly reduced RHOA activity in VSMCs, and improved the cross-sectional area of basilar artery after SAH

(Naraoka et al., 2013). Statins have already been shown to prevent vasospasm via induction of eNOS (Sabri et al., 2011). Pitavastatin alone or in combination with fasudil significantly increased eNOS release, thus preventing cerebral vasospasm, an effect that was absent in animals treated only with fasudil (Wright et al., 1990). The administration of Y-27632, a ROCK inhibitor, attenuated brain injury and ameliorated neurological functions in the early brain injury phase after ICH, which was accompanied with an increased expression of the adherens junction proteins (Huang et al., 2012). However, another report showed that Y-27632 reduced brain edema after SAH without affecting neurological outcomes (Fujii et al., 2012). In this study, the authors have compared the effects of Y-27632 with hydrofasudil, and proposed that hydrofasudil is more potent than Y-27632 in SAH, as it improved neurological recovery (Fujii et al., 2012). Furthermore, hydrofasudil inhibited ROCK activity, which correlated with a reduced BBB permeability associated to an increased expression of occludin and ZO1 (Fujii et al., 2012). Implication of RHOA activation in destabilizing endothelial cell junctions and altering BBB integrity following ICH model was validated using the RHOA inhibitor, transferase C3 (Zhao H. et al., 2016). The intraperitoneal injection of transferase C3 reduced BBB permeability by increasing the expression of occludin, ZO1, and VE-cadherin, and improved the neurological functions in rats after ICH (Zhao H. et al., 2016). The P2X7 receptor, which is known for its cytotoxic activity (Volonté et al., 2012), was activated very early within the peri-hematomal zone after ICH (Zhao H. et al., 2016). Exogenous intraperitoneal delivery of A-438079, a competitive antagonist of P2X7, significantly decreased RHOA activation, and alleviated the neurological deficits after ICH (Zhao H. et al., 2016). In addition, P2X7 receptor was detected in endothelial cells and astrocytes, and its deactivation using A-438079 significantly improved BBB integrity by increasing the expression of occludin, ZO1, and VE-cadherin (Zhao H. et al., 2016). Administration of P2X7 siRNA in mice replicated the effects of A-438079, validating the implication of P2X7 (Zhao H. et al., 2016). Interestingly, these beneficial effects were strongly attenuated when A-438079 was administered in combination with BzATP, an agonist of P2X7 receptor (Zhao H. et al., 2016). Another study reported that P2X7 receptor is expressed as well in neurons after ICH (Wen et al., 2017). The administration of BBG, a P2X7 antagonist, reduced the expression of phosphorylated p38, extracellular signal-regulated kinases (ERKs), and NF-κB; however, expression and phosphorylation of JNK and c-Jun remained unchanged (Wen et al., 2017), suggesting that P2X7 receptor activation modulated essentially RHOA activity. The administration of BBG decreased brain edema as well as the number of Fluoro-Jade (FJB)$^{+}$ cells, and reduced the level of cleaved-caspase-3 (Wen et al., 2017).

The recent findings are suggesting that CaMKII activity, another main component of the non-canonical pathway, might be implicated in artery contraction or vasospasm (House et al., 2008), associated to poor prognosis after hemorrhagic stroke. Indeed, CaMKII expression was reported to increase in the arteries after SAH (Edvinsson et al., 2014). The administration of KN93 attenuated the SAH-induced contractions mediated by endothelin-1 (ET1) and 5-hydroxytryptamine (5-HT), a contractile protein implicated in basilar and MCA arteries, and ameliorated the sensorimotor function of rodents after SAH (Edvinsson et al., 2014). Another report has demonstrated that CaMKII phosphorylation is highly expressed in neurons and microglia in the brain of rodents after SAH (Zhou et al., 2018). The intraperitoneal injection of dihydrolipoic acid (DHLA), an active form of the lipoic acid (LA), reduced CaMKII and JNK activities, and improved the short- and long-term neurological recovery after SAH (Zhou et al., 2018). DHLA administration promoted as well the protective anti-inflammatory phenotype of microglia (Zhou et al., 2018) (**Supplementary Table 2**).

THE Wnt PATHWAY IN TBI

TBI is defined as a brain damage resulting from an external mechanical force, leading to temporary or permanent impairment in cognitive, physical, and psychosocial functions (Lambert et al., 2016). TBI constitutes the main cause of death and disability in the young adults, and contributes to the increasing costs of health care due to its high incidence rate and often long-term sequelae (Hyder et al., 2007; Najem et al., 2018). However, there is still no effective therapy available, in part due to the poor understanding for the pathobiology of this neurological condition (Hyder et al., 2007). TBI is characterized by a complex pathogenesis comprising primary and secondary injury mechanisms (Galgano et al., 2017). The primary injury is the result of the immediate mechanical disruption of the brain tissue that occurs at the time of exposure to the external force and includes contusion, damage to blood vessels, and axonal disorganization (Galgano et al., 2017). The secondary injury evolves over minutes to months after the primary injury, and is the result of cascades of metabolic, molecular and cellular events that ultimately lead to cell death, tissue damage, and brain atrophy (Xiong et al., 2013; Galgano et al., 2017), as well as altered cognitive functions (Lambert et al., 2016). Activation of astrocytes and microglia constitutes an important pathophysiological process after TBI. Indeed, astrocytes are recruited to the lesion site and are quickly activated in response to injury after TBI (Karve et al., 2016). Activated astrocytes have been shown to play an important role in neuroprotection by releasing various trophic factors after TBI (Karve et al., 2016). Autophagy is activated under stress conditions to maintain cell survival by allowing the recycling of macromolecules and metabolites for new protein synthesis modulating (Zhang and Wang, 2018). Autophagy has been shown to be dysfunctional in TBI. Indeed, inhibition of autophagy following TBI reduced cell loss and lesion volume, as well as ameliorated neurological functions (Lipinski et al., 2015; Zhang and Wang, 2018). Importantly, β-catenin negatively regulates autophagy via direct inhibition of autophagosome formation (Zhang et al., 2018). LC3, a key autophagosomal component that is usually upregulated during autophagy, has been shown to form a complex with β-catenin for autolysosomal degradation (Zhang et al., 2018). Moreover, TBI constitutes a major risk factor for AD. Indeed, amyloid-β (Aβ) deposition, which is one of the pathological hallmarks of AD significantly increases following TBI in animal models as well as in humans (Yu et al., 2012b). During the last decade, the overwhelming emerging findings are suggesting that

the Wnt pathway play important roles in TBI pathobiology, thereby constituting a novel target for the development of novel therapeutic interventions.

Implication in TBI Pathobiology

Investigations into the implication of the Wnt pathway in humans with TBI conditions have recently started. In a recent study, it was reported that the levels of Dkk1 were elevated in the serum of patients with severe TBI (Ke et al., 2020). Importantly, Dkk1 elevated levels in the serum were closely associated with increasing severity of the trauma and higher risk of short-term mortality (Ke et al., 2020). Furthermore another study has reported that RHOA was upregulated as early as 24 h after trauma, persisting for several months after TBI (Brabeck et al., 2004). In this study, RHOA was upregulated in various cell types including granulocytes, monocytes, macrophages, as well as reactive astrocytes, and to a lesser extent in neurons (Brabeck et al., 2004).

In the recent years, we began to get better insights into the involvement of Wnt pathway in TBI from experimental studies using different TBI animal models. Most of these studies emphasized on the role of β-catenin, the main effector of the canonical Wnt pathway. Indeed, it has been shown that β-catenin expression was increased in the peri-lesional microvasculature of mice at 1 and 7 days post-TBI, whereas it was reduced in injury site 7 days post-TBI (Salehi et al., 2018). A similar expression pattern was reported in a transgenic mouse line reporter for the canonical Wnt pathway activity, TCF:LEF1:H2B-GFP mice (Salehi et al., 2018). Indeed, β-catenin expression increased 24 h after TBI, and was associated to an enhanced angiogenesis within the peri-lesional zone (Salehi et al., 2018). Importantly, the density and complexity of the microvasculature increased at day 7 after TBI (Jullienne et al., 2018). The mRNA levels of β-catenin and Wnt3a significantly increased following TBI, peaking at day 3 post-TBI for β-catenin and at day 7 for Wnt3a (Wei et al., 2020). Furthermore, several findings have demonstrated that Akt/GSK3β pathway regulates as well β-catenin expression (Zhao et al., 2012). Phosphorylated Akt (p-Akt, i.e., activated) deactivates the kinase activity of GSK3β kinase activity via phosphorylation on serine (Zhao et al., 2012). In the injured cortex of rats, p-Akt increased 4 h after impact, decreasing 72 h later, and was accompanied by increased levels of p-serine-GSK3β 4 h after impact, peaking 72 h later after TBI (Zhao et al., 2012). P-Akt-mediated GSK3β kinase inhibition promoted β-catenin stabilization and accumulation as early as 4 h after the impact and remained constant for 7 days (Zhao et al., 2012). Similar findings were reported in another independent study, which showed in addition that TBI induced a rapid transient increase in LRP6 phosphorylation followed by a slight decrease in β-catenin phosphorylation mediated by GSK3β (Dash et al., 2011). Evidence is suggesting that activated astrocytes limit damage expansion, stimulate tissue repair, and promote synaptic remodeling after TBI (Burda et al., 2016). Using a transgenic mouse line reporter for β-catenin transcriptional activity, BATGAL mice, it has been demonstrated that β-catenin signaling was associated to an enhanced proliferation of neural/glial antigen-2 $(NG2)^+$ progenitors and reactive astrocytes after TBI (White et al., 2010). Moreover, the expression of DIX domain-containing protein-1 (DIXDC1), a positive regulator of the canonical Wnt pathway that activates Wnt3a signaling through Dvl2, was up-regulated in neurons and astrocytes following TBI, and was implicated in reactive astrocyte proliferation (Lu et al., 2017). Interestingly, expression of the C-terminal-binding protein-2 (CtBP2), a protein involved in the transcriptional regulation of Wnts, was induced at the peri-lesional zone after TBI (Zou et al., 2013). CtBP2 was highly expressed in proliferating astrocytes, and was associated to an increased expression of BCL2 (Zou et al., 2013). TBI stressors have been shown to trigger the intracellular accumulation of Ca^{2+} and cyclic adenosine monophosphate (cAMP), activating PKC, CaMKII and protein kinase-A (PKA), which in turn phosphorylate the cAMP response element binding factor (CREB) and serum response factor (SRF), subsequently increasing c-Jun transcriptional activity and cell death (Sheng and Greenberg, 1990; Morgan and Curran, 1991; Raghupathi et al., 2000; Raghupathi, 2004). Interestingly, an increased mRNA expression of c-Jun was observed 5 min after TBI and was maximal 30 min later, persisting for 6 h post-TBI (Raghupathi et al., 1995). Modulation of other components of the non-canonical Wnt pathway was reported after TBI. For instance, CAMKIIδ expression increased within the areas surrounding the impact core, peaking 3 days later and then returned to normal levels (Pan et al., 2014). CAMKIIα plays a key role in regulating the formation of hippocampal-dependent memory, and its activity was reported to increase in the CA1, CA3 and DG regions as early as 30 min after trauma (Atkins et al., 2006; Folkerts et al., 2007). Importantly, CAMKIIα increased activity was accompanied by the phosphorylation and activation of the AMPA-type glutamate receptor (GluR1), and the cytoplasmic polyadenylation element-binding protein (CPEB) in the hippocampus and cortex 1 h after TBI (Atkins et al., 2006). These findings suggest that the biochemical cascades implicated in memory formation are activated in non-selective manner in neurons after TBI (Atkins et al., 2006). However, a proper memory formation requires activation of the CAMKIIα signaling in specific neuronal synapses, and the non-selective activation of this signaling in all synapses may disrupt memory formation, which may account for the memory loss after TBI (Atkins et al., 2006). The recent findings have demonstrated that the RHOA/ROCK pathway is regulated after TBI. RHOA activation was observed from 24 h until 3 days after impact in the cortex, and at 3 days in the hippocampus of the brain of a rat following TBI (Dubreuil et al., 2006). In CamKIIα-Cre;$RHOA^{fl/fl}$ mice, RHOA cKO mice, in which RHOA was specifically depleted in postnatal neurons, motor and cognitive functions were persevered 14 days after TBI without substantially influencing the lesion volume (Mulherkar et al., 2017). These studies highlight an important role of the Wnt pathway in TBI pathobiology, but more research is still needed to fill-in the exiting gaps in the literature (**Figure 3**).

Implication in TBI Therapy

Similar to ischemic stroke, in response to TBI, the brain tries to repair itself by regulating neurogenesis, angiogenesis, and inflammation (Xiong et al., 2010; Russo and McGavern, 2016).

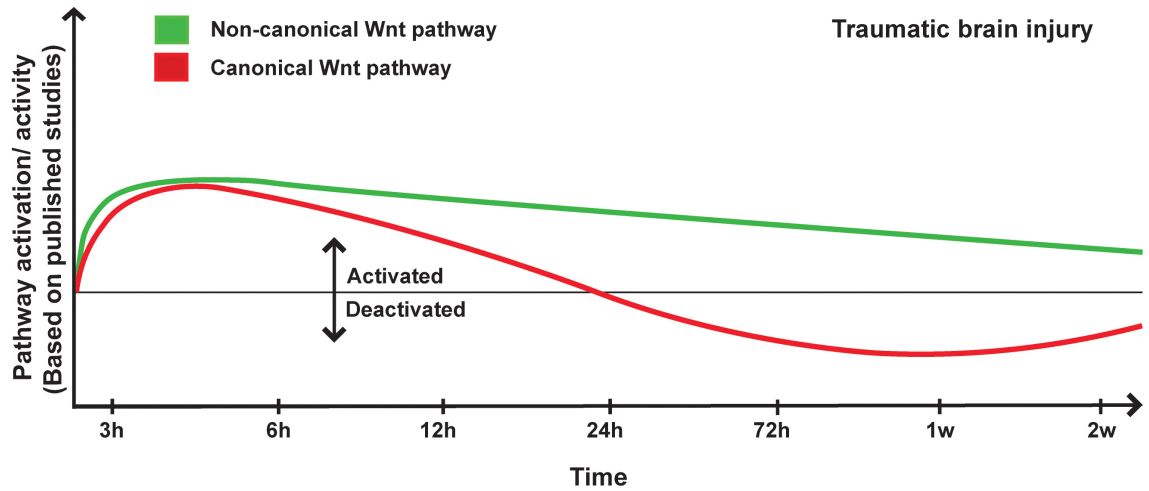

FIGURE 3 | Proposed scheme for Wnt pathway temporal in traumatic brain injury. A representation of canonical and non-canonical Wnt pathways temporal regulation following traumatic brain injury (TBI) onset based on pathway activation (i.e., modulation of pathway's key components) and activity (i.e., regulation of specific target genes), as reported in the different published studies.

After TBI, neurogenesis is stimulated in the SGZ of the DG of the hippocampus and in the SVZ to replace the cells lost by apoptosis or necrosis caused by the impact (Dash et al., 2001; Rice et al., 2003; Sun et al., 2005). Indeed, TBI has been shown to promote the migration of progenitors from the SVZ to the injured site (Ramaswamy et al., 2005). In a rat model of TBI, cell proliferation was reported in the SVZ, corpus callosum, around the cortex and sub-cortical areas connected to the injured site but not inside the lesion site (Kernie et al., 2001). These newborn cells originating from the SVZ were shown to differentiate into neurons or glial cells (Kernie et al., 2001). Cognitive recovery has been observed 2 weeks after TBI, strongly correlating with the integration of newborn cells into the pre-existing network (Emery et al., 2005; Urrea et al., 2007). TBI occasions a serious damage to the microvasculature, which has been shown to occur in both hemispheres (Obenaus et al., 2017). Cerebral hypoperfusion, hypoxia, ischemia, BBB disruption, hemorrhage, and edema formation constitute the main consequences of microvascular dysfunction associated to TBI (Salehi et al., 2017). Interestingly, the endogenous microvascular repair processes were shown to occur in a time course of 2 to 3 weeks starting 2 days post-trauma (Morgan et al., 2007; Beck and Plate, 2009). Importantly, the newly formed capillaries seem to originate from the peri-lesional tissue to penetrate inside the lesion core (Sköld et al., 2005; Park et al., 2009; Hayward et al., 2011). An increased frequency of endothelial progenitor cells (EPCs) has been reported in the blood circulation following TBI, as well as in the microvasculature located inside the lesion site, outlining an active angiogenic response (Guo et al., 2009; Gong et al., 2011; Liu L. et al., 2011). TBI also triggers a strong inflammation response that has been shown, if remained uncontrolled to underlie the chronic neurodegeneration associated to TBI (Johnson et al., 2013; Smith et al., 2013; Faden and Loane, 2015). The resident and peripheral immune cells quickly respond to brain injury and participate to the repair process as well after TBI (Das et al., 2012; Finnie, 2013). Microglia and astrocytes are among the first cells to respond and actively contribute in supporting the survival of stressed neurons, removing of cell debris, releasing trophic mediators, and participating in astroglial scar formation (Corps et al., 2015; Zhou et al., 2020). As Wnt pathway activation after TBI actively contribute in regulating neurogenesis, angiogenesis, and inflammation, research in the field is attempting to anticipate in targeting the pathway in order to promote structural and functional repair after trauma (Marchetti and Pluchino, 2013; Wu et al., 2013; Zhang et al., 2013).

Similar to ischemic and hemorrhagic stroke, several studies were interested in assessing the effects of Wnt ligands in developing TBI therapies, with an emphasis on Wnt3a. When delivered intranasally after TBI, Wnt3a rescued motor function and enhanced the number of $NeuN^+$ cells without affecting the reactivity of astrocytes (Zhang et al., 2018; Chang et al., 2020). Wnt3a exogenous administration efficaciously activated the canonical Wnt pathway by increasing β-catenin nuclear levels, promoted neurogenesis and reduced lesion volume (Zhang et al., 2018; Chang et al., 2020). Similar results were obtained with the intravenous injection of recombinant Wnt3a as well as the intravenous injection of mesenchymal stem cells (MSCs), which enhanced hippocampal neurogenesis by stimulating Wnt3a release after TBI (Zhao Y. et al., 2016). The administration of simvastatin for 2 weeks following TBI increased the expression of p-PKB, CREB, BDNF, and VEGF in the DG (Wu et al., 2008). The increased expression of these factors positively correlated with NPCs proliferation and differentiation into mature neurons in the DG, significantly attenuating spatial learning deficits (Wu et al., 2008). These effects were mediated by canonical Wnt pathway activation associated to the inhibitory effects of simvastatin on GSK3β activity (Wu et al., 2008). Furthermore, simvastatin therapy for 14 days after TBI reduced axonal injury, enhanced neurite outgrowth, and ameliorated neurological recovery (Wu H. et al., 2012).

Interestingly, membrane depolarization plays a decisive role in mediating the survival and maturation of newborn neurons in the DG (Zhao et al., 2018). Optogenetic tools were applied to stimulate the membrane depolarization of Dcx^+ cells via the injection of LV-Dcx-channelrhodopsin-2 (ChR2)-EGFP gene into the brain of TBI mice (Zhao et al., 2018). Optical depolarization of Dcx-$EGFP^+$ cells between 3 and 12 days after TBI attenuated cognitive deficits, accompanied by an enhanced survival and maturation of the newly generated cells in the DG (Zhao et al., 2018). Importantly, these effects were abolished upon Dkk1 administration, confirming that the survival and maturation or newborn neurons were essentially mediated via canonical Wnt pathway activation (Zhao et al., 2018). The intranasal administration of Wnt3a has been shown as well to increase GDNF and VEGF expression, subsequently enhancing angiogenesis after TBI (Zhang et al., 2018). Furthermore, the intranasal administration of Wnt3a reduced cell death and improved functional recovery after TBI (Zhang et al., 2018). Additionally, lithium application for 5 days after TBI improved learning and memory capabilities of animals, associated to a reduced neuronal loss in the CA3 region of the hippocampus (Dash et al., 2011).

Activation of the canonical Wnt pathway via the pharmacological inhibition of GSK3β to stabilize β-catenin after TBI efficaciously reduced cell death, improved locomotor coordination, attenuated depression and anxiety behaviors, and ameliorated overall cognitive functions (Yu et al., 2012a; Shim and Stutzmann, 2016). Indeed, lithium administration has been reported to attenuate BBB disruption following TBI (Yu et al., 2012a). Administration of lithium 15 min after cortical contusion injury (CCI) followed by daily administration for 3 to 6 h or 2 weeks after CCI or once daily for 3 days reduced the inflammatory responses translated by attenuated activation of microglial cells and MMP9 expression (Yu et al., 2012a). This was associated to a reduced lesion size and improved of cognitive functions (Yu et al., 2012a). The authors proposed that injection of lithium within 3 h after TBI provide the best neuroprotective and anti-inflammatory effects (Yu et al., 2012a). Furthermore, a single acute injection of valproic acid (VPA), a potent GSK3β inhibitor, strongly reduced BBB breakdown and diminished the lesion volume after CCI. When injected 5 days after TBI, VPA improved motor function, spatial learning and memory (Dash et al., 2010). Interestingly, the beneficial effects of VPA were time and dose dependent, outlining its potency in activating the canonical Wnt pathway (Dash et al., 2010). As such, the authors suggested that an optimal beneficial effect on structural and functional recovery could be achieved with a first acute injection applied 30 min after TBI followed by daily administration of VPA for at least 5 days (Dash et al., 2010). Since lithium and VPA exhibited beneficial effects in TBI, a co-treatment with sub-effective doses was evaluated. The co-treatment reduced brain lesion, BBB disruption and drastically improved long-term functional recovery (Yu et al., 2013). The authors suggested that a regimen that comprises sub-effective doses might reduce side effects and increase the tolerance (Yu et al., 2013). The prolonged application of VPA after TBI for 3 weeks reduced dendritic loss in the hippocampus (Dash et al., 2010). Similar to lithium, simvastatin and VPA, resveratrol, which is an antioxidant, has been shown to possess inhibitory effects against GSK3β (Lin et al., 2014). Resveratrol mitigated cell death in an *in vitro* model of TBI by suppressing essentially GSK3β-mediated reactive oxygen species (ROS) generation (Lin et al., 2014). Moreover, the co-treatment of lithium and VPA attenuated neurodegeneration after TBI (Yu et al., 2013). Although more investigations are required, the accumulating findings are indicating that GSK3β inhibitors constitute indeed promising candidates for TBI treatment. TBI is a condition that substantially increases the risk of developing dementia-like pathologies, such as AD. For instance, lithium administration 15 min then once daily for up to 3 weeks after TBI attenuated Aβ accumulation, increased beta-site amyloid precursor protein (APP)-cleaving enzyme-1 (BACE1) expression in the hippocampus and the corpus callosum, accompanied by reduced hyper-phosphorylation of tau in the thalamus (Yu et al., 2012b). Application of lithium for 20 days ameliorated short-term memory and learning (Yu et al., 2012b).

Various non-chemical treatments have also been tested to further activate the Wnt pathway after TBI for therapeutic purposes. For instance, acupuncture in rats with TBI induced the mRNA and protein expression of Wnt3a, β-catenin and sex determining region Y-box 2 (SOX2), a transcription factor implicated in the maintenance of NSCs (Zhang et al., 2016). Indeed, this was associated to enhanced proliferation and differentiation of NPCs (Zhang et al., 2016). Interestingly, it has been shown that hyperbaric therapy could restore oxygen supply after TBI, thereby increasing the expression of various antioxidant genes that alleviate inflammation and apoptosis, while promoting neurogenesis, and angiogenesis (Thom, 2009; Godman et al., 2010; Liu W. et al., 2011). Mice in which TBI was induced were placed in a hyperbaric chamber for 90 min. This regimen reduced the number of apoptotic neurons, as well as the mRNA expression of caspase-3 and the level of cleaved-caspase-3 (He et al., 2019). These effects were associated to an increased expression of β-catenin and decreased expression of GSK3β (He et al., 2019).

The non-canonical pathway has also been shown to constitute an interesting therapeutic target for TBI. Fasudil, a RHOA/ROCK inhibitor, as well as RHA depletion prevented TBI-induced spine remodeling and mature spine loss in hippocampal pyramidal neurons, thus improving neurological recovery (Mulherkar et al., 2017). Moreover, docosahexaenoic acid (DHA), which has been shown to inhibit JNK, rescued TBI-mediated hippocampal long-term potentiation (LTP) and improved hippocampus-dependent learning and memory as well as enhanced motor function (Zhu W. et al., 2019). These results are in line with previous studies demonstrating that neuronal dysfunction was alleviated by DHA (Zhu et al., 2017, 2018). A natural supplementation of blueberry for 2 weeks showed mitigated loss of spatial learning and memory performances and improved anxiety (Krishna et al., 2019), associated to increased expression of BDNF, which plays crucial role in neural maturation, and activated CAMKII (Krishna et al., 2019). It is noteworthy to mention that hemorrhage often occurs after TBI due to BBB breakdown. Basic fibroblast growth factor (bFGF)

administration reduced RHOA activity and increased the expression of tight junction proteins, thus preserving BBB integrity after injury (Wang Z.-G. et al., 2016). bFGF increased the expression of claudin-5, occludin, ZO1, and β-catenin in human brain microvascular endothelial cells (HBMECs) exposed to oxygen glucose deprivation (OGD)/re-oxygenation to mimic

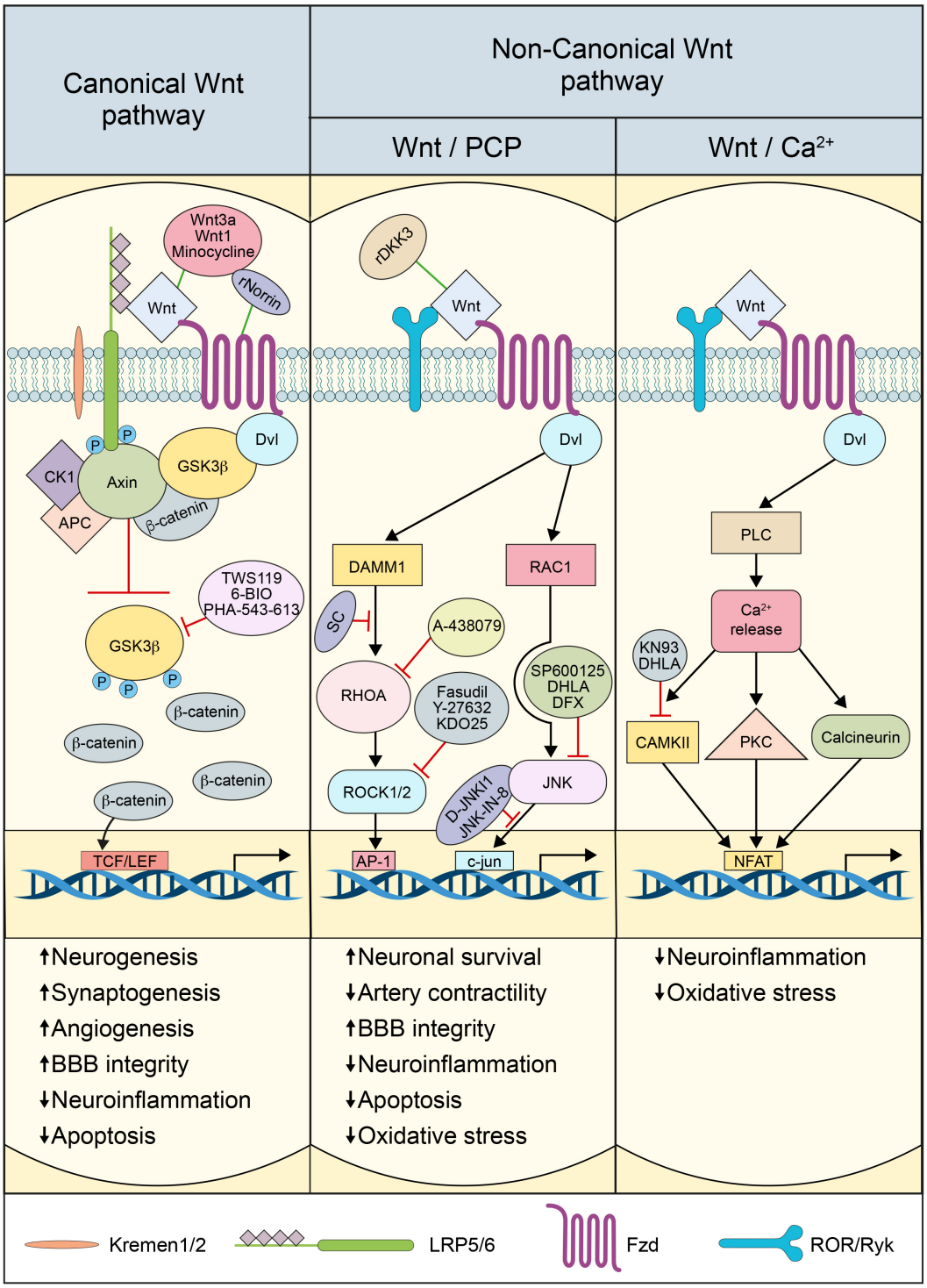

FIGURE 4 | Scheme depicting Wnt pathway modulation for therapeutic purposes: An illustration summarizing the key approaches applied in the literature to modulate canonical and non-canonical Wnt pathways activation and activity, as a strategy to attenuate brain injury, and to ameliorate the post-injury reparative and restorative process.

TBI conditions (Wang Z.-G. et al., 2016). Inhibition of PI3K/Akt pathway or RAC1, using LY-294002 or RAC1 siRNA respectively, abolished the protective effects of bFGF on BBB integrity (Wang Z.-G. et al., 2016). The administration of saikosaponins, which are triterpene saponins isolated from *Bupleurum*, decreased the expression AQP4 expression that is implicated in swelling, MMP9, mitogen-activated protein kinase (MAPK), JNK, TNFα, and IL6 (Mao et al., 2016). Saikosaponins reduced brain edema, BBB breakdown, and inflammation, as well as ameliorated neurological recovery (Mao et al., 2016). Administration of the JNK inhibitor, SP600125, for 7 days after TBI in mice decreased the expression of NF-kB, which in turn reduced caspase3 expression in neurons (Rehman et al., 2018; Bhowmick et al., 2019). On the other hand, ROCK inhibition after TBI in mice promoted acute neuroprotection and functional recovery with only modest impact on neurogenesis, astrocytic reactivity and macrophage/microglial activation (Bye et al., 2016). TBI triggers a cascade of events that increase the concentration of intracellular Ca^{2+}, which is further exacerbated by the increased expression of Wnt5a and Fzd2, a major component of the non-canonical Wnt pathway (Niu et al., 2012). Inhibition of Wnt5a/Fzd2 interaction using Box5, a Wnt5a-derived hexapeptide that antagonizes Wnt5a-mediated cellular activities or Wnt5a siRNA, could constitute a potential therapy to alleviate Ca^{2+} increase and protect neurons (Niu et al., 2012). As mentioned earlier, TBI constitutes a high-risk factor for developing dementia. DHA administration deceased JNK expression, subsequently reducing TBI-mediated tau phosphorylation (Zhu W. et al., 2019). Collectively, these studies suggest that Wnt pathway constitute an important target for the development of efficacious protective and restorative therapies for TBI (**Supplementary Table 3**).

CONCLUSION

The mechanisms underlying brain injury in ischemic and hemorrhagic stroke as well as TBI are very complex and multiphasic, thus constituting a major challenge in the development of efficacious therapeutic interventions. Despite efforts, still no disease-modifying therapy exit for these neurological conditions. This void is frustrating as the emerging findings are indicating that the injured brain tissue is not just passively dying over time, but it is actively trying to recover. Indeed, various developmental and ontogenic processes have been shown to re-emerge upon injury, such as neurogenesis, neural plasticity, angiogenesis, gliosis, and others (Lo, 2008; Hermann and ElAli, 2012; Addington et al., 2015). These processes clearly translate an attempt from the brain to self-repair and regenerate, thus providing a new framework for the development of novel therapeutic interventions. Yet the major challenge remains in identifying a "drugable" target that could be modulated to fine-tune the injury-induced developmental and ontogenic processes. The Wnt pathway regulates crucial biological aspects throughout lifespan. It is critically implicated in regulating the intimate emergence and patterning of the nervous and vascular systems (Hermann and ElAli, 2012; Noelanders and Vleminckx, 2017). The experimental findings are convincingly indicating that the canonical Wnt pathway is of particular interest (**Figure 4**). Indeed, genetic alteration of the pathway drastically impact injury progression, repair and regeneration. Furthermore, pathway activation seems to potently stimulate injured tissue protection and restoration as well as ameliorating already FDA approved therapies, such as thrombolysis via rtPA for ischemic stroke (Jean LeBlanc et al., 2019). Data from patients are indicating that some component of the pathway could be even used as biomarkers or prognostic tools, such as Dkk1 (Seifert-Held et al., 2011; Zhu Z. et al., 2019). The canonical Wnt pathway is an attractive target from pharmacological point of view, as several modulators have been developed in the past decades for other medical conditions, namely neurodegenerative disorders and cancer. The accumulating evidence is suggesting that in order to achieve maximal effects, the implication of some endogenous inhibitors such as Scl and Dkk1 should be taken into consideration. Indeed, the elevated endogenous expression Dkk1 within the injured tissue was sufficient to abolish the biological activity of potent ligands such as Wnt3a (Wei et al., 2018). Dkk1 expression is regulated in an age- and biological sex-dependent manner, thus offering new directions in developing tailored Wnt-dependent therapeutic interventions (Zhang et al., 2008; Seib et al., 2013). On the other hand, the complexity of non-canonical Wnt pathway's intracellular signaling makes it difficult to fully appreciate its exact role as several components of the pathway are shared with Wnt-independent pathways. However, the non-canonical Wnt pathway seems to counteract several of the biological effects of the canonical pathway. Nonetheless, ROCK seems to constitute a very promising target for the therapeutic purposes. It is clear that more research is still needed to fully elucidate with some specificity the implication of the non-canonical Wnt pathway in brain injury and repair.

AUTHOR CONTRIBUTIONS

RM contributed to the writing and figure preparation. SL contributed to the writing. AE contributed to the writing, editing, and finalization of the manuscript. All authors contributed to the article and approved the submitted version.

FUNDING

This work was supported by grants from the Natural Sciences and Engineering Research Council of Canada (NSERC) (Grant # RGPIN-2017-06119), the *Fonds de recherche du Québec - Santé* (*FRQS*), the Heart and Stroke Foundation of Canada (Grant # G-18-0022118), and the Canadian Institutes of Health Research (CIHR) (Grant # 426287) (all to AE).

SUPPLEMENTARY MATERIAL

The Supplementary Material for this article can be found online at: https://www.frontiersin.org/articles/10.3389/fphys.2020.565667/full#supplementary-material

REFERENCES

Abe, T., Zhou, P., Jackman, K., Capone, C., Casolla, B., Hochrainer, K., et al. (2013). Lipoprotein receptor-related protein-6 protects the brain from ischemic injury. *Stroke* 44, 2284–2291. doi: 10.1161/STROKEAHA.113.001320

Adachi, K., Mirzadeh, Z., Sakaguchi, M., Yamashita, T., Nikolcheva, T., Gotoh, Y., et al. (2007). Beta-catenin signaling promotes proliferation of progenitor cells in the adult mouse subventricular zone. *Stem Cells* 25, 2827–2836. doi: 10.1634/stemcells.2007-0177

Addington, C. P., Roussas, A., Dutta, D., and Stabenfeldt, S. E. (2015). Endogenous repair signaling after brain injury and complementary bioengineering approaches to enhance neural regeneration. *Biomark Insights* 10, 43–60. doi: 10.4137/BMI.S20062

Akhter, M., Qin, T., Fischer, P., Sadeghian, H., Kim, H. H., Whalen, M. J., et al. (2018). Rho-kinase inhibitors do not expand hematoma volume in acute experimental intracerebral hemorrhage. *Ann. Clin. Transl. Neurol.* 5, 769–776. doi: 10.1002/acn3.569

Aronowski, J., and Zhao, X. (2011). Molecular pathophysiology of cerebral hemorrhage: secondary brain injury. *Stroke* 42, 1781–1786. doi: 10.1161/STROKEAHA.110.596718

Ashpole, N. M., and Hudmon, A. (2011). Excitotoxic neuroprotection and vulnerability with CaMKII inhibition. *Mol. Cell. Neurosci.* 46, 720–730. doi: 10.1016/j.mcn.2011.02.003

Atkins, C. M., Chen, S., Alonso, O. F., Dietrich, W. D., and Hu, B.-R. (2006). Activation of calcium/calmodulin-dependent protein kinases after traumatic brain injury. *J. Cereb. Blood Flow Metab.* 26, 1507–1518. doi: 10.1038/sj.jcbfm.9600301

Beck, H., and Plate, K. H. (2009). Angiogenesis after cerebral ischemia. *Acta Neuropathol.* 117, 481–496. doi: 10.1007/s00401-009-0483-6

Benakis, C., Bonny, C., and Hirt, L. (2010). JNK inhibition and inflammation after cerebral ischemia. *Brain Behav. Immun.* 24, 800–811. doi: 10.1016/j.bbi.2009.11.001

Bhowmick, S., D'Mello, V., and Abdul-Muneer, P. M. (2019). Synergistic Inhibition of ERK1/2 and JNK, Not p38, phosphorylation ameliorates neuronal damages after traumatic brain injury. *Mol. Neurobiol.* 56, 1124–1136. doi: 10.1007/s12035-018-1132-7

Borsello, T., Clarke, P. G. H., Hirt, L., Vercelli, A., Repici, M., Schorderet, D. F., et al. (2003). A peptide inhibitor of c-Jun N-terminal kinase protects against excitotoxicity and cerebral ischemia. *Nat. Med.* 9, 1180–1186. doi: 10.1038/nm911

Bourhis, E., Tam, C., Franke, Y., Bazan, J. F., Ernst, J., Hwang, J., et al. (2010). Reconstitution of a frizzled8·Wnt3a·LRP6 signaling complex reveals multiple Wnt and Dkk1 binding sites on LRP6. *J. Biol. Chem.* 285, 9172–9179. doi: 10.1074/jbc.M109.092130

Brabeck, C., Beschorner, R., Conrad, S., Mittelbronn, M., Bekure, K., Meyermann, R., et al. (2004). Lesional expression of RhoA and RhoB following traumatic brain injury in humans. *J. Neurotrauma* 21, 697–706. doi: 10.1089/0897715041269597

Brecht, S., Kirchhof, R., Chromik, A., Willesen, M., Nicolaus, T., Raivich, G., et al. (2005). Specific pathophysiological functions of JNK isoforms in the brain. *Eur. J. Neurosci.* 21, 363–377. doi: 10.1111/j.1460-9568.2005.03857.x

Buga, A. M., Margaritescu, C., Scholz, C. J., Radu, E., Zelenak, C., and Popa-Wagner, A. (2014). Transcriptomics of post-stroke angiogenesis in the aged brain. *Front. Aging Neurosci.* 6:44. doi: 10.3389/fnagi.2014.00044

Burda, J. E., Bernstein, A. M., and Sofroniew, M. V. (2016). Astrocyte roles in traumatic brain injury. *Exp. Neurol.* 275(Pt 3), 305–315. doi: 10.1016/j.expneurol.2015.03.020

Bye, N., Christie, K. J., Turbic, A., Basrai, H. S., and Turnley, A. M. (2016). Rho kinase inhibition following traumatic brain injury in mice promotes functional improvement and acute neuron survival but has little effect on neurogenesis, glial responses or neuroinflammation. *Exp. Neurol.* 279, 86–95. doi: 10.1016/j.expneurol.2016.02.012

Cerpa, W., Godoy, J. A., Alfaro, I., Farías, G. G., Metcalfe, M. J., Fuentealba, R., et al. (2008). Wnt-7a Modulates the synaptic vesicle cycle and synaptic transmission in hippocampal neurons. *J. Biol. Chem.* 283, 5918–5927. doi: 10.1074/jbc.M705943200

Chang, C.-Y., Liang, M.-Z., Wu, C.-C., Huang, P.-Y., Chen, H.-I., Yet, S.-F., et al. (2020). WNT3A promotes neuronal regeneration upon traumatic brain injury. *Int. J. Mol. Sci.* 21:1463. doi: 10.3390/ijms21041463

Chang, J., Mancuso, M. R., Maier, C., Liang, X., Yuki, K., Yang, L., et al. (2017). Gpr124 is essential for blood-brain barrier integrity in central nervous system disease. *Nat. Med.* 23, 450–460. doi: 10.1038/nm.4309

Chen, Y., Zhang, Y., Tang, J., Liu, F., Hu, Q., Luo, C., et al. (2015). Norrin Protected Blood–brain barrier via frizzled-4/β-catenin pathway after subarachnoid hemorrhage in rats. *Stroke* 46, 529–536. doi: 10.1161/STROKEAHA.114.007265

Chong, Z. Z., Shang, Y. C., Hou, J., and Maiese, K. (2010). Wnt1 neuroprotection translates into improved neurological function during oxidant stress and cerebral ischemia through AKT1 and mitochondrial apoptotic pathways. *Oxid. Med. Cell. Longev.* 3, 153–165. doi: 10.4161/oxim.3.2.11758

Ciani, L., Boyle, K. A., Dickins, E., Sahores, M., Anane, D., Lopes, D. M., et al. (2011). Wnt7a signaling promotes dendritic spine growth and synaptic strength through Ca2+/Calmodulin-dependent protein kinase II. *Proc. Natl. Acad. Sci. U.S.A.* 108, 10732–10737. doi: 10.1073/pnas.1018132108

Conover, J. C., Doetsch, F., Garcia-Verdugo, J. M., Gale, N. W., Yancopoulos, G. D., and Alvarez-Buylla, A. (2000). Disruption of Eph/ephrin signaling affects migration and proliferation in the adult subventricular zone. *Nat. Neurosci.* 3, 1091–1097. doi: 10.1038/80606

Corps, K. N., Roth, T. L., and McGavern, D. B. (2015). Inflammation and neuroprotection in traumatic brain injury. *JAMA Neurol.* 72, 355–362. doi: 10.1001/jamaneurol.2014.3558

Coultrap, S. J., Vest, R. S., Ashpole, N. M., Hudmon, A., and Bayer, K. U. (2011). CaMKII in cerebral ischemia. *Acta Pharmacol. Sin.* 32, 861–872. doi: 10.1038/aps.2011.68

Croce, J. C., and McClay, D. R. (2008). Evolution of the Wnt pathways. *Methods Mol. Biol.* 469, 3–18. doi: 10.1007/978-1-60327-469-2_1

Daneman, R., Agalliu, D., Zhou, L., Kuhnert, F., Kuo, C. J., and Barres, B. A. (2009). Wnt/ β-catenin signaling is required for CNS, but not non-CNS, angiogenesis. *Proc. Natl. Acad. Sci. U.S.A.* 106, 641–646. doi: 10.1073/pnas.0805165106

Das, M., Mohapatra, S., and Mohapatra, S. S. (2012). New perspectives on central and peripheral immune responses to acute traumatic brain injury. *J. Neuroinflammation* 9:236. doi: 10.1186/1742-2094-9-236

Dash, P. K., Johnson, D., Clark, J., Orsi, S. A., Zhang, M., Zhao, J., et al. (2011). Involvement of the glycogen synthase kinase-3 signaling pathway in TBI pathology and neurocognitive outcome. *PLoS One* 6:e24648. doi: 10.1371/journal.pone.0024648

Dash, P. K., Mach, S. A., and Moore, A. N. (2001). Enhanced neurogenesis in the rodent hippocampus following traumatic brain injury. *J. Neurosci. Res.* 63, 313–319.

Dash, P. K., Orsi, S. A., Zhang, M., Grill, R. J., Pati, S., Zhao, J., et al. (2010). Valproate administered after traumatic brain injury provides neuroprotection and improves cognitive function in rats. *PLoS One* 5:e11383. doi: 10.1371/journal.pone.0011383

Di Carlo, A., Lamassa, M., Baldereschi, M., Pracucci, G., Basile, A. M., Wolfe, C. D. A., et al. (2003). Sex differences in the clinical presentation, resource use, and 3-month outcome of acute stroke in Europe: data from a multicenter multinational hospital-based registry. *Stroke* 34, 1114–1119. doi: 10.1161/01.STR.0000068410.07397.D7

Dirnagl, U., Iadecola, C., and Moskowitz, M. A. (1999). Pathobiology of ischaemic stroke: an integrated view. *Trends Neurosci.* 22, 391–397. doi: 10.1016/S0166-2236(99)01401-0

Dubreuil, C. I., Marklund, N., Deschamps, K., McIntosh, T. K., and McKerracher, L. (2006). Activation of Rho after traumatic brain injury and seizure in rats. *Exp. Neurol.* 198, 361–369. doi: 10.1016/j.expneurol.2005.12.002

Edvinsson, L., Povlsen, G. K., Ahnstedt, H., and Waldsee, R. (2014). CaMKII inhibition with KN93 attenuates endothelin and serotonin receptor-mediated vasoconstriction and prevents subarachnoid hemorrhage-induced deficits in sensorimotor function. *J. Neuroinflammation* 11:207. doi: 10.1186/s12974-014-0207-2

Egea-Guerrero, J. J., Murillo-Cabezas, F., Muñoz-Sánchez, M. Á., Vilches-Arenas, A., Porras-González, C., Castellano, A., et al. (2015). Role of L-type Ca2+ channels, sarcoplasmic reticulum and Rho kinase in rat basilar artery contractile properties in a new model of subarachnoid hemorrhage. *Vascul. Pharmacol.* 72, 64–72. doi: 10.1016/j.vph.2015.04.011

ElAli, A. (2016). The implication of neurovascular unit signaling in controlling the subtle balance between injury and repair following ischemic stroke. *Neural Regen. Res.* 11, 914–915. doi: 10.4103/1673-5374.184485

ElAli, A., Doeppner, T. R., Zechariah, A., and Hermann, D. M. (2011). Increased blood-brain barrier permeability and brain edema after focal cerebral ischemia induced by hyperlipidemia: role of lipid peroxidation and calpain-1/2, matrix metalloproteinase-2/9, and RhoA overactivation. *Stroke* 42, 3238–3244. doi: 10.1161/STROKEAHA.111.615559

ElAli, A., Thériault, P., and Rivest, S. (2014). The Role of pericytes in neurovascular unit remodeling in brain disorders. *IJMS* 15, 6453–6474. doi: 10.3390/ijms15046453

Emery, D. L., Fulp, C. T., Saatman, K. E., Schütz, C., Neugebauer, E., and McIntosh, T. K. (2005). Newly born granule cells in the dentate gyrus rapidly extend axons into the hippocampal CA3 region following experimental brain injury. *J. Neurotrauma* 22, 978–988. doi: 10.1089/neu.2005.22.978

Engelhardt, B. (2003). Development of the blood-brain barrier. *Cell Tissue Res.* 314, 119–129. doi: 10.1007/s00441-003-0751-z

Esfandiari, F., Fathi, A., Gourabi, H., Kiani, S., Nemati, S., and Baharvand, H. (2012). Glycogen synthase kinase-3 inhibition promotes proliferation and neuronal differentiation of human-induced pluripotent stem cell-derived neural progenitors. *Stem Cells Dev.* 21, 3233–3243. doi: 10.1089/scd.2011.0678

Faden, A. I., and Loane, D. J. (2015). Chronic neurodegeneration after traumatic brain injury: Alzheimer disease, chronic traumatic encephalopathy, or persistent neuroinflammation? *Neurotherapeutics* 12, 143–150. doi: 10.1007/s13311-014-0319-5

Fan, R., Enkhjargal, B., Camara, R., Yan, F., Gong, L., Yao, S., et al. (2017). Critical role of EphA4 in early brain injury after subarachnoid hemorrhage in rat. *Exp. Neurol.* 296, 41–48. doi: 10.1016/j.expneurol.2017.07.003

Farías, G. G., Alfaro, I. E., Cerpa, W., Grabowski, C. P., Godoy, J. A., Bonansco, C., et al. (2009). Wnt-5a/JNK signaling promotes the clustering of PSD-95 in hippocampal neurons. *J. Biol. Chem.* 284, 15857–15866. doi: 10.1074/jbc.M808986200

Ferrer, I., Friguls, B., Dalfó, E., and Planas, A. M. (2003). Early modifications in the expression of mitogen-activated protein kinase (MAPK/ERK), stress-activated kinases SAPK/JNK and p38, and their phosphorylated substrates following focal cerebral ischemia. *Acta Neuropathol.* 105, 425–437. doi: 10.1007/s00401-002-0661-2

Feske, S. K., Sorond, F. A., Henderson, G. V., Seto, M., Hitomi, A., Kawasaki, K., et al. (2009). Increased leukocyte ROCK activity in patients after acute ischemic stroke. *Brain Res.* 1257, 89–93. doi: 10.1016/j.brainres.2008.12.045

Finnie, J. W. (2013). Neuroinflammation: beneficial and detrimental effects after traumatic brain injury. *Inflammopharmacology* 21, 309–320. doi: 10.1007/s10787-012-0164-2

Folkerts, M. M., Parks, E. A., Dedman, J. R., Kaetzel, M. A., Lyeth, B. G., and Berman, R. F. (2007). Phosphorylation of calcium calmodulin-dependent protein kinase II following lateral fluid percussion brain injury in rats. *J. Neurotrauma* 24, 638–650. doi: 10.1089/neu.2006.0188

Foulquier, S., Daskalopoulos, E. P., Lluri, G., Hermans, K. C. M., Deb, A., and Blankesteijn, W. M. (2018). WNT signaling in cardiac and vascular disease. *Pharmacol. Rev.* 70, 68–141. doi: 10.1124/pr.117.013896

Fu, Z., Chen, Y., Qin, F., Yang, S., Deng, X., Ding, R., et al. (2014). Increased activity of Rho kinase contributes to hemoglobin-induced early disruption of the blood-brain barrier *in vivo* after the occurrence of intracerebral hemorrhage. *Int. J. Clin. Exp. Pathol.* 7, 7844–7853.

Fujii, M., Duris, K., Altay, O., Soejima, Y., Sherchan, P., and Zhang, J. H. (2012). Inhibition of Rho kinase by hydroxyfasudil attenuates brain edema after subarachnoid hemorrhage in rats. *Neurochem. Int.* 60, 327–333. doi: 10.1016/j.neuint.2011.12.014

Galgano, M., Toshkezi, G., Qiu, X., Russell, T., Chin, L., and Zhao, L.-R. (2017). Traumatic brain injury: current treatment strategies and future endeavors. *Cell Transplant.* 26, 1118–1130. doi: 10.1177/0963689717714102

Godman, C. A., Joshi, R., Giardina, C., Perdrizet, G., and Hightower, L. E. (2010). Hyperbaric oxygen treatment induces antioxidant gene expression. *Ann. N.Y. Acad. Sci.* 1197, 178–183. doi: 10.1111/j.1749-6632.2009.05393.x

Gong, D., Zhang, S., Liu, L., Dong, J., Guo, X., Hao, M., et al. (2011). Dynamic changes of vascular endothelial growth factor and angiopoietin-1 in association with circulating endothelial progenitor cells after severe traumatic brain injury. *J. Trauma* 70, 1480–1484. doi: 10.1097/TA.0b013e31821ac9e1

González-Montelongo, M. D. C., Egea-Guerrero, J. J., Murillo-Cabezas, F., González-Montelongo, R., Ruiz de Azúa-López, Z., Rodríguez-Rodríguez, A., et al. (2018). Relation of RhoA in peripheral blood mononuclear cells with severity of aneurysmal subarachnoid hemorrhage and vasospasm. *Stroke* 49, 1507–1510. doi: 10.1161/STROKEAHA.117.020311

Guo, X., Liu, L., Zhang, M., Bergeron, A., Cui, Z., Dong, J.-F., et al. (2009). Correlation of CD34+ cells with tissue angiogenesis after traumatic brain injury in a rat model. *J. Neurotrauma* 26, 1337–1344. doi: 10.1089/neu.2008.0733

Habas, R., and Dawid, I. B. (2005). Dishevelled and Wnt signaling: is the nucleus the final frontier? *J. Biol.* 4:2. doi: 10.1186/jbiol22

Habas, R., Kato, Y., and He, X. (2001). Wnt/Frizzled activation of Rho regulates vertebrate gastrulation and requires a novel Formin homology protein Daam1. *Cell* 107, 843–854. doi: 10.1016/s0092-8674(01)00614-6

Halleskog, C., Mulder, J., Dahlström, J., Mackie, K., Hortobágyi, T., Tanila, H., et al. (2011). WNT signaling in activated microglia is proinflammatory. *Glia* 59, 119–131. doi: 10.1002/glia.21081

Harriott, A. M., Heckman, M. G., Rayaprolu, S., Soto-Ortolaza, A. I., Diehl, N. N., Kanekiyo, T., et al. (2015). Low density lipoprotein receptor related protein 1 and 6 gene variants and ischaemic stroke risk. *Eur. J. Neurol.* 22, 1235–1241. doi: 10.1111/ene.12735

Hayward, N. M. E. A., Tuunanen, P. I., Immonen, R., Ndode-Ekane, X. E., Pitkänen, A., and Gröhn, O. (2011). Magnetic resonance imaging of regional hemodynamic and cerebrovascular recovery after lateral fluid-percussion brain injury in rats. *J. Cereb. Blood Flow Metab.* 31, 166–177. doi: 10.1038/jcbfm.2010.67

He, H., Li, X., and He, Y. (2019). Hyperbaric oxygen therapy attenuates neuronal apoptosis induced by traumatic brain injury via Akt/GSK3β/β-catenin pathway. *Neuropsychiatr. Dis. Treat.* 15, 369–374. doi: 10.2147/NDT.S183632

He, X., Semenov, M., Tamai, K., and Zeng, X. (2004). LDL receptor-related proteins 5 and 6 in Wnt/beta-catenin signaling: arrows point the way. *Development* 131, 1663–1677. doi: 10.1242/dev.01117

He, X.-W., Wang, E., Bao, Y.-Y., Wang, F., Zhu, M., Hu, X.-F., et al. (2016). High serum levels of sclerostin and Dickkopf-1 are associated with acute ischaemic stroke. *Atherosclerosis* 253, 22–28. doi: 10.1016/j.atherosclerosis.2016.08.003

Hermann, D. M., and Chopp, M. (2012). Promoting brain remodelling and plasticity for stroke recovery: therapeutic promise and potential pitfalls of clinical translation. *Lancet Neurol.* 11, 369–380. doi: 10.1016/S1474-4422(12)70039-X

Hermann, D. M., and ElAli, A. (2012). The abluminal endothelial membrane in neurovascular remodeling in health and disease. *Sci. Signal.* 5:re4. doi: 10.1126/scisignal.2002886

Hiroi, Y., Noma, K., Kim, H.-H., Sladojevic, N., Tabit, C. E., Li, Y., et al. (2018). Neuroprotection mediated by upregulation of endothelial nitric oxide synthase in Rho-associated, coiled-coil-containing kinase 2 deficient mice. *Circ. J.* 82, 1195–1204. doi: 10.1253/circj.CJ-17-0732

House, S. J., Potier, M., Bisaillon, J., Singer, H. A., and Trebak, M. (2008). The non-excitable smooth muscle: calcium signaling and phenotypic switching during vascular disease. *Pflugers Arch.* 456, 769–785. doi: 10.1007/s00424-008-0491-8

Huang, B., Krafft, P. R., Ma, Q., Rolland, W. B., Caner, B., Lekic, T., et al. (2012). Fibroblast growth factors preserve blood-brain barrier integrity through RhoA inhibition after intracerebral hemorrhage in mice. *Neurobiol. Dis.* 46, 204–214. doi: 10.1016/j.nbd.2012.01.008

Huang, C., Lu, X., Wang, J., Tong, L., Jiang, B., and Zhang, W. (2015). Inhibition of endogenous heat shock protein 70 attenuates inducible nitric oxide synthase induction via disruption of heat shock protein 70/Na(+) /H(+) exchanger 1-Ca(2+) -calcium-calmodulin-dependent protein kinase II/transforming growth factor β-activated kinase 1-nuclear factor-κB signals in BV-2 microglia. *J. Neurosci. Res.* 93, 1192–1202. doi: 10.1002/jnr.23571

Hübner, K., Cabochette, P., Diéguez-Hurtado, R., Wiesner, C., Wakayama, Y., Grassme, K. S., et al. (2018). Wnt/β-catenin signaling regulates VE-cadherin-mediated anastomosis of brain capillaries by counteracting S1pr1 signaling. *Nat. Commun.* 9:4860. doi: 10.1038/s41467-018-07302-x

Hur, E.-M., and Zhou, F.-Q. (2010). GSK3 signalling in neural development. *Nat. Rev. Neurosci.* 11, 539–551. doi: 10.1038/nrn2870

Hyder, A. A., Wunderlich, C. A., Puvanachandra, P., Gururaj, G., and Kobusingye, O. C. (2007). The impact of traumatic brain injuries: a global perspective. *Neurorehabilitation* 22, 341–353.

Jaworski, T., Banach-Kasper, E., and Gralec, K. (2019). GSK-3β at the intersection of neuronal plasticity and neurodegeneration. *Neural Plast.* 2019:4209475. doi: 10.1155/2019/4209475

Jean LeBlanc, N., Menet, R., Picard, K., Parent, G., Tremblay, M. -È, and ElAli, A. (2019). Canonical Wnt pathway maintains blood-brain barrier integrity upon ischemic stroke and its activation ameliorates tissue plasminogen activator therapy. *Mol. Neurobiol.* 56, 6521–6538. doi: 10.1007/s12035-019-1539-9

Jessberger, S., Clark, R. E., Broadbent, N. J., Clemenson, G. D., Consiglio, A., Lie, D. C., et al. (2009). Dentate gyrus-specific knockdown of adult neurogenesis impairs spatial and object recognition memory in adult rats. *Learn. Mem.* 16, 147–154. doi: 10.1101/lm.1172609

Johnson, A., and DiPietro, L. A. (2013). Apoptosis and angiogenesis: an evolving mechanism for fibrosis. *FASEB J.* 27, 3893–3901. doi: 10.1096/fj.12-214189

Johnson, G. L., and Nakamura, K. (2007). The c-jun kinase/stress-activated pathway: regulation, function and role in human disease. *Biochim. Biophys. Acta* 1773, 1341–1348. doi: 10.1016/j.bbamcr.2006.12.009

Johnson, V. E., Stewart, J. E., Begbie, F. D., Trojanowski, J. Q., Smith, D. H., and Stewart, W. (2013). Inflammation and white matter degeneration persist for years after a single traumatic brain injury. *Brain* 136, 28–42. doi: 10.1093/brain/aws322

Jullienne, A., Salehi, A., Affeldt, B., Baghchechi, M., Haddad, E., Avitua, A., et al. (2018). Male and female mice exhibit divergent responses of the cortical vasculature to traumatic brain injury. *J. Neurotrauma* 35, 1646–1658. doi: 10.1089/neu.2017.5547

Kang, K., Kim, Y.-J., Kim, Y.-H., Roh, J. N., Nam, J.-M., Kim, P.-Y., et al. (2012). Lithium pretreatment reduces brain injury after intracerebral hemorrhage in rats. *Neurol. Res.* 34, 447–454. doi: 10.1179/1743132812Y.0000000015

Karve, I. P., Taylor, J. M., and Peter J. C. (2016). The contribution of astrocytes and microglia to traumatic brain injury. *Br. J. Pharmacol.* 173, 692–702. doi: 10.1111/bhp.13125

Ke, X., Yang, M., Luo, J.-M., Zhang, Y., and Chen, X.-Y. (2020). The role of serum Dickkopf-1 in predicting 30-day death in severe traumatic brain injury. *Brain Behav.* 10:e01589. doi: 10.1002/brb3.1589

Kelly, S., Zhao, H., Hua Sun, G., Cheng, D., Qiao, Y., Luo, J., et al. (2004). Glycogen synthase kinase 3β inhibitor Chir025 reduces neuronal death resulting from oxygen-glucose deprivation, glutamate excitotoxicity, and cerebral ischemia. *Exp. Neurol.* 188, 378–386. doi: 10.1016/j.expneurol.2004.04.004

Kernie, S. G., Erwin, T. M., and Parada, L. F. (2001). Brain remodeling due to neuronal and astrocytic proliferation after controlled cortical injury in mice. *J. Neurosci. Res.* 66, 317–326. doi: 10.1002/jnr.10013

Kim, J., Kim, J., Kim, D. W., Ha, Y., Ihm, M. H., Kim, H., et al. (2010). Wnt5a induces endothelial inflammation via beta-catenin-independent signaling. *J. Immunol.* 185, 1274–1282. doi: 10.4049/jimmunol.1000181

Koeppen, A. H., Dickson, A. C., and McEvoy, J. A. (1995). The cellular reactions to experimental intracerebral hemorrhage. *J. Neurol. Sci.* 134(Suppl.), 102–112. doi: 10.1016/0022-510x(95)00215-n

Komiya, Y., and Habas, R. (2008). Wnt signal transduction pathways. *Organogenesis* 4, 68–75. doi: 10.4161/org.4.2.5851

Krafft, P. R., Altay, O., Rolland, W. B., Duris, K., Lekic, T., Tang, J., et al. (2012). α7 Nicotinic acetylcholine receptor agonism confers neuroprotection through GSK-3β inhibition in a mouse model of intracerebral hemorrhage. *Stroke* 43, 844–850. doi: 10.1161/STROKEAHA.111.639989

Krafft, P. R., Caner, B., Klebe, D., Rolland, W. B., Tang, J., and Zhang, J. H. (2013). PHA-543613 preserves blood-brain barrier integrity after intracerebral hemorrhage in mice. *Stroke* 44, 1743–1747. doi: 10.1161/STROKEAHA.111.000427

Krishna, G., Ying, Z., and Gomez-Pinilla, F. (2019). Blueberry supplementation mitigates altered brain plasticity and behavior after traumatic brain injury in rats. *Mol. Nutr. Food Res.* 63:e1801055. doi: 10.1002/mnfr.201801055

Kuwabara, T., Hsieh, J., Muotri, A., Yeo, G., Warashina, M., Lie, D. C., et al. (2009). Wnt-mediated activation of NeuroD1 and retro-elements during adult neurogenesis. *Nat. Neurosci.* 12, 1097–1105. doi: 10.1038/nn.2360

Lai, X.-L., Deng, Z.-F., Zhu, X.-G., and Chen, Z.-H. (2019). *Apc* gene suppresses intracranial aneurysm formation and rupture through inhibiting the NF-κB signaling pathway mediated inflammatory response. *Biosci. Rep.* 39:BSR20181909. doi: 10.1042/BSR20181909

Lambert, C., Cisternas, P., and Inestrosa, N. C. (2016). Role of Wnt signaling in central nervous system injury. *Mol. Neurobiol.* 53, 2297–2311. doi: 10.1007/s12035-015-9138-x

Lei, Z.-N., Liu, F., Zhang, L.-M., Huang, Y.-L., and Sun, F.-Y. (2012). Bcl-2 increases stroke-induced striatal neurogenesis in adult brains by inhibiting BMP-4 function via activation of β-catenin signaling. *Neurochem. Int.* 61, 34–42. doi: 10.1016/j.neuint.2012.04.004

Lemmens, R., Jaspers, T., Robberecht, W., and Thijs, V. N. (2013). Modifying expression of EphA4 and its downstream targets improves functional recovery after stroke. *Hum. Mol. Genet.* 22, 2214–2220. doi: 10.1093/hmg/ddt073

Li, L., and Liu, B. (2019). ROCK inhibitor Y-27632 protects rats against cerebral ischemia/reperfusion-induced behavioral deficits and hippocampal damage. *Mol. Med. Rep.* 20, 3395–3405. doi: 10.3892/mmr.2019.10584

Li, T., Qin, J.-J., Yang, X., Ji, Y.-X., Guo, F., Cheng, W.-L., et al. (2017). The ubiquitin E3 ligase TRAF6 exacerbates ischemic stroke by ubiquitinating and activating Rac1. *J. Neurosci.* 37, 12123–12140. doi: 10.1523/JNEUROSCI.1751-17.2017

Li, W., Li, R., Zhao, S., Jiang, C., Liu, Z., and Tang, X. (2018). Lithium posttreatment alleviates blood-brain barrier injury after intracerebral hemorrhage in rats. *Neuroscience* 383, 129–137. doi: 10.1016/j.neuroscience.2018.05.001

Li, Z., Chen, X., Zhang, X., Ren, X., Chen, X., Cao, J., et al. (2017). Small interfering RNA targeting Dickkopf-1 contributes to neuroprotection after intracerebral hemorrhage in rats. *J. Mol. Neurosci.* 61, 279–288. doi: 10.1007/s12031-017-0883-3

Lie, D.-C., Colamarino, S. A., Song, H.-J., Désiré, L., Mira, H., Consiglio, A., et al. (2005). Wnt signalling regulates adult hippocampal neurogenesis. *Nature* 437, 1370–1375. doi: 10.1038/nature04108

Liebner, S., Corada, M., Bangsow, T., Babbage, J., Taddei, A., Czupalla, C. J., et al. (2008). Wnt/β-catenin signaling controls development of the blood–brain barrier. *J. Cell Biol.* 183, 409–417. doi: 10.1083/jcb.200806024

Lin, C.-J., Chen, T.-H., Yang, L.-Y., and Shih, C.-M. (2014). Resveratrol protects astrocytes against traumatic brain injury through inhibiting apoptotic and autophagic cell death. *Cell Death Dis.* 5:e1147. doi: 10.1038/cddis.2014.123

Ling, G.-Q., Li, X.-F., Lei, X.-H., Wang, Z.-Y., Ma, D.-Y., Wang, Y.-N., et al. (2019). c-Jun N-terminal kinase inhibition attenuates early brain injury induced neuronal apoptosis via decreasing p53 phosphorylation and mitochondrial apoptotic pathway activation in subarachnoid hemorrhage rats. *Mol. Med. Rep.* 19, 327–337. doi: 10.3892/mmr.2018.9640

Lipinski, M. M., Wu, J., Faden, A. I., and Sarkar, C. (2015). Function and mechanisms of autophagy in brain and spinal cord trauma. *Antioxid. Redox Signal.* 23, 565–577. doi: 10.1089/ars.2015.6306

Liu, L., Wei, H., Chen, F., Wang, J., Dong, J., and Zhang, J. (2011). Endothelial progenitor cells correlate with clinical outcome of traumatic brain injury. *Crit. Care Med.* 39, 1760–1765. doi: 10.1097/CCM.0b013e3182186cee

Liu, W., Khatibi, N., Sridharan, A., and Zhang, J. H. (2011). Application of medical gases in the field of neurobiology. *Med. Gas. Res.* 1:13. doi: 10.1186/2045-9912-1-13

Liu, Z., and Chopp, M. (2016). Astrocytes, therapeutic targets for neuroprotection and neurorestoration in ischemic stroke. *Prog. Neurobiol.* 144, 103–120. doi: 10.1016/j.pneurobio.2015.09.008

Liu, Z., Li, R., Jiang, C., Zhao, S., Li, W., and Tang, X. (2018). The neuroprotective effect of lithium chloride on cognitive impairment through glycogen synthase kinase-3β inhibition in intracerebral hemorrhage rats. *Eur. J. Pharmacol.* 840, 50–59. doi: 10.1016/j.ejphar.2018.10.019

Llorens-Martín, M., Fuster-Matanzo, A., Teixeira, C. M., Jurado-Arjona, J., Ulloa, F., deFelipe, J., et al. (2013). GSK-3β overexpression causes reversible alterations on postsynaptic densities and dendritic morphology of hippocampal granule neurons *in vivo*. *Mol. Psychiatry* 18, 451–460. doi: 10.1038/mp.2013.4

Lo, E. H. (2008). A new penumbra: transitioning from injury into repair after stroke. *Nat. Med.* 14, 497–500. doi: 10.1038/nm1735

Lu, E., Wang, Q., Li, S., Chen, C., Wu, W., Xu, Y. X. Z., et al. (2020). Profilin 1 knockdown prevents ischemic brain damage by promoting M2 microglial polarization associated with the RhoA/ROCK pathway. *J. Neurosci. Res.* 98, 1198–1212. doi: 10.1002/jnr.24607

Lu, H., Jiang, R., Tao, X., Duan, C., Huang, J., Huan, W., et al. (2017). Expression of Dixdc1 and its role in astrocyte proliferation after traumatic brain injury. *Cell. Mol. Neurobiol.* 37, 1131–1139. doi: 10.1007/s10571-016-0446-0

Ma, B., and Hottiger, M. O. (2016). Crosstalk between Wnt/β-Catenin and NF-κB signaling pathway during inflammation. *Front. Immunol* 7:378. doi: 10.3389/fimmu.2016.00378

MacDonald, B. T., and He, X. (2012). Frizzled and LRP5/6 receptors for Wnt/β-catenin signaling. *Cold Spring Harb. Perspect. Biol.* 4:a007880. doi: 10.1101/cshperspect.a007880

Magistris, F., Bazak, S., and Martin, J. (2013). Intracerebral hemorrhage: pathophysiology, diagnosis and management. *Clin. Rev.* 10, 15–22.

Makino, K., Osuka, K., Watanabe, Y., Usuda, N., Hara, M., Aoyama, M., et al. (2015). Increased ICP promotes CaMKII-mediated phosphorylation of neuronal NOS at Ser847 in the hippocampus immediately after subarachnoid hemorrhage. *Brain Res.* 1616, 19–25. doi: 10.1016/j.brainres.2015.04.048

Manicassamy, S., Reizis, B., Ravindran, R., Nakaya, H., Salazar-Gonzalez, R. M., Wang, Y.-C., et al. (2010). Activation of beta-catenin in dendritic cells regulates immunity versus tolerance in the intestine. *Science* 329, 849–853. doi: 10.1126/science.1188510

Mao, B., Wu, W., Davidson, G., Marhold, J., Li, M., Mechler, B. M., et al. (2002). Kremen proteins are Dickkopf receptors that regulate Wnt/b-catenin signalling. *Nature* 417, 664–667.

Mao, X., Miao, G., Tao, X., Hao, S., Zhang, H., Li, H., et al. (2016). Saikosaponin a protects TBI rats after controlled cortical impact and the underlying mechanism. *Am. J. Transl. Res.* 8, 133–141.

Marchetti, B., and Pluchino, S. (2013). Wnt your brain be inflamed? Yes, it Wnt! *Trends Mol. Med.* 19, 144–156. doi: 10.1016/j.molmed.2012.12.001

Martowicz, A., Trusohamn, M., Jensen, N., Wisniewska-Kruk, J., Corada, M., Ning, F. C., et al. (2019). Endothelial β-catenin signaling supports postnatal brain and retinal angiogenesis by promoting sprouting, tip cell formation, and VEGFR (Vascular Endothelial Growth Factor Receptor) 2 expression. *Arterioscler. Thromb. Vasc. Biol.* 39, 2273–2288. doi: 10.1161/ATVBAHA.119.312749

Mastroiacovo, F., Busceti, C. L., Biagioni, F., Moyanova, S. G., Meisler, M. H., Battaglia, G., et al. (2009). Induction of the Wnt antagonist, Dickkopf-1, contributes to the development of neuronal death in models of brain focal ischemia. *J. Cereb. Blood Flow Metab.* 29, 264–276. doi: 10.1038/jcbfm.2008.111

Matei, N., Camara, J., McBride, D., Camara, R., Xu, N., Tang, J., et al. (2018). Intranasal wnt3a attenuates neuronal apoptosis through Frz1/PIWIL1a/FOXM1 pathway in MCAO rats. *J. Neurosci.* 38, 6787–6801. doi: 10.1523/JNEUROSCI.2352-17.2018

Matias, D., Dubois, L. G., Pontes, B., Rosário, L., Ferrer, V. P., Balça-Silva, J., et al. (2019). GBM-derived Wnt3a induces M2-like phenotype in microglial cells through Wnt/β-catenin signaling. *Mol. Neurobiol.* 56, 1517–1530. doi: 10.1007/s12035-018-1150-5

Michel-Monigadon, D., Bonny, C., and Hirt, L. (2010). c-Jun N-terminal kinase pathway inhibition in intracerebral hemorrhage. *Cerebrovasc. Dis.* 29, 564–570. doi: 10.1159/000306643

Moccia, F., Frost, C., Berra-Romani, R., Tanzi, F., and Adams, D. J. (2004). Expression and function of neuronal nicotinic ACh receptors in rat microvascular endothelial cells. *Am. J. Physiol. Heart Circ. Physiol.* 286, H486–H491. doi: 10.1152/ajpheart.00620.2003

Modi, J. P., Gharibani, P. M., Ma, Z., Tao, R., Menzie, J., Prentice, H., et al. (2014). Protective mechanism of sulindac in an animal model of ischemic stroke. *Brain Res.* 1576, 91–99. doi: 10.1016/j.brainres.2014.06.019

Morgan, J. I., and Curran, T. (1991). Stimulus-transcription coupling in the nervous system: involvement of the inducible proto-oncogenes fos and jun. *Annu. Rev. Neurosci.* 14, 421–451. doi: 10.1146/annurev.ne.14.030191.002225

Morgan, R., Kreipke, C. W., Roberts, G., Bagchi, M., and Rafols, J. A. (2007). Neovascularization following traumatic brain injury: possible evidence for both angiogenesis and vasculogenesis. *Neurol. Res.* 29, 375–381. doi: 10.1179/016164107X204693

Morioka, M., and Orito, K. (2017). Management of spontaneous intracerebral hematoma. *Neurol. Med. Chir. (Tokyo)* 57, 563–574. doi: 10.2176/nmc.ra.2016-0327

Moskowitz, M. A., Lo, E. H., and Iadecola, C. (2010). The science of stroke: mechanisms in search of treatments. *Neuron* 67, 181–198. doi: 10.1016/j.neuron.2010.07.002

Mulherkar, S., Firozi, K., Huang, W., Uddin, M. D., Grill, R. J., Costa-Mattioli, M., et al. (2017). RhoA-ROCK inhibition reverses synaptic remodeling and motor and cognitive deficits caused by traumatic brain injury. *Sci. Rep.* 7:10689. doi: 10.1038/s41598-017-11113-3

Najem, D., Rennie, K., Ribecco-Lutkiewicz, M., Ly, D., Haukenfrers, J., Liu, Q., et al. (2018). Traumatic brain injury: classification, models, and markers. *Biochem. Cell Biol.* 96, 391–406. doi: 10.1139/bcb-2016-0160

Naraoka, M., Munakata, A., Matsuda, N., Shimamura, N., and Ohkuma, H. (2013). Suppression of the Rho/Rho-kinase pathway and prevention of cerebral vasospasm by combination treatment with statin and fasudil after subarachnoid hemorrhage in rabbit. *Transl. Stroke Res.* 4, 368–374. doi: 10.1007/s12975-012-0247-9

Neumann, J., Schaale, K., Farhat, K., Endermann, T., Ulmer, A. J., Ehlers, S., et al. (2010). Frizzled1 is a marker of inflammatory macrophages, and its ligand Wnt3a is involved in reprogramming Mycobacterium tuberculosis-infected macrophages. *FASEB J.* 24, 4599–4612. doi: 10.1096/fj.10-160994

Ng, L. F., Kaur, P., Bunnag, N., Suresh, J., Sung, I. C. H., Tan, Q. H., et al. (2019). WNT signaling in disease. *Cells* 8:826. doi: 10.3390/cells8080826

Niehrs, C. (2012). The complex world of WNT receptor signalling. *Nat. Rev. Mol. Cell. Biol.* 13, 767–779. doi: 10.1038/nrm3470

Niu, L.-J., Xu, R.-X., Zhang, P., Du, M.-X., and Jiang, X.-D. (2012). Suppression of Frizzled-2-mediated Wnt/Ca2+ signaling significantly attenuates intracellular calcium accumulation in vitro and in a rat model of traumatic brain injury. *Neuroscience* 213, 19–28. doi: 10.1016/j.neuroscience.2012.03.057

Noelanders, R., and Vleminckx, K. (2017). How Wnt signaling builds the brain: bridging development and disease. *Neuroscientist* 23, 314–329. doi: 10.1177/1073858416667270

Nusse, R., and Varmus, H. E. (1982). Many tumors induced by the mouse mammary tumor virus contain a provirus integrated in the same region of the host genome. *Cell* 31, 99–109. doi: 10.1016/0092-8674(82)90409-3

Obenaus, A., Ng, M., Orantes, A. M., Kinney-Lang, E., Rashid, F., Hamer, M., et al. (2017). Traumatic brain injury results in acute rarefication of the vascular network. *Sci. Rep.* 7:239. doi: 10.1038/s41598-017-00161-4

Ochs, S. M., Dorostkar, M. M., Aramuni, G., Schön, C., Filser, S., Pöschl, J., et al. (2015). Loss of neuronal GSK3β reduces dendritic spine stability and attenuates excitatory synaptic transmission via β-catenin. *Mol. Psychiatry* 20, 482–489. doi: 10.1038/mp.2014.55

Ohab, J. J., Fleming, S., Blesch, A., and Carmichael, S. T. (2006). A neurovascular niche for neurogenesis after stroke. *J. Neurosci.* 26, 13007–13016. doi: 10.1523/JNEUROSCI.4323-06.2006

Ohnishi, M., Katsuki, H., Fujimoto, S., Takagi, M., Kume, T., and Akaike, A. (2007). Involvement of thrombin and mitogen-activated protein kinase pathways in hemorrhagic brain injury. *Exp. Neurol.* 206, 43–52. doi: 10.1016/j.expneurol.2007.03.030

Okamoto, M., Inoue, K., Iwamura, H., Terashima, K., Soya, H., Asashima, M., et al. (2011). Reduction in paracrine Wnt3 factors during aging causes impaired adult neurogenesis. *FASEB J.* 25, 3570–3582. doi: 10.1096/fj.11-184697

Paganoni, S., Bernstein, J., and Ferreira, A. (2010). Ror1-Ror2 complexes modulate synapse formation in hippocampal neurons. *Neuroscience* 165, 1261–1274. doi: 10.1016/j.neuroscience.2009.11.056

Pan, H., Zhang, J.-J., Xu, D.-D., Gu, Z.-Y., Tao, L.-Y., and Zhang, M.-Y. (2014). [Expression of CaMK II delta in cerebral cortex following traumatic brain injury]. *Fa Yi Xue Za Zhi* 30, 169–171, 177.

Pan, Z., Cui, M., Dai, G., Yuan, T., Li, Y., Ji, T., et al. (2018). Protective effect of anthocyanin on neurovascular unit in cerebral ischemia/reperfusion injury in rats. *Front. Neurosci.* 12:947. doi: 10.3389/fnins.2018.00947

Park, E., Bell, J. D., Siddiq, I. P., and Baker, A. J. (2009). An analysis of regional microvascular loss and recovery following two grades of fluid percussion trauma: a role for hypoxia-inducible factors in traumatic brain injury. *J. Cereb. Blood Flow Metab.* 29, 575–584. doi: 10.1038/jcbfm.2008.151

Peghaire, C., Bats, M. L., Sewduth, R., Jeanningros, S., Jaspard, B., Couffinhal, T., et al. (2016). Fzd7 (Frizzled-7) Expressed by Endothelial Cells Controls Blood Vessel Formation Through Wnt/β-Catenin Canonical Signaling. *Arterioscler. Thromb. Vasc. Biol.* 36, 2369–2380.

Piccin, D., and Morshead, C. M. (2011). Wnt signaling regulates symmetry of division of neural stem cells in the adult brain and in response to injury. *Stem Cells* 29, 528–538. doi: 10.1002/stem.589

Pinzón-Daza, M. L., Salaroglio, I. C., Kopecka, J., Garzòn, R., Couraud, P.-O., Ghigo, D., et al. (2014). The cross-talk between canonical and non-canonical

Wnt-dependent pathways regulates P-glycoprotein expression in human blood-brain barrier cells. *J. Cereb. Blood Flow Metab.* 34, 1258–1269. doi: 10.1038/jcbfm.2014.100

Planutiene, M., Planutis, K., and Holcombe, R. F. (2011). Lymphoid enhancer-binding factor 1, a representative of vertebrate-specific Lef1/Tcf1 sub-family, is a Wnt-beta-catenin pathway target gene in human endothelial cells which regulates matrix metalloproteinase-2 expression and promotes endothelial cell invasion. *Vascular Cell* 3:28. doi: 10.1186/2045-824X-3-28

Qiu, C.-W., Liu, Z.-Y., Hou, K., Liu, S.-Y., Hu, Y.-X., Zhang, L., et al. (2018). Wip1 knockout inhibits neurogenesis by affecting the Wnt/β-catenin signaling pathway in focal cerebral ischemia in mice. *Exp. Neurol.* 309, 44–53. doi: 10.1016/j.expneurol.2018.07.011

Qiu, C.-W., Liu, Z.-Y., Zhang, F.-L., Zhang, L., Li, F., Liu, S.-Y., et al. (2019). Post-stroke gastrodin treatment ameliorates ischemic injury and increases neurogenesis and restores the Wnt/β-Catenin signaling in focal cerebral ischemia in mice. *Brain Res.* 1712, 7–15. doi: 10.1016/j.brainres.2019.01.043

Qu, Q., Sun, G., Murai, K., Ye, P., Li, W., Asuelime, G., et al. (2013). Wnt7a regulates multiple steps of neurogenesis. *Mol. Cell. Biol.* 33, 2551–2559. doi: 10.1128/MCB.00325-13

Qureshi, A. L., Mendelow, A. D., and Hanley, D. F. (2009). Intracerebral haemorrhage. *Lancet* 373, 1632–1644. doi: 10.1016/S0140-6736(09)60371-8

Raghupathi, R. (2004). Cell death mechanisms following traumatic brain injury. *Brain Pathol.* 14, 215–222. doi: 10.1111/j.1750-3639.2004.tb00056.x

Raghupathi, R., Graham, D. I., and McIntosh, T. K. (2000). Apoptosis after traumatic brain injury. *J. Neurotrauma* 17, 927–938. doi: 10.1089/neu.2000.17.927

Raghupathi, R., McIntosh, T. K., and Smith, D. H. (1995). Cellular responses to experimental brain injury. *Brain Pathol.* 5, 437–442. doi: 10.1111/j.1750-3639.1995.tb00622.x

Ramaswamy, S., Goings, G. E., Soderstrom, K. E., Szele, F. G., and Kozlowski, D. A. (2005). Cellular proliferation and migration following a controlled cortical impact in the mouse. *Brain Res.* 1053, 38–53. doi: 10.1016/j.brainres.2005.06.042

Rehman, S. U., Ahmad, A., Yoon, G.-H., Khan, M., Abid, M. N., and Kim, M. O. (2018). Inhibition of c-Jun N-terminal kinase protects against brain damage and improves learning and memory after traumatic brain injury in adult mice. *Cereb. Cortex* 28, 2854–2872. doi: 10.1093/cercor/bhx164

Repici, M., Centeno, C., Tomasi, S., Forloni, G., Bonny, C., Vercelli, A., et al. (2007). Time-course of c-Jun N-terminal kinase activation after cerebral ischemia and effect of D-JNKI1 on c-Jun and caspase-3 activation. *Neuroscience* 150, 40–49. doi: 10.1016/j.neuroscience.2007.08.021

Rice, A. C., Khaldi, A., Harvey, H. B., Salman, N. J., White, F., Fillmore, H., et al. (2003). Proliferation and neuronal differentiation of mitotically active cells following traumatic brain injury. *Exp. Neurol.* 183, 406–417. doi: 10.1016/s0014-4886(03)00241-3

Rikitake, Y., Kim, H.-H., Huang, Z., Seto, M., Yano, K., Asano, T., et al. (2005). Inhibition of Rho kinase (ROCK) leads to increased cerebral blood flow and stroke protection. *Stroke* 36, 2251–2257. doi: 10.1161/01.STR.0000181077.84981.11

Rochefort, G. Y. (2014). The osteocyte as a therapeutic target in the treatment of osteoporosis. *Ther. Adv. Musculoskelet.* 6, 79–91. doi: 10.1177/1759720X14523500

Roquer, J., Campello, A. R., and Gomis, M. (2003). Sex differences in first-ever acute stroke. *Stroke* 34, 1581–1585. doi: 10.1161/01.STR.0000078562.82918.F6

Rosso, S. B., and Inestrosa, N. C. (2013). WNT signaling in neuronal maturation and synaptogenesis. *Front. Cell. Neurosci.* 7:103. doi: 10.3389/fncel.2013.00103

Ruan, W., Hu, J., Zhou, H., Li, Y., Xu, C., Luo, Y., et al. (2020). Intranasal wnt-3a alleviates neuronal apoptosis in early brain injury post subarachnoid hemorrhage via the regulation of wnt target PPAN mediated by the moonlighting role of aldolase C. *Neurochem. Int.* 134:104656. doi: 10.1016/j.neuint.2019.104656

Russo, M. V., and McGavern, D. B. (2016). Inflammatory neuroprotection following traumatic brain injury. *Science* 353, 783–785. doi: 10.1126/science.aaf6260

Sabri, M., Ai, J., Knight, B., Tariq, A., Jeon, H., Shang, X., et al. (2011). Uncoupling of endothelial nitric oxide synthase after experimental subarachnoid hemorrhage. *J. Cereb. Blood Flow Metab.* 31, 190–199. doi: 10.1038/jcbfm.2010.76

Sacco, R. L., and Liao, J. K. (2005). Drug Insight: statins and stroke. *Nat. Clin. Pract. Cardiovasc. Med.* 2, 576–584. doi: 10.1038/ncpcardio0348

Salehi, A., Jullienne, A., Baghchechi, M., Hamer, M., Walsworth, M., Donovan, V., et al. (2018). Up-regulation of Wnt/β-catenin expression is accompanied with vascular repair after traumatic brain injury. *J. Cereb. Blood Flow Metab.* 38, 274–289. doi: 10.1177/0271678X17744124

Salehi, A., Zhang, J. H., and Obenaus, A. (2017). Response of the cerebral vasculature following traumatic brain injury. *J. Cereb. Blood Flow Metab.* 37, 2320–2339. doi: 10.1177/0271678X17701460

Schaale, K., Neumann, J., Schneider, D., Ehlers, S., and Reiling, N. (2011). Wnt signaling in macrophages: augmenting and inhibiting mycobacteria-induced inflammatory responses. *Eur. J. Cell Biol.* 90, 553–559. doi: 10.1016/j.ejcb.2010.11.004

Seib, D. R. M., Corsini, N. S., Ellwanger, K., Plaas, C., Mateos, A., Pitzer, C., et al. (2013). Loss of Dickkopf-1 restores neurogenesis in old age and counteracts cognitive decline. *Cell Stem Cell* 12, 204–214. doi: 10.1016/j.stem.2012.11.010

Seifert-Held, T., Pekar, T., Gattringer, T., Simmet, N. E., Scharnagl, H., Stojakovic, T., et al. (2011). Circulating Dickkopf-1 in acute ischemic stroke and clinically stable cerebrovascular disease. *Atherosclerosis* 218, 233–237. doi: 10.1016/j.atherosclerosis.2011.05.015

Sewduth, R.-N., Jaspard-Vinassa, B., Peghaire, C., Guillabert, A., Franzi, N., Larrieu-Lahargue, F., et al. (2014). The ubiquitin ligase PDZRN3 is required for vascular morphogenesis through Wnt/planar cell polarity signalling. *Nat. Commun.* 5:4832. doi: 10.1038/ncomms5832

Sewduth, R.-N., Kovacic, H., Jaspard-Vinassa, B., Jecko, V., Wavasseur, T., Fritsch, N., et al. (2017). PDZRN3 destabilizes endothelial cell-cell junctions through a PKCζ-containing polarity complex to increase vascular permeability. *Sci. Signal.* 10:eaag3209. doi: 10.1126/scisignal.aag3209

Sheng, M., and Greenberg, M. E. (1990). The regulation and function of c-fos and other immediate early genes in the nervous system. *Neuron* 4, 477–485. doi: 10.1016/0896-6273(90)90106-p

Shibuya, M., Hirai, S., Seto, M., Satoh, S., Ohtomo, E., and Fasudil Ischemic Stroke Study Group. (2005). Effects of fasudil in acute ischemic stroke: results of a prospective placebo-controlled double-blind trial. *J. Neurol. Sci.* 238, 31–39. doi: 10.1016/j.jns.2005.06.003

Shim, S. S., and Stutzmann, G. E. (2016). Inhibition of Glycogen Synthase Kinase-3: an emerging target in the treatment of traumatic brain injury. *J. Neurotrauma* 33, 2065–2076. doi: 10.1089/neu.2015.4177

Shruster, A., Ben-Zur, T., Melamed, E., and Offen, D. (2012). Wnt signaling enhances neurogenesis and improves neurological function after focal ischemic injury. *PLoS One* 7:e40843. doi: 10.1371/journal.pone.0040843

Sköld, M. K., von Gertten, C., Sandberg-Nordqvist, A.-C., Mathiesen, T., and Holmin, S. (2005). VEGF and VEGF receptor expression after experimental brain contusion in rat. *J. Neurotrauma* 22, 353–367. doi: 10.1089/neu.2005.22.353

Sladojevic, N., Yu, B., and Liao, J. K. (2017). ROCK as a therapeutic target for ischemic stroke. *Expert Rev. Neurother.* 17, 1167–1177. doi: 10.1080/14737175.2017.1395700

Smith, C., Gentleman, S. M., Leclercq, P. D., Murray, L. S., Griffin, W. S. T., Graham, D. I., et al. (2013). The neuroinflammatory response in humans after traumatic brain injury. *Neuropathol. Appl. Neurobiol.* 39, 654–666. doi: 10.1111/nan.12008

Song, D., Zhang, X., Chen, J., Liu, X., Xue, J., Zhang, L., et al. (2019). Wnt canonical pathway activator TWS119 drives microglial anti-inflammatory activation and facilitates neurological recovery following experimental stroke. *J. Neuroinflammation* 16:256. doi: 10.1186/s12974-019-1660-8

Sun, D., Colello, R. J., Daugherty, W. P., Kwon, T. H., McGinn, M. J., Harvey, H. B., et al. (2005). Cell proliferation and neuronal differentiation in the dentate gyrus in juvenile and adult rats following traumatic brain injury. *J. Neurotrauma* 22, 95–105. doi: 10.1089/neu.2005.22.95

Sun, J.-D., Li, X.-M., Liu, J.-L., Li, J., and Zhou, H. (2020). Effects of miR-150-5p on cerebral infarction rats by regulating the Wnt signaling pathway via p53. *Eur. Rev. Med. Pharmacol. Sci.* 24, 3882–3891. doi: 10.26355/eurrev_202004_20854

Suryawanshi, A., Manoharan, I., Hong, Y., Swafford, D., Majumdar, T., Taketo, M. M., et al. (2015). Canonical Wnt Signaling in Dendritic Cells Regulates

Th1/Th17 Responses and Suppresses Autoimmune Neuroinflammation. *J. Immunol.* 194, 3295–3304. doi: 10.4049/jimmunol.1402691

Sussman, E. S., and Connolly, E. S. (2013). Hemorrhagic transformation: a review of the rate of hemorrhage in the major clinical trials of acute ischemic stroke. *Front. Neurol.* 4:69. doi: 10.3389/fneur.2013.00069

Swafford, D., and Manicassamy, S. (2016). Wnt signaling in dendritic cells: its role in regulation of immunity and tolerance. *Discov. Med.* 19, 303–310.

Takanari, H., Yosida, T., Morita, J., Izutsu, K., and Ito, T. (1990). Instability of pleomorphic tubulin paracrystals artificially induced by Vinca alkaloids in tissue-cultured cells. *Biol. Cell* 70, 83–90. doi: 10.1016/0248-4900(90)90363-8

Thom, S. R. (2009). Oxidative stress is fundamental to hyperbaric oxygen therapy. *J. Appl. Physiol.* 106, 988–995. doi: 10.1152/japplphysiol.91004.2008

Tran, K. A., Zhang, X., Predescu, D., Huang, X., Machado, R. F., Göthert, J. R., et al. (2016). Endothelial β-catenin signaling is required for maintaining adult blood-brain barrier integrity and central nervous system homeostasis. *Circulation* 133, 177–186. doi: 10.1161/CIRCULATIONAHA.115.015982

Ueba, Y., Aratake, T., Onodera, K.-I., Higashi, Y., Hamada, T., Shimizu, T., et al. (2018). Attenuation of zinc-enhanced inflammatory M1 phenotype of microglia by peridinin protects against short-term spatial-memory impairment following cerebral ischemia in mice. *Biochem. Biophys. Res. Commun.* 507, 476–483. doi: 10.1016/j.bbrc.2018.11.067

Urrea, C., Castellanos, D. A., Sagen, J., Tsoulfas, P., Bramlett, H. M., and Dietrich, W. D. (2007). Widespread cellular proliferation and focal neurogenesis after traumatic brain injury in the rat. *Restor. Neurol. Neurosci.* 25, 65–76.

Van Steenwinckel, J., Schang, A.-L., Krishnan, M. L., Degos, V., Delahaye-Duriez, A., Bokobza, C., et al. (2019). Decreased microglial Wnt/β-catenin signalling drives microglial pro-inflammatory activation in the developing brain. *Brain* 142, 3806–3833. doi: 10.1093/brain/awz319

Varela-Nallar, L., Grabowski, C. P., Alfaro, I. E., Alvarez, A. R., and Inestrosa, N. C. (2009). Role of the Wnt receptor Frizzled-1 in presynaptic differentiation and function. *Neural Dev.* 4:41. doi: 10.1186/1749-8104-4-41

Veeman, M. T., Axelrod, J. D., and Moon, R. T. (2003). A second canon. Functions and mechanisms of beta-catenin-independent Wnt signaling. *Dev. Cell* 5, 367–377. doi: 10.1016/s1534-5807(03)00266-1

Vest, R. S., O'Leary, H., Coultrap, S. J., Kindy, M. S., and Bayer, K. U. (2010). Effective post-insult neuroprotection by a novel Ca(2+)/ calmodulin-dependent protein kinase II (CaMKII) inhibitor. *J. Biol. Chem.* 285, 20675–20682. doi: 10.1074/jbc.M109.088617

Volonté, C., Apolloni, S., Skaper, S. D., and Burnstock, G. (2012). P2X7 receptors: channels, pores and more. *CNS Neurol. Disord. Drug Targets* 11, 705–721. doi: 10.2174/187152712803581137

Wan, S., Zhan, R., Zheng, S., Hua, Y., and Xi, G. (2009). Activation of c-Jun N-terminal kinase in a rat model of intracerebral hemorrhage: the role of iron. *Neurosci. Res.* 63, 100–105. doi: 10.1016/j.neures.2008.10.013

Wang, G., Li, Z., Li, S., Ren, J., Suresh, V., Xu, D., et al. (2019). Minocycline Preserves the Integrity and Permeability of BBB by Altering the Activity of DKK1–Wnt Signaling in ICH Model. *Neuroscience* 415, 135–146. doi: 10.1016/j.neuroscience.2019.06.038

Wang, H., Liu, T., and Malbon, C. C. (2006). Structure-function analysis of Frizzleds. *Cell. Signal.* 18, 934–941. doi: 10.1016/j.cellsig.2005.12.008

Wang, J., Chen, T., and Shan, G. (2017). miR-148b regulates proliferation and differentiation of neural stem cells via Wnt/β-Catenin signaling in rat ischemic stroke model. *Front. Cell. Neurosci.* 11:329. doi: 10.3389/fncel.2017.00329

Wang, L., Geng, J., Qu, M., Yuan, F., Wang, Y., Pan, J., et al. (2020). Oligodendrocyte precursor cells transplantation protects blood-brain barrier in a mouse model of brain ischemia via Wnt/β-catenin signaling. *Cell Death Dis.* 11:9. doi: 10.1038/s41419-019-2206-9

Wang, Q. M., and Liao, J. K. (2012). ROCKs as immunomodulators of stroke. *Expert Opin. Ther. Targets* 16, 1013–1025. doi: 10.1517/14728222.2012.715149

Wang, W., Li, M., Wang, Y., Li, Q., Deng, G., Wan, J., et al. (2016). GSK-3β inhibitor TWS119 attenuates rtPA-induced hemorrhagic transformation and activates the Wnt/β-catenin signaling pathway after acute ischemic stroke in rats. *Mol. Neurobiol.* 53, 7028–7036. doi: 10.1007/s12035-015-9607-2

Wang, X., Tsuji, K., Lee, S.-R., Ning, M., Furie, K. L., Buchan, A. M., et al. (2004). Mechanisms of hemorrhagic transformation after tissue plasminogen activator reperfusion therapy for ischemic stroke. *Stroke* 35, 2726–2730. doi: 10.1161/01.STR.0000143219.16695.af

Wang, Y., Bao, D.-J., Xu, B., Cheng, C.-D., Dong, Y.-F., Wei, X., et al. (2019). Neuroprotection mediated by the Wnt/Frizzled signaling pathway in early brain injury induced by subarachnoid hemorrhage. *Neural Regen. Res.* 14, 1013–1024. doi: 10.4103/1673-5374.250620

Wang, Z.-G., Cheng, Y., Yu, X.-C., Ye, L.-B., Xia, Q.-H., Johnson, N. R., et al. (2016). bFGF protects against blood-brain barrier damage through junction protein regulation via PI3K-Akt-Rac1 pathway following traumatic brain injury. *Mol. Neurobiol.* 53, 7298–7311. doi: 10.1007/s12035-015-9583-6

Wei, C., Luo, Y., Peng, L., Huang, Z., and Pan, Y. (2020). Expression of Notch and Wnt/β-catenin signaling pathway in acute phase severe brain injury rats and the effect of exogenous thyroxine on those pathways. *Eur. J. Trauma Emerg. Surg.* doi: 10.1007/s00068-020-01359-4 [Epub ahead of print].

Wei, Z. Z., Zhang, J. Y., Taylor, T. M., Gu, X., Zhao, Y., and Wei, L. (2018). Neuroprotective and regenerative roles of intranasal Wnt-3a administration after focal ischemic stroke in mice. *J. Cereb. Blood Flow Metab.* 38, 404–421. doi: 10.1177/0271678X17702669

Wen, Z., Mei, B., Li, H., Dou, Y., Tian, X., Shen, M., et al. (2017). P2X7 participates in intracerebral hemorrhage-induced secondary brain injury in rats via MAPKs signaling pathways. *Neurochem. Res.* 42, 2372–2383. doi: 10.1007/s11064-017-2257-1

White, B. D., Nathe, R. J., Maris, D. O., Nguyen, N. K., Goodson, J. M., Moon, R. T., et al. (2010). Beta-catenin signaling increases in proliferating NG2+ progenitors and astrocytes during post-traumatic gliogenesis in the adult brain. *Stem Cells* 28, 297–307. doi: 10.1002/stem.268

Willert, K., and Nusse, R. (2012). Wnt proteins. *Cold Spring Harb. Perspect. Biol.* 4:a007864. doi: 10.1101/cshperspect.a007864

Wright, J. A., Wadsworth, P. F., and Stewart, M. G. (1990). Neuron-specific enolase immunoreactivity in rat and mouse phaeochromocytomas. *J. Comp. Pathol.* 102, 475–478. doi: 10.1016/s0021-9975(08)80168-5

Wu, C., Chen, J., Chen, C., Wang, W., Wen, L., Gao, K., et al. (2015). Wnt/β-catenin coupled with HIF-1α/VEGF signaling pathways involved in galangin neurovascular unit protection from focal cerebral ischemia. *Sci. Rep.* 5:16151. doi: 10.1038/srep16151

Wu, H., Lu, D., Jiang, H., Xiong, Y., Qu, C., Li, B., et al. (2008). Simvastatin-mediated upregulation of VEGF and BDNF, activation of the PI3K/Akt pathway, and increase of neurogenesis are associated with therapeutic improvement after traumatic brain injury. *J. Neurotrauma* 25, 130–139. doi: 10.1089/neu.2007.0369

Wu, H., Mahmood, A., Qu, C., Xiong, Y., and Chopp, M. (2012). Simvastatin attenuates axonal injury after experimental traumatic brain injury and promotes neurite outgrowth of primary cortical neurons. *Brain Res.* 1486, 121–130. doi: 10.1016/j.brainres.2012.09.039

Wu, J., Li, J., Hu, H., Liu, P., Fang, Y., and Wu, D. (2012). Rho-kinase inhibitor, fasudil, prevents neuronal apoptosis via the Akt activation and PTEN inactivation in the ischemic penumbra of rat brain. *Cell. Mol. Neurobiol.* 32, 1187–1197. doi: 10.1007/s10571-012-9845-z

Wu, K.-J., Yu, S., Lee, J.-Y., Hoffer, B., and Wang, Y. (2017). Improving neurorepair in stroke brain through endogenous neurogenesis-enhancing drugs. *Cell Transplant.* 26, 1596–1600. doi: 10.1177/0963689717721230

Wu, X., Mao, H., Liu, J., Xu, J., Cao, J., Gu, X., et al. (2013). Dynamic change of SGK expression and its role in neuron apoptosis after traumatic brain injury. *Int. J. Clin. Exp. Pathol.* 6, 1282–1293.

Xi, G., Keep, R. F., and Hoff, J. T. (2006). Mechanisms of brain injury after intracerebral haemorrhage. *Lancet Neurol.* 5, 53–63. doi: 10.1016/S1474-4422(05)70283-0

Xing, Y., Zhang, X., Zhao, K., Cui, L., Wang, L., Dong, L., et al. (2012). Beneficial effects of sulindac in focal cerebral ischemia: a positive role in Wnt/β-catenin pathway. *Brain Res.* 1482, 71–80. doi: 10.1016/j.brainres.2012.08.057

Xiong, Y., Mahmood, A., and Chopp, M. (2010). Angiogenesis, neurogenesis and brain recovery of function following injury. *Curr. Opin. Investig. Drugs* 11, 298–308.

Xiong, Y., Mahmood, A., and Chopp, M. (2013). Animal models of traumatic brain injury. *Nat. Rev. Neurosci.* 14, 128–142. doi: 10.1038/nrn3407

Xu, Y., Nowrangi, D., Liang, H., Wang, T., Yu, L., Lu, T., et al. (2020). DKK3 attenuates JNK and AP-1 induced inflammation via Kremen-1 and DVL-1 in mice following intracerebral hemorrhage. *J. Neuroinflammation* 17:130. doi: 10.1186/s12974-020-01794-5

Yang, J., Zhao, Y., Zhang, L., Fan, H., Qi, C., Zhang, K., et al. (2018). RIPK3/MLKL-Mediated Neuronal Necroptosis Modulates the M1/M2 Polarization of Microglia/Macrophages in the Ischemic Cortex. *Cereb. Cortex* 28, 2622–2635. doi: 10.1093/cercor/bhy089

Yatsushige, H., Yamaguchi, M., Zhou, C., Calvert, J. W., and Zhang, J. H. (2005). Role of c-Jun N-terminal kinase in cerebral vasospasm after experimental subarachnoid hemorrhage. *Stroke* 36, 1538–1543. doi: 10.1161/01.STR.0000170713.22011.c8

Yatsushige, H., Yamaguchi-Okada, M., Zhou, C., Calvert, J. W., Cahill, J., Colohan, A. R. T., et al. (2008). Inhibition of c-Jun N-terminal kinase pathway attenuates cerebral vasospasm after experimental subarachnoid hemorrhage through the suppression of apoptosis. *Acta Neurochir. Suppl.* 104, 27–31. doi: 10.1007/978-3-211-75718-5_6

Ye, X., Wang, Y., Cahill, H., Yu, M., Badea, T. C., Smallwood, P. M., et al. (2009). Norrin, frizzled-4, and Lrp5 signaling in endothelial cells controls a genetic program for retinal vascularization. *Cell* 139, 285–298. doi: 10.1016/j.cell.2009.07.047

Yi, R., Xiao-Ping, G., and Hui, L. (2015). Atorvastatin prevents angiotensin II-induced high permeability of human arterial endothelial cell monolayers via ROCK signaling pathway. *Biochem. Biophys. Res. Commun.* 459, 94–99. doi: 10.1016/j.bbrc.2015.02.076

Yu, F., Wang, Z., Tanaka, M., Chiu, C.-T., Leeds, P., Zhang, Y., et al. (2013). Posttrauma cotreatment with lithium and valproate: reduction of lesion volume, attenuation of blood-brain barrier disruption, and improvement in motor coordination in mice with traumatic brain injury. *J. Neurosurg.* 119, 766–773. doi: 10.3171/2013.6.JNS13135

Yu, F., Wang, Z., Tchantchou, F., Chiu, C.-T., Zhang, Y., and Chuang, D.-M. (2012a). Lithium Ameliorates Neurodegeneration, Suppresses Neuroinflammation, and Improves Behavioral Performance in a Mouse Model of Traumatic Brain Injury. *J. Neurotrauma* 29, 362–374. doi: 10.1089/neu.2011.1942

Yu, F., Zhang, Y., and Chuang, D.-M. (2012b). Lithium reduces BACE1 overexpression, β amyloid accumulation, and spatial learning deficits in mice with traumatic brain injury. *J. Neurotrauma* 29, 2342–2351. doi: 10.1089/neu.2012.2449

Zhan, L., Liu, D., Wen, H., Hu, J., Pang, T., Sun, W., et al. (2019). Hypoxic postconditioning activates the Wnt/β-catenin pathway and protects against transient global cerebral ischemia through Dkk1 Inhibition and GSK-3β inactivation. *FASEB J.* 33, 9291–9307. doi: 10.1096/fj.201802633R

Zhang, D., Lu, Z., Man, J., Cui, K., Fu, X., and Yu, L. (2019). Wnt-3a alleviates neuroinflammation after ischemic stroke by modulating the responses of microglia/macrophages and astrocytes. *Int. Immunopharmacol.* 75:105760.

Zhang, J. Y., Lee, J. H., Gu, X., Wei, Z. Z., Harris, M. J., Yu, S. P., et al. (2018). Intranasally delivered Wnt3a improves functional recovery after traumatic brain injury by modulating autophagic, apoptotic, and regenerative pathways in the mouse brain. *J. Neurotrauma* 35, 802–813. doi: 10.1089/neu.2016.4871

Zhang, L., and Wang, H. (2018). Autophagy in traumatic brain injury: a new target for therapeutic intervention. *Front. Mol. Neurosci.* 11:190. doi: 10.3389/fnmol.2018.00190

Zhang, L., Yan, R., Zhang, Q., Wang, H., Kang, X., Li, J., et al. (2013). Survivin, a key component of the Wnt/β-catenin signaling pathway, contributes to traumatic brain injury-induced adult neurogenesis in the mouse dentate gyrus. *Int. J. Mol. Med.* 32, 867–875. doi: 10.3892/ijmm.2013.1456

Zhang, Q.-G., Wang, R., Khan, M., Mahesh, V., and Brann, D. W. (2008). Role of Dickkopf-1, an antagonist of the Wnt/beta-catenin signaling pathway, in estrogen-induced neuroprotection and attenuation of tau phosphorylation. *J. Neurosci.* 28, 8430–8441. doi: 10.1523/JNEUROSCI.2752-08.2008

Zhang, Y.-M., Dai, Q., Chen, W., Jiang, S., Chen, S., Zhang, Y.-J., et al. (2016). Effects of acupuncture on cortical expression of Wnt3a, β-catenin and Sox2 in a rat model of traumatic brain injury. *Acupunct. Med.* 34, 48–54. doi: 10.1136/acupmed-2014-010742

Zhao, H., Zhang, X., Dai, Z., Feng, Y., Li, Q., Zhang, J. H., et al. (2016). P2X7 receptor suppression preserves blood-brain barrier through inhibiting RhoA activation after experimental intracerebral hemorrhage in rats. *Sci. Rep.* 6:23286. doi: 10.1038/srep23286

Zhao, J., Zhou, D., Guo, J., Ren, Z., Zhou, L., Wang, S., et al. (2006). Effect of fasudil hydrochloride, a protein kinase inhibitor, on cerebral vasospasm and delayed cerebral ischemic symptoms after aneurysmal subarachnoid hemorrhage. *Neurol. Med. Chir.* 46, 421–428. doi: 10.2176/nmc.46.421

Zhao, J., Zhou, D., Guo, J., Ren, Z., Zhou, L., Wang, S., et al. (2011). Efficacy and safety of fasudil in patients with subarachnoid hemorrhage: final results of a randomized trial of fasudil versus nimodipine. *Neurol. Med. Chir.* 51, 679–683. doi: 10.2176/nmc.51.679

Zhao, M.-L., Chen, S.-J., Li, X.-H., Wang, L.-N., Chen, F., Zhong, S.-J., et al. (2018). Optical depolarization of DCX-expressing cells promoted cognitive recovery and maturation of newborn neurons via the Wnt/β-Catenin Pathway. *J. Alzheimers Dis.* 63, 303–318. doi: 10.3233/JAD-180002

Zhao, S., Fu, J., Liu, X., Wang, T., Zhang, J., and Zhao, Y. (2012). Activation of Akt/GSK-3beta/beta-catenin signaling pathway is involved in survival of neurons after traumatic brain injury in rats. *Neurol. Res.* 34, 400–407. doi: 10.1179/1743132812Y.0000000025

Zhao, Y., Gibb, S. L., Zhao, J., Moore, A. N., Hylin, M. J., Menge, T., et al. (2016). Wnt3a, a protein secreted by mesenchymal stem cells is neuroprotective and promotes neurocognitive recovery following traumatic brain injury. *Stem Cells* 34, 1263–1272. doi: 10.1002/stem.2310

Zhao, Y., Wei, Z. Z., Zhang, J. Y., Zhang, Y., Won, S., Sun, J., et al. (2017). GSK-3β inhibition induced neuroprotection, regeneration, and functional recovery after intracerebral hemorrhagic stroke. *Cell Transplant.* 26, 395–407. doi: 10.3727/096368916X694364

Zhao, Y., and Xu, J. (2020). Sanggenon C ameliorates cerebral ischemia-reperfusion injury by inhibiting inflammation and oxidative stress through regulating RhoA-ROCK signaling. *Inflammation* 43, 1476–1487. doi: 10.1007/s10753-020-01225-w

Zheng, J., Dai, Q., Han, K., Hong, W., Jia, D., Mo, Y., et al. (2020). JNK-IN-8, a c-Jun N-terminal kinase inhibitor, improves functional recovery through suppressing neuroinflammation in ischemic stroke. *J. Cell. Physiol.* 235, 2792–2799. doi: 10.1002/jcp.29183

Zheng, J., Liu, Z., Li, W., Tang, J., Zhang, D., and Tang, X. (2016). Lithium posttreatment confers neuroprotection through glycogen synthase kinase-3β inhibition in intracerebral hemorrhage rats. *J. Neurosurg.* 127, 716–724.

Zhou, J., Cheng, P., Youn, J.-I., Cotter, M. J., and Gabrilovich, D. I. (2009). Notch and wingless signaling cooperate in regulation of dendritic cell differentiation. *Immunity* 30, 845–859. doi: 10.1016/j.immuni.2009.03.021

Zhou, K., Enkhjargal, B., Xie, Z., Sun, C., Wu, L., Malaguit, J., et al. (2018). Dihydrolipoic acid inhibits lysosomal rupture and NLRP3 through LAMP1/CaMKII/TAK1 pathways after subarachnoid hemorrhage in rat. *Stroke* 49, 175–183. doi: 10.1161/STROKEAHA.117.018593

Zhou, L., Deng, L., Chang, N. B., Dou, L., and Yang, C. X. (2014). Cell apoptosis and proliferation in rat brains after intracerebral hemorrhage: role of Wnt/β-catenin signaling pathway. *Turk. J. Med. Sci.* 44, 920–927.

Zhou, X., Zhou, J., Li, X., Guo, C., Fang, T., and Chen, Z. (2011). GSK-3β inhibitors suppressed neuroinflammation in rat cortex by activating autophagy in ischemic brain injury. *Biochem. Biophys. Res. Commun.* 411, 271–275. doi: 10.1016/j.bbrc.2011.06.117

Zhou, Y., Shao, A., Yao, Y., Tu, S., Deng, Y., and Zhang, J. (2020). Dual roles of astrocytes in plasticity and reconstruction after traumatic brain injury. *Cell Commun. Signal.* 18:62. doi: 10.1186/s12964-020-00549-2

Zhou, Y., Wang, Y., Tischfield, M., Williams, J., Smallwood, P. M., Rattner, A., et al. (2014). Canonical WNT signaling components in vascular development and barrier formation. *J. Clin. Invest.* 124, 3825–3846. doi: 10.1172/JCI76431

Zhu, W., Chi, N., Zou, P., Chen, H., Tang, G., and Zhao, W. (2017). Effect of docosahexaenoic acid on traumatic brain injury in rats. *Exp. Ther. Med.* 14, 4411–4416. doi: 10.3892/etm.2017.5054

Zhu, W., Ding, Y., Kong, W., Li, T., and Chen, H. (2018). Docosahexaenoic Acid (DHA) provides neuroprotection in traumatic brain injury models via activating Nrf2-ARE Signaling. *Inflammation* 41, 1182–1193. doi: 10.1007/s10753-018-0765-z

Zhu, W., Zhao, L., Li, T., Xu, H., Ding, Y., and Cui, G. (2019). Docosahexaenoic acid ameliorates traumatic brain injury involving JNK-mediated Tau

phosphorylation signaling. *Neurosci. Res.* doi: 10.1016/j.neures.2019.07.008 [Epub ahead of print].

Zhu, Z., Guo, D., Zhong, C., Wang, A., Xie, X., Xu, T., et al. (2019). Serum Dkk-1 (Dickkopf-1) is a potential biomarker in the prediction of clinical outcomes among patients with acute ischemic stroke. *Arterioscler. Thromb. Vasc. Biol.* 39, 285–293. doi: 10.1161/ATVBAHA.118.311960

Zhu, Z.-F., Wang, Q.-G., Han, B.-J., and William, C. P. (2010). Neuroprotective effect and cognitive outcome of chronic lithium on traumatic brain injury in mice. *Brain Res. Bull.* 83, 272–277. doi: 10.1016/j.brainresbull.2010.07.008

Zou, F., Xu, J., Fu, H., Cao, J., Mao, H., Gong, M., et al. (2013). Different functions of HIPK2 and CtBP2 in traumatic brain injury. *J. Mol. Neurosci.* 49, 395–408. doi: 10.1007/s12031-012-9906-2

Zuo, S., Ge, H., Li, Q., Zhang, X., Hu, R., Hu, S., et al. (2017). Artesunate protected blood-brain barrier via sphingosine 1 phosphate receptor 1/phosphatidylinositol 3 kinase pathway after subarachnoid hemorrhage in rats. *Mol. Neurobiol.* 54, 1213–1228. doi: 10.1007/s12035-016-9732-6

Conflict of Interest: The authors declare that the research was conducted in the absence of any commercial or financial relationships that could be construed as a potential conflict of interest.

frontiers in Physiology

ORIGINAL RESEARCH
published: 26 October 2020
doi: 10.3389/fphys.2020.575598

Increased Immunosignals of Collagen IV and Fibronectin Indicate Ischemic Consequences for the Neurovascular Matrix Adhesion Zone in Various Animal Models and Human Stroke Tissue

Dominik Michalski[1†], Emma Spielvogel[1,2†], Joana Puchta[2,3], Willi Reimann[1,2], Henryk Barthel[4], Björn Nitzsche[4,5], Bianca Mages[6], Carsten Jäger[2], Henrik Martens[7], Anja K. E. Horn[8], Stefan Schob[3] and Wolfgang Härtig[2]*

[1]Department of Neurology, University of Leipzig, Leipzig, Germany, [2]Paul Flechsig Institute for Brain Research, University of Leipzig, Leipzig, Germany, [3]Department of Neuroradiology, University of Leipzig, Leipzig, Germany, [4]Department of Nuclear Medicine, University of Leipzig, Leipzig, Germany, [5]Institute of Anatomy, Histology and Embryology, Faculty of Veterinary Medicine, University of Leipzig, Leipzig, Germany, [6]Institute of Anatomy, University of Leipzig, Leipzig, Germany, [7]Synaptic Systems GmbH, Göttingen, Germany, [8]Institute of Anatomy and Cell Biology I and German Center for Vertigo and Balance Disorders, Ludwig-Maximilians-University, Munich, Germany

OPEN ACCESS

Edited by:
Jean-luc Morel,
Centre National de la Recherche Scientifique (CNRS), France

Reviewed by:
Roxana Octavia Carare,
University of Southampton, United Kingdom
Gautam Bhave,
Vanderbilt University, United States

***Correspondence:**
Dominik Michalski
dominik.michalski@medizin.uni-leipzig.de

†These authors have contributed equally to this work

Specialty section:
This article was submitted to Vascular Physiology, a section of the journal Frontiers in Physiology

Received: 23 June 2020
Accepted: 23 September 2020
Published: 26 October 2020

Citation:
Michalski D, Spielvogel E, Puchta J, Reimann W, Barthel H, Nitzsche B, Mages B, Jäger C, Martens H, Horn AKE, Schob S and Härtig W (2020) Increased Immunosignals of Collagen IV and Fibronectin Indicate Ischemic Consequences for the Neurovascular Matrix Adhesion Zone in Various Animal Models and Human Stroke Tissue. Front. Physiol. 11:575598. doi: 10.3389/fphys.2020.575598

Ischemic stroke causes cellular alterations in the "neurovascular unit" (NVU) comprising neurons, glia, and the vasculature, and affects the blood-brain barrier (BBB) with adjacent extracellular matrix (ECM). Limited data are available for the zone between the NVU and ECM that has not yet considered for neuroprotective approaches. This study describes ischemia-induced alterations for two main components of the neurovascular matrix adhesion zone (NMZ), i.e., collagen IV as basement membrane constituent and fibronectin as crucial part of the ECM, in conjunction with traditional NVU elements. For spatio-temporal characterization of these structures, multiple immunofluorescence labeling was applied to tissues affected by focal cerebral ischemia using a filament-based model in mice (4, 24, and 72 h of ischemia), a thromboembolic model in rats (24 h of ischemia), a coagulation-based model in sheep (2 weeks of ischemia), and human autoptic stroke tissue (3 weeks of ischemia). An increased fibronectin immunofluorescence signal demarcated ischemia-affected areas in mice, along with an increased collagen IV signal and BBB impairment indicated by serum albumin extravasation. Quantifications revealed a region-specific pattern with highest collagen IV and fibronectin intensities in most severely affected neocortical areas, followed by a gradual decline toward the border zone and non-affected regions. Comparing 4 and 24 h of ischemia, the subcortical fibronectin signal increased significantly over time, whereas neocortical areas displayed only a gradual increase. Qualitative analyses confirmed increased fibronectin and collagen IV signals in ischemic areas from all tissues and time points investigated. While the increased collagen IV signal was restricted to vessels, fibronectin appeared diffusely arranged in the parenchyma

with focal accumulations associated to the vasculature. Integrin α_5 appeared enriched in the vicinity of fibronectin and vascular elements, while most of the non-vascular NVU elements showed complementary staining patterns referring to fibronectin. This spatio-temporal characterization of ischemia-related alterations of collagen IV and fibronectin in various stroke models and human autoptic tissue shows that ischemic consequences are not limited to traditional NVU components and the ECM, but also involve the NMZ. Future research should explore more components and the pathophysiological properties of the NMZ as a possible target for novel neuroprotective approaches.

Keywords: stroke, fibronectin, collagen IV, basement membrane, blood-brain barrier, extracellular matrix

INTRODUCTION

Despite enormous efforts concerning a more detailed understanding of pathophysiological mechanisms, ischemic stroke often leads to long-term disability and is still ranging among the three most common causes of death worldwide (Benjamin et al., 2018; Campbell et al., 2019). On the cellular level, excitotoxicity, apoptosis, and inflammation were identified as mechanisms contributing to the ischemia-related tissue damage in a complex time- and region-dependent manner (Dirnagl et al., 1999). Notwithstanding the emerging knowledge on stroke pathophysiology, the development of neuroprotective approaches is rather challenging (Young et al., 2007; Endres et al., 2008). Especially in the era of modern techniques for the recanalization of occluded brain vessels, i.e., intravenous thrombolysis (Hacke et al., 2018) and endovascular treatment (Goyal et al., 2016), additional neuroprotective approaches are needed to facilitate neuronal survival and to reduce bleeding complications.

More than 10 years ago, a group of regionally and functionally associated cells were termed as the "neurovascular unit" (NVU) in order to learn more than their roles and interplay during stroke evolution. Thus, the NVU consists of neurons, astrocytes, oligodendrocytes, microglia, the vasculature with its endothelium, and other cell types (Lo et al., 2003; del Zoppo, 2009, 2010; Iadecola, 2017). Over time, multiple ischemia-associated affections of NVU components were detected (e.g., Härtig et al., 2009; Michalski et al., 2010, 2018; Aleithe et al., 2019; Mages et al., 2019; Kestner et al., 2020). Furthermore, the blood-brain barrier (BBB) attracted interest as a highly dynamic part of the NVU (Yang et al., 2019). Away from the simplified perspective of a layer separating the blood from the brains' parenchyma, the BBB rather represents a complex structure with endothelial cells and basement membranes as its main components (Dyrna et al., 2013). Especially in the setting of stroke, endothelial cells are believed to have a pivotal role in BBB integrity as the leakage of blood-sourced substances was found *via* a transendothelial route together with morphological features like an endothelial swelling (Krueger et al., 2013, 2015, 2019). Overall, abnormalities within the NVU with a consecutive impairment of the BBB integrity are known to increase the risk for secondary hemorrhage associated with recanalizing therapies, and thus critically impact the patients' outcome (Yang and Rosenberg, 2011).

In addition to cellular alterations described in experimental studies, ischemia also affects the extracellular matrix (ECM; Härtig et al., 2017), which is known to have several properties concerning local hemostasis and neuronal function (Soleman et al., 2013). Among the subsumed non-cellular structures, the basement membrane is of special interest because of its close vicinity to the endothelial layer, leading to the assumption of an involvement in regulatory processes within the NVU and thus the BBB integrity (Reed et al., 2019; Xu et al., 2019). In addition to the proteins laminin, nidogen, and heparan sulfate proteoglycans, especially collagen isoforms with predominant collagen IV represent main components of the basement membranes (Thomsen et al., 2017; Gatseva et al., 2019). In this context, integrins were identified as transmembrane proteins with the two subunits α and β linking the endothelial layer with the basement membrane (del Zoppo and Milner, 2006). Considering their special location, integrins can be seen as a connection between the vascular part of the NVU and the adjacent ECM, formerly described in terms of a vascular matrix adhesion complex (del Zoppo et al., 2006). Not surprisingly, integrins might have an important role in BBB stabilization also in the setting of stroke (Guell and Bix, 2014; Edwards and Bix, 2019). From the variety of ECM proteins, especially fibronectin, which provides a fibrillar matrix around cells (White et al., 2008; Singh et al., 2010), was perceived as highly reactive against ischemic stimuli (Edwards and Bix, 2019). Based on a modular composition and different domains, fibronectin interacts with other ECM proteins including other fibronectin molecules and also cell surface receptors (Singh et al., 2010; Mezzenga and Mitsi, 2019). Regarding the dynamic processes within the NVU and the associated ECM, fibronectin appears unique as its complex arrangement is mediated by integrins and other receptors located at the surface of for instance endothelial cells (Mao and Schwarzbauer, 2005; del Zoppo and Milner, 2006).

Overall, both the basement membrane and associated ECM proteins represent structures outside the cell-based NVU perspective that may sensitively react in the setting of ischemia. The few available data in the field indicated alterations of collagen IV and fibronectin after experimental stroke (Hamann et al., 1995), while simultaneous reactions of fibronectin and integrins were observed after focal (Huang et al., 2015) and

global cerebral ischemia (Milner et al., 2008). Further, fibronectin serum levels of stroke patients were associated with hemorrhage as a typical complication following thrombolysis (Castellanos et al., 2004, 2007), suggesting an involvement in BBB dysregulations also in humans. However, additional data on these structures, not necessarily captured by the traditional NVU concept, are needed to generate a hypothesis regarding their functional relevance.

Therefore, the present study aims to explore ischemic consequences for the neurovascular matrix adhesion zone (NMZ) with a special focus on collagen IV as part of the basement membrane and adjacent fibronectin as part of the ECM. To consider potential spatio-temporal effects, quantitative analyses focused on diverse brain regions and different durations of ischemia after experimental stroke in mice. For translational issues, confirmatory analyses included experimental focal cerebral ischemia in rats, sheep, and human stroke tissue.

MATERIALS AND METHODS

Study Design

Various combinations of fluorescence labeling were applied to explore ischemic consequences to the basement membrane and its regionally associated ECM including fibronectin and integrin α_5 in conjunction with diverse components of the NVU, i.e., neurons, oligodendrocytes, micro- and astroglia as well as the vasculature. Details on the used brain tissues and models of focal cerebral ischemia are given below. Analyses were primarily focused on an ischemia duration of 4 h ($n = 6$) and 24 h ($n = 8$) in the mouse model, also used for quantification of collagen IV and fibronectin ($n = 6$ for 4 h, $n = 5$ for 24 h). Confirmative and thus qualitative analyses include an ischemia duration of 72 h in mice ($n = 2$), 24 h in rats ($n = 3$), and 2 weeks in sheep ($n = 6$) as well as 3 weeks in human stroke ($n = 1$). The reporting followed the ARRIVE guidelines for experimental research including animals (Kilkenny et al., 2010).

Animal experiments were carried out in accordance with the European Union Directive 2010/63/EU and the German guideline for care and use of laboratory animals. They had been approved by the Regierungspräsidium Leipzig as local authority (reference numbers: TVV 02/17 for mice and rats, and TVV 56/15 for sheep). For the reporting of histopathological findings in the human sections, prior consent was obtained as described by Kattah et al. (2017).

Experimental Focal Cerebral Ischemia in Rodents

Adult male C57Bl/6J mice with a bodyweight of about 25 g, obtained by Charles River (Sulzfeld, Germany), underwent a filament-based model for permanent right-sided middle cerebral artery occlusion as originally described by Longa et al. (1989) with minor modifications (Hawkes et al., 2013). In brief, right-sided cervical arteries were carefully exposed while using an operation microscope. A standardized silicon-coated 6-0 monofilament (Doccol Corporation, Redlands, CA, United States) was inserted into the internal carotid artery and moved forward until bending was observed or resistance was felt (approximately 9 mm from carotid bifurcation). To induce permanent ischemia, the filament was left in place, and the skin was closed with a surgical suture. Mice were sacrificed at the end of an observation period of 4, 24, or 72 h after ischemia induction.

In adult male Wistar rats with a bodyweight of about 300 g, also provided by Charles River, a thromboembolic model was applied to obtain right-sided middle cerebral artery occlusion as originally described by Zhang et al. (1997) with minor modifications (Michalski et al., 2010). In brief, following the careful exposure of right-sided cervical arteries with an operation microscope, a polyethylene tube with tapered end was introduced into the external carotid artery and moved forward through the internal carotid artery (approximately 16 mm from carotid bifurcation). At this position, a rat blood-sourced clot was injected. Afterwards the catheter was removed, and the skin was closed with a surgical suture. Rats were sacrificed at the end of a 24-h observation period from ischemia induction.

In general, for surgical procedures, mice and rats were anesthetized using about 2–2.5% isoflurane (Isofluran Baxter, Baxter, Unterschleißheim, Germany; mixture 70% N_2O/30% O_2) with a commercial vaporizer (VIP 3000, Matrix, New York, United States) and received a complex pain medication. During surgical procedures, a thermostatically controlled warming pad with rectal probe (Fine Science Tools, Heidelberg, Germany) was used to prevent anesthesia-associated cooling, and the body temperature was kept stable at around 37°C. Sufficient induction of focal cerebral ischemia was ensured by the evaluation of individual neurobehavioral deficits, while animals had to present a score of at least 2 on the Menzies score (Menzies et al., 1992), ranging from 0 (no neuronal deficit) to 4 (spontaneous contralateral circling), which represents a pre-defined study inclusion criterion.

Experimental Focal Cerebral Ischemia in Sheep

In male adult sheep (hornless Merino) with a bodyweight about 70 kg, provided by the Veterinary Faculty of Leipzig University (Lehr- und Versuchsgut Leipzig, Germany), middle cerebral artery occlusion was surgically induced as described by Nitzsche et al. (2016) and Boltze et al. (2008). Briefly, the left temporal bone was carefully exposed, and here, a trepanation with a 6 mm barrel burr at 10,000 rpm (Aesculap microspeed uni, Scil Animal Care Company GmbH, Viernheim, Germany) was performed. The dura mater was incised, and the middle cerebral artery was occluded at the distal M1 segment by electrosurgical coagulation using neurosurgical bipolar forceps (ME 411, KLS Martin, Tuttlingen, Germany). Finally, the dura mater was repositioned while muscles and the skin were sewed with surgical sutures. Sheep were sacrificed after an observation period of 2 weeks from ischemia induction.

For surgical procedure, sheep were anesthetized by an intravenous injection of ketamine (4 mg/kg body weight; Ketamin, Medistar, Holzwicke, Germany), xylazine (0.1 mg/kg body weight; Xylazin, Ceva Sante Animal GmbH, Düsseldorf,

Germany), and diazepam (0.2 mg/kg body weight; Temmler Pharma GmbH, Marburg, Germany). Mechanical ventilation with 2% isoflurane and 40% oxygen (Primus, Dräger AG, Lübeck, Germany) allowed anesthesia during surgery. At the end of surgery, sheep were treated with the antibiotic enrofloxacin (5% Baytril, Bayer AG, Leverkusen, Germany) and the analgesic butorphanol (Alvegesic 1%; CP-pharm, Burgdorf, Germany). The presence of cerebral infarctions was confirmed by MRI.

Human Stroke Tissue

Post-mortem brain tissue affected by an ischemic stroke was originally provided by Jorge C. Kattah (Department of Neurology, University of Illinois, College of Medicine, Peoria, IL, United States) in collaboration with Anja K.E. Horn (Institute of Anatomy and Cell Biology I, University of Munich, Germany). In detail, the autoptic brainstem sections contained ischemia-affected areas of the lateral medulla from a 61-year-old male who passed away 3 weeks after onset of stroke. Further data on the analyzed brain tissue and stroke characterization were summarized by Horn and co-workers in Kattah et al. (2017).

Tissue Preparation

For fluorescence labeling, rodents were transcardially perfused after the respective observation period with saline and 4% phosphate-buffered paraformaldehyde (PFA). Brains were carefully removed from the skull and post-fixed in PFA overnight, followed by equilibration with 30% phosphate-buffered sucrose for a few days. Subsequently, forebrains from rodents were serially cut with a freezing microtome (Leica SM 2000R, Leica Biosystems, Wetzlar, Germany). Thereby, 10 series of 30 µm-thick sections each were collected.

Brains from sacrificed sheep were divided by producing about 10 mm thick slices. After their photo-documentation, each slice was immersion-fixed by 4% buffered formaldehyde for 14 days at 4°C and thereafter equilibrated in 30% phosphate-buffered sucrose. The immersion-fixed tissue blocs were consecutively cut at 40 µm thickness using a freezing microtome (Microm HM 430, Thermo Fisher Scientific, Waltham, MA, United States).

Until histochemical processing, sections from rodents and sheep were stored at 4°C in vials filled with 0.1M Tris-buffered saline (TBS), pH 7.4, containing sodium azide.

Human brain tissue was cut into 5 mm thick slices, fixed by formaldehyde and embedded in paraffin, further sectioned at 5 µm thickness and mounted onto microscope slides. For histochemistry, sections were deparaffinized in xylene and rehydrated in graded alcohols. Antigen retrieval was performed with 0.1M citrate buffer, pH 6, for 15 min in a water bath at 90°C.

Histochemistry

Prior to all histological procedures, free-floating sections were extensively rinsed with TBS. All staining procedures started by blocking non-specific binding sites for subsequently applied immunoreagents with 5% normal donkey serum in TBS containing 0.3% Triton X-100 (NDS-TBS-T) for 1 h. Sections were then incubated for 20 h with mixtures of primary antibodies and biotinylated lectins – diluted in the blocking solution – as listed in **Table 1**. for all procedures, including goat-anti-collagen IV and rabbit-anti-fibronectin. Thereafter, sections were rinsed with TBS followed by incubation with mixtures of appropriate fluorochromated secondary immunoreagents [20 µg/ml TBS containing 2% bovine serum albumin (TBS-BSA); Dianova, Hamburg, Germany] according to **Table 1**.

TABLE 1 | Triple fluorescence staining: marker combinations concomitantly applied with Cy3-stained rabbit-anti-fibronectin*.

First primary antibodies	First visualizing immunoreagents	Second primary antibodies or lectins	Second visualizing immunoreagents
sheep-anti-serum albumin (1:500; Serotec)	Cy2-donkey-anti-goat IgG	biotinylated LEA (20 µg/ml; Vector, Burlingame, CA, United States)	Cy5-streptavidin
goat-anti-collagen IV (1:100; Merck Millipore, Billerica, CA, United States)	Cy2-donkey-anti-goat IgG	biotinylated LEA (20 µg/ml; Vector)	Cy5-streptavidin
guinea pig-anti-NeuN (1:200; Synaptic Systems; Göttingen, Germany)	Cy2-donkey-anti-guinea pig IgG	biotinylated STL (20 µg/ml; Vector)	Cy5-streptavidin
guinea pig-anti-CNP (1:200; Synaptic Systems)	Cy2-donkey-anti-guinea pig IgG	biotinylated STL (20 µg/ml; Vector)	Cy5-streptavidin
guinea pig-anti-Iba (1:100; Synaptic Systems)	Cy2-donkey-anti-guinea pig IgG	biotinylated STL (20 µg/ml; Vector)	Cy5-streptavidin
guinea pig-anti-GFAP (1:200; Synaptic Systems)	Cy2-donkey-anti-guinea pig IgG	biotinylated STL (20 µg/ml; Vector)	Cy5-streptavidin
guinea pig-anti-GFAP (1:300; Synaptic Systems)	Cy2-donkey-anti-guinea pig IgG	biotinylated STL (20 µg/ml; Vector)	Cy5-streptavidin
goat-anti-collagen IV (1:100; Merck Millipore)	Cy2-donkey-anti- goat-IgG	guinea pig-anti-GFAP (1:200; Synaptic Systems)	Cy5-donkey-anti-guinea pig IgG
guinea pig-anti-AQP4 (1:100; Merck Millipore)	Cy2-donkey-anti-guinea pig IgG	goat-anti-collagen IV (1:100; Merck Millipore)	AlexaFluor647-donkey-anti-goat IgG

**Primary antibody: rabbit-anti-fibronectin (1:600, formerly AbD Serotec, Oxford, UK – now Bio-Rad, Munich, Germany); visualizing immunoreagent: Cy3-donkey-anti-rabbit IgG. All fluorescent immunoreagents were obtained from Dianova (Hamburg, Germany) and used at 20 µg/ml. LEA, biotinylated Lycopersicon esculentum agglutinin (= tomato lectin); STL, Solanum tuberosum agglutinin (= potato lectin); NeuN, neuronal nuclei; CNP, 2',3' cyclic nucleotide phosphodiesterase; Iba, ionized calcium binding adapter molecule-1; GFAP, glial fibrillary acidic protein; AQP4, aquaporin-4.*

Additionally, sections from mice were blocked with NDS-TBS-T and processed for 20 h with an antibody cocktail consisting of sheep-anti-fibronectin (R&D Systems, Minneapolis, MN, United States; AF 1918, 1:200 in NDS-TBS-T), rabbit-anti-integrin α_5 (Abcam, Cambridge, UK; ab221606, 1:100), and guinea pig-anti-glial fibrillary acidic protein (GFAP; Synaptic Systems, Göttingen, Germany; 1:200). After extensive rinses with TBS tissues were incubated for 1 h with a cocktail of Cy3-donkey-anti-goat IgG (highly cross-reacting with sheep IgG), Cy2-donkey-anti-rabbit IgG, and Cy5-donkey-anti-guinea pig IgG (all from Dianova; 20 µg/ml TBS-BSA).

In a first set of control experiments, the omission of primary antibodies or biotinylated lectins resulted in the expected absence of cellular labeling. Additional controls were the switch of fluorophores related to the concomitantly detected markers producing no alterations of their stainability. Moreover, immunolabeling of fibronectin with rabbit-anti-fibronectin from Serotec (4470-4339) that was used in the present study (and is now available from Bio-Rad, Munich, Germany) produced nearly the same staining patterns as sheep-anti-fibronectin (R&D) and rabbit-anti-fibronectin from Abcam (ab2413).

Finally, all free-floating sections were extensively rinsed with TBS and briefly with distilled water, mounted onto glass slides, air-dried, and coverslipped with Entellan in toluene (Merck, Darmstadt, Germany). In parallel, stained human paraffin sections underwent a Sudan black B post-treatment for 10 min to quench their autofluorescence. These sections were coverslipped with glycerol gelatin (Sigma, Taufkirchen, Germany).

Microscopy, Image Processing, and Quantification of Fluorescence Signals

For the subsequent imaging process of selected brain regions with different magnifications, the microscope Biorevo BZ-9000 (Keyence, Neu-Isenburg, Germany) was used. Panels of micrographs were generated with Microsoft PowerPoint (Office 365, Version 2018; Microsoft Corp., Redmond, WA, United States). If necessary, brightness and contrast of micrographs were slightly adjusted without the deletion or creation of signals.

Quantitative analyses of the immunofluorescence signals from collagen IV and fibronectin were based on five brain sections from each mouse, while these sections were selected concerning the following criteria: first, an unequivocal ischemic affection as indicated by a regional change of the fluorescence signal typically located in the right-sided neocortex and subcortical areas as known from own earlier studies (e.g., Mages et al., 2018), and second, the absence of tissue damage that prevents immunofluorescence-based analyses in large parts of the ischemia-affected hemisphere. This selection process allowed the analysis of six mice with an ischemia duration of 4 h and five mice with an ischemia duration of 24 h. As prerequisite for the following quantification, in each of the selected brain sections, seven regions of interests (ROIs) were arranged on the ischemia-affected hemisphere including six neocortical ROIs covering the ischemic border zone with most evident changes of the collagen IV immunosignal between ROIs 3 and 4, and a further ROI (number 7) in the subcortex, i.e., the striatum. For control measurements, seven additional ROIs were mirrored on the contralateral, non-affected hemisphere. This method collectively results in 14 ROIs per brain section, while each ROI was captured with a single image using a 40x objective on the Biorevo microscope. The exposure time was routinely adjusted at the level of each section to avoid overexposure, and at the same time, to allow inter-hemispheric comparison. This technique resulted in usually 70 images from each animal, but due to porous infarct material in one mouse, only 60 images were available. Overall, 760 images from 11 mice were included in quantitative analyses.

Immunofluorescence signals of fibronectin were captured by mean values in the obtained images from each ROI using ImageJ (National Institutes of Health, Bethesda, MD, United States). As measuring method for collagen IV, the maximum immunosignal intensity was used to consider the strongly vessel-associated signal that was accompanied by a visually darker background on the affected hemisphere compared to the contralateral side. Finally, rounded mean values of the obtained fluorescence signals of collagen IV and fibronectin were calculated for every ROI of the five sections at the level of each animal. Further calculations included both an inter-hemispheric comparison with reference to ROIs along the ischemic border zone in the neocortex and the striatum in the overall sample, as well as differences between the ischemia- and non-affected hemispheres used for analyses concerning potential time-dependent effects in respective subgroups.

Statistical Analyses

The SPSS software package version 24 (IBM SPSS Statistics for Windows, IBM Corp., Armonk, NY, United States) was used for descriptive analyses and testing concerning statistical significance between groups. Because of the relatively small sample size, non-parametric tests were applied, i.e., the Wilcoxon test and the Mann-Whitney *U* test. To consider multiple testing, the Bonferroni-Holm correction was added to these tests. Further, Pearson correlation coefficients (r) were used to explore statistical relationships between parameters, added by a calculation of the explained variance (r^2). Generally, a value of $p < 0.05$ (if applicable after correction for multiple testing) was considered as statistically significant.

RESULTS

Ischemic Consequences to the Vascular Integrity and Extracellular Matrix

Twenty-four hours of focal cerebral ischemia in mice resulted in a critical affection of the BBB integrity as visualized by an extravasation of serum albumin into the parenchyma in ischemic areas (left upper part in **Figure 1A**), whereas no albumin extravasation was visible in non-affected areas. Concerning the vasculature, lectin-based staining with the tomato lectin (*Lycopersicon esculentum* agglutinin, LEA) showed a homogeneous pattern of vessels in ischemia- and non-affected areas (**Figures 1A**",**B**'). While addressing collagen IV as a major component of basement membranes, an increased and strongly

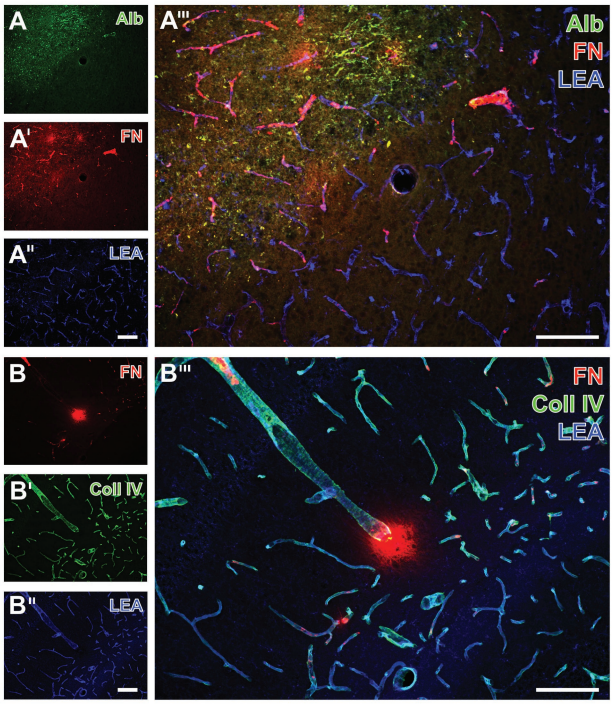

FIGURE 1 | Fluorescence-based visualization of impaired blood-brain barrier integrity with vascular elements as well as collagen IV and fibronectin in mice subjected to 24 h of focal cerebral ischemia. Extravasation of (endogenous) serum albumin (Alb, **A**) into brains' parenchyma is visible in conjunction with an increased immunosignal of fibronectin (FN, **A'**) as a component of the extracellular matrix (ECM). FN also appears in close vicinity to collagen IV (Coll IV, **B'**) as part of the basement membrane 24 h after ischemia onset. FN is thereby visible in the striatum **(A)** and the hippocampus **(B)**. In the area of ischemia, immunosignals for Alb **(A)** and fibronectin **(A',B)** are associated with endothelia, as detected by the lectin-staining with LEA **(A'',B'')**, and are visible within the adjoining neuropil in a carpet-like manner. Ischemia-affected tissue selectively exhibits a strong immunosignal for Coll IV **(B')**. The overlay of staining patterns clearly reveals the border of ischemic affection **(A''')** and different forms of vessel-associated focal condensation of FN. Scale bars: in **A'''** and **B'''** = 100 μm, in **A''** (also valid for **A** and **A'**) and **B''** (also valid for **B** and **B'**) = 100 μm.

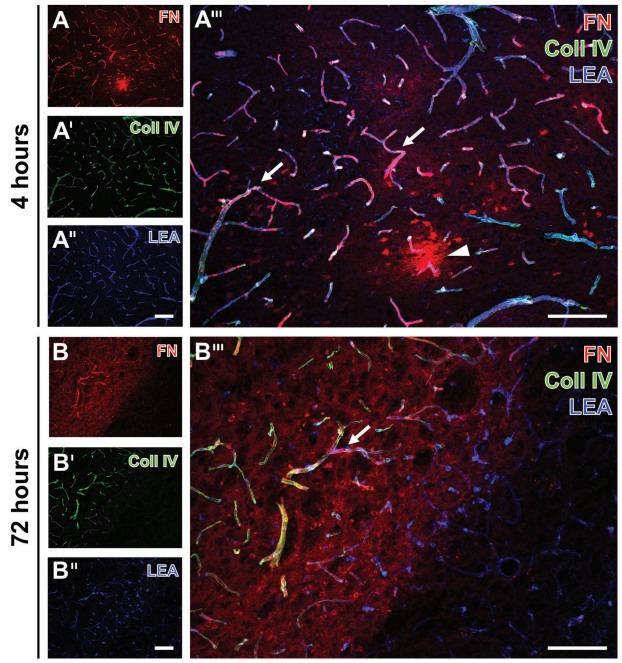

FIGURE 2 | Fluorescence-based detection of collagen IV and fibronectin combined with vessel staining in mice subjected to 4 and 72 h of experimental focal cerebral ischemia. Increased immunosignals of fibronectin (FN) and collagen IV (Coll IV) are visible at both 4 **(A)** and 72 h **(B)** of ischemia in affected areas. At both time points, FN consistently appears associated with the vasculature (arrows in **A'''** and **B'''**) and in a diffuse manner with focal accumulations (arrow head in **A'''**) in close vicinity to vessels. Concomitantly, increased Coll IV immunosignals precisely demarcate the area of ischemic affection **(B')**, which becomes even clearer when merging the staining patterns of FN and Coll IV **(B''')**. Thereby, overlapping signals of FN and Coll IV becomes visible by the purple color **(A''',B''')**. Lectin-based counterstaining using LEA visualizes the vasculature also in ischemic areas **(A'',B'')**. Scale bars: in **A'''** and **B'''** = 100 μm, in **A''** (also valid for **A** and **A'**) and **B''** (also valid for **B** and **B'**) = 100 μm.

vessel-associated immunosignal became evident in areas affected by ischemia (**Figures 1B',B'''**). Concerning fibronectin as part of the ECM, an increased immunosignal was routinely observed in ischemia-affected areas (**Figures 1A',A'''**) with both a strongly vessel-associated pattern and a diffuse appearance in close vicinity to the vasculature not necessarily overlapping with cellular structures (**Figures 1A''',B'''**). These fluorescence-based staining patterns of collagen IV and fibronectin were consistently found in ischemia-affected subcortical, i.e., the striatum, and hippocampal areas (**Figures 1A,B**), as well as the ipsilateral neocortex (not shown).

To explore potential time-dependent alterations, analyses were extended to ischemic tissues from mice subjected to 4 and 72 h of focal cerebral ischemia. In accordance to the findings at 24 h, increased immunosignals of collagen IV and fibronectin were found very early and also 3 days after ischemia onset (**Figure 2**). Thereby, the ischemia-affected striatum displayed an increased immunosignal of fibronectin that was associated with the vasculature as indicated by an overlapping lectin signal (arrows in **Figures 2A''',B'''**). The immunosignal of fibronectin also appeared in a diffuse pattern with some focal accumulations in close vicinity to the vasculature (arrowhead in **Figure 2A'''**). In a more general perspective, the increased fibronectin signal robustly demarcated the area of ischemia (left upper part in **Figures 2B,B'''**). As already demonstrated at 24 h after ischemia onset, lectin-based staining robustly visualized vessels also in areas not affected by ischemia (right bottom in **Figures 2B'',B'''**).

Alterations of Collagen IV and Fibronectin Depending on Brain Region and Duration of Ischemia

With the intention to verify the observed alterations in the immunosignals of collagen IV and fibronectin, quantitative analyses were focused on the ischemic border zone in the neocortex and the ischemia-affected subcortex. For this purpose, on the ischemia-affected hemisphere, six ROIs were used to capture the ischemic border zone in the neocortex, and a

further ROI was applied to capture the ischemic striatum, whereby each of the ROIs was mirrored to the contralateral, non-affected hemisphere for control issues (**Figure 3A**).

In the overall sample used for quantification of mice subjected to 4 and 24 h of focal cerebral ischemia, a gradual decrease was observed for the collagen IV immunoreactivity with a maximum signal in the area of ischemia and the most considerable step toward an immunosignal that is comparable with the non-affected hemisphere in the ischemic border zone (**Figure 3B**). Inter-hemispheric comparison led to significant differences in the first three ROIs starting in the ischemic area with value of p corrected for multiple testing between 0.021 and 0.025. When compared to the non-affected hemisphere, a similar immunosignal of collagen IV was found for the most medial ROIs, assumed

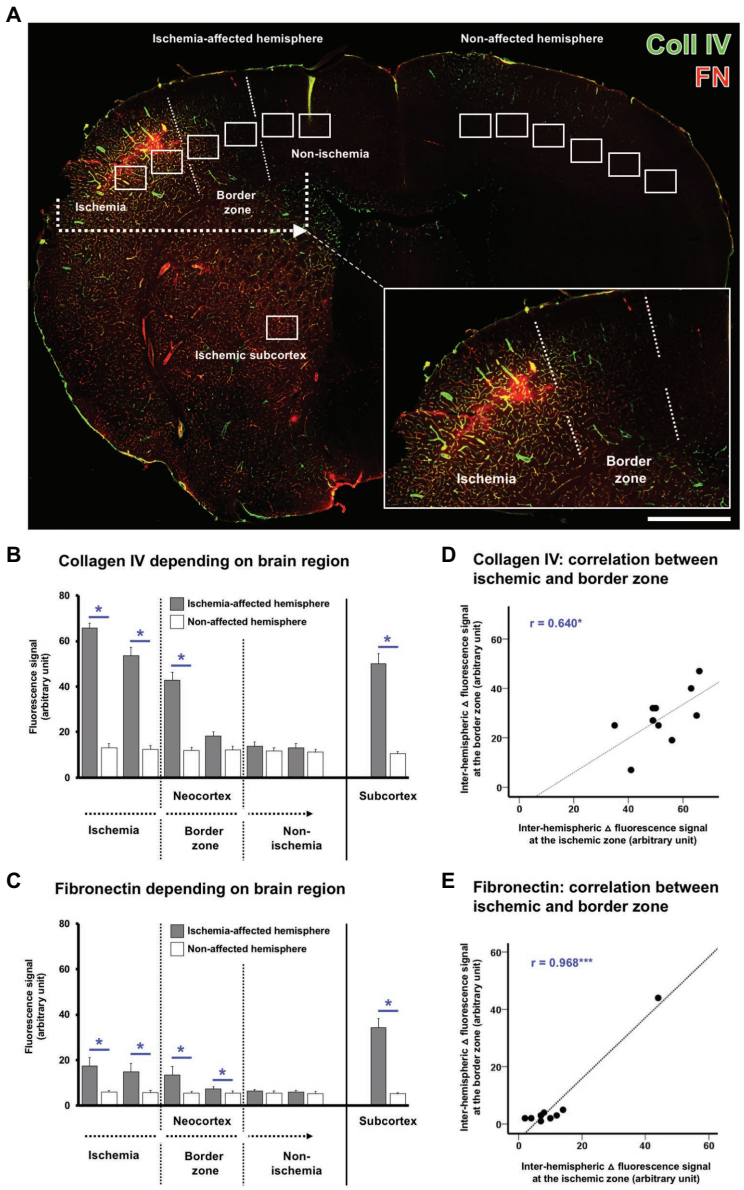

FIGURE 3 | Quantification of collagen IV and fibronectin immunosignals in the overall sample of mice subjected to 4 or 24 h of experimental focal cerebral ischemia. Region-related quantification of both immunosignals based on seven regions of interest (ROIs) located on the ischemia-affected hemisphere, while seven ROIs mirrored to the contralateral, i.e., non-affected hemisphere served as control **(A)**. The ischemia-affected neocortex is captured by six ROIs with the ischemic border zone in the middle part, and the subcortical region is captured by a single ROI **(A)**. Immunosignals of collagen IV **(B)** and fibronectin **(C)** are significantly increased in the neocortical area of maximum ischemic affection with a gradual decline toward the ischemic border zone and the non-affected region. A significantly increased immunosignal is also seen in the subcortical region **(B,C)**. Correlation plots including the area of maximum ischemic affection and the ischemic border zone indicate a strong positive correlation between these regions for the inter-hemispheric differences of collagen IV **(D)** and fibronectin **(E)** indicating commutated changes in both regions at the same time. Scale bar: in **A** = 1 mm. Bars represent means and added lines represent the standard error of means. r: Pearson correlation coefficient. Levels of statistical significance: $^{*}p < 0.05$, $^{***}p < 0.001$.

to be non-altered by ischemia. Along the ischemia-affected neocortex, the stepwise decline of collagen IV immunoreactivity was found as significant between the first (lateral, and thus most ischemia-affected) and the second ROI (p = 0.020), the second and the third ROI (p = 0.020), as well as the third and the fourth ROI (p = 0.015). Subcortically, a significantly increased collagen IV immunosignal was identified in the striatum as compared with the contralateral site (p = 0.021).

A quite similar pattern was observed for fibronectin with a gradual decrease of the immunoreactivity, starting with its maximum in the area of ischemia, and followed by a considerable step in the ischemic border zone, ultimately resulting in signals with good accordance to the non-affected hemisphere (**Figure 3C**). Inter-hemispheric comparison revealed significant differences in the first four ROIs completely covering the area of ischemia and the ischemic border zone with value of p ranging from 0.021 to 0.030. Along the ischemia-affected neocortex, the immunosignal of fibronectin declined in a stepwise manner from the first (most ischemia-affected) to the second ROI (p = 0.028) as well as from the third to the fourth ROI (p = 0.015). In the subcortical region, a significantly increased fibronectin immunosignal was found as compared to the non-affected site (p = 0.021).

Subsequent analyses addressed the correlation between different regions within the ischemia-affected neocortex to explore the statistical relationship, and thus simultaneously occurring changes beyond a single region. For both collagen IV (**Figure 3D**) and fibronectin (**Figure 3E**), a significant correlation was observed between the most severely affected ROI and the ischemic border zone, indicating commutated alterations with an explained variance of 40.9% for collagen IV and remarkable 93.7% for fibronectin.

To explore potential time-dependent effects, altered immunosignals of collagen IV and fibronectin along the ischemia-affected neocortex and the subcortex were separately analyzed for 4 and 24 h of ischemia. Thereby, the inter-hemispheric differences ($\triangle$) of the collagen IV immunosignals confirmed the gradual decline from the most-affected toward the non-affected neocortex without significant differences between the two time points (**Figure 4A**). However, in most affected neocortical regions and the subcortex, the collagen IV immunoreactivity appeared at least numerically increased 24 h after ischemia when compared to the earlier time point (value of p ranged between 0.378 and 0.568). A comparable pattern was observed for the immunosignal of fibronectin that shows a gradual decline along the ischemia-affected neocortex toward non-affected areas without a statistically significant difference between the two time points (**Figure 4B**), while a numeric increase became noticeable in areas of ischemic affection (value of p ranged between 0.120 and 0.724). Remarkably, in the ischemia-affected subcortex, the fibronectin immunoreactivity was significantly increased after 24 h of ischemia when compared to 4 h (p = 0.042).

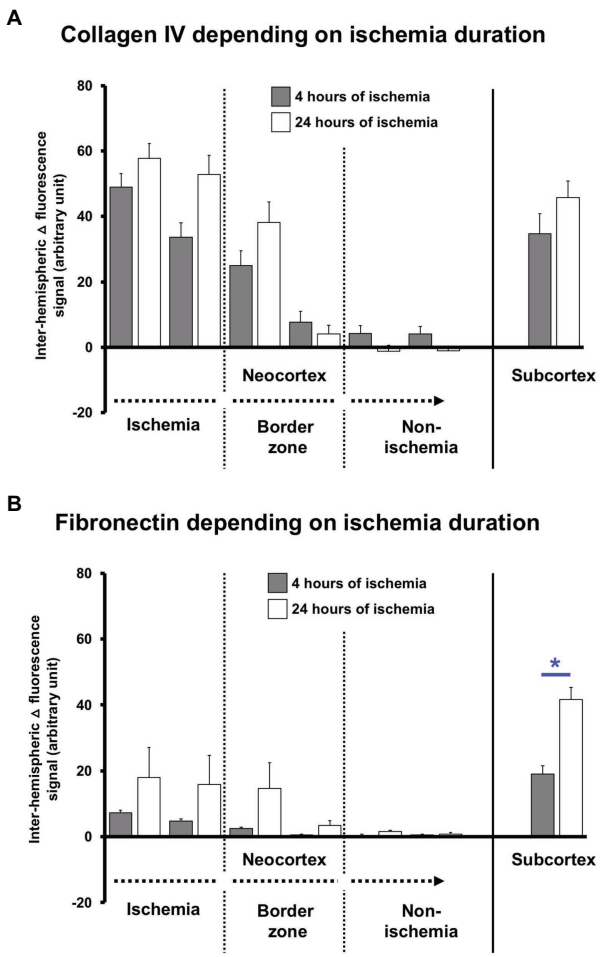

FIGURE 4 | Quantification of collagen IV and fibronectin immunosignals in mice depending on the duration (4 vs. 24 h) of experimental focal cerebral ischemia. Inter-hemispheric differences covering the immunosignals of collagen IV **(A)** and fibronectin **(B)** depending on the duration of ischemia confirms the gradual decrease of the signals along the ischemia-affected neocortex as evaluated in the overall sample. Statistically significant differences are lacking between the 4 and 24 h of ischemia in the neocortex, although a trend is visible for a pronounced signal at the later time point. In the subcortex, the immunosignal of fibronectin increased at 24 h as compared with the earlier time point. Bars represent means and added lines represent the standard error of means. Level of statistical significance: $^*p < 0.05$.

Spatial Relationships Between Fibronectin and the Neurovascular Unit

To explore spatial associations to classical components of the NVU, qualitative analyses based on multiple fluorescence labeling on tissues originating from mice subjected to 24 h of focal cerebral ischemia were added (**Figures 5, 6**).

Starting with neurons, the immunosignal of neuronal nuclei (NeuN) clearly diminished in the area of ischemic affection (left upper part in **Figure 5A'**), while that of fibronectin became visible in a diffuse manner with some focal accumulations and vascular associations. In contrast to the area not affected by ischemia with strong and regular labeling of NeuN (arrows with dashed line in **Figure 5A'''**), signs of neuronal degradation (arrows) and ultimately shrunken NeuN became visible toward the ischemic area (arrowheads in **Figure 5A'''**). Concomitant staining with *Solanum tuberosum* lectin (STL) enabled

(like the tomato lectin LEA) a robust, nearly unaltered visualization of the vasculature (**Figures 5A**",**A**'").

To address oligodendrocytes as part of the glia within the NVU, multiple fluorescence labeling was used to detect the 2',3' cyclic nucleotide phosphodiesterase (CNP) in conjunction with fibronectin and STL. While fibronectin was again found to exhibit a vessel-associated appearance as indicated by the overlapping lectin signal (purple color in **Figure 5B**'"), the ischemia-related increase of the CNP immunoreactivity was observed somewhat distant from fibronectin without evidence for overlapping structures.

As further parts of the glia network, microglia and astrocytes were visualized using the ionized calcium binding adapter molecule-1 (Iba) and GFAP concomitantly with fibronectin immunolabeling. Thereby, microglia were found to be altered with predominantly morphological features in terms of a rounded appearance of GFAP-positive structures together with an overall weakened signal in the ischemia-affected area (upper left part of **Figure 6A**'). As expected, Iba-positive microglia were found unaltered in the non-affected regions (bottom right of **Figure 6A**') as indicated by their ramified appearance. Concerning astroglia, more drastic changes became visible by a nearly disappearing GFAP immunoreactivity in the area of maximum ischemic affection (upper part of **Figure 6B**'), while morphological alterations were evident in the ischemic border zone (arrowheads in **Figure 6B**'"), and the typically branched astroglia was visible in the non-affected region (arrows in **Figure 6B**'"). Remarkably, an overlapping immunoreactivity for fibronectin as well as microglia and astroglia was not evident (**Figures 6A**'",**B**'").

Ischemic Consequences to Collagen IV and Fibronectin in Other Animal Species

With the intention to verify the identified regional arrangement of collagen IV and fibronectin as well as elements of the NVU in a translational perspective, further qualitative analyses included multiple immunofluorescence labeling on tissues originating from rats subjected to 24 h of an embolic-sourced focal cerebral ischemia (**Figures 7, 8**) and sheep subjected to

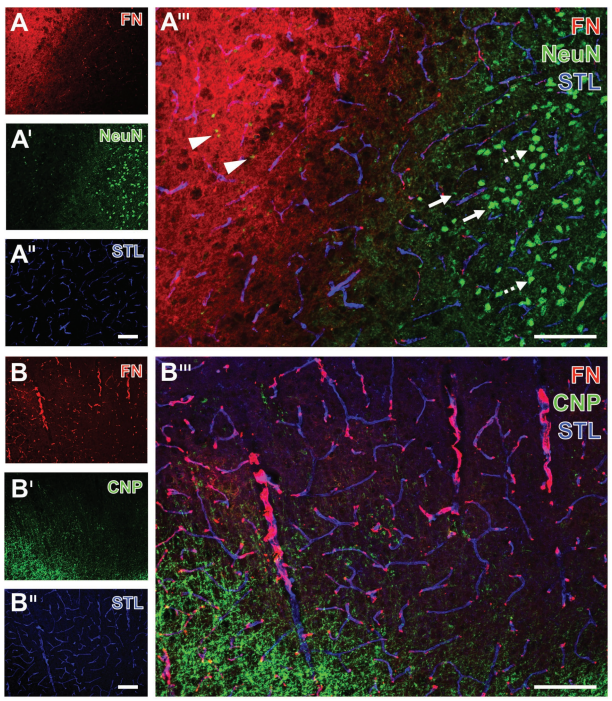

FIGURE 5 | Spatial relationships between fibronectin, the vasculature, neurons, and oligodendroglia in mice subjected to 24 h of experimental focal cerebral ischemia. Staining of fibronectin (FN, **A,B**) and striatal endothelia visualized by a lectin-based technique using *Solanum tuberosum* lectin (STL, **A",B"**) combined with the detection of neurons (NeuN, **A'**) show a regular configuration of NeuN in the non-affected area (arrows with dashed lines in **A'"**). Significant neuronal degeneration is visible toward the ischemic region with a co-occurring increase of the FN signal, starting in the ischemic border zone with shrunken NeuN (arrows in **A'"**) and passing over to the area of maximum ischemic affection with only fragments of NeuN (arrowheads in **A'"**). The concomitant visualization of oligodendroglia in the ischemia-affected neocortex reveals an increased immunosignal of the applied marker CNP **(B')**, not overlapping with FN **(B'")**. Scale bars: in **A'"** and **B'"** = 100 μm, in **A"** (also valid for **A** and **A'**) and **B"** (also valid for **B** and **B'**) = 100 μm.

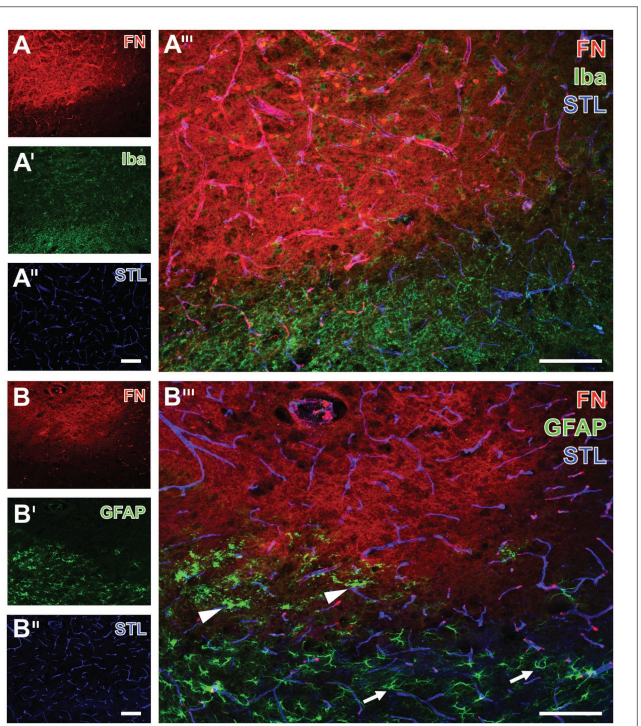

FIGURE 6 | Spatial relationships between fibronectin, the vasculature, microglia, and astrocytes in mice subjected to 24 h of experimental focal cerebral ischemia. Staining of fibronectin (FN, **A,B**) together with the lectin-based visualization of the endothelium by STL **(A",B")** and Iba **(A')** as marker for microglia indicate a mainly morphological alteration of the latter one in the ischemia-affected striatum. Toward the area of ischemia an increase of the FN signal is visible **(A)** in addition to nearly unaltered detection of vessels **(A")**. GFAP immunolabeling displays a loss of astrocytes in the striatum as the region of maximum ischemic affection **(B')** with a simultaneous increase of the FN signal **(B)**. In the ischemic border zone, astrocytes are morphologically altered (arrow heads in **B'"**) when compared to their regular appearance (arrows in **B'"**). Scale bars: in **A'"** and **B'"** = 100 μm, in **A"** (also valid for **A** and **A'**) and **B"** (also valid for **B** and **B'**) = 100 μm.

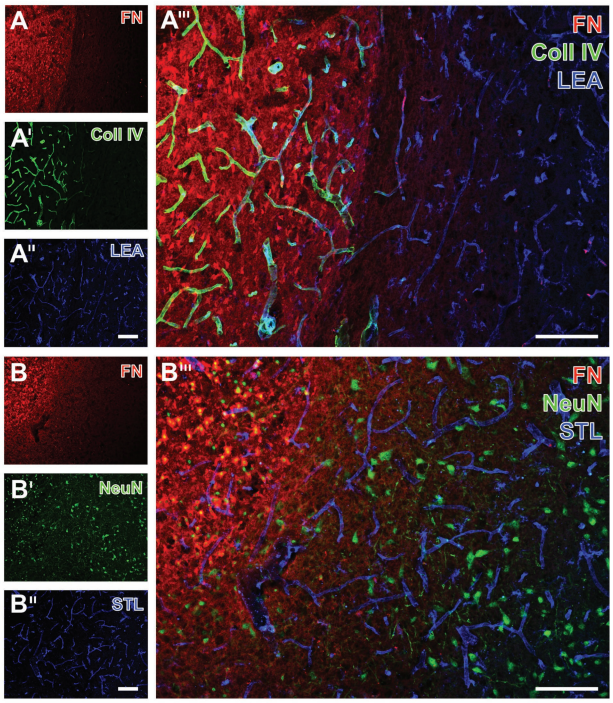

FIGURE 7 | Immunofluorescence-based visualization of fibronectin together with vasculature elements and neurons in rats subjected to 24 h of experimental focal cerebral ischemia. Detection of fibronectin (FN, **A**) in conjunction with collagen IV (Coll IV, **A'**) and neurons using NeuN **(B')** as well as the vasculature as visualized by a lectin-based technique using LEA **(A'')** and STL **(B'')** in the ischemia-affected striatum confirms concomitantly increased immunosignals of FN and Coll IV **(A''')** also in the rat, and neuronal degeneration due to ischemia by an altered NeuN staining in the affected area **(B''')**. Both LEA and STL robustly visualize vessels also in ischemic areas, although STL leads to a somewhat thinner appearance of vessels in ischemic regions **(B''')**. Scale bars: in **A'''** and **B'''** = 100 μm, in **A''** (also valid for **A** and **A'**) and **B''** (also valid for **B** and **B'**) = 100 μm.

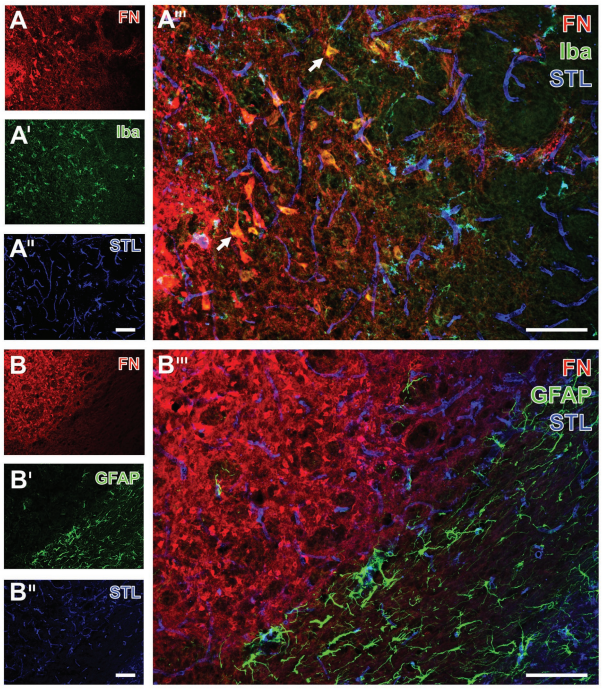

FIGURE 8 | Immunofluorescence-based visualization of microglia and astrocytes combined with fibronectin and vascular elements in rats subjected to 24 h of experimental focal cerebral ischemia. Staining of fibronectin (FN, **A,B**) and lectin-based visualization of vessels using STL **(A'',B'')** together with microglial Iba **(A')** and astroglial GFAP **(B')** confirms for the rat striatum the predominantly morphological alterations of microglia and the nearly disappearing astrocytes in ischemic regions also seen in mice. FN robustly demarcates the area of ischemia **(A,B)**, while the merge with the staining pattern originating from microglia displays an only occasional overlap with the Iba signal (arrow in **A'''**). In contrast, STL appears evenly distributed in differently affected tissue as visualized by merging the staining patterns **(A''',B''')**. Scale bars: in **A'''** and **B'''** = 100 μm, in **A''** (also valid for **A** and **A'**) and **B''** (also valid for **B** and **B'**) = 100 μm.

2 weeks of surgically induced focal cerebral ischemia (**Figure 9**). In general, the obtained data largely resembled the findings observed in the filament-based mouse model of focal cerebral ischemia as described above. They are exemplified for the striatum, while the similar data of the neocortex are not shown.

In the ischemia-affected striatum of rats, a strong collagen IV immunoreactivity was robustly found to demarcate the ischemic area that is also characterized by an enhanced fibronectin signal, appearing in a diffuse manner and some focal accumulations (left part in **Figures 7A**,**A'**). In contrast, in the area that is not affected by ischemia, the vasculature was visualized by LEA (**Figure 7A''**), whereas collagen IV immunoreactivity was widely lacking and fibronectin only displayed a considerably weakened signal toward the ischemic border zone (**Figure 7A'''**). Labeling of NeuN revealed diminished immunosignals and morphologically altered nuclei within the area of ischemic affection that was characterized by an increased fibronectin immunoreactivity (upper left part in **Figures 7B,B'**).

For the visualization of microglia and astroglia in the rat, the detection of Iba and GFAP was combined with fibronectin immunolabeling. In line with the data originating from mice, Iba immunoreactivity indicated morphologically altered microglia in the area of ischemic affection, whereas fibronectin showed increased immunosignals with focal accumulations (**Figures 8A**,**A'**). Additionally, the ischemia-affected area also displayed a few overlapping signals of fibronectin and Iba (arrows in **Figure 8A'''**). Concerning astroglia, a nearly abolished immunosignal of GFAP was observed in the ischemic area along with an increased signal for fibronectin (**Figures 8B,B'**). Thus, overlapping signals of GFAP and fibronectin were not found (**Figure 8B'''**).

To verify the observed alterations of fibronectin in a further species and to gain insights into a later time point following ischemia onset, multiple immunofluorescence labeling was applied to the ischemia-affected neocortex of sheep. At lower magnification, a strong GFAP immunoreactivity was observed at the ischemic border zone probably representing a part of the glia-based scar adjacent to the ischemic area devoid of GFAP (bottom of **Figure 9A**). Remarkably, concomitant staining of fibronectin revealed a strong immunosignal restricted to

the area of ischemia (**Figure 9A'**), whereas the STL-based staining of the vasculature – and in this case additional cells – yielded a pronounced signal toward the ischemic region and did not completely disappear in non-affected areas (**Figure 9A"**). Triple immunofluorescence labeling further showed the presence of morphologically changed ameboid Iba-positive microglia as well as round cells assumed to represent immigrated macrophages in the ischemia-affected area. This tissue was devoid of GFAP-positive astroglia but exhibited strong fibronectin immunoreactivity with both a diffuse appearance and some focal accumulations (**Figure 9B"'**). Overall, in good accordance to the above described findings in rodents, fibronectin and the GFAP-immunoreactive astroglia were found to provide a complementary staining pattern in sheep too (**Figures 9A"',B"'**).

Ischemia-Related Alterations of Collagen IV and Fibronectin in Human Stroke

Autoptic human stroke tissue was used to consider translational aspects of the observed ischemia-related alterations of fibronectin and collagen IV in rodents and sheep (**Figure 10**). In the ischemia-affected area, fibronectin was found strongly associated to vessels and their basement membranes as collagen IV immunoreactivity was regularly found to be encircled by the fibronectin signal, which became exemplarily visible in perpendicularly cut vessels (**Figures 10A,A'**). Astroglia, visualized by GFAP, were arranged farthest from the basement membrane (**Figure 10A"'**).

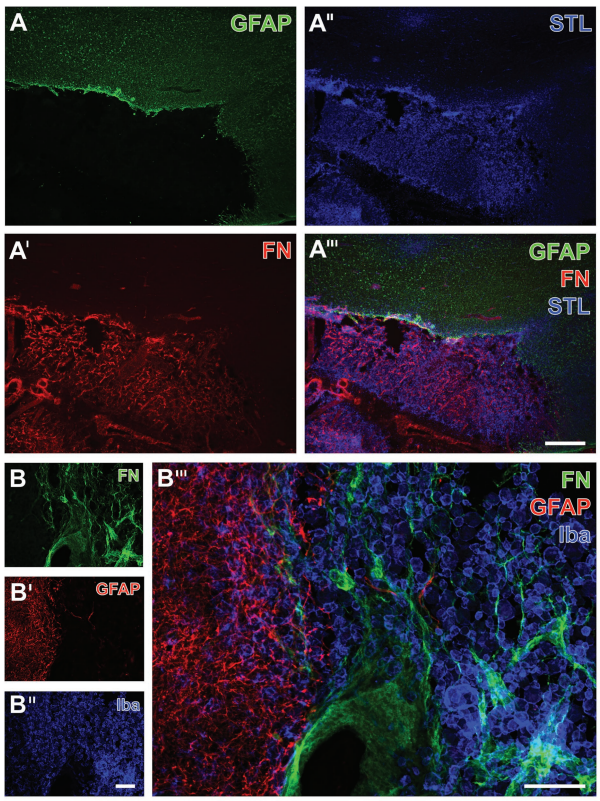

FIGURE 9 | Immunofluorescence-based detection of fibronectin, micro- and astroglia as well as the vasculature in sheep subjected to 14 days of experimental focal cerebral ischemia. Numerous astrocytes as visualized by the GFAP **(A)** with a condensation at the ischemic border zone probably indicate the expected glia scar **(A)**, which is strictly separated from the immunosignal of fibronectin (FN, **A'**) that appears in the ischemic area. As revealed by potato lectin (STL, **A"**), this area also contains several cells presumably representing macrophages in addition to endothelial structures. The overlay verifies the complementary staining patterns of FN and the GFAP-positive astroglia **(A"')**. At higher magnification, the FN immunoreactivity remains not restricted to vessels but is also visible in the surrounding tissue **(B)**; however, nearly disappearing in the area covered by GFAP-positive astroglia **(B')**, which becomes clearly visible in the overlay of staining patterns **(B"')**. Concomitant labeling with antibodies directed against Iba **(B")** visualizes microglia and mainly infiltrated macrophages in the area of ischemia affection that is immunopositive for FN **(B,B"')**. Scale bars: in **A"'** (also valid for **A**, **A'**, and **A"**) = 500 μm, in **B"'** = 100 μm, in **B"** (also valid for **B** and **B'**) = 100 μm.

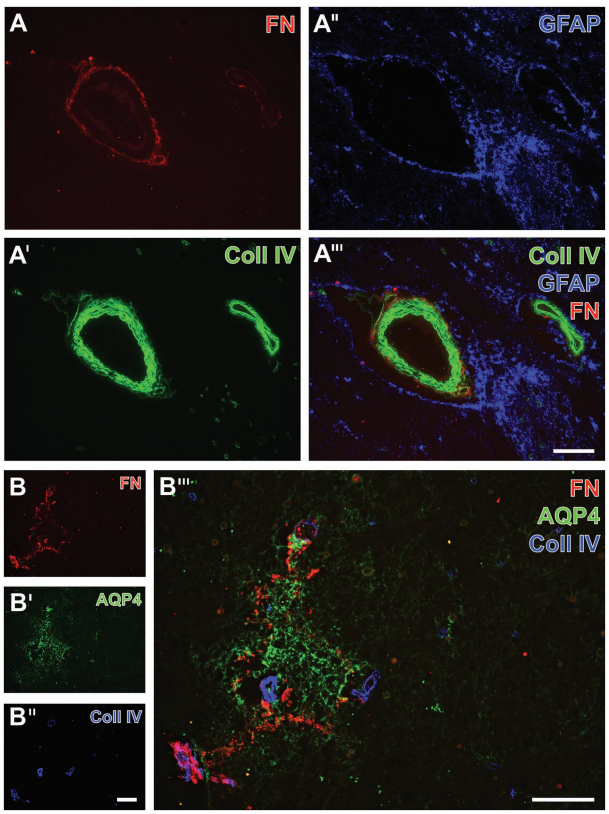

FIGURE 10 | Triple immunofluorescence labeling of fibronectin, collagen IV, and astrocytes in human autoptic tissue affected by a stroke with a post-ischemic period of 3 weeks. Staining of fibronectin (FN, **A,B**) and collagen IV (Coll IV, **A',B"**) combined with astroglial components, i.e., GFAP **(A")** located in cell bodies and AQP4 typically located in astroglial endfeet (AQP4, **B'**), reveals a shell-like pattern of FN and Coll IV in the ischemia-affected brainstem, while the FN signal is encircling Coll IV as obvious at perpendicularly cut vessels **(A"')**. In close vicinity to the vessels, diffusely labeled GFAP-containing astroglial structures are visible **(A",A"')**, not overlapping with FN or Coll IV. The AQP4 immunoreactivity appears in an inhomogeneous manner not following cellular compartments as a sign of significantly degenerated astroglial endfeet in close regional association to the ischemia-related increase of FN signal **(B"')**. Scale bars: in **A"'** (also valid for **A**, **A'**, and **A"**) = 100 μm, in **B"'** = 100 μm, in **B"** (also valid for **B** and **B"**) = 100 μm.

As an approach to explore regional associations of astrocytes as well as fibronectin and collagen IV in more detail, subsequent triple immunofluorescence labeling included aquaporin 4 as an established marker for astrocyte endfeet (**Figure 10B**). In the area of ischemia, the immunosignal of fibronectin regularly appeared in a diffuse manner with some focal accumulations (**Figure 10B**). With reference to the immunosignal of fibronectin, aquaporin-4 (AQP4)-positive astrocytic structures became visible in close regional association in the ischemic area (**Figure 10B'''**), whereas their signal appeared in a disarranged pattern indicating morphologically altered endfeet in terms of cellular degenerations.

Spatial Arrangement of Fibronectin and Integrin α_5

Given the fact that integrins are seen as connecting proteins between the endothelial layer and the ECM with its special component fibronectin, an additional approach focused on their spatial arrangement under ischemic conditions. For this purpose, triple immunofluorescence labeling, also including astroglial GFAP that has shown to demarcate the affected area, was applied to the brain tissue of a mouse subjected to filament-based focal cerebral ischemia with an observation period of 3 days (**Figure 11**). Thereby, an increased fibronectin immunoreactivity consistently appeared in the above described diffuse manner with some focal accumulations in the area of ischemic affection, whereas the GFAP-positive astroglia was mostly lacking (left bottom part of **Figure 11A**). In the area of ischemic affection, the integrin α_5 immunoreactivity appeared in a weak and diffuse pattern, while a regional accumulation was seen associated with the vasculature (**Figure 11A'**) that became even more visible at a higher magnification (arrow in **Figure 11A'''**). This magnification also confirmed the vessel-associated pattern of the fibronectin immunosignal (arrowhead in **Figure 11A'''**).

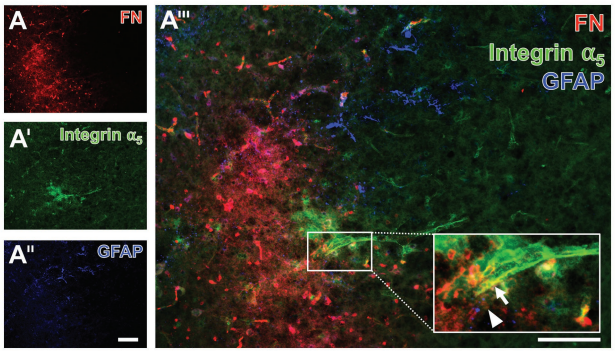

FIGURE 11 | Immunofluorescence labeling of fibronectin and associated integrin α_5 combined with the detection of astroglia in a mouse suffering from 72 h of experimental focal cerebral ischemia. Triple immunofluorescence labeling of fibronectin (FN, **A**), integrin α_5 **(A')**, and astroglia as identified by GFAP **(A'')** confirms the increased immunosignal of FN in the ischemia-affected striatum in an expanded time window of 3 days after ischemia onset. The immunosignal of GFAP-positive astrocytes is clearly diminished in the area of ischemia **(A'')**. FN and integrin α_5 appear vessel-associated, which becomes even clearer at a higher magnification (integrin α_5: arrow in **A'''**, FN: arrowhead in **A'''**). Scale bars: in **A'''** = 100 µm, in **A''** (also valid for **A** and **A'**) = 100 µm.

DISCUSSION

This study addressed ischemic consequences beyond the traditional cellular-based perspective with a special focus on the NMZ, representing the composite of NVU elements, i.e., the vasculature with its endothelium and the adjoined basement membrane, and the ECM (del Zoppo and Milner, 2006; Reed et al., 2019; Xu et al., 2019). Due to limited knowledge regarding the NMZ, neuroprotective approaches have not yet considered this structure, although a strong relationship to the integrity of the BBB with far reaching consequences is deducible already from its physical composition (del Zoppo et al., 2006).

Using multiple immunofluorescence approaches to tissues affected by different durations of focal cerebral ischemia, a spatio-temporal characterization of collagen IV as the major part of the basement membrane (Thomsen et al., 2017; Gatseva et al., 2019), and fibronectin as a major component of the ECM (Singh et al., 2010; Mezzenga and Mitsi, 2019) was performed. To consider the phenomenon of a translational roadblock in the field of stroke research that was at least partially related to artificial models (Young et al., 2007; Endres et al., 2008), efforts have been made to use different animal models with individual strengths and weaknesses (Durukan and Tatlisumak, 2007) as well as different species for this study. Having in mind that some shortcomings naturally remain, i.e., concerning the comparability of animal and human stroke data (Fisher et al., 2009; Sommer, 2017), also human tissue was included in histochemical analyses.

Histomorphological Characterization of Collagen IV and Fibronectin After Ischemia

In the present study, qualitative analyses including different ischemia models and animal species consistently demonstrated visually increased immunosignals of collagen IV and fibronectin in areas affected by focal cerebral ischemia. As expected, collagen IV was associated with the vasculature, whereas fibronectin provided a diffuse staining pattern with focal accumulations in close vicinity to vessels. This finding on collagen IV largely confirms earlier reports describing an increased immunoreactivity of collagen IV in comparable animal models of ischemia (e.g., Hawkes et al., 2013). In contrast, Hamann and co-workers demonstrated in 1995 a decrease of collagen IV due to different durations of ischemia in the non-human primate (Hamann et al., 1995). This opposite finding is likely related to the underlying measurement technique as the number of positive vessels was used as readout, quite different from the signal intensity applied in the present study. Concerning fibronectin, the present study for the first time aims to characterize ischemic consequences in a spatio-temporal manner and thus a comparison to earlier reports is rather challenging. Referring to the few available data, Milner et al. (2008) investigated mice subjected to global hypoxia up to 14 days and reported an up-regulated fibronectin on capillaries as assessed biochemically. Huang et al. (2015) used a transient model of middle cerebral artery occlusion in mice to investigate the angiogenic response after ischemia,

also including an immunofluorescence-based detection of fibronectin to count the number of positive vessels. They were found to be increased over time in the ischemic border zone (penumbra). The angiogenic response to ischemia was further investigated by Li et al. (2012) using a transient model of middle cerebral artery occlusion in mice, which led to significantly augmented fibronectin-positive vessels in the ischemic border zone.

In the present study, added quantitative analyses of immunosignals for collagen IV and fibronectin in mice revealed a significantly increased signal due to focal cerebral ischemia. With reference to regional aspects along the ischemia-affected neocortex, maximum signals were observed in the area of direct ischemia with a gradual decline toward the lesser affected ischemic border zone and the adjoined non-affected area. Significantly increased immunosignals for both collagen IV and fibronectin were observed in the ischemia-affected subcortex, i.e., the striatum. Remarkably, the ischemia-related increase in the immunoreactivities of collagen IV and fibronectin was found in a comparable manner between 4 and 24 h of ischemia, although a trend toward a numerical increase at 24 h was noted. Solely in the ischemia-affected subcortex, the immunosignal of fibronectin increased statistically over time when compared to the contralateral site.

Overall, this study identified significantly enhanced immunosignals for collagen IV and fibronectin following focal cerebral ischemia in mice, rats, sheep, and in human stroke tissue. Derived from the observed close regional association of collagen IV and fibronectin – and considering their primary locations with reference to the basement membrane and the adjoined ECM (del Zoppo and Milner, 2006; Singh et al., 2010; Gatseva et al., 2019) – this study provides robust evidence for an ischemia-induced critical affection of the NMZ. Given the fact of the assumed highly dynamic situation at this site, different patterns of the collagen IV and especially the fibronectin immunosignal would have been expected over time. Although a trend to an increasing immunoreactivity was noted toward an ischemia duration of 24 h when compared to the earlier time point of 4 h, this study revealed consistently increased immunosignals of collagen IV and fibronectin up to 3 weeks following the ischemic event as exemplarily shown by the human stroke sections.

As the present study was designed rather descriptive, a conclusion regarding the causal relationship of altered collagen IV and fibronectin immunosignals remains to be elucidated. However, some thoughts on the potential pathophysiological background might be extracted from earlier reports. Yang et al. (2007) applied a rat model of transient focal cerebral ischemia together with the application of tissue-type plasminogen activator (tPA) as a routinely used thrombolytic substance in the clinical scenario. Thereby, a decreased number of collagen IV-positive vessels were found due to ischemia, and the addition of tPA resulted in a dose-dependent decrease in the tissue content of collagen IV, fibronectin, and other markers. The authors concluded that the observed reduction of collagen IV and other basement membrane constituents reflects the tPA-mediated BBB disruption (Yang et al., 2007). This is very plausible as such BBB alterations are assumed to have a pivotal role for tPA-related bleeding complications (Ishrat et al., 2012; Zhang et al., 2012). With a special focus on fibronectin, Nicosia and co-workers identified fibronectin in cell culture experiments as a promotor for angiogenesis, whereby especially the length of microvessels was found to respond to fibronectin (Nicosia et al., 1993). Further evidence for this perspective was provided from Wang and Milner (2006) as the proliferation but not the survival of capillary endothelia cells was promoted by fibronectin in cell cultures. Consequently, based on the few available data, a role of fibronectin in angiogenesis following hypoxia appears plausible. However, the observation of the present study with an altered immunosignal as early as 4 h after the ischemic event leads to the assumption that properties of fibronectin are not limited to angiogenesis, but may also include acute damaging and long-lasting regenerative processes.

Notably, fibronectins' functional role is still a matter of debate. As for example regarding tissue regeneration, a diversity of beliefs exists ranging from an initial beneficial effect toward an impairment of regeneration in later phases (Stoffels et al., 2013). The remaining difficulties in identifying a clear pathophysiological role of fibronectin might be related to varying properties in different tissues in addition to the brain, such as the skin and the cartilage. Further, different proportions of fibronectin exons like the extra domain A and B due to alternative splicing result in up to 20 different protein variants in human (White and Muro, 2011). In addition, the situation is complicated by the fact that for fibronectin a circulating, soluble form in the plasma has been identified, which is synthesized by hepatocytes, in addition to the cellular-associated, i.e., insoluble form as part of the ECM that is synthesized for instance by endothelial cells (To and Midwood, 2011). Interestingly, Sakai et al. (2001) reported different roles for the circulating fibronectin as mice deficient for this type of fibronectin showed larger infarct areas after a transient model of focal cerebral ischemia, while dermal wound healing was not affected. In an *in vitro* experiment, the soluble fibronectin was further found to impact the formation of fibrin with more and more fibrin matrices in case of increasing fibronectin concentrations (Ramanathan and Karuri, 2014). Circulating fibronectin is thus believed to have a pivotal role on clot formations (To and Midwood, 2011), which is supported by detected fibronectin in proteomic analyses of thrombi that were evacuated by endovascular treatment in human stroke (Muñoz et al., 2018). Additional data on circulating fibronectin recently emerged from an experimental study by Dhanesha et al. (2019): by applying a filament- and clot-based stroke model these authors were able to demonstrate that mice deficient for the fibronectin containing the extra domain A exhibited a decreased thrombo-inflammatory response. Such a reaction is typically linked to secondary thrombosis due to ischemia, which likely represent the key mechanism for the also perceived smaller infarct sizes and improved neurobehavioral deficits. Consistently, several inflammatory processes – as one of the major mechanisms for stroke-related tissue damage (Dirnagl et al., 1999) – were identified in an earlier study applying genetically altered mice including an alternatively spliced extra domain A (Khan et al., 2012). However, a variety of

mainly *in vitro* experiments pointed out the complexity of alternatively spliced isoforms of fibronectin, each of them with distinct properties concerning chemokines and other signaling molecules (White et al., 2008).

Although several studies have focused on fibronectin that measured in the plasma of stroke patients, the currently available data does not support their use for distinguishing between ischemic and hemorrhagic stroke (Bustamante et al., 2017), nor to identify patients for recanalizing treatments (Rodríguez-Yáñez et al., 2011). Basically, a more comprehensive perspective seems reasonable understanding fibronectin as part of the brains' ECM embedded in a complex network of cells related to the NVU. This perspective is supported by studies that identified serum markers of the NVU like GFAP, allowing insights into local processes of the ischemia-affected brain (e.g., Perry et al., 2019).

Spatial Relationships Between Collagen IV, Fibronectin, and the Neurovascular Unit

In the present study, elements of the NVU were addressed by multiple fluorescence labeling based on a variety of antibodies, which have proved their usability in previous studies, in conjunction with collagen IV and fibronectin to explore spatial relationships. In detail, the vasculature was visualized by lectin-histochemistry, while immunolabeling revealed neurons by NeuN, oligodendrocytes by CNP, microglia by Iba, astrocytes by GFAP as well as their endfeet by AQP4.

Overall, the ischemia-induced affections of the NVU elements shown in this study largely confirmed earlier reports from the own group (e.g., Michalski et al., 2010; Härtig et al., 2017; Mages et al., 2019) and others (e.g., Mullen et al., 1992; Matsumoto et al., 2007). With a special focus on collagen IV and fibronectin, both were found without an overlapping signal for astrocytes as indicated by the complementary staining patterns with disappearing astrocytes toward the area of ischemia. At the border zone, morphological features of astrocytes were observed in good accordance to an astrocyte scar formation known for several brain injuries (Anderson et al., 2016; Dias and Göritz, 2018), which was also visible in our study after 2 weeks of focal cerebral ischemia in sheep. Such scar formations are of great interest concerning regenerative aspects. Especially, collagen IV was identified to be involved in the resulting inhibition of for example axon growth (Stichel et al., 1999; Hermanns et al., 2001). The present work revealed fibronectin in the area of ischemia that was only occasionally associated with microglia, whereas overlapping signals of fibronectin and neuronal structures were not unequivocally evident.

Notably, the present study elucidated a close regional association with vessels not only as expected for collagen IV but also for fibronectin that was consistently observed in the applied animal models and human stroke tissue. Qualitative analyses at higher magnification showed that the collagen IV immunoreactivity is encircled by the fibronectin signal in excellent accordance to the concept of the here addressed NMZ. With an additional focus on the regionally associated endothelial cells that were discussed to have a pivotal role in BBB integrity (Krueger et al., 2015), integrins as connecting elements of the endothelial layer and the adjacent basement membrane as well as ECM are of special interest (del Zoppo and Milner, 2006; Edwards and Bix, 2019). In the present study, integrin α_5 was observed in close regional association to the vasculature together with fibronectin. Referring to the time course of BBB opening following focal cerebral ischemia, integrins associated with endothelial cells were found to be also time-dependently expressed (Huang et al., 2015). Thereby, the observed integrin α_5 immunoreactivity 3 days after ischemia in the present study appears in good accordance with the described peak of integrin α_5 at day 4 (Guell and Bix, 2014). With regard to functional consequences of changed integrin levels, the few available reports indicated a relationship to angiogenesis. In detail, Li et al. (2010) applied a mouse model of chronic global hypoxia and a cell culture experiment with endothelial cells to investigate integrins by immunofluorescence labeling and western blot analysis. They observed an increased integrin α_5 expression on angiogenic brain endothelial cells; whereas, the spatio-temporal patterns were found to differ between the ligands associated with the receptors with a clear relevance for α_5/β_1 over α_v/β_3 concerning the proliferation of brain endothelial cells (Li et al., 2010). In a further study, Milner et al. (2008) used a mouse model of chronic global hypoxia and demonstrated integrin α_5 being strongly upregulated on hypoxic capillaries. However, as specific tools targeting integrins are currently lacking, conclusions in terms of causal relationships remain impossible.

Methodological Considerations

This study has some limitations: First, the methodological spectrum is limited to immunofluorescence labeling, which was chosen to explore related signals in both a qualitative and a quantitative manner and to allow comparative analyses at different time points after ischemia onset and diverse animal models or even autoptic human tissue. Consequently, future studies are needed to add analyses comprising protein levels from constituents of the NMZ, which might help to explore functional properties of this special site.

Second, this study is a first attempt to provide a spatio-temporal characterization at the site of the NMZ and thus focused on collagen IV and fibronectin as two representatives. Because collagens represent a large family consisting of several types, as for instance type II, III, or VI, that might exhibit different reactions in the setting of ischemia (Gatseva et al., 2019), further studies might try to cover more than the here addressed collagen IV. Furthermore, other structures associated with the NMZ like β-cadherin, located in close vicinity to integrins, and dystroglycans, related to astrocyte endfeet at the vasculatures' abluminal side (del Zoppo and Milner, 2006), would be of interest concerning their ischemic consequences, and thus need to be addressed in future studies. Thereby, confocal laser scanning microscopy might further help to explore the regional, i.e., three-dimensional arrangement of these structures and the vasculature in more detail.

Third, quantifications were limited to the mouse model with ischemia duration of 4 and 24 h, which was due to the restricted availability of tissues, especially from other species and the human stroke case. Based on the consistent qualitative analyses that emerged from tissues of rat, sheep, and a human stroke,

there are no doubts that an increase of the immunosignals from collagen IV und fibronectin due to focal cerebral ischemia would be quantifiable in these species too. As differences among species might be of relevance for the evaluation of therapeutic approaches, further confirmatory analyses including human brain tissue affected by ischemia seem reasonable. Notably, longitudinal investigations are of special interest to explore the temporal profile of increased fibronectin levels in the human brain after focal cerebral ischemia. As already gradual changes might be associated with different properties concerning the ischemic tolerance, a comparison with imaging parameters that visualize the tissue at risk could help to identify conditions that allow neuroprotective interventions.

Fourth, given the complexity of fibronectin isoforms and on the other hand, the antibodies used in this study, which are considered as pan-fibronectin markers, future efforts should include the detection of fibronectin isoforms in ischemic tissues.

Summary and Outlook

This study for the first time provides a spatio-temporal characterization of ischemia-related alterations for collagen IV and fibronectin as components of the NMZ in various animal models and in human tissue. Because the immunosignals from collagen IV as part of the basal membrane and from fibronectin as a crucial component of the ECM increased concomitantly and in a long-term range after the ischemic event, this study robustly shows that ischemic consequences are not limited to the traditional NVU components and the ECM, but also involve the NMZ. There might be various properties of this special zone including BBB regulations, of which a significant impairment is known to cause severe complications after stroke. As not yet considered for therapeutic approaches in the setting of stroke, the NMZ qualifies for further research to explore its pathophysiological role and opportunities for pharmacological interventions.

DATA AVAILABILITY STATEMENT

The raw data supporting the conclusions of this article will be made available by the authors, without undue reservation.

ETHICS STATEMENT

The animal study was reviewed and approved by Regierungspräsidium Leipzig as local authority (reference numbers: TVV 02/17 for mice and rats, and TVV 56/15 for sheep).

AUTHOR CONTRIBUTIONS

DM and WH designed the study and wrote the manuscript with considerable input from ES. Animal experiments including rodents were performed by DM and BM, whereas the experiments with sheep were carried out by HB and BN. Essential work concerning the human tissue was conducted by AH and CJ. Appropriate immunoreagents for this study were generated and provided by HM and SS. Histochemistry and imaging were conducted by WH, ES, WR and JP. Quantitative analyses and statistical calculations were done by ES, WR and DM. The final figures were generated by DM following proposals from WH. All authors contributed to the article and approved the submitted version.

FUNDING

A part of this study was supported by the Europäischer Sozialfonds (ESF, grant 100270131 to DM). Parts of the sheep experiments were co-funded by the Deutsche Forschungsgemeinschaft (DFG, grant BA 3425/2-3 to HB). Further, a part of the work on human tissue was supported by the Deutsche Forschungsgemeinschaft (DFG, Ho-1639/5-1 to AH).

ACKNOWLEDGMENTS

The authors thank the PET/MRI team from the Department of Nuclear Medicine (University of Leipzig) for the support with the sheep experiments. Further, the authors are thankful to Dr. Susanne Aleithe (University of Leipzig) for technical assistance during tissue preparation. Moreover, Dr. Martin Krueger (University of Leipzig) is gratefully acknowledged for the support of animal experiments with rodents.

REFERENCES

Aleithe, S., Blietz, A., Mages, B., Hobusch, C., Härtig, W., and Michalski, D. (2019). Transcriptional response and morphological features of the neurovascular unit and associated extracellular matrix after experimental stroke in mice. *Mol. Neurobiol.* 56, 7631–7650. doi: 10.1007/s12035-019-1604-4

Anderson, M. A., Burda, J. E., Ren, Y., Ao, Y., O'Shea, T. M., Kawaguchi, R., et al. (2016). Astrocyte scar formation aids central nervous system axon regeneration. *Nature* 532, 195–200. doi: 10.1038/nature17623

Benjamin, E. J., Virani, S. S., Callaway, C. W., Chamberlain, A. M., Chang, A. R., Cheng, S., et al. (2018). Heart disease and stroke statistics-2018 update: a report from the American heart association. *Circulation* 137, e67–e492. doi: 10.1161/CIR.0000000000000558

Boltze, J., Förschler, A., Nitzsche, B., Waldmin, D., Hoffmann, A., Boltze, C. M., et al. (2008). Permanent middle cerebral artery occlusion in sheep: a novel large animal model of focal cerebral ischemia. *J. Cereb. Blood Flow Metab.* 28, 1951–1964. doi: 10.1038/jcbfm.2008.89

Bustamante, A., López-Cancio, E., Pich, S., Penalba, A., Giralt, D., García-Berrocoso, T., et al. (2017). Blood biomarkers for the early diagnosis of stroke: the stroke-chip study. *Stroke* 48, 2419–2425. doi: 10.1161/STROKEAHA.117.017076

Campbell, B. C. V., De Silva, D. A., Macleod, M. R., Coutts, S. B., Schwamm, L. H., Davis, S. M., et al. (2019). Ischaemic stroke. *Nat. Rev. Dis. Primers.* 5:70. doi: 10.1038/s41572-019-0118-8

Castellanos, M., Leira, R., Serena, J., Blanco, M., Pedraza, S., Castillo, J., et al. (2004). Plasma cellular-fibronectin concentration predicts hemorrhagic transformation after thrombolytic therapy in acute ischemic stroke. *Stroke* 35, 1671–1676. doi: 10.1161/01.STR.0000131656.47979.39

Castellanos, M., Sobrino, T., Millán, M., García, M., Arenillas, J., Nombela, F., et al. (2007). Serum cellular fibronectin and matrix metalloproteinase-9 as screening biomarkers for the prediction of parenchymal hematoma after thrombolytic therapy in acute ischemic stroke: a multicenter confirmatory study. *Stroke* 38, 1855–1859. doi: 10.1161/STROKEAHA.106.481556

del Zoppo, G. J. (2009). Relationship of neurovascular elements to neuron injury during ischemia. *Cerebrovasc. Dis.* 27, 65–76. doi: 10.1159/000200442

del Zoppo, G. J. (2010). The neurovascular unit in the setting of stroke. *J. Intern. Med.* 267, 156–171. doi: 10.1111/j.1365-2796.2009.02199.x

del Zoppo, G. J., and Milner, R. (2006). Integrin-matrix interactions in the cerebral microvasculature. *Arterioscler. Thromb. Vasc. Biol.* 26, 1966–1975. doi: 10.1161/01.ATV.0000232525.65682.a2

del Zoppo, G. J., Milner, R., Mabuchi, T., Hung, S., Wang, X., and Koziol, J. A. (2006). Vascular matrix adhesion and the blood-brain barrier. *Biochem. Soc. Trans.* 34, 1261–1266. doi: 10.1042/BST0341261

Dhanesha, N., Chorawala, M. R., Jain, M., Bhalla, A., Thedens, D., Nayak, M., et al. (2019). Fn-EDA (Fibronectin containing extra domain a) in the plasma, but not endothelial cells, exacerbates stroke outcome by promoting thrombo-inflammation. *Stroke* 50, 1201–1209. doi: 10.1161/STROKEAHA.118.023697

Dias, D. O., and Göritz, C. (2018). Fibrotic scarring following lesions to the central nervous system. *Matrix Biol.* 68-69, 561–570. doi: 10.1016/j.matbio.2018.02.009

Dirnagl, U., Iadecola, C., and Moskowitz, M. A. (1999). Pathobiology of ischaemic stroke: an integrated view. *Trends Neurosci.* 22, 391–397. doi: 10.1016/s0166-2236(99)01401-0

Durukan, A., and Tatlisumak, T. (2007). Acute ischemic stroke: overview of major experimental rodent models, pathophysiology, and therapy of focal cerebral ischemia. *Pharmacol. Biochem. Behav.* 87, 179–197. doi: 10.1016/j.pbb.2007.04.015

Dyrna, F., Hanske, S., Krueger, M., and Bechmann, I. (2013). The blood-brain barrier. *J. NeuroImmune Pharmacol.* 8, 763–773. doi: 10.1007/s11481-013-9473-5

Edwards, D. N., and Bix, G. J. (2019). Roles of blood-brain barrier integrins and extracellular matrix in stroke. *Am. J. Phys. Cell Physiol.* 316, C252–C263. doi: 10.1152/ajpcell.00151.2018

Endres, M., Engelhardt, B., Koistinaho, J., Lindvall, O., Meairs, S., Mohr, J. P., et al. (2008). Improving outcome after stroke: overcoming the translational roadblock. *Cerebrovasc. Dis.* 25, 268–278. doi: 10.1159/000118039

Fisher, M., Feuerstein, G., Howells, D. W., Hurn, P. D., Kent, T. A., Savitz, S. I., et al. (2009). Update of the stroke therapy academic industry roundtable preclinical recommendations. *Stroke* 40, 2244–2250. doi: 10.1161/STROKEAHA.108.541128

Gatseva, A., Sin, Y. Y., Brezzo, G., and Van Agtmael, T. (2019). Basement membrane collagens and disease mechanisms. *Essays Biochem.* 63, 297–312. doi: 10.1042/EBC20180071

Goyal, M., Menon, B. K., van Zwam, W. H., Dippel, D. W., Mitchell, P. J., Demchuk, A. M., et al. (2016). Endovascular thromb-ectomy after large-vessel ischaemic stroke: a meta-analysis of individual patient data from five randomised trials. *Lancet* 387, 172317–172331. doi: 10.1016/S0140-6736(16)00163-X

Guell, K., and Bix, G. J. (2014). Brain endothelial cell specific integrins and ischemic stroke. *Expert. Rev. Neurother.* 14, 1287–1292. doi: 10.1586/14737175.2014.964210

Hacke, W., Kaste, M., Bluhmki, E., Brozman, M., Dávalos, A., Guidetti, D., et al. (2018). Thrombolysis with alteplase 3 to 4.5 hours after acute ischemic stroke. *N. Engl. J. Med.* 359, 1317–1329. doi: 10.1056/NEJMoa0804656

Hamann, G. F., Okada, Y., Fitridge, R., and del Zoppo, G. J. (1995). Microvascular basal lamina antigens disappear during cerebral ischemia and reperfusion. *Stroke* 26, 2120–2126. doi: 10.1161/01.str.26.11.2120

Härtig, W., Mages, B., Aleithe, S., Nitzsche, B., Altmann, S., Barthel, H., et al. (2017). Damaged neocortical perineuronal nets due to experimental focal cerebral ischemia in mice, rats and sheep. *Front. Integr. Neurosci.* 11:15. doi: 10.3389/fnint.2017.00015

Härtig, W., Reichenbach, A., Voigt, C., Boltze, J., Bulavina, L., Schuhmann, M. U., et al. (2009). Triple fluorescence labeling of neuronal, glial and vascular markers revealing pathological alterations in various animal models. *J. Chem. Neuroanat.* 37, 128–138. doi: 10.1016/j.jchemneu.2008.10.003

Hawkes, C. A., Michalski, D., Anders, R., Nissel, S., Grosche, J., Bechmann, I., et al. (2013). Stroke induced opposite and age-dependent changes of vessel-associated markers in co-morbid transgenic mice with Alzheimer-like alterations. *Exp. Neurol.* 250, 270–281. doi: 10.1016/j.expneurol.2013.09.020

Hermanns, S., Klapka, N., and Müller, H. W. (2001). The collagenous lesion scar – an obstacle for axonal regeneration in brain and spinal cord injury. *Restor. Neurol. Neurosci.* 19, 139–148.

Huang, Q., Chen, B., Wang, F., Huang, H., Milner, R., and Li, L. (2015). The temporal expression patterns of fibronectin and its receptors-α5β1 and αvβ3 integrins on blood vessels after cerebral ischemia. *Restor. Neurol. Neurosci.* 33, 493–507. doi: 10.3233/RNN-140491

Iadecola, C. (2017). The neurovascular unit coming of age: a journey through neurovascular coupling in health and disease. *Neuron* 96, 17–42. doi: 10.1016/j.neuron.2017.07.030

Ishrat, T., Soliman, S., Guan, W., Saler, M., and Fagan, S. C. (2012). Vascular protection to increase the safety of tissue plasminogen activator for stroke. *Curr. Pharm. Des.* 18, 3677–3684. doi: 10.2174/138161212802002779

Kattah, J. C., Saber Tehrani, A. S., Roeber, S., Gujrati, M., Bach, S. E., Newman Toker, D. E., et al. (2017). Transient vestibulopathy in Wallenberg's syndrome: pathologic analysis. *Front. Neurol.* 8:191. doi: 10.3389/fneur.2017.00191

Kestner, R. I., Mayser, F., Vutukuri, R., Hansen, L., Günther, S., Brunkhorst, R., et al. (2020). Gene expression dynamics at the neurovascular unit during early regeneration after cerebral ischemia/reperfusion injury in mice. *Front. Neurosci.* 14:280. doi: 10.3389/fnins.2020.00280

Khan, M. M., Gandhi, C., Chauhan, N., Stevens, J. W., Motto, D. G., Lentz, S. R., et al. (2012). Alternatively-spliced extra domain a of fibronectin promotes acute inflammation and brain injury after cerebral ischemia in mice. *Stroke* 43, 1376–1382. doi: 10.1161/STROKEAHA.111.635516

Kilkenny, C., Browne, W. J., Cuthill, I. C., Emerson, M., and Altman, D. G. (2010). Improving bioscience research reporting: the ARRIVE guidelines for reporting animal research. *PLoS Biol.* 8:e1000412. doi: 10.1371/journal.pbio.1000412

Krueger, M., Bechmann, I., Immig, K., Reichenbach, A., Härtig, W., and Michalski, D. (2015). Blood-brain barrier breakdown involves four distinct stages of vascular damage in various models of experimental focal cerebral ischemia. *J. Cereb. Blood Flow Metab.* 35, 292–303. doi: 10.1038/jcbfm.2014.199

Krueger, M., Härtig, W., Reichenbach, A., Bechmann, I., and Michalski, D. (2013). Blood-brain barrier breakdown after embolic stroke in rats occurs without ultrastructural evidence for disrupting tight junctions. *PLoS One* 8:e56419. doi: 10.1371/journal.pone.0056419

Krueger, M., Mages, B., Hobusch, C., and Michalski, D. (2019). Endothelial edema precedes blood-brain barrier breakdown in early time points after experimental focal cerebral ischemia. *Acta Neuropathol. Commun.* 7:17. doi: 10.1186/s40478-019-0671-0

Li, L., Liu, F., Welser-Alves, J. V., McCullough, L. D., and Milner, R. (2012). Upregulation of fibronectin and the α5β1 and αvβ3 integrins on blood vessels within the cerebral ischemic penumbra. *Exp. Neurol.* 233, 283–291. doi: 10.1016/j.expneurol.2011.10.017

Li, L., Welser, J. V., and Milner, R. (2010). Absence of the αv β3 integrin dictates the time-course of angiogenesis in the hypoxic central nervous system: accelerated endothelial proliferation correlates with compensatory increases in α5β1 integrin expression. *J. Cereb. Blood Flow Metab.* 30, 1031–1043. doi: 10.1038/jcbfm.2009.276

Lo, E. H., Dalkara, T., and Moskowitz, M. A. (2003). Mechanisms, challenges and opportunities in stroke. *Nat. Rev. Neurosci.* 4, 399–415. doi: 10.1038/nrn1106

Longa, E. Z., Weinstein, P. R., Carlson, S., and Cummins, R. (1989). Reversible middle cerebral artery occlusion without craniectomy in rats. *Stroke* 20, 84–91. doi: 10.1161/01.str.20.1.84

Mages, B., Aleithe, S., Altmann, S., Blietz, A., Nitzsche, B., Barthel, H., et al. (2018). Impaired neurofilament integrity and neuronal morphology in different models of focal cerebral ischemia and human stroke tissue. *Front. Cell. Neurosci.* 12:161. doi: 10.3389/fncel.2018.00161

Mages, B., Aleithe, S., Blietz, A., Krueger, M., Härtig, W., and Michalski, D. (2019). Simultaneous alterations of oligodendrocyte-specific CNP, astrocyte-specific AQP4 and neuronal NF-L demarcate ischemic tissue after experimental stroke in mice. *Neurosci. Lett.* 711:134405. doi: 10.1016/j.neulet.2019.134405

Mao, Y., and Schwarzbauer, J. E. (2005). Fibronectin fibrillogenesis, a cell-mediated matrix assembly process. *Matrix Biol.* 24, 389–399. doi: 10.1016/j.matbio.2005.06.008

Matsumoto, H., Kumon, Y., Watanabe, H., Ohnishi, T., Shudou, M., Ii, C., et al. (2007). Antibodies to CD11b, CD68, and lectin label neutrophils rather than microglia in traumatic and ischemic brain lesions. *J. Neurosci. Res.* 85, 994–1009. doi: 10.1002/jnr.21198

Menzies, S. A., Hoff, J. T., and Betz, A. L. (1992). Middle cerebral artery occlusion in rats: a neurological and pathological evaluation of a reproducible model. *Neurosurgery* 31, 100–107. doi: 10.1227/00006123-199207000-00014

Mezzenga, R., and Mitsi, M. (2019). The molecular dance of fibronectin: conformational flexibility leads to functional versatility. *Biomacromolecules* 20, 55–72. doi: 10.1021/acs.biomac.8b01258

Michalski, D., Grosche, J., Pelz, J., Schneider, D., Weise, C., Bauer, U., et al. (2010). A novel quantification of blood-brain barrier damage and histochemical typing after embolic stroke in rats. *Brain Res.* 1359, 186–200. doi: 10.1016/j.brainres.2010.08.045

Michalski, D., Keck, A. L., Grosche, J., Martens, H., and Härtig, W. (2018). Immunosignals of oligodendrocyte markers and myelin-associated proteins are critically affected after experimental stroke in wild-type and Alzheimer modeling mice of different ages. *Front. Cell. Neurosci.* 12:23. doi: 10.3389/fncel.2018.00023

Milner, R., Hung, S., Erokwu, B., Dore-Duffy, P., LaManna, J. C., and del Zoppo, G. J. (2008). Increased expression of fibronectin and the alpha 5 beta 1 integrin in angiogenic cerebral blood vessels of mice subject to hypobaric hypoxia. *Mol. Cell. Neurosci.* 38, 43–52. doi: 10.1016/j.mcn.2008.01.013

Mullen, R. J., Buck, C. R., and Smith, A. M. (1992). NeuN, a neuronal specific nuclear protein in vertebrates. *Development* 116, 201–211.

Muñoz, R., Santamaría, E., Rubio, I., Ausín, K., Ostolaza, A., Labarga, A., et al. (2018). Mass spectrometry-based proteomic profiling of thrombotic material obtained by endovascular thrombectomy in patients with ischemic stroke. *Int. J. Mol. Sci.* 19:498. doi: 10.3390/ijms19020498

Nicosia, R. F., Bonanno, E., and Smith, M. (1993). Fibronectin promotes the elongation of microvessels during angiogenesis in vitro. *J. Cell. Physiol.* 154, 654–661. doi: 10.1002/jcp.1041540325

Nitzsche, B., Barthel, H., Lobsien, D., Boltze, J., Zeisig, V., and Dreyer, A. Y. (2016). "Focal cerebral ischemia by permanent middle cerebral artery occlusion in sheep: surgical technique, clinical imaging, and histopathological results" in *Experimental neurosurgery in animal models*. ed. M. Janowski (Berlin: Springer), 195–225.

Perry, L. A., Lucarelli, T., Penny-Dimri, J. C., McInnes, M. D., Mondello, S., Bustamante, A., et al. (2019). Glial fibrillary acidic protein for the early diagnosis of intracerebral hemorrhage: systematic review and meta-analysis of diagnostic test accuracy. *Int. J. Stroke* 14, 390–399. doi: 10.1177/1747493018806167

Ramanathan, A., and Karuri, N. (2014). Fibronectin alters the rate of formation and structure of the fibrin matrix. *Biochem. Biophys. Res. Commun.* 443, 395–399. doi: 10.1016/j.bbrc.2013.11.090

Reed, M. J., Damodarasamy, M., and Banks, W. A. (2019). The extracellular matrix of the blood-brain barrier: structural and functional roles in health, aging, and Alzheimer's disease. *Tissue Barriers* 7:1651157. doi: 10.1080/21688370.2019.1651157

Rodríguez-Yáñez, M., Sobrino, T., Arias, S., Vázquez-Herrero, F., Brea, D., Blanco, M., et al. (2011). Early biomarkers of clinical-diffusion mismatch in acute ischemic stroke. *Stroke* 42, 2813–2818. doi: 10.1161/STROKEAHA.111.614503

Sakai, T., Johnson, K. J., Murozono, M., Sakai, K., Magnuson, M. A., Wieloch, T., et al. (2001). Plasma fibronectin supports neuronal survival and reduces brain injury following transient focal cerebral ischemia but is not essential for skin-wound healing and hemostasis. *Nat. Med.* 7, 324–330. doi: 10.1038/85471

Singh, P., Carraher, C., and Schwarzbauer, J. E. (2010). Assembly of fibronectin extracellular matrix. *Annu. Rev. Cell Dev. Biol.* 26, 397–419. doi: 10.1146/annurev-cellbio-100109-104020

Soleman, S., Filippov, M. A., Dityatev, A., and Fawcett, J. W. (2013). Targeting the neural extracellular matrix in neurological disorders. *Neuroscience* 253, 194–213. doi: 10.1016/j.neuroscience.2013.08.050

Sommer, C. J. (2017). Ischemic stroke: experimental models and reality. *Acta Neuropathol.* 133, 245–261. doi: 10.1007/s00401-017-1667-0

Stichel, C. C., Hermanns, S., Luhmann, H. J., Lausberg, F., Niermann, H., D'Urso, D., et al. (1999). Inhibition of collagen IV deposition promotes regeneration of injured CNS axons. *Eur. J. Neurosci.* 11, 632–646. doi: 10.1046/j.1460-9568.1999.00466.x

Stoffels, J. M., Zhao, C., and Baron, W. (2013). Fibronectin in tissue regeneration: timely disassembly of the scaffold is necessary to complete the build. *Cell. Mol. Life Sci.* 70, 4243–4253. doi: 10.1007/s00018-013-1350-0

Thomsen, M. S., Routhe, L. J., and Moos, T. (2017). The vascular basement membrane in the healthy and pathological brain. *J. Cereb. Blood Flow Metab.* 37, 3300–3317. doi: 10.1177/0271678X17722436

To, W. S., and Midwood, K. S. (2011). Plasma and cellular fibronectin: distinct and independent functions during tissue repair. *Fibrogenesis Tissue Repair* 4:21. doi: 10.1186/1755-1536-4-21

Wang, J., and Milner, R. (2006). Fibronectin promotes brain capillary endothelial cell survival and proliferation through α5β1 and αvβ3 integrins via MAP kinase signalling. *J. Neurochem.* 96, 148–159. doi: 10.1111/j.1471-4159.2005.03521.x

White, E. S., Baralle, F. E., and Muro, A. F. (2008). New insights into form and function of fibronectin splice variants. *J. Pathol.* 216, 1–14. doi: 10.1002/path.2388

White, E. S., and Muro, A. F. (2011). Fibronectin splice variants: understanding their multiple roles in health and disease using engineered mouse models. *IUBMB Life* 63, 538–546. doi: 10.1002/iub.493

Xu, L., Nirwane, A., and Yao, Y. (2019). Basement membrane and blood-brain barrier. *Stroke Vasc. Neurol.* 4, 78–82. doi: 10.1136/svn-2018-000198

Yang, C., Hawkins, K. E., Doré, S., and Candelario-Jalil, E. (2019). Neuroinflammatory mechanisms of blood-brain barrier damage in ischemic stroke. *Am. J. Phys. Cell Physiol.* 316, C135–C153. doi: 10.1152/ajpcell.00136.2018

Yang, D. Y., Pan, H. C., Chen, C. J., Cheng, F. C., and Wang, Y. C. (2007). Effects of tissue plasminogen activator on cerebral microvessels of rats during focal cerebral ischemia and reperfusion. *Neurol. Res.* 29, 274–282. doi: 10.1179/016164107X159171

Yang, Y., and Rosenberg, G. A. (2011). Blood-brain barrier breakdown in acute and chronic cerebrovascular disease. *Stroke* 42, 3323–3328. doi: 10.1161/STROKEAHA.110.608257

Young, A. R., Ali, C., Duretête, A., and Vivien, D. (2007). Neuroprotection and stroke: time for a compromise. *J. Neurochem.* 103, 1302–1309. doi: 10.1111/j.1471-4159.2007.04866.x

Zhang, R. L., Chopp, M., Zhang, Z. G., Jiang, Q., and Ewing, J. R. (1997). A rat model of focal embolic cerebral ischemia. *Brain Res.* 766, 83–92. doi: 10.1016/s0006-8993(97)00580-5

Zhang, L., Zhang, Z. G., and Chopp, M. (2012). The neurovascular unit and combination treatment strategies for stroke. *Trends Pharmacol. Sci.* 33, 415–422. doi: 10.1016/j.tips.2012.04.006

Conflict of Interest: The authors declare that the research was conducted in the absence of any commercial or financial relationships that could be construed as a potential conflict of interest.

frontiers in Physiology

ORIGINAL RESEARCH
published: 12 November 2020
doi: 10.3389/fphys.2020.586226

Characterization of the Blood Brain Barrier Disruption in the Photothrombotic Stroke Model

*Rebecca Z. Weber[1,2], Lisa Grönnert[1], Geertje Mulders[1,3], Michael A. Maurer[1], Christian Tackenberg[1,2], Martin E. Schwab[1,2] and Ruslan Rust[1,2]**

[1] *Institute for Regenerative Medicine, University of Zurich, Zurich, Switzerland,* [2] *Neuroscience Center Zurich, University of Zurich and ETH Zurich, Zurich, Switzerland,* [3] *Department of Health Sciences and Technology, ETH Zurich, Zurich, Switzerland*

Blood brain barrier (BBB) damage is an important pathophysiological feature of ischemic stroke which significantly contributes to development of severe brain injury and therefore is an interesting target for therapeutic intervention. A popular permanent occlusion model to study long term recovery following stroke is the photothrombotic model, which so far has not been anatomically characterized for BBB leakage beyond the acute phase. Here, we observed enhanced BBB permeability over a time course of 3 weeks in peri-infarct and core regions of the ischemic cortex. Slight increases in BBB permeability could also be seen in the contralesional cortex, hippocampus and the cerebellum at different time points, regions where lesion-induced degeneration of pathways is prominent. Severe damage of tight and adherens junctions and loss of pericytes was observed within the peri-infarct region. Overall, the photothrombotic stroke model reproduces a variety of features observed in human stroke and thus, represents a suitable model to study BBB damage and therapeutic approaches interfering with this process.

Keywords: photothrombotic stroke, BBB, ischemia, leakage, edema, pericytes, tight junctions

OPEN ACCESS

Edited by:
Jean-luc Morel, Center National de la Recherche Scientifique (CNRS), France

Reviewed by:
Axel Montagne, University of Southern California, United States
Andrew N. Clarkson, University of Otago, New Zealand

****Correspondence:***
Ruslan Rust
ruslan.rust@irem.uzh.ch

Specialty section:
This article was submitted to Vascular Physiology, a section of the journal Frontiers in Physiology

Received: *22 July 2020*
Accepted: *23 October 2020*
Published: *12 November 2020*

Citation:
Weber RZ, Grönnert L, Mulders G, Maurer MA, Tackenberg C, Schwab ME and Rust R (2020) Characterization of the Blood Brain Barrier Disruption in the Photothrombotic Stroke Model. Front. Physiol. 11:586226. doi: 10.3389/fphys.2020.586226

INTRODUCTION

Stroke is a leading cause of disability and death worldwide. There are over 13.7 million strokes every year and one in four people over age 25 will experience a stroke in their lifetime (GBD 2016 Stroke Collaborators, 2019). A majority of stroke victims cannot profit from thrombolysis or thrombectomy, and rehabilitation therapies have often only limited success in restoring the lost functions. Stroke, therefore, remains a global substantial social and clinical burden (Katan and Luft, 2018).

A hallmark of stroke pathology is the breakdown of the blood brain barrier (BBB) that can persist for up to several weeks after stroke and is associated with poor patient outcomes (Kastrup et al., 2008; Brouns et al., 2011). Anatomically, BBB breakdown is characterized by alterations of tight junction protein complexes and damage to cellular components of the neurovascular unit, e.g., pericytes (Bell et al., 2010; Prakash and Carmichael, 2015; Abdullahi et al., 2018; Nation et al., 2019; Montagne et al., 2020). As a result of enhanced BBB permeability, many secondary injury cascades are activated including cytotoxic edema, a disruption in cellular water and ion homeostasis and

vasogenic edema, fluid extravasation into the brain parenchyma (Zhao et al., 2015). BBB integrity is also a safety measure for novel experimental therapies aiming at revascularization of the ischemic brain since newly formed blood vessels can lack barrier functions and may exacerbate brain damage (Rust et al., 2018, 2019c). On the other hand, delivery of therapeutic drugs may be facilitated by the improved accessibility of the brain (Obermeier et al., 2013).

In pre-clinical research different rodent models are used to study various aspects of stroke pathophysiology and to evaluate novel treatment approaches (Carmichael, 2005; Dirnagl, 2010). Apart from the frequently used model of middle cerebral artery occlusion (MCAO), the photothrombotic stroke is an ever-increasingly used model with well-characterized sensory-motor deficits and long-term recovery. However, BBB injury has not yet been studied beyond the acute stage of photothrombotic stroke (Hoff et al., 2005).

Here, we provide a 3-week time course of BBB permeability changes in mice subjected to a cortical photothrombotic stroke within the stroke core and peri-infarct regions. We also assess the permeability in neighboring and contralesional brain regions including contralesional sensorimotor cortex, hippocampus, cerebellum and visual cortex. Moreover, we quantify damage to cellular and major junction protein components in ischemic regions following the injury.

RESULTS

Blood Brain Barrier Leakage Is a Hallmark of the Photothrombotic Stroke Model

Breakdown of the BBB and the risk of hemorrhagic transformation usually occurs within the first days in stroke patients (Nadareishvili et al., 2019). Therefore, we first evaluated the BBB integrity 24 h following the induction of the stroke. Mice received a photothrombotic stroke with a size of 3 x 4 mm in the sensorimotor cortex and were systemically injected with Evans blue (EB), a BBB permeability marker 24 h before sacrifice (**Figure 1A**). EB has a high affinity for serum albumin, which does not cross the intact BBB to the brain parenchyma. 1 day following injury, stroked mouse brains exhibited a strong EB signal in the stroke core in the ipsilesional cortex and a lower signal in the surrounding peri-infarct zone (**Figure 1B**). The EB-positive core covered an area of 7.74 ± 3.52 mm^2 with 11.55 ± 2.43 mm circumference, which was surrounded by an EB-positive peri-infarct region with a total area of 4.08 ± 1.46 mm^2 (core + peri-infarct: 11.82 ± 4.98 mm^2) and 13.756 ± 2.356 mm circumference. In the intact brain no signal of EB was detectable in any region (all $p < 0.01$, **Figure 1C**).

Spatiotemporal Profile of Blood Brain Barrier Permeability Following Photothrombotic Stroke

The spatiotemporal profile of the BBB opening following human stroke is complex and may also occur beyond the acute stage (Merali et al., 2017; Nadareishvili et al., 2019). Re-openings of the BBB have been observed days to weeks following the initial ischemic injury in clinical and pre-clinical research (Huang et al., 1999; Kassner and Merali, 2015; Merali et al., 2017). Moreover, enhanced permeability has also been observed in regions not directly affected by the initial stroke due to retrograde or anterograde pathway degeneration and the associated inflammatory reaction (Ling et al., 2009; Li et al., 2011; Cao et al., 2020). Therefore, we aimed to characterize the spatiotemporal profile of BBB permeability up to 3 weeks following stroke.

Brain tissue was dissected and lysed at 1, 7, and 21 days following a localized unilateral photothrombotic stroke to the sensory-motor cortex. Evans blue was detected at a high sensitivity with a limit of detection (LOD) of 0.006 ng and a limit of quantification (LOQ) of 0.019 ng per mg brain lysate, when administered either 4 or 24 h prior to perfusion (**Figures 2A,B**). A successful stroke procedure was confirmed by severe reduction in cerebral blood perfusion (CBF) of the sensorimotor cortex (<40% of baseline CBF) at 1 dpi (**Figures 2C,D**) using Laser Doppler Imaging (**Figures 2C,D**).

Interestingly, all mice showed up to 1,500-fold upregulation of the EB signal in the ipsilesional cortex 24 h following stroke [intact: 0.03 ± 0.01, $stroke_{(1\ dpi)}$: 42.91 ± 7.79] (**Figure 2E**). At later time points, most of the animals (83–90%) still exhibit enhanced leakage in the ischemic cortex [intact: 0.028, $stroke_{(7\ dpi)}$: 34.01 ± 14.77; $stroke_{(21\ dpi)}$: 31.54 ± 16.06, all $p < 0.01$]. Other brain regions, which were not directly affected by the initial stroke, also displayed enhanced although lower EB signals in individual animals. Most of these EB signals at 24 h after the stroke were detected in the contralesional cortex [intact: 0.05 ± 0.02, $stroke_{(1\ dpi)}$: 17.05 ± 11.92, $p = 0.002$], in the ipsilesional hippocampus [intact: 0.03 ± 0.01, $stroke_{(1\ dpi)}$: 8.98 ± 5.49, $p = 0.03$] and contralesional hippocampus [intact: 0.02 ± 0.01, $stroke_{(1\ dpi)}$: 8.63 ± 3.09, $p = 0.002$] and, at the latest time point, also in the cerebellum [intact: 0.06 ± 0.02, $stroke_{(21\ dpi)}$: 8.29 ± 5.59, $p = 0.003$] (**Figure 2E**). Importantly, signal intensities were not altered to acute time points before 24 h (**Supplementary Figure S1**).

In order to explore the spatial distribution of EB within the brain and to distinguish between core and peri-infarct leakage a histological analysis of vascular permeability in brain sections was performed on the ipsi- and contralesional cortex at day post injury 1, 7, and 21 (**Figures 3A–C**). EB signal strength was measured at the stroke core, the peri-infarct regions, in the contralesional cortex and in intact cortex by fluorescence intensity (**Figure 3C**). The area of EB leakage at the stroke core decreased slightly over time (1 dpi: 8.03 ± 3.83 mm^2, 7 dpi: 6.40 ± 2.20 mm^2, 21 dpi: 5.65 ± 2.80 mm^2, all $p > 0.05$), whereas the EB -positive area in the peri-infarct regions steadily decreased from day 1 (5.79 ± 0.99 mm^2) to day 7 (3.06 ± 1.13 mm^2, $p = 0.007$), and day 21 (2.18 ± 2.01 mm^2, $p = 0.001$) (**Figures 3D,E**). The peri-infarct region was defined by vascular density and ranged 300–600 μm from the stroke core as previously described (Rust et al., 2019b). On the contralesional side the area of EB leakage was 2.39 ± 1.30 mm^2 at day 1 and shrunk to very small dimensions from day 7 on

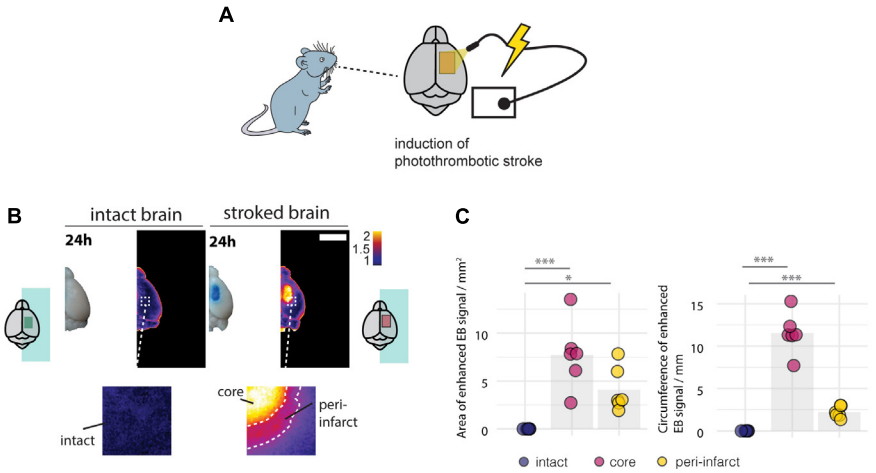

FIGURE 1 | Disruption of the blood brain barrier 24 h following the photothrombotic stroke. **(A)** Schematic representation of photothrombotic stroke induction in the sensorimotor cortex. **(B)** Macroscopic and pseudo-colored image in stroked and non-stroked animals showing the Evans blue (EB) extravasation in stroke core and penumbra. Scale bar: 5 mm. **(C)** Quantitative assessment of area and circumference of EB signals. Each dot in the plots represents one animal and significance of mean differences between the groups was assessed using Tukey's HSD. Asterisks indicate significance: $^{*}P < 0.05$, $^{**}P < 0.01$, $^{***}P < 0.001$.

(**Figure 3E**). No EB signal was detectable in the cortex of intact mice (**Figure 3F**), nor the corpus callosum and other subcortical structures (data not shown).

In conclusion, most damage and vascular permeability in the photothrombotic stroke is present at the site of injury and it weakens gradually with distance to the stroke core. Non-affected brain regions can also show low to moderate leakage at different time points.

Disruption of Peri-Vascular Cells and Junction Proteins Are a Feature of Photothrombotic Stroke

The integrity of the BBB relies on tight and adherens junction protein complexes including Claudin-5, ZO-1, and VE-Cadherin (Jiao et al., 2011; Berndt et al., 2019) and cellular components of the neurovascular unit, especially pericytes (Armulik et al., 2010). Consequently, damage to any of these components may contribute to enhanced vascular leakage and the risk of hemorrhagic transformation. We histologically analyzed pericyte coverage and components of the junction proteins in the ischemic peri-infarct regions and intact animals at 1–21 days following photothrombotic stroke (**Figure 4A**). We observe a considerable ∼80% reduction of the pericyte fraction around blood vessels in the peri-infarct areas (1 dpi: 0.08 ± 0.07, 21 dpi: 0.15 ± 0.08, both $p < 0.001$) compared to intact cortex (0.62 ± 0.11) (**Figure 4B**). The surface ratio of blood vessels covered by tight/adherens junction components also significantly decreased in the peri-infarct region compared to the intact cortex. In particular, there was a decrease of 13% (1 dpi) and 59% (21 dpi) of Claudin-5 (1dpi: 0.069 ± 0.012, $p = 0.832$, 21 dpi: 0.033 ± 0.02 $p = 0.013$), a decrease of 68% (1 dpi) and 41% (21 dpi) of VE-Cadherin (1 dpi: 0.073 ± 0.006, $p < 0.001$; 21 dpi: 0.136 ± 0.05, $p = 0.003$), and a decrease of 85% (1 dpi) and 90% (21 dpi) of ZO-1 (1 dpi: 0.015 ± 0.020, $p < 0.001$; 21 dpi: 0.011 ± 0.007, $p < 0.001$) compared to the intact sensorimotor cortex (Claudin-5: 0.079 ± 0.026, VE-Cadherin: 0.232 ± 0.025, ZO1: 0.096 ± 0.023 (**Figures 4C,D**). Overall, these data indicated a considerable damage to the BBB anatomy also beyond the acute phase.

DISCUSSION

The blood brain barrier (BBB) has a central role in the pathogenesis of stroke. Disruption of the BBB occurs in the acute and subacute phases following stroke and is a precursor to serious clinical consequences such as brain edema and hemorrhagic transformation. Improving the BBB integrity following stroke has recently emerged as a focus for new therapeutic strategies (Sifat et al., 2017). Here, we characterize the spatiotemporal evolution of the BBB breakdown in a photothrombotic stroke model, a popular rodent model of ischemic stroke. While the BBB remained open in the stroke core, permeability decreased over the 3 weeks in the infarcted region. Anatomically, the enhanced permeability was correlated with a decrease of several major membrane constituents of the endothelial tight junctions, and with a reduction in the pericyte-to-blood vessel ratio. A subset of mice also exhibited low to moderate leakage in the contralesional cortex, the ipsi- and contralesional hippocampus and the cerebellum.

In stroke patients the disruption of the BBB was visualized *in vivo* by positron emission tomography (PET) (Okada et al., 2015), dynamic contrast-enhanced (DCE) magnetic resonance imaging (MRI) (Sourbron et al., 2009) and DCE computed tomography (CT) (Hom et al., 2011; Ozkul-Wermester et al., 2014). The dynamics of BBB permeability seem to vary somewhat between the studies. All reports show an acute opening of the

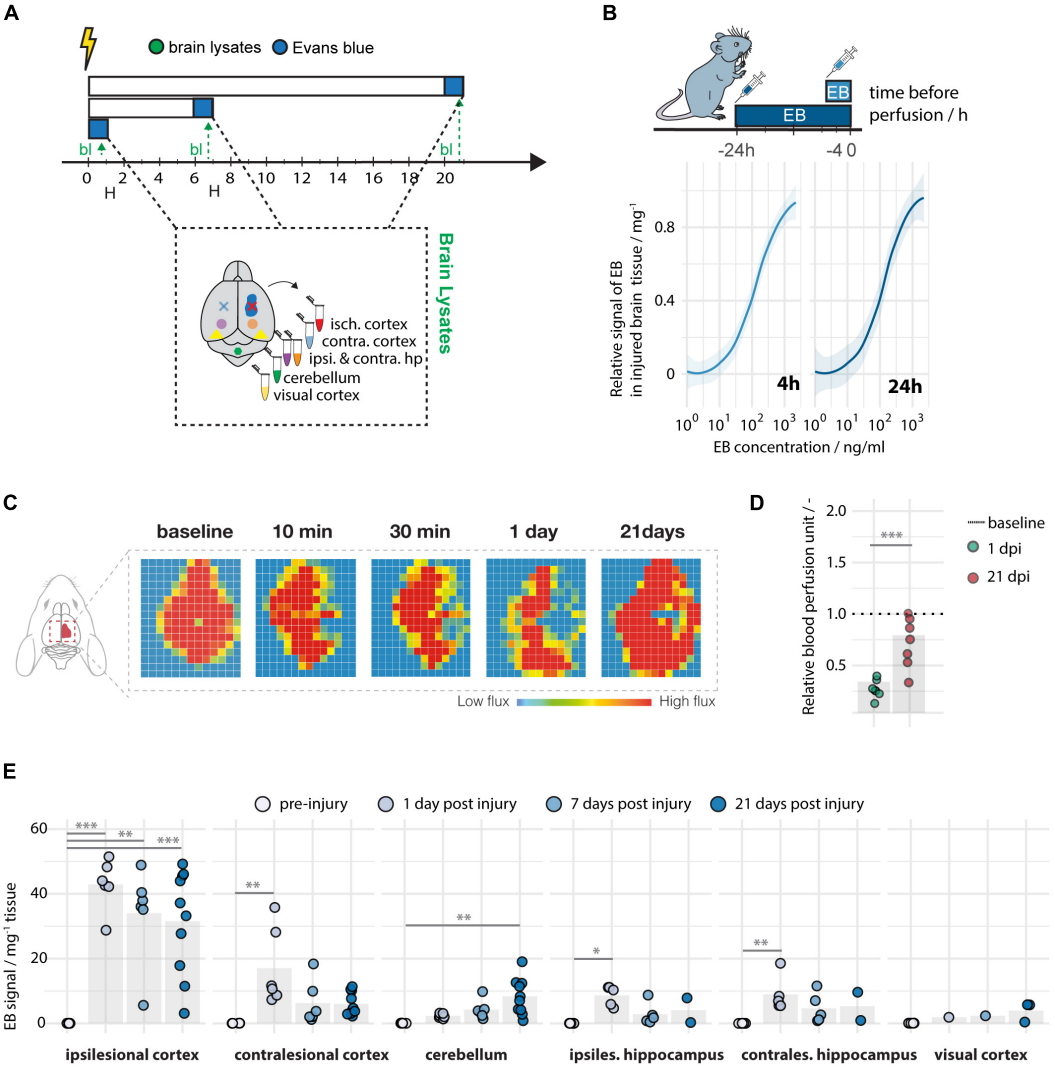

FIGURE 2 | Spatiotemporal leakage following photothrombotic stroke. **(A)** Schematic representation of time course at baseline ($N = 5$), day 1 ($N = 5$–10), day 7 ($N = 5$–7), and day 21 ($N = 2$–10) following stroke. **(B)** Limit of detection and quantification of Evans blue in brain tissue. **(C)** Representative images of images of cerebral blood perfusion at 10, 30 min, 1 and 21 days following stroke. **(D)** Quantification of cerebral blood perfusion relative to baseline. **(E)** Quantitative assessment of Evans blue signal across different brain regions and time points. Data are represented as mean ± SD. Each dot in the plots represents one animal and significance of mean differences between the groups was assessed using Tukey's HSD. Asterisks indicate significance: $^{*}P < 0.05$, $^{**}P < 0.01$, $^{***}P < 0.001$ isch cx; ischemic cortex, contra cx; contralesional cortex, hp; hippocampus, cb; cerebellum, vcx, visual cortex. EB; Evans Blue, bl; brain lysates.

BBB, and many report a bi-phasic or a continuous opening beyond the acute period with a maximum around day 2 and a second peak around day 7 (Merali et al., 2017). Similar results have been observed in animal models with well controlled experimental parameters. BBB openings have been observed in models of middle cerebral artery occlusion to follow bi-phasic course (Belayev et al., 1996; Rosenberg et al., 1998; Huang et al., 1999) or as a continuous opening (Nagel et al., 2004; Strbian et al., 2008).

Although various MCAO models of stroke are sufficiently documented with regard to BBB opening, there is insufficient knowledge in the time course of the photothrombotic stroke. Since the photothrombotic stroke is minimally invasive and reproducibly causes limb use deficits in mice for more than 16 weeks after the infarct, it is an interesting model for assessing long-term functional recovery (Allred et al., 2008). Consequently, efficacy of potential drugs interfering with BBB disruption can be evaluated using the photothrombotic stroke.

In our study, we observed a high variability within the experimental groups: Littermates undergoing the same surgical procedures and without obvious differences in stroke size showed considerable differences in BBB opening. In particular, leakage was clearly reduced in the peri-infarct region already at day 7 after the stroke, comparable to results from previous studies in a transient middle cerebral artery occlusion (MCAO) model (Strbian et al., 2008). However, some leakage, at least in part

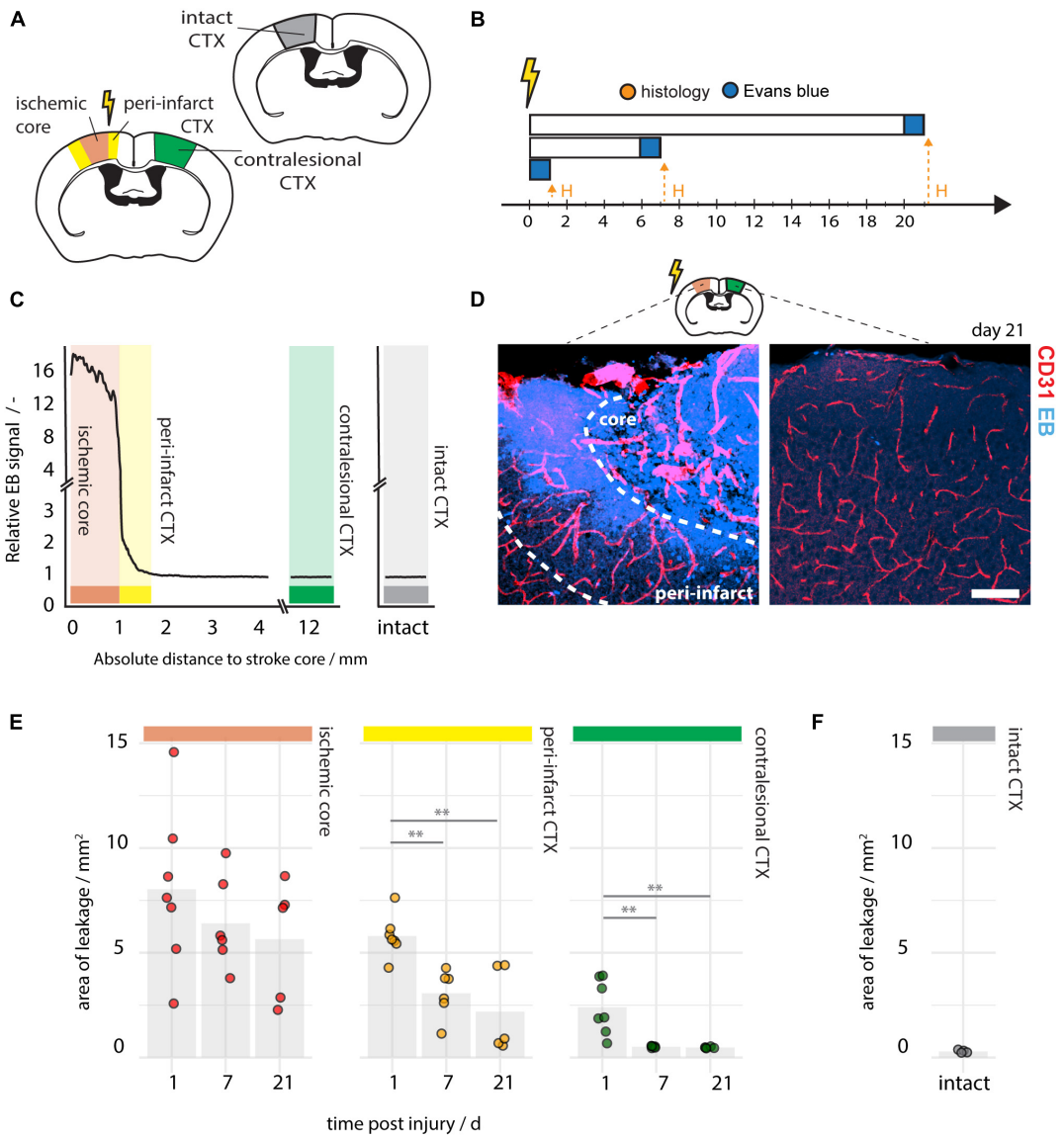

FIGURE 3 | Histological assessment of BBB permeability following photothrombotic stroke. **(A)** Schematic representation of region of interest within the ischemic core (red), the peri-infarct region (yellow), the contralesional cortex (green), and the intact cortex (gray). **(B)** Time course of the experimental pipeline of 1 day ($N = 8$), 7 days ($N = 6$), and 21 days ($N = 5$) following injury. **(C)** Spatial distribution of EB signal along the ischemic, contralesional and intact cortex at 21 dpi. **(D)** Representative images of EB signal in the peri-infarct and contralesional region at 21 dpi. Scale bar: 100 μm. **(E)** Quantification of EB -positive area of the stroke core, the peri-infarct cortex and the contralesional cortex at days 1, 7, and 21 post injury. **(F)** EB -positive area in intact mice ($N = 4$). Each dot in the plots represents one animal and significance of mean differences between the groups was assessed using unpaired two-tailed one-sample Student's *t*-test. Asterisks indicate significance: $^{**}P < 0.01$. Dpi, days post injury; H, histology; ctx, cortex; EB, Evans blue.

of the animals, was still detectable at 21 days in the peri-infarct zone. We found disruption of blood vessel pericytes coverage and tight junction components within the peri-infarct region at 1–21 days following stroke. Pericytes have been previously described to be an essential part of the BBB; pericyte-deficient mutant mice show significantly impaired BBB function (Armulik et al., 2010). Pericytes have also been described to be depleted in the peri-infarct region of MCAO strokes (Fernández-Klett et al., 2013; Nih et al., 2018). Although considerable sex differences have been previously reported in clinical stroke pathology (Reeves et al., 2008) as well as BBB permeability (Castellazzi et al., 2020), we have not observed any differences in BBB disruption between the sex in the photothrombotic stroke model.

Ischemia leads to the release of MMP9 by inflammatory cells in the peri-infarct region which interrupts the tight junctions and increases BBB leakage (Underly et al., 2017). Deficiencies in multiple tight junction proteins are a common observation in other ischemic rodent stroke models (Abdullahi et al., 2018). We have previously observed that sprouted, newly formed vessels in the peri-infarct region are initially immature and

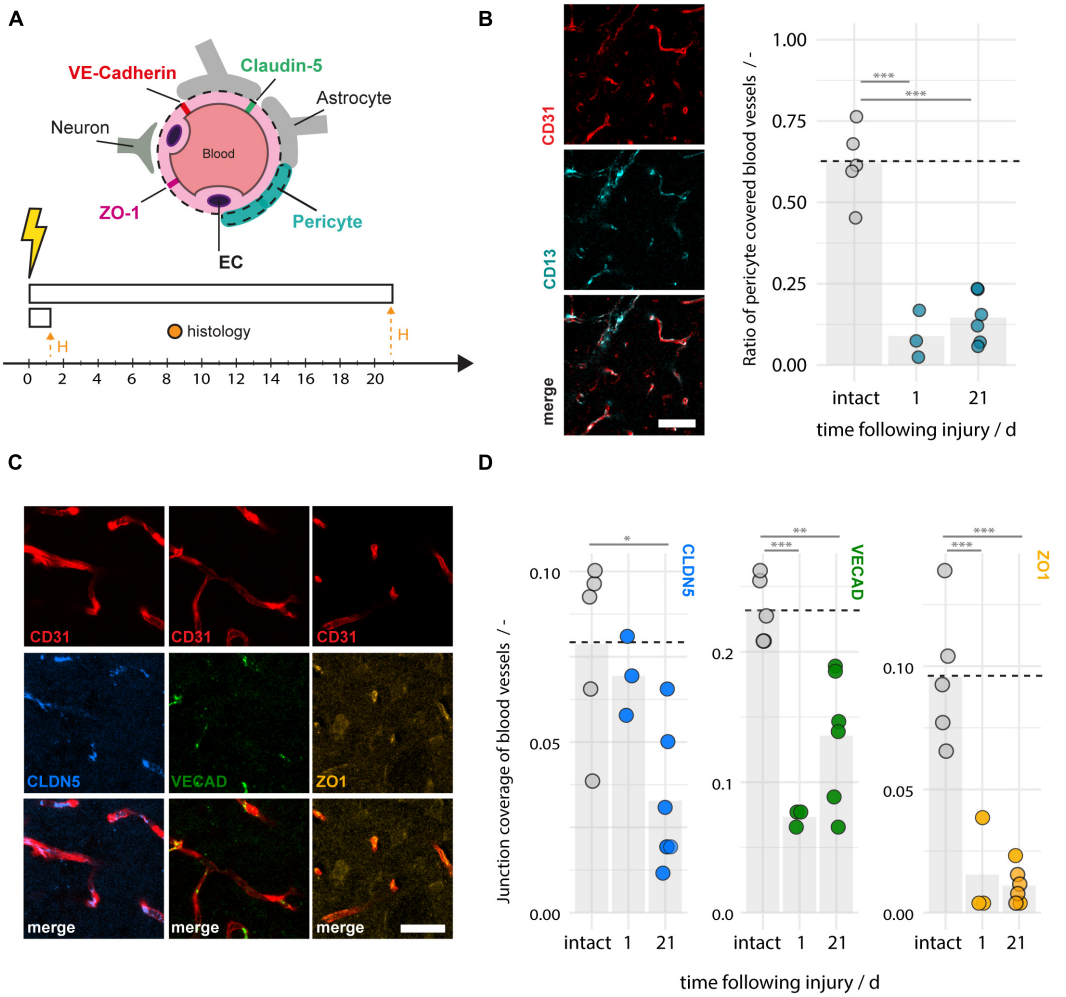

FIGURE 4 | Disruption of pericyte coverage and tight and adherens junction proteins in the peri-infarct region 1–21 days after photothrombotic stroke. **(A)** Schematic representation of blood brain barrier composition and time course of experiment ($N = 3$–6). **(B)** Representative images of blood vessels (CD31, red) covered by pericytes (CD13, cyan) and the quantitative evaluation of pericyte coverage in intact and peri-infarct cortex at 1 and 21dpi. Scale bar: 50 μm. **(C)** Representative images of tight and adherens junction proteins Claudin5 (blue), VE-Cadherin (green), and ZO-1 (yellow) associated with blood vessels (CD31, red). Scale bar: 20 μm. **(D)** Quantitative evaluation of tight and adherens junction coverage of blood vessels in the intact and peri-infarct cortex at 1 and 21 dpi. Each dot in the plots represents one animal and significance of mean differences between the groups was assessed using unpaired two-tailed one-sample Student's *t*-test. Asterisks indicate significance: $^{*}P < 0.05$, $^{**}P < 0.01$, $^{***}P < 0.001$. CTX, cortex, H, histology.

have less pericytes and tight junctions (Rust et al., 2019b,d). Therefore, leakage from these immature vessels may be an additional component of the BBB damage at the 7–21-day time points. However, most likely both events (damaged pre-existing vessels and newly formed immature vessels) contribute to the overall BBB disruption and it requires longitudinal *in vivo* experiments to identify the share of both processes. Moreover, since we performed end-point experiments in the study we have no information about levels of BBB damage outside of our measurements. Dissecting these mechanisms might be addressed in future studies with advancements in genetic models and two-photon microscopy.

An interesting observation in the photothrombotic model was the leakage in several brain regions remote from the stroke at different time points. This has also been observed in patients and other rodent stroke models and was mainly linked to degeneration and subsequent microglia activation and inflammation in projection areas or input systems to the stroke region with retrograde degeneration (Iizuka et al., 1990; Cao et al., 2017; Baumgartner et al., 2018; Jiang et al., 2018). mechanisms are especially known in the secondary thalamic injury affecting thalamus and hippocampus (Holmberg et al., 2009) but have been also observed in the cerebellum in our study. Further studies may address mechanistic basis for this effect in the photothrombotic or MCAO model.

Onset and duration of secondary injury-induced BBB leakage can vary between 3 days after stroke and may be detectable up to 6 months in rodents and 12 months in patients (Cao et al., 2020).

Taken together, the photothrombotic stroke model shows many features of BBB disruption that have been previously

observed in stroke patients and other rodent stroke models. It therefore represents a suitable model to study BBB pathology and to develop therapies to improve BBB integrity following stroke.

MATERIALS AND METHODS

Experimental Design

While BBB dysfunction has been implicated in stroke, the time-course of post-stroke BBB permeability changes is not well known for the photothrombotic stroke model. The present study aims to characterize the long-term temporal evolution of BBB opening following ischemic injury. We histologically and spectrophotometrically analyzed the loss of BBB integrity in different brain regions (affected and non-affected) at 1 days, 7, and 21 after photothrombotic stroke using Evans Blue (EB) dye to measure vascular leakage. To further investigate potential mechanisms underlying BBB damage, pericyte coverage and loss of major tight and adherens junction protein components in ischemic regions were quantified. For the time course experiment mortality rate was 0%. All animals are presented in the study; no statistical outliers were excluded. Data was acquired blinded.

Animals

All animal experiments were performed in accordance with governmental, institutional (University of Zurich), and ARRIVE guidelines and had been approved by the Cantonal Veterinary Office of Zurich. Adult male and female wild type mice (10–14 weeks) of the C57BL/6 strain (16–25 g) were used. No sex-specific differences were observed in any of the experimental readouts. Mice were housed in standard Type II/III cages at least in pairs in a temperature and humidity controlled room with a constant 12/12 h light/dark cycle (light on from 6:00 a.m. until 6:00 p.m.).

Surgical Procedure

Mice were anesthetized using isoflurane (3% induction, 1.5% maintenance; Attane, Provet AG). Analgesic (Novalgin, Sanofi) was administered 24 h prior to the start of the procedure via drinking water. A photothrombotic stroke to unilaterally lesion the sensorimotor cortex was induced on the right hemisphere, as previously described (Labat-gest and Tomasi, 2013; Rust et al., 2019b). Briefly, animals were placed in a stereotactic frame (David Kopf Instruments), the surgical area was sanitized and the skull was exposed through a midline skin incision. A cold light source (Olympus KL 1,500LCS, 150W, 3,000K) was positioned over the right forebrain cortex (anterior/posterior: −1.5–+1.5 mm and medial/lateral 0 –+2 mm relative to Bregma). 5 min prior to illumination, Rose Bengal (10 mg/ml, in 0.9% NaCl, Sigma) was injected intraperitoneally 5 min prior to illumination and the region of interest was subsequently illuminated through the intact skull for 8.5 min. To restrict the illuminated area, an opaque template with an opening of 3 × 4 mm was placed directly on the skull. The wound was closed using a 6/0 silk suture and animals were allowed to recover. For postoperative care, all animals received analgesics (Novalgin, Sanof) for at least 3 days after surgery.

Blood Perfusion by Laser Doppler Imaging

The blood perfusion was measured using Laser Doppler Imaging (Moor Instruments, MOORLDI2-IR). Animals were placed in a stereotactic frame, the surgical area was sanitized and the skull was exposed through a midline skin incision. The brain was scanned using the repeat image measurement mode. All data were exported and quantified in terms of flux in the ROI using Fiji (ImageJ).

Tissue Processing

To characterize the loss of BBB integrity after stroke, ischemic brain tissue was analyzed (1) histologically and (2) spectrophotometrically at day post injury 1, 7, and 21. EB, which was prepared as a 2% solution in saline, was injected intraperitoneally either 4 or 24 h prior to perfusion (6 μg/g body weight, Sigma). For histological analysis, animals were euthanized by intraperitoneal application of pentobarbital (150 mg/kg body weight, Streuli Pharma AG) and perfused with Ringer solution (containing 5 ml/l Heparin, B. Braun) followed by paraformaldehyde (PFA, 4%, in 0.2 M phosphate buffer, pH 7) to wash out intravascular EB. Brains were rapidly harvested and post-fixed for approximately 4 h by exposure to 4% PFA, then transferred to 30% sucrose for cryoprotection and stored at 4°C. Coronal sections with a thickness of 40 μm were cut using a sliding microtome (Microm HM430, Leica), collected and stored as free-floating sections in cryoprotectant solution at −20°C until further processing. For spectrophotometric analysis, animals were perfused with Ringer solution, CNS tissue was isolated (as described before) and stored at −20°C before further processing.

Immunofluorescence

Brain sections were washed with 0.1M phosphate buffer (PB) and incubated with blocking solution containing donkey serum (10%) in PB for 30 min at room temperature. For detection of vascular endothelial cells, sections were incubated overnight at 4°C with monoclonal rat anti-CD31 antibody (BD Biosciences, 1:50). The localization of tight/adherens junction proteins was assessed using the following antibodies: mouse anti-Claudin-5 antibody (1:200, Thermo Fisher Scientific); rat anti-VE-Cadherin antibody (1:100, Thermo Fisher Scientific), and rabbit anti-ZO-1 antibody (1:100, Thermo Fisher Scientific). Pericyte coverage was visualized with goat anti-CD13 (1:200; R&D Systems). The primary antibody incubation was followed by 2 h incubation at room temperature with corresponding fluorescent secondary antibodies (1:500, Thermo Fisher Scientific). Nuclei were counterstained with DAPI (1:2,000 in 0.1 M PB, Sigma). Sections were mounted in 0.1 M PB on Superfrost PlusTM microscope slides and coverslipped using Mowiol.

Spectrophotometric Evans Blue Quantification

Evans Blue dye is an inert tracer frequently used in BBB studies. EB binds rapidly and exclusively to plasma albumin (Yen et al., 2013) when injected peripherally into circulation. Since serum

albumin does not cross the BBB to the brain parenchyma if the barrier is structurally and functionally intact, spectrophotometric determination of EB dye accumulation in brain tissue outside blood vessels reflects the extent of vascular leakage. The isolated CNS tissue samples were homogenized in a lysis buffer (250 µl/mg tissue weight; Tris-HCl, EDTA, NP-40, NaCl, protease inhibitor cocktail) and incubated for 2 h at 4°C, shacking. The mixture was centrifuged to sediment the non-dissolved tissue parts (25 min, 15,000 g, 4°C) and the extracted supernatant was collected in a 96-well plate. Based on a standard curve, EB concentrations could be quantified from their absorbance readings (620 nm) using a standard microplate reader (Spark, Tecan). The results were expressed as micrograms of EB per milligram of brain tissue.

Fluorescence Microscopy and Quantification

Imaging of brain sections was performed 1, 7, and 21 days after stroke with an Olympus FV1000 or Leica SP8 laser scanning confocal microscope equipped with 10×, 20×, and 40× objectives. Images were processed using Fiji (ImageJ), Adobe Photoshop CC and Adobe Illustrator CC. Evans blue signal area in ischemic brain sections was quantified by thresholding at fivefold background signal intensity of the intact sensorimotor cortex (perfused with EB). Pericyte and tight junction coverage of blood vessels was calculated as previously described with an automated Fiji (ImageJ) script (Rust et al., 2019a, 2020) and normalized to the intact cortex. Briefly, 4–6 random ROIs were selected. Area covered by blood vessels was enlarged by 3 µm and pericyte or tight junction signals within this mask were binarized and presented as a ratio. We defined the stroke core region as the region with no surviving neurons that is surrounding by the glial scar. From this region, we defined tissue up to 300 µm distal along the cortex as the ischemic border zone as previously described (Rust et al., 2019b).

Statistical Analysis

Statistical analysis was performed using RStudio and GraphPad Prism 7. Sample sizes were designed with adequate power according to our previous studies (Rust et al., 2019b,d) and to the literature. All data were tested for normal distribution by using the Shapiro-Wilk test. Normally distributed data were tested for differences with a two-tailed unpaired one-sample *t*-test to compare changes between two groups (differences between ipsi- and contra-lesional site) as in **Figures 3E**, **4B–D**. Multiple comparisons as in **Figures 1C**, **2D** were initially tested for normal distribution with the Shapiro-Wilk test. The significance of mean differences between normally distributed multiple comparisons was assessed using Tukey's HSD. Data are expressed as means ± SD, and statistical significance was defined as $^{*}p < 0.05$, $^{**}p < 0.01$, and $^{***}p < 0.001$.

DATA AVAILABILITY STATEMENT

The raw data supporting the conclusions of this article will be made available by the authors, without undue reservation.

ETHICS STATEMENT

The animal study was reviewed and approved by the Cantonal Veterinary Office of Zurich.

AUTHOR CONTRIBUTIONS

RW, LG, and RR designed the study. RR prepared the figures and wrote the manuscript. RW, LG, GM, MM, and RR carried out the experiments. RW, LG, MS, and CT proofread and revised the manuscript. All authors read and approved the final manuscript.

FUNDING

RR and CT were supported by the Mäxi Foundation.

SUPPLEMENTARY MATERIAL

The Supplementary Material for this article can be found online at: https://www.frontiersin.org/articles/10.3389/fphys.2020.586226/full#supplementary-material

REFERENCES

Abdullahi, W., Tripathi, D., and Ronaldson, P. T. (2018). Blood-brain barrier dysfunction in ischemic stroke: targeting tight junctions and transporters for vascular protection. *Am. J. Physiol. Cell Physiol.* 315, C343–C356. doi: 10.1152/ajpcell.00095.2018

Allred, R. P., Adkins, D. L., Woodlee, M. T., Husbands, L. C., Maldonado, M. A., Kane, J. R., et al. (2008). The vermicelli handling test: a simple quantitative measure of dexterous forepaw function in rats. *J. Neurosci. Methods* 170, 229–244. doi: 10.1016/j.jneumeth.2008.01.015

Armulik, A., Genové, G., Mäe, M., Nisancioglu, M. H., Wallgard, E., Niaudet, C., et al. (2010). Pericytes regulate the blood–brain barrier. *Nature* 468, 557–561. doi: 10.1038/nature09522

Baumgartner, P., El Amki, M., Bracko, O., Luft, A. R., and Wegener, S. (2018). Sensorimotor stroke alters hippocampo-thalamic network activity. *Sci. Rep.* 8:15770. doi: 10.1038/s41598-018-34002-9

Belayev, L., Busto, R., Zhao, W., and Ginsberg, M. D. (1996). Quantitative evaluation of blood-brain barrier permeability following middle cerebral artery occlusion in rats. *Brain Res.* 739, 88–96. doi: 10.1016/s0006-8993(96)00815-3

Bell, R. D., Winkler, E. A., Sagare, A. P., Singh, I., LaRue, B., Deane, R., et al. (2010). Pericytes control key neurovascular functions and neuronal phenotype in the adult brain and during brain aging. *Neuron* 68, 409–427. doi: 10.1016/j.neuron.2010.09.043

Berndt, P., Winkler, L., Cording, J., Breitkreuz-Korff, O., Rex, A., Dithmer, S., et al. (2019). Tight junction proteins at the blood–brain barrier: far more than claudin-5. *Cell. Mol. Life Sci.* 76, 1987–2002. doi: 10.1007/s00018-019-03030-7

Brouns, R., Wauters, A., De Surgeloose, D., Mariën, P., and De Deyn, P. P. (2011). Biochemical markers for blood-brain barrier dysfunction in acute ischemic stroke correlate with evolution and outcome. *Eur. Neurol.* 65, 23–31. doi: 10.1159/000321965

Cao, Z., Balasubramanian, A., Pedersen, S. E., Romero, J., Pautler, R. G., and Marrelli, S. P. (2017). TRPV1-mediated pharmacological hypothermia promotes improved functional recovery following ischemic stroke. *Sci. Rep.* 7:17685. doi: 10.1038/s41598-017-17548-y

Cao, Z., Harvey, S. S., Bliss, T. M., Cheng, M. Y., and Steinberg, G. K. (2020). Inflammatory responses in the secondary thalamic injury after cortical ischemic stroke. *Front. Neurol.* 11:236. doi: 10.3389/fneur.2020.00236

Carmichael, S. T. (2005). Rodent models of focal stroke: size. mechanism, and purpose. *NeuroRx* 2, 396–409. doi: 10.1602/neurorx.2.3.396

Castellazzi, M., Morotti, A., Tamborino, C., Alessi, F., Pilotto, S., Baldi, E., et al. (2020). Increased age and male sex are independently associated with higher frequency of blood–cerebrospinal fluid barrier dysfunction using the albumin quotient. *Fluids Barriers CNS* 17:14. doi: 10.1186/s12987-020-0173-2

Dirnagl, U. (2010). *Rodent Models of Stroke*. Available online at: https://www.springer.com/de/book/9781607617495 (accessed July 3, 2020).

Fernández-Klett, F., Potas, J. R., Hilpert, D., Blazej, K., Radke, J., Huck, J., et al. (2013). Early loss of pericytes and perivascular stromal cell-induced scar formation after stroke. *J. Cereb. Blood Flow Metab. Off. J. Int. Soc. Cereb. Blood Flow Metab.* 33, 428–439. doi: 10.1038/jcbfm.2012.187

GBD 2016 Stroke Collaborators (2019). Global, regional, and national burden of stroke, 1990-2016: a systematic analysis for the global burden of disease study 2016. *Lancet Neurol.* 18, 439–458. doi: 10.1016/S1474-4422(19)30034-1

Hoff, E. I., oude Egbrink, M. G. A., Heijnen, V. V. T., Steinbusch, H. W. M., and van Oostenbrugge, R. J. (2005). In vivo visualization of vascular leakage in photochemically induced cortical infarction. *J. Neurosci. Methods* 141, 135–141. doi: 10.1016/j.jneumeth.2004.06.004

Holmberg, P., Liljequist, S., and Wägner, A. (2009). Secondary brain injuries in thalamus and hippocampus after focal ischemia caused by mild, transient extradural compression of the somatosensori cortex in the rat. *Curr. Neurovasc. Res.* 6, 1–11. doi: 10.2174/156720209787466073

Hom, J., Dankbaar, J. W., Soares, B. P., Schneider, T., Cheng, S.-C., Bredno, J., et al. (2011). Blood-brain barrier permeability assessed by perfusion CT predicts symptomatic hemorrhagic transformation and malignant edema in acute ischemic stroke. *Am. J. Neuroradiol.* 32, 41–48. doi: 10.3174/ajnr.A2244

Huang, Z. G., Xue, D., Preston, E., Karbalai, H., and Buchan, A. M. (1999). Biphasic opening of the blood-brain barrier following transient focal ischemia: effects of hypothermia. *Can. J. Neurol. Sci. J. Can. Sci. Neurol.* 26, 298–304. doi: 10.1017/s0317167100000421

Iizuka, H., Sakatani, K., and Young, W. (1990). Neural damage in the rat thalamus after cortical infarcts. *Stroke* 21, 790–794. doi: 10.1161/01.str.21.5.790

Jiang, X., Andjelkovic, A. V., Zhu, L., Yang, T., Bennett, M. V. L., Chen, J., et al. (2018). Blood-brain barrier dysfunction and recovery after ischemic stroke. *Prog. Neurobiol.* 16, 144–171. doi: 10.1016/j.pneurobio.2017.10.001

Jiao, H., Wang, Z., Liu, Y., Wang, P., and Xue, Y. (2011). Specific role of tight junction proteins claudin-5, occludin, and ZO-1 of the blood–brain barrier in a focal cerebral ischemic insult. *J. Mol. Neurosci.* 44, 130–139. doi: 10.1007/s12031-011-9496-4

Kassner, A., and Merali, Z. (2015). Assessment of blood-brain barrier disruption in stroke. *Stroke* 46, 3310–3315. doi: 10.1161/STROKEAHA.115.008861

Kastrup, A., Gröschel, K., Ringer, T. M., Redecker, C., Cordesmeyer, R., Witte, O. W., et al. (2008). Early disruption of the blood-brain barrier after thrombolytic therapy predicts hemorrhage in patients with acute stroke. *Stroke* 39, 2385–2387. doi: 10.1161/STROKEAHA.107.505420

Katan, M., and Luft, A. (2018). Global Burden of Stroke. *Semin. Neurol.* 38, 208–211. doi: 10.1055/s-0038-1649503

Labat-gest, V., and Tomasi, S. (2013). Photothrombotic ischemia: a minimally invasive and reproducible photochemical cortical lesion model for mouse stroke studies. *J. Vis. Exp.* 76:50370. doi: 10.3791/50370

Li, J.-J., Xing, S.-H., Zhang, J., Hong, H., Li, Y.-L., Dang, C., et al. (2011). Decrease of tight junction integrity in the ipsilateral thalamus during the acute stage after focal infarction and ablation of the cerebral cortex in rats. *Clin. Exp. Pharmacol. Physiol.* 38, 776–782. doi: 10.1111/j.1440-1681.2011.05591.x

Ling, L., Zeng, J., Pei, Z., Cheung, R. T. F., Hou, Q., Xing, S., et al. (2009). Neurogenesis and angiogenesis within the ipsilateral thalamus with secondary damage after focal cortical infarction in hypertensive rats. *J. Cereb. Blood Flow Metab. Off. J. Int. Soc. Cereb. Blood Flow Metab.* 29, 1538–1546. doi: 10.1038/jcbfm.2009.76

Merali, Z., Huang, K., Mikulis, D., Silver, F., and Kassner, A. (2017). Evolution of blood-brain-barrier permeability after acute ischemic stroke. *PLoS One* 12:e0171558. doi: 10.1371/journal.pone.0171558

Montagne, A., Nation, D. A., Sagare, A. P., Barisano, G., Sweeney, M. D., Chakhoyan, A., et al. (2020). APOE4 leads to blood–brain barrier dysfunction predicting cognitive decline. *Nature* 581, 71–76. doi: 10.1038/s41586-020-2247-3

Nadareishvili, Z., Simpkins, A. N., Hitomi, E., Reyes, D., and Leigh, R. (2019). Post-stroke blood-brain barrier disruption and poor functional outcome in patients receiving thrombolytic therapy. *Cerebrovasc. Dis.* 47, 135–142. doi: 10.1159/000499666

Nagel, S., Wagner, S., Koziol, J., Kluge, B., and Heiland, S. (2004). Volumetric evaluation of the ischemic lesion size with serial MRI in a transient MCAO model of the rat: comparison of DWI and T1WI. *Brain Res. Brain Res. Protoc.* 12, 172–179. doi: 10.1016/j.brainresprot.2003.11.004

Nation, D. A., Sweeney, M. D., Montagne, A., Sagare, A. P., D'Orazio, L. M., Pachicano, M., et al. (2019). Blood–brain barrier breakdown is an early biomarker of human cognitive dysfunction. *Nat. Med.* 25, 270–276. doi: 10.1038/s41591-018-0297-y

Nih, L. R., Gojgini, S., Carmichael, S. T., and Segura, T. (2018). Dual-function injectable angiogenic biomaterial for the repair of brain tissue following stroke. *Nat. Mater.* 17:642. doi: 10.1038/s41563-018-0083-8

Obermeier, B., Daneman, R., and Ransohoff, R. M. (2013). Development, maintenance and disruption of the blood-brain barrier. *Nat. Med.* 19, 1584–1596. doi: 10.1038/nm.3407

Okada, M., Kikuchi, T., Okamura, T., Ikoma, Y., Tsuji, A. B., Wakizaka, H., et al. (2015). In-vivo imaging of blood-brain barrier permeability using positron emission tomography with 2-amino-[3-11C]isobutyric acid. *Nucl. Med. Commun.* 36, 1239–1248. doi: 10.1097/MNM.0000000000000385

Ozkul-Wermester, O., Guegan-Massardier, E., Triquenot, A., Borden, A., Perot, G., and Gérardin, E. (2014). Increased blood-brain barrier permeability on perfusion computed tomography predicts hemorrhagic transformation in acute ischemic stroke. *Eur. Neurol.* 72, 45–53. doi: 10.1159/000358297

Prakash, R., and Carmichael, S. T. (2015). Blood–brain barrier breakdown and neovascularization processes after stroke and traumatic brain injury. *Curr. Opin. Neurol.* 28, 556–564. doi: 10.1097/WCO.0000000000000248

Reeves, M. J., Bushnell, C. D., Howard, G., Gargano, J. W., Duncan, P. W., Lynch, G., et al. (2008). Sex differences in stroke: epidemiology, clinical presentation, medical care, and outcomes. *Lancet Neurol.* 7, 915–926. doi: 10.1016/S1474-4422(08)70193-5

Rosenberg, G. A., Estrada, E. Y., and Dencoff, J. E. (1998). Matrix metalloproteinases and TIMPs are associated with blood-brain barrier opening after reperfusion in rat brain. *Stroke* 29, 2189–2195. doi: 10.1161/01.str.29.10.2189

Rust, R., Gantner, C., and Schwab, M. E. (2018). Pro- and antiangiogenic therapies: current status and clinical implications. *FASEB J. Off. Publ. Fed. Am. Soc. Exp. Biol* 33, 34-48. doi: 10.1096/fj.201800640RR

Rust, R., Grönnert, L., Dogançay, B., and Schwab, M. E. (2019a). A revised view on growth and remodeling in the retinal vasculature. *Sci. Rep.* 9:3263. doi: 10.1038/s41598-019-40135-2

Rust, R., Grönnert, L., Gantner, C., Enzler, A., Mulders, G., Weber, R. Z., et al. (2019b). Nogo-A targeted therapy promotes vascular repair and functional recovery following stroke. *Proc. Natl. Acad. Sci U.S.A.* 116, 14270-14279. doi: 10.1073/pnas.1905309116

Rust, R., Grönnert, L., Weber, R. Z., Mulders, G., and Schwab, M. E. (2019c). Refueling the ischemic CNS: guidance molecules for vascular repair. *Trends Neurosci* 42, 644-656. doi: 10.1016/j.tins.2019.05.006

Rust, R., Kirabali, T., Grönnert, L., Dogancay, B., Limasale, Y. D. P., Meinhardt, A., et al. (2020). A practical guide to the automated analysis of vascular growth, maturation and injury in the brain. *Front. Neurosci* 14:244. doi: 10.3389/fnins.2020.00244

Rust, R., Weber, R. Z., Grönnert, L., Mulders, G., Maurer, M. A., Hofer, A.-S., et al. (2019d). Anti-Nogo-A antibodies prevent vascular leakage and act as pro-angiogenic factors following stroke. *Sci. Rep.* 9, 1–10. doi: 10.1038/s41598-019-56634-1

Sifat, A. E., Vaidya, B., and Abbruscato, T. J. (2017). Blood-brain barrier protection as a therapeutic strategy for acute ischemic stroke. *AAPS J.* 19, 957–972. doi: 10.1208/s12248-017-0091-7

Sourbron, S., Ingrisch, M., Siefert, A., Reiser, M., and Herrmann, K. (2009). Quantification of cerebral blood flow, cerebral blood volume, and blood–brain-barrier leakage with DCE-MRI. *Magn. Reson. Med.* 62, 205–217. doi: 10.1002/mrm.22005

Strbian, D., Durukan, A., Pitkonen, M., Marinkovic, I., Tatlisumak, E., Pedrono, E., et al. (2008). The blood-brain barrier is continuously open for several weeks following transient focal cerebral ischemia. *Neuroscience* 153, 175–181. doi: 10.1016/j.neuroscience.2008.02.012

Underly, R. G., Levy, M., Hartmann, D. A., Grant, R. I., Watson, A. N., and Shih, A. Y. (2017). Pericytes as inducers of rapid, matrix metalloproteinase-9-dependent capillary damage during Ischemia. *J. Neurosci.* 37, 129–140. doi: 10.1523/JNEUROSCI.2891-16.2016

Yen, L. F., Wei, V. C., Kuo, E. Y., and Lai, T. W. (2013). Distinct patterns of cerebral extravasation by Evans blue and sodium fluorescein in rats. *PLoS One* 8:e68595. doi: 10.1371/journal.pone.0068595

Zhao, Z., Nelson, A. R., Betsholtz, C., and Zlokovic, B. V. (2015). Establishment and dysfunction of the blood-brain barrier. *Cell* 163, 1064–1078. doi: 10.1016/j.cell.2015.10.067

Conflict of Interest: The authors declare that the research was conducted in the absence of any commercial or financial relationships that could be construed as a potential conflict of interest.

frontiers in Physiology

REVIEW
published: 25 November 2020
doi: 10.3389/fphys.2020.601320

The Role of Basement Membranes in Cerebral Amyloid Angiopathy

*Matthew D. Howe†, Louise D. McCullough and Akihiko Urayama**

Department of Neurology, McGovern Medical School, The University of Texas Health Science Center at Houston, Houston, TX, United States

Dementia is a neuropsychiatric syndrome characterized by cognitive decline in multiple domains, often leading to functional impairment in activities of daily living, disability, and death. The most common causes of age-related progressive dementia include Alzheimer's disease (AD) and vascular cognitive impairment (VCI), however, mixed disease pathologies commonly occur, as epitomized by a type of small vessel pathology called cerebral amyloid angiopathy (CAA). In CAA patients, the small vessels of the brain become hardened and vulnerable to rupture, leading to impaired neurovascular coupling, multiple microhemorrhage, microinfarction, neurological emergencies, and cognitive decline across multiple functional domains. While the pathogenesis of CAA is not well understood, it has long been thought to be initiated in thickened basement membrane (BM) segments, which contain abnormal protein deposits and amyloid-β (Aβ). Recent advances in our understanding of CAA pathogenesis link BM remodeling to functional impairment of perivascular transport pathways that are key to removing Aβ from the brain. Dysregulation of this process may drive CAA pathogenesis and provides an important link between vascular risk factors and disease phenotype. The present review summarizes how the structure and composition of the BM allows for perivascular transport pathways to operate in the healthy brain, and then outlines multiple mechanisms by which specific dementia risk factors may promote dysfunction of perivascular transport pathways and increase Aβ deposition during CAA pathogenesis. A better understanding of how BM remodeling alters perivascular transport could lead to novel diagnostic and therapeutic strategies for CAA patients.

Keywords: CAA, basement membrane, amyloid-beta, perivascular transport, dementia

OPEN ACCESS

Edited by:
Fabrice Dabertrand, University of Colorado, United States

Reviewed by:
Humberto Mestre, University of Rochester, United States
Susanne J. Van Veluw, Massachusetts General Hospital and Harvard Medical School, United States

***Correspondence:**
Akihiko Urayama
Akihiko.Urayama@uth.tmc.edu

†Present address:
Matthew D. Howe, Department of Psychiatry and Human Behavior, Brown University, Providence, RI, United States

Specialty section:
This article was submitted to Vascular Physiology, a section of the journal Frontiers in Physiology

Received: *31 August 2020*
Accepted: *28 October 2020*
Published: *25 November 2020*

Citation:
Howe MD, McCullough LD and Urayama A (2020) The Role of Basement Membranes in Cerebral Amyloid Angiopathy. Front. Physiol. 11:601320. doi: 10.3389/fphys.2020.601320

INTRODUCTION

Alzheimer's disease (AD) and vascular cognitive impairment (VCI) nominally represent the most common forms of age-related progressive dementia, and multiple studies have demonstrated that mixed vascular and AD-type amyloid-β (Aβ) pathology is a common finding on autopsy in elderly dementia patients (Jellinger, 2002; White et al., 2005; Schneider et al., 2007). This may be partially explained by epidemiological studies which show that the majority of risk factors for both types of dementia are related to cerebrovascular disease and include APOE-ε4 genotype, advanced age, hypertension, hyperlipidemia, diabetes, obesity, and smoking (Corder et al., 1993; Kivipelto et al., 2006; Gorelick et al., 2011; Viticchi et al., 2015; Santos et al., 2017; Vos et al., 2017; Deckers et al., 2019). These shared risk factors suggest that an interaction between cerebrovascular disease and

Aβ deposition exists, and may help to explain the relatively high incidence of mixed dementia (Deramecourt et al., 2012). While a causal link has yet to be established, a growing body of clinical and pre-clinical evidence suggests that cerebrovascular disease can be a major driver of Aβ deposition and cognitive decline in patients suffering from age-related progressive dementia (Santos et al., 2017).

Cerebral amyloid angiopathy (CAA), which refers to the presence of Aβ plaques in the walls of cerebral vessels, is associated with significant morbidity and mortality in afflicted individuals (Vonsattel et al., 1991; Greenberg and Vonsattel, 1997; Greenberg et al., 2020). CAA affects approximately 82–98% of AD patients on autopsy and is associated with an increased burden of cerebrovascular insults (Jellinger, 2002; Attems and Jellinger, 2014). Neuropathological studies demonstrate that CAA preferentially affects the outer leptomeningeal vessels on the surface of the brain, and can also spread to involve more distal intraparenchymal arteries, arterioles, and capillaries in some patients (Thal et al., 2002; Yamada, 2015; Greenberg et al., 2020). CAA pathology is identified by the formation of small Aβ deposits within the basement membrane (BM), which is a thin perivascular layer of extracellular matrix (ECM) that plays an important role in maintaining the integrity of the blood-brain barrier (Yamaguchi et al., 1992; Reed et al., 2019; Gireud-Goss et al., 2020). As BM remodeling and Aβ deposition progress, CAA impairs cognitive function via multiple mechanisms, including reduced neurovascular coupling, progressive vasculopathy as well as neurological emergencies such as lobar intracerebral hemorrhage.

The pathophysiology of sporadic, age-related CAA is multifactorial and may be driven, in part, by disruption of perivascular Aβ transport along with the remodeled BM. Recent advances in the field have shed light on how specific, early changes in BM morphology and composition may impair the perivascular transport of Aβ. In the present review, we will first describe the anatomy, morphology, molecular composition, and physiology that support perivascular transport through healthy BM. We will then explore how these processes are altered in individuals at-risk of or affected by CAA. Finally, we will highlight multiple potential mechanisms for how BM remodeling could impair perivascular transport and drive CAA pathogenesis. Our hope is that this review will highlight the common molecular pathophysiology of conditions that lead to impaired perivascular transport and early Aβ deposition, which could have major implications for the prevention, early detection and treatment of CAA.

CHANGES IN BM MORPHOLOGY AND COMPOSITION DURING CAA PATHOGENESIS

Anatomical Overview of the Healthy Perivascular Space

The brain contains a dense network of blood vessels and perivascular spaces that act in concert to deliver oxygen and nutrients to the parenchymal tissue, as well as remove waste products. This network can be conceptualized as the cerebrovascular tree (Chandra et al., 2017; Kirst et al., 2020; **Figure 1**). Briefly, the internal carotid and vertebral arteries converge upon the Circle of Willis within the cerebrospinal fluid (CSF)-containing subarachnoid space (SAS) at the base of the skull (Chandra et al., 2017; Kirst et al., 2020). These vessels, along with the SAS, further subdivide and extend around the brain, creating a tortuous network of surface vessels surrounded by large perivascular spaces, called cisterns, that bathe the outside of the brainstem, cerebellum, and cerebral cortex in CSF (Adeeb et al., 2013). These large and medium-sized surface vessels eventually subdivide into smaller leptomeningeal arteries that penetrate the pia mater through Virchow-Robin space, which is a CSF-filled perivascular invagination of cortical tissue that is continuous with the surface cisterns (Shih et al., 2015; Morris et al., 2016; Nakada et al., 2017; Hannocks et al., 2018; Pizzo et al., 2018). As the leptomeningeal arteries pass through Virchow-Robin space, they branch into penetrating arterioles and capillary beds, which subsequently drain into venules, veins, and venous sinuses (Kiliç and Akakin, 2008; Marín-Padilla and Knopman, 2011; Shih et al., 2015). The perivascular space (PVS) continues alongside leptomeningeal arteries and penetrating arterioles, providing an important channel that bathes the cerebral vasculature in CSF and promotes the perivascular clearance of waste products from the brain parenchyma (Alcolado et al., 1988; Zhang et al., 1990; Iliff et al., 2012, 2013a,b; Xie et al., 2013). While the nature of the PVS at the capillary vasculature remains elusive, compelling evidence suggests that the vascular BM serves as a canal for solute clearance (Morris et al., 2016). These important clearance pathways are dependent on a complex interplay between the cells, extracellular BM proteins, and the associated PVSs that together form a unique microenvironment.

Under normal conditions, the healthy PVS consists of three distinct cellular layers that are associated with BM proteins (**Figure 1**, inset). In terms of cellular components, the astrocytic endfeet surround the intracerebral vessels and define the outermost layer of the perivascular tissue, with an additional contribution of microglial processes (Mathiisen et al., 2010; Joost et al., 2019). Additional cell types, including mural cells [referring to vascular smooth muscle cells (VSMCs), pericytes and fibroblasts] as well as perivascular macrophages, comprise the loosely defined middle cellular layer and are embedded within the BM (Goldmann et al., 2016; Nikolakopoulou et al., 2017; Chasseigneaux et al., 2018; Vanlandewijck et al., 2018). Finally, the endothelial cells form a continuous barrier, yet the interface between the CNS and the periphery, which comprises the innermost layer of the perivascular tissue (Ben-Zvi et al., 2014; Banks, 2016). In addition to these separate cellular layers, the PVS includes two major, extracellular components: the protein-rich BM, and the fluid-filled PVS. The composition of the BM is dependent on the cell types contained within each region of the perivasculature and can be divided into anatomically and functionally distinct endothelial, pial, and glial layers (Hannocks et al., 2018). The innermost endothelial layer of the BM is directly apposed to the abluminal surface of the endothelial cell, and extends outward to the PVS

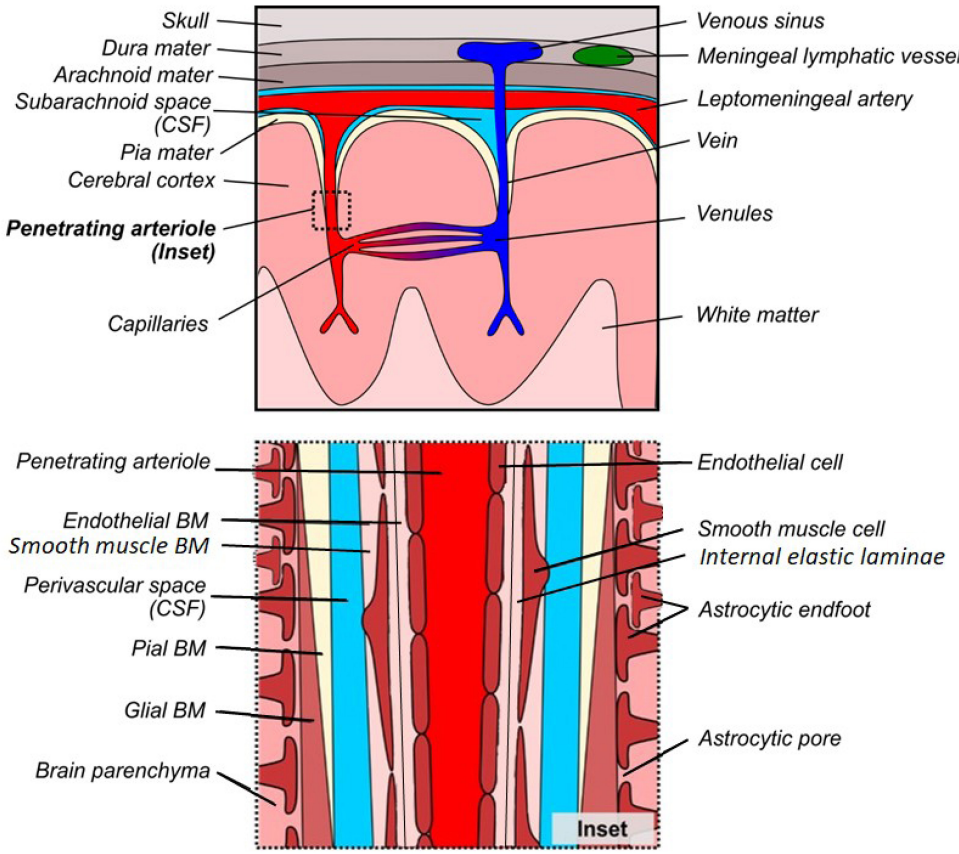

FIGURE 1 | Gross and microscopic anatomy of the perivascular space. **Top:** Gross anatomy of meninges, cortical vessels and associated perivascular networks. **Bottom:** Microscopic anatomy of the perivascular space surrounding a penetrating arteriole in normal cortex. There is debate as to whether the perivascular space is truly distinct from the glial/pial and endothelial BMs, however it has been drawn separately to facilitate understanding of the various models of perivascular transport.

(Sapsford et al., 1983; Abbott et al., 2018). On the opposite side of the PVS, the outer BM is further subdivided into pial and glial layers. The pial layer of the BM is present along the outer surface of the PVS of leptomeningeal arteries and is produced by meningeal epithelial cells and highly attenuated layers of astrocytic endfoot forming the glia limitans (Alcolado et al., 1988; Zhang et al., 1990; Sofroniew, 2015). The glial layer of the BM replaces the pial layer along penetrating arteries and arterioles. This layer is secreted by the perivascular endfeet of astrocytes and forms the prominent outer border of the PVS in arterioles, which eventually merges with the endothelial layer to form a thin capillary BM (Hauw et al., 1975; Watanabe et al., 2010). This separation of layers re-emerges in the post-capillary venule and continues to form a paravenous/extramural perivascular drainage system (Iliff et al., 2012; Hladky and Barrand, 2018).

Composition and Function of the Healthy BM

During development, endothelial cells, astrocytes, and pericytes produce the major components of their respective BM partitions (Chouchkov et al., 1987). In the healthy adult brain, the BM is comprised of large complexes of ECM molecules, including collagen IV, nidogen-1 and -2, various heparan sulfate proteoglycans (HSPGs), and region-dependent laminin isoforms (Engelhardt and Sorokin, 2009; **Table 1**). The BM plays an important role in providing structural support and regulating the activity of the cellular components in the PVS (Thomsen et al., 2017b). The BM regulates local cellular function by binding to integrin receptors, which are a family of cell membrane receptors that contain both α and β subunits. Different classes of integrins are expressed by endothelial cells (α1β1, α3β, α6β1, αvβ1) (Paulus et al., 1993; Milner and Campbell, 2002, 2006; Engelhardt and Sorokin, 2009), pericytes (α4β1) (Grazioli et al., 2006) and astrocytes (α1β1, α5β1, α6β1) (Milner and Campbell, 2006). In addition to their role in maintaining the structure of the PVS, many integrins also transduce signals from surrounding BM proteins, alerting cells to changes in their extracellular environment. For example, α5β1 integrin, which is expressed on the outer surface of astrocytic endfeet, binds to fibronectin within the BM and regulates downstream signaling pathways to promote cellular adhesion and angiogenesis during tissue development and after injury (Wang and Milner, 2006; Yanqing et al., 2006; Mahalingam et al., 2007; Huveneers et al., 2008; Wang et al., 2010; Hielscher et al., 2016; Lee et al., 2019).

TABLE 1 | BM proteins expressed in mature intraparenchymal and meningeal vessels.

	Perivascular Localization	Cellular source
Collagens		
Collagen IV	• Brain microvessels (Urabe et al., 2002) • Choroid plexus (Urabe et al., 2002) • Leptomeningeal arteries (Keable et al., 2016)	• Endothelial cells (Jeanne et al., 2015) • Meningeal cells (Sievers et al., 1994) • Pericytes (Jeanne et al., 2015)
Fibulins		
Fibulin-1	• Brain microvessels (Rauch et al., 2005) • Choroid plexus (Rauch et al., 2005)	• Endothelial cells (Thomsen et al., 2017a)
Fibulin-2	• Larger intraparenchymal vessels (Rauch et al., 2005)	• Endothelial cells (Thomsen et al., 2017a)
Fibulin-5	• Brain microvessels (Guo et al., 2016)	• Astrocytes (Howe et al., 2019) • Endothelial cells (Albig and Schiemann, 2004)
Heparan sulfate proteoglycans		
Perlecan	• Brain microvessels (Endothelial > Glial BM) (Agrawal et al., 2006; Gustafsson et al., 2013)	• Astrocytes (Howe et al., 2019) • Endothelial cells (Thomsen et al., 2017a)
Agrin	• Brain microvessels (Glial > Endothelial BM) (Barber and Lieth, 1997; Agrawal et al., 2006; Wolburg-Buchholz et al., 2009)	• Astrocytes (Howe et al., 2019; Noël et al., 2019) • Endothelial cells (Thomsen et al., 2017a)
Collagen XVIII	• Brain microvessels (Utriainen et al., 2004) • Choroid plexus (Utriainen et al., 2004) • Leptomeningeal arteries (Utriainen et al., 2004)	• Astrocytes (Howe et al., 2019) • Endothelial cells (Thomsen et al., 2017a)
Laminins		
Laminin 111	• Brain microvessels (parenchymal BM) (Jucker et al., 1996; Sixt et al., 2001; Halder et al., 2018; Hannocks et al., 2018)	• Astrocytes (Sixt et al., 2001)
Laminin 211	• Brain microvessels (parenchymal BM) (Jucker et al., 1996; Sixt et al., 2001; Hannocks et al., 2018)	• Astrocytes (Menezes et al., 2014)
Laminin 411	• Brain microvessels (endothelial BM) (Sixt et al., 2001; Halder et al., 2018)	• Endothelial cells (Frieser et al., 1997; Thomsen et al., 2017a)
Laminin 421	• Brain microvessels (endothelial BM) (Sixt et al., 2001; Ljubimova et al., 2006)	• Endothelial cells (Ljubimova et al., 2006)
Laminin 511	• Brain microvessels (endothelial BM) (Sixt et al., 2001)	• Endothelial cells (Thomsen et al., 2017a)
Nidogens		
Nidogen-1	• Brain microvessels (Niquet and Represa, 1996)	• Astrocytes (Grimpe et al., 1999) • Endothelial cells (Thomsen et al., 2017a) • Meningeal cells (Sievers et al., 1994)
Nidogen-2	• Brain microvessels (Keable et al., 2016)	• Endothelial cells (Thomsen et al., 2017a)
Other glycoproteins		
Fibronectin	• Brain microvessels (Keable et al., 2016; Andrews et al., 2018; Howe et al., 2018a, 2019)	• Astrocytes (Howe et al., 2019) • Endothelial cells (Thomsen et al., 2017a; Andrews et al., 2018) • Meningeal cells (Sievers et al., 1994) • VSMCs (Andrews et al., 2018)

Together, the ECM molecules and cellular components at the PVS support tissue homeostasis via a variety of functions in the healthy brain, including maintaining the structural integrity of vessels and permitting the exchange of fluids and solutes between the PVS and the brain parenchyma. In the next section, we will take a detailed look at the molecular and cellular changes that occur within the BM during CAA pathogenesis.

BM Remodeling During CAA Pathogenesis

The pathogenesis of sporadic CAA and AD overlap each other (Greenberg et al., 2020), and this interaction between these two diseases may be centered at the PVS. CAA is associated with profound changes in BM morphology and composition (Okoye and Watanabe, 1982; Snow et al., 1988, 1994; Perlmutter et al., 1990, 1991; Su et al., 1992; Shimizu et al., 2009), which may predispose vessels to the development of Aβ deposits. **Table 2** summarizes the changes in BM protein composition in AD patients as a clinically relevant proxy to CAA as well as APP overexpression animal models which exhibit CAA pathology. Multiple neuropathological studies in human patients and animal models support the hypothesis that BM remodeling sensitizes the perivascular tissue to the development of CAA. Yamaguchi et al. (1992) identified the pial BM layer of large leptomeningeal arteries, as well as the glial BM of small leptomeningeal arteries and penetrating cortical arterioles, as the initial sites of amyloid deposition (**Figures 1**, **2**). The study found that, in sites with more advanced pathology, larger amyloid deposits were found to extend into the endothelial BM, and were associated with mural cell degeneration. Smaller amyloid deposits were also identified in the capillary beds of some patients, and were associated with abnormal thickening of the capillary BM (Yamaguchi et al., 1992). Similar findings were reported in a subsequent study, which identified two distinct subtypes of CAA with and without capillary involvement (Thal et al., 2002). BM thickening and degeneration, abnormal HSPG deposits, and irregular vessel thickness have been noted in multiple studies of AD and CAA

(Okoye and Watanabe, 1982; Snow et al., 1988, 1994; Perlmutter et al., 1990, 1991; Su et al., 1992; Shimizu et al., 2009). Specific changes in BM composition generally include increased collagen IV, fibronectin, agrin, and perlecan expression (**Table 2**). In addition to these molecular changes in BM composition and morphology, multiple cell types associated with the cerebral vasculature exhibit altered morphology and function in CAA. Several studies have found that Aβ pathology was associated with loss of endothelial cells and disruption of blood–brain barrier integrity (De Jager et al., 2013; Magaki et al., 2018), degeneration of mural cells (Yamaguchi et al., 1992; Tian et al., 2006), impairment of pericyte function by oligomeric Aβ (Nortley et al., 2019), as well as increased reactive astrocytosis with dystrophic endfeet surrounding BM amyloid deposits (Giannoni et al., 2016; Yang et al., 2017). Overall, these studies support the claim that CAA is associated with widespread changes to the PVS, including BM composition and cellular morphology.

The pathophysiologic relationship between BM remodeling and Aβ deposition is becoming clearer, as recent advances in our understanding of perivascular amyloid transport have identified fundamental links between these two processes. In the following section, we will explore the evidence for the existence of a perivascular fluid transport system in the brain, and how dysregulation of this system contributes to CAA. With this knowledge in hand, we will then conclude by revisiting how the above changes in BM composition could regulate changes in perivascular transport during CAA pathogenesis.

PERIVASCULAR TRANSPORT NETWORKS IN THE HEALTHY AND DISEASED BRAIN

Perivascular Transport of Solutes in the Brain

The brain extracellular space (ECS) is filled with extracellular matrix components attached to the cellular geometry, forming a multitude of channels where interstitial fluid (ISF) and solutes are transported. The ISF contains secreted $A\beta_{1-40}$ and provides a route for its removal, which is potentially subject to a collection of hydrostatic forces that are generally referred to as "bulk flow," however, it seems such directional flow is confined to the PVSs in the brain (Syková and Nicholson, 2008). Compelling evidence suggests that brain parenchymal solute distribution is predominantly mediated by the thermodynamic free diffusion process through the ECS. *In vivo* visualization of the free diffusion process was established by a series of studies by Nicholson and colleagues (Nicholson and Tao, 1993; Thorne et al., 2004, 2008; Thorne and Nicholson, 2006), which recorded the symmetric diffusion pattern of tracers in the brain.

Earlier studies found that bulk flow may depend on hydrostatic pressure gradients within the brain parenchyma that drive the removal of solutes along with ISF movement. Bulk flow of ISF has been estimated to be relatively fast, occurring at a rate of ∼10.5 μm/min in healthy brain tissue (Rosenberg et al., 1980). Through these studies, the directional fluid movement and the diffusive ECS transport in the brain parenchyma may be controversial, yet the existence of bulk flow was clearly visible in the PVS in an early experiment as well as a recent particle tracking study (Ichimura et al., 1991; Mestre et al., 2018b). While these differing mechanisms for solute translocation require further study, the consensus is that parenchymal solute clearance occurs. Such clearance pathways may be grouped into two general models of perivascular transport, as described below.

The first model, which we will refer to as "peri-arterial drainage," proposes that ISF transport occurs along the outer BM of cerebral arteries (Morris et al., 2014; **Figure 2**). This model is based on a series of studies showing that intraparenchymally injected fluorescent tracers rapidly migrate to the glial BM of capillaries and arterioles, and were transported opposite blood flow to the pial BM surrounding leptomeningeal arteries (Carare et al., 2008; Arbel-Ornath et al., 2013). Additional work found that intraparenchymally injected fluorescent $A\beta_{1-40}$ also distributed along with the BM of capillaries, arterioles, and leptomeningeal arteries, depositing within the vessel wall in a distribution similar to that seen in CAA patients (Hawkes et al., 2011, 2012, 2013, 2015; Morris et al., 2016). A recent study found that, in healthy brain tissue, CSF influx is proposed to take place along the pial/glial BM while ISF efflux occurs along with the smooth muscle BM (tunica media) (Albargothy et al., 2018).

The second model, sometimes referred to as "glial-lymphatic (glymphatic) circulation," posits the existence of circulation of CSF within the PVS surrounding cerebral blood vessels, which we will specifically refer to as *para*-vascular influx/efflux. In this model, para-arterial CSF influx is postulated to drive the clearance of $A\beta_{1-40}$ and other solutes along para-venous routes (Iliff et al., 2012; Jessen et al., 2015), where it is returned to the SAS for transport along multiple pathways, including the recently described meningeal lymphatics (Louveau et al., 2015, 2017; Plog et al., 2015).

Regardless of the driving kinetic model, perivascular $A\beta_{1-40}$ transport provides an intriguing explanation for the arterial distribution of amyloid plaque pathology and also explains why pathology first occurs within the BM (Yamaguchi et al., 1992; Thal et al., 2002; Morris et al., 2014; Keable et al., 2016). In terms of understanding the pathogenesis of CAA, both peri-arterial drainage and glymphatic circulation describe potential mechanisms by which $A\beta_{1-40}$ deposition occurs on the vascular wall. This deposition may be conceptualized as occurring both "directly" and "indirectly." The peri-arterial drainage model provides a "direct" pathway by which $A\beta_{1-40}$ produced by neurons is rapidly deposited within the arterial BM during CAA pathogenesis as a result of impaired clearance from the brain (Morris et al., 2014; Keable et al., 2016). On the other hand, a novel meningeal contribution to the pathogenesis of CAA may be derived from the glymphatic circulation model, in which CSF $A\beta_{1-40}$ may pathologically re-enter the brain along para-arterial influx routes and become deposited along with a similar distribution in an "indirect" manner. In support of the latter model, Peng et al. (2016) found that CSF-derived $A\beta_{1-40}$ colocalizes with existing CAA, and that high levels

TABLE 2 | Changes in BM composition in AD patients and transgenic mouse models compared to age-matched controls.

References	Subjects	Collagen IV	Fibronectin	Agrin	Perlecan	Laminin	Nidogen-2
Kalaria and Pax (1995)	AD patients	↑	–	–	–	–	–
Berzin et al. (2000)	AD patients	–	–	↑	–	–	–
Farkas et al. (2000)	AD patients	↑	–	–	–	–	–
Keable et al. (2016)	AD patients	↔	↔	–	–	–	↓
Lepelletier et al. (2017)	AD Patients	↑	↑	–	↑	–	–
Magaki et al. (2018)	AD patients*	↑	–	–	–	–	–
Singh-Bains et al. (2019)	AD patients	↔	↑	–	–	–	–
Bourasset et al. (2009)	Transgenic mice (3xTg)	↑	–	–	–	–	–
Gama Sosa et al. (2010)	Transgenic mice (P117L)**	↔	↔	–	–	↔	–
Kurata et al. (2011)	Transgenic mice (Tg2576)	↓	–	–	–	–	–
Merlini et al. (2011)	Transgenic mice (Tg-ArcAβ)	–	–	–	–	↑	–
Mehta et al. (2013)	Transgenic mice (3xTg)	↑	–	–	–	–	–

Arrows denote increased, decreased or no significant difference in brain expression relative to controls.
**Significantly increased collagen IV was observed in AD patients without CAA, with a trending increase in AD patients with CAA.*
***P117L mice did not exhibit amyloid pathology.*

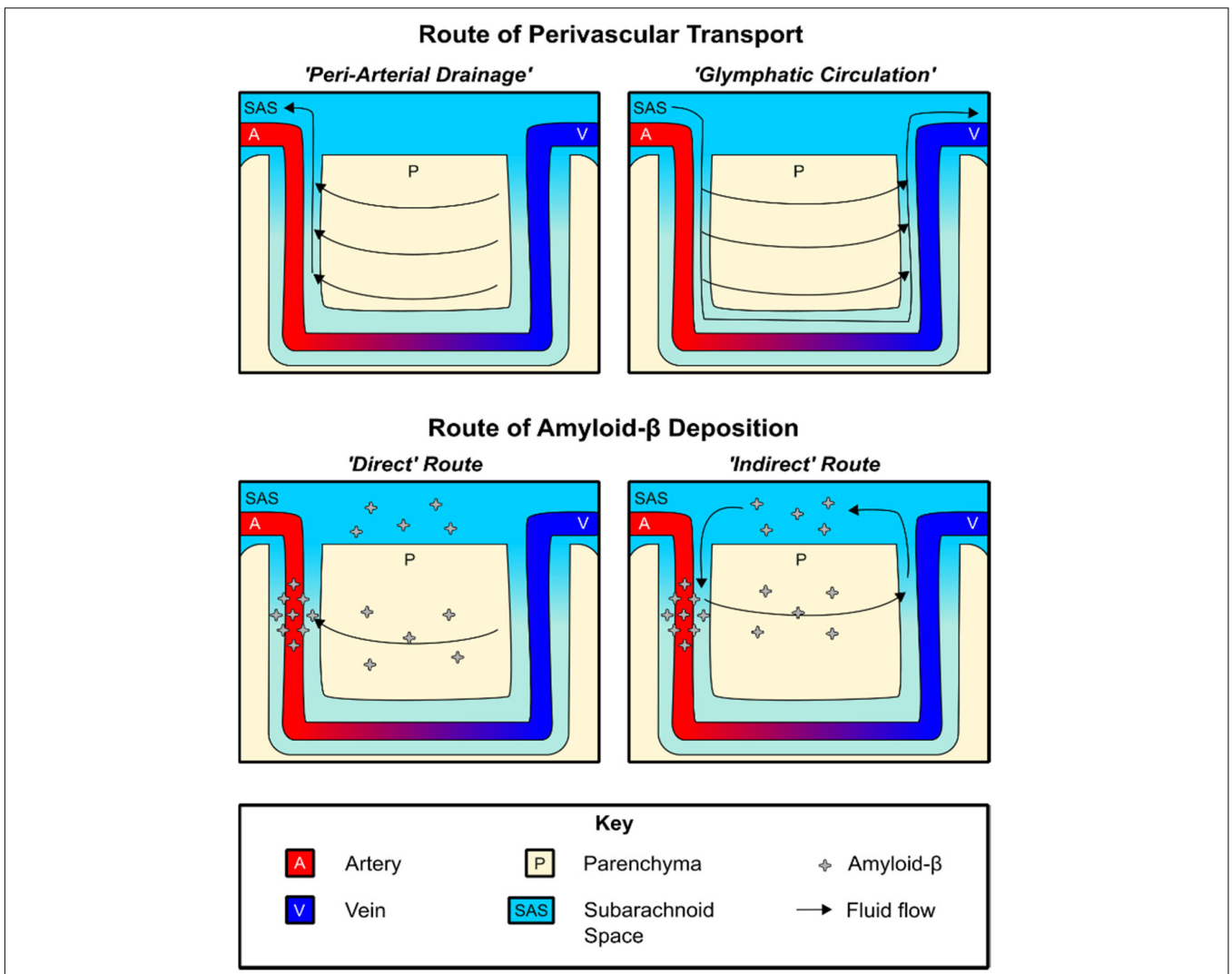

FIGURE 2 | Routes of perivascular fluid transport and Aβ deposition. **Top:** Diagram of perivascular fluid transport under the peri-arterial drainage and glymphatic circulation models, respectively. **Bottom:** Both direct and indirect routes of Aβ deposition may contribute to CAA pathology.

of CSF $A\beta_{1-40}$ can slow the rate of perivascular transport. The importance of this route may further increase in the aged brain, as meningeal drainage pathways become less efficient and could theoretically favor re-circulation of CSF $A\beta_{1-40}$ (Louveau et al., 2015, 2017; Plog et al., 2015; Da Mesquita et al., 2018; Ma et al., 2019). This indirect route of deposition may explain why lower CSF $A\beta_{1-40}$ levels have been found to be a biomarker of CAA, as declining CSF $A\beta_{1-40}$ levels may reflect a disequilibrium between para-venous clearance and para-arterial deposition (Charidimou et al., 2018).

In addition to the above experimental work, both peri-arterial drainage and glymphatic clearance system are equipped with theoretical considerations. The feasibility of the peri-arterial drainage model was estimated by mathematical models, showing that cerebral arterial pulsations, generated by VSMCs, may produce sufficient reflected waves within the BM that drive bulk flow along periarterial vascular routes (Schley et al., 2006; Wang and Olbricht, 2011; Coloma et al., 2016; Aldea et al., 2019). However, several computational studies predicted that the high degree of hydraulic resistances within the BM theoretically limits the distance of ISF transport (Asgari et al., 2015; Faghih and Sharp, 2018; Ray et al., 2019). Also, there is a possibility that that CSF tracer translocation to BM might be associated with spreading depolarizations and tissue processing artifacts as opposed to physiological transport (Bakker et al., 2016; Schain et al., 2017; Mestre et al., 2018b, 2020).

While Faghih and Sharp (2018) also suggested the glymphatic circulation is implausible, this has been rebutted by another study finding that the degree of hydraulic resistance may be overestimated in some models (Tithof et al., 2019), as well as another study that found the diameter of the PVS may be underestimated in other studies due to shrinkage that occurs with tissue fixation (Mestre et al., 2018b). Overall, while mathematical models provide a conflicting picture, the experimental data support a role for glymphatic flow in driving waste clearance under a variety of physiological conditions. Importantly, both peri-arterial efflux and glymphatic circulation may contribute to the pathophysiology of CAA, and these pathways are likely not mutually exclusive from one another.

PERIVASCULAR TRANSPORT IS ALTERED BY AGING AND OTHER DISEASE STATES

Multiple vascular risk factors are associated with CAA, including aging, ApoE-ε4 genotype, cerebrovascular disease, hyperlipidemia, and hypertension. These factors involve changes in the BM which may affect perivascular transport and amyloid clearance as summarized in **Table 3**.

The incidence of CAA increases with aging, affecting 12–100% of patients over the age of 80 (Jellinger, 2002). Interestingly, multiple animal studies also support reductions in perivascular transport in aging. The thickness of the cerebrovascular BM increases with aging, doubling in size by 24 months of age (Ceafalan et al., 2019). Hawkes et al. (2011) found reduced peri-arterial drainage in aged wild-type mice, and Hawkes et al. (2013) reported reduced peri-arterial $A\beta_{1-40}$ drainage. Additionally, Kress et al. (2014) identified reduced para-arterial CSF influx in aged wild-type animals, as well as reduced ISF efflux and $A\beta_{1-40}$ clearance. A recent paper by Da Mesquita et al. (2018) identified impaired meningeal lymphatic outflow in the aging brain as a contributor to reduced CSF influx and ISF efflux.

ApoE genotype is a heritable risk factor for the development of CAA (Yamada, 2002). ApoE isoforms may affect the interaction of Aβ to the BM components, including laminin which facilitates the clearance of Aβ (Thal et al., 2007; Zekonyte et al., 2016). In fact, ApoE-ε4/Aβ complex has been shown to exhibit reduced binding to laminin-511, which may increase the deposition of Aβ (Castillo et al., 2000; Zekonyte et al., 2016). Hawkes et al. (2012) found that humanized ApoE-ε4 mice by the targeted gene replacement exhibited lower levels of laminin and collagen IV in the BM, and increased deposition of intrahippocampally injected $A\beta_{1-40}$ within the walls of leptomeningeal arteries. Finally, Achariyar et al. (2016) found that the para-arterial distribution of ApoE had an isoform specificity, showing that ApoE-ε4 distribution was reduced compared to ApoE-ε2 and ApoE-ε3. These studies point to ApoE/Aβ/laminin interactions as an important regulator of $A\beta_{1-40}$ transport through the BM and PVS.

Cerebrovascular insults and CAA commonly co-occur, with one study reporting that nearly 70% of patients with severe CAA pathology exhibited evidence of either infarction or hemorrhage on autopsy (Jellinger, 2002). Wang et al. (2017) found that stroke increased focal CSF solute trapping within the area of infarction. Venkat et al. (2017) showed that multiple microinfarctions decreased Aquaporin-4 (AQP4) levels resulted in glymphatic dysfunction. Furthermore, Howe et al. (2018a, 2019) reported BM remodeling increased peri-infarct deposition of CSF $A\beta_{1-40}$ in aged animals with stroke. These studies also show a consistent effect of acute stroke on inhibiting perivascular transport and promoting the sequestration of CSF solutes, including $A\beta_{1-40}$, within infarcted brain regions.

Hyperlipidemia may also remodel the cerebrovascular BM through the reduction of collagen IV and other components (de Aquino et al., 2019), which has been shown to also impact perivascular transport pathways. Hawkes et al. (2015) found mice that were first exposed to a maternal diet high in saturated fats, and then subsequently fed a high-fat diet themselves, exhibited impaired perivascular drainage of $A\beta_{1-40}$ in adulthood. Furthermore, Ren et al. (2017) found that fat-1 transgenic mice, which have higher circulating levels of beneficial polyunsaturated fatty acids, exhibited increased rates of both CSF influx and ISF efflux, and that supplementation with fish oil in wild-type mice had a protective effect against CSF $A\beta_{1-40}$ induced injury.

Chronic hypertension causes cerebrovascular BM thickening which may impair perivascular transport mechanisms (Held et al., 2017). Mestre et al. (2018b) found that acute hypertension by angiotensin-2 treatment reduced the efficiency of peri-arterial CSF influx due to increased backflow of solutes within the PVS. The recent studies by Mortensen et al. (2019) and Xue et al. (2020)

TABLE 3 | Studies of perivascular transport in animal models of AD and related dementia risk factors.

References	Subjects	Experimental group	Control group	Tracer influx	Tracer efflux	Aβ deposition	Aβ clearance
CAA							
Hawkes et al. (2011)	Transgenic mice	*Tg2576*	Wild-type	–	↓,↑*	–	–
Peng et al. (2016)	Transgenic mice	*APP/PS1*	Wild-type	↓	↓	↑	↓
van Veluw et al. (2019)	Transgenic mice	*APP/PS1*	Wild-type	–	↓	–	–
Aging							
Hawkes et al. (2011)	Wild-type mice	Aged (22 months-old)	Young (3 months-old)	–	↓	–	–
Hawkes et al. (2013)	Wild-type mice	Aged (22 months-old)	Young (2 months-old)	–	–	–	↓
Kress et al. (2014)	Wild-type mice	Aged (18 months-old)	Young (2 months-old)	↓	↓	–	↓
Da Mesquita et al. (2018)	Wild-type mice	Aged (22 months-old)	Young (2 months-old)	↓	↓	–	–
ApoE-ε4 genotype							
Hawkes et al. (2012)	Transgenic mice	*Hu-APOE4*	*Hu-APOE2*	–	–	↑	–
Achariyar et al. (2016)	Wild-type mice	CSF Hu-APOE4**	CSF Hu-APOE2/3	↓	–	–	–
Cerebrovascular disease							
Gaberel et al. (2014)	Wild-type mice	Stroke (SAH, tMCAO)	Sham	↓	–	–	–
Wang et al. (2017)	Wild-type mice	Stroke (MMI)	Sham	↓	–	–	–
Howe et al. (2018a)	Wild-type mice	Aged stroke (pDMCAO)	Aged sham	↓	–	↑	–
Howe et al. (2019)	Wild-type mice	Stroke (pDMCAO)	Sham	↓	–	–	–
Hyperlipidemia							
Hawkes et al. (2015)	Wild-type mice	High-fat diet	Standard diet	–	–	↑	↓
Ren et al. (2017)	Transgenic mice	*Fat-1*	Wild-type	↑	↑	↓	↑
Hypertension							
Mestre et al. (2018b)	Wild-type mice	Angiotensin-2	Vehicle	↓	–	–	–
Mortensen et al. (2019)	Hypertensive rats	*SHR*	Wild-type	↓	↓	–	–

Tracers refer to injected fluorescent/radiolabeled particles, including dextran, inulin, and/or ovalbumin, unless otherwise noted. The distribution of these tracers is generally taken as a surrogate marker for fluid movement within or between tissue compartments. Tracer influx denotes the movement of intracisternally injected molecules into brain tissue, while tracer efflux denotes the movement of intraparenchymally injected molecules out of brain tissue. The results of fluorescent/radiolabeled Aβ distribution studies are reported in the adjacent columns.

**Decreased peri-arterial dextran efflux with partial compensatory increase in peri-venous efflux noted in aged Tg2576 mice.*

***Fluorescently labeled recombinant ApoE proteins were infused into the CSF and distribution of isoforms was compared (not fluid movement).*

CCI, controlled cortical impact; MMI, multiple microinfarction; pDMCAO, permanent distal middle cerebral artery occlusion; SAH, subarachnoid hemorrhage; SHR, spontaneously hypertensive rats; TBI, traumatic brain injury; tMCAO, transient middle cerebral artery occlusion.

showed that decreased CSF influx in spontaneous hypertensive rats (SHRs), an animal model of chronic hypertension. In addition, Koundal et al. (2020) found reduced glymphatic flow rate and extent in stroke-prone SHRs. The detrimental role of chronic hypertension on perivascular Aβ clearance merits further study, as chronic increases in systemic blood pressure worsens Aβ deposition (Gentile et al., 2009; Carnevale et al., 2012), which may also produce additional changes in the BM in cerebral small vessels that could contribute to altered CSF flow dynamics.

BM REMODELING IMPAIRS PERIVASCULAR SOLUTE TRANSPORT BY MULTIPLE MECHANISMS

In this section, we will summarize the evidence that BM remodeling contributes to the pathogenesis of CAA by impacting at least five distinct physiological parameters that have been demonstrated in the literature to modulate perivascular solute transport (**Figure 3**). BM remodeling may slow the perivascular transport of $A\beta_{1-40}$ and promote CAA via multiple pathophysiologic mechanisms, including (1) specific binding of ECM proteins to soluble $A\beta_{1-40}$, (2) increased tortuosity of the PVS to ISF solute diffusion, reduced vascular reactivity due to, (3) reduced vessel compliance, and (4) impaired contractility of mural cells, as well as (5) altered polarization of AQP4 leading to reduced CSF-ISF exchange. In an attempt to provide a clearer picture of the pathogenesis of CAA, this section will review each of these potential contributions to impaired perivascular flow, with an emphasis on the importance of BM remodeling in driving these processes.

BM Remodeling May Increase Specific Binding of Amyloid Species

BM remodeling may favor amyloid deposition due to changes in BM protein composition that promote the binding of BM proteins to amyloid species (**Figure 3**). CAA is associated with a number of changes in BM composition that may favor the binding of amyloid species to the remodeled BM (**Table 2**). Neuropathological studies in human AD patients consistently report colocalization of amyloid plaques with abnormal deposits

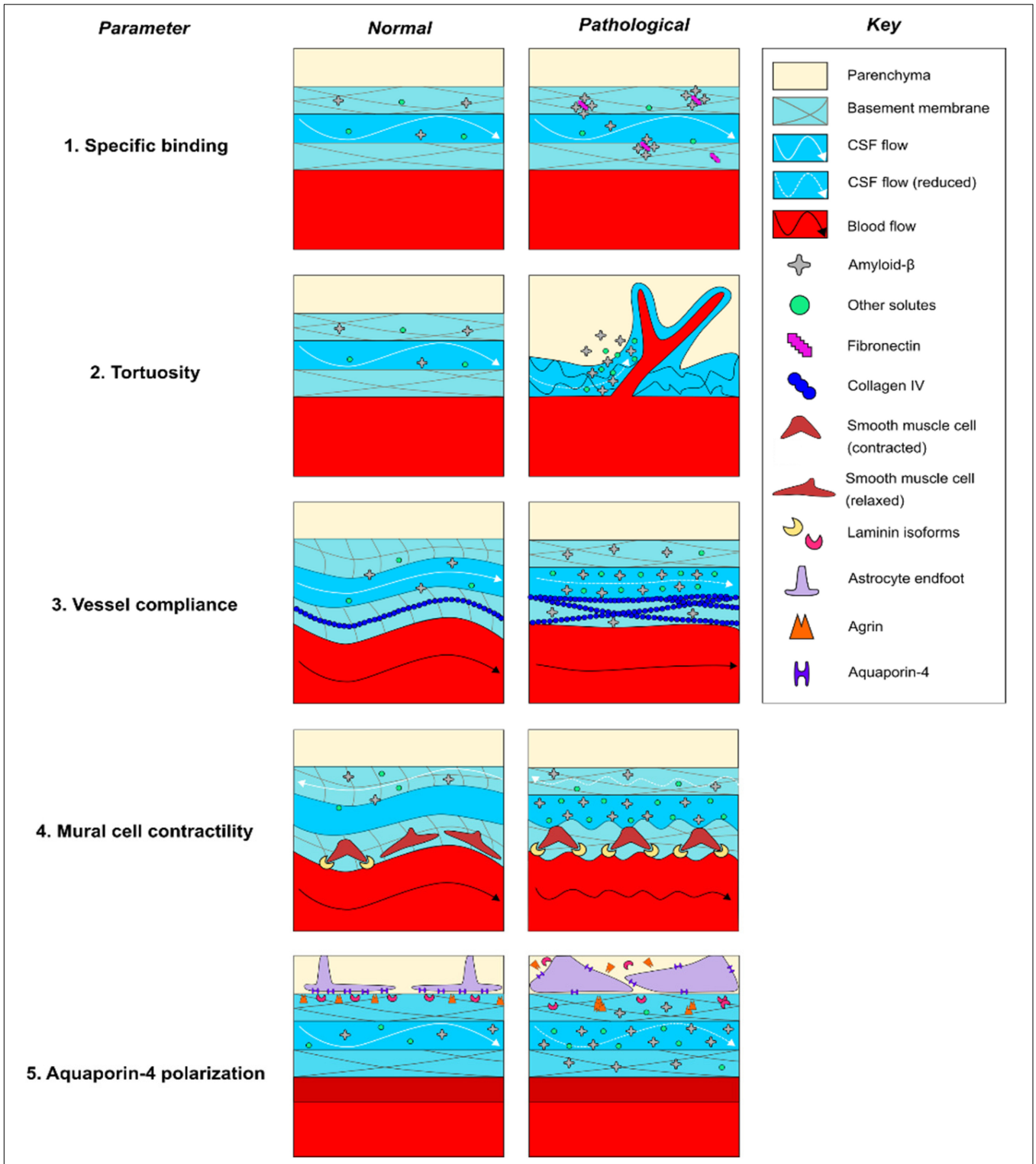

FIGURE 3 | Potential mechanisms of perivascular transport impairment in CAA pathogenesis. (1) Increased expression of fibronectin may specifically favor Aβ deposition within the basement membrane, (2) alterations in the cellular and molecular geometry of the perivascular space may non-specifically trap Aβ and other solutes within areas of reduced flow, (3) increased collagen IV expression may reduce the compliance and alter the pulsatility of vessels, impairing paravascular flow through the PVS, (4) increased laminin expression may pathologically increase vasoconstriction of vessels and reduce peri-arterial BM drainage, and (5) altered laminin and agrin distribution may impair AQP4 polarization along astrocytic endfeet, reducing water permeability and impairing CSF-ISF exchange. Dashed lines indicate reduced rates of CSF flow.

of BM components in the vicinity of brain microvessels; amyloid plaques have been shown to colocalize with staining for HSPGs (Snow et al., 1988; Perlmutter et al., 1991), agrin (Verbeek et al., 1999), perlecan (Lepelletier et al., 2017), collagen IV (Perlmutter et al., 1991; Lepelletier et al., 2017), laminin (Perlmutter et al., 1991), and fibronectin (De Jager et al., 2013; Lepelletier et al., 2017), although colocalization of plaques with fibronectin and perlecan has not always been observed (Koike et al., 1988; Verbeek et al., 1999). Moreover, multiple biochemical studies using C-truncated APP have confirmed specific roles for each of these BM proteins in binding to amyloid species *in vitro* (Narindrasorasak et al., 1991, 1992, 1995). It has also been shown that perlecan and laminin directly bind Aβ (Snow et al., 1995; Castillo et al., 2000). Recent work by our laboratory elucidated a potential pathophysiologic relationship between elevated fibronectin levels and $A\beta_{1-40}$ deposition *in vivo*, finding that intracisternally infused CSF $A\beta_{1-40}$ deposited within thickened, fibronectin-rich segments of the BM in aged mice with stroke, and that fibronectin-$A\beta_{1-40}$ conjugation increased its deposition within the BM of pial vessels (Howe et al., 2018a). Taken together, these studies indicate that deposits containing fibronectin and other BM proteins may create a "trap" for $A\beta_{1-40}$ circulating through the PVS due to specific molecular interactions. However, such binding does not always favor aggregation as laminin binding may inhibit Aβ fibril formation (Castillo et al., 2000). Future work in both wild-type and transgenic models are needed to confirm that changes in BM composition lead to amyloid plaque formation in CAA by a specific binding mechanism.

BM Remodeling May Increase the Tortuosity of the PVS

BM remodeling may also increase the overall tortuosity of the PVS via multiple mechanisms (**Figure 3**). Tortuosity is an experimentally determined variable that reflects the rate of distribution of ISF solutes through the brain ECS, and it has been shown to increase in a variety of pathological states (Syková and Nicholson, 2008). Tortuosity has been shown to correlate with increased geometric path length around cells, increased dead spaces between cells, alterations in the electrical charge of the ECS, and general increases in viscosity due to weak interactions (Syková and Nicholson, 2008). In addition to their impact on diffusional forces, recent mathematical modeling indicates that arterial processes in the PVS are near-optimally located to reduce the hydraulic resistance resulting in an efficient bulk flow (Tithof et al., 2019), although the relative contribution of free diffusion and convective flux of ISF containing parenchymal solutes on their transport remains elusive, and has not been directly confirmed in experimental studies (Nicholson and Hrabìtová, 2017; Faghih and Sharp, 2018). With that said, there is evidence that the projection of cerebral vasculature is altered in CAA, including increased branching of microvessels and regional changes in capillary density. These changes could modify ECS geometry and increase the transit time of solutes contained within the BM, contributing to impairment of solute diffusion and bulk flow (Perlmutter et al., 1990; Yamaguchi et al., 1992; Shimizu et al., 2009; Hawkes et al., 2011; Lepelletier et al., 2017; Hase et al., 2019). One recent experimental study examined the impact of CAA on the geometry of brain microvessels using AD-model TgCRND8 mice. The study found that cortical arterioles exhibited increased branching and decreased diameter with amyloid pathology, which was associated with higher dispersion and elongation of microvascular network transit times of intravenous fluorescent tracers, although perivascular fluid movement through the brain ECS was not measured (Dorr et al., 2012). More directly examining changes in the diffusional properties of the brain ECS in AD-model APP23 mice, Syková et al. (2005) found that aged APP23 mice exhibited increased amyloid pathology, increased ECS volume fraction and decreased apparent diffusion coefficients compared to young controls, all of which is consistent with increased tortuosity (Syková and Nicholson, 2008). More work is needed to determine the impact that increased tortuosity has on the perivascular transport of soluble Aβ.

During CAA pathogenesis, BM remodeling may contribute to these observed increases in tortuosity. Regions of BM thickening have been shown to contain large deposits of collagen IV and HSPGs in human subjects with AD (Perlmutter et al., 1990; Claudio, 1995). Abnormal deposition of these ECM components has been hypothesized to increase tortuosity, but data examining the relationship between specific BM constituents and tortuosity in CAA are limited (Syková and Nicholson, 2008; Nicholson and Hrabìtová, 2017). In a study of human astrocytic tumors, Zámecník et al. (2004) compared ECM composition with tumor grade and then measured the tortuosity of the tissue using tetramethylammonium iontophoresis. They reported that increases in tortuosity positively correlated expression of ECM components, including type IV collagen, laminin, and fibronectin, that localized to the BM. While this study is consistent with the hypothesis that BM remodeling may lead to reduced solute diffusion, further work is needed to assess these relationships in CAA. There is also a need to establish the degree to which solute movement through the BM as well as through the parenchymal ECS is dependent on free diffusion and convective bulk flow, respectively, and whether these change in disease states.

BM Remodeling May Diminish Pulsation Due to Reduced Vessel Compliance

BM remodeling may also act to reduce bulk flow by disrupting the pulsation of brain microvessels (**Figure 3**). Under normal conditions, the ability of pulsatile forces to propagate from the aortic root to the small vessels of the brain is dependent on the compliance of the vascular tree. During aging, reduced compliance of the peripheral vasculature transmits increased pulsatile forces to the cerebral vasculature, which is hypothesized to cause compensatory vasoconstriction and fibrosis that reduces the compliance and pulsation of small vessels (Mitchell et al., 2011; Muhire et al., 2019). The following several studies

have examined the association of cerebrovascular compliance with cognitive function and imaging biomarkers of CAA in human subjects, including white matter hyperintensities and dilation of PVSs. Webb et al. (2012) found that white matter hyperintensities are associated with increased pulsatility of the middle cerebral artery, however, the specific impact on small vessel compliance was not examined. Subsequently, Cooper et al. (2016) found that aortic stiffness was associated with increased resistance of intraparenchymal vessels, white matter hyperintensities, and cognitive impairment. Thomas et al. (2019) found that increased aortic stiffness correlated with dilation of PVSs and decreased small vessel compliance in elderly individuals; cognitive status was not assessed. Finally, Rajna et al. (2019) found that cardiac pulse propagation to the CSF was significantly altered in the lateral ventricles of AD patients, characterized by reduced entropy and increased variance compared to age-matched controls, providing a potential link between reduced pulsation and impairment of CSF flow in human subjects. Overall, these studies point to changes in the pulsation of cerebral vessels in patients with CAA, but more work is needed that specifically examines changes in small vessel pulsatility.

There are limited data available on how brain microvessels respond to increased pulsatility of proximal cerebral arteries, however, there is some evidence that BM remodeling can reduce the compliance of brain microvessels. The majority of studies in AD patients and animal models have identified elevated BM collagen IV levels in the brain (**Table 2**). Studies in collagen IV mutant mice found that loss-of-function mutations increased vessel compliance, leading to distended vessels that are prone to hemorrhage in the perinatal period (Jeanne et al., 2015; Magaki et al., 2018; Ratelade et al., 2018; Hase et al., 2019). Further work in TgAPP mice, an animal model of AD, found increased collagen IV expression in the aorta was associated with reduced aortic responses to pharmacologic treatment with vasodilators (Navarro-Dorado et al., 2016). While the study did report increased collagen IV surrounding brain microvessels, direct physiologic measurements of brain microvessel compliance were not reported in this study. Finally, Iliff et al. (2013b) examined the relationship between the pulsation of intracortical penetrating arterioles and CSF-ISF exchange of fluorescent dextran with two-photon microscopy in anesthetized wild-type mice. The study reported that unilateral carotid ligation reduced the pulsatility of arterioles and limited CSF-ISF exchange, while conversely, acute treatment with the β_1-adrenergic agonist dobutamine increased pulsatility and enhanced CSF-ISF exchange. While compliance was not directly measured, this study provides an important link between altered cerebrovascular pulsation and impairment of CSF-ISF exchange, which may also contribute to CAA pathogenesis. Overall, preclinical work suggests an important role for changes in cerebrovascular pulsation in modulating perivascular CSF-ISF exchange in animal models. While evidence suggests that vessel compliance and pulsatility play an important role in facilitating CSF-ISF exchange, further experiments are required to better establish how increases in collagen IV impact CSF-ISF exchange of Aβ in various stages of CAA pathogenesis.

BM Remodeling May Impair Mural Cell Function and Vasomotion-Assisted Transport Mechanisms

There is emerging evidence showing the activity of mural cells (including pericytes and SMCs), could play an important role in facilitating the transport of solutes through both the PVS and the BM (Schley et al., 2006; Coloma et al., 2016; van Veluw et al., 2019; **Figure 3**). Mathematical modeling suggests that intrinsic vasomotion produces sufficient reflected waves to promote peri-arterial drainage of solutes through the normal BM (Schley et al., 2006; Coloma et al., 2016). During CAA pathogenesis, reduced intrinsic vasomotion of arteries and arterioles might occur in relation to vascular damage (Kisler et al., 2017). These Aβ-related changes may include degeneration of mural cells, which contributes to constriction, hypoperfusion, and BBB breakdown (Kisler et al., 2017), as seen in impaired responses in the neurons and the vasculature in CAA patients (Dumas et al., 2012; Peca et al., 2013; Williams et al., 2017) and in animal models (van Veluw et al., 2019). This is evidenced by Dumas et al. (2012), which found that CAA patients exhibited impaired BOLD responses to visual stimulation, characterized by reduced response amplitude, prolonged time to peak, and prolonged time to baseline, which correlated with white matter hyperintensities and is consistent with impaired neurovascular coupling. Peca et al. (2013) found similar reductions in occipital cortical responses to repetitive visual stimulation in CAA patients, which also correlated with increased white matter hyperintensities and microbleeds. Williams et al. (2017) specifically examined hemodynamic response function (HRF), an integrated measure of neurovascular coupling, and found that multiple parameters of the HRF were associated with CAA and microbleeds. Importantly, emerging research suggests that both neuronal and vascular activities influence perivascular clearance. In a recent study, van Veluw et al. (2019) examined the effect of visual stimulation on the paravascular solute clearance in wild-type and APP/PS1 mice. In this study, fluorescent dextran was first introduced into the PVS of awake animals by the focal laser ablation of a blood vessel, who were subsequently exposed to repetitive visual stimulation. The study identified reduced vascular reactivity in mice with CAA, which correlated with reductions in paravascular clearance and loss of SMC coverage. In summary, the above studies suggest that neurovascular coupling is impaired in both animal models and human subjects with CAA, and play a potentially significant role in modulating perivascular waste clearance.

Reduced cerebrovascular reactivity in CAA may be related to decreased pericyte (Giannoni et al., 2016; Halliday et al., 2016) and SMC (Tian et al., 2006; Miners et al., 2011; Han et al., 2015; Keable et al., 2016; van Veluw et al., 2019) coverage. Multiple studies support a role for the healthy BM in supporting mural cell development, survival, and function under normal conditions. Chen et al. (2013) examined SMC function in astrocyte-specific laminin knockout mice, and found that SMC differentiation and the expression of contractile proteins were reduced in the knockout animals, leading to vasodilation and

hemorrhagic stroke (Chen et al., 2013). In contrast, a subsequent study in pericytes found that inhibition of astrocytic laminin-111 binding to integrin α2 increased pericyte differentiation and contractile protein expression (Yao et al., 2014). Finally, Merlini et al. (2011) found that CAA pathology in AD-model Tg-ArcAβ mice was associated with laminin overexpression, SMC loss, and neuropathological signs of neurovascular decoupling. Laminin expression was found to be highest in vessels impacted by CAA, further suggesting a potential negative effect of laminin on SMC function (Merlini et al., 2011). Taken together, these studies suggest that increased levels of laminin may reduce vasomotion during CAA pathogenesis, although more work is needed to decipher potentially divergent effects of laminin on pericyte and SMC activity and survival, respectively.

BM Remodeling May Impair Perivascular AQP4 Polarization

BM remodeling may also influence para-vascular amyloid transport via indirect effects on AQP4 (Mestre et al., 2018a), a water channel that is expressed on astrocyte endfeet (**Figure 3**). In healthy brain tissue, AQP4 is polarized to the BM-facing surface of astrocytic endfeet (Nakada et al., 2017). Knockout of AQP4 has been shown to inhibit both CSF influx and para-venous efflux in animal models, leading to a reduction in the clearance of $A\beta_{1-40}$ from the brain parenchyma (Iliff et al., 2012). Multiple studies report increased astrocyte reactivity and impaired AQP4 polarization in CAA (Wilcock et al., 2009; Merlini et al., 2011; Zeppenfeld et al., 2017; Boespflug et al., 2018). Yang et al. (2017) found that AQP4 polarization is decreased in AD-model Tg-ArcSwe mice, in part, due to increased expression levels on reactive astrocytes surrounding amyloid plaques. Furthermore, Xu et al. (2015) reported that AQP4 deletion worsened CAA pathology and cognitive deficits in APP/PS1 mice. Zeppenfeld et al. (2017) showed that the degree of AQP4 polarization inversely correlated with amyloid burden in AD brains, and individuals with cognitive impairment had lower levels of AQP4 polarization than age-matched controls on autopsy. Burfeind et al. (2017) identified four single nucleotide polymorphisms in the AQP4 gene that were associated with altered rates of cognitive decline in AD patients. These findings support an important role for dysregulated astrocytic responses and altered AQP4 polarization in CAA.

BM remodeling may impair AQP4 polarization due to altered receptor binding at the astrocytic endfoot. The healthy BM regulates the expression of AQP4. Studies indicate a significant role for multiple BM proteins, including laminin isoforms 111 and 211, as well as agrin and astrocytic β_1–integrin in maintaining AQP4 polarization (Noell et al., 2009; Robel et al., 2009; Fallier-Becker et al., 2011; Menezes et al., 2014; Yao et al., 2014; Gautam et al., 2016; Noël et al., 2019, 2020). Laminins have been shown to promote AQP4 polarization via binding to the dystroglycan associated complex on the cell membrane (Noël et al., 2020), which has been shown to bind AQP4 via α-syntrophin and locally modulate its expression on astrocytic endfeet (Noell et al., 2011; Tham et al., 2016). Interestingly, this process may be disrupted in CAA, as recent transcriptional network analysis of human astrocytic endfoot genes showed reduced levels of dystroglycan, dystrobrevin, and α-syntrophin in AD patients (Simon et al., 2018). In addition to disruption of the dystroglycan pathway, abnormal focal deposits of agrin and laminin could promote the mislocalization of AQP4 to locations outside of the PVS, reducing the polarization of AQP4 to astrocyte endfeet (Noell et al., 2009; Fallier-Becker et al., 2011; Menezes et al., 2014; Yao et al., 2014; Gautam et al., 2016; Noël et al., 2019; **Table 2**). This provides an important link between alterations in BM components, loss of AQP4 polarization and impaired perivascular transport of $A\beta_{1-40}$ observed in CAA.

DISCUSSION AND CLINICAL SIGNIFICANCE

The present review of the literature supports the hypothesis that BM remodeling contributes to the pathogenesis of CAA, in part, by altering the perivascular transport of soluble $A\beta_{1-40}$ from the brain. Perivascular transport is mediated by a complex microenvironment that requires the concerted activity of multiple cell types to maintain effective transport of waste products. BM remodeling, characterized by changes in morphology and composition, occurs early in CAA development and may be an important driver of Aβ deposition due to its effects on perivascular transport pathways relevant to $A\beta_{1-40}$ clearance. The BM provides an important route for perivascular transport, which occurs along multiple pathways, including para-vascular influx and efflux through the PVS, as well as peri-arterial influx and drainage along with the glial/pial BM (influx) and smooth muscle BM (efflux), respectively (Albargothy et al., 2018). Each of these processes may be disrupted in CAA as well as related risk factors and provides a potential explanation for the perivascular distribution of amyloid aggregates. Finally, emerging research indicates that BM remodeling produces changes in multiple parameters relevant to perivascular transport, including increased Aβ affinity, increased tortuosity, altered pulsatility, impaired vasomotor responses, and decreased water permeability.

In addition to perivascular transport, there are numerous other factors that also play a role in CAA pathogenesis that are beyond the scope of this review. Neurodegeneration may be associated with increased APP metabolism and production of Aβ isoforms by neurons and endothelial cells, which is thought to contribute to perivascular amyloid plaques (Kalaria et al., 1996; Bhadbhade and Cheng, 2012). Additionally, microglia and other immune cells have been shown to provoke a neuroinflammatory response and assist with the clearance of amyloid plaques via phagocytosis (Fang et al., 2010; Tarasoff-Conway et al., 2015). Furthermore, alterations in the intracellular degradation of $A\beta_{1-40}$ by endo-lysosomal compartments, which involves the ubiquitin-E3 ligase pathway, may also be affected in AD patients (Tarasoff-Conway et al., 2015; Harris et al., 2020). Alternatively, Aβ may be transported between the ISF and the systemic circulation by transendothelial active transport, assisted by various mediators including p-glycoprotein 1, LRP1, RAGE, alpha2-macroglobulin, clusterin, and apolipoprotein J (Tarasoff-Conway et al., 2015; Reed et al., 2019). Finally,

multiple mutations in the APP gene that increase misfolding and aggregation can predispose individuals to develop hereditary cerebral hemorrhage with amyloidosis (HCHWA), a heritable form of CAA that is associated with early and severe disease onset (Luyendijk et al., 1988; Van Broeckhoven et al., 1990; van Nostrand et al., 1992, 2001; Davis et al., 2004). These factors contribute to disease pathogenesis and have the potential to be integrated into the perivascular transport hypothesis with further study.

The perivascular transport mechanisms have the potential to revolutionize the prevention and early detection of CAA pathology. A recent meta-analysis found that the CSF levels of $A\beta_{1-40}$ and $A\beta_{1-42}$ were significantly lower in symptomatic, sporadic CAA patients compared to healthy controls, which could be related to impaired perivascular clearance or increased re-circulation of waste products along perivascular transport pathways (Charidimou et al., 2018). Furthermore, in a recent study of HCHWA patients, young pre-symptomatic carriers were found to exhibit significantly lower levels of CSF $A\beta_{1-40}$ and $A\beta_{1-42}$ compared to age-matched non-carriers, raising the possibility that declining perivascular Aβ transport could occur decades before the development of symptomatic CAA in affected individuals (van Etten et al., 2017). In addition to direct measurement of CSF proteins, the rapid development of new imaging modalities may soon provide more direct biomarkers of impairment in perivascular transport, potentially improving the detection of pre-symptomatic disease in human patients (Taoka et al., 2017; Ringstad et al., 2018; Rajna et al., 2019). Still more techniques could be used to measure BM remodeling, with specific PET imaging ligands available that provide biomarkers of fibrosis (Beziere et al., 2019), AQP4 levels (Nakamura et al., 2011), and reactive astrogliosis (Cavaliere et al., 2020) that may precede impairment in perivascular transport. Even blood biomarkers could prove useful in diagnosing CAA, as our laboratory has identified serum markers of BM remodeling that may distinguish between CAA and hypertensive intracerebral hemorrhage etiologies (Howe et al., 2018b). Overall, the perivascular transport process may provide a useful model with which to develop novel biomarkers of CAA. When identified, these new biomarkers may help to reduce the burden of dementia in vulnerable populations by identifying patients prior to the development of significant amyloid pathology.

The perivascular transport mechanisms also suggest several therapeutic avenues that may be used to prevent or slow cognitive decline in the elderly. Numerous clinical trials have tested anti-amyloid therapies in human dementia patients, which have shown little improvement in cognitive function despite significant reductions in total brain amyloid levels (van Dyck, 2018). This suggests that targeting amyloid plaques directly may be a suboptimal treatment strategy for age-related dementia. Reversing BM remodeling and boosting perivascular transport via lifestyle modification or pharmacologic treatment could provide an alternative strategy for treating dementia before amyloid accumulation occurs. For example, studies have found that exercise is protective against dementia in humans (Karssemeijer et al., 2017), which may be partially explained by improvements in perivascular transport processes (He et al., 2017; von Holstein-Rathlou et al., 2018). Similarly, treatment with fish oil has been shown to protect against dementia in humans (Zhang et al., 2016), and supplementation has also been shown to boost perivascular transport and protect against CSF amyloid-induced neuroinflammation in mice (Ren et al., 2017). Staying mentally active has been shown to stave off dementia in humans (Bahar-Fuchs et al., 2019), which could be related to neurovascular coupling and perivascular transport (van Veluw et al., 2019). Finally, cerebrovascular disease is a major driver of cognitive impairment in the elderly (Ivan et al., 2004; Mahon et al., 2017), and recently published work by our laboratory found that treatment with a transforming growth factor-β (TGF-β) receptor antagonist reversed BM remodeling and improved perivascular CSF influx in an aged mouse model of stroke, providing a potential tool to mitigate the negative effects of cerebrovascular disease on perivascular transport (Howe et al., 2019). Overall, the above studies showcase the ability of these perivascular transport mechanisms to explain the benefits of lifestyle modification in slowing age-related cognitive decline, as well as identify new potential therapeutic avenues that may prove useful in the primary and secondary prevention of dementia.

In conclusion, the impact of BM remodeling on perivascular transport pathways remains an area of highly active research, with significant potential for improving our understanding of the pathogenesis of CAA. It also provides an important link between cardiovascular risk factors and amyloid accumulation in age-related dementia. While this model represents just a single facet of a complex disease process, it holds promise in guiding future research in two key areas: (1) early detection of individuals who are at-risk of developing CAA, as well as, (2) the development of potential treatments that modify disease-associated BM remodeling before significant neurodegeneration occurs. Accomplishing these two goals could significantly reduce the burden of CAA on our society, and provide improved quality of life to our aging population.

AUTHOR CONTRIBUTIONS

MH and AU conceptualized the review topic and managed the peer review process. MH, LM, and AU wrote the manuscript. All authors contributed to the article and approved the submitted version.

ACKNOWLEDGMENTS

We would like to thank our funding sources; NIH/NIA RF1AG057576 (to AU) and NIH/NIA 1RF1AG058463 (to LDM). MH is currently a research-track resident under R25MH101076 in the Department of Psychiatry and Human Behavior, Brown University.

REFERENCES

Abbott, N. J., Pizzo, M. E., Preston, J. E., Janigro, D., and Thorne, R. G. (2018). The role of brain barriers in fluid movement in the CNS: is there a 'glymphatic' system? *Acta Neuropathol.* 135, 387–407. doi: 10.1007/s00401-018-1812-4

Achariyar, T. M., Li, B., Peng, W., Verghese, P. B., Shi, Y., McConnell, E., et al. (2016). Glymphatic distribution of CSF-derived apoE into brain is isoform specific and suppressed during sleep deprivation. *Mol. Neurodegener.* 11:74. doi: 10.1186/s13024-016-0138-8

Adeeb, N., Deep, A., Griessenauer, C. J., Mortazavi, M. M., Watanabe, K., Loukas, M., et al. (2013). The intracranial arachnoid mater A comprehensive review of its history, anatomy, imaging, and pathology. *Childs Nerv. Syst.* 29, 17–33. doi: 10.1007/s00381-012-1910-x

Agrawal, S., Anderson, P., Durbeej, M., Van Rooijen, N., Ivars, F., Opdenakker, G., et al. (2006). Dystroglycan is selectively cleaved at the parenchymal basement membrane at sites of leukocyte extravasation in experimental autoimmune encephalomyelitis. *J. Exp. Med.* 203, 1007–1016. doi: 10.1084/jem.20051342

Albargothy, N. J., Johnston, D. A., MacGregor-Sharp, M., Weller, R. O., Verma, A., Hawkes, C. A., et al. (2018). Convective influx/glymphatic system: tracers injected into the CSF enter and leave the brain along separate periarterial basement membrane pathways. *Acta Neuropathol.* 136, 139–152. doi: 10.1007/s00401-018-1862-7

Albig, A. R., and Schiemann, W. P. (2004). Fibulin-5 antagonizes vascular endothelial growth factor (VEGF) signaling and angiogenic sprouting by endothelial cells. *DNA Cell Biol.* 23, 367–379. doi: 10.1089/104454904323145254

Alcolado, R., Weller, R. O., Parrish, E. P., and Garrod, D. (1988). The cranial arachnoid and pia mater in man: anatomical and ultrastructural observations. *Neuropathol. Appl. Neurobiol.* 14, 1–17. doi: 10.1111/j.1365-2990.1988.tb00862.x

Aldea, R., Weller, R. O., Wilcock, D. M., Carare, R. O., and Richardson, G. (2019). Cerebrovascular smooth muscle cells as the drivers of intramural periarterial drainage of the brain. *Front. Aging Neurosci.* 11:1. doi: 10.3389/fnagi.2019.00001

Andrews, R. N., Caudell, D. L., Metheny-Barlow, L. J., Peiffer, A. M., Tooze, J. A., Bourland, J. D., et al. (2018). Fibronectin produced by cerebral endothelial and vascular smooth muscle cells contributes to perivascular extracellular matrix in late-delayed radiation-induced brain injury. *Radiat. Res.* 190:361. doi: 10.1667/rr14961.1

Arbel-Ornath, M., Hudry, E., Eikermann-Haerter, K., Hou, S., Gregory, J. L., Zhao, L., et al. (2013). Interstitial fluid drainage is impaired in ischemic stroke and Alzheimer's disease mouse models. *Acta Neuropathol.* 126, 353–364. doi: 10.1007/s00401-013-1145-2

Asgari, M., de Zélicourt, D., and Kurtcuoglu, V. (2015). How astrocyte networks may contribute to cerebral metabolite clearance. *Sci. Rep.* 5:15024. doi: 10.1038/srep15024

Attems, J., and Jellinger, K. A. (2014). The overlap between vascular disease and Alzheimer's disease–lessons from pathology. *BMC Med.* 12:206. doi: 10.1186/s12916-014-0206-2

Bahar-Fuchs, A., Martyr, A., Goh, A. M. Y., Sabates, J., and Clare, L. (2019). Cognitive training for people with mild to moderate dementia. *Cochr. Database Syst. Rev.* 2019:CD013069. doi: 10.1002/14651858.CD013069.pub2

Bakker, E. N., Bacskai, B. J., Arbel-Ornath, M., Aldea, R., Bedussi, B., Morris, A. W., et al. (2016). Lymphatic clearance of the brain: perivascular, paravascular and significance for neurodegenerative diseases. *Cell. Mol. Neurobiol.* 36, 181–194. doi: 10.1007/s10571-015-0273-8

Banks, W. A. (2016). From blood-brain barrier to blood-brain interface: new opportunities for CNS drug delivery. *Nat. Rev. Drug Discov.* 15, 275–292. doi: 10.1038/nrd.2015.21

Barber, A. J., and Lieth, E. (1997). Agrin accumulates in the brain microvascular basal lamina during development of the blood-brain barrier. *Dev. Dyn.* 208, 62–74. doi: 10.1002/(sici)1097-0177(199701)208:1<62::aid-aja6>3.0.co;2-#

Ben-Zvi, A., Lacoste, B., Kur, E., Andreone, B. J., Mayshar, Y., Yan, H., et al. (2014). Mfsd2a is critical for the formation and function of the blood-brain barrier. *Nature* 509, 507–511. doi: 10.1038/nature13324

Berzin, T. M., Zipser, B. D., Rafii, M. S., Kuo-Leblanc, V., Yancopouloš, G. D., Glass, D. J., et al. (2000). Agrin and microvascular damage in Alzheimer's disease. *Neurobiol. Aging* 21, 349–355. doi: 10.1016/S0197-4580(00)00121-4

Beziere, N., Fuchs, K., Maurer, A., Reischl, G., Brück, J., Ghoreschi, K., et al. (2019). Imaging fibrosis in inflammatory diseases: targeting the exposed extracellular matrix. *Theranostics* 9, 2868–2881. doi: 10.7150/thno.28892

Bhadbhade, A., and Cheng, D. W. (2012). Amyloid precursor protein processing in Alzheimer's disease. *Iran. J. Child Neurol.* 6, 1–4. doi: 10.1146/annurev-neuro-061010-113613

Boespflug, E. L., Simon, M. J., Leonard, E., Grafe, M., Woltjer, R., Silbert, L. C., et al. (2018). Targeted assessment of enlargement of the perivascular space in Alzheimer's disease and vascular dementia subtypes implicates astroglial involvement specific to Alzheimer's disease. *J. Alzheimers Dis.* 66, 1587–1597. doi: 10.3233/JAD-180367

Bourasset, F., Ouellet, M., Tremblay, C., Julien, C., Do, T. M., Oddo, S., et al. (2009). Reduction of the cerebrovascular volume in a transgenic mouse model of Alzheimer's disease. *Neuropharmacology* 56, 808–813. doi: 10.1016/j.neuropharm.2009.01.006

Burfeind, K. G., Murchison, C. F., Westaway, S. K., Simon, M. J., Erten-Lyons, D., Kaye, J. A., et al. (2017). The effects of noncoding aquaporin-4 single-nucleotide polymorphisms on cognition and functional progression of Alzheimer's disease. *Alzheimers Dement. Transl. Res. Clin. Interv.* 3, 348–359. doi: 10.1016/j.trci.2017.05.001

Carare, R. O., Bernardes-Silva, M., Newman, T. A., Page, A. M., Nicoll, J. A. R., Perry, V. H., et al. (2008). Solutes, but not cells, drain from the brain parenchyma along basement membranes of capillaries and arteries: significance for cerebral amyloid angiopathy and neuroimmunology. *Neuropathol. Appl. Neurobiol.* 34, 131–144. doi: 10.1111/j.1365-2990.2007.00926.x

Carnevale, D., Mascio, G., D'Andrea, I., Fardella, V., Bell, R. D., Branchi, I., et al. (2012). Hypertension induces brain β-amyloid accumulation, cognitive impairment, and memory deterioration through activation of receptor for advanced glycation end products in brain vasculature. *Hypertension.* 60, 188–197. doi: 10.1161/HYPERTENSIONAHA.112.195511

Castillo, G. M., Lukito, W., Peskind, E., Raskind, M., Kirschner, D. A., Yee, A. G., et al. (2000). Laminin inhibition of β-amyloid protein (Aβ) fibrillogenesis and identification of an Aβ binding site localized to the globular domain repeats on the laminin A chain. *J. Neurosci. Res.* 62, 451–462. doi: 10.1002/1097-4547(20001101)62:3<451::AID-JNR15<3.0.CO;2-F

Cavaliere, C., Tramontano, L., Fiorenza, D., Alfano, V., Aiello, M., and Salvatore, M. (2020). Gliosis and neurodegenerative diseases: the role of PET and MR imaging. *Front. Cell. Neurosci.* 14:75. doi: 10.3389/fncel.2020.00075

Ceafalan, L. C., Fertig, T. E., Gheorghe, T. C., Hinescu, M. E., Popescu, B. O., Pahnke, J., et al. (2019). Age-related ultrastructural changes of the basement membrane in the mouse blood-brain barrier. *J. Cell. Mol. Med.* 23, 819–827. doi: 10.1111/jcmm.13980

Chandra, A., Li, W. A., Stone, C. R., Geng, X., and Ding, Y. (2017). The cerebral circulation and cerebrovascular disease I: anatomy. *Brain Circ.* 3:45. doi: 10.4103/BC.BC_10_17

Charidimou, A., Friedrich, J. O., Greenberg, S. M., and Viswanathan, A. (2018). Core cerebrospinal fluid biomarker profile in cerebral amyloid angiopathy. *Neurology* 90, e754–e762. doi: 10.1212/WNL.0000000000005030

Chasseigneaux, S., Moraca, Y., Cochois-Guégan, V., Boulay, A. C., Gilbert, A., Le Crom, S., et al. (2018). Isolation and differential transcriptome of vascular smooth muscle cells and mid-capillary pericytes from the rat brain. *Sci. Rep.* 8:12272. doi: 10.1038/s41598-018-30739-5

Chen, Z. L., Yao, Y., Norris, E. H., Kruyer, A., Jno-Charles, O., Akhmerov, A., et al. (2013). Ablation of astrocytic laminin impairs vascular smooth muscle cell function and leads to hemorrhagic stroke. *J. Cell Biol.* 202, 381–395. doi: 10.1083/jcb.201212032

Chouchkov, C., Lazarov, N., and Ichev, K. (1987). Localization of newly synthesized protein precursors of basement membrane in the embryonic central nervous system as revealed by radioautography. *Acta Histochem.* 82, 153–158. doi: 10.1016/S0065-1281(87)80021-1

Claudio, L. (1995). Ultrastructural features of the blood-brain barrier in biopsy tissue from Alzheimer's disease patients. *Acta Neuropathol.* 91, 6–14. doi: 10.1007/s004010050386

Coloma, M., Schaffer, J. D., Carare, R. O., Chiarot, P. R., and Huang, P. (2016). Pulsations with reflected boundary waves: a hydrodynamic reverse transport

mechanism for perivascular drainage in the brain. *J. Math. Biol.* 73, 469–490. doi: 10.1007/s00285-015-0960-6

Cooper, L. L., Woodard, T., Sigurdsson, S., Van Buchem, M. A., Torjesen, A. A., Inker, L. A., et al. (2016). Cerebrovascular damage mediates relations between aortic stiffness and memory. *Hypertension* 67, 176–182. doi: 10.1161/HYPERTENSIONAHA.115.06398

Corder, E. H., Saunders, A. M., Strittmatter, W. J., Schmechel, D. E., Gaskell, P. C., Small, G. W., et al. (1993). Gene dose of apolipoprotein E type 4 allele and the risk of Alzheimer's disease in late onset families. *Science* 261, 921–923. doi: 10.1126/science.8346443

Da Mesquita, S., Louveau, A., Vaccari, A., Smirnov, I., Cornelison, R. C., Kingsmore, K. M., et al. (2018). Functional aspects of meningeal lymphatics in ageing and Alzheimer's disease. *Nature* 560, 185–191. doi: 10.1038/s41586-018-0368-8

Davis, J., Xu, F., Deane, R., Romanov, G., Previti, M., Lou, Z. K., et al. (2004). Early-onset and robust cerebral microvascular accumulation of amyloid beta-protein in transgenic mice expressing low levels of a vasculotropic Dutch/Iowa mutant form of amyloid beta-protein precursor. *J. Biol. Chem.* 279, 20296–20306. doi: 10.1074/jbc.M312946200

de Aquino, C. C., Leitão, R. A., Oliveira Alves, L. A., Coelho-Santos, V., Guerrant, R. L., Ribeiro, C. F., et al. (2019). Effect of hypoproteic and high-fat diets on hippocampal blood-brain barrier permeability and oxidative stress. *Front. Nutr.* 5:131. doi: 10.3389/fnut.2018.00131

De Jager, M., van der Wildt, B., Schul, E., Bol, J. G. J. M., van Duinen, S. G., Drukarch, B., et al. (2013). Tissue transglutaminase colocalizes with extracellular matrix proteins in cerebral amyloid angiopathy. *Neurobiol. Aging* 34, 1159–1169. doi: 10.1016/j.neurobiolaging.2012.10.005

Deckers, K., Barbera, M., Kohler, S., Ngandu, T., van Boxtel, M., Rusanen, M., et al. (2019). Long-term dementia risk prediction by the LIBRA score: a 30-year follow-up of the CAIDE study. *Int. J. Geriatr. Psychiatry* 35, 195–203. doi: 10.1002/gps.5235

Deramecourt, V., Slade, J. Y., Oakley, A. E., Perry, R. H., Ince, P. G., Maurage, C. A., et al. (2012). Staging and natural history of cerebrovascular pathology in dementia. *Neurology* 78, 1043–1050. doi: 10.1212/WNL.0b013e31824e8e7f

Dorr, A., Sahota, B., Chinta, L. V., Brown, M. E., Lai, A. Y., Ma, K., et al. (2012). Amyloid-β-dependent compromise of microvascular structure and function in a model of Alzheimer's disease. *Brain* 135, 3039–3050. doi: 10.1093/brain/aws243

Dumas, A., Dierksen, G. A., Gurol, M. E., Halpin, A., Martinez-Ramirez, S., Schwab, K., et al. (2012). Functional magnetic resonance imaging detection of vascular reactivity in cerebral amyloid angiopathy. *Ann. Neurol.* 72, 76–81. doi: 10.1002/ana.23566

Engelhardt, B., and Sorokin, L. (2009). The blood-brain and the blood-cerebrospinal fluid barriers: function and dysfunction. *Semin. Immunopathol.* 31, 497–511. doi: 10.1007/s00281-009-0177-0

Faghih, M. M., and Sharp, M. K. (2018). Is bulk flow plausible in perivascular, paravascular and paravenous channels? *Fluids Barriers CNS* 15:17. doi: 10.1186/s12987-018-0103-8

Fallier-Becker, P., Sperveslage, J., Wolburg, H., and Noell, S. (2011). The impact of agrin on the formation of orthogonal arrays of particles in cultured astrocytes from wild-type and agrin-null mice. *Brain Res.* 1367, 2–12. doi: 10.1016/j.brainres.2010.09.092

Fang, F., Lue, L.-F., Yan, S., Xu, H., Luddy, J. S., Chen, D., et al. (2010). RAGE-dependent signaling in microglia contributes to neuroinflammation, Abeta accumulation, and impaired learning/memory in a mouse model of Alzheimer's disease. *FASEB J.* 24, 1043–1055. doi: 10.1096/fj.09-139634

Farkas, E., De Jong, G. I., De Vos, R. A. I., Jansen Steur, E. N. H., and Luiten, P. G. M. (2000). Pathological features of cerebral cortical capillaries are doubled in Alzheimer's disease and Parkinson's disease. *Acta Neuropathol.* 100, 395–402. doi: 10.1007/s004010000195

Frieser, M., Nöckel, H., Pausch, F., Röder, C., Hahn, A., Deutzmann, R., et al. (1997). Cloning of the mouse laminin α4 cDNA. Expression in a subset of endothelium. *Eur. J. Biochem.* 246, 727–735. doi: 10.1111/j.1432-1033.1997.t01-1-00727.x

Gaberel, T., Gakuba, C., Goulay, R., De Lizarrondo, S. M., Hanouz, J. L., Emery, E., et al. (2014). Impaired glymphatic perfusion after strokes revealed by contrast-enhanced MRI: a new target for fibrinolysis? *Stroke* 45, 3092–3096. doi: 10.1161/STROKEAHA.114.006617

Gama Sosa, M. A., De Gasperi, R., Rocher, A. B., Wang, A. C. J., Janssen, W. G. M., Flores, T., et al. (2010). Age-related vascular pathology in transgenic mice expressing presenilin 1-associated familial Alzheimer's disease mutations. *Am. J. Pathol.* 176, 353–368. doi: 10.2353/ajpath.2010.090482

Gautam, J., Zhang, X., and Yao, Y. (2016). The role of pericytic laminin in blood brain barrier integrity maintenance. *Sci. Rep.* 6:36450. doi: 10.1038/srep36450

Gentile, M. T., Poulet, R., Di Pardo, A., Cifelli, G., Maffei, A., Vecchione, C., et al. (2009). Beta-amyloid deposition in brain is enhanced in mouse models of arterial hypertension. *Neurobiol. Aging* 30, 222–228. doi: 10.1016/j.neurobiolaging.2007.06.005

Giannoni, P., Arango-Lievano, M., Neves, I. D., Rousset, M. C., Baranger, K., Rivera, S., et al. (2016). Cerebrovascular pathology during the progression of experimental Alzheimer's disease. *Neurobiol. Dis.* 88, 107–117. doi: 10.1016/j.nbd.2016.01.001

Gireud-Goss, M., Mack, A. F., Louise, D., McCullough, L. D., and Urayama, A. (2020). Cerebral amyloid angiopathy and blood brain barrier dysfunction. *Neuroscientist*. (in press).

Goldmann, T., Wieghofer, P., Jordão, M. J. C., Prutek, F., Hagemeyer, N., Frenzel, K., et al. (2016). Origin, fate and dynamics of macrophages at central nervous system interfaces. *Nat. Immunol.* 17, 797–805. doi: 10.1038/ni.3423

Gorelick, P. B., Scuteri, A., Black, S. E., Decarli, C., Greenberg, S. M., Iadecola, C., et al. (2011). Vascular contributions to cognitive impairment and dementia: a statement for healthcare professionals from the american heart association/american stroke association. *Stroke* 42, 2672–2713. doi: 10.1161/STR.0b013e3182299496

Grazioli, A., Alves, C. S., Konstantopoulos, K., and Yang, J. T. (2006). Defective blood vessel development and pericyte/pvSMC distribution in alpha 4 integrin-deficient mouse embryos. *Dev. Biol.* 293, 165–177. doi: 10.1016/j.ydbio.2006.01.026

Greenberg, S. M., Bacskai, B. J., Hernandez-Guillamon, M., Pruzin, J., Sperling, R., and van Veluw, S. J. (2020). Cerebral amyloid angiopathy and Alzheimer disease – one peptide, two pathways. *Nat. Rev. Neurol.* 16, 30–42. doi: 10.1038/s41582-019-0281-2

Greenberg, S. M., and Vonsattel, J. P. (1997). Diagnosis of cerebral amyloid angiopathy. Sensitivity and specificity of cortical biopsy. *Stroke* 28, 1418–1422. doi: 10.1161/01.str.28.7.1418

Grimpe, B., Probst, J. C., and Hager, G. (1999). Suppression of nidogen-1 translation by antisense targeting affects the adhesive properties of cultured astrocytes. *Glia* 28, 138–149. doi: 10.1002/(SICI)1098-1136(199911)28:2<138::AID-GLIA5<3.0.CO;2-8

Guo, J., Cheng, C., Chen, C. S., Xing, X., Xu, G., Feng, J., et al. (2016). Overexpression of Fibulin-5 attenuates ischemia/reperfusion injury after middle cerebral artery occlusion in rats. *Mol. Neurobiol.* 53, 3154–3167. doi: 10.1007/s12035-015-9222-2

Gustafsson, E., Almonte-Becerril, M., Bloch, W., and Costell, M. (2013). Perlecan maintains microvessel integrity in vivo and modulates their formation in vitro. *PLoS One* 8:e53715. doi: 10.1371/journal.pone.0053715

Halder, S. K., Kant, R., and Milner, R. (2018). Chronic mild hypoxia increases expression of laminins 111 and 411 and the laminin receptor α6β1 integrin at the blood-brain barrier. *Brain Res.* 1700, 78–85. doi: 10.1016/j.brainres.2018.07.012

Halliday, M. R., Rege, S. V., Ma, Q., Zhao, Z., Miller, C. A., Winkler, E. A., et al. (2016). Accelerated pericyte degeneration and blood-brain barrier breakdown in apolipoprotein E4 carriers with Alzheimer's disease. *J. Cereb. Blood Flow Metab.* 36, 216–227. doi: 10.1038/jcbfm.2015.44

Han, B. H., Zhou, M. L., Johnson, A. W., Singh, I., Liao, F., Vellimana, A. K., et al. (2015). Contribution of reactive oxygen species to cerebral amyloid angiopathy, vasomotor dysfunction, and microhemorrhage in aged Tg2576 mice. *Proc. Natl. Acad. Sci. U.S.A.* 112, E881–E890. doi: 10.1073/pnas.1414930112

Hannocks, M. J., Pizzo, M. E., Huppert, J., Deshpande, T., Abbott, N. J., Thorne, R. G., et al. (2018). Molecular characterization of perivascular drainage pathways in the murine brain. *J. Cereb. Blood Flow Metab.* 38, 669–686. doi: 10.1177/0271678X17749689

Harris, L. D., Jasem, S., and Licchesi, J. D. F. (2020). The ubiquitin system in Alzheimer's disease. *Adv. Exp. Med. Biol.* 1233, 195–221. doi: 10.1007/978-3-030-38266-7_8

Hase, Y., Ding, R., Harrison, G., Hawthorne, E., King, A., Gettings, S., et al. (2019). White matter capillaries in vascular and neurodegenerative dementias. *Acta Neuropathol. Commun.* 7:16. doi: 10.1186/s40478-019-0666-x

Hauw, J. J., Berger, B., and Escourolle, R. (1975). Electron microscopic study of the developing capillaries of human brain. *Acta Neuropathol.* 31, 229–242. doi: 10.1007/BF00684562

Hawkes, C. A., Gatherer, M., Sharp, M. M., Dorr, A., Yuen, H. M., Kalaria, R., et al. (2013). Regional differences in the morphological and functional effects of aging on cerebral basement membranes and perivascular drainage of amyloid-β from the mouse brain. *Aging Cell* 12, 224–236. doi: 10.1111/acel.12045

Hawkes, C. A., Gentleman, S. M., Nicoll, J. A., and Carare, R. O. (2015). Prenatal high-fat diet alters the cerebrovasculature and clearance of β -amyloid in adult offspring. *J. Pathol.* 235, 619–631. doi: 10.1002/path.4468

Hawkes, C. A., Härtig, W., Kacza, J., Schliebs, R., Weller, R. O., Nicoll, J. A., et al. (2011). Perivascular drainage of solutes is impaired in the ageing mouse brain and in the presence of cerebral amyloid angiopathy. *Acta Neuropathol.* 121, 431–443. doi: 10.1007/s00401-011-0801-7

Hawkes, C. A., Sullivan, P. M., Hands, S., Weller, R. O., Nicoll, J. A. R., and Carare, R. O. (2012). Disruption of arterial perivascular drainage of amyloid-β from the brains of mice expressing the human APOE ε4 allele. *PLoS One* 7:e41636. doi: 10.1371/journal.pone.0041636

He, X., Liu, D., Zhang, Q., Liang, F., Dai, G., Zeng, J., et al. (2017). Voluntary exercise promotes glymphatic clearance of amyloid beta and reduces the activation of astrocytes and microglia in aged mice. *Front. Mol. Neurosci.* 10:144. doi: 10.3389/fnmol.2017.00144

Held, F., Morris, A. W. J., Pirici, D., Niklass, S., Sharp, M. M. G., Garz, C., et al. (2017). Vascular basement membrane alterations and β-amyloid accumulations in an animal model of cerebral small vessel disease. *Clin. Sci.* 131, 1001–1013. doi: 10.1042/CS20170004

Hielscher, A., Ellis, K., Qiu, C., Porterfield, J., and Gerecht, S. (2016). Fibronectin deposition participates in extracellular matrix assembly and vascular morphogenesis. *PLoS One* 11:e0147600. doi: 10.1371/journal.pone.0147600

Hladky, S. B., and Barrand, M. A. (2018). Elimination of substances from the brain parenchyma: efflux via perivascular pathways and via the blood-brain barrier. *Fluids Barriers CNS* 15:30. doi: 10.1186/s12987-018-0113-6

Howe, M. D., Atadja, L. A., Furr, J. W., Maniskas, M. E., Zhu, L., McCullough, L. D., et al. (2018a). Fibronectin induces the perivascular deposition of cerebrospinal fluid–derived amyloid-β in aging and after stroke. *Neurobiol. Aging* 72, 1–13. doi: 10.1016/J.NEUROBIOLAGING.2018.07.019

Howe, M. D., Furr, J. W., Munshi, Y., Roy-O'Reilly, M. A., Maniskas, M. E., Koellhoffer, E. C., et al. (2019). Transforming growth factor-β promotes basement membrane fibrosis, alters perivascular cerebrospinal fluid distribution, and worsens neurological recovery in the aged brain after stroke. *GeroScience* 41, 543–559. doi: 10.1007/s11357-019-00118-7

Howe, M. D., Zhu, L., Sansing, L. H., Gonzales, N. R., McCullough, L. D., and Edwards, N. J. (2018b). Serum markers of blood-brain barrier remodeling and fibrosis as predictors of etiology and clinicoradiologic outcome in intracerebral hemorrhage. *Front. Neurol.* 9:746. doi: 10.3389/fneur.2018.00746

Huveneers, S., Truong, H., Fassler, R., Sonnenberg, A., and Danen, E. H. J. (2008). Binding of soluble fibronectin to integrin 5 1 - link to focal adhesion redistribution and contractile shape. *J. Cell Sci.* 121, 2452–2462. doi: 10.1242/jcs.033001

Ichimura, T., Fraser, P. A., and Cserr, H. F. (1991). Distribution of extracellular tracers in perivascular spaces of therat brain. *Brain Res.* 545, 103–113. doi: 10.1016/0006-8993(91)91275-6

Iliff, J. J., Lee, H., Yu, M., Feng, T., Logan, J., Nedergaard, M., et al. (2013a). Brain-wide pathway for waste clearance captured by contrast-enhanced MRI. *J. Clin. Invest.* 123, 1299–1309. doi: 10.1172/JCI67677

Iliff, J. J., Wang, M., Liao, Y., Plogg, B. A., Peng, W., Gundersen, G. A., et al. (2012). A paravascular pathway facilitates CSF flow through the brain parenchyma and the clearance of interstitial solutes, including amyloid β. *Sci. Transl. Med.* 4:147ra111. doi: 10.1126/scitranslmed.3003748

Iliff, J. J., Wang, M., Zeppenfeld, D. M., Venkataraman, A., Plog, B. A., Liao, Y., et al. (2013b). Cerebral arterial pulsation drives paravascular CSF-interstitial fluid exchange in the murine brain. *J. Neurosci.* 33, 18190–18199. doi: 10.1523/JNEUROSCI.1592-13.2013

Ivan, C. S., Seshadri, S., Beiser, A., Au, R., Kase, C. S., Kelly-Hayes, M., et al. (2004). Dementia after stroke: the framingham study. *Stroke* 35, 1264–1268. doi: 10.1161/01.STR.0000127810.92616.78

Jeanne, M., Jorgensen, J., and Gould, D. B. (2015). Molecular and genetic analyses of collagen type IV mutant mouse models of spontaneous intracerebral hemorrhage identify mechanisms for stroke prevention. *Circulation* 131, 1555–1565. doi: 10.1161/CIRCULATIONAHA.114.013395

Jellinger, K. A. (2002). Alzheimer disease and cerebrovascular pathology: an update. *J. Neural Transm.* 109, 813–836. doi: 10.1007/s007020200068

Jessen, N. A., Munk, A. S. F., Lundgaard, I., and Nedergaard, M. (2015). The glymphatic system: a beginner's guide. *Neurochem. Res.* 40, 2583–2599. doi: 10.1007/s11064-015-1581-6

Joost, E., Jordão, M. J. C., Mages, B., Prinz, M., Bechmann, I., and Krueger, M. (2019). Microglia contribute to the glia limitans around arteries, capillaries and veins under physiological conditions, in a model of neuroinflammation and in human brain tissue. *Brain Struct. Funct.* 224, 1301–1314. doi: 10.1007/s00429-019-01834-8

Jucker, M., Tian, M., Norton, D. D., Sherman, C., and Kusiak, J. W. (1996). Laminin α2 is a component of brain capillary basement membrane: reduced expression in dystrophic dy mice. *Neuroscience* 71, 1153–1161. doi: 10.1016/0306-4522(95)00496-3

Kalaria, R. N., and Pax, A. B. (1995). Increased collagen content of cerebral microvessels in Alzheimer's disease. *Brain Res.* 705, 349–352. doi: 10.1016/0006-8993(95)01250-8

Kalaria, R. N., Premkumar, D. R. D., Pax, A. B., Cohen, D. L., and Lieberburg, I. (1996). Production and increased detection of amyloid β protein and amyloidogenic fragments in brain microvessels, meningeal vessels and choroid plexus in Alzheimer's disease. *Mol. Brain Res.* 35, 58–68. doi: 10.1016/0169-328X(95)00180-Z

Karssemeijer, E., Aaronson, J., Bossers, W., Smits, T., Olde Rikkert, M., and Kessels, R. (2017). Positive effects of combined cognitive and physical exercise training on cognitive function in older adults with mild cognitive impairment or dementia: a meta-analysis. *Ageing Res. Rev.* 40, 75–83. doi: 10.1016/j.arr.2017.09.003

Keable, A., Fenna, K., Yuen, H. M., Johnston, D. A., Smyth, N. R., Smith, C., et al. (2016). Deposition of amyloid β in the walls of human leptomeningeal arteries in relation to perivascular drainage pathways in cerebral amyloid angiopathy. *Biochim. Biophys. Acta* 1862, 1037–1046. doi: 10.1016/j.bbadis.2015.08.024

Kiliç, T., and Akakin, A. (2008). Anatomy of cerebral veins and sinuses. *Front. Neurol. Neurosci.* 23:4–15. doi: 10.1159/000111256

Kirst, C., Skriabine, S., Vieites-Prado, A., Topilko, T., Bertin, P., Gerschenfeld, G., et al. (2020). Mapping the fine-scale organization and plasticity of the brain vasculature. *Cell* 180, 780–795.e25. doi: 10.1016/j.cell.2020.01.028

Kisler, K., Nelson, A. R., Montagne, A., and Zlokovic, B. V. (2017). Cerebral blood flow regulation and neurovascular dysfunction in Alzheimer disease. *Nat. Rev. Neurosci.* 18, 419–434. doi: 10.1038/nrn.2017.48

Kivipelto, M., Ngandu, T., Laatikainen, T., Winblad, B., Soininen, H., and Tuomilehto, J. (2006). Risk score for the prediction of dementia risk in 20 years among middle aged people: a longitudinal, population-based study. *Lancet Neurol.* 5, 735–741. doi: 10.1016/S1474-4422(06)70537-3

Koike, F., Kunishita, T., Nakayama, H., and Tabira, T. (1988). Immunohistochemical study of Alzheimer's disease using antibodies to synthetic amyloid and fibronectin. *J. Neurol. Sci.* 85, 9–15. doi: 10.1016/0022-510X(88)90031-7

Koundal, S., Elkin, R., Nadeem, S., Xue, Y., Constantinou, S., Sanggaard, S., et al. (2020). Optimal mass transport with lagrangian workflow reveals advective and diffusion driven solute transport in the glymphatic system. *Sci. Rep.* 10:1990. doi: 10.1038/s41598-020-59045-9

Kress, B. T., Iliff, J. J., Xia, M., Wang, M., Wei, H. S., Zeppenfeld, D., et al. (2014). Impairment of paravascular clearance pathways in the aging brain. *Ann. Neurol.* 76, 845–861. doi: 10.1002/ana.24271

Kurata, T., Miyazaki, K., Kozuki, M., Morimoto, N., Ohta, Y., Ikeda, Y., et al. (2011). Progressive neurovascular disturbances in the cerebral cortex of Alzheimer's disease-model mice: protection by atorvastatin and pitavastatin. *Neuroscience* 197, 358–368. doi: 10.1016/j.neuroscience.2011.09.030

Lee, T. H., Hsieh, S. T., and Chiang, H. Y. (2019). Fibronectin inhibitor pUR4 attenuates tumor necrosis factor α-induced endothelial hyperpermeability by modulating β1 integrin activation. *J. Biomed. Sci.* 26:37. doi: 10.1186/s12929-019-0529-6

Lepelletier, F.-X., Mann, D. M. A., Robinson, A. C., Pinteaux, E., and Boutin, H. (2017). Early changes in extracellular matrix in Alzheimer's disease. *Neuropathol. Appl. Neurobiol.* 43, 167–182. doi: 10.1111/nan.12295

Ljubimova, J. Y., Fujita, M., Khazenzon, N. M., Ljubimov, A. V., and Black, K. L. (2006). Changes in laminin isoforms associated with brain tumor invasion and angiogenesis. *Front. Biosci.* 11:81–88. doi: 10.2741/1781

Louveau, A., Plog, B. A., Antila, S., Alitalo, K., Nedergaard, M., and Kipnis, J. (2017). Understanding the functions and relationships of the glymphatic system and meningeal lymphatics. *J. Clin. Invest.* 127, 3210–3219. doi: 10.1172/JCI90603

Louveau, A., Smirnov, I., Keyes, T. J., Eccles, J. D., Rouhani, S. J., Peske, J. D., et al. (2015). Structural and functional features of central nervous system lymphatic vessels. *Nature* 523, 337–341. doi: 10.1038/nature14432

Luyendijk, W., Bots, G. T., Vegter-van der Vlis, M., Went, L. N., and Frangione, B. (1988). Hereditary cerebral haemorrhage caused by cortical amyloid angiopathy. *J. Neurol. Sci.* 85, 267–280. doi: 10.1016/0022-510x(88)90186-4

Ma, Q., Ries, M., Decker, Y., Müller, A., Riner, C., Bücker, A., et al. (2019). Rapid lymphatic efflux limits cerebrospinal fluid flow to the brain. *Acta Neuropathol.* 137, 151–165. doi: 10.1007/s00401-018-1916-x

Magaki, S., Tang, Z., Tung, S., Williams, C. K., Lo, D., Yong, W. H., et al. (2018). The effects of cerebral amyloid angiopathy on integrity of the blood-brain barrier. *Neurobiol. Aging* 70, 70–77. doi: 10.1016/j.neurobiolaging.2018.06.004

Mahalingam, Y., Gallagher, J. T., and Couchman, J. R. (2007). Cellular adhesion responses to the heparin-binding (HepII) domain of fibronectin require heparan sulfate with specific properties. *J. Biol. Chem.* 282, 3221–3230. doi: 10.1074/jbc.M604938200

Mahon, S., Parmar, P., Barker-Collo, S., Krishnamurthi, R., Jones, K., Theadom, A., et al. (2017). Determinants, prevalence, and trajectory of long-term post-stroke cognitive impairment: results from a 4-year follow-up of the ARCOS-IV study. *Neuroepidemiology* 49, 129–134. doi: 10.1159/000484606

Marín-Padilla, M., and Knopman, D. S. (2011). Developmental aspects of the intracerebral microvasculature and perivascular spaces: insights into brain response to late-life diseases. *J. Neuropathol. Exp. Neurol.* 70, 1060–1069. doi: 10.1097/NEN.0b013e31823ac627

Mathiisen, T. M., Lehre, K. P., Danbolt, N. C., and Ottersen, O. P. (2010). The perivascular astroglial sheath provides a complete covering of the brain microvessels: an electron microscopic 3D reconstruction. *Glia* 58, 1094–1103. doi: 10.1002/glia.20990

Mehta, D. C., Short, J. L., and Nicolazzo, J. A. (2013). Altered brain uptake of therapeutics in a triple transgenic mouse model of alzheimer's disease. *Pharm. Res.* 30, 2868–2879. doi: 10.1007/s11095-013-1116-2

Menezes, M. J., McClenahan, F. K., Leiton, C. V., Aranmolate, A., Shan, X., and Colognato, H. (2014). The extracellular matrix protein laminin α2 regulates the maturation and function of the blood–brain barrier. *J. Neurosci.* 34, 15260–15280. doi: 10.1523/JNEUROSCI.3678-13.2014

Merlini, M., Meyer, E. P., Ulmann-Schuler, A., and Nitsch, R. M. (2011). Vascular β-amyloid and early astrocyte alterations impair cerebrovascular function and cerebral metabolism in transgenic arcAβ mice. *Acta Neuropathol.* 122, 293–311. doi: 10.1007/s00401-011-0834-y

Mestre, H., Hablitz, L. M., Xavier, A. L. R., Feng, W., Zou, W., Pu, T., et al. (2018a). Aquaporin-4-dependent glymphatic solute transport in the rodent brain. *Elife* 7:e40070. doi: 10.7554/eLife.40070

Mestre, H., Mori, Y., and Nedergaard, M. (2020). The brain's glymphatic system: current controversies. *Trends Neurosci.* 43, 458–466. doi: 10.1016/j.tins.2020.04.003

Mestre, H., Tithof, J., Du, T., Song, W., Peng, W., Sweeney, A. M., et al. (2018b). Flow of cerebrospinal fluid is driven by arterial pulsations and is reduced in hypertension. *Nat. Commun.* 9:4878. doi: 10.1038/s41467-018-07318-3

Milner, R., and Campbell, I. L. (2002). Developmental regulation of beta1 integrins during angiogenesis in the central nervous system. *Mol. Cell. Neurosci.* 20, 616–626. doi: 10.1006/mcne.2002.1151

Milner, R., and Campbell, I. L. (2006). Increased expression of the beta4 and alpha5 integrin subunits in cerebral blood vessels of transgenic mice chronically producing the pro-inflammatory cytokines IL-6 or IFN-alpha in the central nervous system. *Mol. Cell. Neurosci.* 33, 429–440. doi: 10.1016/j.mcn.2006.09.004

Miners, J. S., Kehoe, P., and Love, S. (2011). Neprilysin protects against cerebral amyloid angiopathy and aβ-induced degeneration of cerebrovascular smooth muscle cells. *Brain Pathol.* 21, 594–605. doi: 10.1111/j.1750-3639.2011.00486.x

Mitchell, G. F., Van Buchem, M. A., Sigurdsson, S., Gotal, J. D., Jonsdottir, M. K., Kjartansson, Ó, et al. (2011). Arterial stiffness, pressure and flow pulsatility and brain structure and function: the age, gene/environment susceptibility-reykjavik study. *Brain* 134, 3398–3407. doi: 10.1093/brain/awr253

Morris, A. W. J., Carare, R. O., Schreiber, S., and Hawkes, C. A. (2014). The cerebrovascular basement membrane: role in the clearance of β-amyloid and cerebral amyloid angiopathy. *Front. Aging Neurosci.* 6:251. doi: 10.3389/fnagi.2014.00251

Morris, A. W. J., Sharp, M. M., Albargothy, N. J., Fernandes, R., Hawkes, C. A., Verma, A., et al. (2016). Vascular basement membranes as pathways for the passage of fluid into and out of the brain. *Acta Neuropathol.* 131, 725–736. doi: 10.1007/s00401-016-1555-z

Mortensen, K. N., Sanggaard, S., Mestre, H., Lee, H., Kostrikov, S., Xavier, A. L. R., et al. (2019). Impaired glymphatic transport in spontaneously hypertensive rats. *J. Neurosci.* 39, 6365–6377. doi: 10.1523/JNEUROSCI.1974-18.2019

Muhire, G., Iulita, M. F., Vallerand, D., Youwakim, J., Gratuze, M., Petry, F. R., et al. (2019). Arterial stiffness due to carotid calcification disrupts cerebral blood flow regulation and leads to cognitive deficits. *J. Am. Heart Assoc.* 8:e011630. doi: 10.1161/JAHA.118.011630

Nakada, T., Kwee, I. L., Igarashi, H., and Suzuki, Y. (2017). Aquaporin-4 functionality and virchow-robin space water dynamics: physiological model for neurovascular coupling and glymphatic flow. *Int. J. Mol. Sci.* 18:1798. doi: 10.3390/ijms18081798

Nakamura, Y., Suzuki, Y., Tsujita, M., Huber, V. J., Yamada, K., and Nakada, T. (2011). Development of a novel ligand, [11C]TGN-020, for aquaporin 4 positron emission tomography imaging. *ACS Chem. Neurosci.* 2, 568–571. doi: 10.1021/cn2000525

Narindrasorasak, S., Altman, R. A., Gonzalez-DeWhitt, P., Greenberg, B. D., and Kisilevsky, R. (1995). An interaction between basement membrane and Alzheimer amyloid precursor proteins suggests a role in the pathogenesis of Alzheimer's disease. *Lab. Invest.* 72, 272–282.

Narindrasorasak, S., Lowery, D., Gonzalez-DeWhitt, P., Poorman, R. A., Greenberg, B., and Kisilevsky, R. (1991). High affinity interactions between the Alzheimer's beta-amyloid precursor proteins and the basement membrane form of heparan sulfate proteoglycan. *J. Biol. Chem.* 266, 12878–12883.

Narindrasorasak, S., Lowery, D. E., Altman, R. A., Gonzalez-DeWhitt, P. A., Greenberg, B. D., and Kisilevsky, R. (1992). Characterization of high affinity binding between laminin and Alzheimer's disease amyloid precursor proteins. *Lab. Invest.* 67, 643–652.

Navarro-Dorado, J., Villalba, N., Prieto, D., Brera, B., Martín-Moreno, A. M., Tejerina, T., et al. (2016). Vascular dysfunction in a transgenic model of Alzheimer's disease: effects of CB1R and CB2R cannabinoid agonists. *Front. Neurosci.* 10:422. doi: 10.3389/fnins.2016.00422

Nicholson, C., and Hrabìtová, S. (2017). Brain extracellular space: the final frontier of neuroscience. *Biophys. J.* 113, 2133–2142. doi: 10.1016/j.bpj.2017.06.052

Nicholson, C., and Tao, L. (1993). Hindered diffusion of high molecular weight compounds in brain extracellular microenvironment measured with integrative optical imaging. *Biophys. J.* 65, 2277–2290. doi: 10.1016/S0006-3495(93)81324-9

Nikolakopoulou, A. M., Zhao, Z., Montagne, A., and Zlokovic, B. V. (2017). Regional early and progressive loss of brain pericytes but not vascular smooth muscle cells in adult mice with disrupted platelet-derived growth factor receptor-β signaling. *PLoS One* 12:e0176225. doi: 10.1371/journal.pone.0176225

Niquet, J., and Represa, A. (1996). Entactin immunoreactivity in immature and adult rat brain. *Dev. Brain Res.* 95, 227–233. doi: 10.1016/0165-3806(96)00089-2

Noël, G., Tham, D. K. L., Guadagno, E., MacVicar, B. A., and Moukhles, H. (2020). The laminin-induced phosphorylation of PKCδ regulates AQP4 distribution

and water permeability in rat astrocytes. *Cell. Mol. Neurobiol.* doi: 10.1007/s10571-020-00944-w

Noël, G., Tham, D. K. L., MacVicar, B. A., and Moukhles, H. (2019). Agrin plays a major role in the coalescence of the aquaporin-4 clusters induced by gamma-1-containing laminin. *J. Comp. Neurol.* 528, 407–418. doi: 10.1002/cne.24763

Noell, S., Fallier-Becker, P., Deutsch, U., MacK, A. F., and Wolburg, H. (2009). Agrin defines polarized distribution of orthogonal arrays of particles in astrocytes. *Cell Tissue Res.* 337, 185–195. doi: 10.1007/s00441-009-0812-z

Noell, S., Wolburg-Buchholz, K., Mack, A. F., Beedle, A. M., Satz, J. S., Campbell, K. P., et al. (2011). Evidence for a role of dystroglycan regulating the membrane architecture of astroglial endfeet. *Eur. J. Neurosci.* 33, 2179–2186. doi: 10.1111/j.1460-9568.2011.07688.x

Nortley, R., Korte, N., Izquierdo, P., Hirunpattarasilp, C., Mishra, A., Jaunmuktane, Z., et al. (2019). Amyloid b oligomers constrict human capillaries in Alzheimer's disease via signaling to pericytes. *Science* 365:eaav9518. doi: 10.1126/science.aav9518

Okoye, M. I., and Watanabe, I. (1982). Ultrastructural features of cerebral amyloid angiopathy. *Hum. Pathol.* 13, 1127–1132. doi: 10.1016/S0046-8177(82)80251-7

Paulus, W., Baur, I., Schuppan, D., and Roggendorf, W. (1993). Characterization of integrin receptors in normal and neoplastic human brain. *Am. J. Pathol.* 143, 154–163.

Peca, S., McCreary, C. R., Donaldson, E., Kumarpillai, G., Shobha, N., Sanchez, K., et al. (2013). Neurovascular decoupling is associated with severity of cerebral amyloid angiopathy. *Neurology* 81, 1659–1665. doi: 10.1212/01.wnl.0000435291.49598.54

Peng, W., Achariyar, T. M., Li, B., Liao, Y., Mestre, H., Hitomi, E., et al. (2016). Suppression of glymphatic fluid transport in a mouse model of Alzheimer's disease. *Neurobiol. Dis.* 93, 215–225. doi: 10.1016/j.nbd.2016.05.015

Perlmutter, L. S., Barrón, E., Saperia, D., and Chui, H. C. (1991). Association between vascular basement membrane components and the lesions of Alzheimer's disease. *J. Neurosci. Res.* 30, 673–681. doi: 10.1002/jnr.490300411

Perlmutter, L. S., Chui, H. C., Saperia, D., and Athanikar, J. (1990). Microangiopathy and the colocalization of heparan sulfate proteoglycan with amyloid in senile plaques of Alzheimer's disease. *Brain Res.* 508, 13–19. doi: 10.1016/0006-8993(90)91111-S

Pizzo, M. E., Wolak, D. J., Kumar, N. N., Brunette, E., Brunnquell, C. L., Hannocks, M. J., et al. (2018). Intrathecal antibody distribution in the rat brain: surface diffusion, perivascular transport and osmotic enhancement of delivery. *J. Physiol.* 596, 445–475. doi: 10.1113/JP275105

Plog, B. A., Dashnaw, M. L., Hitomi, E., Peng, W., Liao, Y., Lou, N., et al. (2015). Biomarkers of traumatic injury are transported from brain to blood via the glymphatic system. *J. Neurosci.* 35, 518–526. doi: 10.1523/JNEUROSCI.3742-14.2015

Rajna, Z., Raitamaa, L., Tuovinen, T., Heikkila, J., Kiviniemi, V., and Seppanen, T. (2019). 3D multi-resolution optical flow analysis of cardiovascular pulse propagation in human brain. *IEEE Trans. Med. Imaging* 38, 2028–2036. doi: 10.1109/TMI.2019.2904762

Ratelade, J., Mezouar, N., Domenga-Denier, V., Rochey, A., Plaisier, E., and Joutel, A. (2018). Severity of arterial defects in the retina correlates with the burden of intracerebral haemorrhage in COL4A1-related stroke. *J. Pathol.* 244, 408–420. doi: 10.1002/path.5023

Rauch, U., Zhou, X. H., and Roos, G. (2005). Extracellular matrix alterations in brains lacking four of its components. *Biochem. Biophys. Res. Commun.* 328, 608–617. doi: 10.1016/j.bbrc.2005.01.026

Ray, L., Iliff, J. J., and Heys, J. J. (2019). Analysis of convective and diffusive transport in the brain interstitium. *Fluids Barriers CNS.* 16:6. doi: 10.1186/s12987-019-0126-9

Reed, M. J., Damodarasamy, M., and Banks, W. A. (2019). The extracellular matrix of the blood–brain barrier: structural and functional roles in health, aging, and Alzheimer's disease. *Tissue Barriers* 7:1651157. doi: 10.1080/21688370.2019.1651157

Ren, H., Luo, C., Feng, Y., Yao, X., Shi, Z., Liang, F., et al. (2017). Omega-3 polyunsaturated fatty acids promote amyloid-b clearance from the brain through mediating the function of the glymphatic system. *FASEB J.* 31, 282–293. doi: 10.1096/fj.201600896

Ringstad, G., Valnes, L. M., Dale, A. M., Pripp, A. H., Vatnehol, S. A. S., Emblem, K. E., et al. (2018). Brain-wide glymphatic enhancement and clearance in humans assessed with MRI. *JCI Insight* 3:e121537. doi: 10.1172/jci.insight.121537

Robel, S., Mori, T., Zoubaa, S., Schlegel, J., Sirko, S., Faissner, A., et al. (2009). Conditional deletion of β1-integrin in astroglia causes partial reactive gliosis. *Glia* 57, 1630–1647. doi: 10.1002/glia.20876

Rosenberg, G. A., Kyner, W. T., and Estrada, E. (1980). Bulk flow of brain interstitial fluid under normal and hyperosmolar conditions. *Am. J. Physiol.* 238, F42–F49. doi: 10.1152/ajprenal.1980.238.1.F42

Santos, C. Y., Snyder, P. J., Wu, W.-C., Zhang, M., Echeverria, A., and Alber, J. (2017). Pathophysiologic relationship between Alzheimer's disease, cerebrovascular disease, and cardiovascular risk: a review and synthesis. *Alzheimers Dement.* 7, 69–87. doi: 10.1016/j.dadm.2017.01.005

Sapsford, I., Buontempo, J., and Weller, R. O. (1983). Basement membrane surfaces and perivascular compartments in normal human brain and glial tumors. A scanning electron microscope study. *Neuropathol. Appl. Neurobiol.* 9, 181–194. doi: 10.1111/j.1365-2990.1983.tb00106.x

Schain, A. J., Melo-Carrillo, A., Strassman, A. M., and Burstein, R. (2017). Cortical spreading depression closes paravascular space and impairs glymphatic flow: implications for migraine headache. *J. Neurosci.* 37, 2904–2915. doi: 10.1523/JNEUROSCI.3390-16.2017

Schley, D., Carare-Nnadi, R., Please, C. P., Perry, V. H., and Weller, R. O. (2006). Mechanisms to explain the reverse perivascular transport of solutes out of the brain. *J. Theor. Biol.* 238, 962–974. doi: 10.1016/j.jtbi.2005.07.005

Schneider, J. A., Arvanitakis, Z., Bang, W., and Bennett, D. A. (2007). Mixed brain pathologies account for most dementia cases in community-dwelling older persons. *Neurology* 69, 2197–2204. doi: 10.1212/01.wnl.0000271090.28148.24

Shih, A. Y., Rühlmann, C., Blinder, P., Devor, A., Drew, P. J., Friedman, B., et al. (2015). Robust and fragile aspects of cortical blood flow in relation to the underlying angioarchitecture. *Microcirculation* 22, 204–218. doi: 10.1111/micc.12195

Shimizu, H., Ghazizadeh, M., Sato, S., Oguro, T., and Kawanami, O. (2009). Interaction between b-amyloid protein and heparan sulfate proteoglycans from the cerebral capillary basement membrane in Alzheimer's disease. *J. Clin. Neurosci.* 16, 277–282. doi: 10.1016/j.jocn.2008.04.009

Sievers, J., Pehlemann, F. W., Gude, S., and Berry, M. (1994). Meningeal cells organize the superficial glia limitans of the cerebellum and produce components of both the interstitial matrix and the basement membrane. *J. Neurocytol.* 23, 135–149. doi: 10.1007/BF01183867

Simon, M. J., Wang, M. X., Murchison, C. F., Roese, N. E., Boespflug, E. L., Woltjer, R. L., et al. (2018). Transcriptional network analysis of human astrocytic endfoot genes reveals region-specific associations with dementia status and tau pathology. *Sci. Rep.* 8:12389. doi: 10.1038/s41598-018-30779-x

Singh-Bains, M. K., Linke, V., Austria, M. D. R., Tan, Y. S., Scotter, E. L., Mehrabi, N. F., et al. (2019). Altered microglia and neurovasculature in the Alzheimer's disease cerebellum. *Neurobiol. Dis.* 132:104589. doi: 10.1016/j.nbd.2019.104589

Sixt, M., Engelhardt, B., Pausch, F., Hallmann, R., Wendler, O., and Sorokin, L. M. (2001). Endothelial cell laminin isoforms, laminins 8 and 10, play decisive roles in T cell recruitment across the blood-brain barrier in experimental autoimmune encephalomyelitis. *J. Cell Biol.* 153, 933–945. doi: 10.1083/jcb.153.5.933

Snow, A. D., Kinsella, M. G., Parks, E., Sekiguchi, R. T., Miller, J. D., Kimata, K., et al. (1995). Differential binding of vascular cell-derived proteoglycans (Perlecan, Biglycan, Decorin, and Versican) to the beta-amyloid protein of Alzheimer's disease. *Arch. Biochem. Biophys.* 320, 84–95. doi: 10.1006/abbi.1995.1345

Snow, A. D., Mar, H., Nochlin, D., Kimata, K., Kato, M., Suzuki, S., et al. (1988). The presence of heparan sulfate proteoglycans in the neuritic plaques and congophilic angiopathy in Alzheimer's disease. *Am. J. Pathol.* 133, 456–463.

Snow, A. D., Sekiguchi, R. T., Nochlin, D., Kalaria, R. N., and Kimata, K. (1994). Heparan sulfate proteoglycan in diffuse plaques of hippocampus but not of cerebellum in Alzheimer's disease brain. *Am. J. Pathol.* 144, 337–347.

Sofroniew, M. V. (2015). Astrocyte barriers to neurotoxic inflammation. *Nat. Rev. Neurosci.* 16, 249–263. doi: 10.1038/nrn3898

Su, J. H., Cummings, B. J., and Cotman, C. W. (1992). Localization of heparan sulfate glycosaminoglycan and proteoglycan core protein in aged brain and Alzheimer's disease. *Neuroscience* 51, 801–813. doi: 10.1016/0306-4522(92)90521-3

Syková, E., and Nicholson, C. (2008). Diffusion in brain extracellular space. *Physiol. Rev.* 88, 1277–1340. doi: 10.1152/physrev.00027.2007

Syková, E., Vorísek, I., Antonova, T., Mazel, T., Meyer-Luehmann, M., Jucker, M., et al. (2005). Changes in extracellular space size and geometry in APP23 transgenic mice: a model of Alzheimer's disease. *Proc. Natl. Acad. Sci. U.S.A.* 102, 479–484. doi: 10.1073/pnas.0408235102

Taoka, T., Masutani, Y., Kawai, H., Nakane, T., Matsuoka, K., Yasuno, F., et al. (2017). Evaluation of glymphatic system activity with the diffusion MR technique: diffusion tensor image analysis along the perivascular space (DTI-ALPS) in Alzheimer's disease cases. *Jpn. J. Radiol.* 35, 172–178. doi: 10.1007/s11604-017-0617-z

Tarasoff-Conway, J. M., Carare, R. O., Osorio, R. S., Glodzik, L., Butler, T., Fieremans, E., et al. (2015). Clearance systems in the brain –implications for Alzheimer disease. *Nat. Rev. Neurol.* 11, 457–470. doi: 10.1038/nrneurol.2015.119

Thal, D. R., Ghebremedhin, E., Rüb, U., Yamaguchi, H., Del Tredici, K., and Braak, H. (2002). Two types of sporadic cerebral amyloid angiopathy. *J. Neuropathol. Exp. Neurol.* 61, 282–293. doi: 10.1093/jnen/61.3.282

Thal, D. R., Larionov, S., Abramowski, D., Wiederhold, K. H., Van Dooren, T., Yamaguchi, H., et al. (2007). Occurrence and co-localization of amyloid β-protein and apolipoprotein E in perivascular drainage channels of wild-type and APP-transgenic mice. *Neurobiol. Aging* 28, 1221–1230. doi: 10.1016/j.neurobiolaging.2006.05.029

Tham, D. K. L., Joshi, B., and Moukhles, H. (2016). Aquaporin-4 cell-surface expression and turnover are regulated by dystroglycan, dynamin, and the extracellular matrix in astrocytes. *PLoS One* 11:e0165439. doi: 10.1371/journal.pone.0165439

Thomas, O., Cain, J., Nasralla, M., and Jackson, A. (2019). Aortic pulsatility propagates intracranially and correlates with dilated perivascular spaces and small vessel compliance. *J. Stroke Cerebrovasc. Dis.* 28, 1252–1260. doi: 10.1016/j.jstrokecerebrovasdis.2019.01.020

Thomsen, M. S., Birkelund, S., Burkhart, A., Stensballe, A., and Moos, T. (2017a). Synthesis and deposition of basement membrane proteins by primary brain capillary endothelial cells in a murine model of the blood-brain barrier. *J. Neurochem.* 140, 741–754. doi: 10.1111/jnc.13747

Thomsen, M. S., Routhe, L. J., and Moos, T. (2017b). The vascular basement membrane in the healthy and pathological brain. *J. Cereb. Blood Flow Metab.* 37, 3300–3317. doi: 10.1177/0271678X17722436

Thorne, R. G., Hrabìtová, S., and Nicholson, C. (2004). Diffusion of epidermal growth factor in rat brain extracellular space measured by integrative optical imaging. *J. Neurophysiol.* 92, 3471–3481. doi: 10.1152/jn.00352.2004

Thorne, R. G., Lakkaraju, A., Rodriguez-Boulan, E., and Nicholson, C. (2008). *In vivo* diffusion of lactoferrin in brain extracellular space is regulated by interactions with heparan sulfate. *Proc. Natl. Acad. Sci. U.S.A.* 105, 8416–8421. doi: 10.1073/pnas.0711345105

Thorne, R. G., and Nicholson, C. (2006). *In vivo* diffusion analysis with quantum dots and dextrans predicts the width of brain extracellular space. *Proc. Natl. Acad. Sci. U.S.A.* 103, 5567–5572. doi: 10.1073/pnas.0509425103

Tian, J., Shi, J., Smallman, R., Iwatsubo, T., and Mann, D. M. A. (2006). Relationships in Alzheimer's disease between the extent of Aβ deposition in cerebral blood vessel walls, as cerebral amyloid angiopathy, and the amount of cerebrovascular smooth muscle cells and collagen. *Neuropathol. Appl. Neurobiol.* 32, 332–340. doi: 10.1111/j.1365-2990.2006.00732.x

Tithof, J., Kelley, D. H., Mestre, H., Nedergaard, M., and Thomas, J. H. (2019). Hydraulic resistance of periarterial spaces in the brain. *Fluids Barriers CNS* 16:19. doi: 10.1186/s12987-019-0140-y

Urabe, N., Naito, I., Saito, K., Yonezawa, T., Sado, Y., Yoshioka, H., et al. (2002). Basement membrane type IV collagen molecules in the choroid plexus, pia mater and capillaries in the mouse brain. *Arch. Histol. Cytol.* 65, 133–143. doi: 10.1679/aohc.65.133

Utriainen, A., Sormunen, R., Kettunen, M., Carvalhaes, L. S., Sajanti, E., Eklund, L., et al. (2004). Structurally altered basement membranes and hydrocephalus in a type XVIII collagen deficient mouse line. *Hum. Mol. Genet.* 13, 2089–2099. doi: 10.1093/hmg/ddh213

Van Broeckhoven, C., Haan, J., Bakker, E., Hardy, J. A., Van Hul, W., Wehnert, A., et al. (1990). Amyloid beta protein precursor gene and hereditary cerebral hemorrhage with amyloidosis (Dutch). *Science* 248, 1120–1122. doi: 10.1126/science.1971458

van Dyck, C. H. (2018). Anti-Amyloid-β monoclonal antibodies for Alzheimer's disease: pitfalls and promise. *Biol. Psychiatry* 83, 311–319. doi: 10.1016/j.biopsych.2017.08.010

van Etten, E. S., Verbeek, M. M., van der Grond, J., Zielman, R., van Rooden, S., van Zwet, E. W., et al. (2017). β-Amyloid in CSF. *Neurology* 88, 169–176. doi: 10.1212/WNL.0000000000003486

van Nostrand, W. E., Melchor, J. P., Cho, H. S., Greenberg, S. M., and Rebeck, G. W. (2001). Pathogenic effects of D23N Iowa mutant amyloid beta -protein. *J. Biol. Chem.* 276, 32860–32866. doi: 10.1074/jbc.M104135200

van Nostrand, W. E., Wagner, S. L., Haan, J., Bakker, E., and Roos, R. A. C. (1992). Alzheimer's disease and hereditary cerebral hemorrhage with amyloidosis-dutch type share a decrease in cerebrospinal fluid levels of amyloid-protein precursor. *Ann. Neurol.* 32, 215–218. doi: 10.1002/ana.410320214

van Veluw, S. J., Hou, S. S., Calvo-Rodriguez, M., Arbel-Ornath, M., Snyder, A. C., Frosch, M. P., et al. (2019). Vasomotion as a driving force for paravascular clearance in the awake mouse brain. *Neuron* 105, 549–561.e5. doi: 10.1016/j.neuron.2019.10.033

Vanlandewijck, M., He, L., Mäe, M. A., Andrae, J., Ando, K., Del Gaudio, F., et al. (2018). A molecular atlas of cell types and zonation in the brain vasculature. *Nature* 554, 475–480. doi: 10.1038/nature25739

Venkat, P., Chopp, M., Zacharek, A., Cui, C., Zhang, L., Li, Q., et al. (2017). White matter damage and glymphatic dysfunction in a model of vascular dementia in rats with no prior vascular pathologies. *Neurobiol. Aging* 50, 96–106. doi: 10.1016/j.neurobiolaging.2016.11.002

Verbeek, M. M., Otte-Höller, I., van den Born, J., van den Heuvel, L. P. W. J., David, G., Wesseling, P., et al. (1999). Agrin is a major heparan sulfate proteoglycan accumulating in Alzheimer's disease brain. *Am. J. Pathol.* 155, 2115–2125. doi: 10.1016/S0002-9440(10)65529-0

Viticchi, G., Falsetti, L., Buratti, L., Boria, C., Luzzi, S., Bartolini, M., et al. (2015). Framingham risk score can predict cognitive decline progression in Alzheimer's disease. *Neurobiol. Aging* 36, 2940–2945. doi: 10.1016/j.neurobiolaging.2015.07.023

von Holstein-Rathlou, S., Petersen, N. C., and Nedergaard, M. (2018). Voluntary running enhances glymphatic influx in awake behaving, young mice. *Neurosci. Lett.* 662, 253–258. doi: 10.1016/j.neulet.2017.10.035

Vonsattel, J. P., Myers, R. H., Hedley-Whyte, E. T., Ropper, A. H., Bird, E. D., and Richardson, E. P. (1991). Cerebral amyloid angiopathy without and with cerebral hemorrhages: a comparative histological study. *Ann. Neurol.* 30, 637–649. doi: 10.1002/ana.410300503

Vos, S. J. B., Van Boxtel, M. P. J., Schiepers, O. J. G., Deckers, K., De Vugt, M., Carrière, I., et al. (2017). Modifiable risk factors for prevention of dementia in midlife, late life and the oldest-old: validation of the LIBRA index. *J. Alzheimers Dis.* 58, 537–547. doi: 10.3233/JAD-161208

Wang, J., and Milner, R. (2006). Fibronectin promotes brain capillary endothelial cell survival and proliferation through alpha5beta1 and alphavbeta3 integrins via MAP kinase signalling. *J. Neurochem.* 96, 148–159. doi: 10.1111/j.1471-4159.2005.03521.x

Wang, M., Ding, F., Deng, S. Y., Guo, X., Wang, W., Iliff, J. J., et al. (2017). Focal solute trapping and global glymphatic pathway impairment in a murine model of multiple microinfarcts. *J. Neurosci.* 37, 2870–2877. doi: 10.1523/JNEUROSCI.2112-16.2017

Wang, P., and Olbricht, W. L. (2011). Fluid mechanics in the perivascular space. *J. Theor. Biol.* 274, 52–57. doi: 10.1016/j.jtbi.2011.01.014

Wang, Z., Collighan, R. J., Gross, S. R., Danen, E. H. J., Orend, G., Telci, D., et al. (2010). RGD-independent cell adhesion via a tissue transglutaminase-fibronectin matrix promotes fibronectin fibril deposition and requires syndecan-4/2 and α5β1 integrin Co-signaling. *J. Biol. Chem.* 285, 40212–40229. doi: 10.1074/jbc.M110.123703

Watanabe, K., Takeishi, H., Hayakawa, T., and Sasaki, H. (2010). Three-dimensional organization of the perivascular glial limiting membrane and its relationship with the vasculature: a scanning electron microscope study. *Okajimas Folia Anat. Jpn.* 87, 109–121. doi: 10.2535/ofaj.87.109

Webb, A. J. S., Simoni, M., Mazzucco, S., Kuker, W., Schulz, U., and Rothwell, P. M. (2012). Increased cerebral arterial pulsatility in patients with leukoaraiosis: arterial stiffness enhances transmission of aortic pulsatility. *Stroke* 43, 2631–2636. doi: 10.1161/STROKEAHA.112.655837

White, L., Small, B. J., Petrovitch, H., Ross, G. W., Masaki, K., Abbott, R. D., et al. (2005). Recent clinical-pathologic research on the causes of dementia in late life: update from the Honolulu-Asia Aging study. *J. Geriatr. Psychiatry Neurol.* 18, 224–227. doi: 10.1177/0891988705281872

Wilcock, D. M., Vitek, M. P., and Colton, C. A. (2009). Vascular amyloid alters astrocytic water and potassium channels in mouse models and humans with Alzheimer's disease. *Neuroscience* 159, 1055–1069. doi: 10.1016/j.neuroscience.2009.01.023

Williams, R. J., Goodyear, B. G., Peca, S., McCreary, C. R., Frayne, R., Smith, E. E., et al. (2017). Identification of neurovascular changes associated with cerebral amyloid angiopathy from subject-specific hemodynamic response functions. *J. Cereb. Blood Flow Metab.* 37, 3433–3445. doi: 10.1177/0271678X17691056

Wolburg-Buchholz, K., Mack, A. F., Steiner, E., Pfeiffer, F., Engelhardt, B., and Wolburg, H. (2009). Loss of astrocyte polarity marks blood-brain barrier impairment during experimental autoimmune encephalomyelitis. *Acta Neuropathol.* 118, 219–233. doi: 10.1007/s00401-009-0558-4

Xie, L., Kang, H., Xu, Q., Chen, M. J., Liao, Y., Thiyagarajan, M., et al. (2013). Sleep drives metabolite clearance from the adult brain. *Science* 342, 373–377. doi: 10.1126/science.1241224

Xue, Y., Liu, N., Zhang, M., Ren, X., Tang, J., and Fu, J. (2020). Concomitant enlargement of perivascular spaces and decrease in glymphatic transport in an animal model of cerebral small vessel disease. *Brain Res. Bull.* 161, 78–83. doi: 10.1016/j.brainresbull.2020.04.008

Xu, Z., Xiao, N., Chen, Y., Huang, H., Marshall, C., Gao, J., et al. (2015). Deletion of aquaporin-4 in APP/PS1 mice exacerbates brain Aβ accumulation and memory deficits. *Mol. Neurodegener.* 10, 58. doi: 10.1186/s13024-015-0056-1

Yamada, M. (2002). Risk factors for cerebral amyloid angiopathy in the elderly. *Ann. N. Y. Acad. Sci.* 977, 37–44. doi: 10.1111/j.1749-6632.2002.tb04797.x

Yamada, M. (2015). Cerebral amyloid angiopathy: emerging concepts. *J. Stroke* 17, 17–30. doi: 10.5853/jos.2015.17.1.17

Yamaguchi, H., Yamazaki, T., Lemere, C. A., Frosch, M. P., and Selkoe, D. J. (1992). Beta amyloid is focally deposited within the outer basement membrane in the amyloid angiopathy of Alzheimer's disease. An immunoelectron microscopic study. *Am. J. Pathol.* 141, 249–259.

Yang, J., Zhang, R., Shi, C., Mao, C., Yang, Z., Suo, Z., et al. (2017). AQP4 association with amyloid deposition and astrocyte pathology in the Tg-ArcSwe mouse model of Alzheimer's disease. *J. Alzheimers Dis.* 57, 157–169. doi: 10.3233/JAD-160957

Yanqing, Z., Yu-Min, L., Jian, Q., Bao-Guo, X., and Chuan-Zhen, L. (2006). Fibronectin and neuroprotective effect of granulocyte colony-stimulating factor in focal cerebral ischemia. *Brain Res.* 1098, 161–169. doi: 10.1016/j.brainres.2006.02.140

Yao, Y., Chen, Z. L., Norris, E. H., and Strickland, S. (2014). Astrocytic laminin regulates pericyte differentiation and maintains blood brain barrier integrity. *Nat. Commun.* 5:3413. doi: 10.1038/ncomms4413

Zámecník, J., Vargová, L., Homola, A., Kodet, R., and Syková, E. (2004). Extracellular matrix glycoproteins and diffusion barriers in human astrocytic tumours. *Neuropathol. Appl. Neurobiol.* 30, 338–350. doi: 10.1046/j.0305-1846.2003.00541.x

Zekonyte, J., Sakai, K., Nicoll, J. A. R., Weller, R. O., Carare, R. O., Murphy, M. P., et al. (2016). Quantification of molecular interactions between ApoE, amyloid-beta (Aβ) and laminin: relevance to accumulation of Aβ in Alzheimer's disease. *Biochim. Biophys. Acta J.* 1862, 1047–1053. doi: 10.1016/j.bbadis.2015.08.025

Zeppenfeld, D. M., Simon, M., Haswell, J. D., D'Abreo, D., Murchison, C., Quinn, J. F., et al. (2017). Association of perivascular localization of aquaporin-4 with cognition and Alzheimer disease in aging brains. *JAMA Neurol.* 74, 91–99. doi: 10.1001/jamaneurol.2016.4370

Zhang, E. T., Inman, C. B., and Weller, R. O. (1990). Interrelationships of the pia mater and the perivascular (Virchow-Robin) spaces in the human cerebrum. *J. Anat.* 170, 111–123.

Zhang, Y., Chen, J., Qiu, J., Li, Y., Wang, J., and Jiao, J. (2016). Intakes of fish and polyunsaturated fatty acids and mild-to-severe cognitive impairment risks: a dose-response meta-analysis of 21 cohort studies 1-3. *Am. J. Clin. Nutr.* 103, 330–370. doi: 10.3945/ajcn.115.124081

Conflict of Interest: The authors declare that the research was conducted in the absence of any commercial or financial relationships that could be construed as a potential conflict of interest.

frontiers in Physiology

REVIEW
published: 03 December 2020
doi: 10.3389/fphys.2020.600767

The Expanding Cell Diversity of the Brain Vasculature

*Jayden M. Ross[1,2,3,4], Chang Kim[2,3,4], Denise Allen[2,3,4], Elizabeth E. Crouch[5], Kazim Narsinh[6], Daniel L. Cooke[6], Adib A. Abla[1], Tomasz J. Nowakowski[2,3,4,6] and Ethan A. Winkler[1]**

[1] Department of Neurological Surgery, University of California, San Francisco, San Francisco, CA, United States, [2] Department of Anatomy, University of California, San Francisco, San Francisco, CA, United States, [3] Department of Psychiatry and Behavioral Sciences, University of California, San Francisco, San Francisco, CA, United States, [4] The Eli and Edythe Broad Center for Regeneration Medicine and Stem Cell Research, University of California, San Francisco, San Francisco, CA, United States, [5] Department of Pediatrics, University of California, San Francisco, San Francisco, CA, United States, [6] Department of Radiology, University of California, San Francisco, San Francisco, CA, United States, [7] Chan Zuckerberg Biohub, San Francisco, CA, United States

The cerebrovasculature is essential to brain health and is tasked with ensuring adequate delivery of oxygen and metabolic precursors to ensure normal neurologic function. This is coordinated through a dynamic, multi-directional cellular interplay between vascular, neuronal, and glial cells. Molecular exchanges across the blood–brain barrier or the close matching of regional blood flow with brain activation are not uniformly assigned to arteries, capillaries, and veins. Evidence has supported functional segmentation of the brain vasculature. This is achieved in part through morphologic or transcriptional heterogeneity of brain vascular cells—including endothelium, pericytes, and vascular smooth muscle. Advances with single cell genomic technologies have shown increasing cell complexity of the brain vasculature identifying previously unknown cell types and further subclassifying transcriptional diversity in cardinal vascular cell types. Cell-type specific molecular transitions or zonations have been identified. In this review, we summarize emerging evidence for the expanding vascular cell diversity in the brain and how this may provide a cellular basis for functional segmentation along the arterial-venous axis.

Keywords: neurovascular unit, single cell sequencing, endothelial cells, pericytes and vascular smooth muscle cells, perivascular macrophages, perivascular fibroblasts, astrocytes, blood brain barrier

OPEN ACCESS

Edited by:
Fabrice Dabertrand, University of Colorado, United States

Reviewed by:
Julie Siegenthaler, University of Colorado, United States
Zhen Zhao, University of Southern California, Los Angeles, United States

****Correspondence:***
Ethan A. Winkler
Ethan.winkler@ucsf.edu

Specialty section:
This article was submitted to Vascular Physiology, a section of the journal Frontiers in Physiology

Received: *31 August 2020*
Accepted: *10 November 2020*
Published: *03 December 2020*

Citation:
Ross JM, Kim C, Allen D, Crouch EE, Narsinh K, Cooke DL, Abla AA, Nowakowski TJ and Winkler EA (2020) The Expanding Cell Diversity of the Brain Vasculature. Front. Physiol. 11:600767. doi: 10.3389/fphys.2020.600767

INTRODUCTION

Continued expansion and sophistication of the mammalian brain has resulted in an astonishing level of cell diversity (Zeisel et al., 2015, 2018; Neubauer et al., 2018; Saunders et al., 2018; Tasic et al., 2018; Cadwell et al., 2019; Hodge et al., 2019). It is believed that this cell diversity helps provide the sub-specialization of cellular function required to face the everchanging contexts of life—such as brain development, aging, and responses to injury or environmental insults. Despite this sophistication, the brain remains vitally dependent on the cerebrovasculature for metabolic exchange with circulating blood—including the delivery of oxygen, glucose, and other metabolites and clearance of toxic metabolic by-products (Winkler et al., 2014a, 2015; Iadecola, 2017; Sweeney et al., 2018). Disruption of the cerebral circulation for even minutes may have profound neurologic implications (Campbell et al., 2019). To meet dynamic metabolic needs, the cerebrovasculature

has developed a highly evolved blood–brain barrier (BBB) to permit regulated molecular transport while preventing influx of circulating blood cells or potentially toxic pathogens or plasma proteins (Zhao et al., 2015; Sweeney et al., 2019). Coordinated communication between neurons, glial, and vascular cells facilitates local regulation of cerebral blood flow (CBF) to ensure blood supply is tightly matched with metabolic demand—a process known as "neurovascular coupling" (Uhlirova et al., 2016; Iadecola, 2017).

Over the past two decades, increased recognition that interconnection between multiple cell types is essential for brain vascular function and has resulted in advancement of the concept of the "neurovascular unit" (Iadecola, 2017; Sweeney et al., 2018). Much of this work, however, has focused on cardinal cell types without acknowledgment of further sub-specialization or vascular cellular diversity. Development of single cell RNA sequencing (scRNAseq) technologies have now allowed unbiased characterization of transcriptional heterogeneity in brain vascular cells (Zeisel et al., 2015, 2018; Sabbagh et al., 2018; Saunders et al., 2018; Vanlandewijck et al., 2018). While heterogeneity in glial and neurons have been reviewed elsewhere (Miller, 2018; Cembrowski and Spruston, 2019; Masuda et al., 2020), we summarize the emerging evidence of added cell diversity within brain vascular cells highlighting how cellular sub-specialization contributes to regionalized vascular function along the arterial-venous axis.

Cardinal Cell Types of the Cerebrovasculature

The cerebrovasculature consists of multiple cell types—including endothelial cells (ECs), pericytes (PCs), and vascular smooth muscle cells (vSMCs) (Winkler et al., 2011, 2019; Zhao et al., 2015; Iadecola, 2017; Sweeney et al., 2018; **Figure 1**). Newly defined perivascular macrophages (PVMs) and perivascular fibroblast-like cells (PVFBs) also reside along the vascular wall (Zeisel et al., 2015; Saunders et al., 2018; Vanlandewijck et al., 2018). Astrocyte foot processes wrap around the vessel wall and create the Virchow Robin space—a perivascular space important for brain interstitial fluid and cerebrospinal fluid exchange known as the "glymphatic system" (Wardlaw et al., 2020). Parenchymal glial or neuronal cell bodies are closely apposed to the brain vasculature and rarely exceed > 15 μm from each vessel (Tsai et al., 2009). Here, we summarize established characteristics of vascular cells and briefly highlight their brain-specific features and functions.

Endothelial Cells

Blood vessels are made up of a single layer of ECs that form a tubular structure (Zhao et al., 2015; Sweeney et al., 2019). The blood facing surface, or luminal surface, is covered by the glycocalyx—a gel-like covering comprised of glycoproteins, proteoglycans, and glycosaminoglycans (Ando et al., 2018; Kutuzov et al., 2018). Most brain ECs have a continuous cell membrane which lacks pores or fenestrations. Adjacent ECs are securely connected to one another by adherens junctional protein complexes and tight junction protein complexes occludes the intercellular cleft. Brain ECs have a high density of tight junction proteins which precludes significant paracellular flow and is a key feature regulating size-restricted transcellular passage of molecules (Zhao et al., 2015; Sweeney et al., 2019). Unlike other organs, ECs also display lower rates of pinocytosis or non-specific bulk-flow vesicular transport (Ben-Zvi et al., 2014; Andreone et al., 2017; Chow and Gu, 2017). The brain-facing or abluminal EC membrane is embedded in a protein-rich basement membrane (BM) serving as a cellular scaffolding essential for interactions with neighboring cells (Thomsen et al., 2017).

Low rates of pinocytosis and membrane permeability make brain ECs the anatomic site of the BBB. The BBB permits gases, e.g., carbon dioxide and oxygen, and lipophilic and small molecules (< 400 Da) to freely enter the brain, but limits circulating cells and other molecules from crossing the endothelium without regulated transport systems (Banks, 2009; Sweeney et al., 2019). ECs contain a number of different transmembrane transporters to regulate influx of circulating nutrients and proteins—including carrier-mediated, receptor-mediated, and active transporter proteins (Sweeney et al., 2019; Tjakra et al., 2019). Active efflux transporters or other transport proteins also help remove potentially toxic waste products from brain into the blood (Hladky and Barrand, 2018). ECs sense shear stress from blood flow or receive signaling cues from neurons or glia to secrete vasoactive substances to help modulate vasomotor responses in adjacent mural cells and titrate local blood flow (Chen et al., 2014; Iadecola, 2017; Chow et al., 2020).

Pericytes

In the microvasculature, e.g., capillaries, venules, and select arterioles, PCs are embedded in the shared BM and extend foot processes which cover much of the vessel wall (Winkler et al., 2012, 2014a; Grant et al., 2019). Unlike vSMCs which surround blood vessels circumferentially, PCs generally extend thin longitudinal processes with further delicate elaborations to cover more of the vascular surface. Interestingly, PCs cover the vasculature in a mutually exclusive pattern and do not overlap; upon experimental ablation of one pericyte, the neighboring pericytes will then grow their surface area to take over the newly absent territory (Berthiaume et al., 2018). Pericytes contribute to endothelial BBB properties through upregulation of tight junctional protein complexes and/or downregulation of transcytotic pathways—such as those mediated by plasmalemma vesicle associated protein (*Plvap*) or caveolin-1 (Hellstrom et al., 2001; Armulik et al., 2010; Bell et al., 2010; Daneman et al., 2010). They also secrete BM proteins to stabilize vessels (Thomsen et al., 2017). To further regulate brain molecular exchanges, PCs are enriched in multiple carrier- and receptor-mediated transporters, active transporter proteins, or ion channels (He et al., 2016; Vanlandewijck et al., 2018; Sweeney et al., 2019).

PCs modulate capillary diameter in response to neuronal or astrocytic cues (Peppiatt et al., 2006; Hall et al., 2014; Cai et al., 2018), but the functional significance of this is unclear. Some have shown that PCs regulate local CBF regulation and neurovascular coupling (Kisler et al., 2017b, 2020). Others have found this is principally the role of vSMCs, such as those in arterioles, or pre-capillary sphincters (Fernandez-Klett et al., 2010; Hill et al., 2015; Grubb et al., 2020). This discrepancy likely stems from a lack of clarity in regards to the exact definition

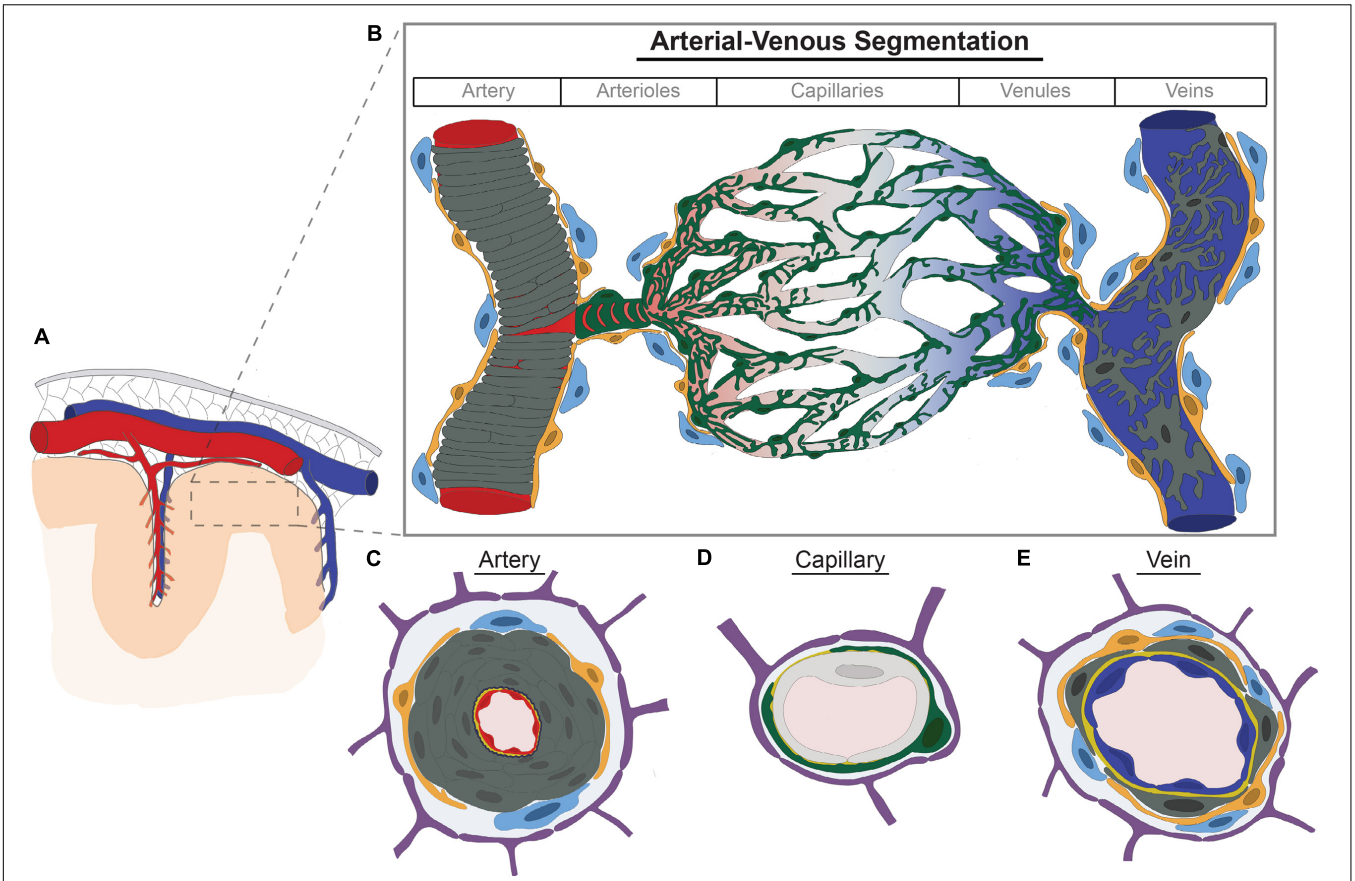

FIGURE 1 | Brain vascular cell diversity along the arterial-venous axis. **(A)** Large arteries (red) and cortical veins (blue) course within the subarachnoid space (gray mesh) inside the dura mater (gray). Cerebral arteries course along the brain's pial surface and within sulci giving rise to pial and penetrating arterioles which pierce the brain parenchyma. **(B)** Arterioles progressively branch to form capillaries. Capillaries then converge to form venules which converge further to form veins. Each vessel segment along the arterial-venous axis are comprised of different cell types—including endothelium (shown in red, gray, and blue to denote transcriptional zonations), vascular smooth muscle cells (dark gray, vSMCs), pericytes (green), perivascular fibroblasts (yellow), and perivascular macrophages (light blue). Pericytes further adopt different morphologic configurations along the arteriovenous axis, such as ensheathing pericytes (pre-capillary arterioles) and mesh-like and stellate pericytes in more distal arterioles, capillaries, and venules. vSMCs form concentric rings in arteries but are discrete and stellate shaped in veins. Perivascular fibroblasts and macrophages are found in arteries, arterioles, venules, and veins, but not capillaries. **(C–E)** Cross section of cellular components of artery **(C)**, capillary **(D)**, and veins **(E)**. Endothelium depicted in artery, capillary, and vein are shown in red, light gray, and blue, respectively, to denote transcriptional differences or molecular zonations defined and validated by independent groups with single cell RNA-sequencing. Dark gray, vascular smooth muscle cells; Navy blue, internal elastic lamina; Green, pericytes; Orange, perivascular fibroblasts; Light blue, perivascular macrophages; Yellow, basement membrane; Purple, astrocyte end feet.

of vSMCs vs. PCs. PCs supply trophic support to neurons and also modulate immune responses (Rustenhoven et al., 2017; Nikolakopoulou et al., 2019; Uemura et al., 2020). For example, PCs modulate expression of endothelial cell adhesion molecules, such as intercellular adhesion molecule-1 (*Icam1*), and may also play a direct role in the phagocytosis of extracellular proteins (Bell et al., 2010; Sagare et al., 2013; Ma et al., 2018). This has been suggested to increase after brain injury, such as ischemic stroke, and pericytes may assume a microglial-like phenotype (Ozen et al., 2014; Sakuma et al., 2016). Others have suggested pericytes may serve as multi-potent stem cells *in vitro* (Dore-Duffy et al., 2006; Crisan et al., 2008; Karow et al., 2018). However, lineage tracing has shown that pericytes do not significantly contribute to other cell lineages *in vivo* and do not differentiate into microglia following acute brain injuries (Guimaraes-Camboa et al., 2017; Huang et al., 2020).

Vascular Smooth Muscle Cells

vSMCs from concentric rings in larger arteries and become less layered and more sparse as vessels progressively branch to form pial and penetrating arterioles (Iadecola, 2017; Frosen and Joutel, 2018). In veins, vSMCs remain as discrete cells. Due to their location and composition, vSMCs contribute much of structural stability to the vessel wall and mediate synthesis and turnover of extracellular matrix proteins, such as collagen and elastin (Iadecola, 2017; Frosen and Joutel, 2018).

vSMCs serve as contractile cells and express a number of contractile proteins or associated regulatory proteins, such as smooth muscle alpha actin (*ACTA2*), and receptors to numerous vasoactive molecules, including adenosine, prostaglandins, or catecholamines, and to myogenic or flow-related stimuli (Koller and Toth, 2012; He et al., 2016; Kisler et al., 2017a; Chasseigneaux et al., 2018). Through these contractile properties,

vSMCs contribute to regulation of cerebral blood flow and autoregulation (Fernandez-Klett et al., 2010; Hill et al., 2015; Iadecola, 2017). Arterial pulsations and/or oscillations in relaxation or contraction of vSMCs contribute to perivascular fluid flow via the glymphatic system (Iliff et al., 2013; Aldea et al., 2019; Wardlaw et al., 2020). Studies have supported that arteriolar vSMCs are the predominate site of regional CBF regulation (Hill et al., 2015; Grutzendler and Nedergaard, 2019), but the relative contributions of vSMCs and PCs to neurovascular coupling continues to be debated (Hamilton et al., 2010; Hall et al., 2014; Hill et al., 2015; Kisler et al., 2017b; Winkler et al., 2017).

Perivascular Fibroblast-Like Cells

A recent constellation of unbiased scRNAseq studies have identified PVFBs on all vessels except capillaries (Marques et al., 2016; Saunders et al., 2018; Vanlandewijck et al., 2018; Zeisel et al., 2018). PVFBs are located within the Virchow-Robin space and loosely adhere to vessels through small, fine cellular processes (Soderblom et al., 2013; Vanlandewijck et al., 2018; Rajan et al., 2020). PVFBs express platelet-derived growth factor receptor-α (*Pdgfrα*) and a number of extracellular matrix proteins—including fibrillar and non-fibrillar collagens, collagen-modifying enzymes, and small leucin-rich proteoglycans, such as lumican (*lum*) and decorin (*Dcn*) (Vanlandewijck et al., 2018; Rajan et al., 2020). The function of these new-defined cells has not been completely characterized. Emerging evidence early in zebrafish development in other vascular beds, such as intersegmental vessels, has suggested that PVFBs stabilize the vasculature prior to appearance of PCs, and lineage tracing has suggested a subpopulation of PVFBs may serve as PC progenitor cells (Rajan et al., 2020). In the mouse brain, however, collagen type 1 alpha 1 chain (*Col1a1*)-positive PVFBs are not detected until after the birth (Kelly et al., 2016). Therefore, it is presently unclear as to the role if any PVFBs play in the developing or adult mammalian brain vasculature under physiologic conditions. In response to traumatic injury, PVFBs have been suggested to contribute to scar formation (Soderblom et al., 2013). Others have ascribed scar formation to a subpopulation of PCs which may highlight difficulties in distinguishing perivascular cell types (Goritz et al., 2011; Dias et al., 2018).

Perivascular Macrophages

PVMs are myeloid cells distinct from microglia that reside in the Virchow-Robin space surrounding arterioles and venules (Lapenna et al., 2018; Yang et al., 2019). PVMs serve a vital role in the phagocytosis of blood-borne pathogens and antigen presentation to induce protective immune responses (Lapenna et al., 2018; Kierdorf et al., 2019). They also limit EC production of pro-inflammatory mediators suggesting a dual regulatory role in immune response (Serrats et al., 2010). PVMs promote EC BBB properties and tight junction protein expression (Zenker et al., 2003). Others have shown that PVMS modulate EC expression of nutrient receptors—such as solute carrier family 2 member 1 (*Slc2a*)—playing a homeostatic role in cerebral glucose metabolism (Jais et al., 2016). In brain regions devoid of a BBB, such as the circumventricular organs, PVM uptake restricts influx of blood-borne proteins and macromolecules providing a size selective barrier (Willis et al., 2007). Phagocytic properties are not limited to blood-borne molecules and may help clear other extracellular proteins, such as amyloid-β (Hawkes and McLaurin, 2009).

Astrocytes

Brain vascular cells are ensheathed by astrocyte end feet which form the outer limit of the perivascular Virchow-Robin space (Iliff et al., 2012; Rasmussen et al., 2018). Adjacent astrocyte end feet are connected via both tight and gap junctions which create a semi-permeable barrier—known as the glia limitans (Horng et al., 2017; Kutuzov et al., 2018). This secondary barrier further restricts radial diffusion of large solutes and circulating inflammatory cells (Nuriya et al., 2013; Horng et al., 2017; Kutuzov et al., 2018). Expression of transmembrane pores within astrocyte end feet, e.g., aquaporin-4, or ion pumps, e.g., Kir 4.1 potassium channels, regulate molecular exchanges between cerebrospinal fluid (CSF) within the perivascular space and brain interstitial fluid underlying the "glymphatic system" (Iliff et al., 2012; Rasmussen et al., 2018; Wardlaw et al., 2020). Interactions with adjacent PCs help maintain astrocyte end foot polarity and transport systems (Armulik et al., 2010; Gundersen et al., 2014). Astrocytes also contribute directly to EC BBB properties and secrete BM proteins, such as laminin (Abbott et al., 2006; Yao et al., 2014).

Astrocytes express metabotropic glutamate receptors (mGluR) and purinergic receptors (P2YR) which detect neuronal by-products of neuronal activation, such as glutamate or adenosine triphosphate, which help trigger section of vasoactive molecules—including arachidonic acid, associated derivatives, and prostaglandin E2 (Abbott et al., 2006; Iadecola, 2017; Kisler et al., 2017a). Low frequency stimuli or resting state fluctuations in neuronal activity have been shown to not provoke calcium signaling in astrocytes (Gu et al., 2018). Thus, it has been hypothesized that slow hemodynamic fluctuations in blood flow are driven largely by neurons and astrocytes play a modulating, but not triggering role in neurovascular coupling (Gu et al., 2018).

Variations in Cytoarchitecture and Cell Morphology

Large muscular arteries, such as the internal carotid arteries and vertebral arteries which coalesce to form the basilar artery, enter the subarachnoid space and form a complex anastomotic loop known as the "circle of Willis." Large cerebral arteries course along the brain's pial surface tapering and branching giving rise to pial and penetrating arterioles. Arterioles branch to give rise to an immense capillary tree. Capillaries ultimately converge to form venules which further converge to form veins. Large cortical veins within the subarachnoid space ultimately connect to venous sinuses contained within the dura mater to facilitate egress of blood from the brain. In the ensuing subsection, we describe the diversity in cell morphology of each cell type along these vascular transitions or regional variations when described in the central nervous system (summarized in **Figure 1**).

Endothelial Cells

For most brain regions, the EC membrane remains continuous without interruption (Zhao et al., 2015; Sweeney et al., 2019). Expression of the tight junction proteins remains constant throughout the arterial-venous axis in the brain, but show some ultrastructural differences—such as a greater overlap in arteries (Hanske et al., 2017). Higher permeability and reduced tight junction protein expression is reported for select CNS regions—such as the spinal cord (Winkler et al., 2012). In brain circumventricular organs—such as the subfornical organ, organum vasculosum of the lamina terminalis and area postrema—or choroid-plexus, ECs contain fenestrations or intracellular pores which permit high permeability (Ghersi-Egea et al., 2018).

Preservation of BBB integrity also occurs through suppression of caveolae and transcytosis (Ben-Zvi et al., 2014; Andreone et al., 2017; Chow and Gu, 2017). Classically low rates of vesicular transport were thought to be uniform. However, higher rates of vesicular transport have been observed in arteries/arterioles whereas receptor-mediated transcytosis is primarily detected in post-capillary venules (Hanske et al., 2017; Kucharz et al., 2020). A recent work has shown that suppression is not uniform and that abundant caveolae are selectively abundant in arteriolar ECs—which facilitates the signaling between neurons, ECs, and vSMCs underlying neurovascular coupling (Chow et al., 2020). Whether this phenomenon varies regionally has not been reported.

Mural Cells

Considerable variation is observed in mural cells—a term referring to both vSMCs and PCs in part to account for varying cell identity along the arterial-venous axis (Winkler et al., 2011, 2019; **Figures 1B–E**). In arteries with diameters > 100 μm, vSMCs are spindle shaped and form concentric rings ∼ 4–10 cells thick (Shiraishi et al., 1986). As arteries progressively branch and taper forming arterioles, vSMC cell layers become thinner and ultimately become discontinuous cells with rod-like or thin lateral processes in more terminal branches (Shiraishi et al., 1986; Iadecola, 2017; **Figures 1C,D**). In venules and veins, vSMCs remain discontinuous and are stellate in configuration (Hill et al., 2015; Smyth et al., 2018; Vanlandewijck et al., 2018; **Figure 1E**).

Whether a continuum of mural cell phenotypes exists and the point of transition between vSMC to pericyte remains controversial. Some have suggested that the transition from vSMCs to pericytes is discrete (Hill et al., 2015; Zeisel et al., 2015; Vanlandewijck et al., 2018). Others have described a transitional cell with shared attributes between both cell types (Hartmann et al., 2015; Grant et al., 2019; Grubb et al., 2020; Ratelade et al., 2020). Transitional cells have also been suggested in humans (Smyth et al., 2018; Ratelade et al., 2020). However, classification of these or closely related cells differs between groups with a number of other terms—including ensheathing PCs, pre-capillary PCs, vSMC-PCs hybrids, or precapillary vSMCs (Uemura et al., 2020). Despite these differences, most agree that the contractile cells in pre-capillary arterioles are responsible for regional CBF regulation and neurovascular coupling (Fernandez-Klett et al., 2010; Hill et al., 2015; Kisler et al., 2017b; Hartmann et al., 2020).

Brain PCs also display considerable morphologic heterogeneity—including ensheathing or transitional, mesh, thin-strand, or helical and stellate configurations (Hartmann et al., 2015; Arango-Lievano et al., 2018; Smyth et al., 2018; Grant et al., 2019; Uemura et al., 2020; **Figure 1B**). Ensheathing PCs—analogous to the transitional cells above—predominately localize to pre-capillary arterioles. Like other PCs, they have an ovoid cell body, but with cell processes that are larger and broader which enwrap and cover much of the endothelial wall (> 90%). They also express contractile proteins—such as smooth muscle α-actin (αSMA) (Hartmann et al., 2015; Smyth et al., 2018; Grant et al., 2019). Contractile protein expression terminates as arterioles branch further to form smaller capillaries. Throughout capillaries and post-capillary venules, PC cell processes assume a mesh-like or thin-strand appearance which covers ∼70 or ∼50% of the endothelial cell well, respectively (Hartmann et al., 2015; Smyth et al., 2018; Grant et al., 2019). The functional significance of these configurations is presently unknown but may reflect a facilitatory role in transport.

PC abundance and coverage of the EC wall is relatively constant in the adult brain—including the cortex, hippocampus, striatum, and cerebellum (Bell et al., 2010; Winkler et al., 2010, 2012). However, PCs are less abundant in the spinal cord and most reduced in the gray matter of the anterior horn (Winkler et al., 2012, 2013). Whether these alterations are the result of the relative abundance or presence of different pericyte subtypes is presently unknown. Much of this work has also been done in rodents and whether species-specific differences as with other cell types exists has also yet to be determined (O'Brown et al., 2018).

Perivascular Fibroblast-Like Cells

PVFBs share some cell marker expression with PCs—including N-aminopeptidase (also known as CD13, encoded by *Anpep*) and platelet-derived growth factor receptor-β (*Pdgfr*β) (Soderblom et al., 2013). Unlike PCs, they are found along all vessels expect capillaries (**Figures 1B,C,E**). Morphologically they are more globular appearance with shorter and finer processes which enwrap the vessel wall. They are also more loosely associated with the vessels—described to be an "awkward hug" (Vanlandewijck et al., 2018; Rajan et al., 2020). Whether different morphologic subtypes exist along the arterial-venous axis or in different brain regions remains to be characterized.

Perivascular Macrophages

PVMs are confined to arterioles and venules and are one of several specialized macrophages known as "border associated macrophages"—including leptomeningeal, dural, and choroid plexus macrophages (Goldmann et al., 2016; Utz et al., 2020; **Figures 1B,C,E**). PVMs adopt a relatively simple ameboid morphology (Zeisel et al., 2015; Kierdorf et al., 2019). They are non-motile, but able to extend cellular processes along the Virchow-Robin Space (Goldmann et al., 2016). Other border associated macrophages are stellate or dendriform appearance (Goldmann et al., 2016; Kierdorf et al., 2019). Whether PVMs has regional or arterial-venous variation in morphology has not been reported.

Astrocytes

Morphologic variations in astrocytes have been described for > 100 years and were first introduced by Golgi and Cajal (Garcia-Lopez et al., 2010). Classically astrocytes were divided into two morphologic groups. Protoplasmic astrocytes of the gray matter are highly ramified contacting neuronal cell bodies, dendrites, and the vasculature, whereas fibrous astrocytes characterized as smaller with fewer branches are organized largely around white matter tracts (Oberheim et al., 2006; Miller, 2018; Matias et al., 2019). Between species, protoplasmic astrocytes are larger and extend 10-fold as many cellular processes in humans than rodents (Oberheim et al., 2009). Even greater morphological diversity is observed in different cortical layers (Oberheim et al., 2006, 2009; Lanjakornsiripan et al., 2018). For example, layer 1 astrocytes known as subpial or marginal zone astrocytes display unique molecular expression patterns (Garcia-Marques and Lopez-Mascaraque, 2013; Batiuk et al., 2020). Another subgroup of astrocytes unique to primates—known as interlaminar astrocytes—are located in layer 1 and extend long fibers which extend throughout the cortex and terminate in layers 3/4 (Oberheim et al., 2006, 2009). Extent of ramification or synaptic ensheathment of protoplasmic astrocytes varies between cortical layers (Lanjakornsiripan et al., 2018). In layers 5–6, varicose projection astrocytes also extend long fibers with regularly spaced varicosities (Oberheim et al., 2006, 2009).

With respect to the brain vasculature, astrocyte cell bodies rarely exceed ∼6–10 μm from blood vessels and foot processes form a continuous sheathe around all vessels below the pia—including arterioles, capillaries, and venules (McCaslin et al., 2011). Within the somatosensory cortex, the perivascular astrocytic sheath is thickest for arterioles and thinnest for capillaries. However, capillaries had the greatest density of astrocyte foot processes and separation between astrocytes and capillaries decreased with increasing cortical depth (McCaslin et al., 2011). In other CNS regions, e.g., the retina, astrocytes along veins are large and occur with greater density than arteries (Jammalamadaka et al., 2015). Whether this relationship is maintained in the brain or differs between CNS regions remains to be characterized. During development, the vasculature has been shown to interact with different subtypes of astrocytes or astrocyte-like radial-glial cells depending on location, such as truncated and outer radial glia (Marin-Padilla, 1995; Nowakowski et al., 2016). How different subtypes of astrocytes interact with different aspects of the arterial-venous axis in the adult brain has yet to be completely characterized.

Transcriptomic Diversification and Subspecialization

Cell diversity in brain vascular cells transcends what can be seen with conventional histologic evaluations. Development of high-throughput single cell transcriptomic technologies identified considerable transcriptional variability of subpopulations within cardinal cell types. Distinct vascular segments have unique functional properties. For example, terminal or pre-capillary arterioles are believed to be the site of regional CBF regulation (Fernandez-Klett et al., 2010; Hill et al., 2015; Kisler et al., 2017b). Capillaries are the site of bidirectional molecular transport (Sweeney et al., 2019). Venules and veins are the site of leukocyte migration and vascular immune responses (Filippi et al., 2018; Lapenna et al., 2018). Dural based sinuses facilitate continued immune surveillance through meningeal lymphatics (Louveau et al., 2015, 2016). In this subsection, we summarize newly defined transcriptional variation and functional distinctions within subpopulations of brain vascular cells (summarized in **Table 1**).

Endothelial Cells

EC heterogeneity is observed across organs (Augustin and Koh, 2017). Brain ECs display a number of distinct attributes consistent with their specialized function. For example, brain ECs specifically express a number of transmembrane transporters—such as those involved in the transport of glucose (*Slc2a1*), amino acids (*Slc3a2*, *Slc7a5),* and fatty acids (*Mfsd2a*) (Sabbagh et al., 2018; Feng et al., 2019; Jambusaria et al., 2020; Kalucka et al., 2020). Brain ECs also demonstrate a unique metabolic gene signature (Kalucka et al., 2020). Others have demonstrated enrichment of translated transcripts specific to neurotransmission, such as synapse organization and neurotransmitter transport (Jambusaria et al., 2020). Enrichment for Wnt signaling and brain EC-specific transcription factors associated with maturation of the BBB are also observed, such as forkhead box F2 (*Foxf2*), forkhead box Q1 (*Foxq1*) or zic family member 3 (*Zic3*) (Hupe et al., 2017; Sabbagh et al., 2018; Kalucka et al., 2020). Brain specific epigenetic regulatory networks, including chromatin accessibility and DNA methylome landscapes, have also been described in brain ECs suggesting added regulatory mechanisms (Sabbagh et al., 2018).

Within the brain, EC gene expression changes along the arterial-venous axis. Capillary and venule ECs preferentially express solute transporters and inflammatory mediators, respectively (Macdonald et al., 2010). scRNAseq studies have demonstrated a transcriptional continuum or zonation characterized by gradual phenotypic changes along the arterial-venous axis. Closer analyses showed that transcription factors were overrepresented in arterial ECs, while transporters were enriched in ECs from capillary and veins. Three additional EC clusters were also identified but were outside the arteriovenous zone and the significance of these were unclear (Vanlandewijck et al., 2018).

scRNAseq technologies have evolved to permit characterization of a greater number of cells, such as droplet based scRNAseq. Studies employing these techniques in the adult murine brain vasculature have similarly showed continuous gene expression changes consistent with smooth EC molecular transitions along the arterial-venous axis (Saunders et al., 2018; Kalucka et al., 2020). A recent study has identified nine distinct EC clusters. Seven correspond to arterial-venous graduation—such as large arteries, arterial shear stress, capillary artery, capillary, capillary venous, and large vein. Two additional clusters were also noted—including choroid plexus ECs and interferon-activated ECs (Kalucka et al., 2020). Others have identified seven distinct subclusters of brain ECs. In addition to observing an arterial-venous continuum, the authors

TABLE 1 | Enriched cellular markers of transcriptionally-defined subpopulations of brain vascular cells.

Cardinal cell identity	Sub-stratification	Selected enriched markers	References
Endothelial	Arterial	*Gkn3, Hey1, Bmx, Efnb2, Vegfc, Sema3g, Mgp, Fbln2, Fbln5, Cytl1 Tm4sf1*	Sabbagh et al., 2018; Saunders et al., 2018; Vanlandewijck et al., 2018; Zeisel et al., 2018; Kalucka et al., 2020
	Capillary	*Mfsd2a, Tfrc, Meox1, Rgcc*	Sabbagh et al., 2018; Saunders et al., 2018; Vanlandewijck et al., 2018; Zeisel et al., 2018; Kalucka et al., 2020
	Venous	*Slc38a5, Nr2f2, Lcn2, Ccl19, Mafb, Mmm 1, Vwf*	Sabbagh et al., 2018; Saunders et al., 2018; Vanlandewijck et al., 2018; Zeisel et al., 2018; Kalucka et al., 2020
	Tip Cells	*Plaur, Angpt2, Lcp2, Cxcr4, Apln, Kcne3, Mcam, Lamb1, Trp53i11*	Sabbagh et al., 2018
	Choroid plexus	*Plvap, Plpp3, Esm1, Plpp1, Cd24a, Nrp1, Rgcc*	Kalucka et al., 2020
Pericytes		*Abcc9, Kcnj8, Vtn, Ifitm1, Ggt1*	Saunders et al., 2018; Vanlandewijck et al., 2018; Zeisel et al., 2018
Vascular smooth muscle cells	Arterial	*Acta, Tagln, Cnn1, Tinagl1, Fos*	Saunders et al., 2018; Vanlandewijck et al., 2018
	Venous	*Kcnj8, Abcc9, Car4, Slc5a5*	Saunders et al., 2018; Vanlandewijck et al., 2018
Fibroblasts	Perivascular	*Col1a1, Col1a2, Lum, Dcn, Pdgfra*	Saunders et al., 2018; Vanlandewijck et al., 2018;
	Pial	*S100a6, Col18a1, Postn, Lama2, Ngfr*	DeSisto et al., 2020
	Arachnoid	*Ptgds, Aldh1a2, Crabp2, Ogn*	DeSisto et al., 2020
	Dura	*Alpl, Foxc2, Fxyd5, Dkk2, Mgp, Crabp2*	DeSisto et al., 2020
Perivascular macrophages		*Mrc, Lyve1, Lyl1, Spic*	Zeisel et al., 2015

found evidence for further functional subspecialization within subclusters. For example, a subcluster of arterial ECs displayed selective expression of genes implicated in growth factor dependent remodeling, such as matrix gla protein (*Mgp*), fibulin 5 (*Fbln5*), elastin (*Eln*), insulin-like growth factor binding protein 4 (*Igfbp4*), and clusterin (*Clu*). Other processes, such as host immunity or interferon signaling, showed similar expression across vessel types (Saunders et al., 2018).

In the early postnatal brain vasculature, others have demonstrated six EC clusters or subtypes—including arterial, capillary-arterial, capillary-venous, venous, mitotic, and tip cells (Sabbagh et al., 2018). Angiogenic cues specify some endothelial cells to become tip cells—which are motile and able to navigate through tissues. These are followed by less motile stalk ECs which maintain connections with the preexisting vasculature (Hasan et al., 2017; Pitulescu et al., 2017). scRNAseq has shown tip cells are enriched for transcripts encoding membrane or secreted proteins—including ion channels, cell adhesion proteins, receptor tyrosine kinases, extracellular matrix proteins, and other signaling molecules (Sabbagh et al., 2018). Lineage tracing demonstrated that tip cells are more closely related to arterial than venous ECs (Sabbagh et al., 2018). During angiogenesis, proliferating cells have recently been shown to arise from veins (Xu et al., 2014). Consistent with this, shared expression patterns are observed between mitotic, capillary venous, and venous ECs (Sabbagh et al., 2018).

Regional variability has also been reported in the brain EC transcriptome. For example, brain EC expression of transporter genes was upregulated in arterial, capillary, and venous ECs, but not in choroid plexus (Kalucka et al., 2020). Consistent with their fenestrated morphology, there were also selective upregulation in high permeability genes—such as *Plvap* (Kalucka et al., 2020). Other studies have shown similar relative abundances of EC subtypes across 9 distinct brain regions—including the frontal cortex, posterior cortex, hippocampus, striatum, thalamus, globus pallidus externus, and nucleus basalis, subthalamic nucleus, substantia nigra, and ventral tegmental area, and cerebellum (Saunders et al., 2018). Other targeted scRNA approaches geared toward the neuronal-stem cell enriched subventricular zone show EC expression of certain stem cell markers—such as prominin 1 (*Prom1*) and nestin (*Nes*) (Zywitza et al., 2018).

Mural Cells

RNAseq experiments have confirmed a number of transcriptomic differences between vSMCs and PCs (Zeisel et al., 2015; He et al., 2016; Chasseigneaux et al., 2018; Saunders et al., 2018; Vanlandewijck et al., 2018). For example, arteriolar vSMCs show enrichment in gene products involved in pathways mediating cell contractility, vascular remodeling, and responses to hypoxia or oxidative stress, whereas mid-capillary PCs are enriched for immune regulatory processes and responses to viruses or toxic substances (Chasseigneaux et al., 2018). Early scRNAseq studies distinguished vSMCs from PCs based on expression of the contractile protein smooth muscle α-actin (*Acta2*) (Zeisel et al., 2015). In contrast to ECs, a more recent scRNAseq study has suggested a punctuated continuum for mural cells with an abrupt transition between arterial/arteriolar vSMCs and PCs. However, PCs appear to form a transcriptional continuum with venous vSMCs (Vanlandewijck et al., 2018). This study also

demonstrated differences in expression between arterial and venous vSMCs, such as levels of calponin-1 (*Cnn1)*, *Acta2*, and smooth muscle protein 22-α (*Tagln*) (Vanlandewijck et al., 2018). With different scRNAseq methodologies, others have shown even greater mural size diversity and identified seven distinct subpopulations (Saunders et al., 2018). These approaches have identified specific markers for brain PCs in rodents—such as ATP binding cassette subfamily C member 9 (*Abcc9*), gamma-glutamyltransferase 1 (*Ggt1*), potassium inwardly rectifying channel subfamily J member 8 (*Kcnj8),* vitronectin (*vtn*) and interferon-induced transmembrane protein 1 (*Ifitm1*) (He et al., 2016; Chasseigneaux et al., 2018; Vanlandewijck et al., 2018), and have found differences in brain PCs in comparison to other organs—such as enrichment in SLC, ABC, and ATP transporters (He et al., 2018; Vanlandewijck et al., 2018).

Many scRNAseq studies have not found transcriptionally distinct brain PC subtypes as supported by morphologic studies (Saunders et al., 2018; Vanlandewijck et al., 2018). A more recent scRNAseq mouse brain atlas has shown three distinct PC populations which vary in relative abundance across brain regions (Zeisel et al., 2018). Techniques—such as fluorescent activated cell sorting—have supported molecularly distinct PC subtypes based on transmembrane protein expression (Park et al., 2016). Others have shown that another subpopulation of brain PCs express the gap junction protein connexin 30 (Mazare et al., 2018). A separate group has classified PCs into two subtypes—type A and type B subtypes—based on expression of *Pdgfrα, Pdgfr*β, *Anpep*, desmin (*Des*) and αSMA (Goritz et al., 2011). Type A PCs have been shown to form scars after spinal cord and/or brain injury (Goritz et al., 2011; Birbrair et al., 2014; Dias et al., 2018). However, some have suggested that this classification are not distinct PC populations, but rather more newly defined PVFBs (Soderblom et al., 2013; Vanlandewijck et al., 2018). These studies support distinct subpopulations of brain pericytes. However, future studies are need to more completely characterize regulatory mechanisms contributing to pericyte diversity.

Perivascular Fibroblast-Like Cells

scRNAseq first identified 2 PVFBs subpopulations defined by expression of collagens [e.g., collagen type I alpha 1 chain (*Col1a1*) and collagen type I alpha 2 chain (*Col1a2*)], lumican (*Lum*), decorin (*Dcn*), and *Pdgfr*α (Vanlandewijck et al., 2018). With newer droplet-based scRNAseq, up to 7 distinct subtypes have been identified (Saunders et al., 2018). Two subclusters were enriched in membrane transporters and pumps, while others showed higher levels in collagen genes or different extracellular matrix proteins, angiogenesis, and contraction (Saunders et al., 2018). This suggests possible functional subspecialization which has been shown to vary regionally. PVFBs enriched for membrane transport functions and collagen expression were observed with higher relative abundance in the hippocampus/cortex and basal ganglia/thalamus, respectively (Saunders et al., 2018). Others have shown PVFBs are transcriptionally similar to populations of vascular leptomeningeal cells (pial and arachnoid cells) that reside in the meninges (Marques et al., 2016; DeSisto et al., 2020). Expression of the cytokine interleukin 33 (*Il33*) and the prostaglandin D2 synthetase (*Ptgds*) and markers of pial, arachnoid, and dural meningeal fibroblasts, may also help distinguish between PVFBs subpopulations located in the brain vs. fibroblasts in the meninges (Zeisel et al., 2018; DeSisto et al., 2020). Both *Col1a1*-positive and *Rgs5*-positive populations of mural cells representing PVFBs and PCs, respectively, can sense inflammatory stimuli and signal to the brain through C–C motif chemokine ligand 2 (*Ccl2*) (Duan et al., 2018). Apart from this study, however, the functional significance of this heterogeneity has yet to be defined and future studies are needed.

Perivascular Macrophages

PVMs are transcriptionally closely related to microglial, but may be distinguished by expression of mannose receptor C-type 1 (*Mrc,* encodes CD206) and lymphatic vessel endothelial hyaluronan receptor 1 (*Lyve1)* or *Cd36* (Zeisel et al., 2015; Goldmann et al., 2016). Some have shown that expression of LYL1 basic helix-loop-helix family member (*Lyl1*) and Spi-C transcription factor (*Spic*) were specific to PVMs in the brain (Zeisel et al., 2015). Others have distinguished CNS-associated macrophages from peripheral immune cells through an absence of α4-integrin (*Itga4*) and *Cd44* (Butovsky et al., 2012; Ajami et al., 2018; Jordao et al., 2019; Kierdorf et al., 2019).

Profiling of all CNS-associated macrophage populations—perivascular, meningeal, and choroid plexus, demonstrates three transcriptionally distinct clusters which share a core signature consisting of *Mrc1,* platelet factor 4 *(Pf4)*, membrane-spanning four domains subfamily A member 7 (*Ms4a7*), stabilin 1 (*Stab1*), and carbonyl reductase 2 (*Cbr2)* (Jordao et al., 2019). Other distinct PVM subclasses have also been defined in neuroinflammation—such as expression of antigen-presenting MHC class II molecules (Jordao et al., 2019). Other brain inflammatory cells—such as microglia—are transcriptional similar across brain regions in adults but display added heterogeneity in different developmental periods (Li et al., 2019). Whether regional or context-dependent heterogeneity exists specifically within PVMs has yet to be reported.

Astrocytes

Astrocyte heterogeneity has been identified both morphologically and transcriptionally (Bayraktar et al., 2014). For example, fibrous astrocytes of the white matter more highly express glial fibrillary acidic protein (Gfap) than protoplasmic astrocytes of cortical gray matter (Cahoy et al., 2008). Early scRNA seq experiments transcriptional defined two separate populations of cortical astrocytes distinguished by expression of glial fibrillary acidic protein (*Gfap*) and milk fat globule-EGF factor 8 protein (*Mfge8*) (Zeisel et al., 2015). A more recent scRNAseq study in the cortex and hippocampus has identified 5 transcriptionally distinct astrocyte subtypes in adult rodents (Batiuk et al., 2020). Each with a unique spatial distribution, and with some exceptions roughly coincide with morphologically defined subtypes (Lanjakornsiripan et al., 2018). Others have similarly supported the presence of five molecularly distinct astrocytes with different techniques—such as fluorescence-activated cell sorting (John Lin et al., 2017).

With inclusion of additional brain regions, others have found seven distinct subtypes of astrocytes with scRNAseq—including Bergmann glia of the cerebellum, olfactory-specific astrocytes, two telencephalon specific astrocytes, two non-telencephalon astrocytes, and a myocilin (*Myoc*) expressing astrocyte of the dorsal midbrain (Zeisel et al., 2018). Expression of *Mfge8* and angiotensinogen (*Agt*) sharply distinguished astrocytes from the telencephalon and diencephalon (Zeisel et al., 2018). Others have defined further regionally distinct astrocyte subtypes in other CNS regions—such as the spinal cord and retina (Hochstim et al., 2008; Menon et al., 2019). Additional astrocytic transcriptional heterogeneity has also been identified within cytoarchitecturally defined brain subregions. For example, laminar spatial gene expression is observed within astrocytes from distinct cortical layers which also varies between functionally distinct regions of cortex (Bayraktar et al., 2020). With emerging sequencing technologies it is therefore likely additional astrocyte subtypes will be defined. How different transcriptional diversity of astrocytes influences vascular interactions has yet to be systematically studied.

DISCUSSION AND FUTURE DIRECTIONS

Advances in scRNAseq technology have identified heterogeneity within cells comprising the brain vasculature beyond what can be seen with a microscope. The functional significance of transcriptomic variation has been implied based on enriched signaling or ontologic pathways. Future studies with subtype specific enhancer constructs and/or viruses are needed to directly understand the functional delineation of cell subtypes (Blankvoort et al., 2018; Nott et al., 2019). Platforms to survey the function of vascular cells are also lacking. While organoids have rapidly increased in popularity to study neuronal brain cell types, these "mini-brains" have only been vascularized with ECs from other organs to date and further lack blood flow (Khakipoor et al., 2020). Regulatory mechanism responsible for the genesis or maintenance of transcriptomic diversity in the context of brain vascular cells is also presently poorly defined. Only a single report has described epigenetic regulatory mechanisms in brain ECs (Sabbagh et al., 2018). Studies have supported that signaling from neighboring glia and neurons contribute to brain specific transcriptomic networks (Hupe et al., 2017; Sabbagh et al., 2018; Jambusaria et al., 2020; Kalucka et al., 2020). Alterations in blood flow-induced wall shear stress may lead to further transcriptional augmentation and in part help delineate cells along the arterial-venous axis (Masumura et al., 2009; Vatine et al., 2019). However, the relative contributions of flow-mediated biomechanical properties, circulating blood cells, and/or brain parenchyma to these observations is presently unknown.

Much of the variation of brain vasculature has been defined in rodents. Whether further diversity is seen in other species—such as humans—is also presently unknown. A number of studies have described alterations of vascular cells in neurovascular disorders—such as neurodegenerative diseases (Alzheimer's disease and amyotrophic lateral sclerosis), intracerebral hemorrhage, and vascular malformations (Goritz et al., 2011; Winkler et al., 2011, 2013, 2014b, 2015, 2018; Dias et al., 2018; Montagne et al., 2018; Sweeney et al., 2018; Ratelade et al., 2020). How vascular cell heterogeneity is altered in diseases affecting the cerebrovasculature has yet to be defined, and continued efforts are also needed to create *in vitro* human models which retain vascular cell diversity are needed to facilitate disease modeling.

AUTHOR CONTRIBUTIONS

JR, CK, and EW designed the review outline, performed the literature search, and wrote the manuscript. DA, EC, KN, DC, AA, and TN provided the critical reviews, revised the manuscript, and provided relevant edits. All authors contributed to the article and approved the submitted version.

FUNDING

The work of EW was supported by a Brain Vascular Malformation Consortium (BVMC) Pilot Feasibility Project Grant and Brain Aneurysm Foundation grant. The BVMC (U54NS065705) was a part of the NCATS Rare Diseases Clinical Research Network (RDCRN) and was supported by the RDCRN Data Management and Coordinating Center (DMCC) (U2CTR002818). RDCRN was an initiative of the Office of Rare Diseases Research (ORDR), NCATS, funded through a collaboration between NCATS and NINDS.

REFERENCES

Abbott, N. J., Ronnback, L., and Hansson, E. (2006). Astrocyte-endothelial interactions at the blood-brain barrier. *Nat. Rev. Neurosci.* 7, 41–53. doi: 10.1038/nrn1824

Ajami, B., Samusik, N., Wieghofer, P., Ho, P. P., Crotti, A., Bjornson, Z., et al. (2018). Single-cell mass cytometry reveals distinct populations of brain myeloid cells in mouse neuroinflammation and neurodegeneration models. *Nat. Neurosci.* 21, 541–551. doi: 10.1038/s41593-018-0100-x

Aldea, R., Weller, R. O., Wilcock, D. M., Carare, R. O., and Richardson, G. (2019). Cerebrovascular smooth muscle cells as the drivers of intramural periarterial drainage of the brain. *Front. Aging Neurosci.* 11:1. doi: 10.3389/fnagi.2019.00001

Ando, Y., Okada, H., Takemura, G., Suzuki, K., Takada, C., Tomita, H., et al. (2018). Brain-specific ultrastructure of capillary endothelial glycocalyx and its possible contribution for blood brain barrier. *Sci. Rep.* 8:17523.

Andreone, B. J., Chow, B. W., Tata, A., Lacoste, B., Ben-Zvi, A., Bullock, K., et al. (2017). Blood-brain barrier permeability is regulated by lipid transport-dependent suppression of caveolae-mediated transcytosis. *Neuron* 94, 581–594.e5.

Arango-Lievano, M., Boussadia, B., De Terdonck, L. D. T., Gault, C., Fontanaud, P., Lafont, C., et al. (2018). Topographic reorganization of cerebrovascular mural cells under seizure conditions. *Cell Rep.* 23, 1045–1059. doi: 10.1016/j.celrep.2018.03.110

Armulik, A., Genove, G., Mae, M., Nisancioglu, M. H., Wallgard, E., Niaudet, C., et al. (2010). Pericytes regulate the blood-brain barrier. *Nature* 468, 557–561.

Augustin, H. G., and Koh, G. Y. (2017). Organotypic vasculature: from descriptive heterogeneity to functional pathophysiology. *Science* 357:eaal2379. doi: 10.1126/science.aal2379

Banks, W. A. (2009). Characteristics of compounds that cross the blood-brain barrier. *BMC Neurol.* 9(Suppl. 1):S3. doi: 10.1186/1471-2377-9-S1-S3

Batiuk, M. Y., Martirosyan, A., Wahis, J., De Vin, F., Marneffe, C., Kusserow, C., et al. (2020). Identification of region-specific astrocyte subtypes at single cell resolution. *Nat. Commun.* 11:1220.

Bayraktar, O. A., Bartels, T., Holmqvist, S., Kleshchevnikov, V., Martirosyan, A., Polioudakis, D., et al. (2020). Astrocyte layers in the mammalian cerebral cortex revealed by a single-cell in situ transcriptomic map. *Nat. Neurosci.* 23, 500–509. doi: 10.1038/s41593-020-0602-1

Bayraktar, O. A., Fuentealba, L. C., Alvarez-Buylla, A., and Rowitch, D. H. (2014). Astrocyte development and heterogeneity. *Cold Spring Harb. Perspect. Biol.* 7:a020362. doi: 10.1101/cshperspect.a020362

Bell, R. D., Winkler, E. A., Sagare, A. P., Singh, I., Larue, B., Deane, R., et al. (2010). Pericytes control key neurovascular functions and neuronal phenotype in the adult brain and during brain aging. *Neuron* 68, 409–427. doi: 10.1016/j.neuron.2010.09.043

Ben-Zvi, A., Lacoste, B., Kur, E., Andreone, B. J., Mayshar, Y., Yan, H., et al. (2014). Mfsd2a is critical for the formation and function of the blood-brain barrier. *Nature* 509, 507–511. doi: 10.1038/nature13324

Berthiaume, A. A., Grant, R. I., Mcdowell, K. P., Underly, R. G., Hartmann, D. A., Levy, M., et al. (2018). Dynamic remodeling of pericytes in vivo maintains capillary coverage in the adult mouse brain. *Cell Rep.* 22, 8–16. doi: 10.1016/j.celrep.2017.12.016

Birbrair, A., Zhang, T., Files, D. C., Mannava, S., Smith, T., Wang, Z. M., et al. (2014). Type-1 pericytes accumulate after tissue injury and produce collagen in an organ-dependent manner. *Stem Cell Res. Ther.* 5:122. doi: 10.1186/scrt512

Blankvoort, S., Witter, M. P., Noonan, J., Cotney, J., and Kentros, C. (2018). Marked diversity of unique cortical enhancers enables neuron-specific tools by enhancer-driven gene expression. *Curr. Biol.* 28, 2103–2114.e5.

Butovsky, O., Siddiqui, S., Gabriely, G., Lanser, A. J., Dake, B., Murugaiyan, G., et al. (2012). Modulating inflammatory monocytes with a unique microRNA gene signature ameliorates murine ALS. *J. Clin. Invest.* 122, 3063–3087. doi: 10.1172/jci62636

Cadwell, C. R., Bhaduri, A., Mostajo-Radji, M. A., Keefe, M. G., and Nowakowski, T. J. (2019). Development and arealization of the cerebral cortex. *Neuron* 103, 980–1004. doi: 10.1016/j.neuron.2019.07.009

Cahoy, J. D., Emery, B., Kaushal, A., Foo, L. C., Zamanian, J. L., Christopherson, K. S., et al. (2008). A transcriptome database for astrocytes, neurons, and oligodendrocytes: a new resource for understanding brain development and function. *J. Neurosci.* 28, 264–278. doi: 10.1523/jneurosci.4178-07.2008

Cai, C., Fordsmann, J. C., Jensen, S. H., Gesslein, B., Lonstrup, M., Hald, B. O., et al. (2018). Stimulation-induced increases in cerebral blood flow and local capillary vasoconstriction depend on conducted vascular responses. *Proc. Natl. Acad. Sci. U.S.A.* 115, E5796–E5804.

Campbell, B. C. V., De Silva, D. A., Macleod, M. R., Coutts, S. B., Schwamm, L. H., Davis, S. M., et al. (2019). Ischaemic stroke. *Nat. Rev. Dis. Primers* 5:70.

Cembrowski, M. S., and Spruston, N. (2019). Heterogeneity within classical cell types is the rule: lessons from hippocampal pyramidal neurons. *Nat. Rev. Neurosci.* 20, 193–204. doi: 10.1038/s41583-019-0125-5

Chasseigneaux, S., Moraca, Y., Cochois-Guegan, V., Boulay, A. C., Gilbert, A., Le Crom, S., et al. (2018). Isolation and differential transcriptome of vascular smooth muscle cells and mid-capillary pericytes from the rat brain. *Sci. Rep.* 8:12272.

Chen, B. R., Kozberg, M. G., Bouchard, M. B., Shaik, M. A., and Hillman, E. M. (2014). A critical role for the vascular endothelium in functional neurovascular coupling in the brain. *J. Am. Heart Assoc.* 3:e000787.

Chow, B. W., and Gu, C. (2017). Gradual suppression of transcytosis governs functional blood-retinal barrier formation. *Neuron* 93, 1325–1333.e3.

Chow, B. W., Nunez, V., Kaplan, L., Granger, A. J., Bistrong, K., Zucker, H. L., et al. (2020). Caveolae in CNS arterioles mediate neurovascular coupling. *Nature* 579, 106–110. doi: 10.1038/s41586-020-2026-1

Crisan, M., Yap, S., Casteilla, L., Chen, C. W., Corselli, M., Park, T. S., et al. (2008). A perivascular origin for mesenchymal stem cells in multiple human organs. *Cell Stem Cell* 3, 301–313. doi: 10.1016/j.stem.2008.07.003

Daneman, R., Zhou, L., Kebede, A. A., and Barres, B. A. (2010). Pericytes are required for blood-brain barrier integrity during embryogenesis. *Nature* 468, 562–566. doi: 10.1038/nature09513

DeSisto, J., O'rourke, R., Jones, H. E., Pawlikowski, B., Malek, A. D., Bonney, S., et al. (2020). Single-cell transcriptomic analyses of the developing meninges reveal meningeal fibroblast diversity and function. *Dev. Cell* 54, 43–59.e4.

Dias, D. O., Kim, H., Holl, D., Werne Solnestam, B., Lundeberg, J., Carlen, M., et al. (2018). Reducing pericyte-derived scarring promotes recovery after spinal cord injury. *Cell* 173, 153–165.e22.

Dore-Duffy, P., Katychev, A., Wang, X., and Van Buren, E. (2006). CNS microvascular pericytes exhibit multipotential stem cell activity. *J. Cereb. Blood Flow Metab.* 26, 613–624. doi: 10.1038/sj.jcbfm.9600272

Duan, L., Zhang, X. D., Miao, W. Y., Sun, Y. J., Xiong, G., Wu, Q., et al. (2018). PDGFRbeta cells rapidly relay inflammatory signal from the circulatory system to neurons via chemokine CCL2. *Neuron* 100, 183–200.e8.

Feng, W., Chen, L., Nguyen, P. K., Wu, S. M., and Li, G. (2019). Single cell analysis of endothelial cells identified organ-specific molecular signatures and heart-specific cell populations and molecular features. *Front. Cardiovasc. Med.* 6:165. doi: 10.3389/fcvm.2019.00165

Fernandez-Klett, F., Offenhauser, N., Dirnagl, U., Priller, J., and Lindauer, U. (2010). Pericytes in capillaries are contractile in vivo, but arterioles mediate functional hyperemia in the mouse brain. *Proc. Natl. Acad. Sci. U.S.A.* 107, 22290–22295. doi: 10.1073/pnas.1011321108

Filippi, M., Bar-Or, A., Piehl, F., Preziosa, P., Solari, A., Vukusic, S., et al. (2018). Multiple sclerosis. *Nat. Rev. Dis. Primers* 4:43.

Frosen, J., and Joutel, A. (2018). Smooth muscle cells of intracranial vessels: from development to disease. *Cardiovasc. Res.* 114, 501–512. doi: 10.1093/cvr/cvy002

Garcia-Lopez, P., Garcia-Marin, V., and Freire, M. (2010). The histological slides and drawings of cajal. *Front. Neuroanat.* 4:9. doi: 10.3389/neuro.05.009.2010

Garcia-Marques, J., and Lopez-Mascaraque, L. (2013). Clonal identity determines astrocyte cortical heterogeneity. *Cereb. Cortex* 23, 1463–1472. doi: 10.1093/cercor/bhs134

Ghersi-Egea, J. F., Strazielle, N., Catala, M., Silva-Vargas, V., Doetsch, F., and Engelhardt, B. (2018). Molecular anatomy and functions of the choroidal blood-cerebrospinal fluid barrier in health and disease. *Acta Neuropathol.* 135, 337–361. doi: 10.1007/s00401-018-1807-1

Goldmann, T., Wieghofer, P., Jordao, M. J., Prutek, F., Hagemeyer, N., Frenzel, K., et al. (2016). Origin, fate and dynamics of macrophages at central nervous system interfaces. *Nat. Immunol.* 17, 797–805. doi: 10.1038/ni.3423

Goritz, C., Dias, D. O., Tomilin, N., Barbacid, M., Shupliakov, O., and Frisen, J. (2011). A pericyte origin of spinal cord scar tissue. *Science* 333, 238–242. doi: 10.1126/science.1203165

Grant, R. I., Hartmann, D. A., Underly, R. G., Berthiaume, A. A., Bhat, N. R., and Shih, A. Y. (2019). Organizational hierarchy and structural diversity of microvascular pericytes in adult mouse cortex. *J. Cereb. Blood Flow Metab.* 39, 411–425. doi: 10.1177/0271678x17732229

Grubb, S., Cai, C., Hald, B. O., Khennouf, L., Murmu, R. P., Jensen, A. G. K., et al. (2020). Precapillary sphincters maintain perfusion in the cerebral cortex. *Nat. Commun.* 11:395.

Grutzendler, J., and Nedergaard, M. (2019). Cellular control of brain capillary blood flow: in vivo imaging veritas. *Trends Neurosci.* 42, 528–536. doi: 10.1016/j.tins.2019.05.009

Gu, X., Chen, W., Volkow, N. D., Koretsky, A. P., Du, C., and Pan, Y. (2018). Synchronized astrocytic Ca(2+) responses in neurovascular coupling during somatosensory stimulation and for the resting state. *Cell Rep.* 23, 3878–3890. doi: 10.1016/j.celrep.2018.05.091

Guimaraes-Camboa, N., Cattaneo, P., Sun, Y., Moore-Morris, T., Gu, Y., Dalton, N. D., et al. (2017). Pericytes of multiple organs do not behave as mesenchymal stem cells in vivo. *Cell Stem Cell* 20, 345–359.e5.

Gundersen, G. A., Vindedal, G. F., Skare, O., and Nagelhus, E. A. (2014). Evidence that pericytes regulate aquaporin-4 polarization in mouse cortical astrocytes. *Brain Struct. Funct.* 219, 2181–2186. doi: 10.1007/s00429-013-0629-0

Hall, C. N., Reynell, C., Gesslein, B., Hamilton, N. B., Mishra, A., Sutherland, B. A., et al. (2014). Capillary pericytes regulate cerebral blood flow in health and disease. *Nature* 508, 55–60. doi: 10.1038/nature13165

Hamilton, N. B., Attwell, D., and Hall, C. N. (2010). Pericyte-mediated regulation of capillary diameter: a component of neurovascular coupling in health and disease. *Front. Neuroenergetics* 2:5. doi: 10.3389/fnene.2010.00005

Hanske, S., Dyrna, F., Bechmann, I., and Krueger, M. (2017). Different segments of the cerebral vasculature reveal specific endothelial specifications, while tight junction proteins appear equally distributed. *Brain Struct. Funct.* 222, 1179–1192. doi: 10.1007/s00429-016-1267-0

Hartmann, D. A., Berthiaume, A. A., Grant, R. I., Harrill, S. A., Noonan, T., Costello, J., et al. (2020). Brain capillary pericytes exert a substantial but slow influence on blood flow. *bioRxiv [Preprint]* doi: 10.1101/2020.03.26.008763

Hartmann, D. A., Underly, R. G., Grant, R. I., Watson, A. N., Lindner, V., and Shih, A. Y. (2015). Pericyte structure and distribution in the cerebral cortex revealed by high-resolution imaging of transgenic mice. *Neurophotonics* 2:041402. doi: 10.1117/1.nph.2.4.041402

Hasan, S. S., Tsaryk, R., Lange, M., Wisniewski, L., Moore, J. C., Lawson, N. D., et al. (2017). Endothelial Notch signalling limits angiogenesis via control of artery formation. *Nat. Cell Biol.* 19, 928–940. doi: 10.1038/ncb3574

Hawkes, C. A., and McLaurin, J. (2009). Selective targeting of perivascular macrophages for clearance of beta-amyloid in cerebral amyloid angiopathy. *Proc. Natl. Acad. Sci. U.S.A.* 106, 1261–1266. doi: 10.1073/pnas.0805453106

He, L., Vanlandewijck, M., Mae, M. A., Andrae, J., Ando, K., Del Gaudio, F., et al. (2018). Single-cell RNA sequencing of mouse brain and lung vascular and vessel-associated cell types. *Sci. Data* 5:180160.

He, L., Vanlandewijck, M., Raschperger, E., Andaloussi Mae, M., Jung, B., Lebouvier, T., et al. (2016). Analysis of the brain mural cell transcriptome. *Sci. Rep.* 6:35108.

Hellstrom, M., Gerhardt, H., Kalen, M., Li, X., Eriksson, U., Wolburg, H., et al. (2001). Lack of pericytes leads to endothelial hyperplasia and abnormal vascular morphogenesis. *J. Cell Biol.* 153, 543–553. doi: 10.1083/jcb.153.3.543

Hill, R. A., Tong, L., Yuan, P., Murikinati, S., Gupta, S., and Grutzendler, J. (2015). Regional blood flow in the normal and ischemic brain is controlled by arteriolar smooth muscle cell contractility and not by capillary pericytes. *Neuron* 87, 95–110. doi: 10.1016/j.neuron.2015.06.001

Hladky, S. B., and Barrand, M. A. (2018). Elimination of substances from the brain parenchyma: efflux via perivascular pathways and via the blood-brain barrier. *Fluids Barriers CNS* 15:30.

Hochstim, C., Deneen, B., Lukaszewicz, A., Zhou, Q., and Anderson, D. J. (2008). Identification of positionally distinct astrocyte subtypes whose identities are specified by a homeodomain code. *Cell* 133, 510–522. doi: 10.1016/j.cell.2008.02.046

Hodge, R. D., Bakken, T. E., Miller, J. A., Smith, K. A., Barkan, E. R., Graybuck, L. T., et al. (2019). Conserved cell types with divergent features in human versus mouse cortex. *Nature* 573, 61–68.

Horng, S., Therattil, A., Moyon, S., Gordon, A., Kim, K., Argaw, A. T., et al. (2017). Astrocytic tight junctions control inflammatory CNS lesion pathogenesis. *J. Clin. Invest.* 127, 3136–3151. doi: 10.1172/jci91301

Huang, W., Bai, X., Meyer, E., and Scheller, A. (2020). Acute brain injuries trigger microglia as an additional source of the proteoglycan NG2. *Acta Neuropathol. Commun.* 8:146.

Hupe, M., Li, M. X., Kneitz, S., Davydova, D., Yokota, C., Kele, J., et al. (2017). Gene expression profiles of brain endothelial cells during embryonic development at bulk and single-cell levels. *Sci. Signal.* 10:eaag2476.

Iadecola, C. (2017). The neurovascular unit coming of age: a journey through neurovascular coupling in health and disease. *Neuron* 96, 17–42. doi: 10.1016/j.neuron.2017.07.030

Iliff, J. J., Wang, M., Liao, Y., Plogg, B. A., Peng, W., Gundersen, G. A., et al. (2012). A paravascular pathway facilitates CSF flow through the brain parenchyma and the clearance of interstitial solutes, including amyloid beta. *Sci. Transl. Med.* 4:147ra111. doi: 10.1126/scitranslmed.3003748

Iliff, J. J., Wang, M., Zeppenfeld, D. M., Venkataraman, A., Plog, B. A., Liao, Y., et al. (2013). Cerebral arterial pulsation drives paravascular CSF-interstitial fluid exchange in the murine brain. *J. Neurosci.* 33, 18190–18199. doi: 10.1523/jneurosci.1592-13.2013

Jais, A., Solas, M., Backes, H., Chaurasia, B., Kleinridders, A., Theurich, S., et al. (2016). Myeloid-cell-derived VEGF maintains brain glucose uptake and limits cognitive impairment in obesity. *Cell* 165, 882–895. doi: 10.1016/j.cell.2016.03.033

Jambusaria, A., Hong, Z., Zhang, L., Srivastava, S., Jana, A., Toth, P. T., et al. (2020). Endothelial heterogeneity across distinct vascular beds during homeostasis and inflammation. *eLife* 9:e51413.

Jammalamadaka, A., Suwannatat, P., Fisher, S. K., Manjunath, B. S., Hollerer, T., and Luna, G. (2015). Characterizing spatial distributions of astrocytes in the mammalian retina. *Bioinformatics* 31, 2024–2031. doi: 10.1093/bioinformatics/btv097

John Lin, C. C., Yu, K., Hatcher, A., Huang, T. W., Lee, H. K., Carlson, J., et al. (2017). Identification of diverse astrocyte populations and their malignant analogs. *Nat. Neurosci.* 20, 396–405. doi: 10.1038/nn.4493

Jordao, M. J. C., Sankowski, R., Brendecke, S. M., Sagar, Locatelli, G., Tai, Y. H., et al. (2019). Single-cell profiling identifies myeloid cell subsets with distinct fates during neuroinflammation. *Science* 363:eaat7554. doi: 10.1126/science.aat7554

Kalucka, J., De Rooij, L., Goveia, J., Rohlenova, K., Dumas, S. J., Meta, E., et al. (2020). Single-cell transcriptome atlas of murine endothelial cells. *Cell* 180, 764–779.e20.

Karow, M., Camp, J. G., Falk, S., Gerber, T., Pataskar, A., Gac-Santel, M., et al. (2018). Direct pericyte-to-neuron reprogramming via unfolding of a neural stem cell-like program. *Nat. Neurosci.* 21, 932–940. doi: 10.1038/s41593-018-0168-3

Kelly, K. K., Macpherson, A. M., Grewal, H., Strnad, F., Jones, J. W., Yu, J., et al. (2016). Col1a1+ perivascular cells in the brain are a source of retinoic acid following stroke. *BMC Neurosci.* 17:49. doi: 10.1186/s12868-016-0284-5

Khakipoor, S., Crouch, E. E., and Mayer, S. (2020). Human organoids to model the developing human neocortex in health and disease. *Brain Res.* 1742:146803. doi: 10.1016/j.brainres.2020.146803

Kierdorf, K., Masuda, T., Jordao, M. J. C., and Prinz, M. (2019). Macrophages at CNS interfaces: ontogeny and function in health and disease. *Nat. Rev. Neurosci.* 20, 547–562. doi: 10.1038/s41583-019-0201-x

Kisler, K., Nelson, A. R., Montagne, A., and Zlokovic, B. V. (2017a). Cerebral blood flow regulation and neurovascular dysfunction in Alzheimer disease. *Nat. Rev. Neurosci.* 18, 419–434. doi: 10.1038/nrn.2017.48

Kisler, K., Nelson, A. R., Rege, S. V., Ramanathan, A., Wang, Y., Ahuja, A., et al. (2017b). Pericyte degeneration leads to neurovascular uncoupling and limits oxygen supply to brain. *Nat. Neurosci.* 20, 406–416. doi: 10.1038/nn.4489

Kisler, K., Nikolakopoulou, A. M., Sweeney, M. D., Lazic, D., Zhao, Z., and Zlokovic, B. V. (2020). Acute ablation of cortical pericytes leads to rapid neurovascular uncoupling. *Front. Cell. Neurosci.* 14:27. doi: 10.3389/fncel.2020.00027

Koller, A., and Toth, P. (2012). Contribution of flow-dependent vasomotor mechanisms to the autoregulation of cerebral blood flow. *J. Vasc. Res.* 49, 375–389. doi: 10.1159/000338747

Kucharz, K., Kristensen, K., Johnsen, K. B., Lund, M. A., Lonstrup, M., Moos, T., et al. (2020). Post-capillary venules is the locus for transcytosis of therapeutic nanoparticles to the brain. *bioRxiv [Preprint]* doi: 10.1101/2020.06.05.133819

Kutuzov, N., Flyvbjerg, H., and Lauritzen, M. (2018). Contributions of the glycocalyx, endothelium, and extravascular compartment to the blood-brain barrier. *Proc. Natl. Acad. Sci. U.S.A.* 115, E9429–E9438.

Lanjakornsiripan, D., Pior, B. J., Kawaguchi, D., Furutachi, S., Tahara, T., Katsuyama, Y., et al. (2018). Layer-specific morphological and molecular differences in neocortical astrocytes and their dependence on neuronal layers. *Nat. Commun.* 9:1623.

Lapenna, A., De Palma, M., and Lewis, C. E. (2018). Perivascular macrophages in health and disease. *Nat. Rev. Immunol.* 18, 689–702. doi: 10.1038/s41577-018-0056-9

Li, Q., Cheng, Z., Zhou, L., Darmanis, S., Neff, N. F., Okamoto, J., et al. (2019). Developmental heterogeneity of microglia and brain myeloid cells revealed by deep single-cell RNA sequencing. *Neuron* 101, 207–223.e10.

Louveau, A., Da Mesquita, S., and Kipnis, J. (2016). Lymphatics in neurological disorders: a neuro-lympho-vascular component of multiple sclerosis and Alzheimer's disease? *Neuron* 91, 957–973. doi: 10.1016/j.neuron.2016.08.027

Louveau, A., Smirnov, I., Keyes, T. J., Eccles, J. D., Rouhani, S. J., Peske, J. D., et al. (2015). Structural and functional features of central nervous system lymphatic vessels. *Nature* 523, 337–341. doi: 10.1038/nature14432

Ma, Q., Zhao, Z., Sagare, A. P., Wu, Y., Wang, M., Owens, N. C., et al. (2018). Blood-brain barrier-associated pericytes internalize and clear aggregated amyloid-beta42 by LRP1-dependent apolipoprotein E isoform-specific mechanism. *Mol. Neurodegener.* 13:57.

Macdonald, J. A., Murugesan, N., and Pachter, J. S. (2010). Endothelial cell heterogeneity of blood-brain barrier gene expression along the cerebral microvasculature. *J. Neurosci. Res.* 88, 1457–1474.

Marin-Padilla, M. (1995). Prenatal development of fibrous (white matter), protoplasmic (gray matter), and layer I astrocytes in the human cerebral cortex: a Golgi study. *J. Comp. Neurol.* 357, 554–572. doi: 10.1002/cne.903570407

Marques, S., Zeisel, A., Codeluppi, S., Van Bruggen, D., Mendanha Falcao, A., Xiao, L., et al. (2016). Oligodendrocyte heterogeneity in the mouse juvenile and adult central nervous system. *Science* 352, 1326–1329. doi: 10.1126/science.aaf6463

Masuda, T., Sankowski, R., Staszewski, O., and Prinz, M. (2020). Microglia heterogeneity in the single-cell era. *Cell Rep.* 30, 1271–1281. doi: 10.1016/j.celrep.2020.01.010

Masumura, T., Yamamoto, K., Shimizu, N., Obi, S., and Ando, J. (2009). Shear stress increases expression of the arterial endothelial marker ephrinB2 in murine ES cells via the VEGF-Notch signaling pathways. *Arterioscler. Thromb. Vasc. Biol.* 29, 2125–2131. doi: 10.1161/atvbaha.109.193185

Matias, I., Morgado, J., and Gomes, F. C. A. (2019). Astrocyte heterogeneity: impact to brain aging and disease. *Front. Aging Neurosci.* 11:59. doi: 10.3389/fnagi.2019.00059

Mazare, N., Gilbert, A., Boulay, A. C., Rouach, N., and Cohen-Salmon, M. (2018). Connexin 30 is expressed in a subtype of mouse brain pericytes. *Brain Struct. Funct.* 223, 1017–1024. doi: 10.1007/s00429-017-1562-4

McCaslin, A. F., Chen, B. R., Radosevich, A. J., Cauli, B., and Hillman, E. M. (2011). In vivo 3D morphology of astrocyte-vasculature interactions in the somatosensory cortex: implications for neurovascular coupling. *J. Cereb. Blood Flow Metab.* 31, 795–806. doi: 10.1038/jcbfm.2010.204

Menon, M., Mohammadi, S., Davila-Velderrain, J., Goods, B. A., Cadwell, T. D., Xing, Y., et al. (2019). Single-cell transcriptomic atlas of the human retina identifies cell types associated with age-related macular degeneration. *Nat. Commun.* 10:4902.

Miller, S. J. (2018). Astrocyte heterogeneity in the adult central nervous system. *Front. Cell. Neurosci.* 12:401. doi: 10.3389/fncel.2018.00401

Montagne, A., Nikolakopoulou, A. M., Zhao, Z., Sagare, A. P., Si, G., Lazic, D., et al. (2018). Pericyte degeneration causes white matter dysfunction in the mouse central nervous system. *Nat. Med.* 24, 326–337. doi: 10.1038/nm.4482

Neubauer, S., Hublin, J. J., and Gunz, P. (2018). The evolution of modern human brain shape. *Sci. Adv.* 4:eaao5961. doi: 10.1126/sciadv.aao5961

Nikolakopoulou, A. M., Montagne, A., Kisler, K., Dai, Z., Wang, Y., Huuskonen, M. T., et al. (2019). Pericyte loss leads to circulatory failure and pleiotrophin depletion causing neuron loss. *Nat. Neurosci.* 22, 1089–1098. doi: 10.1038/s41593-019-0434-z

Nott, A., Holtman, I. R., Coufal, N. G., Schlachetzki, J. C. M., Yu, M., Hu, R., et al. (2019). Brain cell type-specific enhancer-promoter interactome maps and disease-risk association. *Science* 366, 1134–1139. doi: 10.1126/science.aay0793

Nowakowski, T. J., Pollen, A. A., Sandoval-Espinosa, C., and Kriegstein, A. R. (2016). Transformation of the radial glia scaffold demarcates two stages of human cerebral cortex development. *Neuron* 91, 1219–1227. doi: 10.1016/j.neuron.2016.09.005

Nuriya, M., Shinotsuka, T., and Yasui, M. (2013). Diffusion properties of molecules at the blood-brain interface: potential contributions of astrocyte endfeet to diffusion barrier functions. *Cereb. Cortex* 23, 2118–2126. doi: 10.1093/cercor/bhs198

Oberheim, N. A., Takano, T., Han, X., He, W., Lin, J. H., Wang, F., et al. (2009). Uniquely hominid features of adult human astrocytes. *J. Neurosci.* 29, 3276–3287. doi: 10.1523/jneurosci.4707-08.2009

Oberheim, N. A., Wang, X., Goldman, S., and Nedergaard, M. (2006). Astrocytic complexity distinguishes the human brain. *Trends Neurosci.* 29, 547–553. doi: 10.1016/j.tins.2006.08.004

O'Brown, N. M., Pfau, S. J., and Gu, C. (2018). Bridging barriers: a comparative look at the blood-brain barrier across organisms. *Genes Dev.* 32, 466–478. doi: 10.1101/gad.309823.117

Ozen, I., Deierborg, T., Miharada, K., Padel, T., Englund, E., Genove, G., et al. (2014). Brain pericytes acquire a microglial phenotype after stroke. *Acta Neuropathol.* 128, 381–396. doi: 10.1007/s00401-014-1295-x

Park, T. I., Feisst, V., Brooks, A. E., Rustenhoven, J., Monzo, H. J., Feng, S. X., et al. (2016). Cultured pericytes from human brain show phenotypic and functional differences associated with differential CD90 expression. *Sci. Rep.* 6:26587.

Peppiatt, C. M., Howarth, C., Mobbs, P., and Attwell, D. (2006). Bidirectional control of CNS capillary diameter by pericytes. *Nature* 443, 700–704. doi: 10.1038/nature05193

Pitulescu, M. E., Schmidt, I., Giaimo, B. D., Antoine, T., Berkenfeld, F., Ferrante, F., et al. (2017). Dll4 and Notch signalling couples sprouting angiogenesis and artery formation. *Nat. Cell Biol.* 19, 915–927. doi: 10.1038/ncb3555

Rajan, A. M., Ma, R. C., Kocha, K. M., Zhang, D. J., and Huang, P. (2020). Dual function of perivascular fibroblasts in vascular stabilization in zebrafish. *bioRxiv [Preprint]* doi: 10.1101/2020.04.27.063792

Rasmussen, M. K., Mestre, H., and Nedergaard, M. (2018). The glymphatic pathway in neurological disorders. *Lancet Neurol.* 17, 1016–1024. doi: 10.1016/s1474-4422(18)30318-1

Ratelade, J., Klug, N. R., Lombardi, D., Angelim, M., Dabertrand, F., Domenga-Denier, V., et al. (2020). Reducing hypermuscularization of the transitional segment between arterioles and capillaries protects against spontaneous intracerebral hemorrhage. *Circulation* 141, 2078–2094. doi: 10.1161/circulationaha.119.040963

Rustenhoven, J., Jansson, D., Smyth, L. C., and Dragunow, M. (2017). Brain pericytes as mediators of neuroinflammation. *Trends Pharmacol. Sci.* 38, 291–304. doi: 10.1016/j.tips.2016.12.001

Sabbagh, M. F., Heng, J. S., Luo, C., Castanon, R. G., Nery, J. R., Rattner, A., et al. (2018). Transcriptional and epigenomic landscapes of CNS and non-CNS vascular endothelial cells. *eLife* 7:e36187.

Sagare, A. P., Bell, R. D., Zhao, Z., Ma, Q., Winkler, E. A., Ramanathan, A., et al. (2013). Pericyte loss influences Alzheimer-like neurodegeneration in mice. *Nat. Commun.* 4:2932.

Sakuma, R., Kawahara, M., Nakano-Doi, A., Takahashi, A., Tanaka, Y., Narita, A., et al. (2016). Brain pericytes serve as microglia-generating multipotent vascular stem cells following ischemic stroke. *J. Neuroinflammation* 13:57.

Saunders, A., Macosko, E. Z., Wysoker, A., Goldman, M., Krienen, F. M., De Rivera, H., et al. (2018). Molecular diversity and specializations among the cells of the adult mouse brain. *Cell* 174, 1015–1030.e16.

Serrats, J., Schiltz, J. C., Garcia-Bueno, B., Van Rooijen, N., Reyes, T. M., and Sawchenko, P. E. (2010). Dual roles for perivascular macrophages in immune-to-brain signaling. *Neuron* 65, 94–106. doi: 10.1016/j.neuron.2009.11.032

Shiraishi, T., Sakaki, S., and Uehara, Y. (1986). Architecture of the media of the arterial vessels in the dog brain: a scanning electron-microscopic study. *Cell Tissue Res.* 243, 329–335.

Smyth, L. C. D., Rustenhoven, J., Scotter, E. L., Schweder, P., Faull, R. L. M., Park, T. I. H., et al. (2018). Markers for human brain pericytes and smooth muscle cells. *J. Chem. Neuroanat.* 92, 48–60. doi: 10.1016/j.jchemneu.2018.06.001

Soderblom, C., Luo, X., Blumenthal, E., Bray, E., Lyapichev, K., Ramos, J., et al. (2013). Perivascular fibroblasts form the fibrotic scar after contusive spinal cord injury. *J. Neurosci.* 33, 13882–13887. doi: 10.1523/jneurosci.2524-13.2013

Sweeney, M. D., Kisler, K., Montagne, A., Toga, A. W., and Zlokovic, B. V. (2018). The role of brain vasculature in neurodegenerative disorders. *Nat. Neurosci.* 21, 1318–1331. doi: 10.1038/s41593-018-0234-x

Sweeney, M. D., Zhao, Z., Montagne, A., Nelson, A. R., and Zlokovic, B. V. (2019). Blood-brain barrier: from physiology to disease and back. *Physiol. Rev.* 99, 21–78. doi: 10.1152/physrev.00050.2017

Tasic, B., Yao, Z., Graybuck, L. T., Smith, K. A., Nguyen, T. N., Bertagnolli, D., et al. (2018). Shared and distinct transcriptomic cell types across neocortical areas. *Nature* 563, 72–78.

Thomsen, M. S., Routhe, L. J., and Moos, T. (2017). The vascular basement membrane in the healthy and pathological brain. *J. Cereb. Blood Flow Metab.* 37, 3300–3317. doi: 10.1177/0271678x17722436

Tjakra, M., Wang, Y., Vania, V., Hou, Z., Durkan, C., Wang, N., et al. (2019). Overview of crosstalk between multiple factor of transcytosis in blood brain barrier. *Front. Neurosci.* 13:1436. doi: 10.3389/fnins.2019.01436

Tsai, P. S., Kaufhold, J. P., Blinder, P., Friedman, B., Drew, P. J., Karten, H. J., et al. (2009). Correlations of neuronal and microvascular densities in murine cortex revealed by direct counting and colocalization of nuclei and vessels. *J. Neurosci.* 29, 14553–14570. doi: 10.1523/jneurosci.3287-09.2009

Uemura, M. T., Maki, T., Ihara, M., Lee, V. M. Y., and Trojanowski, J. Q. (2020). Brain microvascular pericytes in vascular cognitive impairment and dementia. *Front. Aging Neurosci.* 12:80. doi: 10.3389/fnagi.2020.00080

Uhlirova, H., Kilic, K., Tian, P., Thunemann, M., Desjardins, M., Saisan, P. A., et al. (2016). Cell type specificity of neurovascular coupling in cerebral cortex. *eLife* 5:e14315.

Utz, S. G., See, P., Mildenberger, W., Thion, M. S., Silvin, A., Lutz, M., et al. (2020). Early fate defines microglia and non-parenchymal brain macrophage development. *Cell* 181, 557–573.e18.

Vanlandewijck, M., He, L., Mae, M. A., Andrae, J., Ando, K., Del Gaudio, F., et al. (2018). A molecular atlas of cell types and zonation in the brain vasculature. *Nature* 554, 475–480. doi: 10.1038/nature25739

Vatine, G. D., Barrile, R., Workman, M. J., Sances, S., Barriga, B. K., Rahnama, M., et al. (2019). Human iPSC-derived blood-brain barrier chips enable disease modeling and personalized medicine applications. *Cell Stem Cell* 24, 995–1005.e6.

Wardlaw, J. M., Benveniste, H., Nedergaard, M., Zlokovic, B. V., Mestre, H., Lee, H., et al. (2020). Perivascular spaces in the brain: anatomy, physiology and pathology. *Nat. Rev. Neurol.* 16, 137–153.

Willis, C. L., Garwood, C. J., and Ray, D. E. (2007). A size selective vascular barrier in the rat area postrema formed by perivascular macrophages and the extracellular matrix. *Neuroscience* 150, 498–509. doi: 10.1016/j.neuroscience.2007.09.023

Winkler, E. A., Bell, R. D., and Zlokovic, B. V. (2010). Pericyte-specific expression of PDGF beta receptor in mouse models with normal and deficient PDGF beta receptor signaling. *Mol. Neurodegener.* 5:32. doi: 10.1186/1750-1326-5-32

Winkler, E. A., Bell, R. D., and Zlokovic, B. V. (2011). Central nervous system pericytes in health and disease. *Nat. Neurosci.* 14, 1398–1405. doi: 10.1038/nn.2946

Winkler, E. A., Birk, H., Burkhardt, J. K., Chen, X., Yue, J. K., Guo, D., et al. (2018). Reductions in brain pericytes are associated with arteriovenous malformation vascular instability. *J. Neurosurg.* 129, 1464–1474. doi: 10.3171/2017.6.jns17860

Winkler, E. A., Lu, A. Y., Raygor, K. P., Linzey, J. R., Jonzzon, S., Lien, B. V., et al. (2019). Defective vascular signaling & prospective therapeutic targets in brain arteriovenous malformations. *Neurochem. Int.* 126, 126–138.

Winkler, E. A., Nishida, Y., Sagare, A. P., Rege, S. V., Bell, R. D., Perlmutter, D., et al. (2015). GLUT1 reductions exacerbate Alzheimer's disease vasculo-neuronal dysfunction and degeneration. *Nat. Neurosci.* 18, 521–530. doi: 10.1038/nn.3966

Winkler, E. A., Rutledge, W. C., Kalani, M. Y. S., and Rolston, J. D. (2017). Pericytes regulate cerebral blood flow and neuronal health at a capillary level. *Neurosurgery* 81, N37–N38.

Winkler, E. A., Sagare, A. P., and Zlokovic, B. V. (2014a). The pericyte: a forgotten cell type with important implications for Alzheimer's disease? *Brain Pathol.* 24, 371–386. doi: 10.1111/bpa.12152

Winkler, E. A., Sengillo, J. D., Sagare, A. P., Zhao, Z., Ma, Q., Zuniga, E., et al. (2014b). Blood-spinal cord barrier disruption contributes to early motor-neuron degeneration in ALS-model mice. *Proc. Natl. Acad. Sci. U.S.A.* 111, E1035–E1042.

Winkler, E. A., Sengillo, J. D., Bell, R. D., Wang, J., and Zlokovic, B. V. (2012). Blood-spinal cord barrier pericyte reductions contribute to increased capillary permeability. *J. Cereb. Blood Flow Metab.* 32, 1841–1852. doi: 10.1038/jcbfm.2012.113

Winkler, E. A., Sengillo, J. D., Sullivan, J. S., Henkel, J. S., Appel, S. H., and Zlokovic, B. V. (2013). Blood-spinal cord barrier breakdown and pericyte reductions in amyotrophic lateral sclerosis. *Acta Neuropathol.* 125, 111–120. doi: 10.1007/s00401-012-1039-8

Xu, C., Hasan, S. S., Schmidt, I., Rocha, S. F., Pitulescu, M. E., Bussmann, J., et al. (2014). Arteries are formed by vein-derived endothelial tip cells. *Nat. Commun.* 5:5758.

Yang, T., Guo, R., and Zhang, F. (2019). Brain perivascular macrophages: recent advances and implications in health and diseases. *CNS Neurosci. Ther.* 25, 1318–1328. doi: 10.1111/cns.13263

Yao, Y., Chen, Z. L., Norris, E. H., and Strickland, S. (2014). Astrocytic laminin regulates pericyte differentiation and maintains blood brain barrier integrity. *Nat. Commun.* 5:3413.

Zeisel, A., Hochgerner, H., Lonnerberg, P., Johnsson, A., Memic, F., Van Der Zwan, J., et al. (2018). Molecular architecture of the mouse nervous system. *Cell* 174, 999–1014.e22.

Zeisel, A., Munoz-Manchado, A. B., Codeluppi, S., Lonnerberg, P., La Manno, G., Jureus, A., et al. (2015). Brain structure. Cell types in the mouse cortex and hippocampus revealed by single-cell RNA-seq. *Science* 347, 1138–1142. doi: 10.1126/science.aaa1934

Zenker, D., Begley, D., Bratzke, H., Rubsamen-Waigmann, H., and Von Briesen, H. (2003). Human blood-derived macrophages enhance barrier function of cultured primary bovine and human brain capillary endothelial cells. *J. Physiol.* 551, 1023–1032. doi: 10.1113/jphysiol.2003.045880

Zhao, Z., Nelson, A. R., Betsholtz, C., and Zlokovic, B. V. (2015). Establishment and dysfunction of the blood-brain barrier. *Cell* 163, 1064–1078. doi: 10.1016/j.cell.2015.10.067

Zywitza, V., Misios, A., Bunatyan, L., Willnow, T. E., and Rajewsky, N. (2018). Single-cell transcriptomics characterizes cell types in the subventricular zone and uncovers molecular defects impairing adult neurogenesis. *Cell Rep.* 25, 2457–2469.e8.

Conflict of Interest: The authors declare that the research was conducted in the absence of any commercial or financial relationships that could be construed as a potential conflict of interest.

frontiers in Physiology

BRIEF RESEARCH REPORT
published: 10 December 2020
doi: 10.3389/fphys.2020.611884

Heterogeneity of Sensory-Induced Astrocytic Ca^{2+} Dynamics During Functional Hyperemia

*Kushal Sharma[1], Grant R. J. Gordon[2] and Cam Ha T. Tran[1]**

[1]Department of Physiology and Cell Biology, Center for Molecular and Cellular Signaling in the Cardiovascular System, University of Nevada, Reno School of Medicine, Reno, NV, United States, [2]Department of Physiology and Pharmacology, School of Medicine, Hotchkiss Brain Institute, University of Calgary, Calgary, AB, Canada

Astrocytic Ca^{2+} fluctuations associated with functional hyperemia have typically been measured from large cellular compartments such as the soma, the whole arbor and the endfoot. The most prominent Ca^{2+} event is a large magnitude, delayed signal that follows vasodilation. However, previous work has provided little information about the spatio-temporal properties of such Ca^{2+} transients or their heterogeneity. Here, using an awake, *in vivo* two-photon fluorescence-imaging model, we performed detailed profiling of delayed astrocytic Ca^{2+} signals across astrocytes or within individual astrocyte compartments using small regions of interest next to penetrating arterioles and capillaries along with vasomotor responses to vibrissae stimulation. We demonstrated that while a 5-s air puff that stimulates all whiskers predominantly generated reproducible functional hyperemia in the presence or absence of astrocytic Ca^{2+} changes, whisker stimulation inconsistently produced astrocytic Ca^{2+} responses. More importantly, these Ca^{2+} responses were heterogeneous among subcellular structures of the astrocyte and across different astrocytes that resided within the same field of view. Furthermore, we found that whisker stimulation induced discrete Ca^{2+} "hot spots" that spread regionally within the endfoot. These data reveal that astrocytic Ca^{2+} dynamics associated with the microvasculature are more complex than previously thought, and highlight the importance of considering the heterogeneity of astrocytic Ca^{2+} activity to fully understanding neurovascular coupling.

Keywords: two-photon imaging, cerebral blood flow, calcium, awake *in vivo*, functional hyperemia, astrocyte

OPEN ACCESS

Edited by:
Fabrice Dabertrand, University of Colorado School of Medicine, United States

Reviewed by:
Andy Shih, Seattle Children's Research Institute, United States
William F. Jackson, Michigan State University, United States

****Correspondence:***
Cam Ha T. Tran
camt@unr.edu

Specialty section:
This article was submitted to Vascular Physiology, a section of the journal Frontiers in Physiology

Received: *29 September 2020*
Accepted: *24 November 2020*
Published: *10 December 2020*

Citation:
Sharma K, Gordon GRJ and Tran CHT (2020) Heterogeneity of Sensory-Induced Astrocytic Ca^{2+} Dynamics During Functional Hyperemia. Front. Physiol. 11:611884. doi: 10.3389/fphys.2020.611884

INTRODUCTION

Functional hyperemia is a fundamental control mechanism that provides a rapid local increase in blood flow in response to increased neuronal activity. It is well established that neurotransmission can directly affect the vasculature through innervation (Hamel, 2006; Schummers et al., 2008; Nimmerjahn et al., 2009) or through neuromodulators (Bekar et al., 2008; Takata et al., 2011; Ding et al., 2013; Paukert et al., 2014). These processes are critical in cerebral blood flow (CBF) regulation and serve to ensure that the blood supply matches temporally and spatially changing metabolic demands of neurons. It has been proposed that astrocytes are mediators that relay neuronal information to the vasculature – perhaps on slower timescales – helping to control vessel diameter in addition to neurons and, in turn, regulate blood flow (Zonta et al., 2003;

Mulligan and MacVicar, 2004; Straub and Nelson, 2007; Gordon et al., 2008). Our previous study has reported that the delayed astrocytic endfoot Ca^{2+} signal is mediated by both neurons and vasculature, suggesting a complex interplay between multiple mechanisms that must temporally and spatially coincide to cause a large activation of endfeet. This intriguing finding necessitates further detailed analysis of endfoot Ca^{2+} dynamics to gain insights into their contributions to functional hyperemia (Tran et al., 2018).

The work performed on *ex vivo* brain slice preparations has shown that increases in cytosolic Ca^{2+} concentration [(Ca^{2+})], produced by uncaging caged Ca^{2+} compounds (Mulligan and MacVicar, 2004; Straub et al., 2006) or through neuronal stimulation (Simard et al., 2003; Zonta et al., 2003; Gordon et al., 2008), are critical mediators of functional hyperemia, suggesting that activity-dependent vascular changes are facilitated by an astrocyte-mediated Ca^{2+}-dependent process. Some *in vivo* two-photon imaging studies in anesthetized animals have provided support for this notion, demonstrating rapid astrocytic Ca^{2+} transients followed by vasodilation (Winship et al., 2007; Lind et al., 2013, 2018) or an increase in red blood cell (RBC) velocity (Otsu et al., 2015) in various regions of the cerebral cortex in response to sensory stimuli. However, other *in vivo* studies in anesthetized or slightly sedated animals have provided evidence that functional hyperemia can be achieved in the absence of astrocytic Ca^{2+} increases (Schulz et al., 2012; Takata et al., 2013; Bonder and McCarthy, 2014), or precedes the occasional astrocyte Ca^{2+} transients (Nizar et al., 2013). In awake, resting animals using astrocyte AAV lck-GCaMP6f tools, whisker stimulation triggered both a fast and slow Ca^{2+} signals during functional hyperemia (Stobart et al., 2018a). Our own work in awake and active animals using astrocyte Rhod-2 AM, GCaMP3, or GCaMP6s, revealed that whisker stimulation elicited large astrocytic Ca^{2+} signals that followed rather than preceded vasodilation (Tran et al., 2018). Remarkably, these astrocytic endfoot Ca^{2+} events were mediated by both glutamatergic transmission and vascular-derived nitric oxide. These data signify that astrocytic Ca^{2+} dynamics and its contributions to functional hyperemia maybe more complex than previously thought. It has been shown that astrocytic Ca^{2+} activity is dynamic and heterogeneous (Bindocci et al., 2017; Stobart et al., 2018b). Characterizations of Ca^{2+} activity in astrocytes have commonly focused on the soma, processes, microdomains or macrodomains (Shigetomi et al., 2013; Srinivasan et al., 2015), but rarely on the astrocytic endfoot. This critical subcellular structure of the neurovascular unit has functional relevance to the astro-vascular relationship. Here, we characterized the cortical astrocyte Ca^{2+} dynamics, in particular astrocytic endfoot Ca^{2+}, and examined its relationship with functional hyperemia in completely awake mice *in vivo* using two-photon imaging.

MATERIALS AND METHODS

Animals

The Animal Care and Use Committee of the University of Calgary approved all the animal procedures. All studies were either performed on male GLAST-Cre ERTx LSL-GCaMP3 mice (Jax#014538) between postnatal day 30 (P30) and P60. Animals were injected on three consecutive days with tamoxifen (100 mg/kg, Sigma), prepared as a 10 mg/ml stock in corn oil. Injections started between P19 and P35. Animals were kept on a normal 12-h light/12-h dark cycle and had *ad libitum* access to food and water.

Awake *in vivo* Preparation

All surgical procedures and isoflurane anesthesia were performed as previously described (Tran and Gordon, 2015). Briefly, 1 week before the imaging session, a head bar was surgically installed on the animal, after which the animal was returned to its home cage to recover. Mice were initially trained on a passive air-supported Styrofoam ball treadmill under head restraint for 30 min and habituated to whisker stimulation with an air puff on contralateral vibrissae once every minute for 5 s using a Picospritzer III (General Valve Corp.) for 2 consecutive days. After training, the animal was returned to its home cage. On imaging day, bone and dura over the primary somatosensory cortex were removed and a ∼3 × 3mm cover glass (thickness #0) was installed over the cranial window.

Vessel Indicators

Rhodamine B isothiocyanate (RhodB)-dextran (MW 70,000; Sigma) was injected *via* the tail vein (100–200 µl of a 2.3% (w/v) solution in saline) to visualize the blood plasma. The animal was allowed to recover on the treadmill, with its head immobilized, for 30 min prior to imaging.

Two-Photon Fluorescence Imaging and Whisker Stimulations

Fluorescence images were obtained using a custom-built *in vivo* two-photon microscope (Rosenegger et al., 2014) illuminated with a tunable Ti:sapphire laser (Coherent Chameleon, Ultra II), equipped with GaAsP PMTs (Hamamatsu) and controlled by an open-source ScanImage software. A Nikon 16X objective lens (0.8NA, 3 mm WD) or a Zeiss 40X objective lens (1.0NA, 2.5 mm WD) was used. GCaMP3 and Rhodamine B dextran were excited at 920 nm. Green fluorescence signals were obtained using a 525/50 nm band-pass filter, and an orange/red light was obtained using a 605/70 nm band-pass filter (Chroma Technology). Bidirectional xy raster scanning was used at a frame rate of 3.91 Hz. Animal behaviors were captured using a near-infrared LED (780 nm) and a camera at 14 Hz. A 5-s air puff that deflected all whiskers on the contralateral side without impacting the face was applied using a Picospritzer while vasodilation and astrocytic Ca^{2+} responses were monitored in the barrel cortex (layers 1–3).

Data Analysis and Statistics

All data were processed using ImageJ. Movement artifacts in the xy plane were corrected for using the align_slices plugin.

ROIs corresponding to astrocyte endfeet, soma, and arbor were analyzed separately. Small ROIs (2.5×2.5 μm) placed next to one and another around the endfoot was analyzed to obtain temporal sequence of Ca^{2+} signals around the endfoot. Ca^{2+} responses were calculated as $\Delta F/F = (F_t - F_{rest})/F_{rest}$, where F_t is the measured fluorescence at any given time and F_{rest} is the average fluorescence obtained over 2 s prior to whisker stimulation. Ca^{2+} signals with an intensity that crossed a 3-standard deviation (SD) threshold (average 3SD: $\Delta F/F_{ef} = 5.9$; $\Delta F/F_{soma} = 3.8$; $\Delta F/F_{arbor} = 2.6$ and the associated coefficient of variation: 56.5, 65.6, and 63.5% respectively) relative to signal fluctuations during a 2-s prestimulus baseline and remained above the threshold for at least 0.5 s were detected as astrocyte Ca^{2+} increases. Penetrating arteriole cross-sectional area was analyzed by using the threshold feature in imageJ, after which particle analysis was used to measure the area of the lumen filled with RhodB-dextran. Cross-sectional area changes were calculated as $\Delta d/d = (d_t - d_{rest})/d_{rest}$ where d_t is the area obtained at any given time and d_{rest} is the average baseline area obtained over 2 s prior to whisker stimulation. Area change with an intensity that crossed a 3-SD threshold (average SD for $\Delta d/d = 2.8$; coefficient of variation: 50.8%); relative to signal fluctuations during a 2-s prestimulus baseline, and remained above the threshold for at least 0.5 s were detected as vasodilation. Onset corresponds to the first time point at which the signal reached the threshold and remained over it for at least 0.5 s. Duration was calculated as the difference between response onset and response offset. Statistical analyses used a paired or unpaired *t*-test or one-way analysis of variance (ANOVA) followed by Tukey's multiple comparisons test as appropriate. Statistical "n" constituted a single experimental trial or an experimental animal, as indicated. Data are expressed as means ± SEM. values of $p < 0.05$ were considered statistically significant. All statistical analyses were done using GraphPad. A 95% confidence interval (CI) was calculated using modified Wald method.

RESULTS

Contralateral Whisker Stimulation Predominantly Elicits Reliable Arteriolar Dilation, but Generates Heterogeneous Astrocytic Ca^{2+} Responses

We previously showed that sensory stimulation induces rapid functional hyperemic response that is followed by delayed astrocytic Ca^{2+} (Tran et al., 2018). In this previous study, we primarily focused on a single penetrating arteriole enwrapped by an endfoot and associated soma and arbor. Since other astrocytes, and in particular endfeet, that enwrapped nearby capillaries within the same cortical layer as that of penetrating arterioles were not examined, it remained unclear whether sensory stimulation induced a global effect that elicited homogeneous Ca^{2+} changes in all astrocytes. In the present study, we extended these analyses, examining Ca^{2+} dynamics in as many astrocytes within the field of view as possible and monitoring endfoot Ca^{2+} changes associated with penetrating arterioles and capillaries in the same cortical layer and focal plane. We used a genetically engineered Ca^{2+} indicator, a cytosolic form of GCaMP3, driven by the tamoxifen-inducible astrocyte-specific promoter, *Slc1a3*-Cre/ERT (GLAST-ERT), to assess local intracellular astrocyte Ca^{2+} dynamics, with concurrent tail vein injection of RhodB-dextran to visualize the vasculature and monitor vascular responses (**Figures 1A**,**B**,**D**). A 5-s whisker stimulation of contralateral side vibrissae predominantly induced a rapid functional hyperemic response that was followed by a rise in astrocytic Ca^{2+} (**Figures 1C**,**E**,**G**, $n = 9$ mice; number of trials: vessels, 25; endfoot at penetrating arteriole, 33; endfoot at capillaries, 68; soma, 28; arbor, 37). Even though stimulation of vibrissae did not elicit arteriole dilation in all cases, it induced more vasodilatory responses (74%, CI: 0.55–0.87) than Ca^{2+} rises (48%, CI: 0.33–0.65) in endfeet, enveloping the penetrating arterioles (**Figure 1F**). Sensory-induced increases in Ca^{2+} rises were observed in some, but not all, soma (68%, CI: 0.49–0.82), endfeet (at cap: 60%, CI: 0.48–0.71) and arbors (62%, CI: 0.46–0.76; **Figure 1F**). Interestingly, there were more cases where sensory-associated Ca^{2+} increases were observed at endfeet wrapping around the capillaries than at those enwrapping the penetrating arterioles (**Figure 1F**). More importantly, the spatial and temporal profiles of Ca^{2+} signals in a given subcellular structure were not always similar from one astrocyte to another when they were imaged simultaneously within the same field of view (**Figures 1G–K**). While whisker stimulation elicited a rise in astrocytic Ca^{2+} in all regions of interest (ROIs) from the subcellular compartments in some trials (endfoot at penetrating arterioles: three trials, CI: 0.18–0.81; endfoot at capillaries: 10 trials, CI: 0.23–0.59; soma: four trials, CI: 0.24–0.84; arbor: three trials, CI: 0.12–0.65), it did not trigger Ca^{2+} changes in any ROIs in other trials. There were also trials in which at least one ROI did not exhibit a rise in Ca^{2+} (**Figure 1G**). An increase in endfoot Ca^{2+} associated with penetrating arterioles was not always accompanied by an increase in endfoot Ca^{2+} at the capillaries and similarly, a lack of endfoot Ca^{2+} increases at the penetrating arterioles did not always correspond to a lack in endfoot Ca^{2+} changes at the capillaries when they were imaged simultaneously within the same field of view (an increase in endfoot Ca^{2+} at both penetrating arterioles and capillaries: 12 trials, CI: 0.65– >0.99; no increase in endfoot Ca^{2+} at penetrating arterioles with an increase in endfoot Ca^{2+} at capillaries: 10 trials, CI: 0.45–0.89; **Figure 1H**). Functional hyperemic responses were not only more frequently observed than Ca^{2+} rises, but were also initiated before endfoot Ca^{2+} increased (onset: 2.2 ± 1.1 s and 3.4 ± 2.3 s for diameter and endfoot Ca^{2+} response respectively; $p = 0.02$; **Figure 1I**), a finding that is consistent with our previous observation (Tran et al., 2018). Although the onset of functional hyperemia was faster than that of endfoot, soma or arbor Ca^{2+} increases, the durations and time to peak of all responses were comparable (Data not shown). The distribution of onset time for sensory-induced astrocytic Ca^{2+} changes was more widespread than that of functional hyperemic responses (**Figure 1J**). While the majority of trials displayed an onset time between 1 and 3 s for functional hyperemia, the onset

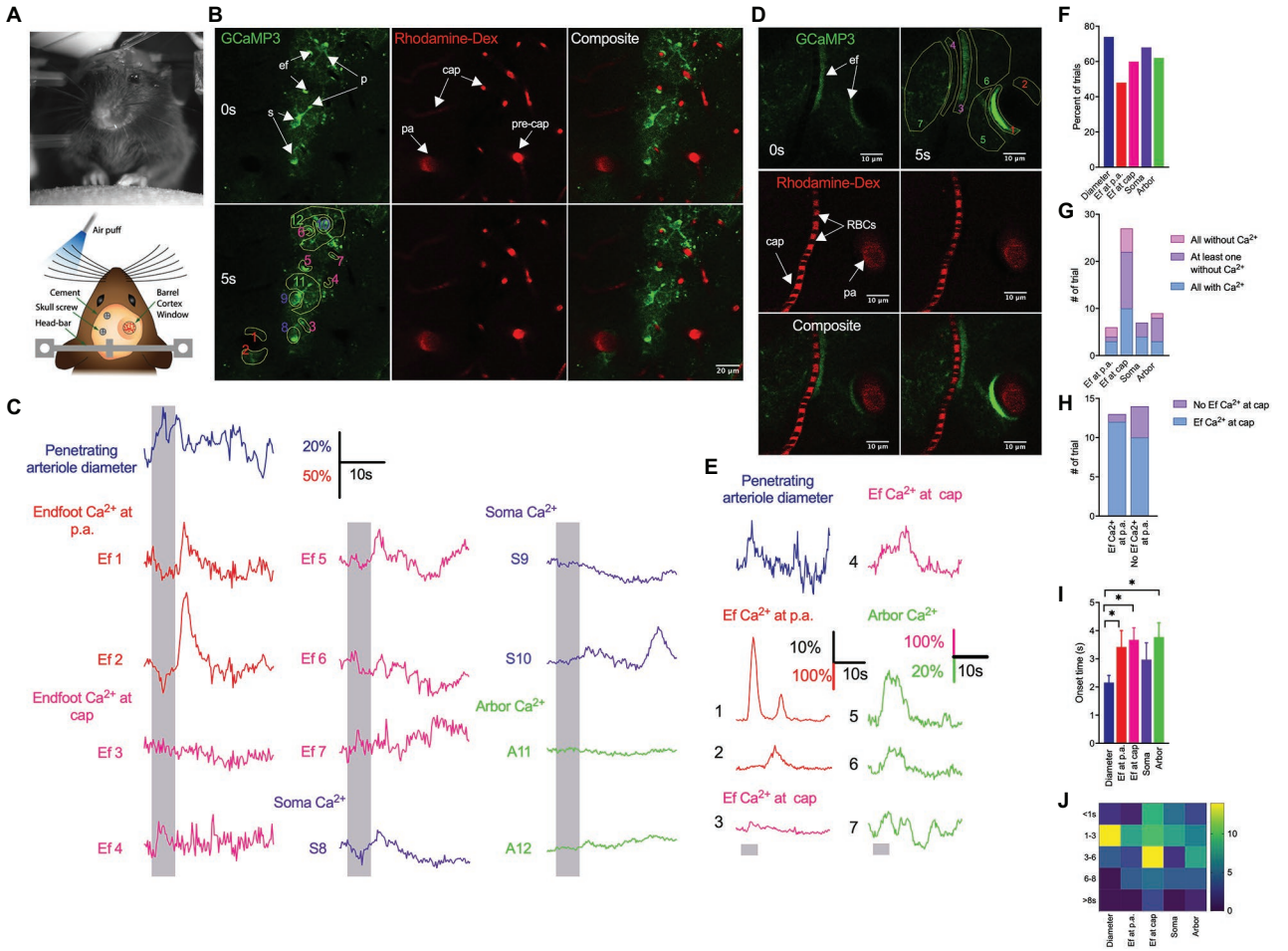

FIGURE 1 | Contralateral whisker stimulation predominantly elicits reliable arteriole dilation but generates heterogeneous astrocytic Ca^{2+} responses. **(A)** Image of an awake mouse and schematics showing the *in vivo* experimental setup. **(B)** Representative images from a cranial window over the barrel cortex of a GLAST-Cre ERT x GCaMP3 mouse showing Ca^{2+} fluctuations (green) from endfoot (ef), soma (s), process (p) and vessel response in penetrating arterioles (pa), pre-capillaries (pre-cap) and capillaries (cap) [labeled with Rhod-B dextran (red)] before (top images) and during (bottom images) a 5 s whisker stimulation. Regions of interest (ROIs) (bottom left) correspond to representative traces in **(C)**. **(C)** Representative traces from a GLAST-Cre ERT x GCaMP3 mouse (from ROIs as indicated in **B**) showing the percent change in peak diameter of a penetrating arteriole (navy) and Ca^{2+} activity from an endfoot at the penetrating arteriole (red), endfoot at the capillaries (magenta), soma (purple), and arbor (green) in response to a 5-s whisker stimulation. Vertical shaded areas indicate periods of whisker stimulation. **(D)** Higher-magnification images of a penetrating arteriole and nearby capillary enveloped by an astrocytic endfoot from a different mouse showing responses immediately prior to (0 s) and during (5 s) whisker stimulation. ROIs (top right) correspond to representative traces in **(E)**. **(E)** Representative traces showing changes in penetrating arteriole diameter change and astrocytic Ca^{2+} fluctuations (from ROIs as indicated in D (top right)) in different subcellular compartments in response to whisker stimulation. **(F)** Plot showing the percentage of trials generating arteriole dilation and Ca^{2+} increases in response to a 5-s whisker stimulation. **(G)** Summary showing the number of trials that displayed Ca^{2+} changes in all, all but one (at least one) or none from a given subcellular structure among several astrocytes observed within a single field of view. **(H)** Summary showing heterogeneity of Ca^{2+} increases observed at endfeet wrapping around the penetrating arterioles and those enwrapping capillaries when they were imaged simultaneously. **(I)** Summary showing arteriole dilation onset time and that of Ca^{2+} changes in all subcellular compartments of the astrocyte in response to a 5 s whisker stimulation. **(J)** Heat map showing the distribution of onset time of arteriole dilation and Ca^{2+} changes in all subcellular compartments of the astrocyte.

time of astrocytic Ca^{2+} rise could be varied from less than 1 s to more than 8 s (**Figure 1J**).

Whisker Stimulation-Induced Arteriole Dilation Occurs in the Absence of Astrocytic Endfoot Ca^{2+}

Although some *in vivo* studies have reported that arteriole dilation is associated with a rapid rise in endfoot Ca^{2+} (Lind et al., 2013, 2018; Stobart et al., 2018a), others have shown that a majority of vasodilatory responses to sensory stimulation lack an associated astrocytic Ca^{2+} response (Nizar et al., 2013; Bonder and McCarthy, 2014). In the present work, vasodilation in response to a 5-s whisker stimulation was observed in both the presence and absence of a rise in endfoot Ca^{2+} (**Figures 2A**,**B**). Of the total 175 trials in 22 mice, 95 exhibited an endfoot Ca^{2+} increase and 80 lacked it. Trials with a rise in endfoot Ca^{2+} were more frequently associated with vasodilation (42%) than those without an endfoot Ca^{+} increase

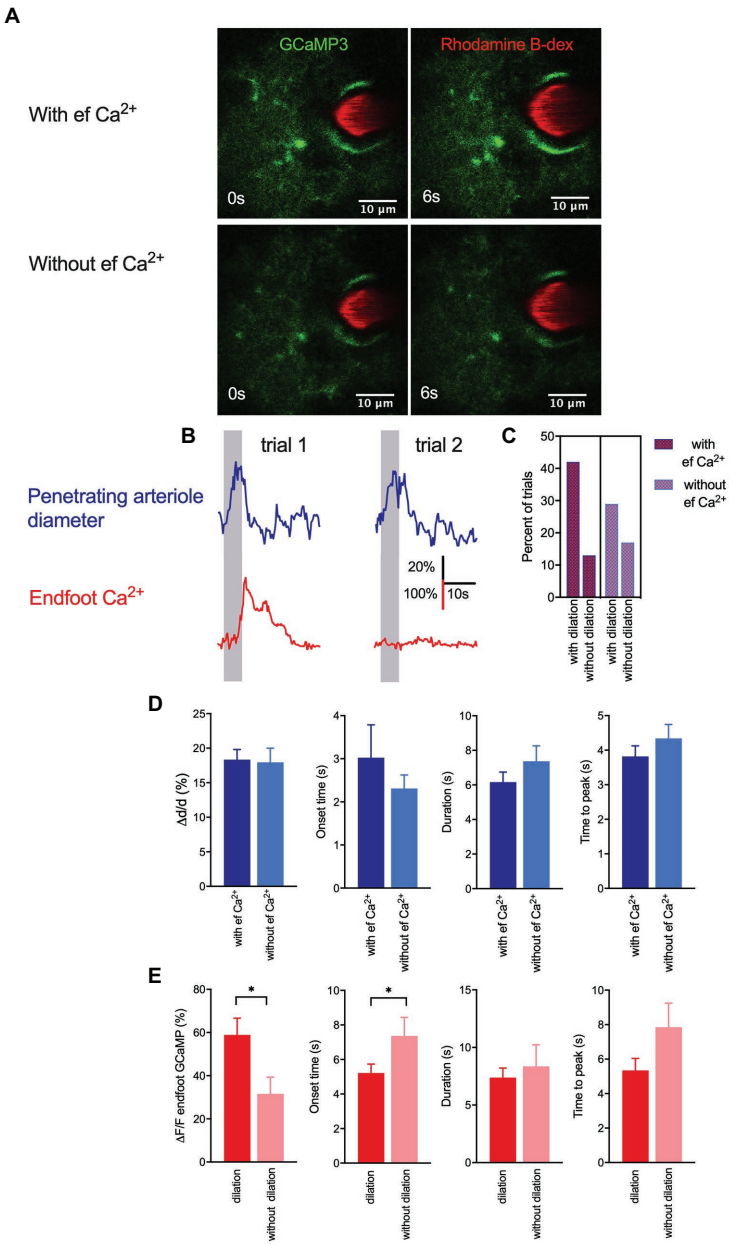

FIGURE 2 | Whisker stimulation-induced arteriole dilation occurs in the absence of astrocytic endfoot Ca^{2+} but vasodilation augmented endfoot Ca^{2+}. **(A)** Representative images from two different trials showing a penetrating arteriole enwrapped by an endfoot of a GLAST-Cre ERT x GCaMP3 mouse immediately prior to (0 s) and in response to (6 s) whisker stimulation. **(B)** Representative traces showing penetrating arteriole diameter and changes in endfoot Ca^{2+} (from **A**) from the same mouse but different trials in response to a 5-s whisker stimulation. **(C)** Percentage of trials with and without dilation in the presence and absence of endfoot Ca^{2+}. **(D)** Summary of percent peak change (i), onset time (ii), duration (iii), and time to peak (iv) of penetrating arteriole diameter in response to whisker stimulation in the presence or absence of endfoot Ca^{2+}. **(E)** Summary of percent peak change (i), onset time (ii), duration (iii) and time to peak (iv) of endfoot Ca^{2+} in response to whisker stimulation in the presence or absence of vasodilation.

(29%; **Figure 2C**), but we found no significant differences in peak percentage increase in arteriole cross-sectional area, onset time or duration of dilation, or time to peak dilation between these two trial groups (**Figure 2D**). These data suggest that changes in local endfoot Ca^{2+} are not directly linked to arteriole dilation during experimentally evoked sensory stimulation in completely awake behaving mice. On the other hand, arteriole dilation significantly enhanced endfoot Ca^{2+} ($\Delta F/F = 58.9 \pm 7.8\%$ with vasodilation vs. $31.6 \pm 7.7\%$ without vasodilation; $p = 0.02$, $n = 22$ mice, 175 trials; **Figure 2E**). Furthermore, the onset of endfoot Ca^{2+} elevations was significantly faster in cases when there was an associated

vasodilation (5.2 ± 0.5 s vs. 7.4 ± 1.1 s, p = 0.04, n = 22 mice, 175 trials). These observations further support our previous findings that changes in arteriole diameter evoked endfoot Ca^{2+} transients (Tran et al., 2018).

Whisker Stimulation Elicits Discrete Endfoot Ca^{2+} Signals That Subsequently Spread

We next performed a detailed analysis of endfoot Ca^{2+} dynamics in response to a 5-s whisker stimulation. Previous studies have shown that astrocytic Ca^{2+} activity is heterogeneous across different subcellular structures within an astrocyte (Bindocci et al., 2017). Under basal conditions, gliapil, the peripheral region of an astrocyte composed of fine processes, exhibit the highest activity, whereas, soma exhibit the lowest activity. Given their close proximity to the vessel wall, endfeet could conceivably directly modulate, or be modulated by, the vasculature. A detailed analysis of Ca^{2+} activity within a cross-section of an endfoot enwrapping a penetrating arteriole that dilated in response to whisker stimulation revealed heterogeneous Ca^{2+} signals (**Figure 3**). The discrete nature of these Ca^{2+} signals are revealed in 3-D surface plots that also display, once initiated, how these Ca^{2+} signals spread (**Figures 3Ai,Bi,Ci**). Subsequently, we analyzed Ca^{2+} responses in small regions of interest (ROIs) positioned next to one and another around the endfoot (**Figures 3A**,**B**,**Cii-iv**). Interestingly, sensory stimulation did not initiate a global rise in endfoot Ca^{2+}; instead, it triggered Ca^{2+} "hot spots" at various discrete regions of the endfoot, from which Ca^{2+} signals then spread either bidirectionally or unidirectionally (**Figure 3E**). While some endfeet had several Ca^{2+} "hot spots" with different onsets (**Figures 3A**,**F**), others had only a single hot spot (**Figures 3B**,**F**). Occasionally, endfoot Ca^{2+} increases were observed without any discernable "hot spots" (**Figure 3D**; n = 10 animals). In some instances, a soma appeared to be physically part of the endfoot; in this particular scenario, Ca^{2+} signals increased within the soma region either remained localized or did not spread far (**Figure 3Ai**). This behavior is similar to that observed by Bindocci and colleagues under basal conditions where Ca^{2+} signals were relatively confined to the boundary of the soma (Bindocci et al., 2017). In another instance in which we could clearly see the endfoot, its associated processes and a soma, 3-D surface plots revealed the spread of Ca^{2+} signals from different hot spots within each subcellular structure of the astrocyte. However, signals from these astrocytic compartments appeared to be independent of each other (**Figure 3C**).

DISCUSSION

In this study, we revealed that (1) sensory stimulation did not generate a global effect that elicited homogeneous Ca^{2+} changes in all astrocytes or subcellular compartments of an astrocyte; (2) although the absence of endfoot Ca^{2+} around the penetrating arteriole did not preclude arteriole dilation, stronger endfoot Ca^{2+} rises were observed in the presence of vasodilation; (3) sensory stimulation did not elicit a global rise in endfoot Ca^{2+}, but instead triggered discrete Ca^{2+} "hot spots" that typically spread around the endfoot and occasionally remained localized. These findings indicate that astrocytic Ca^{2+} dynamics are heterogeneous across different astrocytes as well as between astrocytic subcellular compartments, and suggest that these Ca^{2+} signals may be compartmentalized during sensory-induced functional hyperemia. They further suggest that the close proximity between the endfoot and the vessel wall of a penetrating arteriole does not necessarily translate to direct effects of local endfoot Ca^{2+} on arteriole dilation.

In the past decade, studies performed *in vivo* have presented polarized views on the involvement of astrocytic Ca^{2+} in functional hyperemia. Some of these studies in anesthetized or slightly sedated animals have shown that fast astrocytic Ca^{2+} transients precede functional hyperemic responses to sensory stimulation (Takano et al., 2006; Winship et al., 2007; Petzold et al., 2008; Lind et al., 2013, 2018; Stobart et al., 2018a), whereas others have shown that such signals are absent (Schummers et al., 2008; Schulz et al., 2012; Nizar et al., 2013; Bonder and McCarthy, 2014). Our earlier *in vivo* studies in awake active mice in which we focused on dynamic interactions between a small region of a single penetrating arteriole and its associated endfoot using cross-section imaging showed that a 5-s whisker stimulation induced a rapid functional hyperemic response followed by a delayed increase in endfoot Ca^{2+} (Tran et al., 2018). The current study in awake animals not only showed that vibrissae stimulation produced fast vasodilation followed by less reliable astrocytic Ca^{2+} increases but it also revealed the heterogeneous characteristic of astrocytic Ca^{2+} signals across different astrocytes within a single field of view (**Figure 1**). These whisker stimulation-induced Ca^{2+} signals appeared to be asynchronous and regional. Our findings are in agreement with previous studies (Bindocci et al., 2017; Stobart et al., 2018b) that demonstrated some fundamental differences in Ca^{2+} dynamics between individual structures of an astrocyte. These observations implicate a compartmentalizing effect in astrocyte Ca^{2+} dynamics. They also call attention to the fact that the majority of prior *in vivo* studies monitored Ca^{2+} changes selectively at small regions of astrocytic subcellular structures or assessed bulk changes in Ca^{2+} in the entire astrocyte, but nonetheless concluded that these observations were representatives of the whole-cell activity or the activity of the entire network. In the current study, simultaneous measurements of vascular reactivity and astrocytic Ca^{2+} changes revealed that continuous vibrissae stimulation for 5 s predominantly induced arteriole dilation that was accompanied by a rise in endfoot Ca^{2+}. However, a significant number of trials showed vasodilation in the absence of endfoot Ca^{2+} change, a finding in agreement with previous studies (Schulz et al., 2012; Nizar et al., 2013; Bonder and McCarthy, 2014). Nevertheless, our data showed the likelihood of observing vasodilation with endfoot Ca^{2+} vs. that without endfoot Ca^{2+} was ~42% vs. 29% instead of 10% vs. 90%, as reported from Nizar and colleagues (Nizar et al., 2013). They are also clearly distinct from a previous report that endfoot Ca^{2+} responses

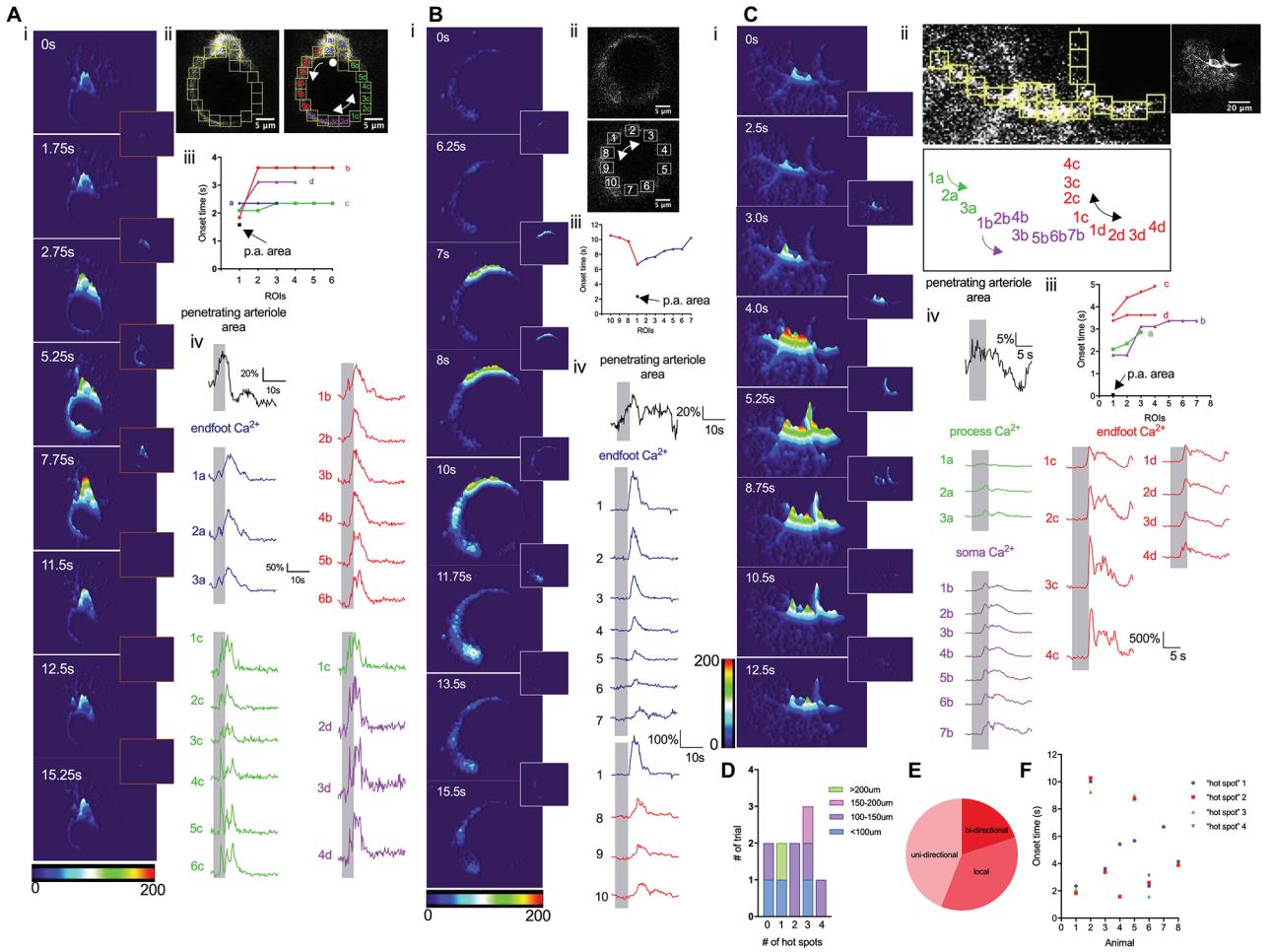

FIGURE 3 | Whisker stimulation elicits discrete endfoot Ca^{2+} signals that subsequently spread. **(A)** Detailed analysis of Ca^{2+} dynamics in response to a 5 s whisker stimulation. (i). 3-D surface plot of astrocyte Ca^{2+} fluctuations in an astrocyte at different time points immediately prior to (0 s), during (1.75 s, 2.75 s), or after (5.25 s, 7.75 s, 11.5 s, 12.5 s, and 15.25 s) a 5-s whisker stimulation. Insets showed the differential images between the two time points. (ii) Higher magnification image of an endfoot and consecutive ROIs from which Ca^{2+} measurements were obtained. Double-headed arrow indicates the bidirectional spread of the Ca^{2+} "hot spot" spread. Single-headed arrow indicates the uni-directional spread of the Ca^{2+} "hot spot". A dot indicates Ca^{2+} signals remain localized. (iii) Onset times from different ROIs showing regional Ca^{2+} activity and vasodilation. (iv) Penetrating arteriole cross-sectional area trace (black) and Ca^{2+} traces (colors) from different ROIs. Vertical shaded areas indicate periods of whisker stimulation. **(B)** Detailed analysis similar to that in A, but from a different animal displaying only the endfoot enwrapping a penetrating arteriole. (i) 3-D surface plot of astrocyte Ca^{2+} fluctuations at different time points immediately prior to (0 s) and after (6.25 s, 7 s, 8 s, 10s, 11.75 s, 13.5 s, and 15.5 s) a 5 s whisker stimulation. Insets showed the differential images between the two time points. (ii) Higher-magnification image of the endfoot and consecutive ROIs (right) from which Ca^{2+} measurements were obtained. Double-headed arrow indicates bidirectional spread of the Ca^{2+} "hot spot". (iii) Onset times from different ROIs showing endfoot Ca^{2+} activity and vasodilation. (iv) Penetrating arteriole cross-sectional area trace (black) and Ca^{2+} traces (colors) from different ROIs. Vertical shaded areas indicate periods of 5 s whisker stimulation periods. **(C)** Detailed analysis similar to that in **(A)** and **(B)**, but from a different animal showing all subcellular compartments of an astrocyte. (i) 3-D surface plot showing astrocytic Ca^{2+} fluctuations at different time points immediately prior to (0 s), during (2.5 s, 3 s, and 4 s) and after (5.25 s, 8.75 s, 10.5 s, and 12.5 s) a 5 s whisker stimulation. Insets showed the differential images between the two time points. (ii) Higher-magnification image of an endfoot and consecutive ROIs (top left) from which Ca^{2+} measurements were obtained. Labels of all the ROIs (bottom) indicated previously. Double-headed arrow indicates bidirectional spread of the Ca^{2+} "hot spot". Lower magnification image of the entire astrocyte (top right). (iii) Onset times from different ROIs showing regional Ca^{2+} activity and vasodilation. (iv) Penetrating arteriole cross-sectional area trace (black) and Ca^{2+} traces (colors) from different subcellular compartments. Vertical shaded areas indicate periods of whisker stimulation. **(D)** Summary showing the number of "hot spots" detected associated with the area of the endfoot. **(E)** Pie chart showing the percentage of how those "hot spots" spread. **(F)** Scatter plot of onset time for each "hot spot" from individual mouse.

were completely absent in all trials (Bonder and McCarthy, 2014). These discrepancies could be attributable partly to the use of anesthesia (Thrane et al., 2011). These findings do not necessarily refute the role of endfoot Ca^{2+} in regulating functional hyperemia on a whole. In fact, they highlight the heterogeneity of astrocytic Ca^{2+} dynamics and suggest that the close proximity of the endfoot and vessel wall does not universally translate to a direct effect of endfoot Ca^{2+} changes on local vasodilation. The dilation of penetrating arterioles observed in layers I–III of the cortex reported here could be due to the retrograde

vascular conduction that was initiated deep in the cortex (Uhlirova et al., 2016; Longden et al., 2017), and the endfoot Ca^{2+} increases subsequently observed in deeper cortical layers could exhibit different dynamics from those observed in the relatively superficial layer of the cortex. Interestingly, we found here that sensory-induced endfoot Ca^{2+} increases were significantly stronger when they were accompanied by vasodilation of the penetrating arterioles (**Figure 2**), further supporting our previous observations that vasodilation obtained independent of neural activity modulates endfoot Ca^{2+} (Tran et al., 2018). The changes in astrocytic Ca^{2+} in response to changes in vasomotor tone suggest a potential arteriole-to-astrocyte communication as previously suggested by our work and others (Kim et al., 2016; Tran et al., 2018).

Situated as they are between neurons and the vasculature, forming a tripartite architecture, astrocytes are ideally positioned to facilitate neuron-vascular communication and have been increasingly viewed as a hub of integrated activity that modulates neuronal and vascular responses. Activity-dependent astrocytic Ca^{2+} responses are typically reported as global events (Zonta et al., 2003; Lind et al., 2013), in which increased neuronal activity triggers a global rise in Ca^{2+} throughout the whole astrocyte or individual compartment. A recent work described more localized events that spread within the confined boundaries of the subcellular structures (Bindocci et al., 2017). Similar to these latter studies, our work reported here using cross-section imaging explored Ca^{2+} dynamics in some of the endfeet that almost completely ensheathed the vessel (**Figure 3**). Although an initial analysis appeared to show a global rise in endfoot Ca^{2+} in response to a 5-s whisker stimulation; a detailed analysis of these Ca^{2+} responses revealed discrete Ca^{2+} "hot spots" that typically spread. The majority of these "hot spots" spread uni-directionally, while others spread bidirectionally around the endfoot. Yet, in some instances, the "hot spot" remained as a single discrete Ca^{2+} signal. There were also cases where no discernible "hot spot" was observed. In agreement with a previous work (Bindocci et al., 2017), we found that astrocytic Ca^{2+} signals were compartmentalized. For example, in cases where the soma was a part of an endfoot, the somatic Ca^{2+} signal seemed to remain confined to the region defined as a soma. Similar observations were noted in other soma that were not physically a part of the endfoot. These findings suggest that astrocyte can assemble as multiple local units that function heterogeneously, implying that astrocytes can locally sense features of their surrounding environment, whether it is a nearby neuron or a vessel wall, and respond accordingly. Studies have further shown that resting Ca^{2+} differs in different astrocytic regions (Zheng et al., 2015), suggesting that there might be some regional control. These observations suggest that there are specific regions within the soma, endfoot and process where plasma membrane channels (e.g., transient receptor potential vanilloid 4, TRPV4) and/or intracellular organelles possessing the machinery, such as the mitochondria (Agarwal et al., 2017), to initiate Ca^{2+} changes reside, and that these are responsible for inducing the spread of Ca^{2+} signals, perhaps *via* Ca^{2+}-induced Ca^{2+} release. Similarly, these subcellular structures may have organelles, such as endoplasmic reticulum (ER) or mitochondria that buffer Ca^{2+} and prevent the signals from spreading beyond a boundary. Other studies have described global events observed in all subcellular compartments (Ding et al., 2013; Paukert et al., 2014; Srinivasan et al., 2015). However, these events appeared to be associated with specific physiological conditions, in this case, a startle response (Ding et al., 2013; Bonder and McCarthy, 2014; Paukert et al., 2014; Srinivasan et al., 2015). This implies that an astrocyte needs to reach a certain threshold before it can trigger the coordination between different compartments and, potentially, between different astrocytes. In the quiescent state, astrocytes have a high threshold for activation such that other systems, such as noradrenergic (Paukert et al., 2014) and/or cholinergic (Takata et al., 2011) circuits, must be recruited to enhance local signals.

Our work has unveiled the complexity of astrocytic Ca^{2+} dynamics and addressed the relationship between such Ca^{2+} signals and NVC. We do not dispute the role of astrocytic Ca^{2+} in regulating vascular response; however, for several reasons, we recommend caution in universally interpreting NVC based on data from an isolated subpopulation of astrocytes imaged at a certain layer of the cortex. First, since astrocytic Ca^{2+} activity is heterogeneous, it would be inaccurate to take observations from a single compartment or a single astrocyte as being representative of the whole cell or the whole network. Second, somatosensory cortical activation is significantly different between layers of the cortex (Krupa et al., 2004). Finally, different levels of the vascular network are structurally and functionally reflected in differences in architecture (Shih et al., 2015), anastomoses, level of neuronal innervation (Hamel, 2006), and expression of receptors and ion channels (Sercombe et al., 1990). Collectively, this vascular architecture serves to provide a supply of blood to every single neural cell sufficient to match the metabolic needs of the cell. In fact, recent studies have demonstrated temporal differences in sensory-induced vasodilation across different layers of the cortex, with the fastest onset of dilation observed below layer IV (Uhlirova et al., 2016). It has been proposed that upstream penetrating arterioles or pial arterioles dilate in response to signals initiated few 100 μm away achieved *via* a retrograde vascular conduction mechanism (Longden et al., 2017). Nevertheless, this does not imply that conduction is the only process that mediates upstream dilation nor does it rule out the possible involvement of NVC at all cortical depths. There are some important caveats that we need to acknowledge: (1) all two-photon fluorescence imaging were conducted at a frame rate of 3.91 Hz. This might have prevented us from detecting faster discrete Ca^{2+} signals; (2) we acknowledge that the fact that small ROIs used to detect discrete Ca^{2+} were done manually could contribute to the under-detection of the signals. In conclusions, our findings further emphasize that examining NVC in 3-Ds and at different layers of the cortex in awake animals is necessary to obtain accurate assessments of astrocytic Ca^{2+}. Furthermore, they highlight the need to have an automation of Ca^{2+} analysis designed to better detect all signals from all subcellular compartments of the astrocyte.

DATA AVAILABILITY STATEMENT

The original contributions presented in the study are included in the article/supplementary materials, further inquiries can be directed to the corresponding author.

ETHICS STATEMENT

The animal study was reviewed and approved by The Animal Care and Use Committee of the University of Calgary.

AUTHOR CONTRIBUTIONS

CT and GG: conceptualization, methodology, writing – review and editing. CT: investigation. CT and KS: formal analysis, writing – original draft. All authors contributed to the article and approved the submitted version.

FUNDING

This work was supported by operating grants from the Canadian Institute of Health Research to GG (130233) and the Centers of Biomedical Research Excellence (COBRE) to CT (1P20GM130459).

ACKNOWLEDGMENTS

We thank the developers and distributers of ScanImage open-source control and acquisition software for two-photon laser-scanning microscopy as well as ImageJ for data analysis. We also want to thank Eslam M F Mehina for her contributions.

REFERENCES

Agarwal, A., Wu, P. -H., Hughes, E. G., Fukaya, M., Tischfield, M. A., Langseth, A. J., et al. (2017). Transient opening of the mitochondrial permeability transition pore induces microdomain calcium transients in astrocyte processes. *Neuron* 93, 587–605.e7. doi: 10.1016/j.neuron.2016.12.034

Bekar, L. K., He, W., and Nedergaard, M. (2008). Locus coeruleus alpha-adrenergic-mediated activation of cortical astrocytes in vivo. *Cereb. Cortex* 18, 2789–2795. doi: 10.1093/cercor/bhn040

Bindocci, E., Savtchouk, I., Liaudet, N., Becker, D., Carriero, G., and Volterra, A. (2017). Three-dimensional Ca^{2+} imaging advances understanding of astrocyte biology. *Science* 356:eaai8185. doi: 10.1126/science.aai8185

Bonder, D. E., and McCarthy, K. D. (2014). Astrocytic Gq-GPCR-linked IP3R-dependent Ca^{2+} signaling does not mediate neurovascular coupling in mouse visual cortex in vivo. *J. Neurosci.* 34, 13139–13150. doi: 10.1523/JNEUROSCI.2591-14.2014

Ding, F., O'Donnell, J., Thrane, A. S., Zeppenfeld, D., Kang, H., Xie, L., et al. (2013). α1-adrenergic receptors mediate coordinated Ca^{2+} signaling of cortical astrocytes in awake, behaving mice. *Cell Calcium* 54, 387–394. doi: 10.1016/j.ceca.2013.09.001

Gordon, G. R. J., Choi, H. B., Rungta, R. L., Ellis-Davies, G. C. R., and MacVicar, B. A. (2008). Brain metabolism dictates the polarity of astrocyte control over arterioles. *Nature* 456, 745–749. doi: 10.1038/nature07525

Hamel, E. (2006). Perivascular nerves and the regulation of cerebrovascular tone. *J. Appl. Physiol.* 100, 1059–1064. doi: 10.1152/japplphysiol.00954.2005

Kim, K. J., Ramiro Diaz, J., Iddings, J. A., and Filosa, J. A. (2016). Vasculo-neuronal coupling: retrograde vascular communication to brain neurons. *J. Neurosci.* 36, 12624–12639. doi: 10.1523/JNEUROSCI.1300-16.2016

Krupa, D. J., Wiest, M. C., Shuler, M. G., Laubach, M., and Nicolelis, M. A. L. (2004). Layer-specific somatosensory cortical activation during active tactile discrimination. *Science* 304, 1989–1992. doi: 10.1126/science.1093318

Lind, B. L., Brazhe, A. R., Jessen, S. B., Tan, F. C. C., and Lauritzen, M. J. (2013). Rapid stimulus-evoked astrocyte Ca^{2+} elevations and hemodynamic responses in mouse somatosensory cortex in vivo. *Proc. Natl. Acad. Sci. U. S. A.* 110, E4678–E4687. doi: 10.1073/pnas.1310065110

Lind, B. L., Jessen, S. B., Lønstrup, M., Joséphine, C., Bonvento, G., and Lauritzen, M. (2018). Fast Ca^{2+} responses in astrocyte end-feet and neurovascular coupling in mice. *Glia* 66, 348–358. doi: 10.1002/glia.23246

Longden, T. A., Dabertrand, F., Koide, M., Gonzales, A. L., Tykocki, N. R., Brayden, J. E., et al. (2017). Capillary K^+-sensing initiates retrograde hyperpolarization to increase local cerebral blood flow. *Nat. Neurosci.* 20, 717–726. doi: 10.1038/nn.4533

Mulligan, S. J., and MacVicar, B. A. (2004). Calcium transients in astrocyte endfeet cause cerebrovascular constrictions. *Nature* 431, 195–199. doi: 10.1038/nature02827

Nimmerjahn, A., Mukamel, E. A., and Schnitzer, M. J. (2009). Motor behavior activates Bergmann glial networks. *Neuron* 62, 400–412. doi: 10.1016/j.neuron.2009.03.019

Nizar, K., Uhlirova, H., Tian, P., Saisan, P. A., Cheng, Q., Reznichenko, L., et al. (2013). In vivo stimulus-induced vasodilation occurs without IP3 receptor activation and may precede astrocytic calcium increase. *J. Neurosci.* 33, 8411–8422. doi: 10.1523/JNEUROSCI.3285-12.2013

Otsu, Y., Couchman, K., Lyons, D. G., Collot, M., Agarwal, A., Mallet, J. -M., et al. (2015). Calcium dynamics in astrocyte processes during neurovascular coupling. *Nat. Neurosci.* 18, 210–218. doi: 10.1038/nn.3906

Paukert, M., Agarwal, A., Cha, J., Doze, V. A., Kang, J. U., and Bergles, D. E. (2014). Norepinephrine controls astroglial responsiveness to local circuit activity. *Neuron* 82, 1263–1270. doi: 10.1016/j.neuron.2014.04.038

Petzold, G. C., Albeanu, D. F., Sato, T. F., and Murthy, V. N. (2008). Coupling of neural activity to blood flow in olfactory glomeruli is mediated by astrocytic pathways. *Neuron* 58, 897–910. doi: 10.1016/j.neuron.2008.04.029

Rosenegger, D. G., Tran, C. H. T., LeDue, J., Zhou, N., and Gordon, G. R. (2014). A high performance, cost-effective, open-source microscope for scanning two-photon microscopy that is modular and readily adaptable. *PLoS One* 9:e110475. doi: 10.1371/journal.pone.0110475.s005

Schulz, K., Sydekum, E., Krueppel, R., Engelbrecht, C. J., Schlegel, F., Schröter, A., et al. (2012). Simultaneous BOLD fMRI and fiber-optic calcium recording in rat neocortex. *Nat. Methods* 9, 597–602. doi: 10.1038/nmeth.2013

Schummers, J., Yu, H., and Sur, M. (2008). Tuned responses of astrocytes and their influence on hemodynamic signals in the visual cortex. *Science* 320, 1638–1643. doi: 10.1126/science.1156120

Sercombe, R., Hardebo, J. E., Kåhrström, J., and Seylaz, J. (1990). Amine-induced responses of pial and penetrating cerebral arteries: evidence for heterogeneous responses. *J. Cereb. Blood Flow Metab.* 10, 808–818. doi: 10.1038/jcbfm.1990.137

Shigetomi, E., Bushong, E. A., Haustein, M. D., Tong, X., Jackson-Weaver, O., Kracun, S., et al. (2013). Imaging calcium microdomains within entire astrocyte territories and endfeet with GCaMPs expressed using adeno-associated viruses. *J. Gen. Physiol.* 141, 633–647. doi: 10.1085/jgp.201210949

Shih, A. Y., Rühlmann, C., Blinder, P., Devor, A., Drew, P. J., Friedman, B., et al. (2015). Robust and fragile aspects of cortical blood flow in relation to the underlying angioarchitecture. *Microcirculation* 22, 204–218. doi: 10.1111/micc.12195

Simard, M., Arcuino, G., Takano, T., Liu, Q. -S., and Nedergaard, M. (2003). Signaling at the gliovascular interface. *J. Neurosci.* 23, 9254–9262. doi: 10.1523/JNEUROSCI.23-27-09254.2003

Srinivasan, R., Huang, B. S., Venugopal, S., Johnston, A. D., Chai, H., Zeng, H., et al. (2015). Ca^{2+} signaling in astrocytes from $Ip3r2^{(-/-)}$ mice in brain slices and during startle responses in vivo. *Nat. Neurosci.* 18, 708–717. doi: 10.1038/nn.4001

Stobart, J. L., Ferrari, K. D., Barrett, M. J. P., Glück, C., Stobart, M. J., Zuend, M., et al. (2018a). Cortical circuit activity evokes rapid astrocyte calcium signals on a similar timescale to neurons. *Neuron* 98, 726–735.e4. doi: 10.1016/j.neuron.2018.03.050

Stobart, J. L., Ferrari, K. D., Barrett, M. J. P., Stobart, M. J., Looser, Z. J., Saab, A. S., et al. (2018b). Long-term in vivo calcium imaging of astrocytes reveals distinct cellular compartment responses to sensory stimulation. *Cereb. Cortex* 28, 184–198. doi: 10.1093/cercor/bhw366

Straub, S. V., Bonev, A. D., Wilkerson, M. K., and Nelson, M. T. (2006). Dynamic inositol trisphosphate-mediated calcium signals within astrocytic endfeet underlie vasodilation of cerebral arterioles. *J. Gen. Physiol.* 128, 659–669. doi: 10.1085/jgp.200609650

Straub, S. V., and Nelson, M. T. (2007). Astrocytic calcium signaling: the information currency coupling neuronal activity to the cerebral microcirculation. *Trends Cardiovasc. Med.* 17, 183–190. doi: 10.1016/j.tcm.2007.05.001

Takano, T., Tian, G. -F., Peng, W., Lou, N., Libionka, W., Han, X., et al. (2006). Astrocyte-mediated control of cerebral blood flow. *Nat. Neurosci.* 9, 260–267. doi: 10.1038/nn1623

Takata, N., Mishima, T., Hisatsune, C., Nagai, T., Ebisui, E., Mikoshiba, K., et al. (2011). Astrocyte calcium signaling transforms cholinergic modulation to cortical plasticity in vivo. *J. Neurosci.* 31, 18155–18165. doi: 10.1523/JNEUROSCI.5289-11.2011

Takata, N., Nagai, T., Ozawa, K., Oe, Y., Mikoshiba, K., and Hirase, H. (2013). Cerebral blood flow modulation by basal forebrain or whisker stimulation can occur independently of large cytosolic Ca^{2+} signaling in astrocytes. *PLoS One* 8:e66525. doi: 10.1371/journal.pone.0066525

Thrane, A. S., Rappold, P. M., Fujita, T., Torres, A., Bekar, L. K., Takano, T., et al. (2011). Critical role of aquaporin-4 (AQP4) in astrocytic Ca^{2+} signaling events elicited by cerebral edema. *Proc. Natl. Acad. Sci. U. S. A.* 108, 846–851. doi: 10.1073/pnas.1015217108

Tran, C. H. T., and Gordon, G. R. (2015). Acute two-photon imaging of the neurovascular unit in the cortex of active mice. *Front. Cell. Neurosci.* 9:11. doi: 10.3389/fncel.2015.00011/abstract

Tran, C. H. T., Peringod, G., and Gordon, G. R. (2018). Astrocytes integrate behavioral state and vascular signals during functional hyperemia. *Neuron* 100, 1133–1148.e3. doi: 10.1016/j.neuron.2018.09.045

Uhlirova, H., Kılıç, K., Tian, P., Thunemann, M., Desjardins, M., Saisan, P. A., et al. (2016). Cell type specificity of neurovascular coupling in cerebral cortex. *elife* 5:e14315. doi: 10.7554/eLife.14315

Winship, I. R., Plaa, N., and Murphy, T. H. (2007). Rapid astrocyte calcium signals correlate with neuronal activity and onset of the hemodynamic response in vivo. *J. Neurosci.* 27, 6268–6272. doi: 10.1523/JNEUROSCI.4801-06.2007

Zheng, K., Bard, L., Reynolds, J. P., King, C., Jensen, T. P., Gourine, A. V., et al. (2015). Time-resolved imaging reveals heterogeneous landscapes of Nanomolar Ca^{2+} in neurons and astroglia. *Neuron* 88, 277–288. doi: 10.1016/j.neuron.2015.09.043

Zonta, M., Angulo, M. C., Gobbo, S., Rosengarten, B., Hossmann, K. -A., Pozzan, T., et al. (2003). Neuron-to-astrocyte signaling is central to the dynamic control of brain microcirculation. *Nat. Neurosci.* 6, 43–50. doi: 10.1038/nn980

Conflict of Interest: The authors declare that the research was conducted in the absence of any commercial or financial relationships that could be construed as a potential conflict of interest.

frontiers in Cellular Neuroscience

REVIEW
published: 18 December 2020
doi: 10.3389/fncel.2020.601324

The Ion Channel and GPCR Toolkit of Brain Capillary Pericytes

Ashwini Hariharan[1†], Nick Weir[1†], Colin Robertson[1], Liqun He[2], Christer Betsholtz[2,3] and Thomas A. Longden[1]*

[1] Department of Physiology, School of Medicine, University of Maryland, Baltimore, MD, United States, [2] Rudbeck Laboratory, Department of Immunology, Genetics and Pathology, Uppsala University, Uppsala, Sweden, [3] Department of Medicine Huddinge (MedH), Karolinska Institutet & Integrated Cardio Metabolic Centre, Huddinge, Sweden

Brain pericytes reside on the abluminal surface of capillaries, and their processes cover ~90% of the length of the capillary bed. These cells were first described almost 150 years ago (Eberth, 1871; Rouget, 1873) and have been the subject of intense experimental scrutiny in recent years, but their physiological roles remain uncertain and little is known of the complement of signaling elements that they employ to carry out their functions. In this review, we synthesize functional data with single-cell RNAseq screens to explore the ion channel and G protein-coupled receptor (GPCR) toolkit of mesh and thin-strand pericytes of the brain, with the aim of providing a framework for deeper explorations of the molecular mechanisms that govern pericyte physiology. We argue that their complement of channels and receptors ideally positions capillary pericytes to play a central role in adapting blood flow to meet the challenge of satisfying neuronal energy requirements from deep within the capillary bed, by enabling dynamic regulation of their membrane potential to influence the electrical output of the cell. In particular, we outline how genetic and functional evidence suggest an important role for G_s-coupled GPCRs and ATP-sensitive potassium (K_{ATP}) channels in this context. We put forth a predictive model for long-range hyperpolarizing electrical signaling from pericytes to upstream arterioles, and detail the TRP and Ca^{2+} channels and G_q, $G_{i/o}$, and $G_{12/13}$ signaling processes that counterbalance this. We underscore critical questions that need to be addressed to further advance our understanding of the signaling topology of capillary pericytes, and how this contributes to their physiological roles and their dysfunction in disease.

Keywords: pericytes, ion channels, GPCRs (G protein coupled receptors), neurovascular coupling (NVC), cerebral blood flow (CBF), K_{ATP} channels, brain metabolism

OPEN ACCESS

Edited by:
Fabrice Dabertrand, University of Colorado, United States

Reviewed by:
Chiara Bianca Maria Platania, University of Catania, Italy
Frank Faraci, The University of Iowa, United States

***Correspondence:**
Thomas A. Longden
thomas.longden@som.umaryland.edu

[†]These authors have contributed equally to this work

Specialty section:
This article was submitted to Non-Neuronal Cells, a section of the journal Frontiers in Cellular Neuroscience

Received: *31 August 2020*
Accepted: *13 November 2020*
Published: *18 December 2020*

Citation:
Hariharan A, Weir N, Robertson C, He L, Betsholtz C and Longden TA (2020) The Ion Channel and GPCR Toolkit of Brain Capillary Pericytes. Front. Cell. Neurosci. 14:601324. doi: 10.3389/fncel.2020.601324

INTRODUCTION

A combination of autonomic signaling (Cipolla et al., 2004; Hamel, 2006) and intrinsic pressure sensing and metabolic autoregulatory mechanisms (Bayliss, 1902; Paulson et al., 1990) drives continual adjustments in global and local blood flow in the brain. Importantly, as the brain lacks substantial energy stores it must be able to rapidly adapt local blood flow to fluctuating neuronal metabolic needs to provide adequate oxygen and glucose delivery. This is achieved through the on-demand process of functional hyperemia (FH), where increases in neural activity—which can span orders of magnitude in milliseconds—are met with an increase in local blood flow within seconds. This call-and-response phenomenon is underlain by a complex range of stratified mechanisms, collectively termed neurovascular coupling (NVC), which have inbuilt redundancy to ensure the fidelity of the blood flow response.

Significant inroads toward a full understanding of these NVC mechanisms have been made in recent years (Iadecola, 2017), and in particular ion channel and GPCR signaling networks within and between the cells of the neurovascular unit [NVU; neurons, astrocytes, smooth muscle cells (SMCs), endothelial cells (ECs), and pericytes] are emerging as major contributors (Longden et al., 2016). However, capillary pericytes represent a relative blind spot in our knowledge, and our understanding of their involvement in brain blood flow control is less well-developed than that for other cells of the NVU. Accordingly, the purpose of this review is to survey the signaling toolkit that mesh and thin-strand pericytes may employ to contribute to the control of blood flow throughout the brain. To this end, we leverage data from recent brain single-cell RNAseq (scRNAseq) screens (He et al., 2018; Vanlandewijck et al., 2018; Zeisel et al., 2018) to profile the expression of ion channels (**Table 1**) and GPCRs (**Table 2**) in brain capillary pericytes which, when synthesized with functional results, may aid in delineating their physiological roles.

An important caveat with this approach is that mRNA expression does not necessarily predict protein levels (Liu et al., 2016), and we thus stress that it is essential that the hypotheses generated by transcriptomic data be subject to further experimental scrutiny. Accordingly, while the following discussion is based on robust mRNA expression data, we highlight where there is question of whether gene expression translates into functional channels or receptors. A second putative caveat relates to the quality of the scRNAseq data. Specifically, it is important to ask if low-level mRNA counts reflect true and physiologically meaningful expression or artifacts such as contamination of the pericyte transcriptomes by mRNA from other cell types. Pericytes in particular are sensitive to endothelial contamination because of the tight physical association between these two cell types. With these caveats in mind, to arrive at a list of genes with reasonable likelihood of pericyte expression we first selected genes detected at levels >1 average count per cell in the 1,088 adult brain pericytes present in the Vanlandewijck et al. dataset (http://betsholtzlab.org/VascularSingleCells/database.html; He et al., 2018; Vanlandewijck et al., 2018) and compared this to their expression in the Zeisel dataset (http://mousebrain.org; Zeisel et al., 2018). In the latter, three pericyte clusters are provided (PER1, PER2, PER3) of which PER1 and PER2 are endothelial cell contaminated, whereas PER3 appears pure. After manually checking for signs of contamination by comparing the expression level in pericytes with expression in other brain cell types, we selected the following criteria as qualifying: (i) expression in >3% of the pericytes in the Vanlandewijck dataset and; (ii) detectable expression (>0) in the Zeisel et al. PER3 dataset (**Figure 1**).

Below, we focus our discussion on the ion channels and GPCRs that are likely to be most pertinent to blood flow control. We center our discussion on studies using acute and *in vivo* preparations, as cultured pericytes may exhibit phenotypic drift which confounds interpretation. Accordingly, we note instances in which we refer to cultured pericytes. We begin by briefly reviewing the key features of the brain vasculature and pericytes before exploring their ion channel and GPCR complement in detail.

THE VASCULAR NETWORK OF THE BRAIN

Fundamental Angioarchitecture

From pial arteries on the brains surface, penetrating arterioles branch orthogonally and dive into the parenchyma (Duvernoy et al., 1981; Cipolla, 2009; **Figure 2**). Arteries and arterioles are composed of a lumen lined by electrically-coupled cobblestone–morphology ECs (Haas and Duling, 1997) that directly interface with the blood. These ECs are surrounded by a fenestrated internal elastic lamina (IEL), composed mainly of elastin and collagen (Schwartz et al., 1981), through which they extend projections to directly contact overlying contractile smooth muscle cells (SMCs) (Aydin et al., 1991).

As the penetrating arteriole extends deeper into the tissue, further vessels sprout from its length at regular intervals (Blinder et al., 2013). These initial branch points are sites of precapillary sphincters which are regulated over short time scales to control blood flowing into the capillary bed (Grubb et al., 2020). From this point, extensive ramification of the vascular bed greatly expands the surface area of the network, facilitating efficient exchange of nutrients and waste to rapidly satisfy the intense metabolic requirements of every neuron. The capillary bed—consisting of capillary ECs (cECs; Garcia and Longden, 2020) and overlying pericytes (see below) embedded in the basement membrane (a dense network of glycoproteins, collagens and secreted factors; Pozzi et al., 2017)—is incredibly dense, and each microliter of cortex holds approximately 1 m of blood vessels (Shih et al., 2015). Of these, around 90% by volume are capillaries (Gould et al., 2017). Accordingly, ECs are estimated to comprise around 30% of the non-neuronal cell mass in the gray matter, forming a network of 20–25 billion ECs throughout the entire human brain (von Bartheld et al., 2016). This places cECs in close apposition with all neurons, with each neuronal cell body lying within ∼15 μm of a vessel (Tsai et al., 2009). Red blood cells (RBCs) traverse this network, releasing oxygen to diffuse down its concentration gradient into the tissue, while glucose is transported by ECs from the blood plasma into the parenchyma. After negotiating the capillary bed, oxygen-depleted RBCs eventually reach a vertically-oriented venule, which drain to veins at the cortical surface on the path back to the heart.

Mural Cell Properties Transition Gradually With Increasing Branch Order

As the vascular bed ramifies from the penetrating arteriole, there is gradation in the morphology and functional characteristics of the mural cells associated with vessels. The first 3–4 branches of the vascular network (1st to 4th order) originating from the penetrating arteriole constitute a "transitional zone" (Ratelade et al., 2020). These vessels are covered by cells expressing high levels of α-smooth muscle actin (α-SMA) with ovoid cell bodies and multiple broad processes that almost completely ensheathe the underlying vessel (Grant et al., 2019; **Figure 3A**). Given that the identity of these cells is unresolved, and that they have been referred to as both pericytes (Peppiatt et al., 2006; Hall et al., 2014; Attwell et al., 2016; Grant et al., 2019) and SMCs (Hill et al., 2015; Grutzendler and Nedergaard, 2019), we refer to these cells here as "contractile mural cells" and to the segments of the vasculature

TABLE 1 | Ion channels expressed by CNS capillary pericytes.

Channel protein	Gene	mRNA average counts/cell*	Ion selectivity	Endogenous activators and key modulators	Key properties	Key references
$K_{ir}6.1$	*Kcnj8*	1670.21	K^+	ATP:ADP, UDP, G_q/G_s signaling	Weakly rectifying; Forms K_{ATP} channel with SUR2 to mediate metabolism-electrical coupling	Ishizaki et al., 2009
$K_{ir}2.2$	*Kcnj12*	31.01	K^+	K^+, hyperpolarization	Strongly rectifying; Propagation of hyperpolarizing signals	Matsushita and Puro, 2006; Longden and Nelson, 2015; Longden et al., 2017
$K_v1.2$	*Kcna2*	1.25	K^+			
$K_v2.1$	*Kcnb1*	4.11	K^+			
$K_v6.1$	*Kcng1*	8.75	K^+		Negative feedback regulation of V_m; K_v currents have been reported in peripheral pericytes	Nelson and Quayle, 1995; von Beckerath et al., 2000; Quignard et al., 2003
$K_v7.4$	*Kcnq4*	7.7	K^+	Depolarization		
$K_v7.5$	*Kcnq5*	1.48	K^+			
$K_v9.1$	*Kcns1*	1.66	K^+			
$K_v9.3$	*Kcns3*	3.21	K^+			
$K_{2P}3.1$	*Kcnk3*	9.8	K^+	pH	Activation in response to moderate rise in pH	Duprat et al., 1997
$K_{Na}1.2$	*Kcnt2*	5.87	K^+	Intracellular Na^+, Cl^-	Maintaining resting V_m; Sensitive to cell volume changes; Inactivated by ADP and ATP	Bhattacharjee et al., 2003; Tejada et al., 2014
$K_{Ca}2.3$	*Kcnn3*	1.81	K^+	Intracellular Ca^{2+}	Hyperpolarization in response to Ca^{2+} elevation;	Taylor et al., 2003; Adelman et al., 2012
TRPC1	*Trpc1*	16.04	Na^+, K^+, Ca^{2+}	n.d[a]	Store-operated Ca^{2+} entry in association with STIM1 and Orai1	Huang et al., 2006; Cheng et al., 2008
TRPC3	*Trpc3*	266.99	***p*Ca^{2+}/*p*Na^+: 1.6** Na^+, K^+, Ca^{2+}	G_q signaling, DAG	Facilitates Ca^{2+} entry; Depolarizes V_m	Xi et al., 2009; Kochukov et al., 2014
TRPC4	*Trpc4*	67.83	***p*Ca^{2+}/*p*Na^+: 1.1-7.7** Na^+, K^+, Ca^{2+}	$G_{i/o}/G_q$ signaling	Activated by $G_{i/o}$-GPCR signaling	Albert, 2011; Jeon et al., 2012
TRPC6	*Trpc6*	5.94	***p*Ca^{2+}/*p*Na^+: 5** Na^+, K^+, Ca^{2+}	G_q signaling, arachidonic acid, lysophosphatidylcholine, 20-HETE	Mechanosensation; Ca^{2+} influx through TRPC6 can sensitize IP_3R to cause Ca^{2+} release	Gonzales et al., 2014
TRPM3	*Trpm3*	1.04	***p*Ca^{2+}/*p*Na^+: 1.6** Na^+, K^+, Ca^{2+}, Mg^{2+}**	Sphingosine, sphinganine, NN-dimethyl-D-erythrosphingosine, pregnenolone sulfate	Steroid signaling; Lipid signaling; Mechanosensation	Grimm et al., 2005; Wagner et al., 2008
TRPM4	*Trpm4*	21.32	Na^+, K^+	PIP_2, intracellular Ca^{2+}	Permeable to monovalent cations; Depolarizes V_m in response to Ca^{2+} elevations	Gonzales et al., 2014
TRPM7	*Trpm7*	104.35	***p*Ca^{2+}/*p*Na^+: 0.34** Na^+, K^+, Ca^{2+}, Mg^{2+}	PIP_2	Mg^{2+} homeostasis; Can modulate store-operated Ca^{2+} entry; pH sensitive;	Schlingmann et al., 2007; Souza Bomfim et al., 2020
TRPML1	*Mcoln1*	39.53	Na^+, K^+, Ca^{2+}, Mg^{2+}	Phosphatidyl (3,5) inositol bisphosphate	Lysosomal ion homeostasis	Venkatachalam et al., 2015
TRPP1	*Pkd2*	117.24	Na^+, K^+, Ca^{2+}	Intracellular Ca^{2+}	Large Ca^{2+} conductance; Mechanosensation in association with PKD1	Sharif-Naeini et al., 2009; Narayanan et al., 2013

(Continued)

TABLE 1 | Continued

Channel protein	Gene	mRNA average counts/cell*	Ion selectivity	Endogenous activators and key modulators	Key properties	Key references
TRPP3	*Pkd2l2*	1.3	**pCa^{2+}/pNa^{+}: 4-4.3** Na^{+}, K^{+}, Ca^{2+}, Mg^{2+}	n.d	pH sensitive	Inada et al., 2008
TRPV2	*Trpv2*	98.6	**pCa^{2+}/pNa^{+}: 0.9-2.9** Na^{+}, K^{+}, Ca^{2+}, Mg^{2+}	n.d	Mechanosensitive - detects cell swelling/stretch	Perálvarez-Marín et al., 2013
IP_3R1	*Itpr1*	209.62	Ca^{2+}	IP_3, cytosolic Ca^{2+}	Mediate Ca^{2+} release from endoplasmic reticulum upon binding of IP_3; Participate in many intracellular Ca^{2+} signaling processes	Foskett et al., 2007; Berridge, 2016
IP_3R2	*Itpr2*	250.43	Ca^{2+}			
IP_3R3	*Itpr3*	1.73	Ca^{2+}			
$Ca_v1.2$	*Cacna1c*	99.46	Ca^{2+}	Depolarization	Ca^{2+} entry in response to depolarization or at resting; V_m; L-type Ca^{2+} currents recorded in retinal pericytes	Sakagami et al., 1999; Perez-Reyes, 2003
$Ca_v1.3$	*Cacna1d*	2.48				
$Ca_v2.1$	*Cacna1a*	1.05				
$Ca_v3.1$	*Cacna1g*	1.73				
$Ca_v3.2$	*Cacna1h*	42.59				
Orai1	*Orai1*	22.88	Ca^{2+}	ER Ca^{2+} depletion	Store operated Ca^{2+} entry channels; Associate with STIM1 to permit Ca^{2+} entry upon store depletion	Prakriya and Lewis, 2015
Orai3	*Orai3*	99.94				
CaCC (TMEM16A)	*Ano1*	329.91	Cl^{-}	Intracellular Ca^{2+}	Membrane depolarization in response to increased Ca^{2+}; CaCC currents reported in retinal and peripheral pericytes	Sakagami et al., 1999; Hashitani et al., 2018
ClC-2	*Clcn2*	19.95	Cl^{-}	Hyperpolarization, arachidonic acid	Repolarization of V_m; Sensitive to intracellular ATP and ADP	Nilius and Droogmans, 2003; Stölting et al., 2013; Bi et al., 2014
ASIC2	*Asic2*	4.52	**pNa^{+}/pCa^{2+}: 20** **pNa^{+}/pK^{+}: 10** Na^{+}, K^{+}, Ca^{2+}	Extracellular H^{+}	Activated by extracellular acidification	Gannon et al., 2008; Sherwood et al., 2012
$Na_v1.2$	*Scn2a*	3.02	Na^{+}	Depolarization	Na^{+} influx in response to membrane depolarization; $Na_v1.3$ is expressed in peripheral pericytes	Yu and Catterall, 2003; Lee-Kwon et al., 2007
$Na_v1.3$	*Scn3a*	1.53	Na^{+}			
P2X1	*P2rx1*	10.53	Na^{+}, K^{+}, Ca^{2+}	ATP	Local ATP sensors	Khakh et al., 2001
P2X4	*P2rx4*	23.6				
Piezo1	*Piezo1*	2.09	Na^{+}, K^{+}, Ca^{2+}, Mg^{2+}	Mechanically activated	Senses and couples shear stress with cation entry	Coste et al., 2010; Li et al., 2014
TPC1	*Tpcn1*	36.44	Na^{+}, K^{+}, Ca^{2+}	Phosphatidyl (3,5) inositol bisphosphate	Located on endosomal/lysosomal membranes; NAADP-induced Ca^{2+} release	Calcraft et al., 2009; Pitt et al., 2016
TPC2	*Tpcn2*	6.01				

Naming conventions used throughout conform to those outlined in the IUPHAR/BPS Guide to Pharmacology (Armstrong et al., 2020). Permeability ratios are noted in bold where appropriate. Abbreviations not used elsewhere: NAADP, nicotinic acid adenine dinucleotide phosphate.

[a] *n.d., no data.*

**Data from He et al. (2018) and Vanlandewijck et al. (2018), expressed as average counts per cell annotated as a brain pericyte. Cells were isolated from adult mice of either sex aged 10–19 weeks.*

***Permeability for short-pore sequence isoform TRPM3α2.*

TABLE 2 | G protein coupled receptors expressed by CNS capillary pericytes.

Receptor	Gene	mRNA average counts/cell*	Principal G-protein**	GPCR sub-class	Endogenous agonists	Signal transduction effects; roles	Key references
Adenosine receptors							
A_1 receptor	*Adora1*	1.96	$G_{i/o}$	A	Adenosine	↓ cAMP; Arterial vasoconstriction	Borea et al., 2018
A_{2A} receptor	*Adora2a*	85.45	G_s			↑ cAMP; Arterial vasorelaxation	
A_{2B} receptor	*Adora2b*	6.52	G_s			↑ cAMP; Arterial vasorelaxation	
Adrenoceptors							
α_{1A}-adrenoreceptor	*Adra1a*	1.44	G_q	A	Epinephrine > norepinephrine	↑ IP_3/DAG; Arterial vasoconstriction	Hieble and Ruffolo, 1997; Guimarães and Moura, 2001; Muszkat et al., 2005; Silva and Zanesco, 2010; de Oliveira et al., 2019
α_{1B}-adrenoreceptor	*Adra1b*	1.29	G_q				
α_{2A}-adrenoreceptor	*Adra2a*	1.73	$G_{i/o}$			↓ cAMP; Arterial vasoconstriction	
α_{2B}-adrenoreceptor	*Adra2b*	2.03	$G_{i/o}$				
β2-adrenoreceptor	*Adrb2*	1.65	G_s			↑ cAMP; Vasodilation	
Calcitonin receptor-like receptor	*Calcrl*	37.46	G_s	B	CGRP > Adrenomedullin	Non-functional alone, requires a RAMP. Likely colocalizes with RAMP2 to form AM_1 receptors in pericytes	Poyner et al., 2002
Chemerin receptor 1	*Cmklr1*	3.49	$G_{i/o}$	A	Resolvin E1 > Chemerin	↓ cAMP; Vasoconstrictor with a role in inflammation	De Henau et al., 2016; Kennedy et al., 2016
Chemokine receptors							
CCR9	*Ccr9*	25.5	$G_{i/o}$	A	CCL25	↑ Ca^{2+}; Activation of adaptive immune response; Leukocyte recruitment	Watts et al., 2013; Mazzotti et al., 2017
CXCR4	*Cxcr4*	1.44	$G_{i/o}$		CXCL12		
CCRL2	*Ccrl2*	85.53	n.d[a]		CCL19	Anchors and presents chemerin to Cmklr1-expressing cells	
Endothelin receptors							
ET_A receptor	*Ednra*	236.01	G_q	A	Endothelin-1 > endothelin-2 > endothelin-3	Vasoconstriction in SMCs; Extracellular matrix production and inflammation	Patel et al., 2014; Maguire and Davenport, 2015; Urtatiz and Van Raamsdonk, 2016
ET_B receptor	*Ednrb*	20.99	G_s, $G_{i/o}$, G_q			↑ IP_3/DAG/PLA_2/PLD; Vasodilation in ECs, vasoconstriction in SMCs	
FFA2 receptor	*Ffar2*	6.47	G_q	A	Free fatty acids	↑ IP_3/DAG; Roles in metabolism and inflammation	Li et al., 2018
GIP receptor	*Gipr*	8.48	G_s	B	Gastric inhibitory polypeptide	↑ cAMP; Increases blood flow in adipose microvessels	Asmar et al., 2019
GPER	*Gper1*	716.19	$G_{i/o}$	A	17β-estradiol	Diverse genomic and non-genomic roles; Vasodilation, likely via secondary G_s coupling	Prossnitz and Arterburn, 2015; Evans et al., 2016
Kisspeptin receptor	*Kiss1r*	1.93	G_q	A	Kisspeptin-10,−13,−14,−54,−52	↑ IP_3/DAG; Vasoconstrictor, inhibits angiogenesis	Sawyer et al., 2011; Cvetković et al., 2013

(Continued)

TABLE 2 | Continued

Receptor	Gene	mRNA average counts/cell*	Principal G-protein**	GPCR sub-class	Endogenous agonists	Signal transduction effects; roles	Key references
Leukotriene receptors							
$CysLT_1$	*Cysltr1*	9	G_q	A	$LTD_4 > LTC_4 > LTE_4$	↑ IP_3/DAG; Vascular permeability, SMC contraction, immune cell activation	Zhang et al., 2006; Woszczek et al., 2007; Thiriet, 2013
$CysLT_2$	*Cysltr2*	35.81	G_q		$LTC_4 > LTD_4 > LTE_4$		
Lysophospholipid receptors							
LPA_1	*Lpar1*	8.29	$G_{i/o}$, G_q, $G_{12/13}$	A	LPA	↓ cAMP; ↑IP_3/DAG and PLA_2; Vasoconstrictor	Means and Brown, 2009; Cheng et al., 2012; Aoki et al., 2016; Pébay and Wong, 2017; Masago et al., 2018
LPA_6	*Lpar6*	19.76	$G_{12/13}$	A	LPA	↑ cAMP; ↑ IP_3/DAG; BBB permeability	
$S1P_1$	*S1pr1*	5.88	$G_{i/o}$	A	S1P > sphingosylphosphoryl-choline > LPA	↓ cAMP; ↑ IP3/DAG and PLD; Leukocyte recruitment, ↓ vascular permeability	
$S1P_2$	*S1pr2*	20.32	$G_{i/o}$, G_q, $G_{12/13}$	A	S1P > sphingosylphosphoryl-choline	↑ cAMP; ↑ IP_3/DAG; ↓ chemotaxis, ↑ vascular permeability	
$S1P_3$	*S1pr3*	936.18	$G_{i/o}$, G_q, $G_{12/13}$	A	S1P > sphingosylphosphoryl-choline	↓ cAMP; ↑ IP_3/DAG; Vasoconstriction via SMCs, vasorelaxation via ECs; Angiogenesis	
Metabotropic glutamate receptors							
$mGlu_3$ receptor	*Grm3*	206.24	$G_{i/o}$	C	Glutamate > NAAG	↓ cAMP; Inhibits glial non-vesicular glutamate release and neuronal synaptic plasticity	Wroblewska et al., 1998; Harrison et al., 2008; Palazzo et al., 2016; Yudin and Rohacs, 2018
$mGlu_7$ receptor	*Grm7*	94.26	$G_{i/o}$	C	Glutamate > L-serine-O-phosphate	↓ cAMP; Low glutamate affinity, auto-inhibition of glutamate release	
NOP receptor	*Oprl1*	12.02	$G_{i/o}$	A	Nociceptin/orphanin FQ	↓ cAMP; Bradycardia, hypotension upon systemic administration of agonist	Kapusta et al., 2002
PAC_1 receptor	*Adcyap1r1*	35.51	G_s, G_q	B	PACAP-27 = PACAP-38 > VIP, PHI, PHM, PHV	↑ cAMP; Potent vasodilator	May et al., 2010; Koide et al., 2014
PAR1	*F2r*	141.17	$G_{i/o}$, G_q, $G_{12/13}$	A	Thrombin activated protein C, MMP1, MMP13	Haematopoietic development, vascular development, peripheral vasodilation, hypotension, bradycardia	Cheung et al., 1998; Yue et al., 2012
PTH1 receptor	*Pth1r*	226.03	G_s	B	PTH = PTHrP-1, TIP39	↑ cAMP; Systemic mineral homeostasis	Mahon, 2012
Prostanoid receptors							
DP_2 receptor	*Ptgdr2*	2	$G_{i/o}$	A	$PGD_2 > PGF_{2\alpha} > PGE_2 > PGI_2$, thromboxane A_2 PGD_3, PGJ_2	↓ cAMP; Vasodilation, role in angiogenesis	Praticò and Dogné, 2005; Kaczynski et al., 2016; Longden et al., 2019; Upchurch and Leitinger, 2019; Ozen et al., 2020
EP_1 receptor	*Ptger1*	10.87	G_q	A	$PGE_2 > PGE_1 > PGF_{2\alpha} > PGI_2 > PGD_2$ > thromboxane A_2	↑ IP_3/DAG; Role in NVC	
EP_3 receptor	*Ptger3*	5.74	$G_{i/o}$	A	$PGE_2 > PGE_1 > PGF_{2\alpha} > PGI_2 > PGD_2$ > thromboxane A_2	↓ cAMP	

(Continued)

TABLE 2 | Continued

Receptor	Gene	mRNA average counts/cell*	Principal G-protein**	GPCR sub-class	Endogenous agonists	Signal transduction effects; roles	Key references
FP receptor	*Ptgfr*	13.26	G_q	A	$PGF_{2\alpha}$ > PGD_2 > PGE_2, PGI_2 > thromboxane A_2	↑ IP_3/DAG; Angiogenesis, matrix remodeling	
IP receptor	*Ptgir*	2.7	G_s	A	PGI_2 > PGE_1 > PGD_2, $PGF_{2\alpha}$ > thromboxane A_2 PGE_2	↑ cAMP; Released from ECs, drives vasodilation, angiogenesis	
TP receptor	*Tbxa2r*	282.65	G_q	A	Thromboxane A_2 = PGH_2 > PGD_2, PGE_2, $PGF_{2\alpha}$, PGI_2,	↑ IP_3/DAG; vasoconstriction	
Purinergic receptors							
$P2Y_{12}$ receptor	*P2ry12*	3.56	$G_{i/o}$	A	ADP > ATP	↓ cAMP; Platelet aggregation; Microglial migration; Vasoconstriction	Sasaki et al., 2003; Wihlborg et al., 2004
$P2Y_{14}$ receptor	*P2ry14*	1291.7	$G_{i/o}$	A	UDP = UDP-glucose > UDP-galactose > UDP-glucoronic acid > UDP-N-acetyl-glucosamine	↓ cAMP; inflammatory/immune responses	Harden et al., 2010
V_{1A} receptor	*Avpr1a*	1.08	G_q	A	Vasopressin > oxytocin	↑ IP_3/DAG; Vasoconstriction	Yang et al., 2010
Y_1 receptor	*Npy1r*	39.94	$G_{i/o}$	A	Neuropeptide Y = peptide YY > pancreatic polypeptide	↓ cAMP; Inhibits glutamatergic neurotransmission; Vascular remodeling; Vasoconstriction	Crnkovic et al., 2014; Huang and Thathiah, 2015
Adhesion receptors							
CELSR2	*Celsr2*	1.03	n.d	Adhesion	Orphan	↑ Ca^{2+}; CamKII and Jun kinase activity	Shima et al., 2007; Cortijo et al., 2012; Sugimura et al., 2012
Frizzled receptors							
FZD_1	*Fzd1*	4.86	Canonical Wnt signaling	Frizzled	Wnt-1, Wnt-2, Wnt-3A, Wnt-5A, Wnt-7B	Pericyte motility and polarity during angiogenesis	Nichols et al., 2013; Dijksterhuis et al., 2014; Kilander et al., 2014; Yuan et al., 2015; Corda and Sala, 2017; Henno et al., 2017; Hot et al., 2017; Zimmerli, 2018; Kozielewicz et al., 2020
FZD_3	*Fzd3*	14.53	G_s	Frizzled	Wnt-2, Wnt-3A, Wnt-5A	Decoy receptor, dampens Wg signaling	
FZD_6	*Fzd6*	129.87	$G_{i/o}$, $G_{q/11}$	Frizzled	Wnt-3A, Wnt-4, Wnt-5A, Wnt-5B, Wnt-7A	Cell proliferation, differentiation and polarity	
FZD_7	*Fzd7*	3.72	G_s, $G_{i/o}$, Canonical Wnt signaling	Frizzled	Wnt-3, Wnt-3A, Wnt-5A, Wnt-7A	Pericyte motility and polarity during angiogenesis	
FZD_8	*Fzd8*	4.83	Putative Canonical Wnt signaling	Frizzled	Wnt-2, Wnt-3A, Wnt-9B	n.d	
FZD_{10}	*Fzd10*	1.36	Canonical Wnt signaling	Frizzled	Wnt7A, Wnt-7B	Putative role in CNS angiogenesis	
SMO	*Smo*	19.64	$G_{i/o}$, $G_{12/13}$	Frizzled	Constitutively active; oxysterols?	Angiogenesis, remodeling, proliferation and NO release in ECs	

(Continued)

TABLE 2 | Continued

Receptor	Gene	mRNA average counts/cell*	Principal G-protein**	GPCR sub-class	Endogenous agonists	Signal transduction effects; roles	Key references
Orphan receptors							
GPR4	*Gpr4*	85.06	G_s, $G_{i/o}$, G_q, $G_{12/13}$	A	H^+	↑ cAMP ↑ IP_3/DAG Pro-inflammatory in ECs	Tobo et al., 2007; Li et al., 2015; Weiß et al., 2017; Carvalho et al., 2020
GPR19	*Gpr19*	15.87	G_s	A	H^+	↑ cAMP; Pro-inflammatory in ECs	
GPR20	*Gpr20*	4.93	n.d	A	n.d	n.d	
GPR157	*Gpr157*	1.18	n.d	None	n.d	n.d	
GPR182	*Gpr182*	17.83	n.d	A	Adrenomedullin	n.d	
GPRC5B	*Gprc5b*	1.04	n.d	C	n.d	Regulation of vascular SMC tone	
GPRC5C	*Gprc5c*	385.48	$G_{12/13}$	C	n.d	Reinforces β-catenin and Wnt signaling	
LGR4	*Lgr4*	10.67	Non-classical	A	R-spondin1-4	Implicated role in lipid metabolism	
OPN3	*Opn3*	1.59	n.d	A	n.d	n.d	
TPRA1	*Tpra1*	52.7	$G_{i/o}$	7TM	N/A	n.d	Singh et al., 2015

The $GABA_B$ subunit $GABA_{B1}$ is also expressed by pericytes, but is not included here due to the apparent absence of $GABA_{B2}$, required for functional receptors. Abbreviations not used elsewhere: LPA, lysophosphatidic acid; MMP, matrix metalloproteinase; NAAG, N-acetylaspartylglutamate; PHI, peptide histidine-isoleucine; PHM, peptide histidine-methionine; PHV, peptide histidine-valine; PLD, phospholipase D; TIP39, Tuberoinfundibular peptide of 39 residues; VIP, vasoactive intestinal peptide.

[a]*n.d, no data.*

**Data from He et al. (2018) and Vanlandewijck et al. (2018), expressed as average counts per cell annotated as a brain pericyte. Cells were isolated from adult mice of either sex aged 10–19 weeks.*

***We note here the principal transduction G-protein, although many receptors are promiscuous and couple to secondary transduction pathways. Frizzled receptors canonically couple to Wnt signaling but may also interact with a rage of G proteins. Where there is no clear primary pathway, we list all possibilities. Readers are referred to Alexander et al. (2019) for further details.*

that they cover as "vessels." Expression of α-SMA permits these cells to rapidly regulate the diameter of the underlying vessel and therefore blood flow. Indeed, multiple studies have illustrated the importance of contractile mural cells in mediating dilation (of ∼10–30%) in response to neuronal stimulation (Hill et al., 2015; Mishra et al., 2016; Kisler et al., 2017; Cai et al., 2018; Rungta et al., 2018).

Beyond this point in the vasculature, mural cells do not express high levels of α-SMA, although one recent study suggested that retinal mural cells retain expression of a low level of this protein (Alarcon-Martinez et al., 2018) and they do express very low levels of the *Acta2* gene in the brain (He et al., 2018; Vanlandewijck et al., 2018). As a result, these cells are not equipped to regulate vessel diameter over abrupt time scales, but there is clear evidence that they may contract slowly under certain circumstances (reducing the diameter of the underlying vessel by up to ∼25%; Fernández-Klett et al., 2010; Gonzales et al., 2020). Thus, we consider the relatively static diameter vessels downstream of the α-SMA terminus (which typically occurs between the 1st and 4th order branch in immunostaining experiments; Grant et al., 2019) to be capillaries. The identity of mural cells on these so-defined capillaries is unambiguous, and there is consensus that these cells are pericytes.

The pericytes residing on capillaries display at least two distinct morphologies: (i) Immediately adjacent to the α-SMA terminus, pericytes take on a mesh-like appearance, and are thus known as "mesh pericytes" (**Figure 3B**); (ii) beyond these are cells that project long, thin processes along the vasculature, and accordingly these are referred to as "thin-strand pericytes" (Grant et al., 2019; **Figures 3C,D**).

CELLULAR ANATOMY OF MESH AND THIN-STRAND PERICYTES

Despite differing morphologies (**Figure 3**), mesh and thin-strand pericytes are indistinguishable at the level of single-cell transcriptomics, possibly due to the fact that mesh pericytes represent only a small fraction of capillary pericytes (Chasseigneaux et al., 2018). Pericyte cell bodies have a highly stereotyped shape, appearing as a large ovoid that protrudes from the wall of the capillary, which is often referred to as a "bump-on-a-log" (Grant et al., 2019). Mesh pericytes are few in number relative to thin-strand pericytes and have fewer, shorter longitudinal processes (their primary trunks averaging 40 μm in length; Hartmann et al., 2015) that cover ∼70% of the underlying capillary. This contrasts with upstream contractile mural cells which cover 95% of the underlying vessel (Grant et al., 2019). Thin-strand pericytes extend long, thin, strand-like processes that are ∼1.5 μm in diameter and cover on average around 250 μm in total capillary distance, in some instances

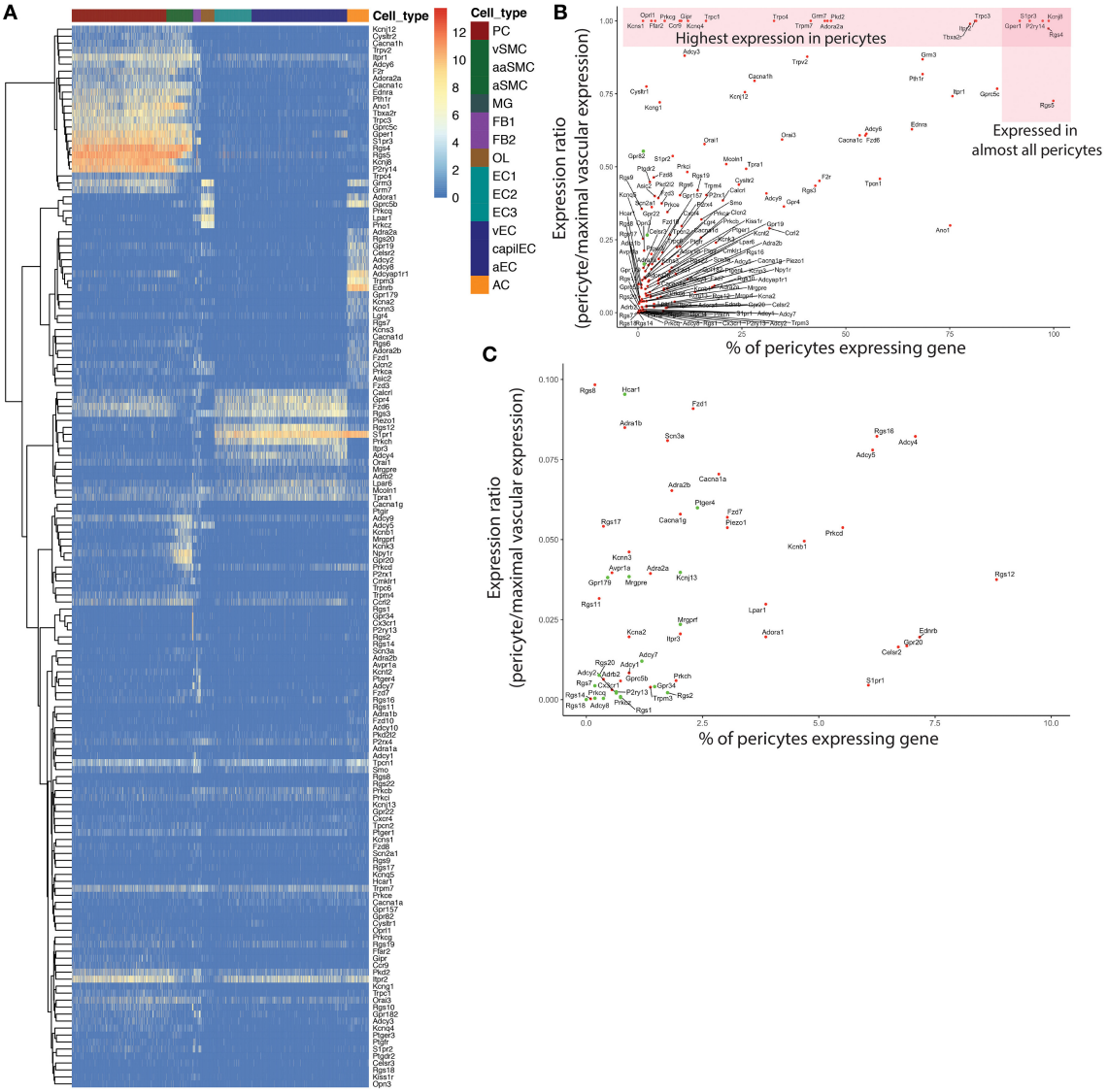

FIGURE 1 | Overview of gene qualification process for pericyte ion channels and GPCRs and other genes of interest. An initial filter of 1 average count/cell was applied to exclude genes with extremely low expression. **(A)** Heatmap of expression of the remaining genes throughout the neurovascular unit. A small subset of these genes were highly enriched in pericytes (*top left*), while many showed higher expression in other cell types. To filter out potential contamination, genes that were expressed in <3% of pericytes, and were absent from the PER3 cluster of Zeisel et al. (2018) were excluded. **(B)** Relationship between pericyte-specificity of expression and fraction of pericytes expressing each gene considered. Genes represented by green circles were excluded according to the above criteria. **(C)** High resolution view of genes with a <0.1 expression ratio in pericytes, that were expressed in fewer than 10% of pericytes, corresponding to the bottom left corner in **(B)**. Genes represented by green circles were excluded from further consideration as potential contamination.

exceeding 300 μm (Berthiaume et al., 2018). Together, the thin-strand pericyte cell body and its processes cover between one third (Mathiisen et al., 2010) and one half (Grant et al., 2019) of the abluminal surface area of the endothelium. A typical thin-strand process has a stable "non-terminal core" of ∼50 μm in length that bifurcates into slightly shorter, dynamic terminal processes that may extend or retract up to 20 μm over the course of days to weeks (Berthiaume et al., 2018). At their terminal ends, thin-strand processes appear to come into close proximity with those of neighboring pericytes (Berthiaume et al., 2018), possibly allowing for direct contact between adjacent pericytes, although this awaits direct experimental confirmation. Changes in the length of processes of one cell appear to evoke opposite changes in the length of adjacent pericyte processes, preventing the formation of substantial gaps (Berthiaume et al., 2018).

These processes are for the most part prevented from making direct contact with the underlying endothelium by the basement membrane. However, electron microscopy has revealed that—similar to the IEL of arteries and arterioles—the capillary basement membrane is dotted with many fenestrations, with an average area of 1.5 μm^2, ranging from 100 to 450 nm in diameter (Carlson, 1989; **Figure 3D**). In arteries, similar fenestrations are

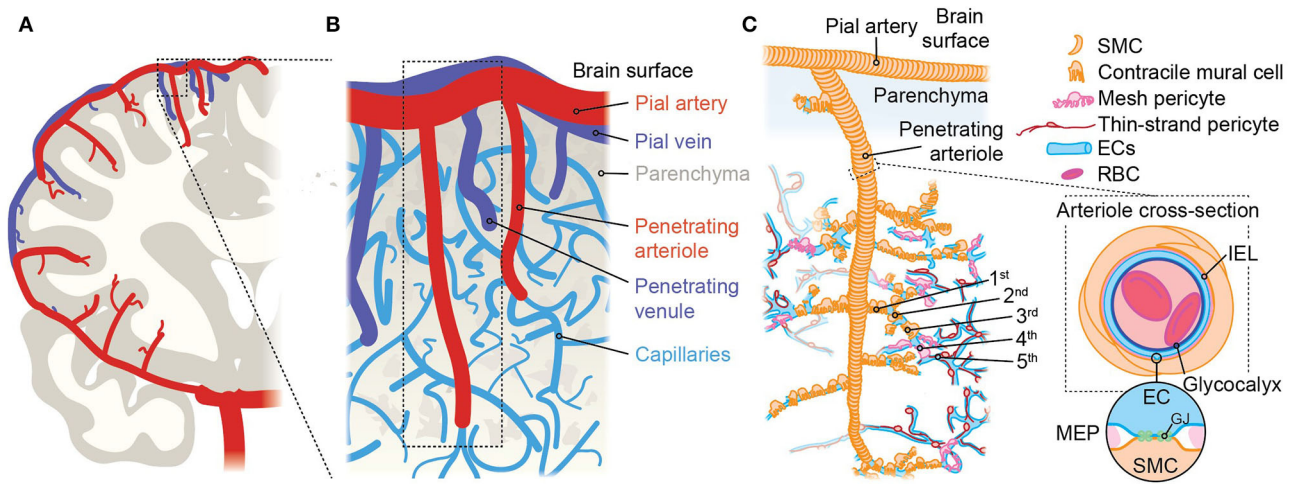

FIGURE 2 | An overview of brain angioarchitecture. **(A)** Cross-section of one brain hemisphere illustrating macroscopic vascular architecture. The carotid artery joins the circle of Willis at the base of the brain, then gives rise to major pial arteries which course over the brain surface, from which multiple penetrating arterioles arise and dive into the tissue. **(B)** Close up view of the components of the vascular network approximating the area in the boxed region in *A* showing the interconnected organization of pial arteries, penetrating arterioles, the dense capillary network, and venules. The vessel labeling system we use takes the penetrating arteriole as the 0-order vessel and primary reference point, and vessels are numbered sequentially with regard to this. Vessel number automatically increases each time a vessel branches and thus, after vessel *n* branches, the daughter branches—regardless of diameter or orientation—are labeled vessel $n + 1$. **(C)** Illustration approximating the boxed region in **(B)**, showing the cellular elements that make up the arteriolar side of the brain vasculature. Arteries and arterioles consist of SMCs surrounding ECs, which are in direct contact with the blood. The first 3–4 vessels emanating from the penetrating arteriole are a transitional zone and are covered with contractile mural cells that are positive for α-SMA and can change diameter abruptly. Immediately after the α-actin terminus are capillaries covered by mesh pericytes, following which are capillaries where thin-strand pericytes reside. The cross-section at right shows a section through an artery/arteriole and illustrates the presence of the internal elastic lamina (IEL) which separates ECs and SMCs. Occasional fenestrations dot the IEL, through which ECs and SMCs make direct contact via myoendothelial projections (MEPs, *circular inset*). These are sites of gap junctions (GJs) permitting chemical and electrical cell-cell communication.

the sites of myoendothelial junctions, optimized for EC-SMC communication by the presence of a number of key enzymes, ion channels, and gap junction (GJ) proteins (Straub et al., 2014). In the capillary bed, these fenestrations are the site of "peg-socket" interdigitations where either the pericyte or the EC sends a projection to make contact with the adjacent cell (Tilton et al., 1979; Cuevas et al., 1984; Armulik et al., 2005). These contact points are thought to be the sites of GJ communication between the two cell types (see **Box 1**), and may be the location of key signaling events, such as local calcium (Ca^{2+}) or cyclic adenosine monophosphate (cAMP) elevations. Moreover, they may be sites of macromolecular signaling complex assembly, containing ion channels, and GPCRs positioned to facilitate cell-cell communication.

ION CHANNEL EXPRESSION IN BRAIN CAPILLARY PERICYTES

A cursory review of the brain capillary pericyte ion channel expression data provided by He et al. (2018) and Vanlandewijck et al. (2018) reveals that potassium (K^+) channels are the dominant ion channel species in pericytes. Remarkably, this is due to the adenosine triphosphate (ATP)-sensitive K^+ (K_{ATP}) channel inward rectifier (K_{ir}) subunit, $K_{ir}6.1$, accounting for nearly half of the total ion channel gene expression in these cells. Transient receptor potential (TRP), Ca^{2+}, and chloride (Cl^-) channels make up the remaining half, along with lower expression of a handful of other channel subunits including two-pore channels (TPCs), voltage-gated sodium (Na^+; Na_v) channels, P2X receptors, acid sensing ion channels (ASICs), and Piezo1 (**Table 1** and **Figure 4**).

PERICYTE K^+ CHANNELS

Focusing initially on the K^+ channel superfamily, capillary pericytes express K_{ir}, two-pore domain (K_{2P}), voltage-gated (K_v), Na^+-activated (K_{Na}), and Ca^{2+}-activated (K_{Ca}) K^+ channel genes.

K_{ir}-Family Channels May Enable Pericyte Metabolism-Electrical Coupling and Facilitate Rapid, Long-Range Electrical Signaling

K_{ir} channels have the defining biophysical property of inward rectification, preferentially conducting large currents into the cell at voltages negative to the K^+ equilibrium potential (E_K), the magnitude of which depend on the electrochemical gradient for K^+ [i.e., the difference between V_m and E_K] (Katz, 1949; Hibino et al., 2010). At potentials positive to E_K some degree of rectification occurs, ranging from strong—in which almost no current passes from the interior of the cell to the exterior—to weak, in which rectification is only seen at very positive potentials. Accordingly, K_{ir} channels can be classified by their

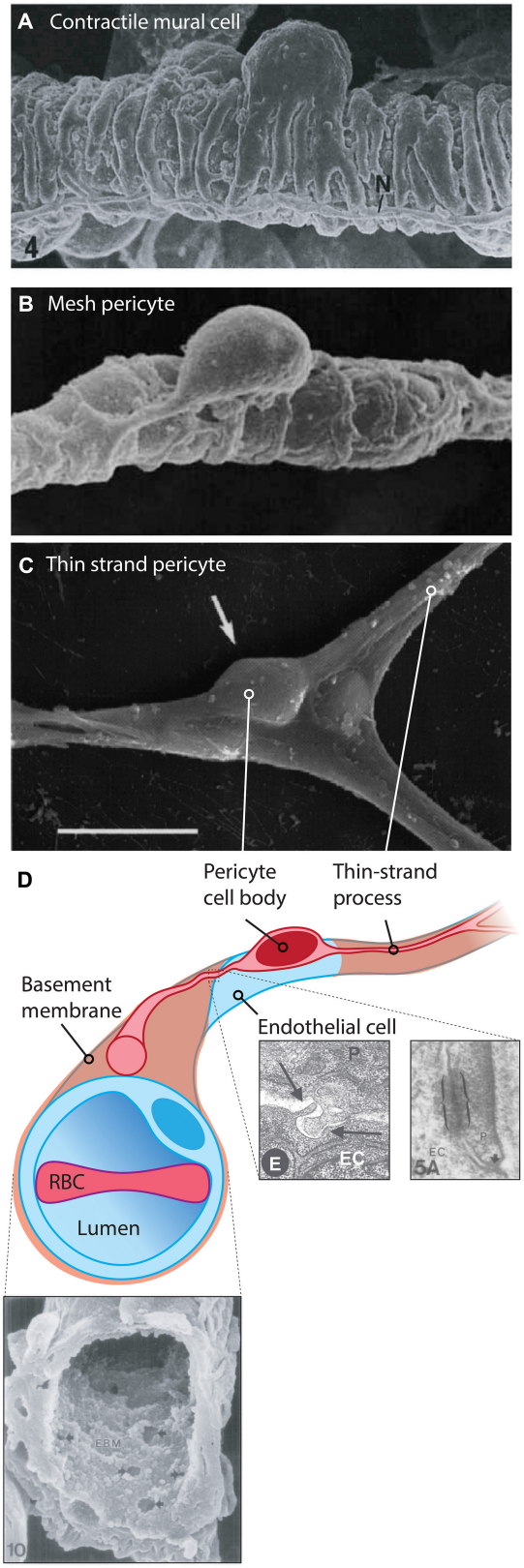

FIGURE 3 | Cytoarchitecture and microenvironment of pericytes. **(A)** Mural cells with a 'bump-on-a-log' cell body, with multiple contractile processes that *(Continued)*

FIGURE 3 | almost completely encase the underlying vessel. 6,000x, rat mammary gland vasculature. Reproduced with permission from Fujiwara and Uehara (1984). **(B)** A 4,400x magnification scanning electron micrograph of a putative mesh pericyte of the rat mammary gland. Multiple sparse processes enwrap the underlying capillary. Reproduced with permission from Fujiwara and Uehara (1984). **(C)** A thin-strand pericyte atop a rat retinal capillary, extending fine processes away from the ovoid cell body. Adapted with permission from Sakagami et al. (1999). Scale bar: 10 μm. **(D)** Illustration of a thin-strand pericyte. The bulk of the volume of the cell body is occupied by the nucleus. The pericyte is prevented from making direct contact with the underlying EC by the basement membrane, shown in the SEM at *bottom left*, reproduced with permission from Carlson (1989). Multiple small fenestrations are seen in this structure, allowing for pericyte and endothelial projections to make direct contact with one another, forming so-called 'peg-socket junctions' which are also sites of gap junction formation. At *bottom right* electron micrographs depicting a peg-socket junction (left) and a pericyte-endothelial gap junction (right) are shown, reproduced with permission from Díaz-Flores et al. (2009) and Carlson (1989). Abbreviations in micrographs: EC, endothelial cell; N, nerve; P, pericyte.

degree of rectification as strongly-rectifying ($K_{ir}2.x$, $K_{ir}3.x$), intermediately-rectifying ($K_{ir}4.x$) or weakly-rectifying ($K_{ir}1.1$, $K_{ir}6.x$, $K_{ir}7.x$). Alternatively, this group of channels can be classified according to function into classic ($K_{ir}2.x$), G-protein sensitive ($K_{ir}3.x$), K_{ATP} ($K_{ir}6.x$), or K^+ transport ($K_{ir}1.x$, $K_{ir}4.x$, $K_{ir}5.x$, $K_{ir}7.x$) channels (Hibino et al., 2010). Of the K_{ir} channel family, capillary pericytes express extremely high levels of $K_{ir}6.1$—far exceeding that of any other ion channel gene expressed by brain pericytes—and to a lesser extent $K_{ir}2.2$ (Bondjers et al., 2006; He et al., 2018; Vanlandewijck et al., 2018).

As $K_{ir}6.1$ is a component of K_{ATP} channels, this suggests that the two key roles of these channels—providing membrane hyperpolarization and coupling metabolism to membrane electrical activity—could be major contributors to pericyte physiology. Functional K_{ATP} channels are hetero-octameric assemblies of four two-transmembrane spanning pore–forming $K_{ir}6.x$ subunits (either $K_{ir}6.1$ or $K_{ir}6.2$, encoded by *Kcnj8* and *Kcnj11*, respectively), each associated with a regulatory 17-transmembrane spanning ATP-binding cassette subfamily sulfonylurea subunit (SUR1 or SUR2, respectively encoded by *Abcc8* and *Abcc9*—the latter of which is also highly expressed in brain pericytes; **Figure 5A**; Seino and Miki, 2003; Li et al., 2017). SURs are required for membrane trafficking of the channel (Burke et al., 2008) and impart sensitivity to K_{ATP} agonists and antagonists and intracellular nucleotides. Alternative splicing yields a number of SUR2 variants with SUR2A and SUR2B as the major forms, differing by just 42 amino acids in their C-terminal domains (Seino and Miki, 2003). Thus, the available expression data suggest that K_{ATP} channels native to brain pericytes are composed of $K_{ir}6.1$ and SUR2—often referred to as the "vascular" form of K_{ATP}–and indicates that these are expressed much more highly in pericytes than they are in cerebral SMCs and ECs (**Figure 4C**).

K^+ currents through K_{ATP} channels are weakly rectifying at potentials very positive to E_K–the result of voltage-dependent intracellular magnesium (Mg^{2+}) block (Findlay, 1987). The defining biophysical feature of K_{ATP} channels is that open probability (P_o) decreases with increasing

BOX 1 | Potential gap junction configurations between capillary pericytes and cECs.

According to expression data (He et al., 2018; Vanlandewijck et al., 2018), pericytes predominantly express mRNA for connexin (Cx)37 and Cx45, along with much lower expression of Cx26 and Cx43. Capillary ECs, on the other hand, robustly express Cx43 and Cx45, with low levels of Cx37, whereas Cx26 is undetectable (see Figure). Electron microscopy has been used to visualize putative GJ sites between pericytes and ECs at peg-socket interdigitations. In contrast, similar sites between the processes of neighboring pericytes have yet to be clearly demonstrated. Nonetheless, a recent dye transfer study (Kovacs-Oller et al., 2020), has shown that the cells of the capillary bed form a syncytium. Accordingly, two configurations for cell-cell communication can be postulated: (i) Pericyte-EC GJs alone permit bidirectional transfer of intracellular materials and charge between cells of the capillary wall; (ii) both pericyte-EC GJs and pericyte-pericyte GJs permit intercellular communication along two parallel, closely adjacent paths. The latter configuration would provide redundancy in the event of cell-cell communication failing in one cell type.

GJs are homo- or hetero-dodecameric assemblies of Cx subunits (Koval et al., 2014), formed from two hexameric hemichannels that dock to yield intercellular channels. GJs can be homotypic, with both hemichannels composed of the same Cx isoform(s), or heterotypic, with each hemichannel consisting of a distinct assembly of 6 Cx subunits. Moreover, a given hemichannel may be homomeric (composed Cx monomers of the same isoform) or heteromeric (consisting of multiple Cx isoforms), a property that depends on the propensity of the locally expressed Cxs to co-assemble. These complexities yield channels with distinct attributes, which may further oligomerize into large GJ plaques with discrete population characteristics.

Considering pericyte connexins in isolation, α-class Cxs 37 and 45 are not known to assemble into heteromers, but both of these will heteromerize with the much more modestly expressed α Cx43. The β Cx26, on the other hand, is not compatible with α Cx isoforms. Thus, the available data suggest that the typical pericyte hemichannel is most likely to be a homomeric assembly of Cx37 or Cx45, with perhaps a low level of heteromerization involving Cx43. Similarly, the EC-expressed Cx43 will form heteromers with Cx37 and Cx45, but again the latter are not compatible with one another. Thus, the possibility of heteromerization appears to be higher for ECs. In terms of heterotypic compatibility in the formation of GJs, Cx37, Cx43, and Cx45 are known to readily assemble together, whereas Cx26 hemichannels will not dock with any of these.

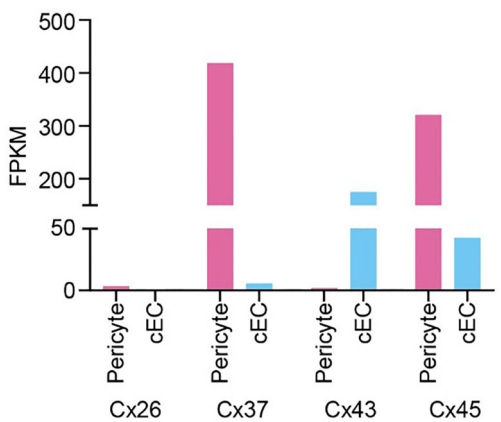

Taken together, this complexity underscores the great deal of further work needed to firmly establish the nature and properties of GJs in the capillary wall.

intracellular ATP levels, with ATP stabilizing the closed state of the channel (Enkvetchakul and Nichols, 2003). Thus, when cellular ATP demands are low and free cytosolic ATP is high, the channel is closed. In contrast, when cell activity increases or metabolism drops, the ADP:ATP ratio rises and the channel may open to hyperpolarize the membrane (Quayle et al., 1997). Consistent with these channels being saturated by ATP to keep them closed under resting conditions, the K_{ATP} channel blocker glibenclamide has no effects on resting CBF but levcromakalim, a K_{ATP} channel opener, increases global CBF by 14% (Al-Karagholi et al., 2020).

Nucleotide regulation of K_{ATP} channels is complex and has been best characterized for $K_{ir}6.2$/SUR1-containing channels, which we review briefly here. Intracellular nucleotides are sensed by an array of sites throughout the channel complex: ATP has been shown to bind to an inhibitory site of the $K_{ir}6.2$ subunit (Tucker et al., 1997; Tanabe et al., 2000) with just one of four subunits of the channel needing to bind ATP to effect closure (Markworth et al., 2000). The SUR1 subunit has two nucleotide binding domains (Li et al., 2017), where Mg^{2+}-bound adenosine diphosphate (MgADP) occupancy increases channel activity (Tung and Kurachi, 1991; Gribble et al., 1997; Shyng et al., 1997). MgATP also has a stimulatory effect here, likely through hydrolysis to MgADP, although this is normally masked by the much more potent inhibitory effect of free ATP (Gribble et al., 1998; Proks et al., 2010). Thus, as might be expected, increasing intracellular Mg^{2+} antagonizes the inhibitory effect of free ATP (Gribble et al., 1998). Conversely, in the absence of Mg^{2+}, ADP may have an inhibitory effect (Findlay, 1988). Comparatively less is known about the fine details of nucleotide regulation of $K_{ir}6.1$/SUR2B channels, which have a smaller conductance than their $K_{ir}6.2$-containing counterparts (~15–30 pS for $K_{ir}6.1$/SUR2B-containing channels vs. ~50–90 pS for the $K_{ir}6.2$/SUR2A form, for example; Hibino et al., 2010). However, it is clear that the presence of a nucleotide diphosphate and Mg^{2+} is a requirement for channel activity, and that these channels are also sensitive to ATP inhibition (Kajioka et al., 1991; Kovacs and Nelson, 1991; Beech et al., 1993; Kamouchi and Kitamura, 1994; Nelson and Quayle, 1995; Zhang and Bolton, 1996; Yamada et al., 1997).

One of the consequences of the nucleotide sensitivity of K_{ATP} channels is that they may act as sensors of the metabolic state of the cell and transduce changes in this parameter into adjustments of membrane voltage. This is perhaps best characterized in pancreatic β cells, where K_{ATP} channels composed of $K_{ir}6.2$ and SUR1 subunits couple glucose concentration with insulin secretion (Tarasov et al., 2004). Here, elevated glucose leads to an increase in intracellular ATP due to increased glucose metabolism. This closes K_{ATP} channels, which depolarizes the cell and drives Ca^{2+}-mediated insulin secretion through the activation of L-type voltage-dependent Ca^{2+} channels (VDCCs; MacDonald et al., 2005). Conversely, if glucose concentrations decrease the channel opens, hyperpolarizing the membrane to

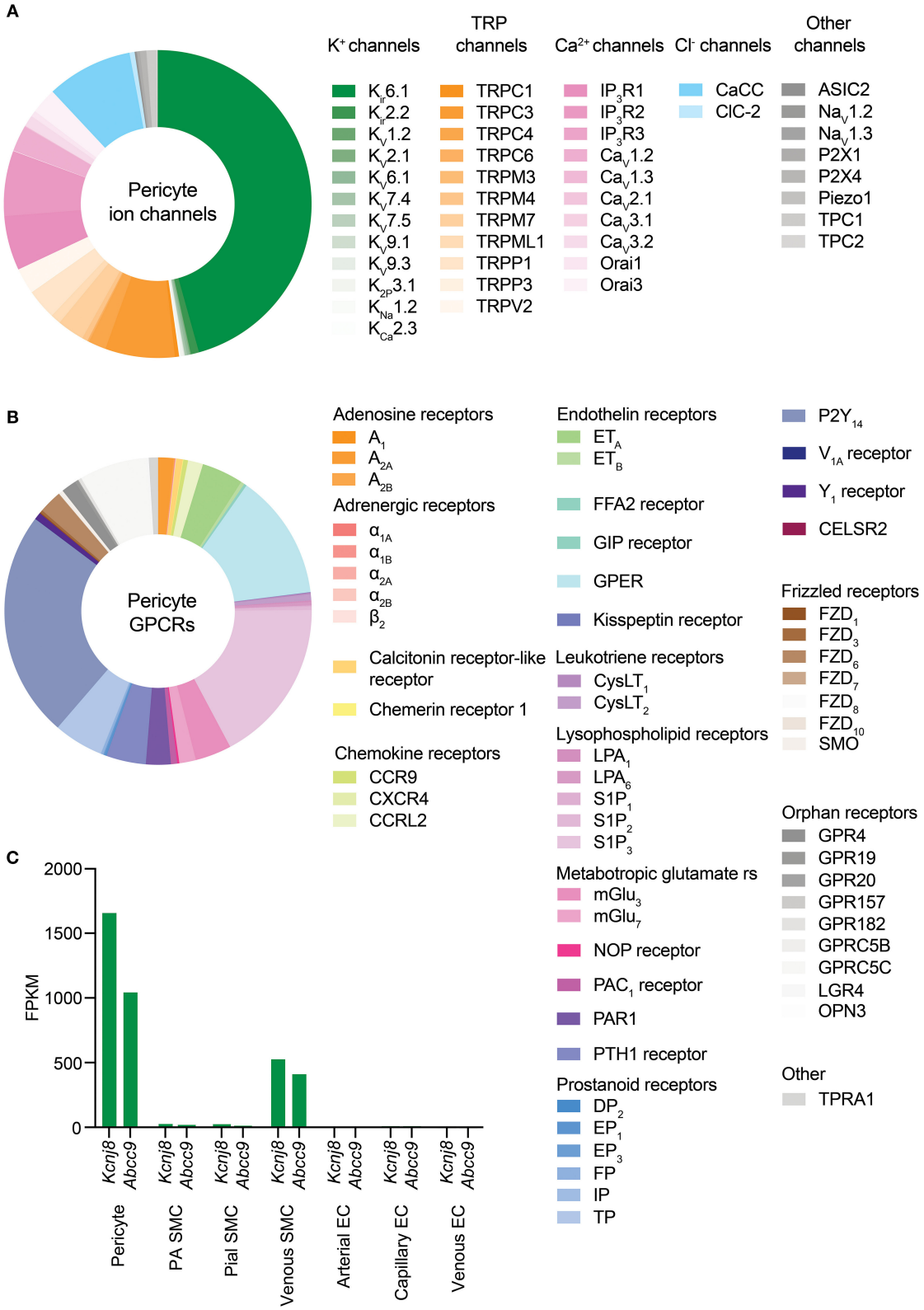

FIGURE 4 | Overview of CNS pericyte ion channel and GPCR expression. **(A)** Relative abundance of mRNA for all ion channel subunits meeting our inclusion criteria. The size of each segment represents the relative expression of the underlying gene. Channels are clustered on the basis of the ion species that the corresponding

(Continued)

FIGURE 4 | functional channel conducts (denoted by shading of the same color) and are then grouped by family/subfamily. K^+ channels are the predominant ion channel class due to extremely high expression of *Kcnj8* which forms the pore of vascular K_{ATP} channels. The non-selective TRP channels are the next highest expressed, followed by Ca^{2+} channels, Cl^- channels, and lower expression of other channels. **(B)** Relative expression of pericyte GPCRs. Here, receptors are organized by ligand sensitivity or class. **(C)** Expression of the K_{ATP} channel genes *Kcnj8* and *Abcc9* throughout the brain vasculature. Pericytes express both genes at much higher levels than arterial SMCs or ECs. However, venous SMCs also express high levels of K_{ATP} channel-forming genes.

prevent insulin release. In an analogous situation, K_{ATP} channels composed of $K_{ir}6.2$ and SUR1 are involved in glucose sensing and glucagon secretion in the ventromedial hypothalamic neurons of the hypothalamus (Miki et al., 2001).

Like many other channels (Hille et al., 2015; Dickson and Hille, 2019), K_{ATP} channels containing $K_{ir}6.2$ pore-forming subunits are also influenced by the concentration of intracellular phosphoinositides, such as phosphoinositol-4,5-bisphosphate (PIP_2; Fan and Makielski, 1997). In $K_{ir}6.2$-containing channels, ATP and PIP_2 compete for residues on overlapping binding sites on the pore forming subunit, each subtly altering channel conformation to stabilize closed or open states, respectively (Enkvetchakul and Nichols, 2003), with PIP_2 additionally uncoupling the pore-forming subunit from its SUR companion (Li et al., 2017). Exposure of these K_{ATP} channels to PIP_2 decreases ATP affinity ($K_{0.5}$) in excess of two orders of magnitude from ∼10 μM to ∼3.5 mM, and furthermore in the absence of ATP increases channel P_o (Shyng and Nichols, 1998). As the abundance of PIP_2 thus regulates P_o, this raises the possibility that cell signaling that impinges upon PIP_2 levels may subsequently affect channel activity. $K_{ir}6.1$/SUR2B channels, in contrast, appear to have a much higher affinity for PIP_2 than $K_{ir}6.2$ channels. Accordingly, PIP_2 is thought to bind so tightly here as to be saturating, and thus physiological fluctuations of this phospholipid do not influence channel activity (Quinn et al., 2003; Harraz et al., 2020). However, a number of intracellular signaling pathways have been established to dramatically influence vascular K_{ATP} activity. Indeed, phosphorylation by protein kinase C (PKC), lying downstream of DAG, decreases the P_o of $K_{ir}6.1$/SUR2B channels (Bonev and Nelson, 1996; Shi et al., 2008b) and in stark contrast, protein kinase A (PKA), which is stimulated as a result of G_s-coupled GPCR engagement, phosphorylates K_{ATP} to increase P_o (Kleppisch and Nelson, 1995; Bonev and Nelson, 1996; Quinn et al., 2004; Shi et al., 2007, 2008a).

Accordingly, there appear to be two major possible avenues through which vascular K_{ATP} channels could be engaged in pericytes:

i) Changes in metabolism may couple K_{ATP} channel activity to membrane hyperpolarization.

It is possible that brain pericyte K_{ATP} channels act as sensors of the metabolic state of the cell and adjust membrane potential in response to perturbations in energy supply. Notably, the expression of the glucose transporter GLUT1 is incredibly high in astrocytes and brain ECs compared to pericytes, which express much lower levels of GLUTs 1, 3 and 4 (He et al., 2018; Vanlandewijck et al., 2018). Therefore, while astrocytes and capillary endothelial cells are well equipped for glucose import, the comparatively lower expression of GLUTs in the pericytes situated between them could make them more sensitive to subtle changes in glucose levels, such as local depletions that occur during neural activity (Hu and Wilson, 1997; Paulson et al., 2010; Li and Freeman, 2015; Pearson-Leary and McNay, 2016). Such decreases in glucose could impact pericyte metabolism, increasing the ADP:ATP ratio to open K_{ATP} channels and hyperpolarize the membrane.

However, as glucose can be transmitted via gap junctions (Rouach et al., 2008) it is possible that pericyte glucose needs are instead satisfied directly by the underlying ECs, enabling them to continually maintain a high level of cytosolic ATP. This latter possibility, coupled with evidence that metabolic regulation of vascular K_{ATP} channels in arteriolar SMCs requires either anoxia or extreme ATP consumption (Quayle et al., 2006)—circumstances of energetic compromise that are unlikely to be seen under physiological conditions (Quayle et al., 1997)—suggests that K_{ATP} metabolism-electrical coupling may be primarily relevant in pathological situations (e.g., stroke). In this context, metabo-electrical coupling may represent a last-ditch effort to stimulate blood flow and therefore replenish O_2 and glucose to regions in deep metabolic crisis. Further studies are needed to understand metabolic contributions to the control of pericyte K_{ATP} channels.

ii) Molecules that stimulate G_s signaling may engage pericyte K_{ATP} channels.

Pericytes express a broad repertoire of receptors that couple to the G_s signaling pathway, including those for purines, polyadenylate cyclase activating peptide (PACAP), parathyroid hormone (PTH) and prostaglandins (discussed in detail below, see **Table 2**). The release of these molecules into the paravascular space during neuronal activity could thus engage G_s signaling in local pericytes, culminating in the phosphorylation of K_{ATP} and channel opening. Indeed, in the retina (often used as a model of the NVU; see **Box 2**) the inhibitory neurotransmitter and metabolic byproduct adenosine hyperpolarizes the rat retinal pericyte membrane potential by ∼30 mV through K_{ATP} channel engagement resulting from A_1 and A_{2a} adenosine receptor activation (Li and Puro, 2001), likely through engagement of cAMP and PKA.

What would be the physiological consequence of such profound membrane hyperpolarization in pericytes? It has been proposed that K_{ATP}-generated hyperpolarization of pericytes in the retinal vasculature could be transmitted over long distances to close VDCCs in the mural cells of upstream vessels, thereby causing vasorelaxation and an increase in blood flow (Ishizaki et al., 2009). Such a mechanism could

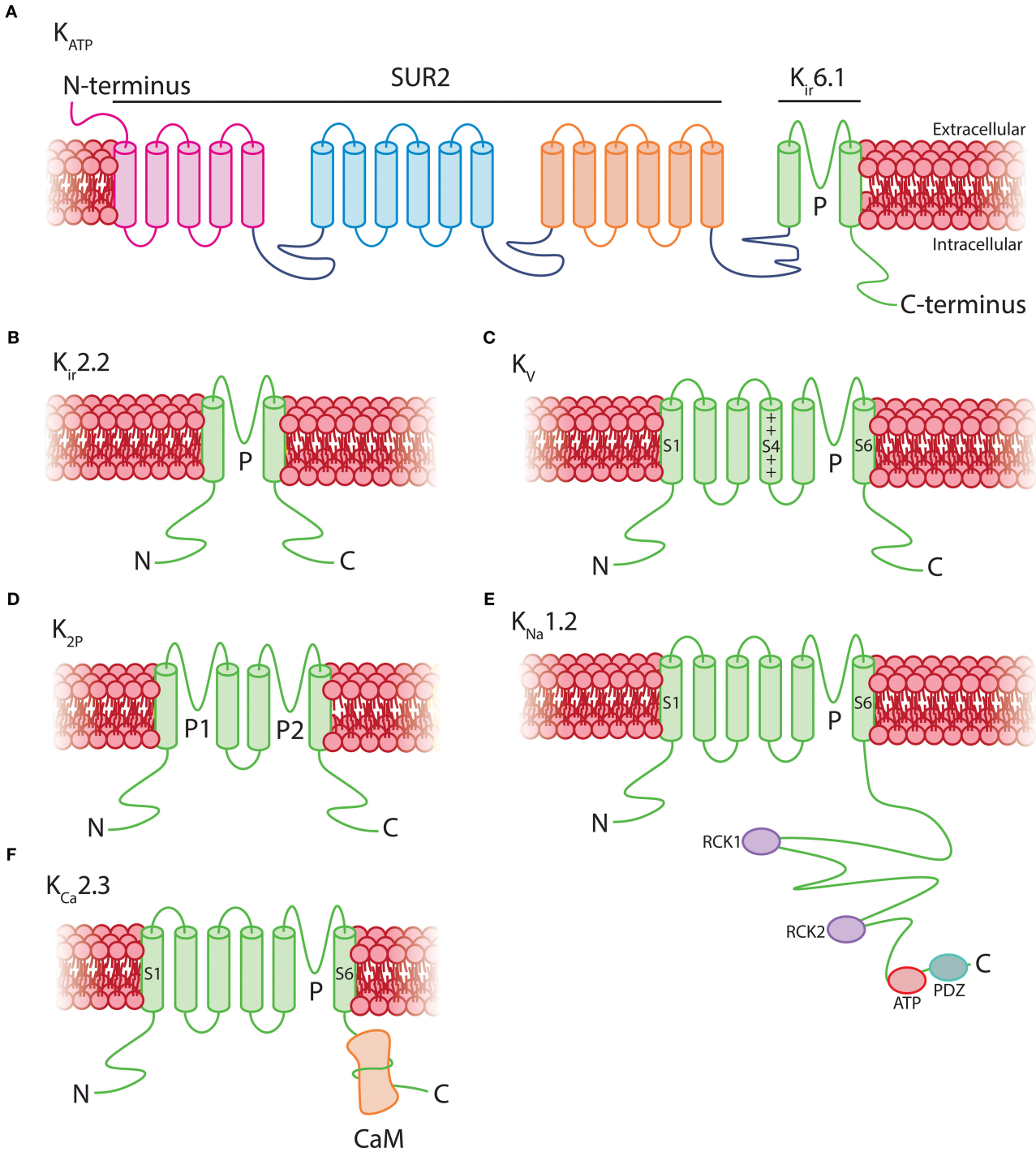

FIGURE 5 | Structural topology of K^+ channels expressed by pericytes. **(A)** Vascular K_{ATP} channels are octamers consisting of four 17-transmembrane SUR2 subunits associated with four 2-transmembrane pore-forming $K_{ir}6.1$ subunits. **(B)** $K_{ir}2.2$ channels consist of homo or heteromeric assemblies of four 2-transmembrane subunits. **(C)** K_v channels are composed of four 6-transmembrane alpha subunits with a positively charged voltage sensor at S4 which transduces changes in V_m into conformational alterations. **(D)** K_{2P} channels are tetramers of two-pore domain four-transmembrane subunits. **(E)** K_{Na} channels have a 6-transmembrane structure that lacks a voltage sensor, with multiple regulatory sites in the long intracellular COOH-terminus including two RCK domains, an ATP binding site, and a PDZ domain. **(F)** $K_{Ca}2.3$ channels consist of four 6-transmembrane domains which lack a voltage-sensor at S4. The COOH-terminus of each is associated with a calmodulin monomer, which imparts Ca^{2+} sensitivity to the channel.

BOX 2 | A brief comparison of retinal and brain vasculatures.

The retinal vasculature consists of two vascular beds—the outer layer of retinal photoreceptors is nourished by the choroidal vasculature, and the multilayered inner retinal vasculature provides oxygen and nutrients to the inner cell layers. The latter has a tightly regulated blood-retinal barrier, akin to the BBB, which pericytes help to maintain (Trost et al., 2016). Vascular density in the cerebral cortex varies according to the metabolic demand of the brain region it supplies (e.g., white vs. gray matter), whereas in the retina, capillary density tends to be greater in the center of the tissue and decreases toward the periphery (Patton et al., 2005). Both retinal and cerebral vascular cells have identical embryological origins: pericytes and SMCs derive from neuroectodermal neural crest cells and ECs derive from mesodermal hemangioblasts (Kurz, 2009; Dyer and Patterson, 2010). Structurally, the cortical and inner retinal vascular beds share a similar overall architecture, with a post-arteriolar transitional zone of 3–4 branches that are covered by contractile mural cells, leading to thin strand pericyte-covered deep capillaries (Ratelade et al., 2020). A distinction between these vascular beds is that the retinal vasculature is highly organized into two parallel plexi (Ramos et al., 2013), whereas cerebral capillaries form more elaborate three-dimensional geometries (Blinder et al., 2013). These structural differences could dictate differences in the flow of blood through each circulation and may necessitate distinctions in the signaling mechanisms that are utilized to direct blood flow through either bed. However, the vasculatures in both retina and cortex respond similarly to neuronal activity with elevations in blood flow (Newman, 2013), and similar mechanisms underpinning these responses appear to be at play in either bed. K^+, PGE_2, and EETs, for example, have been implicated in control of blood flow in both circulations (Newman, 2013; Longden et al., 2017; Gonzales et al., 2020). Recent studies have also indicated the utility of non-invasive examinations of the retinal vasculature as a marker for detecting cerebrovascular diseases, due to a similar susceptibility of both circulations to vascular risk factors such as hypertension or diabetes (Patton et al., 2005; van de Kreeke et al., 2018; McGrory et al., 2019; Querques et al., 2019). Data on gene expression in vascular cells of the retina are currently lacking, but would provide a useful standpoint for deeper comparisons of the similarities and differences between these vascular beds.

Studies on retinal pericytes (Li and Puro, 2001; Kawamura et al., 2002, 2003; Wu et al., 2003; Matsushita and Puro, 2006), on cerebral pericytes (Peppiatt et al., 2006; Fernández-Klett et al., 2010; Hill et al., 2015; Rungta et al., 2018), or both (Gonzales et al., 2020; Kovacs-Oller et al., 2020) have thus informed our current understanding of blood flow control and pericyte physiology. Although it is clear that a high degree of similarity exists between these vascular beds, the possibility of yet-to-be-identified differences between these networks should be borne in mind when attempting to draw generalizations from data from both vascular beds. To this end, we note explicitly where data on pericytes in this review were drawn from studies performed in retina.

be enabled by transmission of hyperpolarizing signals either between pericytes themselves, or between pericytes and ECs. Indeed, hyperpolarizations transmitted to cECs are predicted to engage $K_{ir}2.1$ channels, which we have recently shown to rapidly propagate hyperpolarizing signals over long distances through the brain endothelium to upstream arterioles, causing their dilation and an increase in blood flow (Longden and Nelson, 2015; Longden et al., 2017). A similar mechanism involving both K_{ATP} and $K_{ir}2.1$ channels has also recently been shown to be critical for control of blood flow in the heart (Zhao et al., 2020). In the brain, connexin (Cx)37, and Cx45 are highly expressed in pericytes (He et al., 2018; Vanlandewijck et al., 2018; see **Box 1**), and thus these likely form cell-cell GJs that facilitate long-range transmission of K_{ATP}-mediated electrical signals (**Figure 6**).

$K_{ir}2$ channels are activated not only by membrane hyperpolarization, but also by external K^+, which is an important mediator of NVC (Filosa et al., 2006; Longden and Nelson, 2015; Longden et al., 2017). Neurons or astrocytes release K^+ into the perivascular space during NVC, and its concentration can reach ∼10 mM during concerted activity (Orkand et al., 1966; Newman, 1986; Ballanyi et al., 1996; Kofuji and Newman, 2004). Interestingly, $K_{ir}2.2$ channels are expressed in pericytes (**Table 1** and **Figure 5B**) and K_{ir} currents with the expected biophysical characteristics and sensitivity to micromolar barium (Ba^{2+}) have been reported in cultured retinal and heart pericytes (von Beckerath et al., 2000; Quignard et al., 2003), and retinal and kidney pericytes from microvessels (Cao et al., 2006; Matsushita and Puro, 2006). Strong rectification in $K_{ir}2$ channels results from intracellular polyamine and Mg^{2+} block of the channel pore at depolarized membrane potentials, limiting outward current. This block is relieved by elevating external K^+ to levels that are typically seen during neuronal activity, initiating rapid and self-perpetuating hyperpolarization that drives V_m toward E_K (Longden and Nelson, 2015). Thus, pericyte $K_{ir}2.2$ channels could contribute to transmitted hyperpolarizations in several ways. On one hand, K^+ elevations resulting from neural activity may directly activate $K_{ir}2.2$ channels on pericytes (**Figure 6**). Alternatively, engagement of pericyte K_{ATP} channels could cause a K^+ or hyperpolarization-mediated recruitment of $K_{ir}2.2$ channels, which would serve to amplify hyperpolarization. $K_{ir}2.2$ channels could then propagate hyperpolarizing signals from capillary pericytes to upstream vessels by means of pericyte-pericyte communication through their thin-strand processes or by passing hyperpolarization to neighboring ECs via pericyte-endothelial GJs. PIP_2 is also central to $K_{ir}2$ channel function (D'Avanzo et al., 2010; Hansen et al., 2011), and its depletion via G_qPCR signaling has recently been shown to play an important role in regulating $K_{ir}2.1$ channel activity in cECs (Harraz et al., 2018). Accordingly, signaling processes that influence PIP_2 levels are anticipated to factor in to $K_{ir}2.2$ channel activity in pericytes.

Collectively, genetic and functional data to date argue for an important role of K_{ATP} and $K_{ir}2.2$ channels in regulating pericyte electrical activity, and we thus propose that the activity of these channels plays a central role in the control of capillary blood flow (**Figure 6**).

Voltage-Gated K^+ (K_v) Channels Provide Graded Opposition to Membrane Depolarization

K_v channels are formed by 4 identical subunits that surround a central pore. Each subunit is composed of six transmembrane segments (S1–S6) of which four form the voltage sensor domain (S1–S4) with several regularly spaced positively-charged amino acids in the S4 helix playing a central role in transducing voltage into conformational changes that gate the channel. The

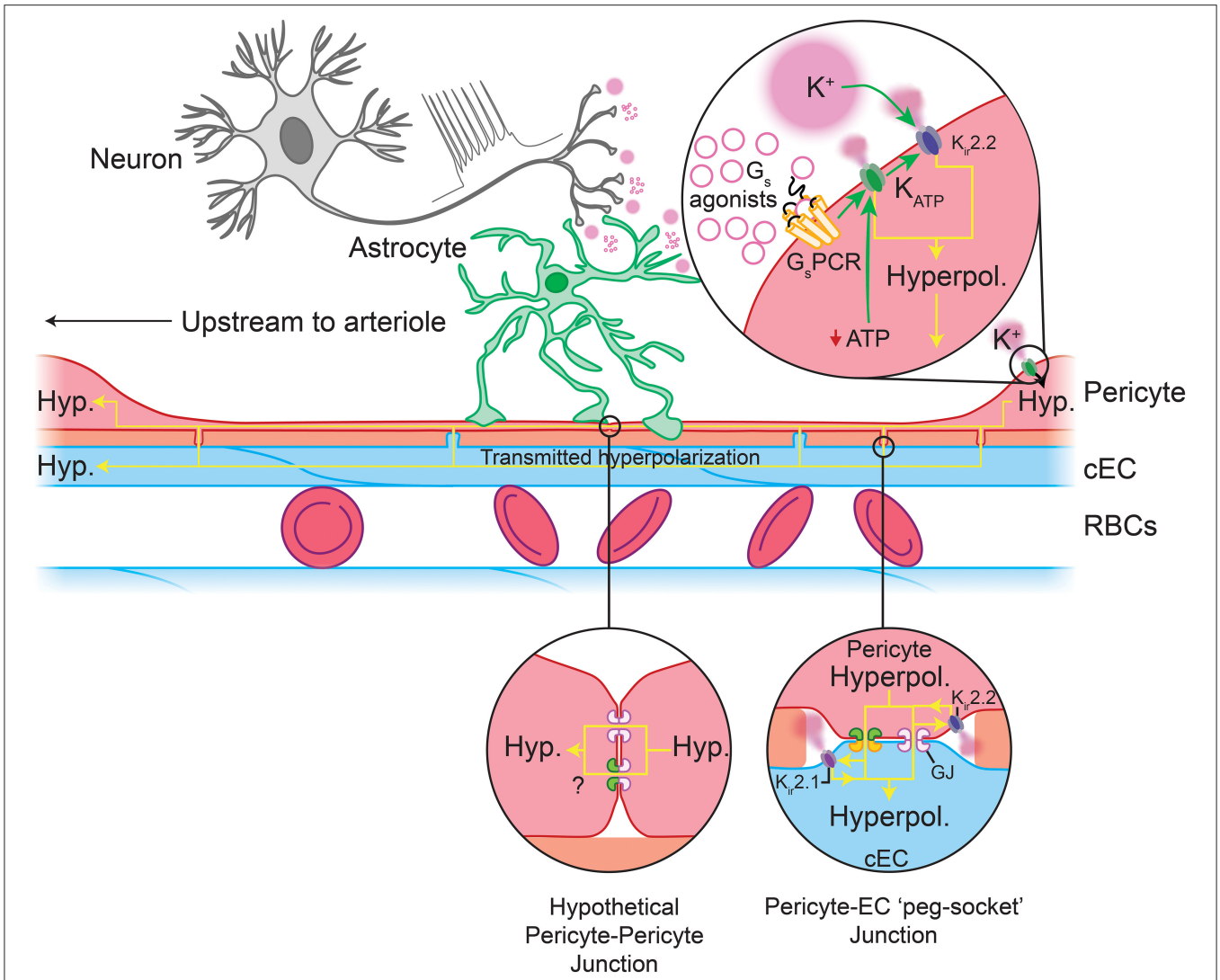

FIGURE 6 | Predicted capillary pericyte-EC interactions to control local blood flow. Neuronal activity drives the release of K^+ and G_sPCR agonists. *Top inset:* These are predicted to engage pericyte $K_{ir}2.2$ and their cognate GPCRs, respectively. G_sPCR activity activates K_{ATP} channels, the hyperpolarization by which may feed forward to evoke further $K_{ir}2.2$ activity (a sufficient fall in ATP:ADP would also engage K_{ATP} channels). The hyperpolarization generated by these channels may then be passed via gap junctions to cECs (*bottom right inset*) or possibly to adjacent pericytes, though direct pericyte-pericyte gap junctions have not been observed to date. In cECs, the incoming hyperpolarization will engage $K_{ir}2.1$ channels to amplify hyperpolarization to a sufficient level to pass to adjacent cECs and pericytes. Hyperpolarization-mediated activation of $K_{ir}2.1$ and $K_{ir}2.2$ in these cells will rapidly regenerate the current so that it can be passed to the next cell, and so on upstream to the arteriole. Upon arrival at the arteriole and its first few offshoots, hyperpolarization will be passed via GJs at MEPs to SMCs and to contractile mural cells, which will close VDCCs, leading to a fall in intracellular Ca^{2+}, relaxation of their actin-myosin contractile machinery, vasodilation, and an increase in blood flow.

remaining two transmembrane regions line the K^+-selective pore (S5–S6; **Figure 5C**; Jiang et al., 2003; Chen et al., 2010).

In order of mRNA abundance, cerebral pericytes express modest to low levels of genes encoding: $K_v6.1$, $K_v7.4$, $K_v2.1$, $K_v9.3$, $K_v9.1$, $K_v7.5$, and $K_v1.2$, in the absence of K_v beta subunits (**Table 1**). Outward K^+ currents attributable to K_v channels have been measured in these cells, for example in guinea pig cochlear stria vascularis and cultured bovine retinal pericytes (von Beckerath et al., 2000; Quignard et al., 2003; Liu et al., 2018). K_v channels are crucial for negative feedback regulation of V_m, their P_o and unitary currents increasing with membrane depolarization to provide a counterbalancing hyperpolarizing influence (Nelson and Quayle, 1995; Koide et al., 2018). Their activity can also be modulated by a range of intracellular signaling cascades that engage varied effectors such as PKC, c-SRC or Rho-kinase (which inhibit K_v channels) or cAMP-PKA and cyclic guanosine monophosphate(cGMP)-protein kinase G (PKG) signaling pathways (which promote channel activity) (Jackson, 2018). Of note, nitric oxide (NO) can exert major signaling effects via soluble guanylate cyclase (sGC) and cGMP-PKG in pericytes (Denninger and Marletta, 1999). As adjacent cECs are a major source of local NO (Longden et al., 2019), its

elevation may be sufficient to engage pericyte PKG signaling to promote activity of K_V and other PKG-sensitive channels.

Cerebral arteriolar SMCs are each estimated to express ∼3,000 K_v channels/cell (Dabertrand et al., 2015) composed principally of K_v1.2 and K_v1.5 (Straub et al., 2009) with activation initially detectable above −40 mV and increasing e-fold per 11-13 mV, exhibiting half-activation between approximately −10 and 0 mV (Robertson and Nelson, 1994; Straub et al., 2009). These channels also exhibit substantial steady-state inactivation over the physiological voltage range (Robertson and Nelson, 1994). K_v currents with similar characteristics have been described in cultured retinal pericytes (Quignard et al., 2003), whereas the half-maximal activation of K_v channels recorded in cultured coronary pericytes is substantially more negative at −40.9 mV, along with a steeper voltage-dependence of activation (e-fold per 4.6 mV) and only modest inactivation at physiological membrane potentials (von Beckerath et al., 2000). Thus, K_v current characteristics in pericytes appear to be regionally dependent, likely a result of differential expression and assembly of distinct K_v isoforms. Direct characterization of K_v currents in native brain pericytes is therefore critical to furthering our understanding of their role in the control of pericyte V_m, where these channels are anticipated to provide negative feedback to limit depolarization effected by the activity of depolarizing ion channels in pericytes, such as those of the TRP family.

K_{2P}3.1 Channels Provide a Background K^+ Conductance and May Impart pH Sensitivity

K_{2P} channels contribute to maintenance of resting membrane potential due to steady outward K^+ "leak" at potentials positive to E_K. They comprise a family of 15 members, and are composed of two identical subunits, each with four transmembrane domains with two pore-forming loops making up a central K^+-conducting pore (**Figure 5D**; Miller and Long, 2012; Lolicato et al., 2014). K_{2P}3.1, also known as the two-pore domain weakly inwardly-rectifying K^+ channel (*T*WIK)-related *a*cid-sensitive *K*$^+$ (TASK)-1 channel (Duprat et al., 1997), is the only K_{2P} isoform expressed in capillary pericytes, and is also expressed in cerebral SMCs (He et al., 2018; Vanlandewijck et al., 2018). In SMCs, its steady current contributes to maintaining a relatively negative V_m by counterbalancing depolarizing influences (Gurney et al., 2003).

Perhaps the most well-studied characteristic of TASK-1 is its sensitivity to pH within the range of ∼6.5–8. Acidic pH inhibits channel activity while alkaline pH increases it, with half-maximal activation occurring at pH 7.4 and ∼90% of maximal TASK-1 current recorded at pH 7.7 (Duprat et al., 1997). Synchronous neuronal activity can cause rapid changes in pH. For example, alkalization in extracellular pH has been observed in the hippocampus, cerebellum and some cortical areas, by up to 0.2 units (Chesler and Kaila, 1992; Makani and Chesler, 2010). Thus, it is possible that in addition to setting resting V_m, K_{2P}3.1 imparts sensitivity to pericytes in these regions to such shifts, which could hyperpolarize V_m to modulate blood flow through the mechanisms described above.

Na^+- and Ca^{2+}-Activated K^+ Channels Are Expressed at Low Levels in Pericytes

Capillary pericytes also express low levels of genes encoding the Na^+-activated K_{Na}1.2 channel and the Ca^{2+}-activated K_{Ca}2.3 channel (**Table 1**). K_{Na}1.2 channels (**Figure 5E**) are sensitive to intracellular Na^+ and Cl^-, and are dramatically stimulated by cell swelling and inhibited by a decrease in cell volume (Bhattacharjee et al., 2003; Tejada et al., 2014). Thus, they could impart sensitivity to pericyte volume changes, and may respond to fluctuations in intracellular ion concentrations or metabolic state.

K_{Ca}2.3 (also known as SK3) belongs to the family of small-conductance Ca^{2+}-activated K^+ (SK) channels that share overall transmembrane topology with K_v channels, yet lack a functional voltage-sensor at S4 (**Figure 5F**; Adelman et al., 2012). Each subunit in the tetrameric channel is associated with a calmodulin (CaM) monomer via a CaM binding domain in the C-terminal region. Ca^{2+} binding to CaM induces a conformational change which leads to rapid channel opening, with an EC_{50} for Ca^{2+} of 300–500 nM (Ledoux et al., 2006; Adelman et al., 2012). If functional SK channels in native pericytes are confirmed, they are expected to facilitate coupling between Ca^{2+} elevations and membrane hyperpolarization.

PERICYTE TRP CHANNELS

The TRP channel family mediates cellular responses to a wide range of stimuli (Clapham, 2003). These are non-selective cation channels that depolarize the membrane upon activation and, in many cases, conduct significant amounts of Ca^{2+}. In mammals there are six subfamilies of TRP channels encoded by 28 genes, 11 of which are expressed by capillary pericytes. These are canonical (TRPC1, TRPC3, TRPC4, TRPC6), melastatin (TRPM3, TRPM4, TRPM7), mucolipin (TRPML1), poly-cystin (TRPP1, TRPP3), and vanilloid (TRPV2) channels (Earley and Brayden, 2010; He et al., 2018; Vanlandewijck et al., 2018). Functional TRP channels are tetramers of subunits with a common six transmembrane structure, which can assemble into homomeric or heteromeric functional channels. Their tendency to heteromerize, generally with closely related members, can give rise to channels with unique sensing capabilities and biophysical properties (Venkatachalam and Montell, 2007). Overall, subfamily members share ∼35% amino acid sequence homology, with the majority of this diversity arising from differences in their cytoplasmic domains (**Figure 7**; Clapham, 2003; Nilius and Owsianik, 2011). While they have been traditionally described as "non-selective," the pattern of ion selectivity for different cations varies between subfamilies (Hill-Eubanks et al., 2014; see **Table 1**).

Broadly speaking, TRP channels are major downstream effectors for GPCR signaling (Clapham, 2003; Veldhuis et al., 2015), with particular second messenger systems both activating or sensitizing some TRP channels, and decreasing the activity of others. TRPC channels are Ca^{2+} permeable and typically activated by plasmalemmal GPCRs or tyrosine kinase receptors that activate PLC isoforms (Albert, 2011). TRPC3/6 channels are directly activated by DAG, which is liberated by G_q signaling, and inhibited by PIP_2, which decreases during G_q

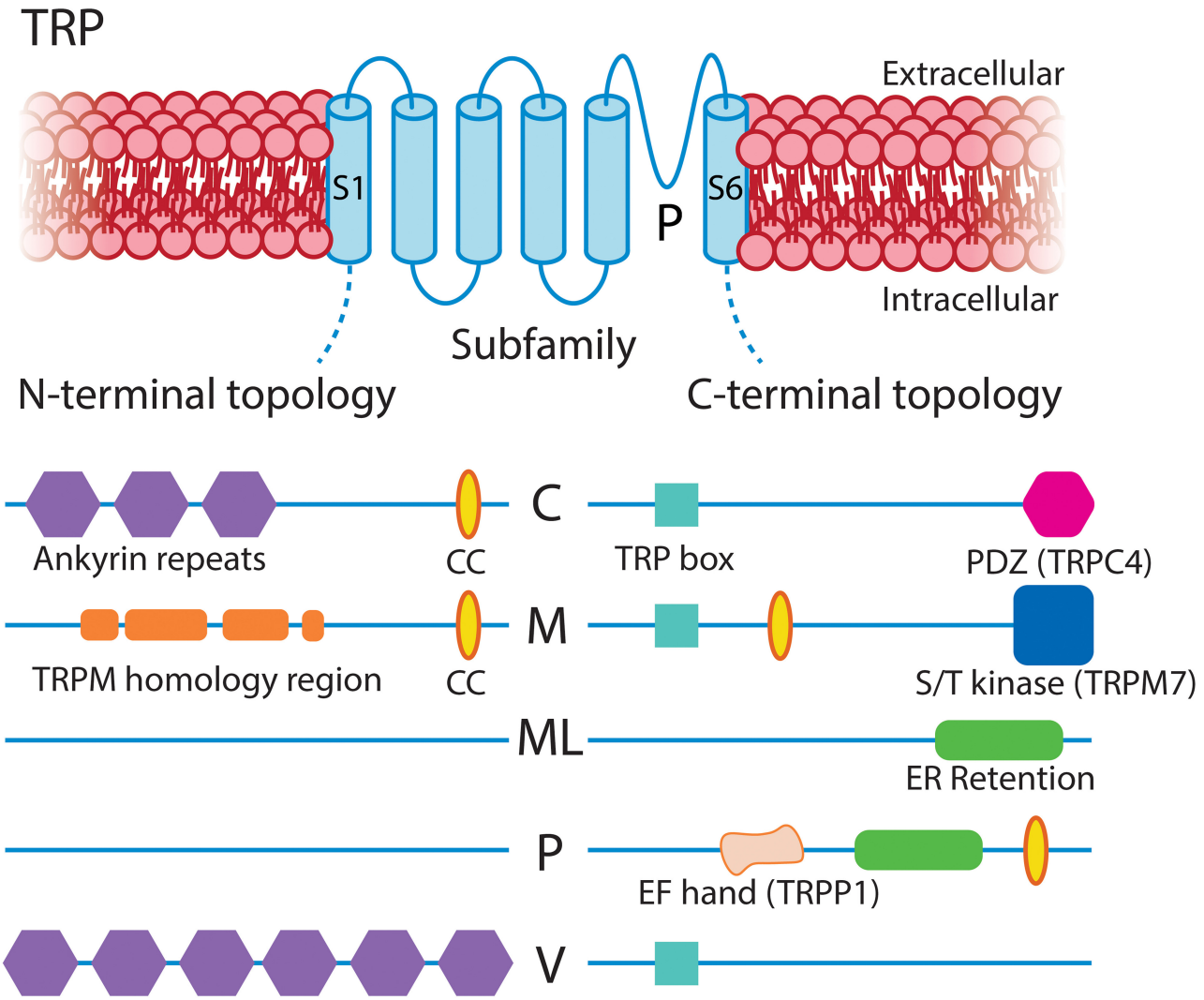

FIGURE 7 | Structural overview of the TRP families expressed in CNS capillary pericytes, adapted with permission from Clapham (2003). All TRP channels share a common and typical 6-transmembrane structure with profoundly varying intracellular N- and C-terminal domains, the major features of which are illustrated. CC, coiled-coil domain.

activity (Hofmann et al., 1999; Albert, 2011). The activation mechanisms of TRPC4 are less clear, whereas TRPC1-containing channels are unresponsive to DAG and are instead gated by PIP_2 in a PKC-dependent manner (Hofmann et al., 1999; Albert, 2011), although heteromultimerization with TRPC3 can convey DAG sensitivity (Lintschinger et al., 2000). TRPC3 is the most robustly expressed TRP channel in capillary pericytes (**Table 1**) and is thus likely to be engaged during G_qPCR-DAG signaling. This channel permits robust Ca^{2+} entry, although it has relatively low selectivity for Ca^{2+} over Na^+ (pCa^{2+}:pNa^+ ~1.5; Pedersen et al., 2005). At the arteriolar level, TRPC3 has been implicated in mediating vasodilation through elevations of EC Ca^{2+} leading to $K_{Ca}2.3$ activation (Kochukov et al., 2014), whereas its activation in SMCs mediates arteriolar constriction through a mechanism involving an IP_3R-activated (sarcoplasmic reticulum (SR) Ca^{2+} release independent) TRPC3-dependent Na^+ current that depolarizes V_m and activates VDCCs (Xi et al., 2009). Similar couplings may occur in capillary pericytes, likely depending on the macromolecular organization of TRPC3 with other local signaling elements.

Members of the TRPC subfamily, in particular TRPC1, have also been suggested to participate in store-operated Ca^{2+} entry (SOCE)—an event activated by the depletion of endoplasmic reticulum (ER) Ca^{2+} stores that depends on Orai1 and the ER-Ca^{2+} status sensing protein stromal interaction molecule 1 (STIM1; Huang et al., 2006; Soboloff et al., 2006; Cheng et al., 2008, 2013). Capillary pericytes express STIM1 and Orai1 and 3 (**Table 1**), and thus a functional interaction between TRPC1 and these proteins could be important for SOCE in pericytes. Recent work also shows TRPM7 activation, although not essential, can positively modulate SOCE (Souza Bomfim et al., 2020).

The melastatin channel TRPM4 is unique in its exclusive permeability to monovalent cations. Na^+ currents through TRPM4 are voltage-dependent and activated by intracellular Ca^{2+} (EC_{50} ~20 μM) with the Ca^{2+} sensitivity of the channel regulated by multiple factors including cytosolic ATP, PKC-dependent phosphorylation and calmodulin (Nilius et al., 2005; Ullrich et al., 2005). In cerebral SMCs, membrane stretch indirectly activates TRPM4 (and TRPC6) current through angiotensin II AT_1 receptor activation and a resultant IP_3-mediated Ca^{2+} elevation (Gonzales et al., 2014). Pericytes also express the AT_1 receptor, and thus a similar mechanism may be present in capillary pericytes which could contribute to the mild, slow constrictions these cells are capable of Fernández-Klett et al. (2010). In contrast to the monovalent conductance of TRPM4, the closely related TRPM3 and TRPM7 channels are also permeable to Ca^{2+} and Mg^{2+} (Pedersen et al., 2005). TRPM3 is activated by cell swelling, the neurosteroid pregnenolone sulfate, and the metabolite D-erythro-sphingosine and related sphingosine analogs and thus may impart sensitivity to steroid and lipid signals to pericytes (Grimm et al., 2005; Wagner et al., 2008). As pericytes also robustly express the $S1P_3$ receptor (discussed below), it is likely that TRPM3 and $S1P_3$ respond in concert to locally released lipids, such as those released constitutively by ECs and RBCs (Selim et al., 2011; Ksiazek et al., 2015). TRPM7, in contrast, is ubiquitously expressed and plays a major role in Mg^{2+} homeostasis (Schlingmann et al., 2007).

Functional TRPP1 channels (encoded by the *Pkd2* gene) have a large conductance and conduct a significant amount of Ca^{2+} (Earley and Brayden, 2015). This channel has been implicated in mechanosensation when expressed alongside polycystic kidney disease (PKD)1 (Giamarchi and Delmas, 2007; Sharif-Naeini et al., 2009; Narayanan et al., 2013). As PKD1 is also present in pericytes, these channels may aid in the detection of local mechanical forces, such as paravascular fluid shear from the glymphatic system (Mestre et al., 2018), or those imparted through the very thin endothelium by changes in blood flow during neuronal activity, or through subtle changes in diameter of the underlying capillary. Similarly, the vanilloid family member TRPV2, also expressed in SMCs throughout the vasculature (Muraki et al., 2003), has been suggested to play a role in mechanosensation-evoked Ca^{2+} entry (Perálvarez-Marín et al., 2013). Continuing this theme, mechanosensory contributions have also been reported for TRPC1, TRPC6, and TRPM4 (Yin and Kuebler, 2010). Combined with the fact that pericytes also express Piezo1 (see below), this represents a broad mechanosensing repertoire, suggesting that pericytes may be exquisitely sensitive to a range of mechanical perturbations. The resultant Ca^{2+} elevation and depolarizing currents through the activity of these channels could couple to a number of processes, including driving further Ca^{2+} release from stores, and activation of VDCCs, $K_{Ca}2.3$ channels, or Ca^{2+}-activated Cl^- channels (CaCCs; discussed below). As recent work demonstrates that pericytes can subtly influence tone throughout the capillary bed (Fernández-Klett et al., 2010), mechanosensing and Ca^{2+}-mediated mechanisms may play an important role in influencing this process.

PERICYTE Ca^{2+} CHANNELS

The overall expression level of Ca^{2+} channels is similar to that of TRP channels in pericytes, composed of message for IP_3R subtypes and a range of VDCCs.

IP_3Rs Permit a Versatile Range of Ca^{2+} Signaling Behaviors in Response to Extracellular Signals

The vast majority of intracellular Ca^{2+} signals arise from either Ca^{2+} influx across the plasmalemma, or release from the SR/ER via IP_3Rs or ryanodine receptors (RyRs). IP_3Rs are enormous proteins (~1.3 MDa) formed by four IP_3R subunits. Three subunit isoforms—IP_3R1-3—exist, which are able to homo- or heterotetramize. Each individual subunit has six transmembrane segments: The fifth and sixth segments form a central ion-conducting pore that is connected via a linker to the peripheral bundle formed by transmembrane domains 1-4. The large cytoplasmic N-terminal domain contains the IP_3 binding site and a putative Ca^{2+} sensor region, and binding of IP_3 and Ca^{2+} leads to conformational changes which are transmitted to the pore to gate the channel (**Figure 8**; Fan et al., 2015; Baker et al., 2017; Hamada et al., 2017). IP_3R subtypes share ~70% homology and differ in their affinity for IP_3, with IP_3R2 being more sensitive than IP_3R1, and both of these subtypes being more sensitive than IP_3R3 (Tu et al., 2005; Iwai et al., 2007). Brain capillary pericytes express the genes encoding IP_3Rs 1 and 2 robustly, and a much lower level of IP_3R3, whereas RyRs are not appreciably expressed by these cells (He et al., 2018; Vanlandewijck et al., 2018; **Table 1**).

As described briefly above, G_qPCRs activating phospholipase Cβ (PLCβ) (Fisher et al., 2020), or receptor tyrosine kinases (RTKs) activating PLCγ, can mediate the formation of IP_3 and DAG from PIP_2. IP_3 then binds to IP_3Rs on the ER membrane, leading to Ca^{2+} release from the ER lumen (where Ca^{2+} is maintained between 100 and 800 μM; Burdakov et al., 2005) down its electrochemical gradient into the cytosol (<100 nM basal Ca^{2+}; Berridge, 2016). IP_3 and Ca^{2+} act as co-agonists at IP_3Rs (Bezprozvanny et al., 1991; Finch et al., 1991; Foskett et al., 2007) and channels display a biphasic sensitivity to Ca^{2+}, resulting in a characteristic bell-shaped concentration-response curve. In the presence of very low IP_3 levels, IP_3Rs are extremely sensitive to Ca^{2+} inhibition. However, a small increase in IP_3 concentration (to ~100 nM) profoundly reduces the sensitivity of the channel to Ca^{2+} inhibition, permitting dramatic increases in activity (Iino, 1990; Bezprozvanny et al., 1991; Finch et al., 1991; Foskett et al., 2007).

The resultant release of stored Ca^{2+} can take on a broad range of spatiotemporal profiles, which depend on many factors. To name just a few, these include the concentration of local IP_3 and Ca^{2+}, ER Ca^{2+} load, the type, and number of IP_3Rs expressed, their splice variation, whether they are homomers or heteromers, and the topology of the local microenvironment. Such intricacies provide the versatility to potentially generate a huge variety of Ca^{2+} signals that encode information through their amplitudes,

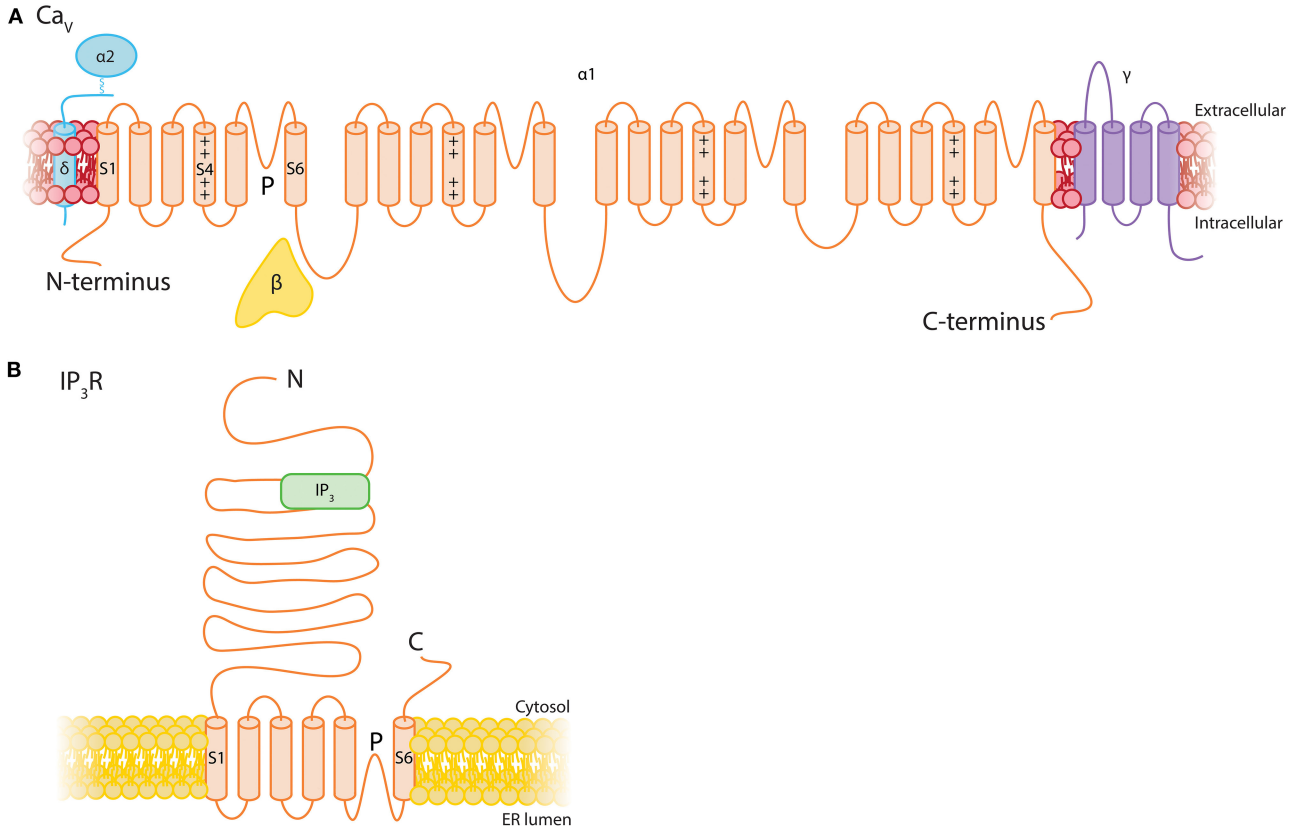

FIGURE 8 | Structural topology of Ca^{2+} channels expressed by pericytes. **(A)** The general structure of Ca_v channels consists of a single 24-transmembrane α subunit which is a repeat of a 6-transmembrane motif with an embedded voltage sensor connected by intracellular loops. This is accompanied by associated β, γ, and α2δ subunits. **(B)** IP_3Rs consist of a tetrameric assembly of 6- transmembrane subunits with a large N-terminal domain that contains the IP_3 binding site.

durations, frequencies, and spatial characteristics (Bootman and Bultynck, 2020). Despite these inherent complexities, a range of stereotyped IP_3R-mediated Ca^{2+} signals typically emerge. These range from the opening of single IP_3R (termed a "blip"), to the coordinated, weakly cooperative openings of a cluster of around 6 IP_3Rs within a release site (a "puff"), to finally—with sufficient IP_3–a long-range regenerative Ca^{2+} "wave" arising due to the recruitment of successive sites through the process of Ca^{2+}-induced Ca^{2+} release (CICR) (Berridge et al., 2000; Smith and Parker, 2009; Lock and Parker, 2020).

Store-mediated Ca^{2+} release has been observed in pericytes in a range of contexts. For example, pericytes of the ureter display long-duration IP_3R-mediated Ca^{2+} transients in response to the G_qPCR agonists endothelin-1 and arginine vasopressin. These signals are suppressed by elevations of Ca^{2+} in adjacent cECs, which are suggested to inhibit IP_3R activity through a NO-dependent mechanism (Borysova et al., 2013). Spontaneous ER Ca^{2+} release-dependent Ca^{2+} transients have also been observed in suburothelial capillary pericytes, which activate CaCCs to depolarize the membrane, subsequently recruiting VDCCs (Hashitani et al., 2018).

In the brain, recent studies have revealed that capillary pericytes generate microdomain Ca^{2+} oscillations under ambient conditions, and that neural activity evoked by odor leads to a transient cessation of these signals and a decrease in basal Ca^{2+}, which correlates with an increase in RBC velocity (Hill et al., 2015; Rungta et al., 2018). However, it is worthy of note that a decrease was not observed in similar experiments in which whisker stimulation was used to drive activity (Hill et al., 2015), suggesting the possibility of heterogeneity in the Ca^{2+} signaling machinery deployed by pericytes in different regions of the cortex. The specific ion channels and broader mechanisms that underlie these ambient signals have not yet been delineated, but IP_3Rs are obvious potential candidates. Elucidation of the mechanistic basis and roles of these Ca^{2+} signals in brain capillaries is critical, and awaits further experimentation.

Voltage-Dependent Ca^{2+} Channels Directly Link V_m to Ca^{2+} Entry

VDCCs are composed of four to five distinct subunits (α_1, β, $\alpha_2\delta$, and γ; **Figure 7**). The α_1 subunits are pore forming and responsible for the pharmacological diversity of different VDCC subtypes. These are associated with an intracellular β subunit, a disulphide-linked $\alpha_2\delta$ subunit, and in some cases a transmembrane γ subunit, each of which regulate surface

expression and tune the biophysical properties of the channel (Catterall et al., 2005). The large α_1 subunit is organized into four homologous domains, each comprising six transmembrane segments (S1-S6) with intracellular N- and C- termini. Similar to K_v channels, the S4 segment of each of these domains comprises the voltage sensor and the S5-S6 regions form the ion conducting pore (Catterall et al., 2005). Capillary pericytes express genes encoding the α subunits for L-type ($Ca_v1.2$, $Ca_v1.3$), P/Q-type ($Ca_v2.1$), and T-type ($Ca_v3.1$, $Ca_v3.2$) channels and thus we briefly review the salient properties of these here. They also express low levels of several genes encoding β and $\alpha_2\delta$ auxiliary subunits (He et al., 2018; Vanlandewijck et al., 2018).

As with K_v channels, VDCC activity depends on membrane potential: P_o steeply increases with depolarization, balanced by multiple feedback mechanisms that act to limit Ca^{2+} entry at depolarized potentials. Prominent among these are voltage- and Ca^{2+}-dependent inactivation. Voltage-dependent inactivation (VDI) is inherent to the α_1 subunit but is modulated by the ancillary β subunit and others, whereas Ca^{2+}-dependent inactivation (CDI) is conferred by a CaM monomer associated with the α_1 carboxy tail (Peterson et al., 1999; An and Zamponi, 2005; Dick et al., 2008; Tadross and Yue, 2010; Tadross et al., 2010). Regulation is additionally complicated by the panoply of alternative splice variants that can be expressed, which impact the biophysical properties of the functional channel, including sensitivity to CDI and VDI.

L-type channels are widely expressed, including in the heart, in skeletal and smooth muscle, and in neurons (Zamponi et al., 2015). $Ca_v1.2$ and $Ca_v1.3$ have distinct biophysical and pharmacological differences (Lipscombe et al., 2004)—$Ca_v1.3$ channels open and close on faster timescales than $Ca_v1.2$ (Helton et al., 2005), and are less sensitive to inhibition by dihydropyridines (Xu and Lipscombe, 2001). A C-terminal modulatory (CTM) domain can structurally interfere with CaM binding to decrease P_o and reduce CDI, an effect that is more pronounced in $Ca_v1.3$ than $Ca_v1.2$ (Striessnig et al., 2014). Moreover, in alternatively spliced $Ca_v1.3$ channels, the absence of a CTM domain can shift the voltage of half-maximal activation by ∼+10 mV by decreasing the slope factor of the activation curve without any effects on activation threshold (Singh et al., 2008). At physiological extracellular Ca^{2+} levels, the activation threshold of $Ca_v1.3$ is much more negative (-55 mV) than $Ca_v1.2$ (-25 to −30 mV) (Xu and Lipscombe, 2001). Thus, at pericyte resting V_m of around −45 mV, as measured in the retina (Zhang et al., 2011), $Ca_v1.3$ channels could be active and contribute to Ca^{2+} entry.

In addition to voltage- and Ca^{2+}-dependent inhibition, L-type VDCC activity is heavily regulated by GPCR signaling. Prominent among these, G_s-cAMP-PKA signaling has long been known to play an important role in stimulating channel activity, and has been studied extensively in the heart. Here, it was recently shown that the target of PKA phosphorylation is not the core channel itself, as mutation of all PKA consensus phosphorylation sites to alanine resulted in channels that retained PKA regulation. Rather, PKA acts via the small G protein Rad, a constitutive inhibitor of VDCCs. Phosphorylation of Rad relieves its interaction with β subunits, and allows channel activity (Liu et al., 2020). Further regulation of L-type channels by PKC, stimulated by DAG liberated as a result of G_qPCR activity, is also a possibility, with both inhibitory and potentiating effects having been observed (Kamp and Hell, 2000).

P- and Q-type currents are both attributable to $Ca_v2.1$, with the β subunit accompanying the pore-forming subunit thought to account for their differences (Zamponi et al., 2015). These channels have been best characterized in the nerve terminals and dendrites of neurons where they couple Ca^{2+} entry with neurotransmitter release (Zamponi et al., 2015) and also play a role in coupling Ca^{2+} entry to gene transcription via engagement of CaM kinase II (Wheeler et al., 2012). They open in response to similar depolarization levels as $Ca_v1.2$ channels, with an activation threshold of approximately −40 mV (Adams et al., 2009). Upon repetitive/tetanic stimulation, as occurs during neuronal activity, CaM can bind to two adjacent sites on the $Ca_v2.1$ α_1 subunit to mediate an initial Ca^{2+}-dependent facilitation (CDF) of P/Q-type current, followed by progressive CDI, with a relatively slow (30 s−1 min) recovery from this (Lee et al., 1999, 2000). While CDI of $Ca_v2.1$ requires a global Ca^{2+} increase, CDF can be promoted by Ca^{2+} entry through an individual $Ca_v2.1$ channel and results in an enhancement of channel P_o, enabling stimulation-evoked increases in amplitude and duration of Ca^{2+} currents (Chaudhuri et al., 2007). Slow and fast modes of $Ca_v2.1$ gating have been proposed. The slow mode exhibits longer mean closed times and latency to first opening, slower kinetics of inactivation, and necessitates larger depolarizations to open the channel. Inactivation also occurs at more depolarized potentials in the slow compared to fast mode (Luvisetto et al., 2004). The type of β subunit modulates the prevalence of these modes, with fast and slow gating mediated by β_{3a} and β_{4a} subunits, respectively (Luvisetto et al., 2004), the latter of which is expressed more robustly by brain pericytes (He et al., 2018; Vanlandewijck et al., 2018). $Ca_v2.1$ channels are inhibited by GPCR activity through several distinct mechanisms—direct binding of the G protein βγ dimer can augment VDI, while voltage-independent mechanisms such as phosphorylation, depletion of essential lipids, and trafficking mechanisms also play important roles (Zamponi and Currie, 2013).

T-type ($Ca_v3.1$ and $Ca_v3.2$) channels are activated at more negative potentials, around −60 mV, with rapid gating kinetics and small single channel amplitudes (Iftinca and Zamponi, 2009; Rossier, 2016). At membrane potentials of −65 to −55 mV, these channels exhibit window currents in which the channels open but do not inactivate completely, permitting ongoing Ca^{2+} entry (Perez-Reyes, 2003). These channels can be modulated by the activity of a broad range of GPCRs, including those with Gα subunits that couple to PKA, PKC, and PKG, along with direct effects of Gβγ subunits (Iftinca and Zamponi, 2009).

Both L- and T-type VDCCs are expressed in cerebral SMCs (Hill-Eubanks et al., 2011; Harraz and Welsh, 2013; Harraz et al., 2014). Here, L-type channels provide Ca^{2+} for contraction (Nelson et al., 1990), whereas T-type channels provide negative feedback by coupling Ca^{2+} entry to RyR activity. Subsequent Ca^{2+} release via RyRs in turn activates large-conductance Ca^{2+}-activated K^+ (BK) channels to hyperpolarize the membrane (Harraz and Welsh, 2013; Harraz et al., 2014). T- and P/Q-type

channel currents have not yet been observed in native pericytes, but L-type VDCC currents have been measured in the retina (Sakagami et al., 1999). Variance in the magnitude of L-type VDCC Ca^{2+} currents across the microvascular network has functional consequences for the degree of Ca^{2+} entry via these channels (Matsushita et al., 2010; Burdyga and Borysova, 2014). In the retina, L-type VDCC currents are 7.5-fold higher in SMCs as compared to capillary pericytes, suggesting that V_m changes influence intracellular Ca^{2+} levels to a greater degree at the level of arterioles (Matsushita et al., 2010). Indeed, extracellular K^+ at 10 mM (a concentration that evokes K_{ir}-mediated hyperpolarization) and 97.5 mM (which depolarizes the membrane to drive VDCC activity) significantly decreased and increased intracellular Ca^{2+} in arteriolar SMCs, respectively, but had only a marginal effect on capillary pericyte Ca^{2+} (Matsushita et al., 2010). Thorough characterization of native brain capillary pericyte VDCC currents and their densities is needed to advance our understanding of the contribution of these channels to pericyte Ca^{2+} handling.

PERICYTE Cl^- CHANNELS

Cl^- channels are found in the plasma membrane and that of intracellular organelles and have been implicated in the regulation of cell excitability and volume, acidification of intracellular organelles, control of muscle tone, and synaptic transmission (Jentsch et al., 1999; Nilius and Droogmans, 2003). While they are permeable to other anions (such as iodide, bromide, or nitrate), they are referred to as Cl^- channels since this is the most abundant permeating anion species (Jentsch et al., 2002). Capillary pericytes express the CaCC formerly known as TMEM16A or anoctamin (Ano)1, and several members of the voltage-dependent chloride channel (ClC) family—ClC-2,−3,−4,−6, and−7 (He et al., 2018; Vanlandewijck et al., 2018). The latter four of these are Cl^-/H^+ antiporters and are not considered further here. Capillary pericytes also express other anoctamins that have been implicated in lipid scrambling: Ano4 and Ano6, as well as the poorly understood Ano10 (He et al., 2018; Vanlandewijck et al., 2018). Reports indicate that Ano6 may act as a Ca^{2+}-activated Cl^- and non-selective cation channel with scramblase activity (Suzuki et al., 2010; Yang et al., 2012; Grubb et al., 2013) and Ano4 was recently shown to be a Ca^{2+}-dependent non-specific cation channel with similar scrambling capabilities (Reichhart et al., 2019).

CaCC Channels Couple Intracellular Ca^{2+} Increases to Depolarizing Cl^- Efflux

The CaCC TMEM16A is a homodimer of two pores and ten transmembrane domains, cytosolic N- and C-termini, and an extracellular domain (Dang et al., 2017; Paulino et al., 2017). Ca^{2+} binding to a transmembrane region of the pore induces a conformational rearrangement that gates the channel and leads to Cl^- permeation, generating a current that is outwardly rectifying with a slope conductance of ∼8 pS (Yang et al., 2008; Xiao et al., 2011; Paulino et al., 2017). Ca^{2+} and voltage gating are closely coupled, with a stretch of 8 amino acids controlling both Ca^{2+} sensitivity and voltage-dependence of the channel (Xiao et al., 2011). Indeed, a remarkable feature of this channel is the voltage-dependence of Ca^{2+} sensitivity, with an EC_{50} of 2.6 μM at −60 mV and 400 nM at +60 mV. At physiological voltages, the channel is maximally activated by around 10 μM intracellular Ca^{2+} but concentrations exceeding this lower activation. Strong depolarization (above ∼100 mV), in contrast, opens the channel even in the absence of Ca^{2+}, despite the lack of a classic voltage sensor in the CaCC structure (Yang et al., 2008; Xiao et al., 2011). The kinetics of activation are slow at positive potentials, but are sharpened by an elevation of Ca^{2+}, and at negative potentials channels display deactivation (Nilius and Droogmans, 2003). This interplay between V_m and intracellular Ca^{2+} makes the CaCC an attractive candidate for regulation of V_m in response to elevations intracellular Ca^{2+}.

Since CaCC is sensitive to micromolar-range intracellular Ca^{2+} at typical resting potentials, it seems plausible that it is stimulated by local Ca^{2+} elevations (as opposed to global increases) such as those occurring through nearby TRPs, VDCCs, Orai channels, or IP_3Rs. In keeping with this notion, cerebral SMC CaCCs are activated by TRPC6-mediated Ca^{2+} entry which drives vasoconstriction (Wang et al., 2016). Coupling of IP_3R activity to CaCCs has also been reported in response to purinergic receptor activation, wherein CaCC-containing membrane domains are closely localized with ER regions via a physical linkage between this protein and IP_3R1, facilitating exclusive communication between the two and exposing the CaCC to high Ca^{2+} concentrations during its release from the ER (Jin et al., 2013; Cabrita et al., 2017).

Underscoring their important role in the vasculature, targeted disruption of CaCCs from contractile vascular SMCs, mural cells and pericytes lowers systemic blood pressure (Heinze et al., 2014), whereas conversely CaCC overexpression drives hypertension (Wang et al., 2015). In vascular SMCs, the driving force for depolarizing Cl^- currents comes from $Cl^-/HCO3^-$ exchange and $Na^+/K^+/Cl^-$ cotransport which enable high intracellular Cl^- concentrations (30–50 mM; Owen, 1984; Chipperfield and Harper, 2000; Kitamura and Yamazaki, 2001). Capillary pericytes in the brain express mRNA for genes encoding two of the SLC4 family $Cl^-/HCO3^-$ exchangers (*Slc4a2, Slc4a3*) and the NKCC1 $Na^+/K^+/Cl^-$ cotransporter (*Slc12a2*) (He et al., 2018; Vanlandewijck et al., 2018), which raise the potential for similarly high intracellular Cl^- concentrations. E_{Cl} with 30–50 mM intracellular Cl^- and 133 mM extracellular Cl^- (Longden et al., 2016) is between approximately −35 and −25 mV—more positive than resting V_m of pericytes (∼-45 mV, as measured in the retina; Zhang et al., 2011), therefore under these conditions activation of CaCC would cause Cl^- efflux and membrane depolarization, as seen in SMCs (Kitamura and Yamazaki, 2001; Bulley and Jaggar, 2014). While direct evidence for CaCCs in cortical capillary pericytes is currently lacking, in bladder pericytes ER Ca^{2+} release activates CaCCs and the resulting depolarization propagates to upstream SMCs of pre-capillary arterioles via gap junctions, where they depolarize the membrane to activate L-type VDCCs (Hashitani et al., 2018). In the pericytes of descending vasa recta, angiotensin II causes cytoplasmic Ca^{2+} oscillations that activate CaCC channels and depolarize V_m to

approximately −30 mV (Zhang et al., 2008; Lin et al., 2010). CaCC current and membrane depolarization have also been recorded in retinal pericytes, where CaCC activation depends on unidentified non-selective cation channels (Sakagami et al., 1999) and can be evoked by G_qPCR stimulation with endothelin (Kawamura et al., 2002). Thus, CaCCs in brain pericytes are predicted to depolarize V_m by coupling to a number of potential Ca^{2+} sources, including IP_3Rs and TRP channels.

ClC Channels May Repolarize the Membrane Following Electrical Signaling

ClCs are double-barreled homodimeric channels with one ion conduction pore per monomer (Dutzler et al., 2002). Each subunit is made up of 18 α-helices which display an interesting internal anti-parallel architecture, and many of these helices are shortened and tilted which permits disparate parts of the polypeptide to come together to form the Cl^- selectivity filter of the pore (Dutzler et al., 2002). The C-terminus also contains two cystathione-β-synthase domains, which regulate gating by binding ATP and ADP to decelerate the kinetics of activation and deactivation (Estévez et al., 2004; Stölting et al., 2013). ClC-2 has a unitary conductance of 2-3 pS and displays strong inward rectification. A remarkable biophysical characteristic of this channel is its slow hyperpolarization-mediated activation at potentials negative to around−40 mV, giving rise to currents that are only very slowly inactivating (Nilius and Droogmans, 2003; Bi et al., 2014). In addition to its hyperpolarization activation, it is sensitive to changes in cell volume and extracellular pH and is also activated by PKA (Nilius and Droogmans, 2003; Bi et al., 2014). As we have suggested previously for hyperpolarizing electrical signals generated in cECs, ClC-2 is an attractive candidate for mediating membrane repolarization (Garcia and Longden, 2020), in that its slow activation kinetics would enable K_{ir}-mediated electrical signals to be generated and sent upstream before ClC-2 mediated Cl^- current fully develops to repolarize the membrane. Accordingly, ClC-2 may fulfill a similar role in pericytes to initiate membrane repolarization in the wake of electrical signals generated by K_{ATP} and K_{ir} channels.

FURTHER CHANNELS IN PERICYTES

Capillary pericytes express an array of other ion channels, including the ubiquitous two-pore channels (TPCs), voltage-gated Na^+ (Na_v) channels, P2X receptors, and acid-sensing ion channels (ASICs; **Table 1** and **Figure 4**). Due to their lower expression and dearth of functional data in capillary pericytes, detailed discussion of these channels is beyond the scope of this review, although we touch briefly upon the function of Piezo1 channels and P2X receptors.

P2X Receptors

The ubiquitous purine ATP has received attention as a putative gliotransmitter (Pelligrino et al., 2011) and acts as an endogenous agonist at P2Y GPCRs and the cation-selective ionotropic P2X receptors, permeable to Na^+, K^+, and Ca^{2+} (Khakh et al., 2001). P2X receptors are trimmers consisting of intracellular N- and C-termini, a large extracellular domain containing the ATP binding site, and two transmembrane segments that line an integral ion pore (Kawate et al., 2009). Capillary pericytes express mRNA for P2X1 and P2X4 receptors (**Table 1**), which have a pCa^{2+}/pNa^+ of ∼5 and 4.2, respectively (Khakh et al., 2001). Thus, pericyte P2X receptors could function as sensors transducing ATP released into the local environment into Ca^{2+} elevations. Several studies have also suggested P2X7 receptors are functionally expressed in cultured human and freshly isolated rat retinal pericytes (Kawamura et al., 2003; Sugiyama et al., 2005; Platania et al., 2017), though it should be noted that our expression data do not unambiguously support the expression of this P2X isoform in CNS pericytes.

Piezo1

Piezo1 is a large (2,521 amino acids in humans) mechanosensitive cation channel, with three identical subunits, thought to have 38 transmembrane segments, that form a central ion conduction pore with surrounding peripheral domains shaped like propeller blades (Coste et al., 2010; Zhao et al., 2016, 2018; Wu et al., 2017). Functional channels have a single channel conductance of 29 pS and a current that rapidly activates and then decays on a millisecond timescale (Coste et al., 2010, 2015; Zhao et al., 2018). In ECs, piezo1 can be activated by fluid shear stress, and has been implicated in blood flow regulation, vascular development and remodeling, and permeability (Li et al., 2014; Ranade et al., 2014; Friedrich et al., 2019). Piezo1 may play similar roles in capillary pericytes to mechanosensitive TRP channels in detecting changes in blood flow, vessel diameter, or paravascular fluid shear stress.

A BIRDS-EYE VIEW OF PERICYTE G-PROTEIN COUPLED RECEPTORS

Pericytes express a huge variety of GPCRs (**Table 2** and **Figure 4**) enabling them to transduce a vast array of extracellular stimuli into intracellular responses. As outlined above, many of the signaling pathways triggered by GPCR signaling impinge upon ion channel activity and thus regulate pericyte V_m and intracellular Ca^{2+}.

Assessment of the general characteristics of the list of GPCRs expressed by pericytes is revealing. The majority of pericyte GPCRs primarily interact with $G_{i/o}$ α subunits. This is closely followed by G_q-coupled GPCRs, then those that are G_s-coupled, and the remainder couple primarily to $G_{12/13}$. Perhaps tellingly, expression of the *Gnas* gene, encoding the G_s α subunit, is ∼5 times higher than those collectively encoding $G_{q/11}$ α subunits, more than double that of $G_{i/o}$ α subunit genes, and more than 12 times in excess of $G_{12/13}$ genes (He et al., 2018; Vanlandewijck et al., 2018). Thus, while a wider variety of pericyte receptors may couple to depolarizing, Ca^{2+}-elevating processes, it appears that hyperpolarizing G_s signaling may be a favored intracellular transduction pathway.

Around 12% of the receptor subtypes expressed by pericytes are promiscuous/pleiotropic in their G-protein coupling, the degree of which will depend on the expression levels of the signaling elements involved and their local densities and organization within GPCR signaling platforms. One such example is the highly-expressed A_{2A} adenosine receptor which couples primarily to G_s, but also interacts with G_q and others (Olah, 1997; Fresco et al., 2004). Such promiscuity could represent an inbuilt feedback mechanism to prevent V_m being locked at hyperpolarized potentials by K^+ channel activity, by facilitating recruitment of additional transduction pathways to promote repolarization. In contrast, the promiscuity in signaling exhibited among receptors that couple to G_q, $G_{i/o}$, and $G_{12/13}$ would serve to reinforce depolarization. For example, the highly expressed $S1P_3$ and PAR1 receptors frequently exhibit coupling to not just $G_{i/o}$, but also to both G_q and $G_{12/13}$ α subunits (Tobo et al., 2007; Means and Brown, 2009; Yue et al., 2012).

At the time of writing, a significant portion of GPCRs expressed by pericytes (**Table 2**) remain orphan receptors with little functional data available. Strikingly, one such orphan, GPRC5C, is the 4th most robustly expressed GPCR in these cells. Given this lack of data, we omit this group from further discussion.

G-PROTEIN COUPLED RECEPTOR STRUCTURE AND SUBCLASSES

The GPCR family represents the largest family of mammalian proteins (Lagerström and Schiöth, 2008; Katritch et al., 2014) sharing a common 7-transmembrane topology with an extracellular N-terminus and intracellular C-terminus. G-protein heterotrimers are organized into four principal categories based on the similarity of function and homology in their α subunits: G_s, $G_{i/o}$, $G_{q/11}$, and $G_{12/13}$ (Simon et al., 1991; Dupré et al., 2009). Broadly, the roles of these Gα subunits are to stimulate/inhibit production of cAMP by adenylate cyclase (AC; G_s and $G_{i/o}$, respectively), to activate PLC ($G_{q/11}$), and to activate Rho guanine nucleotide exchange factors (GEFs) ($G_{12/13}$) (Hanlon and Andrew, 2015). The Gβγ subunit also activates downstream signaling elements and plays a role in GPCR mediated intracellular signaling (Dupré et al., 2009). Below, we outline how signaling through these pathways may modulate the activity of pericyte ion channel activity and consequently V_m and Ca^{2+} signaling, and we explore what the GPCRs expressed by pericytes might be able to tell us about NVC mechanisms.

PKA AS A G_s- AND $G_{i/o}$-CONTROLLED MODULATOR OF ION CHANNEL FUNCTION

In pericytes, G_s stimulation and subsequent PKA engagement is likely to drive phosphorylation of a number of ion channel targets including K_{ATP}, a range of TRP channels, VDCCs, and IP_3Rs—modulating their activity and thus V_m and cellular behavior (**Figure 9**). G_sPCR activation leads to association of the $G\alpha_s$ subunit with a cleft in the C2 domain of AC, catalyzing the conversion of ATP to cAMP (Sadana and Dessauer, 2009). cAMP then activates PKA by binding to its two regulatory subunits, inducing the dissociation of two catalytic subunits, enabling their subsequent phosphorylation of downstream targets (Sassone-Corsi, 2012). In contrast, $G_{i/o}$ activation inhibits AC, opposing G_sPCR activity. Here, $G\alpha_{i/o}$ binds to the C1 domain of AC to inhibit enzymatic activity, although this is limited to the AC-I, -V, and -VI isoforms (Sadana and Dessauer, 2009).

G_s-cAMP-PKA Signaling Augments Hyperpolarizing K^+ Currents in Pericytes

K_{ir} channels are likely key determinants of pericyte V_m, and as noted previously K_{ATP} channel activity is bidirectionally modulated by cAMP levels. At tonic, low concentrations of cAMP, PKA increases vascular K_{ATP} channel activity by phosphorylating multiple sites on the pore-forming and regulatory subunits (Quinn et al., 2004; Shi et al., 2007, 2008b). At higher concentrations, cAMP conversely inhibits K_{ATP} channel activity in a Ca^{2+}-dependent manner via engagement of the ubiquitous exchange protein activated by cAMP (Epac)-1 (Purves et al., 2009). PKA is preferentially activated by cAMP over Epac1, exhibiting a 30-fold lower EC_{50} (∼1 vs. 30 μM; Purves et al., 2009). Accordingly, it seems that G_s activity will preferentially favor membrane hyperpolarization through K_{ATP} engagement. Consistent with this, activation of G_s-coupled adenosine receptors leads to a dramatic increase in retinal pericyte K^+ currents (Li and Puro, 2001). High-level accumulation of cAMP might in turn be expected to act as an inbuilt concentration-based feedback mechanism to inhibit the channel through Epac1 engagement.

In addition to such concentration-dependent regulation of channel activity, spatial considerations are important in determining the functional outcome of cAMP elevations. The assembly of ACs and phosphodiesterases into membrane-bound scaffolds organized around A-kinase anchoring proteins (AKAPs) has been suggested to facilitate the generation of microdomains of cAMP (Arora et al., 2013; Lefkimmiatis and Zaccolo, 2014). Such compartmentalization may facilitate specific, local adjustment of, for example, K_{ATP} channel activity in a select part of the cell (e.g., a thin-strand process or around a peg-socket junction in the case of pericytes) without impacting ion channels in other regions.

Complementary to the activation by PKA that K_{ATP} channels exhibit, $K_{ir}2.2$ is also positively regulated by PKA (Zitron et al., 2004). Moreover, several K_v isoforms expressed by pericytes exhibit PKA sensitivity, in that the activity of $K_v7.4/7.5$ heteromers or $K_v7.5$ homomers is potentiated by PKA activation (Mani et al., 2016). $K_v2.1$ membrane trafficking is also controlled by a PKA-dependent mechanism (Wu et al., 2015). Collectively, these data suggest a key stimulatory role for G_s-cAMP-PKA signaling in the regulation of pericyte K^+

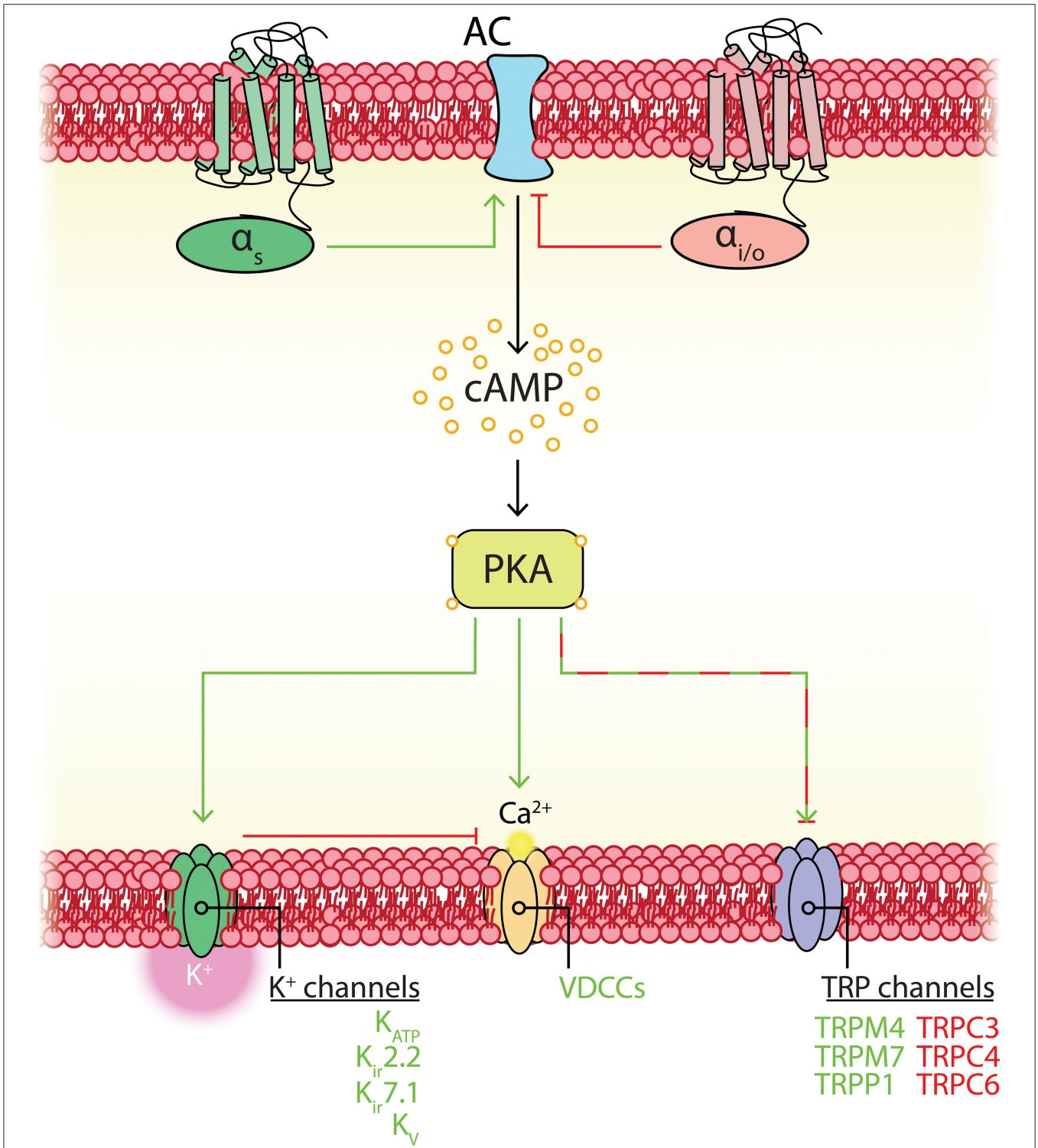

FIGURE 9 | Potential G_s- and $G_{i/o}$-coupled GPCR–ion channel interactions in capillary pericytes. G_sPCR activation promotes (green) adenylate cyclase (AC) activity, whereas $G_{i/o}$PCR activation inhibits (red) AC. AC in turn generates cAMP from ATP, which stimulates PKA activity. PKA interacts with a broad range of ion channels. In pericytes, its activity is expected to couple to plasma membrane K^+ and VDCC activity, with mixed effects on TRP channel activity. K^+ channel hyperpolarization will oppose VDCC activity and thus the overall effect of G_s stimulation is membrane hyperpolarization.

channels, along with potential negative feedback mechanisms to prevent over-activation.

G_s-Mediated Reduction of TRP Channel Activity Complements K^+ Channel Engagement

TRP channels are extensively regulated by G_s activity, and in contrast to K^+ channels this typically leads to a decrease in activity. Focusing on the TRP isoforms expressed by pericytes, TRPC3, TRPC4, TRPC6, and TRPML1 are all inhibited by PKA phosphorylation (Vergarajauregui et al., 2008; Nishioka et al., 2011; Sung et al., 2011). In contrast, TRPM4 exhibits activation as a result of G_s stimulation in an Epac1-and IP_3R-mediated Ca^{2+} release-dependent manner (Mironov and Skorova, 2011), and TRPM7 can also be potentiated by PKA (Takezawa et al., 2004). Phosphorylation of TRPP1 by PKA also increases channel P_o (Cantero del Rocío et al., 2015).

Thus, regulation of TRP channels via PKA is complex but it appears that this will to lean toward PKA-dependent inhibition of currents in pericytes. This reinforces the notion that engagement of PKA will shift the balance of ion channel activity to favor membrane hyperpolarization via K^+ channel activity, while reducing Na^+ and Ca^{2+} influx via TRP channels.

G_s Activation May Promote Increases in Intracellular Ca^{2+}

As noted, augmentation of $Ca_v1.2$ is primarily dependent on PKA phosphorylation of Rad to relieve channel inhibition (Liu et al., 2020). PKA phosphoregulation of $Ca_v1.2$ is also dependent on the AKAP isoform present in the macromolecular environment of the channel: AKAP15 permits sensitization of the channel whereas calcineurin associated with AKAP79 suppresses PKA-mediated increases in $Ca_v1.2$ activity via dephosphorylation (Fuller et al., 2014). scRNAseq data (He et al., 2018; Vanlandewijck et al., 2018) indicate that pericytes express AKAP79 at low levels whilst expressing high levels of AKAP15, suggesting G_s-stimulation in pericytes will favor increases in $Ca_v1.2$ channel activity. Along similar lines, an increase in PKA activity induces sensitization of $Ca_v1.3$ (Mahapatra et al., 2012), and $Ca_v3.1$ currents are augmented in a cAMP/PKA-dependent manner (Li et al., 2012). Moreover, the current of $Ca_v3.2$ is increased by cAMP, an effect that depends upon AKAP79/150, and its gene expression is also up-regulated by G_s-signaling, suggesting a mechanism for long term T-type VDCC regulation (Liu et al., 2010; Sekiguchi and Kawabata, 2013). Accordingly, PKA activity should increase VDCC channel activity but, due to its voltage-dependence, in the broader context of the pericyte ion channel repertoire this must be weighed against simultaneous increases in activity of multiple K^+ channels which will hyperpolarize V_m and keep VDCCs closed.

IP_3Rs also possess phosphorylation sites for PKA (Ferris et al., 1991a; Vanderheyden et al., 2009) and can also be directly influenced by cAMP (Tovey et al., 2010), allowing for direct crosstalk between cAMP and Ca^{2+} release pathways. Indeed, phosphorylation by PKA induces an increase in sensitivity of the receptor for IP_3, promoting IP_3-induced Ca^{2+} release, while Epac1 activation also potentiates Ca^{2+} release (Vanderheyden et al., 2009; Mironov and Skorova, 2011).

Drawing all of these threads together, the complement of PKA targets and their relative expression levels in pericytes suggests that the G_s-coupled receptors here likely primarily transduce stimuli into V_m hyperpolarization, but may in some cases also elevate intracellular Ca^{2+} via release from stores.

The G_s Receptor Complement of Pericytes Suggest a Range of Potential Mediators for the Regulation of Blood Flow

Pericytes express a range of receptors that couple to G_s–of particular note are the adenosine A_{2A} receptor, the PACAP receptor, PAC_1, the prostacyclin IP receptor and the PTH-type 1 receptor (PTHR1). The expression of these suggests the possibility that their endogenous agonists could be released onto pericytes during neuronal activity to evoke membrane hyperpolarization and electrical signaling to increase blood flow (**Figure 6**).

The vasodilatory effects of adenosine, an abundant metabolic byproduct, have long been appreciated (Drury and Szent-Györgyi, 1929). In the brain, adenosine is released into the extracellular space by widely-expressed nucleoside transporters, or more commonly accumulates through the extracellular catabolism of ATP by ectonucleotidases (Cunha, 2016). Recent *in vivo* work showing a reliable correlation between extracellular adenosine accumulation and rapid increases in local O_2 suggest that adenosine is capable of acting as a neurovascular coupling mediator (Wang and Venton, 2017), and clear links have been established between sensory stimulation, adenosine receptor engagement, and increases in cerebral blood flow (Ko et al., 1990; Dirnagl et al., 1994). The precise cellular and molecular mechanisms underlying this linkage remain to be determined, and actions through pericyte adenosine receptors are a strong candidate for mediating these effects.

Considering prostanoids also, blockade of G_s-coupled IP receptors impairs neuronal activity-evoked vasodilation (Lacroix et al., 2015), which suggests a role for the classic vasodilator prostacyclin—produced in the same metabolic pathway as PGE_2—in NVC. This possibility remains little explored, but the expression of IP receptors in pericytes provides a potential target for capillary endothelium-generated prostacyclin.

PACAP is a 27- or 38-amino acid neuropeptide that is an extremely potent vasodilatory agent (Koide et al., 2014). PACAP polypeptides are produced throughout the brain where they act as neurotransmitters and also have neurotrophic effects. These peptides are released by both neurons and astrocytes during activity and thus PACAP accumulation in the paravascular space could feasibly activate pericyte G_s-coupled PAC_1 receptors (Johnson et al., 2020), warranting further exploration of their potential involvement in NVC.

Finally, PTHR1 binds the endocrine ligand PTH and the paracrine ligand PTH-related protein-1 (PTHrP-1) (Vilardaga et al., 2011). Intriguingly, PTH binding to PTHR1 triggers sustained and prolonged cAMP production by retaining the intact ligand-receptor complex even after

endocytosis (Ferrandon et al., 2009). This could have important implications for pericyte G_s signaling if PTH is released during neuronal activity.

$G_{i/o}$-Coupled $P2Y_{14}$ Receptor Signaling May Impart Sensitivity to Local Metabolic Substrate Availability

The purinergic family $P2Y_{14}$ receptor is the most robustly expressed GPCR in pericytes. This receptor signals through $G_{i/o}$ and is activated by uridine diphosphate (UDP) and nucleotide sugars—most potently by UDP-glucose (Harden et al., 2010). UDP-glucose is synthesized from glucose and acts as a glucose donor in the synthesis of glycogen, which is present at modest levels in the brain (Leloir et al., 1959; Breckenridge and Crawford, 1960; Öz et al., 2015). This and related nucleotide sugars also act as donors for glycosylation in the ER lumen and Golgi apparatus (Berninsone and Hirschberg, 1998), and as a consequence these molecules are thought to be released under basal and simulated conditions from a broad range of cells, primarily through vesicular transport accompanying glycoconjugate delivery to the cell membrane (Harden et al., 2010; Lazarowski, 2012). The released nucleotide sugars have been hypothesized to act in an autocrine or paracrine manner on local $P2Y_{14}$ receptors (Lazarowski and Harden, 2015), and as the hydrolyzation of UDP-glucose is three times slower than that of ATP, this has been suggested to result in long-duration signaling (Lazarowski, 2006). As its synthesis is dependent on glucose, we speculate that UDP-glucose signaling through $P2Y_{14}$ may function to notify pericytes of local energy substrate availability: in conditions of ample glucose, UDP-glucose maintains activity of $P2Y_{14}$, which through $G_{i/o}$ signaling would counterbalance cAMP generation and prevent PKA activation of K_{ATP} and other K^+ channels. In the event that glucose levels fall, such as during neuronal activity (Hu and Wilson, 1997; Paulson et al., 2010; Li and Freeman, 2015; Pearson-Leary and McNay, 2016) or in situations of metabolic stress, the loss of this negative feedback could be relieved, leading to cAMP elevations and engagement of K_{ATP} and other K^+ channels to increase blood flow and replenish local glucose.

$mGluR_3$ and $mGluR_7$ May Impart Glutamate Sensing Capabilities to Pericytes

The $G_{i/o}$-coupled metabotropic glutamate receptors $mGluR_3$ and $mGluR_7$ are both localized in presynaptic terminals of GABAergic and glutamatergic synapses, and $mGluR_3$ is also found in glia (Harrison et al., 2008; Palazzo et al., 2016). Like other mGluRs, these receptors contain a large N-terminal venus flytrap domain with a glutamate binding site that dimerizes with that of neighboring mGluRs. $mGluR_7$ has a comparatively low affinity for glutamate and is thus activated only by its accumulation at high extracellular concentrations, but is also activated by elevations of intracellular Ca^{2+} through CaM interactions with its C-terminal tail. In neurons activity of these receptors exerts a hyperpolarizing influence that depresses synaptic activity through the lowering of cAMP, activation of G protein-coupled K_{ir} (GIRK) channels and the inhibition of VDCCs (Niswender and Conn, 2010). Pericytes do not express GIRKs, but they do express a range of VDCCs (**Table 1**). Thus, although the physiological roles of mGluRs in pericytes remain to be ascertained, their expression here implies that any glutamate elevations in the vicinity of pericytes could drive cAMP inhibition via $mGluR_3$ and $mGluR_7$ activation, and a reduction in Ca^{2+} entry via VDCCs.

PKC TARGETS: G_q-DEPENDENT MODULATION OF PERICYTE ION CHANNELS

Activation of the G_q α subunit stimulates phospholipase C (PLC), which mediates the conversion of membrane phospholipids to DAG and IP_3, inducing PKC activation and Ca^{2+} release, respectively, which may affect a broad range of ion channels (**Figure 10**). We focus below on the ramifications of PKC signaling.

G_q-DAG-PKC Signaling Will Promote Depolarizing Currents in Pericytes

Activated PKC phosphorylates a diverse range of ion channels and is thus capable of exerting considerable influence on V_m. PKCs are divided into three subfamilies depending on their activation requirements: conventional PKCs require DAG, Ca^{2+} and a phospholipid for activation; novel PKCs require DAG but are independent of Ca^{2+}; atypical PKCs require neither of these (Newton, 2010). CNS capillary pericytes express PKC isoforms from each of these subfamilies (**Table 3**).

All three IP_3R isoforms can be phosphorylated by PKC. PKC phosphorylation of IP_3R1 is potentiated by prior phosphorylation by PKA and increases Ca^{2+} release (Ferris et al., 1991a,b; Vermassen et al., 2004; Vanderheyden et al., 2009). In contrast, IP_3R2 and IP_3R3 are each inhibited by Ca^{2+}-sensitive, conventional PKCs (Arguin et al., 2007; Caron et al., 2007).

K_{ir} channels are also extensively regulated by PKC, where phosphorylation inhibits $K_{ir}6.1$-containing K_{ATP} channels, contrasting starkly with the stimulatory effects of PKA. This phosphorylation is graded—multiple serine residues (ser-354,−379,−385,−397, and−397 in the $K_{ir}6.1$ C-terminal domain) can be phosphorylated, and the degree of inhibition is proportional to the number of these sites that receive a phosphoryl group from PKC (Shi et al., 2008b). In pericytes this graded response to PKC for the highly expressed K_{ATP} channel could provide a means to fine tune activity, by permitting the degree of local G_q signaling to oppose the stimulatory effects or PKA or ATP depletion. PKC also regulates the membrane density of $K_{ir}6.1$, in that the PKCε isoform induces internalization of the receptor in a caveolin-dependent manner (Jiao et al., 2008), providing another avenue to decrease K_{ATP} channel activity. Likewise, $K_{ir}2.2$ has multiple sites that inhibit channel current upon phosphorylation by PKC, but the graded PKC phosphorylation observed for $K_{ir}6.1$ is absent (Kim et al., 2015; Scherer et al., 2016).

TRP channels are subject to complex regulation by G_q activity, with important roles for DAG, detailed above, and

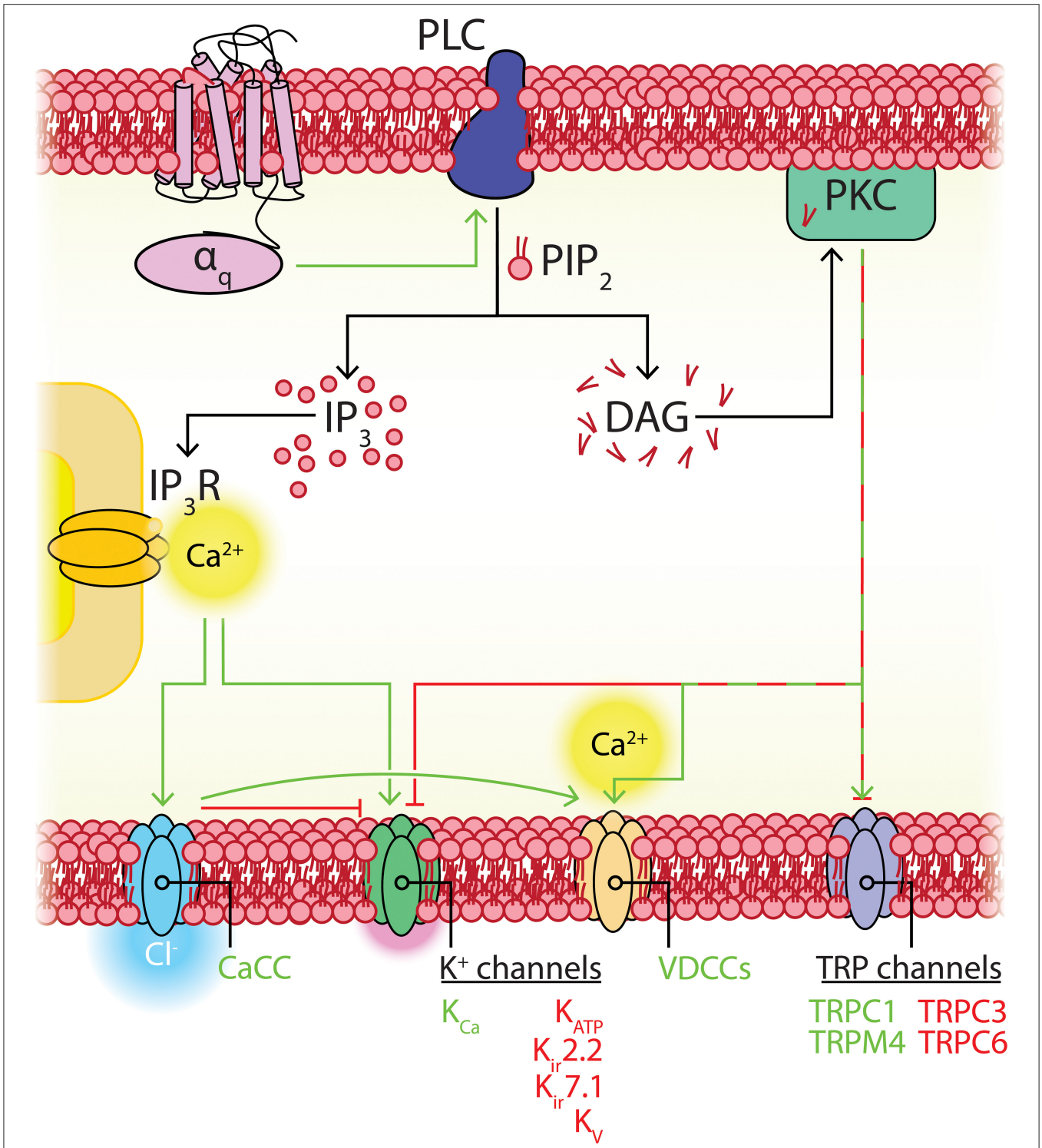

FIGURE 10 | Potential G_qPCR-ion channel interactions in capillary pericytes. G_qPCR activation engages PLC, leading to the hydrolysis of PIP_2 into IP_3 and DAG. IP_3 evokes Ca^{2+} release from the ER via resident IP_3Rs, which may engage CaCCs and K_{Ca} channels. DAG stimulates PKC which has mixed effects on the TRP channels expressed by pericytes, promotes VDCC activity, and inhibits K_{ATP}, K_{ir}, and K_v channels. The net effect of engagement of G_qPCRs is thus membrane depolarization and intracellular Ca^{2+} elevation.

TABLE 3 | Expression of PKC isoforms in brain capillary pericytes, and their modes of activation and regulation.

PKC isoform	Gene name	Average counts/cell (annotated as a pericyte)	Class	Ca^{2+} activation	DAG activation	Phospholipid activation	Regulation by arachidonic acid
PKC-α	*Prkca*	6.57	Conventional	Yes	Yes	Yes	+
PKC-β1	*Prkcb*	17.45	Conventional	Yes	Yes	Yes	+
PKC-β2	*Prkcb*		Conventional	Yes	Yes	Yes	+
PKC-γ	*Prkcg*	13.19	Conventional	Yes	Yes	Yes	+
PKC-δ	*Prkcd*	5.93	Novel	No	Yes	No	–
PKC-ε	*Prkce*	6.65	Novel	No	Yes	No	Insensitive
PKC-η	*Prkch*	1.25	Novel	No	Yes	No	+
PKC-θ	*Prkcq*	0.04	Novel	No	Yes	No	Insensitive
PKC-ι	*Prkci*	22.30	Atypical	Insensitive	Insensitive	Yes	Insensitive
PKC-ζ	*Prkcz*	0.06	Atypical	Insensitive	Insensitive	Yes	Insensitive

mRNA average counts per cell were mined from He et al. (2018) and Vanlandewijck et al. (2018). For regulation by arachidonic acid, "+" denotes an increase in enzymatic activity, while "–" represents a decrease in enzymatic activity.

PKC. TRPC3 and TRPC6 in particular are inhibited by PKC despite activation by other elements of the G_q signaling cascade (Bousquet et al., 2010; Earley and Brayden, 2015), and TRPC1 is in contrast activated by PKC (Xiao et al., 2017). TRPM4 can be phosphorylated by PKC to sensitize the receptor to Ca^{2+} (Nilius et al., 2005), which augments Na^+ entry in response to subsequent local Ca^{2+} elevations.

$Ca_v1.2$ currents are enhanced by phosphorylation at Ser1928 by PKC isoforms from each subfamily (PKCα, PKCε, and PKCζ), permitting a broad range of conditions to regulate VDCC activity (Yang et al., 2005). As pericytes express members of all three subfamilies of PKC, regulation of $Ca_v1.2$ activity may be similarly robust in these cells. $Ca_v1.2$ surface expression is also increased within minutes of G_q stimulation via a PKC-dependent increase in channel trafficking to the plasma membrane (Raifman et al., 2017). In contrast, $Ca_v1.3$ is negatively regulated by both conventional and atypical PKC isoforms (PKCβ2 and the PKCε, respectively), both of which are expressed in CNS pericytes (**Table 3**). As for T-type channels, $Ca_v3.1$ activity is stimulated by PKC phosphorylation, independently of trafficking (Park et al., 2006), and $Ca_v3.2$ is negatively regulated by Ca^{2+}-independent PKCη phosphorylation (Zhang Y. et al., 2018), although PKCη is absent in pericytes.

PKCα also activates CaCCs to promote Cl^- efflux, where phosphorylation shifts the EC_{50} of intracellular Ca^{2+} from 349 to 63 nM for channel activation at −80 mV (Dutta et al., 2016).

Pulling these threads together, it seems that PKC activation as a result of G_q activity in pericytes will contrast with the effects of G_s-cAMP-PKA signaling by enhancing activity of depolarizing ion channels such as VDCCs, TRP channels, and CaCCs while inhibiting hyperpolarizing channels such as K_{ATP} and K_{ir}. Given that G_q activity also induces the release of Ca^{2+} from intracellular stores via IP_3Rs, Ca^{2+}-sensitive PKC activation may act as a further amplification loop to increase the signal:noise ratio of G_q signaling and promote Ca^{2+} accumulation and depolarization.

Thromboxane and ET_A Receptors Are G_q-Coupled Mediators of SMC Constriction That Are Robustly Expressed by Capillary Pericytes

The G_q-coupled thromboxane (TP) receptor is well-known to induce vasoconstriction by SMCs (Dorn and Becker, 1993) and contractile mural cells of 1st−4th order vessels (Mishra et al., 2016). The TP receptor's endogenous agonists include a range of eicosanoid lipids that are generated from arachidonic acid (AA), which is initially mobilized from membrane phospholipid pools by the action of Ca^{2+}-dependent phospholipase A_2 (PLA_2; Balsinde et al., 2002). Subsequently, cyclooxygenase or prostaglandin H_2 (PGH_2) synthase enzymes convert AA to PGH_2, a potent agonist of the TP receptor. Further processing of PGH_2 yields thromboxane-A_2 (TxA_2), a still more potent agonist (Bos et al., 2004; Woodward et al., 2011). Alternatively, AA can be shuttled down a cytochrome P450 ω-hydroxylase pathway to generate the TP agonist 20-HETE (Miyata and Roman, 2005). The contractile influence of 20-HETE has been suggested to play a major role in determining the diameter of cerebral arterioles and thus controlling brain blood flow (Attwell et al., 2010), and the activation of TP receptors has also been suggested to cause mild, slow contractions of capillary pericytes (Fernández-Klett et al., 2010). It is unknown whether pericyte TP receptors are basally active to produce this effect *in vivo*, but subtle changes in capillary diameter induced by this process could regulate local blood flow over the long term, dependent on the local levels of these agonists.

The ET_A receptor shares broad similarities with the TP receptor. Its principal transduction pathway is also G_q—although coupling to other G proteins such as $G_{12/13}$ has been noted—and similar to the TP receptor, its activation evokes robust SMC contractions (Sokolovsky, 1995; Horinouchi et al., 2013; Davenport et al., 2016). The agonist of the ET_A receptor, Endothelin-1, is constitutively released by ECs, SMCs, neurons and astrocytes (Russell and Davenport, 1999; Thorin and Webb,

2010; Freeman et al., 2014). In culture, release of endothelin-1 from ECs has been noted to drive changes in pericyte morphology through reorganization of F-actin and intermediate filaments (Dehouck et al., 1997), suggesting that ECs could regulate their coverage by pericyte processes through ET_A signaling. In the context of Alzheimer's disease, aberrant ET_A signaling caused by amyloid β accumulation results in capillary constriction by overlying pericytes which may limit oxygen and glucose delivery to the parenchyma (Nortley et al., 2019).

As described above, signaling through these receptors is expected to oppose G_s-cAMP-PKA signaling while promoting membrane depolarization and elevation of Ca^{2+}.

Crosstalk and Control of G Protein Signaling Pathways

The preceding discussion illustrates that many channels expressed by pericytes are differentially regulated by PKA and PKC phosphorylation, and thus their activity will depend in part on the balance of activity between these pathways. Crosstalk between these pathways also occurs at the level of effectors, in addition to ultimate phosphorylation targets. For example, the G_q and $G_{i/o}$ pathways oppose the G_s pathway at the level of AC, which can be Ca^{2+} sensitive and modulated by PKC, dependent on isoform (Chern, 2000). Indeed, the most highly expressed AC isoform in brain pericytes is ACVI (**Table 4**), which is regulated by PKC, $G_{i/o}$, Ca^{2+}, and $G\beta\gamma$ (Chern, 2000; Sadana and Dessauer, 2009). This regulation is mirrored for G_s acting on the G_q pathway, where PKA can directly inhibit the activity of PLC via phosphorylation (Nalli et al., 2014). Accordingly, G_s- and G_q-coupled receptors functionally oppose one another at multiple levels of their transduction pathways, which will help push the membrane potential toward either hyperpolarization or depolarization, respectively.

Another layer of control is provided by regulators of GPCR signaling (RGS)—small proteins that regulate the duration and intensity of GPCR signaling by driving GTPase activity of the Gα subunit and accelerating the hydrolysis of GTP, thereby inactivating their target (Ross and Wilkie, 2000; Kach et al., 2012). Capillary pericytes express high levels of RGS4 and 5 (Bondjers et al., 2003; He et al., 2018; Vanlandewijck et al., 2018) that act as GTPase activating proteins for $G_{i/o}$ and $G_{q/11}$ subunits, while seemingly sparing G_s (Berman et al., 1996; Watson et al., 1996; Hepler et al., 1997; Huang et al., 1997; Cho et al., 2003; Gunaje et al., 2011). Intriguingly, RGS4 is known to be phosphorylated by PKA and PKG, which stimulate its activity, accelerating the deactivation of $G_{q/11}$ and inhibiting the hydrolysis of phosphoinositide to IP_3 (Huang et al., 2007). Therefore, RGS engagement in pericytes may complement and amplify the hyperpolarizing effects of G_s signaling by stifling the depolarizing influences of $G_{i/o}$ and $G_{q/11}$.

TABLE 4 | Expression of isoforms of adenylate cyclase (AC) by CNS pericytes.

AC isoform	Gene name	Average counts/cell (annotated as a pericyte)
AC-I	*Adcy1*	0.79
AC-II	*Adcy2*	0.31
AC-III	*Adcy3*	15.18
AC-IV	*Adcy4*	11.33
AC-V	*Adcy5*	8.27
AC-VI	*Adcy6*	89.98
AC-VII	*Adcy7*	1.34
AC-VIII	*Adcy8*	0.05
AC-IX	*Adcy9*	55.32
AC-X	*Adcy10*	0.34

mRNA average counts per cell were mined from He et al. (2018) and Vanlandewijck et al. (2018).

RhoA TARGETS: $G_{12/13}$-SIGNALING

Capillary pericytes express several $G_{12/13}$-coupled receptors, including a range of lysophospholipid receptors with important roles in lipid signaling, the promiscuous protease activated receptor PAR1, and several orphan receptors (**Table 2**). $G_{12/13}$ activation couples to a number of interacting partners including cadherins, AKAPs, non-receptor tyrosine kinases and protein phosphatases, though its interaction with Ras homolog family member A (RhoA) is the best characterized (Worzfeld et al., 2008). In SMCs, RhoA engagement of its downstream effector Rho-associated kinase is known to contribute to a range of receptor-mediated contractile responses (Swärd et al., 2003).

RhoA is also frequently observed to be activated downstream of ion channel engagement, including TRPC6 and TRPM7 channels (Canales et al., 2019) and VDCCs (Fernández-Tenorio et al., 2011). RhoA modulating ion channel activity is less frequently reported, but RhoA may indirectly modulate V_m on slow time scales by promoting the endocytosis and translocation of channels such as $K_v1.2$, IP_3Rs, and TRPC1 (Mehta et al., 2003; Mayor and Pagano, 2007; Stirling et al., 2009) and possibly K_{ATP} channels (Foster and Coetzee, 2015). Effects of RhoA on $K_{ir}2.1$ channel activity have also been reported, although the mechanistic details of this interaction have not been fully clarified (Jones, 2003).

Gβγ SIGNALING AND PERICYTE FUNCTION

Initially, the Gβγ subunit was viewed as a negative regulator of the Gα subunit, serving to increase signal:noise ratio and specificity of signaling by preventing aberrant Gα activity in the absence of an agonist, but has since been found to be an active effector in its own right (Dupré et al., 2009), and may play important roles in pericyte physiology. Gβγ interacts with a range of canonical effectors (for example PLCβ, AC, GIRKs; Chern, 2000; Smrcka, 2008) along with a growing list of non-canonical effectors such as mitochondrial ATP synthase, a range of nuclear transcription factors, cytoskeletal regulators involved in motility, and constituents of the extracellular signal regulated kinase (ERK) pathway. These interactions implicate Gβγ in signaling roles as diverse as regulation of transcriptional

activity, modulation of mRNA processing, control of nuclear import/export, cell motility, and oxidative phosphorylation (Khan et al., 2016). In addition to regulation of AC VI (Sadana and Dessauer, 2009)—the most highly expressed pericyte AC isoform (**Table 4**)—Gβγ signaling may also exert direct effects on pericyte V_m through activation of $K_v7.4$ (Stott et al., 2015). In contrast $Ca_v2.1$, $Ca_v3.2$, and TRPM3 can be inhibited through Gβγ-dependent mechanisms (Hu et al., 2009; Zamponi and Currie, 2013; Alkhatib et al., 2019).

PERICYTE GPCRs THAT COUPLE TO MULTIPLE G PROTEINS

The previously discussed GPCRs are largely selective in their G protein coupling, allowing for precise intracellular signaling in response to a range of stimuli. However, many GPCRs that are highly expressed in pericytes are capable of signaling through multiple G proteins. This may represent pleiotropy—physiological activation of different G proteins in response to differing signals—or promiscuity, i.e., engaging in non-preferred G protein interactions due to high levels of receptor expression or excessive stimulation (Maudsley et al., 2005). Here, we review examples of highly-expressed pericyte GPCRs with a tendency to couple to multiple G proteins.

S1P Receptors

Sphingosine-1-phosphate (S1P) is a lipid mediator formed through the action of ceramidase on lipids of the plasma membrane (Ksiazek et al., 2015). S1P is constitutively released by erythrocytes and its plasma concentration strongly correlates with hematocrit (Selim et al., 2011; Ksiazek et al., 2015). The transporter-mediated release of S1P from ECs has also been documented (Kerage et al., 2014) along with the export of the enzyme that catalyzes its formation, sphingosine kinase (Ancellin et al., 2002). This leads to S1P signaling in the vasculature, which is particularly important for maintenance of the BBB (Janiurek et al., 2019), vasoconstriction (Salomone et al., 2010), angiogenesis, and regulation of vascular tone at the level of arterioles (Kerage et al., 2014).

Pericytes are ideally positioned to sense the release of S1P from local ECs. The actions of S1P are mediated through a family of receptors that act through $G_{i/o}$, G_q, and $G_{12/13}$ signaling, with $S1P_2$ and the robustly expressed $S1P_3$ coupling to each of these (Means and Brown, 2009). Accordingly, S1P sensed by pericytes is expected to promote PLC engagement, Ca^{2+} elevations, a fall in cAMP, and depolarization, but further information as to the physiological roles of signaling through these receptors awaits experimental attention. As pericytes are critical for the maintenance of blood-brain barrier tightness (Armulik et al., 2010), it is possible that S1P signaling contributes to this process. S1P signaling also strengthens contact between ECs and pericytes in culture through a mechanism involving the trafficking and activation of the adhesion molecule N-cadherin by ECs (Paik et al., 2004), and it is thus possible that this is mirrored in pericytes to contribute to this interaction and maintain peg-socket junctions.

PAR1 May Regulate Pericyte Thin-Strand Processes

Protease-activated receptor (PAR) 1 is a member of the PAR family and is stimulated by external proteases such as thrombin and trypsin. The proteolytic action of these enzymes on the extracellular domain of the receptor reveal an N-terminal tethered ligand sequence, exposure of which results in irreversible activity of the receptor that is halted only by its internalization (Soh et al., 2010). PARs are broadly expressed in the neurovascular unit, found in neurons, glia, ECs and SMCs, as well as pericytes. PAR1 couples to G_q, $G_{i/o,}$ and $G_{12/13}$, and while the release or activation of agonists for these receptors is typically associated with injury or inflammatory responses (Ma and Dorling, 2012; Yue et al., 2012), they have also been implicated in cell proliferation and differentiation, synaptic plasticity (Noorbakhsh et al., 2003), and driving vasodilation (Villari et al., 2017). Interestingly, thrombin signaling regulates morphology of fine processes in astrocytes through RhoA, and similar effects have been noted in neurons (Noorbakhsh et al., 2003). In line with this, it is possible that PAR1 signaling regulates the dynamics of pericyte process extension and retraction on capillaries (Berthiaume et al., 2018).

FRIZZLED AND ADHESION GPCRs IN PERICYTES

Finally, pericytes also express a range of members of the frizzled family of GPCRs. These are receptors for Wnt proteins, and G-protein coupling is of less importance in this group. Instead, canonical frizzled signaling occurs through the β-catenin pathway (MacDonald et al., 2009), but G protein coupling through signaling platforms assembled around the FZD-associated phosphoprotein Disheveled is also possible. The latter facilitates activation of G_q- and $G_{i/o}$-proteins to produce Ca^{2+} elevations and PKC engagement (Schulte, 2010; Kilander et al., 2014). Further research is required to infer the functional implications of pericyte expression of frizzled receptors, but developmental and homeostatic roles seem likely, as these are major aspects of Wnt signaling (Yang, 2012). Low levels of the adhesion class cadherin EGF lag seven pass receptors (CELSR)2 are also seen in pericytes.

CONTROL OF PERICYTE V_m BY PERICYTE ION CHANNELS AND GPCRs—CONCLUSIONS AND FUTURE PERSPECTIVES

The ion channels and GPCRs expressed by capillary pericytes represent a toolkit for the dynamic control of pericyte membrane potential and function. Among a panoply of roles for these signaling elements, the robust expression of genes encoding K^+ channels and G_sPCRs and their second messenger components implies an important role for pericyte membrane hyperpolarization, which we suggest contributes to long-range electrical signaling to control blood flow (**Figure 6**). Importantly,

disturbances in blood flow and the processes that regulate it are increasingly appreciated to play a key role in a variety of pathological conditions. These include dementias such as Alzheimer's disease (AD) (Alsop et al., 2000; Iadecola, 2004; Nicolakakis and Hamel, 2011; Iturria-Medina et al., 2016), small vessel disease of the brain (Dabertrand et al., 2015; Capone et al., 2016; Huneau et al., 2018), psychological conditions such as schizophrenia (Mathew et al., 1988; Zhu et al., 2017) and chronic stress (Longden et al., 2014; Han et al., 2019), plus diabetes (Mogi and Horiuchi, 2011; Vetri et al., 2012), hypertension (Girouard and Iadecola, 2006; Capone et al., 2012), and stroke (Girouard and Iadecola, 2006; Koide et al., 2012; Balbi et al., 2017), and pericytes appear to be exceptionally sensitive to pathological perturbations (Winkler et al., 2011).

The ion channels and GPCRs that are highly expressed by brain pericytes thus have the potential to be pharmacological targets for vascular disorders, metabolic diseases, and neurodegenerative and neurological disorders (wherein for example K_{ATP} channels, IP_3Rs, VDCCs, TRP channels, and GPCRs such as A_{2A} and ET_A receptors have been implicated, to name but a few; Hübner and Jentsch, 2002; Jacobson and Gao, 2006; Nilius et al., 2007; Ohkita et al., 2012; Aziz et al., 2014; Mikoshiba, 2015). Thus, furthering our understanding of the mechanisms through which pericytes contribute to blood flow control in the brain is a critical step in the search for ways in which to prevent decline or restore function in these disease contexts. The data we have discussed underscore that we are at an early stage in our understanding of how pericyte ion channels and GPCRs contribute to these functions, and warrant further studies to reveal novel mechanisms and therapeutic targets.

In the future, it will be important to determine the precise effects of both hyperpolarization and depolarization on pericyte functional outputs, for which optogenetic technologies or traditional electrophysiological approaches (Zhang et al., 2011) can be leveraged. At a deeper level, questions regarding the organization of pericyte ion channels and GPCRs await exploration—are these organized into macromolecular signaling complexes to facilitate privileged communication between complementary molecular players? Are these elements concentrated at sites to optimize cell-cell communication, such as peg-socket junctions, or distributed more broadly throughout the cell? What are the mechanisms that modulate the fidelity and gain of signaling (control of gene expression, protein trafficking, cell surface expression levels, and so on) and how are these affected in cerebrovascular disorders? The present survey of pericyte ion channels and GPCRs provides a map that can be used to guide these deeper explorations.

AUTHOR CONTRIBUTIONS

All authors listed have made a substantial, direct and intellectual contribution to the work, and approved it for publication.

FUNDING

Support for this work was provided by the NIH National Institute on Aging and National Institute of Neurological Disorders and Stroke (1R01AG066645 and 1DP2NS121347, to TL), the American Heart Association (17SDG33670237 and 19IPLOI34660108 to TL), and the Swedish Cancer Society (to CB).

ACKNOWLEDGMENTS

The authors thank B. Huang for data organization and proofreading the manuscript.

REFERENCES

Adams, P. J., Garcia, E., David, L. S., Mulatz, K. J., Spacey, S. D., and Snutch, T. P. (2009). $Ca_v2.1$ P/Q-type calcium channel alternative splicing affects the functional impact of familial hemiplegic migraine mutations: implications for calcium channelopathies. *Channels* 3, 110–121. doi: 10.4161/chan.3.2.7932

Adelman, J. P., Maylie, J., and Sah, P. (2012). Small-conductance Ca^{2+}-activated K^+ channels: form and function. *Annu. Rev. Physiol.* 74, 245–269. doi: 10.1146/annurev-physiol-020911-153336

Alarcon-Martinez, L., Yilmaz-Ozcan, S., Yemisci, M., Schallek, J., Kil,iç, K., Can, A., et al. (2018). Capillary pericytes express α-smooth muscle actin, which requires prevention of filamentous-actin depolymerization for detection. *Elife* 7:e34861. doi: 10.7554/eLife.34861.017

Albert, A. P. (2011). "Gating mechanisms of canonical transient receptor potential channel proteins: role of phosphoinositols and diacylglycerol," in *Transient Receptor Potential Channels. Advances in Experimental Medicine and Biology,* ed M. Islam (Dordrecht: Springer), 391–411. doi: 10.1007/978-94-007-0265-3_22

Alexander, S. P. H., Christopoulos, A., Davenport, A. P., Kelly, E., Mathie, A., Peters, J. A., et al. (2019). The concise guide to pharmacology 2019/20: G protein-coupled receptors. *Br. J. Pharmacol.* 176, S21–S141. doi: 10.1111/bph.14748

Al-Karagholi, M. A.-M., Ghanizada, H., Nielsen, C. A. W., Ansari, A., Gram, C., Younis, S., et al. (2020). Cerebrovascular effects of glibenclamide investigated using high-resolution magnetic resonance imaging in healthy volunteers. *J. Cereb. Blood Flow Metab.* doi: 10.1177/0271678X20959294. [Epub ahead of print].

Alkhatib, O., da Costa, R., Gentry, C., Quallo, T., Bevan, S., and Andersson, D. A. (2019). Promiscuous G-protein-coupled receptor inhibition of transient receptor potential melastatin 3 ion channels by Gβγ subunits. *J. Neurosci.* 39, 7840–7852. doi: 10.1523/JNEUROSCI.0882-19.2019

Alsop, D. C., Detre, J. A., and Grossman, M. (2000). Assessment of cerebral blood flow in Alzheimer's disease by spin-labeled magnetic resonance imaging. *Ann. Neurol.* 47, 93–100. doi: 10.1002/1531-8249(200001)47:1<93::AID-ANA15>3.0.CO;2-8

An, M. T., and Zamponi, G. W. (2005). "Voltage-dependent inactivation of voltage gated calcium channels," in *Voltage-Gated Calcium Channels. Molecular Biology Intelligence Unit*, ed G. W. Zamponi (Boston, MA: Springer), 194–204. doi: 10.1007/0-387-27526-6_12

Ancellin, N., Colmont, C., Su, J., Li, Q., Mittereder, N., Chae, S. S., et al. (2002). Extracellular export of sphingosine kinase-1 enzyme. Sphingosine 1-phosphate generation and the induction of angiogenic vascular maturation. *J. Biol. Chem.* 277, 6667–6675. doi: 10.1074/jbc.M102841200

Aoki, M., Aoki, H., Ramanathan, R., Hait, N. C., and Takabe, K. (2016). Sphingosine-1-phosphate signaling in immune cells and inflammation: roles and therapeutic potential. *Mediators Inflamm.* 2016:8606878. doi: 10.1155/2016/8606878

Arguin, G., Regimbald-Dumas, Y., Fregeau, M. O., Caron, A. Z., and Guillemette, G. (2007). Protein kinase C phosphorylates the inositol 1,4,5-trisphosphate

receptor type 2 and decreases the mobilization of Ca^{2+} in pancreatoma AR4-2J cells. *J. Endocrinol.* 192, 659–668. doi: 10.1677/JOE-06-0179

Armstrong, J. F., Faccenda, E., Harding, S. D., Pawson, A. J., Southan, C., Sharman, J. L., et al. (2020). The iuphar/bps guide to pharmacology in 2020: extending immunopharmacology content and introducing the iuphar/mmv guide to malaria pharmacology. *Nucleic Acids Res.* 48, D1006–D1021. doi: 10.1093/nar/gkz951

Armulik, A., Abramsson, A., and Betsholtz, C. (2005). Endothelial/pericyte interactions. *Circ. Res.* 97, 512–523. doi: 10.1161/01.RES.0000182903.16652.d7

Armulik, A., Genové, G., Mäe, M., Nisancioglu, M. H., Wallgard, E., Niaudet, C., et al. (2010). Pericytes regulate the blood-brain barrier. *Nature* 468, 557–561. doi: 10.1038/nature09522

Arora, K., Sinha, C., Zhang, W., Ren, A., Moon, C. S., Yarlagadda, S., et al. (2013). Compartmentalization of cyclic nucleotide signaling: a question of when, where, and why? *Pflugers Arch.* 465, 1397–1407. doi: 10.1007/s00424-013-1280-6

Asmar, M., Asmar, A., Simonsen, L., Dela, F., Holst, J. J., and Bülow, J. (2019). GIP-induced vasodilation in human adipose tissue involves capillary recruitment. *Endocr. Connect.* 8, 806–813. doi: 10.1530/EC-19-0144

Attwell, D., Buchan, A. M., Charpak, S., Lauritzen, M., MacVicar, B. A., and Newman, E. A. (2010). Glial and neuronal control of brain blood flow. *Nature* 468, 232–243. doi: 10.1038/nature09613

Attwell, D., Mishra, A., Hall, C. N., O'Farrell, F. M., and Dalkara, T. (2016). What is a pericyte? *J. Cereb. Blood Flow Metab.* 36, 451–455. doi: 10.1177/0271678X15610340

Aydin, F., Rosenblum, W. I., and Povlishock, J. T. (1991). Myoendothelial junctions in human brain arterioles. *Stroke* 22, 1592–1597. doi: 10.1161/01.STR.22.12.1592

Aziz, Q., Thomas, A. M., Gomes, J., Ang, R., Sones, W. R., Li, Y., et al. (2014). The ATP-sensitive potassium channel subunit, $K_{ir}6.1$, in vascular smooth muscle plays a major role in blood pressure control. *Hypertension* 64, 523–529. doi: 10.1161/HYPERTENSIONAHA.114.03116

Baker, M. R., Fan, G., and Serysheva, I. I. (2017). Structure of IP_3R channel: high-resolution insights from cryo-EM. *Curr. Opin. Struct. Biol.* 46, 38–47. doi: 10.1016/j.sbi.2017.05.014

Balbi, M., Koide, M., Wellman, G. C., and Plesnila, N. (2017). Inversion of neurovascular coupling after subarachnoid hemorrhage *in vivo*. *J. Cereb. Blood Flow Metab.* 37, 3625–3634. doi: 10.1177/0271678X16686595

Ballanyi, K., Doutheil, J., and Brockhaus, J. (1996). Membrane potentials and microenvironment of rat dorsal vagal cells *in vitro* during energy depletion. *J. Physiol.* 495, 769–784. doi: 10.1113/jphysiol.1996.sp021632

Balsinde, J., Winstead, M. V., and Dennis, E. A. (2002). Phospholipase A_2 regulation of arachidonic acid mobilization. *FEBS Lett.* 531, 2–6. doi: 10.1016/S0014-5793(02)03413-0

Bayliss, W. M. (1902). On the local reactions of the arterial wall to changes of internal pressure. *J. Physiol.* 28, 220–231. doi: 10.1113/jphysiol.1902.sp000911

Beech, D. J., Zhang, H., Nakao, K., and Bolton, T. B. (1993). K channel activation by nucleotide diphosphates and its inhibition by glibenclamide in vascular smooth muscle cells. *Br. J. Pharmacol.* 110, 573–582. doi: 10.1111/j.1476-5381.1993.tb13849.x

Berman, D. M., Wilkie, T. M., and Gilman, A. G. (1996). GAIP and RGS4 are GTPase-activating proteins for the G_i subfamily of G protein α subunits. *Cell* 86, 445–452. doi: 10.1016/S0092-8674(00)80117-8

Berninsone, P., and Hirschberg, C. B. (1998). Nucleotide sugars, nucleotide sulfate, and ATP transporters of the endoplasmic reticulum and Golgi apparatus. *Ann. N. Y. Acad. Sci.* 842, 91–99. doi: 10.1111/j.1749-6632.1998.tb09636.x

Berridge, M. (2016). The inositol trisphosphate/calcium signaling pathway in health and disease. *Physiol. Rev.* 96, 1261–1296. doi: 10.1152/physrev.00006.2016

Berridge, M. J., Lipp, P., and Bootman, M. D. (2000). The versatility and universality of calcium signalling. *Nat. Rev. Mol. Cell Biol.* 1, 11–21. doi: 10.1038/35036035

Berthiaume, A. A., Grant, R. I., McDowell, K. P., Underly, R. G., Hartmann, D. A., Levy, M., et al. (2018). Dynamic remodeling of pericytes *in vivo* maintains capillary coverage in the adult mouse brain. *Cell Rep.* 22, 8–16. doi: 10.1016/j.celrep.2017.12.016

Bezprozvanny, L., Watras, J., and Ehrlich, B. E. (1991). Bell-shaped calcium-response curves of $Ins(1,4,5)P_3$- and calcium-gated channels from endoplasmic reticulum of cerebellum. *Nature* 351, 751–754. doi: 10.1038/351751a0

Bhattacharjee, A., Joiner, W. J., Wu, M., Yang, Y., Sigworth, F. J., and Kaczmarek, L. K. (2003). Slick (Slo2.1), a rapidly-gating sodium-activated potassium channel inhibited by ATP. *J. Neurosci.* 23, 11681–11691. doi: 10.1523/JNEUROSCI.23-37-11681.2003

Bi, M. M., Hong, S., Zhou, H. Y., Wang, H. W., Wang, L. N., and Zheng, Y. J. (2014). Chloride channelopathies of ClC-2. *Int. J. Mol. Sci.* 15, 218–249. doi: 10.3390/ijms15010218

Blinder, P., Tsai, P. S., Kaufhold, J. P., Knutsen, P. M., Suhl, H., and Kleinfeld, D. (2013). The cortical angiome: an interconnected vascular network with noncolumnar patterns of blood flow. *Nat. Neurosci.* 16, 889–897. doi: 10.1038/nn.3426

Bondjers, C., He, L., Takemoto, M., Norlin, J., Asker, N., Hellström, M., et al. (2006). Microarray analysis of blood microvessels from PDGF-B and PDGF-Rβ mutant mice identifies novel markers for brain pericytes. *FASEB J.* 20, E1005–E1013. doi: 10.1096/fj.05-4944fje

Bondjers, C., Kalén, M., Hellström, M., Scheidl, S. J., Abramsson, A., Renner, O., et al. (2003). Transcription profiling of platelet-derived growth factor-B-deficient mouse embryos identifies RGS5 as a novel marker for pericytes and vascular smooth muscle cells. *Am. J. Pathol.* 162, 721–729. doi: 10.1016/S0002-9440(10)63868-0

Bonev, A. D., and Nelson, M. T. (1996). Vasoconstrictors inhibit ATP-sensitive K^+ channels in arterial smooth muscle through protein kinase C. *J. Gen. Physiol.* 108, 315–323. doi: 10.1085/jgp.108.4.315

Bootman, M. D., and Bultynck, G. (2020). Fundamentals of cellular calcium signaling: a primer. *Cold Spring Harb. Perspect. Biol.* 12:a038802. doi: 10.1101/cshperspect.a038802

Borea, P. A., Gessi, S., Merighi, S., Vincenzi, F., and Varani, K. (2018). Pharmacology of adenosine receptors: the state of the art. *Physiol. Rev.* 98, 1591–1625. doi: 10.1152/physrev.00049.2017

Borysova, L., Wray, S., Eisner, D. A., and Burdyga, T. (2013). How calcium signals in myocytes and pericytes are integrated across *in situ* microvascular networks and control microvascular tone. *Cell Calcium* 54, 163–174. doi: 10.1016/j.ceca.2013.06.001

Bos, C. L., Richel, D. J., Ritsema, T., Peppelenbosch, M. P., and Versteeg, H. H. (2004). Prostanoids and prostanoid receptors in signal transduction. *Int. J. Biochem. Cell Biol.* 36, 1187–1205. doi: 10.1016/j.biocel.2003.08.006

Bousquet, S. M., Monet, M., and Boulay, G. (2010). Protein kinase C-dependent phosphorylation of transient receptor potential canonical 6 (TRPC6) on serine 448 causes channel inhibition. *J. Biol. Chem.* 285, 40534–40543. doi: 10.1074/jbc.M110.160051

Breckenridge, B. M., and Crawford, E. J. (1960). Glycogen synthesis from uridine diphosphate glucose in brain. *J. Biol. Chem.* 235, 3054–3057.

Bulley, S., and Jaggar, J. H. (2014). Cl^- channels in smooth muscle cells. *Pflügers Arch.* 466, 861–872. doi: 10.1007/s00424-013-1357-2

Burdakov, D., Petersen, O. H., and Verkhratsky, A. (2005). Intraluminal calcium as a primary regulator of endoplasmic reticulum function. *Cell Calcium* 38, 303–310. doi: 10.1016/j.ceca.2005.06.010

Burdyga, T., and Borysova, L. (2014). Calcium signalling in pericytes. *J. Vasc. Res.* 51, 190–199. doi: 10.1159/000362687

Burke, M. A., Mutharasan, R. K., and Ardehali, H. (2008). The sulfonylurea receptor, an atypical ATP-binding cassette protein, and its regulation of the K_{ATP} channel. *Circ. Res.* 102, 164–176. doi: 10.1161/CIRCRESAHA.107.165324

Cabrita, I., Benedetto, R., Fonseca, A., Wanitchakool, P., Sirianant, L., Skryabin, B. V., et al. (2017). Differential effects of anoctamins on intracellular calcium signals. *FASEB J.* 31, 2123–2134. doi: 10.1096/fj.201600797RR

Cai, C., Fordsmann, J. C., Jensen, S. H., Gesslein, B., Lønstrup, M., Hald, B. O., et al. (2018). Stimulation-induced increases in cerebral blood flow and local capillary vasoconstriction depend on conducted vascular responses. *Proc. Natl. Acad. Sci. U.S.A.* 115, E5796–E5804. doi: 10.1073/pnas.1707702115

Calcraft, P. J., Arredouani, A., Ruas, M., Pan, Z., Cheng, X., Hao, X., et al. (2009). NAADP mobilizes calcium from acidic organelles through two-pore channel. *Nature* 459, 596–600. doi: 10.1038/nature08030

Canales, J., Morales, D., Blanco, C., Rivas, J., Diaz, N., Angelopoulos, I., et al. (2019). A tr(i)p to cell migration: new roles of trp channels in mechanotransduction and cancer. *Front. Physiol.* 10:757. doi: 10.3389/fphys.2019.00757

Cantero del Rocío, M., Velázquez, I. F., Streets, A. J., Ong, A. C. M., and Cantiello, H. F. (2015). The cAMP signaling pathway and direct protein kinase a phosphorylation regulate polycystin-2 (TRPP2) channel function. *J. Biol. Chem.* 290, 23888–23896. doi: 10.1074/jbc.M115.661082

Cao, C., Goo, J. H., Lee-Kwon, W., and Pallone, T. L. (2006). Vasa recta pericytes express a strong inward rectifier K^+ conductance. *Am. J. Physiol. Regul. Integr. Comp. Physiol.* 290, R1601–R1607. doi: 10.1152/ajpregu.00877.2005

Capone, C., Dabertrand, F., Baron-Menguy, C., Chalaris, A., Ghezali, L., Domenga-Denier, V., et al. (2016). Mechanistic insights into a TIMP3-sensitive pathway constitutively engaged in the regulation of cerebral hemodynamics. *Elife* 5:e17536. doi: 10.7554/eLife.17536.042

Capone, C., Faraco, G., Peterson, J. R., Coleman, C., Anrather, J., Milner, T. A., et al. (2012). Central cardiovascular circuits contribute to the neurovascular dysfunction in angiotensin II hypertension. *J. Neurosci.* 32, 4878–4886. doi: 10.1523/JNEUROSCI.6262-11.2012

Carlson, E. (1989). Fenestrated subendothelial basement membranes in human retinal capillaries. *Investig. Opthalmology Vis. Sci.* 30, 1923–1932.

Caron, A. Z., Chaloux, B., Arguin, G., and Guillemette, G. (2007). Protein kinase C decreases the apparent affinity of the inositol 1,4,5-trisphosphate receptor type 3 in RINm5F cells. *Cell Calcium* 42, 323–331. doi: 10.1016/j.ceca.2007.01.002

Carvalho, J., Chennupati, R., Li, R., Günther, S., Kaur, H., Zhao, W., et al. (2020). Orphan G protein-coupled receptor GPRC5B controls smooth muscle contractility and differentiation by inhibiting prostacyclin receptor signaling. *Circulation* 141, 1168–1183. doi: 10.1161/CIRCULATIONAHA.119.043703

Catterall, W. A., Perez-Reyes, E., Snutch, T. P., and Striessnig, J. (2005). International Union of Pharmacology. *XLVIII. Nomenclature and structure-function relationships of voltage-gated calcium channels. Pharmacol. Rev.* 57, 411–425. doi: 10.1124/pr.57.4.5

Chasseigneaux, S., Moraca, Y., Cochois-Guégan, V., Boulay, A. C., Gilbert, A., Crom, S., et al. (2018). Isolation and differential transcriptome of vascular smooth muscle cells and mid-capillary pericytes from the rat brain. *Sci. Rep.* 8:12272. doi: 10.1038/s41598-018-30739-5

Chaudhuri, D., Issa, J. B., and Yue, D. T. (2007). Elementary mechanisms producing facilitation of $Ca_v2.1$ (P/Q-type) channels. *J. Gen. Physiol.* 129, 385–401. doi: 10.1085/jgp.200709749

Chen, X., Wang, Q., Ni, F., and Ma, J. (2010). Structure of the full-length Shaker potassium channel $K_v1.2$ by normal-mode-based X-ray crystallographic refinement. *Proc. Natl. Acad. Sci. U.S.A.* 107, 11352–11357. doi: 10.1073/pnas.1000142107

Cheng, H. Y., Dong, A., Panchatcharam, M., Mueller, P., Yang, F., Li, Z., et al. (2012). Lysophosphatidic acid signaling protects pulmonary vasculature from hypoxia-induced remodeling. *Arterioscler. Thromb. Vasc. Biol.* 32, 24–32. doi: 10.1161/ATVBAHA.111.234708

Cheng, K. T., Liu, X., Ong, H. L., and Ambudkar, I. S. (2008). Functional requirement for Orai1 in store-operated TRPC1-STIM1 channels. *J. Biol. Chem.* 283, 12935–12940. doi: 10.1074/jbc.C800008200

Cheng, K. T., Ong, H. L., Liu, X., and Ambudkar, I. S. (2013). Contribution and regulation of TRPC channels in store-operated Ca^{2+} entry. *Curr. Top. Membr.* 71, 149–179. doi: 10.1016/B978-0-12-407870-3.00007-X

Chern, Y. (2000). Regulation of adenylyl cyclase in the central nervous system. *Cell. Signal.* 12, 195–204. doi: 10.1016/S0898-6568(99)00084-4

Chesler, M., and Kaila, K. (1992). Modulation of pH by neuronal activity. *Trends Neurosci.* 15, 396–402. doi: 10.1016/0166-2236(92)90191-A

Cheung, W., Andrade-Gordon, P., Derian, C. K., and Damiano, B. P. (1998). Receptor-activating peptides distinguish thrombin receptor (PAR-1) and protease activated receptor 2 (PAR-2) mediated hemodynamic responses *in vivo*. *Can. J. Physiol. Pharmacol.* 76, 16–25. doi: 10.1139/y97-176

Chipperfield, A. R., and Harper, A. A. (2000). Chloride in smooth muscle. *Prog. Biophys. Mol. Biol.* 74, 175–221. doi: 10.1016/S0079-6107(00)00024-9

Cho, H., Kozasa, T., Bondjers, C., Betsholtz, C., and Kehrl, J. H. (2003). Pericyte-specific expression of Rgs5: implications for PDGF and EDG receptor signaling during vascular maturation. *FASEB J.* 17, 440–442. doi: 10.1096/fj.02-0340fje

Cipolla, M. (2009). "Chapter 2: Anatomy and Ultrastructure," in *The Cerebral Circulation* (San Rafael, CA: Morgan & Claypool Life Sciences).

Cipolla, M., Li, R., and Vitullo, L. (2004). Perivascular innervation of penetrating brain parenchymal arterioles. *J. Cardiovasc. Pharmacol.* 44, 1–8. doi: 10.1097/00005344-200407000-00001

Clapham, D. E. (2003). TRP channels as cellular sensors. *Nature* 426, 517–524. doi: 10.1038/nature02196

Corda, G., and Sala, A. (2017). Non-canonical WNT/PCP signalling in cancer: Fzd6 takes centre stage. *Oncogenesis* 6:e364. doi: 10.1038/oncsis.2017.69

Cortijo, C., Gouzi, M., Tissir, F., and Grapin-Botton, A. (2012). Planar cell polarity controls pancreatic beta cell differentiation and glucose homeostasis. *Cell Rep.* 2, 1593–1606. doi: 10.1016/j.celrep.2012.10.016

Coste, B., Mathur, J., Schmidt, M., Earley, T. J., Ranade, S., Petrus, M. J., et al. (2010). Piezo1 and Piezo2 are essential components of distinct mechanically activated cation channels. *Science* 330, 55–60. doi: 10.1126/science.1193270

Coste, B., Murthy, S. E., Mathur, J., Schmidt, M., Mechioukhi, Y., Delmas, P., et al. (2015). Piezo1 ion channel pore properties are dictated by C-terminal region. *Nat. Commun.* 6:7223. doi: 10.1038/ncomms8223

Crnkovic, S., Egemnazarov, B., Jain, P., Seay, U., Gattinger, N., Marsh, L. M., et al. (2014). NPY/Y1 receptor-mediated vasoconstrictory and proliferative effects in pulmonary hypertension. *Br. J. Pharmacol.* 171, 3895–3907. doi: 10.1111/bph.12751

Cuevas, P., Gutierrez-Diaz, J. A., Reimers, D., Dujovny, M., Diaz, F. G., and Ausman, J. I. (1984). Pericyte endothelial gap junctions in human cerebral capillaries. *Anat. Embryol.* 170, 155–159. doi: 10.1007/BF00319000

Cunha, R. A. (2016). How does adenosine control neuronal dysfunction and neurodegeneration? *J. Neurochem.* 139, 1019–1055. doi: 10.1111/jnc.13724

Cvetković, D., Babwah, A. V., and Bhattacharya, M. (2013). Kisspeptin/KISSIR system in breast cancer. *J. Cancer* 4, 653–661. doi: 10.7150/jca.7626

Dabertrand, F., Krøigaard, C., Bonev, A. D., Cognat, E., Dalsgaard, T., Domenga-Denier, V., et al. (2015). Potassium channelopathy-like defect underlies early-stage cerebrovascular dysfunction in a genetic model of small vessel disease. *Proc. Natl. Acad. Sci. U.S.A.* 112, E796–E805. doi: 10.1073/pnas.1420765112

Dang, S., Feng, S., Tien, J., Peters, C. J., Bulkley, D., Lolicato, M., et al. (2017). Cryo-EM structures of the TMEM16A calcium-activated chloride channel. *Nature* 552, 426–429. doi: 10.1038/nature25024

D'Avanzo, N., Cheng, W. W. L., Doyle, D. A., and Nichols, C. G. (2010). Direct and specific activation of human inward rectifier K^+ channels by membrane phosphatidylinositol 4,5-Bisphosphate. *J. Biol. Chem.* 285, 37129–37132. doi: 10.1074/jbc.C110.186692

Davenport, A. P., Hyndman, K. A., Dhaun, N., Southan, C., Kohan, D. E., Pollock, J. S., et al. (2016). Endothelin. *Pharmacol. Rev.* 68, 357–418. doi: 10.1124/pr.115.011833

De Henau, O., Degroot, G. N., Imbault, V., Robert, V., De Poorter, C., McHeik, S., et al. (2016). Signaling properties of chemerin receptors CMKLR1, GPR1 and CCRL2. *PLoS ONE* 11:e0164179. doi: 10.1371/journal.pone.0164179

de Oliveira, P. G., Ramos, M. L. S., Amaro, A. J., Dias, R. A., and Vieira, S. I. (2019). $G_{i/o}$-protein coupled receptors in the aging brain. *Front. Aging Neurosci.* 11:89. doi: 10.3389/fnagi.2019.00089

Dehouck, M. P., Vigne, P., Torpier, G., Breittmayer, J. P., Cecchelli, R., and Frelin, C. (1997). Endothelin-1 as a mediator of endothelial cell-pericyte interactions in bovine brain capillaries. *J. Cereb. Blood Flow Metab.* 17, 464–469. doi: 10.1097/00004647-199704000-00012

Denninger, J. W., and Marletta, M. A. (1999). Guanylate cyclase and the NO/cGMP signaling pathway. *Biochim. Biophys. Acta Bioenerg.* 1411, 334–350. doi: 10.1016/S0005-2728(99)00024-9

Díaz-Flores, L., Gutiérrez, R., Madrid, J. F., Varela, H., Valladares, F., Acosta, E., et al. (2009). Pericytes. Morphofunction, interactions and pathology in a quiescent and activated mesenchymal cell niche. *Histol. Histopathol.* 24, 909–969. doi: 10.14670/HH-24.909

Dick, I. E., Tadross, M. R., Liang, H., Tay, L. H., Yang, W., and Yue, D. T. (2008). A modular switch for spatial Ca^{2+} selectivity in the calmodulin regulation of Ca_v channels. *Nature* 451, 830–834. doi: 10.1038/nature06529

Dickson, E. J., and Hille, B. (2019). Understanding phosphoinositides: rare, dynamic, and essential membrane phospholipids. *Biochem. J.* 476, 1–23. doi: 10.1042/BCJ20180022

Dijksterhuis, J. P., Petersen, J., and Schulte, G. (2014). WNT/Frizzled signalling: Receptor-ligand selectivity with focus on FZD-G protein signalling and its physiological relevance: IUPHAR review 3. *Br. J. Pharmacol.* 171, 1195–1209. doi: 10.1111/bph.12364

Dirnagl, U., Niwa, K., Lindauer, U., and Villringer, A. (1994). Coupling of cerebral blood flow to neuronal activation: role of adenosine and nitric oxide. *Am. J. Physiol. Hear. Circ. Physiol.* 267, H296–H301. doi: 10.1152/ajpheart.1994.267.1.H296

Dorn, G. W. II., and Becker, M. W. (1993). Thromboxane A_2 stimulated signal transduction in vascular smooth muscle. *J. Pharmacol. Exp. Ther.* 265, 447–456.

Drury, A. N., and Szent-Györgyi, A. (1929). The physiological activity of adenine compounds with especial reference to their action upon the mammalian heart. *J. Physiol.* 68, 213–237. doi: 10.1113/jphysiol.1929.sp002608

Duprat, F., Lesage, F., Fink, M., Reyes, R., Heurteaux, C., and Lazdunski, M. (1997). TASK, a human background K^+ channel to sense external pH variations near physiological pH. *EMBO J.* 16, 5464–5471. doi: 10.1093/emboj/16.17.5464

Dupré, D. J., Robitaille, M., Rebois, R. V., and Hébert, T. E. (2009). The role of Gβγ subunits in the organization, assembly, and function of GPCR signaling complexes. *Annu. Rev. Pharmacol. Toxicol.* 49, 31–56. doi: 10.1146/annurev-pharmtox-061008-103038

Dutta, A. K., Khimji, A. K., Liu, S., Karamysheva, Z., Fujita, A., Kresge, C., et al. (2016). PKCα regulates TMEM16A-mediated Cl^- secretion in human biliary cells. *Am. J. Physiol. Gastrointest. Liver Physiol.* 310, G34–G42. doi: 10.1152/ajpgi.00146.2015

Dutzler, R., Campbell, E. B., Cadene, M., Chait, B. T., and MacKinnon, R. (2002). X-ray structure of a ClC chloride channel at 3.0 Å reveals the molecular basis of anion selectivity. *Nature* 415, 287–294. doi: 10.1038/415287a

Duvernoy, H. M., Delon, S., and Vannson, J. L. (1981). Cortical blood vessels of the human brain. *Brain Res. Bull.* 7, 519–579. doi: 10.1016/0361-9230(81)90007-1

Dyer, L. A., and Patterson, C. (2010). Development of the endothelium: An emphasis on heterogeneity. *Semin. Thromb. Hemost.* 36, 227–235. doi: 10.1055/s-0030-1253446

Earley, S., and Brayden, J. E. (2010). Transient receptor potential channels and vascular function. *Clin. Sci.* 119, 19–36. doi: 10.1042/CS20090641

Earley, S., and Brayden, J. E. (2015). Transient receptor potential channels in the vasculature. *Physiol. Rev.* 95, 645–690. doi: 10.1152/physrev.00026.2014

Eberth, C. (1871). Handbuch der lehre von der gewegen des menschen und der tiere Vol. 1. Leipzig: Engelmann

Enkvetchakul, D., and Nichols, C. G. (2003). Gating mechanism of K_{ATP} channels: function fits form. *J. Gen. Physiol.* 122, 471–480. doi: 10.1085/jgp.200308878

Estévez, R., Pusch, M., Ferrer-Costa, C., Orozco, M., and Jentsch, T. J. (2004). Functional and structural conservational of CBS domains from CLC chloride channels. *J. Physiol.* 557, 363–378. doi: 10.1113/jphysiol.2003.058453

Evans, N. J., Bayliss, A. L., Reale, V., and Evans, P. D. (2016). Characterisation of signalling by the endogenous GPER1 (GPR30) receptor in an embryonic mouse hippocampal cell line (mHippoE-18). *PLoS ONE* 11:e0152138. doi: 10.1371/journal.pone.0152138

Fan, G., Baker, M. L., Wang, Z., Baker, M. R., Sinyagovskiy, P. A., Chiu, W., et al. (2015). Gating machinery of $InsP_3R$ channels revealed by electron cryomicroscopy. *Nature* 527, 336–341. doi: 10.1038/nature15249

Fan, Z., and Makielski, J. C. (1997). Anionic phospholipids activate ATP-sensitive potassium channels. *J. Biol. Chem.* 272, 5388–5395. doi: 10.1074/jbc.272.9.5388

Fernández-Klett, F., Offenhauser, N., Dirnagl, U., Priller, J., and Lindauer, U. (2010). Pericytes in capillaries are contractile *in vivo*, but arterioles mediate functional hyperemia in the mouse brain. *Proc. Natl. Acad. Sci. U.S.A.* 107, 22290–22295. doi: 10.1073/pnas.1011321108

Fernández-Tenorio, M., Porras-González, C., Castellano, A., Del Valle-Rodríguez, A., López-Barneo, J., and Ureña, J. (2011). Metabotropic regulation of RhoA/Rho-associated kinase by L-type Ca^{2+} channels: new mechanism for depolarization-evoked mammalian arterial contraction. *Circ. Res.* 108, 1348–1357. doi: 10.1161/CIRCRESAHA.111.240127

Ferrandon, S., Feinstein, T. N., Castro, M., Wang, B., Bouley, R., Potts, J. T., et al. (2009). Sustained cyclic AMP production by parathyroid hormone receptor endocytosis. *Nat. Chem. Biol.* 5, 734–742. doi: 10.1038/nchembio.206

Ferris, C. D., Cameron, A. M., Bredt, D. S., Huganir, R. L., and Snyder, S. H. (1991a). Inositol 1,4,5-trisphosphate receptor is phosphorylated by cyclic AMP-dependent protein kinase at serines 1755 and 1589. *Biochem. Biophys. Res. Commun.* 175, 192–198. doi: 10.1016/S0006-291X(05)81219-7

Ferris, C. D., Huganir, R. L., Bredt, D. S., Cameron, A. M., and Snyder, S. H. (1991b). Inositol trisphosphate receptor: phosphorylation by protein kinase C and calcium calmodulin-dependent protein kinases in reconstituted lipid vesicles. *Proc. Natl. Acad. Sci. U.S.A.* 88, 2232–2235. doi: 10.1073/pnas.88.6.2232

Filosa, J. A., Bonev, A. D., Straub, S. V., Meredith, A. L., Wilkerson, M. K., Aldrich, R. W., et al. (2006). Local potassium signaling couples neuronal activity to vasodilation in the brain. *Nat. Neurosci.* 9, 1397–1403. doi: 10.1038/nn1779

Finch, E., Turner, T., and Goldin, S. (1991). Calcium as a coagonist of inositol 1,4,5-trisphosphate-induced calcium release. *Science* 252, 443–446. doi: 10.1126/science.2017683

Findlay, I. (1987). The effects of magnesium upon adenosine triphosphate-sensitive potassium channels in a rat insulin-secreting cell line. *J. Physiol.* 391, 611–629. doi: 10.1113/jphysiol.1987.sp016759

Findlay, I. (1988). Effects of ADP upon the ATP-sensitive K^+ channel in rat ventricular myocytes. *J. Membr. Biol.* 101, 83–92. doi: 10.1007/BF01872823

Fisher, I., Jenkins, M. L., Tall, G. G., Burke, J. E., and Smrcka, A. V. (2020). Activation of phospholipase C β by Gβγ and $G\alpha_q$ involves C-terminal rearrangement to release auto-inhibition. *Structure* 28, 1–10. doi: 10.1101/810994

Foskett, J. K., White, C., Cheung, K. H., and Mak, D. O. (2007). Inositol trisphosphate receptor Ca^{2+} release channels. *Physiol. Rev.* 87, 593–658. doi: 10.1152/physrev.00035.2006

Foster, M. N., and Coetzee, W. A. (2015). K_{ATP} channels in the cardiovascular system. *Physiol. Rev.* 96, 177–252. doi: 10.1152/physrev.00003.2015

Freeman, B. D., Machado, F. S., Tanowitz, H. B., and Desruisseaux, M. S. (2014). Endothelin-1 and its role in the pathogenesis of infectious diseases. *Life Sci.* 118, 110–119. doi: 10.1016/j.lfs.2014.04.021

Fresco, P., Diniz, C., and Gonçalves, J. (2004). Facilitation of noradrenaline release by activation of adenosine A_{2A} receptors triggers both phospholipase C and adenylate cyclase pathways in rat tail artery. *Cardiovasc. Res.* 63, 739–746. doi: 10.1016/j.cardiores.2004.05.015

Friedrich, E. E., Hong, Z., Xiong, S., Zhong, M., Di, A., Rehman, J., et al. (2019). Endothelial cell Piezo1 mediates pressure-induced lung vascular hyperpermeability via disruption of adherens junctions. *Proc. Natl. Acad. Sci. U.S.A.* 116, 12980–12985. doi: 10.1073/pnas.1902165116

Fujiwara, T., and Uehara, Y. (1984). The cytoarchitecture of the wall and the innervation pattern of the microvessels in the rat mammary gland: A scanning electron microscopic observation. *Am. J. Anat.* 170, 39–54. doi: 10.1002/aja.1001700104

Fuller, M. D., Fu, Y., Scheuer, T., and Catterall, W. A. (2014). Differential regulation of $Ca_v1.2$ channels by cAMP-dependent protein kinase bound to A-kinase anchoring proteins 15 and 79/150. *J. Gen. Physiol.* 143, 315–324. doi: 10.1085/jgp.201311075

Gannon, K. P., Vanlandingham, L. G., Jernigan, N. L., Grifoni, S. C., Hamilton, G., and Drummond, H. A. (2008). Impaired pressure-induced constriction in mouse middle cerebral arteries of ASIC2 knockout mice. *Am. J. Physiol. Hear. Circ. Physiol.* 294, H1793–H1803. doi: 10.1152/ajpheart.01380.2007

Garcia, D. C. G., and Longden, T. A. (2020). "Ion channels in capillary endothelium," in *Current Topics in Membranes. Ion Channels and Calcium Signaling in the Microcirculation,* ed W. F. Jackson (Cambridge, MA: Academic Press), 261–300. doi: 10.1016/bs.ctm.2020.01.005

Giamarchi, A., and Delmas, P. (2007). "Activation mechanisms and functional roles of TRPP2 cation channels," in *TRP Ion Channel Function in Sensory Transduction and Cellular Signaling Cascades,* eds W. Liedtke and S. Heller (Boca Raton FL: CRC Press/Taylor & Francis).

Girouard, H., and Iadecola, C. (2006). Neurovascular coupling in the normal brain and in hypertension, stroke, and Alzheimer disease. *J. Appl. Physiol.* 100, 328–335. doi: 10.1152/japplphysiol.00966.2005

Gonzales, A. L., Klug, N. R., Moshkforoush, A., Lee, J. C., Lee, F. K., Shui, B., et al. (2020). Contractile pericytes determine the direction of blood flow at capillary junctions. *Proc. Natl. Acad. Sci. U.S.A.* 117, 27022–27033. doi: 10.1073/pnas.1922755117

Gonzales, A. L., Yang, Y., Sullivan, M. N., Sanders, L., Dabertrand, F., Hill-Eubanks, D. C., et al. (2014). A PLCγ1-dependent, force-sensitive signaling network in the myogenic constriction of cerebral arteries. *Sci. Signal.* 7:ra49. doi: 10.1126/scisignal.2004732

Gould, I. G., Tsai, P., Kleinfeld, D., and Linninger, A. (2017). The capillary bed offers the largest hemodynamic resistance to the cortical blood supply. *J. Cereb. Blood Flow Metab.* 37, 52–68. doi: 10.1177/0271678X16671146

Grant, R. I., Hartmann, D. A., Underly, R. G., Berthiaume, A. A., Bhat, N. R., and Shih, A. Y. (2019). Organizational hierarchy and structural diversity of microvascular pericytes in adult mouse cortex. *J. Cereb. Blood Flow Metab.* 39, 411–425. doi: 10.1177/0271678X17732229

Gribble, F. M., Tucker, S. J., and Ashcroft, F. M. (1997). The essential role of the walker A motifs of SUR1 in K-ATP channel activation by Mg-ADP and diazoxide. *EMBO J.* 16, 1145–1152. doi: 10.1093/emboj/16.6.1145

Gribble, F. M., Tucker, S. J., Haug, T., and Ashcroft, F. M. (1998). MgATP activates the β cell K_{ATP} channel by interaction with its SUR1 subunit. *Proc. Natl. Acad. Sci. U.S.A.* 95, 7185–7190. doi: 10.1073/pnas.95.12.7185

Grimm, C., Kraft, R., Schultz, G., and Harteneck, C. (2005). Activation of the melastatin-related cation channel TRPM3 by D-erythro-sphingosine [Corrected]. *Mol. Pharmacol.* 67, 798–805. doi: 10.1124/mol.104.006734

Grubb, S., Cai, C., Hald, B. O., Khennouf, L., Murmu, R. P., Jensen, A. G. K., et al. (2020). Precapillary sphincters maintain perfusion in the cerebral cortex. *Nat. Commun.* 11:395. doi: 10.1038/s41467-020-14330-z

Grubb, S., Poulsen, K. A., Juul, C. A., Kyed, T., Klausen, T. K., Larsen, E. H., et al. (2013). TMEM16F (Anoctamin 6), an anion channel of delayed Ca^{2+} activation. *J. Gen. Physiol.* 141, 585–600. doi: 10.1085/jgp.201210861

Grutzendler, J., and Nedergaard, M. (2019). Cellular control of brain capillary blood flow: *in vivo* imaging veritas. *Trends Neurosci.* 42, 528–536. doi: 10.1016/j.tins.2019.05.009

Guimarães, S., and Moura, D. (2001). Vascular adrenoceptors: an update. *Pharmacol. Rev.* 53, 319–356.

Gunaje, J. J., Bahrami, A. J., Schwartz, S. M., Daum, G., and Mahoney, W. M. (2011). PDGF-dependent regulation of regulator of G protein signaling-5 expression and vascular smooth muscle cell functionality. *Am. J. Physiol. Cell Physiol.* 301, C478–C489. doi: 10.1152/ajpcell.00348.2010

Gurney, A. M., Osipenko, O. N., MacMillan, D., McFarlane, K. M., Tate, R. J., and Kempsill, F. E. J. (2003). Two-pore domain K channel, TASK-1, in pulmonary artery smooth muscle cells. *Circ. Res.* 93, 957–964. doi: 10.1161/01.RES.0000099883.68414.61

Haas, T. L., and Duling, B. R. (1997). Morphology favors an endothelial cell pathway for longitudinal conduction within arterioles. *Microvasc. Res.* 53, 113–120. doi: 10.1006/mvre.1996.1999

Hall, C. N., Reynell, C., Gesslein, B., Hamilton, N. B., Mishra, A., Sutherland, B. A., et al. (2014). Capillary pericytes regulate cerebral blood flow in health and disease. *Nature* 508, 55–60. doi: 10.1038/nature13165

Hamada, K., Miyatake, H., Terauchi, A., and Mikoshiba, K. (2017). IP_3-mediated gating mechanism of the IP_3 receptor revealed by mutagenesis and X-ray crystallography. *Proc. Natl. Acad. Sci. U.S.A.* 114, 4661–4666. doi: 10.1073/pnas.1701420114

Hamel, E. (2006). Perivascular nerves and the regulation of cerebrovascular tone. *J. Appl. Physiol.* 100, 1059–1064. doi: 10.1152/japplphysiol.00954.2005

Han, K., Min, J., Lee, M., Kang, B.-M., Park, T., Hahn, J., et al. (2019). Neurovascular coupling under chronic stress is modified by altered GABAergic interneuron activity. *J. Neurosci.* 39, 10081–10095. doi: 10.1523/JNEUROSCI.1357-19.2019

Hanlon, C. D., and Andrew, D. J. (2015). Outside-in signaling - a brief review of GPCR signaling with a focus on the Drosophila GPCR family. *J. Cell Sci.* 128, 3533–3542. doi: 10.1242/jcs.175158

Hansen, S. B., Tao, X., and MacKinnon, R. (2011). Structural basis of PIP_2 activation of the classical inward rectifier K^+ channel $K_{ir}2.2$. *Nature* 477, 495–498. doi: 10.1038/nature10370

Harden, T. K., Sesma, J. I., Fricks, I. P., and Lazarowski, E. R. (2010). Signalling and pharmacological properties of the $P2Y_{14}$ receptor. *Acta Physiol.* 199, 149–160. doi: 10.1111/j.1748-1716.2010.02116.x

Harraz, O. F., Abd El-Rahman, R. R., Bigdely-Shamloo, K., Wilson, S. M., Brett, S. E., Romero, M., et al. (2014). $Ca_v3.2$ channels and the induction of negative feedback in cerebral arteries. *Circ. Res.* 115, 650–661. doi: 10.1161/CIRCRESAHA.114.304056

Harraz, O. F., Hill-Eubanks, D., and Nelson, M. T. (2020). PIP_2: a critical regulator of vascular ion channels hiding in plain sight. *Proc. Natl. Acad. Sci. U.S.A.* doi: 10.1073/pnas.2006737117. [Epub ahead of print].

Harraz, O. F., Longden, T. A., Dabertrand, F., Hill-Eubanks, D., and Nelson, M. T. (2018). Endothelial G_qPCR activity controls capillary electrical signaling and brain blood flow through PIP_2 depletion. *Proc. Natl. Acad. Sci. U.S.A.* 115, E3569–E3577. doi: 10.1073/pnas.1800201115

Harraz, O. F., and Welsh, D. G. (2013). T-Type Ca^{2+} channels in cerebral arteries: approaches, hypotheses, and speculation. *Microcirculation* 20, 299–306. doi: 10.1111/micc.12038

Harrison, P. J., Lyon, L., Sartorius, L. J., Burnet, P. W. J., and Lane, T. A. (2008). The group II metabotropic glutamate receptor 3 (mGluR3, mGlu3, GRM3): expression, function and involvement in schizophrenia. *J. Psychopharmacol.* 22, 308–322. doi: 10.1177/0269881108089818

Hartmann, D. A., Underly, R. G., Grant, R. I., Watson, A. N., Lindner, V., and Shih, A. Y. (2015). Pericyte structure and distribution in the cerebral cortex revealed by high-resolution imaging of transgenic mice. *Neurophotonics* 2:041402. doi: 10.1117/1.NPh.2.4.041402

Hashitani, H., Mitsui, R., Miwa-Nishimura, K., and Lam, M. (2018). Role of capillary pericytes in the integration of spontaneous Ca^{2+} transients in the suburothelial microvasculature *in situ* of the mouse bladder. *J. Physiol.* 596, 3531–3552. doi: 10.1113/JP275845

He, L., Vanlandewijck, M., Mäe, M., Andrae, J., Ando, K., Gaudio, F., et al. (2018). Single cell RNAseq of mouse brain and lung vascular and vessel-associated cell types. *Sci. Data* 5:180160. doi: 10.1038/sdata.2018.160

Heinze, C., Seniuk, A., Sokolov, M. V., Huebner, A. K., Klementowicz, A. E., Szijárt,ó, I. A., et al. (2014). Disruption of vascular Ca^{2+}-activated chloride currents lowers blood pressure. *J. Clin. Invest.* 124, 675–686. doi: 10.1172/JCI70025

Helton, T. D., Xu, W., and Lipscombe, D. (2005). Neuronal L-type calcium channels open quickly and are inhibited slowly. *J. Neurosci.* 25, 10247–10251. doi: 10.1523/JNEUROSCI.1089-05.2005

Henno, P., Grassin-Delyle, S., Belle, E., Brollo, M., Naline, E., Sage, E., et al. (2017). In smokers, Sonic hedgehog modulates pulmonary endothelial function through vascular endothelial growth factor. *Respir. Res.* 18:102. doi: 10.1186/s12931-017-0590-1

Hepler, J. R., Berman, D. M., Gilman, A. G., and Kozasa, T. (1997). RGS4 and GAIP are GTPase-activating proteins for $G_q\alpha$ and block activation of phospholipase Cβ by γ-thio-GTP-$G_q\alpha$. *Proc. Natl. Acad. Sci. U.S.A.* 94, 428–432. doi: 10.1073/pnas.94.2.428

Hibino, H., Inanobe, A., Furutani, K., Murakami, S., Findlay, I., and Kurachi, Y. (2010). Inwardly rectifying potassium channels: their structure, function, and physiological roles. *Physiol. Rev.* 90, 291–366. doi: 10.1152/physrev.00021.2009

Hieble, J. P., and Ruffolo, R. R. Jr. (1997). Recent advances in the identification of α_1- and α_2-adrenoceptor subtypes: therapeutic implications. *Expert Opin. Investig. Drugs* 6, 367–387. doi: 10.1517/13543784.6.4.367

Hill, R. A., Tong, L., Yuan, P., Murikinati, S., Gupta, S., and Grutzendler, J. (2015). Regional blood flow in the normal and ischemic brain is controlled by arteriolar smooth muscle cell contractility and not by capillary pericytes. *Neuron* 87, 95–110. doi: 10.1016/j.neuron.2015.06.001

Hille, B., Dickson, E. J., Kruse, M., Vivas, O., and Suh, B. C. (2015). Phosphoinositides regulate ion channels. *Biochim. Biophys. Acta* 1851, 844–856. doi: 10.1016/j.bbalip.2014.09.010

Hill-Eubanks, D. C., Gonzales, A. L., Sonkusare, S. K., and Nelson, M. T. (2014). Vascular TRP channels: performing under pressure and going with the flow. *Physiology* 29, 343–360. doi: 10.1152/physiol.00009.2014

Hill-Eubanks, D. C., Werner, M. E., Heppner, T. J., and Nelson, M. T. (2011). Calcium signaling in smooth muscle. *Cold Spring Harb. Perspect. Biol.* 3:a004549. doi: 10.1101/cshperspect.a004549

Hofmann, T., Obukhov, A. G., Schaefer, M., Harteneck, C., Gudermann, T., and Schultz, G. (1999). Direct activation of human TRPC6 and TRPC3 channels by diacylglycerol. *Nature* 397, 259–263. doi: 10.1038/16711

Horinouchi, T., Terada, K., Higashi, T., and Miwa, S. (2013). Endothelin receptor signaling: new insight into its regulatory mechanisms. *J. Pharmacol. Sci.* 123, 85–101. doi: 10.1254/jphs.13R02CR

Hot, B., Valnohova, J., Arthofer, E., Simon, K., Shin, J., Uhlén, M., et al. (2017). FZD_{10}-Gα13 signalling axis points to a role of FZD_{10} in CNS angiogenesis. *Cell. Signal.* 32, 93–103. doi: 10.1016/j.cellsig.2017.01.023

Hu, C., DePuy, S. D., Yao, J., McIntire, W. E., and Barrett, P. Q. (2009). Protein kinase A activity controls the regulation of T-type $Ca_v3.2$ channels by Gβγ dimers. *J. Biol. Chem.* 284, 7465–7473. doi: 10.1074/jbc.M808049200

Hu, Y., and Wilson, G. S. (1997). Rapid changes in local extracellular rat brain glucose observed with an *in vivo* glucose sensor. *J. Neurochem.* 68, 1745–1752. doi: 10.1046/j.1471-4159.1997.68041745.x

Huang, C., Hepler, J. R., Gilman, A. G., and Mumby, S. M. (1997). Attenuation of G_i- and G_q-mediated signaling by expression of RGS4 or GAIP in mammalian cells. *Proc. Natl. Acad. Sci. U.S.A.* 94, 6159–6163. doi: 10.1073/pnas.94.12.6159

Huang, G. N., Zeng, W., Kim, J. Y., Yuan, J. P., Han, L., Muallem, S., et al. (2006). STIM1 carboxyl-terminus activates native SOC, I_{crac} and TRPC1 channels. *Nat. Cell Biol.* 8, 1003–1010. doi: 10.1038/ncb1454

Huang, J., Zhou, H., Mahavadi, S., Sriwai, W., and Murthy, K. S. (2007). Inhibition of $G\alpha_q$-dependent PLC-β1 activity by PKG and PKA is mediated by phosphorylation of RGS4 and GRK2. *Am. J. Physiol. Cell Physiol.* 292, C200–C208. doi: 10.1152/ajpcell.00103.2006

Huang, Y., and Thathiah, A. (2015). Regulation of neuronal communication by G protein-coupled receptors. *FEBS Lett.* 589, 1607–1619. doi: 10.1016/j.febslet.2015.05.007

Hübner, C. A., and Jentsch, T. J. (2002). Ion channel diseases. *Hum. Mol. Genet.* 11, 2435–2445. doi: 10.1093/hmg/11.20.2435

Huneau, C., Houot, M., Joutel, A., Béranger, B., Giroux, C., Benali, H., et al. (2018). Altered dynamics of neurovascular coupling in cadasil. *Ann. Clin. Transl. Neurol.* 5, 788–802. doi: 10.1002/acn3.574

Iadecola, C. (2004). Neurovascular regulation in the normal brain and in Alzheimer's disease. *Nat. Rev. Neurosci.* 5, 347–360. doi: 10.1038/nrn1387

Iadecola, C. (2017). The neurovascular unit coming of age: a journey through neurovascular coupling in health and disease. *Neuron* 96, 17–42. doi: 10.1016/j.neuron.2017.07.030

Iftinca, M. C., and Zamponi, G. W. (2009). Regulation of neuronal T-type calcium channels. *Trends Pharmacol. Sci.* 30, 32–40. doi: 10.1016/j.tips.2008.10.004

Iino, M. (1990). Biphasic Ca^{2+} dependence of inositol 1,4,5-trisphosphate-induced Ca release in smooth muscle cells of the guinea pig taenia caeci. *J. Gen. Physiol.* 95, 1103–1122. doi: 10.1085/jgp.95.6.1103

Inada, H., Kawabata, F., Ishimaru, Y., Fushiki, T., Matsunami, H., and Tominaga, M. (2008). Off-response property of an acid-activated cation channel complex PKD1L3-PKD2L1. *EMBO Rep.* 9, 690–697. doi: 10.1038/embor.2008.89

Ishizaki, E., Fukumoto, M., and Puro, D. G. (2009). Functional K_{ATP} channels in the rat retinal microvasculature: topographical distribution, redox regulation, spermine modulation and diabetic alteration. *J. Physiol.* 587, 2233–2253. doi: 10.1113/jphysiol.2009.169003

Iturria-Medina, Y., Sotero, R. C., Toussaint, P. J., Mateos-Pérez, J. M., Evans, A. C., and Alzheimer's Disease Neuroimaging Initiative (2016). Early role of vascular dysregulation on late-onset Alzheimer's disease based on multifactorial data-driven analysis. *Nat. Commun.* 21:11934. doi: 10.1038/ncomms11934

Iwai, M., Michikawa, T., Bosanac, I., Ikura, M., and Mikoshiba, K. (2007). Molecular basis of the isoform-specific ligand-binding affinity of inositol 1,4,5-trisphosphate receptors. *J. Biol. Chem.* 282, 12755–12764. doi: 10.1074/jbc.M609833200

Jackson, W. F. (2018). K_v channels and the regulation of vascular smooth muscle tone. *Microcirculation* 25:e12421. doi: 10.1111/micc.12421

Jacobson, K. A., and Gao, Z. G. (2006). Adenosine receptors as therapeutic targets. *Nat. Rev. Drug Discov.* 5, 247–264. doi: 10.1038/nrd1983

Janiurek, M. M., Soylu-Kucharz, R., Christoffersen, C., Kucharz, K., and Lauritzen, M. (2019). Apolipoprotein M-bound sphingosine-1-phosphate regulates blood–brain barrier paracellular permeability and transcytosis. *Elife* 8:e49405. doi: 10.1101/684894

Jentsch, T. J., Friedrich, T., Schriever, A., and Yamada, H. (1999). The CLC chloride channel family. *Pflügers Arch.* 437, 783–795. doi: 10.1007/s004240050847

Jentsch, T. J., Stein, V., Weinreich, F., and Zdebik, A. A. (2002). Molecular structure and physiological function of chloride channels. *Physiol. Rev.* 82, 503–568. doi: 10.1152/physrev.00029.2001

Jeon, J. P., Hong, C., Park, E. J., Jeon, J. H., Cho, N. H., Kim, I. G., et al. (2012). Selective $G\alpha_i$ subunits as novel direct activators of transient receptor potential canonical (TRPC)4 and TRPC5 channels. *J. Biol. Chem.* 287, 17029–17039. doi: 10.1074/jbc.M111.326553

Jiang, Y., Lee, A., Chen, J., Ruta, V., Cadene, M., Chait, B. T., et al. (2003). X-ray structure of a voltage-dependent K^+ channel. *Nature* 423, 33–41. doi: 10.1038/nature01580

Jiao, J., Garg, V., Yang, B., Elton, T. S., and Hu, K. (2008). Protein kinase C-ε; induces caveolin-dependent internalization of vascular adenosine 5′-triphosphate-sensitive K^+ channels. *Hypertension* 52, 499–506. doi: 10.1161/HYPERTENSIONAHA.108.110817

Jin, X., Shah, S., Liu, Y., Zhang, H., Lees, M., Fu, Z., et al. (2013). Activation of the Cl^- channel ANO1 by localized calcium signals in nociceptive sensory neurons requires coupling with the IP_3 receptor. *Sci. Signal.* 6, ra73. doi: 10.1126/scisignal.2004184

Johnson, G. C., Parsons, R., May, V., and Hammack, S. E. (2020). The role of pituitary adenylate cyclase-activating polypeptide (PACAP) signaling in the hippocampal dentate gyrus. *Front. Cell. Neurosci.* 14:111. doi: 10.3389/fncel.2020.00111

Jones, S. V. P. (2003). Role of the small GTPase Rho in modulation of the inwardly rectifying potassium channel $K_{ir}2.1$. *Mol. Pharmacol.* 64, 987–993. doi: 10.1124/mol.64.4.987

Kach, J., Sethakorn, N., and Dulin, N. O. (2012). A finer tuning of G-protein signaling through regulated control of RGS proteins. *Am. J. Physiol. Hear. Circ. Physiol.* 303, H19–H35. doi: 10.1152/ajpheart.00764.2011

Kaczynski, P., Kowalewski, M. P., and Waclawik, A. (2016). Prostaglandin $F_{2\alpha}$ promotes angiogenesis and embryo-maternal interactions during implantation. *Reproduction* 151, 539–552. doi: 10.1530/REP-15-0496

Kajioka, S., Kitamura, K., and Kuriyama, H. (1991). Guanosine diphosphate activates an adenosine 5'-triphosphate-sensitive K^+ channel in the rabbit portal vein. *J. Physiol.* 444, 397–418. doi: 10.1113/jphysiol.1991.sp018885

Kamouchi, M., and Kitamura, K. (1994). Regulation of ATP-sensitive K^+ channels by ATP and nucleotide diphosphate in rabbit portal vein. *Am. J. Physiol. Hear. Circ. Physiol.* 266, H1687–H1698. doi: 10.1152/ajpheart.1994.266.5.H1687

Kamp, T. J., and Hell, J. W. (2000). Regulation of Cardiac L-type calcium channels by protein kinase A and protein kinase C. *Circ. Res.* 87, 1095–1102. doi: 10.1161/01.RES.87.12.1095

Kapusta, D. R., Dayan, L. A., and Kenigs, V. A. (2002). Nociceptin/orphanin FQ modulates the cardiovascular, but not renal, responses to stress in spontaneously hypertensive rats. *Clin. Exp. Pharmacol. Physiol.* 29, 254–259. doi: 10.1046/j.1440-1681.2002.03639.x

Katritch, V., Fenalti, G., Abola, E. E., Roth, B. L., Cherezov, V., and Stevens, R. C. (2014). Allosteric sodium in class A GPCR signaling. *Trends Biochem. Sci.* 39, 233–244. doi: 10.1016/j.tibs.2014.03.002

Katz, B. (1949). Les constantes electriques de la membrane du muscle. *Arch. Sci. Physiol.* 3, 285–299.

Kawamura, H., Sugiyama, T., Wu, D. M., Kobayashi, M., Yamanishi, S., Katsumura, K., et al. (2003). ATP: a vasoactive signal in the pericyte-containing microvasculature of the rat retina. *J. Physiol.* 551, 787–799. doi: 10.1113/jphysiol.2003.047977

Kawamura, H., Oku, H., Li, Q., Sakagami, K., and Puro, D. G. (2002). Endothelin-induced changes in the physiology of retinal pericytes. *Invest. Opthalmol. Vis. Sci.* 43, 882–888. Available online at: https://iovs.arvojournals.org/article.aspx?articleid=2200149

Kawate, T., Michel, J. C., Birdsong, W. T., and Gouaux, E. (2009). Crystal structure of the ATP-gated P2X4 ion channel in the closed state. *Nature* 460, 592–598. doi: 10.1038/nature08198

Kennedy, A. J., Yang, P., Read, C., Kuc, R. E., Yang, L., Taylor, E. J. A., et al. (2016). Chemerin elicits potent constrictor actions via chemokine-like receptor 1 (CMKLR1), not G-protein-coupled receptor 1 (GPR1), in human and rat vasculature. *J. Am. Heart Assoc.* 5:e004421. doi: 10.1161/JAHA.116.004421

Kerage, D., Brindley, D. N., and Hemmings, D. G. (2014). Review: Novel insights into the regulation of vascular tone by sphingosine 1-phosphate. *Placenta* 35, S86–S92. doi: 10.1016/j.placenta.2013.12.006

Khakh, B. S., Burnstock, G., Kennedy, C., King, B. F., North, R. A., Séguéla, P., et al. (2001). International union of pharmacology. XXIV. Current status of the nomenclature and properties of P2X receptors and their subunits. *Pharmacol. Rev.* 53, 107–118.

Khan, S. M., Sung, J. Y., and Hébert, T. E. (2016). Gβγ subunits—different spaces, different faces. *Pharmacol. Res.* 111, 434–441. doi: 10.1016/j.phrs.2016.06.026

Kilander, M. B. C., Petersen, J., Andressen, K. W., Ganji, R. S., Levy, F. O., Schuster, J., et al. (2014). Disheveled regulates precoupling of heterotrimeric G proteins to Frizzled 6. *FASEB J.* 28, 2293–2305. doi: 10.1096/fj.13-246363

Kim, K. S., Jang, J. H., Lin, H., Choi, S. W., Kim, H. R., Shin, D. H., et al. (2015). Rise and fall of $K_{ir}2.2$ current by TLR4 signaling in human monocytes: PKC-dependent trafficking and PI3K-mediated PIP_2 decrease. *J. Immunol.* 195, 3345–3354. doi: 10.4049/jimmunol.1500056

Kisler, K., Nelson, A. R., Rege, S. V., Ramanathan, A., Wang, Y., Ahuja, A., et al. (2017). Pericyte degeneration leads to neurovascular uncoupling and limits oxygen supply to brain. *Nat. Neurosci.* 20, 406–441. doi: 10.1038/nn.4489

Kitamura, K., and Yamazaki, J. (2001). Chloride channels and their functional roles in smooth muscle tone in the vasculature. *Jpn. J. Pharmacol.* 85, 351–357. doi: 10.1254/jjp.85.351

Kleppisch, T., and Nelson, M. T. (1995). Adenosine activates ATP-sensitive potassium channels in arterial myocytes via A_2 receptors and cAMP-dependent protein kinase. *Proc. Natl. Acad. Sci. U.S.A.* 92, 12441–12445. doi: 10.1073/pnas.92.26.12441

Ko, K. R., Ngai, A. C., and Winn, H. R. (1990). Role of adenosine in regulation of regional cerebral blood flow in sensory cortex. *Am. J. Physiol. Hear. Circ. Physiol.* 259, H1703-H1708. doi: 10.1152/ajpheart.1990.259.6.H1703

Kochukov, M. Y., Balasubramanian, A., Abramowitz, J., Birnbaumer, L., and Marrelli, S. P. (2014). Activation of endothelial transient receptor potential C3 channel is required for small conductance calcium-activated potassium channel activation and sustained endothelial hyperpolarization and vasodilation of cerebral artery. *J. Am. Heart Assoc.* 3:e000913. doi: 10.1161/JAHA.114.000913

Kofuji, P., and Newman, E. A. (2004). Potassium buffering in the central nervous system. *Neuroscience* 129, 1045–1056. doi: 10.1016/j.neuroscience.2004.06.008

Koide, M., Bonev, A. D., Nelson, M. T., and Wellman, G. C. (2012). Inversion of neurovascular coupling by subarachnoid blood depends on large-conductance Ca^{2+}-activated K^+ (BK) channels. *Proc. Natl. Acad. Sci. U.S.A.* 109, E1387–E1395. doi: 10.1073/pnas.1121359109

Koide, M., Syed, A. U., Braas, K. M., May, V., and Wellman, G. C. (2014). Pituitary adenylate cyclase activating polypeptide (PACAP) dilates cerebellar arteries through activation of large-conductance Ca^{2+}-activated (BK) and ATP-sensitive (K_{ATP}) K^+ channels. *J. Mol. Neurosci.* 54, 443–450. doi: 10.1007/s12031-014-0301-z

Koide, M., Moshkforoush, A., Tsoukias, N. M., Hill-Eubanks, D. C., Wellman, G. C., Nelson, M. T., et al. (2018). The yin and yang of K_v channels in cerebral small vessel pathologies. *Microcirculation* 25, 1–10. doi: 10.1111/micc.12436

Kovacs, R. J., and Nelson, M. T. (1991). ATP-sensitive K^+ channels from aortic smooth muscle incorporated into planar lipid bilayers. *Am. J. Physiol. Hear. Circ. Physiol.* 261, H604–H609. doi: 10.1152/ajpheart.1991.261.2.H604

Kovacs-Oller, T., Ivanova, E., Bianchimano, P., and Sagdullaev, B. T. (2020). The pericyte connectome: spatial precision of neurovascular coupling is driven by selective connectivity maps of pericytes and endothelial cells and is disrupted in diabetes. *Cell Discov.* 6:39. doi: 10.1038/s41421-020-0180-0

Koval, M., Molina, S. A., and Burt, J. M. (2014). Mix and match: investigating heteromeric and heterotypic gap junction channels in model systems and native tissues. *FEBS Lett.* 588, 1193–1204. doi: 10.1016/j.febslet.2014.02.025

Kozielewicz, P., Turku, A., and Schulte, G. (2020). Molecular pharmacology of class F receptor activation. *Mol. Pharmacol.* 97, 62–71. doi: 10.1124/mol.119.117986

Ksiazek, M., Chacińska, M., Chabowski, A., and Baranowski, M. (2015). Sources, metabolism, and regulation of circulating sphingosine-1-phosphate. *J. Lipid Res.* 56, 1271–1281. doi: 10.1194/jlr.R059543

Kurz, H. (2009). Cell lineages and early patterns of embryonic CNS vascularization. *Cell Adhes. Migr.* 3, 205–210. doi: 10.4161/cam.3.2.7855

Lacroix, A., Toussay, X., Anenberg, E., Lecrux, C., Ferreirós, N., Karagiannis, A., et al. (2015). COX-2-derived prostaglandin E_2 produced by pyramidal neurons contributes to neurovascular coupling in the rodent cerebral cortex. *J. Neurosci.* 35, 11791–11810. doi: 10.1523/JNEUROSCI.0651-15.2015

Lagerström, M. C., and Schiöth, H. B. (2008). Structural diversity of G protein coupled receptors and significance for drug discovery. *Nat. Rev. Drug Discov.* 7, 339–357. doi: 10.1038/nrd2518

Lazarowski, E. (2006). Regulated release of nucleotides and UDP sugars from astrocytoma cells. *Novartis Found. Symp.* 276, 73–84. doi: 10.1002/9780470032244.ch7

Lazarowski, E. R. (2012). Vesicular and conductive mechanisms of nucleotide release. *Purinergic Signal.* 8, 359–373. doi: 10.1007/s11302-012-9304-9

Lazarowski, E. R., and Harden, T. K. (2015). UDP-sugars as extracellular signaling molecules: cellular and physiologic consequences of $P2Y_{14}$ receptor activation. *Mol. Pharmacol.* 88, 151–160. doi: 10.1124/mol.115.098756

Ledoux, J., Werner, M. E., Brayden, J. E., and Nelson, M. T. (2006). Calcium-activated potassium channels and the regulation of vascular tone. *Physiology* 21, 69–78. doi: 10.1152/physiol.00040.2005

Lee, A., Scheuer, T., and Catterall, W. A. (2000). Ca^{2+}/calmodulin-dependent facilitation and inactivation of P/Q-type Ca^{2+} channels. *J. Neurosci.* 20, 6830–6838. doi: 10.1523/JNEUROSCI.20-18-06830.2000

Lee, A., Wong, S. T., Gallagher, D., Li, B., Storm, D. R., Scheuer, T., et al. (1999). Ca^{2+}/calmodulin binds to and modulates P/Q-type calcium channels. *Nature* 399, 155–159. doi: 10.1038/20194

Lee-Kwon, W., Goo, J. H., Zhang, Z., Silldorff, E. P., and Pallone, T. L. (2007). Vasa recta voltage-gated Na^+ channel $Na_v1.3$ is regulated by calmodulin. *Am. J. Physiol. Ren. Physiol.* 292, F404–F414. doi: 10.1152/ajprenal.00070.2006

Lefkimmiatis, K., and Zaccolo, M. (2014). cAMP signaling in subcellular compartments. *Pharmacol. Ther.* 143, 295–304. doi: 10.1016/j.pharmthera.2014.03.008

Leloir, L. F., Olavarría, J. M., Goldemberg, S. H., and Carminatti, H. (1959). Biosynthesis of glycogen from uridine diphosphate glucose. *Arch. Biochem. Biophys.* 81, 508–520. doi: 10.1016/0003-9861(59)90232-2

Li, B., and Freeman, R. D. (2015). Neurometabolic coupling between neural activity, glucose and lactate in activated visual cortex. *J. Neurochem.* 135, 742–754. doi: 10.1111/jnc.13143

Li, J., Hou, B., Tumova, S., Muraki, K., Bruns, A., Ludlow, M. J., et al. (2014). Piezo1 integration of vascular architecture with physiological force. *Nature* 515, 279–282. doi: 10.1038/nature13701

Li, M., van Esch, B. C. A. M., Henricks, P. A. J., Folkerts, G., and Garssen, J. (2018). The anti-inflammatory effects of short chain fatty acids on lipopolysaccharide- or tumor necrosis factor α-stimulated endothelial cells via activation of GPR41/43 and inhibition of HDACs. *Front. Pharmacol.* 9:533. doi: 10.3389/fphar.2018.00533

Li, N., Wu, J. X., Ding, D., Cheng, J., Gao, N., and Chen, L. (2017). Structure of a pancreatic ATP-sensitive potassium channel. *Cell* 168, 101–110. doi: 10.1016/j.cell.2016.12.028

Li, Q., and Puro, D. G. (2001). Adenosine activates ATP-sensitive K^+ currents in pericytes of rat retinal microvessels: role of A_1 and A_{2a} receptors. *Brain Res.* 907, 93–99. doi: 10.1016/S0006-8993(01)02607-5

Li, Y., Wang, F., Zhang, X., Qi, Z., Tang, M., Szeto, C., et al. (2012). β-adrenergic stimulation increases $Ca_v3.1$ activity in cardiac myocytes through protein kinase A. *PLoS ONE* 7:e39965. doi: 10.1371/journal.pone.0039965

Li, Z., Zhang, W., and Mulholland, M. W. (2015). LGR4 and its role in intestinal protection and energy metabolism. *Front. Endocrinol.* 6:131. doi: 10.3389/fendo.2015.00131

Lin, H., Pallone, T. L., and Cao, C. (2010). Murine vasa recta pericyte chloride conductance is controlled by calcium, depolarization, and kinase activity. *Am. J. Physiol. Regul. Integr. Comp. Physiol.* 299, R1317–R1325. doi: 10.1152/ajpregu.00129.2010

Lintschinger, B., Balzer-Geldsetzer, M., Baskaran, T., Graier, W. F., Christoph, R., Zhu, M. X., et al. (2000). Coassembly of Trp1 and Trp3 proteins generates diacylglycerol- and Ca^{2+}-sensitive cation channels. *J. Biol. Chem.* 275, 27799–27805. doi: 10.1074/jbc.M002705200

Lipscombe, D., Helton, T. D., and Xu, W. (2004). L-type calcium channels: the low down. *J. Neurophysiol.* 92, 2633–2641. doi: 10.1152/jn.00486.2004

Liu, G., Papa, A., Katchman, A. N., Zakharov, S. I., Roybal, D., Hennessey, J. A., et al. (2020). Mechanism of adrenergic $Ca_v1.2$ stimulation revealed by proximity proteomics. *Nature* 577, 695–700. doi: 10.1038/s41586-020-1947-z

Liu, H., Enyeart, J. A., and Enyeart, J. J. (2010). ACTH induces $Ca_v3.2$ current and mRNA by cAMP-dependent and cAMP-independent mechanisms. *J. Biol. Chem.* 285, 20040–20050. doi: 10.1074/jbc.M110.104190

Liu, Y., Beyer, A., and Aebersold, R. (2016). On the dependency of cellular protein levels on mRNA abundance. *Cell* 165, 535–550. doi: 10.1016/j.cell.2016.03.014

Liu, Y., Zhang, Z., Wang, Y., Song, J., Ma, K., Si, J., et al. (2018). Electrophysiological properties of strial pericytes and the effect of aspirin on pericyte K^+ channels. *Mol. Med. Rep.* 17, 2861–2868. doi: 10.3892/mmr.2017.8194

Lock, J. T., and Parker, I. (2020). IP_3 mediated global Ca^{2+} signals arise through two temporally and spatially distinct modes of Ca^{2+} release. *Elife* 9:e55008. doi: 10.7554/eLife.55008.sa2

Lolicato, M., Riegelhaupt, P. M., Arrigoni, C., Clark, K. A., and Minor Jr., D. L. (2014). Transmembrane helix straightening and buckling underlies activation of mechanosensitive and thermosensitive K_2P channels. *Neuron* 84, 1198–1212. doi: 10.1016/j.neuron.2014.11.017

Longden, T., Harraz, O., Hennig, G., Shui, B., Lee, F., Lee, J., et al. (2019). Neural activity drives dynamic Ca^{2+} signals in capillary endothelial cells that shape local brain blood flow. *FASEB J.* 33:688. doi: 10.1096/fasebj.2019.33.1_supplement.688.8

Longden, T. A., Dabertrand, F., Hill-Eubanks, D. C., Hammack, S. E., and Nelson, M. T. (2014). Stress-induced glucocorticoid signaling remodels neurovascular coupling through impairment of cerebrovascular inwardly rectifying K^+ channel function. *Proc. Natl. Acad. Sci. U.S.A.* 111, 7462–7467. doi: 10.1073/pnas.1401811111

Longden, T. A., Dabertrand, F., Koide, M., Gonzales, A. L., Tykocki, N. R., Brayden, J. E., et al. (2017). Capillary K^+-sensing initiates retrograde hyperpolarization to locally increase cerebral blood flow. *Nat. Neurosci.* 20, 717–726. doi: 10.1038/nn.4533

Longden, T. A., Hill-Eubanks, D. C., and Nelson, M. T. (2016). Ion channel networks in the control of cerebral blood flow. *J. Cereb. Blood Flow Metab.* 36, 492–512. doi: 10.1177/0271678X15616138

Longden, T. A., and Nelson, M. T. (2015). Vascular inward rectifier K^+ channels as external K^+ sensors in the control of cerebral blood flow. *Microcirculation* 22, 183–196. doi: 10.1111/micc.12190

Luvisetto, S., Fellin, T., Spagnolo, M., Hivert, B., Brust, P. F., Harpold, M. M., et al. (2004). Modal gating of human $Ca_v2.1$ (P/Q-type) calcium channels: I. *The slow and the fast gating modes and their modulation by β subunits. J. Gen. Physiol.* 124, 445–461. doi: 10.1085/jgp.200409034

Ma, L., and Dorling, A. (2012). The roles of thrombin and protease-activated receptors in inflammation. *Semin. Immunopathol.* 34, 63–72. doi: 10.1007/s00281-011-0281-9

MacDonald, B., Tamai, K., and He, X. (2009). Wnt/beta-catenin signaling: components, mechanisms, and diseases. *Dev. Cell* 17, 9–26. doi: 10.1016/j.devcel.2009.06.016

MacDonald, P. E., Joseph, J. W., and Rorsman, P. (2005). Glucose-sensing mechanisms in pancreatic β-cells. *Philos. Trans. R. Soc. London. Ser. B, Biol. Sci.* 360, 2211–2225. doi: 10.1098/rstb.2005.1762

Maguire, J. J., and Davenport, A. P. (2015). Endothelin receptors and their antagonists. *Semin. Nephrol.* 35, 125–136. doi: 10.1016/j.semnephrol.2015.02.002

Mahapatra, S., Marcantoni, A., Zuccotti, A., Carabelli, V., and Carbone, E. (2012). Equal sensitivity of $Ca_v1.2$ and $Ca_v1.3$ channels to the opposing modulations of PKA and PKG in mouse chromaffin cells. *J. Physiol.* 590, 5053–5073. doi: 10.1113/jphysiol.2012.236729

Mahon, M. J. (2012). The parathyroid hormone receptorsome and the potential for therapeutic intervention. *Curr. Drug Targets* 13, 116–128. doi: 10.2174/138945012798868416

Makani, S., and Chesler, M. (2010). Rapid rise of extracellular pH evoked by neural activity is generated by the plasma membrane calcium ATPase. *J. Neurophysiol.* 103, 667–676. doi: 10.1152/jn.00948.2009

Mani, B. K., Robakowski, C., Brueggemann, L. I., Cribbs, L. L., Tripathi, A., Majetschak, M., et al. (2016). $K_v7.5$ potassium channel subunits are the primary targets for PKA-Dependent enhancement of vascular smooth muscle K_v7 currents. *Mol. Pharmacol.* 89, 323–334. doi: 10.1124/mol.115.101758

Markworth, E., Schwanstecher, C., and Schwanstecher, M. (2000). ATP4-mediates closure of pancreatic beta-cell ATP-sensitive potassium channels by interaction with 1 of 4 identical sites. *Diabetes* 49, 1413–1418. doi: 10.2337/diabetes.49.9.1413

Masago, K., Kihara, Y., Yanagida, K., Hamano, F., Nakagawa, S., Niwa, M., et al. (2018). Lysophosphatidic acid receptor, LPA6, regulates endothelial blood-brain barrier function: implication for hepatic encephalopathy. *Biochem. Biophys. Res. Commun.* 501, 1048–1054. doi: 10.1016/j.bbrc.2018.05.106

Mathew, R. J., Wilson, W. H., Tant, S. R., Robinson, L., and Prakash, R. (1988). Abnormal resting regional cerebral blood flow patterns and their correlates in schizophrenia. *Arch. Gen. Psychiatry* 45, 542–549. doi: 10.1001/archpsyc.1988.01800300038004

Mathiisen, T. M., Lehre, K. P., Danbolt, N. C., and Ottersen, O. P. (2010). The perivascular astroglial sheath provides a complete covering of the brain microvessels: an electron microscopic 3D reconstruction. *Glia* 58, 1094–1103. doi: 10.1002/glia.20990

Matsushita, K., Fukumoto, M., Kobayashi, T., Kobayashi, M., Ishizaki, E., Minami, M., et al. (2010). Diabetes-induced inhibition of voltage-dependent calcium channels in the retinal microvasculature: role of spermine. *Investig. Opthalmology Vis. Sci.* 51, 5979–5990. doi: 10.1167/iovs.10-5377

Matsushita, K., and Puro, D. G. (2006). Topographical heterogeneity of K_{ir} currents in pericyte-containing microvessels of the rat retina: effect of diabetes. *J. Physiol.* 573, 483–495. doi: 10.1113/jphysiol.2006.107102

Maudsley, S., Martin, B., and Luttrell, L. M. (2005). The origins of diversity and specificity in G protein-coupled receptor signaling. *J. Pharmacol. Exp. Ther.* 314, 485–494. doi: 10.1124/jpet.105.083121

May, V., Lutz, E., MacKenzie, C., Schutz, K. C., Dozark, K., and Braas, K. M. (2010). Pituitary adenylate cyclase-activating polypeptide (PACAP)/PAC 1HOP1 receptor activation coordinates multiple neurotrophic signaling pathways: akt activation through phosphatidylinositol 3-kinase γ and vesicle endocytosis for neuronal survival. *J. Biol. Chem.* 285, 9749–9761. doi: 10.1074/jbc.M109.043117

Mayor, S., and Pagano, R. E. (2007). Pathways of clathrin-independent endocytosis. *Nat. Rev. Mol. Cell Biol.* 8, 603–612. doi: 10.1038/nrm2216

Mazzotti, C., Gagliostro, V, Bosisio, D., Del Prete, A., Tiberio, L., Thelen, M. M., et al. (2017). The atypical receptor CCRL2 (C-C Chemokine Receptor-Like 2) does not act as a decoy receptor in endothelial cells. *Front. Immunol.* 8:1233. doi: 10.3389/fimmu.2017.01233

McGrory, S., Ballerini, L., Doubal, F. N., Staals, J., Allerhand, M., Valdes-Hernandez, M., et al. (2019). Retinal microvasculature and cerebral small vessel disease in the lothian birth cohort 1936 and mild stroke study. *Sci. Rep.* 9:6320. doi: 10.1038/s41598-019-42534-x

Means, C. K., and Brown, J. H. (2009). Sphingosine-1-phosphate receptor signalling in the heart. *Cardiovasc. Res.* 82, 193–200. doi: 10.1093/cvr/cvp086

Mehta, D., Ahmmed, G. U., Paria, B. C., Holinstat, M., Voyno-Yasenetskaya, T., Tiruppathi, C., et al. (2003). RhoA interaction with inositol 1,4,5-trisphosphate receptor and transient receptor potential channel-1 regulates Ca^{2+} entry: role in signaling increased endothelial permeability. *J. Biol. Chem.* 278, 33492–33500. doi: 10.1074/jbc.M302401200

Mestre, H., Tithof, J., Du, T., Song, W., Peng, W., Sweeney, A. M., et al. (2018). Flow of cerebrospinal fluid is driven by arterial pulsations and is reduced in hypertension. *Nat. Commun.* 9:4878. doi: 10.1038/s41467-018-07318-3

Miki, T., Liss, B., Minami, K., Shiuchi, T., Saraya, A., Kashima, Y., et al. (2001). ATP-sensitive K^+ channels in the hypothalamus are essential for the maintenance of glucose homeostasis. *Nat. Neurosci.* 4, 507–512. doi: 10.1038/87455

Mikoshiba, K. (2015). Role of IP_3 receptor signaling in cell functions and diseases. *Adv. Biol. Regul.* 57, 217–227. doi: 10.1016/j.jbior.2014.10.001

Miller, A. N., and Long, S. B. (2012). Crystal structure of the human two-pore domain potassium channel $K_{2P}1$. *Science* 335, 432–436. doi: 10.1126/science.1213274

Mironov, S. L., and Skorova, E. Y. (2011). Stimulation of bursting in pre-Bötzinger neurons by Epac through calcium release and modulation of TRPM4 and K-ATP channels. *J. Neurochem.* 117, 295–308. doi: 10.1111/j.1471-4159.2011.07202.x

Mishra, A., Reynolds, J. P., Chen, Y., Gourine, A. V., Rusakov, D. A., and Attwell, D. (2016). Astrocytes mediate neurovascular signaling to capillary pericytes but not to arterioles. *Nat. Neurosci.* 19, 1619–1627. doi: 10.1038/nn.4428

Miyata, N., and Roman, R. J. (2005). Role of 20-hydroxyeicosatetraenoic acid (20-HETE) in vascular system. *J. Smooth Muscle Res.* 41, 175–193. doi: 10.1540/jsmr.41.175

Mogi, M., and Horiuchi, M. (2011). Neurovascular coupling in cognitive impairment associated with diabetes mellitus. *Circ. J.* 75, 1042–1048. doi: 10.1253/circj.CJ-11-0121

Muraki, K., Iwata, Y., Katanosaka, Y., Ito, T., Ohya, S., Shigekawa, M., et al. (2003). TRPV2 is a component of osmotically sensitive cation channels in murine aortic myocytes. *Circ. Res.* 93, 829–838. doi: 10.1161/01.RES.0000097263.10220.0C

Muszkat, M., Kurnik, D., Solus, J., Sofowora, G. G., Xie, H. G., Jiang, L., et al. (2005). Variation in the α_{2B}-adrenergic receptor gene (ADRA2B) and its relationship to vascular response *in vivo*. *Pharmacogenet. Genomics* 15, 407–414. doi: 10.1097/01213011-200506000-00006

Nalli, A. D., Kumar, D. P., Al-Shboul, O., Mahavadi, S., Kuemmerle, J. F., Grider, J. R., et al. (2014). Regulation of $G\beta\gamma_i$-dependent PLC-β3 activity in smooth muscle: inhibitory phosphorylation of PLC-β3 by PKA and PKG and stimulatory phosphorylation of $G\alpha_i$-GTPase-activating protein RGS2

by PKG. *Cell Biochem. Biophys.* 70, 867–880. doi: 10.1007/s12013-014-9992-6

Narayanan, D., Bulley, S., Leo, M. D., Burris, S. K., Gabrick, K. S., Boop, F. A., et al. (2013). Smooth muscle cell transient receptor potential polycystin-2 (TRPP2) channels contribute to the myogenic response in cerebral arteries. *J. Physiol.* 591, 5031–5046. doi: 10.1113/jphysiol.2013.258319

Nelson, M. T., Patlak, J. B., Worley, J. F., and Standen, N. B. (1990). Calcium channels, potassium channels, and voltage dependence of arterial smooth muscle tone. *Am. J. Physiol. Cell Physiol.* 259, C3–C18. doi: 10.1152/ajpcell.1990.259.1.C3

Nelson, M. T., and Quayle, J. M. (1995). Physiological roles and properties of potassium channels in arterial smooth muscle. *Am. J. Physiol. Cell Physiol.* 268, C799–C822. doi: 10.1152/ajpcell.1995.268.4.C799

Newman, E. (1986). High potassium conductance in astrocyte endfeet. *Science* 233, 453–454. doi: 10.1126/science.3726539

Newman, E. A. (2013). Functional hyperemia and mechanisms of neurovascular coupling in the retinal vasculature. *J. Cereb. Blood Flow Metab.* 33, 1685–1695. doi: 10.1038/jcbfm.2013.145

Newton, A. C. (2010). Protein kinase C: poised to signal. *Am. J. Physiol. Endocrinol. Metab.* 298, E395–E402. doi: 10.1152/ajpendo.00477.2009

Nichols, A. S., Floyd, D. H., Bruinsma, S. P., Narzinski, K., and Baranski, T. J. (2013). Frizzled receptors signal through G proteins. *Cell. Signal.* 25, 1468–1475. doi: 10.1016/j.cellsig.2013.03.009

Nicolakakis, N., and Hamel, E. (2011). Neurovascular function in Alzheimer's disease patients and experimental models. *J. Cereb. Blood Flow Metab.* 31, 1354–1370. doi: 10.1038/jcbfm.2011.43

Nilius, B., and Droogmans, G. (2003). Amazing chloride channels: an overview. *Acta Physiol. Scand.* 177, 119–147. doi: 10.1046/j.1365-201X.2003.01060.x

Nilius, B., and Owsianik, G. (2011). The transient receptor potential family of ion channels. *Genome Biol.* 12:218. doi: 10.1186/gb-2011-12-3-218

Nilius, B., Owsianik, G., Voets, T., and Peters, J. A. (2007). Transient receptor potential cation channels in disease. *Physiol. Rev.* 87, 165–217. doi: 10.1152/physrev.00021.2006

Nilius, B., Prenen, J., Tang, J., Wang, C., Owsianik, G., Janssens, A., et al. (2005). Regulation of the Ca^{2+} sensitivity of the nonselective cation channel TRPM4. *J. Biol. Chem.* 280, 6423–6433. doi: 10.1074/jbc.M411089200

Nishioka, K., Nishida, M., Ariyoshi, M., Jian, Z., Saiki, S., Hirano, M., et al. (2011). Cilostazol suppresses angiotensin II-induced vasoconstriction via protein kinase A-mediated phosphorylation of the transient receptor potential canonical 6 channel. *Arterioscler. Thromb. Vasc. Biol.* 31, 2278–2286. doi: 10.1161/ATVBAHA.110.221010

Niswender, C. M., and Conn, P. J. (2010). Metabotropic glutamate receptors: physiology, pharmacology, and disease. *Annu. Rev. Pharmacol. Toxicol.* 50, 295–322. doi: 10.1146/annurev.pharmtox.011008.145533

Noorbakhsh, F., Vergnolle, N., Hollenberg, M. D., and Power, C. (2003). Proteinase-activated receptors in the nervous system. *Nat. Rev. Neurosci.* 4, 981–990. doi: 10.1038/nrn1255

Nortley, R., Mishra, A., Jaunmuktane, Z., Kyrargyri, V., Madry, C., Gong, H., et al. (2019). Amyloid? *oligomers constrict human capillaries in Alzheimer's disease via signalling to pericytes. Science* 365:300. doi: 10.1126/science.aav9518

Ohkita, M., Tawa, M., Kitada, K., and Matsumura, Y. (2012). Pathophysiological roles of endothelin receptors in cardiovascular diseases. *J. Pharmacol. Sci.* 119, 302–313. doi: 10.1254/jphs.12R01CR

Olah, M. E. (1997). Identification of A_{2a} adenosine receptor domains involved in selective coupling to G_s: analysis of chimeric A_1/A_{2a} adenosine receptors. *J. Biol. Chem.* 272, 337–344. doi: 10.1074/jbc.272.1.337

Orkand, R. K., Nicholls, J. G., and Kuffler, S. W. (1966). Effect of nerve impulses on the membrane potential of glial cells in the central nervous system of amphibia. *J. Neurophysiol.* 29, 788–806. doi: 10.1152/jn.1966.29.4.788

Owen, N. E. (1984). Regulation of Na/K/Cl cotransport in vascular smooth muscle cells. *Biochem. Biophys. Res. Commun.* 125, 500–508. doi: 10.1016/0006-291X(84)90568-0

Öz, G., DiNuzzo, M., Kumar, A., Moheet, A., and Seaquist, E. R. (2015). Revisiting glycogen content in the human brain. *Neurochem. Res.* 40, 2473–2481. doi: 10.1007/s11064-015-1664-4

Ozen, G., Benyahia, C., Amgoud, Y., Patel, J., Abdelazeem, H., Bouhadoun, A., et al. (2020). Interaction between PGI_2 and ET-1 pathways in vascular smooth muscle from Group-III pulmonary hypertension patients. *Prostaglandins Other Lipid Mediat.* 146:106388. doi: 10.1016/j.prostaglandins.2019.106388

Paik, J. H., Skoura, A., Chae, S. S., Cowan, A. E., Han, D. K., Proia, R. L., et al. (2004). Sphingosine 1-phosphate receptor regulation of N-cadherin mediates vascular stabilization. *Genes Dev.* 18, 2392–2403. doi: 10.1101/gad.1227804

Palazzo, E., Marabese, I., de Novellis, V., Rossi, F., and Maione, S. (2016). Metabotropic glutamate receptor 7: from synaptic function to therapeutic implications. *Curr. Neuropharmacol.* 14, 504–513. doi: 10.2174/1570159X13666150716165323

Park, J. Y., Kang, H. W., Moon, H. J., Huh, S. U., Jeong, S. W., Soldatov, N. M., et al. (2006). Activation of protein kinase C augments T-type Ca^{2+} channel activity without changing channel surface density. *J. Physiol.* 577, 513–523. doi: 10.1113/jphysiol.2006.117440

Patel, C., Narayanan, S. P., Zhang, W., Xu, Z., Sukumari-Ramesh, S., Dhandapani, K. M., et al. (2014). Activation of the endothelin system mediates pathological angiogenesis during ischemic retinopathy. *Am. J. Pathol.* 184, 3040–3051. doi: 10.1016/j.ajpath.2014.07.012

Patton, N., Aslam, T., MacGillivray, T., Pattie, A., Deary, I. J., and Dhillon, B. (2005). Retinal vascular image analysis as a potential screening tool for cerebrovascular disease: A rationale based on homology between cerebral and retinal microvasculatures. *J. Anat.* 206, 319–348. doi: 10.1111/j.1469-7580.2005.00395.x

Paulino, C., Kalienkova, V., Lam, A. K. M., Neldner, Y., and Dutzler, R. (2017). Activation mechanism of the calcium-activated chloride channel TMEM16A revealed by cryo-EM. *Nature* 552, 421–425. doi: 10.1038/nature24652

Paulson, O. B., Hasselbalch, S. G., Rostrup, E., Knudsen, G. M., and Pelligrino, D. (2010). Cerebral blood flow response to functional activation. *J. Cereb. Blood Flow Metab.* 30, 2–14. doi: 10.1038/jcbfm.2009.188

Paulson, O. B., Strandgaard, S., and Edvinsson, L. (1990). Cerebral autoregulation. *Cerebrovasc. Brain Metab. Rev.* 2, 161–192.

Pearson-Leary, J., and McNay, E. C. (2016). Novel roles for the insulin-regulated glucose transporter-4 in hippocampally dependent memory. *J. Neurosci.* 36, 11851–11864. doi: 10.1523/JNEUROSCI.1700-16.2016

Pébay, A., and Wong, R. C. B. (2017). *Lipidomics of Stem Cells*. *Cham*: *Humana Press*. doi: 10.1007/978-3-319-49343-5

Pedersen, S. F., Owsianik, G., and Nilius, B. (2005). TRP channels: an overview. *Cell Calcium* 38, 233–252. doi: 10.1016/j.ceca.2005.06.028

Pelligrino, D. A., Vetri, F., and Xu, H. L. (2011). Purinergic mechanisms in gliovascular coupling. *Semin. Cell Dev. Biol.* 22, 229–236. doi: 10.1016/j.semcdb.2011.02.010

Peppiatt, C. M., Howarth, C., Mobbs, P., and Attwell, D. (2006). Bidirectional control of CNS capillary diameter by pericytes. *Nature* 443, 700–704. doi: 10.1038/nature05193

Perálvarez-Marín, A., Doñate-Macian, P., and Gaudet, R. (2013). What do we know about the transient receptor potential vanilloid 2 (TRPV2) ion channel? *FEBS J.* 280, 5471–5487. doi: 10.1111/febs.12302

Perez-Reyes, E. (2003). Molecular physiology of low-voltage-activated T-type calcium channels. *Physiol. Rev.* 83, 117–161. doi: 10.1152/physrev.00018.2002

Peterson, B. Z., DeMaria, C. D., and Yue, D. T. (1999). Calmodulin is the Ca^{2+} sensor for Ca^{2+}-dependent inactivation of L-type calcium channels. *Neuron* 22, 549–558. doi: 10.1016/S0896-6273(00)80709-6

Pitt, S. J., Reilly-O'Donnell, B., and Sitsapesan, R. (2016). Exploring the biophysical evidence that mammalian two-pore channels are NAADP-activated calcium-permeable channels. *J. Physiol.* 594, 4171–4179. doi: 10.1113/JP270936

Platania, C. B. M., Giurdanella, G., Di Paola, L., Leggio, G. M., Drago, F., Salomone, S., et al. (2017). $P2X_7$ receptor antagonism: implications in diabetic retinopathy. *Biochem. Pharmacol.* 138, 130–139. doi: 10.1016/j.bcp.2017.05.001

Poyner, D. R., Sexton, P. M., Marshall, I., Smith, D. M., Quirion, R., Born, W., et al. (2002). International Union of Pharmacology. *XXXII. The mammalian calcitonin gene-related peptides, adrenomedullin, amylin, and calcitonin receptors. Pharmacol. Rev.* 54, 233–246. doi: 10.1124/pr.54.2.233

Pozzi, A., Yurchenco, P. D., and Iozzo, R. V. (2017). The nature and biology of basement membranes. *Matrix Biol.* 57–58, 1–11. doi: 10.1016/j.matbio.2016.12.009

Prakriya, M., and Lewis, R. S. (2015). Store-operated calcium channels. *Physiol. Rev.* 95, 1383–1436. doi: 10.1152/physrev.00020.2014

Praticò, D., and Dogné, J. M. (2005). Selective cyclooxygenase-2 inhibitors development in cardiovascular medicine. *Circulation* 112, 1073–1079. doi: 10.1161/CIRCULATIONAHA.104.524231

Proks, P., de Wet, H., and Ashcroft, F. M. (2010). Activation of the K(ATP) channel by Mg-nucleotide interaction with SUR1. *J. Gen. Physiol.* 136, 389–405. doi: 10.1085/jgp.201010475

Prossnitz, E. R., and Arterburn, J. B. (2015). International union of basic and clinical pharmacology. *XCVII. G protein–coupled estrogen receptor and its pharmacologic modulators. Pharmacol. Rev.* 67, 505–540. doi: 10.1124/pr.114.009712

Purves, G. I., Kamishima, T., Davies, L. M., Quayle, J. M., and Dart, C. (2009). Exchange protein activated by cAMP (Epac) mediates cAMP-dependent but protein kinase A-insensitive modulation of vascular ATP-sensitive potassium channels. *J. Physiol.* 587, 3639–3650. doi: 10.1113/jphysiol.2009.173534

Quayle, J. M., Nelson, M. T., and Standen, N. B. (1997). ATP-sensitive and inwardly rectifying potassium channels in smooth muscle. *Physiol. Rev.* 77, 1165–1232. doi: 10.1152/physrev.1997.77.4.1165

Quayle, J. M., Turner, M. R., Burrell, H. E., and Kamishima, T. (2006). Effects of hypoxia, anoxia, and metabolic inhibitors on K_{ATP} channels in rat femoral artery myocytes. *Am. J. Physiol. Hear. Circ. Physiol.* 291, H71–H80. doi: 10.1152/ajpheart.01107.2005

Querques, G., Borrelli, E., Sacconi, R., De Vitis, L., Leocani, L., Santangelo, R., et al. (2019). Functional and morphological changes of the retinal vessels in Alzheimer's disease and mild cognitive impairment. *Sci. Rep.* 9:63. doi: 10.1038/s41598-018-37271-6

Quignard, J., Harley, E., Duhault, J., Vanhoutte, P., and Félétou, M. (2003). K^+ channels in cultured bovine retinal pericytes: effects of β-adrenergic stimulation. *J. Cardiovasc. Pharmacol.* 42, 379–388. doi: 10.1097/00005344-200309000-00009

Quinn, K. V., Cui, Y., Giblin, J. P., Clapp, L. H., and Tinker, A. (2003). Do anionic phospholipids serve as cofactors or second messengers for the regulation of activity of cloned ATP-sensitive K^+ channels? *Circ. Res.* 93, 646–655. doi: 10.1161/01.RES.0000095247.81449.8E

Quinn, K. V., Giblin, J. P., and Tinker, A. (2004). Multisite phosphorylation mechanism for protein kinase A activation of the smooth muscle ATP-sensitive K^+ channel. *Circ. Res.* 94, 1359–1366. doi: 10.1161/01.RES.0000128513.34817.c4

Raifman, T. K., Kumar, P., Haase, H., Klussmann, E., Dascal, N., and Weiss, S. (2017). Protein kinase C enhances plasma membrane expression of cardiac L-type calcium channel, $Ca_v1.2$. *Channels* 11, 604–615. doi: 10.1080/19336950.2017.1369636

Ramos, D., Navarro, M., Mendes-Jorge, L., Carretero, A., López-Luppo, M., Nacher, V., et al. (2013). "The use of confocal laser microscopy to analyze mouse retinal blood vessels," in *Confocal Laser Microscopy - Principles and Applications in Medicine, Biology, and the Food Sciences*, ed N. Lagali (London: IntechOpen), 19–37. doi: 10.5772/56131

Ranade, S. S., Qiu, Z., Woo, S. H., Hur, S. S., Murthy, S. E., Cahalan, S. M., et al. (2014). Piezo1, a mechanically activated ion channel, is required for vascular development in mice. *Proc. Natl. Acad. Sci. U.S.A.* 111, 10347–10352. doi: 10.1073/pnas.1409233111

Ratelade, J., Klug, N. R., Lombardi, D., Angelim, M. K. S. C., Dabertrand, F., Domenga-Denier, V., et al. (2020). Reducing hypermuscularization of the transitional segment between arterioles and capillaries protects against spontaneous intracerebral hemorrhage. *Circulation* 141, 2078–2094. doi: 10.1161/CIRCULATIONAHA.119.040963

Reichhart, N., Schöberl, S., Keckeis, S., Alfaar, A. S., Roubeix, C., Cordes, M., et al. (2019). Anoctamin-4 is a bona fide Ca^{2+}-dependent non-selective cation channel. *Sci. Rep.* 9:2257. doi: 10.1038/s41598-018-37287-y

Robertson, B. E., and Nelson, M. T. (1994). Aminopyridine inhibition and voltage dependence of K^+ currents in smooth muscle cells from cerebral arteries. *Am. J. Physiol. Cell Physiol.* 267, C1589–C1597. doi: 10.1152/ajpcell.1994.267.6.C1589

Ross, E. M., and Wilkie, T. M. (2000). GTPase-activating proteins for heterotrimeric G proteins: regulators of G protein signaling (RGS) and RGS-like proteins. *Annu. Rev. Biochem.* 69, 795–827. doi: 10.1146/annurev.biochem.69.1.795

Rossier, M. F. (2016). T-type calcium channel: a privileged gate for calcium entry and control of adrenal steroidogenesis. *Front. Endocrinol.* 7:43. doi: 10.3389/fendo.2016.00043

Rouach, N., Koulakoff, A., Abudara, V., Willecke, K., and Giaume, C. (2008). Astroglial metabolic networks sustain hippocampal synaptic transmission. *Science* 322, 1551–1555. doi: 10.1126/science.1164022

Rouget, C. (1873). Mémoire sur le développement, la structure et les proprietés physiologiques des capillaires sanguins et lymphatiques. *Arch. Physiol. Norm. Pathol.* 5, 603–663.

Rungta, R. L., Chaigneau, E., Osmanski, B.-F., and Charpa, S. (2018). Vascular compartmentalization of functional hyperemia from the synapse to the pia. *Neuron* 99, 362–337. doi: 10.1016/j.neuron.2018.06.012

Russell, F. D., and Davenport, A. P. (1999). Secretory pathways in endothelin synthesis. *Br. J. Pharmacol.* 126, 391–398. doi: 10.1038/sj.bjp.0702315

Sadana, R., and Dessauer, C. W. (2009). Physiological roles for G protein-regulated adenylyl cyclase isoforms: insights from knockout and overexpression studies. *NeuroSignals* 17, 5–22. doi: 10.1159/000166277

Sakagami, K., Wu, D. M., and Puro, D. G. (1999). Physiology of rat retinal pericytes: modulation of ion channel activity by serum-derived molecules. *J. Physiol.* 521, 637–650. doi: 10.1111/j.1469-7793.1999.00637.x

Salomone, S., Soydan, G., Ip, P. C. T., Hopson, K. M. P., and Waeber, C. (2010). Vessel-specific role of sphingosine kinase 1 in the vasoconstriction of isolated basilar arteries. *Pharmacol. Res.* 62, 465–474. doi: 10.1016/j.phrs.2010.09.002

Sasaki, Y., Hoshi, M., Akazawa, C., Nakamura, Y., Tsuzuki, H., Inoue, K., et al. (2003). Selective expression of $G_{i/o}$-coupled ATP receptor P2Y12 in microglia in rat brain. *Glia* 44, 242–250. doi: 10.1002/glia.10293

Sassone-Corsi, P. (2012). The cyclic AMP pathway. *Cold Spring Harb. Perspect. Biol.* 4:a011148. doi: 10.1101/cshperspect.a011148

Sawyer, I., Smillie, S. J., Bodkin, J. V., Fernandes, E., O'Byrne, K. T., and Brain, S. D. (2011). The vasoactive potential of kisspeptin-10 in the peripheral vasculature. *PLoS ONE* 6:e14671. doi: 10.1371/journal.pone.0014671

Scherer, D., Seyler, C., Xynogalos, P., Scholz, E. P., Thomas, D., Backs, J., et al. (2016). Inhibition of cardiac K_{ir} current (I_{K1}) by protein kinase C critically depends on PKCβ and $K_{ir}2.2$. *PLoS ONE* 11:e0156181. doi: 10.1371/journal.pone.0156181

Schlingmann, K. P., Waldegger, S., Konrad, M., Chubanov, V., and Gudermann, T. (2007). TRPM6 and TRPM7–gatekeepers of human magnesium metabolism. *Biochim. Biophys. Acta* 1772, 813–821. doi: 10.1016/j.bbadis.2007.03.009

Schulte, G. (2010). International Union of Basic and Clinical Pharmacology. *LXXX. The class frizzled receptors. Pharmacol. Rev.* 62, 632–667. doi: 10.1124/pr.110.002931

Schwartz, E., Adamany, A. M., and Blumenfeld, O. O. (1981). Isolation and characterization of the internal elastic lamina from calf thoracic aorta. *Exp. Mol. Pathol.* 34, 299–306. doi: 10.1016/0014-4800(81)90047-2

Seino, S., and Miki, T. (2003). Physiological and pathophysiological roles of ATP-sensitive K^+ channels. *Prog. Biophys. Mol. Biol.* 81, 133–176. doi: 10.1016/S0079-6107(02)00053-6

Sekiguchi, F., and Kawabata, A. (2013). T-type calcium channels: functional regulation and implication in pain signaling. *J. Pharmacol. Sci.* 122, 244–250. doi: 10.1254/jphs.13R05CP

Selim, S., Sunkara, M., Salous, A. K., Leung, S. W., Berdyshev, E. V., Bailey, A., et al. (2011). Plasma levels of sphingosine 1-phosphate are strongly correlated with haematocrit, but variably restored by red blood cell transfusions. *Clin. Sci.* 121, 565–572. doi: 10.1042/CS20110236

Sharif-Naeini, R., Folgering, J. H. A., Bichet, D., Duprat, F., Lauritzen, I., Arhatte, M., et al. (2009). Polycystin-1 and−2 dosage regulates pressure sensing. *Cell* 139, 587–596. doi: 10.1016/j.cell.2009.08.045

Sherwood, T. W., Frey, E. N., and Askwith, C. C. (2012). Structure and activity of the acid-sensing ion channels. *Am. J. Physiol. Cell Physiol.* 303, C699–C710. doi: 10.1152/ajpcell.00188.2012

Shi, Y., Chen, X., Wu, Z., Shi, W., Yang, Y., Cui, N., et al. (2008a). cAMP-dependent protein kinase phosphorylation produces interdomain movement in SUR2B leading to activation of the vascular K_{ATP} channel. *J. Biol. Chem.* 283, 7523–7530. doi: 10.1074/jbc.M709941200

Shi, Y., Cui, N., Shi, W., and Jiang, C. (2008b). A short motif in $K_{ir}6.1$ consisting of four phosphorylation repeats underlies the vascular K_{ATP} channel inhibition by protein kinase C. *J. Biol. Chem.* 283, 2488–2494. doi: 10.1074/jbc.M708769200

Shi, Y., Wu, Z., Cui, N., Shi, W., Yang, Y., Zhang, X., et al. (2007). PKA phosphorylation of SUR2B subunit underscores vascular K_{ATP} channel activation by beta-adrenergic receptors. *Am. J. Physiol. Regul. Integr. Comp. Physiol.* 293, R1205–R1214. doi: 10.1152/ajpregu.00337.2007

Shih, A. Y., Rühlmann, C., Blinder, P., Devor, A., Drew, P. J., Friedman, B., et al. (2015). Robust and fragile aspects of cortical blood flow in relation to the underlying angioarchitecture. *Microcirculation* 22, 204–218. doi: 10.1111/micc.12195

Shima, Y., Kawaguchi, S. Y., Kosaka, K., Nakayama, M., Hoshino, M., Nabeshima, Y., et al. (2007). Opposing roles in neurite growth control by two seven-pass transmembrane cadherins. *Nat. Neurosci.* 10, 963–969. doi: 10.1038/nn1933

Shyng, S. L., Ferrigni, T., and Nichols, C. G. (1997). Regulation of K_{ATP} channel activity by diazoxide and MgADP. *Distinct functions of the two nucleotide binding folds of the sulfonylurea receptor. J. Gen. Physiol.* 110, 643–654. doi: 10.1085/jgp.110.6.643

Shyng, S. L., and Nichols, C. G. (1998). Membrane phospholipid control of nucleotide sensitivity of K_{ATP} channels. *Science* 282, 1138–1141. doi: 10.1126/science.282.5391.1138

Silva, A. S., and Zanesco, A. (2010). Physical exercise, β-adrenergic receptors, and vascular response. *J. Vasc. Bras.* 9, 47–56. doi: 10.1590/S1677-54492010000200007

Simon, M. I., Strathmann, M. P., and Gautam, N. (1991). Diversity of G proteins in signal transduction. *Science* 252, 802–808. doi: 10.1126/science.1902986

Singh, A., Gebhart, M., Fritsch, R., Sinnegger-Brauns, M. J., Poggiani, C., Hoda, J. C., et al. (2008). Modulation of voltage- and Ca^{2+}-dependent gating of $Ca_v1.3$ L-type calcium channels by alternative splicing of a C-terminal regulatory domain. *J. Biol. Chem.* 283, 20733–20744. doi: 10.1074/jbc.M802254200

Singh, J., Wen, X., and Scales, S. J. (2015). The orphan G protein-coupled receptor Gpr175 (Tpra40) enhances Hedgehog signaling by modulating cAMP levels. *J. Biol. Chem.* 290, 29663–29675. doi: 10.1074/jbc.M115.665810

Smith, I. F., and Parker, I. (2009). Imaging the quantal substructure of single IP_3R channel activity during Ca^{2+} puffs in intact mammalian cells. *Proc. Natl. Acad. Sci. U.S.A.* 106, 6404–6409. doi: 10.1073/pnas.0810799106

Smrcka, A. V. (2008). G protein βγ subunits: Central mediators of G protein-coupled receptor signaling. *Cell. Mol. Life Sci.* 65, 2191–2214. doi: 10.1007/s00018-008-8006-5

Soboloff, J., Spassova, M. A., Tang, X. D., Hewavitharana, T., Xu, W., and Gill, D. L. (2006). Orai1 and STIM reconstitute store-operated calcium channel function. *J. Biol. Chem.* 281, 20661–20665. doi: 10.1074/jbc.C600126200

Soh, U. J., Dores, M. R., Chen, B., and Trejo, J. (2010). Signal transduction by protease-activated receptors. *Br. J. Pharmacol.* 160, 191–203. doi: 10.1111/j.1476-5381.2010.00705.x

Sokolovsky, M. (1995). Endothelin receptor subtypes and their role in transmembrane signaling mechanisms. *Pharmacol. Ther.* 68, 435–471. doi: 10.1016/0163-7258(95)02015-2

Souza Bomfim, G. H., Costiniti, V., Li, Y., Idaghdour, Y., and Lacruz, R. S. (2020). TRPM7 activation potentiates SOCE in enamel cells but requires ORAI. *Cell Calcium* 87:102187. doi: 10.1016/j.ceca.2020.102187

Stirling, L., Williams, M. R., and Morielli, A. D. (2009). Dual roles for RhoA/Rho-kinase in the regulated trafficking of a voltage-sensitive potassium channel. *Mol. Biol. Cell* 20, 2991–3002. doi: 10.1091/mbc.e08-10-1074

Stölting, G., Teodorescu, G., Begemann, B., Schubert, J., Nabbout, R., Toliat, M. R., et al. (2013). Regulation of ClC-2 gating by intracellular ATP. *Pflügers Arch.* 465, 1423–1437. doi: 10.1007/s00424-013-1286-0

Stott, J. B., Povstyan, O. V., Carr, G., Barrese, V., and Greenwood, I. A. (2015). G-protein βγ subunits are positive regulators of $K_v7.4$ and native vascular K_v7 channel activity. *Proc. Natl. Acad. Sci. U.S.A.* 112, 6497–6502. doi: 10.1073/pnas.1418605112

Straub, A., Zeigler, A., and Isakson, B. (2014). The myoendothelial junction: connections that deliver the message. *Physiology* 29, 242–249. doi: 10.1152/physiol.00042.2013

Straub, S. V., Girouard, H., Doetsch, P. E., Hannah, R. M., Wilkerson, M. K., and Nelson, M. T. (2009). Regulation of intracerebral arteriolar tone by K_v channels: effects of glucose and PKC. *Am. J. Physiol. Cell Physiol.* 297, C788–C796. doi: 10.1152/ajpcell.00148.2009

Striessnig, J., Pinggera, A., Kaur, G., Bock, G., and Tuluc, P. (2014). L-type Ca^{2+} channels in heart and brain. *Wiley Interdiscip. Rev. Membr. Transp. Signal.* 3, 15–38. doi: 10.1002/wmts.102

Sugimura, R., He, X. C., Venkatraman, A., Arai, F., Box, A., Semerad, C., et al. (2012). Noncanonical Wnt signaling maintains hematopoietic stem cells in the niche. *Cell* 150, 351–365. doi: 10.1016/j.cell.2012.05.041

Sugiyama, T., Kawamura, H., Yamanishi, S., Kobayashi, M., Katsumura, K., and Puro, D. G. (2005). Regulation of $P2X_7$-induced pore formation and cell death in pericyte-containing retinal microvessels. *Am. J. Physiol.* 288, C568–C576. doi: 10.1152/ajpcell.00380.2004

Sung, T. S., Jeon, J. P., Kim, B. J., Hong, C., Kim, S. Y., Kim, J., et al. (2011). Molecular determinants of PKA-dependent inhibition of TRPC5 channel. *Am. J. Physiol. Cell Physiol.* 301, C823–C832. doi: 10.1152/ajpcell.00351.2010

Suzuki, J., Umeda, M., Sims, P. J., and Nagata, S. (2010). Calcium-dependent phospholipid scrambling by TMEM16F. *Nature* 468, 834–838. doi: 10.1038/nature09583

Swärd, K., Mita, M., Wilson, D. P., Deng, J. T., Susnjar, M., and Walsh, M. P. (2003). The role of RhoA and Rho-associated kinase in vascular smooth muscle contraction. *Curr. Hypertens. Rep.* 5, 66–72. doi: 10.1007/s11906-003-0013-1

Tadross, M. R., Johny, M., Ben, and Yue, D. T. (2010). Molecular endpoints of Ca^{2+}/calmodulin- and voltage-dependent inactivation of $Ca_v1.3$ channels. *J. Gen. Physiol.* 135, 197–215. doi: 10.1085/jgp.200910308

Tadross, M. R., and Yue, D. T. (2010). Systematic mapping of the state dependence of voltage- and Ca^{2+}-dependent inactivation using simple open-channel measurements. *J. Gen. Physiol.* 135, 217–227. doi: 10.1085/jgp.200910309

Takezawa, R., Schmitz, C., Demeuse, P., Scharenberg, A. M., Penner, R., and Fleig, A. (2004). Receptor-mediated regulation of the TRPM7 channel through its endogenous protein kinase domain. *Proc. Natl. Acad. Sci. U.S.A.* 101, 6009–6014. doi: 10.1073/pnas.0307565101

Tanabe, K., Tucker, S. J., Ashcroft, F. M., Proks, P., Kioka, N., Amachi, T., et al. (2000). Direct photoaffinity labeling of $K_{ir}6.2$ by [gamma-(32)P]ATP-[gamma]4-azidoanilide. *Biochem. Biophys. Res. Commun.* 272, 316–319. doi: 10.1006/bbrc.2000.2780

Tarasov, A., Dusonchet, J., and Ashcroft, F. (2004). Metabolic regulation of the pancreatic beta-cell ATP-sensitive K^+ channel: a pas de deux. *Diabetes* 53, S113–S122. doi: 10.2337/diabetes.53.suppl_3.S113

Taylor, M. S., Bonev, A. D., Gross, T. P., Eckman, D. M., Brayden, J. E., Bond, C. T., et al. (2003). Altered expression of small-conductance Ca^{2+}-activated K^+ (SK3) channels modulates arterial tone and blood pressure. *Circ. Res.* 93, 124–131. doi: 10.1161/01.RES.0000081980.63146.69

Tejada, M. A., Stople, K., Bomholtz, S. H., Meinild, A.-K., Poulsen, A. N., and Klaerke, D. A. (2014). Cell volume changes regulate slick (Slo2.1), but not slack (Slo2.2) K^+ channels. *PLoS ONE* 9:e110833. doi: 10.1371/journal.pone.0110833

Thiriet, M. (2013). *Tissue Functioning and Remodeling in the Circulatory and Ventilatory Systems.* Verlag; New York, NY: Springer. doi: 10.1007/978-1-4614-5966-8

Thorin, E., and Webb, D. J. (2010). Endothelium-derived endothelin-1. *Pflugers Arch.* 459, 951–958. doi: 10.1007/s00424-009-0763-y

Tilton, R. G., Kilo, C., and Williamson, J. R. (1979). Pericyte-endothelial relationships in cardiac and skeletal muscle capillaries. *Microvasc. Res.* 18, 325–335. doi: 10.1016/0026-2862(79)90041-4

Tobo, M., Tomura, H., Mogi, C., Wang, J. Q., Liu, J. P., Komachi, M., et al. (2007). Previously postulated "ligand-independent" signaling of GPR4 is mediated through proton-sensing mechanisms. *Cell. Signal.* 19, 1745–1753. doi: 10.1016/j.cellsig.2007.03.009

Tovey, S. C., Dedos, S. G., Rahman, T., Taylor, E. J. A., Pantazaka, E., and Taylor, C. W. (2010). Regulation of inositol 1,4,5-trisphosphate receptors by cAMP independent of cAMP-dependent protein kinase. *J. Biol. Chem.* 285, 12979–12989. doi: 10.1074/jbc.M109.096016

Trost, A., Lange, S., Schroedl, F., Bruckner, D., Motloch, K. A., Bogner, B., et al. (2016). Brain and retinal pericytes: Origin, function and role. *Front. Cell. Neurosci.* 10:20. doi: 10.3389/fncel.2016.00020

Tsai, P. S., Kaufhold, J. P., Blinder, P., Friedman, B., Drew, P. J., Karten, H. J., et al. (2009). Correlations of neuronal and microvascular densities in murine cortex revealed by direct counting and colocalization of nuclei and vessels. *J. Neurosci.* 29, 14553–14570. doi: 10.1523/JNEUROSCI.3287-09.2009

Tu, H., Wang, Z., Nosyreva, E., Smedt, H., De, and Bezprozvanny, I. (2005). Functional characterization of mammalian inositol 1,4,5-trisphosphate receptor isoforms. *Biophys. J.* 88, 1046–1055. doi: 10.1529/biophysj.104.049593

Tucker, S. J., Gribble, F. M., Zhao, C., Trapp, S., and Ashcroft, F. M. (1997). Truncation of $K_{ir}6.2$ produces ATP-sensitive K^+ channels in the absence of the sulphonylurea receptor. *Nature* 387, 179–183. doi: 10.1038/387179a0

Tung, R. T., and Kurachi, Y. (1991). On the mechanism of nucleotide diphosphate activation of the ATP-sensitive K^+ channel in ventricular cell of guinea-pig. *J. Physiol.* 437, 239–256. doi: 10.1113/jphysiol.1991.sp018593

Ullrich, N. D., Voets, T., Prenen, J., Vennekens, R., Talavera, K., Droogmans, G., et al. (2005). Comparison of functional properties of the Ca^{2+}-activated cation channels TRPM4 and TRPM5 from mice. *Cell Calcium* 37, 267–278. doi: 10.1016/j.ceca.2004.11.001

Upchurch, C., and Leitinger, N. (2019). "Biologically active lipids in vascular biology," in *Fundamentals of Vascular Biology. Learning Materials in Biosciences,* ed M. Geiger (Cham: Springer), 171–193. doi: 10.1007/978-3-030-12270-6_9

Urtatiz, O., and Van Raamsdonk, C. D. (2016). Gnaq and Gna11 in the Endothelin signaling pathway and melanoma. *Front. Genet.* 7:59. doi: 10.3389/fgene.2016.00059

van de Kreeke, J. A., Nguyen, H. T., Konijnenberg, E., Tomassen, J., den Braber, A., ten Kate, M., et al. (2018). Retinal and cerebral microvasculopathy: Relationships and their genetic contributions. *Investig. Ophthalmol. Vis. Sci.* 59, 5025–5031. doi: 10.1167/iovs.18-25341

Vanderheyden, V., Devogelaere, B., Missiaen, L., De Smedt, H., Bultynck, G., and Parys, J. B. (2009). Regulation of inositol 1,4,5-trisphosphate-induced Ca^{2+} release by reversible phosphorylation and dephosphorylation. *Biochim. Biophys. Acta* 1793, 959–970. doi: 10.1016/j.bbamcr.2008.12.003

Vanlandewijck, M., He, L., Mäe, M. A., Andrae, J., Ando, K., Gaudio, F., et al. (2018). A molecular atlas of cell types and zonation in the brain vasculature. *Nature* 554, 475–480. doi: 10.1038/nature25739

Veldhuis, N. A., Poole, D. P., Grace, M., McIntyre, P., Bunnett, N. W., and Christopoulos, A. (2015). The G protein–coupled receptor–transient receptor potential channel axis: molecular insights for targeting disorders of sensation and inflammation. *Pharmacol. Rev.* 67, 36–73. doi: 10.1124/pr.114.009555

Venkatachalam, K., and Montell, C. (2007). TRP Channels. *Annu. Rev. Biochem.* 76, 387–417. doi: 10.1146/annurev.biochem.75.103004.142819

Venkatachalam, K., Wong, C.-O., and Zhu, M. X. (2015). The role of TRPMLs in endolysosomal trafficking and function. *Cell Calcium* 58, 48–56. doi: 10.1016/j.ceca.2014.10.008

Vergarajauregui, S., Oberdick, R., Kiselyov, K., and Puertollano, R. (2008). Mucolipin 1 channel activity is regulated by protein kinase A-mediated phosphorylation. *Biochem. J.* 410, 417–425. doi: 10.1042/BJ20070713

Vermassen, E., Fissore, R. A., Kasri, N. N., Vanderheyden, V., Callewaert, G., Missiaen, L., et al. (2004). Regulation of the phosphorylation of the inositol 1,4,5-trisphosphate receptor by protein kinase C. *Biochem. Biophys. Res. Commun.* 319, 888–893. doi: 10.1016/j.bbrc.2004.05.071

Vetri, F., Xu, H., Paisansathan, C., and Pelligrino, D. A. (2012). Impairment of neurovascular coupling in type 1 diabetes mellitus in rats is linked to PKC modulation of BK_{Ca} and K_{ir} channels. *Am. J. Physiol. Hear. Circ. Physiol.* 302, H1274–H1284. doi: 10.1152/ajpheart.01067.2011

Vilardaga, J. P., Romero, G., Friedman, P. A., and Gardella, T. J. (2011). Molecular basis of parathyroid hormone receptor signaling and trafficking: a family B GPCR paradigm. *Cell. Mol. Life Sci.* 68, 1–13. doi: 10.1007/s00018-010-0465-9

Villari, A., Giurdanella, G., Bucolo, C., Drago, F., and Salomone, S. (2017). Apixaban enhances vasodilatation mediated by protease-activated receptor 2 in isolated rat arteries. *Front. Pharmacol.* 8:480. doi: 10.3389/fphar.2017.00480

von Bartheld, C. S., Bahney, J., and Herculano-Houzel, S. (2016). The search for true numbers of neurons and glial cells in the human brain: a review of 150 years of cell counting. *J. Comp. Neurol.* 524, 3865–3895. doi: 10.1002/cne.24040

von Beckerath, N., Nees, S., Neumann, F. J., Krebs, B., Juchem, G., and Schömig, A. (2000). An inward rectifier and a voltage-dependent K^+ current in single, cultured pericytes from bovine heart. *Cardiovasc. Res.* 46, 569–578. doi: 10.1016/S0008-6363(00)00055-9

Wagner, T. F. J., Loch, S., Lambert, S., Straub, I., Mannebach, S., Mathar, I., et al. (2008). Transient receptor potential M3 channels are ionotropic steroid receptors in pancreatic β cells. *Nat. Cell Biol.* 10, 1421–1430. doi: 10.1038/ncb1801

Wang, B., Li, C., Huai, R., and Qu, Z. (2015). Overexpression of ANO1/TMEM16A, an arterial Ca^{2+}-activated Cl^- channel, contributes to spontaneous hypertension. *J. Mol. Cell. Cardiol.* 82, 22–32. doi: 10.1016/j.yjmcc.2015.02.020

Wang, Q., Leo, M. D., Narayanan, D., Kuruvilla, K. P., and Jaggar, J. H. (2016). Local coupling of TRPC6 to ANO1/TMEM16A channels in smooth muscle cells amplifies vasoconstriction in cerebral arteries. *Am. J. Physiol. Cell Physiol.* 310, C1001–C1009. doi: 10.1152/ajpcell.00092.2016

Wang, Y., and Venton, B. J. (2017). Correlation of transient adenosine release and oxygen changes in the caudate-putamen. *J. Neurochem.* 140, 13–23. doi: 10.1111/jnc.13705

Watson, N., Linder, M. E., Druey, K. M., Kehrl, J. H., and Blumer, K. J. (1996). RGS family members: GTPase-activating proteins for heterotrimeric G- protein α-subunits. *Nature* 383, 172–175. doi: 10.1038/383172a0

Watts, A. O., Verkaar, F., Van Der Lee, M. M. C., Timmerman, C. A. W., Kuijer, M., Offenbeek, J., et al. (2013). β-Arrestin recruitment and G protein signaling by the atypical human chemokine decoy receptor CCX-CKR. *J. Biol. Chem.* 288, 7169–7181. doi: 10.1074/jbc.M112.406108

Weiß, K. T., Fante, M., Köhl, G., Schreml, J., Haubner, F., Kreutz, M., et al. (2017). Proton-sensing G protein-coupled receptors as regulators of cell proliferation and migration during tumor growth and wound healing. *Exp. Dermatol.* 26, 127–132. doi: 10.1111/exd.13209

Wheeler, D. G., Groth, R. D., Ma, H., Barrett, C. F., Owen, S. F., Safa, P., et al. (2012). Ca_v1 and Ca_v2 channels engage distinct modes of Ca^{2+} signaling to control CREB-dependent gene expression. *Cell* 149, 1112–1124. doi: 10.1016/j.cell.2012.03.041

Wihlborg, A. K., Wang, L., Braun, O. Ö., Eyjolfsson, A., Gustafsson, R., Gudbjartsson, T., et al. (2004). ADP receptor P2Y12 is expressed in vascular smooth muscle cells and stimulates contraction in human blood vessels. *Arterioscler. Thromb. Vasc. Biol.* 24, 1810–1815. doi: 10.1161/01.ATV.0000142376.30582.ed

Winkler, E. A., Bell, R. D., and Zlokovic, B. V. (2011). Central nervous system pericytes in health and disease. *Nat. Neurosci.* 14, 1398–1405. doi: 10.1038/nn.2946

Woodward, D. F., Jones, R. L., and Narumiya, S. (2011). International union of basic and clinical pharmacology. LXXXIII: classification of prostanoid receptors, updating 15 years of progress. *Pharmacol. Rev.* 63, 471–538. doi: 10.1124/pr.110.003517

Worzfeld, T., Wettschureck, N., and Offermanns, S. (2008). G_{12}/G_{13}-mediated signalling in mammalian physiology and disease. *Trends Pharmacol. Sci.* 29, 582–589. doi: 10.1016/j.tips.2008.08.002

Woszczek, G., Chen, L.-Y., Nagineni, S., Alsaaty, S., Harry, A., Logun, C., et al. (2007). IFN-γ induces cysteinyl leukotriene receptor 2 expression and enhances the responsiveness of human endothelial cells to cysteinyl leukotrienes. *J. Immunol.* 178, 5262–5270. doi: 10.4049/jimmunol.178.8.5262

Wroblewska, B., Santi, M. R., and Neale, J. H. (1998). N-acetylaspartylglutamate activates cyclic AMP-coupled metabotropic glutamate receptors in cerebellar astrocytes. *Glia* 24, 172–179. doi: 10.1002/(SICI)1098-1136(199810)24:2<172::AID-GLIA2>3.0.CO;2-6

Wu, D. M., Kawamura, H., Sakagami, K., Kobayashi, M., and Puro, D. G. (2003). Cholinergic regulation of pericyte-containing retinal microvessels. *Am. J. Physiol. Hear. Circ. Physiol.* 284, H2083–H2090. doi: 10.1152/ajpheart.01007.2002

Wu, J., Lewis, A. H., and Grandl, J. (2017). Touch, tension, and transduction – the function and regulation of piezo ion channels. *Trends Biochem. Sci.* 42, 57–71. doi: 10.1016/j.tibs.2016.09.004

Wu, Y., Shyng, S. L., and Chen, P. C. (2015). Concerted trafficking regulation of $K_v2.1$ and K_{ATP} channels by leptin in pancreatic β-cells. *J. Biol. Chem.* 290, 29676–29690. doi: 10.1074/jbc.M115.670877

Xi, Q., Adebiyi, A., Zhao, G., Chapman, K. E., Waters, C. M., Hassid, A., et al. (2009). IP_3 constricts cerebral arteries via IP_3 receptor-mediated TRPC3 channel activation and independently of sarcoplasmic reticulum Ca^{2+} release. *Circ. Res.* 105:e1. doi: 10.1161/CIRCRESAHA.108.173948

Xiao, Q., Yu, K., Perez-Cornejo, P., Cui, Y., Arreola, J., and Hartzell, H. C. (2011). Voltage- and calcium-dependent gating of TMEM16A/Ano1 chloride channels are physically coupled by the first intracellular loop. *Proc. Natl. Acad. Sci. U.S.A.* 108, 8891–8896. doi: 10.1073/pnas.1102147108

Xiao, X., Liu, H. X., Shen, K., Cao, W., and Li, X. Q. (2017). Canonical transient receptor potential channels and their link with cardio/cerebro-vascular diseases. *Biomol. Ther.* 25, 471–481. doi: 10.4062/biomolther.2016.096

Xu, W., and Lipscombe, D. (2001). Neuronal $Ca_v1.3\alpha_1$ L-type channels activate at relatively hyperpolarized membrane potentials and are

incompletely inhibited by dihydropyridines. *J. Neurosci.* 21, 5944–5951. doi: 10.1523/JNEUROSCI.21-16-05944.2001

Yamada, M., Isomoto, S., Matsumoto, S., Kondo, C., Shindo, T., Horio, Y., et al. (1997). Sulphonylurea receptor 2B and $K_{ir}6.1$ form a sulphonylurea-sensitive but ATP-insensitive K^+ channel. *J. Physiol.* 499, 715–720. doi: 10.1113/jphysiol.1997.sp021963

Yang, G., Xu, J., Li, T., Ming, J., Chen, W., and Liu, L. (2010). Role of V_{1a} receptor in AVP-induced restoration of vascular hyporeactivity and its relationship to MLCP-MLC_{20} phosphorylation pathway. *J. Surg. Res.* 161, 312–320. doi: 10.1016/j.jss.2009.01.005

Yang, H., Kim, A., David, T., Palmer, D., Jin, T., Tien, J., et al. (2012). TMEM16F forms a Ca^{2+}-activated cation channel required for lipid scrambling in platelets during blood coagulation. *Cell* 151, 111–122. doi: 10.1016/j.cell.2012.07.036

Yang, L., Liu, G., Zakharov, S. I., Morrow, J. P., Rybin, V. O., Steinberg, S. F., et al. (2005). Ser1928 is a common site for $Ca_v1.2$ phosphorylation by protein kinase C isoforms. *J. Biol. Chem.* 280, 207–214. doi: 10.1074/jbc.M410509200

Yang, Y. (2012). Wnt signaling in development and disease. *Cell Biosci.* 2:14. doi: 10.1186/2045-3701-2-14

Yang, Y. D., Cho, H., Koo, J. Y., Tak, M. H., Cho, Y., Shim, W. S., et al. (2008). TMEM16A confers receptor-activated calcium-dependent chloride conductance. *Nature* 455, 1210–1215. doi: 10.1038/nature07313

Yin, J., and Kuebler, W. M. (2010). Mechanotransduction by TRP channels: general concepts and specific role in the vasculature. *Cell Biochem. Biophys.* 56, 1–18. doi: 10.1007/s12013-009-9067-2

Yu, F. H., and Catterall, W. A. (2003). Overview of the voltage-gated sodium channel family. *Genome Biol.* 4:207. doi: 10.1186/gb-2003-4-3-207

Yuan, K., Orcholski, M. E., Panaroni, C., Shuffle, E. M., Huang, N. F., Jiang, X., et al. (2015). Activation of the wnt/planar cell polarity pathway is required for pericyte recruitment during pulmonary angiogenesis. *Am. J. Pathol.* 185, 69–84. doi: 10.1016/j.ajpath.2014.09.013

Yudin, Y., and Rohacs, T. (2018). Inhibitory $G_{i/o}$-coupled receptors in somatosensory neurons: potential therapeutic targets for novel analgesics. *Mol. Pain* 14:1744806918763646. doi: 10.1177/1744806918763646

Yue, R., Li, H., Liu, H., Li, Y., Wei, B., Gao, G., et al. (2012). Thrombin receptor regulates hematopoiesis and endothelial-to-hematopoietic transition. *Dev. Cell* 22, 1092–1100. doi: 10.1016/j.devcel.2012.01.025

Zamponi, G. W., and Currie, K. P. M. (2013). Regulation of Ca_v2 calcium channels by G protein coupled receptors. *Biochim. Biophys. Acta* 1828, 1629–1643. doi: 10.1016/j.bbamem.2012.10.004

Zamponi, G. W., Striessnig, J., Koschak, A., Dolphin, A. C., and Sibley, D. R. (2015). The physiology, pathology, and pharmacology of voltage-gated calcium channels and their future therapeutic potential. *Pharmacol. Rev.* 67, 821–870. doi: 10.1124/pr.114.009654

Zeisel, A., Hochgerner, H., Lönnerberg, P., Johnsson, A., Memic, F., van der Zwan, J., et al. (2018). Molecular architecture of the mouse nervous system. *Cell 174*, 999.e22–1014.e22. doi: 10.1016/j.cell.2018.06.021

Zhang, H. L., and Bolton, T. B. (1996). Two types of ATP-sensitive potassium channels in rat portal vein smooth muscle cells. *Br. J. Pharmacol.* 118, 105–114. doi: 10.1111/j.1476-5381.1996.tb15372.x

Zhang, Q., Cao, C., Zhang, Z., Wier, W. G., Edwards, A., and Pallone, T. L. (2008). Membrane current oscillations in descending vasa recta pericytes. *Am. J. Physiol. Ren. Physiol.* 294, F656–F666. doi: 10.1152/ajprenal.00493.2007

Zhang, T., Wu, D. M., Xu, G., and Puro, D. G. (2011). The electrotonic architecture of the retinal microvasculature: modulation by angiotensin II. *J. Physiol.* 589, 2383–2399. doi: 10.1113/jphysiol.2010.202937

Zhang, Y., Ji, H., Wang, J., Sun, Y., Qian, Z., Jiang, X., et al. (2018). Melatonin-mediated inhibition of $Ca_v3.2$ T-type Ca^{2+} channels induces sensory neuronal hypoexcitability through the novel protein kinase C-eta isoform. *J. Pineal Res.* 64:e12476. doi: 10.1111/jpi.12476

Zhang, Y. J., Zhang, L., Ye, Y. L., Fang, S. H., Zhou, Y., Zhang, W. P., et al. (2006). Cysteinyl leukotriene receptors CysLT1 and CysLT2 are upregulated in acute neuronal injury after focal cerebral ischemia in mice. *Acta Pharmacol. Sin.* 27, 1553–1560. doi: 10.1111/j.1745-7254.2006.00458.x

Zhao, G., Joca, H. C., Nelson, M. T., and Lederer, W. J. (2020). ATP- And voltage-dependent electro-metabolic signaling regulates blood flow in heart. *Proc. Natl. Acad. Sci. U. S. A.* 117, 7461–7470. doi: 10.1073/pnas.1922095117

Zhao, Q., Wu, K., Geng, J., Chi, S., Wang, Y., Zhi, P., et al. (2016). Ion permeation and mechanotransduction mechanisms of mechanosensitive piezo channels. *Neuron* 89, 1248–1263. doi: 10.1016/j.neuron.2016.01.046

Zhao, Q., Zhou, H., Chi, S., Wang, Y., Wang, J., Geng, J., et al. (2018). Structure and mechanogating mechanism of the Piezo1 channel. *Nature* 554, 487–492. doi: 10.1038/nature25743

Zhu, J., Zhuo, C., Xu, L., Liu, F., Qin, W., and Yu, C. (2017). Altered coupling between resting-state cerebral blood flow and functional connectivity in schizophrenia. *Schizophr. Bull.* 43, 1363–1374. doi: 10.1093/schbul/sbx051

Zimmerli, D. (2018). *Elucidating the Roles of Wnt-Secretion and β-Catenin's Interaction Partners in Development and Disease*. University of Zurich.

Zitron, E., Kiesecker, C., Lück, S., Kathöfer, S., Thomas, D., Kreye, V. A. W., et al. (2004). Human cardiac inwardly rectifying current $I_{Kir2.2}$ is upregulated by activation of protein kinase A. *Cardiovasc. Res.* 63, 520–527. doi: 10.1016/j.cardiores.2004.02.015

Conflict of Interest: The authors declare that the research was conducted in the absence of any commercial or financial relationships that could be construed as a potential conflict of interest.

frontiers in Physiology

MINI REVIEW
published: 21 December 2020
doi: 10.3389/fphys.2020.599897

Cellular and Molecular Mechanisms of Spinal Cord Vascularization

*Jose Ricardo Vieira[1,2†], Bhavin Shah[1†] and Carmen Ruiz de Almodovar[1,3]**

[1]European Center for Angioscience, Medicine Faculty Mannheim, Heidelberg University, Mannheim, Germany, [2]Faculty of Biosciences, Heidelberg University, Heidelberg, Germany, [3]Interdisciplinary Center for Neurosciences, Heidelberg University, Heidelberg, Germany

During embryonic central nervous system (CNS) development, the neural and the vascular systems communicate with each other in order to give rise to a fully functional and mature CNS. The initial avascular CNS becomes vascularized by blood vessel sprouting from different vascular plexus in a highly stereotypical and controlled manner. This process is similar across different regions of the CNS. In particular for the developing spinal cord (SC), blood vessel ingression occurs from a perineural vascular plexus during embryonic development. In this review, we provide an updated and comprehensive description of the cellular and molecular mechanisms behind this stereotypical and controlled patterning of blood vessels in the developing embryonic SC, identified using different animal models. We discuss how signals derived from neural progenitors and differentiated neurons guide the SC growing vasculature. Lastly, we provide a perspective of how the molecular mechanisms identified during development could be used to better understand pathological situations.

Keywords: neurovascular, angiogenesis, spinal cord, VEGF, neural progenitors, blood brain barrier, CNS pathology

OPEN ACCESS

Edited by:
Jean-luc Morel, Centre National de la Recherche Scientifique (CNRS), France

Reviewed by:
Yoshiko Takahashi, Kyoto University, Japan
Frrédéric Clarençon, Hôpitaux Universitaires Pitié Salpêtrière, France

***Correspondence:**
Carmen Ruiz de Almodovar carmen.ruizdealmodovar@medma.uni-heidelberg.de

[†]These authors have contributed equally to this work

Specialty section:
This article was submitted to Vascular Physiology, a section of the journal Frontiers in Physiology

Received: *28 August 2020*
Accepted: *24 November 2020*
Published: *21 December 2020*

Citation:
Vieira JR, Shah B and Ruiz de Almodovar C (2020) Cellular and Molecular Mechanisms of Spinal Cord Vascularization. Front. Physiol. 11:599897. doi: 10.3389/fphys.2020.599897

SPINAL CORD DEVELOPMENT

The development of the central nervous system (CNS) of vertebrates starts with the formation of the neural tube, an ectoderm-derived embryonic structure that gives rise to the brain and the spinal cord (SC). In mouse, this process starts at E7.5–E8 (embryonic day) and, as the neural tube grows and matures along the anterio-posterior axis, it partitions into the rostral and caudal vesicles. While the rostral vesicles form the prosencephalon, mesencephalon, and the rhombencephalon (together, the brain), the caudal vesicle matures into the SC (Lumsden and Krumlauf, 1996; Purves, 2008). At around E9.5, the neural tube acquires a dorsal-ventral patterning by the controlled secretion of morphogens in a time and concentration dependent manner, establishing 13 different neural progenitor domains (Jessell, 2000; Dessaud et al., 2008). The identity of these progenitors is characterized by a unique expression profile of transcription factors, essential for the specification of the different neuronal subtypes that each domain generates. These individual expression profiles result from the combination of different morphogens: the floor plate and the notochord generate a gradient of Sonic Hedgehog (SHH), the key player for the ventral axis, while the roof plate creates a gradient of Wingless-related integration site (WNTs) family members and bone morphogenic proteins (BMPs), required for dorsal SC patterning. Other important factors, such as fibroblast growth factors (FGFs) and retinoic acid (RA), have been shown to contribute to a correct positioning of the neural

progenitors (Diez del Corral et al., 2003; Duester, 2008; Diez Del Corral and Morales, 2017). For more details on neural development of the SC, we refer the readers to excellent reviews (Jessell, 2000; Wilson and Maden, 2005; Dessaud et al., 2007, 2008; Sagner and Briscoe, 2019).

Interestingly, as the neural progenitors undergo active proliferation and differentiation, the developing CNS starts to be simultaneously vascularized to meet the increasing demand of nutrients and oxygen. The avascular CNS starts to be vascularized at E8.5–E9.5 in mice by the formation of the perineural vascular plexus (PNVP) from mesoderm-derived angioblasts that completely covers the entire neural tube (Hogan et al., 2004; Engelhardt and Liebner, 2014). Between E9.5 and E10.5, the first blood vessels from the PNVP start ingressing into the developing SC in a stereotypical growth pattern (Nakao et al., 1988; Himmels et al., 2017). Unlike the SC, where vessels ingress from a single vascular plexus, the neocortex is vascularized by the ingression of vessels from the PNVP and an additional periventricular plexus (PVP) (Vasudevan et al., 2008). There, intrinsic transcriptional factors (Nkx2.1, Dlx1/2, and Pax6) expressed in endothelial cells are crucial for such vessel patterning from the PVP (Vasudevan et al., 2008).

Research from the last decade suggests that during development the nervous and vascular systems actively and vitally crosstalk with each other to build a fully functional organ system (Paredes et al., 2018; Segarra et al., 2019). In the next sections, we will focus on those interactions that occur during SC development in coordination with vascularization. From the current knowledge of developmental studies in SC using different animal models, we also introduce the readers with SC pathologies and the molecular targets discovered during development that could prove beneficial during injuries and diseases.

SPINAL CORD VASCULARIZATION: FROM A SIMPLE PLEXUS TO A COMPLEX NETWORK

Development of the PNVP

The early development of the SC vasculature begins at around E8.5 in mouse embryos and around E3 in avian embryos with the formation of the PNVP, a primitive vascular network formed *via* the process of vasculogenesis (Noden, 1988; Kurz et al., 1996). The assembling of this vascular bed initially requires proliferation, migration, and differentiation of mesoderm-derived angioblasts, a mesenchymal cell type giving rise to the endothelial cell lineage (Noden, 1988; Kurz et al., 1996). The identification of the first key factors contributing for this process, FGF-2 and vascular endothelial growth factor (VEGF), was initially identified by experimentation in quail (Cox and Poole, 2000; Hogan et al., 2004). In avian and mouse embryos, the first primordial vascular structures neighboring the SC and fusing to the PNVP are the dorsal aorta (the major artery) and the cardinal vein (the major vein). Mice and avians present two dorsal aortas, one dorsal aorta in each side of the midline (defined by the notochord) – but fusing into a single artery in the mid-trunk region – and two cardinal veins, similarly one in each side of the midline along the entire body (Hogan and Bautch, 2004; Kurz, 2009). In avians, primitive arterial tracts connect each of the dorsal aortas to the ventral part of the PNVP, laterally to the FP, precisely where the first sprouts from the PNVP ingress into the SC. Afterward, the SC vascular circuit is closed and drained into the cardinal veins, which are connected to the PNVP in the lateral sides of the SC (Kurz, 2009). For the best of our knowledge, a similar vascular circuit in mouse has not been demonstrated yet.

In zebrafish, the PNVP forms, however, a bit different. In zebrafish, the dorsal aorta and the cardinal vein are single vessels located below the notochord and extend throughout the entire anterior-posterior axis. The PNVP surrounding the SC arises by the combination of sprouts from arterial and venous intersegmental vessels (ISVs; which sprout from the previously formed dorsal aorta and posterior cardinal vein) and vertebral arteries (VTAs; Isogai et al., 2001, 2003; Matsuoka et al., 2016, 2017; Wild et al., 2017). Bilateral VTAs are formed along the SC by sprouting from the previously established ISVs. Genetically-ablation studies have shown that this process in zebrafish is regulated by VEGF secreted from radial glia cells located in the SC (Matsuoka et al., 2017). Interestingly, not only radial glia but also SC neurons were also shown to similarly control sprouting of venous ISVs around the developing SC in zebrafish (Wild et al., 2017). SC neurons simultaneously secrete VEGF and SFLT1 and, in case of a shift in the balance toward the former, ectopic sprouting of venous ISVs (not arterial ISVs) arise and surround the SC, suggesting that the VEGF signaling affects specifically venous ECs during this development stage window (Wild et al., 2017).

Vessel Ingression Into the SC

In avians, single angioblasts are able to invade and migrate into the SC and thus contribute, together with the sprouting from the PNVP, to SC vascularization (Kurz et al., 1996). In mice, in contrast, once the PNVP is formed, vessel ingression into of the SC only occurs from new sprouts arising from the PNVP – *via* sprouting angiogenesis (Nakao et al., 1988; Himmels et al., 2017).

Blood vessel ingression into the SC occurs in a highly stereotypical way. At around E10.5 in mouse embryos, sprouting blood vessels from the PNVP invade the neural tissue in a very specific pattern: the first sprouts invade the ventral part of the SC in between the floor plate and MN columns and also from the lateral-ventral side in proximity with the MNs (**Figure 1**). VEGF, demonstrated to be important for PNVP formation, also plays a role in this initial blood vessel ingression. Interestingly, different VEGFA isoforms perturbed SC angiogenesis at different levels. While ectopic expression of VEGFA165 and VEGFA189 in quail embryos resulted in a considerable increase of vessel ingression, only a mild phenotype is observed after ectopic expression of VEGFA121 (James et al., 2009). Although VEGFA plays a role in blood

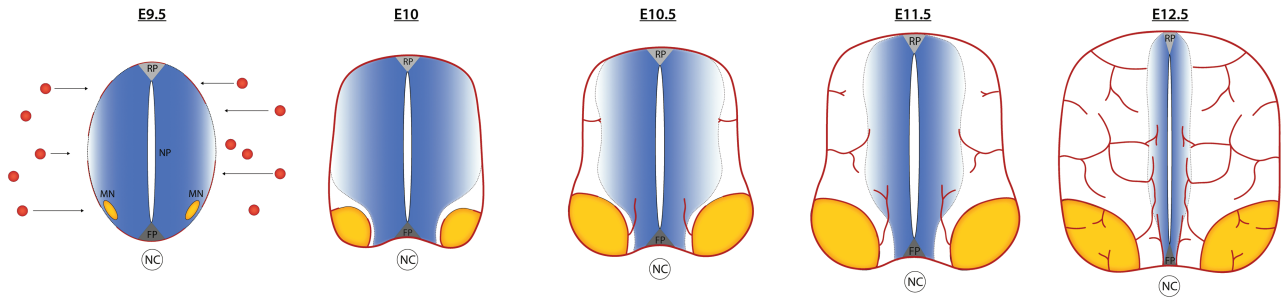

Factors involved in spinal cord vascularization

E9.5 - Development of the PNVP	E10 to E10.5 - Vessel ingression into the SC	E11.5 onwards - Stereotypical vessel patterning within the SC
FGF-2 (Cox and Poole., 2000) **VEGFA** (Hogan et al., 2004; Matsuoka et al., 2017)	**WNT7a/b** (Daneman et al., 2009; Stenman et al, 2008) **GPR124** (Kuhnert et al., 2010; Posokhova et al., 2015; Vanhollebeke et al., 2015; Zhou and Nathans, 2014) **RECK-Norrin** (Cho et al., 2017; Vanhollebeke et al., 2015) **VEGFA** (James et al., 2009) **sFLT1** (Wild et al., 2017)	**sFLT1** (Himmels et al., 2017; Matsuoka et al., 2016; Wild et al., 2017) **VEGFA** (Himmels et al., 2017; Takahashi et al., 2015)

FIGURE 1 | Stereotypical patterning of spinal cord (SC) vascularization. In normal conditions, the avascular SC starts to be vascularized at embryonic day 8.5–9.5 in mice by the formation of the perineural vascular plexus (PNVP). Between E9.5 and E10.5, blood vessels ingressing from the PNVP follow a specific invading pattern: the first vessel sprouts enter between the floor plate (FP) and motor neuron (MN) columns; subsequently they surround the MN columns and continue growing towards dorsal areas, but continuously avoiding the MNs region, the FP and part of the neural progenitors' area (NP) for a particular development time window. At E12.5 MN columns are finally vascularized and a dense network of vessels sustains the continuous growth of the SC. Factors involved in the different steps are indicated in the table.

vessel ingression, its expression is not specifically localized to areas of ingression, instead is broadly expressed in dorsal and ventral areas of the SC. This suggests that VEGFA is necessary but may not be the only factor controlling the location and timing of blood vessel sprouting from the PNVP (James et al., 2009). In fact, recent studies show that sFLT1 expression is also important to control the initial vascular sprouting into the SC in mouse (Himmels et al., 2017) and zebrafish (Wild et al., 2017). SC neurons (MNs in the case of mouse embryos) simultaneously secrete VEGF and sFLT1 to control the regions and timing of vessel ingression from the PNVP (Himmels et al., 2017; Wild et al., 2017).

WNT ligands play a major role in the initial sprouting of vessels into the SC. WNT7a and WNT7b, as other family members of the WNT family, are expressed in specific regions of the SC coincident with the time of ingression of the first vessel sprouts (Parr et al., 1993; Hollyday et al., 1995; Stenman et al., 2008; Daneman et al., 2009). WNT7a/b are expressed by several ventral and dorsal neural progenitors surrounding the ventricle at E10.5 and, while single null mutants for WNT7a or WNT7b do not present any phenotype, WNT7a/b double mutants show defects in their CNS-specific vasculature with the embryos dying around E12.5 (Stenman et al., 2008; Daneman et al., 2009). Remarkably, double mutant embryos were completely devoid of vessels and pericytes in the ventral part of the SC, but presented vessels (however with abnormal morphology) in dorsal regions of the SC. The fact that vessels continue to ingress into dorsal areas after deletion of WNT7a/b might suggested a role in SC vascularization for other WNT ligands expressed by the dorsal domains (Stenman et al., 2008). Consistently, blocking the canonical WNT signaling pathway by the removal of β-catenin from endothelial cells results in a more severe phenotype with the complete absence of blood vessels in the entire SC (Stenman et al., 2008; Daneman et al., 2009). Interestingly, in those mutants PNVP formation occurs normally, indicating that WNT signaling plays a role in the initial vessel ingression but not in PNVP formation (Stenman et al., 2008). Additionally, WNT7a/b also promote blood-brain barrier (BBB) formation, as lack of WNT7 leads to a reduction of GLUT1, the main glucose transporter in ECs of the CNS (Stenman et al., 2008). Wnt7a/b signal *via* Frizzled receptors (Zerlin et al., 2008) and RECK (reversion-inducing cysteine-rich protein), a GPI-anchored plasma membrane protein, was shown to act as a specific co-receptor for WNT7a/b in ECs (Vanhollebeke et al., 2015; Ulrich et al., 2016; Cho et al., 2017).

GPR124 is expressed by endothelial cells and pericytes and GPR124 null mice present severe hemorrhages as early as E12.5 and embryonic lethality at E15.5 (Kuhnert et al., 2010). Interestingly, GPR124 null mice present the same developmental defects observed in WNT7a/b and β-catenin null mice, suggesting that both signaling pathways share a common mechanism (Kuhnert et al., 2010). Indeed, independent groups showed that GPR124 acts as a co-activator of WNT7a/b-specific canonical pathway in endothelial cells (Zhou and Nathans, 2014; Posokhova et al., 2015; Vanhollebeke et al., 2015). Further studies have shown that a synergetic action of RECK-Norrin-GPR124 receptors in WNT7a/b signaling to promote vascular development, and the absence of either one is enough

to reduce, but not completely abolish, WNT7a/b signaling (Vanhollebeke et al., 2015; Cho et al., 2017).

Vessel Patterning Within the SC

As indicated above, the first vessel sprouts invade the ventral part of the SC in between the floor plate and MN columns and also from the lateral-ventral side in proximity with the MNs (**Figure 1**). At E11.5, vessels ingressing from both sites migrate toward each other and completely surround the MN columns, whereas at the same time additional sprouts branch from the previous vessels and also extend into dorsal areas of the SC, always along and in close contact with the ventricular zone occupied by the neural progenitors. Initially vessels do not ingress from the most dorsal part of the PNVP (Feeney and Watterson, 1946; James et al., 2009; Himmels et al., 2017). A considerable amount of research has been developed to try to understand this well-defined vascular patterning but still little is known about how the neural cells and growing blood vessels communicate to each other to orchestrate a correct SC vascularization pattern. Interestingly, we and others found that it is in the areas that blood vessels initially avoid (the floor plate, neural progenitors, and MN columns), where the highest amount of VEGF is detected (James et al., 2009; Ruiz de Almodovar et al., 2011; Himmels et al., 2017). This suggested that together with VEGF other factors were involved in blood vessel patterning. In line with this idea, we demonstrated how MNs control their own vascularization during a particular development time window (E10.5–E12.5) by simultaneously secreting VEGF and its decoy receptor sFLT1 in a hypoxia-inducible factor 1 (HIF1α) and neuropilin-1 (NRP1) dependent manner, respectively (Himmels et al., 2017). The importance of a perfect balance of these molecules is visible when overexpressing of VEGF in neural cells in mouse embryos or when reducing sFLT1 or NRP1 by knocking down their expression using *in ovo* experiments. Under those different conditions premature blood vessel ingression into MN columns occurs, showing an example of a neural-to-vessel communication mechanism that shapes SC development (Himmels et al., 2017). The importance of the balance VEGF-sFLT1 for a correct SC vascularization has also been described in zebrafish (Matsuoka et al., 2016, 2017; Wild et al., 2017).

As mentioned above blood vessels ingress from the ventral region and migrate toward dorsal areas along a well-defined path: in mice, vessels grow in close contact to the undifferentiated neural progenitors next to the ventricle while in avian vessels extend in between the undifferentiated neural progenitor zone ($Sox2^+$) and the differentiated zone ($Sox2^-$ $Tuj\text{-}1^+$; Takahashi et al., 2015; Himmels et al., 2017). Manipulation of these two areas in avian by locally disturbing neurogenesis originates a change in vascular patterning, suggesting that this particular growth path is controlled by the surrounding neural cells (Takahashi et al., 2015). Further, gain-of-function studies in chick embryos demonstrated that the stereotypical pattern along the neural progenitor area is achieved by the secretion of VEGF from the neural progenitors, attracting growing sprouts, but simultaneously endothelial cell response to VEGF is fine-tuned by sFLT1 secretion by ECs (Takahashi et al., 2015).

Notably, the degree of angiogenesis needs to be controlled as negative effects on the neural compartment can arise when too much VEGF is available. As shown in Himmels et al. (2017), MNs secrete VEGF and sFLT1 simultaneously to ensure that a correct level and timing of angiogenesis takes place. When this balance of factors is disrupted and excessive angiogenesis occurs, MNs are distributed incorrectly and MN axons leave the SC defasciculated (Himmels et al., 2017). When extrapolating this to situations, where axon regrowth is needed, it is possible that simply inducing regeneration of axons and angiogenesis is not enough to promote proper axon regrowth, but that angiogenesis needs to be limited to not disrupt the other process.

With respect to the specific pattern of arteries, veins, and capillaries, it is well-defined that in the adult SC the main arterial supply is achieved by the presence of segmental spinal arteries arising from the vertebral arteries, dorsal intercostal arteries, and lumbar arteries. Blood flows in the SC through these arteries and is further drained into the large and dorsal and posterior spinal veins in the SC (Farrar et al., 2015; Mazensky et al., 2017). Yet, it remains to be further characterized how the pattern of these three different vessel types appears during development.

COMMON MOLECULAR FACTORS IN DEVELOPMENT AND PATHOLOGY

CNS pathologies are multifaceted and complex pathologies characterized by cell death, axon damage/degeneration, loss of vascular integrity, disruption of the BBB and blood-spinal cord barrier (BSCB), inflammation, and ECM (extracellular matrix) remodeling (Griffin and Bradke, 2020). The BBB and BSCB are sophisticated barrier systems in which ECs and their tight junctions play a central part in association with astrocyte end-feet, perivascular macrophages, pericytes, and basement lamina (Bartanusz et al., 2011). However, they are heterogenous in concern to their expression of barrier-specific proteins and their functional permeability. Compared to brain, ECs in the SC seem to have decreased expression of adherens junction (AJ) and tight junction (TJs) proteins and show a corresponding increase in permeability to low-molecular-weight tracers (Bartanusz et al., 2011).

It is by now understood that neuronal regeneration events during pathology and embryonic development by NPCs elicit very similar transcriptomic response making them fairly similar processes (Poplawski et al., 2020). Comparably, pathways that regulate vascular development and BBB properties are also active in pathological conditions. We provide here some examples of these molecules and their signaling pathways that play a significant role during vascularization and BBB formation in the SC and also during its pathology. Due to space limitations, we took as examples the experimental autoimmune encephalomyelitis (EAE), amyotrophic later sclerosis (ALS), and arteriovenous malformations (AVMs) in the SC.

Among the available experimental models to understand the BSCB pathology, the **EAE mouse model**, characterized

by autoimmune attack to oligodendrocytes in the CNS leading to their loss and demyelination of axons, is one of the most commonly used (Tonra et al., 2001; Muller et al., 2005; Schellenberg et al., 2007; Aube et al., 2014). Multiple reports describe changes in endothelial proliferation, vessel morphology, and increased blood vessel density in the SC and brain with EAE (Kirk and Karlik, 2003; Roscoe et al., 2009; Seabrook et al., 2010). In addition, a recent study applying the EAE model in Claudin5-GFP reporter line (with ECs expressing GFP) shows that remodeling of TJs in ECs and paracellular BSCB leakage precedes the EAE disease onset. (Lutz et al., 2017). Changes in VEGF expression and increased levels of VEGF have been described in EAE and in multiple sclerosis (MS) patients (Proescholdt et al., 2002; Su et al., 2006; Shimizu et al., 2012) and may eventually be responsible for the increase in EC proliferation and vessel density as well as for the leaky barrier (Argaw et al., 2009; Luissint et al., 2012). Once the immune system gets activated, it further exacerbates VEGF signaling cascade ending into a feedback loop that would further promote BSCB leakage and inflammation (Argaw et al., 2006, 2012). Based on this increase in VEGF expression, one of the strategies to balance the VEGF availability, learned from developmental studies, would be to promote the expression of sFLT1 that could titrate the excess of VEGF from the system (Himmels et al., 2017; Wild et al., 2017).

As mentioned above, WNT ligands are known for their specific role in CNS angiogenesis and BBB formation (Stenman et al., 2008; Daneman et al., 2009). Consistent with its role as a co-receptor for WNT ligands, GPR124 also participates in BBB formation (Kuhnert et al., 2010; Anderson et al., 2011; Cullen et al., 2011). The WNT/β-catenin signaling pathway is important for adult BBB maintenance as shown in multiple reports (Tran et al., 2016; Chang et al., 2017; Griveau et al., 2018) and is activated in CNS endothelium also in EAE and human MS during the course of disease progression (Lengfeld et al., 2017; Niu et al., 2019). The re-activation of this pathway in pathological conditions may suggest a rapid endothelial response toward restoring the barrier properties of the damaged vessels. Consistent with this hypothesis, *in vivo* inhibition of WNT signaling in ECs exacerbated EAE pathology with increased mortality, greater infiltration of CD4+ T cells into the CNS and more drastic myelin loss (Lengfeld et al., 2017). Interestingly, in postnatal or adult mice conditional deletion of endothelial GPR124 resulted in no defects in CNS angiogenesis, BBB development or maintenance; making GPR124 dispensable for vascular homeostasis in adult CNS (Chang et al., 2017). However, deficiency of GPR124 in a pathological mouse model of ischemic stroke or glioblastoma leads to extensive BBB leakage and hemorrhage, microvascular damage accompanied by pericyte, ECM, and TJ deficits. Thus, similar as the re-activation of the WNT signaling pathway, the GPR124-WNT signaling axis is important in maintaining vascular homeostasis during injury in adult. Considering that BSCB leakage is a primary feature of several diseases, one approach to target leakage, suggested by those studies, and by the role of the WNT/β-catenin signaling in BBB formation during development, could be to promote the activation of this pathway in ECs in pathological conditions (Liu et al., 2014; Jia et al., 2019). This was already shown in the above mentioned GPR124 deletion mouse pathology-model, where EC-specific constitutive activation of WNT signaling *via* activated β-catenin restored the vascular defects (Chang et al., 2017). In line with this idea, it was recently also shown that the activation of β-catenin in ECs from circumventricular organs of the CNS, which under physiological conditions lack BBB properties and are permeable, results in a tightened BBB in those regions and augmented neuronal activity (Benz et al., 2019).

Amyotrophic lateral sclerosis (ALS) is another SC and brain related disease, where the progression of MN degeneration leads to muscle atrophy, paralysis, and death. In ALS, BSCB impairment is also shown (Taylor et al., 2016). The disruption of endothelial TJ proteins like ZO1, occludin, and claudin5 seems to be the primary cause of microhemorrhages, reduced microcirculation, prior to the MN degeneration and the inflammatory response (Zhong et al., 2008). There is increasing evidence suggesting that MN degeneration is not only due to intrinsic defects, but also that the surrounding cell types like microglia, astrocytes, oligodendrocytes, and ECs may also be involved. A variety of growth and neurotrophic factors are also reported to mediate the ALS pathology (Bruijn et al., 2004). Of note, VEGF and WNTs are well studied. Mice with reduced VEGF levels ($Vegf^{\delta/\delta}$ mice) present reduced neural vascular perfusion and progressive MN degeneration, mimicking the human ALS (Oosthuyse et al., 2001). Multiple studies have shown the importance of VEGF in decelerating the disease outcome and providing a protective effect for MNs by both maintaining proper vessel perfusion and by acting directly on MNs as a survival factor (Lange et al., 2016). The underlying pathophysiological mechanisms leading to the MN degeneration and fatal outcome observed in ALS also seems to be linked to WNTs (Chen et al., 2012; Yu et al., 2013; Tury et al., 2014; Gonzalez-Fernandez et al., 2016, 2020; Bhinge et al., 2017). $SOD1^{G93A}$ ALS mice, as well as ALS patients, present a dysregulation in WNT signaling with upregulation or downregulation of certain ligands, receptors, and coreceptors depending on the distinct cell of the CNS analyzed (Gonzalez-Fernandez et al., 2020). As WNT ligands can act and exert different functions in different cellular context, close examination of their effect in astrocytes, neurons, and blood vessels in ALS conditions is required to understand their overall outcome. In this regard, upregulation of canonical WNT signaling seems to promote glial proliferation, that is, eventually neuroprotective during ALS (Chen et al., 2012; Li et al., 2013; Yu et al., 2013). In a similar manner, extrapolating from their role in blood vessel and BBB formation in the CNS, upregulated WNT ligands could be a defense mechanism to also promote a tighter BBB. However, their role in conjunction with the CNS vessels in this pathology needs further investigation.

Arteriovenous malformations (AVMs) are characterized by abnormal tangles of blood vessels connecting arteries and veins, where blood flow is thus shunted from arteries to veins without

passing through a capillary network (Mouchtouris et al., 2015). While AVMs can develop anywhere in our body, they occur most often in the CNS (being more common in the brain than in the SC). Spinal AVMs are mainly represented during the adulthood, however, they may also appear as a juvenile form, which can be intramedullary, extramedullary, and extraspinal (Ferch et al., 2001). Most of the molecular studies on CNS AVMs have been in the brain and indicate that similar mechanisms involved in CNS vascularization are de-regulated in AVMs. Although not described in the SC AVMs, here, we will describe those main findings.

Multiple studies suggest active angiogenesis as a feature of AVMs. Similarly, inflammation is a major contributor toward the pathogenesis and active angiogenesis of AVMs. The inflammatory response triggered by hemodynamic factors and/or genetic predisposition in the formation and rupture of AVMs involves different cytokines (IL-6, IL-1β, TNFα, and IL-8), neutrophils, and macrophages (Mouchtouris et al., 2015) that eventually upregulate the expression of VEGF. IL-6, IL-1β, and TNFα also induce NF-kB expression, which further exacerbates VEGF levels (Angelo and Kurzrock, 2007). Moreover, it is possible that this AVM niche itself may contribute to the stimulation of pathological angiogenesis, where the occurrence of focal ischemia leads to a hypoxic environment that in turn leads to angiogenesis by the expression of VEGF and VEGFR1 (Rothbart et al., 1996; Koizumi et al., 2002; Jabbour et al., 2009; Mouchtouris et al., 2015; Gamboa et al., 2017). Worth to mention, the NF-kB-VEGF cascade in AVMs is also stimulated under hypoxia by HIF-1 (Ng et al., 2005). Consistently, VEGF has been reported in patients suffering from recurrent cerebral AVMs (Rothbart et al., 1996) and VEGF receptors (VEGFR1 and VEGFR2), matrix metalloproteinases-MMP9 and ECM proteins like Collagen IV (Rothbart et al., 1996; Pyo et al., 2000; Hashimoto et al., 2003; Gamboa et al., 2017) are further thought to play a primary role in the pathogenesis of AVMs. As Notch signaling plays a critical role in the determining the arterio-venous cell fate during vascular development, it is thus crucial in AVMs also (Murphy et al., 2008; ZhuGe et al., 2009; Tetzlaff and Fischer, 2018). Manipulations in the notch signaling pathway leads to development of hallmark features of AVMs in the brain (Murphy et al., 2008; Nielsen et al., 2014). Recently a few studies have also shed light on the role of Wnt signaling in AVMs. β-catenin gain-of-function in ECs can cause arterial defects, including the loss of venous marker expression, arterialization of veins, and formation of AVMs (Corada et al., 2010). These ECs show a strong increase in Dll4/Notch signaling along with reduced sprouting activity, indicating a requirement for fine-tuning Wnt and Notch signaling pathways in the pathogenesis of AVMs. Additionally, a very recent study on whole-exome RNA sequencing in human samples of brain AVMs also showed an activation of canonical Wnt signaling *via* the activity of increased FZD10 and MYOC (Huo et al., 2019). All in all, the current understanding in AVM pathology, diagnoses, and treatment is increasing, but the molecular players and its regulation require further investigation. In addition, whether the same molecular mechanisms that lead to AVMs in the brain are also active in spinal AVMs is also something that remains to be investigated.

These examples show that VEGF and WNT signaling, that are important for blood vessel growth and BBB formation, during development are also involved in distinct pathologies.

CONCLUDING REMARKS

Research in the past recent years has provided further mechanistic insight into neuro-vascular interactions and into the importance of those interactions for proper development and function of the CNS. Here, studies in the SC have been fundamental. To advance in our understanding of SC development and function further studies focused on delineating angiogenic cues and potential bidirectional signaling pathways are needed. Spinal cord injuries are debilitating and fatal in many cases. Understanding SC development from a neural-vascular interaction perspective, and the potential reactivation or inhibition of those molecular signaling pathways in pathological conditions will be important for further developing therapeutic strategies.

AUTHOR CONTRIBUTIONS

JRV, BS, and CRA wrote the manuscript. All authors contributed to the article and approved the submitted version.

FUNDING

This work was supported by the EU: ERC-CoG grant (ref: 864875) and the DFG: DFG grants from SFB1366 (project number 394046768-SFB 1366), and from SFB 1158.

REFERENCES

Anderson, K. D., Pan, L., Yang, X. M., Hughes, V. C., Walls, J. R., Dominguez, M. G., et al. (2011). Angiogenic sprouting into neural tissue requires Gpr124, an orphan G protein-coupled receptor. *Proc. Natl. Acad. Sci. U. S. A.* 108, 2807–2812. doi: 10.1073/pnas.1019761108

Angelo, L. S., and Kurzrock, R. (2007). Vascular endothelial growth factor and its relationship to inflammatory mediators. *Clin. Cancer Res.* 13, 2825–2830. doi: 10.1158/1078-0432.CCR-06-2416

Argaw, A. T., Asp, L., Zhang, J., Navrazhina, K., Pham, T., Mariani, J. N., et al. (2012). Astrocyte-derived VEGF-A drives blood-brain barrier disruption in CNS inflammatory disease. *J. Clin. Invest.* 122, 2454–2468. doi: 10.1172/JCI60842

Argaw, A. T., Gurfein, B. T., Zhang, Y., Zameer, A., and John, G. R. (2009). VEGF-mediated disruption of endothelial CLN-5 promotes blood-brain barrier breakdown. *Proc. Natl. Acad. Sci. U. S. A.* 106, 1977–1982. doi: 10.1073/pnas.0808698106

Argaw, A. T., Zhang, Y., Snyder, B. J., Zhao, M. L., Kopp, N., Lee, S. C., et al. (2006). IL-1beta regulates blood-brain barrier permeability via reactivation

of the hypoxia-angiogenesis program. *J. Immunol.* 177, 5574–5584. doi: 10.4049/jimmunol.177.8.5574

Aube, B., Levesque, S. A., Pare, A., Chamma, E., Kebir, H., Gorina, R., et al. (2014). Neutrophils mediate blood-spinal cord barrier disruption in demyelinating neuroinflammatory diseases. *J. Immunol.* 193, 2438–2454. doi: 10.4049/jimmunol.1400401

Bartanusz, V., Jezova, D., Alajajian, B., and Digicaylioglu, M. (2011). The blood-spinal cord barrier: morphology and clinical implications. *Ann. Neurol.* 70, 194–206. doi: 10.1002/ana.22421

Benz, F., Wichitnaowarat, V., Lehmann, M., Germano, R. F., Mihova, D., Macas, J., et al. (2019). Low wnt/beta-catenin signaling determines leaky vessels in the subfornical organ and affects water homeostasis in mice. *elife* 8:e43818. doi: 10.7554/eLife.43818

Bhinge, A., Namboori, S. C., Zhang, X., VanDongen, A. M. J., and Stanton, L. W. (2017). Genetic correction of SOD1 mutant iPSCs reveals ERK and JNK activated AP1 as a driver of neurodegeneration in amyotrophic lateral sclerosis. *Stem Cell Reports.* 8, 856–869. doi: 10.1016/j.stemcr.2017.02.019

Bruijn, L. I., Miller, T. M., and Cleveland, D. W. (2004). Unraveling the mechanisms involved in motor neuron degeneration in ALS. *Annu. Rev. Neurosci.* 27, 723–749. doi: 10.1146/annurev.neuro.27.070203.144244

Chang, J., Mancuso, M. R., Maier, C., Liang, X., Yuki, K., Yang, L., et al. (2017). Gpr124 is essential for blood-brain barrier integrity in central nervous system disease. *Nat. Med.* 23, 450–460. doi: 10.1038/nm.4309

Chen, Y., Guan, Y., Liu, H., Wu, X., Yu, L., Wang, S., et al. (2012). Activation of the Wnt/beta-catenin signaling pathway is associated with glial proliferation in the adult spinal cord of ALS transgenic mice. *Biochem. Biophys. Res. Commun.* 420, 397–403. doi: 10.1016/j.bbrc.2012.03.006

Cho, C., Smallwood, P. M., and Nathans, J. (2017). Reck and Gpr124 are essential receptor cofactors for Wnt7a/Wnt7b-specific signaling in mammalian CNS angiogenesis and blood-brain barrier regulation. *Neuron* 95, 1056–1073. doi: 10.1016/j.neuron.2017.07.031

Corada, M., Nyqvist, D., Orsenigo, F., Caprini, A., Giampietro, C., Taketo, M. M., et al. (2010). The Wnt/beta-catenin pathway modulates vascular remodeling and specification by upregulating Dll4/notch signaling. *Dev. Cell* 18, 938–949. doi: 10.1016/j.devcel.2010.05.006

Cox, C. M., and Poole, T. J. (2000). Angioblast differentiation is influenced by the local environment: FGF-2 induces angioblasts and patterns vessel formation in the quail embryo. *Dev. Dyn.* 218, 371–382. doi: 10.1002/(SICI)1097-0177(200006)218:2<371::AID-DVDY10>3.0.CO;2-Z

Cullen, M., Elzarrad, M. K., Seaman, S., Zudaire, E., Stevens, J., Yang, M. Y., et al. (2011). GPR124, an orphan G protein-coupled receptor, is required for CNS-specific vascularization and establishment of the blood-brain barrier. *Proc. Natl. Acad. Sci. U. S. A.* 108, 5759–5764. doi: 10.1073/pnas.1017192108

Daneman, R., Agalliu, D., Zhou, L., Kuhnert, F., Kuo, C. J., and Barres, B. A. (2009). Wnt/beta-catenin signaling is required for CNS, but not non-CNS, angiogenesis. *Proc. Natl. Acad. Sci. U. S. A.* 106, 641–646. doi: 10.1073/pnas.0805165106

Dessaud, E., McMahon, A. P., and Briscoe, J. (2008). Pattern formation in the vertebrate neural tube: a sonic hedgehog morphogen-regulated transcriptional network. *Development* 135, 2489–2503. doi: 10.1242/dev.009324

Dessaud, E., Yang, L. L., Hill, K., Cox, B., Ulloa, F., Ribeiro, A., et al. (2007). Interpretation of the sonic hedgehog morphogen gradient by a temporal adaptation mechanism. *Nature* 450, 717–720. doi: 10.1038/nature06347

Diez Del Corral, R., and Morales, A. V. (2017). The multiple roles of FGF signaling in the developing spinal cord. *Front. Cell Dev. Biol.* 5:58. doi: 10.3389/fcell.2017.00058

Diez del Corral, R., Olivera-Martinez, I., Goriely, A., Gale, E., Maden, M., and Storey, K. (2003). Opposing FGF and retinoid pathways control ventral neural pattern, neuronal differentiation, and segmentation during body axis extension. *Neuron* 40, 65–79. doi: 10.1016/s0896-6273(03)00565-8

Duester, G. (2008). Retinoic acid synthesis and signaling during early organogenesis. *Cell* 134, 921–931. doi: 10.1016/j.cell.2008.09.002

Engelhardt, B., and Liebner, S. (2014). Novel insights into the development and maintenance of the blood-brain barrier. *Cell Tissue Res.* 355, 687–699. doi: 10.1007/s00441-014-1811-2

Farrar, M. J., Rubin, J. D., Diago, D. M., and Schaffer, C. B. (2015). Characterization of blood flow in the mouse dorsal spinal venous system before and after dorsal spinal vein occlusion. *J. Cereb. Blood Flow Metab.* 35, 667–675. doi: 10.1038/jcbfm.2014.244

Feeney, J. F. Jr., and Watterson, R. L. (1946). The development of the vascular pattern within the walls of the central nervous system of the chick embryo. *J. Morphol.* 78, 231–303. doi: 10.1002/jmor.1050780205

Ferch, R. D., Morgan, M. K., and Sears, W. R. (2001). Spinal arteriovenous malformations: a review with case illustrations. *J. Clin. Neurosci.* 8, 299–304. doi: 10.1054/jocn.2000.0914

Gamboa, N. T., Taussky, P., Park, M. S., Couldwell, W. T., Mahan, M. A., and Kalani, M. Y. S. (2017). Neurovascular patterning cues and implications for central and peripheral neurological disease. *Surg. Neurol. Int.* 8:208. doi: 10.4103/sni.sni_475_16

Gonzalez-Fernandez, C., Gonzalez, P., and Rodriguez, F. J. (2020). New insights into Wnt signaling alterations in amyotrophic lateral sclerosis: a potential therapeutic target? *Neural Regen. Res.* 15, 1580–1589. doi: 10.4103/1673-5374.276320

Gonzalez-Fernandez, C., Mancuso, R., Del Valle, J., Navarro, X., and Rodriguez, F. J. (2016). Wnt signaling alteration in the spinal cord of amyotrophic lateral sclerosis transgenic mice: special focus on Frizzled-5 cellular expression pattern. *PLoS One* 11:e0155867. doi: 10.1371/journal.pone.0155867

Griffin, J. M., and Bradke, F. (2020). Therapeutic repair for spinal cord injury: combinatory approaches to address a multifaceted problem. *EMBO Mol. Med.* 12:e11505. doi: 10.15252/emmm.201911505

Griveau, A., Seano, G., Shelton, S. J., Kupp, R., Jahangiri, A., Obernier, K., et al. (2018). A glial signature and Wnt7 signaling regulate glioma-vascular interactions and tumor microenvironment. *Cancer Cell* 33, 874–889 e7. doi: 10.1016/j.ccell.2018.03.020

Hashimoto, T., Wen, G., Lawton, M. T., Boudreau, N. J., Bollen, A. W., Yang, G. Y., et al. (2003). Abnormal expression of matrix metalloproteinases and tissue inhibitors of metalloproteinases in brain arteriovenous malformations. *Stroke* 34, 925–931. doi: 10.1161/01.STR.0000061888.71524.DF

Himmels, P., Paredes, I., Adler, H., Karakatsani, A., Luck, R., Marti, H. H., et al. (2017). Motor neurons control blood vessel patterning in the developing spinal cord. *Nat. Commun.* 8:14583. doi: 10.1038/ncomms14583

Hogan, K. A., Ambler, C. A., Chapman, D. L., and Bautch, V. L. (2004). The neural tube patterns vessels developmentally using the VEGF signaling pathway. *Development* 131, 1503–1513. doi: 10.1242/dev.01039

Hogan, K. A., and Bautch, V. L. (2004). Blood vessel patterning at the embryonic midline. *Curr. Top. Dev. Biol.* 62, 55–85. doi: 10.1016/S0070-2153(04)62003-5

Hollyday, M., McMahon, J. A., and McMahon, A. P. (1995). Wnt expression patterns in chick embryo nervous system. *Mech. Dev.* 52, 9–25. doi: 10.1016/0925-4773(95)00385-E

Huo, R., Fu, W., Li, H., Jiao, Y., Yan, Z., Wang, L., et al. (2019). RNA sequencing reveals the activation of Wnt signaling in low flow rate brain arteriovenous malformations. *J. Am. Heart Assoc.* 8:e012746. doi: 10.1161/JAHA.119.012746

Isogai, S., Horiguchi, M., and Weinstein, B. M. (2001). The vascular anatomy of the developing zebrafish: an atlas of embryonic and early larval development. *Dev. Biol.* 230, 278–301. doi: 10.1006/dbio.2000.9995

Isogai, S., Lawson, N. D., Torrealday, S., Horiguchi, M., and Weinstein, B. M. (2003). Angiogenic network formation in the developing vertebrate trunk. *Development* 130, 5281–5290. doi: 10.1242/dev.00733

Jabbour, M. N., Elder, J. B., Samuelson, C. G., Khashabi, S., Hofman, F. M., Giannotta, S. L., et al. (2009). Aberrant angiogenic characteristics of human brain arteriovenous malformation endothelial cells. *Neurosurgery* 64, 139–146. doi: 10.1227/01.NEU.0000334417.56742.24

James, J. M., Gewolb, C., and Bautch, V. L. (2009). Neurovascular development uses VEGF-A signaling to regulate blood vessel ingression into the neural tube. *Development* 136, 833–841. doi: 10.1242/dev.028845

Jessell, T. M. (2000). Neuronal specification in the spinal cord: inductive signals and transcriptional codes. *Nat. Rev. Genet.* 1, 20–29. doi: 10.1038/35049541

Jia, L., Pina-Crespo, J., and Li, Y. (2019). Restoring Wnt/beta-catenin signaling is a promising therapeutic strategy for Alzheimer's disease. *Mol. Brain* 12: 104. doi: 10.1186/s13041-019-0525-5

Kirk, S. L., and Karlik, S. J. (2003). VEGF and vascular changes in chronic neuroinflammation. *J. Autoimmun.* 21, 353–363. doi: 10.1016/S0896-8411(03)00139-2

Koizumi, T., Shiraishi, T., Hagihara, N., Tabuchi, K., Hayashi, T., and Kawano, T. (2002). Expression of vascular endothelial growth factors and their receptors in and around intracranial arteriovenous malformations. *Neurosurgery* 50, 117–124. doi: 10.1097/00006123-200201000-00020

Kuhnert, F., Mancuso, M. R., Shamloo, A., Wang, H. T., Choksi, V., Florek, M., et al. (2010). Essential regulation of CNS angiogenesis by the orphan G protein-coupled receptor GPR124. *Science* 330, 985–989. doi: 10.1126/science.1196554

Kurz, H. (2009). Cell lineages and early patterns of embryonic CNS vascularization. *Cell Adhes. Migr.* 3, 205–210. doi: 10.4161/cam.3.2.7855

Kurz, H., Gartner, T., Eggli, P. S., and Christ, B. (1996). First blood vessels in the avian neural tube are formed by a combination of dorsal angioblast immigration and ventral sprouting of endothelial cells. *Dev. Biol.* 173, 133–147. doi: 10.1006/dbio.1996.0012

Lange, C., Storkebaum, E., de Almodovar, C. R., Dewerchin, M., and Carmeliet, P. (2016). Vascular endothelial growth factor: a neurovascular target in neurological diseases. *Nat. Rev. Neurol.* 12, 439–454. doi: 10.1038/nrneurol.2016.88

Lengfeld, J. E., Lutz, S. E., Smith, J. R., Diaconu, C., Scott, C., Kofman, S. B., et al. (2017). Endothelial Wnt/beta-catenin signaling reduces immune cell infiltration in multiple sclerosis. *Proc. Natl. Acad. Sci. U. S. A.* 114, E1168–E1177. doi: 10.1073/pnas.1609905114

Li, X., Guan, Y., Chen, Y., Zhang, C., Shi, C., Zhou, F., et al. (2013). Expression of Wnt5a and its receptor Fzd2 is changed in the spinal cord of adult amyotrophic lateral sclerosis transgenic mice. *Int. J. Clin. Exp. Pathol.* 6, 1245–1260.

Liu, L., Wan, W., Xia, S., Kalionis, B., and Li, Y. (2014). Dysfunctional Wnt/beta-catenin signaling contributes to blood-brain barrier breakdown in Alzheimer's disease. *Neurochem. Int.* 75, 19–25. doi: 10.1016/j.neuint.2014.05.004

Luissint, A. C., Artus, C., Glacial, F., Ganeshamoorthy, K., and Couraud, P. O. (2012). Tight junctions at the blood brain barrier: physiological architecture and disease-associated dysregulation. *Fluids Barriers CNS.* 9:23. doi: 10.1186/2045-8118-9-23

Lumsden, A., and Krumlauf, R. (1996). Patterning the vertebrate neuraxis. *Science* 274, 1109–1115. doi: 10.1126/science.274.5290.1109

Lutz, S. E., Smith, J. R., Kim, D. H., Olson, C. V. L., Ellefsen, K., Bates, J. M., et al. (2017). Caveolin1 is required for Th1 cell infiltration, but not tight junction remodeling, at the blood-brain barrier in autoimmune neuroinflammation. *Cell Rep.* 21, 2104–2117. doi: 10.1016/j.celrep.2017.10.094

Matsuoka, R. L., Marass, M., Avdesh, A., Helker, C. S., Maischein, H. M., Grosse, A. S., et al. (2016). Radial glia regulate vascular patterning around the developing spinal cord. *elife* 5:e20253. doi: 10.7554/eLife.20253

Matsuoka, R. L., Rossi, A., Stone, O. A., and Stainier, D. Y. R. (2017). CNS-resident progenitors direct the vascularization of neighboring tissues. *Proc. Natl. Acad. Sci. U. S. A.* 114, 10137–10142. doi: 10.1073/pnas.1619300114

Mazensky, D., Flesarova, S., and Sulla, I. (2017). Arterial blood supply to the spinal cord in animal models of spinal cord injury. A review. *Anat. Rec.* 300, 2091–2106. doi: 10.1002/ar.23694

Mouchtouris, N., Jabbour, P. M., Starke, R. M., Hasan, D. M., Zanaty, M., Theofanis, T., et al. (2015). Biology of cerebral arteriovenous malformations with a focus on inflammation. *J. Cereb. Blood Flow Metab.* 35, 167–175. doi: 10.1038/jcbfm.2014.179

Muller, D. M., Pender, M. P., and Greer, J. M. (2005). Blood-brain barrier disruption and lesion localisation in experimental autoimmune encephalomyelitis with predominant cerebellar and brainstem involvement. *J. Neuroimmunol.* 160, 162–169. doi: 10.1016/j.jneuroim.2004.11.011

Murphy, P. A., Lam, M. T., Wu, X., Kim, T. N., Vartanian, S. M., Bollen, A. W., et al. (2008). Endothelial Notch4 signaling induces hallmarks of brain arteriovenous malformations in mice. *Proc. Natl. Acad. Sci. U. S. A.* 105, 10901–10906. doi: 10.1073/pnas.0802743105

Nakao, T., Ishizawa, A., and Ogawa, R. (1988). Observations of vascularization in the spinal cord of mouse embryos, with special reference to development of boundary membranes and perivascular spaces. *Anat. Rec.* 221, 663–677. doi: 10.1002/ar.1092210212

Ng, I., Tan, W. L., Ng, P. Y., and Lim, J. (2005). Hypoxia inducible factor-1alpha and expression of vascular endothelial growth factor and its receptors in cerebral arteriovenous malformations. *J. Clin. Neurosci.* 12, 794–799. doi: 10.1016/j.jocn.2005.02.005

Nielsen, C. M., Cuervo, H., Ding, V. W., Kong, Y., Huang, E. J., and Wang, R. A. (2014). Deletion of Rbpj from postnatal endothelium leads to abnormal arteriovenous shunting in mice. *Development* 141, 3782–3792. doi: 10.1242/dev.108951

Niu, J., Tsai, H. H., Hoi, K. K., Huang, N., Yu, G., Kim, K., et al. (2019). Aberrant oligodendroglial-vascular interactions disrupt the blood-brain barrier, triggering CNS inflammation. *Nat. Neurosci.* 22, 709–718. doi: 10.1038/s41593-019-0369-4

Noden, D. M. (1988). Interactions and fates of avian craniofacial mesenchyme. *Development* 103, 121–140.

Oosthuyse, B., Moons, L., Storkebaum, E., Beck, H., Nuyens, D., Brusselmans, K., et al. (2001). Deletion of the hypoxia-response element in the vascular endothelial growth factor promoter causes motor neuron degeneration. *Nat. Genet.* 28, 131–138. doi: 10.1038/88842

Paredes, I., Himmels, P., and Ruiz de Almodovar, C. (2018). Neurovascular communication during CNS development. *Dev. Cell* 45, 10–32. doi: 10.1016/j.devcel.2018.01.023

Parr, B. A., Shea, M. J., Vassileva, G., and McMahon, A. P. (1993). Mouse Wnt genes exhibit discrete domains of expression in the early embryonic CNS and limb buds. *Development* 119, 247–261.

Poplawski, G. H. D., Kawaguchi, R., Van Niekerk, E., Lu, P., Mehta, N., Canete, P., et al. (2020). Injured adult neurons regress to an embryonic transcriptional growth state. *Nature* 581, 77–82. doi: 10.1038/s41586-020-2200-5

Posokhova, E., Shukla, A., Seaman, S., Volate, S., Hilton, M. B., Wu, B., et al. (2015). GPR124 functions as a WNT7-specific coactivator of canonical beta-catenin signaling. *Cell Rep.* 10, 123–130. doi: 10.1016/j.celrep.2014.12.020

Proescholdt, M. A., Jacobson, S., Tresser, N., Oldfield, E. H., and Merrill, M. J. (2002). Vascular endothelial growth factor is expressed in multiple sclerosis plaques and can induce inflammatory lesions in experimental allergic encephalomyelitis rats. *J. Neuropathol. Exp. Neurol.* 61, 914–925. doi: 10.1093/jnen/61.10.914

Purves, D. (2008). Neuroscience. Sinauer, Sunderland, Mass. xvii, 857, G-816, IC-857, I-829 p.

Pyo, R., Lee, J. K., Shipley, J. M., Curci, J. A., Mao, D., Ziporin, S. J., et al. (2000). Targeted gene disruption of matrix metalloproteinase-9 (gelatinase B) suppresses development of experimental abdominal aortic aneurysms. *J. Clin. Invest.* 105, 1641–1649. doi: 10.1172/JCI8931

Roscoe, W. A., Welsh, M. E., Carter, D. E., and Karlik, S. J. (2009). VEGF and angiogenesis in acute and chronic MOG((35-55)) peptide induced EAE. *J. Neuroimmunol.* 209, 6–15. doi: 10.1016/j.jneuroim.2009.01.009

Rothbart, D., Awad, I. A., Lee, J., Kim, J., Harbaugh, R., and Criscuolo, G. R. (1996). Expression of angiogenic factors and structural proteins in central nervous system vascular malformations. *Neurosurgery* 38, 915–924. doi: 10.1097/00006123-199605000-00011

Ruiz de Almodovar, C., Fabre, P. J., Knevels, E., Coulon, C., Segura, I., Haddick, P. C., et al. (2011). VEGF mediates commissural axon chemoattraction through its receptor Flk1. *Neuron* 70, 966–978. doi: 10.1016/j.neuron.2011.04.014

Sagner, A., and Briscoe, J. (2019). Establishing neuronal diversity in the spinal cord: a time and a place. *Development* 146:dev182154. doi: 10.1242/dev.182154

Schellenberg, A. E., Buist, R., Yong, V. W., Del Bigio, M. R., and Peeling, J. (2007). Magnetic resonance imaging of blood-spinal cord barrier disruption in mice with experimental autoimmune encephalomyelitis. *Magn. Reson. Med.* 58, 298–305. doi: 10.1002/mrm.21289

Seabrook, T. J., Littlewood-Evans, A., Brinkmann, V., Pollinger, B., Schnell, C., and Hiestand, P. C. (2010). Angiogenesis is present in experimental autoimmune encephalomyelitis and pro-angiogenic factors are increased in multiple sclerosis lesions. *J. Neuroinflammation* 7:95. doi: 10.1186/1742-2094-7-95

Segarra, M., Aburto, M. R., Hefendehl, J., and Acker-Palmer, A. (2019). Neurovascular interactions in the nervous system. *Annu. Rev. Cell Dev. Biol.* 35, 615–635. doi: 10.1146/annurev-cellbio-100818-125142

Shimizu, F., Sano, Y., Takahashi, T., Haruki, H., Saito, K., Koga, M., et al. (2012). Sera from neuromyelitis optica patients disrupt the blood-brain barrier. *J. Neurol. Neurosurg. Psychiatry* 83, 288–297. doi: 10.1136/jnnp-2011-300434

Stenman, J. M., Rajagopal, J., Carroll, T. J., Ishibashi, M., McMahon, J., and McMahon, A. P. (2008). Canonical Wnt signaling regulates organ-specific assembly and differentiation of CNS vasculature. *Science* 322, 1247–1250. doi: 10.1126/science.1164594

Su, J. J., Osoegawa, M., Matsuoka, T., Minohara, M., Tanaka, M., Ishizu, T., et al. (2006). Upregulation of vascular growth factors in multiple sclerosis: correlation with MRI findings. *J. Neurol. Sci.* 243, 21–30. doi: 10.1016/j.jns.2005.11.006

Takahashi, T., Takase, Y., Yoshino, T., Saito, D., Tadokoro, R., and Takahashi, Y. (2015). Angiogenesis in the developing spinal cord: blood vessel exclusion from neural progenitor region is mediated by VEGF and its antagonists. *PLoS One* 10:e0116119. doi: 10.1371/journal.pone.0116119

Taylor, J. P., Brown, R. H. Jr., and Cleveland, D. W. (2016). Decoding ALS: from genes to mechanism. *Nature* 539, 197–206. doi: 10.1038/nature20413

Tetzlaff, F., and Fischer, A. (2018). Control of blood vessel formation by notch signaling. *Adv. Exp. Med. Biol.* 1066, 319–338. doi: 10.1007/978-3-319-89512-3_16

Tonra, J. R., Reiseter, B. S., Kolbeck, R., Nagashima, K., Robertson, R., Keyt, B., et al. (2001). Comparison of the timing of acute blood-brain barrier breakdown to rabbit immunoglobulin G in the cerebellum and spinal cord of mice with experimental autoimmune encephalomyelitis. *J. Comp. Neurol.* 430, 131–144. doi: 10.1002/1096-9861(20010129)430:1<131::AID-CNE1019>3.0.CO;2-K

Tran, K. A., Zhang, X., Predescu, D., Huang, X., Machado, R. F., Gothert, J. R., et al. (2016). Endothelial beta-catenin signaling is required for maintaining adult blood-brain barrier integrity and central nervous system homeostasis. *Circulation* 133, 177–186. doi: 10.1161/CIRCULATIONAHA.115.015982

Tury, A., Tolentino, K., and Zou, Y. (2014). Altered expression of atypical PKC and Ryk in the spinal cord of a mouse model of amyotrophic lateral sclerosis. *Dev. Neurobiol.* 74, 839–850. doi: 10.1002/dneu.22137

Ulrich, F., Carretero-Ortega, J., Menendez, J., Narvaez, C., Sun, B., Lancaster, E., et al. (2016). Reck enables cerebrovascular development by promoting canonical Wnt signaling. *Development* 143, 147–159. doi: 10.1242/dev.123059

Vanhollebeke, B., Stone, O. A., Bostaille, N., Cho, C., Zhou, Y., Maquet, E., et al. (2015). Tip cell-specific requirement for an atypical Gpr124- and reck-dependent Wnt/beta-catenin pathway during brain angiogenesis. *elife* 4:e06489. doi: 10.7554/eLife.06489

Vasudevan, A., Long, J. E., Crandall, J. E., Rubenstein, J. L., and Bhide, P. G. (2008). Compartment-specific transcription factors orchestrate angiogenesis gradients in the embryonic brain. *Nat. Neurosci.* 11, 429–439. doi: 10.1038/nn2074

Wild, R., Klems, A., Takamiya, M., Hayashi, Y., Strahle, U., Ando, K., et al. (2017). Neuronal sFlt1 and Vegfaa determine venous sprouting and spinal cord vascularization. *Nat. Commun.* 8:13991. doi: 10.1038/ncomms13991

Wilson, L., and Maden, M. (2005). The mechanisms of dorsoventral patterning in the vertebrate neural tube. *Dev. Biol.* 282, 1–13. doi: 10.1016/j.ydbio.2005.02.027

Yu, L., Guan, Y., Wu, X., Chen, Y., Liu, Z., Du, H., et al. (2013). Wnt signaling is altered by spinal cord neuronal dysfunction in amyotrophic lateral sclerosis transgenic mice. *Neurochem. Res.* 38, 1904–1913. doi: 10.1007/s11064-013-1096-y

Zerlin, M., Julius, M. A., and Kitajewski, J. (2008). Wnt/frizzled signaling in angiogenesis. *Angiogenesis* 11, 63–69. doi: 10.1007/s10456-008-9095-3

Zhong, Z., Deane, R., Ali, Z., Parisi, M., Shapovalov, Y., O'Banion, M. K., et al. (2008). ALS-causing SOD1 mutants generate vascular changes prior to motor neuron degeneration. *Nat. Neurosci.* 11, 420–422. doi: 10.1038/nn2073

Zhou, Y., and Nathans, J. (2014). Gpr124 controls CNS angiogenesis and blood-brain barrier integrity by promoting ligand-specific canonical wnt signaling. *Dev. Cell* 31, 248–256. doi: 10.1016/j.devcel.2014.08.018

ZhuGe, Q., Zhong, M., Zheng, W., Yang, G. Y., Mao, X., Xie, L., et al. (2009). Notch-1 signalling is activated in brain arteriovenous malformations in humans. *Brain* 132, 3231–3241. doi: 10.1093/brain/awp246

Conflict of Interest: The authors declare that the research was conducted in the absence of any commercial or financial relationships that could be construed as a potential conflict of interest.

frontiers in Physiology

REVIEW
published: 22 December 2020
doi: 10.3389/fphys.2020.605398

Blood-Brain Barrier Damage in Ischemic Stroke and Its Regulation by Endothelial Mechanotransduction

Keqing Nian[1†], Ian C. Harding[1†], Ira M. Herman[2,3] and Eno E. Ebong[1,4,5]*

[1]Department of Bioengineering, Northeastern University, Boston, MA, United States, [2]Department of Development, Molecular, and Chemical Biology, Tufts Sackler School of Graduate Biomedical Sciences, Boston, MA, United States, [3]Center for Innovations in Wound Healing Research, Tufts University School of Medicine, Boston, MA, United States, [4]Department of Chemical Engineering, Northeastern University, Boston, MA, United States, [5]Department of Neuroscience, Albert Einstein College of Medicine, New York, NY, United States

Ischemic stroke, a major cause of mortality in the United States, often contributes to disruption of the blood-brain barrier (BBB). The BBB along with its supportive cells, collectively referred to as the "neurovascular unit," is the brain's multicellular microvasculature that bi-directionally regulates the transport of blood, ions, oxygen, and cells from the circulation into the brain. It is thus vital for the maintenance of central nervous system homeostasis. BBB disruption, which is associated with the altered expression of tight junction proteins and BBB transporters, is believed to exacerbate brain injury caused by ischemic stroke and limits the therapeutic potential of current clinical therapies, such as recombinant tissue plasminogen activator. Accumulating evidence suggests that endothelial mechanobiology, the conversion of mechanical forces into biochemical signals, helps regulate function of the peripheral vasculature and may similarly maintain BBB integrity. For example, the endothelial glycocalyx (GCX), a glycoprotein-proteoglycan layer extending into the lumen of bloods vessel, is abundantly expressed on endothelial cells of the BBB and has been shown to regulate BBB permeability. In this review, we will focus on our understanding of the mechanisms underlying BBB damage after ischemic stroke, highlighting current and potential future novel pharmacological strategies for BBB protection and recovery. Finally, we will address the current knowledge of endothelial mechanotransduction in BBB maintenance, specifically focusing on a potential role of the endothelial GCX.

Keywords: blood-brain barrier, ischemic stroke, endothelial cells, mechanotransduction, neuroprotection, neurovascular unit, endothelial glycocalyx

OPEN ACCESS

Edited by:
Clotilde Lecrux, McGill University, Canada

Reviewed by:
Pedro Campinho, University of Lisbon, Portugal
Jingjing Zhang, Affiliated Hospital of Guangdong Medical University, China

***Correspondence:**
Eno E. Ebong
e.ebong@northeastern.edu

[†]These authors have contributed equally to this work

Specialty section:
This article was submitted to Vascular Physiology, a section of the journal Frontiers in Physiology

Received: *12 September 2020*
Accepted: *27 November 2020*
Published: *22 December 2020*

Citation:
Nian K, Harding IC, Herman IM and Ebong EE (2020) Blood-Brain Barrier Damage in Ischemic Stroke and Its Regulation by Endothelial Mechanotransduction. Front. Physiol. 11:605398. doi: 10.3389/fphys.2020.605398

INTRODUCTION

Despite significant progression in treatment strategies, stroke remains one of the most common causes of death worldwide and accounts for 55% of all neurological disabilities (Posada-Duque et al., 2014). In the United States alone, approximately 800,000 people suffer from stroke yearly, accounting for $34 billion in medical expenses and lost productivity (Kassner and Merali, 2015;

Shi et al., 2016). The majority of observed strokes are classified as ischemic strokes, which occur when a clot within a blood vessel interrupts the cerebral blood flow that supplies vital ions, oxygen, and nutrients to the brain (Obermeier et al., 2013). It is well established that one of the hallmarks of acute ischemic stroke is the disruption of the blood-brain barrier (BBB; Sifat et al., 2017), which leads to the subsequent disruption of ion homeostasis and transporter functions in the brain. The mechanisms of BBB damage in the setting of stroke include modification of tight junction (TJ) proteins, modulation of transporters expression, and inflammatory damage (Abdullahi et al., 2018). Structural injury of TJs combined with BBB transporter dysfunction can collectively lead to increased paracellular solute permeability, ultimately resulting in tissue edema and exacerbating brain injury associated with cognitive impairment (Abdullahi et al., 2018). Therefore, it is necessary to develop therapeutic strategies protecting against BBB dysfunction.

One area of BBB maintenance that has received limited attention is its regulation *via* endothelial mechanotransduction, the conversion of mechanical forces into endothelial cell (EC) biochemical signals (Lam et al., 2012). In the peripheral vasculature, endothelial mechanotransduction has been shown to support proper vessel function *via* the regulation of inflammation, vessel tone, and permeability (Chien, 2008; Jones, 2010; Glen et al., 2012). However, while several studies have demonstrated the presence and function of endothelial mechanotransducers in the BBB (Zaragoza et al., 2012; Conway et al., 2013), more research is necessary to determine the extent and mechanisms by which endothelial mechanotransduction precisely regulates BBB function.

In this review, we first highlight the current understanding of BBB structure. Then, we describe ischemic stroke and its relationship with BBB dysfunction, noting current and potential future therapeutic strategies. Finally, we will put emphasis on studies implicating endothelial mechanotransduction in BBB function and its possibility as a target for novel approaches for BBB protection.

BBB: STRUCTURE AND FUNCTION

The Neurovascular Unit

The blood-brain barrier is an important dynamic and metabolic interface that precisely regulates ion homeostasis in the central nervous system (CNS) and protects delicate neural tissue from potentially toxic substances and pathogens (Jiang et al., 2018). For example, the BBB controls the entry and exit of essential nutrients and waste materials *via* the expression of various channels and transporters to regulate CNS concentrations of ions, neurotransmitters, neuroactive agents, and many other molecules (Jeong et al., 2006). Typically, the BBB primarily refers to the endothelium of the CNS vasculature. However, the development and maintenance of the BBB not only requires ECs and their associated TJs but also requires supporting pericytes, astrocytes, neurons, and extracellular matrix (ECM) that surround the BBB (**Table 1**). This intricate cellular grouping is referred to as the "neurovascular unit (NVU)" and each cell within the NVU helps promote the proper function of the BBB (**Figure 1**; Obermeier et al., 2013). Here, we will discuss the function of each cell type in relation to BBB function.

While ECs of the BBB largely mimic their counterparts in the peripheral vasculature, BBB endothelium also present several phenotypic differences that make them ideal for permeability regulation. For example, BBB ECs have increased mitochondrial content leading to an increased production of biological energy. This energy is required to strictly regulate transport processes through the expression of many receptors and ion channels. Additionally, BBB ECs are characterized by a lack of fenestrations, minimal pinocytotic activity with a small number of endocytotic vesicles, unique receptor-mediated endocytosis, and a heightened presence of TJ proteins. Collectively, these properties help restrict BBB permeability (Bicker et al., 2014; Knowland et al., 2014).

Pericytes of the NVU are located along the basement membrane of BBB ECs, encircling the vessel wall and promoting overall BBB function (**Figure 1**; Dalkara et al., 2011). For example, pericytes induce occludin and multidrug resistance-associated protein (MRP) expression in ECs and contribute to blood flow regulation *via* their contractile nature. Pericytes also exist in the peripheral vasculature, but the CNS microvasculature has the highest degree of pericyte coverage, potentially contributing to the observed vascular permeability and small vessel stability (Daneman et al., 2010). In addition to their impact on BBB EC function, pericytes exhibit phagocytic activity relevant to the clearance of toxic proteins and can also regulate the influx of immune cells into the nervous system (Rustenhoven et al., 2017). They also display an ability to self-renew and differentiate into neural and vascular lineage cells in the setting of stroke, thereby functioning as pluripotent stem cells (Nakagomi et al., 2015).

Another NVU cell type implicated in promoting BBB function are astrocytes. Astrocytes are the most common glial cell in the brain and have a variety of different morphologies and phenotypes dependent on their location within the brain and association with other cell types. Their close interaction with ECs within the BBB, particularly *via* astrocyte end feet, strengthens the regulation and maturation of the BBB and has been shown to contribute to cerebral blood flow control (Liu and Chopp, 2016). For example, astrocytes release many bioactive substances and regulatory factors that promote BBB function (Alvarez et al., 2013) including sonic hedgehog (Shh), which regulates TJ development and BBB permeability; nitric oxide (NO), which regulates vasodilation (Iadecola and Nedergaard, 2007); and vascular endothelial growth factor (VEGF), which is involved in angiogenesis and vasogenic edema during stroke (Davis et al., 2010). As previously mentioned, astrocytes regulate EC function mainly through their astrocytic end-feet, which extend from their cell body and connect to the basolateral surface of ECs (**Figure 1**). One astrocyte end-foot protein strongly implicated in BBB function is the water channel aquaporin 4 (AQP4). AQP4, which is involved in the pathogenesis of cerebral edema, facilitates water movement through the plasma membrane of

Abbreviations: TJ, Tight junction; EC, Endothelial cell; AJ, Adherens junction; GCX, Glycocalyx; NBP, Dl-3-n-butylphthalide; Cop-1, Copolymer 1; GAG, Glycosaminoglycan.

TABLE 1 | Components and their functions of the NVU.

Component	Function	Reference
Endothelial cells (ECs)	Main permeability regulators of the neurovascular unit. Possess increased mitochondrial content to increase production of biological energy. Characterized by a lack of fenestrations, minimal pinocytotic activity, enhanced receptor-mediated endocytosis, and increased presence of tight junction proteins, which help with permeability regulation.	Bicker et al., 2014; Knowland et al., 2014
Pericytes	Regulate blood flow and vascular permeability *via*, for example, the induction of occludin and multidrug resistance-associated protein (MRP) expression. Also regulate migration of immune cells. Self-renew and differentiate into neural and vascular lineage cells in the setting of stroke.	Daneman et al., 2010; Dalkara et al., 2011; Nakagomi et al., 2015; Rustenhoven et al., 2017
Astrocytes	Closely interact with ECs *via* astrocyte end feet. Regulate cerebral blood flow and promote BBB function through the release of bioactive substances and regulatory factors, including sonic hedgehog, nitric oxide, and vascular endothelial growth factor. Express the water channel aquaporin 4 (AQP4), assisting with permeability regulation.	Ishida et al., 2006; Iadecola and Nedergaard, 2007; Davis et al., 2010; Alvarez et al., 2013; Liu and Chopp, 2016
Neurons	Communicate with astrocytes to regulate vascular tone and cerebral blood flow.	Koehler et al., 2006
Microglia	Resident immune cell of the brain. Microglia activation contributes to BBB dysfunction.	da Fonseca et al., 2014; Zhou et al., 2006
Extracellular matrix (ECM)	Connects and separates ECs from pericytes and astrocytes to allow proper cellular orientation. Mediates the movement of cells and helps maintain brain homeostasis. The basement membrane of the extracellular matrix connects ECs to astrocytic end-feet to help maintain BBB integrity.	del Zoppo and Milner, 2006; Sandoval and Witt, 2008; Zobel et al., 2016

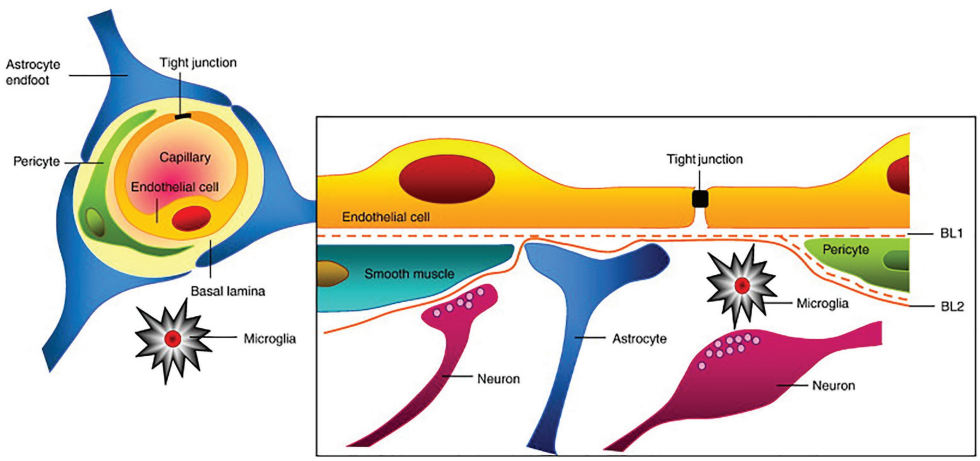

FIGURE 1 | Structure of the neurovascular unit (NVU). Endothelial cells (ECs) form the inner most layer of the NVU and are connected to each other *via* tight junctions (TJs). Surrounding the ECs are pericytes in the case of capillaries or smooth muscle cells in the case of larger cerebrovasculature such as veins and arteries. Additionally, astrocytes and neurons of the NVU extend foot-processes or axons, respectively, that also help regulate NVU function. Finally, microglia, which are the brain's resident immune cells, also contribute to NVU regulation. Collectively, ECs and these supportive cells help maintain the proper function of the blood-brain barrier (BBB). This figure is reprinted from Abbott et al. (2010)) "Structure and function of the blood-brain barrier," Neurobiology of Disease, 37 (1): 12–25, with permission from Elsevier.

several cell types in the brain, including ECs, and therefore contributes to permeability regulation (Ishida et al., 2006). Additionally, astrocytes play a substantial role in mediating neuroinflammation and thus are significant in neuroinflammatory pathologies including ischemic stroke (Colombo and Farina, 2016).

Neurons have also been reported to regulate BBB function. Although, while direct neuronal contact with the endothelium has been implicated, the incorporation of neurons into the NVU is thought to mainly occur *via* astrocytes. When necessary, neurons will communicate with astrocytes to influence BBB function. For instance, neurons have been suggested to tightly regulate vascular tone and cerebral blood flow *via* astrocytes, which is justifiable given the metabolic demands of nervous tissue; however, neuronal contributions to other BBB structures and function, such as TJ regulation, remain unknown (Koehler et al., 2006).

Although a non-cellular component, the ECM, which is composed of several major proteins including hyaluronan, lecticans, collagen IV, and fibronectin, is an integral component of the BBB and NVU. The ECM functions by connecting and functionally separating brain capillary ECs from pericytes and astrocytes, thereby allowing proper cellular orientation (Zobel et al., 2016). In addition, the ECM mediates the movement of cells within and outside of the NVU and maintains brain homeostasis due to its buffering properties. It is well established that disruption of the ECM and alterations in matrix adhesion receptors, such as integrins, contributes to increased BBB

permeability during stroke (del Zoppo and Milner, 2006; Sandoval and Witt, 2008). The basement membrane, a thin layer of ECM that lines the parenchymal side of NVU, connects ECs to astrocytic end-feet and has been implicated in BBB maintenance. Specifically, damage of the basement membrane caused by increased expression of matrix metalloproteinases (MMPs) is believed to be related to alterations in BBB permeability in numerous pathologies (Wang and Shuaib, 2007; Sandoval and Witt, 2008; Lau et al., 2013).

Finally, the NVU also contains microglia, which are the primary immune cells of the CNS (Graeber and Streit, 2010). While the impact of microglia on BBB function in physiological conditions is not well known, activation of microglia *via* neuronal or BBB damage has been shown to contribute to and exacerbate BBB dysfunction (da Fonseca et al., 2014; Thurgur and Pinteaux, 2019). For example, microglial activation resulting in the release of pro-inflammatory cytokines, such as IL-1β and TNF-α, can lead to increased BBB permeability *via* disrupted TJs and increased neutrophil recruitment (Zhou et al., 2006; Chen et al., 2019). Thus, microglia are important to consider when discussing CNS pathologies associated with neuroinflammation.

Endothelial Cell Junctions

Tight Junctions

Tight junctions are large, multiprotein junctional cell-cell complexes composed of three major membrane proteins, claudins, occludin, and junction adhesion molecules (JAMs), along with the accessory proteins zonula occludins (ZO; **Figure 2**). TJs are particularly significant in regulating permeability by inducing EC polarization and restricting the paracellular movement of ions, such as Na^+ and Cl^-, as well as macromolecules across the BBB. TJ efficacy in the BBB, specifically compared to the peripheral vasculature, is evidenced by a considerably high value of BBB transendothelial electrical resistance (TEER) and low paracellular permeability (Ronaldson and Davis, 2015).

The tight junction protein family claudins are 20–24-kDa proteins with four transmembrane domains (**Figure 2**). To date, more than 24 members have been identified (Ballabh et al., 2004). However, in brain ECs, the major isoforms are claudin-1, -3, -5 and -12, all of which play important roles in barrier function (Yang and Rosenberg, 2011). Claudin-5, in particular, significantly limits paracellular diffusion of small substances in the BBB (Greene et al., 2019). Specifically, increased claudin-5 can increase TEER and decrease BBB permeability. To regulate TJ function, the carboxy terminal (intracellular tail) of claudins bind to cytoplasmic proteins including ZO-1, ZO-2, and ZO-3, forming TJ scaffolds between extracellular neighboring proteins and the cell cytoskeleton, thus providing an anchorage to maintain cell-cell contacts (**Figure 2**; Honda et al., 2006).

A second major transmembrane TJ protein is occludin, a 65-kDa protein involved in TJ stabilization to regulate BBB functional integrity (**Figure 2**; Nag et al., 2007). Similar to other TJ proteins, occludin is highly expressed in cerebral endothelium but more sparsely distributed in non-neural endothelia (Nag et al., 2007) and is associated with increased electrical resistance in TJ-containing tissues and decreased

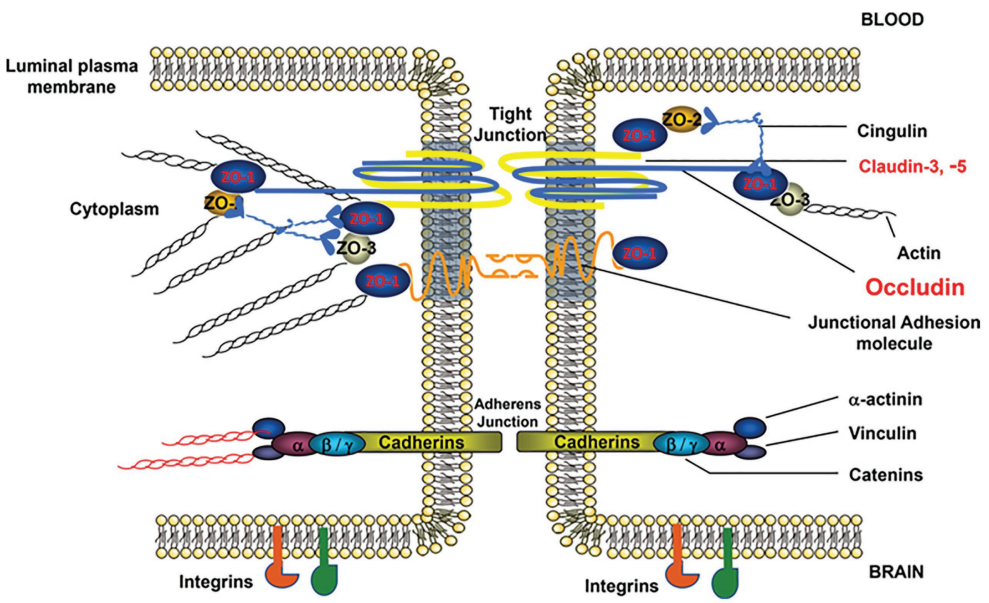

FIGURE 2 | Structure of brain EC-cell junctions. EC-to-EC junctions consist of permeability regulating protein complexes in both tight and adherens junctions (AJs). TJs, which are more strongly associated with permeability regulation, consist of the occludin, junctional adhesion molecule, and claudin families of proteins linked to the cytoskeleton *via* zona occludens (ZO) proteins. AJs, which also play a role in permeability regulation, are composed of vascular endothelial (VE)-cadherin dimers similarly linked to the cytoskeleton *via* an array of linker proteins, such as catenin. In addition to these major junctional components, EC junctions also contain numerous supporting proteins such as cingulin, vinculin, and integrins, among others. This figure is reprinted from a previous publication (Abdullahi et al., 2018), with permission from the previous publisher, the American Physiological Society.

paracellular diffusion (Nag et al., 2007). As with claudins, ZO proteins also localize occludin to the cellular membrane, creating an intercellular bridge (**Figure 2**). Interestingly, the function of occludins is suggested to be a function of dynamic phosphorylation, which can affect the assembly/disassembly of TJs (Dorfel and Huber, 2012). Combined with claudins and junctional adhesion molecules, occludins within the BBB strictly regulate BBB permeability to promote CNS homeostasis.

Adherens Junctions

Adherens junctions (AJs), located toward the basolateral side of EC TJs, are adhesive cell-cell interactions composed of cadherins along with their associated proteins, which are important for both the localization and stabilization of AJs (**Figure 2**). The transmembrane cadherin protein and, more specifically, cadherin-mediated signaling plays a key role in numerous EC processes, including endothelial layer integrity and the organization of microvessels during development (Lampugnani and Dejana, 2007). The regulation of these cadherin functions also relies on other AJ components, namely α-actinin and vinculin (**Figure 2**), which similarly have been implicated in maintaining BBB function (Abu Taha and Schnittler, 2014). Out of the numerous cadherin proteins in humans, VE-cadherin is specifically expressed by ECs and is required for endothelial survival and stabilization (Tietz and Engelhardt, 2015) and is also associated with paracellular permeability (Beard et al., 2011). Interestingly, despite the correlation between VE-cadherin expression and permeability regulation, one particular study suggested that partial loss of VE-cadherin may lead to long-term stroke protection (Gertz et al., 2016).

Transporters

Endothelial cells of the BBB express many transporters that, in addition to junctional proteins, play an important role in regulating the transport of endogenous and exogenous materials, such as glucose, which cannot permeate cell-cell junctions. Major transporters include nutrient transporters, ion transporters, and the ATP-binding cassette (ABC) transporters, which will be discussed here (**Table 2**; Jiang et al., 2018).

Nutrient Transporters

D-glucose is the main energy source for brain metabolism and a continuous supply is therefore required to maintain normal brain function. The main glucose transporter in the BBB is the glucose transporter 1 (GLUT1) protein (**Table 2**), which is expressed and localized to brain ECs. Many pathophysiological conditions, including chronic hypoxia and ischemia, are capable of altering glucose transporter expression, including GLUT1. However, whether these changes in expression are beneficial or detrimental to BBB and neuronal function varies (Vemula et al., 2009). For example, one study found that hypoxia-ischemia can elevate GLUT1 expression, which in previous studies has been demonstrated to serve a neuroprotective role by reducing focal ischemic lesion size (Shi et al., 1997; Li et al., 2013). Another type of glucose transporter expressed in the BBB is the sodium-glucose transporter (SGLT) protein (**Table 2**), which contributes to materials transport and cell depolarization and has been shown to help maintain glucose levels during stroke (Yamazaki et al., 2015). However, contrary to the observed beneficial effects of GLUT1, several studies have shown that SGLT is relevant to increased edema formation and can actually exacerbate cerebral ischemic neuronal injury due to the influx of sodium ions (Yamazaki et al., 2016; Sifat et al., 2017). Other studies have corroborated these findings, suggesting that inhibition of SGLT during stroke may improve stroke outcome (Vemula et al., 2009). Thus, regulation of glucose transporters within the BBB can have complex consequences on CNS homeostasis.

TABLE 2 | EC transporters and their functions.

Component		Function	Diseased condition	Expression	Reference
Nutrient transporters	Glucose transporter 1 (GLUT1) protein	Regulates glucose level in brain	Hypoxia-ischemia elevates GLUT1 expression, which serves a neuroprotective role by reducing focal ischemia	Disperse	Shi et al., 1997; Vemula et al., 2009; Li et al., 2013
	Sodium-glucose transporter (SGLT) protein	Materials transport; cell depolarization; glucose level maintenance	Increases edema formation and exacerbates cerebral ischemic neuronal injury; inhibition of SGLT during stroke improves outcome		Vemula et al., 2009; Yamazaki et al., 2015; Yamazaki et al., 2016; Sifat et al., 2017
Ion transporters	Na^+-K^+-Cl^- co-transporter	Maintain CNS ion content	Hypoxia stimulates Na^+-K^+-Cl^- cotransporter expression leading to brain edema formation	Luminal	Foroutan et al., 2005; Jayakumar and Norenberg, 2010
	Na^+/K^+-ATPase		Decreased Na^+/K^+-ATPase expression causes the accumulation of Na^+ leading to endothelial swelling and cytotoxic edema	Abluminal	Babsky et al., 2008; Hladky and Barrand, 2016; Jiang et al., 2018
	Ca^{2+}-ATPase		Ca^{2+}-ATPase fails to maintain ion homeostasis in the setting of stroke due to ATP loss	Luminal	Jiang et al., 2018
ATP-binding cassette (ABC) transporters	P-glycoprotein (P-gp) Breast cancer resistance protein (Bcrp) Multidrug resistance-associated proteins (Mrps)	Efflux pumps most notably regulating drug transport	Differentially expressed in neurological disorders	Luminal	Abbott et al., 2010; Qosa et al., 2015; Jiang et al., 2018

Ion Transporters

Ion transporters, which are predominantly expressed at BBB ECs' abluminal surface, have important effects on vectorial transport across the cell membrane and, subsequently, on CNS ion homeostasis and fluid movement. The major ions in the nervous system are Na^+, K^+, Cl^-, and Ca^{2+}, all of which are critical to the regulation of neuronal activity (Hladky and Barrand, 2016). The transport of Na^+, Cl^-, and other ions combined with the associated water influx is responsible for approximately 30% of the interstitial fluid in a healthy brain. One common ion transporter is the Na^+-K^+-Cl^- co-transporter (NKCC; **Table 2**), which is important in maintaining CNS homeostasis (Jayakumar and Norenberg, 2010). It has been reported that hypoxia can stimulate the expression of the Na^+-K^+-Cl^- cotransporter, leading to ischemia-induced brain edema formation (Foroutan et al., 2005; Jayakumar and Norenberg, 2010). As such, in stroke patients, the entry of extracellular Na^+ caused by the alteration of these ion transporters, such as decreased Na^+/K^+-ATPase expression and function, has a profound impact on endothelial swelling and cytotoxic edema (Babsky et al., 2008; Hladky and Barrand, 2016). Other ion transporters are also implicated in stroke and BBB dysfunction (Hom et al., 2007; O'Donnell, 2014; Jiang et al., 2018). For example, in an ischemic episode, the Na^+/K^+-ATPase and Ca^{2+}-ATPase ion transporters (**Table 2**) fail to conserve ionic balance due to ATP depletion caused by the blockage of oxidative phosphorylation (Jiang et al., 2018). Collectively, these studies highlight the importance of ion transporters in regulating BBB function and in pathophysiological events such as stroke.

ATP-Binding Cassette Transporters

The ABC transporters (**Table 2**), which are located at the EC luminal membrane, are a protein superfamily that transports neurotoxins against concentration gradients, thereby requiring biological energy. This protein superfamily contains 48 members and is divided into seven sub-families (Jiang et al., 2018). Major ABC transporters relevant to the BBB include P-glycoprotein (P-gp; **Table 2**), which transports a variety of structurally diverse compounds; breast cancer resistance protein (Bcrp; **Table 2**), which is able to recognize variable organic anions; and MRPs (**Table 2**), which are associated with cellular efflux of anionic drugs as well as their metabolites (Abbott et al., 2010). While ABC transporters protect the CNS by restricting toxin permeability through the BBB, they have also been found to hinder therapeutic strategies targeting the CNS as they similarly limit the transport of drugs through the BBB. It has also been shown that ABC transporter expression varies in neurological disorders such as Alzheimer's, Parkinson's, and stroke (Qosa et al., 2015). Thus, while the role of ABC transporters in both proper BBB function and neurological disorders is complex, it is clear that alterations in their expression can have significant consequences on BBB and neural tissue function.

ISCHEMIC STROKE

Ischemic Stroke Pathology

Stroke is the second leading cause of death in the world behind cardiovascular diseases and annually contributes to 5.5 million deaths globally (Alishahi et al., 2019). Stroke incidence has also increased more than 100% in developing countries, suggesting that stroke prevalence will likely increase over the coming years (Tsai et al., 2016). At present, there are two major types of stroke: ischemic strokes and hemorrhagic strokes. In this review, we focus on ischemic strokes.

Ischemic strokes amount to approximately 87% of all strokes and are classified as strokes that occur due to vessel obstruction *via* a blood clot (Sevick et al., 2017). These clots can either form directly at the site of insult or result from the rupture of a larger clot at an upstream region of the vasculature. When ischemic strokes occur, blood flow to the brain is interrupted leading to decreased oxygen delivery and reduced nutritional supply (e.g., glucose) to the affected part of the brain (Chauhan and Debette, 2016). The affected areas of the brain resulting from ischemic stroke are referred to as the ischemic, or infarct, core, and penumbra, which collectively form the term "brain ischemia" (**Figure 3**; Bandera et al., 2006). The ischemic or infarct core is defined as the area of irreversible tissue injury, typically characterized by blood flow with perfusion rates below 10 ml/100 g of tissue per minute (Latchaw et al., 2003; Bandera et al., 2006). Outside of the infarct core is the penumbra, which also contains the benign oligemia (**Figure 3**), and is defined as functionally impaired tissue that is still viable. Typically, tissue within the penumbra is perfused at rates below 25 ml/100 g tissue per minute (Bandera et al., 2006; Fisher and Bastan, 2012). While tissue within the benign oligemia will recover spontaneously, tissue outside of the benign oligemia but within the penumbra requires clinical intervention. Therefore, therapeutics aimed at preventing CNS damage as result of ischemic stroke target these areas of the brain, whereas the infarct core is beyond treatment due to the rapid development of necrosis (Bandera et al., 2006).

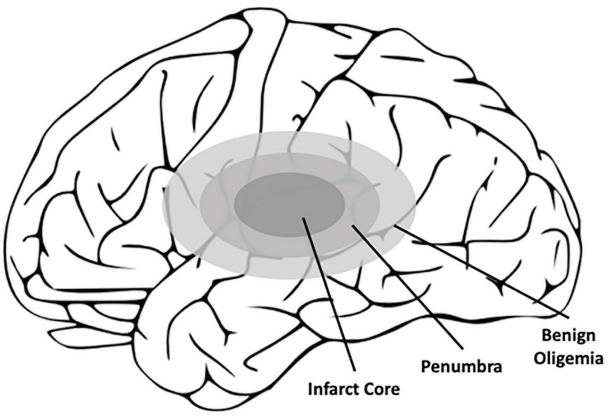

FIGURE 3 | Schematic of the affected areas of the brain after ischemic stroke. Closest to the location of the blood clot, and thus the loss of blood flow, is the infarct core, which contains irreversibly damaged tissue. Outside of the infarct core lies the penumbra, which also contains the benign oligemia, and defines the area of reversible tissue damage. While the benign oligemia specifies tissue that will recover function on its own, tissue within the penumbra but outside of the benign oligemia requires therapeutic intervention for full recovery.

The first contributors to the rate of infarct progression are the degree of collateral arterial circulation, duration of insult, and the functional and metabolic cellular state (Bandera et al., 2006). Collectively, these factors determine the likelihood of success of common ischemic stroke therapeutics.

In addition to the initial insults of ischemic stroke, following ischemic stroke metabolic disturbances and energy imbalance can cause secondary injury such as inflammation and gliosis leading to further neuronal and vascular cell death. Inflammation, in particular, is believed to play a critical role in the pathogenesis of ischemic stroke. For example, the initial ischemic insult leads to the activation of microglia (Ma et al., 2017) and astrocytes (Choudhury and Ding, 2016) as well as the recruitment and infiltration of inflammatory cells such as leukocytes (Gronberg et al., 2013). Interestingly, while some studies have indicated beneficial impacts of several of these inflammatory mechanisms on brain recovery, overall the inflammatory response is believed to have a detrimental effect, particularly under prolonged inflammation (Jin et al., 2010). This is supported by the effective use of anti-inflammatory therapeutics to limit neurological deficits in animal models of ischemic stroke (Lakhan et al., 2009), although these therapeutics have not translated into the clinic. These and other therapeutic options for ischemic stroke will be further discussed later in the review.

Although not well studied, endothelial mechanotransduction within the BBB may also play a major role in ischemic stroke pathology and potentially its initial occurrence. In the peripheral vasculature, endothelial exposure to physiological shear stress promotes vessel function through the regulation of vascular permeability (Himburg et al., 2004; Warboys et al., 2010), vasoconstriction/vasodilation (Uematsu et al., 1995; Muller et al., 1997), and inflammatory phenotype (Chen et al., 2003). Recent studies have similarly demonstrated that brain-derived ECs similarly benefit from shear stress exposure *via* observed increases in barrier integrity (Colgan et al., 2007; Siddharthan et al., 2007; Cucullo et al., 2011; Walsh et al., 2011). Thus, stroke-induced hypoperfusion may lead to inadequate mechanotransduction that could further compromise BBB integrity. Additionally, mechanotransducers, such as the endothelial glycocalyx (GCX), have been shown to be degraded in response to ischemia-reperfusion (Rubio-Gayosso et al., 2006), which may exacerbate issues of proper mechanotransduction. Impaired mechanotransduction may even contribute to the occurrence of ischemic stroke, as the development of blood vessel plaques, which can rupture and lead to ischemic stroke, are known to occur in areas of disturbed blood flow characterized by altered mechanotransduction and degraded GCX layers (van den Berg et al., 2009; Cancel et al., 2016; Harding et al., 2018; Mitra et al., 2018). It is therefore vital to understand the impact of endothelial mechanotransduction in both stroke pathology and occurrence, which will be addressed later in the review.

BBB Dysfunction in Ischemic Stroke

A major hallmark of stroke is its associated BBB disruption, which is initiated due to ischemia but continual deteriorates with sustained hypoperfusion. This deterioration is largely attributed to a lack of nutrients (e.g., oxygen and glucose), but altered mechanotransduction may also play a role. This is evidenced by the fact that even after the restoration of blood flow, albeit below baseline levels, BBB permeability does not revert but instead persists. Furthermore, degradation of the mechanotransductive GCX layer has been shown to be degraded in ischemia/reperfusion (Chappell et al., 2009; van Golen et al., 2012), implicating its potential role in BBB maintenance. The exact time course of increased BBB permeability in ischemic stroke is widely debated. Initial studies in animal models identified a biphasic nature of BBB permeability, in which initial increases in permeability are followed by a reduction in permeability to baseline levels but eventual return to increased permeability (Kuroiwa et al., 1985; Huang et al., 1999). While more recent studies have supported this theory (Pillai et al., 2009), other studies, including in human subjects, suggest that BBB permeability remains elevated post-stroke potentially for several weeks (Strbian et al., 2008; Merali et al., 2017). Regardless, initial breakdown of the BBB is believed to occur at least partially through the overexpression of matrix metalloproteinases (MMPs), which can have numerous detrimental effects including the degradation of the endothelial GCX, a known mechanotransducer (Ramnath et al., 2014; Yang and Rosenberg, 2015; Zhang et al., 2018). GCX degradation has been shown to disrupt junctional protein expression and function (Thi et al., 2004; Mensah et al., 2017). Following this initial breakdown, a sustained increase in permeability likely occurs due to a neuroinflammatory response, which, combined with other consequences such as brain edema, contributes to longer-term permanent loss of neurological function (Abdullahi et al., 2018). To better understand the observed increase in BBB permeability following stroke, we will discuss the mechanisms of this process, focusing on the role of junctional and transporter proteins.

Junctional Proteins

The overall increase in BBB permeability in stroke is largely attributed to differences in junctional protein expression and function. For example, stroke is associated with decreased expression of the TJ proteins claudin-5, occludin, and ZO-1, among others (Jiao et al., 2011). This is evidenced by the increased uptake of ^{14}C-sucrose, a membrane impermeant marker, in the brain parenchyma after stroke (Hau et al., 2004; McCaffrey et al., 2009; Abdullahi et al., 2018). It has also been suggested that occludin redistribution, in addition to changes in expression, induced by VEGF may occur and is associated with increased paracellular permeability in ECs (Murakami et al., 2009). Caveolin-1, a coat protein of pinocytotic caveolae vesicles implicated in molecular trafficking, mediates the redistribution and localization of junctional proteins, such as ZO-1, claudin-5, and occludin, as previously mentioned (Choi et al., 2016; Abdullahi et al., 2018; Zhang et al., 2018). Additionally, while TJs are more widely known for their role in maintaining BBB permeability, the AJ protein VE-cadherin has also been shown to have decreased expression after stroke, contributing to the overall increase in permeability (Abdullahi et al., 2018). The observed changes in VE-cadherin expression following stroke may be regulated by sphingosine kinase (SphK2),

as SphK2-null mice display reduced levels of VE-cadherin and other junctional proteins (Wacker et al., 2012).

Initial disruption in junctional protein expression is believed to be due to MMPs and, on a lesser basis, reactive oxygen species (ROS). This initial, short-term increase in permeability in some cases reverts to baseline levels and is thus often classified as "reversible" (**Figure 4**). However, as the molecular response shifts in response to stroke, longer-term BBB opening, referred to as "irreversible," can persist for several days or longer (**Figure 4**). What determines the length of increased BBB permeability is not fully known, but molecules such as MMPs and cytokines are implicated in the process. For example, MMP-2 activation is believed to be responsible for initial disruption of TJ proteins (**Figure 4**). However, in later phases of BBB disruption resulting from stroke, MMP-9 expression is induced and results in more intense and irreversible damage (**Figure 4**; Yang and Rosenberg, 2015). The role of MMPs in stroke-induced BBB dysfunction was evidenced by Shuai et al., who found that stroke results in decreased ZO-1 expression and translocation of ZO-1 from the cell junctions to the cytoplasm, which occurs due to increased MMP-2/9 and caveolin-1 expression (Zhang et al., 2018). Another study suggested that reduction in brain permeability is highly associated with decreased expression of MMP-2/9 (Zeng et al., 2020). In addition to increased MMP expression and activity, increased concentrations of ROS such as superoxide, which is substantially produced by the NADPH oxidase (Nox) proteins (Revuelta et al., 2019), has similarly been shown to reduce the expression of junctional proteins such as claudin-5 and occludin. For example, Zhanying et al. found that upregulation of TJ protein expression owing to attenuated generation of ROS contributed to improvement of BBB function (Ye et al., 2019). ROS has also been shown to cause caspase-3-mediated damage of TJs and microvascular endothelial hyperpermeability *in vitro* (Alluri et al., 2014). In addition to the short- and long-term impacts of MMPs and ROS on BBB integrity, other inflammatory regulators, such as the cytokines TNF-α (Yang et al., 1999; Pan and Kastin, 2007) and IL-1β (Anthony et al., 1997; Ferrari et al., 2004), as well as neutrophils (Rosell et al., 2008; Joice et al., 2009; Jickling et al., 2015) have been implicated in BBB maintenance following stroke. Due to the proven detrimental effects of these factors, therapeutics targeting these molecules have drawn significant interest to maintain BBB integrity.

Endogenous BBB Transporters

Changes in the expression and function of endogenous BBB transporters also impact stroke-induced BBB permeability and the resulting pathophysiological processes such as edema. Major BBB transporters associated with stroke include the glucose transporter proteins and ion transporters. For instance, the GLUT1 and GLUT3 glucose transporters are significantly elevated in the short and long term time periods following severe hypoxic-ischemic insults (Vannucci et al., 1998). Increased expression of the SGLT glucose transporter has also been observed and inhibition of this and the GLUT1 transporter can reduce edema formation despite the beneficial nutrient transport roles of these proteins (Vemula et al., 2009). Also implicated in permeability regulation in stroke and subsequent edema formation are ion transporters, particularly the Na^+ transporters. For instance, increased expression and phosphorylation of the Na^+-K^+-Cl^- transporter is associated with severe ischemic conditions (Foroutan et al., 2005). Furthermore, the inhibition of various ion transporters, including Na^+-K^+-Cl^- (Huang et al., 2019), NHE1 (Park et al., 2010), and KCa3.1 (Chen et al., 2015), have been shown to reduce edema or infarct size, highlighting their importance in stroke. In addition to alternations in specific transporter proteins, elevation of pinocytosis within the endothelium occurs post ischemia-reperfusion (Shinozuka et al., 2013), further contributing to increased permeability (Xia et al., 2012). A study by Knowland et al. (2014) even suggested that

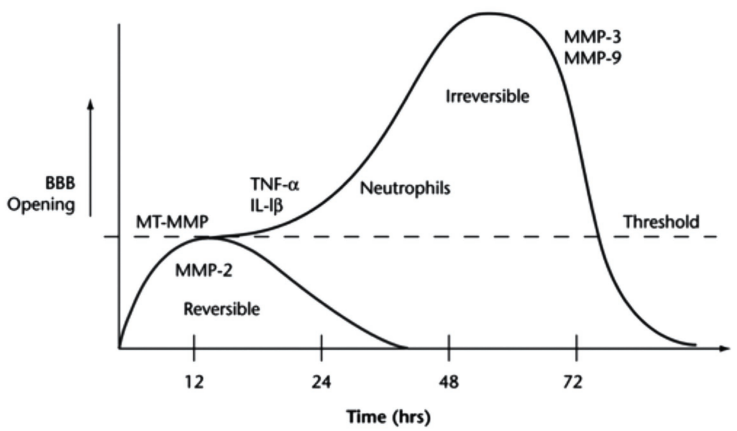

FIGURE 4 | The time course of BBB opening and associated expression of pro-inflammatory mediators of BBB damage. Initial opening of the BBB is likely caused, at least in part, by increases in MMPs, specifically MMP-2. This initial phase occurs over ~24 h and is referred to as "reversible." Over time, continuous production of pro-inflammatory molecules, such as TNF-alpha, IL-1beta, and MMPs 3 and 9, can lead to prolonged opening (72+ h) of the BBB, potentially contributing to long-term tissue damage. This phase is thus referred to as "irreversible." Reprinted from Yang and Rosenberg, "Matrix metalloproteinases as therapeutic targets for stroke," Brain Research, 2015, 1,623:30–38, with permission from Elsevier.

increased transcellular transport *via* caveolae and other pinocytotic vesicles occurs before TJ disruption.

Other Mechanisms

In addition to the common permeability pathways controlled by junctional proteins and EC transporters, other molecules, such as integrins and EC adhesion molecules, also play a role in regulating BBB permeability after stroke, albeit to a lesser extent. Integrins, transmembrane proteins that interact with the ECM to stabilize ECs to their environment, have been shown to contribute to BBB permeability regulation. For example, Osada et al. (2011) demonstrated that antibody neutralization of b_1-integrin leads to a significant decrease in BBB barrier integrity, specifically through a reduction in transepithelial electrical resistance and increased permeability. Studies suggest that integrins are able to regulate BBB integrity through both the downstream regulation of TJ proteins, specifically claudin-5 (Osada et al., 2011), and by promoting EC-astrocyte interactions, which are crucial for proper BBB function (Almutairi et al., 2016).

Endothelial cell adhesion molecules, such as intercellular adhesion molecule 1 (ICAM-1), also play a role in regulating transport in the BBB in particular through their role in leukocyte transendothelial migration. After focal brain ischemia, EC adhesion molecules, mainly ICAM-1, are upregulated potentially *via* the local and systemic release of pro-inflammatory factors (Lindsberg et al., 1996). Combined with increased leukocyte production in response to stroke (Ross et al., 2007), this promotes increased transendothelial migration of leukocytes, such as neutrophils. While short term increases in neutrophils and other white blood cells may help resolve vascular and CNS damage, prolonged neutrophil accumulation, and activity actually worsens long term outcomes (Buck et al., 2008; Kumar et al., 2013).

THERAPEUTIC STRATEGIES FOR ISCHEMIC STROKE

Current therapeutic strategies for ischemic stroke fall into four categories: clinical care, neuroprotection, neurorestoration strategies, and rehabilitation therapy (Patel and McMullen, 2017). To date, the only major treatment strategies approved by the United States Food and Drug Administration (FDA) and used in the clinic are thrombolysis *via* tissue plasminogen activator (r-TPA) and endovascular treatment. However, while these treatments have been successful in improving clinical outcome, they are not able to resolve prolonged neuronal dysfunction and degeneration of still viable tissue. Therefore, many studies and experimental trials have been focused on developing neuroprotective therapies to retain function of viable tissue after an ischemic episode. Yet, while many animal studies have demonstrated promising results, they have met limited success in clinical trials. In this review, we will first address stroke management in the clinic and then elaborate on both previous and promising neuroprotective treatment options currently being assessed (**Table 3**). Furthermore, we will briefly discuss neurorestorative therapies.

Clinical Care

Two major thrombolytic therapeutic strategies, either *via* the use of pharmacological agents or *via* mechanical thrombectomy (Jovin et al., 2015; Saver et al., 2016), are currently used for recanalization and reperfusion for stroke patients (**Table 3**). The treatment of choice for each patient depends on the time to treatment and the etiology of the injury. At present, the most common pharmacological treatment is thrombolysis *via* r-tPA, known as alteplase (**Table 3**), which is approved by the FDA

TABLE 3 | Current and promising therapeutics for treatment of ischemic stroke.

Therapy	Functionality	Reference
Alteplase	Tissue plasminogen activator used for thrombolysis. Only FDA approved pharmacological treatment. Only utilized within 3–4.5 h of stroke.	Bansal et al., 2013; Sifat et al., 2017; Clarke and Ayala, 2019
Mechanical thrombectomy	An FDA approved treatment that utilizes a catheter to navigate blood vessels to the site of the clot for mechanical disruption. Has shown efficacy, but is a difficult procedure and only 10% of patients fit the criteria for treatment.	Mokin et al., 2014; Lapergue et al., 2020
Cerebrolysin	A mixture of brain-derived neuropeptides that exhibits anti-excitatory, anti-inflammatory, and anti-apoptotic activity. Approved in over 40 countries outside of the United States.	Goenka et al., 2019
Magnesium sulfate	An anti-excitatory treatment designed for neuroprotection. Has demonstrated a mixture of success and failure in clinical trials.	Lampl et al., 2001; Muir et al., 2004; Saver et al., 2015
Minocycline	An antibiotic designed for neuroprotection that displays anti-inflammatory and anti-apoptotic properties. It has demonstrated success in animal models but has been met with mediocre success in clinical trials.	Fagan et al., 2010; Karsy et al., 2017
Edaravone	An anti-oxidant therapy approved for the treatment of ischemic stroke in Japan, but not the US. Has demonstrated some success in clinical trials.	Kimura et al., 2012; Kikuchi et al., 2013
DI-3-n-butylphthalide (NBP)	A synthetic compound with intrinsic anti-inflammatory, anti-oxidative, and anti-apoptotic properties approved for the treatment of stroke in China and currently in clinical trials in the United States.	Li et al., 2019; Wang et al., 2019
Liraglutide/exenatide	Glucagon-like peptide-1 agonists that reduce infarct size and improve neurological function in animals. Ongoing clinical trials.	Sato et al., 2013; Zhu et al., 2016
Neurotophin-3	A neurorestorative therapy that has demonstrated neurogenesis in animal models but no success in humans.	Vilar and Mira, 2016; Duricki et al., 2019

(Sifat et al., 2017). When administered intravenously, alteplase provides local fibrinolytic effects by first binding to fibrin clots and then hydrolyzing peptide bonds in surrounding plasminogen, thus converting it to plasmin and subsequently disintegrating the clot (Bansal et al., 2013; Clarke and Ayala, 2019). While studies have demonstrated that alteplase does reduce tissue infarct volume, it does not alter other associated pathophysiologies such as ischemic brain edema (Broocks et al., 2020). While r-tPA has been demonstrated as an efficient and cost-effective thrombolytic agent, its short therapeutic time window of up to 4.5 h, association with severe deleterious events, especially hemorrhagic transformation and brain injury, and candidates' eligibility for treatment (e.g., delayed identification in the emergency department; Sung et al., 2013) greatly limit the safety and application of r-tPA (Mendez et al., 2018). Regarding deleterious events associated with tPA, it has been proposed that tPA exacerbates neuron death in the hippocampus due to inter-neuronal laminin degradation and pro-survival cell-matrix signaling disruption (Lo et al., 2004). Additionally, evidence suggests that a compromised BBB may limit the efficacy of r-tPA because it may exacerbate hemorrhagic transformation and promote brain edema and neuroinflammation. Due to these limitations, alternatives to alteplase, such as tenecteplase, have been investigated but have not shown any significant improvements in clinical trials (Logallo et al., 2017). Still, it is clear that areas for improvement exist.

Aside from r-TPA, other minor pharmacological treatment options are available, most notably aspirin. Aspirin treatment, which is only used for secondary prophylaxis, must be delivered within 24–48 h after stroke onset but has been reported to lower the potential risk of recurrent stroke and vascular events than non-users (Kong et al., 2019). However, it is suggested to be useless for the treatment of an ongoing acute ischemic stroke and, thus, alternative pharmacological therapeutic options remain the primary mode of treatment (Powers et al., 2018).

In addition to these pharmacological treatment options, endovascular mechanical thrombectomy treatment (**Table 3**), which utilizes micronavigation of catheters into the cerebral vasculature to mechanically disrupt clots (Akins et al., 2014), provides a more direct way to the occlusive lesion and has a longer therapeutic time window-up to 8 h (Jovin et al., 2015). Furthermore, it is reported that endovascular treatment combined with intravenous pharmacological thrombolysis may provide increased efficacy to many patients with ischemic stroke (Lowhagen Henden et al., 2017). Endovascular mechanical thrombectomy has also shown great benefits in large vessel occlusion *via* a combination of contact aspiration and stent retrievers (Mokin et al., 2014; Lapergue et al., 2020). However, despite the potential benefits, endovascular mechanical thrombectomy treatment is limited by high costs, its need for trained personnel, and its inability to restore tissue function within the penumbra.

Neuroprotection

Neuroprotective treatments are defined as therapeutics administered during the acute ischemic phase with the overall goal of protecting from further neuronal tissue injury. These therapeutics typically target the penumbra as this tissue is still viable but may require clinical intervention for complete functional recovery. Neuroprotective treatments as defined here are in contrast with neurorestoration techniques, which aim to restore tissue functionality through the stimulation of neurogenesis and neuroplasticity. There are two types of neuroprotection: pharmacologic neuroprotection and non-pharmacologic neuroprotection. Non-pharmacologic neuroprotective methods, such as transcranial laser therapy (Patel and McMullen, 2017), have shown some promise but will not be discussed in this review. For pharmacologic neuroprotection, our understanding of the mechanisms of tissue damage following ischemic stroke has advanced, providing scientists with viable targets for neuroprotective therapeutics. Many developed and tested therapeutics have targeted the modulation of inflammation, oxidative stress, excitotoxicity, or apoptosis, all of which have been implicated in post-stroke tissue damage (Goenka et al., 2019; Wang et al., 2019). However, despite the relatively high levels of therapeutic benefits identified by these treatments in animal models, limited success has been observed in the clinic despite the hundreds of clinical trials run. The low degree of therapeutic translation from animal models to human subjects is likely due to a combination of reasons relating to differences between animal models and human subjects (e.g., age of treatment and presence of comorbidities), the employed experimental methods, the quality of experimental or clinical trial design, the outcome measures utilized, and others. Thus, future research efforts attempting to identify neuroprotective therapeutics not only need to identify the novel therapeutics themselves but also enforce proper pre-clinical and clinical methods to properly evaluate the efficacies of these treatment options. Here, we will discuss several drugs that may prove to be promising therapeutics or may provide insight into the development of other future therapeutics.

While the only FDA-approved pharmacological therapeutic for ischemic stroke is tPA, a variety of other neuroprotective molecules have been approved for clinical use for other indications or in other countries. Still, the therapeutic efficacy of these treatments is controversial. For example, cerebrolysin (**Table 3**) is a mixture of brain-derived neuropeptide that exhibits anti-excitotoxicity, antioxidant, and anti-apoptotic activity that is approved for the treatment of stroke in more than 40 countries (Goenka et al., 2019). Several animal studies have demonstrated that cerebrolysin can improve outcome from stroke, for example, by reducing infarct size (Ren et al., 2007; Zhang et al., 2010). However, clinical trials for cerebrolysin have returned mixed results. Specifically, while the drug has demonstrated safety in Phase 1 and Phase 2 clinical trials, several later stage trials failed to demonstrate any improvement in neurological outcome. Although, a combination of cerebrolysin and physical rehabilitation therapy was shown to improve motor recovery in individuals with severe motor impairment.

Magnesium sulfate (**Table 3**), which modulates excitotoxicity, has also demonstrated success in animal studies but has been met with both success and failure in a clinical setting. An initial pilot clinical trial from 2001 found a significant correlation between magnesium sulfate and improved neurological outcome (Lampl et al., 2001). However, another larger future study

identified no relationship between the drug and neurological outcomes (Muir et al., 2004). Because the administration time in this study was in some cases significantly delayed, an additional clinical trial utilizing magnesium sulfate treatment in the field within 2 h of stroke onset was therefore performed and demonstrated a significant improvement in neurological outcomes (Saver et al., 2015). Other promising drugs, such as minocycline (**Table 3**), an antibiotic drug approved in the United States for numerous non-stroke indications, and edaravone (**Table 3**), an antioxidant therapy, have similarly demonstrated promise in animal trials but mixed results in clinical trials (Fagan et al., 2010; Sharma et al., 2011; Kimura et al., 2012; Kikuchi et al., 2013; Karsy et al., 2017). These studies, among many others, demonstrate both the difficulty of identifying promising stroke therapeutics and the importance of proper pre-clinical and clinical study design. Currently, new therapeutics are being tested in clinical trials around the world that will hopefully prove to be more successful than previous waves.

One such molecule is Dl-3-n-butylphthalide (NBP; **Table 3**), a synthetic compound that possesses anti-inflammatory, anti-oxidative, and anti-apoptotic properties and has been approved for treatment of ischemic strokes in China (Wang et al., 2019). Animal models evaluating NBP as a stroke therapeutic have found positive results. For example, Wang et al. (2019) identified increased neurological functional recovery after NBP treatment for ischemic stroke in mice, which was associated with increased white matter integrity and the upregulation of the TJ protein occludin. Similarly, Jiamin et al. demonstrated that NBP greatly reduces BBB permeability *via* the upregulation of claudin-5 and ZO-1 and downregulation of caveolin-1 in ischemic stroke mice (Li et al., 2019). These and other results have supported the use of NBP as a therapeutic, which is currently being evaluated in the clinic in a Phase 2 trial. Another promising therapeutic option, liraglutide (**Table 3**), a glucagon-like peptide-1 receptor agonist, is supported by a significant body of work which has identified both its beneficial effects on neurological function in animal models of stroke and its mechanism. For instance, numerous studies have demonstrated improved behavioral scores/neurological deficits and reduced infarct size in animal models of stroke treated with liraglutide (Sato et al., 2013; Zhu et al., 2016). These improved outcomes are believed to be due to reductions in oxidative stress, improved mitochondrial function, and reduced cell apoptosis *via* neuronal sirtuin 1 and activation of the PI3K/AKT and MAPK pathways (Sato et al., 2013; Zhu et al., 2016; He et al., 2020b). A phase 3 clinical trial evaluating the efficacy of liraglutide for treatment of ischemic stroke is currently underway. Another glucagon-like peptide-1 receptor agonist, exenatide (**Table 3**), has also met success in animal models and has an ongoing phase 3 clinical trial. Other recent therapeutic options, such as alpha lipoic acid, verapamil, soyateltide, and JPI-289, have also recently demonstrated success in animal models and currently have ongoing clinical trials. However, whether these new therapeutics will have higher success than previous neuroprotective therapies is still yet to be seen.

Neurorestoration

While neuroprotection focuses on preventing further damage to tissue, neurorestoration aims to restore function to damaged neurons *via* the use of neurotrophins, a group of proteins associated with the maintenance and survival of the CNS. The most abundant neurotrophin in the adult brain is brain-derived neurotrophic factor (BDNF), which participates in proliferation and neuronal differentiation, among other functions (Liu et al., 2020). Another common and well-studied neurotrophin, neurotrophin-3 (NT-3; **Table 3**), is specifically involved in cell proliferation as well as the processes of memory and learning (Vilar and Mira, 2016). As a stroke therapeutic, NT-3 has demonstrated excellent translational potential. For example, studies have shown that peripheral infusion of NT-3 can increase sensorimotor function after stroke. Additionally, phase 1 and phase 2 clinical trials have already been performed for NT-3, demonstrating its safety as a therapeutic (Duricki et al., 2019). Combined with NT-3's ability to be transported to the CNS through the BBB, these findings make it a promising future therapeutic. Metformin, another potential neurorestorative therapy, has also been shown to induce recovery of memory and learning by increasing the expression of the neutrophin BDNF (Ghadernezhad et al., 2016). Interestingly, metformin has also been shown to regenerate the GCX (Eskens et al., 2013; Targosz-Korecka et al., 2020). However, whether or not metformin-induced GCX regeneration plays a role in neurorestoration following stroke has not been studied. Other therapies, such as copolymer-1 (Cop-1), can similarly increase NT-3 and other neurotrophins to promote neurogenesis (Cruz et al., 2015). However, while some of these treatments have demonstrated efficacy *in vitro* or in animal models, further research is necessary to support their testing in clinical trials.

ENDOTHELIAL MECHANOBIOLOGY IN THE PERIPHERAL VASCULATURE, BBB MAINTENANCE, AND ISCHEMIC STROKE

One regulatory mechanism of vascular function that has been well studied in the peripheral vasculature but not in the context of the brain vasculature (i.e., the BBB), neither in physiological nor pathological conditions, is endothelial mechanobiology. Endothelial mechanobiology is the process by which ECs sense mechanical forces and convert these forces into biochemical signals (Davies, 1995; Ando and Yamamoto, 2009). These forces include shear stress created by blood flow and tension created by vessel contraction/dilation and changes in the ECM (He et al., 2020a). In the peripheral vasculature, endothelial mechanobiology promotes proper function of the vasculature by regulating permeability, vascular tone, inflammatory state, and other important vascular functions implicated in vascular disease (Chien, 2008; Jones, 2010; Glen et al., 2012). For example, in the peripheral vasculature, both *in vitro* and *in vivo* studies have demonstrated that exposure to physiological levels of fluid shear stresses

strengthens vascular barrier integrity (Himburg et al., 2004; Warboys et al., 2010). *Via* a novel *in vivo*/*ex vivo* permeability technique, Himburg et al. (2004) specifically found that increasing levels of physiological time-averaged shear stress leads to decreased endothelial permeability. Shear stress exposure has also been shown to increase nitric oxide production (Uematsu et al., 1995) and reduce the production of reactive oxygen species (Chen et al., 2003) when compared to samples maintained in static, no-flow conditions. In contrast, impaired mechanotransduction in the peripheral vasculature may promote the development of cardiovascular diseases such as atherosclerosis. In the case of atherosclerosis, a disease characterized by plaque formation in vessel walls, plaque development preferentially occurs in areas of the vasculature that experience abnormal flow patterns. Blood flow in these regions is typically characterized by multi-directional flow and low time-averaged shear stresses, leading to impaired mechanotransduction (Zarins et al., 1983; Ku et al., 1985).

Endothelial mechanotransduction has also been proven beneficial in the BBB. Specifically, several studies have demonstrated that exposure of brain EC monocultures or co-cultures to shear stress leads to increased TEER, reduced permeability, and increased expression of junctional proteins (Colgan et al., 2007; Siddharthan et al., 2007; Cucullo et al., 2011; Walsh et al., 2011). For example, Cucullo et al. (2011) found that shear stress application of 6.2 dynes/cm^2 to a co-culture of human brain microvascular ECs and astrocytes leads to increased expression of TJ proteins, such as occludin and claudin-5, while simultaneously upregulating protective transporter proteins such as the ABC transporter family. This led to reduced permeability of numerous molecules including mannitol and d-glucose. Although, while this and other studies have correlated shear stress exposure with increased barrier integrity, many of these studies utilize sub-physiological shear stress magnitudes or do not include important supportive cells such as pericytes and astrocytes. Furthermore, while the impacts of shear stress exposure have been demonstrated, the mechanostransducers responsible for the observed impacts are largely unknown. In this section, we will address a prominent endothelial mechanotransducing structure, the GCX, and elaborate upon the potential of this and other mechanotransducers as future therapeutic targets for the treatment of stroke and other diseases associated with BBB dysfunction.

Endothelial Glycocalyx Structure

The endothelial GCX is a transmembrane, proteoglycan-glycoprotein layer extending from the luminal surface of ECs with a reported thickness ranging from 20 nm to 11 mm *in vitro* and *in vivo*, depending on the size and location of the vessel, as well as the method of GCX preservation and visualization (**Figure 5**; Chignalia et al., 2016; Mitra et al., 2017; Harding et al., 2019). Due to its position, the GCX serves as a barrier to vascular permeability (Butler et al., 2020), can regulate the movement and absorption of blood-borne molecules, and can even affect the resistance to blood flow (Mitra et al., 2017; Zhu et al., 2018). These and other GCX functions are understandably largely dependent on the structural composition and stability of the GCX itself.

Glycoproteins of the GCX are protein-glycan conjugates that facilitate interactions with surrounding molecules and cells and include common adhesion molecules located at the base of the GCX. Three types of adhesion molecules play an important role in GCX structure: the selectin family, including E-selectin and P-selectin, which is highly associated with the interaction of leukocytes with the endothelium; the integrin family, which regulates platelet-EC interactions; and the immunoglobulin superfamily, which serve as ligands for integrins and additional mediators of adhesion to the endothelium (**Figure 5**; Mitra et al., 2017). Another major GCX component, proteoglycans, are core proteins to which many glycosaminoglycan (GAG) chains are covalently attached (**Figure 5**; Uchimido et al., 2019). Therefore, these proteins control the incorporation of extracellular GCX components into the EC body. The syndecan family of proteoglycans, which is composed of four members, is a unique transmembrane proteoglycan family involved in many biological processes like wound healing and inflammation (Chignalia et al., 2016). The glypican family, another proteoglycan family, is composed of six members and can be bound to glycosyl-phosphatidylinositol anchors within the cell membrane, which may contribute to its functional roles (**Figure 5**). The GAGs attached to these proteoglycans are composed of repeating disaccharide units and include heparan sulfate, which is the most common GAG on the GCX, chondroitin sulfate, which is believed to be the second most common GAG, and hyaluronic acid, which contributes to the structural integrity of the GAG-protein matrix. Additionally, GAGs and other GCX constituents are extensively modified with sialic acid residues, imparting a net negative charge to the structure. Collectively, these GCX components are highly associated with EC protection in the peripheral vasculature and several studies have even implicated the GCX as a critical component of the BBB, as discussed below (Ando et al., 2018).

Endothelial Glycocalyx and BBB Function

Previous investigations in the peripheral vasculature, mainly using transmission electron microscopy, identified robust expression of the GCX *ex vivo* (Luft, 1966; van den Berg et al., 2003; Ueda et al., 2004; Ebong et al., 2011). Subsequent studies have implicated GCX of the peripheral vasculature in regulating key EC functions. For instance, abundant GCX expression has been shown to reduce endothelial permeability in multiple vascular beds, including the mesenteric capillaries and glomerular vasculature (Adamson, 1990; Singh et al., 2007). GCX expression in the peripheral vasculature has also been shown to mediate shear stress-induced increases in nitric oxide formation, which promotes vasodilation and in general is associated with vascular health (Ebong et al., 2014; Harding et al., 2018). Specifically, shear stress exposure was shown to increase endothelial nitric oxide synthase activation and expression in a heparan sulfate-dependent nature (Harding et al., 2018). However, whether the GCX is expressed at the BBB and, if so, its thickness and composition had until recently

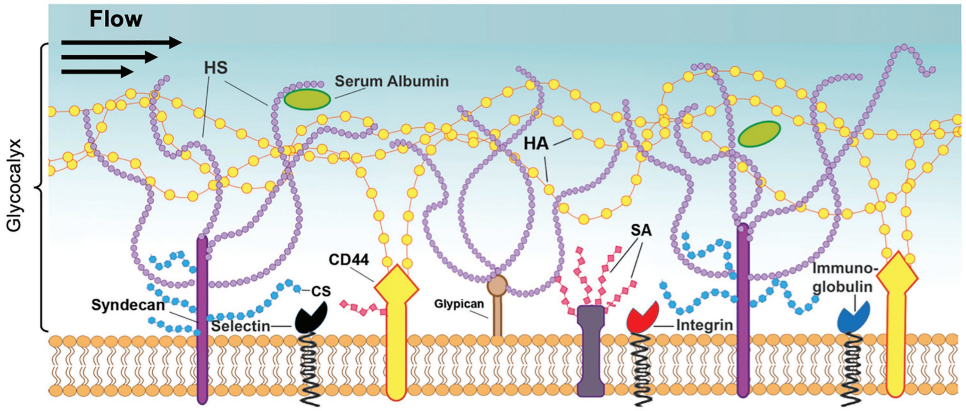

FIGURE 5 | Structure of the endothelial glycocalyx. The glycocalyx, a mechanotransducer implicated in BBB regulation, extends from the membrane of ECs into the vessel lumen and is largely composed of proteoglycans and glycoproteins. The proteoglycans consist of the core proteins, syndecans, and glypicans, along with their attached glycosaminoglycans: heparan sulfate (HS), chondroitin sulfate (CS), and hyaluronic acid (HA). These chains are also modified by sialic acid (SA), which provides a net negative charge to the structure. Additionally, the glycocalyx contains glycoproteins, such as integrins and immunoglobulins, and soluble proteins, such as albumin. Reprinted from Harding et al., 2019 "Endothelial barrier reinforcement relies on flow-regulated glycocalyx, a potential therapeutic target," Biorheology, 56 (2–3): 131–149, with permission from IOS Press. The publication is available at IOS Press through http://dx.doi.org/10.3233/BIR-180205.

not been studied. The first confirmation of GCX expression in the BBB came in 2017 by Yoon et al. (2017) who identified GCX expression *in vivo via* fluorescence microscopy. By labeling the GCX with wheat germ agglutinin and performing 2-photon microscopy, which allows for *in vivo* imaging at sufficient depth, Yoon identified a fluorescent dextran permeation-resistant GCX layer of approximately 1 mm in thickness. In agreement with these findings, another investigation found that GCX within the BBB resists permeation of larger molecules, such as dextran, but not smaller molecules, such as fluorescein and Alexa Fluor antibodies (Kutuzov et al., 2018). The Yoon study also suggested that GCX expression varies in the cerebrovasculature, with the highest expression in arteries and no detectable expression in veins and venules. In 2018, Ando et al. (2018) validated the presence of the GCX in the BBB using electron microscopy. Specifically, transmission electron microscopy demonstrated a robust expression of the GCX in brain capillaries that was greater than the expression in the peripheral vasculature of similar diameter. Furthermore, the study determined that GCX of the BBB is more resistant to inflammation-induced degradation, which is known to occur in numerous indications. These results suggest that GCX integrity may play an even more significant role in regulating BBB function when compared to the peripheral vasculature.

In addition to these studies confirming the presence of the GCX *in vivo*, other studies have implicated the GCX in regulation of BBB function in physiological conditions. For example, DeOre et al. (2020) recently found that CD44, a hyaluronic acid binding protein, promotes BBB function by regulating BBB permeability in response to fluid shear stress. Specifically, CD44 knockdown led to increased permeability and decreased TEER after 24 h of flow exposure at 0.7 dynes/cm^2, demonstrating the importance of CD44 expression in physiological conditions for proper mechanotransduction. In contrast to the beneficial effects of GCX expression in physiological conditions, GCX degradation has been identified in numerous pathologies, such as stroke and traumatic brain injury (TBI), suggesting that GCX degradation may play a functional role in the development of these conditions. For example, one study identified a degraded GCX layer in individuals with cerebral small vessel disease coinciding with white matter lesions (Martens et al., 2013). Another study in rats found that TBI significantly elevates levels of syndecan-1, a major GCX component, in serum samples compared to healthy controls (Jepsen et al., 2014). This is in agreement with other studies, including one using human subjects that identified increased syndecan shedding in response to TBI (Gonzalez Rodriguez et al., 2018). It was even found that repeated, low intensity TBI is sufficient to reduce both GCX thickness and density, which correlated with downstream behavioral deficits (Hall et al., 2017). GCX degradation is also associated with ischemia/reperfusion as occurs in ischemic stroke (Chappell et al., 2009; van Golen et al., 2012). Furthermore, a recent study by Zhu et al. (2018) found that hyaluronic acid degradation in rats *via* hyaluronidase treatment increases BBB permeability. While these studies demonstrate a correlation between GCX degradation and several neurological conditions, few studies have directly confirmed the role of the GCX in BBB function in physiological conditions. Furthermore, although GCX degradation is associated with ischemia/reperfusion as occurs in ischemic stroke, to our knowledge, no studies have extensively investigated the relationship between GCX expression and ischemic stroke pathology. Thus, future research should focus in these areas.

Other Mechanotransducers Implicated in BBB Maintenance

In addition to the GCX, other endothelial mechanosensors are involved in the maintenance of BBB integrity and

permeability. For example, it has been demonstrated that ion channels, particularly the transient receptor potential (TRP) channels, which are mechanosensitive, non-selective, calcium-permeable, cation channels, are heavily expressed on brain microvascular ECs (Chang et al., 2018) and serve as critical regulators of the intact BBB. Specifically, studies have demonstrated that transient receptor potential polycystin-2 (TRPP2; encoded by the PKD2 gene; AbouAlaiwi et al., 2009) and transient receptor potential channel 1 (TRPC1), which are responsible for calcium influx mediation, are highly involved in the response for BBB damage induced by TBI (Berrout et al., 2012). Both channels were suggested to modulate stretch-induced injury *via* nitric oxide (NO) production and action stress fiber formation in brain microvessel ECs. Marked decrease of the injury-induced calcium response, NO production, and stress fiber formation were observed after interfering with the function of TRPP2 and TRPC1 channel *via* TRPP2 and TRPC1 channel blockers or siRNA knockdown (Berrout et al., 2012). Ellaine et al. also demonstrated that stretch injury and oxygen glucose deprivation induced a significant increase in calcium ion concentration inside ECs (Salvador et al., 2015). Collectively, these studies suggest that ion channels may serve as potential therapeutic targets for BBB disruption. VE-cadherin has also been shown to regulate BBB function *via* endothelial mechanotransduction (Walsh et al., 2011). Specifically, Walsh et al. (2011) demonstrated for the first time that VE-cadherin transmits shear signals to occludin *via* Rac1, leading to BBB stabilization. This mechanosensory function of VE-cadherin likely occurs as part of the junctional mechanosensory complex, which has previously been shown to mediate EC responses to fluid shear stress (Conway et al., 2013).

Endothelial Glycocalyx Regeneration as a Therapeutic Option

To date, limited therapies targeting GCX restoration or protection exist. However, recent *in vitro* and *in vivo* animal studies have demonstrated potential promise for GCX-targeted therapeutics aiming to restore endothelial and vascular function associated with endothelial mechanotransduction. For example, spingosine-1-phosphate (S1P), which is a membrane phospholipid metabolite, can protect against shedding of the GCX and induce biosynthesis of GCX components after their shedding (Zeng et al., 2015; Araibi et al., 2020). Specifically, Zeng et al. (2015) found that S1P induces the synthesis of syndecan-1 and incorporates heparan sulfate and chondroitin sulfate chains on ECs. This function was modulated by the phosphoinositide 3-kinase (PI3K) pathway. However, other findings have suggested that S1P induction of cardioprotection against ischemia-reperfusion injury is not relevant to the integrity of syndecan-1 in adult rats but instead *via* alternative S1P functions (Araibi et al., 2020). Future examination of the effects of S1P will provide greater insight into the mechanisms and potential usage of S1P for GCX recovery and potentially for conditions such as ischemic stroke associated with GCX degradation.

Another treatment strategy referred to as GAG replacement includes GCX repair through the administration of exogenous GAGs, such as heparan sulfate. These include sulodexide, which contains heparin (80%) and dermatan sulfate (20%), and can lead to the reconstruction of endothelium barrier function and inhibition of GCX degrading enzymes (Mitra et al., 2017). Similarly, experiments performed by our research group have shown that heparan sulfate-degraded rat ECs can be treated with exogenous heparan sulfate and S1P to restore GCX structure. Furthermore, not only was this treatment able to restore GCX structure, but it was also able to restore EC function, particularly cell-cell gap junction communication (Mensah et al., 2017). Taken together, these studies demonstrate the potential for GCX protection as a novel approach for treatment of diseases associated with vascular dysfunction. Future work further identifying the mechanisms of GCX-induced regulation of vascular function will corroborate the GCX as a target for vascular related disease. Combining these findings with the development of accurate therapeutics to protect or restore GCX expression may thus aid in the identification of GCX-based therapeutics for BBB protection or regeneration in diseases such as ischemic stroke.

CONCLUSION

Over the past decade, our understanding of normal BBB and NVU functions and the mechanisms underlying BBB disruption during stroke has rapidly increased. It is well known that TJ proteins are complex and dynamic in nature and can be modulated in response to ischemic stroke while alterations of TJs can promote BBB permeability and oxidative stress-associated injury. In addition, endogenous BBB transporters further play a role in regulating BBB permeability and may be disrupted during ischemic stroke. Many therapeutic strategies have been investigated for their usage for ischemic stroke but with the exception of thrombolysis *via* recombinant tissue plasminogen activator (r-tPA) and endovascular mechanical thrombectomy treatment, these treatments have failed to pass clinical trials. New treatments targeting neuroprotection and neurorestoration, such as NBP and neurotrophins, respectively, are thus needed to help protect tissue injury from increasing in the setting of ischemic stroke. Additionally, endothelial mechanobiology, notably the endothelial GCX mechanotransducer, has been found to modulate BBB integrity and permeability, suggesting its high potential as a therapeutic target for BBB protection and recovery following ischemic stroke. However, the complete role of the GCX in BBB regulation has not been comprehensively studied, and few drugs have been developed for the protection or restoration of GCX components. Future research should further clarify the role of the GCX and other mechanotransducers in regulating BBB function and advance the development of novel therapeutics that target mechanotransducers in hopes of alleviating the impact of ischemic stroke.

AUTHOR CONTRIBUTIONS

KN, ICH, IMH, and EE were involved in the genesis of the review topic. KN and ICH drafted the manuscript. KN, ICH, EE, and IMH reviewed, edited, and approved the manuscript. All authors contributed to the article and approved the submitted version.

FUNDING

This manuscript was made possible by funding from the National Institutes of Health (K01 HL125499 awarded to EE), the American Heart Association (18PRE33960461 awarded to ICH), and Tufts University Office of the Provost (Inflammation-Based Collaborative Grant awarded to lead Principal Investigator (PI) IMH and co-PIs Luis Dorfmann and Tinatin Chabrashvili. The funders had no role in data or information collection and analysis, decision to publish, or preparation of the manuscript.

ACKNOWLEDGMENTS

We would like to thank members of the Ebong lab, specifically Ronodeep Mitra and Chinedu Okorafor, for providing input on the manuscript.

REFERENCES

Abbott, N. J., Patabendige, A. A., Dolman, D. E., Yusof, S. R., and Begley, D. J. (2010). Structure and function of the blood-brain barrier. *Neurobiol. Dis.* 37, 13–25. doi: 10.1016/j.nbd.2009.07.030

Abdullahi, W., Tripathi, D., and Ronaldson, P. T. (2018). Blood-brain barrier dysfunction in ischemic stroke: targeting tight junctions and transporters for vascular protection. *Am. J. Physiol. Cell Physiol.* 315, C343–C356. doi: 10.1152/ajpcell.00095.2018

AbouAlaiwi, W. A., Takahashi, M., Mell, B. R., Jones, T. J., Ratnam, S., Kolb, R. J., et al. (2009). Ciliary polycystin-2 is a mechanosensitive calcium channel involved in nitric oxide signaling cascades. *Circ. Res.* 104, 860–869. doi: 10.1161/CIRCRESAHA.108.192765

Abu Taha, A., and Schnittler, H. J. (2014). Dynamics between actin and the VE-cadherin/catenin complex: novel aspects of the ARP2/3 complex in regulation of endothelial junctions. *Cell Adhes. Migr.* 8, 125–135. doi: 10.4161/cam.28243

Adamson, R. H. (1990). Permeability of frog mesenteric capillaries after partial pronase digestion of the endothelial glycocalyx. *J. Physiol.* 428, 1–13. doi: 10.1113/jphysiol.1990.sp018197

Akins, P. T., Amar, A. P., Pakbaz, R. S., Fields, J. D., and Investigators, S. (2014). Complications of endovascular treatment for acute stroke in the SWIFT trial with solitaire and Merci devices. *AJNR Am. J. Neuroradiol.* 35, 524–528. doi: 10.3174/ajnr.A3707

Alishahi, M., Ghaedrahmati, F., Kolagar, T. A., Winlow, W., Nikkar, N., Farzaneh, M., et al. (2019). Long non-coding RNAs and cell death following ischemic stroke. *Metab. Brain Dis.* 34, 1243–1251. doi: 10.1007/s11011-019-00423-2

Alluri, H., Stagg, H. W., Wilson, R. L., Clayton, R. P., Sawant, D. A., Koneru, M., et al. (2014). Reactive oxygen species-caspase-3 relationship in mediating blood-brain barrier endothelial cell hyperpermeability following oxygen-glucose deprivation and reoxygenation. *Microcirculation* 21, 187–195. doi: 10.1111/micc.12110

Almutairi, M. M., Gong, C., Xu, Y. G., Chang, Y., and Shi, H. (2016). Factors controlling permeability of the blood-brain barrier. *Cell. Mol. Life Sci.* 73, 57–77. doi: 10.1007/s00018-015-2050-8

Alvarez, J. I., Katayama, T., and Prat, A. (2013). Glial influence on the blood brain barrier. *Glia* 61, 1939–1958. doi: 10.1002/glia.22575

Ando, Y., Okada, H., Takemura, G., Suzuki, K., Takada, C., Tomita, H., et al. (2018). Brain-specific ultrastructure of capillary endothelial glycocalyx and its possible contribution for blood brain barrier. *Sci. Rep.* 8:17523. doi: 10.1038/s41598-018-35976-2

Ando, J., and Yamamoto, K. (2009). Vascular mechanobiology: endothelial cell responses to fluid shear stress. *Circ. J.* 73, 1983–1992. doi: 10.1253/circj.cj-09-0583

Anthony, D. C., Bolton, S. J., Fearn, S., and Perry, V. H. (1997). Age-related effects of interleukin-1 beta on polymorphonuclear neutrophil-dependent increases in blood-brain barrier permeability in rats. *Brain* 120, 435–444. doi: 10.1093/brain/120.3.435

Araibi, H., van der Merwe, E., Gwanyanya, A., and Kelly-Laubscher, R. (2020). The effect of sphingosine-1-phosphate on the endothelial glycocalyx during ischemia-reperfusion injury in the isolated rat heart. *Microcirculation* 27:e12612. doi: 10.1111/micc.12612

Babsky, A. M., Topper, S., Zhang, H., Gao, Y., James, J. R., Hekmatyar, S. K., et al. (2008). Evaluation of extra- and intracellular apparent diffusion coefficient of sodium in rat skeletal muscle: effects of prolonged ischemia. *Magn. Reson. Med.* 59, 485–491. doi: 10.1002/mrm.21568

Ballabh, P., Braun, A., and Nedergaard, M. (2004). The blood-brain barrier: an overview: structure, regulation, and clinical implications. *Neurobiol. Dis.* 16, 1–13. doi: 10.1016/j.nbd.2003.12.016

Bandera, E., Botteri, M., Minelli, C., Sutton, A., Abrams, K. R., and Latronico, N. (2006). Cerebral blood flow threshold of ischemic penumbra and infarct core in acute ischemic stroke: a systematic review. *Stroke* 37, 1334–1339. doi: 10.1161/01.STR.0000217418.29609.22

Bansal, S., Sangha, K. S., and Khatri, P. (2013). Drug treatment of acute ischemic stroke. *Am. J. Cardiovasc. Drugs* 13, 57–69. doi: 10.1007/s40256-013-0007-6

Beard, R. S. Jr., Reynolds, J. J., and Bearden, S. E. (2011). Hyperhomocysteinemia increases permeability of the blood-brain barrier by NMDA receptor-dependent regulation of adherens and tight junctions. *Blood* 118, 2007–2014. doi: 10.1182/blood-2011-02-338269

Berrout, J., Jin, M., and O'Neil, R. G. (2012). Critical role of TRPP2 and TRPC1 channels in stretch-induced injury of blood-brain barrier endothelial cells. *Brain Res.* 1436, 1–12. doi: 10.1016/j.brainres.2011.11.044

Bicker, J., Alves, G., Fortuna, A., and Falcao, A. (2014). Blood-brain barrier models and their relevance for a successful development of CNS drug delivery systems: a review. *Eur. J. Pharm. Biopharm.* 87, 409–432. doi: 10.1016/j.ejpb.2014.03.012

Broocks, G., Kniep, H., Kemmling, A., Flottmann, F., Nawabi, J., Elsayed, S., et al. (2020). Effect of intravenous alteplase on ischaemic lesion water homeostasis. *Eur. J. Neurol.* 27, 376–383. doi: 10.1111/ene.14088

Buck, B. H., Liebeskind, D. S., Saver, J. L., Bang, O. Y., Yun, S. W., Starkman, S., et al. (2008). Early neutrophilia is associated with volume of ischemic tissue in acute stroke. *Stroke* 39, 355–360. doi: 10.1161/STROKEAHA.107.490128

Butler, M. J., Down, C. J., Foster, R. R., and Satchell, S. C. (2020). The pathological relevance of increased endothelial glycocalyx permeability. *Am. J. Pathol.* 190, 742–751. doi: 10.1016/j.ajpath.2019.11.015

Cancel, L. M., Ebong, E. E., Mensah, S., Hirschberg, C., and Tarbell, J. M. (2016). Endothelial glycocalyx, apoptosis and inflammation in an atherosclerotic mouse model. *Atherosclerosis* 252, 136–146. doi: 10.1016/j.atherosclerosis.2016.07.930

Chang, S. L., Huang, W., Mao, X., and Mack, M. L. (2018). Ethanol's effects on transient receptor potential channel expression in brain microvascular endothelial cells. *J. NeuroImmune Pharmacol.* 13, 498–508. doi: 10.1007/s11481-018-9796-3

Chappell, D., Jacob, M., Hofmann-Kiefer, K., Rehm, M., Welsch, U., Conzen, P., et al. (2009). Antithrombin reduces shedding of the endothelial glycocalyx following ischaemia/reperfusion. *Cardiovasc. Res.* 83, 388–396. doi: 10.1093/cvr/cvp097

Chauhan, G., and Debette, S. (2016). Genetic risk factors for ischemic and hemorrhagic stroke. *Curr. Cardiol. Rep.* 18:124. doi: 10.1007/s11886-016-0804-z

Chen, A. Q., Fang, Z., Chen, X. L., Yang, S., Zhou, Y. F., Mao, L., et al. (2019). Microglia-derived TNF-alpha mediates endothelial necroptosis aggravating blood brain-barrier disruption after ischemic stroke. *Cell Death Dis.* 10:487. doi: 10.1038/s41419-019-1716-9

Chen, X. L., Varner, S. E., Rao, A. S., Grey, J. Y., Thomas, S., Cook, C. K., et al. (2003). Laminar flow induction of antioxidant response element-mediated

genes in endothelial cells. A novel anti-inflammatory mechanism. *J. Biol. Chem.* 278, 703–711. doi: 10.1074/jbc.M203161200

Chen, Y. J., Wallace, B. K., Yuen, N., Jenkins, D. P., Wulff, H., and O'Donnell, M. E. (2015). Blood-brain barrier KCa3.1 channels: evidence for a role in brain Na uptake and edema in ischemic stroke. *Stroke* 46, 237–244. doi: 10.1161/STROKEAHA.114.007445

Chien, S. (2008). Role of shear stress direction in endothelial mechanotransduction. *Mol. Cell. Biomech.* 5, 1–8. doi: 10.3970/mcb.2008.005.001

Chignalia, A. Z., Yetimakman, F., Christiaans, S. C., Unal, S., Bayrakci, B., Wagener, B. M., et al. (2016). The glycocalyx and trauma: a review. *Shock* 45, 338–348. doi: 10.1097/SHK.0000000000000513

Choi, K. H., Kim, H. S., Park, M. S., Kim, J. T., Kim, J. H., Cho, K. A., et al. (2016). Regulation of caveolin-1 expression determines early brain edema after experimental focal cerebral ischemia. *Stroke* 47, 1336–1343. doi: 10.1161/STROKEAHA.116.013205

Choudhury, G. R., and Ding, S. (2016). Reactive astrocytes and therapeutic potential in focal ischemic stroke. *Neurobiol. Dis.* 85, 234–244. doi: 10.1016/j.nbd.2015.05.003

Clarke, J. D., and Ayala, J. P. (2019). Hemifacial angioedema following alteplase for acute stroke. *Pract. Neurol.* 19, 272–273. doi: 10.1136/practneurol-2018-002112

Colgan, O. C., Ferguson, G., Collins, N. T., Murphy, R. P., Meade, G., Cahill, P. A., et al. (2007). Regulation of bovine brain microvascular endothelial tight junction assembly and barrier function by laminar shear stress. *Am. J. Physiol. Heart Circ. Physiol.* 292, H3190–H3197. doi: 10.1152/ajpheart.01177.2006

Colombo, E., and Farina, C. (2016). Astrocytes: key regulators of neuroinflammation. *Trends Immunol.* 37, 608–620. doi: 10.1016/j.it.2016.06.006

Conway, D. E., Breckenridge, M. T., Hinde, E., Gratton, E., Chen, C. S., and Schwartz, M. A. (2013). Fluid shear stress on endothelial cells modulates mechanical tension across VE-cadherin and PECAM-1. *Curr. Biol.* 23, 1024–1030. doi: 10.1016/j.cub.2013.04.049

Cruz, Y., Lorea, J., Mestre, H., Kim-Lee, J. H., Herrera, J., Mellado, R., et al. (2015). Copolymer-1 promotes neurogenesis and improves functional recovery after acute ischemic stroke in rats. *PLoS One* 10:e0121854. doi: 10.1371/journal.pone.0121854

Cucullo, L., Hossain, M., Puvenna, V., Marchi, N., and Janigro, D. (2011). The role of shear stress in blood-brain barrier endothelial physiology. *BMC Neurosci.* 12:40. doi: 10.1186/1471-2202-12-40

da Fonseca, A. C., Matias, D., Garcia, C., Amaral, R., Geraldo, L. H., Freitas, C., et al. (2014). The impact of microglial activation on blood-brain barrier in brain diseases. *Front. Cell. Neurosci.* 8:362. doi: 10.3389/fncel.2014.00362

Dalkara, T., Gursoy-Ozdemir, Y., and Yemisci, M. (2011). Brain microvascular pericytes in health and disease. *Acta Neuropathol.* 122, 1–9. doi: 10.1007/s00401-011-0847-6

Daneman, R., Zhou, L., Kebede, A. A., and Barres, B. A. (2010). Pericytes are required for blood-brain barrier integrity during embryogenesis. *Nature* 468, 562–566. doi: 10.1038/nature09513

Davies, P. F. (1995). Flow-mediated endothelial mechanotransduction. *Physiol. Rev.* 75, 519–560. doi: 10.1152/physrev.1995.75.3.519

Davis, B., Tang, J., Zhang, L., Mu, D., Jiang, X., Biran, V., et al. (2010). Role of vasodilator stimulated phosphoprotein in VEGF induced blood-brain barrier permeability in endothelial cell monolayers. *Int. J. Dev. Neurosci.* 28, 423–428. doi: 10.1016/j.ijdevneu.2010.06.010

del Zoppo, G. J., and Milner, R. (2006). Integrin-matrix interactions in the cerebral microvasculature. *Arterioscler. Thromb. Vasc. Biol.* 26, 1966–1975. doi: 10.1161/01.ATV.0000232525.65682.a2

DeOre, B. J., Partyka, P. P., Fan, F., and Galie, P. A. (2020). CD44 regulates blood-brain barrier integrity in response to fluid shear stress. bioRxiv [Preprint]. doi:10.1101/2020.01.28.924043

Dorfel, M. J., and Huber, O. (2012). Modulation of tight junction structure and function by kinases and phosphatases targeting occludin. *J. Biomed. Biotechnol.* 2012:807356. doi: 10.1155/2012/807356

Duricki, D. A., Drndarski, S., Bernanos, M., Wood, T., Bosch, K., Chen, Q., et al. (2019). Stroke recovery in rats after 24-hour-delayed intramuscular neurotrophin-3 infusion. *Ann. Neurol.* 85, 32–46. doi: 10.1002/ana.25386

Ebong, E. E., Lopez-Quintero, S. V., Rizzo, V., Spray, D. C., and Tarbell, J. M. (2014). Shear-induced endothelial NOS activation and remodeling via heparan sulfate, glypican-1, and syndecan-1. *Integr. Biol.* 6, 338–347. doi: 10.1039/c3ib40199e

Ebong, E. E., Macaluso, F. P., Spray, D. C., and Tarbell, J. M. (2011). Imaging the endothelial glycocalyx in vitro by rapid freezing/freeze substitution transmission electron microscopy. *Arterioscler. Thromb. Vasc. Biol.* 31, 1908–1915. doi: 10.1161/ATVBAHA.111.225268

Eskens, B. J., Zuurbier, C. J., van Haare, J., Vink, H., and van Teeffelen, J. W. (2013). Effects of two weeks of metformin treatment on whole-body glycocalyx barrier properties in db/db mice. *Cardiovasc. Diabetol.* 12:175. doi: 10.1186/1475-2840-12-175

Fagan, S. C., Waller, J. L., Nichols, F. T., Edwards, D. J., Pettigrew, L. C., Clark, W. M., et al. (2010). Minocycline to improve neurologic outcome in stroke (MINOS): a dose-finding study. *Stroke* 41, 2283–2287. doi: 10.1161/STROKEAHA.110.582601

Ferrari, C. C., Depino, A. M., Prada, F., Muraro, N., Campbell, S., Podhajcer, O., et al. (2004). Reversible demyelination, blood-brain barrier breakdown, and pronounced neutrophil recruitment induced by chronic IL-1 expression in the brain. *Am. J. Pathol.* 165, 1827–1837. doi: 10.1016/S0002-9440(10)63438-4

Fisher, M., and Bastan, B. (2012). Identifying and utilizing the ischemic penumbra. *Neurology* 79(Suppl. 1), S79–S85. doi: 10.1212/WNL.0b013e3182695814

Foroutan, S., Brillault, J., Forbush, B., and O'Donnell, M. E. (2005). Moderate-to-severe ischemic conditions increase activity and phosphorylation of the cerebral microvascular endothelial cell Na^+-K^+-Cl^- cotransporter. *Am. J. Phys. Cell Physiol.* 289, C1492–C1501. doi: 10.1152/ajpcell.00257.2005

Gertz, K., Kronenberg, G., Uhlemann, R., Prinz, V., Marquina, R., Corada, M., et al. (2016). Partial loss of VE-cadherin improves long-term outcome and cerebral blood flow after transient brain ischemia in mice. *BMC Neurol.* 16:144. doi: 10.1186/s12883-016-0670-8

Ghadernezhad, N., Khalaj, L., Pazoki-Toroudi, H., Mirmasoumi, M., and Ashabi, G. (2016). Metformin pretreatment enhanced learning and memory in cerebral forebrain ischaemia: the role of the AMPK/BDNF/P70SK signalling pathway. *Pharm. Biol.* 54, 2211–2219. doi: 10.3109/13880209.2016.1150306

Glen, K., Luu, N. T., Ross, E., Buckley, C. D., Rainger, G. E., Egginton, S., et al. (2012). Modulation of functional responses of endothelial cells linked to angiogenesis and inflammation by shear stress: differential effects of the mechanotransducer CD31. *J. Cell. Physiol.* 227, 2710–2721. doi: 10.1002/jcp.23015

Goenka, L., Uppugunduri Satyanarayana, C. R., Suresh Kumar, S., and George, M. (2019). Neuroprotective agents in acute ischemic stroke-A reality check. *Biomed. Pharmacother.* 109, 2539–2547. doi: 10.1016/j.biopha.2018.11.041

Gonzalez Rodriguez, E., Cardenas, J. C., Cox, C. S., Kitagawa, R. S., Stensballe, J., Holcomb, J. B., et al. (2018). Traumatic brain injury is associated with increased syndecan-1 shedding in severely injured patients. *Scand. J. Trauma Resusc. Emerg. Med.* 26:102. doi: 10.1186/s13049-018-0565-3

Graeber, M. B., and Streit, W. J. (2010). Microglia: biology and pathology. *Acta Neuropathol.* 119, 89–105. doi: 10.1007/s00401-009-0622-0

Greene, C., Hanley, N., and Campbell, M. (2019). Claudin-5: gatekeeper of neurological function. *Fluids Barriers CNS* 16:3. doi: 10.1186/s12987-019-0123-z

Gronberg, N. V., Johansen, F. F., Kristiansen, U., and Hasseldam, H. (2013). Leukocyte infiltration in experimental stroke. *J. Neuroinflammation* 10:115. doi: 10.1186/1742-2094-10-115

Hall, A. A., Mendoza, M. I., Zhou, H., Shaughness, M., Maudlin-Jeronimo, E., McCarron, R. M., et al. (2017). Repeated low intensity blast exposure is associated with damaged endothelial glycocalyx and downstream behavioral deficits. *Front. Behav. Neurosci.* 11:104. doi: 10.3389/fnbeh.2017.00104

Harding, I. C., Mitra, R., Mensah, S. A., Herman, I. M., and Ebong, E. E. (2018). Pro-atherosclerotic disturbed flow disrupts caveolin-1 expression, localization, and function via glycocalyx degradation. *J. Transl. Med.* 16:364. doi: 10.1186/s12967-018-1721-2

Harding, I. C., Mitra, R., Mensah, S. A., Nersesyan, A., Bal, N. N., and Ebong, E. E. (2019). Endothelial barrier reinforcement relies on flow-regulated glycocalyx, a potential therapeutic target. *Biorheology* 56, 131–149. doi: 10.3233/BIR-180205

Hau, V. S., Huber, J. D., Campos, C. R., Davis, R. T., and Davis, T. P. (2004). Effect of lambda-carrageenan-induced inflammatory pain on brain uptake of codeine and antinociception. *Brain Res.* 1018, 257–264. doi: 10.1016/j.brainres.2004.05.081

He, M., Martin, M., Marin, T., Chen, Z., and Gongol, B. (2020a). Endothelial mechanobiology. *APL Bioeng.* 4:010904. doi: 10.1063/1.5129563

He, W., Wang, H., Zhao, C., Tian, X., Li, L., and Wang, H. (2020b). Role of liraglutide in brain repair promotion through Sirt1-mediated mitochondrial improvement in stroke. *J. Cell. Physiol.* 235, 2986–3001. doi: 10.1002/jcp.29204

Himburg, H. A., Grzybowski, D. M., Hazel, A. L., LaMack, J. A., Li, X. M., and Friedman, M. H. (2004). Spatial comparison between wall shear stress measures and porcine arterial endothelial permeability. *Am. J. Physiol. Heart Circ. Physiol.* 286, H1916–H1922. doi: 10.1152/ajpheart.00897.2003

Hladky, S. B., and Barrand, M. A. (2016). Fluid and ion transfer across the blood-brain and blood-cerebrospinal fluid barriers; a comparative account of mechanisms and roles. *Fluids Barriers CNS* 13:19. doi: 10.1186/s12987-016-0040-3

Hom, S., Fleegal, M. A., Egleton, R. D., Campos, C. R., Hawkins, B. T., and Davis, T. P. (2007). Comparative changes in the blood-brain barrier and cerebral infarction of SHR and WKY rats. *Am. J. Physiol. Regul. Integr. Comp. Physiol.* 292, R1881–R1892. doi: 10.1152/ajpregu.00761.2005

Honda, M., Nakagawa, S., Hayashi, K., Kitagawa, N., Tsutsumi, K., Nagata, I., et al. (2006). Adrenomedullin improves the blood-brain barrier function through the expression of claudin-5. *Cell. Mol. Neurobiol.* 26, 109–118. doi: 10.1007/s10571-006-9028-x

Huang, H., Bhuiyan, M. I. H., Jiang, T., Song, S., Shankar, S., Taheri, T., et al. (2019). A novel Na^+-K^+-Cl^- cotransporter 1 inhibitor STS66* reduces brain damage in mice after ischemic stroke. *Stroke* 50, 1021–1025. doi: 10.1161/STROKEAHA.118.024287

Huang, Z. G., Xue, D., Preston, E., Karbalai, H., and Buchan, A. M. (1999). Biphasic opening of the blood-brain barrier following transient focal ischemia: effects of hypothermia. *Can. J. Neurol. Sci.* 26, 298–304. doi: 10.1017/s0317167100000421

Iadecola, C., and Nedergaard, M. (2007). Glial regulation of the cerebral microvasculature. *Nat. Neurosci.* 10, 1369–1376. doi: 10.1038/nn2003

Ishida, H., Takemori, K., Dote, K., and Ito, H. (2006). Expression of glucose transporter-1 and aquaporin-4 in the cerebral cortex of stroke-prone spontaneously hypertensive rats in relation to the blood-brain barrier function. *Am. J. Hypertens.* 19, 33–39. doi: 10.1016/j.amjhyper.2005.06.023

Jayakumar, A. R., and Norenberg, M. D. (2010). The Na-K-Cl Co-transporter in astrocyte swelling. *Metab. Brain Dis.* 25, 31–38. doi: 10.1007/s11011-010-9180-3

Jeong, S. M., Hahm, K. D., Shin, J. W., Leem, J. G., Lee, C., and Han, S. M. (2006). Changes in magnesium concentration in the serum and cerebrospinal fluid of neuropathic rats. *Acta Anaesthesiol. Scand.* 50, 211–216. doi: 10.1111/j.1399-6576.2006.00925.x

Jepsen, C. H., deMoya, M. A., Perner, A., Sillesen, M., Ostrowski, S. R., Alam, H. B., et al. (2014). Effect of valproic acid and injury on lesion size and endothelial glycocalyx shedding in a rodent model of isolated traumatic brain injury. *J. Trauma Acute Care Surg.* 77, 292–297. doi: 10.1097/TA.0000000000000333

Jiang, X., Andjelkovic, A. V., Zhu, L., Yang, T., Bennett, M. V. L., Chen, J., et al. (2018). Blood-brain barrier dysfunction and recovery after ischemic stroke. *Prog. Neurobiol.* 163–164, 144–171. doi: 10.1016/j.pneurobio.2017.10.001

Jiao, H., Wang, Z., Liu, Y., Wang, P., and Xue, Y. (2011). Specific role of tight junction proteins claudin-5, occludin, and ZO-1 of the blood-brain barrier in a focal cerebral ischemic insult. *J. Mol. Neurosci.* 44, 130–139. doi: 10.1007/s12031-011-9496-4

Jickling, G. C., Liu, D., Ander, B. P., Stamova, B., Zhan, X., and Sharp, F. R. (2015). Targeting neutrophils in ischemic stroke: translational insights from experimental studies. *J. Cereb. Blood Flow Metab.* 35, 888–901. doi: 10.1038/jcbfm.2015.45

Jin, R., Yang, G., and Li, G. (2010). Inflammatory mechanisms in ischemic stroke: role of inflammatory cells. *J. Leukoc. Biol.* 87, 779–789. doi: 10.1189/jlb.1109766

Joice, S. L., Mydeen, F., Couraud, P. O., Weksler, B. B., Romero, I. A., Fraser, P. A., et al. (2009). Modulation of blood-brain barrier permeability by neutrophils: in vitro and in vivo studies. *Brain Res.* 1298, 13–23. doi: 10.1016/j.brainres.2009.08.076

Jones, E. A. V. (2010). Mechanotransduction and blood fluid dynamics in developing blood vessels. *Can. J. Chem. Eng.* 88, 136–143. doi: 10.1002/cjce.20290

Jovin, T. G., Chamorro, A., Cobo, E., de Miquel, M. A., Molina, C. A., Rovira, A., et al. (2015). Thrombectomy within 8 hours after symptom onset in ischemic stroke. *N. Engl. J. Med.* 372, 2296–2306. doi: 10.1056/NEJMoa1503780

Karsy, M., Brock, A., Guan, J., Taussky, P., Kalani, M. Y., and Park, M. S. (2017). Neuroprotective strategies and the underlying molecular basis of cerebrovascular stroke. *Neurosurg. Focus* 42:E3. doi: 10.3171/2017.1.FOCUS16522

Kassner, A., and Merali, Z. (2015). Assessment of blood-brain barrier disruption in stroke. *Stroke* 46, 3310–3315. doi: 10.1161/STROKEAHA.115.008861

Kikuchi, K., Miura, N., Kawahara, K. I., Murai, Y., Morioka, M., Lapchak, P. A., et al. (2013). Edaravone (Radicut), a free radical scavenger, is a potentially useful addition to thrombolytic therapy in patients with acute ischemic stroke. *Biomed. Rep.* 1, 7–12. doi: 10.3892/br.2012.7

Kimura, K., Aoki, J., Sakamoto, Y., Kobayashi, K., Sakai, K., Inoue, T., et al. (2012). Administration of edaravone, a free radical scavenger, during t-PA infusion can enhance early recanalization in acute stroke patients—a preliminary study. *J. Neurol. Sci.* 313, 132–136. doi: 10.1016/j.jns.2011.09.006

Knowland, D., Arac, A., Sekiguchi, K. J., Hsu, M., Lutz, S. E., Perrino, J., et al. (2014). Stepwise recruitment of transcellular and paracellular pathways underlies blood-brain barrier breakdown in stroke. *Neuron* 82, 603–617. doi: 10.1016/j.neuron.2014.03.003

Koehler, R. C., Gebremedhin, D., and Harder, D. R. (2006). Role of astrocytes in cerebrovascular regulation. *J. Appl. Physiol.* 100, 307–317. doi: 10.1152/japplphysiol.00938.2005

Kong, T., Chen, J., Sun, K., Zhang, W., Wang, J., Song, L., et al. (2019). Aspirin reduced recurrent stroke risk in patients with lacunar stroke. *Acta Neurol. Scand.* 140, 78–83. doi: 10.1111/ane.13105

Ku, D. N., Giddens, D. P., Zarins, C. K., and Glagov, S. (1985). Pulsatile flow and atherosclerosis in the human carotid bifurcation. Positive correlation between plaque location and low oscillating shear stress. *Arteriosclerosis* 5, 293–302. doi: 10.1161/01.atv.5.3.293

Kumar, A. D., Boehme, A. K., Siegler, J. E., Gillette, M., Albright, K. C., and Martin-Schild, S. (2013). Leukocytosis in patients with neurologic deterioration after acute ischemic stroke is associated with poor outcomes. *J. Stroke Cerebrovasc. Dis.* 22, e111–e117. doi: 10.1016/j.jstrokecerebrovasdis.2012.08.008

Kuroiwa, T., Ting, P., Martinez, H., and Klatzo, I. (1985). The biphasic opening of the blood-brain barrier to proteins following temporary middle cerebral artery occlusion. *Acta Neuropathol.* 68, 122–129. doi: 10.1007/BF00688633

Kutuzov, N., Flyvbjerg, H., and Lauritzen, M. (2018). Contributions of the glycocalyx, endothelium, and extravascular compartment to the blood-brain barrier. *Proc. Natl. Acad. Sci. U. S. A.* 115, E9429–E9438. doi: 10.1073/pnas.1802155115

Lakhan, S. E., Kirchgessner, A., and Hofer, M. (2009). Inflammatory mechanisms in ischemic stroke: therapeutic approaches. *J. Transl. Med.* 7:97. doi: 10.1186/1479-5876-7-97

Lam, R. H., Sun, Y., Chen, W., and Fu, J. (2012). Elastomeric microposts integrated into microfluidics for flow-mediated endothelial mechanotransduction analysis. *Lab Chip* 12, 1865–1873. doi: 10.1039/c2lc21146g

Lampl, Y., Gilad, R., Geva, D., Eshel, Y., and Sadeh, M. (2001). Intravenous administration of magnesium sulfate in acute stroke: a randomized double-blind study. *Clin. Neuropharmacol.* 24, 11–15. doi: 10.1097/00002826-200101000-00003

Lampugnani, M. G., and Dejana, E. (2007). Adherens junctions in endothelial cells regulate vessel maintenance and angiogenesis. *Thromb. Res.* 120, S1–S6. doi: 10.1016/s0049-3848(07)70124-x

Lapergue, B., Labreuche, J., Blanc, R., Marnat, G., Consoli, A., Rodesch, G., et al. (2020). Combined use of contact aspiration and the stent retriever technique versus stent retriever alone for recanalization in acute cerebral infarction: the randomized ASTER 2 study protocol. *J. Neurointerv. Surg.* 12, 471–476. doi: 10.1136/neurintsurg-2019-014735

Latchaw, R. E., Yonas, H., Hunter, G. J., Yuh, W. T., Ueda, T., Sorensen, A. G., et al. (2003). Guidelines and recommendations for perfusion imaging in cerebral ischemia: a scientific statement for healthcare professionals by the writing group on perfusion imaging, from the Council on Cardiovascular Radiology of the American Heart Association. *Stroke* 34, 1084–1104. doi: 10.1161/01.STR.0000064840.99271.9E

Lau, L. W., Cua, R., Keough, M. B., Haylock-Jacobs, S., and Yong, V. W. (2013). Pathophysiology of the brain extracellular matrix: a new target for remyelination. *Nat. Rev. Neurosci.* 14, 722–729. doi: 10.1038/nrn3550

Li, X., Han, H., Hou, R., Wei, L., Wang, G., Li, C., et al. (2013). Progesterone treatment before experimental hypoxia-ischemia enhances the expression of glucose transporter proteins GLUT1 and GLUT3 in neonatal rats. *Neurosci. Bull.* 29, 287–294. doi: 10.1007/s12264-013-1298-y

Li, J., Liu, Y., Zhang, X., Chen, R., Zhang, L., Xue, J., et al. (2019). Dl-3-N-butylphthalide alleviates the blood-brain barrier permeability of focal cerebral

ischemia reperfusion in mice. *Neuroscience* 413, 99–107. doi: 10.1016/j.neuroscience.2019.06.020

Lindsberg, P. J., Carpen, O., Paetau, A., Karjalainen-Lindsberg, M. L., and Kaste, M. (1996). Endothelial ICAM-1 expression associated with inflammatory cell response in human ischemic stroke. *Circulation* 94, 939–945. doi: 10.1161/01.cir.94.5.939

Liu, Z., and Chopp, M. (2016). Astrocytes, therapeutic targets for neuroprotection and neurorestoration in ischemic stroke. *Prog. Neurobiol.* 144, 103–120. doi: 10.1016/j.pneurobio.2015.09.008

Liu, W., Wang, X., O'Connor, M., Wang, G., and Han, F. (2020). Brain-derived neurotrophic factor and its potential therapeutic role in stroke comorbidities. *Neural Plast.* 2020, 1–13. doi: 10.1155/2020/1969482

Lo, E. H., Broderick, J. P., and Moskowitz, M. A. (2004). tPA and proteolysis in the neurovascular unit. *Stroke* 35, 354–356. doi: 10.1161/01.STR.0000115164.80010.8A

Logallo, N., Novotny, V., Assmus, J., Kvistad, C. E., Alteheld, L., Rønning, O. M., et al. (2017). Tenecteplase versus alteplase for management of acute ischaemic stroke (NOR-TEST): a phase 3, randomised, open-label, blinded endpoint trial. *Lancet Neurol.* 16, 781–788. doi: 10.1016/s1474-4422(17)30253-3

Lowhagen Henden, P., Rentzos, A., Karlsson, J. E., Rosengren, L., Leiram, B., Sundeman, H., et al. (2017). General anesthesia versus conscious sedation for endovascular treatment of acute ischemic stroke: the AnStroke trial (anesthesia during stroke). *Stroke* 48, 1601–1607. doi: 10.1161/STROKEAHA.117.016554

Luft, J. H. (1966). Fine structures of capillary and endocapillary layer as revealed by ruthenium red. *Fed. Proc.* 25, 1773–1783.

Ma, Y., Wang, J., Wang, Y., and Yang, G. Y. (2017). The biphasic function of microglia in ischemic stroke. *Prog. Neurobiol.* 157, 247–272. doi: 10.1016/j.pneurobio.2016.01.005

Martens, R. J. H., Vink, H., van Oostenbrugge, R. J., and Staals, J. (2013). Sublingual microvascular glycocalyx dimensions in lacunar stroke patients. *Cerebrovasc. Dis.* 35, 451–454. doi: 10.1159/000348854

McCaffrey, G., Willis, C. L., Staatz, W. D., Nametz, N., Quigley, C. A., Hom, S., et al. (2009). Occludin oligomeric assemblies at tight junctions of the blood-brain barrier are altered by hypoxia and reoxygenation stress. *J. Neurochem.* 110, 58–71. doi: 10.1111/j.1471-4159.2009.06113.x

Mendez, A. A., Samaniego, E. A., Sheth, S. A., Dandapat, S., Hasan, D. M., Limaye, K. S., et al. (2018). Update in the early management and reperfusion strategies of patients with acute ischemic stroke. *Crit. Care Res. Pract.* 2018:9168731. doi: 10.1155/2018/9168731

Mensah, S. A., Cheng, M. J., Homayoni, H., Plouffe, B. D., Coury, A. J., and Ebong, E. E. (2017). Regeneration of glycocalyx by heparan sulfate and sphingosine 1-phosphate restores inter-endothelial communication. *PLoS One* 12:e0186116. doi: 10.1371/journal.pone.0186116

Merali, Z., Huang, K., Mikulis, D., Silver, F., and Kassner, A. (2017). Evolution of blood-brain-barrier permeability after acute ischemic stroke. *PLoS One* 12:e0171558. doi: 10.1371/journal.pone.0171558

Mitra, R., O'Neil, G. L., Harding, I. C., Cheng, M. J., Mensah, S. A., and Ebong, E. E. (2017). Glycocalyx in atherosclerosis-relevant endothelium function and as a therapeutic target. *Curr. Atheroscler. Rep.* 19:63. doi: 10.1007/s11883-017-0691-9

Mitra, R., Qiao, J., Madhavan, S., O'Neil, G. L., Ritchie, B., Kulkarni, P., et al. (2018). The comparative effects of high fat diet or disturbed blood flow on glycocalyx integrity and vascular inflammation. *Transl. Med. Commun.* 3:10. doi: 10.1186/s41231-018-0029-9

Mokin, M., Khalessi, A. A., Mocco, J., Lanzino, G., Dumont, T. M., Hanel, R. A., et al. (2014). Endovascular treatment of acute ischemic stroke: the end or just the beginning? *Neurosurg. Focus* 36:E5. doi: 10.3171/2013.10.FOCUS13374

Muir, K. W., Lees, K. R., Ford, I., and Davis, S.Intravenous Magnesium Efficacy in Stroke Study Investigators (2004). Magnesium for acute stroke (Intravenous Magnesium Efficacy in Stroke trial): randomised controlled trial. *Lancet* 363, 439–445. doi: 10.1016/S0140-6736(04)15490-1

Muller, J. M., Chilian, W. M., and Davis, M. J. (1997). Integrin signaling transduces shear stress—dependent vasodilation of coronary arterioles. *Circ. Res.* 80, 320–326. doi: 10.1161/01.res.80.3.320

Murakami, T., Felinski, E. A., and Antonetti, D. A. (2009). Occludin phosphorylation and ubiquitination regulate tight junction trafficking and vascular endothelial growth factor-induced permeability. *J. Biol. Chem.* 284, 21036–21046. doi: 10.1074/jbc.M109.016766

Nag, S., Venugopalan, R., and Stewart, D. J. (2007). Increased caveolin-1 expression precedes decreased expression of occludin and claudin-5 during blood-brain barrier breakdown. *Acta Neuropathol.* 114, 459–469. doi: 10.1007/s00401-007-0274-x

Nakagomi, T., Kubo, S., Nakano-Doi, A., Sakuma, R., Lu, S., Narita, A., et al. (2015). Brain vascular pericytes following ischemia have multipotential stem cell activity to differentiate into neural and vascular lineage cells. *Stem Cells* 33, 1962–1974. doi: 10.1002/stem.1977

O'Donnell, M. E. (2014). Blood-brain barrier Na transporters in ischemic stroke. *Adv. Pharmacol.* 71, 113–146. doi: 10.1016/bs.apha.2014.06.011

Obermeier, B., Daneman, R., and Ransohoff, R. M. (2013). Development, maintenance and disruption of the blood-brain barrier. *Nat. Med.* 19, 1584–1596. doi: 10.1038/nm.3407

Osada, T., Gu, Y. H., Kanazawa, M., Tsubota, Y., Hawkins, B. T., Spatz, M., et al. (2011). Interendothelial claudin-5 expression depends on cerebral endothelial cell-matrix adhesion by beta(1)-integrins. *J. Cereb. Blood Flow Metab.* 31, 1972–1985. doi: 10.1038/jcbfm.2011.99

Pan, W., and Kastin, A. J. (2007). Tumor necrosis factor and stroke: role of the blood-brain barrier. *Prog. Neurobiol.* 83, 363–374. doi: 10.1016/j.pneurobio.2007.07.008

Park, S. L., Lee, D. H., Yoo, S. E., and Jung, Y. S. (2010). The effect of Na^+/H^+ exchanger-1 inhibition by sabiporide on blood-brain barrier dysfunction after ischemia/hypoxia in vivo and in vitro. *Brain Res.* 1366, 189–196. doi: 10.1016/j.brainres.2010.09.077

Patel, R. A. G., and McMullen, P. W. (2017). Neuroprotection in the treatment of acute ischemic stroke. *Prog. Cardiovasc. Dis.* 59, 542–548. doi: 10.1016/j.pcad.2017.04.005

Pillai, D. R., Dittmar, M. S., Baldaranov, D., Heidemann, R. M., Henning, E. C., Schuierer, G., et al. (2009). Cerebral ischemia-reperfusion injury in rats—a 3 T MRI study on biphasic blood-brain barrier opening and the dynamics of edema formation. *J. Cereb. Blood Flow Metab.* 29, 1846–1855. doi: 10.1038/jcbfm.2009.106

Posada-Duque, R. A., Barreto, G. E., and Cardona-Gomez, G. P. (2014). Protection after stroke: cellular effectors of neurovascular unit integrity. *Front. Cell. Neurosci.* 8:231. doi: 10.3389/fncel.2014.00231

Powers, W. J., Rabinstein, A. A., Ackerson, T., Adeoye, O. M., Bambakidis, N. C., Becker, K., et al. (2018). 2018 guidelines for the early management of patients with acute ischemic stroke: a guideline for healthcare professionals from the American Heart Association/American Stroke Association. *Stroke* 49, e46–e110. doi: 10.1161/STR.0000000000000158

Qosa, H., Miller, D. S., Pasinelli, P., and Trotti, D. (2015). Regulation of ABC efflux transporters at blood-brain barrier in health and neurological disorders. *Brain Res.* 1628, 298–316. doi: 10.1016/j.brainres.2015.07.005

Ramnath, R., Foster, R. R., Qiu, Y., Cope, G., Butler, M. J., Salmon, A. H., et al. (2014). Matrix metalloproteinase 9-mediated shedding of syndecan 4 in response to tumor necrosis factor alpha: a contributor to endothelial cell glycocalyx dysfunction. *FASEB J.* 28, 4686–4699. doi: 10.1096/fj.14-252221

Ren, J., Sietsma, D., Qiu, S., Moessler, H., and Finklestein, S. P. (2007). Cerebrolysin enhances functional recovery following focal cerebral infarction in rats. *Restor. Neurol. Neurosci.* 25, 25–31.

Revuelta, M., Elicegui, A., Moreno-Cugnon, L., Buhrer, C., Matheu, A., and Schmitz, T. (2019). Ischemic stroke in neonatal and adult astrocytes. *Mech. Ageing Dev.* 183:111147. doi: 10.1016/j.mad.2019.111147

Ronaldson, P. T., and Davis, T. P. (2015). Targeting transporters: promoting blood-brain barrier repair in response to oxidative stress injury. *Brain Res.* 1623, 39–52. doi: 10.1016/j.brainres.2015.03.018

Rosell, A., Cuadrado, E., Ortega-Aznar, A., Hernandez-Guillamon, M., Lo, E. H., and Montaner, J. (2008). MMP-9-positive neutrophil infiltration is associated to blood-brain barrier breakdown and basal lamina type IV collagen degradation during hemorrhagic transformation after human ischemic stroke. *Stroke* 39, 1121–1126. doi: 10.1161/STROKEAHA.107.500868

Ross, A. M., Hurn, P., Perrin, N., Wood, L., Carlini, W., and Potempa, K. (2007). Evidence of the peripheral inflammatory response in patients with transient ischemic attack. *J. Stroke Cerebrovasc. Dis.* 16, 203–207. doi: 10.1016/j.jstrokecerebrovasdis.2007.05.002

Rubio-Gayosso, I., Platts, S. H., and Duling, B. R. (2006). Reactive oxygen species mediate modification of glycocalyx during ischemia-reperfusion injury. *Am. J. Physiol. Heart Circ. Physiol.* 290, H2247–H2256. doi: 10.1152/ajpheart.00796.2005

Rustenhoven, J., Jansson, D., Smyth, L. C., and Dragunow, M. (2017). Brain pericytes as mediators of neuroinflammation. *Trends Pharmacol. Sci.* 38, 291–304. doi: 10.1016/j.tips.2016.12.001

Salvador, E., Burek, M., and Forster, C. Y. (2015). Stretch and/or oxygen glucose deprivation (OGD) in an in vitro traumatic brain injury (TBI) model induces calcium alteration and inflammatory cascade. *Front. Cell. Neurosci.* 9:323. doi: 10.3389/fncel.2015.00323

Sandoval, K. E., and Witt, K. A. (2008). Blood-brain barrier tight junction permeability and ischemic stroke. *Neurobiol. Dis.* 32, 200–219. doi: 10.1016/j.nbd.2008.08.005

Sato, K., Kameda, M., Yasuhara, T., Agari, T., Baba, T., Wang, F., et al. (2013). Neuroprotective effects of liraglutide for stroke model of rats. *Int. J. Mol. Sci.* 14, 21513–21524. doi: 10.3390/ijms141121513

Saver, J. L., Goyal, M., van der Lugt, A., Menon, B. K., Majoie, C. B., Dippel, D. W., et al. (2016). Time to treatment with endovascular thrombectomy and outcomes from ischemic stroke: a meta-analysis. *JAMA* 316, 1279–1288. doi: 10.1001/jama.2016.13647

Saver, J. L., Starkman, S., Eckstein, M., Stratton, S. J., Pratt, F. D., Hamilton, S., et al. (2015). Prehospital use of magnesium sulfate as neuroprotection in acute stroke. *N. Engl. J. Med.* 372, 528–536. doi: 10.1056/NEJMoa1408827

Sevick, L. K., Ghali, S., Hill, M. D., Danthurebandara, V., Lorenzetti, D. L., Noseworthy, T., et al. (2017). Systematic review of the cost and cost-effectiveness of rapid endovascular therapy for acute ischemic stroke. *Stroke* 48, 2519–2526. doi: 10.1161/STROKEAHA.117.017199

Sharma, P., Sinha, M., Shukla, R., Garg, R. K., Verma, R., and Singh, M. K. (2011). A randomized controlled clinical trial to compare the safety and efficacy of edaravone in acute ischemic stroke. *Ann. Indian Acad. Neurol.* 14, 103–106. doi: 10.4103/0972-2327.82794

Shi, Y., Leak, R. K., Keep, R. F., and Chen, J. (2016). Translational stroke research on blood-brain barrier damage: challenges, perspectives, and goals. *Transl. Stroke Res.* 7, 89–92. doi: 10.1007/s12975-016-0447-9

Shi, J., Zhang, Y. Q., and Simpkins, J. W. (1997). Effects of 17beta-estradiol on glucose transporter 1 expression and endothelial cell survival following focal ischemia in the rats. *Exp. Brain Res.* 117, 200–206. doi: 10.1007/s002210050216

Shinozuka, K., Dailey, T., Tajiri, N., Ishikawa, H., Kim, D. W., Pabon, M., et al. (2013). Stem cells for neurovascular repair in stroke. *J. Stem Cell Res. Ther.* 4:12912. doi: 10.4172/2157-7633.S4-004

Siddharthan, V., Kim, Y. V., Liu, S., and Kim, K. S. (2007). Human astrocytes/astrocyte-conditioned medium and shear stress enhance the barrier properties of human brain microvascular endothelial cells. *Brain Res.* 1147, 39–50. doi: 10.1016/j.brainres.2007.02.029

Sifat, A. E., Vaidya, B., and Abbruscato, T. J. (2017). Blood-brain barrier protection as a therapeutic strategy for acute ischemic stroke. *AAPS J.* 19, 957–972. doi: 10.1208/s12248-017-0091-7

Singh, A., Satchell, S. C., Neal, C. R., McKenzie, E. A., Tooke, J. E., and Mathieson, P. W. (2007). Glomerular endothelial glycocalyx constitutes a barrier to protein permeability. *J. Am. Soc. Nephrol.* 18, 2885–2893. doi: 10.1681/ASN.2007010119

Strbian, D., Durukan, A., Pitkonen, M., Marinkovic, I., Tatlisumak, E., Pedrono, E., et al. (2008). The blood-brain barrier is continuously open for several weeks following transient focal cerebral ischemia. *Neuroscience* 153, 175–181. doi: 10.1016/j.neuroscience.2008.02.012

Sung, S. F., Huang, Y. C., Ong, C. T., and Chen, W. (2013). Validity of a computerised five-level emergency triage system for patients with acute ischaemic stroke. *Emerg. Med. J.* 30, 454–458. doi: 10.1136/emermed-2012-201423

Targosz-Korecka, M., Malek-Zietek, K. E., Kloska, D., Rajfur, Z., Stepien, E. L., Grochot-Przeczek, A., et al. (2020). Metformin attenuates adhesion between cancer and endothelial cells in chronic hyperglycemia by recovery of the endothelial glycocalyx barrier. *Biochim. Biophys. Acta Gen. Subj.* 1864:129533. doi: 10.1016/j.bbagen.2020.129533

Thi, M. M., Tarbell, J. M., Weinbaum, S., and Spray, D. C. (2004). The role of the glycocalyx in reorganization of the actin cytoskeleton under fluid shear stress: a "bumper-car" model. *Proc. Natl. Acad. Sci. U. S. A.* 101, 16483–16488. doi: 10.1073/pnas.0407474101

Thurgur, H., and Pinteaux, E. (2019). Microglia in the neurovascular unit: blood-brain barrier-microglia interactions after central nervous system disorders. *Neuroscience* 405, 55–67. doi: 10.1016/j.neuroscience.2018.06.046

Tietz, S., and Engelhardt, B. (2015). Brain barriers: crosstalk between complex tight junctions and adherens junctions. *J. Cell Biol.* 209, 493–506. doi: 10.1083/jcb.201412147

Tsai, C. F., Anderson, N., Thomas, B., and Sudlow, C. L. (2016). Comparing risk factor profiles between intracerebral hemorrhage and ischemic stroke in Chinese and white populations: systematic review and meta-analysis. *PLoS One* 11:e0151743. doi: 10.1371/journal.pone.0151743

Uchimido, R., Schmidt, E. P., and Shapiro, N. I. (2019). The glycocalyx: a novel diagnostic and therapeutic target in sepsis. *Crit. Care* 23:16. doi: 10.1186/s13054-018-2292-6

Ueda, A., Shimomura, M., Ikeda, M., Yamaguchi, R., and Tanishita, K. (2004). Effect of glycocalyx on shear-dependent albumin uptake in endothelial cells. *Am. J. Physiol. Heart Circ. Physiol.* 287, H2287–H2294. doi: 10.1152/ajpheart.00808.2003

Uematsu, M., Ohara, Y., Navas, J. P., Nishida, K., Murphy, T. J., Alexander, R. W., et al. (1995). Regulation of endothelial cell nitric oxide synthase mRNA expression by shear stress. *Am. J. Physiol.* 269, C1371–C1378. doi: 10.1152/ajpcell.1995.269.6.C1371

van den Berg, B. M., Spaan, J. A., and Vink, H. (2009). Impaired glycocalyx barrier properties contribute to enhanced intimal low-density lipoprotein accumulation at the carotid artery bifurcation in mice. *Pflugers Arch.* 457, 1199–1206. doi: 10.1007/s00424-008-0590-6

van den Berg, B. M., Vink, H., and Spaan, J. A. (2003). The endothelial glycocalyx protects against myocardial edema. *Circ. Res.* 92, 592–594. doi: 10.1161/01.RES.0000065917.53950.75

van Golen, R. F., van Gulik, T. M., and Heger, M. (2012). Mechanistic overview of reactive species-induced degradation of the endothelial glycocalyx during hepatic ischemia/reperfusion injury. *Free Radic. Biol. Med.* 52, 1382–1402. doi: 10.1016/j.freeradbiomed.2012.01.013

Vannucci, S. J., Reinhart, R., Maher, F., Bondy, C. A., Lee, W. H., Vannucci, R. C., et al. (1998). Alterations in GLUT1 and GLUT3 glucose transporter gene expression following unilateral hypoxia-ischemia in the immature rat brain. *Brain Res. Dev. Brain Res.* 107, 255–264. doi: 10.1016/s0165-3806(98)00021-2

Vemula, S., Roder, K. E., Yang, T., Bhat, G. J., Thekkumkara, T. J., and Abbruscato, T. J. (2009). A functional role for sodium-dependent glucose transport across the blood-brain barrier during oxygen glucose deprivation. *J. Pharmacol. Exp. Ther.* 328, 487–495. doi: 10.1124/jpet.108.146589

Vilar, M., and Mira, H. (2016). Regulation of neurogenesis by neurotrophins during adulthood: expected and unexpected roles. *Front. Neurosci.* 10:26. doi: 10.3389/fnins.2016.00026

Wacker, B. K., Freie, A. B., Perfater, J. L., and Gidday, J. M. (2012). Junctional protein regulation by sphingosine kinase 2 contributes to blood-brain barrier protection in hypoxic preconditioning-induced cerebral ischemic tolerance. *J. Cereb. Blood Flow Metab.* 32, 1014–1023. doi: 10.1038/jcbfm.2012.3

Walsh, T. G., Murphy, R. P., Fitzpatrick, P., Rochfort, K. D., Guinan, A. F., Murphy, A., et al. (2011). Stabilization of brain microvascular endothelial barrier function by shear stress involves VE-cadherin signaling leading to modulation of pTyr-occludin levels. *J. Cell. Physiol.* 226, 3053–3063. doi: 10.1002/jcp.22655

Wang, Y., Shen, Y., Liu, Z., Gu, J., Xu, C., Qian, S., et al. (2019). Dl-NBP (Dl-3-N-butylphthalide) treatment promotes neurological functional recovery accompanied by the upregulation of white matter integrity and HIF-1alpha/VEGF/Notch/Dll4 expression. *Front. Pharmacol.* 10:1595. doi: 10.3389/fphar.2019.01595

Wang, C. X., and Shuaib, A. (2007). Critical role of microvasculature basal lamina in ischemic brain injury. *Prog. Neurobiol.* 83, 140–148. doi: 10.1016/j.pneurobio.2007.07.006

Warboys, C. M., Eric Berson, R., Mann, G. E., Pearson, J. D., and Weinberg, P. D. (2010). Acute and chronic exposure to shear stress have opposite effects on endothelial permeability to macromolecules. *Am. J. Physiol. Heart Circ. Physiol.* 298, H1850–H1856. doi: 10.1152/ajpheart.00114.2010

Xia, C. Y., Liu, Y. H., Wang, P., and Xue, Y. X. (2012). Low-frequency ultrasound irradiation increases blood-tumor barrier permeability by transcellular pathway in a rat glioma model. *J. Mol. Neurosci.* 48, 281–290. doi: 10.1007/s12031-012-9770-0

Yamazaki, Y., Harada, S., Wada, T., Yoshida, S., and Tokuyama, S. (2016). Sodium transport through the cerebral sodium-glucose transporter exacerbates neuron damage during cerebral ischaemia. *J. Pharm. Pharmacol.* 68, 922–931. doi: 10.1111/jphp.12571

Yamazaki, Y., Ogihara, S., Harada, S., and Tokuyama, S. (2015). Activation of cerebral sodium-glucose transporter type 1 function mediated by post-ischemic hyperglycemia exacerbates the development of cerebral ischemia. *Neuroscience* 310, 674–685. doi: 10.1016/j.neuroscience.2015.10.005

Yang, G. Y., Gong, C., Qin, Z., Liu, X. H., and Lorris Betz, A. (1999). Tumor necrosis factor alpha expression produces increased blood-brain barrier permeability following temporary focal cerebral ischemia in mice. *Brain Res. Mol. Brain Res.* 69, 135–143. doi: 10.1016/s0169-328x(99)00007-8

Yang, Y., and Rosenberg, G. A. (2011). MMP-mediated disruption of claudin-5 in the blood-brain barrier of rat brain after cerebral ischemia. *Methods Mol. Biol.* 762, 333–345. doi: 10.1007/978-1-61779-185-7_24

Yang, Y., and Rosenberg, G. A. (2015). Matrix metalloproteinases as therapeutic targets for stroke. *Brain Res.* 1623, 30–38. doi: 10.1016/j.brainres.2015.04.024

Ye, Z. Y., Xing, H. Y., Wang, B., Liu, M., and Lv, P. Y. (2019). DL-3-n-butylphthalide protects the blood-brain barrier against ischemia/hypoxia injury via upregulation of tight junction proteins. *Chin. Med. J.* 132, 1344–1353. doi: 10.1097/CM9.0000000000000232

Yoon, J. H., Lee, E. S., and Jeong, Y. (2017). In vivo imaging of the cerebral endothelial glycocalyx in mice. *J. Vasc. Res.* 54, 59–67. doi: 10.1159/000457799

Zaragoza, C., Marquez, S., and Saura, M. (2012). Endothelial mechanosensors of shear stress as regulators of atherogenesis. *Curr. Opin. Lipidol.* 23, 446–452. doi: 10.1097/MOL.0b013e328357e837

Zarins, C. K., Giddens, D. P., Bharadvaj, B. K., Sottiurai, V. S., Mabon, R. F., and Glagov, S. (1983). Carotid bifurcation atherosclerosis. Quantitative correlation of plaque localization with flow velocity profiles and wall shear stress. *Circ. Res.* 53, 502–514. doi: 10.1161/01.res.53.4.502

Zeng, Y., Liu, X. H., Tarbell, J., and Fu, B. (2015). Sphingosine 1-phosphate induced synthesis of glycocalyx on endothelial cells. *Exp. Cell Res.* 339, 90–95. doi: 10.1016/j.yexcr.2015.08.013

Zeng, C., Wang, D., Chen, C., Chen, L., Chen, B., Li, L., et al. (2020). Zafirlukast protects blood-brain barrier integrity from ischemic brain injury. *Chem. Biol. Interact.* 316:108915. doi: 10.1016/j.cbi.2019.108915

Zhang, S., An, Q., Wang, T., Gao, S., and Zhou, G. (2018). Autophagy- and MMP-2/9-mediated reduction and redistribution of ZO-1 contribute to hyperglycemia-increased blood-brain barrier permeability during early reperfusion in stroke. *Neuroscience* 377, 126–137. doi: 10.1016/j.neuroscience.2018.02.035

Zhang, C., Chopp, M., Cui, Y., Wang, L., Zhang, R., Zhang, L., et al. (2010). Cerebrolysin enhances neurogenesis in the ischemic brain and improves functional outcome after stroke. *J. Neurosci. Res.* 88, 3275–3281. doi: 10.1002/jnr.22495

Zhou, H., Lapointe, B. M., Clark, S. R., Zbytnuik, L., and Kubes, P. (2006). A requirement for microglial TLR4 in leukocyte recruitment into brain in response to lipopolysaccharide. *J. Immunol.* 177, 8103–8110. doi: 10.4049/jimmunol.177.11.8103

Zhu, J., Li, X., Yin, J., Hu, Y., Gu, Y., and Pan, S. (2018). Glycocalyx degradation leads to blood-brain barrier dysfunction and brain edema after asphyxia cardiac arrest in rats. *J. Cereb. Blood Flow Metab.* 38, 1979–1992. doi: 10.1177/0271678X17726062

Zhu, H., Zhang, Y., Shi, Z., Lu, D., Li, T., Ding, Y., et al. (2016). The neuroprotection of liraglutide against ischaemia-induced apoptosis through the activation of the PI3K/AKT and MAPK pathways. *Sci. Rep.* 6:26859. doi: 10.1038/srep26859

Zobel, K., Hansen, U., and Galla, H. J. (2016). Blood-brain barrier properties in vitro depend on composition and assembly of endogenous extracellular matrices. *Cell Tissue Res.* 365, 233–245. doi: 10.1007/s00441-016-2397-7

Conflict of Interest: The authors declare that the research was conducted in the absence of any commercial or financial relationships that could be construed as a potential conflict of interest.

frontiers in Physiology

ORIGINAL RESEARCH
published: 22 December 2020
doi: 10.3389/fphys.2020.593026

Blood–Brain Barrier Leakage Is Increased in Parkinson's Disease

*Sarah Al-Bachari[1,2,3], Josephine H. Naish[4,5], Geoff J. M. Parker[5,6], Hedley C. A. Emsley[1,2,3] and Laura M. Parkes[3,7]**

[1] Lancaster Medical School, Faculty of Health and Medicine, Lancaster University, Lancaster, United Kingdom, [2] Department of Neurology, Lancashire Teaching Hospitals NHS Foundation Trust, Preston, United Kingdom, [3] Division of Neuroscience and Experimental Psychology, Faculty of Biology, Medicine and Health, The University of Manchester, Manchester, United Kingdom, [4] Division of Cardiovascular sciences, Faculty of Biology, Medicine and Health, The University of Manchester, Manchester, United Kingdom, [5] Bioxydyn Limited, Manchester, United Kingdom, [6] Centre for Medical Image Computing, Department of Computer Science and Department of Neuroinflammation, University College London, London, United Kingdom, [7] Geoffrey Jefferson Brain Research Centre, Manchester Academic Health Science Centre, Manchester, United Kingdom

Background: Blood–brain barrier (BBB) disruption has been noted in animal models of Parkinson's disease (PD) and forms the basis of the vascular hypothesis of neurodegeneration, yet clinical studies are lacking.

Objective: To determine alterations in BBB integrity in PD, with comparison to cerebrovascular disease.

Methods: Dynamic contrast enhanced magnetic resonance images were collected from 49 PD patients, 15 control subjects with cerebrovascular disease [control positive (CP)] and 31 healthy control subjects [control negative (CN)], with all groups matched for age. Quantitative maps of the contrast agent transfer coefficient across the BBB (K^{trans}) and plasma volume (v_p) were produced using Patlak analysis. Differences in K^{trans} and v_p were assessed with voxel-based analysis as well as in regions associated with PD pathophysiology. In addition, the volume of white matter lesions (WMLs) was obtained from T_2-weighted fluid attenuation inversion recovery (FLAIR) images.

Results: Higher K^{trans}, reflecting higher BBB leakage, was found in the PD group than in the CN group using voxel-based analysis; differences were most prominent in the posterior white matter regions. Region of interest analysis confirmed K^{trans} to be significantly higher in PD than in CN, predominantly driven by differences in the substantia nigra, normal-appearing white matter, WML and the posterior cortex. WML volume was significantly higher in PD compared to CN. K^{trans} values and WML volume were similar in PD and CP, suggesting a similar burden of cerebrovascular disease despite lower cardiovascular risk factors.

Conclusion: These results show BBB disruption in PD.

Keywords: blood–brain barrier, cerebrovascular disease, dynamic contrast enhanced MRI, Parkinson's disease, neurovascular unit

OPEN ACCESS

Edited by:
Fabrice Dabertrand, University of Colorado, United States

Reviewed by:
Axel Montagne, University of Southern California, Los Angeles, United States
Walter Backes, Maastricht University Medical Centre, Netherlands

***Correspondence:**
Laura M. Parkes
Laura.Parkes@manchester.ac.uk

Specialty section:
This article was submitted to Vascular Physiology, a section of the journal Frontiers in Physiology

Received: *09 August 2020*
Accepted: *24 November 2020*
Published: *22 December 2020*

Citation:
Al-Bachari S, Naish JH, Parker GJM, Emsley HCA and Parkes LM (2020) Blood–Brain Barrier Leakage Is Increased in Parkinson's Disease. Front. Physiol. 11:593026. doi: 10.3389/fphys.2020.593026

INTRODUCTION

The blood–brain barrier (BBB) consists of highly specialised, metabolically active cells forming a selectively permeable, highly resistant barrier to diffusion of blood products (Pardridge, 2005). It is closely coupled with glial cells (i.e., pericytes, microglia, oligodendroglia, and astrocyte end-feet), all in close proximity to a neuron; collectively termed the neurovascular unit (Lo and Rosenberg, 2009; Alvarez et al., 2013). Normal functioning of the neurovascular unit ensures healthy function of the BBB and adequate cerebral blood flow, it also maintains the neuronal "milieu" which is required for proper functioning of neuronal circuits and ensures the metabolic needs of the neurons are met (Zlokovic, 2008, 2011). In the neurovascular unit, BBB permeability and cerebral blood flow are mainly controlled by endothelial cells, smooth muscle cells and pericytes; damage to which have been associated with accumulation of neurotoxins and hypoxia leading to neuronal injury and loss (Bell et al., 2010; Montagne et al., 2018).

Neurodegeneration is now understood to be the consequence of multiple factors acting and interacting over time to lead to neuronal dysfunction and death (Carvey et al., 2006; Collins et al., 2012; Sweeney et al., 2019). Neurovascular unit dysfunction, unsurprisingly, contributes to neuronal dysfunction and death; this forms the basis of the "vascular model of neurodegeneration" (Grammas et al., 2011; Zlokovic, 2011; Andreone et al., 2015; Nelson et al., 2015; Zhao et al., 2015; Hachinski et al., 2019). The two pillars of this model are hypoperfusion and BBB disruption, both contributing to the vicious circle of neuronal loss. Studies particularly in the preclinical setting, suggest microvascular pathology and hypoperfusion occurs in the context of neurodegenerative diseases (Brown and Thore, 2011; Zlokovic, 2011; Di Marco et al., 2015; Iadecola, 2017; Kisler et al., 2017). In addition studies in Parkinson's disease (PD) have revealed vascular remodelling, altered vasculature and abnormal angiogenesis (Faucheux et al., 1999; Farkas et al., 2000; Wada et al., 2006; Chao et al., 2009; Patel et al., 2011; Guan et al., 2013; Janelidze et al., 2015).

Understanding of the pathogenesis of PD centres around the selective and progressive loss of dopaminergic neurons in the substantia nigra pars compacta (SNpc) and its connections with other basal ganglia structures. BBB disruption contributing to neurodegeneration in the SNpc has been reported in PD in animal studies (Barcia et al., 2005; Rite et al., 2007; Chao et al., 2009). In humans, a relatively small positron emission tomography (PET) study in PD patients revealed dysfunction of the BBB transporter system (Kortekaas et al., 2005). A histological study revealed significantly increased permeability of the BBB in the post commissural putamen of PD patients (Gray and Woulfe, 2015). Thus the areas implicated in PD pathology have been shown to demonstrate BBB disruption, yet studies remain few and predominantly in animal models.

Many studies describe hypoperfusion in the posterior cortices in PD, in particular in the posterior parieto-occipital cortex, precuneus and cuneus and temporal regions with variable patterns in the frontal lobe (Ma et al., 2010; Kamagata et al., 2011; Melzer et al., 2011; Borghammer, 2012; Fernandez-Seara et al., 2012). The extent to which BBB disruption impacts perfusion and vice versa (hypoperfusion influencing BBB disruption) is poorly understood. However, both occur at the microvascular level and may be linked. If this is the case, this then suggests that alterations in BBB may also be expected in these posterior regions as well as in regions implicated in PD pathology such as the basal ganglia, where neuronal loss and loss of nigrostriatal projections occurs.

Advances in neuroimaging techniques, in particular quantitative MRI techniques such as arterial spin labelling and dynamic contrast enhanced magnetic resonance imaging (DCE-MRI), have paved the way for studies of the microcirculation in the clinical setting, with DCE-MRI specifically probing BBB integrity (Tofts and Kermode, 1991). Previously applied to measure BBB disruption in tumours, multiple sclerosis and acute ischaemic stroke, recent applications have used this technique to probe more subtle and chronic BBB disruption. Studies include small vessel disease (Wardlaw et al., 2008), Alzheimer's disease (Starr et al., 2009), mild cognitive impairment and normal ageing (Montagne et al., 2015), vascular cognitive impairment (Taheri et al., 2011) and diabetes (Starr et al., 2003); its value in these settings has been systematically reviewed (Heye et al., 2014). To our knowledge there is no published work on DCE-MRI measures in PD.

We used DCE-MRI to investigate regional alterations in BBB permeability in the context of PD. PD was compared with a control group with known cerebrovascular disease [control positive (CP)] and a control group without known cerebrovascular disease or PD [control negative (CN)]. Our aim was to investigate whether potential changes are simply attributable to co-existing cerebrovascular disease in an ageing population or if a pattern of BBB alterations specific to PD is revealed. Inclusion of the CP group allows us to do this by comparing the pattern of BBB disruption in the PD and CP groups with reference to the burden of cerebrovascular disease in each group, defined by white matter lesion (WML) volume as an accepted surrogate marker of small vessel disease. We hypothesised that BBB disruption in PD would occur in the basal ganglia structures due to the pathophysiology of PD being centred around selective and progressive loss of dopaminergic neurons in the SNpc and nigrostriatal pathways. Therefore, based on the vascular hypothesis of neurodegeneration, these areas should display BBB disruption. We also expected BBB disruption to occur in posterior and frontal cortices given that hypoperfusion, which potentially impacts BBB function, has been noted in these regions in PD. Finally, as BBB alterations in

Abbreviations: ANOVA, analysis of variance; BBB, blood–brain barrier; CA, caudate; CN, control negative; CP, control positive; CSF, cerebral spinal fluid; DCE-MRI, dynamic contrast enhanced magnetic resonance imaging; FLAIR, fluid attenuation inversion recovery; FC, frontal cortex; FWE, family wise error; Hct, haematocrit; K^{trans}, contrast agent endothelial transfer coefficient; LEDD, levodopa equivalent daily dose; MNI, Montreal Neurological Institute; MoCA, Montreal cognitive assessment; NAWM, normal appearing white matter; NHS, National Health Service; P, pallidum; PET, positron emission tomography; PC, posterior cortices; PD, Parkinson's disease; PU, putamen; ROI, region of interest; SN, substantia nigra; SNpc, substantia nigra pars compacta; SPM, statistical parametric mapping; T_1-FFE, T_1 fast field echo; TE, echo time; 3 T, 3 tesla; TR, repetition time; UPDRS, Unified Parkinson's Disease Rating Scale; v_p, plasma volume; VEGF, vascular endothelial growth factor; WML, white matter lesion.

cerebrovascular disease have been found within WML and in the normal appearing white matter (NAWM) (Wardlaw et al., 2017) we also considered alterations in these regions. Hence we investigated BBB changes in basal ganglia, posterior and frontal cortex regions, NAWM and WML, along with a more exploratory voxel-wise analysis across the entire brain.

MATERIALS AND METHODS

Approvals, Recruitment, Eligibility and Consent

Relevant approvals were obtained including National Health Service (NHS) ethical approval (North West – Preston Research Ethics Committee), research governance and local university approvals. PD patients were recruited from Lancashire Teaching Hospitals NHS Foundation Trust and Salford Royal NHS Foundation Trust. Eligibility criteria for PD participants were a clinical diagnosis of PD fulfilling United Kingdom PD society brain bank criteria[1] without known clinical cerebrovascular disease (no history of transient ischaemic attack or stroke) or dementia (Emre et al., 2007). Participants with cerebrovascular disease were recruited from patients attending Lancashire Teaching Hospitals with a clinical diagnosis of stroke or transient ischaemic attack within the previous 2 years (and at least 3 months prior to participation) supported by relevant brain imaging (CP). Controls without a history of either PD or clinical cerebrovascular disease were also recruited from the local community (CN). All groups were matched for age. All participants were required to provide written informed consent and had capacity to do so.

Clinical Assessments

Parkinson's disease assessment included the Unified Parkinson's Disease Rating Scale (UPDRS)[2] during the scan visit. Disease severity was measured using the Hoehn and Yahr rating scale (Hoehn and Yahr, 1967). No alterations were made to the participants' medications for the study protocol. Routine clinical baseline data were also recorded and the levodopa equivalent daily dose (LEDD) calculated (Tomlinson et al., 2010). A battery of clinical scales was also administered, including the Montreal Cognitive Assessment (MoCA)[3] to measure cognition. Demographics and clinical data were compared between PD and control participants using unpaired Student's *t*-test for continuous variables or Fisher's exact test for categorical variables with p value set at <0.05.

MRI Protocol

Participants were scanned on one of two systems running the same software version: a 3.0 T Philips Achieva scanner with an eight channel head coil at Salford Royal Hospital or a separate 3.0 T Philips Achieva scanner with a 32 channel head coil at the Manchester Clinical Research Facility. Involuntary movements in participants were minimised using padding within the head coil.

Both scanners ran an identical MRI protocol. A DCE-MRI dynamic series of 160 3D T_1-weighted images [T_1 Fast Field Echo (T_1-FFE)] were acquired with a temporal resolution of 7.6 s, spatial resolution of $1.5 \times 1.5 \times 4$ mm, and total duration of approximately 20 min. On the 8th dynamic, a gadolinium-based contrast agent (Dotarem) bolus was administered using a power injector. The volume administered was proportional to the weight of the subject with a dose of 0.1 mmol/kg.

Prior to the dynamic scan, a series of additional 3D T_1-FFE images were acquired at three flip angles (2, 5, and 10 degrees) in order to calculate a pre-contrast T_1 map using the variable flip angle method. A B_1 map was also collected in order to correct for B_1 field inhomogeneities.

In addition, a 1 mm isotropic 3D T_1-weighted image and a T_2-weighted fluid attenuation inversion recovery (FLAIR) image were acquired. Please see supplementary material for full details of acquisition parameters.

MRI Analysis

White Matter Lesion Volume Estimation

White matter lesion volume was calculated as an established marker of small vessel disease (Wardlaw et al., 2013). WML volume was estimated using the lesion segmentation toolbox (Schmidt et al., 2012) in SPM8 using both T_2-weighted FLAIR images and T_1-weighted images as inputs. A threshold of 0.3 was chosen as it gave the most accurate estimates in a sub-study comparing WML volume estimates from the lesion segmentation toolbox with those from semi-automated lesion-growing methods on a subset of the data (n = 51, including representation from all groups, unpublished)[4]. WML volumes were positively skewed and were therefore cube-root transformed as is commonly done (Stefaniak et al., 2018) before group comparisons using un-paired *t*-tests.

DCE Analysis

The dynamic series of 160 images were first corrected for motion using the "realignment" option in SPM12[5], which aligned all DCE-MRI images to the first image in the time-series. A vascular input function was derived from the sagittal sinus (Lavini and Verhoeff, 2010), which was delineated using MRIcro on the final image of the motion-corrected dynamic time series. Regions of approximately 50 voxels were selected. A voxel-by-voxel fit of the dynamic data for both the contrast agent transfer coefficient (K^{trans}) and plasma volume (v_p) was performed using the uptake or "Patlak" model assuming unidirectional transport of the tracer from the blood plasma to the extravascular, extracellular space. Further details regarding DCE-MRI analysis can be found in Supplementary Material.

Mean images of K^{trans} and v_p in each of the three groups were created following spatial smoothing using a 3D 3 mm

[1]https://www.ncbi.nlm.nih.gov/projects/gap/cgi-bin/GetPdf.cgi?id=phd000042

[2]https://www.movementdisorders.org/MDS/MDS-Rating-Scales/MDS-Unified-Parkinsons-Disease-Rating-Scale-MDS-UPDRS.htm

[3]www.MoCAtest.org

[4]https://www.statistical-modelling.de/lst.html

[5]www.fil.ion.ucl.ac.uk/spm

full-width-half-maximum kernel in and visually inspected for differences. Voxel-wise analysis was performed using the SPM12 PET toolbox to determine regional differences in K^{trans} and v_p between the groups. K^{trans} and v_p maps were co-registered to the high resolution 3D T_1-weighted image and then normalised to Montreal Neurological Institute (MNI) space. The normalised K^{trans} and v_p maps were spatially smoothed using an 8 mm full-width-half-maximum kernel. Voxel-wise comparisons of K^{trans} and v_p between the groups were performed, without intensity normalisation, using a two-sample unpaired *t*-test (unequal variances). Group comparisons were performed between: CN and PD, CP and PD and CP and CN. Regions were considered to show significant group differences at a voxel-level threshold of $p < 0.001$ uncorrected, and a minimum cluster size of 50 voxels, masked to the intra-cranial volume. Further analysis using family wise error (FWE) correction for multiple comparisons at the cluster level was performed. The MNI coordinates were used to identify regions showing group differences using xjview V 8.14[6].

Group differences in K^{trans} and v_p were also assessed in region of interest (ROI) including the basal ganglia, frontal and posterior cortices, WML and NAWM. WML regions were obtained using the co-registered binary lesion masks from the lesion segmentation (see section "White Matter Lesion Volume Estimation") and care was taken to remove regions of WML from all other ROIs. The caudate (CA), putamen (PU), and pallidum (P) regions were obtained from MNI atlases (Tzourio-Mazoyer et al., 2002; Prodoehl et al., 2008). The substantia nigra (SN) region was manually drawn on the T_2-weighted template image from SPM by an experienced researcher. Frontal and selected posterior cortical regions were also defined (in keeping with regions of hypoperfusion in other studies) (Melzer et al., 2011; Fernandez-Seara et al., 2012; Gray and Woulfe, 2015; Al-Bachari et al., 2017) using a combination of regions from the automatic anatomical labelling atlas (Tzourio-Mazoyer et al., 2002). The frontal region consisted of superior and middle frontal gyri and the posterior region of pre-cuneus, cuneus, lingual, superior, and middle occipital gyri. Finally, NAWM was also selected, defined using the mask from the segmentation of the co-registered T_1-weighted image, in order to determine the significance of any diffuse differences between the groups. **Figure 1** depicts the location of these ROIs. Mean K^{trans} and v_p values were extracted from each of these regions for each subject. Repeated measures analysis of variance (ANOVA) was performed with factors "group" and "region" to determine any significant difference in K^{trans} and v_p between the groups with "subject" included as a random effect. A second ANOVA was performed with the addition of age, gender and the cube-root of WML volume as covariates to determine if these factors could explain any variance in K^{trans} and v_p. Where significant group differences were found, *post hoc t*-tests were performed with Bonferroni correction where stated. Statistical analyses were conducted using R-Studio Version 1.3.959[7].

[6]https://www.alivelearn.net/xjview/

[7]https://rstudio.com/products/rstudio/

Correlation With Cognitive and Clinical Parameters

Any association between the DCE-MRI parameters and cognitive deficit, medication and disease severity within the PD group was evaluated with a linear mixed effects model and ANOVA. Region (as a factor), MoCA score, LEDD dose and UPDRS score (as continuous variables) and their interaction with region were modelled as fixed effects, and subject was set as a random effect. Where significant interactions with region were found, the fixed effects *t*-tests and corresponding *p* values for each region were considered, calculated using Satterthwaite's approximation in the lmerTest package (Kuznetsova et al., 2017) in R-studio.

RESULTS

Fifty-one PD patients were recruited, 17 CP subjects with cerebrovascular disease (13 with ischaemic stroke, 4 with single or multiple transient ischaemic attacks; mean time since symptom onset and where applicable most recent known transient ischaemic attack = 1.1 ± 0.7 years) and 34 CN subjects. Twenty-eight participants were scanned at Salford Royal Hospital and 74 participants at the Manchester Clinical Research Facility (37 PD, 20 CN, and 17 CP).

Data from seven participants could not be analysed due to (i) participants not tolerating the complete scan procedure ($n = 2$) (ii) failure of the contrast agent injection ($n = 3$), resulting in either absent, very low or very distorted vascular input function and (iii) non-physiological values of plasma volume ($n = 2$); leaving data from 95 participants (49 PD, 31 CN, 15 CP). Summary demographic information from these patients is given in **Table 1**, along with the WML volume measurements. There were no significant differences in age between the groups. As expected the CP group had more cerebrovascular risk factors than either the PD or CN groups but there was no difference in risk factors between the PD and CN groups. WML volume was significantly higher in the PD group than the CN group, suggesting that, although vascular risk factors are similar, there was increased microvascular pathology in the PD group. WML volume was also higher in the CP group that the CN group, as expected, but not significantly different from the PD group. The PD group had significantly lower MoCA score compared to the CN group, but was not significantly different from the CP group. It is noted that there are significant gender differences between the PD and CN groups, which is addressed directly in a sub-analysis (see Supplementary Materials).

Voxel-Wise Analysis

Figure 2 shows mean images of K^{trans} and v_p in the three groups. It can be seen that K^{trans} is generally higher in PD than in the control groups. The v_p maps look similar between the PD and CN group, but the CP group has noticeably lower v_p.

The voxel-wise comparisons revealed significantly higher K^{trans} in the PD group than in the CN group (**Figure 3** and **Supplementary Table 1**) in regions including white matter regions of the pre-cuneus bilaterally. Only the largest region

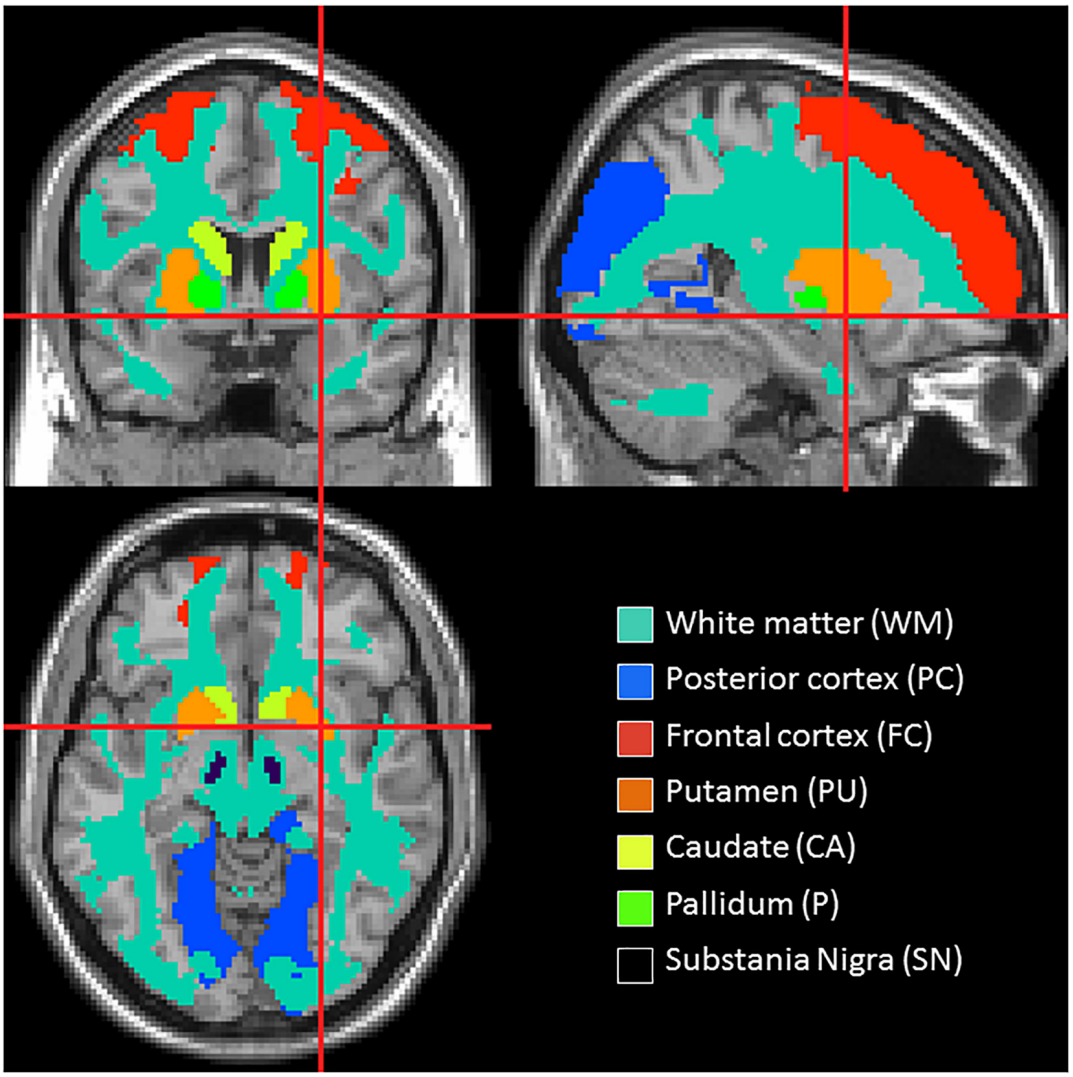

FIGURE 1 | Location of the regions of interest.

in the right pre-cuneus survived cluster-level FWE correction. There were no regions of significantly lower K^{trans} in PD than in CN. K^{trans} was also significantly higher in the PD group than in the CP group in one region of white matter in the right temporal lobe (**Supplementary Table 2**). Significantly higher K^{trans} was also seen in the CP group than in the CN group (**Supplementary Table 3**), in the mid cingulum and R cerebellum. Aside from for the PD vs. CN comparison, none of these regions survived the cluster-level FWE correction.

Control positive showed regions of significantly lower v_p than CN (**Supplementary Table 4**) and PD (**Supplementary Table 5**) in white matter regions of the left and right temporal lobes. No significant voxel-wise differences in v_p were seen for PD vs. CN.

ROI Analysis

Figure 4 shows group mean regional values for K^{trans} and v_p. There was a significant effect of group ($F = 3.3$, $p = 0.04$) and region ($F = 54.1$, $p < 0.0001$) on K^{trans} with *post hoc* tests showing K^{trans} to be significantly higher in PD than in CN ($p = 0.03$, Bonferroni corrected) and no significant differences between the other two pairwise comparisons. The NAWM, posterior cortex and SN show elevated K^{trans} in PD compared to CN when considering differences on a region-by-region basis ($p < 0.05$, uncorrected). K^{trans} is also higher *within* the WML in PD in comparison to CN. A second ANOVA with WML volume, age and gender included as covariates showed a similar effect of group ($F = 3.9$, $p = 0.02$) and region ($F = 54.1$, $p < 0.0001$) and no significant effect of WML volume ($F = 1.0$ $p = 0.3$), age ($F = 1.1$, $p = 0.3$) or gender ($F = 0.1$, $p = 0.8$). *Post hoc* tests again showed K^{trans} to be significantly higher in PD than in CN ($p = 0.02$, Bonferroni corrected).

There was a significant effect of region ($F = 90.0$, $p < 0.0001$) but not group ($F = 1.1$, $p = 0.3$) on v_p. The second ANOVA with WML volume, age and gender included as covariates showed a

TABLE 1 | Demographics and clinical and radiological characteristics of the study group.

	CN (n = 31)	CP (n = 15)	PD (n = 49)	p value PD vs. CN	p value PD vs. CP	p value CP vs. CN
n (F:M)	16:15	4:11	12:37	0.01	0.25	0.07
Age (years): mean (range)	66.4 (52–81)	69.1 (53–84)	68.9 (52–85)	0.23	0.84	0.26
No. of cardiovascular risk factors: mean (SD)	1.52 (1.12)	2.93 (1.16)	1.72 (1.52)	0.55	0.002	<0.0001
Cardiovascular Risk Factors (% of group):						
Hypertension	29.0	73.3	26.5	0.13	0.02	0.005
Diabetes mellitus	6.5	13.3	6.1	0.36	0.43	0.46
FH of CVD	45.2	46.7	22.4	0.10	0.15	0.25
Smoker	29.0	66.7	28.6	0.15	0.03	0.01
Hypercholesterolaemia	45.2	68.9	22.4	0.08	0.004	0.05
Ischaemic heart disease	6.5	13.3	12.2	0.13	0.31	0.30
Atrial fibrillation	0	20.0	2.0	0.61	0.04	0.03
Disease Duration (years): mean (SD)	N/A	1.1 (0.77)	7.2 (4.45)	N/A	N/A	N/A
Hoehn and Yahr Score: mean (SD)	N/A	N/A	2.60 (0.09)	N/A	N/A	N/A
UPDRS Score: mean (SD)	N/A	N/A	29.2 (12.7)	N/A	N/A	N/A
LEDD (mg): mean (SD)	N/A	N/A	583.5 (399.6)	N/A	N/A	N/A
MoCA Score: mean (SD)	27.9 (2.3)	26.1 (2.9)	25.2 (3.9)	0.0004	0.39	0.04
Cube-root of WML volume (mm): mean (SD)	1.26 (0.83)	2.11 (0.72)	1.80 (0.95)	0.008	0.19	0.001

AF, atrial fibrillation; CN, control negative; CP, control positive; CV, cardiovascular; DM, diabetes mellitus; FH of CVD, family history of cardiovascular disease; Hyperchol., hypercholesterolaemia; IHD, ischaemic heart disease; LEDD, levodopa equivalent daily dose; MoCA, Montreal Cognitive Assessment; RF, risk factors; PD, Parkinson's disease; TD, tremor dominant; UPDRS 111, unified Parkinson's disease rating scale motor score; WML, white matter lesion.

similar result with an impact of region ($F = 90.0$, $p < 0.0001$) but not group ($F = 1.1$, $p = 0.3$) on v_p and no significant effect of WML volume ($F = 0.1$. $p = 0.8$), age ($F = 2.2$, $p = 0.1$) or gender ($F = 0.2$, $p = 0.6$).

To check that differences were not driven by the differences in gender-matching or by the use of two scanners, the regional analysis was repeated with gender-matched groups and with data from only one scanner. Broadly the same regional and group effects were seen for both K^{trans} and v_p (see supplementary materials).

Correlation With Cognitive and Clinical Parameters

Table 2 summaries the ANOVA findings evaluating the impact of cognitive deficit (MoCA score), medication (LEDD dose) and disease severity (UPDRS score) on the DCE-MRI parameters within the PD group. There are no significant associations between these parameters and K^{trans}. In particular, LEDD dose was not associated with K^{trans} suggesting that the increased BBB leakage seen in the PD group is not a consequence of medication. A significant effect of LEDD dose on v_p was found with higher LEDD dose associated with higher v_p.

DISCUSSION

The aim of this study was to determine alterations in BBB permeability in PD, by comparison with controls, and to investigate whether potential changes are simply attributable to co-existing cerebrovascular disease in an ageing population or if a pattern of BBB alteration specific to PD is revealed. The results show higher K^{trans}, reflecting higher BBB leakage, in PD than in CN (**Figures 2**, **3** and **Supplementary Table 1**), with a somewhat different spatial pattern to the differences seen between individuals with known cerebrovascular disease (CP) and CN (**Supplementary Table 3**). Direct comparison of PD and CP shows higher K^{trans} for PD in the white matter of the right temporal lobe (**Supplementary Table 2**). Blood plasma volume, v_p, is similar in PD and CN, with some evidence of lower v_p in the CP group (**Supplementary Tables 4, 5** and **Figure 4**). Collectively these data demonstrate BBB disruption in PD can be detected in the clinical setting in keeping with evidence from studies in animal models and post mortem human brain. The K^{trans} values (**Figure 4**) are within the wide range of published values which seem dependent on the specific acquisition and analysis methods and contrast agents used (Raja et al., 2018). A study using the same contrast agent and similar method shows very comparable values (Heye et al., 2016).

Both the voxel-based and the ROI analysis showed higher K^{trans} in PD when compared with CN. These results are in keeping with several studies showing altered components of the BBB in PD (Barcia et al., 2005; Carvey et al., 2005; Chao et al., 2009; Sarkar et al., 2014) such as loss of capillaries, an alteration in the capillary calibre and thickened basement membrane (making the BBB less competent) (Brown and Thore, 2011). Our voxel-based analysis approach allows a whole brain view of BBB dysfunction, and, in the whole brain maps, we see a fairly diffuse pattern of BBB disruption in PD, compared to CN. K^{trans} differences only reach statistical significance in posterior regions; however, given the requirement for multiple

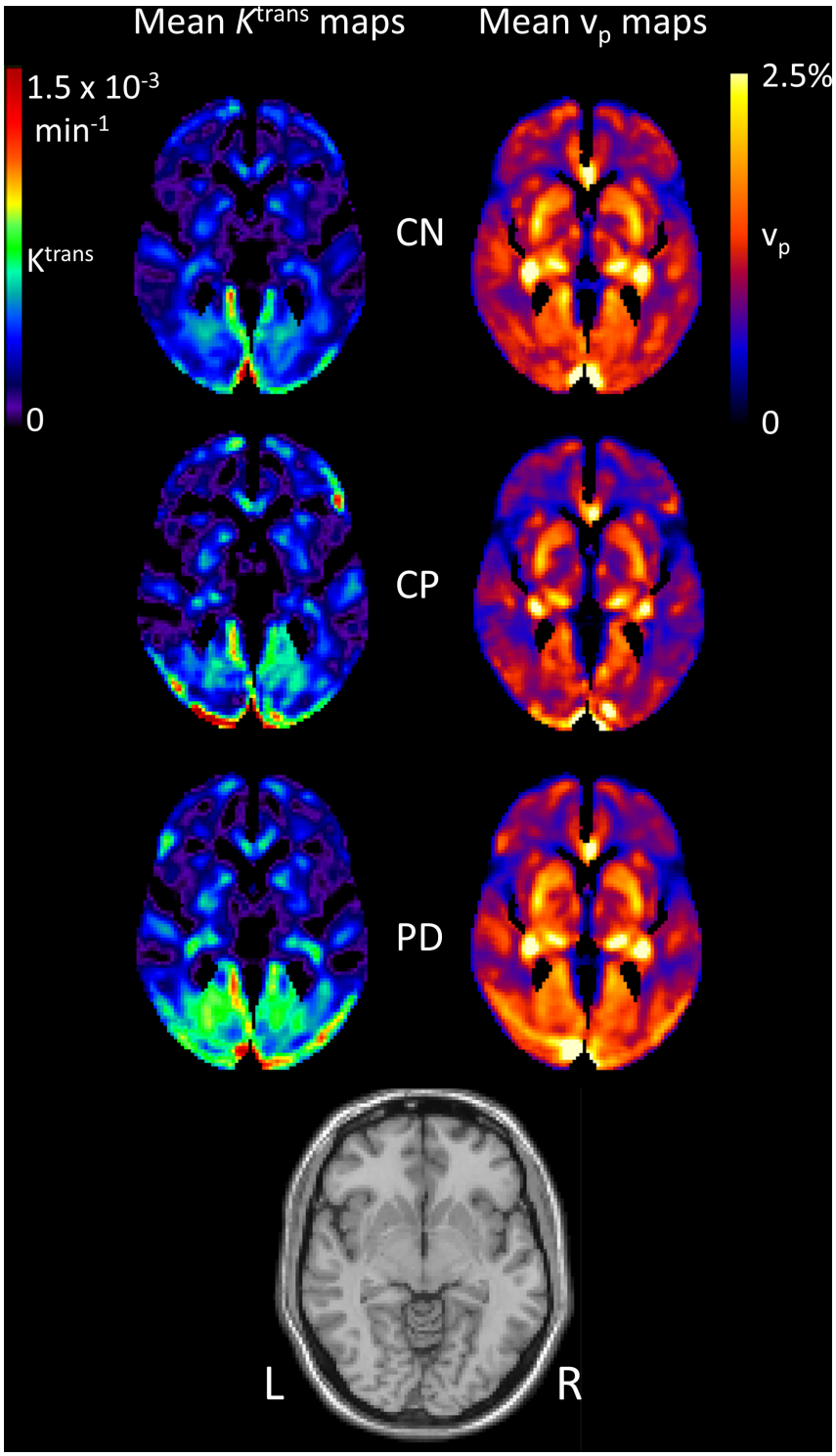

FIGURE 2 | Mean images of K^{trans} and v_p for each group. Images of the mean contrast agent transfer coefficient K^{trans} and the plasma volume v_p for each group. Individual images were first normalised to MNI space before averaging. A T_1-weighted image is shown for reference.

comparisons correction, it would likely require a much larger study for smaller brain regions such as basal ganglia nuclei to survive the statistical threshold. The ROI approach focussed on areas expected to display disease pathology based on our understanding of the pathophysiology of PD. It revealed K^{trans} to be generally higher in the PD group than in the CN group.

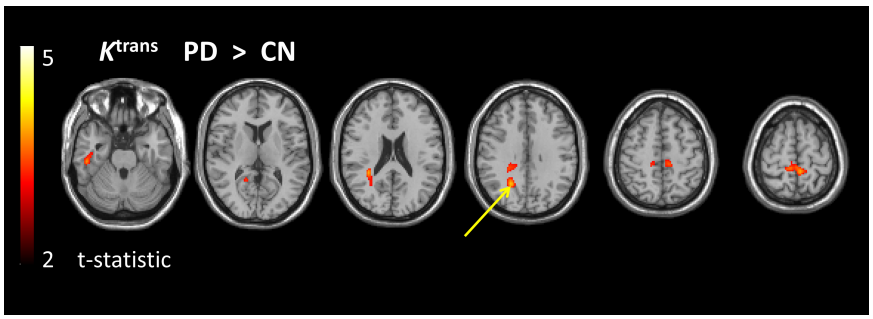

FIGURE 3 | Regions of higher K^{trans} in the PD group compared to the CN group. t-statistic map overlaid on structural image showing the regions of significantly higher K^{trans} in the PD group than in the CN group. Map is thresholded with voxel-level $p < 0.001$ (uncorrected) and minimum cluster size of 50 voxels. The arrow indicates the cluster that survives cluster-level family wise error correction for multiple comparisons ($p < 0.05$).

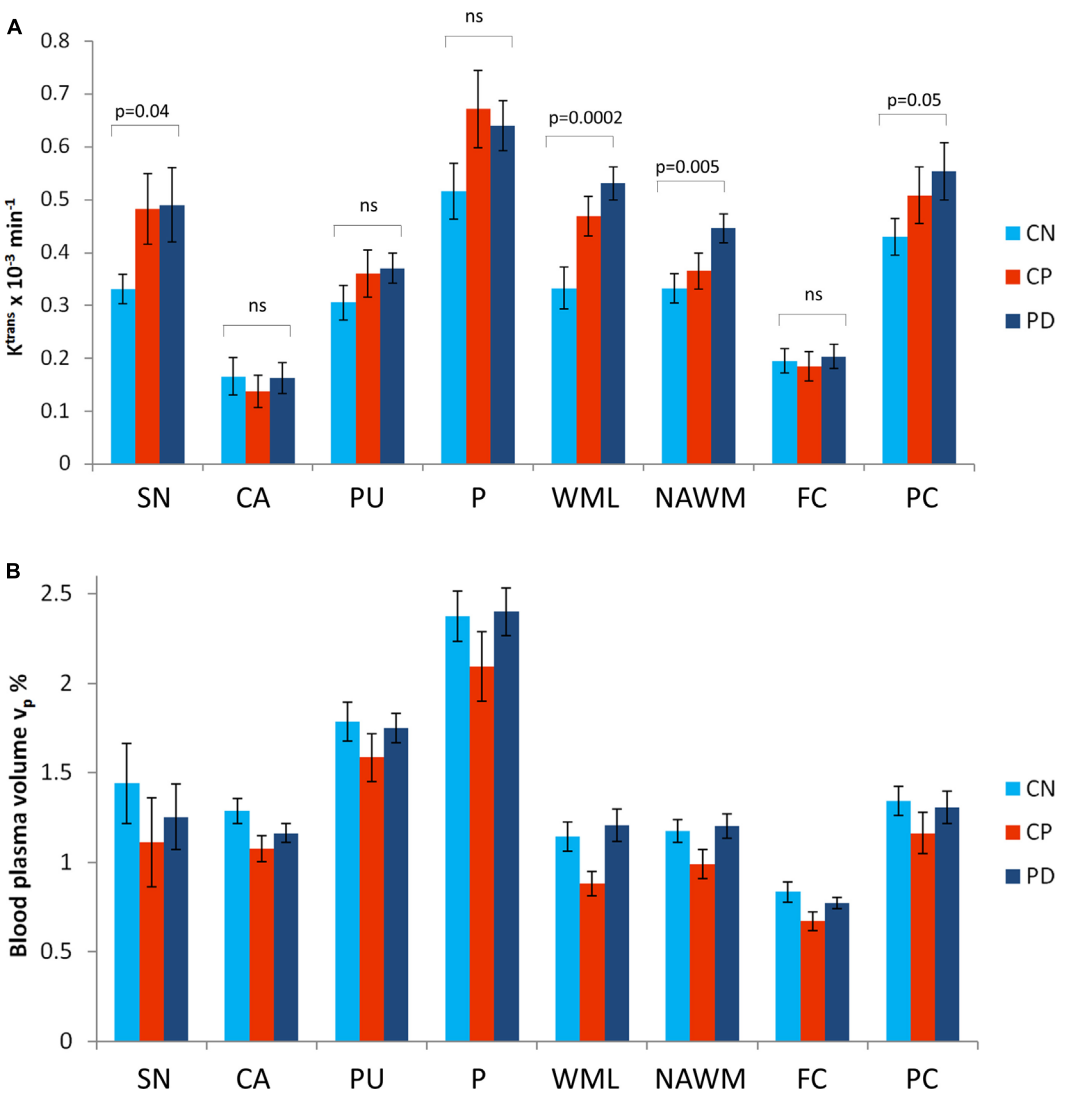

FIGURE 4 | Mean values for K^{trans} and v_p in regions of interest for each group. Mean values are given for **(A)** the contrast agent transfer coefficient K^{trans} and **(B)** the plasma volume v_p. Error bars show the standard error in the mean. The significance of *post hoc t*-tests (uncorrected) between K^{trans} in the PD and CN group are shown. SN, substantia nigra; CA, caudate; PU, putamen; P, pallidum; WMLs, white matter lesions; NAWM, normal-appearing white matter; FC, frontal cortex; PC, posterior cortices.

TABLE 2 | Analysis of variance for the impact of cognitive deficit (MoCA score), medication (LEDD dose) and disease severity (UPDRS score) on regional DCE-MRI parameters within the PD group.

Factor		K^{trans} as dependent variable		V_p as dependent variable	
	Deg. freedom	*F* value	*p* value	*F* value	*p* value
Region	6	0.3	1.0	3.5	0.002
MoCA	1	3.8	0.06	0.4	0.52
LEDD	1	0.4	0.5	6.1	0.02
UPDRS	1	0.5	0.5	0.02	0.9
Region: MoCA	6	0.1	1.0	1.7	0.1
Region: LEDD	6	0.5	0.8	1.0	0.4
Region: UPDRS	6	0.4	0.9	0.8	0.5

Considering the magnitude and significance of regional K^{trans} differences between PD and CN (**Figure 4**), this is driven mainly by differences in SN, NAWM, WML and the posterior cortex. Alterations in SN and posterior cortex are in keeping with BBB breakdown playing a role in the pathophysiology of PD.

The increased K^{trans} in posterior cortical regions in PD is particularly noteworthy as these are the same regions that display hypoperfusion (Borghammer et al., 2010; Melzer et al., 2011; Fernandez-Seara et al., 2012; Al-Bachari et al., 2017) i.e., the results strengthen the argument of a link between BBB leakage and hypoperfusion. Hypoperfusion has been attributed to altered vasculature (string vessels, shorter/loss of capillaries, tortuous vessels), which can hinder normal BBB function (Rite et al., 2007; Guan et al., 2013; Gray and Woulfe, 2015; Fang, 2018). BBB disruption has been attributed to alterations in key components such as tight junctions, potentially caused by pro-inflammatory cytokines and altered vascular endothelial growth factor (VEGF) (Carvey et al., 2009; Matsumoto et al., 2017; Chen et al., 2018). Interestingly a study using albumin (mg/L)/plasma albumin (g/L) ratio in the cerebral spinal fluid (CSF) to measure BBB dysfunction, revealed increased BBB dysfunction in PD compared to controls which was associated with increased CSF biomarkers of angiogenesis (e.g., VEGF) (Janelidze et al., 2015). These substances can also alter perfusion, with enhanced angiogenesis resulting in abnormal vascular permeability in PD. Future longitudinal imaging studies will be important to understand whether hypoperfusion leads to altered BBB function, or vice versa, or in fact whether BBB and perfusion changes have a common cause, for example, inflammation. Furthermore, it will be important to determine what downstream effects these microvascular changes may have on neuronal loss. We did not observe any statistically significant differences in K^{trans} between CP and CN unlike other studies which have reported elevated K^{trans} post-stroke (Wardlaw et al., 2017). However, the small sample size and high heterogeneity of the CP group may have contributed to this.

White matter lesion have been used as a surrogate marker of SVD (Wardlaw et al., 2013). We find higher WML volume in the PD group than the CN group despite the fact the groups have no significant differences in cardiovascular risk factors. Previous studies of WML in PD however show mixed results (Rabbitt et al., 2006; de Schipper et al., 2019). To investigate whether the WML volume was driving the K^{trans} group differences, we used ANOVA with WML volume, age, and gender as covariates and found that there was no significant association between WML volume (or age or gender) and K^{trans}. The main finding of higher K^{trans} in the PD group than CN was maintained. Recent work has tried to understand the link between BBB dysfunction and WML revealing a continuum of BBB disruption leading to myelin loss and fibrinogen accumulation resulting in WML formation (Muñoz Maniega et al., 2017; Wardlaw and William, 2018; Wardlaw et al., 2019). Indeed NAWM (particularly that surrounding the WML) has been shown to have increased BBB leakage suggesting BBB disruption can precede WML formation (Wardlaw et al., 2017). We do not find a significant association between WML volume and K^{trans}, which alongside the higher K^{trans} in NAWM in the PD group compared to CN, supports this notion that BBB disruption is diffuse throughout the white matter and perhaps precedes WML formation. It is interesting to note that, within the lesions, K^{trans} is significantly higher in the PD group than in the CN group suggesting more severe underlying pathology.

Our measurements of blood plasma volume, v_p are not significantly different between PD and healthy controls, which may seem contradictory to the well-reported hypoperfusion in PD, given that blood volume and perfusion are closely related. However, blood flow also depends on the blood velocity within the capillaries which may underlie the observed differences. Indeed, we have previously found significantly prolonged arterial transit time in posterior brain regions in PD, suggesting lower blood velocity (Al-Bachari et al., 2017). Furthermore, v_p estimation may also be affected by the rate of *trans*-endothelial water exchange leading to possible underestimation of v_p in the CN group in comparison to the PD group due to the relatively more intact BBB, potentially contributing to the lack of group difference seen. As the K^{trans} and v_p patterns differed between CP and PD this would suggest that the BBB alterations do not simply occur due to co-existing cerebrovascular disease (indeed PD patients with known cerebrovascular disease were not included in the study and the PD group had significantly fewer cerebrovascular risk factors) but plays an independent role in PD pathophysiology. Together with the increased WML volume in the PD group, this supports the hypothesis that microvascular pathology occurs in PD.

We explored the impact of cognitive deficit (MoCA score), medication (LEDD dose) and disease severity (UPDRS score) on K^{trans} and v_p within the PD group. LEDD dose was associated with higher v_p, which is in keeping with studies that suggest L-dopa increases blood flow in certain regions (Ohlin et al., 2012; Ko et al., 2015). There were no significant associations between any parameter and K^{trans} and we conclude that the K^{trans} differences between the PD and CN groups are not driven by the differences in MoCA score or by levodopa medications.

One limitation of this study is the significant gender imbalance between the PD and CN groups (**Table 1**) with relatively more men in the PD group. However, we do not believe this compromises our findings as there are no reports of gender

differences in K^{trans} values, and secondary analysis of our own data shows consistent findings in a gender-matched subgroup (Supplementary Materials). Likewise we collected data on two different scanners which may have influenced the results; however secondary analysis shows consistent findings in analysis of data from a single scanner (Supplementary Materials). We interpret the higher K^{trans} in PD as relating to higher endothelial leakage, but note that K^{trans} is also affected by cerebral blood flow. However cerebral blood flow is lower than normal in posterior regions in PD (Barcia et al., 2005; Kortekaas et al., 2005; Tomlinson et al., 2010; Gray and Woulfe, 2015) which would lead to lower K^{trans}, and yet we see higher K^{trans} in the PD group, implying that the differences are not due to blood flow differences.

CONCLUSION

In conclusion, this study has shown subtle BBB disruption in PD, in key regions implicated in the pathophysiology including the SN, white matter and posterior cortical regions. Further research is needed, including longitudinal clinical imaging studies combining neuronal, metabolic and vascular measurements to better understand disease mechanisms and so identify potential therapeutic targets in PD.

DATA AVAILABILITY STATEMENT

Data including images, imaging metrics and participant metadata are available on request. Please email the corresponding author: Laura.Parkes@manchester.ac.uk.

ETHICS STATEMENT

The studies involving human participants were reviewed and approved by NHS ethical approval (North West – Preston Research Ethics Committee), United Kingdom. The patients/participants provided their written informed consent to participate in this study.

AUTHOR CONTRIBUTIONS

SA-B contributed to the conception of the study, organised and executed the study, collected all data, performed the majority of the data analysis and interpretation, wrote the first draft of the manuscript, and contributed to further editing. JN and GP contributed to the execution of the study and the data analysis and interpretation as well as reviewing the manuscript. HE conceived of and organised the study, contributed to data interpretation, and reviewed and edited the manuscript. LP contributed to the conception, organisation and execution of the study, contributed to the data analysis and interpretation, and reviewed and edited the manuscript. All authors contributed to the article and approved the submitted version.

FUNDING

Salary (SA-B) and research costs for this work were provided through support from: Lancaster University, Sydney Driscoll Neuroscience Foundation, The University of Manchester and Medical Research Council Studentship, Lancashire Teaching Hospitals NHS Foundation Trust, and the Engineering and Physical Sciences Research Council (EP/M005909/1). HE is supported by Lancashire Teaching Hospitals NHS Foundation Trust and Lancaster University. LP, JN, and GP were supported by The University of Manchester.

SUPPLEMENTARY MATERIAL

The Supplementary Material for this article can be found online at: https://www.frontiersin.org/articles/10.3389/fphys.2020.593026/full#supplementary-material

REFERENCES

Al-Bachari, S., Vidyasagar, R., Emsley, H. C., and Parkes, L. M. (2017). Structural and physiological neurovascular changes in idiopathic Parkinson's disease and its clinical phenotypes. *J. Cereb. Blood Flow Metab.* 37, 3409–3421. doi: 10.1177/0271678x16688919

Alvarez, J. I., Katayama, T., and Prat, A. (2013). Glial influence on the blood brain barrier. *Glia* 61, 1939–1958. doi: 10.1002/glia.22575

Andreone, B. J., Lacoste, B., and Gu, C. (2015). Neuronal and vascular interactions. *Annu. Rev. Neurosci.* 38, 25–46. doi: 10.1146/annurev-neuro-071714-033835

Barcia, C., Bautista, V., Sanchez-Bahillo, A., Fernandez-Villalba, E., Faucheux, B., Poza y Poza, M., et al. (2005). Changes in vascularization in substantia nigra pars compacta of monkeys rendered parkinsonian. *J. Neural Transm.* 112, 1237–1248. doi: 10.1007/s00702-004-0256-2

Bell, R. D., Winkler, E. A., Sagare, A. P., Singh, I., LaRue, B., Deane, R., et al. (2010). Pericytes control key neurovascular functions and neuronal phenotype in the adult brain and during brain aging. *Neuron* 68, 409–427. doi: 10.1016/j.neuron.2010.09.043

Borghammer, P. (2012). Perfusion and metabolism imaging studies in Parkinson's disease. *Dan. Med. J.* 59:B4466.

Borghammer, P., Chakravarty, M., Jonsdottir, K. Y., Sato, N., Matsuda, H., Ito, K., et al. (2010). Cortical hypometabolism and hypoperfusion in Parkinson's disease is extensive: probably even at early disease stages. *Brain Struct. Funct.* 214, 303–317. doi: 10.1007/s00429-010-0246-0

Brown, W. R., and Thore, C. R. (2011). Review: cerebral microvascular pathology in ageing and neurodegeneration. *Neuropathol. Appl. Neurobiol.* 37, 56–74. doi: 10.1111/j.1365-2990.2010.01139.x

Carvey, P. M., Hendey, B., and Monahan, A. J. (2009). The blood-brain barrier in neurodegenerative disease: a rhetorical perspective. *J. Neurochem.* 111, 291–314. doi: 10.1111/j.1471-4159.2009.06319.x

Carvey, P. M., Punati, A., and Newman, M. B. (2006). Progressive dopamine neuron loss in Parkinson's disease: the multiple hit hypothesis. *Cell Transplant.* 15, 239–250. doi: 10.3727/000000006783981990

Carvey, P. M., Zhao, C. H., Hendey, B., Lum, H., Trachtenberg, J., Desai, B. S., et al. (2005). 6-Hydroxydopamine-induced alterations in blood-brain barrier permeability. *Eur. J. Neurosci.* 22, 1158–1168. doi: 10.1111/j.1460-9568.2005.04281.x

Chao, Y. X., He, B. P., and Tay, S. S. (2009). Mesenchymal stem cell transplantation attenuates blood brain barrier damage, and neuroinflammation. (and). protects dopaminergic neurons against MPTP toxicity in the substantia nigra in a model

of Parkinson's disease. *J. Neuroimmunol.* 216, 39–50. doi: 10.1016/j.jneuroim.2009.09.003

Chen, C., Li, X., Ge, G., Liu, J., Biju, K. C., Laing, S. D., et al. (2018). GDNF-expressing macrophages mitigate loss of dopamine neurons and improve Parkinsonian symptoms in MitoPark mice. *Sci. Rep.* 8:5460.

Collins, L. M., Toulouse, A., Connor, T. J., and Nolan, Y. M. (2012). Contributions of central and systemic inflammation to the pathophysiology of Parkinson's disease. *Neuropharmacology* 62, 2154–2168. doi: 10.1016/j.neuropharm.2012.01.028

de Schipper, L. J., Hafkemeijer, A., Bouts, M., van der Grond, J., Marinus, J., Henselmans, J. M. L., et al. (2019). Age- and disease-related cerebral white matter changes in patients with Parkinson's disease. *Neurobiol. Aging* 80, 203–209. doi: 10.1016/j.neurobiolaging.2019.05.004

Di Marco, L. Y., Venneri, A., Farkas, E., Evans, P. C., Marzo, A., and Frangi, A. F. (2015). Vascular dysfunction in the pathogenesis of Alzheimer's disease–A review of endothelium-mediated mechanisms and ensuing vicious circles. *Neurobiol. Dis.* 82, 593–606. doi: 10.1016/j.nbd.2015.08.014

Emre, M., Aarsland, D., Brown, R., Burn, D. J., Duyckaerts, C., Mizuno, Y., et al. (2007). Clinical diagnostic criteria for dementia associated with Parkinson's disease. *Mov. Disord* 22, 1689–1707.

Fang, X. (2018). Impaired tissue barriers as potential therapeutic targets for Parkinson's disease and amyotrophic lateral sclerosis. *Metab. Brain Dis.* 33, 1031–1043. doi: 10.1007/s11011-018-0239-x

Farkas, E., De Jong, G. I., de Vos, R. A., Jansen Steur, E. N., and Luiten, P. G. (2000). Pathological features of cerebral cortical capillaries are doubled in Alzheimer's disease and Parkinson's disease. *Acta Neuropathol.* 100, 395–402. doi: 10.1007/s004010000195

Faucheux, B. A., Bonnet, A. M., Agid, Y., and Hirsch, E. C. (1999). Blood vessels change in the mesencephalon of patients with Parkinson's disease. *Lancet* 353, 981–982. doi: 10.1016/s0140-6736(99)00641-8

Fernandez-Seara, M. A., Mengual, E., Vidorreta, M., Aznarez-Sanado, M., Loayza, F. R., Villagra, F., et al. (2012). Cortical hypoperfusion in Parkinson's disease assessed using arterial spin labeled perfusion MRI. *Neuroimage* 59, 2743–2750. doi: 10.1016/j.neuroimage.2011.10.033

Grammas, P., Martinez, J., and Miller, B. (2011). Cerebral microvascular endothelium and the pathogenesis of neurodegenerative diseases. *Expert Rev. Mol. Med.* 13:e19.

Gray, M. T., and Woulfe, J. M. (2015). Striatal blood-brain barrier permeability in Parkinson's disease. *J. Cereb. Blood Flow Metab.* 35, 747–750. doi: 10.1038/jcbfm.2015.32

Guan, J., Pavlovic, D., Dalkie, N., Waldvogel, H. J., O'Carroll, S. J., Green, C. R., et al. (2013). Vascular degeneration in Parkinson's disease. *Brain Pathol.* 23, 154–164. doi: 10.1111/j.1750-3639.2012.00628.x

Hachinski, V., Einhäupl, K., Ganten, D., Alladi, S., Brayne, C., Stephan, B. C. M., et al. (2019). Special topic section: linkages among cerebrovascular, cardiovascular, and cognitive disorders: preventing dementia by preventing stroke: The Berlin Manifesto. *Int. J. Stroke*. doi: 10.1177/1747493019871915 [Epub ahead of print].

Heye, A. K., Culling, R. D., Valdés Hernández, M. D. C., Thrippleton, M. J., and Wardlaw, J. M. (2014). Assessment of blood–brain barrier disruption using dynamic contrast-enhanced MRI. A systematic review. *Neuroimage Clin.* 6, 262–274. doi: 10.1016/j.nicl.2014.09.002

Heye, A. K., Thrippleton, M. J., Armitage, P. A., Valdés Hernández, M. D. C., Makin, S. D., Glatz, A., et al. (2016). Tracer kinetic modelling for DCE-MRI quantification of subtle blood-brain barrier permeability. *Neuroimage* 125, 446–455. doi: 10.1016/j.neuroimage.2015.10.018

Hoehn, M. M., and Yahr, M. D. (1967). Parkinsonism: onset, progression and mortality. *Neurology* 17, 427–442. doi: 10.1212/wnl.17.5.427

Iadecola, C. (2017). The neurovascular unit coming of age: a journey through neurovascular coupling in health and disease. *Neuron* 96, 17–42. doi: 10.1016/j.neuron.2017.07.030

Janelidze, S., Lindqvist, D., Francardo, V., Hall, S., Zetterberg, H., Blennow, K., et al. (2015). Increased CSF biomarkers of angiogenesis in Parkinson disease. *Neurology* 85, 1834–1842. doi: 10.1212/wnl.0000000000002151

Kamagata, K., Motoi, Y., Hori, M., Suzuki, M., Nakanishi, A., Shimoji, K., et al. (2011). Posterior hypoperfusion in Parkinson's disease with and without dementia measured with arterial spin labeling MRI. *J. Magn. Reson. Imaging* 33, 803–807. doi: 10.1002/jmri.22515

Kisler, K., Nelson, A. R., Montagne, A., and Zlokovic, B. V. (2017). Cerebral blood flow regulation and neurovascular dysfunction in Alzheimer disease. *Nat. Rev. Neurosci.* 18, 419–434. doi: 10.1038/nrn.2017.48

Ko, J. H., Lerner, R. P., and Eidelberg, D. (2015). Effects of levodopa on regional cerebral metabolism and blood flow. *Mov. Disord.* 30, 54–63. doi: 10.1002/mds.26041

Kortekaas, R., Leenders, K. L., van Oostrom, J. C., Vaalburg, W., Bart, J., Willemsen, A. T., et al. (2005). Blood-brain barrier dysfunction in parkinsonian midbrain *in vivo*. *Ann. Neurol.* 57, 176–179. doi: 10.1002/ana.20369

Kuznetsova, A., Brockhoff, P. B., and Christensen, R. H. B. (2017). lmerTest package: tests in linear mixed effects models. *J. Stat. Softw.* 82, 1–26.

Lavini, C., and Verhoeff, J. J. (2010). Reproducibility of the gadolinium concentration measurements and of the fitting parameters of the vascular input function in the superior sagittal sinus in a patient population. *Magn. Reson. Imaging* 28, 1420–1430. doi: 10.1016/j.mri.2010.06.017

Lo, E. H., and Rosenberg, G. A. (2009). The neurovascular unit in health and disease: introduction. *Stroke*40(3 Suppl.), S2–S3.

Ma, Y., Huang, C., Dyke, J. P., Pan, H., Alsop, D., Feigin, A., et al. (2010). Parkinson's disease spatial covariance pattern: noninvasive quantification with perfusion MRI. *J. Cereb. Blood Flow Metab.* 30, 505–509. doi: 10.1038/jcbfm.2009.256

Matsumoto, J., Stewart, T., Sheng, L., Li, N., Bullock, K., Song, N., et al. (2017). Transmission of alpha-synuclein-containing erythrocyte-derived extracellular vesicles across the blood-brain barrier via adsorptive mediated transcytosis: another mechanism for initiation and progression of Parkinson's disease? *Acta Neuropathol. Commun.* 5:71.

Melzer, T. R., Watts, R., MacAskill, M. R., Pearson, J. F., Rueger, S., Pitcher, T. L., et al. (2011). Arterial spin labelling reveals an abnormal cerebral perfusion pattern in Parkinson's disease. *Brain* 134(Pt 3), 845–855. doi: 10.1093/brain/awq377

Montagne, A., Barnes, S. R., Sweeney, M. D., Halliday, M. R., Sagare, A. P., Zhao, Z., et al. (2015). Blood-brain barrier breakdown in the aging human hippocampus. *Neuron* 85, 296–302. doi: 10.1016/j.neuron.2014.12.032

Montagne, A., Nikolakopoulou, A. M., Zhao, Z., Sagare, A. P., Si, G., Lazic, D., et al. (2018). Pericyte degeneration causes white matter dysfunction in the mouse central nervous system. *Nat. Med.* 24, 326–337. doi: 10.1038/nm.4482

Muñoz Maniega, S., Chappell, F. M., Valdés Hernández, M. C., Armitage, P. A., Makin, S. D., Heye, A. K., et al. (2017). Integrity of normal-appearing white matter: influence of age, visible lesion burden and hypertension in patients with small-vessel disease. *J. Cereb. Blood Flow Metab.* 37, 644–656. doi: 10.1177/0271678x16635657

Nelson, A. R., Sweeney, M. D., Sagare, A. P., and Zlokovic, B. V. (2015). Neurovascular dysfunction and neurodegeneration in dementia and Alzheimer's disease. *Biochim. Biophys. Acta* 1862, 887–900. doi: 10.1016/j.bbadis.2015.12.016

Ohlin, K. E., Sebastianutto, I., Adkins, C. E., Lundblad, C., Lockman, P. R., and Cenci, M. A. (2012). Impact of L-DOPA treatment on regional cerebral blood flow and metabolism in the basal ganglia in a rat model of Parkinson's disease. *Neuroimage* 61, 228–239. doi: 10.1016/j.neuroimage.2012.02.066

Pardridge, W. M. (2005). Molecular biology of the blood-brain barrier. *Mol. Biotechnol.* 30, 57–70.

Patel, A., Toia, G. V., Colletta, K., Bradaric, B. D., Carvey, P. M., and Hendey, B. (2011). An angiogenic inhibitor, cyclic RGDfV, attenuates MPTP-induced dopamine neuron toxicity. *Exp. Neurol.* 231, 160–170. doi: 10.1016/j.expneurol.2011.06.004

Prodoehl, J., Yu, H., Little, D. M., Abraham, I., and Vaillancourt, D. E. (2008). Region of interest template for the human basal ganglia: comparing EPI and standardized space approaches. *Neuroimage* 39, 956–965. doi: 10.1016/j.neuroimage.2007.09.027

Rabbitt, P. M., Scott, M., Thacker, N., Lowe, C., Horan, M., Pendleton, N., et al. (2006). Balance marks cognitive changes in old age because it reflects global brain atrophy and cerebro-arterial blood-flow. *Neuropsychologia* 44, 1978–1983. doi: 10.1016/j.neuropsychologia.2005.08.017

Raja, R., Rosenberg, G. A., and Caprihan, A. (2018). MRI measurements of Blood-Brain Barrier function in dementia: a review of recent studies. *Neuropharmacology* 134(Pt B), 259–271. doi: 10.1016/j.neuropharm.2017.10.034

Rite, I., Machado, A., Cano, J., and Venero, J. L. (2007). Blood-brain barrier disruption induces in vivo degeneration of nigral dopaminergic neurons. *J. Neurochem.* 101, 1567–1582. doi: 10.1111/j.1471-4159.2007.04567.x

Sarkar, S., Raymick, J., Mann, D., Bowyer, J. F., Hanig, J. P., Schmued, L. C., et al. (2014). Neurovascular changes in acute, sub-acute and chronic mouse models of Parkinson's disease. *Curr. Neurovasc. Res.* 11, 48–61. doi: 10.2174/1567202610666131124234506

Schmidt, P., Gaser, C., Arsic, M., Buck, D., Förschler, A., Berthele, A., et al. (2012). An automated tool for detection of FLAIR-hyperintense white-matter lesions in Multiple Sclerosis. *Neuroimage* 59, 3774–3783. doi: 10.1016/j.neuroimage.2011.11.032

Starr, J. M., Farrall, A. J., Armitage, P., McGurn, B., and Wardlaw, J. (2009). Blood-brain barrier permeability in Alzheimer's disease: a case-control MRI study. *Psychiatry Res.* 171, 232–241. doi: 10.1016/j.pscychresns.2008.04.003

Starr, J. M., Wardlaw, J., Ferguson, K., MacLullich, A., Deary, I. J., and Marshall, I. (2003). Increased blood-brain barrier permeability in type II diabetes demonstrated by gadolinium magnetic resonance imaging. *J. Neurol. Neurosurg. Psychiatry* 74, 70–76. doi: 10.1136/jnnp.74.1.70

Stefaniak, J. D., Parkes, L. M., Parry- Jones, A. R., Potter, G. M., Vail, A., Jovanovic, A., et al. (2018). Enzyme replacement therapy and white matter hyperintensity progression in Fabry disease. *Neurology* 91, e1413–e1422.

Sweeney, M. D., Zhao, Z., Montagne, A., Nelson, A. R., and Zlokovic, B. V. (2019). Blood-brain barrier: from physiology to disease and back. *Physiol. Rev.* 99, 21–78. doi: 10.1152/physrev.00050.2017

Taheri, S., Gasparovic, C., Huisa, B. N., Adair, J. C., Edmonds, E., Prestopnik, J., et al. (2011). Blood-brain barrier permeability abnormalities in vascular cognitive impairment. *Stroke* 42, 2158–2163. doi: 10.1161/strokeaha.110.611731

Tofts, P. S., and Kermode, A. G. (1991). Measurement of the blood-brain barrier permeability and leakage space using dynamic MR imaging. 1. Fundamental concepts. *Magn. Reson. Med.* 17, 357–367. doi: 10.1002/mrm.1910170208

Tomlinson, C. L., Stowe, R., Patel, S., Rick, C., Gray, R., and Clarke, C. E. (2010). Systematic review of levodopa dose equivalency reporting in Parkinson's disease. *Mov. Disord.* 25, 2649–2653. doi: 10.1002/mds.23429

Tzourio-Mazoyer, N., Landeau, B., Papathanassiou, D., Crivello, F., Etard, O., Delcroix, N., et al. (2002). Automated anatomical labeling of activations in SPM using a macroscopic anatomical parcellation of the MNI MRI single-subject brain. *Neuroimage* 15, 273–289. doi: 10.1006/nimg.2001.0978

Wada, K., Arai, H., Takanashi, M., Fukae, J., Oizumi, H., Yasuda, T., et al. (2006). Expression levels of vascular endothelial growth factor and its receptors in Parkinson's disease. *Neuroreport* 17, 705–709. doi: 10.1097/01.wnr.0000215769.71657.65

Wardlaw, J. M., Farrall, A., Armitage, P. A., Carpenter, T., Chappell, F., Doubal, F., et al. (2008). Changes in background blood-brain barrier integrity between lacunar and cortical ischemic stroke subtypes. *Stroke* 39, 1327–1332. doi: 10.1161/strokeaha.107.500124

Wardlaw, J. M., Makin, S. J., Valdés Hernández, M. C., Armitage, P. A., Heye, A. K., Chappell, F. M., et al. (2017). Blood-brain barrier failure as a core mechanism in cerebral small vessel disease and dementia: evidence from a cohort study. *Alzheimers Dement.* 13, 634–643. doi: 10.1016/j.jalz.2016.09.006

Wardlaw, J. M., Smith, C., and Dichgans, M. (2019). Small vessel disease: mechanisms and clinical implications. *Lancet Neurol.* 18, 684–696. doi: 10.1016/s1474-4422(19)30079-1

Wardlaw, J. M., Smith, E. E., Biessels, G. J., Cordonnier, C., Fazekas, F., Frayne, R., et al. (2013). Neuroimaging standards for research into small vessel disease and its contribution to ageing and neurodegeneration. *Lancet Neurol.* 12, 822–838.

Wardlaw, J. M., and William, M. (2018). Feinberg award for excellence in clinical stroke: small vessel disease; a big problem, but fixable. *Stroke* 49, 1770–1775. doi: 10.1161/strokeaha.118.021184

Zhao, Z., Nelson, A. R., Betsholtz, C., and Zlokovic, B. V. (2015). Establishment and dysfunction of the blood-brain barrier. *Cell* 163, 1064–1078. doi: 10.1016/j.cell.2015.10.067

Zlokovic, B. V. (2008). The blood-brain barrier in health and chronic neurodegenerative disorders. *Neuron* 57, 178–201. doi: 10.1016/j.neuron.2008.01.003

Zlokovic, B. V. (2011). Neurovascular pathways to neurodegeneration in Alzheimer's disease and other disorders. *Nat. Rev. Neurosci.* 12, 723–738. doi: 10.1038/nrn3114

Conflict of Interest: Authors JN and GP were part employed by the company Bioxydyn and hold shares in the company.

The remaining authors declare that the research was conducted in the absence of any commercial or financial relationships that could be construed as a potential conflict of interest.

frontiers in Physiology

ORIGINAL RESEARCH
published: 11 January 2021
doi: 10.3389/fphys.2020.619230

Rapid, Nitric Oxide Synthesis-Dependent Activation of MMP-9 at Pericyte Somata During Capillary Ischemia *in vivo*

Robert G. Underly[1] *and Andy Y. Shih*[1,2,3,4]*

[1] Department of Neuroscience, Medical University of South Carolina, Charleston, SC, United States, [2] Center for Developmental Biology and Regenerative Medicine, Seattle Children's Research Institute, Seattle, WA, United States, [3] Department of Pediatrics, University of Washington, Seattle, WA, United States, [4] Department of Bioengineering, University of Washington, Seattle, WA, United States

Nitric oxide serves essential roles in normal vascular physiology, but paradoxically contributes to vascular pathology in disease. During brain ischemia, aberrant nitric oxide levels can cause cellular injury through induction of nitrosative/oxidative stress and post-translational activation of matrix-metalloproteinase-9 (MMP-9). We recently demonstrated that brain pericyte somata were associated with very early and localized MMP-9 activation along capillaries during cerebral ischemia, leading to focal blood-brain barrier disruption. Here, we tested whether this effect was dependent upon nitric oxide production. *In vivo* two-photon imaging was used to directly visualize MMP9 activity using a FITC-gelatin probe and leakage of intravenous dye during photothrombotically induced capillary ischemia. Results showed that the NOS inhibitor, L-NIL, at concentrations affecting both iNOS and constitutive NOS isoforms, attenuated capillary leakage at pericyte soma-specific locations and substantially reduced FITC-gelatin cleavage. We also found that combined administration of L-NIL and anisomycin, an inhibitor of protein synthesis, led to near complete elimination of FITC-gelatin cleavage and vascular leakage. These results indicate that both nitric oxide synthase and new protein synthesis are involved in the rapid activation of MMP-9 at somata of capillary pericytes during ischemia.

Keywords: pericyte, blood-brain barrier, ischemia, matrix-metalloproteinase-9, capillary, two-photon imaging, nitric oxide, stroke

OPEN ACCESS

Edited by:
Fabrice Dabertrand, University of Colorado, United States

Reviewed by:
Muge Yemisci, Hacettepe University, Turkey
Elizabeth Anne Vincent Jones, KU Leuven, Belgium

***Correspondence:**
Andy Y. Shih
Andy.Shih@SeattleChildrens.org

Specialty section:
This article was submitted to Vascular Physiology, a section of the journal Frontiers in Physiology

Received: *19 October 2020*
Accepted: *10 December 2020*
Published: *11 January 2021*

Citation:
Underly RG and Shih AY (2021) Rapid, Nitric Oxide Synthesis-Dependent Activation of MMP-9 at Pericyte Somata During Capillary Ischemia in vivo. Front. Physiol. 11:619230. doi: 10.3389/fphys.2020.619230

INTRODUCTION

During stroke, rapid activation of the proteolytic enzyme, matrix-metalloproteinase-9 (MMP9) leads to degradation of the neurovascular unit and compromise of the blood-brain barrier (BBB) (Gasche et al., 1999; Planas et al., 2001; Montaner, 2003; Fukuda et al., 2004). This process can occur within minutes to hours, and worsens stroke outcome by allowing brain entry of toxic

Abbreviations: BBB, blood-brain barrier; MMP-9, matrix metalloproteinase-9; NOS, nitric oxide synthase; iNOS, inducible nitric oxide synthase; eNOS, endothelial nitric oxide synthase; nNOS, neuronal nitric oxide synthase; PDGFRβ, platelet-derived growth factor beta; L-NIL, L-N6-(1-Iminoethyl)lysine.

blood molecules and by shortening the time window for thrombolytic treatment. Delineating the mechanisms of early BBB disruption in stroke may identify potential targets for therapeutic intervention. Pericytes, the mural cells of the brain's capillary bed, have been identified as cellular targets in treatment of acute stroke (Dalkara and Arsava, 2012; Zheng et al., 2020). Pericytes are uniquely sensitive to oxidative/nitrosative stress (Yemisci et al., 2009), and their death or aberrant contraction causes impaired cerebral perfusion during both ischemia and reperfusion phases of stroke (Hall et al., 2014; Hill et al., 2015). However, pericytes also appear to induce MMP-9 activity during neuroinflammation (Bell et al., 2012; Machida et al., 2015) and ischemia (Underly et al., 2017). Using *in vivo* two-photon imaging techniques, we recently showed that pericytes are spatially associated with rapid MMP-9 activation (within 10 min) during ischemia (Underly et al., 2017). This was an unexpected result considering that most prior studies have reported MMP-9 activation hours to days after the ischemic event (Weekman and Wilcock, 2015). To study rapid MMP-9 activity *in vivo*, we used two-photon microscopy to image mice with labeled pericytes, in combination with a well established probe of MMP-9 activity (FITC-gelatin). This was coupled with a photothrombotic model of capillary occlusion to induce ischemia during imaging, and then rapidly track its pathological consequence. These studies revealed extensive overlap between the somata of capillary pericytes, FITC-gelatin cleavage and leakage of blood plasma. These findings point to pericytes as a trigger for rapid MMP-9 activation, likely through induction of existing pools of MMP-9 or rapid MMP-9 expression. However, the prior studies did not delineate the upstream signals involved in pericyte-associated MMP-9 activation.

Nitric oxide (NO) is a diffusible signaling molecule integral for regulation and maintenance of vascular homeostasis (Bredt et al., 1990; Alderton et al., 2001). Nitric oxide is produced through the oxidation of L-arginine by three isoforms of nitric oxide synthase (NOS) which include neuronal NOS (nNOS), endothelial NOS (eNOS), and inducible NOS (iNOS). Two isoforms, nNOS and eNOS, are considered constitutively active in resting cells and also calcium dependent, while iNOS is activated through stimulation by pro-inflammatory cytokines and is calcium independent. Nitric oxide contributes to rapid post-translational modifications, including S-nitrosylation, tyrosine nitration, and S-glutathionylation, which can result in activation of a wide variety of proteins (Martínez-Ruiz et al., 2011; Bradley and Steinert, 2015). S-nitrosylation is the process by which NO reacts with cysteine thiol residues on proteins to form an S-nitrosylated derivative of the protein. Matrix metalloproteinases (MMPs) are a target for S-nitrosylation during pathological conditions involving rapid increases in NO bioavailability through activation of NOS. S-nitrosylation of MMP-9 has been shown to play a role in neuronal cell death (Gu et al., 2002), and may therefore also be involved in the rapid induction of MMP-9 by pericytes during microvascular ischemia. The purpose of this study was to determine if NOS inhibition is sufficient to reduce MMP-9 activation and vascular leakage associated with pericytes during capillary ischemia *in vivo*.

RESULTS

Photothrombotically Induced Capillary Ischemia and FITC-Gelatin Imaging *in vivo*

We previously established a method to induce capillary ischemia *in vivo* during two-photon imaging, by using focal photothrombotic approach to occlude small regions of capillary bed in the cerebral cortex (**Figure 1A**; Underly and Shih, 2017). In this model, capillary ischemia results in cessation of flow in a population of capillaries (∼10–12 capillary segments) that are collectively contacted by ∼3–5 capillary pericytes. These ischemic capillary segments experience rapid peri-vascular activation of MMP-9, followed by blood plasma leakage. The sites of MMP-9 activation and leakage appear focal, and occur with twofold to threefold greater likelihood at capillary regions occupied by pericyte somata (Underly et al., 2017). Pericyte soma location was ascertained by using a mouse line in which pericytes were fluorescently labeled (PDGFRβ-tdTomato). These mice were intravenously injected with a 70 kDa Texas red-dextran dye to visualize the microvasculature (**Figures 1B–D**). The mice were further intracortically injected with a small volume of MMP-2/9 sensitive probe, FITC-gelatin, at the time of cranial window implantation. Altogether, this preparation enabled concurrent imaging of capillary pericyte location, MMP-2/9 activity, microvascular structure, and BBB breakdown with high spatiotemporal resolution *in vivo*. In conjunction with the photothrombotic model, which allows imaging immediately post-occlusion, very early pathological events associated with ischemia could be observed.

Plasma Leakage Occurs Predominately at Pericyte Somata While FITC-Gelatin Cleavage Occurs at All Leakage Sites

We first sought to reproduce results observed previously (Underly et al., 2017). We tracked the regions of capillary ischemia before photothrombosis, and every 15 min after photothrombosis for a period of 60 min (**Figure 1B**). As ischemia progressed, heterogeneous plasma leakage was observed, which manifested as bright fluorescent foci at the site of leakage onset, surrounded by a diffuse border of fluorescence. Since multiple time-points were imaged, we could identify the original location of leakage, even if the leaked dye diffused away in later time-points. Leakage sites occurred only following complete cessation of flow in the associated capillary segment (**Figure 1C**). We counted the number of leakage sites at locations containing pericyte somata and those devoid of pericyte somata. Consistent with our prior study, leakage sites occurred with significantly greater frequency (twofold) at pericyte somata compared to regions lacking somata (**Figure 1D**). All leakage sites contained localized increases in FITC-gelatin fluorescence, irrespective of pericyte location (**Figure 1E**). At very early time-points following photothrombosis, FITC-gelatin fluorescence could be seen prior to vascular leakage (**Figure 1E**, FITC-gelatin, 2nd row). In many cases, clear spatial overlap could be seen between this early

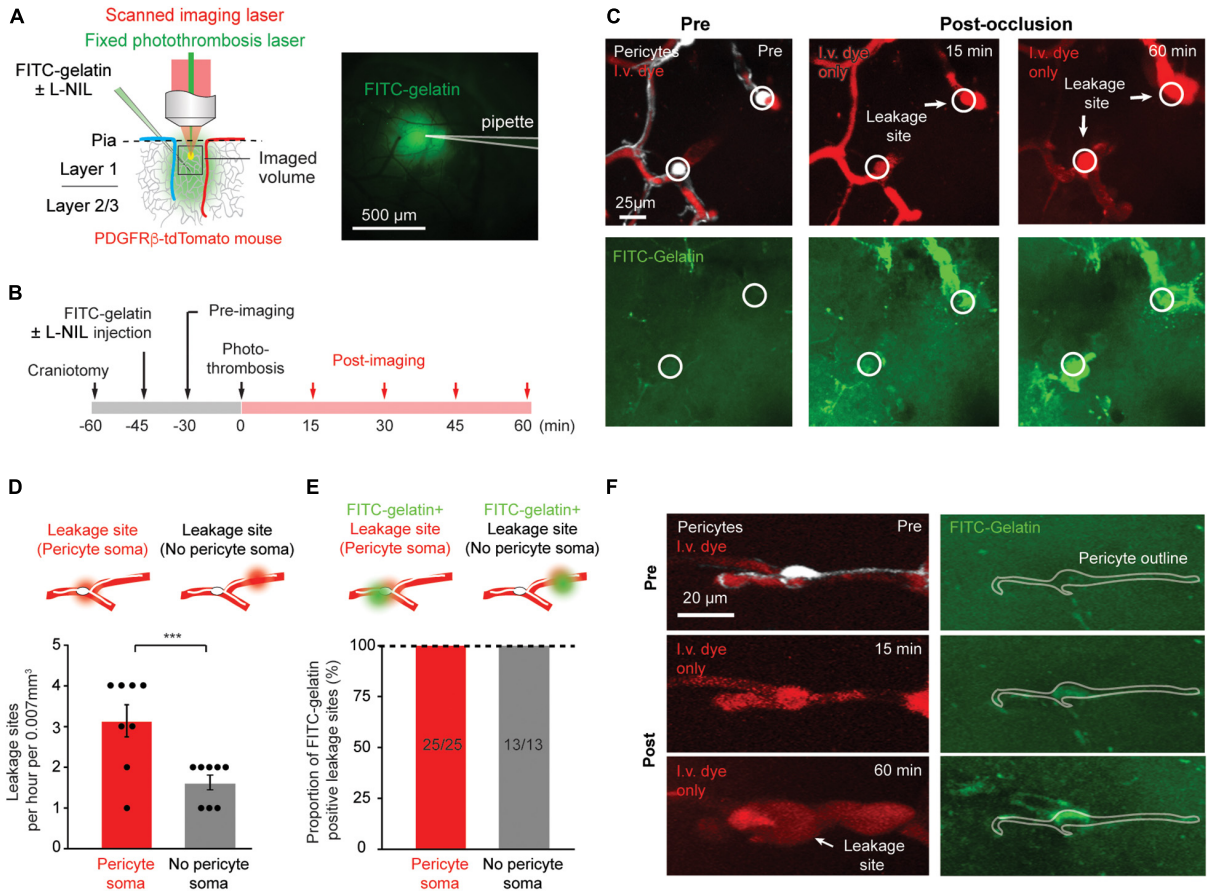

FIGURE 1 | Rapid MMP-9 activation and localized capillary leakage occurs preferentially at pericyte somata. **(A)** Left, Schematic of experimental approach. *In vivo* two-photon imaging is used to visualize multiple structures/processes: PDFGRβ-tdTomato mice for visualization of pericytes, intravenous Texas red-dextran dye for capillary structure and BBB leakage, FITC-gelatin for MMP-9 activity. A Ti:Sapphire scanned laser was used for imaging, while a fixed green continuous wave laser was used for photothrombotic occlusion of capillaries. Right, area of tissue labeled by intracortical FITC-gelatin pressure injection (with or without L-NIL). **(B)** Experimental timeline for surgical procedures and imaging. **(C)** Example of *in vivo* imaging data, with pericytes and/or i.v. dye visible in upper row, and FITC-gelatin fluorescence increase due to its cleavage by active MMP-2/9 in the bottom row. The locations of pericyte somata are marked with a circle. **(D)** Number of focal BBB leakage events occurring at pericyte soma or in non-soma regions. Leakage sites per hour per 0.007 mm^3: 3.125 ± 0.398 (pericyte soma), 1.625 ± 0.183 (no pericyte soma). Paired *t*-test: $t(7) = 5.612$, $^{***}p = 0.0008$, $N = 8$ mice (one region imaged per mouse) for each treatment group. Data is presented as mean ± S.E.M. **(E)** Proportion of leakage sites that are positive for FITC-gelatin cleavage. Each bar shows FITC-gelatin positive leakage sites over total number of leakage sites observed. **(F)** Example of marked co-localization between pericyte soma and early FITC-gelatin activation.

FITC-gelatin accumulation and the tdTomato-positive pericyte soma, suggesting that the pericytes themselves might be a source of active MMP-9 (**Figure 1F**). Critically, our past work also showed that FITC-gelatin cleavage at pericyte somata was dependent on MMP-9, rather than MMP-2 using isoform specific inhibitors (Underly et al., 2017). We therefore refer to FITC-gelatin cleavage also as MMP9 activation in this context.

Pericyte Leakage Is Attenuated With a Concentration of L-NIL That Inhibits eNOS/nNOS, but Not iNOS Alone

To determine if NOS activity could be involved in the observed rapid activation of MMP-9, we intra-cortically injected the moderately selective iNOS inhibitor, L-N6-(1-Iminoethyl)lysine (L-NIL), together with FITC-gelatin 30 min prior to photothrombosis. Two doses of L-NIL were tested: A lower dose expected to inhibit primarily iNOS (3.8 µM) and a higher dose (19 µM) expected to begin inhibiting constitutive forms, nNOS and eNOS as well. The low-dose of 3.8 µM affected neither the occurrence of vascular leakage nor MMP-9 activation (**Figures 2A,B,D,E**). However, the higher dose (19 µM) significantly reduced leakage events and MMP-9 activation occurring at pericyte soma locations (**Figures 2C–E**). High-dose L-NIL had no effect on vascular leakage at locations lacking pericyte somata. FITC-gelatin cleavage was also reduced at leakage sites lacking pericyte somata, albeit to a lesser extent than at pericyte soma locations. Collectively, these data suggests that constitutive NOS forms (probably eNOS, for which L-NIL is slightly more selective) may be contributing to the overproduction of NO and rapid activation of MMP-9 at pericyte somata during capillary ischemia.

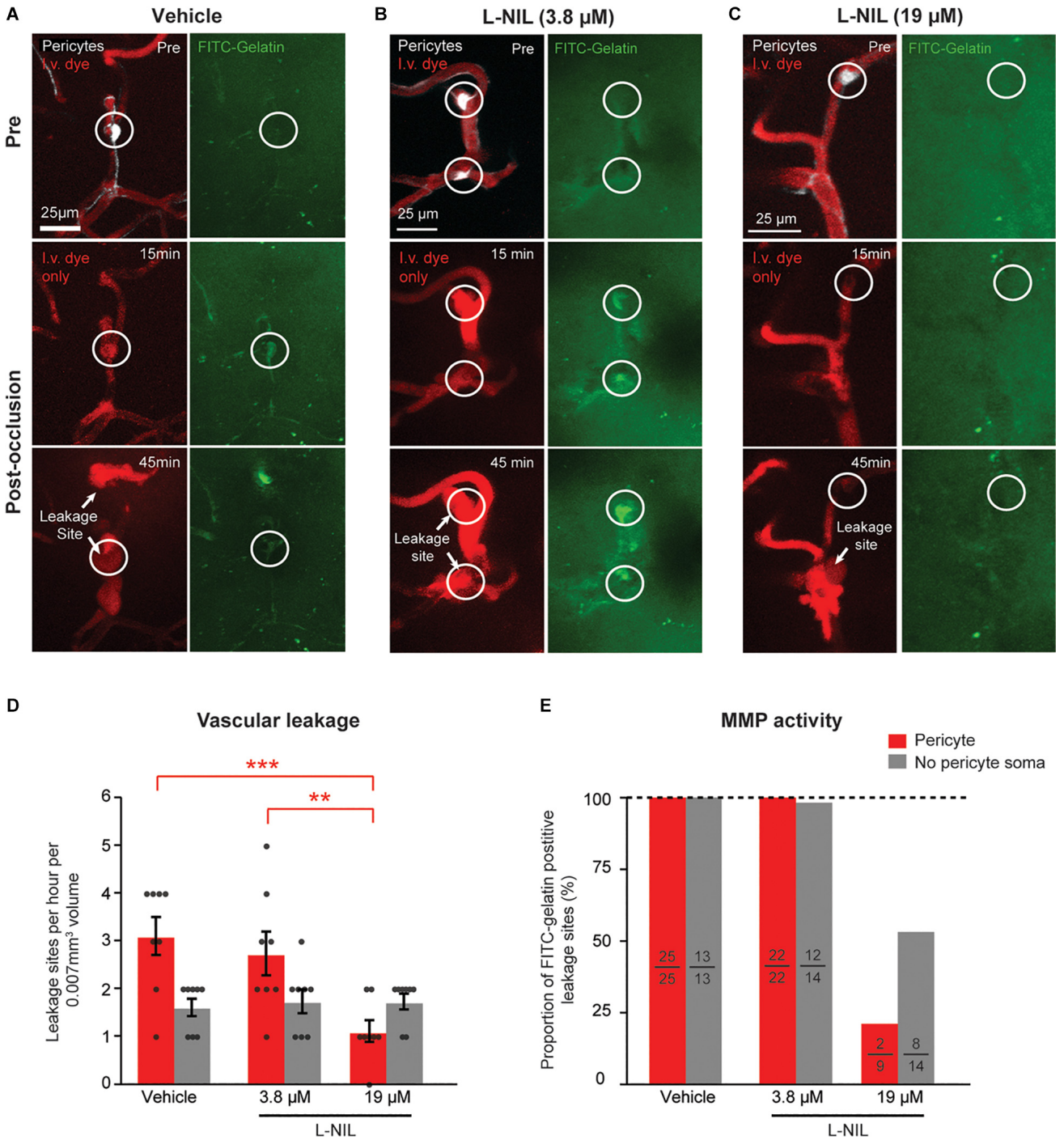

FIGURE 2 | Dose-dependent reduction of pericyte-associated BBB leakage and MMP-9 activity with intracortical L-NIL injection. **(A)** Representative example of vehicle injected control mouse (same example as in panel of **Figure 1F**). **(B,C)** Representative example of mice receiving low-dose (3.8 μM) and high-dose (19 μM) L-NIL. **(D)** Effect of L-NIL on number of BBB leakage occurring at pericyte soma and non-soma locations. Pericyte soma leakage sites per hour per 0.007 mm^3: 3.125 ± 0.398 (vehicle), 2.750 ± 0.453 (3.8 μM L-NIL), 1.125 ± 0.227 (19 μM L-NIL); No pericyte soma leakage sites per hour per 0.007 mm^3: 1.625 ± 0.183 (vehicle), 1.750 ± 0.250 (3.8 μM L-NIL), 1.750 ± 0.164 (19 μM L-NIL). One-way ANOVA with Bonferroni *post hoc* test; $F(5, 42) = 6.373$, $^*p = 0.045$ overall, $^{***}p = 0.0004$ (vehicle soma vs. 19 μM L-NIL soma), $^{**}p = 0.0052$ (3.8 μM L-NIL soma vs. 19 μM L-NIL soma); $N = 8$ mice (one region imaged per mouse) for each treatment group. Data is presented as mean ± S.E.M. **(E)** Proportion of leakage sites with FITC-gelatin cleavage at pericyte soma and non-soma locations with and without L-NIL. Each bar shows FITC-gelatin positive leakage sites over total number of leakage sites observed.

NOS Activity and Protein Synthesis Additively Inhibit Vascular Leakage and FITC-Gelatin Cleavage

We further asked whether rapid MMP-9 activation was entirely a post-translational process or also involved new protein synthesis. To test this, we administered the protein synthesis inhibitor, anisomycin (75 mg/kg, i.p.), either alone or in combination with intra-cortical injection of 19 μM L-NIL (**Figure 3**). Anisomycin is known the pass the BBB following i.p. injection, and has been shown to inhibit brain protein synthesis by ∼90% within 10 min after peripheral injection (Flood et al., 1973). Anisomycin reduced the number of leakage sites at pericyte somata significantly (**Figure 3E**), but had no effect on leakage sites away from pericyte somata (**Figure 3F**). The combination of high-dose L-NIL and anisomycin produced an additive reduction in leakage sites at pericyte somata, nearly eliminating their occurrence entirely (**Figures 3E,F**). The combination treatment had no effect on leakage sites lacking pericyte somata (**Figure 3F**).

We further compared the effects of anisomycin, alone or in combination with L-NIL on MMP-9 activity at leakage locations (**Figure 4**). Anisomycin reduced the percentage of FITC-gelatin positive leakage sites at pericyte somata by 25% (**Figure 4E**) and the percentage of non-pericyte leakage sites by 29% (**Figure 4F**). When the inhibitors were administered together, pericyte-specific leakage sites that were FITC-gelatin positive were completely eliminated (**Figure 4E**) and FITC-gelatin positive non-pericyte leakage sites were reduced by 87% (**Figure 4F**). Collectively, these results suggest that post-translation modification of MMPs, via NO, contributes more than protein synthesis in the activation of MMP 2/9 during capillary ischemia. However, both post-translational modification and new expression of MMP-9 may be involved in rapid activation of MMP-9 activity.

DISCUSSION

We have previously shown that pericytes are involved in very early BBB damage during ischemia, and that the vascular damage near their somata corresponds to rapid increases MMP-9 activity (Underly et al., 2017). The speed of this activation implied a post-translational modification of existing pro-MMP-9 pools. We extend these prior studies by examining NO production as a potential upstream signal that leads to this MMP-9 activation. Specifically, we show that pharmacological inhibition of NOS with L-NIL significantly reduces the number of sites of BBB breakdown. A low-dose that inhibits iNOS selectively had no effect, while higher dose that begins to inhibit both nNOS and eNOS as well, blocked both leakage and MMP-9 activity. We also find that MMP-9 activation can be further ameliorated with an inhibitor of protein synthesis, although NO-dependent mechanisms seemed to be the predominant pathway. The combination of both L-NIL and anisomycin led to an additive effect and led to near complete blockade of MMP-9 activity and leakage at pericyte somata, suggesting both mechanisms are at play. From this evidence we speculate that a post-translational modification of MMP-9 by NO (Gu et al., 2002) may be one of the key mechanisms of pericyte-associated BBB breakdown during ischemia. It also suggests that some of the salutary actions of NO inhibition in experimental stroke studies may, in part, be through reduction of pericyte-associated MMP9 activation and BBB disruption (Willmot et al., 2005).

Our findings add further weight to the notion of pericyte sensitivity in vascular pathology by showing that NO can act on pericyte MMP-9 activation very rapidly after ischemic onset. This is complementary to prior work showing that pericytes are exquisitely sensitive to nitrosative/oxidative stress during brain ischemia and (Yemisci et al., 2009). Yemisci et al. (2009) used NO scavengers to reduce aberrant pericyte contraction that could lead to impaired microcirculatory perfusion. More recently, it was shown that amyloid beta induces oxidase stress in pericytes in part through activation of NADPH oxidase 4 (Nox4) in pericytes, leading to their aberrant contraction (Nortley et al., 2019). In the context of amyloid beta toxicity, the NOS blocker L-NNA did not alter pericyte contraction, suggesting against a role for reactive nitrogen species in pericyte contraction and death. However, this may be different in the more rapid and severe pathology of ischemia, where reactive nitrogen species are likely to be produced. Indeed, a recent study by Nishimura et al. (2016) showed marked increase of Nox4 expression in brain pericytes after middle cerebral artery occlusion stroke, which corresponded with BBB breakdown. In parallel studies using pericyte culture, they linked Nox4 over-expression to upregulation of MMP9 gene expression through increased phosphorylation of NFκB. These gene expression changes were seen over longer durations of time after stroke (24–48 h) than the very acute stages studied here. However, they delineate a potential pathway through which anisomycin could block rapid, protein synthesis-dependent MMP9 activity in pericytes during ischemia.

While the source of NO is not entirely clear, it could conceivably be produced by the endothelium, which expresses RNA for eNOS (Nos1) at high levels, but also iNOS (Nos2) at lower levels in the normal brain microvasculature (Vanlandewijck et al., 2018). The proximate localization of the endothelium and pericytes makes for effective NO-MMP-9 interaction. Over-abundance of NO could also be derived from locally affected neurons that express nNOS. Though less well understood, mitochondrial NOS (mtNOS) may also be a potential source of NO from pericytes. Curiously, pericytes are more densely packed with mitochondria, compared to other neurovascular cell types, suggesting that mtNOS may be more prevalent in pericytes (Mathiisen et al., 2010). We further speculate that pericytes are a source of MMP-9 that can be rapidly expressed, or deployed in existing pro-enzyme pools. This is as opposed to infiltration of neutrophils, which have been described as a major source of MMP-9 in cerebral ischemia (reviewed by Turner and Sharp, 2016). Evidence for this comes from observation of clear co-localization in shape between tdTomato-positive pericytes and early FITC-gelatin activation. Also, the initiation of MMP-9 activity occurs in capillaries lacking blood flow, which could not support the recruitment of neutrophils. Other studies have also suggested that pericytes are a source of MMP-9 *in vivo* (Bell et al., 2012). However, further genetic studies to delete MMP-9 specifically

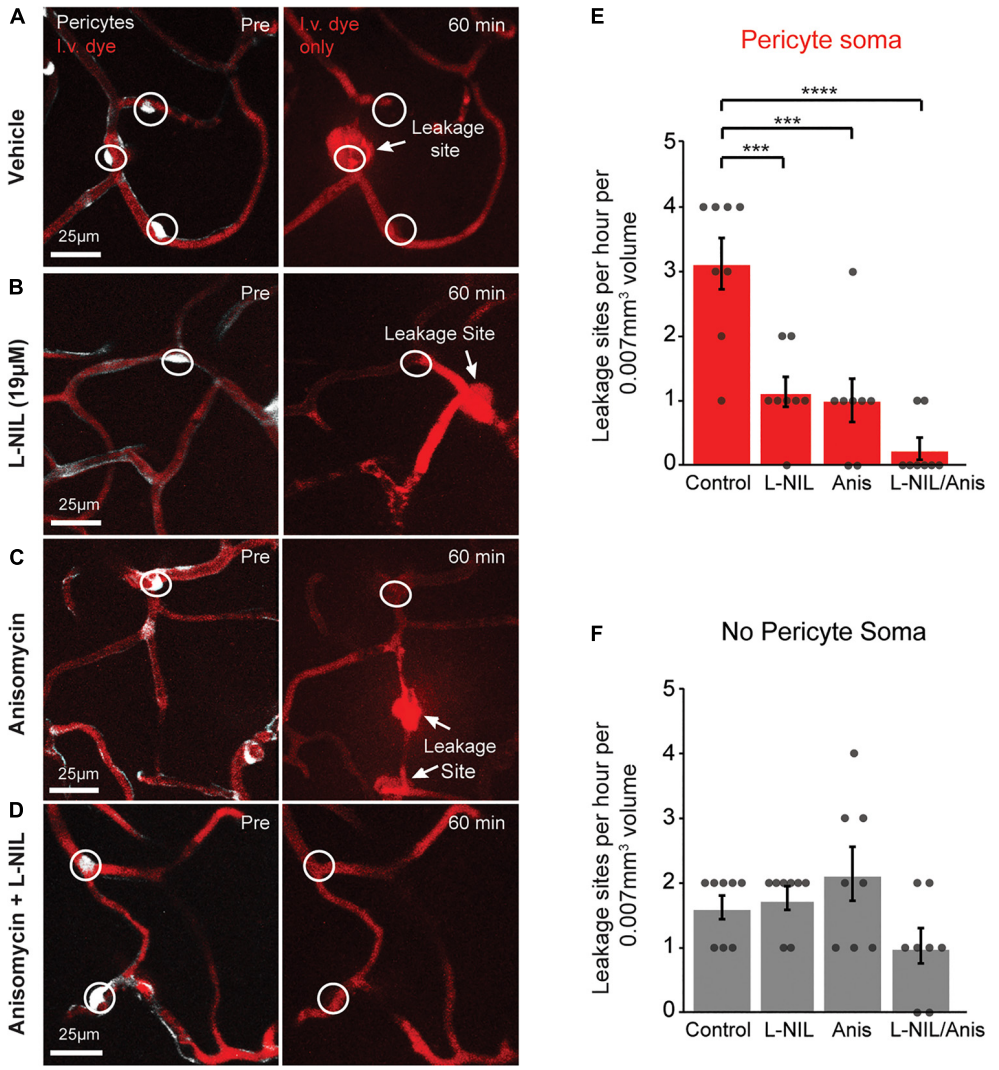

FIGURE 3 | Additive effect of L-NIL and anisomycin on pericyte-associated BBB leakage. **(A–D)** Representative examples of pericyte-associated BBB leakage in the vehicle group **(A)**, and with administration of high-dose L-NIL **(B)**, anisomycin **(C)**, and L-NIL + anisomycin **(D)**. **(E)** Effect of inhibitors on incidence of BBB leakage at pericyte somata. Pericyte soma leakage sites per hour per 0.007 mm^3: 3.125 ± 0.398 (veh), 1.125 ± 0.227 (19 μM L-NIL), 1.000 ± 0.327 (anisomycin), 0.250 ± 0.164 (19 μM L-NIL + anisomycin). One-way ANOVA with Bonferroni *post hoc* test; $F(3, 28) = 17.58$, $^{***}p < 0.0001$ overall, $^{***}p = 0.0003$ (vehicle vs. 19 μM L-NIL), $^{***}p = 0.001$ (vehicle vs. anisomycin), $^{****}p < 0.0001$ (vehicle vs. L-NIL + anisomycin); $N = 8$ mice (one region imaged per mouse) for each treatment group. Data is presented as mean ± S.E.M. **(F)** Effect of inhibitors on incidence of BBB leakage at non-soma locations. Non-soma leakage sites per hour per 0.007 mm^3: 1.625 ± 0.183 (veh), 1.750 ± 0.164 (19 μM L-NIL), 2.125 ± 0.398 (anisomycin), 1.000 ± 0.267 (19 μM L-NIL + anisomycin). One-way ANOVA with Bonferroni *post hoc* test; $F(3, 28) = 3.015$, $p = 0.05$ overall, non-significant; $N = 8$ mice (one region imaged per mouse) for each treatment group. Data is presented as mean ± SEM.

in pericytes at adulthood will be required to fully assess this possibility. Additionally, future work is also necessary to prove that the direct S-nitrosylation of MMP-9 occurs in pericytes. A further limitation is that anisomycin does not solely block the synthesis of MMP9. It is possible that inhibition of other MMP9 regulating proteins was involved in the observed reduction of MMP9 activity.

In summary, our results provide a basis for deeper mechanistic studies on pericytes as inducers of BBB disruption in stroke, and potentially other cerebrovascular diseases were MMP-9 has been implicated in microvascular pathology (Weekman and Wilcock, 2015). Pericytes are in direct apposition to the capillary endothelium making them a particularly ill-placed source of unchecked proteolytic activity. If they are indeed the source of rapid MMP-9 activation during ischemia, their pathological contributions to BBB damage may be significant, widespread, and readily overlooked by other biochemical approaches lacking spatiotemporal resolution to resolve the process. While aberrant NO and MMP-9 are well-established moderators of BBB damage during acute ischemia, our work has added pericytes as a site of convergence for these mechanisms.

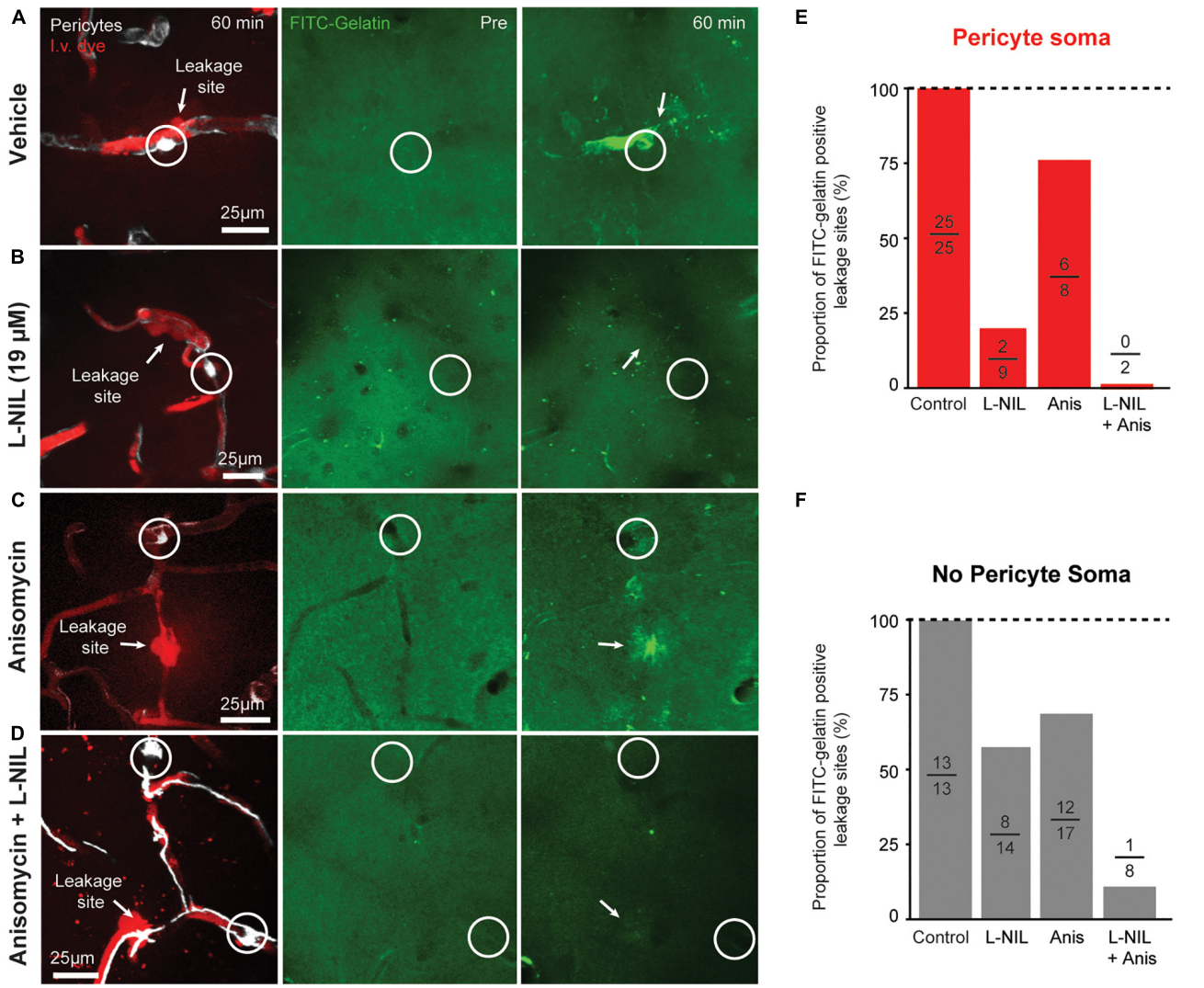

FIGURE 4 | Additive effect of L-NIL and anisomycin on MMP-9 activity at both pericyte soma and non-soma locations. **(A–D)** Representative examples of pericyte-associated FITC-gelatin activation in the vehicle group **(A)**, and with administration of high-dose L-NIL **(B)**, anisomycin **(C)**, and L-NIL + anisomycin **(D)**. **(E,F)** Effect of inhibitors on proportion of leakage sites with FITC-gelatin activity at pericyte soma or non-soma locations. Each bar shows FITC-gelatin positive leakage sites over total number of leakage sites observed.

METHODS

Mice

Tdtomato reporter mice (Ai14) on a C57/Bl6 background were purchased from Jackson Labs (Jax #: 007914) (Madisen et al., 2010). These mice were crossed with PDGFRβ-Cre mice (Cuttler et al., 2011) to achieve transgene expression in pericytes. Mice were maintained in standard cages on a 12 h light-dark cycle, and housed five or less per cage. Both male and female mice were used, and all mice used were between 2 and 5 months of age.

Surgery

Skull-removed, dura-intact craniotomies (Mostany and Portera-Cailliau, 2008) were generated over the sensorimotor cortex to achieve optical access for two-photon imaging. Intracortical injections of FITC-gelatin and other drugs were performed (see below) when the craniotomies were generated and animals were imaged immediately after sealing the craniotomy with a coverslip. Anesthesia was induced with isoflurane (Patterson Veterinary) at 3% mean alveolar concentration in 100% oxygen and maintained at 1–2% during surgery. Body temperature was maintained at 37°C with a feedback-regulated heat pad. All animals were administered buprenorphine for analgesia prior to surgery at a concentration of 0.025 mg/kg.

In vivo Two-Photon Microscopy

Two-photon imaging was performed with a Sutter Moveable Objective Microscope and a Coherent Ultra II Ti:Sapphire

laser source. A wavelength of 800 nm was used for excitation of FITC-gelatin and Texas red-dextran. Excitation was tuned to 975 nm to successively capture tdTomato fluorescence at the start of each experiment. Green and red emission was simultaneously collected using ET525/70m and ET605/70m filter sets, respectively (Chroma Corp.). Throughout the duration of imaging, mice were maintained under light isoflurane (0.75%) supplied in medical air (20–22% oxygen and 78% nitrogen, moisturized by bubbling through water; AirGas Inc.). Pulse oximetry (MouseOx; Starr Life Sciences) was used to monitor blood oxygen saturation and heart rate to ensure that cardiovascular function was normal during imaging.

Procedures for vascular imaging and analysis have been described previously (Shih et al., 2012). Briefly, the blood plasma was labeled by infraorbital vein injection of 0.025 mL of Texas red-dextran (70 kDa, D-1830; Life Technologies) prepared at a concentration of 5% (w/v) in sterile saline. A 4-X, 0.13 NA air objective lens (UPLFLN 4X; Olympus) was used to generate vascular maps of the entire window for navigational purposes. High-resolution imaging was performed using a water immersion 20-X, 1.0 NA objective lens (XLUMPLFLN 20XW; Olympus). Image stacks for data analysis consisted of 200 μm (x) × 200 μm (y) × 150 μm (z) volumes of cortex (sensory region) starting from the pial surface. FITC-gelatin was homogeneously seen throughout this volume of tissue.

Photothrombotic Occlusions

Restricted photothrombotic capillary occlusions have been previous described (Underly and Shih, 2017). Briefly, a focused green laser (1 mW, 20 μm diameter at focal plane) was applied directly to the superficial capillary bed (avoiding pericyte somata) for 25 s following an infraorbital injection of Rose Bengal (0.013 mg/kg). This led to the diffuse irradiation of a population of capillaries surrounding the focal point of the laser.

Quantification of Capillary Leakage Sites

Image stacks collected *in vivo* using two-photon microscopy were rendered in 3-D using Imaris 7.7 Software (Bitplane). Lateral sampling was 0.41 μm per pixel and axial sampling was 1 μm per pixel. Vascular leakage was quantified from 3-D renderings of the Texas red-dextran labeled channel, and also confirmed in 2-dimensional images by scrolling through z-stacks with Fiji/ImageJ software. This method of quantification was previous described (Underly et al., 2017; Underly and Shih, 2017). Briefly, leakage events were defined as the localized permeation of Texas red-dextran from the intravascular space into the surrounding parenchyma. The sites of leakage were separated into pericyte soma-specific and non-pericyte soma leakage sites based on the localization of the pericyte soma to the central portion of the intravascular dye extravasation. These leakage sites were counted at each time point to give a cumulative total of the number of sites during the 1 h duration of the experiment.

In vivo Gelatin Zymography

A FITC-gelatin probe (Bozdagi et al., 2007) (DQ-Gelatin, D12054; Life Technologies), diluted to a concentration of 1 mg/mL in sterile PBS, was pressure injected into the cortex using a pulled glass pipette (10–20 μm tip diameter). The pipette tip was lowered 250 μm into the cortex following the removal of a circular portion of skull (∼2 mm) over the somatosensory area. A small incision was made in the dura mater using a 26-gauge syringe needle tip to facilitate entry of the glass pipette. FITC-gelatin was injected over 5 min using a Picospritzer (10–20 ms pulses, 5–15 psi, 0.5–2 Hz pulse frequency) until 200 nL was delivered. The injection pipette was then left in place for 10 min before removal from the cortex. The craniotomy was then overlaid with 1.5% agarose, as described previously (Shih et al., 2012), followed by a circular coverslip. The coverslip was fixed in position with dental cement prior to two-photon imaging. Quantification of "MMP-positive" cells was previously described (Underly et al., 2017). Cells that co-localized with pericyte somata (tdTomato) were counted as FITC-gelatin positive pericytes. Areas of heightened FITC-fluorescence that did not co-localize with pericyte somata, but exhibited some cellular morphology, were counted as FITC-gelatin positive non-pericytes.

Nitric Oxide Synthase Inhibition

L-NIL was prepared into stock solutions by dissolving 1 mg/mL L-NIL in sterile PBS and then diluting to working concentrations (3.8, 19 μM) in PBS, together with the FITC-gelatin, which was then injected intracortically.

Protein Synthesis Inhibition

Anisomycin was administered intraperitoneally at a concentration of 75 mg per kg of mouse body weight. Anisomycin was prepared by adding the minimum amount of 1 M HCL required to bring the drug into solution. Sodium hydroxide (1 M) was then added to bring the solution to a neutral pH. Saline was then added to bring the solution to the appropriate concentration (Wanisch and Wotjak, 2008). Intraperitoneal administration of anisomycin was done 30 min prior to taking the pre-occlusion imaging stack for the experiments. Capillary occlusions were made ∼35 min following anisomycin administration.

Statistics

All statistical analyses were performing using Graphpad PRISM 9 software. Statistical details are provided in the legend of each figure.

DATA AVAILABILITY STATEMENT

The raw data supporting the conclusions of this article will be made available by the authors, without undue reservation, to any qualified researcher. Source data is provided in **Supplementary Material**.

ETHICS STATEMENT

The animal study was reviewed and approved by IACUC of the Medical University of South Carolina.

AUTHOR CONTRIBUTIONS

RU performed the data collection and analysis. RU and AS wrote the manuscript. Both authors contributed to the article and approved the submitted version.

FUNDING

This work was supported by grants to AS from the NIH/NINDS (NS096997, NS106138, and NS097775) and NIH/NIA (AG063031 and AG062738).

SUPPLEMENTARY MATERIAL

The Supplementary Material for this article can be found online at: https://www.frontiersin.org/articles/10.3389/fphys.2020.619230/full#supplementary-material

REFERENCES

Alderton, W. K., Cooper, C. E., and Knowles, R. G. (2001). Nitric oxide synthases: structure, function and inhibition. *Biochem. J.* 357, 593–615. doi: 10.1042/bj3570593

Bell, R. D., Winkler, E. A., Singh, I., Sagare, A. P., Deane, R., Wu, Z., et al. (2012). Apolipoprotein E controls cerebrovascular integrity via cyclophilin A. *Nature* 485, 512–516. doi: 10.1038/nature11087

Bozdagi, O., Nagy, V., Kwei, K. T., and Huntley, G. W. (2007). In vivo roles for matrix metalloproteinase-9 in mature hippocampal synaptic physiology and plasticity. *J. Neurophysiol.* 98, 334–344. doi: 10.1152/jn.00202.2007

Bradley, S. A., and Steinert, J. R. (2015). Nitric Oxide-Mediated Posttranslational Modifications: Impacts at the Synapse. *Oxidative Med. Cell. longevity* 2016:5681036.

Bredt, D. S., Hwang, P. M., and Snyder, S. H. (1990). Localization of nitric oxide synthase indicating a neural role for nitric oxide. *Nature* 347, 768–770. doi: 10.1038/347768a0

Cuttler, A. S., Leclair, R. J., Stohn, J. P., Wang, Q., Sorenson, C. M., Liaw, L., et al. (2011). Characterization of Pdgfrb-Cre transgenic mice reveals reduction of ROSA26 reporter activity in remodeling arteries. *Genesis* 49, 673–680. doi: 10.1002/dvg.20769

Dalkara, T., and Arsava, E. M. (2012). Can restoring incomplete microcirculatory reperfusion improve stroke outcome after thrombolysis? *J. Cereb. Blood Flow Metabol.* 32, 2091–2099. doi: 10.1038/jcbfm.2012.139

Flood, J. F., Rosenzweig, M. R., Bennett, E. L., and Orme, A. E. (1973). The influence of duration of protein synthesis inhibition on memory. *Physiol. Behav.* 10, 555–562. doi: 10.1016/0031-9384(73)90221-7

Fukuda, S., Fini, C. A., Mabuchi, T., Koziol, J. A., Eggleston, L. L. J., and Del Zoppo, G. J. (2004). Focal cerebral ischemia induces active proteases that degrade microvascular matrix. *Stroke* 35:4.

Gasche, Y., Fujimura, M., Morita-Fujimura, Y., Copin, J.-C., Kawase, M., Massengale, J., et al. (1999). Early appearance of activated matrix metalloproteinase-9 after focal cerebral ischemia in mice: a possible role in blood—brain barrier dysfunction. *J. Cereb. Blood Flow Metabol.* 19, 1020–1028. doi: 10.1097/00004647-199909000-00010

Gu, Z., Kaul, M., Yan, B., Kridel, S. J., Cui, J., Strongin, A. Y., et al. (2002). S-nitrosylation of matrix metalloproteinases: Signaling pathway to neuronal cell death. *Science* 297, 1186–1190. doi: 10.1126/science.1073634

Hall, C. N., Reynell, C., Gesslein, B., Hamilton, N. B., Mishra, A., Sutherland, B. A., et al. (2014). Capillary pericytes regulate cerebral blood flow in health and disease. *Nature* 508, 55–60. doi: 10.1038/nature13165

Hill, R. A., Tong, L., Yuan, P., Murikinati, S., Gupta, S., and Grutzendler, J. (2015). Regional Blood Flow in the Normal and Ischemic Brain Is Controlled by Arteriolar Smooth Muscle Cell Contractility and Not by Capillary Pericytes. *Neuron* 87, 95–110. doi: 10.1016/j.neuron.2015.06.001

Machida, T., Takata, F., Matsumoto, J., Takenoshita, H., Kimura, I., Yamauchi, A., et al. (2015). Brain pericytes are the most thrombin-sensitive matrix metalloproteinase-9-releasing cell type constituting the blood-brain barrier in vitro. *Neurosci. Lett.* 599, 109–114. doi: 10.1016/j.neulet.2015.05.028

Madisen, L., Zwingman, T. A., Sunkin, S. M., Oh, S. W., Zariwala, H. A., Gu, H., et al. (2010). A robust and high-throughput Cre reporting and characterization system for the whole mouse brain. *Nat. Neurosci.* 13, 133–140. doi: 10.1038/nn.2467

Martínez-Ruiz, A., Cadenas, S., and Lamas, S. (2011). Nitric oxide signaling: classical, less classical, and nonclassical mechanisms. *Free Radical Biol. Med.* 51, 17–29. doi: 10.1016/j.freeradbiomed.2011.04.010

Mathiisen, T. M., Lehre, K. P., Danbolt, N. C., and Ottersen, O. P. (2010). The perivascular astroglial sheath provides a complete covering of the brain microvessels: An electron microscopic 3D reconstruction. *Glia* 9, 1094–1103. doi: 10.1002/glia.20990

Montaner, J. (2003). Matrix Metalloproteinase-9 Pretreatment Level Predicts Intracranial Hemorrhagic Complications After Thrombolysis in Human Stroke. *Circulation* 107, 598–603. doi: 10.1161/01.cir.0000046451.38849.90

Mostany, R., and Portera-Cailliau, C. (2008). A method for 2-photon imaging of blood flow in the neocortex through a cranial window. *J. Visualiz. Exp.* 2008:678.

Nishimura, A., Ago, T., Kuroda, J., Arimura, K., Tachibana, M., Nakamura, K., et al. (2016). Detrimental role of pericyte Nox4 in the acute phase of brain ischemia. *J. Cereb. Blood Flow Metabol.* 36, 1143–1154. doi: 10.1177/0271678x15606456

Nortley, R., Korte, N., Izquierdo, P., Hirunpattarasilp, C., Mishra, A., Jaunmuktane, Z., et al. (2019). Amyloid β oligomers constrict human capillaries in Alzheimer's disease via signaling to pericytes. *Sci.* 365:2020.

Planas, A. M., Solé, S., and Justicia, C. (2001). Expression and activation of matrix metalloproteinase-2 and -9 in rat brain after transient focal cerebral ischemia. *Neurobiol. Dis.* 8, 834–846. doi: 10.1006/nbdi.2001.0435

Shih, A. Y., Driscoll, J. D., Drew, P. J., Nishimura, N., Schaffer, C. B., and Kleinfeld, D. (2012). Two-photon microscopy as a tool to study blood flow and neurovascular coupling in the rodent brain. *J. Cereb. Blood Flow Metabol.* 32, 1277–1309. doi: 10.1038/jcbfm.2011.196

Turner, R. J., and Sharp, F. R. (2016). Implications of MMP9 for Blood Brain Barrier Disruption and Hemorrhagic Transformation Following Ischemic Stroke. *Front. Cell. Neurosci.* 10:56. doi: 10.3389/fncel.2016.00056

Underly, R. G., and Shih, A. Y. (2017). Photothrombotic induction of capillary ischemia in mouse cortex during in vivo two-photon imaging. *Bio Protoc.* 7:e2378.

Underly, R. G., Levy, M., Hartmann, D. A., Grant, R. I., Watson, A. N., and Shih, A. Y. (2017). Pericytes as inducers of rapid, matrix metalloproteinase-9 dependent capillary damage during ischemia. *J. Neurosci.* 37, 129–140. doi: 10.1523/jneurosci.2891-16.2017

Vanlandewijck, M., He, L., Mäe, M. A., Andrae, J., Ando, K., Del Gaudio, F., et al. (2018). A molecular atlas of cell types and zonation in the brain vasculature. *Nature* 554, 475–480. doi: 10.1038/nature25739

Wanisch, K., and Wotjak, C. T. (2008). Time course and efficiency of protein synthesis inhibition following intracerebral and systemic anisomycin treatment. *Neurobiol. Learning Memory* 90, 485–494. doi: 10.1016/j.nlm.2008.02.007

Weekman, E. M., and Wilcock, D. M. (2015). Matrix Metalloproteinase in Blood-Brain Barrier Breakdown in Dementia. *J. Alzheimer's Dis.* 49, 893–903. doi: 10.3233/jad-150759

Willmot, M., Gibson, C., Gray, L., Murphy, S., and Bath, P. (2005). Nitric oxide synthase inhibitors in experimental ischemic stroke and their effects on infarct

size and cerebral blood flow: a systematic review. *Free Rad. Biol. Med.* 39, 412–425. doi: 10.1016/j.freeradbiomed.2005.03.028

Yemisci, M., Gursoy-Ozdemir, Y., Vural, A., Can, A., Topalkara, K., and Dalkara, T. (2009). Pericyte contraction induced by oxidative-nitrative stress impairs capillary reflow despite successful opening of an occluded cerebral artery. *Nat. Med.* 15, 1031–1037. doi: 10.1038/nm.2022

Zheng, Z., Chopp, M., and Chen, J. (2020). Multifaceted roles of pericytes in central nervous system homeostasis and disease. *J. Cereb. Blood Flow Metabol.* 40, 1381–1401. doi: 10.1177/0271678x20911331

Conflict of Interest: The authors declare that the research was conducted in the absence of any commercial or financial relationships that could be construed as a potential conflict of interest.

frontiers in Cellular Neuroscience

ORIGINAL RESEARCH
published: 12 January 2021
doi: 10.3389/fncel.2020.610714

DL-3n-Butylphthalide Improves Blood–Brain Barrier Integrity in Rat After Middle Cerebral Artery Occlusion

Muyassar Mamtilahun[1], Zhenyu Wei[2], Chuan Qin[1], Yongting Wang[1], Yaohui Tang[1], Fan-xia Shen[3], Heng-Li Tian[4], Zhijun Zhang[1] and Guo-Yuan Yang[1,3]**

[1] Shanghai Jiao Tong University Affiliated Sixth People's Hospital, School of Biomedical Engineering, Shanghai Jiao Tong University, Shanghai, China, [2] University of Shanghai for Science and Technology Affiliated Shidong Hospital, Shanghai, China, [3] Department of Neurology, Ruijin Hospital, School of Medicine, Shanghai Jiao Tong University, Shanghai, China, [4] Department of Neurosurgery, Shanghai Jiao Tong University Affiliated Sixth People's Hospital, Shanghai Jiao Tong University, Shanghai, China

OPEN ACCESS

Edited by:
Daniela Carnevale,
Sapienza University of Rome, Italy

Reviewed by:
Giuseppe Faraco,
Weill Cornell Medicine, United States
Shinya Dohgu,
Fukuoka University, Japan

***Correspondence:**
Guo-Yuan Yang
gyyang@sjtu.edu.cn
Zhijun Zhang
zhangzj@sjtu.edu.cn

Specialty section:
This article was submitted to Non-Neuronal Cells, a section of the journal Frontiers in Cellular Neuroscience

Received: 29 September 2020
Accepted: 23 November 2020
Published: 12 January 2021

Citation:
Mamtilahun M, Wei Z, Qin C, Wang Y, Tang Y, Shen F-x, Tian H-L, Zhang Z and Yang G-Y (2021) DL-3n-Butylphthalide Improves Blood–Brain Barrier Integrity in Rat After Middle Cerebral Artery Occlusion. Front. Cell. Neurosci. 14:610714. doi: 10.3389/fncel.2020.610714

Objective: DL-3n-butylphthalide (NBP) has beneficial effects in different stages of ischemic stroke. Our previous studies have demonstrated that NBP promoted angiogenesis in the perifocal region of the ischemic brain. However, the molecular mechanism of NBP for blood–brain barrier protection in acute ischemic stroke was unclear. Here, we explored the neuroprotective effects of NBP on blood–brain barrier integrity in the acute phase of ischemic stroke in a rat model.

Methods: Adult male Sprague–Dawley rats ($n = 82$) underwent 2 h of transient middle cerebral artery occlusion and received 90 mg/kg of NBP for 3 days. Brain edema, infarct volume, surface blood flow, and neurological severity score were evaluated. Blood–brain barrier integrity was evaluated by Evans blue leakage and changes in tight junction proteins. We further examined AQP4 and eNOS expression, MMP-9 enzyme activity, and possible signaling pathways for the role of NBP after ischemic stroke.

Results: NBP treatment significantly increased eNOS expression and surface blood flow in the brain, reduced brain edema and infarct volume, and improved neurological severity score compared to the control group ($p < 0.05$). Furthermore, NBP attenuated Evans blue and IgG leakage and increased tight junction protein expression compared to the control after 1 and 3 days of ischemic stroke ($p < 0.05$). Finally, NBP decreased AQP4 expression, MMP-9 enzyme activity, and increased MAPK expression during acute ischemic stroke.

Conclusion: NBP protected blood–brain barrier integrity and attenuated brain injury in the acute phase of ischemic stroke by decreasing AQP4 expression and MMP-9 enzyme activity. The MAPK signaling pathway may be associated in this process.

Keywords: AQP4, blood-brain barrier, dl-3n-butylphthalide, edema, ischemic stroke

INTRODUCTION

Stroke is one of the leading causes of death and disability worldwide (Feigin et al., 2017). Due to a narrow treatment window, complex pathology, and limited treatment options, stroke ultimately causes patient disability or death, proving to be an enormous economic burden to families and society (Writing Group et al., 2016; Feigin et al., 2017). Approximately 87% of stroke cases are ischemic strokes in the clinic; from the moment cerebral vascular occlusion occurs, the brain tissue suffers a series of pathological cascades including energy failure, increase in reactive oxygen species (ROS), free radical formation, inflammation, and neuronal apoptosis, which could last for several days (Kalogeris et al., 2016). These pathological processes upregulate aquaporin 4 (AQP4) expression and enhance matrix metalloproteinase-9 (MMP-9) enzyme activity. Both AQP4 and MMP-9 increase water uptake and degradation of protein in the blood–brain barrier (BBB) tight junction, which is the main cause of brain edema (Ribeiro et al., 2006; Lakhan et al., 2013; Turner and Sharp, 2016). Brain edema leads to cerebral parenchymal swelling, increased intracranial pressure, and decreased blood flow (Rosenberg, 1999; Mamtilahun et al., 2019). Without medical treatment, edema can result in secondary brain injury and aggravate stroke prognosis.

In the normal brain, the BBB facilitates brain homeostasis by separating the brain tissues from the peripheral circulation. BBB disruption is a canonical pathological characteristic in the acute stage of stroke. It not only causes brain edema but also allows the passage of phagocytes, red blood cells, and metabolic products that induce inflammatory responses and neuronal cell death, which together contribute to the high mortality of ischemic stroke (Yang and Rosenberg Gary, 2011; Obermeier et al., 2013). Hence, targeting BBB protection may be a viable approach for acute ischemic stroke therapy.

Dl-3n-butylphthalide (NBP) is a synthesized drug that was first extracted from *Apium graveolens* Linn seeds (celery) and approved for clinical usage in China by the National Medical Products Administration of China in 2002 (Wang et al., 2018). Clinical and experimental studies have shown that NBP attenuates cerebral infarct size and neurobehavioral deficiency through multitargeted effects, including antiplatelet aggregation (Wang et al., 2016), improvement of mitochondrial functions, antithrombosis (Qin et al., 2019), and reduction of both neurovascular inflammation (Yang et al., 2019) and apoptosis (Zhang et al., 2010). Previously, we found that NBP treatment promoted middle cerebral artery (MCA) dilation and increased microvessel density in ischemic rats (Qin et al., 2019; Zhou et al., 2019). NBP was approved for acute ischemic stroke stage II clinical studies by the Food and Drug Administration (FDA) in 2016 (Wang et al., 2018). Even though there are extensive studies on the therapeutic effects of NBP in ischemic stroke, more robust evidence regarding its effects and underlying mechanisms is required to recommend universal clinical use. Particularly, the neuroprotective effects of NBP on BBB integrity and its underlying mechanism remain unclear. In the present study, we explored the effect of NBP on the functional and structural integrity of the BBB, and whether AQP4 and MMP-9 are involved in this process.

Abbreviations: AQP4, Aquaporin4; BBB, blood–brain barrier; EB, Evans blue; eNOS, endothelial nitric oxide synthase; LSCI, Laser speckle contrast imaging; MCAO, middle cerebral artery occlusion; MMP-9, matrix metalloproteinase-9; NBP, dl-3n-butylphthalide; mNSS, modified neurological severity scores; ROS, reactive oxygen species; CBF, cerebral blood flow; PFA, paraformaldehyde; ZO-1, zonula occludens-1.

MATERIALS AND METHODS

Experimental Design

The rat brain surgery procedure and experimental protocol were approved by the Institutional Animal Care and Use Committee (IACUC) of Shanghai Jiao Tong University, Shanghai, China. Adult male Sprague–Dawley (SD) rats ($n = 82$, Jiesijie Laboratory Animal Co., Shanghai, China), weighing 250–280 g, were used in this study. All rats were kept in a humidity-controlled house at 22–25°C with 12-h dark/light cycling, and were allowed to eat and drink freely. The SD rats underwent 2 h of transient middle cerebral artery occlusion (tMCAO) and were randomly assigned to NBP or vehicle (vegetable oil) treatment by daily oral gavage for 3 consecutive days. Cerebral blood flow was assessed using laser speckle contrast imaging (LSCI) at the five indicated time points (**Figure 1A**). Neurobehavioral outcomes of tMCAO rats were evaluated by neurological severity score (NSS) on days 1 and 3 after tMCAO, following which, rats were euthanized for further immunohistochemistry analysis. For Western blot and Evans blue analysis, the samples were collected from the indicated parts of the brain (**Figure 1B**). For immunostaining, five to seven animals in each group, with four brain sections from each animal were used. Next, four peri-infarct areas of each brain section were randomly chosen to take confocal images (**Figure 1C**).

Surgical Procedure for Transient Middle Cerebral Artery Occlusion

Ischemic brain injury was induced by tMCAO, as described in our previous studies (Li et al., 2013). Briefly, the rat was anesthetized with 4% isoflurane, and anesthesia was maintained with 2% isoflurane during the entire surgical procedure. The body temperature was maintained at 37 ± 0.5°C using a heating pad (RWD Life Science Co., Shenzhen, China). The left common carotid, internal carotid, and external carotid arteries were carefully isolated. A silicon coded 4-0 round top nylon suture (Covidien, Mansfield, MA, USA) was carefully inserted from the left external carotid artery into the internal carotid artery and the origin of the middle cerebral artery. The surface cerebral blood flow (CBF) was monitored, and a decrease to 80% of the baseline value was considered as MCA occlusion. Reperfusion was performed using a suture draw after 2 h of MCAO. To ensure reproducibility of the tMCAO model, the surface blood flow was monitored before and after MCAO, and after reperfusion. Blood oxygen (PO_2), blood carbon dioxide (PCO_2), blood pH, glucose (Glu), sodium (Na), and potassium (K) were determined using an i-STAT system (Abbott Point of Care Inc., Princeton, NJ, USA). NBP (purity > 99.5%) was obtained as a gift from Shijiazhuang Pharmaceutical Group Co. Ltd., China, and dissolved in vegetable oil. tMCAO rats were randomly divided into two groups: NBP

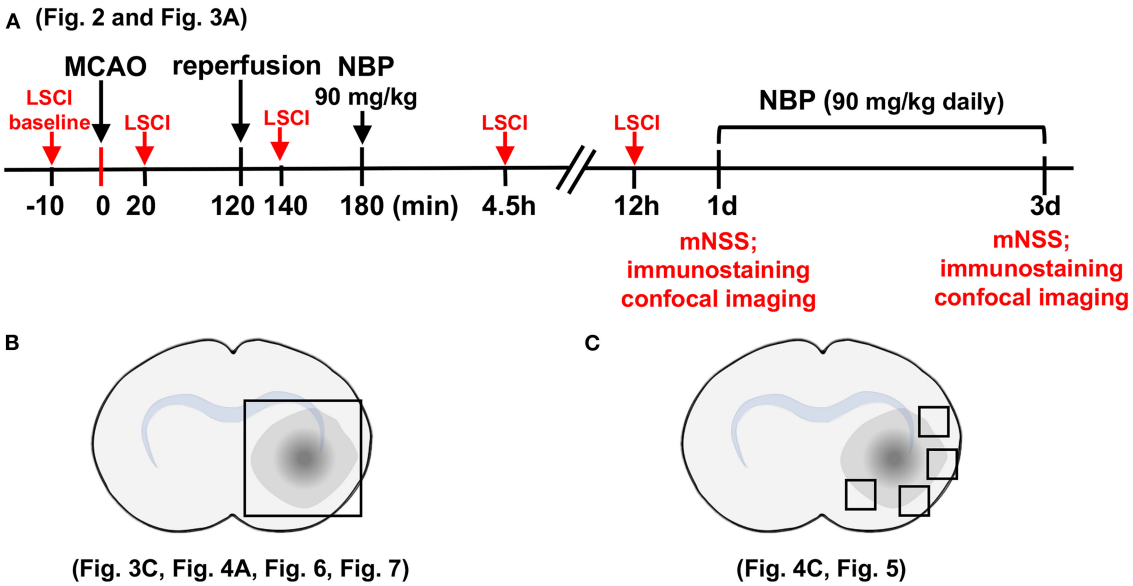

FIGURE 1 | Schematic for experimental design and brain regions used for immunofluorescence analysis. **(A)** Graph illustrates the experimental design and sample collection schedule. Male SD rats underwent transient middle cerebral artery occlusion (tMCAO) for 2 h; 90 mg/kg of dl-3n-butylphthalide (NBP) or vehicle was orally administered at 3 h after MCAO (1 h after reperfusion) for the first time, and then twice daily. The modified neurological severity scores (mNSS) scores were evaluated on day 1 and day 3 after tMCAO. **(B)** Photographs illustrate the brain samples collected after the neurobehavioral tests to evaluate gap formation in the blood–brain barrier (BBB) tight junction proteins. **(C)** Photographs illustrate brain regions used for immunostaining and analysis.

treated and control group. NBP (90 mg/kg) or equal volume of vegetable oil was orally administered 3 h after MCAO for the first-time treatment, and then twice daily until sacrificing the animals. MAPK signaling inhibitor PD98059 (10 mg/kg, Meilun, Dalian, China) were tail intravenously injected to rats 1 h before tMCAO as per manufacturers' instruction.

Evaluation of Neurological Severity Score

At 1 and 3 days after tMCAO, modified NSS (mNSS) was examined to evaluate animal neurological status including sensory, motor, reflex, and balance tests (Tang et al., 2014). The normal mNSS was 0, and the maximal deficit score was 14 (Li et al., 2000). Rats were raised by the tail, and the flexion of the forelimb was tested for motor function evaluation (0–3). Rats' gait was examined by placing them on the floor (0–3). For the beam balance test, rats were placed on a 60-cm-long beam, and their posture was examined (0–6). The sensory tests (0–2) for touch-reflex were used to assess the pinna and corneal reflex.

Laser Speckle Contrast Imaging

LSCI was performed using a high-resolution laser speckle contrast imaging system (LSCI-2 system, Dolphin BioTech Ltd., Shanghai, China). The imaging protocol has been described previously (Lin et al., 2013). After anesthetizing the rats, a midline incision was made on the scalp, and the skull was exposed. A dental drill was used to remove the surface of the skull until surface blood vessels were detected beneath the skull. Raw speckle images (696 × 512 pixels, 40 μm/pixel) were acquired at 23 fps (exposure time $T = 5$ ms) under 780 nm laser illumination. In each measurement, 20 consecutive frames of speckle images were detected and recorded. Image processing was carried out offline using MatLab software. In order to reduce the noise, the raw LSCI images were aligned using the registered laser speckle contrast analysis method (Wang et al., 2019). The registered speckle images were then analyzed using a random process estimator method to detect the contrast image with improved signal-to-noise ratio (Miao et al., 2010). Relative blood flow was calculated as described in our previous study (Lin et al., 2013). The CBF was detected using LSCI before MCAO, 10 min after occlusion, 20 min after reperfusion, and 4.5 and 12 h after occlusion in NBP-treated and control rats.

Assessment of Brain Edema and Ischemic Infarct Volume

Frozen brain sections 20 μm in thickness from the anterior commissure to the hippocampus were collected for immunohistochemistry. Serial frozen sections, 20 μm in thickness and 200 μm in interval from the frontal cortex were stained with 0.1% cresyl violet (Meilun Chemical Reagent Co., Dalian, China). Infarct volume was determined by subtracting the area stained with cresyl violet in the ipsilateral hemisphere from that of the contralateral hemisphere using the Image J software (NIH, Bethesda, MD, USA, RRID: SCR_003070), and then multiplying by section interval thickness.

$$\upsilon = \sum_{1}^{n} \left[\left(s_n + \sqrt{s_n \times s_{n+1}} + s_{n+1} \right) \times \frac{h}{3} \right]$$

The $h = 0.2$ mm represents the distance between each section, and S represents the area (mm^2) in each brain section.

Determining Permeability of the Blood-Brain Barrier

Rats were sacrificed after 1 and 3 days of tMCAO using a high dose of chloral hydrate (10%) anesthesia. The extravasation of Evans Blue (EB, Sigma-Aldrich, St. Louis, MO, USA) and IgG were used to assess BBB permeability. EB dye solution (2% EB dye in saline, 4 ml/kg) was injected through the left jugular vein at 4.5 h, 1 day, and 3 days after tMCAO (Tang et al., 2014). The rats were sacrificed via cardiac perfusion after 2 h of EB circulation under anesthetized conditions. Both brain hemispheres were weighed, and the samples were homogenized in 1 ml of 50% trichloroacetic acid solution to extract EB, followed by centrifugation at 12,000 g for 20 min. The supernatant was diluted with 100% ethanol at a ratio of 1:3. The amount of EB was quantified at 610 nm using a spectrophotometer (Bio-Tek, Winooski, VT).

IgG was examined as previously described (Tanno et al., 1992; Tang et al., 2014). Briefly, brain slices were fixed in 4% paraformaldehyde (PFA) solution, blocked in 10% bovine serum albumin (BSA), incubated in biotinylated antibody for 30 min at room temperature, and incubated in Avidin: Biotinylated Enzyme Complex (ABC) reagent (Vector Labs, Burlingame, CA, USA) for 30 min. DAB staining was used for the visualization of immune reactivity (Vector Labs, Burlingame, CA, USA), and the sections were counterstained with hematoxylin. We randomly chose four fields from the area of interest in each section and used the Image J software (NIH, Bethesda, MD, RRID: SCR_003070) for mean integrated optical density (IOD) analysis.

Immunohistochemistry

Brain sections were fixed for 10 min in cold methanol at 4°C, then blocked with 10% BSA for 1 h at room temperature after washing with PBS thrice. The brain sections were then incubated with antibodies against occludin (1:100, Invitrogen Cat# 33-1500, RRID: AB_87033), zonula occludens-1 (ZO-1, 1:100, Invitrogen Cat# 61-7300, RRID: AB_138452), and CD-31 (1:200, R&D Systems Cat# AF3628, RRID: AB_2161028) overnight at 4°C. The sections were stained with fluorescence-conjugated secondary antibodies for 1 h at 37°C after washing with PBS thrice. The gap length was shown as a percentage (%) of the whole tight junction staining. Similarly, four brain sections were stained for each animal, and four fields were randomly selected from each brain section (upper, middle, and bottom of the peri-infarct region), using confocal microscopy. Data were analyzed using the Image J software (NIH, Bethesda, MD, USA, RRID: SCR_003070).

Western Blot Analysis

At 1 and 3 days after tMCAO, fresh rat brains were collected and sectioned into 2-mm slices that included the ischemic core and peri-infarct areas in a rat brain mold (RWD Company, Shenzhen, China), and peri-infarct areas were collected from the ipsilateral cerebral hemisphere for the Western blotting experiments. Homogenizing buffer (RIPA with protease cocktail inhibitor, phosphatase inhibitor, and phenylmethanesulfonyl fluoride) was used for the brain sample collection. The homogenate was centrifuged at 12,000 *g*, and the pellets were discarded. Protein concentration was examined using a BCA kit (Meilun, Dalian, China), and 40 μg of protein from each group was loaded onto 10% resolving gel for electrophoresis. Then protein was transferred to a nitrocellulose membrane (GE Healthcare Life Sciences, Pittsburgh, PA, USA), and 5% skim milk was used for blocking. Next, the membranes were incubated with primary antibodies against AQP4 (1:1,000, Santa Cruz Biotechnology Cat# sc-58612, RRID:AB_781471), occludin (1:1,000, Invitrogen Cat# 33-1500, RRID: AB_87033), zonula occludens-1 (ZO-1, 1:1,000, Invitrogen Cat# 61-7300, RRID: AB_138452), eNOS (1:1,000, BD Biosciences Cat# 610298, RRID:AB_397692), phospho-MAPK (1:1,000, Cell Signaling Technology Cat# 4370, RRID:AB_2315112), MAPK (1:1,000, Cell Signaling Technology Cat# 4695, RRID:AB_390779), and β-actin (1:1,000, Santa Cruz Biotechnology Cat# sc-47778 HRP, RRID:AB_2714189) overnight at 4°C. HRP-conjugated secondary antibody and enhanced chemiluminescence substrate (Pierce, Rockford, IL, USA, www.piercenet.com) were used for visualization after washing thrice with TBST buffer. The results of chemiluminescence were assessed with an imaging system (Bio-Rad, Hercules, CA, USA, www.bio-rad.com). The relative levels of AQP4, occludin, ZO-1, and eNOS were normalized to that of β-actin. The pMAPK levels were normalized to those of total MAPK.

TABLE 1 | Analysis of blood parameters.

	Baseline		MCAO		Reperfusion		
	Oil	NBP	Oil	NBP	Oil	NBP	
sO_2	95.5 ± 0.5	95.1 ± 0.3	96.5 ± 0.2	95.2 ± 0.3	96.1 ± 0.9	95.6 ± 0.8	95–98%
PCO_2	51.4 ± 1.7	49.2 ± 1.2	42.8 ± 1.5	42.4 ± 1.1	46.2 ± 1.3	46.7 ± 1.7	41–51 mmHg
pH	7.35 ± 0.01	7.34 ± 0.01	7.40 ± 0.02	7.37 ± 0.01	7.37 ± 0.01	7.32 ± 0.02	7.31–7.41
PO_2	82 ± 0.38	82 ± 0.38	92.57 ± 3.21	92.57 ± 3.21	92.57 ± 2.89	92.57 ± 2.89	80–105 mmHg
Na	139.75 ± 0.75	138.57 ± 0.61	138.63 ± 0.63	138.71 ± 0.84	138.13 ± 0.77	139.5 ± 0.76	138–146
K	4.83 ± 0.12	4.84 ± 0.18	4.83 ± 0.17	4.89 ± 0.14	4.83 ± 0.23	4.74 ± 0.34	3.5–4.9
Glu	92.25 ± 8.11	97.0 ± 15.16	99.63 ± 6.31	93.20 ± 5.32	96.43 ± 8.69	90.86 ± 8.69	70–105

Blood parameters (sO_2, pO_2, pCO_2, K, Na, Glu) before and during the occlusion, and after reperfusion. Data are mean ± SD; n = 8 per group.

Real-Time PCR Analysis

Total RNA from brain tissue samples was isolated using TRIzol Reagent (Life Technologies). RNA concentration was examined using a spectrophotometer (NanoDrop 1000, Thermo Fisher) followed by a reverse transcription process using the PrimeScript RT reagent kit (TaKaRa, Dalian, China, www.takara.com.cn). SYBR Premix Ex Tag Kit (TaKaRa, Dalian, China) was used to perform real-time PCR. A two-stage RT-PCR amplification reaction was performed under the following conditions: 95°C for 30 s, followed by 40 cycles at 95°C for 5 s, and at 60°C for 30 s. The primer sequences were: AQP4 forward primer: 5′-GGGTTGGACCAATCATAGG CG-3′, reverse primer: 5′-GCAGGAAATCTGAGGCCAGTTCTAGG-3′; MMP-9 forward primer: 5′-CGCTGACAAGAAGTGGGGTTT−3′, reverse primer: 5′-TACAGATGGTGGATGCCTTTTA G−3′; GAPDH forward primer: 5′-TGAACGGGAAGCTCACTGG−3′, reverse primer: 5′-GCTTCACCACCTTCTTGATGTC-3′.

Gelatin Zymography

Previous zymography protocol was followed here (Cai et al., 2015). Briefly, 50 μg samples were diluted in the zymogram sample buffer (Bio-Rad) and electrophoresed using SDS-PAGE for ∼2.5 h. Then the gels were incubated four times in renaturing buffer (2.5% Triton X- 100, 50 mmol/L Tris-HCl) for 15 min each with gentle shaking, and then moved to developing buffer for 30 min with gentle shaking at room temperature. Next, gels were stained with Coomassie Blue (0.05% Coomassie Brilliant Blue, 30% methanol, 10% acetic acid) for 3 h after incubation in fresh developing buffer for 3 days at 37°C, and then 30% methanol containing 10% acetic acid was used for de-staining to achieve proper color contrast. The final bands were quantified using the Image J software (NIH, Bethesda, MD, USA, RRID: SCR_003070).

Statistical Analysis

Data are shown as mean ± SD. Statistical analysis was performed using SPSS and GraphPad PRISM 6.0 software (RRID: SCR_002798) for both parametric and non-parametric comparisons. Unpaired two-tailed Student's *t*-test (between two groups) and one-way ANOVA followed by Student–Newman–Keuls (among multiple groups) were used to evaluate statistical significance. Differences with $p < 0.05$ were considered significant.

RESULTS

NBP Attenuated Brain Edema, Increased Cerebral Blood Flow, and Improved Neurobehavioral Outcomes in Transient Middle Cerebral Artery Occlusion Rats

Blood parameters including pH, PCO_2, PO_2, sodium, potassium, and glucose concentration were measured before the surgery, 10 min after occlusion, and immediately after reperfusion. No significant changes in physiological parameters were detected

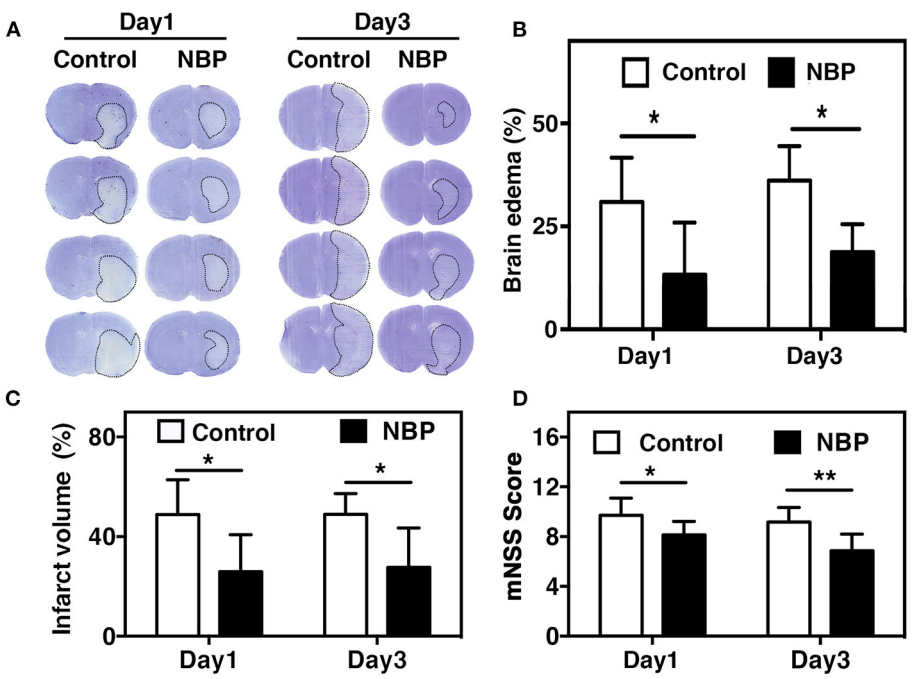

FIGURE 2 | NBP reduced edema and improved neurobehavioral outcomes in tMCAO rats. **(A)** Photomicrography represents the cresyl violet staining in NBP-treated and the control rats at 1 and 3 days after tMCAO. The dashed line indicates the border of the infarct area. Semi-quantification of the brain edema volume **(B)** and the infarct volume **(C)** in the NBP-treated and the control rats at 1 and 3 days after tMCAO. (**D)** Bar graph shows the mNSS assessment in the NBP-treated and the control rats at 1 and 3 days after tMCAO. Data are mean ± SD; $n = 8$ per group; $^*p < 0.05$ and $^{**}p < 0.01$; NBP-treated rats vs. control rats.

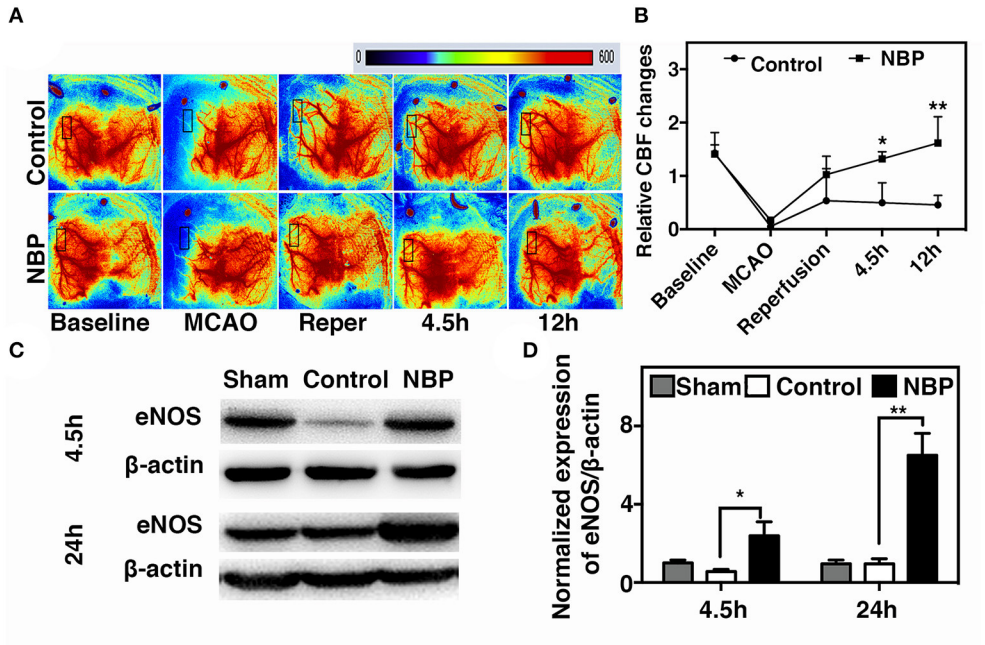

FIGURE 3 | NBP increased cerebral blood flow (CBF) in rats after tMCAO. **(A)** Photomicrographs show CBF measured by Laser speckle contrast imaging (LSCI) at the baseline, 10 min after MCAO, 10 min after reperfusion, and 4.5 and 12 h after occlusion in NBP-treated and control animals. **(B)** Bar graph shows the change in surface CBF in the ipsilateral hemisphere at different time points. Data are mean ± SD; $n = 5$ per group; $^{*}p < 0.05$ and $^{**}p < 0.01$; NBP-treated group vs. control animals. Bar graphs show Western blot images **(C)** and eNOS protein expression **(D)** in the NBP-treated and the control rats at 2.5 and 24 h after reperfusion. Data are mean ± SD; $n = 3$ per group; $^{*}p < 0.05$ and $^{**}p < 0.01$; NBP-treated group vs. control animals.

before and after tMCAO operation (**Table 1**). Since ischemia-induced BBB disruption could lead to brain edema, we measured brain edema and brain infarct volume in NBP-treated rats at 1 and 3 days after tMCAO. The results showed that the ischemic infarct area decreased in the NBP-treated rats compared to that of the control (**Figure 2A**). It was noted that the infarct area was limited to the striatum in the NBP-treated rats, while it was larger in both the cortex and striatum of control rats. NBP treatment also decreased the brain edema volume and infarct volume (**Figures 2B,C**) compared to the control after 1 and 3 days of tMCAO ($p < 0.05$). Meanwhile, the mNSS evaluation showed that NBP treatment reduced neurobehavioral deficiency after ischemic brain injury both at 1 and 3 days of tMCAO ($p < 0.01$, **Figure 2D**).

A laser speckle contrast imaging system was used to monitor CBF during tMCAO surgery and assess the CBF dynamic changes after NBP treatment. The results showed that NBP treatment significantly increased CBF after reperfusion ($p < 0.05$) and maintained the increase until 12 h after tMCAO ($p < 0.01$). Meanwhile, the control group showed a decreasing tendency in CBF changes after reperfusion (**Figures 3A,B**). To further explore which molecular mechanism induces increase in CBF, we examined endothelial nitric oxide synthase (eNOS) expression due to its role in vasodilation (Coletta et al., 2012). Our results showed that NBP treatment increased eNOS protein expression compared to the control at 4.5 and 24 h after occlusion (**Figures 3C,D**, $p < 0.05$), which could explain why CBF increased after NBP treatment.

DL-3n-Butylphthalide Protected Blood–Brain Barrier Integrity After Transient Middle Cerebral Artery Occlusion

To evaluate BBB functional integrity, we injected 2% Evans blue (EB) in the rats using the jugular vein on 4.5 h, day 1, and day 3 after tMCAO. EB extravasation was limited to the striatum of the ipsilateral hemisphere after NBP treatment, while EB extravasation was detected in both the striatum and cortex in the control group (**Figure 4A**), which was consistent with the cresyl violet staining results (**Figure 2A**). The quantification of EB results showed that the total amount of extravasated EB decreased in NBP-treated rats compared to the control at 1 and 3 days after tMCAO ($p < 0.01$, $p < 0.001$, **Figure 4B**). To further evaluate BBB permeability, we stained the brain sections with the IgG antibody to assess the severity of the IgG invasion at 1 and 3 days after tMCAO. Results showed that IgG invasion mainly occurred in the striatum of NBP-treated rat brains, while both striatum and cortex showed IgG invasion in the control (**Figure 4C**). Semi-quantification analyses showed that NBP treatment decreased IgG invasion compared to the control at 1 and 3 days after tMCAO ($p < 0.01$, $p < 0.05$, **Figure 4D**). Furthermore, to investigate whether NBP protected BBB structural integrity,

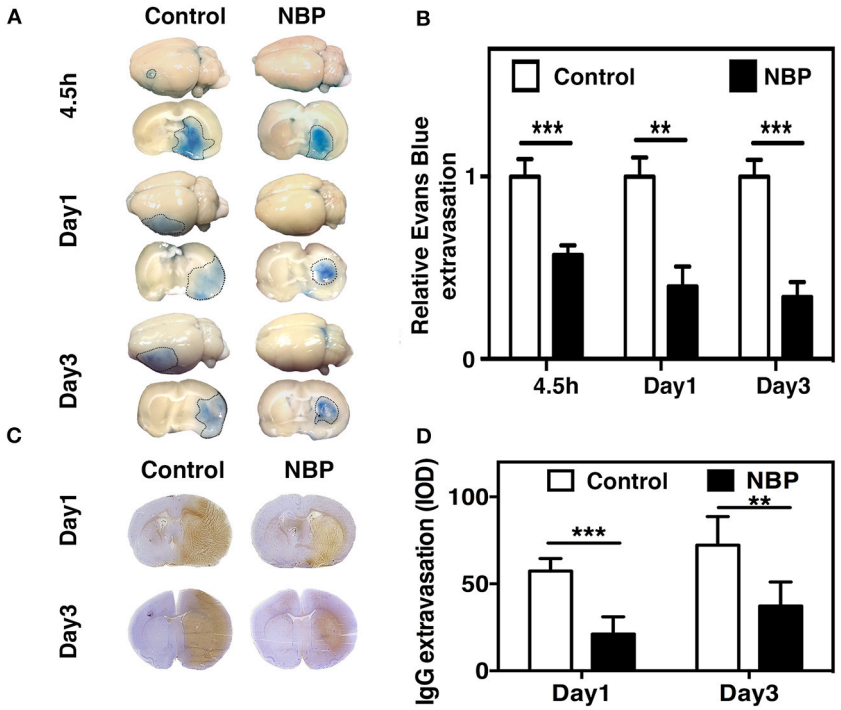

FIGURE 4 | NBP reduced BBB leakage in rats after tMCAO. **(A)** Photographs shows Evans blue (EB) exudation for the whole brain and brain sections in the NBP-treated and control rats at 1 and 3 days after tMCAO. The value of extravasated EB was recorded by a spectrophotometer at 610 nm (g). **(B)** Bar graph shows semi-quantification for the relative EB extravasation in the NBP-treated and the control rats at 4.5 h, 1 day, and 3 days after tMCAO. Data are mean ± SD; $n = 8$ per group; $^{**}p < 0.01$ and $^{***}p < 0.001$; NBP-treated rats vs. control rats. **(C)** Photographs show the IgG leakage in the ipsilateral hemisphere of NBP-treated and control rats following 1 and 3 days after tMCAO. **(D)** Bar graph shows semi-quantification of IgG extravasation in the NBP-treated and control rats. Data are mean ± SD; $n = 7$ per group; $^{**}p < 0.01$, and $^{***}p < 0.001$; NBP-treated rats vs. the control rats.

we stained the tight junction proteins ZO-1 and occludin with endothelial cell marker CD31. The confocal microscopy images showed that NBP treatment significantly attenuated ZO-1 and occludin-mediated gap formation in the microvessel wall induced by stroke, thereby preserving tight junction protein structural integrity at 1 and 3 days after tMCAO (**Figures 5A–D**).

DL-3n-Butylphthalide Preserved Blood–Brain Barrier Integrity by Decreasing AQP4 Expression and MMP-9 Activity After Transient Middle Cerebral Artery Occlusion

AQP4 overexpression and disruption of ionic balance contribute to brain edema after ischemic brain injury (Yang et al., 2007; Kleffner et al., 2008). Our results demonstrated that NBP could downregulate AQP4 expression at both the protein ($p < 0.01$, $p < 0.05$, **Figures 6A–D**) and mRNA levels ($p < 0.01$, **Figure 6E**). Occludin expression increased in NBP-treated rats at 1 and 3 days after tMCAO, while ZO-1 expression only increased at 3 days after tMCAO (**Figures 6A–D**, $p < 0.05$).

MMP-9 mediates BBB permeability by degrading tight junction proteins in the acute stage of stroke (Yang et al., 2007; Rosell et al., 2008). We next examined whether NBP had a protective effect on BBB permeability by reducing MMP-9 activity after ischemic brain injury. First, we found that MMP-9 at the mRNA levels decreased in the NBP-treated rats compared to the control after 1 and 3 days after tMCAO ($p < 0.05$, **Figure 6F**). Second, to evaluate the MMP-9 enzyme activity, gelatin zymography was performed in the NBP-treated and control rats at 1 and 3 days after tMCAO. Results showed that MMP-9 activity was reduced in the NBP-treated rats compared to the control rats at 3 days after tMCAO ($p < 0.01$, **Figures 7A,B**).

MAPK Signaling Pathway Involved in the Protective Role of DL-3n-Butylphthalide After Transient Middle Cerebral Artery Occlusion

To further explore the signaling pathway involved in the protective role of NBP on BBB integrity after tMCAO, we examined the MAPK signaling pathway. The results showed that MAP kinase phosphorylation decreased in the NBP-treated rats compared to the control at 3 days after tMCAO (**Figures 7C,D**, $p < 0.05$). PD98059 inhibited MAPK phosphorylation in PD98059+NBP-treated group compared to the control group after tMCAO and diminished the effect of NBP on MAPK phosphorylation (**Figures 7E,F**, $p < 0.05$).

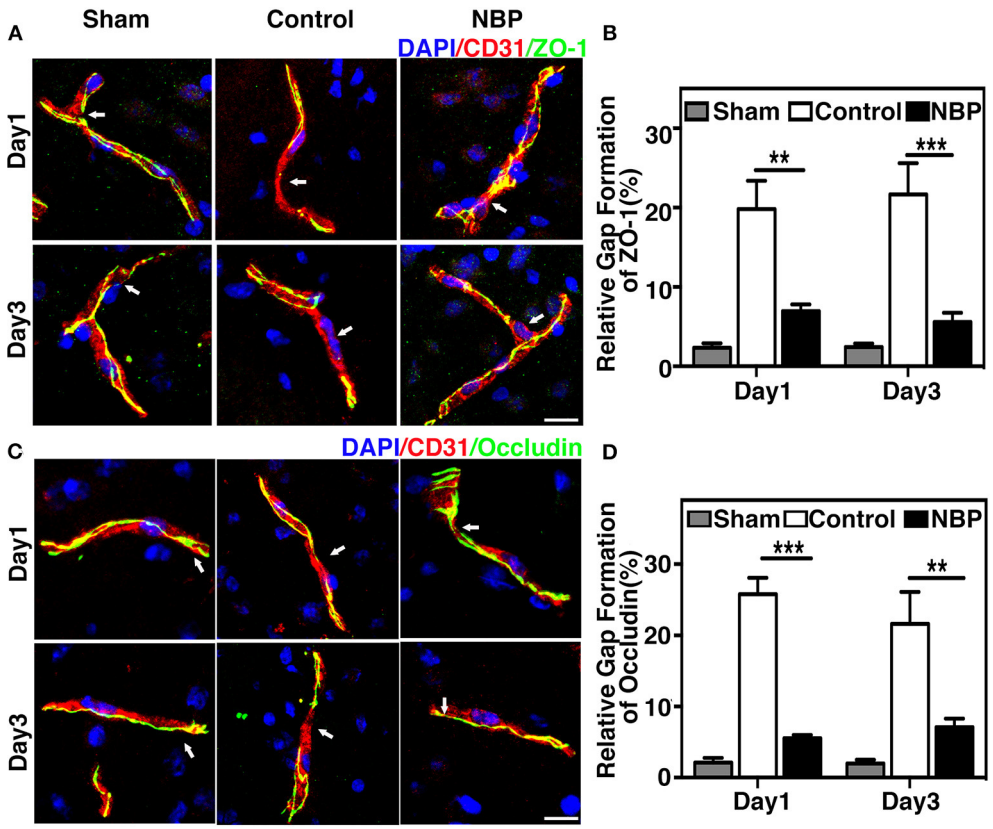

FIGURE 5 | NBP reduced BBB tight junction disruption in rats after tMCAO. **(A)** Photomicrographs show the ZO-1 (green) and CD31 (red) double immunostaining in the NBP treated and control rats at 1 and 3 days after tMCAO. Scale bar = 25 μm. **(B)** Bar graph shows the semi-quantification of gap length for ZO-1-positive staining. **(C)** Photomicrographs showed the occludin (green) and CD31 (red) double immunostaining in the NBP-treated and control rats at 1 and 3 days after tMCAO. Scale bar = 25 μm. **(D)** Bar graph shows the semi-quantification of gap length for occludin-positive staining. Data are mean ± SD; $n = 5$ per group; $^{**}p < 0.01$, $^{***}p < 0.001$; NBP-treated rats vs. the control rats.

DISCUSSION

In the present study, we demonstrated that NBP (1) attenuated ischemia-induced brain edema and neuronal death; (2) improved neurological function recovery; (3) inhibited AQP4 expression in the ischemic brain and reduced tight junction protein loss; (4) and partially inhibited MMP-9 expression and activity (5) through the possible MAPK signaling pathway associated in BBB disruption (**Figure 8**). Our results provide experimental evidence that NBP improves the damaged BBB integrity during brain edema, suggesting that NBP could be used for BBB disruption induced by ischemia or other brain diseases.

Ischemic brain injury is common; it causes neuronal apoptosis, inflammatory response, free radical oxidants, and BBB disruption (Feigin et al., 2017). The disrupted BBB allows vasculature-derived substances to infiltrate the brain, induces secondary brain injury and edema, and aggravates ischemic stroke outcomes (Sandoval and Witt, 2008). We chose days 1 and 3 after tMCAO because BBB damage occurs in the early stage after stroke (Rosenberg, 1999; Khatri et al., 2012). We present the data at days 1 and 3 to interpret the effect of NBP on BBB integrity after ischemia. NBP has been used in the acute phase after ischemic stroke after several studies demonstrated its neuroprotective effects including dilation of blood vessels, promotion of angiogenesis, suppression of inflammation, antioxidative stress, protection of the structure and function of mitochondria, and inhibition of thrombosis (Abdoulaye and Guo, 2016; Qin et al., 2019; Yang et al., 2019; Zhou et al., 2019). NBP also attenuated ischemic brain injury by decreasing infarct volume, neuronal apoptosis, and neurological deficits in the peri-infarct areas in a rat disease model (Li et al., 2010; Zhang et al., 2012a,b). Clinical and experimental studies showed that as a lipid-soluble drug, NBP could directly pass through the BBB and exert its protective effects on the brain (Liu et al., 2007; Cao et al., 2009; Liao et al., 2009; Wang et al., 2011; Zhang et al., 2012a, 2017). *In vitro* study showed that NBP could protect BBB tight junction protein by decreasing the endothelial intracellular ROS generation (Ye et al., 2019). Our results demonstrated that NBP had protective effects on the BBB in an acute ischemic stroke animal model. The results showed that NBP reduced tight junction protein loss and AQP4 expression. Since the inhibition of AQP4 protein ameliorated

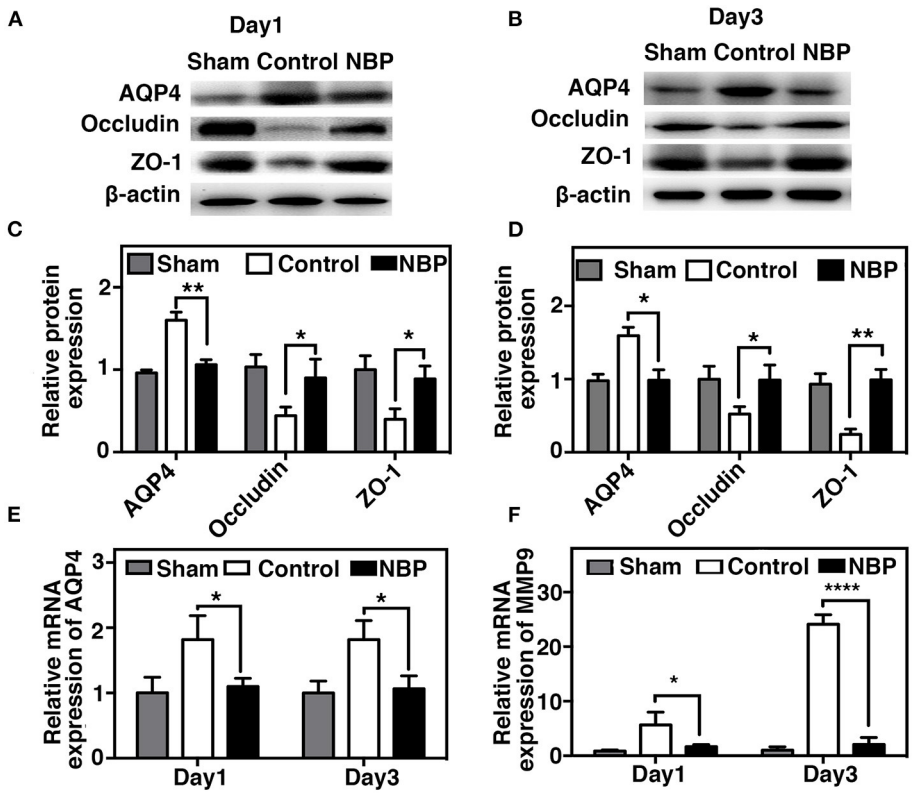

FIGURE 6 | NBP decreased AQP4 expression and tight junction protein loss after tMCAO. Photomicrographs showing the Western blot of AQP4, ZO-1, and occludin expression in the NBP-treated and control rats at 1 **(A)** and 3 days **(B)** after tMCAO. Bar graphs show the semi-quantification of AQP4, ZO-1, and occludin expression in the NBP-treated and control rats at 1 day **(C)** and 3 days **(D)** after tMCAO, and relative AQP4 **(E)** and matrix metalloproteinase-9 (MMP-9) **(F)** mRNA expression in the NBP-treated and control rats. Data are presented as mean ± SD; $n = 3$ per group; $^{*}p < 0.05$, $^{**}p < 0.01$, $^{****}p < 0.0001$; NBP-treated rats vs. control rats.

ischemic brain injury by reducing early cytotoxic brain edema, NBP may further protect the BBB from ischemia and reperfusion injury by downregulating AQP4. Preservation of the BBB tight junction proteins is essential for maintaining BBB integrity, which prevents secondary brain injury and is closely correlated with AQP4 downregulation (Tang et al., 2014; Filchenko et al., 2020). NBP has a therapeutic effect on the disrupted BBB in the early phase of ischemic stroke.

MMP-9 also plays a critical role in maintaining BBB integrity (Cai et al., 2015). Studies have shown that MMP-9 is not only involved in the pathogenesis of BBB disruption and subsequent vasogenic edema following stroke but also in hemorrhagic transformation (Lakhan et al., 2013; Shi et al., 2016). MMP-9 upregulation results in the degradation of tight junction proteins such as ZO-1, occludin, and the basal lamina, ultimately triggering BBB disruption and brain edema in the acute stage of stroke (Yang et al., 2007; Lee et al., 2013; Mamtilahun et al., 2019). The inhibition of MMP-9 could reverse this effect (Wang et al., 2012). Here, we found that NBP could inhibit MMP-9 mRNA expression and MMP-9 enzyme activity. NBP-mediated MMP-9 activity downregulation could reduce BBB tight junction protein degradation and protect BBB integrity.

Additionally, we found that NBP increased MAP kinase phosphorylation. Studies have shown that MAP kinase ERK1/2 modulates the internalization and degradation of tight junction proteins claudin-2, claudin-4, occludin, and ZO-1 (Rincon-Heredia et al., 2014; Stamatovic et al., 2017). Phosphorylation of MAPK is usually induced by pro-inflammatory stimuli; it also can be activated by growth factor (Sun and Nan, 2016). In the present study, we found that NBP treatment modulated the MAPK phosphorylation to the same level as the sham group after tMCAO, and treating with MAPK inhibitor reversed the result. Previous studies showed that NBP treatment upregulates the VEGF and basic fibroblast growth factor (bFGF) expressions in ischemic stroke patients and improve neurobehavioral recovery in rat ischemic stroke model (Liao et al., 2009; Tang et al., 2017; Zhou et al., 2019); growth factor binds to its receptor to activate MAPK by B-Raf (Kao et al., 2001). Taken together, the increased phosphorylation of MAPK may be due to the upregulated growth factor after NBP treatment, which is closely related to angiogenesis and long-term recovery after stroke. Our results support that NBP protects BBB integrity by increasing the phosphorylation of MAP kinase pathway after stroke.

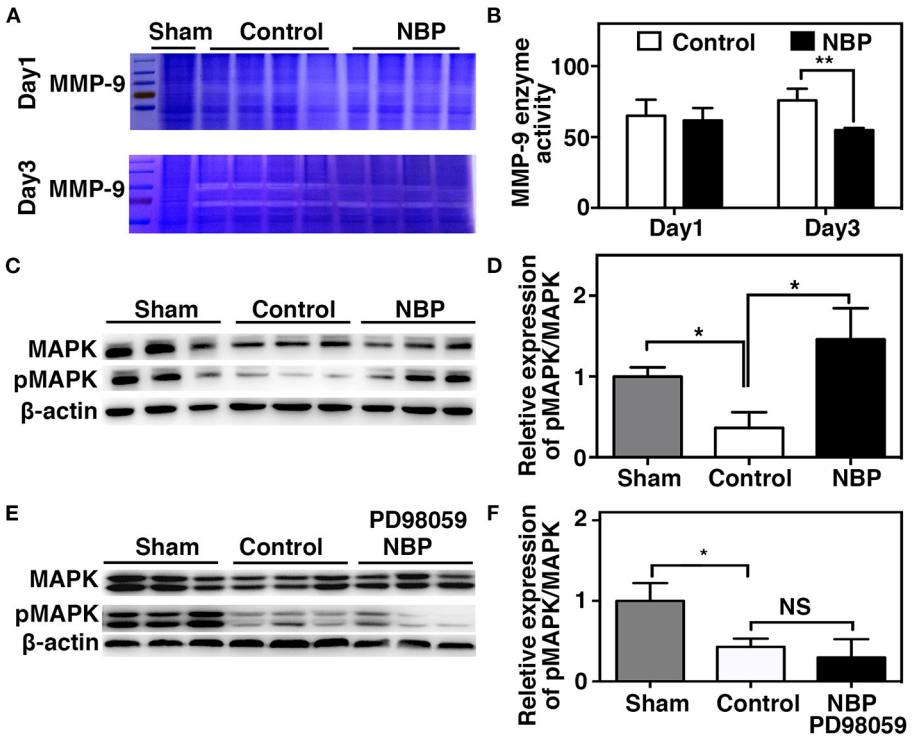

FIGURE 7 | NBP decreased MMP-9 enzyme activity, increased MAP kinases phosphorylation after tMCAO. **(A)** Photomicrograph shows zymography in NBP-treated and control rats at 1 and 3 days after tMCAO. **(B)** Bar graph shows the semi-quantification of active MMP-9 levels. Data are mean ± SD; $n = 4$ per group; $^{**}p < 0.01$; NBP-treated rats vs. control rats. **(C)** Photomicrograph showed a Western blot of MAP kinases phosphorylation in the NBP-treated, control, and sham rats. **(D)** Bar graph shows semi-quantification of phospho-MAP kinase at 3 days after tMCAO. **(E)** Photomicrograph showed a Western blot of MAP kinases phosphorylation in the sham, Control, and PD98059+NBP-treated rats. **(F)** Bar graph shows semi-quantification of phospho-MAP kinase at 3 days after tMCAO. Data are mean ± SD, $n =$ 3 per group; $^{*}p < 0.05$, $^{**}p < 0.01$; NBP-treated rats vs. control rats.

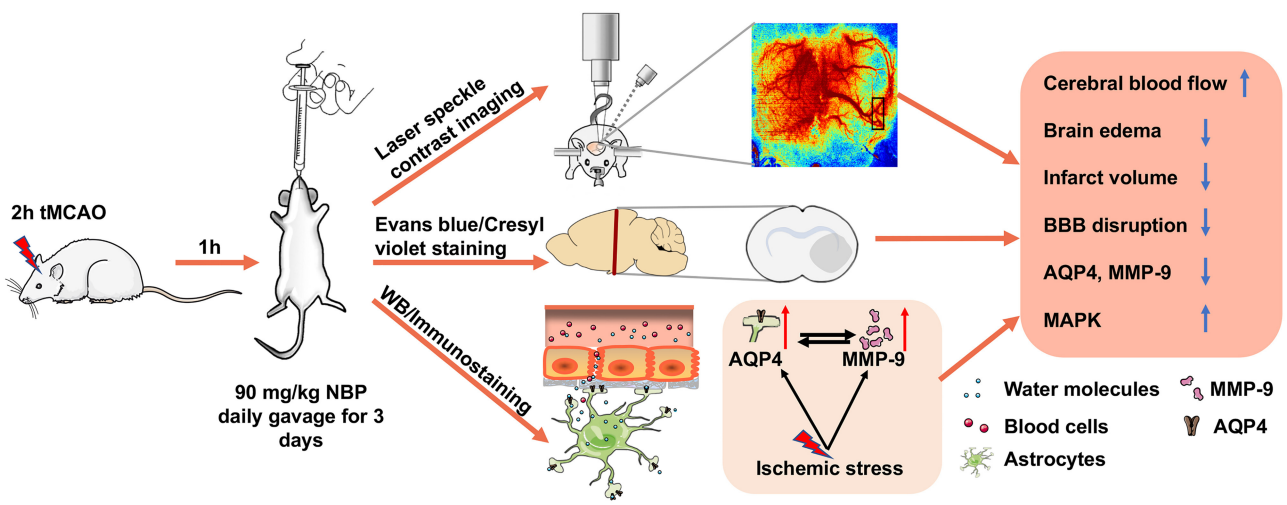

FIGURE 8 | Therapeutic effect of NBP during tMCAO. Diagram illustrates that adult SD rats underwent tMCAO and were treated with NBP for 3 days. The results demonstrated that NBP treatment could increase CBF of the ipsilateral hemisphere, attenuate infarct volume and brain edema, reduce BBB disruption, and inhibit ischemia-induced increase in AQP4 and MMP-9 expression, which is associated with MAP kinase phosphorylation.

CONCLUSION

Our study demonstrated that NBP treatment increased CBF and preserved BBB integrity by inhibiting AQP4 and MMP-9 enzyme activity. MAP kinases signaling pathways are possibly associated in this mechanism.

DATA AVAILABILITY STATEMENT

The original contributions presented in the study are included in the article/supplementary materials, further inquiries can be directed to the corresponding authors.

ETHICS STATEMENT

The animal surgery and experimental protocol were approved by the Institutional Animal Care and Use Committee (IACUC), Shanghai Jiao Tong University, Shanghai, China.

AUTHOR CONTRIBUTIONS

MM participated in the research design, all experimental procedures, animal surgery, data analysis, and drafting of the first manuscript. ZW and CQ contributed to animal surgery, behavioral tests, and data collection. YT provided technical assistance for *in vivo* and *in vitro* experiments. H-LT and YW were involved in discussion of the research design, the results, and edited the manuscript. G-YY and ZZ supervised all aspects including research design, data analysis, and manuscript preparation. All authors read and agreed to the final manuscript.

FUNDING

This study was supported by grants from the National Key Research and Development Program of China (2016YFC1300600), scientific research and innovation program of Shanghai Education Commission (2019-01-07-00-02-E00064, G-YY), the National Natural Science Foundation of China (81771244, ZZ; 81771251, G-YY; 81974179, ZZ; 81771281, F-xS; 81801170, YT; 81870921, YW), and the K. C. Wong Education Foundation (G-YY).

ACKNOWLEDGMENTS

We thank Peng Miao and Bing Bo for assisting the laser speckle contrast imaging data analysis and Shijiazhuang Pharmaceutical Group Co. Ltd. for providing NBP.

REFERENCES

Abdoulaye, I. A., and Guo, Y. J. (2016). A review of recent advances in neuroprotective potential of 3-N-butylphthalide and its derivatives. *Biomed. Res. Int*. 2016:5012341. doi: 10.1155/2016/5012341

Cai, H., Mu, Z., Jiang, Z., Wang, Y., Yang, G.-Y., and Zhang, Z. (2015). Hypoxia-controlled matrix metalloproteinase-9 hyperexpression promotes behavioral recovery after ischemia. *Neurosci. Bull.* 31, 550–560. doi: 10.1007/s12264-015-1533-1

Cao, W. Y., Deji, Q. Z., Li, Q. F., He, L., and Zhou, D. (2009). Effects of dl-3n-butylphthalide on the expression of VEGF and bFGF in transient middle cerebral artery occlusion rats. *Sichuan Da Xue Xue Bao Yi Xue Ban* 40, 403–407. doi: 10.1360/972009-495

Coletta, C., Papapetropoulos, A., Erdelyi, K., Olah, G., Módis, K., Panopoulos, P., et al. (2012). Hydrogen sulfide and nitric oxide are mutually dependent in the regulation of angiogenesis and endothelium-dependent vasorelaxation. *Proc. Natl. Acad. Sci. U.S.A.* 109, 9161–9166. doi: 10.1073/pnas.1202916109

Feigin, V. L., Norrving, B., and Mensah, G. A. (2017). Global burden of stroke. *Circ. Res.* 120, 439–448. doi: 10.1161/CIRCRESAHA.116.308413

Filchenko, I., Blochet, C., Buscemi, L., Price, M., Badaut, J., and Hirt, L. (2020). Caveolin-1 regulates perivascular aquaporin-4 expression after cerebral ischemia. *Front. Cell Develop. Biol.* 8:371. doi: 10.3389/fcell.2020.00371

Kalogeris, T., Baines, C. P., Krenz, M., and Korthuis, R. J. (2016). Ischemia/reperfusion. *Compr. Physiol.* 7, 113–170. doi: 10.1002/cphy.c160006

Kao, S., Jaiswal, R. K., Kolch, W., and Landreth, G. E. (2001). Identification of the mechanisms regulating the differential activation of the mapk cascade by epidermal growth factor and nerve growth factor in PC12 cells. *J. Biol. Chem.* 276, 18169–18177. doi: 10.1074/jbc.M008870200

Khatri, R., McKinney, A. M., Swenson, B., and Janardhan, V. (2012). Blood-brain barrier, reperfusion injury, and hemorrhagic transformation in acute ischemic stroke. *Neurology* 79, 52–57. doi: 10.1212/WNL.0b013e3182697e70

Kleffner, I., Bungeroth, M., Schiffbauer, H., Schäbitz, W.-R., Ringelstein, E. B., and Kuhlenbäumer, G. (2008). The role of aquaporin-4 polymorphisms in the development of brain edema after middle cerebral artery occlusion. *Stroke* 39, 1333–1335. doi: 10.1161/STROKEAHA.107.500785

Lakhan, S., Kirchgessner, A., Tepper, D., and Aidan, L. (2013). Matrix metalloproteinases and blood-brain barrier disruption in acute ischemic stroke. *Front. Neurol.* 4:32. doi: 10.3389/fneur.2013.00032

Lee, J. H., Cui, H. S., Shin, S. K., Kim, J. M., Kim, S. Y., Lee, J. E., et al. (2013). Effect of propofol post-treatment on blood–brain barrier integrity and cerebral edema after transient cerebral ischemia in rats. *Neurochem. Res.* 38, 2276–2286. doi: 10.1007/s11064-013-1136-7

Li, J., Li, Y., Ogle, M., Zhou, X., Song, M., Yu, S. P., et al. (2010). DL-3-n-butylphthalide prevents neuronal cell death after focal cerebral ischemia in mice via the JNK pathway. *Brain Res.* 1359, 216–226. doi: 10.1016/j.brainres.2010.08.061

Li, Q., Tang, G., Xue, S., He, X., Miao, P., Li, Y., et al. (2013). Silica-coated superparamagnetic iron oxide nanoparticles targeting of EPCs in ischemic brain injury. *Biomaterials* 34, 4982–4992. doi: 10.1016/j.biomaterials.2013.03.030

Li, Y., Chopp, M., Chen, J., Wang, L., Gautam, S. C., Xu, Y.-X., et al. (2000). Intrastriatal transplantation of bone marrow nonhematopoietic cells improves functional recovery after stroke in adult mice. *J. Cereb. Blood Flow Metabol.* 20, 1311–1319. doi: 10.1097/00004647-200009000-00006

Liao, S. J., Lin, J. W., Pei, Z., Liu, C. L., Zeng, J. S., and Huang, R. X. (2009). Enhanced angiogenesis with dl-3n-butylphthalide treatment after focal cerebral ischemia in RHRSP. *Brain Res.* 1289, 69–78. doi: 10.1016/j.brainres.2009.06.018

Lin, X., Miao, P., Wang, J., Yuan, F., Guan, Y., Tang, Y., et al. (2013). Surgery-related thrombosis critically affects the brain infarct volume in mice following transient middle cerebral artery occlusion. *PLoS ONE* 8:e75561. doi: 10.1371/journal.pone.0075561

Liu, C. L., Liao, S. J., Zeng, J. S., Lin, J. W., Li, C. X., Xie, L. C., et al. (2007). dl-3n-butylphthalide prevents stroke via improvement of cerebral microvessels in RHRSP. *J. Neurol. Sci.* 260, 106–113. doi: 10.1016/j.jns.2007.04.025

Mamtilahun, M., Tang, G., Zhang, Z., Wang, Y., Tang, Y., and Yang, G.-Y. (2019). Targeting water in the brain: role of aquaporin-4 in ischemic brain edema. *Curr. Drug Targets* 20, 748–755. doi: 10.2174/1389450120666190214115309

Miao, P., Li, N., Thakor, N. V., and Tong, S. (2010). Random process estimator for laser speckle imaging of cerebral blood flow. *Opt. Express*. 18, 218–236. doi: 10.1364/OE.18.000218

Obermeier, B., Daneman, R., and Ransohoff, R. M. (2013). Development, maintenance and disruption of the blood-brain barrier. *Nat. Med.* 19, 1584–1596. doi: 10.1038/nm.3407

Qin, C., Zhou, P., Wang, L., Mamtilahun, M., Li, W., Zhang, Z., et al. (2019). Dl-3-N-butylphthalide attenuates ischemic reperfusion injury by improving the function of cerebral artery and circulation. *J. Cereb. Blood Flow Metab.* 39, 2011–2021. doi: 10.1177/0271678X18776833

Ribeiro, M. d. C., Hirt, L., Bogousslavsky, J., Regli, L., and Badaut, J. (2006). Time course of aquaporin expression after transient focal cerebral ischemia in mice. *J. Neurosci. Res.* 83, 1231–1240. doi: 10.1002/jnr.20819

Rincon-Heredia, R., Flores-Benitez, D., Flores-Maldonado, C., Bonilla-Delgado, J., García-Hernández, V., Verdejo-Torres, O., et al. (2014). Ouabain induces endocytosis and degradation of tight junction proteins through ERK1/2-dependent pathways. *Exp. Cell Res.* 320, 108–118. doi: 10.1016/j.yexcr.2013.10.008

Rosell, A., Cuadrado, E., Ortega-Aznar, A., Hernández-Guillamon, M., Lo Eng, H., and Montaner, J. (2008). MMP-9–positive neutrophil infiltration is associated to blood–brain barrier breakdown and basal lamina type IV collagen degradation during hemorrhagic transformation after human ischemic stroke. *Stroke* 39, 1121–1126. doi: 10.1161/STROKEAHA.107.500868

Rosenberg, G. A. (1999). Ischemic brain edema. *Prog. Cardiovasc. Dis.* 42, 209–216. doi: 10.1016/S0033-0620(99)70003-4

Sandoval, K. E., and Witt, K. A. (2008). Blood-brain barrier tight junction permeability and ischemic stroke. *Neurobiol. Dis.* 32, 200–219. doi: 10.1016/j.nbd.2008.08.005

Shi, Y., Leak, R. K., Keep, R. F., and Chen, J. (2016). Translational stroke research on blood-brain barrier damage: challenges, perspectives, and goals. *Transl. Stroke Res.* 7, 89–92. doi: 10.1007/s12975-016-0447-9

Stamatovic, S. M., Johnson, A. M., Sladojevic, N., Keep, R. F., and Andjelkovic, A. V. (2017). Endocytosis of tight junction proteins and the regulation of degradation and recycling. *Ann. N. Y. Acad. Sci.* 1397, 54–65. doi: 10.1111/nyas.13346

Sun, J., and Nan, G. (2016). The mitogen-activated protein kinase (MAPK) signaling pathway as a discovery target in stroke. *J. Mol. Neurosci.* 59, 90–98. doi: 10.1007/s12031-016-0717-8

Tang, G., Liu, Y., Zhang, Z., Lu, Y., Wang, Y., Huang, J., et al. (2014). Mesenchymal stem cells maintain blood-brain barrier integrity by inhibiting aquaporin-4 upregulation after cerebral ischemia. *Stem Cells* 32, 3150–3162. doi: 10.1002/stem.1808

Tang, S. C., Luo, C. J., Zhang, K. H., Li, K., Fan, X. H., Ning, L. P., et al. (2017). Effects of dl-3-n-butylphthalide on serum VEGF and bFGF levels in acute cerebral infarction. *Eur. Rev. Med. Pharmacol. Sci.* 21, 4431–4436.

Tanno, H., Nockels, R. P., Pitts, L. H., and Noble, L. J. (1992). Breakdown of the blood–brain barrier after fluid percussive brain injury in the rat. Part 1: distribution and time course of protein extravasation. *J. Neurotrauma* 9, 21–32. doi: 10.1089/neu.1992.9.21

Turner, R. J., and Sharp, F. R. (2016). Implications of MMP9 for blood brain barrier disruption and hemorrhagic transformation following ischemic stroke. *Front. Cell. Neurosci.* 10:56. doi: 10.3389/fncel.2016.00056

Wang, J., Lin, X., Mu, Z., Shen, F., Zhang, L., Xie, Q., et al. (2019). Rapamycin increases collateral circulation in rodent brain after focal ischemia as detected by multiple modality dynamic imaging. *Theranostics* 9, 4923–4934. doi: 10.7150/thno.32676

Wang, S., Ma, F., Huang, L., Zhang, Y., Peng, Y., Xing, C., et al. (2018). Dl-3-n-butylphthalide (NBP): a promising therapeutic agent for ischemic stroke. *CNS Neurol. Disord. Drug Targets* 17, 338–347. doi: 10.2174/1871527317666180612125843

Wang, X., Li, Y., Zhao, Q., Min, Z., Zhang, C., Lai, Y., et al. (2011). Design, synthesis and evaluation of nitric oxide releasing derivatives of 3-n-butylphthalide as antiplatelet and antithrombotic agents. *Org. Biomol. Chem.* 9, 5670–5681. doi: 10.1039/c1ob05478c

Wang, X.-L., Wang, Z.-Y., Ling, J.-J., Zhang, Y.-H., and Yin, J. (2016). Synthesis and biological evaluation of nitric oxide (NO)-hydrogen sulfide (H(2)S) releasing derivatives of (S)-3-n-butylphthalide as potential antiplatelet agents. *Chin. J. Nat. Med.* 14, 946–953. doi: 10.1016/S1875-5364(17)30021-3

Wang, Z., Meng, C.-J., Shen, X.-M., Shu, Z., Ma, C., Zhu, G.-Q., et al. (2012). Potential contribution of hypoxia-inducible factor-1α, aquaporin-4, and matrix metalloproteinase-9 to blood-brain barrier disruption and brain edema after experimental subarachnoid hemorrhage. *J. Mol. Neurosci.* 48, 273–280. doi: 10.1007/s12031-012-9769-6

Writing Group, M., Mozaffarian, D., Benjamin, E. J., Go, A. S., Arnett, D. K., Blaha, M. J., et al. (2016). Heart disease and stroke statistics-2016 update: a report from the american heart association. *Circulation* 133, e38–e360. doi: 10.1161/CIR.0000000000000350

Yang, C.-S., Guo, A., Li, Y., Shi, K., Shi, F.-D., and Li, M. (2019). Dl-3-n-butylphthalide reduces neurovascular inflammation and ischemic brain injury in mice. *Aging Dis.* 10, 964–976. doi: 10.14336/AD.2019.0608

Yang, Y., Estrada, E. Y., Thompson, J. F., Liu, W., and Rosenberg, G. A. (2007). Matrix metalloproteinase-mediated disruption of tight junction proteins in cerebral vessels is reversed by synthetic matrix metalloproteinase inhibitor in focal ischemia in rat. *J. Cereb. Blood Flow Metab.* 27, 697–709. doi: 10.1038/sj.jcbfm.9600375

Yang, Y., and Rosenberg Gary, A. (2011). Blood–brain barrier breakdown in acute and chronic cerebrovascular disease. *Stroke* 42, 3323–3328. doi: 10.1161/STROKEAHA.110.608257

Ye, Z. Y., Xing, H. Y., Wang, B., Liu, M., and Lv, P. Y. (2019). DL-3-n-butylphthalide protects the blood-brain barrier against ischemia/hypoxia injury via upregulation of tight junction proteins. *Chin. Med. J.* 132, 1344–1353. doi: 10.1097/CM9.0000000000000232

Zhang, C., Zhao, S., Zang, Y., Gu, F., Mao, S., Feng, S., et al. (2017). The efficacy and safety of Dl-3n-butylphthalide on progressive cerebral infarction: a randomized controlled STROBE study. *Medicine* 96:e7257. doi: 10.1097/MD.0000000000007257

Zhang, L., Lü, L., Chan, W. M., Huang, Y., Wai, M. S., and Yew, D. T. (2012a). Effects of DL-3-n-butylphthalide on vascular dementia and angiogenesis. *Neurochem. Res.* 37, 911–919. doi: 10.1007/s11064-011-0663-3

Zhang, L., Yu, W. H., Wang, Y. X., Wang, C., Zhao, F., Qi, W., et al. (2012b). DL-3-n-Butylphthalide, an anti-oxidant agent, prevents neurological deficits and cerebral injury following stroke per functional analysis, magnetic resonance imaging and histological assessment. *Curr. Neurovasc. Res.* 9, 167–175. doi: 10.2174/156720212801618956

Zhang, T., Jia, W., and Sun, X. (2010). 3-n-Butylphthalide (NBP) reduces apoptosis and enhances vascular endothelial growth factor (VEGF) up-regulation in diabetic rats. *Neurol. Res.* 32, 390–396. doi: 10.1179/016164110X12670144526264

Zhou, P.-T., Wang, L.-P., Qu, M.-J., Shen, H., Zheng, H.-R., Deng, L.-D., et al. (2019). Dl-3-N-butylphthalide promotes angiogenesis and upregulates sonic hedgehog expression after cerebral ischemia in rats. *CNS Neurosci. Therap.* 25, 748–758. doi: 10.1111/cns.13104

Conflict of Interest: The authors declare that the research was conducted in the absence of any commercial or financial relationships that could be construed as a potential conflict of interest.

frontiers in Physiology

METHODS
published: 22 January 2021
doi: 10.3389/fphys.2020.612678

Chronic Cranial Windows for Long Term Multimodal Neurovascular Imaging in Mice

Kıvılcım Kılıç[1], Michèle Desjardins[2], Jianbo Tang[1,3], Martin Thunemann[1], Smrithi Sunil[1], Şefik Evren Erdener[1,4], Dmitry D. Postnov[1,5], David A. Boas[1] and Anna Devor[1]*

[1] Biomedical Engineering, Boston University, Boston, MA, United States, [2] Centre de recherche du CHU de Québec, Université Laval, Quebec City, QC, Canada, [3] Department of Biomedical Engineering, SUSTech, Shenzhen, China, [4] Institute of Neurological Sciences and Psychiatry, Hacettepe Üniversitesi, Ankara, Turkey, [5] Department of Biomedical Sciences, University of Copenhagen, Copenhagen, Denmark

Chronic cranial windows allow for longitudinal brain imaging experiments in awake, behaving mice. Different imaging technologies have their unique advantages and combining multiple imaging modalities offers measurements of a wide spectrum of neuronal, glial, vascular, and metabolic parameters needed for comprehensive investigation of physiological and pathophysiological mechanisms. Here, we detail a suite of surgical techniques for installation of different cranial windows targeted for specific imaging technologies and their combination. Following these techniques and practices will yield higher experimental success and reproducibility of results.

Keywords: imaging, multimodal, vascular, neural, mice, awake, chronic

OPEN ACCESS

Edited by:
Clotilde Lecrux, McGill University, Canada

Reviewed by:
Kazuto Masamoto, The University of Electro-Communications, Japan
Bernd Kuhn, Okinawa Institute of Science and Technology Graduate University, Japan

****Correspondence:***
Kıvılcım Kılıç
kkilic@bu.edu

Specialty section:
This article was submitted to Vascular Physiology, a section of the journal Frontiers in Physiology

Received: *30 September 2020*
Accepted: *18 December 2020*
Published: *22 January 2021*

Citation:
Kılıç K, Desjardins M, Tang J, Thunemann M, Sunil S, Erdener ŞE, Postnov DD, Boas DA and Devor A (2021) Chronic Cranial Windows for Long Term Multimodal Neurovascular Imaging in Mice. Front. Physiol. 11:612678. doi: 10.3389/fphys.2020.612678

INTRODUCTION

The utilization of multiple imaging modalities in neuroscience enables comprehensive investigation of brain structure and function. Each imaging technology has unique advantages and disadvantages. For example, while ultrasound (US) allows whole-brain imaging of cerebral blood flow, it cannot achieve micron resolution. On the other hand, two-photon (2-P) microscopy yields micron resolution but is limited by relatively shallow penetration (in common practice, limited to the upper cortical layers) and relatively small field of view (usually, <1 mm).

Previous studies have described design and surgical implantation of chronic cranial windows in mice enabling longitudinal measurements (Mostany and Portera-Cailliau, 2008; Holtmaat et al., 2009; Andermann et al., 2010; Goldey et al., 2014; Roome and Kuhn, 2014; Heo et al., 2016). These window implants allow imaging of awake mice, which is important for investigation of brain function without the confounding effects of anesthesia on the physiology of nervous and cardiovascular systems. Although some of these protocols are highly detailed, they usually employ imaging with one system. Here, we expand on these previous publications and describe a spectrum of surgical methods in mice suited for multiple imaging modalities, used alone or in combination, including 2-P microscopy, laser speckle contrast imaging (LSCI), intrinsic optical signal imaging (IOSI), optical coherence tomography (OCT), and functional US (fUS). These optical windows can last for a span of up to 6 months after surgery and can be made MRI-safe for combined optical imaging or optogenetic (OG) stimulation in awake mice undergoing fMRI.

METHODS

The protocols described below contain surgical procedures as well as pre- and post-operative measures. Common procedures are presented in the main text. Procedures specific for individual imaging modalities are presented in the **Supplementary Material**. All surgical procedures and imaging protocols were approved by the institutional Animal Care and Use Committee.

Pre-operative Measures

Adequate planning and preparation decrease the time spent during surgery and the risk of infection or inflammation leading to an overall increase in the success rate of surgery.

4 A's: Anesthesia, Analgesia, Antibiotics, and Anti-inflammatories

In our procedures we have used isoflurane for anesthesia, buprenorphine for analgesia, ibuprofen for analgesic, and anti-inflammatory properties, dexamethasone for prevention of inflammation and brain edema (Hedley-Whyte and Hsu, 1986) and cefazolin and trimethioprim-sulfametoxazole as broad-spectrum antibiotics. For details, please see the **Supplementary Material**.

Sterilization and Preparation of the Surgical Room

The surgery room should be prepared before the start of the surgery. Surfaces should be cleaned with antiseptic solution and clutter should be avoided. There should not be any non-essential personnel traffic into the room. Surgical chair should be comfortable and adjustable. Surgeon should don personal protective equipment including lab coat, surgical mask, and gloves.

All tools and supplies used for surgery, starting from dissection of the skin, need to be sterile. Surgical tools and metal head bars should be autoclaved. If a surgical tool tip touches a non-sterile surface during the surgery, it should be bead sterilized. A metal tool tray should be autoclaved. Batches of paper cleaning wipes (e.g., Kimwipes) and glass pipettes can be autoclaved. Saline can be autoclaved in glass bottles (∼10 ml) or purchased in sterile 10-mL batches. Gelatin absorbable hemostatic sponge (e.g., Surgifoam), cotton-tipped applicators, and bone wax are purchased in sterile batches. Thirty minutes before surgery, heating blanket, and hot bead sterilizer are switched on. The surgical microscope is adjusted (height and focus are in the middle of their dynamic range). Surfaces, trays, and handles are cleaned with an antiseptic solution.

Although every surgeon may feel more comfortable with a different set of tools and supplies, we recommend keeping the number of sterile tools as low as possible to avoid accidental contamination. Tools are supplies commonly used in our laboratories are listed in the **Supplementary Material**.

Intraoperative Measures

Induction of Anesthesia

After the mouse has rested for at least 15 min following the transport, it is weighed and the tail is marked with a marker pen for easier identification, when multiple mice are housed in the same cage. Having a calm subject during the induction of anesthesia increases the chances of stable anesthesia. Mouse is lifted from the cage by the proximal tail. The body is immediately rested on a flat surface or the palm or the back of the opposite hand of the researcher since tail suspension is stressful for the mice (Yapıcı-Eser et al., 2018) If the mouse is going to receive inhalation anesthesia, it is slowly placed in an induction chamber that is not pre-filled with anesthetic. Anesthesia is induced with isoflurane at 3% followed by 1–1.5% maintenance. Alternatively, ketamine-xylazine (K/X) injection (i.p.) can be used for induction and can be supplemented with extra doses of ketamine throughout surgery, or isoflurane. K/X has been used as a standard anesthetic for surgical procedures, but the short half life makes it less practical for longer procedures (Jaber et al., 2014). On the other hand, isoflurane anesthesia is reported to increase brain edema (Thal et al., 2012), but in our protocols with the use of preoperative dexamethasone, we have not experienced significant brain edema.

Surgical Procedure

The mouse is placed on the heating blanket and secured in the stereotaxic frame (please see the **Supplementary Material**). A sterile ointment is applied to the eyes. The application of this ointment can be repeated as often as necessary. Not only does this ointment protects the eyes from keratitis, it also protects against accidental exposure to povidone-iodine solution (P-I) and alcohol. For many behavioral experiments, facial whiskers play an important role for sensing and task performance. The whiskers can be weighed down with some lubricant so that they are not accidentally cut during surgery.

Cefazolin and buprenorphine are injected. Hair is removed with depilatory cream, and the skin is wiped with wet surgical sponges to remove remaining hair. The bare skin is cleaned with a 5% P-I solution (e.g., Betadine) followed by alcohol swabs repeatedly for three times with alternating wipes. P-I solution should be completely rinsed off since it may cause the mouse to itch when dried up. The skin is marked with a semi-permanent marker (e.g., fine tip Sharpie) to define the surgical borders slightly smaller than the intended size, because the skin will stretch after the cut, which makes the incision larger. The skin is cut with a #11 blade and scissors following the markings. Sub-cutaneous tissue is dissected with scissors. The remaining subcutaneous tissue is pushed aside with sterile cotton tip applicators starting from the middle and moving toward the edges until the bone is dry. The periosteum is removed by scratching with a #15 blade. This procedure is repeated until no loose connective tissue is left. A crosshatch pattern is carved on the skull with a blade sparing the exposure and surroundings to improve adherence. The skull is dried completely with pressurized air and covered with cyanoacrylate glue (Loctite 4014). For better control, a drop of glue is placed in the middle of the skull and dragged to the edge of the skin with a sterile wooden applicator (the handle of sterile cotton tipped applicator could be used after sharpening the tip with a sterile blade). It is best to position the skin in place before the application of the glue and drag the glue just until the skin edge to attach it in place.

The exposure is marked using a semi-permanent marker (e.g., fine tip Sharpie). Marking the exposure on dried glue has the advantage as the marking can be cleaned with a sterile cotton tip applicator and alcohol before drawn again for adjustments to the drawing. Head bar is attached with glue (Loctite 401) and dental acrylic. Applying the acrylic before the glue completely dries promotes a chemical reaction between the two yielding a stronger bond (Winkler et al., 2006). The details for the adjustments and attachment of different head bars are described in the **Supplementary Material**. When the head bar is secured in its place, the bone on the exposure is thinned along the marked craniotomy perimeter using a surgical drill and tungsten carbide burrs with 0.3-0.5 mm diameter. It is important to drill slowly (up to 15,000 rpm) and softly to prevent heating of the bone which would exaggerate inflammatory processes. A standard craniotomy takes about 15–30 min. The drill bit should be regularly dipped in chilled saline to avoid excessive heating. The bone should regularly be chilled with chilled saline prior to removal. The bone dust should be removed by washing the area with sterile saline. The excess liquid could be removed from the area using sterile wipes. Alternatively, a vacuum aspiration system equipped with a sterile blunt tip could be used. In case of bleeding from the bone, sterile sponges in saline and bone wax are utilized. It is recommended to stop drilling until the bleeding is completely under control. The thickness of the bone along the drilled perimeter can be checked by pressing on the bone gently. When the bone is thin enough along the drilled perimeter, the central piece is easily depressed when gently pushed. Prior to removal of the central piece, a drop of saline at 37° C is placed on the exposure. Using a craniotomy forceps, gently check for an edge which can be pierced. Slowly pry the edge and follow around. It is important to proceed slow to avoid bleeding from the dura. When the bone is loose enough, tear the remaining edge and remove the bone. At this point a piece of saline-soaked gel foam may be used to keep the dura moist, promote coagulation, and remove small residues of bone dust, and blood clots.

When all the bleeding is under control, the borosilicate glass or polymer is placed on the exposure replacing the bone. The window is pushed down and inside the craniotomy such that the bottom surface of the window comes in touch with the brain surface. A stereotaxic frame manipulator equipped with a sterile plastic pipette tip or a sterile wooden stick can be used to hold the glass in place. For soft polymer windows, manual handling may be needed. The details for the attachment of specific glass or polymer windows is described in the **Supplementary Material**. The cover is then sealed with glue, dental acrylic, and a second layer of glue. The whole skull surface and the part of the head bar that is attached to the skull are covered with dental acrylic and a thin layer of glue. 0.1 ml of 5% dextrose is injected subcutaneously for surgeries up to 2 h. If the surgery takes longer than that, this injection is repeated every 2 h.

After the glue and acrylic are completely dry and the animal is marked (e.g., by ear notch), the exposure is covered by a protective cap (please see the following section). The animal is then placed in a clean cage that is positioned on top of a heating blanket set to 37°C and is monitored until it regains motor control before being returned to the vivarium. In case of isoflurane, the mouse should regain some motor control within 10 min and eating/drinking within 1 h after a successful surgery. In case of K/X, the mouse is expected to recover some motor functions after ∼30 min following the last supplemental K injection, but the time course of recovery can vary between animals.

Protective Caps

For chronically prepared animals we suggest using a protective cap on top of the exposure. This prevents the possible break in the glass and protects soft exposure covers like polymers.

In the case of glass windows, regardless of the head bar design, casting silicone can be used right before the end of surgery. Casting silicone components are mixed 1:1, and a large drop is applied to cover the glass windows and surrounding acrylic. This polymer helps keep the glass safe and clean and acts as a thermal insulation barrier. The anesthesia is discontinued when the silicone is set (∼5 min following application). This silicone can be gently peeled for imaging sessions leaving no residue behind and can be reapplied when the session is over and before the animal is released to the home cage.

When using the polymer covers, we suggest using harder materials to cover the surface. While 3-D printed caps are the most convenient ones to use, custom machined caps can also be used. Cap can be mounted on the head bar using interlocking designs or magnets (not MRI safe). For an exemplary design please see the **Supplementary Material**.

Post-operative Measures (∼<10days)

Monitoring

Monitor the mouse daily for 5 days following surgery assessing general appearance, weight, and pain scale (Langford et al., 2010). TMP-SMX/Ibuprofen is supplied in drinking water during this period. If there are signs of pain, additional buprenorphine injections should be given in 12-h periods for up to 3 days. It is also helpful to give some softened pellets of food immersed in medicated drinking solution or gel food or hydrogel to feed and hydrate the mouse.

Training for Head Fixation

Training sessions can start when the initial monitoring of the animal is completed (post-operative ∼7 days). The mouse is handled until calm and trained to sit still in the cradle for up to 1 h with increasing duration (e.g., 15, 30, 45 min, 1 h). On imaging days, once the animal sits in the cradle, it is quickly fixed and left to rest for 5 min before moving the cradle under the microscope. It is rewarded with a treat (e.g., sweetened condensed milk). The cradle is positioned in the imaging setup and reward is offered about every 15 min. If the mouse shows signs of discomfort or anxiety, the session is aborted, and the mouse is released. Forceful movement and struggling can lead to the mouse detaching its head bar.

Imaging Under Light Anesthesia

The mouse can be imaged under light anesthesia (K/X or isoflurane) when no functional data is needed. Eyes should be protected with ointment. The glass window can be wiped

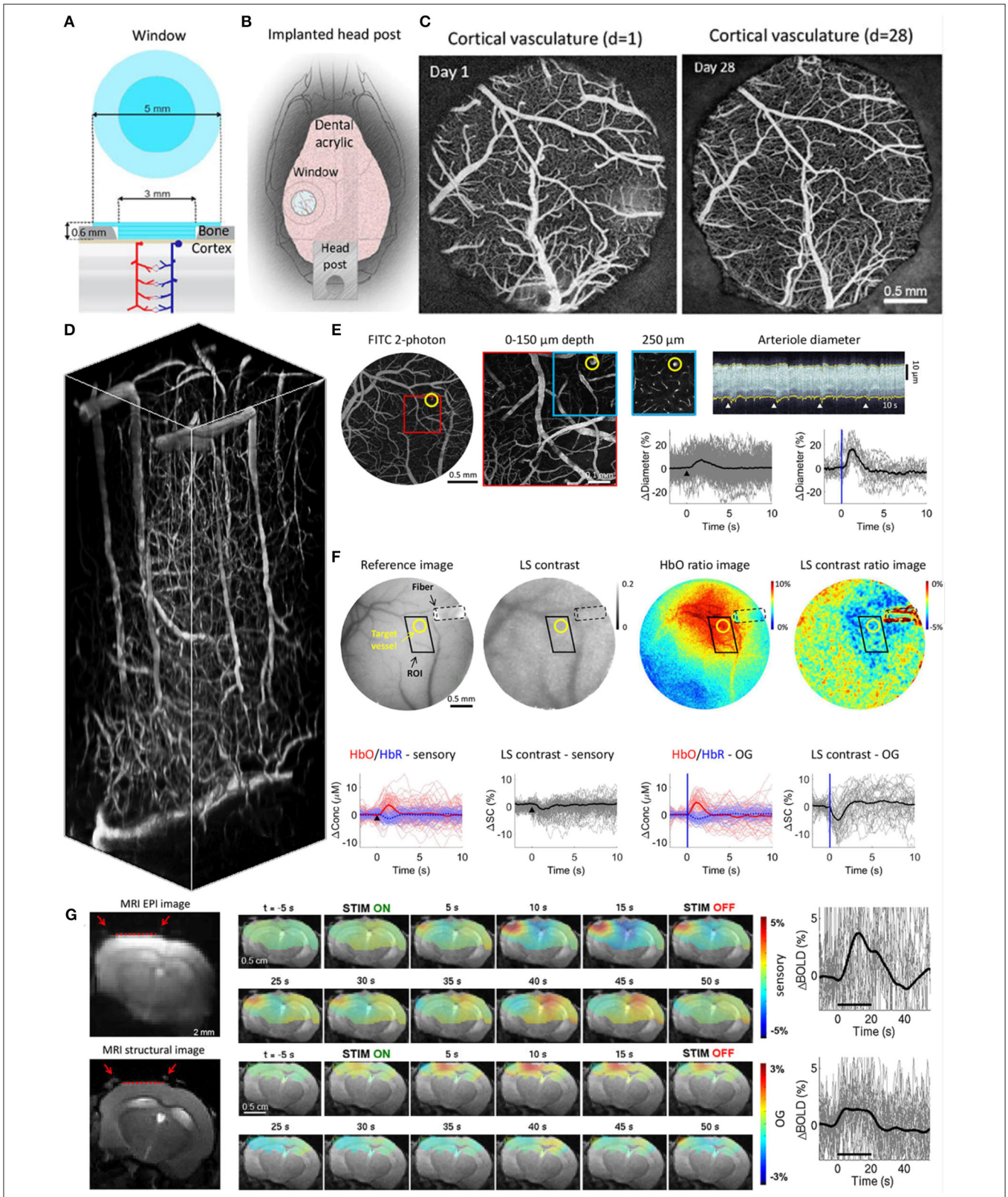

FIGURE 1 | (A) Schematics of the borosilicate glass window implant. **(B)** Schematic illustration of the window implant over the whisker representation within the primary somatosensory cortex (SI) and the headpost fixed to the skull overlaying the other (contralateral) hemisphere. **(C)** Images of the brain vasculature through the

(Continued)

FIGURE 1 | glass window implant obtained by 2-photon imaging of fluorescein isothiocyanate (FITC)-labeled dextran injected intravenously. The images illustrate preserved integrity of the vasculature between days 1 (left) and 28 (right) following surgical implantation. **(D)** Two-photon image stack obtained with Alexa 680 labeled dextran injected intravenously illustrating the capability of deep imaging. The resolution for presented images was ∼1 μm/pixel. **(E)** Top: Image of the surface vasculature calculated as a maximum intensity projection (MIP) of an image stack 0–300 μm in depth using a 4× objective. Individual images were acquired every 10 μm (top, left). A zoomed-in view of the region within the red square acquired with a 20× objective (top, middle, left). A plane 250 μm below the surface corresponding to the region outlined in blue (top, middle, right). The yellow circle indicates a small diving arteriole. An example temporal diameter change profile acquired from the arteriole outlined by the yellow circle imaged 250 μm below the surface (top, right). The vessel diameter was captured by repeated line-scans across the vessel. These line-scans form a space-time image when stacked sequentially, from left to right. White arrowheads indicate the onset of stimulus trials (air puffs to the whisker pad); four trials are shown. Graphs: Single-vessel dilation time-courses extracted from data. Time-courses for individual trials are overlaid for sensory stimuli (left, $n = 160$ trials) and OG stimuli (right, $n = 19$ trials); the thick lines show the average. The stimulus onset is indicated by the black arrowhead and the blue vertical line for the sensory and OG panels, respectively. **(F)** Concurrent IOSI and LSCI in the same subject. A CCD reflectance image of the surface vasculature (left). The corresponding LS contrast image (middle, left). Ratio images of HbO (extracted from the OIS data, see Methods) and LS contrast showing the region of activation following OG stimulation (middle, right, and right). The location of optical fiber is indicated on all images (black dotted line). The same arteriole is outlined by yellow circles. The black parallelogram indicates the region of interest (ROI) used for extraction of time-courses. The resolution for presented images was 5.5 μm/pixel. Graphs: Time-courses of HbO and HbR (shown in red and blue, respectively), and LS contrast (shown in black) in response to sensory and OG stimulation. These time-courses were extracted from the polygonal ROI shown in top images. **(G)** Corrected GE EPI image (left, top) and a corresponding structural image (TurboRARE, left, bottom). The resolution for EPI and TurboRARE is 200 μm/pixel 100 × 50 and ∼75 μm/pixel, slice thickness = 1 mm. Red arrows point to the peripheral edges of the implant, i.e., the glass/bone boundary. The red line indicates the bottom of the glass implant, i.e., the glass/brain boundary. The BOLD signal in response to sensory stimuli in a fully awake mouse (top, middle). Spatiotemporal evolution of the BOLD signal change from a single slice cutting through the center of the evoked response, presented as trial-averaged ratio maps, in response to a 20-s train of 100-ms light pulses delivered at 1 Hz ("blocked" OG stimulus) in a single Emx1-Cre/Ai32 subject. EPI images were thresholded to reflect the sensitivity of the surface RF coil (for display purposes only). The ratio images are overlaid on the structural (TurboRARE) image of the same slice. BOLD response time-courses extracted from the active ROI (top, right). Fifty seven stimulus trials are superimposed. The average is overlaid in thick black. The BOLD signal in response to OG stimuli in a fully awake mouse (bottom, middle). Spatiotemporal evolution of the BOLD signal change from a single slice cutting through the center of the evoked response, presented as trial-averaged ratio maps, in response to a 20-s train of 100-ms light pulses delivered at 1 Hz ("blocked" OG stimulus) in a single Emx1-Cre/Ai32 subject. EPI images were thresholded to reflect the sensitivity of the surface RF coil (for display purposes only). The ratio images are overlaid on the structural (TurboRARE) image of the same slice. BOLD response time-courses extracted from the active ROI (bottom, right). Twenty eight stimulus trials are superimposed. The average is overlaid in thick black. Modified from Desjardins et al. (2019).

with alcohol and, if necessary, it can be gently scraped with a blade. Soft polymer windows should not be treated with alcohol. Instead, sterile saline can be used. This imaging protocol is suitable for morphological imaging where small movements may cause imaging artifacts the researcher wants to avoid.

Over the course of days 1–10 after surgery, exposure may become inflamed and some dural vessels could develop from the sides, but this should resolve, and the exposure should be ready to image around day 10–14 after surgery. High-quality exposures allow imaging of intravascular fluorescent tracer fluorescein isothiocyanate (FITC)-dextran (2 MDa) down to at least 500 μm with 900 nm excitation.

Imaging (∼Day 10+)

Delivery of Contrast Agents

For imaging protocols that involve i.v. contrast agents, a brief anesthesia is induced with 3% isoflurane in O_2 or air. Retro-orbital injection (Yardeni et al., 2011) of contrast agents (e.g., 0.05 ml FITC at 5% in PBS) is performed using a tuberculin syringe 31 G, 0.5″ needle. Care is taken not to scratch the orbital fossa (bone), because this may cause irritation and pain when anesthesia is discontinued. Alternatively, intravenous injections can be given through the tail vein, however, this may result in local inflammation with imperfect application and is not recommended for novice researchers.

Awake Imaging

In cases where an i.v. injection is performed, the mouse is allowed to wake up and recover from anesthesia for 15–60 min. The mouse is handled until it becomes calm. After that, the head bar is fixed in the mouse holder and brought in the imaging setup. Reward is offered in line with the experimental protocol. The imaging session should not last longer than 60–90 min. The mouse should be released and returned to its home cage when the frequency of its movement starts increasing. Movement can be detected via cameras and/or accelerometer (Bergel et al., 2018). The mouse is returned to its cage and the cage to vivarium after the imaging session is over.

Euthanasia

Whenever, the experimental study is completed or if the exposure is no longer imageable, euthanasia is performed in accordance with Institutional Animal Care and Use Committee guidelines.

RESULTS

In this section, we will present example imaging data that were acquired from chronically prepared animals. Details of specific surgical procedures and imaging protocols are described in the **Supplementary Material**.

Glass Windows Used in 2-Photon Microscopy, IOSI, LSCI, and MRI-Compatible Optical Imaging in Conjunction With OG Stimulation

This preparation is a modification of the design described by Chen et al. (2015). It has been used by our group in several studies including Desjardins et al. (2019). A glass plug constructed from one 5-mm round coverslip and two or three 3-mm round coverslip is used in this surgery (**Figures 1A,B**). Structural imaging demonstrating the state of the surface vessels 1 and 28 days after the surgery is obtained after i.v. (retroorbital) injection of FITC-dextran (**Figure 1C**). The quality of the window can

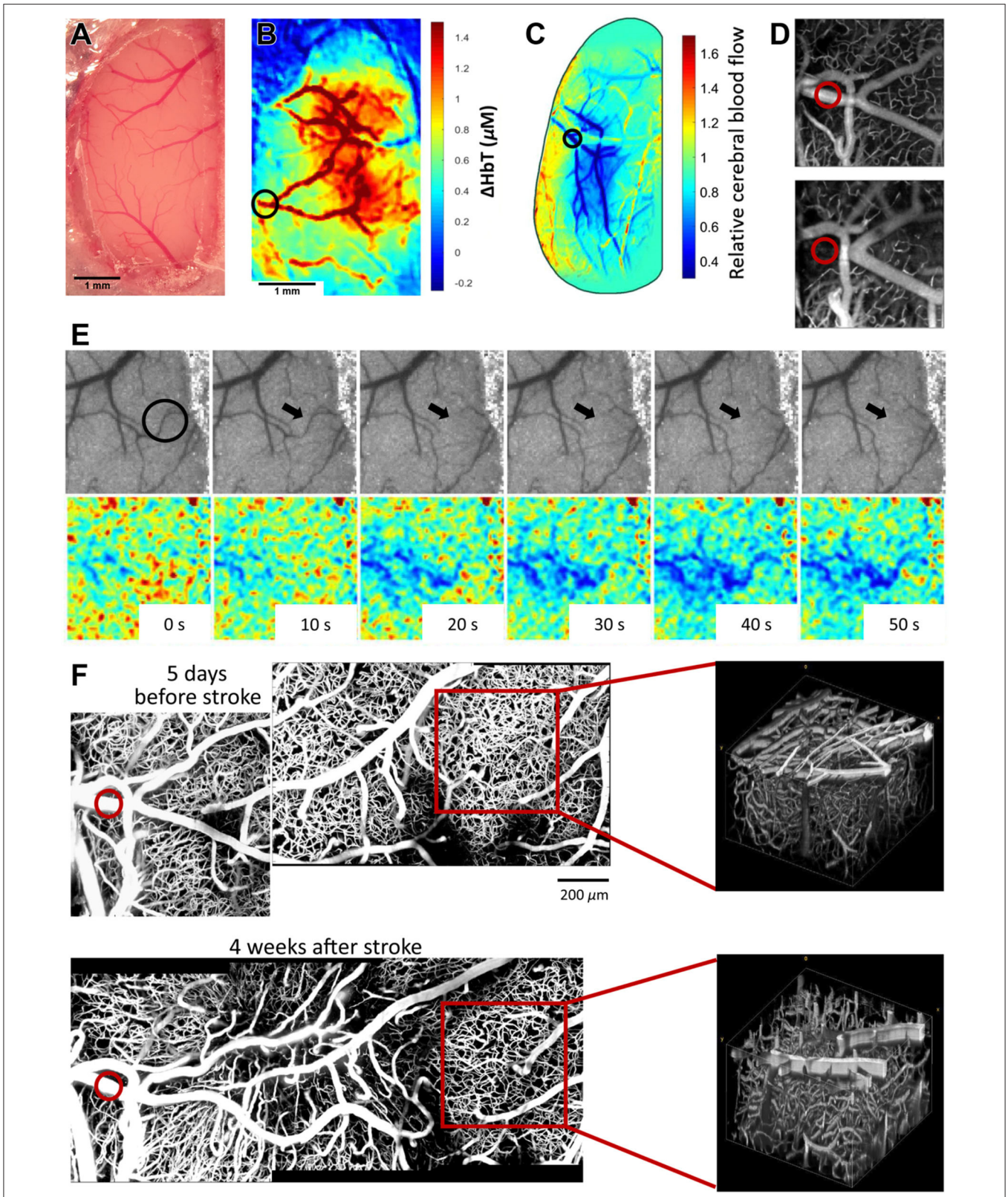

FIGURE 2 | (A) Representative image of cranial window immediately after surgery. In this preparation, animal was implanted with a one-point secured flat head bar and half Crystal Skull glass (please see **Supplementary Material** for details). **(B)** Intrinsic optical signal imaging of change in total hemoglobin concentration during air

(Continued)

FIGURE 2 | puff stimulation of the contralateral forelimb. Black circle indicates the vessel targeted for photothrombotic occlusion. The resolution for presented images was 5.5 μm/pixel. **(C)** Relative CBF detected by LSCI at 1 h after photothrombosis. The resolution for presented images was 5.5 μm/pixel. **(D)** OCT angiograms of flowing vessel before stroke (top) and 1-h after photothrombotic stroke (bottom). Transverse and axial resolutions of the OCT system using a 10× objective (Mitutoyo) were 3.5 and 3.5 μm. **(E)** Representative images showing collateral occlusion (circled in black). Top panel shows laser speckle contrast images as visualized in real time. Bottom panel shows relative blood flow changes associated with the occlusion. **(F)** Two-photon maximum intensity projections (left) and volumes (right) of 400 μm stack 5 days before photothrombosis (top) and 4 weeks after photothrombosis. Red circle indicates vessel targeted for photothrombosis. Red square indicates regions chosen for volume projections. The resolution for presented images was ∼1.5 μm/pixel. Modified from Sunil et al. (2020).

be further appreciated in a 3D vascular stack that was obtained after injecting Alexa 680-dextran (**Figure 1D**). Functional data were obtained with 2-photon imaging of vasodilation in response to sensory stimuli applied to the whiskers as well as OG stimuli stimulation in animals expressing VGAT-ChR2 (**Figure 1E**). The same animals can be used for measurements of oxygenated hemoglobin (HbO), reduced hemoglobin (HbR), and total hemoglobin (HbT) concentrations using IOSI and cortical blood flow using LSCI in response to sensory and OG stimuli (**Figure 1F**). Finally, the same animals can be used for optical imaging and OG stimulation performed simultaneously with fMRI when headposts are made from polyether ether ketone (PEEK) plastic (**Figure 1G**). For details, please see the **Supplementary Material** and Desjardins et al. (2019).

We have also modified these glass windows with polymer sealed ports for injection of drugs or various fluorophores (Roome and Kuhn, 2014). These ports also allowed insertion of thin electrodes or optical fibers. Please see the **Supplementary Material** for details.

Half Crystal Skull Covered Craniotomy Used in 2-Photon Microscopy, IOSI, LSCI, and OCT Imaging to Evaluate the Effects of Stroke Caused by Photothrombosis

This preparation is a modification of the design described in Kim et al. (2016) where they have created a curved glass replacement to dorsal cranium and termed it the "Crystal Skull." We have modified this protocol using half of this commercially available curved glass (labmaker.org) to prevent the disruption of blood flow in sagittal sinus while extending the coverage to visualize the distal branching points of MCA and the entirety of barrel cortex which are more laterally positioned than the original design of Crystal Skull placement. We have used our version of preparation in several studies including Sunil et al. (2020). In cases where a large cortical area is desired to be imaged, surgery using crystal skull glass can be performed (Kim et al., 2016). However, due to high risk of bleeding or thrombosis, researchers may wish to avoid preparations involving the sagittal sinus. We have successfully implemented a modified procedure that allows us to image one hemisphere, which is sufficient for our application (**Figure 2A**). This preparation prevents drilling over the sagittal sinus, and small displacement of the glass in the lateral direction allows covering the hemisphere up to the lateral ridge, which cannot be achieved with the original method. Here we present results from experiments involving IOSI (**Figure 2B**), LSCI (**Figures 2C,E**), OCT (**Figure 2D**), and 2-photon microscopy (**Figure 2F**). We leveraged these large windows in studies of recovery from experimentally induced photothrombotic stroke in chronic, awake animals. The half crystal skull window allowed us to longitudinally image the stroke area after distal middle cerebral artery (**Figures 2B–D,F**, circles) and collateral occlusion (**Figure 2E**, arrow). Both the stroked and surrounding healthy tissue (**Figure 2F**) was accessible in the same animal for a month after the stroke was induced, allowing for long-term assessment of the pathology. For details, please see the **Supplementary Material** and Sunil et al. (2020).

Soft Polymer Window Used in 2-Photon Microscopy, IOSI, LSCI, OCT, and fUS Imaging

This preparation is a modification of the "soft window" design described in Boido et al. (2019). We used this preparation in several studies including Kılıç et al. (2020) and Tang et al. (2020). Although glass craniotomies are preferred because of the durability, glass has properties incompatible with US imaging. Here, we show typical results from animals prepared with a polymethypentene (PMP) polymer soft window (**Figure 3A**). This type of window is compatible with 2-P microscopy (**Figure 3B**), LSCI and IOSI (**Figure 3C**), OCT (**Figure 3D**), ultrasound localization microscopy (ULM, **Figure 3E**), and fUSG (**Figure 3F**). In contrast with the soft windows made from PDMS (Heo et al., 2016), PMP windows are less permeable to air and have no air bubbles formed on the cortical surface which makes them more suitable for US imaging since the air bubbles will lead to loss of signal. Although these windows are very stable, compared to glass counterparts, the optical imaging quality may degrade faster over time. For example, 2-P microscopy imaging at 800 nm with FITC-dextran in a glass preparation, can acquire good images down to 500–600 μm in cortex with quality comparable in first and the sixth month. However, with PMP windows, while penetration in the first month with the same imaging modality is comparable, we have experienced that we could only image 300–400 μm deep after 6 months and 150–200 μm after 1 year (data not shown). For details, please see the **Supplementary Material** and Kılıç et al. (2020) and Tang et al. (2020).

DISCUSSION

The surgical procedures described in this manuscript and the **Supplementary Material** are easy to follow for an experienced surgeon. For novice surgeons, we recommend starting surgical training using healthy, wild type, young adult mice (8–12 weeks). For the first training sessions, avoiding the sutures between

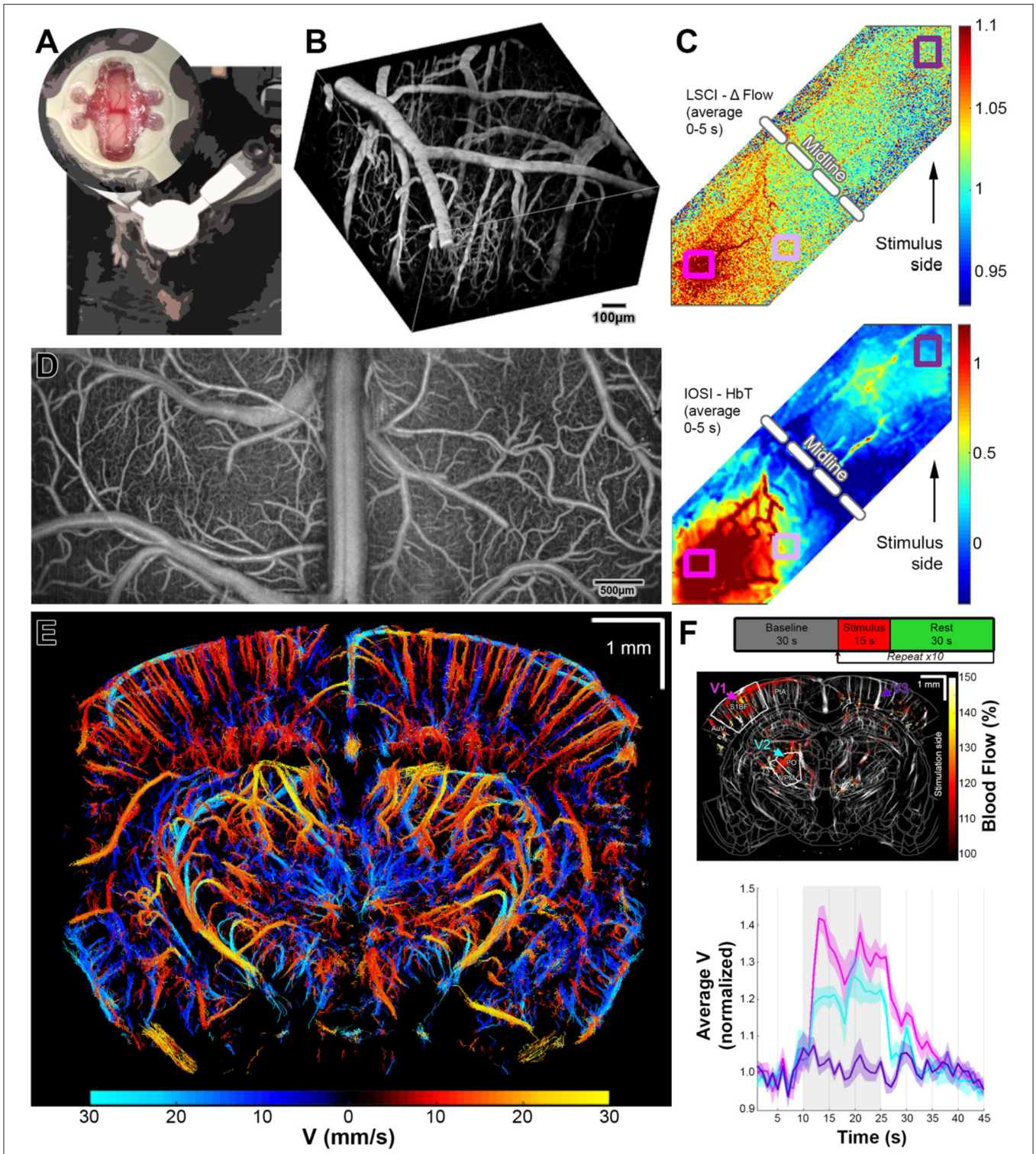

FIGURE 3 | (A) Representative images of US compatible craniotomy (top) and the position of an awake mouse for training and imaging. In this preparation, animal was implanted with a two-point secured machined head bar and a PMP strip (please see **Supplementary Material** for details). **(B)** 2-P vascular stack taken with i.v. FITC injection. The resolution for presented images was ∼1.5 μm/pixel. **(C)** LSCI (top) and IOSI (bottom) of both hemispheres during whisker stimulation. The resolution for presented images was 5.5 μm/pixel. **(D)** Full field OCT angiography. Transverse and axial resolutions of the OCT system using a 5× objective (Mitutoyo) were 7 and 3.5 μm. **(E)** ULM images acquired by US. The resolution for presented images was ∼10 μm/pixel. **(F)** Experimental paradigm for fUS imaging (top). Trial average of fUS images acquired during whisker stimuli (middle). The resolution for presented images was ∼100 μm/pixel. Time series of average velocity values calculated for marked vessels (middle) during whisker stimuli. Note that contralateral cortical and subcortical activation is visible while ipsilateral cortex is not activated. Modified from Tang et al. (2020).

skull bones will increase the success rate. During training, a surgeon also gets accustomed to a varying bone thickness across the dorsal surface of the mouse skull. After the goals of this training are achieved, craniotomies crossing the midline may be attempted. Here, the main challenge is to meticulously remove the bone without damaging the underlying sagittal sinus. Even for experienced surgeons, using two half crystal skull windows instead of making a single bilateral exposure may be preferable. This is because exposing the midline entails high risk of bleeding and thrombosis of the sagittal sinus.

The window quality depends not only on the optimization of the craniotomy procedure but also on the proficiency in sealing the window. This step may take some time to master. Once all the procedures are mastered, a mouse with a chronic window implant can be imaged routinely up to 6 months with good outcome, although instances where imaging was performed for up-to 1.5 years after surgery have been reported (Füger et al., 2017).

Researchers should keep in mind that inflammation peaks around the third day post-operatively and usually takes a few weeks to resolve. While the inflammatory processes are ongoing, the tissue will remain opaque and not suitable for optical imaging. Therefore, imaging should start around 3 weeks after the surgery, although training sessions can start earlier but not within the first week after the surgery. In our experience, the best efficiency is achieved when the mouse is given 1 week to recover before starting the training and at least 4 training sessions in the upcoming 10–14 days before starting the imaging. The exact schedule may vary slightly depending on the subject.

Lastly, performing a craniotomy can be more invasive compared to the thinned skull preparations (Shih et al., 2012); but may give more flexibility with different imaging modalities. Removing the skull completely eliminates a problem of inconsistent thickness of the thinned skull preparations, provides less scattering and therefore deeper optical penetration. Also, most thinned skull preparations (Drew et al., 2010; Shih et al., 2012) require the used of reinforcement which makes them not suitable or less desirable for some imaging methods like fUS or for optical imaging performed simultaneously with MRI.

Although truly simultaneous application with all of the imaging/stimulation techniques mentioned here is not feasible, one mouse can rotate between imaging instruments, sometimes on the same day, provided that it is given enough time to rest in between imaging sessions in the home cage. Some of the abovementioned imaging modalities can be readily combined in a multimodal setup that allow simultaneous use of the systems. Examples include (1) LSCI, IOSI and photothrombosis (Kazmi et al., 2013; Sunil et al., 2020) (2) 2-P microscopy and optogenetic stimulation (Bovetti et al., 2017; Yang et al., 2018), and (3) MRI and optical imaging and/or optogenetic stimulation (Lin et al., 2016; Schlegel et al., 2018; Chen et al., 2019).

CONCLUSION

Even though it was introduced around 60 years ago, the 3R (Replacement, Reduction, Refinement) principle is exceedingly relevant and important to the current *in vivo* data acquisition protocols (De Angelis et al., 2019). These principles serve as gatekeepers on the way of improving both the quality of life of the animals used, as well as the quality of the data collected. The surgical procedures described here are designed to maximize the spectrum of imaging techniques that can be applied on the same subject. They are also modified to decrease the complications after surgery, morbidity, and mortality therefore decreasing the number of the experimental subjects.

We hope these detailed protocols will be helpful for increasing the rigor and repeatability in imaging studies and decreasing the number of animals utilized by these studies.

DATA AVAILABILITY STATEMENT

The raw data supporting the conclusions of this article will be made available by the authors, without undue reservation.

ETHICS STATEMENT

The animal study was reviewed and approved by UCSD and Boston University. Some parts of this study are conducted at University of California, San Diego (UCSD).

AUTHOR CONTRIBUTIONS

KK: development of surgical methods, acquisition of data, analysis of data, and writing the manuscript. MD, MT, SS, and ŞE: acquisition of data, analysis of data, and writing the manuscript. JT and DP: development of imaging algorithms, acquisition of data, analysis of data, and writing the manuscript. DB and AD: supervising the experiments and writing the manuscript. All authors contributed to the article and approved the submitted version.

FUNDING

Authors gratefully acknowledge support from the NIH (BRAIN Initiative R01MH111359, R01NS108472, R01NS057198, and K99AG063762).

ACKNOWLEDGMENTS

Authors would like to acknowledge Qun Chen, Céline Mateo, An Na Kim, Takaki Komiyama, Anderson Chen, John T. Giblin, Blaire S. Lee, Su Jin Kim for their creative designs and support for the development of these surgical protocols and the members of the DB and the AD labs for helpful discussions.

SUPPLEMENTARY MATERIAL

The Supplementary Material for this article can be found online at: https://www.frontiersin.org/articles/10.3389/fphys.2020.612678/full#supplementary-material

REFERENCES

Andermann, M. L., Kerlin, A. M., and Reid, R. C. (2010). Chronic cellular imaging of mouse visual cortex during operant behavior and passive viewing. *Front. Cell. Neurosci.* 4:3. doi: 10.3389/fncel.2010.00003

Bergel, A., Deffieux, T., Demené C., Tanter, M., and Cohen, I. (2018). Local hippocampal fast gamma rhythms precede brain-wide hyperemic patterns during spontaneous rodent REM sleep. *Nat. Commun.* 9:5364. doi: 10.1038/s41467-018-07752-3

Boido, D., Rungta, R. L., Osmanski, B. F., Roche, M., Tsurugizawa, T., Le Bihan, D., et al. (2019). Mesoscopic and microscopic imaging of sensory responses in the same animal. *Nat. Commun.* 10:1110. doi: 10.1038/s41467-019-09082-4

Bovetti, S., Moretti, C., Zucca, S., Dal Maschio, M., Bonifazi, P., and Fellin, T. (2017). Simultaneous high-speed imaging and optogenetic inhibition in the intact mouse brain. *Sci. Rep.* 7:40041. doi: 10.1038/srep46122

Chen, S. X., Kim, A. N., Peters, A. J., and Komiyama, T. (2015). Subtype-specific plasticity of inhibitory circuits in motor cortex during motor learning. *Nat. Neurosci.* 18, 1109–1115. doi: 10.1038/nn.4049

Chen, X., Sobczak, F., Chen, Y., Jiang, Y., Qian, C., Lu, Z., et al. (2019). Mapping optogenetically-driven single-vessel fMRI with concurrent neuronal calcium recordings in the rat hippocampus. *Nat. Commun.* 10:5239. doi: 10.1038/s41467-019-12850-x

De Angelis, I., Ricceri, L., and Vitale, A. (2019). The 3R principle: 60 years taken well. Preface. *Ann. Ist. Super. Sanita*. 55, 398–399. doi: 10.4415/ANN_19_04_15

Desjardins, M., Kılıç, K., Thunemann, M., Mateo, C., Holland, D., Ferri, C. G. L., et al. (2019). *Awake mouse imaging: from two-photon microscopy to blood oxygen level-dependent functional magnetic resonance imaging. Biol. Psychiatry Cogn. Neurosci. Neuroimaging* 4, 533–542. doi: 10.1016/j.bpsc.2018.12.002

Drew, P. J., Shih, A. Y., Driscoll, J. D., Knutsen, P. M., Blinder, P., Davalos, D., et al. (2010). Chronic optical access through a polished and reinforced thinned skull. *Nat. Methods* 7, 981–984. doi: 10.1038/nmeth.1530

Füger, P., Hefendehl, J. K., Veeraraghavalu, K., Wendeln, A. C., Schlosser, C., Obermüller, U., et al. (2017). Microglia turnover with aging and in an alzheimer's model via long-term *in vivo* single-cell imaging. *Nat. Neurosci.* 20, 1371–1376. doi: 10.1038/nn.4631

Goldey, G. J., Roumis, D. K., Glickfeld, L. L., Kerlin, A. M., Reid, R. C., Bonin, V., et al. (2014). Removable cranial windows for long-term imaging in awake mice. *Nat. Protoc.* 9, 2515–2538. doi: 10.1038/nprot.2014.165

Hedley-Whyte, E. T., and Hsu, D. W. (1986). Effect of dexamethasone on blood-brain barrier in the normal mouse. *Ann. Neurol.* 19, 373–377. doi: 10.1002/ana.410190411

Heo, C., Park, H., Kim, Y. T., Baeg, E., Kim, Y. H., Kim, S. G., et al. (2016). A soft, transparent, freely accessible cranial window for chronic imaging and electrophysiology. *Sci. Rep.* 6:27818. doi: 10.1038/srep27818

Holtmaat, A., Bonhoeffer, T., Chow, D. K., Chuckowree, J., De Paola, V., Hofer, S. B., et al. (2009). Long-term, high-resolution imaging in the mouse neocortex through a chronic cranial window. *Nat. Protoc.* 4, 1128–1144. doi: 10.1038/nprot.2009.89

Jaber, S. M., Hankenson, F. C., Heng, K., McKinstry-Wu, A., Kelz, M. B., and Marx, J. O. (2014). Dose regimens, variability, and complications associated with using repeat-bolus dosing to extend a surgical plane of anesthesia in laboratory mice. *J. Am. Assoc. Lab. Anim. Sci.* 53, 684–691.

Kazmi, S. M., Parthasarthy, A. B., Song, N. E., Jones, T. A., and Dunn, A. K. (2013). Chronic imaging of cortical blood flow using multi-exposure speckle imaging. *J. Cereb. Blood Flow Metab.* 33, 798–808. doi: 10.1038/jcbfm.2013.57

Kılıç, K., Tang, J., Erdener, Ş. E., Sunil, S., Giblin, J. T., Lee, B. S., et al. (2020). Chronic imaging of mouse brain: from optical systems to functional ultrasound. *Curr. Protoc. Neurosci.* 93:e98. doi: 10.1002/cpns.98

Kim, T. H., Zhang, Y., Lecoq, J., Jung, J. C., Li, J., Zeng, H., et al. (2016). Long-term optical access to an estimated one million neurons in the live mouse cortex. *Cell Rep.* 17, 3385–3394. doi: 10.1016/j.celrep.2016.12.004

Langford, D. J., Bailey, A. L., Chanda, M. L., Clarke, S. E., Drummond, T. E., Echols, S., et al. (2010). *Coding of facial expressions of pain in the laboratory mouse. Nat. Methods* 7, 447–449. doi: 10.1038/nmeth.1455

Lin, P., Fang, Z., Liu, J., and Lee, J. H. (2016). Optogenetic functional MRI. *J. Vis. Exp.* 19:53346. doi: 10.3791/53346

Mostany, R., and Portera-Cailliau, C. (2008). A craniotomy surgery procedure for chronic brain imaging. *J. Vis. Exp.* 15:680. doi: 10.3791/680

Roome, C. J., and Kuhn, B. (2014). Chronic cranial window with access port for repeated cellular manipulations, drug application, and electrophysiology. *Front. Cell. Neurosci.* 8:379. doi: 10.3389/fncel.2014.00379

Schlegel, F., Sych, Y., Schroeter, A., Stobart, J., Weber, B., Helmchen, F., et al. (2018). Fiber-optic implant for simultaneous fluorescence-based calcium recordings and BOLD fMRI in mice. *Nat. Protoc.* 13, 840–855. doi: 10.1038/nprot.2018.003

Shih, A. Y., Mateo, C., Drew, P. J., Tsai, P. S., and Kleinfeld, D. (2012). A polished and reinforced thinned-skull window for long-term imaging of the mouse brain. *J. Vis. Exp.* 7:3742. doi: 10.3791/3742

Sunil, S., Erdener, S. E., Lee, B. S., Postnov, D., Tang, J., Kura, S., et al. (2020). *Awake chronic mouse model of targeted pial vessel occlusion via photothrombosis. Neurophotonics* 7:015005. doi: 10.1117/1.NPh.7.1.015005

Tang, J., Postnov, D. D., Kilic, K., Erdener, S. E., Lee, B., Giblin, J. T., et al. (2020). Functional ultrasound speckle decorrelation-based velocimetry of the brain. *Adv. Sci.* 7:2001044. doi: 10.1002/advs.202001044

Thal, S. C., Luh, C., Schaible, E. V., Timaru-Kast, R., Hedrich, J., Luhmann, H. J., et al. (2012). Volatile anesthetics influence blood-brain barrier integrity by modulation of tight junction protein expression in traumatic brain injury. *PLoS ONE* 7:e50752. doi: 10.1371/journal.pone.0050752

Winkler, S., Wood, R., Facchiano, A. M., Boberick, K. G., and Patel, A. R. (2006). Prosthodontic self-treatment with acrylic resin super glue: a case report. *J. Oral Implantol.* 32, 132–136. doi: 10.1563/788.1

Yang, W., Carrillo-Reid, L., Bando, Y., Peterka, D. S., and Yuste, R. (2018). Simultaneous two-photon imaging and two-photon optogenetics of cortical circuits in three dimensions. *Elife*. 7:e32671. doi: 10.7554/eLife.32671

Yapıcı-Eser, H., Dönmez-Demir, B., Kılıç, K., Eren-Koçak, E., and Dalkara, T. (2018). Stress modulates cortical excitability via α-2 adrenergic and glucocorticoid receptors: as assessed by spreading depression. *Exp. Neurol.* 307, 45–51. doi: 10.1016/j.expneurol.2018.05.024

Yardeni, T., Eckhaus, M., Morris, H. D., Huizing, M., and Hoogstraten-Miller, S. (2011). Retro-orbital injections in mice. *Lab Anim.* 40, 155–160. doi: 10.1038/laban0511-155

Conflict of Interest: The authors declare that the research was conducted in the absence of any commercial or financial relationships that could be construed as a potential conflict of interest.

frontiers in Physiology

BRIEF RESEARCH REPORT
published: 01 February 2021
doi: 10.3389/fphys.2021.611984

A Longitudinal Pilot Study on Cognition and Cerebral Hemodynamics in a Mouse Model of Preeclampsia Superimposed on Hypertension: Looking at Mothers and Their Offspring

Lianne J. Trigiani[1], Clotilde Lecrux[1], Jessika Royea[1], Julie L. Lavoie[2], Frédéric Lesage[3], Louise Pilote[4] and Edith Hamel[1]**

[1] Laboratory of Cerebrovascular Research, Montreal Neurological Institute, McGill University, Montréal, QC, Canada, [2] Centre de Recherche du Centre Hospitalier de l'Universite de Montreal and School of Kinesiology and physical activity sciences, Université de Montréal, Montréal, QC, Canada, [3] Biomedical Engineering Institute, École Polytechnique de Montréal, Montréal, QC, Canada, [4] Department of Medicine, Centre for Outcomes Research and Evaluation, McGill University Health Centre, Montréal, QC, Canada

OPEN ACCESS

Edited by:
Carlos Alonso Escudero,
University of the Bío Bío, Chile

Reviewed by:
Robert Gros,
University of Western Ontario, Canada
Matthew Ratsep,
McMaster University, Canada

***Correspondence:**
Lianne J. Trigiani
Lianne.trigiani@mail.mcgill.ca
Edith Hamel
Edith.hamel@mcgill.ca

Specialty section:
This article was submitted to Vascular Physiology, a section of the journal Frontiers in Physiology

Received: 29 September 2020
Accepted: 06 January 2021
Published: 01 February 2021

Citation:
Trigiani LJ, Lecrux C, Royea J, Lavoie JL, Lesage F, Pilote L and Hamel E (2021) A Longitudinal Pilot Study on Cognition and Cerebral Hemodynamics in a Mouse Model of Preeclampsia Superimposed on Hypertension: Looking at Mothers and Their Offspring. Front. Physiol. 12:611984. doi: 10.3389/fphys.2021.611984

Preeclampsia is a common hypertensive disorder in pregnant women and whose causes and consequences have focused primarily on cardiovascular outcomes on the mother and offspring, often without taking into consideration the possible effects on the brain. One possible cause of preeclampsia has been attributed to alterations in the renin-angiotensin system, which has also been linked to cognitive decline. In this pilot study, we use a transgenic mouse model that chronically overexpresses human angiotensinogen and renin (R^+A^+ mice) that displayed characteristics of preeclampsia such as proteinuria during gestation. Offspring of these mothers as well as from control mothers were also examined. We were primarily interested in detecting whether cognitive deficits were present in the mothers and offspring in the long term and used a spatial learning and memory task as well as an object recognition task at three timepoints: 3, 8, and 12 months post-partum or post-natal, while measuring blood pressure and performing urine analysis after each timepoint. While we did not find significant deficits in preeclamptic mothers at the later timepoints, we did observe negative consequences in the pups of R^+A^+ mice that coincided with hemodynamic alterations whereby pups had higher whisker-evoked oxygenated hemoglobin levels and increased cerebral blood flow responses compared to control pups. Our study provides validation of this preeclampsia mouse model for future studies to decipher the underlying mechanisms of long-term cognitive deficits found in offspring.

Keywords: preeclampsia, cerebrovascular function, cognition, renin—angiotensin—aldosterone system, cerebral hemodynamics

INTRODUCTION

Preeclampsia is a common hypertensive disorder in pregnant women, with a worldwide incidence rate of just under 3% but varying between 2.7 and 8.2% depending on the region studied (Kongwattanakul et al., 2018) and this incidence rate continues to grow (Fox et al., 2019). Considering these statistics, and despite the connection between hypertension and cognitive

impairment and dementia (Obisesan, 2009; Walker et al., 2017; Wright and Harding, 2019), little is known about the long-term neurological consequences of preeclampsia on both mothers and even less so in children. What is well known in the preeclampsia field is the increased risk of cardiovascular incidents in mothers, including increased risk of long-term hypertension and stroke, and increased mortality due to major cardiovascular events, as well as early onset hypertension, increased risk of ischemic heart disease and strokes in children (Bokslag et al., 2016; Goffin et al., 2018). The focus of studies evaluating the risks associated with preeclampsia has thus been on cardiovascular health, often disregarding the relationship between cardiovascular disease and late-life dementia (Justin et al., 2013). Cognitive effects of preeclampsia on mothers revealed only subjective memory complaints in the short term with no significant long-term consequences after adjusting for other relevant risk actors, while developmental and behavioral consequences in offspring are evident, but not often studied beyond the age of 12 years old, again focusing mostly on short-term effects (Figueiro-Filho et al., 2017; Dayan et al., 2018; Elharram et al., 2018).

In part due to a lack of understanding underlying the etiology of preeclampsia and its multifactorial nature, different animal models have been used to mimic different aspects of this condition. These models recapitulate alterations in angiogenesis, immune responses, disrupted oxygen metabolism, and abnormal trophoblast invasion seen in humans (Pennington et al., 2012; Marshall et al., 2018). Of interest, the renin-angiotensin system (RAS) has been implicated in the development of preeclampsia (Shah, 2005) and alterations in the RAS have been linked to cognitive decline and dementia (Wright and Harding, 2019). Here, we used transgenic female mice overexpressing human angiotensinogen and renin (R^+A^+ females) that are chronically hypertensive. This is a realistic disease model of preeclampsia superimposed on chronic hypertension, not only because chronic hypertension represents a major risk factor for developing preeclampsia during pregnancy, but because these mice mimic several aspects of preeclampsia, including aggravated hypertension during pregnancy, glomerular endotheliosis, proteinuria, placental necrosis, lower pup weights, impaired angiogenesis of uteroplacental vessels, and increased circulating anti-angiogenic factors (Falcao et al., 2009; Marshall et al., 2018). This pilot study aimed to assess whether preeclampsia incurs any behavioral consequences in the long term in R^+A^+ mothers, and whether this is also imparted on their offspring. Our study corroborates findings from human studies and reveals the presence of cognitive impairment later in life in offspring born from preeclamptic mothers, thus providing further validation of this mouse model for future studies to decipher the underlying mechanisms of these cognitive deficits in mothers and offspring.

MATERIALS AND METHODS

Study Design

Mice were produced by breeding transgenic male mice heterozygous for human renin (Ren9 line) with female mice heterozygous for overexpressing human angiotensinogen (204/1 line) (Falcao et al., 2009). An equal number (n = 15/group, 4 months of age) of control females (a mixture of R^-A^-, R^-A^+, and R^+A^- genotypes) and transgenic females with the R^+A^+ genotype, predisposed to become preeclamptic during pregnancy, entered the study. Baseline blood pressure (BP) was measured, and urine samples collected to assess proteinuria prior to mating. All females were then paired with a wild type (C57BL/6 background) male for breeding, and a female was deemed pregnant by the presence of a vaginal plug and later confirmed by weight gain. After 2 months of mating 13/15 control females became pregnant (average litter size of 5.69 $\pm$ 0.47), while only 8/15 R^+A^+ were pregnant (average litter size of 6.38 $\pm$ 0.65). Fifteen and eighteen days following the initial plug, a urine sample was collected, and BP was measured; this was also performed 5 days after giving birth, at which point pups were weighed. Urine samples and BP were taken in mothers 3, 6, and 12 months postpartum (PP). Cognitive testing on mothers was performed at 9, 14, and 18 months of age (or 3, 8, and 12 months PP) alongside a subset of their offspring (3, 8, and 12 months of age, equally distributed males and females). Likely due to R^+A^+ females being chronically hypertensive, we found a higher death rate over time in this group, leaving us with n = 5 at study endpoint (12 months PP). Due to differences in cognitive function in offspring at 12 months of age and sufficient group sizes, we used optical imaging of intrinsic signals (n = 6/group) to asses cerebral hemodynamic function. Experiments were approved by the Animal Ethics Committee of the Montreal Neurological Institute (McGill University, Montréal, Québec, Canada) and complied with the Canadian Council on Animal Care.

Assessing Preeclampsia Traits in Mouse Model

Proteinuria

Urine samples (~100 μL) were collected in 1.5 mL centrifuge tubes from mothers prior to being impregnated (baseline), and then after 15 days of gestation (day 1 defined by the presence of a plug), 18 days of gestation, 5 days PP and before the first behavioral test, 3 and 8 months PP. Samples were kept at −80°C, and then thawed and diluted 1:10 before measurements were made in duplicate. Proteinuria was determined as the ratio of albumin:creatinine using Albuwell and Creatinine companion mouse ELISA kits (Exocell, Philadelphia, PA) according to manufacturer's protocol.

Blood Pressure (BP)

Blood pressure was measured (n = 10 mice/group) after each behavioral timepoint in mothers, and at 6 months of age in a subset of offspring using non-invasive tail-cuff plethysmography (Kent Scientific Company). Mice were habituated to the restraining device and tail cuffs for 10 min/d for 3 days before measurements were recorded. Ten additional acclimation cycles were performed before acquiring five measurements of systolic, diastolic, and mean blood pressure. This was performed 1 week prior to each behavioral testing session.

Pup Weight

Five days after birth, pups were individually weighed on a scale tarred with a small piece of nesting material and immediately returned to their mother's nest. The average weight of the pups from individual mothers was calculated, and then compared based on mother's genotype.

Morris Water Maze (MWM)

Spatial cognitive function was evaluated in the MWM (Deipolyi et al., 2008) at 2 time points in mothers and offspring. A pool (1.4 m diameter) was filled with water (18 ± 1°C) made opaque with inert white Tempera paint. Three initial visible platform training days were performed: On each day, the mice were given three trials of 60 s separated by approximately 45 min to find the platform (15 cm diameter). Before the 5-days learning phase of the task began, the visual cues in the room were changed, as was the location of the platform, which was completely submerged (1 cm below the surface of the water). Mice were given three trials of 90 s to find the hidden platform. On the final day (day 9 for first timepoint), a probe trial was conducted to assess spatial memory. The platform was removed from the pool and the mice were given 60 s of free swim in which the time they spent swimming and the distance they swam in the quadrant that contained the platform was recorded as well as the number of times they would have landed on the platform if it were present. All data was recorded using the 2020 Plus tracking system and Water 2020 software (Ganz FC62D video camera; HVS Image, Buckingham, United Kingdom). When the MWM was conducted at the second time point (8 months postpartum or 8 months of age for the pups), the only differences in the test were that the mice were only provided with one training day to locate the platform before it was hidden (the probe trial being performed on day 7), and the locations of the spatial cues and platform were changed. Due to the sample size of R^+A^+ mothers decreasing to $n = 5$ at 12 months PP, along with no cognitive deficits observed at 8 months PP, no MWM was conducted at this last timepoint.

Novel Object Recognition (NOR)

Following the MWM, mothers and offspring were habituated (10 min) to the NOR testing arena (45 cm wide × 45 cm long × 50 cm high). The following day, mice underwent both the familiarization and test phases. During familiarization, each mouse was given 5 min to explore 2 identical objects placed in opposite corners of the arena, equidistant from the center. Two hours after familiarization, one of the objects was replaced with a novel object and another 5 min exploration period was allotted. Both the location of the novel object and the objects were counterbalanced. Behavior was recorded using iSpy software and ODLog to record the amount of time spent exploring each object. An investigation ratio was calculated by dividing the time spent with the novel object by the total time investigating both objects during the test phase. This test was conducted at 3 separate time points using different pairs of objects at each time.

Imaging of Optical Intrinsic Signals (OIS)

A subset of pups ($n = 6$/group, 12 months) were implanted with a cranial window made of a cover glass glued on a thinned bone preparation over the left barrel cortex and allowed 2 weeks to recover before imaging. Mice were anesthetized (ketamine 85 mg/kg/xylazine 3 mg/kg, i.m.) and fixed with ear bars on a physiological platform (Harvard Apparatus #75–1,500, Saint-Laurent, QC, Canada) with online recording of body temperature, heart rate and respiratory rate. The platform was then moved to the imaging system (OIS200 from LabeoTech, Montréal, QC, Canada); the mouse cranial window placed parallel to the camera. Whisker-evoked changes in total, oxy- and deoxyhemoglobin (HbT, HbO, and HbR, respectively) were measured with three light emitting diodes (LEDs, 525, 590, and 625 nm) placed 8 cm from the cranial window. Whisker-evoked changes in cerebral blood flow (CBF) were measured with laser speckle contrast imaging using a 780 nm laser diode. Images were acquired at a frame rate of 30 Hz in total (7.5 Hz for each wavelength), with a 14 ms exposure time. Each recording consisted of 7 blocks of right whisker stimulation (8 Hz, 10 s followed by a rest period of 40 s using a piezo actuator). We included a jitter of 3 s to avoid habituation to the stimulation timing for the mice. Data were lowpass filtered at 0.3 Hz to suppress high frequency noise (mouse respiration) and analyzed using MATLAB to obtain whisker-evoked changes in cerebral blood volume and CBF from baseline. Analysis was as described in Dubeau et al. (2011). Briefly, reflectance signals were converted to changes in absorption $\Delta A = \log(R/R_0)$, and a pseudo-inverse and the modified Beer–Lambert law were used to extract relative changes in HbR and HbO. CBF was computed by quantifying the spatial contrast during laser illumination, defined as the ratio of the standard deviation to the mean intensity in a given spatial area. For each animal, the spatial location of the response in the contralateral barrel cortex was first identified. A region of interest around the maximum response was manually delineated avoiding medium, large arteries, and veins, and the signal averaged over all pixels to recover an impulse response function for each component: HbO, HbR, and CBF.

Statistical Analysis

All behavioral and imaging experiments were performed blind to the identity of the mice. Independent samples t-tests were conducted using GraphPad Prism 7, a $p = 0.05$ was considered statistically significant.

RESULTS

Model Characterization of Mothers

Due to chronic overexpression of human angiotensinogen and renin, the mouse model used in this study of preeclampsia superimposed on chronic hypertension, is not only hypertensive during gestation, with a slight increase in BP from D15 to D18, but is chronically hypertensive as shown by elevated mean BP prior to pregnancy (baseline) and continued elevated BP levels when measured PP (**Figure 1A**). The majority of offspring (19/23) were negative for human renin and/or angiotensinogen, however 4 pups had the R^+A^+ genotype and were hypertensive when measured at 6 months of age

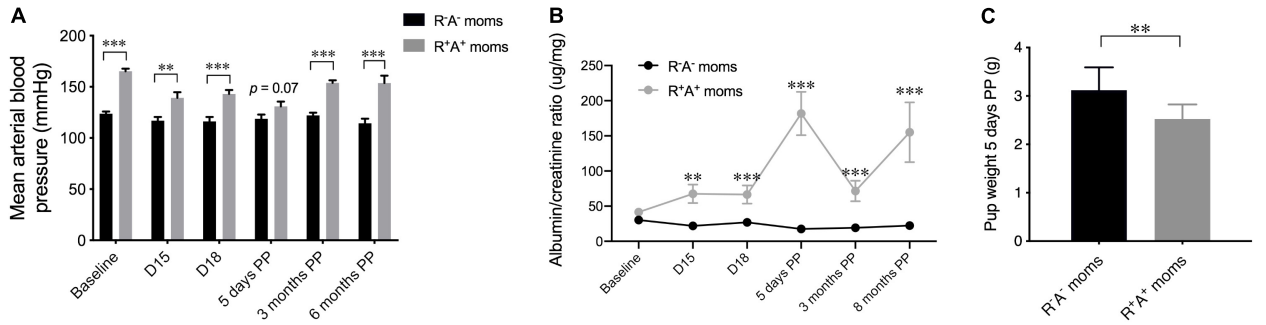

FIGURE 1 | Preeclampsia model characteristics. **(A)** Mean arterial blood pressure shown at different timepoints for the mothers throughout the study beginning at baseline prior to mating, two times during pregnancy and three postpartum (PP) timepoints, revealing that this model is chronically hypertensive. **(B)** Urinalysis quantification over the same timepoints in mothers revealing an increased albumin:creatine ratio in R^+A^+ mothers during pregnancy that persisted up to 8 months PP. **(C)** The average pup weight 5 days PP from individual mothers was averaged and shown here indicating R^+A^+ birthed smaller pups than control mothers. N = 10–13 for control mothers and n = 5–8 for preeclamptic (R^+A^+) mothers, $^{**}p < 0.01$ and $^{***}p < 0.001$.

(mean BP of 160.36 mmHg ± 3.2 compared to control pups 124.30 mmHg ± 3.49). These hypertensive pups were examined with caution following all measures, but they did not significantly differ from normotensive pups birthed by the same R^+A^+ mothers. A cardinal feature of preeclampsia is the presence of proteinuria during pregnancy, assessed here by the ratio of albumin to creatine (**Figure 1B**), which not only showed increases during gestation (D15 $p < 0.01$, and D18 $p < 0.001$) but also PP, spiking sharply at 5 days PP ($p < 0.001$) and remaining elevated at 3 months PP ($p < 0.01$), and even more so at 8 months PP ($p < 0.001$), prolonged or persistent proteinuria has been found as long as 2 years after delivery in preeclamptic women (Berks et al., 2009; Unverdi et al., 2013). Another indication of preeclampsia is a lower birth weight of the offspring, measured here 5 days PP, that revealed pups from preeclamptic mothers weighing significantly less ($p < 0.01$) than those from control mothers (**Figure 1C**).

Behavioral Consequences on Mothers and Offspring

When tested on the MWM for spatial learning and memory, a primarily hippocampal-dependent task, preeclamptic mothers did not differ from control mothers on the visible platform training days (days 1–3) 3 months PP, indicating that they were capable of performing the task. However, when the platform was hidden, preeclamptic mothers took significantly more time to locate the platform on days 4–6 (**Figure 2A**) before learning the location to the same capacity as the control mothers on days 7 and 8, where there is no difference in escape latency. On day 9 when assessed for spatial memory, there were no differences between groups on any parameter measured (**Figure 2A**). Interestingly, the differences observed in spatial learning did not persist at 8 months PP in the mothers, and no difference in spatial memory was observed (**Figure 2B**). When comparing the pups of these mothers on the same MWM task at both 3 and 8 months of age, no differences were observed in spatial learning nor in spatial memory (**Figures 2C,D**). When testing for object recognition memory at 3 months PP in the dams and 3 months of age for the pups (**Figure 3A**), only preeclamptic mothers showed a deficit ($p < 0.05$). Despite a trend ($p = 0.09$) this deficit was no longer present at 8 months PP (**Figure 3B**) nor at 12 months PP in mothers (**Figure 3C**). However the pups from preeclamptic mothers presented a different tendency such that they began to display a significant deficit on this object memory task (investigation ratio of 0.42 ± 0.06 compared to 0.59 ± 0.05 in controls, $p < 0.05$) at 8 months, and not only did this deficit persist but also worsened when tested at 12 months of age (investigation ratio of 0.37 ± 0.06 compared to 0.69 ± 0.05 in controls, $p < 0.001$).

Hemodynamic Alterations in Offspring

Due to the presence of a cognitive deficit in the pups at the 12-months endpoint, offspring were examined for possible hemodynamic alterations that could be contributing to worse cognitive performance. Surprisingly, we found there was a larger whisker-evoked CBF response in the contralateral barrel cortex (11.22% ± 0.49 increase from baseline) in pups from preeclamptic mothers compared to that elicited in the offspring of control mothers (6.93% ± 0.89, **Figure 4A**) and quantified in **Figure 4C**. In line with this finding, whisker stimulation elicited an enhanced response in total hemoglobin (HbT) during the stimulation period [$t(10) = 4.51$, $p < 0.01$] in the offspring of preeclamptic mothers, largely driven by an increase in oxygenated Hb (HbO) by nearly twofold: HbO during whisker-stimulation of pups from preeclamptic mothers being 4.16 mM ± 0.17, and 2.50 mM ± 0.30 from control pups $t(10) = 4.22$, $p < 0.01$. No differences in deoxygenated Hb (HbR) were observed between groups. These findings are consistent with whisker-evoked increases in CBF driving the surge in HbO, corresponding to fresh supply of arterial blood, with HbR, typically in veins, being washed out of the activated region, as illustrated by the decreased HbR (**Figure 4B** for raw images and **Figure 4D** for traces and quantification) (Ma et al., 2016).

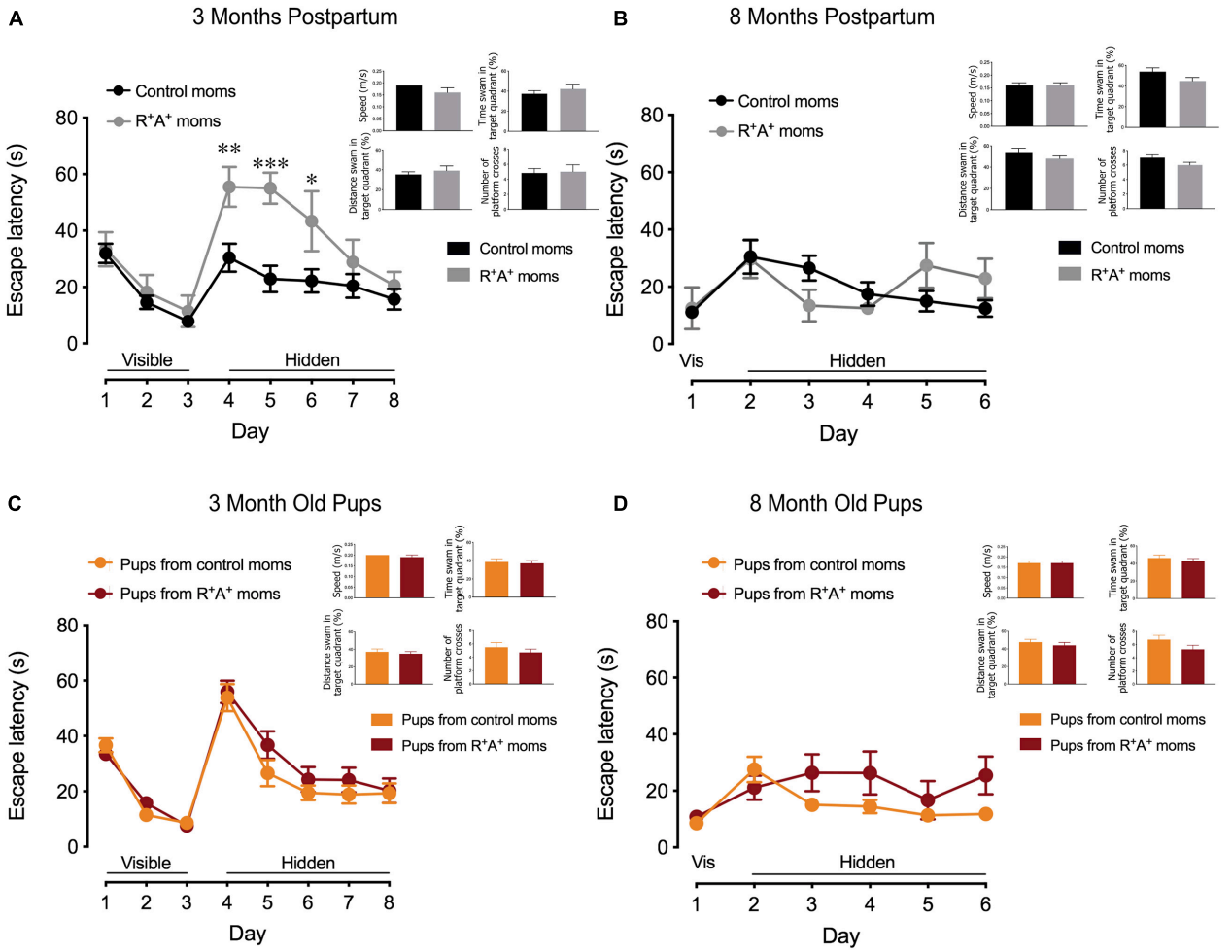

FIGURE 2 | Spatial learning and memory testing in mothers and offspring. **(A)** Spatial learning portion of MWM in mothers 3 months PP showing deficits in preeclamptic mothers (R^+A^+, $n = 7$) early during the learning phase but without any spatial memory deficits measured during the probe trial compared to control mothers ($n = 12$). **(C)** Regardless of the genotype of their birth mother, 3-months old pups ($n = 18$–26/group) showed no differences in spatial learning nor memory. **(B)** At 8 months PP another MWM was conducted, revealing no spatial learning and memory deficits in the mothers nor in the pups **(D)**. Sample size at 8 months PP, control mothers $n = 10$, R^+A^+ mothers $n = 6$. Due to no observed sex differences in pups at 3 months of age, group sizes were reduced at random when tested at 8 months to $n = 11$/group. $^*p < 0.05$, $^{**}p < 0.01$, and $^{***}p < 0.001$.

DISCUSSION

In this pilot study, we investigated the long-term cognitive consequences in both preeclamptic transgenic R^+A^+ mothers and their offspring, and found evidence that supports the notion that mothers experience short-term deficits, while offspring showed longer lasting impairments on an object recognition task as far as 12-months of age. Moreover, we provide new evidence for alterations in cerebrovascular function in offspring at a time when they display cognitive deficits.

One link worth further exploring between altered cerebrovascular and behavioral function in offspring of preeclamptic mothers stems from the fact that levels of placental growth factor (PGF) were markedly low during a preeclamptic pregnancy. One group has used PGF knockout mice as a preclinical model for offspring of preeclamptic mothers and found working memory deficits along with increased vascular density and length at the capillary level, without any changes in cerebral blood volume (Kay et al., 2018). Furthermore, when challenged with a common carotid artery ligation, CBF was lower in the PGF knockout mice, as measured by laser Doppler flowmetry (Luna et al., 2016). Other factors implicated in preeclamptic pregnancies include a hypoxic fetal environment, increased exposure to cortisol, altered production of angiogenic factors, and increased production of pro-inflammatory cytokines, all of which could impact the development of the cerebrovascular system (Kay et al., 2019; Maher et al., 2019). Furthermore, epigenetic alterations have been described in the preeclamptic placenta, mostly in the context of disease development and associated to the environmental changes listed above. Hence, the possibility that abnormal DNA methylation during preeclamptic placental development is involved in long-term cognitive

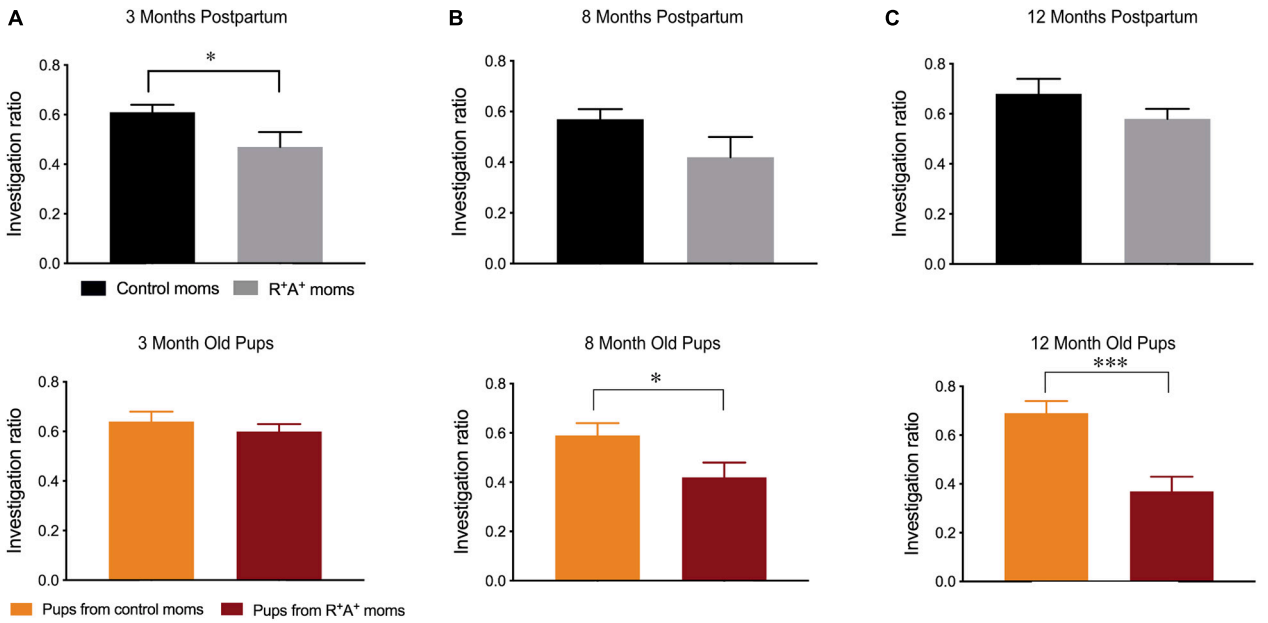

FIGURE 3 | Novel object recognition memory testing in mothers and offspring. **(A)** NOR investigation ratios for mothers 3 months PP (R^+A^+ $n = 7$, controls $n = 12$) and pups at 3 months of age ($n = 18$–26/group) revealing a deficit in preeclamptic mothers. While no deficits were observed in mothers at 8 **(B)** nor 12 months PP **(C)**, pups born from preeclamptic mothers had impaired performance at these two age points **(B,C)**. Samples sizes at 8 and 12 months: control mothers $n = 10$, R^+A^+ mothers $n = 5$–6, pups $n = 11$/group. $^*p < 0.05$ $^{***}p < 0.001$.

consequences merits further investigation (Apicella et al., 2019; Kamrani et al., 2019). While we acknowledge that there could be many factors at play that caused the offspring of preeclamptic mothers to show cognitive deficits, we explored the possibility that a consequence of these *in utero* alterations could be associated with altered cerebral hemodynamics, which have been found to underlay cognitive impairment in different contexts related to cardiovascular disease and dementia.

The regulation of CBF is altered by pregnancy, and even further by hypertension; both hypo- and hyperperfusion have been observed in preeclamptic mothers (Jones-Muhammad and Warrington, 2019), and this seems to be related to the severity of the condition, whereby more severe preeclampsia resulted in hyperperfusion measured in the middle cerebral artery by transcranial laser Doppler prior to delivery (Belfort et al., 1999; van Veen et al., 2015). Although we did not measure baseline perfusion, we found elevated whisker-evoked CBF responses and cerebral blood volume characterized by enhanced evoked relative oxygenated hemoglobin levels in 12 month-old offspring of R^+A^+ preeclamptic mothers. Interestingly, while we found an enhanced hyperemic response, hyperperfusion has been observed in preeclamptic patients and has been linked to decreased vascular resistance, which can further lead to disruptions of the blood brain barrier and negative neurological outcomes (Hammer and Cipolla, 2015). While the resistance in an individual capillary is quite high, when there is a dense capillary bed with several small vessels running parallel to one another, vascular resistance drops (Mandeville and Rosen, 2002). It is therefore possible that if the offspring in our study also experienced altered angiogenesis as seen in the PGF model (Kay et al., 2018), then global cerebral vascular resistance could be decreased, thus providing an explanation for the observed increased perfusion in response to whisker stimulation compared to control offspring. In a hypertensive environment, cerebral vessels are remodeled to protect against sudden spikes in blood pressure, however this could impair their general function at lower blood pressures (Jones-Muhammad and Warrington, 2019). Due to the offspring developing in a hypertensive environment and thus exposed to circulating factors that cross the placental barrier, despite the majority not being hypertensive themselves, this could also help to explain the elevated hemodynamic responses.

There exists a tight communication between neural cells and blood vessels termed neurovascular coupling, and here we observe an altered hemodynamic response whereby too much blood is being sent to the activated somatosensory cortex. We found that oxygenated hemoglobin levels were elevated in response to the same sensory stimulus in offspring of preeclamptic mothers. Capillaries are comprised mainly of endothelial cells, which play an important role in neurovascular coupling (Chen et al., 2014), and are the site of oxygen exchange, making it tempting to suggest that this is the primary site of dysfunction in the offspring, whereby either too much oxygen is being extracted into the parenchyma or that blood flow is too fast, and thus preventing oxygen extraction, leading to high levels in the blood. Either way, there is a clear lack of control over CBF that resulted in an elevated, unfocused/diffuse response in the parenchyma, and such hyperperfusion has been proposed as a

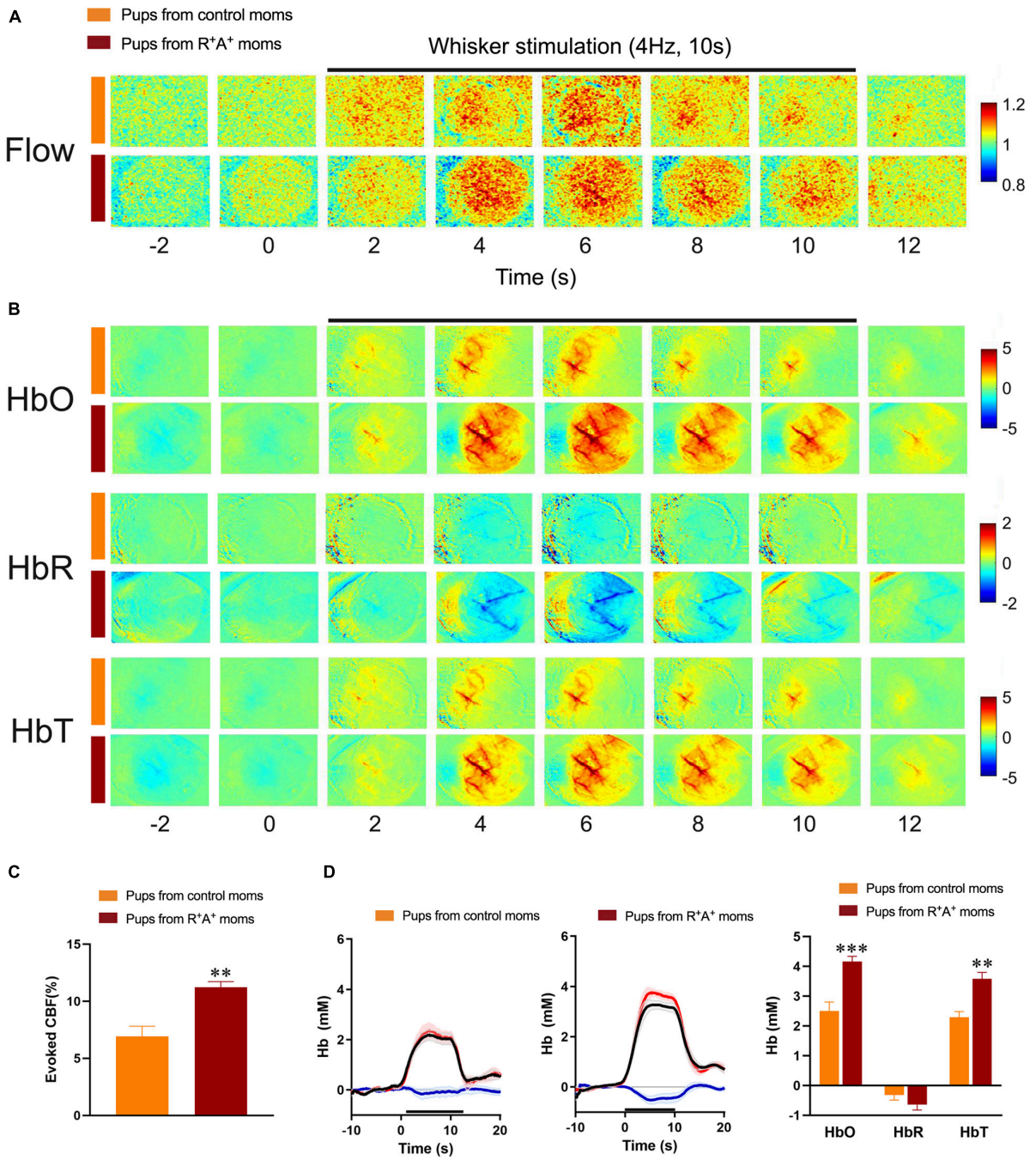

FIGURE 4 | Evaluation of hemodynamic alterations in offspring at 12 months of age. **(A)** Functional laser speckle contrast imaging maps representative of cerebral blood flow (CBF) changes in the barrel cortex in response to whisker stimulation. **(B)** Functional imaging maps of oxygenated (HbO), deoxygenated (HbR) and total hemoglobin (HbT) levels from 4 s prior to stimulus to 2 s after a 10 s whisker stimulation (4 Hz) in offspring of preeclamptic (red bars) and control mothers (orange bars). **(C)** Quantification of laser Speckle contrast imaging showing an increased evoked CBF response in pups from preeclamptic mothers. **(D)** Average traces and quantification of peak concentrations (mM) of HbO (red line), HbR (blue line), and HbT (black line) from offspring revealing a significant increase in HbO and HbT levels in pups from preeclamptic mothers. $N = 6$/group $^{**}p < 0.01$ and $^{***}p < 0.001$.

compensatory mechanism in asymptomatic individuals at risk for late life dementia (Ostergaard et al., 2013).

In this pilot study we used the pups from an established model of preeclampsia and validated their use for future studies as a realistic model of offspring of preeclamptic mothers in terms of their cognitive outcome. Our findings are in line with cognition being altered in preeclamptic mothers in the short-term without any lasting deficits (Dayan et al., 2018; Elharram et al., 2018).

They also draw attention to the necessity for more research focusing on children born under preeclamptic conditions to better understand the cerebrovascular mechanisms that may accompany cognitive deficits to try and establish treatments that could be used to actively counteract them from transpiring.

DATA AVAILABILITY STATEMENT

The raw data supporting the conclusions of this article will be made available by the authors, without undue reservation, to any qualified researcher.

ETHICS STATEMENT

The animal study was reviewed and approved by the Animal Ethics Committee of the Montreal Neurological Institute.

AUTHOR CONTRIBUTIONS

LT assisted in the design of the study, conducted all behavioral experiments, measured blood pressure and took urine samples at all time points excluding baseline, analyzed data, and wrote and finalized the manuscript. CL implanted mice with cranial windows and performed optical imaging experiments and analysis. JR assisted in the study design and acquired baseline urine and blood pressure measurements. JL provided the mouse model used in this pilot study and provided equipment for urine analysis to assess proteinuria. FL provided their expertise and codes for analysis of optical. LP helping to initiated the study and contributed to the editing of the final manuscript. EH supervised the project, assisted in the design of the study, contributed to the writing, and editing of the final manuscript. All authors contributed to the article and approved the submitted version.

FUNDING

This work was supported by grants (EH) from the Canadian Institutes of Health Research (CIHR-MOP-126001), the Canadian Vascular Network (EH and LP), and studentships (LT) from the Canadian Vascular Network, McGill Healthy Brains for Healthy Lives and the Fonds de recherche du Québec—Santé (FRQS).

ACKNOWLEDGMENTS

We would like to acknowledge Brent Fortin-Boily for his work on the code for OIS data analysis and to Émilie Pepin for performing genotyping and biochemical analysis on urine samples.

REFERENCES

Apicella, C., Ruano, C. S. M., Méhats, C., Miralles, F., and Vaiman, D. (2019). The role of epigenetics in placental development and the etiology of preeclampsia. *Int. J. Mol. Sci.* 20:2837. doi: 10.3390/ijms20112837

Belfort, M. A., Grunewald, C., Saade, G. R., Varner, M., and Nisell, H. (1999). Preeclampsia may cause both overperfusion and underperfusion of the brain. *Acta Obstet. Gynecol. Scand.* 78, 586–591. doi: 10.1034/j.1600-0412.1999.780705.x

Berks, D., Steegers, E. A. P., Molas, M., and Visser, W. (2009). Resolution of hypertension and proteinuria after preeclampsia. *Obstet. Gynecol.* 114, 1307–1311. doi: 10.1097/aog.0b013e3181c14e3e

Bokslag, A., van Weissenbruch, M., Mol, B. W., and de Groot, C. J. (2016). Preeclampsia; short and long-term consequences for mother and neonate. *Early Hum. Dev.* 102, 47–50.

Chen, B. R., Kozberg, M. G., Bouchard, M. B., Shaik, M. A., and Hillman, E. M. (2014). A critical role for the vascular endothelium in functional neurovascular coupling in the brain. *J. Am. Heart Assoc.* 3:e000787.

Dayan, N., Kaur, A., Elharram, M., Rossi, A. M., and Pilote, L. (2018). Impact of preeclampsia on long-term cognitive function. *Hypertension* 72, 1374–1380. doi: 10.1161/hypertensionaha.118.11320

Deipolyi, A. R., Fang, S., Palop, J. J., Yu, G. Q., Wang, X., Mucke, L., et al. (2008). Altered navigational strategy use and visuospatial deficits in hAPP transgenic mice. *Neurobiol. Aging* 29, 253–266. doi: 10.1016/j.neurobiolaging.2006.10.021

Dubeau, S., Desjardins, M., Pouliot, P., Beaumont, E., Gaudreau, P., Ferland, G., et al. (2011). Biophysical model estimation of neurovascular parameters in a rat model of healthy aging. *Neuroimage* 57, 1480–1491. doi: 10.1016/j.neuroimage.2011.04.030

Elharram, M., Dayan, N., Kaur, A., Landry, T., and Pilote, L. (2018). Long-term cognitive impairment after preeclampsia: a systematic review and meta-analysis. *Obstet. Gynecol.* 132, 355–364. doi: 10.1097/aog.0000000000002686

Falcao, S., Stoyanova, E., Cloutier, G., Maurice, R. L., Gutkowska, J., Lavoie, J. L., et al. (2009). Mice overexpressing both human angiotensinogen and human renin as a model of superimposed preeclampsia on chronic hypertension. *Hypertension* 54, 1401–1407. doi: 10.1161/hypertensionaha.109.137356

Figueiro-Filho, E. A., Mak, L. E., Reynolds, J. N., Stroman, P. W., Smith, G. N., Forkert, N. D., et al. (2017). Neurological function in children born to preeclamptic and hypertensive mothers–a systematic review. *Pregnancy Hypertens.* 10, 1–6. doi: 10.1016/j.preghy.2017.07.144

Fox, R., Kitt, J., Leeson, P., Aye, C. Y. L., and Lewandowski, A. J. (2019). Preeclampsia: risk factors, diagnosis, management, and the cardiovascular impact on the offspring. *J. Clin. Med.* 8:1625. doi: 10.3390/jcm8101625

Goffin, S. M., Derraik, J. G. B., Groom, K. M., and Cutfield, W. S. (2018). Maternal pre-eclampsia and long-term offspring health: is there a shadow cast? *Pregnancy Hypertens.* 12, 11–15. doi: 10.1016/j.preghy.2018.02.003

Hammer, E. S., and Cipolla, M. J. (2015). Cerebrovascular dysfunction in preeclamptic pregnancies. *Curr. Hypertens. Rep.* 17:64.

Jones-Muhammad, M., and Warrington, J. P. (2019). Cerebral blood flow regulation in pregnancy, hypertension, and hypertensive disorders of pregnancy. *Brain Sci.* 9:224. doi: 10.3390/brainsci9090224

Justin, B. N., Turek, M., and Hakim, A. M. (2013). Heart disease as a risk factor for dementia. *Clin. Epidemiol.* 5, 135–145. doi: 10.2147/clep.s30621

Kamrani, A., Alipourfard, I., Ahmadi-Khiavi, H., Yousefi, M., Rostamzadeh, D., Izadi, M., et al. (2019). The role of epigenetic changes in preeclampsia. *Biofactors* 45, 712–724. doi: 10.1002/biof.1542

Kay, V. R., Rätsep, M. T., Cahill, L. S., Hickman, A. F., Zavan, B., Newport, M. E., et al. (2018). Effects of placental growth factor deficiency on behavior, neuroanatomy, and cerebrovasculature of mice. *Physiol. Genomics* 50, 862–875. doi: 10.1152/physiolgenomics.00076.2018

Kay, V. R., Wedel, N., and Smith, G. N. (2019). Preeclampsia may influence offspring neuroanatomy and cognitive function: a role for placental growth factor. *Biol. Reprod.* 101, 271–283. doi: 10.1093/biolre/ioz095

Kongwattanakul, K., Saksiriwuttho, P., Chaiyarach, S., and Thepsuthammarat, K. (2018). Incidence, characteristics, maternal complications, and perinatal outcomes associated with preeclampsia with severe features and HELLP syndrome. *Int. J. Womens Health* 10, 371–377. doi: 10.2147/IJWH.S168569

Luna, R. L., Kay, V. R., Rätsep, M. T., Khalaj, K., Bidarimath, M., Peterson, N., et al. (2016). Placental growth factor deficiency is associated with impaired

cerebral vascular development in mice. *Mol. Hum. Reprod.* 22, 130–142. doi: 10.1093/molehr/gav069

Ma, Y., Shaik, M. A., Kim, S. H., Kozberg, M. G., Thibodeaux, D. N., Zhao, H. T., et al. (2016). Wide-field optical mapping of neural activity and brain haemodynamics: considerations and novel approaches. *Philos. Trans. R. Soc. Lond. B Biol. Sci.* 371:20150360. doi: 10.1098/rstb.2015.0360

Maher, G. M., McCarthy, F. P., McCarthy, C. M., Kenny, L. C., Kearney, P. M., Khashan, A. S., et al. (2019). A perspective on pre-eclampsia and neurodevelopmental outcomes in the offspring: does maternal inflammation play a role? *Int. J. Dev. Neurosci.* 77, 69–76. doi: 10.1016/j.ijdevneu.2018.10.004

Mandeville, J. B., and Rosen, B. R. (2002). *Brain Mapping: The Methods*, 2nd Edn. Cambridge, MA: Academic Press.

Marshall, S. A., Hannan, N. J., Jelinic, M., Nguyen, T. P. H., Girling, J. E., Parry, L. J., et al. (2018). Animal models of preeclampsia: translational failings and why. *Am. J. Physiol. Regul. Integr. Comp. Physiol.* 314, R499–R508.

Obisesan, T. O. (2009). Hypertension and cognitive function. *Clin. Geriatr. Med.* 25, 259–288.

Ostergaard, L., Aamand, R., Gutiérrez-Jiménez, E., Ho, Y. C., Blicher, J. U., Madsen, S. M., et al. (2013). The capillary dysfunction hypothesis of Alzheimer's disease. *Neurobiol. Aging* 34, 1018–1031.

Pennington, K. A., Schlitt, J. M., Jackson, D. L., Schulz, L. C., and Schust, D. J. (2012). Preeclampsia: multiple approaches for a multifactorial disease. *Dis. Model. Mech.* 5, 9–18. doi: 10.1242/dmm.008516

Shah, D. M. (2005). Role of the renin-angiotensin system in the pathogenesis of preeclampsia. *Am. J. Physiol. Renal. Physiol.* 288, F614–F625.

Unverdi, S., Ceri, M., Unverdi, H., Yilmaz, R., Akcay, A., Duranay, M., et al. (2013). Postpartum persistent proteinuria after preeclampsia: a single-center experience. *Wien. Klin. Wochenschr.* 125, 91–95. doi: 10.1007/s00508-013-0320-8

van Veen, T. R., Panerai, R. B., Haeri, S., Singh, J., Adusumalli, J. A., Zeeman, G. G., et al. (2015). Cerebral autoregulation in different hypertensive disorders of pregnancy. *Am. J. Obstet. Gynecol.* 212, e1–e7.

Walker, K. A., Power, M. C., and Gottesman, R. F. (2017). Defining the relationship between hypertension, cognitive decline, and dementia: a review. *Curr. Hypertens Rep.* 19:24.

Wright, J. W., and Harding, J. W. (2019). Contributions by the brain renin-angiotensin system to memory, cognition, and Alzheimer's disease. *J. Alzheimers Dis.* 67, 469–480. doi: 10.3233/jad-181035

Conflict of Interest: The authors declare that the research was conducted in the absence of any commercial or financial relationships that could be construed as a potential conflict of interest.

Advantages of publishing in Frontiers

OPEN ACCESS
Articles are free to read for greatest visibility and readership

FAST PUBLICATION
Around 90 days from submission to decision

HIGH QUALITY PEER-REVIEW
Rigorous, collaborative, and constructive peer-review

TRANSPARENT PEER-REVIEW
Editors and reviewers acknowledged by name on published articles

Frontiers
Avenue du Tribunal-Fédéral 34
1005 Lausanne | Switzerland

Visit us: www.frontiersin.org
Contact us: frontiersin.org/about/contact

REPRODUCIBILITY OF RESEARCH
Support open data and methods to enhance research reproducibility

DIGITAL PUBLISHING
Articles designed for optimal readership across devices

FOLLOW US
@frontiersin

IMPACT METRICS
Advanced article metrics track visibility across digital media

EXTENSIVE PROMOTION
Marketing and promotion of impactful research

LOOP RESEARCH NETWORK
Our network increases your article's readership